Transactions of the ASME®

Journal of Applied Mechanics

Published Quarterly by The American Society of Mechanical Engineers

VOLUME 56 • NUMBER 2 • JUNE 1989

Transactions of the ASME, Journal of Applied Mechanics (ISSN 0021-8936) is published quarterly (Mar., June, Sept., Dec.) for $120 per year by The American Society of Mechanical Engineers, 345 East 47th Street, New York, NY 10017. Second class postage paid at New York, NY and additional mailing offices. POSTMASTER: Send address changes to Transactions of the ASME, Journal of Applied Mechanics, c/o THE AMERICAN SOCIETY OF MECHANICAL ENGINEERS, 22 Law Drive, Box 2300, Fairfield, NJ 07007-2300.

CHANGES OF ADDRESS must be received at Society headquarters seven weeks before they are to be effective. Please send old label and new address.

PRICES: To members, $29.00, annually; to nonmembers, $120.00. Add $15.00 for postage to countries outside the United States and Canada.

INDEXED by Applied Mechanics Reviews and Engineering Information, Inc.

(Contents continued on Inside Back Cover)

CONTENTS (Continued)

BRIEF NOTES

BOOK REVIEWS

ERRATA

In Memoriam

Eli Sternberg

Eli Sternberg, perhaps the best known scholar in the field of elasticity during most of the past half-century, died suddenly in Pasadena, California, on October 8, 1988, shortly before his seventy-first birthday.

Sternberg was born in Vienna in 1917. He left Europe for the United States during the late 1930s, taking his bachelor's degree in civil engineering at North Carolina State University in 1941. After receiving the Ph.D. in mechanics from Illinois Institute of Technology in 1945, he remained at that institution as a member of the faculty, becoming a full professor in 1951. He left I.I.T. in 1956 to join Brown University's Division of Applied Mathematics, which had recently been developed by William Prager into one of the world's foremost centers of activity in continuum mechanics. Upon returning from sabbatical leave in Japan in 1964, Sternberg joined the faculty at the California Institute of Technology, where he spent the rest of his career, becoming Professor of Mechanics, Emeritus, in July, 1988. In addition to his sabbatical stay in Japan, he also spent academic years in the Netherlands and in Chile.

Eli Sternberg

After his dissertation on elastic fields with linear kinematics but nonlinear stress-strain relations, Sternberg and his Ph.D. research adviser M. A. Sadowsky wrote several papers in the late 1940s on three-dimensional stress concentration at an ellipsoidal cavity. These papers have remained of great interest because of their relevance to issues of interest in fracture mechanics.

A 1952 paper with F. Rosenthal devoted to the elastic sphere under concentrated loads marked the beginning of Sternberg's interest in singular problems in elasticity, an interest that was to persist in a variety of contexts throughout his career. His work on concentrated loads was aimed primarily at clarifying the formulation of such problems, with special concern for questions of uniqueness.

One of the best known early papers of Sternberg, *On Saint-Venant's Principle*, appeared in 1954; in it, he gave mathematical form and proof to the version of the principle put forward shortly before by von Mises. This, too, was a subject to which Sternberg would return in later years.

Elastodynamics occupied Sternberg at various stages of his career. His paper *On the Integration of the Equations of Motion in the Classical Theory of Elasticity*, concerned with representations of the elastodynamic displacement field in terms of potentials, remains the definitive work on this subject today. Indeed, Sternberg's fascination with questions about the completeness of the many classes of displacement and stress potentials in the classical linear theory of elasticity persisted throughout his career.

Together with some of his Ph.D. students, Sternberg undertook sustained studies in thermoelasticity in the late 1950s and viscoelasticity in the 1960s. As in other areas of his research, here, too, he was concerned both with issues at the foundation of his subjects as well as with applications to specific problems of engineering interest.

In later years, Sternberg's interest turned primarily to the theory of finite elasticity, where he studied the effect of nonlinearity on singular elastostatic fields, as well as conservation laws that follow from variational principles.

A noteworthy aspect of Sternberg's career was the presence of several sustained collaborations, especially those with M. E. Gurtin (who was a Ph. D. student of Sternberg's), with J. K. Knowles and with R. Muki. The first of these was with Muki; initially, it was primarily concerned with thermal stress problems. Later, they explored the effect of couple stresses on singular fields, while later still, their interests turned to load transfer problems in fiber-reinforced composites. Shortly after the collaboration with Muki began, Gurtin and Sternberg undertook joint research over a period of several years on a variety of topics, including fundamental theorems in linear elastostatics and elastodynamics, thermoelasticity, and viscoelasticity. The collaborations with Muki and with Gurtin began at Brown; the one with Knowles, devoted primarily to singular problems and problems involving loss of equilibrium ellipticity in finite elasticity, began shortly after Sternberg came to Caltech. It was to last for nearly twenty-five years.

Sternberg's scholarly achievements were recognized through several prestigious awards. He held Fulbright and Guggenheim Fellowships, he was a Fellow of the American Academy of Arts and Sciences, and he was elected to membership in both the National Academy of Engineering and the National Academy of Sciences. He held honorary degrees from North Carolina State University and The Technion in Israel. He received the Timoshenko Medal of the American Society of Mechanical Engineers in 1985.

Sternberg was a superb teacher whose lectures, like his research writings, were distinguished by uncommon clarity, conviction and integrity. His influence on students—even those who were not his research students—was enormous. This enviable academic legacy is aptly illustrated by a quotation taken from the acknowledgment in a recent Ph.D. dissertation written by an exceptionally able Caltech Ph.D. student for whom the research supervisor was *not* Sternberg: after expressing appreciation to the research mentor, the acknowledgment goes on to thank ". . . Professor Eli Sternberg, whose course in elasticity caused me to start thinking about mechanics in an entirely new way."

James K. Knowles
California Institute of Technology

John Dundurs
Professor,
Civil Engineering and
Mechanical Engineering,
Northwestern University,
Evanston, Ill. 60208
Fellow, ASME

Xanthippi Markenscoff
Professor,
Applied Mechanics Division,
University of California, San Diego,
La Jolla, Calif. 92093
Mem. ASME

The Sternberg-Koiter Conclusion and Other Anomalies of the Concentrated Couple

A notable conclusion reached by Sternberg and Koiter 30 years ago is that an elastic wedge loaded by a concentrated couple at its vertex remains a well-posed elasticity problem only as long as the wedge does not degenerate into a reentrant corner. A closely related problem is that of a concentrated couple approaching the tip of a crack. It is shown in this article that the corresponding limits in the stress fields do not exist, but that the Bueckner weight function is obtained by appropriately diminishing the magnitude of the couple. It is also shown that the elastic fields, when a concentrated couple approaches an interface between two materials, depend on the direction from which the interface is approached. Moreover, the elastic wedge embedded in another material is discussed.

Dedication: Eli Sternberg died on the 8th of October 1988. He was the eminent American elastician. As we mourn his death, we cherish remembering him as a scientist and a unique man. We dedicate this paper to his memory.

1 Introduction

We discuss a plane elasticity problem that by now has a long history. The solution for the infinite wedge loaded at its vertex by a concentrated couple was given by Carothers (1912) more than 75 years ago, and apparently rediscovered a decade later by Inglis (1922). In terms of an Airy stress function it is

$$\phi = \frac{M}{D}\left(\theta \cos 2\gamma - \frac{1}{2} \sin 2\theta\right) \tag{1}$$

$$D = \sin 2\gamma - 2\gamma \cos 2\gamma \tag{2}$$

with the symbols used shown in Fig. 1. The corresponding displacement and stress components are

$$2\mu u_r = -\frac{M}{2Dr}(\kappa+1)\sin 2\theta \tag{3}$$

$$2\mu u_\theta = -\frac{M}{2Dr}\{2\cos 2\gamma + (\kappa-1)\cos 2\theta\} \tag{4}$$

$$\sigma_{rr} = \frac{M}{Dr^2} 2\sin 2\theta \tag{5}$$

$$\sigma_{r\theta} = \frac{M}{Dr^2}(\cos 2\gamma - \cos 2\theta) \tag{6}$$

$$\sigma_{\theta\theta} = 0 \tag{7}$$

where μ is the shear modulus, and, with ν denoting Poisson's ratio, $\kappa = 3-4\nu$ for plane strain and $\kappa = (3-\nu)/(1+\nu)$ for plane stress. It was noted eventually by Fillunger (1930) that all is not well with the Carothers solution, because $D=0$ and the elastic fields explode for the special angle $\gamma^* = 0.715\pi = 128.7$ deg which still falls within the admissible range $0 < \gamma \leq \pi$.

The Carothers solution satisfies the vulgar formulation of problems of this type: The tractions vanish on both flanks of

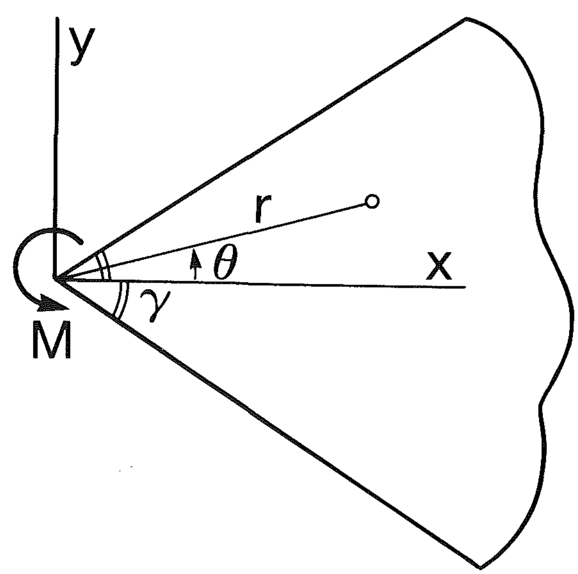

Fig. 1 Wedge subjected to a concentrated couple

Contributed by the Applied Mechanics Division of The American Society of Mechanical Engineers for publication in the Journal of Applied Mechanics.
Discussion on this paper should be addressed to the Editorial Department, ASME, United Engineering Center, 345 East 47th Street, New York, N.Y. 10017, and will be accepted until two months after final publication of the paper itself in the Journal of Applied Mechanics. Manuscript received by ASME Applied Mechanics Division, March 14, 1988; final revision, August 5, 1988.

the wedge, and their resultant on any simple contour around the vertex is equipollent to a couple with the moment M. Moreover, the stresses are proportional to r^{-2} as they should be according to dimensional analysis, since there is no characteristic length in the problem. However, nothing is said in this kind of formulation what a concentration couple actually is. It also may be noted that the two biharmonic functions θ and $\sin 2\theta$ in (1) correspond, respectively, to a concentrated moment and a center of shear acting at an interior point. For $0<\gamma\leq\pi/2$, the shear tractions on a circle centered at the vertex of the wedge are of the same sign. In contrast for $\pi/2<\gamma\leq\pi$, the center of shear causes a twofold reversal in sign of the shear tractions which makes the Carothers solution suspect also on physical grounds when the wedge becomes a reentrant corner.[1]

In the late 1950s, the dilemma noted by Fillunger was considered by Sternberg and Koiter (1958) from the point of view that the concentrated couple applied at the vertex should be a meaningful limit of suitable distributed tractions acting on the flanks of the wedge. Their conclusion, based on a detailed analysis, was that the Carothers solution is valid and that the notion of a concentrated couple applied at the vertex remains meaningful only for wedges up to half plane, or $0<\gamma\leq\pi/2$, and that there is a mathematical breakdown for reentrant corners ($\pi/2<\gamma\leq\pi$).

Since the Sternberg-Koiter conclusion contradicts the notion of perfect order in elasticity, it is not surprising that it led to an extensive discussion[2] and several attempts to explain and possibly mend the situation. We find it impossible to summarize the follow-up papers in detail, and suggest that the interested reader consult the following articles: Sonntag (1961a)—a photoelastic experiment, reentrant corner with the critical angle $\gamma=0.715\,\pi$, couple applied by twisting a glued-in dowel, no signs of anything peculiar happening; Sonntag (1961b)—more photoelastic experiments for other wedge angles and some analytical considerations for $\gamma=\pi/2$ necessitated by the load transmitting dowel, no indication of the twofold sign reversal in the shear tractions predicted by the Carothers solution; Neuber (1963)—a massive article attempting to mend the Carothers solution by applying the couple through a dowel of finite size, succeeds in eliminating the twofold reversal in the sign of shear tractions, but throws no light on the dilemma explored by Sternberg and Koiter; Buchwald (1965)—analysis of the eigenfunction expansion for the wedge, proposed that the solution for $\gamma>\pi/2$ should contain several eigenfunctions even if their fields show a slow decay at infinity, the point that a concentrated couple applied at the vertex must be a limit of a well-posed problem is missed; Barenblatt and Zeldovich (1972) and Barenblatt (1979)—considerations based on self-similarity confirming the Sternberg-Koiter results; Budiansky and Carrier (1973)—wedge loaded through a dowel, shown that satisfactory results can be achieved for the stiffness of the wedge by adding to the Carothers solution eigenfunctions for the wedge with free flanks; and Ting (1985)—attempt to mend the Carothers solution by introducing additional eigenfunctions and using the traditional formulation.

Two points may be made in connection with the Sternberg-Koiter conclusion:

(1) The singularity induced by a concentrated action is very often a physically meaningful elasticity solution for the unbounded domain. But this is not an *a priori* requirement on the singularity, and there are examples to the contrary. For instance, the singularity for a wedge disclination is given by the Airy stress function (Dundurs, 1969)

[1]This observation is due to R. D. Mindlin (see the discussion of the Sternberg-Koiter paper, p. 473).

[2]*Journal of Applied Mechanics*, Vol. 26, 1959, pp. 472–474.

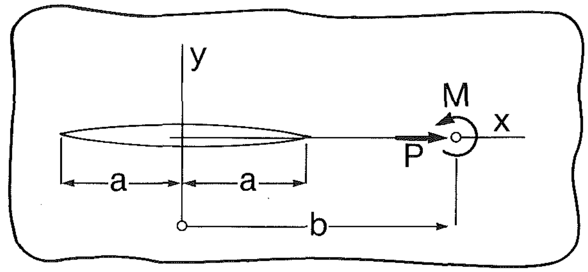

Fig. 2 Concentrated force and couple in the vicinity of a crack tip

$$\phi=\frac{\omega\mu}{\pi(\kappa+1)}\,r^2\log r \tag{8}$$

where ω is the angle of the wedge-shaped material cut out before closing the gap. The stresses corresponding to (8) become logarithmically infinite at large distances from the singular point, and (8) by itself is in no acceptable sense a solution to any problem. It is intriguing to note in this connection that nature seems to know about this "result," and that disclinations in crystalline solids are observed only when the body has a dimension that is not extremely large in comparison to the atomic spacing (whiskers, dust-like particles). Although Sternberg and Koiter (1958) do not touch directly upon the question whether the concentrated couple at a reentrant corner could be made meaningful in this narrower sense, their analysis leaves little room for optimism.

(2) The line of reasoning followed by Sternberg and his collaborators (Sternberg and Rosenthal, 1952; Sternberg and Eubanks, 1955) in dealing with singularities induced by concentrated actions applied to the surface of the body is that the elastic fields must be meaningful limits of distributed surface tractions. This approach cannot be contested. However, if the singularity is to be completely satisfactory, one should also obtain the same result when the concentrated action approaches the surface from an interior point of the body.

Both points are pursued in this paper by considering a concentrated couple near the tip of a crack which, in a sense, corresponds to a wedge angle $\gamma=\pi$. This problem has the attraction that it can be solved in closed form, and the limit of the couple approaching the tip of the crack explored in detail. It also seems intuitively that the problem of a crack of finite length should somehow be mathematically more stable than a cut running to infinity or, for that matter, the general shape of a reentrant corner.

The crack problems in this paper are solved using a formulation in terms of distributed dislocations. We recall for this purpose that, if edge dislocations are distributed on the x-axis, the induced traction components on $y=0$ are (Mura, 1982)

$$\sigma_{xy}^{D}(x,0)=-\frac{2\mu}{\pi(\kappa+1)}\int_{-\infty}^{\infty}\frac{B_x(\xi)d\xi}{\xi-x} \tag{9}$$

$$\sigma_{yy}^{D}(x,0)=-\frac{2\mu}{\pi(\kappa+1)}\int_{-\infty}^{\infty}\frac{B_y(\xi)d\xi}{\xi-x} \tag{10}$$

where B_x and B_y are the densities (B_x corresponds to a glide array with Burgers vectors in the x-direction, and B_y to a climb array with Burgers vectors in the y-direction), and the superscript D is added to emphasize that these stress components are due to a dislocation distribution.

2 Concentrated Couple and a Crack

For mathematical simplicity we place the concentrated couple in line of the crack (see Fig. 2) and consider only the stress component $\sigma_{xy}(x,0)$. The concentrated couple applied at the interior point (Timoshenko and Goodier, 1970) gives the traction components

$$\sigma_{xy}^{M}(x,0) = -\frac{M}{2\pi}\frac{1}{(x-b)^2}, \quad \sigma_{yy}^{M}(x,0)=0. \tag{11}$$

Simulating the crack as distributed glide dislocations on $|x|<a$, the total stress is $\sigma_{xy}^{M}(x,0)+\sigma_{xy}^{D}(x,0)$, and the requirement that the faces of the crack be free of tractions gives immediately the integral equation

$$\int_{-a}^{a}\frac{B_x(\xi)d\xi}{\xi-x} = -\frac{M(\kappa+1)}{4\mu}\frac{1}{(x-b)^2}, \quad |x|<a<b \tag{12}$$

with the side condition

$$\int_{-a}^{a}B_x(x)dx=0. \tag{13}$$

The solution of this system obtained by a well-known approach (Muskhelishvili, 1953) is

$$B_x(x) = -\frac{M(\kappa+1)}{4\mu}\frac{bx-a^2}{(b^2-a^2)^{1/2}(a^2-x^2)^{1/2}(b-x)^2}, \quad |x|<a<b. \tag{14}$$

Finally, backsubstituting (14) into (9) and adding (11) yields the total stress

$$\sigma_{xy}(x,0) = -\frac{M}{2\pi}\frac{(bx-a^2)\operatorname{sgn} x\, H(|x|-a)}{(b^2-a^2)^{1/2}(x^2-a^2)^{1/2}(x-b)^2}, \quad |x|<\infty. \tag{15}$$

Before considering the limit $b\to a$, it may be noted that the shear stress in the plane of the crack given by (15) has precisely the features that should be anticipated. In the vicinity of $x=a+$,

$$\sigma_{xy}(x,0) \sim -\frac{M}{2\pi}\frac{a^{1/2}}{2^{1/2}(b^2-a^2)^{1/2}(b-a)(x-a)^{1/2}} \tag{16}$$

showing the customary square-root singularity at a crack tip. In the vicinity of $x=b$,

$$\sigma_{xy}(x,0) \sim -\frac{M}{2\pi}\frac{1}{(x-b)^2} \tag{17}$$

which is the same as (11), and corresponds to the singularity of a concentrated couple. In the vicinity of $x=+\infty$,

$$\sigma_{xy}(x,0) \sim -\frac{M}{2\pi}\frac{b}{(b^2-a^2)^{1/2}x^2} \tag{18}$$

The decay of stresses as r^{-2} far away is typical of both a crack and the concentrated couple. However, it is notable that (18) contains the magnification factor $(b^2-a^2)^{-1/2}$.

It is obvious from (14) and (15) that the limit $b\to a$ does not exist as both the dislocation density and the shear stress simply become infinite. This in a sense confirms the Sternberg-Koiter conclusion, and also shows that a singularity for a concentrated couple applied at the tip of a cut cannot be defined in some weaker sense.

Finite limits for $b\to a$ can be achieved, however, by diminishing the magnitude of the couple as it approaches the tip by taking $M(b^2-a^2)^{-1/2}=Q=\text{const}$. Then from (14) and (15)

$$B_x(x) = \frac{Q(\kappa+1)}{4\mu}\frac{a}{(a+x)^{1/2}(a-x)^{3/2}}, \quad x<a \tag{19}$$

which no longer satisfies (13), meaning that the crack is dislocated, and

$$\sigma_{xy}(x,0) = -\frac{Q}{2\pi}\frac{a\operatorname{sgn} x\, H(|x|-a)}{(x+a)^{1/2}(x-a)^{3/2}}, \quad |x|<\infty. \tag{20}$$

The presence of the $r^{-3/2}$ type singularity at the right crack tip suggests that (19) and (20) correspond to the Bueckner weight function in fracture mechanics (Bueckner 1971; Rice 1972; Paris, McMeeking, and Tada 1976). Indeed, this is accomplished by setting $Q\sqrt{a}/2\sqrt{2}=B_{II}$ in the Paris, McMeeking, and Tada paper. The $r^{-3/2}$ singularity in (20) is also obtained in the Mellin transform analyses of Sternberg and Koiter (1958), and Barenblatt (1979) if a fractional power moment, but not the ordinary moment, is set equal to a constant. This is seen from equation (10.31) in Barenblatt's book, and equation (57) in the Sternberg-Koiter paper using the eigenvalue $\lambda=-1/2$ for a crack.

3 Concentrated Force and a Crack

It is instructive to contrast the situation for the couple with that for a concentrated force (see Fig. 2). The force is taken in line with the crack, because the force perpendicular to the crack is less revealing.

The force applied at an interior point gives the traction components (Timoshenko and Goodier, 1970)

$$\sigma_{xy}^{P}(x,0)=0, \qquad \sigma_{yy}^{P}(x,0)=\frac{P(\kappa-1)}{2\pi(\kappa+1)}\frac{1}{x-b}. \tag{21}$$

Cancelling these tractions on the faces of the crack by distributed dislocations, (10) gives immediately the integral equation

$$\int_{-a}^{a}\frac{B_y(\xi)d\xi}{\xi-x} = -\frac{P(\kappa-1)}{4\mu}\frac{1}{b-x}, \qquad |x|<a. \tag{22}$$

The solution of (22) satisfying the side condition

$$\int_{-a}^{a}B_y(x)dx=0 \tag{23}$$

is

$$B_y(x) = \frac{P(\kappa-1)}{4\pi\mu}\frac{1}{(a^2-x^2)^{1/2}}\left[1 - \frac{(b-a^2)^{1/2}}{b-x}\right], \qquad |x|<a<b. \tag{24}$$

Now it is more interesting to compute $\sigma_{xx}(x,0)$. The concentrated force by itself gives

$$\sigma_{xx}^{P}(x,0) = -\frac{P(\kappa+3)}{2\pi(\kappa+1)}\frac{1}{x-b}. \tag{25}$$

The distributed dislocations give

$$\sigma_{xx}^{D}(x,0) = -\frac{2\mu}{\pi(\kappa+1)}\int_{-a}^{a}\frac{B_y(\xi)d\xi}{\xi-x}. \tag{26}$$

Substituting (24) into (26) and adding the two contributions, the result is

$$\sigma_{xx}(x,0) = \frac{P}{\pi}\left\{-\frac{1}{x-b} + \frac{\kappa-1}{2(\kappa+1)}\left[1 + \frac{(b^2-a^2)^{1/2}}{x-b}\right]\frac{\operatorname{sgn} x}{(x^2-a^2)^{1/2}}H(|x|-a)\right\}, \qquad |x|<\infty. \tag{27}$$

In the vicinity $x=a+$,

$$\sigma_{xx}(x,0) \sim \frac{P(\kappa-1)}{2\pi(2a)^{1/2}(\kappa+1)}\left[1 - \left(\frac{b+a}{b-a}\right)^{1/2}\right]\frac{1}{(x-a)^{1/2}} \tag{28}$$

and it exhibits the customary singularity of a crack tip. In the vicinity $x=b$,

$$\sigma_{xx}(x,0) \sim -\frac{P(\kappa+3)}{2\pi(\kappa+1)}\frac{1}{x-b} \tag{29}$$

which is the same as (25). In the vicinity $x=+\infty$ we have, to the first order

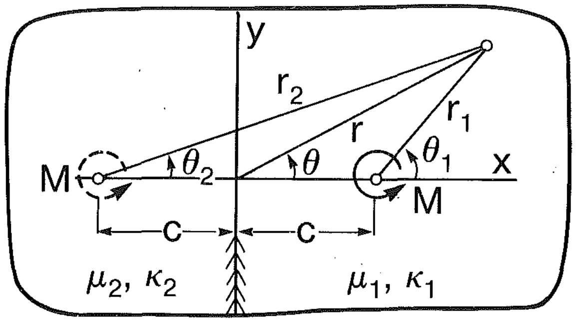

Fig. 3 Concentrated couple in the vicinity of an interface

$$\sigma_{xx}(x,0) \sim -\frac{P(\kappa+3)}{2\pi(\kappa+1)}\frac{1}{x} \tag{30}$$

and, in contrast to the couple, there is no magnification factor involved.

Finally, in the limit $b \to a$,

$$B_y(x) = \frac{P(\kappa-1)}{4\pi\mu}\frac{1}{(a^2-x^2)^{1/2}}, \qquad |x| < a \tag{31}$$

$$\sigma_{xx}(x,0) = \frac{P}{\pi}\left\{-\frac{1}{x-a} + \frac{\kappa-1}{2(\kappa+1)}\frac{\operatorname{sgn} x}{(x^2-a^2)^{1/2}}H(|x|-a)\right\}, \qquad |x| < \infty \tag{32}$$

Now there are two singularities at the right crack tip. The dominant singularity corresponding to the first term in (32) is the same as in the Michell solution for the wedge with $\gamma = \pi$ that is loaded by a concentrated force (Michell, 1901). The second term gives the weaker singularity of a crack tip.

Thus there are no surprises when a concentrated force approaches the tip of the crack, and the results have precisely the structure that would be anticipated intuitively. It should be noted that one should not attempt the limit $b \to a$ in (28) because the asymptotic expression valid only in the vicinity of $x = a$ precludes a change to the singularity in Michell's solution as the concentrated force approaches the crack tip. The proper limit sequence for the force approaching the crack tip is $b \to a$ in (27) and then $x \to a$ to explore the stresses near the crack tip.

4 Concentrated Couple and a Bimaterial Interface

The solution for a concentrated couple that is applied in the vicinity of a bonded bimaterial interface is known (Fukui, Dundurs, and Fukui, 1967). When the couple is applied at the point $(c,0)$ (see Fig. 3), the Airy stress functions for the two regions are

$$\phi_1 = -\frac{M}{2\pi}\left\{\theta_1 - \frac{\alpha-\beta}{1+\beta}\left[\theta_2 + \sin 2\theta_2 - 2c\frac{\sin\theta_2}{r_2}\right]\right\} \tag{33}$$

$$\phi_2 = -\frac{M}{2\pi}\frac{1+\alpha}{1+\beta}\theta_1 \tag{34}$$

where

$$\alpha = \frac{\mu_2(\kappa_1+1)-\mu_1(\kappa_2+1)}{\mu_2(\kappa_1+1)+\mu_1(\kappa_2+1)},$$

$$\beta = \frac{\mu_2(\kappa_1-1)-\mu_1(\kappa_2-1)}{\mu_2(\kappa_1+1)+\mu_1(\kappa_2+1)}. \tag{35}$$

It can be deduced from (33) and (34) (looking at Fig. 3 from behind, returning to θ_1 and θ_2 as measured in Fig. 3, and noting that α changes to $-\alpha$ and β to $-\beta$ upon interchange of materials) that when the couple is applied at the point $(-c,0)$, the Airy stress functions are

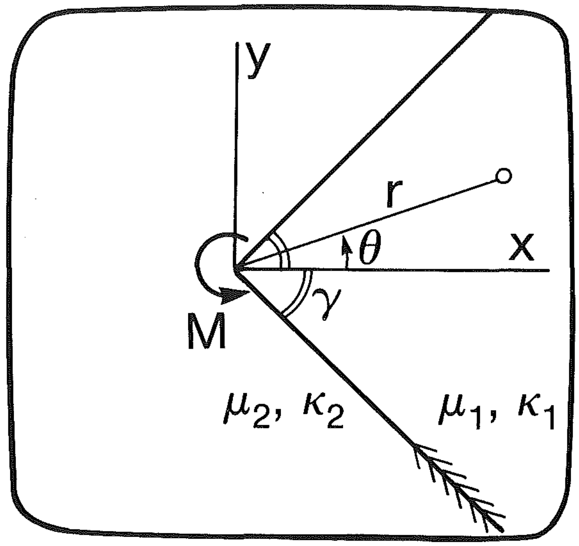

Fig. 4 Embedded wedge subjected to a concentrated couple

$$\phi_1 = -\frac{M}{2\pi}\frac{1-\alpha}{1-\beta}\theta_2 \tag{36}$$

$$\phi_2 = -\frac{M}{2\pi}\left\{\theta_2 + \frac{\alpha-\beta}{1-\beta}\left[\theta_1 + \sin 2\theta_1 + 2c\frac{\sin\theta_1}{r_1}\right]\right\}. \tag{37}$$

Next, let the concentrated couples approach the interface (see Fig. 3). For approach from the left, the Airy stress functions are

$$\phi_1^L = -\frac{M}{2\pi(1-\beta)}(1-\alpha)\theta \tag{38}$$

$$\phi_2^L = -\frac{M}{2\pi(1-\beta)}\{(1+\alpha-2\beta)\theta + (\alpha-\beta)\sin 2\theta\}. \tag{39}$$

In contrast, for approach from the right, the result is

$$\phi_1^R = -\frac{M}{2\pi(1+\beta)}\{(1-\alpha+2\beta)\theta - (\alpha-\beta)\sin 2\theta\} \tag{40}$$

$$\phi_2^R = -\frac{M}{2\pi(1+\beta)}(1+\alpha)\theta. \tag{41}$$

The unexpected outcome is now that the elastic fields depend on the direction of approach (except when $\alpha = \beta$, or $\mu_1 = \mu_2$). There is a way to explain this. The concentrated couple at an interior point can be constructed by adding two force doublets with moment, which themselves are obtained by differention with respect to the coordinates of the point of application (Timoshenko and Goodier, 1970). Although the resulting singularity has perfect axial symmetry, it apparently remembers that such an operation would give two different results if it were done directly at the interface. For $\mu_2 = 0$, ϕ_1^R yields the well-known result for a concentrated couple applied at a free boundary (Timoshenko and Goodier, 1970). The same is obtained from ϕ_2^L for $\mu_1 = 0$, and there is evidently no difficulty with the free surface.

It is also clear that the vulgar formulation can throw little light on this anomaly of the concentrated couple. Both ϕ^L and ϕ^R, or for that matter, any linear combination of the form $k\phi^L + (1-k)\phi^R$ satisfy it.

Another consequence of this anomaly is that two concentrated couples of same magnitude, but turning in opposite directions, do not cancel if they meet at the interface. Reversing the direction of the couple at $(-c,0)$ in Fig. 3, and letting the two couples go to the interface, gives the Airy stress functions

$$\phi_1 = -\frac{M}{2\pi}(\alpha-\beta)\left\{\frac{2\beta}{1-\beta^2}\theta - \frac{1}{1+\beta}\sin 2\theta\right\} \quad (42)$$

$$\phi_2 = -\frac{M}{2\pi}(\alpha-\beta)\left\{-\frac{2\beta}{1-\beta^2}\theta - \frac{1}{1+\beta}\sin 2\theta\right\} \quad (43)$$

which correspond to a self-equilibrated singularity. It may be noted that the two opposite couples cancel for the special combination of materials with $\alpha=\beta$, or $\mu_1=\mu_2$.

No anomalies of this kind are encountered with concentrated forces, as is readily confirmed by using the Airy stress functions derived by Dundurs and Hetényi (Dundurs and Hetényi, 1961; Hetényi and Dundurs, 1962).

5 Embedded Wedge

Suppose that an elastic wedge is embedded in another material (see Fig. 4), and the vertex in the two materials is loaded by a concentrated couple. Since the special case of identical materials is well posed, a natural question is whether the vulgar formulation would yield acceptable results at least for small mismatches in the elastic constants of the two materials.

The only biharmonic functions that give stresses proportional to r^{-2}, as predicted by dimensional analysis, and that have the required symmetry-antisymmetry properties are θ and $\sin 2\theta$. Taking the Airy stress functions for the two regions as linear combinations of these two terms (subscripts 1 and 2 are used to refer to the two regions $-\gamma<\theta<\gamma$ and $\gamma<\theta<2\pi-\gamma$, and the corresponding elastic constants of the two materials),

$$\phi_1 = A\theta + B\sin 2\theta \quad (44)$$

$$\phi_2 = C\theta + D\sin 2\theta. \quad (45)$$

The requirement that tractions and displacements be continuous on $\theta=\pm\gamma$ gives the three equations (only three, because $\sigma_{\theta\theta}=0$ for all terms in the Airy stress functions)

$$A+2B\cos 2\gamma - C - 2D\cos 2\gamma = 0 \quad (46)$$

$$B\Gamma(\kappa_1+1)\sin 2\gamma - D(\kappa_2+1)\sin 2\gamma = 0 \quad (47)$$

$$A\Gamma - B\Gamma(\kappa_1-1)\cos 2\gamma - C + D(\kappa_2-1)\cos 2\gamma = 0 \quad (48)$$

where $\Gamma=\mu_2/\mu_1$. The fourth condition for finding the unknown coefficients is, of course, the requirement that the stress resultant on a circle around the origin be a couple of moment M.

The system (46)–(48) has degeneracies for $\gamma=\pi/2$ (two half planes) and $\Gamma=1$ which have to be dealt with separately. Excluding these special cases the solution is

$$\phi_1 = \frac{M(1-\alpha)}{2\Delta}(-2\theta\cos 2\gamma + \sin 2\theta) \quad (49)$$

$$\phi_2 = \frac{M(1+\alpha)}{2\Delta}(-2\theta\cos 2\gamma + \sin 2\theta) \quad (50)$$

$$\Delta = 2\{[(1+\alpha)\pi - 2\alpha\gamma]\cos 2\gamma + \alpha\sin 2\gamma\} \quad (51)$$

where the constant α is defined by (35). This solution suffers from the same defects as the Carothers solution: The quantity Δ can vanish for special values of γ (in fact it vanishes for two values of γ when $-1<\alpha<0$), and it predicts shear tractions on a circle around the vertex that involve sign reversals. It is, in fact, a fake solution: The interfaces between the two wedges transmit no tractions; the moment M is simply split between the two regions so that the displacements are continuous on $\theta=\pm\gamma$. Thus, no matter how small the mismatch in the elastic constants is, the vulgar formulation does no better than for a single wedge.

It is still worthwhile to consider the two special cases mentioned before. For $\gamma=\pi/2$, (46)–(48) collapse into the two equations

$$A-2B-C+2D=0 \quad (52)$$

$$A\Gamma + B\Gamma(\kappa_1-1) - C - D(\kappa_2-1) = 0. \quad (53)$$

Now there are not enough conditions to determine the unknown coefficients uniquely. This is obviously connected with the fact that, for half planes, it matters whether the couple approaches the interface from one side or the other, as discussed in Section 4. It goes to the credit of the vulgar formulation, however, that it can, in a sense, anticipate this result.

For $\Gamma=1$ and $\cos 2\gamma\neq 0$, the result is

$$\phi_1 = \phi_2 = -\frac{M}{2\pi}\theta \quad (54)$$

which is the same as for a homogeneous body. No objections can be raised against it.

For $\Gamma=1$ and $\cos 2\gamma=0$, however, system (46)–(48) collapses into the equations

$$A-C=0 \quad (55)$$

$$B\Gamma(\kappa_1+1) - D(\kappa_2+1) = 0 \quad (56)$$

and the solution is no longer unique. The choice $A=C$ and $B=D=0$, corresponding to (54), may be the best on physical grounds, because it avoids the terms related to a center of shear, and gives constant shear tractions on a circle around the vertex.

It may be of interest to note that there are no dilemmas when the tip of the embedded wedge is loaded by a concentrated force (Dundurs, 1962).

6 Conclusion

Contrasted to a concentrated force, the concentrated couple exhibits various anomalies when it approaches either a discontinuity in the elastic constants or a singular point in the geometry. In the latter case, infinite stresses are created everywhere in the material. This anomaly includes, besides the classical "paradox" of the wedge, the couple approaching the tip of a crack, the vertex of a wedge embedded in another elastic material, and the tip of an anticrack. The anticrack (rigid lamellar inclusion of negligible thickness) is discussed in a separate paper (Dundurs and Markenscoff, 1989). It appears that what is important in this phenomenon are only the orders of the interacting singularities of the loading and geometry. If the load-induced singularity at an interior point has a local stress field of the order $r^{-\lambda}$, and the geometric singularity is of order $r^{-\mu}$ (note that $\mu<1$, because the geometric singularity must have an integrable strain energy density), a unique limit exists only if $\lambda+\mu<2$. In this connection, the geometrically smooth interface between two materials corresponds to $\mu=0$.

References

Barenblatt, G. I., 1979, *Similarity, Self-similarity, and Intermediate Asymptotics*, translated from Russian by Norman Stein, Consultants Bureau, New York.

Barenblatt, G. I., and Zeldovich, Y. B., 1972, "Self-similar Solutions as Intermediate Asymptotics," *Annual Review of Fluid Mechanics*, Vol. 4, pp. 285–312.

Budiansky, B., and Carrier, G. F., 1973, "The Pointless Wedge," *SIAM Journal on Applied Mathematics*, Vol. 25, pp. 378–387.

Buchwald, V. T., 1965, "Eigenfunctions of Plane Elastostatics III—The Wedge," *Journal of the Australian Mathematical Society*, Vol. 5, pp. 241–257.

Bueckner, H. F., 1971, "Weight Functions for the Notched Bar," *Zeitschrift für angewandte Mathematik und Mechanik*, Vol. 51, pp. 97–109.

Carothers, S. D., 1912, "Plane Strain in a Wedge," *Proceedings of the Royal Society of Edinburgh*, Vol. 23, p. 292.

Dundurs, J., 1962, "Die seitlich elastisch eingebettete keilförmige Scheibe unter Spitzenbelastung," *Ingenieur-Archiv*, Vol. 31, pp. 144–148.

Dundurs, J., 1969, "Elastic Interaction of Dislocations with Inhomogeneities," *Mathematical Theory of Dislocations*, T. Mura, ed., ASME, New York, pp. 70–115.

Dundurs, J., and Hetényi, M., 1961, "The Elastic Plane with a Circular Insert, Loaded by a Radial Force," ASME JOURNAL OF APPLIED MECHANICS, Vol. 28, pp. 103–111.

Dundurs, J., and Markenscoff, 1989, "A Green's Function Formulation of

Anticracks and Their Interaction with Load Induced Singularities," ASME Journal of Applied Mechanics, in press.

Fillunger, P., 1930, "Über die Spannungen in Mittelschnitt eines Eisenbahnzughakens," *Zeitschrift für angewandte Mathematik und Mechanik*, Vol. 10, pp. 218–227.

Fukui, K., Dundurs, J., and Fukui, T., 1967, "The Elastic Plane with a Circular Insert, Loaded by a Concentrated Moment, *Bulletin of JSME*, Vol. 10, pp. 9–14.

Hetényi, M., and Dundurs, J., 1962, "The Elastic Plane with a Circular Insert, Loaded by a Tangentially Directed Force," ASME Journal of Applied Mechanics, Vol. 29, pp. 363–368.

Inglis, C. E., 1922, "Some Special Cases of Two-dimensional Stress and Strain," *Transactions of the Institution of Naval Architects*, Vol. 64, p. 253.

Michell, J. H., 1901, "Elementary Distributions of Plane Stress," *Proceedings of the London Mathematical Society*, Vol. 32, pp. 35–61.

Mura, T., 1982, *Micromechanics of Defects in Solids*, Martinus Nijhoff Publishers.

Muskhelishvili, N. I., 1953, *Singular Integral Equations*, (translated by J. R. M. Radok), P. Noordhoff, Groningen.

Neuber, H., 1963, "Lösung des Carothers-Problems mittels Prinzipien der Kraftübertragung (Keil mit Moment an der Spitze)," *Zeitschrift für angewandte Mathematik und Mechanik*, Vol. 43, pp. 211–228.

Paris, P. C., McMeeking, R. M., and Tada, H., 1976, "The Weight Function Method for Determining Stress Intensity Factors," *Cracks and Fracture*, ASTM STP 601, American Society for Testing and Materials, pp. 471–489.

Rice, J. R., 1972, "Some Remarks on Elastic Crack-tip Stress Fields," *International Journal of Solids and Structures*, Vol. 8, pp. 751–758.

Sonntag, G., 1961a, "Beitrag zum Keil mit einem Moment an der Spitze," *Zeitschrift für angewandte Mathematik und Mechanik*, Vol. 41, pp. T110-T112.

Sonntag, G., 1961b, "Beitrag zum Keil mit einem Moment an der Spitze," *Forschung auf dem Gebiete des Ingenieurwesens*, Vol. 27, pp. 175–179.

Sternberg, E., and Eubanks, R. A., 1955, "On the Concept of Concentrated Loads and an Extension of the Uniqueness Theorem in the Linear Theory of Elasticity," *Journal of Rational Mechanics and Analysis*, Vol. 4, pp. 135–168.

Sternberg, E., and Koiter, W. T., 1958, "The Wedge Under a Concentrated Couple: A Paradox in the Two-Dimensional Theory of Elasticity," ASME Journal of Applied Mechanics, Vol. 25, pp. 575–581.

Sternberg, E., and Rosenthal, F., 1952, "The Elastic Sphere Under Concentrated Loads," ASME Journal of Applied Mechanics, Vol. 19, pp. 413–421.

Timoshenko, S. P., and Goodier, J. N., 1970, *Theory of Elasticity*, 3rd ed., McGraw-Hill Book Co., New York.

Ting, T. C. T., 1985, "A Paradox of the Elastic Wedge Subjected to a Concentrated Couple and the Jeffrey-Hamel Viscous Flow Problem," *Zeitschrift für angewandte Mathematik und Mechanik*, Vol. 65, pp. 188–190.

Chein H. Wu
Professor.
Fellow, ASME

Chao-Hsun Chen
Graduate Student.

Department of Civil Engineering, Mechanics, and Metallurgy,
University of Illinois at Chicago,
Chicago, Ill. 60680

Wedge-Apex Crack in an Angularly Inhomogeneous Wedge

An edge crack surrounded by a slender, triangularly-shaped elastic inclusion is used to represent an experimentally-observed crack layer generated by constant amplitude fatigue conditions. Approximate but explicit formula is derived for the stress-intensity factor. As a byproduct, the exact stress-intensity factor for the title problem is explicitly obtained.

1 Introduction

In a series of constant amplitude fatigue crack propagation tests reported by Chudnovsky (1984, 1987), the propagation of a crack is observed to be accompanied by the propagation of a crack layer, using Chudnovsky's terminology. A typical experimental result is reproduced in Fig. 1. It is seen that the crack layer assumes the shape of a round-tipped slender triangle. An extensive experimental study of fatigue crack layer propagation may be found in Botsis, Chudnovsky, and Moet (1987).

We propose to model the crack layer via a "strength of materials" approach by assuming that the crack layer is actually an isotropic and homogeneous elastic inclusion with a modulus softer than that of the sample material. The elasticity problem depicted in Fig. 2(*a*) must then be solved. This problem is solved in this paper.

In the process of solving the aforementioned problem, we realized the need of the solution to the elasticity problem depicted in Fig. 2(*b*). The SIF of this problem is determined exactly. In fact, the exact SIF for the problem depicted in Fig. 3 can be determined even if the material is angularly inhomogeneous with respect to the origin. This solution is presented in Section 3. What is central to the analysis is the solution to an angularly inhomogeneous wedge subjected to a wedge-apex load. This solution is given in the Appendix. The steps needed in completing the stress-intensity factor calculation follow straightforwardly from an energy-momentum formulation (Eshelby, 1951, 1956, 1970 and Wu, 1988) which is summarized in Section 2.

2 Energy-Momentum Tensor in Plane Elastostatics

Let O-(z_1, z_2) be rectangular cartesian coordinates and let $(\mathbf{i}_1, \mathbf{i}_2)$ be the associated unit vectors. A polar coordinate system (r, θ) is also erected at O, and the associated vectors are denoted by $(\mathbf{e}_r, \mathbf{e}_\theta)$. A typical two-dimensional region is denoted by R, its boundary by ∂R, and the outward unit normal to ∂R by $\mathbf{n}$. The displacement, strain, and stress are denoted by u_α, $\epsilon_{\alpha\beta}$ and $\tau_{\alpha\beta}$, respectively. We assume that the elastic material is inhomogeneous in θ and that the stresses may be derived from the strain energy density $W(u_{\alpha,\beta}, \theta)$ via

$$\tau_{\alpha\beta} = \frac{\partial W}{\partial u_{\alpha,\beta}}. \tag{1}$$

In the absence of body forces, the symmetric stress tensor satisfies the equations of equilibrium

$$\tau_{\beta\alpha,\beta} = 0. \tag{2}$$

Using equation (1) and (2), we obtain

$$p_{\beta\alpha,\beta} = \frac{\partial W}{\partial \theta}\theta_{,\alpha} \tag{3}$$

where

$$p_{\beta\alpha} = W\delta_{\beta\alpha} - \tau_{\beta\lambda}u_{\lambda,\alpha} \tag{4}$$

is just the energy-momentum tensor which is not symmetric.

The energy-momentum traction vector $\mathbf{p}$ along a curve C with unit normal $\mathbf{n}$ is defined by

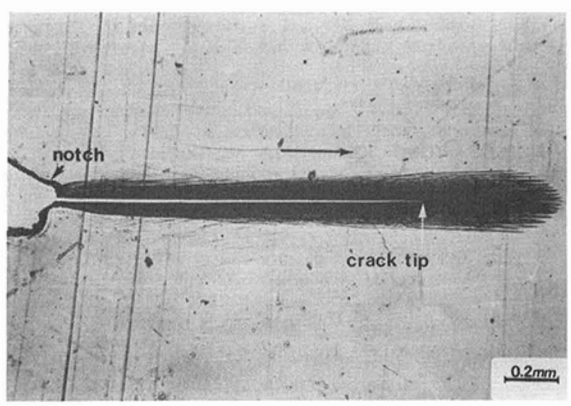

Fig. 1 Fatigue crack—polystyrene

Contributed by the Applied Mechanics Division of THE AMERICAN SOCIETY OF MECHANICAL ENGINEERS for presentation at the Joint ASCE/ASME Applied Mechanics, Biomechanics, and Fluids Engineering Conference, San Diego, Calif., July 9 to 12, 1989.

Discussion of this paper should be addressed to the Editorial Department, ASME, United Engineering Center, 345 East 47th Street, New York, N.Y. 10017, and will be accepted until two months after final publication of the paper itself in the JOURNAL OF APPLIED MECHANICS. Manuscript received by the ASME Applied Mechanics Division, September 9, 1987; final revision, September 28, 1988.

Paper No. 89-APM-33.

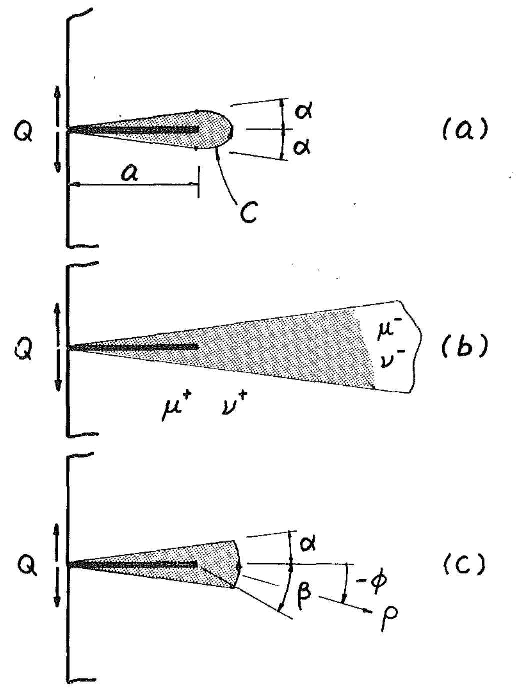

Fig. 2 Crack-layer geometry; R is the half plane with the edge crack

$$\mathbf{p} = p_\alpha \mathbf{i}_\alpha = p_{\beta\alpha} n_\beta \mathbf{i}_\alpha \tag{5}$$

which is directly involved in the various known conservation integrals. In particular, the M-integral reads

$$\int_{\partial R} z_\alpha p_\alpha d\sigma = \int_R z_\alpha \frac{\partial W}{\partial \theta} \theta_{,\alpha} da. \tag{6}$$

We note in passing that for the angularly inhomogeneous material considered in this paper,

$$\frac{\partial W}{\partial \theta} \theta_{,\alpha} \mathbf{i}_\alpha = \frac{1}{r} \frac{\partial W}{\partial \theta} \mathbf{e}_\theta. \tag{7}$$

3 Wedge-Apex Crack in an Angularly Inhomogeneous Wedge

Consider now the elasticity problem depicted in Fig. 3. The material is angularly inhomogeneous with respect to the origin. The problem, however, is completely symmetric with respect to the crack orientation in that the geometry, load, and material inhomogeneity are symmetric with respect to the z_1-axis. Our objective is to determine the Mode-I SIF K. The pertinent results for homogeneous material may be found in Freund (1978) and Tada et al., (1970).

Let us apply the M-integral (6) to the region R depicted in Fig. 3. In view of (7), the area integral is identically zero. Since the energy-momentum traction $\mathbf{p}$ along a traction-free boundary is normal to the boundary, the line integrals along the crack and wedge boundaries are also zero. It follows that the M-integral is merely given by

$$I_\infty + I_t + 2I_w = 0 \tag{8}$$

where I_∞, I_t, and I_w are the line integrals along the circular arcs at infinity, around the crack tip, and around the upper portion of the wedge apex, respectively.

The stress field at infinity may be deduced from the formula given in the Appendix by letting

$$-\theta_1 = \theta_2 = \theta_o, \mathbf{F} = 2P\mathbf{i}_1. \tag{9}$$

It is

$$\tau_{rr} = \frac{16\mu(\theta)P}{[1+\kappa(\theta)]a_{11}^\infty} \frac{\cos\theta}{r} \qquad (r \to \infty) \tag{10}$$

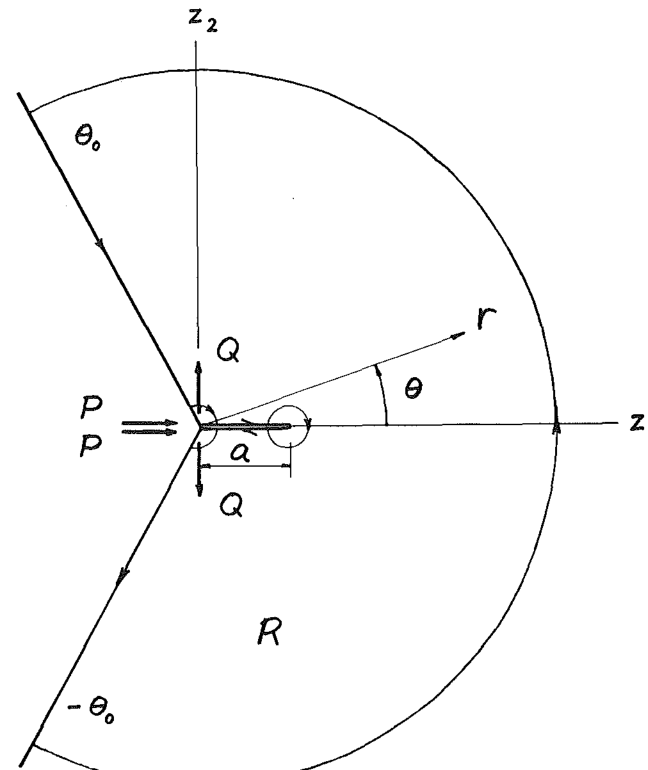

Fig. 3 An angularly inhomogeneous isotropic wedge

where

$$a_{11}^\infty = -\int_{-\theta_o}^{\theta_o} \frac{8\mu(\theta)}{1+\kappa(\theta)} \cos^2\theta d\theta. \tag{11}$$

The value of I_∞ is just

$$I_\infty = \int_{-\theta_o}^{\theta_o} -\frac{1}{2} \tau_{rr} \epsilon_{rr} r^2 d\theta = 2P^2/a_{11}^\infty. \tag{12}$$

In stress field near the origin and for $0 < \theta < \theta_o$ may be deduced from the formula given in the Appendix by letting

$$\theta_1 = 0, \theta_2 = \theta_o, \mathbf{F} = P\mathbf{i}_1 + Q\mathbf{i}_2. \tag{13}$$

It is

$$\tau_{rr} = \frac{8\mu(\theta)}{[1+\kappa(\theta)]r}(A_1 \cos\theta + A_2 \sin\theta), \ (r \to 0, \ 0 < \theta < \theta_o), \tag{14}$$

where A_1 and A_2 are given by (A8) and (A9). The value of I_w is just

$$I_w = \int_0^{\theta_o} \frac{1}{2} \tau_{rr} \epsilon_{rr} r^2 d\theta = -\frac{1}{2}(A_1 P + A_2 Q). \tag{15}$$

The properties of the material at the crack tip are governed by $\mu(0)$ and $\kappa(0)$ where the 0 stands for $\theta = 0$. It follows that I_t may be expressed in terms of the J_1-integral (Rice, 1968) and

$$I_t = -\frac{\kappa(0)+1}{8\mu(0)} K^2 a \tag{16}$$

where K is the Mode-I SIF. Substituting the above results into (8), we obtain

$$K = \left\{ \frac{8\mu(0)}{\kappa(0)+1} \left[-A_2 Q + \left(-A_1 + \frac{2P}{a_{11}^\infty} \right) P \right] \frac{1}{a} \right\}^{1/2} \tag{17}$$

which is the exact SIF for the problem posed in Fig. 3. For the case of a homogeneous wedge, (17) becomes the known results given by (Tada et al., 1970) and (Freund, 1978).

Let us now apply (17) to the case depicted in Fig. 2(*b*) where the wedge angle is 2α. Moreover, we assume that $\alpha << 1$ so that only terms linear in α are retained. The result is

$$K = Q\left[\frac{4\pi(1-\delta)}{(\pi^2-4)a}\right]^{1/2}\left[1+\frac{8}{\pi(\pi^2-4)}\alpha\delta\right] \tag{18}$$

where

$$\delta = 1 - \frac{(1+\kappa^+)\mu^-}{(1+\kappa^-)\mu^+} \tag{19}$$

is a composite parameter. We note in passing that for the problem under consideration there are two independent composite parameters (Dundurs, 1969).

The homogeneous-wedge counterpart of (18), denoted by K_H may be deduced from (18) by setting $\delta = 0$, i.e.,

$$K_H = Q\left[\frac{4\pi}{(\pi^2-4)a}\right]^{1/2} \tag{20}$$

which is the result of Freund (1978). Using K_H as a normalizing factor, we obtain from (18)

$$K_o(\alpha,\delta) = \frac{K}{K_H} = (1-\delta)^{1/2}\left[1+\frac{8}{\pi(\pi^2-4)}\alpha\delta\right]. \tag{21}$$

Thus, for α small, K_o may be approximated by

$$K_o(0,\delta) \simeq (1-\delta)^{1/2} = \left[\frac{(1+\kappa^+)\mu^-}{(1+\kappa^-)\mu^+}\right]^{1/2}. \tag{22}$$

4 The Crack Layer As An Elastic Inclusion

We proceed to determine the SIF, associated with the situation given in Fig. 2(*a*), where the crack layer is bounded by two radial lines and a smooth curve C. To fix ideas, let C be defined by

$$C: z_\alpha = y_\alpha(\eta) \tag{23}$$

where η is the arc length along C. The unit tangent and normal to C are denoted by $\boldsymbol{\eta}$ and $\boldsymbol{\xi}$, respectively. We shall also use ξ to denote the distance from C along $\boldsymbol{\xi}$. It follows that (ξ, η) form a set of orthogonal curvilinear coordinates. We shall use $\tau_{\xi\xi}$, $\tau_{\eta\eta}$ and $\tau_{\xi\eta}$ to denote the stresses relative to the curvilinear system.

It was shown by Wu (1988) that the energy-momentum traction jump along C may be represented by

$$[p^+_{\beta\alpha}(0,\eta) - p^-_{\beta\alpha}(0,\eta)]\,\xi_\beta(\eta)\mathbf{i}_\alpha = q(\eta)\boldsymbol{\xi} \tag{24}$$

where $\boldsymbol{\xi} = \xi_\beta \mathbf{i}_\beta$ is the normal to C and $f^\pm(0,\eta) \equiv f(\xi,\eta)$ evaluated at $\xi = \pm 0$. Moreover,

$$\frac{8\mu^-}{1+\kappa^-}q(\eta) = \frac{1}{2}(\delta_1-\delta_2)(\tau_{\xi\xi}+\tau_{\eta\eta})^2 - \delta_1(\tau_{\xi\xi}+\tau_{\eta\eta})\tau_{\xi\xi} + \frac{\delta_1}{1+\delta_1-\delta_2}\tau^2_{\xi\eta} + \frac{\delta_1(2+\delta_1)}{2(1+\delta_1-\delta_2)}\tau^2_{\xi\xi} \tag{25}$$

where

$$\delta_1 = \frac{4}{1+\kappa^+}\left(\frac{\mu^+}{\mu^-}-1\right),\ \delta_2 = \frac{3-\kappa^+}{1+\kappa^+}\left(\frac{3-\kappa^-}{3-\kappa^+}\ \frac{\mu^+}{\mu^-}-1\right) \tag{26}$$

are two new composite parameters and all τ's are evaluated at $\xi = -0$.

Let us now apply the M-integral (6) to the region R depicted in Fig. 2(*a*). In view of (7), the right-hand side of (6) is identically zero except along C where a jump in energy-momentum traction takes place. The result is

$$I_t + 2I_w = \int_C y_\alpha \xi_\alpha q(\eta)d\eta \tag{27}$$

where I_t is given by (16) with κ (0) and $\mu(0)$ replaced by κ^{-1} and μ^-, respectively, and I_w by (15) with $P=0$ and $\theta_o = \pi/2$. We recall that C is only the curved portion of the crack-layer boundary. The needed SIF will be computed from (27).

The function $q(\eta)$ needed in completing the calculation is defined by (25) in which the values of the stresses are unknown. However, if the distance between C and the crack tip is relatively small, the needed stresses may be approximated by the crack tip K-field $\tau_{\rho\rho}$, $\tau_{\phi\phi}$, and $\tau_{\rho\phi}$ where (ρ, ϕ) is the crack-tip polar coordinate system. The accuracy of such an approximation has been favorably substantiated by a benchmark solution by Wu (1988). In view of the stated approximation and the specific configuration, the curve C is chosen to be a circular arc to facilitate the ensuing computations, viz.,

$$C: z_\alpha \mathbf{i}_\alpha = a\mathbf{i}_1 + ka\alpha\mathbf{e}_\rho \tag{28}$$

where $\mathbf{e}_\rho$ is the crack-tip radial direction, Fig. 2(*c*), and k an aspect ratio greater than 1. The polar system (ρ, ϕ) may now be identified with the curvilinear system (ξ, η), and (27) yields

$$\tilde{K}(\alpha,\delta,k) = \frac{K}{K_H} = \left\{\frac{(1-\delta)\left[1+\frac{16}{\pi(\pi^2-4)}\alpha\delta\right]}{1+\frac{1}{2\pi}[I_1(\alpha,k)+\alpha k I_2(\alpha,k)]}\right\}^{1/2} \tag{29}$$

where

$$I_1 = \frac{2\pi k a\alpha}{K^2}\int_{-\beta}^{\beta}\frac{8\mu^-}{1+\kappa^-}q(\phi)\cos\phi d\phi, \tag{30}$$

$$I_2 = \frac{2\pi k a\alpha}{K^2}\int_{-\beta}^{\beta}\frac{8\mu^-}{1+\kappa^-}q(\phi)d\phi, \tag{31}$$

and $\beta = \sin^{-1}[\alpha + (1/k)]$. Since I_2 is multiplied by α, the value of $I_2(\alpha, k)$ may be replaced by $I_2(0,k)$. Using the K-field τ's to approximate the τ's needed in the q expression, we obtain

$$\begin{aligned} I_1 &= \frac{\delta_1}{16(1+\delta_1-\delta_2)}\left(\frac{1}{2}\beta + \sin\beta - \frac{1}{3}\sin3\beta - \frac{1}{8}\sin4\beta\right) \\ &- \frac{\delta_1}{2}\left(2\beta + \frac{9}{2}\sin\beta + \sin2\beta - \frac{1}{6}\sin3\beta\right) + (\delta_1-\delta_2) \\ &\times\left(\beta + 2\sin\beta + \frac{1}{2}\sin2\beta\right) + \frac{\delta_1(2+\delta_1)}{8(1+\delta_1-\delta_2)} \\ &\times\left(\frac{15}{8}\beta + \frac{21}{4}\sin\beta + \sin2\beta - \frac{5}{12}\sin3\beta + \frac{1}{32}\sin4\beta\right) \end{aligned} \tag{32}$$

$$\begin{aligned} I_2 &= \frac{\delta_1}{16(1+\delta_1-\delta_2)}\left(2\beta + \sin\beta - \sin2\beta - \frac{1}{3}\sin3\beta\right) \\ &- \frac{\delta_1}{2}\left(5\beta + 4\sin\beta - \frac{1}{2}\sin2\beta\right) \\ &+ (\delta_1-\delta_2)(2\beta + 2\sin\beta) + \frac{\delta_1(2+\delta_2)}{8(1+\delta_1-\delta_2)} \\ &\times\left(\frac{13}{2}\beta + \frac{15}{4}\sin\beta - \frac{5}{4}\sin2\beta + \frac{1}{12}\sin3\beta\right). \end{aligned} \tag{33}$$

Finally, the composite parameter δ, (19), is related to δ_1 and δ_2 by

$$\delta = (\delta_1-\delta_2)/(1+\delta_1-\delta_2), \tag{34}$$

as there are only two independent parameters (Dundurs, 1969).

The normalized SIF $\tilde{K}(\alpha,\delta,k)$ defined by (29) is plotted as a function of the shear modulus ratio μ^-/η^+ for $\nu^- = \nu^+ = 0.2$, $\alpha = 5\pi/180$ and $k = 1$ to 2 at 0.2 increments in Fig. 4. It is

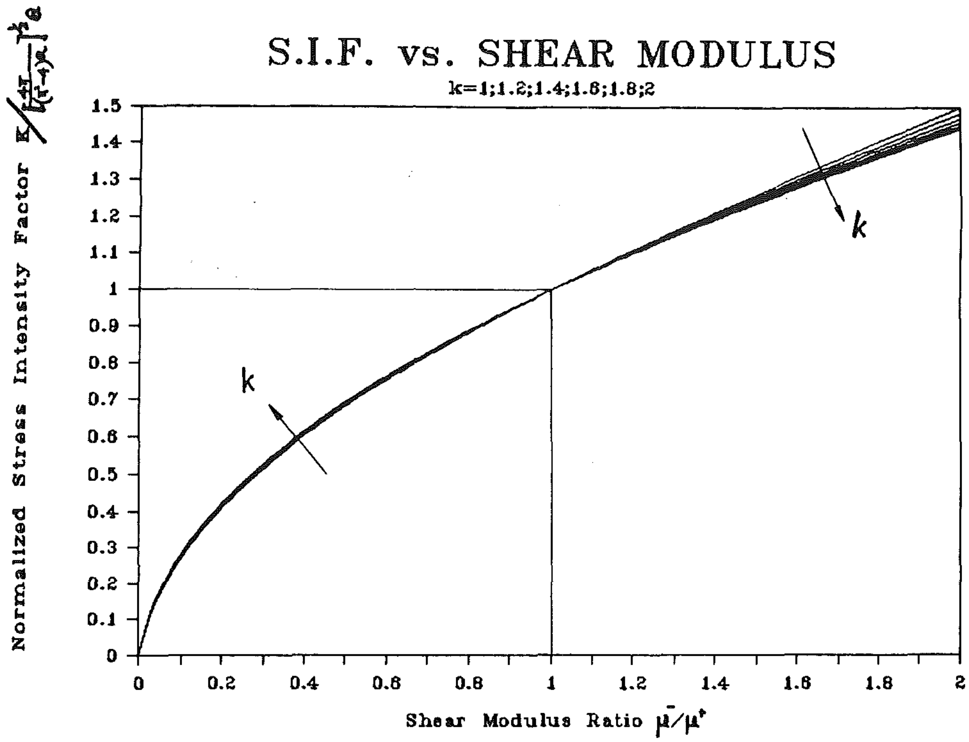

Fig. 4 Normalized SIF versus shear modulus ratio for $\nu^- = \nu^+ = 0.2$, $\alpha = 5\pi/180$, and $k = 1$, 1.2, 1.4, 1.6, 1.8, and 2.0

noted that $\tilde{K}(\alpha, \delta, k)$ approaches to a limiting curve very rapidly as k increases. While (29) is approximate, the exact $\tilde{K}$ must satisfy the condition

$$\lim_{k\to\infty} \lim_{\alpha\to\infty} \tilde{K}(\alpha, \delta, k) = K_o(0, \delta) = \left(\frac{\mu^-}{\mu^+}\right)^{1/2} \tag{35}$$

where K_o is given by (21). The approximate $\tilde{K}$ plotted in Fig. 4 does appear to tend to the above limit.

When a crack layer is modeled by a homogeneous inclusion, the inclusion modulus μ^- must be less than μ^+. It is noted that in this region $(\mu^-/\mu^+ < 1)$ the layer shields the crack and decreases the SIF.

5 Acknowledgment

The authors are most grateful to their colleague John Botsis for the opportunity of viewing many of his published and unpublished micrographs. In particular, Fig. 1 was supplied by John Botsis.

References

Botsis, J., Chudnovsky, A., and Moet, A., 1987, "Fatigue Crack Layer Propagation in Polystyrene—Part I: Experimental Observations," *Int. J. Fracture*, Vol. 33, pp. 263–276.

Chudnovsky, A., 1984, "Crack Layer Theory," NASA Report 174634.

Chudnovsky, A., 1987, "Crack Layer," ASME Journal of Applied Mechanics, to appear.

Dundurs, J., 1969, "Edge-Bonded Dissimilar Orthogonal Elastic Wedges Under Normal and Shear Loading—Discussion," ASME Journal of Applied Mechanics, Vol. 36, pp. 650–652.

Eshelby, J. D., 1951, "The Force on an Elastic Singularity," *Phil. Trans. Roy. Soc. Lond.*, Vol. 244A, pp. 87–112.

Eshelby, J. D., 1956, "The Continuum Theory of Lattice Defects," *Solid State Physics, Advances in Research and Applications*, F. Seitz and D. Turnbull eds., Vol. III, Academic Press, New York, pp. 79–114.

Eshelby, J. D., 1970, "Energy Relations and the Energy-Momentum Tensor in Continuum Mechanics," *Inelastic Behavior of Solids*, M. F. Kanninen, W. F. Adler, A. R. Rosenfield, and R. I. Jaffee eds., McGraw-Hill, New York, pp. 77–114.

Freund, L. B., 1978, "Stress Intensity Factor Calculations Based on a Conservation Integral," *Int. J. Solids Structures*, Vol. 14, pp. 241–250.

Rice, J. R., 1968, "A Path Independent Integral and the Approximate Analysis of Strain Concentration by Notches and Cracks," ASME Journal of Applied Mechanics, Vol. 35, pp. 379–386.

Tada, H., Paris, P., and Irwin, G., 1970, *The Stress Analysis of Cracks Handbook*, Del Research Corporation, Hellertown.

Wu, C. H., 1988, "A Semi-Infinite Crack Penetrating an Inclusion," ASME Journal of Applied Mechanics, to appear.

APPENDIX

An Angularly Inhomogeneous Isotropic Wedge

Consider an infinite wedge occupying the region $0 < r < \infty$ and $\theta_1 < \theta < \theta_2$ where (r, θ) are the polar coordinates relative to a Cartesian frame $(\mathbf{i}_1, \mathbf{i}_2)$. The elastic wedge is angularly inhomogeneous so that the shear modulus μ and Poisson's ratio ν are functions of the polar angle θ. It follows that the plane-elasticity constant κ defined by

$$\kappa = \begin{cases} 3-4\nu & \text{plane strain} \\ (3-\nu)/(1+\nu) & \text{plane stress} \end{cases} \tag{A1}$$

is also a function of θ.

The wedge is loaded at the apex by a concentrated force $\mathbf{F} = F_\alpha \mathbf{i}_\alpha$. It can be shown that the stress field defined by

$$\tau_{rr} = \tau(\theta)/r, \;\; \tau_{r\theta} = \tau_{\theta\theta} = 0 \tag{A2}$$

satisfies the equilibrium identically. The compatibility condition is satisfied if

$$\left[\frac{1+\kappa(\theta)}{8\mu(\theta)}\tau(\theta)\right]_{,\theta\theta} + \left[\frac{1+\kappa(\theta)}{8\mu(\theta)}\tau(\theta)\right] = 0 \tag{A3}$$

which governs the single unknown function $\tau(\theta)$. The general solution is

$$\tau_{rr} = \frac{8\mu(\theta)}{[1+\kappa(\theta)]r}(A_1\cos\theta + A_2\sin\theta) \tag{A4}$$

$$u_r = (A_1 \cos\theta + A_2 \sin\theta)\ln r + G'(\theta) \quad (A5)$$

$$u_\theta = Br - (A_1 \sin\theta - A_2 \cos\theta)\ln r - \int \frac{3-\kappa(\theta)}{1+\kappa(\theta)} [A_1 \cos\theta + A_2 \sin\theta]\, d\theta - G(\theta) \quad (A6)$$

where A_1, A_2, B are constants and $G(\theta)$ satisfies

$$G''(\theta) + G(\theta) = A_1 \sin\theta - A_2 \cos\theta - \int \frac{3-\kappa(\theta)}{1+\kappa(\theta)} (A_1 \cos\theta + A_2 \sin\theta) d\theta. \quad (A7)$$

The constants A_1 and A_2 may be expressed in terms of the concentrated load $\mathbf{F}$, viz.,

$$a_{\alpha\beta} A_\beta = -F_\alpha \quad (A8)$$

where

$$a_{11} = \int_{\theta_1}^{\theta_2} \frac{8\mu(\theta)}{1+\kappa(\theta)} \cos^2\theta d\theta,\ a_{22} = \int_{\theta_1}^{\theta_2} \frac{8\mu(\theta)}{1+\kappa(\theta)} \sin^2\theta d\theta$$

$$a_{12} = a_{21} = \int_{\theta_1}^{\theta_2} \frac{8\mu(\theta)}{1+\kappa(\theta)} \cos\theta \sin\theta d\theta. \quad (A9)$$

Multiple Region Contact Solutions for a Flat Indenter on a Layered Elastic Half Space: Plane-Strain Case

T. W. Shield[1]

D. B. Bogy
Mem. ASME

University of California,
Berkeley, Calif. 94720

The plane-strain problem of a smooth, flat rigid indenter contacting a layered elastic half space is examined. It is mathematically formulated using integral transforms to derive a singular integral equation for the contact pressure, which is solved by expansion in orthogonal polynomials. The solution predicts complete contact between the indenter and the surface of the layered half space only for a restricted range of the material and geometrical parameters. Outside of this range, solutions exist with two or three contact regions. The parameter space divisions between the one, two, or three contact region solutions depend on the material and geometrical parameters and they are found for both the one and two layer cases. As the modulus of the substrate decreases to zero, the two contact region solution predicts the expected result that contact occurs only at the corners of the indenter. The three contact region solution provides an explanation for the nonuniform approach to the half space solution as the layer thickness vanishes.

1 Introduction

A common method of protecting a soft material is to coat it with a layer of harder material. This is done in many applications where wear and damage due to sliding contact of solids are a problem. Examples include the hard overcoats which are used to protect the magnetic layers on the platters of hard disk files. In order to design an overcoat for maximum protection of an underlying layer, one must have a clear understanding of the effect of the layered structure on the stresses.

The solutions for rigid round and flat indenters contacting a homogeneous half space of an elastic material have been known for a century. Correct solutions of some contact problems on layered structures, however, have not yet been published. The contact problem of a single layer bonded to a half space was considered by Chen and Engel (1972), who obtained a solution assuming that the top surface of the layer remains in complete contact with the indenter. For certain combinations of parameters they calculated normal stresses under the indenter that were tensile. The correct solution must allow separation between the indenter and the contacting surface. The contact region must be found as part of the solution and it depends on the relative dimensions and material parameters. This type of contact problem is termed a *stationary receding* contact problem by Dundurs and Stippes (see Gladwell (1980), page 183). It is *receding* because the contact region is a subset of the whole face of the indenter and *stationary* because the region size does not depend on the load.

The problem is considered in the context of linear elasticity. The layers and the substrate are assumed to be isotropic, homogeneous, and perfectly-bonded at their interfaces. The indenter is assumed to be rigid with a perfectly-plane face and sharp corners, which lead to singularities in the contact pressure.

The problem is solved by the use of integral transforms. After the transformed field equations are solved and the boundary conditions applied, the inverse transform leads to a singular integral equation for the pressure under the indenter. The integral equation has Cauchy singularities, but methods for numerical solutions exist. They involve expansion in the orthogonal polynomials that are appropriate to the characteristic behavior of the solution.

The solution of the contact problem that assumes contact over the entire face of the indenter is not always the physically relevant one. Indeed, solutions with one, two, or three contact regions between the indenter and the layer surface are found. These solutions exist only for certain combinations of the

[1] Currently at the Department of Theoretical and Applied Mechanics, University of Illinois, Urbana, Ill. 61801.

Contributed by the Applied Mechanics Division of THE AMERICAN SOCIETY OF MECHANICAL ENGINEERS for presentation at the Joint ASCE/ASME Applied Mechanics, Biomechanics, and Fluids Engineering Conference, San Diego, Calif., July 9 to 12, 1989.

Discussion of this paper should be addressed to the Editorial Department, ASME, United Engineering Center, 345 East 47th Street, New York, N.Y. 10017, and will be accepted until two months after final publication of the paper itself in the JOURNAL OF APPLIED MECHANICS. Manuscript received by ASME Applied Mechanics Division, May 27, 1988; final revision, October 7, 1988.

Paper No. 89-APM-26.

material and geometrical parameters for the layered media. In a case of a single layer, the number of contact regions in the solution depends on the elastic moduli and the layer thickness. Underlying layers have the effect of changing the effective modulus of the substrate under the top layer. Based on the solutions obtained, the modulus-thickness parameter space is divided into zones where the solution has one, two, or three contact regions. It is found that the number of contact regions cannot exceed three.

In all cases the problem is reduced to one of determining the contact pressure. Therefore, the fundamental results to be presented are the pressure profiles under the indenter and the parameter space divisions between the one, two, and three contact region solutions. The dependence of the contact region dimensions on the layer properties are considered in detail. The other results to be presented are the stress intensity factors at the corners of the indenter.

2 The Problem Formulation in the Theory of Linear Elasticity

The following equations give the relevant displacement and stress components for plane strain in terms of the two unknown harmonic functions ϕ and Ψ. The first component of the displacement is denoted by u and the third by w, while the stress components have double subscripts, corresponding to the appropriate coordinates.

$$2\mu u = -\frac{\partial}{\partial x}(z\Psi+\phi), \tag{1}$$

$$2\mu w = \kappa\Psi - z\frac{\partial\Psi}{\partial z} - \frac{\partial\phi}{\partial z}, \tag{2}$$

$$\tau_{xx} = 2\nu\frac{\partial\phi}{\partial z} - z\frac{\partial^2\Psi}{\partial x^2} - \frac{\partial^2\phi}{\partial x^2}, \tag{3}$$

$$\tau_{xz} = (1-2\nu)\frac{\partial\Psi}{\partial x} - z\frac{\partial^2\Psi}{\partial x\partial z} - \frac{\partial^2\phi}{\partial x\partial z}, \tag{4}$$

$$\tau_{zz} = 2(1-\nu)\frac{\partial\Psi}{\partial z} - z\frac{\partial^2\Psi}{\partial z^2} - \frac{\partial^2\phi}{\partial z^2}. \tag{5}$$

2.1 Boundary Conditions. At the top layer surface, $z=0$, the frictionless contact with the indenter is described by

$$\begin{aligned} &w^1(x,0)=\delta, && x\in A_c \\ &\tau^1_{zz}(x,0)=0, && x\in\tilde{A}_c, \\ &\tau^1_{xz}(x,0)=0, && \text{all } x \end{aligned} \tag{6}$$

where A_c is the contact region and δ is the indentation. A numerical superscript on a dependent variable denotes the number of the layer in which the quantity is defined, with 1 being the top layer. Quantities in the half space are denoted with a superscript s. Parameters and other quantities carry this information with use of a subscript.

Since the layers are bonded to each other and to the half space (substrate), the displacements and stress components involved in the tractions are continuous across these interfaces. The number of layers is N_l. Thus, the boundary conditions at the interfaces are

$$\left.\begin{aligned} &u^i(x,z_i)=u^{i+1}(x,z_i) \\ &w^i(x,z_i)=w^{i+1}(x,z_i) \\ &\tau^i_{xz}(x,z_i)=\tau^{i+1}_{xz}(x,z_i) \\ &\tau^i_{zz}(x,z_i)=\tau^{i+1}_{zz}(x,z_i) \end{aligned}\right\}, \quad i=1,2,\ldots,N_l, \tag{7}$$

where z_i is the z coordinate of the interface between the ith and $(i+1)$th layer, and the equations hold for all values of the coordinate x. An index value of N_l+1 denotes quantities in the substrate. The layer thicknesses are given by

$$h_i = z_i - z_{i-1}, \quad i=1,2,\ldots,N_l, \tag{8}$$

where z_0 is zero.

The final condition on the solution is overall equilibrium, which requires that the stresses decay to zero for large $\mathbf{x}$ in such a way as to make the integral of the tractions finite over the boundary of an arbitrarily large semicircle. Since the displacements involve the integral of the stresses, they are not globally bounded, and the problem therefore has to be formulated in terms of the surface slope.

Overall equilibrium also requires that the integral of the pressure over the contact region equals the total load, L, applied to the indenter. This condition is

$$L = \int_{A_c} \tau^1_{zz}(x,0)dx. \tag{9}$$

2.2 Application of Integral Transforms. The method of solution of the field equations, supplemented by the boundary conditions (6) and (7), employs the Fourier transform in the coordinate x to reduce the problem to a singular integral equation. First, the transformed field equations are solved analytically in terms of exponentials and unknown functions of the transform variable, which are determined by the transformed boundary conditions. The inverse transform is then applied to recover the dependence on the x coordinate in the form of an integral equation. This is a well-known technique (see Gladwell (1980), for example). The application of the boundary conditions can be simplified by a judicious ordering of the calculations. Brekhovskikh (1980) provides a useful method for this ordering in the context of elastic wave solutions for layered media.

The Fourier transform of a general harmonic function is known and thus ϕ can be written as

$$\hat{\phi}(\xi,z) = A(\xi)e^{z|\xi|} + B(\xi)e^{-z|\xi|}, \tag{10}$$

where the absolute values are employed for later convenience. Similarly, the transform of Ψ is

$$\hat{\Psi}(\xi,z) = C(\xi)e^{z|\xi|} + D(\xi)e^{-z|\xi|}. \tag{11}$$

The transforms of u, w, τ_{xz}, and τ_{zz} are needed in order to apply the boundary conditions (6) and (7). These are written in terms of the four unknown functions $A(\xi)$, $B(\xi)$, $C(\xi)$, and $D(\xi)$, by substituting equations (10) and (11) into the transforms of equations (1), (2), (4), and (5). The result of these operations for a given layer can be written as

$$\mathbf{f}(\xi,z) = \mathbf{T}(\xi,z)\mathbf{a}(\xi), \tag{12}$$

where

$$\mathbf{f}(\xi,z) = \begin{Bmatrix} \hat{u}(\xi,z) \\ \hat{w}(\xi,z) \\ \hat{\tau}_{xz}(\xi,z) \\ \hat{\tau}_{zz}(\xi,z) \end{Bmatrix}, \quad \mathbf{a}(\xi) = \begin{Bmatrix} A(\xi) \\ B(\xi) \\ C(\xi) \\ D(\xi) \end{Bmatrix} \tag{13}$$

and

$$\mathbf{T}=\begin{bmatrix} \frac{i\xi}{2\mu}e^{z|\xi|} & \frac{i\xi}{2\mu}e^{-z|\xi|} & \frac{i\xi z}{2\mu}e^{z|\xi|} & \frac{i\xi z}{2\mu}e^{-z|\xi|} \\ \frac{-|\xi|}{2\mu}e^{z|\xi|} & \frac{|\xi|}{2\mu}e^{-z|\xi|} & \frac{(\kappa-z|\xi|)}{2\mu}e^{z|\xi|} & \frac{(\kappa+z|\xi|)}{2\mu}e^{-z|\xi|} \\ i\xi|\xi|e^{z|\xi|} & -i\xi|\xi|e^{-z|\xi|} & -i\xi((1-2\nu)-z|\xi|)e^{z|\xi|} & -i\xi((1-2\nu)+z|\xi|)e^{-z|\xi|} \\ -\xi^2e^{z|\xi|} & -\xi^2e^{-z|\xi|} & (2(1-\nu)|\xi|-z\xi^2)e^{z|\xi|} & -(2(1-\nu)|\xi|+z\xi^2)e^{-z|\xi|} \end{bmatrix}. \tag{14}$$

These expressions are valid in the layers and the substrate provided the appropriate material constants are used. When needed for clarity, a subscript will be attached to the vectors **f** and **a** and the matrix **T**.

In the substrate, the regularity condition at infinity requires that the coefficients of the $e^{z|\xi|}$ terms vanish in the solutions for Ψ_s and ϕ_s, so that

$$\mathbf{a}_s(\xi)=\begin{Bmatrix} 0 \\ B_s(\xi) \\ 0 \\ D_s(\xi) \end{Bmatrix}. \tag{15}$$

2.3 Transfer Matrix Approach. The idea of the transfer matrix approach is to eliminate the unknown functions of ξ in the layers and write the surface values of the physical quantities directly in terms of the substrate functions $B_s(\xi)$ and $D_s(\xi)$. The boundary conditions (6) are then used to solve for these two remaining functions.

Using the interface boundary conditions to eliminate the unknown functions of ξ in the layers, we find the transfer matrix between the substrate and the top surface of the first layer to be

$$\mathbf{H}(\xi,h_1,h_2,\ldots,h_{N_l})=\Big(\prod_{i=1}^{N_l}\mathbf{A}_i(\xi,h_i)\Big)\mathbf{T}_s(\xi,z_{N_l}), \tag{16}$$

where the single layer transfer matrix is given by

$$\mathbf{A}_i(\xi,h_i)=\mathbf{T}_i(\xi,z_{i-1})\mathbf{T}_i^{-1}(\xi,z_i). \tag{17}$$

The matrix **H** gives the physical quantities at $z=0$ in terms of the two unknown functions in the substrate as

$$\begin{Bmatrix} U(\xi) \\ W(\xi) \\ Q(\xi) \\ -P(\xi) \end{Bmatrix}=\mathbf{H}(\xi,h_1,h_2,\ldots,h_{N_l})\begin{Bmatrix} 0 \\ B_s(\xi) \\ 0 \\ D_s(\xi) \end{Bmatrix}. \tag{18}$$

Here we have also used the notation U and W to refer to the transforms of the surface tangential and normal displacements and Q and $-P$ to refer to the transforms of the shear and normal tractions on the surface $z=0$. The minus sign appears because of the convention that positive contact pressure means compressive stress. The dependence of **H** on the layer thicknesses has been displayed explicitly in equation (18), but it should be remembered that **H** also depends on the elastic parameters of all the layers and the substrate.

Next, the no shear boundary condition in (6) is used to eliminate the unknown functions of ξ in the substrate and write the transform of the surface displacement directly in terms of the transform of the contact pressure as

$$W(\xi)=-\left[\frac{H_{24}H_{32}-H_{22}H_{34}}{H_{44}H_{32}-H_{42}H_{34}}\right]P(\xi), \tag{19}$$

where the H_{ij} are the components of **H**. The function of ξ multiplying $P(\xi)$ in equation (19) is the transform, $G(\xi)$, of the Green's function, $g(x,t)$, that relates the surface displacement to a surface normal force,

$$G(\xi)=-\frac{H_{24}H_{32}-H_{22}H_{34}}{H_{44}H_{32}-H_{42}H_{34}}. \tag{20}$$

If there is only one layer bonded to the substrate the function $G(\xi)$ can readily be evaluated analytically. Using the symbolic manipulation program REDUCE, we obtain the result

$$G(\xi)=\frac{\alpha_1+e^{-2h_1\xi}(\alpha_2(h_1\xi)+\alpha_3e^{-2h_1\xi})}{2\mu_1[\beta_1+e^{-2h_1\xi}(\beta_2(h_1\xi)^2+\beta_3+\beta_4e^{-2h_1\xi})]\,|\xi|} \tag{21}$$

where the constants α_i and β_i depend only on the four material parameters as given in the Appendix. It will be useful later to have the following limit

$$\lim_{\xi\to\infty}\xi G(\xi)=\frac{\alpha_1}{2\mu_1\beta_1}\equiv\frac{1-\nu_1}{\mu_1}. \tag{22}$$

This is the short wavelength limit of the Green's function (ξ is similar to a wave number), which also corresponds to the case of $h_1\to\infty$. Thus, we obtain the known result that the transform of the Green's function for a half space with shear modulus μ_1 and Poisson's ratio ν_1 is

$$G_0(\xi)=\frac{1-\nu_1}{\mu_1\,|\xi|}. \tag{23}$$

When more than one layer is present, equation (20) is used to numerically calculate the values of $G(\xi)$ as explained in Shield (1988).

2.4 Reduction of the Problems to Singular Integral Equations. In this section the two remaining equations in the boundary conditions (6) are used to derive a singular integral equation for the contact pressure.

The pressure and its transform are related by

$$P(\xi)=\frac{1}{\sqrt{2\pi}}\int_{A_c}p(x)e^{ix\xi}dx, \tag{24}$$

where the integral is taken over the contact region. Equation (19) relates the surface slope in terms of the transform of the pressure as

$$\frac{\partial w(x)}{\partial x}=\frac{1}{\sqrt{2\pi}}\int_{-\infty}^{+\infty}-i\xi G(\xi)P(\xi)e^{-ix\xi}d\xi. \tag{25}$$

The surface slope, given by (25), must be zero for $x\epsilon A_c$ by the first of (6). Equations (24) and (25) therefore yield dual integral equations for the pressure and its transform, which can be reduced to a single integral equation,

$$0 = \frac{1-\nu_1}{\pi\mu_1}\int_{A_c} g'(x,t)p(t)dt,\ x\epsilon A_c, \tag{26}$$

where

$$g'(x,t) = \frac{1}{t-x} + n(x,t). \tag{27}$$

The layer term $n(x,t)$ is given by

$$n(x,t) = -\int_0^{+\infty} N(\xi)\sin(x-t)\xi d\xi, \tag{28}$$

where the function $N(\xi)$ is the exponentially decaying part of $G(\xi)$, given by

$$N(\xi) = \frac{\mu_1}{1-\nu_1}\xi G(\xi) - \mathrm{sgn}(\xi). \tag{29}$$

Equation (26) is the convolution of the pressure with the Green's function, given by equation (27), and it is the desired singular integral equation for the problem.

2.5 Nondimensionalization. In order to solve numerically the integral equations, it is desirable to nondimensionalize the variables. The length scale for the problem is the half width of the indenter, denoted by a. The stresses are referenced to the substrate shear modulus μ_s, as are the shear moduli of the layers. With this choice, a layer stiffer than the substrate has a modulus greater than one, while a softer layer has a modulus less than one. The constant factor multiplying the integrals in the integral equations will be denoted by θ, given by

$$\theta = \frac{1-\nu_1}{\pi\mu_1}. \tag{30}$$

The equations in nondimensional form are not repeated here, but they will be exhibited in the sections in which they next appear and it is understood henceforth that all quantities are dimensionless.

3 Numerical Solution of the Singular Integral Equations

3.1 Properties of the Solution of a Cauchy-Type Equation. The Cauchy singular integral equations derived above have been considered in general by Muskhelishvili (1953) and an overview of their application to elastic contact problems has been given by Gladwell (1980). The fundamental results are given in Section 29 of (1953) and their application to elastic contact problems is explained in Chapter 3 of (1980). The key result from these analyses is that the form of the solution of the integral equation depends only on the strongest singularity in the kernel, the Cauchy singularity. The theory of Cauchy line integrals determines the characteristic part of the solution to a singular integral equation of the form

$$F(x) = \int_{A_c}\left(\frac{1}{t-x} + K_0(x,t)\right)p(t)dt,\ x\epsilon A_c, \tag{31}$$

where K_0, can contain logarithmic singularities. The contact region can have the general multicontact form

$$A_c = [b_1,a_1] \cup [b_2,a_2] \cup \ldots \cup [b_{N_c},a_{N_c}], \tag{32}$$

where N_c is the number of separate contact regions. The form of the solution in each subregion is

$$p_i(x) = g_i(x)\,|a_i - x|^{\pm 1/2}\,|b_i - x|^{\pm 1/2},\ i = 1,\ \ldots,N_c, \tag{33}$$

where the functions $g_i(x)$ are bounded on $[b_i,a_i]$. The signs of the exponents are determined by the boundary conditions of the problem. In the case of a sharp-cornered indenter, the negative signs should be chosen for the exponents of the factor involving the coordinate of the corner. If all exponents are negative, the contact is referred to as complete and the extent of the contact region is known beforehand; it is the same as the indenter, which can have separate contact regions. If a corner is rounded or if the surface of the elastic material recedes smoothly from the surface of the indenter, the contact is termed incomplete and the positive sign is chosen for the appropriate exponent. In this case, the extent of the contact region must be determined as part of the solution of the problem by requiring that the pressure vanish at that boundary of the contact region.

3.2 The Method of Solution. A numerical method for solving an equation of the form of equation (31) was first proposed by Erdogan and Gupta (1972) and is summarized in Erdogan, Gupta, and Cook (1973). This method is a simplification of the classical method of expansion in orthogonal polynomials. It is based on the fact that a Gauss-Chebyshev integration scheme can be used to evaluate the singular integral in (31) for a discrete set of values of x. Thus, we have the approximation that

$$\int_{-1}^{+1}\frac{p(t)}{t-y_k}dt = \sum_{i=1}^{N} W_i\frac{g(s_i)}{s_i - y_k} \tag{34}$$

where $p(t)$ has the form (33). The expressions for the W_i, s_i, and y_k are given in (1973) for the various combinations of exponents in (33). This method implicitly assumes that the regular part of the pressure can be represented to sufficient accuracy by

$$g(t) = \sum_{n=0}^{N-1} g_n\pi_n(t), \tag{35}$$

where the $\pi_n(t)$ are polynomials whose weight function is the coefficient of $g(t)$ in (33). Applying this method to equation (31) we obtain

$$F(y_k) = \sum_{i=1}^{N} W_i g(s_i)\left[\frac{1}{s_i - y_k} + K_0(y_k,s_i)\right],\ k = 1,\ \ldots,N-1. \tag{36}$$

This is a set of $N-1$ linear equations in the unknowns $g(s_i)$, the load equation provides the Nth equation.

In the following it will be useful to solve directly for the coefficients g_n instead of the values for $g(t)$ at the points s_i. To accomplish this we first rewrite equation (36) as

$$F(y_k) = \frac{\pi}{N}\sum_{i=1}^{N} g(s_i)\frac{1}{s_i - y_k} + \int_{-1}^{+1}\frac{g(t)K_0(y_k,t)}{\sqrt{1-t^2}}dt,$$

$$k = 1,\ \ldots,N-1, \tag{37}$$

by removing the approximation to the integral of the second term in (31). (Here, we are using as an example the case of $A_c = [-1,1]$ with complete contact.) Using the expansion in equation (35), with the polynomials $\pi_n(t)$ identified as the Chebyshev polynomials of the first kind, $T_n(t)$, in place of $g(s_i)$ and $g(t)$ and interchanging the order of summation, we obtain from equation (37)

$$F(y_k) = \sum_{n=0}^{N-1} g_n\left[\frac{\pi}{N}\sum_{i=1}^{N} T_n(s_i)\frac{1}{s_i - y_k} + \int_{-1}^{+1}\frac{T_n(t)K_0(y_k,t)}{\sqrt{1-t^2}}dt\right]\quad k = 1,\ \ldots,N-1. \tag{38}$$

The remaining integral can be evaluated with the Gauss-Chebyshev integrator suited to the behavior of the integrand (see Abramowitz and Stegun (1965), for example) to yield

$$F(y_k)=\sum_{n=0}^{N-1} g_n\left[\frac{\pi}{N}\sum_{i=1}^{N} T_n(s_i)\left(\frac{1}{s_i-y_k}+K_0(y_k,s_i)\right)\right]$$

$$k=1,\ \ldots\ ,N-1. \tag{39}$$

These are $N-1$ equations in the N unknowns g_n.

If the solution of the problem is symmetric with respect to the origin, half of the computational effort can be saved. In this case we write $g(t)$ as

$$g(t)=\sum_{n=0}^{N/2-1} g_n T_{2n}(t), \tag{40}$$

where N is assumed to be even. Using this in the aforementioned derivation leads to the same result, equation (39), with the range of summation on n reduced by half and T_n replaced by T_{2n}. Since there are only $N/2$ unknowns, it is only necessary to generate $N/2$ equations. The load equation is retained and we consider only positive y_k, given by $k=1,\ \ldots\ ,N/2-1$. The remaining values of k would produce redundant equations.

3.3 Numerical Inversion of the Layer Kernel. In order to use the methods presented for solving singular integral equations, it is necessary to calculate the values of the kernel $n(x,t)$ given by (28). The function $N(\xi)$ in the integrand of (28) is bounded and is $O(e^{-h_1\xi})$ as $\xi\to\infty$. The integrand of the integral depends on the term $x-t$, which can have values in the interval $[-2,2]$ for the numerical schemes just presented. This term can never be identically zero, but as the order of the numerical scheme becomes large, the minimum value of y_k-s_i approaches zero. This combination of results makes (28) difficult to evaluate. Also, as the layer thickness gets small, many cycles of the trigonometric function occur before $N(\xi)$ becomes sufficiently small for truncation. As h_1 becomes large, $N(\xi)$ decays more rapidly as $\xi\to\infty$, making the value of the integral smaller. In the limit of infinite h_1, the value of $N(\xi)$ is zero. This suggests that the integrator used to numerically evaluate (28) should depend on the value of h_1. If h_1 is small, the number of integration points should be related to the shortest period of the trigonometric function. For large h_1 the step size for the integrator should depend only on the decay rate of $N(\xi)$ as $\xi\to\infty$. The large h_1 case is not critical, because in this case the value of $N(\xi)$ is small and the layer has little effect on the solution. In the most interesting case of $h_1<1$, many cycles in $N(\xi)$ can occur before it decays to zero. Since all of the functions involved in the integrands are smooth, a high order integration scheme is not necessary if this behavior of the integrands is taken into account. Therefore, we use a trapezoidal integrator with a step size $\Delta\xi$ that is an integer fraction of the shortest period of the cyclic functions,

$$\Delta\xi=\frac{\pi}{N_h}. \tag{41}$$

The shortest period occurs for $x-t=2$. The integration is truncated at $\xi_{\max}$, which is chosen such that

$$|N(\xi_{\max})|<\epsilon_h, \tag{42}$$

where ϵ_h is a tolerance for the integration scheme. The contribution to the integral for $\xi>\xi_{\max}$ is neglected.

For small values of h_1, the method just outlined can be very time consuming, and it must be remembered that the numerical method for the solution of the integral equation requires approximately N^2 evaluations of this integral. In the case of more than one layer, considerable time is involved in the calculation of $N(\xi)$. Examination of the method presented shows that the N^2 evaluations all use the values of $N(\xi)$ at the same points; only the values of x and t change. Thus, if the values of $N(\xi)$ at the integration points are stored in an array when the integral is first evaluated, considerable time can be saved in successive evaluations.

As $h_1\to 0$, the function $n(x,t)$ becomes large for x near t, as is revealed if one integrates equation (28) by parts to get

$$n(x,t)=\frac{N(0)}{x-t}+\frac{1}{x-t}\int_0^{+\infty} N'(\xi)\cos(t-x)\xi d\xi, \tag{43}$$

where

$$N(0)=\frac{\mu_1^*(1-\nu_s)}{1-\nu_1}-1. \tag{44}$$

The first term in (43), when combined with the first term in $g'(x,t)$ of equation (27), gives

$$\theta\left(\frac{1}{t-x}+\frac{N(0)}{t-x}\right)=\frac{1-\nu_s}{\pi}\frac{1}{t-x}. \tag{45}$$

As $h_1\to\infty$, for which $n(x,t)=0$ in equation (27), we obtain the Green's function for a half space with the material properties of the layer, $\theta/(t-x)$. Comparing this with the right-hand side of equation (45), we see that (45) is the Green's function for a half space of material properties ν_s and μ_s (the nondimensionalization has $\mu_s^*=1$). Thus, the leading term in the Green's function for a layered half space with a very thin layer is the half space Green's function for the substrate. This should be expected because for $h_1=0$, we must recover the result for a half space of the substrate material. Equation (42) is not useful for numerical calculations until h_1 is as small as 0.01, which is much smaller than we consider here. The reason for this is that the coefficient of the second term in equation (43), $1/(t-x)$, can be very large. Thus, h_1 must be small enough to override and make the integral correspondingly small. This factor also magnifies any errors in the calculation of the integral.

4 Solutions for Specific Contact Regions

In this section, we specialize the problem to three specific cases of A_c. First, we consider the single contact region case, which has been treated previously in the literature. Its solution is characterized by non-negative pressure over the entire face of the indenter, which contacts the top layer over the region $[-1,+1]$. Next, we examine the two contact region solutions. These solutions involve contact of the indenter with the surface of the top layer only over the region $c\le|x|\le 1$. Finally, the three contact region solution is presented. In this solution the indenter contacts the top layer surface for $|x|\le d$ and $c\le|x|\le 1$. Each of these solutions exist only for a certain ranges of geometry and materials.

4.1 The Solution With One Contact Region. The one contact region solution, with $A_c=[-1,1]$, is given in the Section 3.2. The solution has the form

$$p(t)=\frac{1}{\sqrt{1-t^2}}\sum_{n=0}^{N/2-1} g_n T_{2n}(t),\ t\in[-1,1]. \tag{46}$$

The set of algebraic linear equations for this case is given by (39) specialized to the symmetric form of the pressure given in (46). We write this set of linear equations as ${}^1A\mathbf{g}=\mathbf{b}$, where

$$\mathbf{g}=\left\{\begin{array}{c} g_0 \\ g_1 \\ \cdots \\ g_{N/2-1} \end{array}\right\},\quad \mathbf{b}=\left\{\begin{array}{c} 0 \\ \cdots \\ 0 \\ 1 \end{array}\right\}, \tag{47}$$

and the first $N/2-1$ rows of the matrix ${}^1A$ are determined by equation (39) to be

$${}^1A_{kn}=\frac{\pi}{N}\sum_{i=1}^{N}T_{2n}(s_i)\left(\frac{1}{s_i-y_k}+n(y_k,s_i)\right),$$

$$k=1,\ldots,N/2-1,\quad n=0,\ldots,N/2-1. \tag{48}$$

The presuperscript on the matrix A indicates one contact region. The points s_i and the y_k are given by (7.56) of Erdogan, Gupta, and Cook (1973). The $(N/2)$th row of the matrix ${}^1A$ is given by the coefficients of g_n in the load equation, which becomes

$$1=\pi g_0. \tag{49}$$

The nondimensional load has the value of one, without loss of generality.

To be valid the solution must satisfy the condition that the pressure is non-negative over the entire contact region. Thus, if we define a function that is $+1$ when $p(t)\geq 0$ for all $t\in[-1,1]$ and -1 otherwise, a simple bisection root-finding routine can be used to determine the parameter values such that $p(t)=0$ for some t. The parameters that determine this root are the layer thicknesses h_i and the material constants μ_i and ν_i. The root-finding routine varies one parameter, usually the top layer modulus μ_1, while all the others are fixed. The curve found (a surface in the $3N_l+2$ parameter space) is the boundary of the zone of validity of the one contact region solution.

4.2 The Solution With Two Contact Regions. If the pressure predicted by the one contact region solution is negative in some symmetric region about $t=0$, then this solution is not valid. The correct solution has contact between the indenter and the surface only over the region $c\leq |x|\leq 1$ for some unknown value of c. In order to solve the problem under these conditions, we must consider the solution of the integral equation (31) after it has been symmetrized with respect to the origin. Thus, we write equation (31) as

$$0=\int_c^{+1}\left(\frac{2x}{t^2-x^2}+n^*(x,t)\right)p(t)dt,\ x\in[c,1]. \tag{50}$$

The kernel $n^*(x,t)$ is

$$n^*(x,t)=-2\int_0^{+\infty}N(\xi)\sin(x\xi)\cos(t\xi)d\xi. \tag{51}$$

The pressure for the two contact region solution is zero at $x=c$ and has a square root singularity at $x=1$. Thus, we assume that

$$p(t)=\sqrt{\frac{t^2-c^2}{1-t^2}}\,tg(s), \tag{52}$$

where the function $g(s)$ is given by

$$g(s)=\sigma^{-1}\sum_{n=0}^{N-1}g_nT_{2n+1}(\sigma), \tag{53}$$

where

$$\sigma=\sqrt{\frac{s+1}{2}}. \tag{54}$$

The variable s is related to the variable t through the relation Gladwell (1980)

$$s=\frac{2t^2-1-c^2}{1-c^2}. \tag{55}$$

This map takes the interval $[c,1]$ onto $[-1,1]$. After this change of variables equation (50) yields

$$0=\int_{-1}^{+1}\sqrt{\frac{1+s}{1-s}}g(s)\left(\frac{x}{s-y}+\frac{1-c^2}{4}n^*(x,t)\right)ds,\ y\in[-1,1], \tag{56}$$

where we have also related y to x according to (55).

Equation (56) has the same form as equation (31), only the characteristic part of the pressure is different and the numerical approximation of equation (56) is

$$0=\frac{\pi}{2N+1}\sum_{n=0}^{N-1}g_n{}^2A_{kn},\ k=1,\ldots,N, \tag{57}$$

where

$${}^2A_{kn}=\sum_{i=1}^{N}(1+s_i)\sigma_i^{-1}T_{2n+1}(\sigma_i)\left(\frac{x_k}{s_i-y_k}+\frac{1-c^2}{4}n^*(x_k,t_i)\right)$$

$$n=0,\ldots,N-1,\quad k=1,\ldots,N, \tag{58}$$

and s_i and y_k are given in Erdogan, Gupta, and Cook (1973) by equation (7.47). The variable σ_i is given by (54) with s replaced by s_i. The untransformed variables t_i and x_k are given by the inverse of equation (55), applied to s_i and y_k, respectively.

The load equation (9) transforms, with use of the orthogonality of the T_{2n+1}, to

$$1=\frac{1-c^2}{4}\int_{-1}^{+1}\sqrt{\frac{1+s}{1-s}}g(s)ds=\frac{\pi(1-c^2)}{2}g_0. \tag{59}$$

We have found $N+1$ equations involving the N unknowns g_n. Equation (57) has N equations and the load equation provides the other one. The number of equations is not excessive because there is another unknown, c, the inner contact dimension, that must be determined as part of the solution. In order for a unique nontrivial solution to be found the rank of the $N+1$ equations must be N. Because the load equation is not related to the other N equations, we must find a value of c such that one of the equations in (57) is redundant. That is, we require

$$\det({}^2A)=0. \tag{60}$$

This is a nonlinear equation giving c as a function of the material and geometrical parameters of the problem. A bisection root-finding algorithm is also used to solve this equation. The determinate is found using a Gaussian decomposition of the matrix ${}^2A$. The determinate is the product of the diagonal elements of the upper diagonal result of the decomposition. After the proper value of c has been found, any one of the rows of ${}^2A$ can be replaced by the load equation, and the set of linear equations can be solved for the g_n. After the value of c is found and one row of ${}^2A$ is replaced by the load equation, the matrix is denoted by ${}_L{}^2A$.

The solutions of the contact problems posed here are known to be unique (Shield, 1982), and the value of c determined from equation (60) should therefore be unique. The zone in the parameter space where this equation has no roots corresponds to the zone of validity of the one contact region solution. Thus, the zone of validity in the parameter space for the two contact region solution is bounded by the set of values of the parameters for which the number of roots of equation (60) changes from one to zero or two. The curve in the parameter space across which the number of roots changes from one to two is the boundary between the zones of validity for the two and three contact region solutions. These curves are found by defining a function that is $+1$ if equation (60) has one root and -1 otherwise. A bisection root-finding routine is used to find the value of a parameter for which the number of roots changes while the other parameters are held fixed. The number of roots is determined by counting the number of sign changes that occur in $\det(^2A)$ as c is varied from 0 to 1. The boundary between the zones for the one and two contact solutions obtained using this method agrees with the results found in the previous section using the sign of the pressure.

4.3 The Solution With Three Contact Regions. For three contact regions $A_c = [-1, -c] \cup [-d, d] \cup [c, 1]$. The motivation for finding a two contact region solution was the observation that the one contact region solution predicts negative pressure near $x=0$ for some choices of the parameters. It was also observed that the one contact region solution may predict negative pressure over a region that does not include the origin. This occurs if the top layer is too thin for the two contact region solution to exist. Therefore, there is a zone in the parameter space in which neither the one nor the two contact region solution is valid. This is the zone where the three contact region solutions exist.

We were able to solve the two contact region problem by using symmetry to reduce the two integrals to a single integral. It will not be possible here to reduce the three integrals to one, but the same method can be used to reduce from three to two integrals. Equation (31) specialized to this form of A_c and symmetrized as in the two contact region case becomes

$$0 = \int_c^{+1} \left(\frac{2x}{t^2 - x^2} + n^*(x,t)\right) p_1(t) dt$$

$$+ \int_0^d \left(\frac{2x}{t^2 - x^2} + n^*(x,t)\right) p_2(t) dt \tag{61}$$

and is valid for x in $[0,d]$ or $[c,1]$. Only one of these integrals is singular for a given value of x. This means that the techniques for evaluating the singular integrals given in Section 3 need only be applied to one integral at a time. In (61) the subscript on the pressure refers to the contact region over which it is defined.

The pressure, $p_1(t)$, defined in the region $[c,1]$ is the same as in the two contact region solution, and is given by equations (52) and (53). The pressure $p_2(t)$ defined in $[0,d]$, has a square root zero at the points $\pm d$,

$$p_2(t) = \sqrt{d^2 - t^2}\, g_2(s'), \tag{62}$$

where the function $g_2(s')$ is given by

$$g_2(s') = (\sigma')^{-1} \sum_{n=0}^{N-1} g'_n T_{2n+1}(\sigma'). \tag{63}$$

The variable s' is related to t by

$$s' = \frac{2t^2 - d^2}{d^2}, \tag{64}$$

and σ' is given by equation (54) evaluated at s'. The prime is used on subscripted variables to denote quantities associated with the region $[-d,d]$. By examining the transformed integral, we find that the proper integrator has $\alpha = \beta = -1/2$, the same as used for the two contact region integral. Thus we have $s'_i = s_i$. Using this integrator and the form of $p_2(t)$, we obtain for the approximation of the second integral in equation (61)

$$\frac{2\pi}{2N+1} \sum_{n=0}^{N-1} g'_n \sum_{i=1}^{N} (1+s_i)(\sigma_i)^{-1} T_{2n+1}(\sigma_i)$$

$$\times \left(\frac{x}{s_i - y} + \frac{d^2}{4} n^*(x, t'_i)\right). \tag{65}$$

This equation is valid for $x = x'_k$ or $x = x_k$. The x'_k are given by

$$x'_k = \left(\frac{d^2 (y_k - 1)}{2}\right)^{1/2} \tag{66}$$

and the t'_i are similarly related to s_i. The coefficient matrix of the g'_n in equation (65) is denoted by $^3A^{22}_{kn}$ when x is replaced by x'_k and by $^3A^{12}_{kn}$ when $x = x_k$. This postsuperscript notation refers to the region in which a given pressure has effect. Thus, 22 refers to the slope produced in $[-d, d]$ by the pressure p_2 and 12 refers to the slope produced in $[c, 1]$ by the pressure p_2. The matrix given in equation (58) in this notation is $^3A^{11}_{kn}$. The remaining submatrix is given by

$$^3A^{21}_{kn} = \sum_{i=1}^{N} (1+s_i)\sigma_i^{-1} T_{2n+1}(\sigma_i)$$

$$\times \left(\frac{x'_k}{s_i - y'_k} + \frac{1-c^2}{4} n^*(x'_k, t_i)\right)$$

$$n = 0, \ldots, N-1,\ k = 1, \ldots, N. \tag{67}$$

These four submatrices makeup the complete set of equations with coefficient matrix ^3A and the vector of unknows, $\mathbf{g}$, given by

$$^3A = \begin{bmatrix} ^3A^{11} & ^3A^{12} \\ ^3A^{21} & ^3A^{22} \end{bmatrix}, \quad \mathbf{g} = \begin{Bmatrix} g_0 \\ \cdots \\ g_{N-1} \\ g'_0 \\ \cdots \\ g'_{N-1} \end{Bmatrix}. \tag{68}$$

The matrix ^3A has $2N$ nonzero rows. The number of unknowns in this problem is $2N+2$. There are $2N$ entries in $\mathbf{g}$, and the two contact region dimensions c and d must also be determined as part of the solution. The extra equations are the resultant load equation for the indenter, involving the sum of the integrals of p_1 and p_2, and a consistency condition. The consistency condition is a mathematical statement that there is only one indenter, that is, that the normal displacement in each region must be the same. This condition can be stated as

$$\int_d^c \frac{\partial w(x)}{\partial x}\, dx = 0, \tag{69}$$

that is, $w(c) = w(d)$. In the region $d \le x \le c$ neither integral in equation (61) is singular. Thus, an integrator appropriate to the forms of the pressure can be used for any x value in this region. Using the integral representation of the slope in terms of the pressures we obtain from (69)

$$0 = \int_c^{+1} p_1(t) I(t) dt + \int_0^d p_2(t) I(t) dt \tag{70}$$

where

$$I(t) = \theta \int_d^c \left(\frac{2x}{t^2 - x^2} + n^*(x,t)\right) dx,\ t \in A_c. \tag{71}$$

The order of integration has been interchanged so that equation (70) can be written as a linear equation in elements of $\mathbf{g}$. The integral in (71) can be calculated using a Gaussian integration scheme given by Abramowitz and Stegun in Table 25.4, and it yields

$$I(t)=\theta\,\frac{c-d}{2}\sum_{i=1}^{N}W_i^G\left(\frac{2x_i^G}{t^2-(x_i^G)^2}+n^*(x_i^G,t)\right), \tag{72}$$

where x_i^G is given by

$$x_i^G=\frac{(c-d)t_i^G+c+d}{2}. \tag{73}$$

Equation (70) can then be integrated numerically using the integrators appropriate to the forms of the pressure to give

$$0=\frac{\pi(1-c^2)}{2(2N+1)}\sum_{n=0}^{N-1}g_n\sum_{i=1}^{N}(1+s_i)\sigma_i^{-1}T_{2n+1}(\sigma_i)I(t_i)$$

$$+\frac{\pi d^2}{2(2N+1)}\sum_{n=0}^{N-1}g_n'\sum_{i=1}^{N}(1+s_i')(\sigma_i')^{-1}T_{2n+1}(\sigma_i')I(t_i'). \tag{74}$$

The coefficients of the g_n and g_n' in equation (74) form the row of the matrix ${}^3A$ for the consistency equation.

We now have $2N+2$ equations for the $2N+2$ unknowns, however, they include implicit nonlinear equations for the two contact dimensions. If the correct values of the contact dimensions were known, then the $2N+2$ equations would have rank $2N$ for there to exist in nontrivial unique solution for **g**. This suggests that the proper conditions to determine c and d are both of

$$\det({}^3A)=0,\ \det({}^3_dA)=0, \tag{75}$$

where ${}^3_dA$ is the matrix ${}^3A$ with one row replaced by (74). Finding the simultaneous root of these equations directly is difficult, but it is possible with an iterative procedure. This procedure requires that one of c and d be held fixed, and with a bisection root finding routine the other is varied until one of the equations is solved. This second parameter is then held fixed while the root-finding routine is applied to the other equation. This procedure is repeated until the result converges to the simultaneous root of the two equations. After the simultaneous root of these two equations is found, one row of ${}^3_dA$ can be replaced by the load equation to solve for **g**. This load equation is

$$1=L_1+L_2, \tag{76}$$

where L_1 is given by the right-hand side of equation (59). The contribution to the load by $p_2(t)$ is given by

$$L_2=\frac{\pi d^2}{2}g_0'. \tag{77}$$

After the coefficients in the pressure expansion and the contact dimensions have been obtained using the procedures just given, the stress intensity factor at the corners of the indenter,

$$K_I=\lim_{t\to 1}(1-t)^{1/2}p(t), \tag{78}$$

can be found. The stress intensity factor for the half space solution is easily calculated analytically and it is found to be 0.2250.

5 Results

In this section we present the results of the calculations. Typical solutions for the three types of contact regions are given, then we determine the zones in the parameter space in which each solution is valid. After this is done, the contact dimensions and other quantities of interest are calculated, and the limiting behavior in various cases is discussed. Finally, the stress intensity factors are obtained.

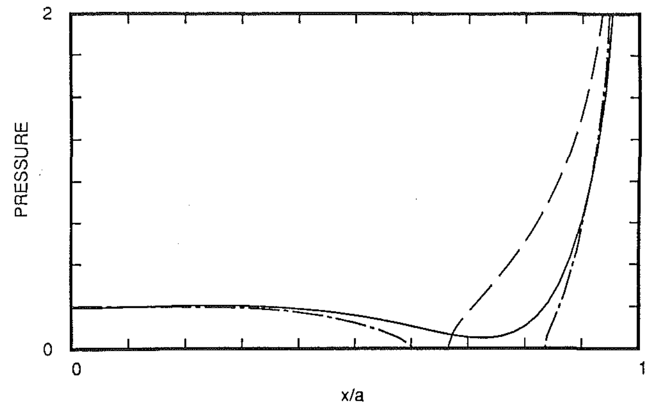

Fig. 1 Typical solutions for each type of contact region: one contact region, $h=0.25$, $\mu=10.0$, (solid), two contact regions, $h=.75$, $\mu=15.0$, (dashed), three contact regions, $h=.25$, $\mu=15.0$, (dot-dashed).

The number of geometrical and material parameters involved in the solutions is $3N_l+1$: the thickness, Poisson's ratio and modulus ratio for each layer, and the Poisson's ratio of the substrate. To reduce the number of combinations, the values of all Poisson's ratios are fixed at 1/3. The behavior of the solutions are examined in detail for the case of a single layer, but in the two-layer case only the parameter space divisions for selected examples are presented.

5.1 Examples of the Three Solutions. Figure 1 shows typical pressure distributions under the indenter for the three types of contact regions. The one contact region solution has positive pressure over the entire face of the indenter. The two contact region solution has contact for $1\geq|x|\geq c$, where $c=0.666$ in this example. The three contact region solution has contact for $|x|\leq d$ and $1\geq|x|\geq c$. Both the two and three contact region solutions have regions of zero pressure where the surface of the top layer does not contact the indenter.

5.2 Numerical Accuracy. The numerical schemes presented in the earlier sections have several parameters that must be determined in order for the solutions to be suitably accurate. These parameters are N_h and ϵ_h for the layer term integrator and N, the order of the series expansions for $g(t)$. The integrator used for the layer term is well behaved and the suitable values of the parameters are easily found for accurate evaluations. Examination of the values of $n(x,t)$ calculated with the integrator shows that the values $N_h=20$ and $\epsilon_h=0.01$ are suitable for all calculations. The number of terms in the expansion for $g(t)$ is also important to the speed and accuracy of the solution. The suitability of a given value of N is checked by examining the size of the highest order coefficient in the expansion, g_{N-1}. $N=10$ was suitable for all the calculations performed here.

5.3 Parameter Space. For the one-layer problem, the two parameters are the layer modulus ratio, μ, and thickness, h. The subscripts are omitted when only one layer is involved. The most important issue is the type of solution as regards the number of contact regions for given layer properties. In Section 4 the conditions for each of the three types of solutions were stated. The one contact region solution is valid when the calculated pressure is non-negative over the entire face of the indenter. Thus, the boundary of this zone is the parameter space is characterized by solutions in which the pressure is zero at a single point under the indenter. The two contact region solution exists when equation (60) has a single root. The boundary of this zone in the (μ, h) plane is the curve across which the number of roots of (60) changes from one to zero or two. The three contact region solution is valid in the parameter zone where there is a single simultaneous root of equations

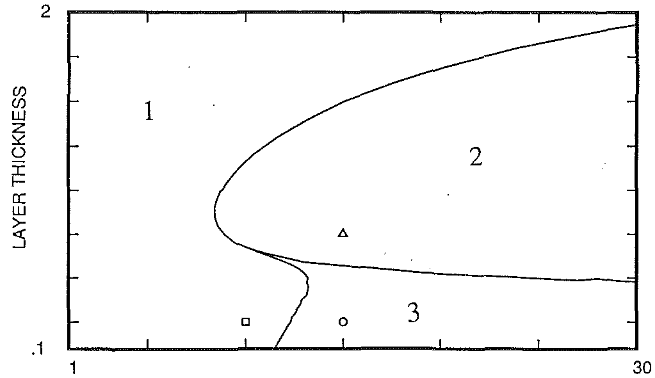

Fig. 2 The parameter space for a single layer showing the zones of existence of the three types of solutions for $\nu=\nu_s=1/3$. The labels are explained in the text and the symbols correspond to the solutions presented in Fig. 1.

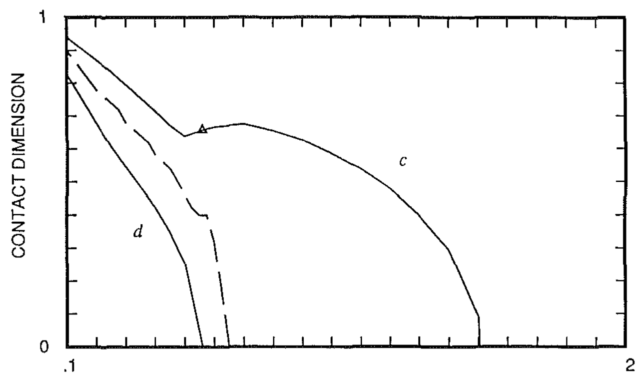

Fig. 3 The values of $c=d$ along the 1-3 boundary (dashed). The variations of c and d with layer thickness along the $\mu=15.0$ line (solid). The 2-3 boundary is marked by the triangular symbol.

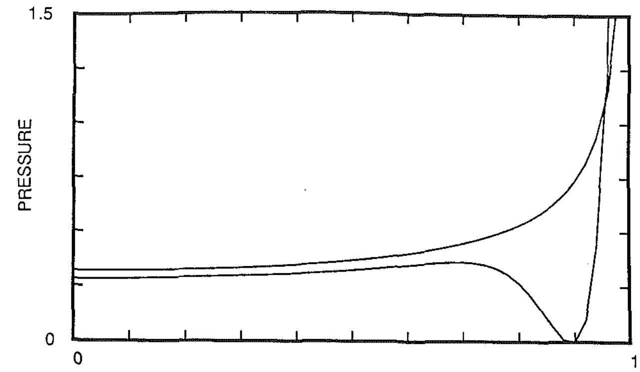

Fig. 4 Comparison of the solutions for the half space case and for $h=0.1$, $\mu=11.48$

(75). Figure 2 shows these zones in the (μ, h) plane. We observe that one curve generally separates the zone of lower modulus from the rest of the plane. It divides the plane into the domains of low-modulus, single-contact-region solutions and the high-modulus multiple-contact-region solutions. Because all of the modulus ratios shown in Fig. 2 are greater than one, it follows that multiple-contact-region solutions occur only when the layer is stiffer than the substrate. The curve that is almost parallel to the modulus axis in the high-modulus zone divides the multiple-contact-region zone into the two- and three-contact-region zones.

The single-multiple contact-region solution separation curve in Fig. 2 on which $p(t)=0$ for some isolated t, can be divided into two parts. If, as μ increases for fixed h, the zero pressure occurs first for $t=0$, then crossing the curve in the direction of increasing modulus changes the type of solution from one to two contact regions. This curve is called the 1-2 boundary in Fig. 2. If in this process of increasing μ for fixed h the zero in pressure occurs first for $t\neq 0$, then further increasing the modulus causes the solution to change from a one to a three-contact-region solution. This curve is called the 1-3 boundary. The 1-3 boundary occurs for thinner layers than the 1-2 boundary. The point at which the 1-2 and 1-3 boundary curves meet is also the intersection point with the 2-3 boundary curve, which is defined as the curve across which the number of roots of (60) changes from one to two. At exactly this triple point all three solutions exist for the contact dimensions of $c=d=0$.

5.3.1 Dependence of Contact Regions on the Physical Parameters. Obtaining the two- and three-contact-region solutions involves finding the contact region as well as the pressure distributions. The contact dimensions are easiest to determine on the boundaries of the zones in the (μ, h) plane. At points on the 1-2 boundary the value of c, which determines the point of contact in the outer contact region, is zero. The parameter d determines the point of contact in the inner contact region of the three contact region solution. On the 1-3 boundary, c is equal to d and they can be determined by finding the point at which the pressure first becomes zero as the modulus is increased for fixed h. Along the 2-3 boundary the value of c must be determined by finding the root of (60), and the value of d is zero.

The dependence of c and d on the layer properties will be discussed next. Figure 3 shows the common values of $c=d$ versus the layer thickness along the 1-3 boundary. As the layer thickness approaches zero, the value of $c=d$ approaches unity. Figure 4 shows the contact pressure for the point on the 1-3 curve in Fig. 2 corresponding to $h=0.1$. It also shows for comparison the contact pressure for the half space solution ($h=0$). As can be seen the pressure is close to the half space solution away from the corners of the indenter. As $h\rightarrow 0$ the point zero pressure moves to the corner and the solution approaches the half space solution over the entire indenter in a somewhat singular manner. The size of the region near the corner where the layer has a large effect is on the order of the layer thickness, indicating a boundary layer type of phenomenon. The convergence to the half space solution is nonuniform, because for any finite layer thickness there is always a large difference in the solutions near the corner. For a given layer thickness this difference is proportional to the modulus ratio of the layer, but there is no difference for a modulus ratio of unity.

Referring again to Fig. 2, d is zero on the 2-3 boundary and moving away from this curve by decreasing h while holding μ fixed causes d to increase. The dependencies of both c and d on h along the $\mu=15.0$ line in the parameter space of Fig. 2 are also given in Fig. 3. The contact dimension d is zero until the 2-3 boundary is crossed, marked by a triangle at the corresponding c value. As the layer thickness decreases the contact dimensions both approach one, exhibiting the same type of behavior in the contact pressure as seen in Fig. 4 along the 1-3 boundary curve.

At points on the 2-3 boundary in the (μ, h) plane, the contact dimension, d, is zero. Figure 5 shows the value of c versus layer modulus, found along the 2-3 boundaries as shown in Fig. 2. As the layer modulus increases, c approaches 1, that is, the extent of the contact goes to a point at the corner of the indenter. This is also the case for any fixed value fo h as $\mu\rightarrow\infty$, not just along the 2-3 boundary. This is also shown in Fig. 5 for the case of $h=0.5$. This means that regardless of the values of h, the contact can be forced to the limiting case of only

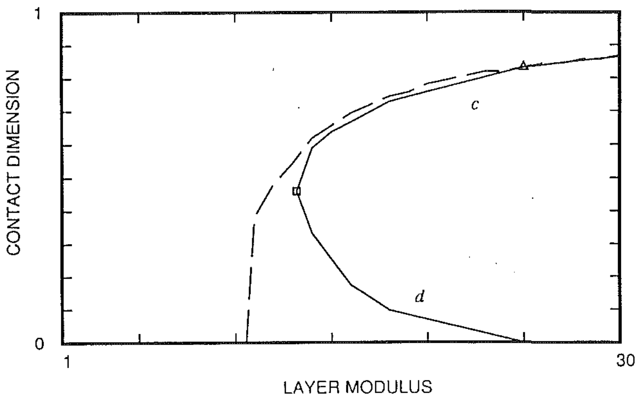

Fig. 5 The contact dimension c versus modulus along the 2-3 boundary (dashed). The variation of c and d with layer modulus along the $h=0.5$ line (solid). The square symbol marks the 1-3 boundary, and the triangular symbol marks the 2-3 boundary.

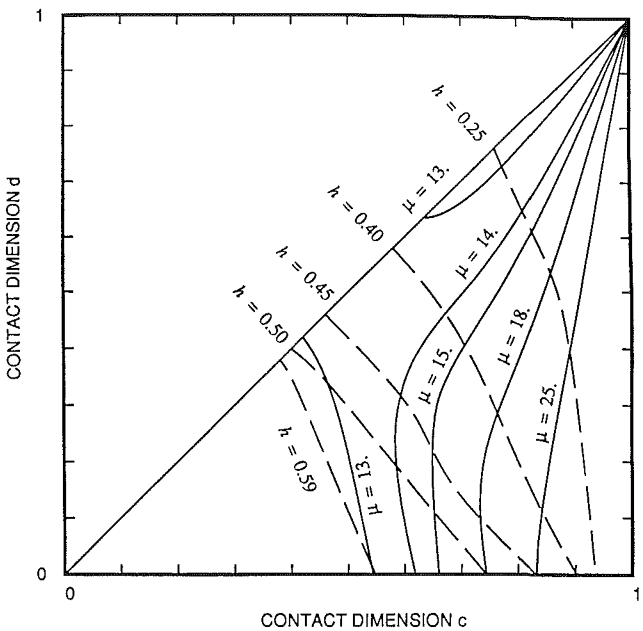

Fig. 6 The simultaneous root of equations (75), (c,d), for various layers. The layer modulus is constant along the solid lines and the thickness is constant along the dashed lines.

point contacts at the corners of the indenter if the layer modulus is made sufficiently large. In Fig. 5, the values of c and d are equal at the 1-3 boundary, marked with the square symbol (see also Fig. 2). As the modulus increases from this point, d decreases and c increases. The 2-3 boundary in Fig. 2 has a slight negative slope. Thus, increasing the modulus at constant thickness will eventually result in a crossing of the 2-3 boundary. There the value of d becomes zero at the 2-3 boundary, but c continues to increase from this point, which is marked with a triangle, as the modulus increases. The behavior of the solution as $\mu \rightarrow \infty$ was just discussed.

The dependence of the contact dimensions c and d on h and μ can also be displayed by marking the locations of the roots of equations (75) in a (c, d) plane for various combinations of the layer thickness and modulus. Figure 6 presents such a plot. Five values of the layer modulus are represented by the solid lines, along which the layer thickness varies. Along the dashed lines the layer thickness is held constant while the modulus is varied. The $c=d$ diagonal is the 1-3 boundary in the μ versus h space of Fig. 2. The 2-3 boundary is the $d=0$ axis. The $c=d=1$ point corresponds to the limit as the layer thickness

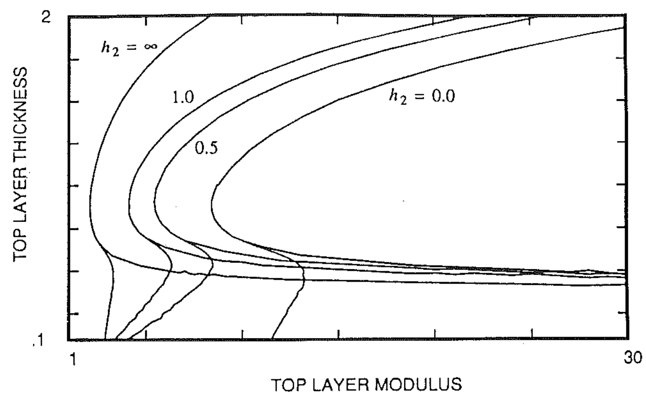

Fig. 7 The parameter space divisions for a midlayer modulus of 0.25 and thicknesses of ∞, 1.0, 0.5, and 0.0

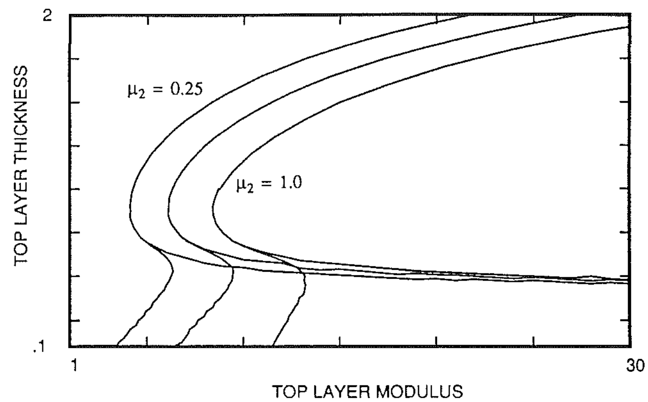

Fig. 8 The parameter space divisions for a midlayer thickness of 1.0 and moduli of 0.25, 0.5, and 1.0

goes to zero. The $c=d=0$ point is the intersection point of the 1-3, 1-2, and 2-3 boundary curves in Fig. 2.

5.3.2 The Effect of a Second Layer. In the previous sections we considered the case of a single layer bonded to a substrate. In this section the (μ, h) parameter space divisions for two layers will be examined. We only consider middle layers with moduli less than one. Thus the shear moduli of the middle layers are less than that of the substrate. The top layer must be stiffer than the effective modulus of the midlayer substrate combination for multiple contact region solutions to exist, however, the minimum top layer modulus necessary for multiple contact decreases for increasing middle layer thickness. If the middle layer is infinitely thick this minimum modulus is reduced, compared to the case of no middle layer, by a factor equal to the midlayer modulus. This can be seen in Fig. 7, which presents the results for a middle layer with $\mu_2=0.25$. The right-most curves are the results for a single layer, $h_1=0$. The left-most curves are for infinite midlayer thickness, which agree with the one layer results with the modulus reduced by a factor of 0.25. The intermediate curves are for midlayer thickness of 1.0 and 0.5. The results for all intermediate thickness will lie between the curves for zero and infinite thickness. A feature of interest is that the 1-3 portions of the curves for the intermediate thicknesses of the midlayer approach the 1-3 curve for an infinitely thick midlayer as the top layer thickness goes to zero. This is the expected behavior because as the top layer becomes thinner, a finite thickness midlayer becomes relatively thicker and influences the solution to a greater degree.

If the thickness of the midlayer is fixed and the parameter space curves are found for various moduli of the midlayer, the results obtained are as shown in Fig. 8. In this figure the right-most curves are the single layer results, since the midlayer has

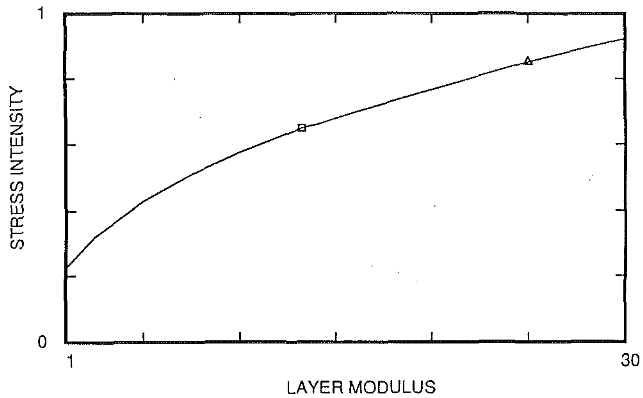

Fig. 9 The stress intensity factor at the corner of the indenter for a single layer of thickness $h = 0.5$. The symbols correspond to the boundaries in Fig. 2.

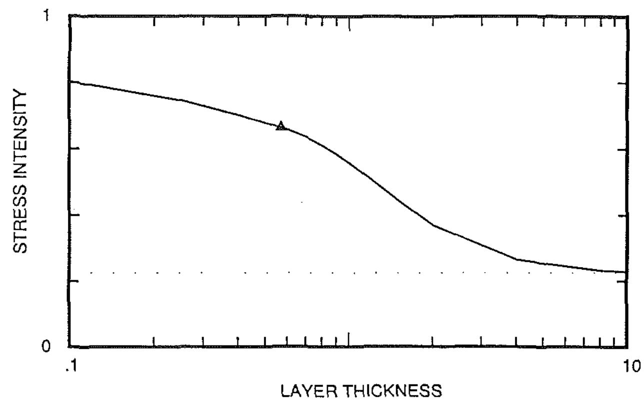

Fig 10 The stress intensity factor at the corner of the indenter for a single layer of modulus $\mu = 15.0$. The triangle marks the 2-3 boundary in Fig. 2.

a modulus of one. As the modulus of the midlayer is reduced from one, the top layer modulus at which multiple contact region solutions exist is decreased. The division between the low-modulus, single-contact-region zone and the high-modulus, multiple-contact-region zone in the limit of zero midlayer modulus can not be to the left of the straight line $\mu_1 = 0.0$. This will be the dividing line for thin layers and for thicker layers the layer will have to have a correspondingly higher modulus. Plate theory predicts the behavior of the thinner layers.

5.4 Stress Intensity Factors. The stress intensity factors defined in equation (78) are a measure of the strength of the pressure singularity at the corners of the indenter. A common use of stress intensity factors is in problems involving cracks in linearly elastic material. Figure 9 shows the stress intensity factor versus layer modulus for a single layer of thickness 0.5. As the layer modulus is increased, the stress intensities increase. The square symbol corresponds to the 1-3 boundary and the triangular symbol occurs at the 2-3 boundary in the (μ, h) parameter space of Fig. 2. Since the contact dimension c approaches one as the layer modulus increases for fixed layer thickness, the increase in stress intensity factor is expected because the load is carried by a smaller region. Figure 10 shows the variation in the stress intensity factor with layer thickness for a fixed layer modulus of 15.0. An infinitely thick layer gives the result for a half-space of modulus 15.0. A layer thickness of zero recovers the half-space result of 1.0.

6 Summary and Conclusions

The effect of one or more layers on the solution for contact by a flat smooth indenter is presented. For such a layered structure the solution may have one, two, or three contact regions under the indenter and the choice is determined by the layer's elastic properties and thickness. The parameter space of layer modulus versus layer thickness is divided into three zones, corresponding to the three types of solutions. For multiple-layered structures, the solution depends on many parameters. If only the top layer's parameters are varied, the parameter space divisions are very similar to the single layer case. Only the modulus at which the transitions between solution types is affected, because the effective modulus of the foundation under the top layer is changed.

The parameter space for a single layer is divided into three zones. In each zone the contact configuration is different. For low moduli layers there is only one contact region, the entire face of the indenter. Depending on the layer thickness, two contact regions are possible for stiffer layers. Here, for thickness layers the two contact region solution is valid, for thinner layers the three contact region solution exists. On the boundaries of these zones in the parameter space, where two solutions are valid simultaneously, the various pairs of solutions agree.

The contact regions under the indenter were completely determined for the two and three contact region solutions. The limits of zero layer thickness and infinite layer modulus agree with expectations. This leads to the conclusion that only one, two, or three contact region solutions are possible for this problem. As the thickness of a layer of fixed modulus decreases, the solution approaches that for a half space. However, this limit is approached in a nonuniform manner. Boundary layer phenomena exist near the corners of the indenter, where the solution for a thin layer always differs from the half space solution by a large amount, while away from the corners the difference is small. An asymptotic analysis of thin layer behavior of this problem may be of interest. As the modulus increases, for a layer of fixed thickness, the contact region shrinks until only the region very close to the corners is in contact with the layer surface. This limit agrees with the result predicted by plate theory.

Acknowledgment

The first author, T. W. Shield, would like to thank the National Science Foundation and the University of California at Berkeley for fellowship support during the course of this research. This work was also partially supported by the Center for Magnetic Recording Research at the University of California at San Diego through contract UCB ENG-5730 with the University of California at Berkeley.

7 References

Abramowitz, M., and Stegun, I. A., 1965, *Handbook of Mathematical Functions*, Dover, New York.

Brekhovshikh, L. M., 1980, *Waves in Layered Media*, Academic Press, New York.

Chen, W. T., and Engle, P. A., 1972, "Impact and Contact Stress Analysis in a Multilayer Media," *Internal Journal of Solids and Structures*, Vol. 8, pp. 1257–1281.

Erdogan, F., Gupta, G. D., 1972, "On the Numerical Solution of Singular Integral Equations," ASME Journal of Applied Mechanics, Vol. 29, pp. 525–534.

Erdogan, F., Gupta, G. D., and Cook, T. S., 1973, "Numerical Solutions of Singular Integral Equations," *Methods of Analysis and Solutions of Crack Problems*, Vol. 1 in the series Mechanics of Fracture, G. C. Sih, ed., Nordhoff International Publ., Leyden, pp. 368–425.

Gladwell, G. M. L., 1980, *Contact Problems in the Theory of Elasticity*, Sijthoff and Noordhoff, Maryland.

Mushelishvili, N. I., 1953, *Singular Integral Equations*, English translation by J. M. R. Radok, Noordhoff, Groningen.

Shield, T. W., 1988, "Multiple Contact Region Solutions for a Flat Indenter on a Layered Elastic Half Space," Ph.D., Thesis, University of California at Berkeley.

Shield, R. T., 1982, "Uniqueness of Elastic Crack and Punch Problems," ASME Journal of Applied Mechanics, Vol. 49, pp. 516–518.

APPENDIX

Listed here are the coefficients in the analytical solution for the Green's function for a single layer on a half space. The modulus ratio for the single layer is α, where

$$\alpha = \frac{\mu_s}{\mu_1}. \tag{A1}$$

$$\alpha_1 = 2(-4\alpha^2\nu^2 + 7\alpha^2\nu - 3\alpha^2 + 16\alpha\nu^2\nu_s - 12\alpha\nu^2 - 28\alpha\nu\nu_s + 22\alpha\nu + 12\alpha\nu_s - 10\alpha - 4\nu\nu_s + 3\nu + 4\nu_s - 3) \tag{A2}$$

$$\alpha_2 = 8(-\alpha^2\nu + \alpha^2 + 4\alpha\nu\nu_s - 2\alpha\nu - 4\alpha\nu_s + 2\alpha - 4\nu\nu_s + 3\nu + 4\nu_s - 3) \tag{A3}$$

$$\alpha_3 = 2(4\alpha^2\nu^2 - 7\alpha^2\nu + 3\alpha^2 - 4\alpha\nu^2 - 4\alpha\nu\nu_s + 10\alpha\nu + 4\alpha\nu_s - 6\alpha + 4\nu\nu_s - 3\nu - 4\nu_s + 3) \tag{A4}$$

$$\beta_1 = (4\alpha^2\nu - 3\alpha^2 - 16\alpha\nu\nu_s + 12\alpha\nu + 12\alpha\nu_s - 10\alpha + 4\nu_s - 3) \tag{A5}$$

$$\beta_2 = 4(-\alpha^2 + 4\alpha\nu_s - 2\alpha - 4\nu_s + 3) \tag{A6}$$

$$\beta_3 = 2(-8\alpha^2\nu^2 + 12\alpha^2\nu - 5\alpha^2 + 8\alpha\nu\nu_s - 4\alpha\nu - 4\alpha\nu_s + 2\alpha - 4\nu_s + 3) \tag{A7}$$

$$\beta_4 = (4\alpha^2\nu - 3\alpha^2 - 4\alpha\nu - 4\alpha\nu_s + 6\alpha + 4\nu_s - 3) \tag{A8}$$

On the Flexure of a Partially Embedded Bar Under Lateral Loads

Ronald Y. S. Pak
University of Colorado,
Boulder, Colo. 80309-0428
Assoc. Mem. ASME

This investigation is concerned with a laterally-loaded bar which is partially embedded in a three-dimensional elastic half space. The loading is assumed to be applied at the unembedded end of the bar and may, in general, be a combination of horizontal shear forces and moments. On the adoption of a one-dimensional theory for the bar and the classical theory of elasticity for the semi-infinite solid, the structure-medium interaction problem is reduced to a Fredholm integral equation of the second kind whose solution is then computed. Selected results are presented to illustrate various features of the solution. A set of compliance charts is also included.

1 Introduction

Analysis concerning the deformation of a partially embedded bar in an elastic half space under external loads is relevant to a number of engineering applications. In civil engineering, this class of problems is closely related to the mechanics of piles and anchors used in foundation designs. In the context of solid mechanics, this type of investigation is conducive to a better understanding of the behavior of fiber-reinforced composites, to which the load transfer characteristics between the matrix and the reinforcement is of importance. The underlying mechanical interaction between an embedded bar and its surrounding medium depends on the properties of both media and, in particular, on the mode of deformation as induced by the external forces. Of interest in this paper is the response of the system under the action of asymmetric loadings such as those incurred by lateral forces and moments.

Owing to various analytical difficulties, rigorous attempts to this class of three-dimensional load diffusion problems have been limited. On the axisymmetric problems of axial extension and torsion, the works by Luco (1976) and Luk and Keer (1979) are some of the noteworthy contributions. For simplicity, the embedded bars in these studies are assumed to be rigid. As a consequence, the influence of the deformability of the embedment on its mechanical interaction with the surrounding medium has not been addressed. The general need to account for the foregoing aspect in practical problems, however, is illustrated in the treatment of Muki and Sternberg (1969) on an axially-loaded infinite rod embedded in a medium of infinite extent. Of greater importance, though, is their subsequent contribution to the more difficult problem of axial load diffusion from a partially embedded rod in a semi-infinite medium (Muki and Sternberg, 1970). In that treatment they have shown that it is possible to obtain a consistent formulation for the structure-medium interaction problem on the occasion that the engineering approach of treating the rod as a one-dimensional elastic continuum is adopted. The present work is an effort in the same direction.

This paper is concerned with the analysis of the response of a partially embedded bar under lateral loadings. A mathematical formulation for the structure-medium interaction problem is presented in Section 2 which culminates in a derivation of the governing Fredholm integral equation. An important ingredient of the analysis is an influence field which describes the response of an elastic half space to the action of an internal, distributed, horizontal body-force field. By a method of strain potentials, the required result can be derived in closed form, the details of which is furnished in Section 3. In Section 4, illustrative numerical results based on the solution of the Fredholm integral equation are presented.

2 Mathematical Formulation

In this section a mathematical formulation is presented for the structure-medium interaction problem under consideration. To this end, a rectangular Cartesian coordination frame $\{0; x_1, x_2, x_3\}$ is used that spans the three-dimensional Euclidean space E. The position vector of points in E is denoted by $\mathbf{x}=(x_1, x_2, x_3)$ and the unit base vectors in the x_1-, x_2-, x_3-directions are designated by $\mathbf{e}_1$, $\mathbf{e}_2$, $\mathbf{e}_3$, respectively.

In this investigation, one considers a circular cylindrical bar B of length L and radius a, whose longitudinal centroidal axis is coincident with the x_3-axis (see Fig. 1). For reference, the open cross-sectional region of the bar is denoted by Π; the open half space is defined by $H=\{\mathbf{x}\,|\,\mathbf{x}\epsilon E,\ x_3>0\}$; the cylin-

Contributed by the Applied Mechanics Division of The American Society of Mechanical Engineers for presentation at the Joint ASCE/ASME Applied Mechanics, Biomechanics, and Fluids Engineering Conference, San Diego, CA, July 9 to 12, 1989.

Discussion of this paper should be addressed to the Editorial Department, ASME, United Engineering Center, 345 East 47th Street, New York, N.Y. 10017, and will be accepted until two months after final publication of the paper itself in the Journal of Applied Mechanics. Manuscript received by ASME Applied Mechanics Division, March 17, 1987; final revision, September 26, 1988.

Paper No. 89-APM-27.

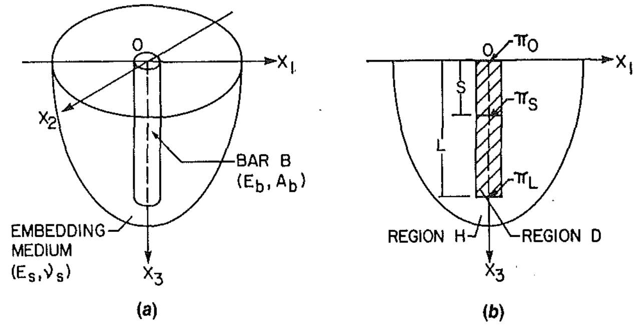

Fig. 1 Bar and medium configurations

drical subdomain of H occupied by the bar is designated by $D=\{\mathbf{x}\,|(x_1, x_2)\epsilon\Pi,\ 0<x_3<L\}$; and the open cross-section of D located at $x_3=z$ is labeled as $\Pi_z=\{\mathbf{x}\,|(x_1, x_2)\epsilon\Pi,\ x_3=z\}$. The loads under consideration are assumed to be applied at the top end of the bar and may, in general, be a combination of a lateral shear force V_0 and a moment M_0 acting in the x_1-x_3 plane. The present treatment aims at a bar whose diameter or lateral dimension is suitably small compared to the length of embedment. As in the treatment by Muki and Sternberg (1970), the embedding medium is extended throughout the half space $\bar{H}$, and an elastic body S with the same material properties as the original material is assumed to occupy this extended region. To account for the presence of the embedded bar, a fictitious reinforcement B_* is introduced throughout D such that the *composite solid* occupying the region is *equivalent* to the actual embedment. Since flexure is the mode of deformation under consideration, *equivalence* is taken to mean that the reinforced region will have the same flexural properties as B. Accordingly, for a solid bar the reinforcement B_* is assigned a Young's modulus of

$$E_*=E_b-E_s>0 \tag{1}$$

where the subscripts b and s denote the corresponding quantities of the bar and of the embedding medium, respectively, (see Fig. 2). In what follows, the extended medium is treated as a three-dimensional continuum within the framework of linear elastostatics. In contrast, the reinforcement B_* is regarded as a one-dimensional elastic structure. On the adoption of the Bernoulli-Euler bending beam theory for its behavior, B_* is governed by the constitutive relation

$$E_*I\frac{d^2u_*(z)}{dz^2}=M_*(z), \tag{2}$$

and the equilibrium equations

$$\frac{dM_*(z)}{dz}=V_*(z), \tag{3}$$

$$\frac{dV_*(z)}{dz}=-p_*(z), \tag{4}$$

where the notation and sign conventions are explained in Fig. 3. On the basis of the response of the reinforcement, the response of the embedded bar can be obtained, within the approximation under consideration, as the sum of those of B_* and D. Specifically, one may write

$$M(z)=M_*(z)-\int_{\Pi_z}\sigma_{33}(\mathbf{x})x_1\,dA \tag{5}$$

$$V(z)=V_*(z)-\int_{\Pi_z}\sigma_{31}(\mathbf{x})dA. \tag{6}$$

Here, $M(z)$ and $V(z)$ denote the bending moment and internal shear in the bar B, respectively; σ_{ij} are the components of the Cauchy stress tensor associated with the extended medium.

For a proper account of the interaction forces between the bar and the medium, it is important to first introduce the notion of direct load transfers which may occur at both ends of the embedment. Here, direct load transfer refers to the direct transmission of loads from the bar to its embedding medium through concentrated bond forces. The possibility of such mechanisms arising in load transfer problems is first suggested by Reissner (1940) and later clarified by Muki and Sternberg (1968). Providing for this possibility while treating the circumferential surface of the bar as frictionless, one may consider the external forces acting on B_* as composed of: (*i*) $-p_*(z)\mathbf{e}_1$, the distributed normal force per unit length exerted by S on B_*, (*ii*) $V_*(0^+)\mathbf{e}_1$, the resultant shear force at the top of the bar after a possible direct shear transfer, (*iii*) $-M_*(0^+)\mathbf{e}_2$, the resultant bending moment at the top end of the bar after a possible direct moment transfer, (*iv*) $-V_*(L)\mathbf{e}_1$, the terminal shear force at the bottom end of the bar, and (*v*) $M_*(L)\mathbf{e}_2$, the terminal moment at the bottom of the bar (see Fig. 4). In accordance to the foregoing account and the law of action and reaction, the forces acting on the half space are: (*i*) $p_*(z)\mathbf{e}_1$, (*ii*) $[V_0-V_*(0^+)]\mathbf{e}_1$, the direct shear transfer to the half space from the bar at Π_0, (*iii*) $-[M_0-M_*(0^+)]\mathbf{e}_2$, the direct moment transfer to the half space from the bar at Π_0, (*iv*) $V_*(L)\mathbf{e}_1$, the terminal shear transfer from B_*, and (*v*) $-M_*(L)\mathbf{e}_2$, the terminal moment transfer from B_*. If the additional assumption of small cross-sectional rotation of the bar is made, the analysis can be simplified further as the effects of the direct moment transfers at the ends become negligible. In such circumstances, it is thus reasonable to assume that

$$M_*(L)=0, \tag{7}$$

and

$$M(0)-M_*(0^+)=0. \tag{8}$$

For the description of the response of the extended medium to the foregoing interaction forces, it is convenient to employ an influence field $\hat{u}_i(\mathbf{x};s)$ which is defined as the displacement at a point $\mathbf{x}\epsilon S$ due to a suitably distributed body-force field on Π_s, acting in the x_1-direction, with a unit resultant (see Fig. 5). As the in-plane stiffness of the cross-section of the bar is usually substantially higher than that of the medium in most

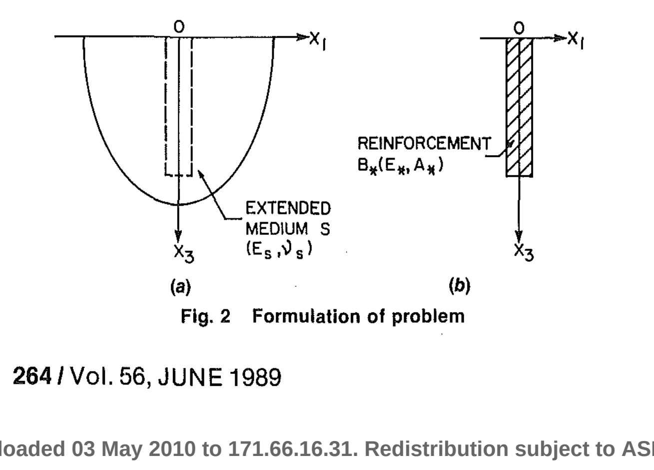

Fig. 2 Formulation of problem

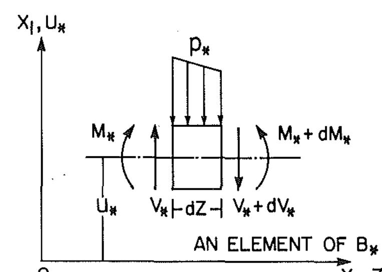

Fig. 3 Beam theory for B_*

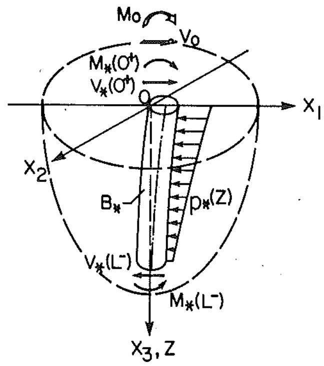

Fig. 4 Forces on B_* and sign conventions

applications, the body-force field distribution corresponding to a laterally-loaded rigid disc embedded in an elastic medium is adopted in this treatment. With the aid of the foregoing influence field, the displacement in the half space can be written as

$$u_i(\mathbf{x}) = [V_0 - V_*(0^+)]\hat{u}_i(\mathbf{x};0) + V_*(L)\hat{u}_i(\mathbf{x};L)$$

$$+ \int_0^L p_*(s)\hat{u}_i(\mathbf{x};s)ds, \quad \mathbf{x}\epsilon S. \tag{9}$$

In particular, along the centroidal axis of the bar where $\mathbf{x} = (0,0,x_3)$, the displacement in the x_1-direction is

$$u_1(x_3) = [V_0 - V_*(0^+)]\hat{u}_1(x_3;0) + V_*(L)\hat{u}_1(x_3;L)$$

$$+ \int_0^L p_*(s)\hat{u}_1(x_3;s)ds, \quad 0 \le x_3 \le \infty. \tag{10}$$

To render the deformation of B_* compatible with that of S, the imposition of a suitable bond condition is necessary. To this end, the requirement is adopted that the lateral displacement of the bar and the half space be equal along the x_3-axis over the length of embedment; i.e.,

$$u_*(x_3) = u_1(x_3), \quad 0 \le x_3 \le L. \tag{11}$$

In addition to its intuitive appeal, this condition leads to, as will be shown later, a governing equation which is amenable to simple treatments.

With the aid of (10), the bond condition (11) can be written as

$$u_*(z) = [V_0 - V_*(0^+)]\hat{u}_1(z;0) + V_*(L)\hat{u}_1(z;L)$$

$$+ \int_0^L p_*(s)\hat{u}_1(z;s)ds, \quad 0 \le z \le L. \tag{12}$$

Equation (12) represents the primary governing equation for the structure-medium interaction problem under consideration.

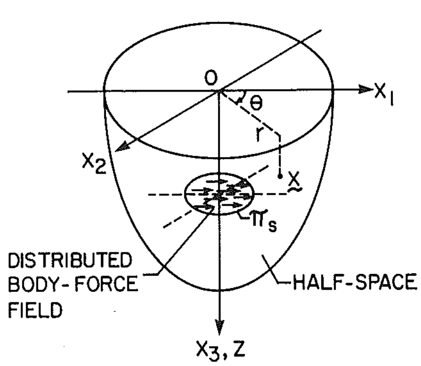

Fig. 5 Problem definition for influence field $\hat{u}_i(\bar{x};s)$

Reduction to a Fredholm Integral Equation. By virtue of (4), (12) can be written as

$$u_*(z) = [V_0 - V_*(0^+)]\hat{u}_1(z;0) + V_*(L)\hat{u}_1(z;L)$$

$$- \int_0^L \frac{dV_*(s)}{ds}\hat{u}_1(z;s)ds, \; 0 \le z \le L. \tag{13}$$

With proper account of the discontinuity of the integrand during an integration by parts, one can show that (13) yields, upon application of (7) and (8),

$$u_*(z) = V_0\hat{u}_1(z;0) - M_0\frac{\partial \hat{u}_1}{\partial s}(z;0) - M_*(z)\left[\frac{\partial \hat{u}_1}{\partial s}(z;s)\right]_{z^-}^{z^+}$$

$$- \int_0^L M_*(s)\frac{\partial^2 \hat{u}_1}{\partial s^2}(z;s)ds, \; 0 \le z \le L. \tag{14}$$

With the aid of (14) and the representation of u_* as

$$u_*(z) = -\int_0^L g(z;s)M_*(s)ds + u_*(0)\left(1 - \frac{z}{L}\right) + u_*(L)\left(\frac{z}{L}\right) \tag{15}$$

where

$$g(z;s) = \frac{1}{E_*I}\begin{Bmatrix} \left(1 - \frac{s}{L}\right)z, & z < s \\ \left(1 - \frac{z}{L}\right)s, & z > s \end{Bmatrix}, \tag{16}$$

the structure-medium interaction problem under consideration can be reduced to a single equation. For further considerations, however, it is appropriate at this point to formulate the analysis in dimensionless form. To this end, the following dimensionless parameters are defined:

$$\bar{z} = \frac{z}{a}; \; \bar{s} = \frac{s}{a}; \; \bar{L} = \frac{L}{a}; \; \bar{E} = \frac{E_b}{E_s}; \; \kappa = \frac{8}{(1+\nu_s)(\bar{E}-1)};$$

$$\bar{M}_0 = \frac{M_0}{4\pi\mu_s a^3}; \; \bar{M} = \frac{M_*}{4\pi\mu_s a^3}; \; \bar{u} = \frac{u_*}{a};$$

$$\bar{V}_0 = \frac{V_0}{4\pi\mu_s a^2}; \; \bar{V} = \frac{V_*}{4\pi\mu_s a^2}. \tag{17}$$

In the above, μ_s and ν_s are the shear modulus and the Poisson's ratio of the embedding medium, respectively. In terms of these parameters, the governing equation that fully describes the problem under consideration can be expressed as

$$A(\bar{z})\bar{M}(\bar{z}) + B(\bar{z})\bar{u}(0) + C(\bar{z})\bar{u}(\bar{L}) + \int_0^L K(\bar{z};\bar{s})\bar{M}(\bar{s})ds$$

$$= \bar{V}_0\hat{U}(\bar{z};0) - \bar{M}_0\frac{\partial \hat{U}}{\partial \bar{s}}(\bar{z};0), \; 0 \le \bar{z} \le \bar{L}, \tag{18}$$

where

$$A(\bar{z}) = \left[\frac{\partial \hat{U}}{\partial \bar{s}}(\bar{z},\bar{s})\right]_{\bar{z}^-}^{\bar{z}^+}, \quad B(\bar{z}) = \left(1 - \frac{\bar{z}}{\bar{L}}\right), \tag{19}$$

$$C(\bar{z}) = \frac{\bar{z}}{\bar{L}}, \quad G(\bar{z};\bar{s}) = \begin{Bmatrix} \left(1 - \frac{\bar{s}}{\bar{L}}\right)\bar{z}, & \bar{z} < \bar{s} \\ \left(1 - \frac{\bar{z}}{\bar{L}}\right)\bar{s}, & \bar{z} > \bar{s} \end{Bmatrix}, \tag{20}$$

$$\hat{U}(\bar{z};\bar{s}) = 4\pi\mu_s a\hat{u}_1(z;s), \tag{21}$$

$$K(\bar{z};\bar{s}) = \frac{\partial^2 \hat{U}}{\partial \bar{s}^2}(\bar{z};\bar{s}) - \kappa G(\bar{z};\bar{s}). \tag{22}$$

The integral equation in (18) is one of Fredholm's second kind, the solution of which furnishes the bending moment and the top and bottom displacements of B_*. In turn, they render the response of the whole system determinate by virtue of (2) to (9).

3 Influence Field

To determine the influence field $\hat{u}_i(z;s)$ required in the preceding formulation, it is convenient to employ a procedure based on the strain-potential approach proposed by Muki (1960) for asymmetric problems in the theory of elasticity. As a specific reduction of the general Boussinesq-Somigliano-Galerkin solution in the classical theory, the method entails representing the solutions to the displacement equations of equilibrium for an elastic medium with vanishing body forces in terms of a biharmonic function $\Phi(r,\theta,z)$ and a harmonic function $\Psi(r,\theta,z)$, i.e.,

$$\nabla^4\Phi(r,\theta,z) = 0, \quad \nabla^2\Psi(r,\theta,z) = 0, \tag{23}$$

where

$$\nabla^4 = \nabla^2\nabla^2, \quad \nabla^2 = \frac{\partial^2}{\partial r^2} + \frac{1}{r}\frac{\partial}{\partial r} + \frac{1}{r^2}\frac{\partial^2}{\partial\theta^2} + \frac{\partial^2}{\partial z^2} \tag{24}$$

in circular cylindrical coordinates. To obtain the solution of interest, proper account must be given to the traction-free boundary conditions at $z = 0$, the regularity conditions at infinity, and the stress discontinuities induced by the distributed body-force field acting on Π_s, i.e.,

$$\hat{\sigma}_{zz}(r,\theta,0) = \hat{\sigma}_{rz}(r,\theta,0) = \hat{\sigma}_{z\theta}(r,\theta,0) = 0, \ \forall r,\theta \tag{25}$$

$$\hat{\sigma} \to 0, \quad \sqrt{r^2+z^2} \to \infty; \tag{26}$$

$$\hat{\sigma}_{zr}(r,\theta,s^-) - \hat{\sigma}_{zr}(r,\theta,s^+) = \frac{1}{2\pi a\sqrt{a^2-r^2}}\cos\theta, \ (r,\theta)\in\Pi_s; \tag{27}$$

$$\hat{\sigma}_{z\theta}(r,\theta,s^-) - \hat{\sigma}_{z\theta}(r,\theta,s^+) = -\frac{1}{2\pi a\sqrt{a^2-r^2}}\sin\theta, \ (r,\theta)\in\Pi_s. \tag{28}$$

On the assumption that the stresses and displacements are continuous throughout the medium except for those specified in (27) and (28), it can be shown, with the aid of Hankel transforms and the foregoing method of potentials, that the requisite dimensionless influence function $\hat{U}$ admits the following integral representation:

$$\hat{U}(\bar{z};\bar{s}) = \int_0^\infty \left[A(\xi)e^{-\xi d_1} + B(\xi)e^{-\xi d_2}\right]\frac{\sin(\xi)}{\xi}d\xi \tag{29}$$

where

$$A(\xi) = \frac{1}{8(1-\nu_s)}\{(7-8\nu_s) - \xi d_1\}, \tag{30}$$

$$B(\xi) = \frac{\{(9-16\nu_s+8\nu_s^2) - (3-4\nu_s)\xi d_2 + 2\xi^2\bar{z}\bar{s}d_2\}}{8(1-\nu_s)}, \tag{31}$$

$$d_1 = |\bar{z}-\bar{s}|, \quad d_2 = (\bar{z}+\bar{s}). \tag{32}$$

Involved in (29) are integrals that can all be evaluated in terms of elementary functions. Accordingly, one finds

$$\hat{U}(\bar{z};\bar{s}) = \frac{1}{8(1-\nu_s)} \left\{ \begin{array}{l} (7-8\nu_s)\tan^{-1}\left(\dfrac{1}{d_1}\right) + (9-16\nu_s+8\nu_s^2)\tan^{-1}\left(\dfrac{1}{d_2}\right) \\ -\dfrac{d_1}{(1+d_1^2)} - (3-4\nu_s)\dfrac{d_2}{(1+d_2^2)} + \dfrac{4\bar{z}\bar{s}d_2}{(1+d_2^2)^2} \end{array} \right\}. \tag{33}$$

By virtue of (33), the derivatives of $\hat{U}(\bar{z};\bar{s})$ required in the formulation can also be computed in closed form. In addition to its mathematical appeal, this distinctive feature renders an accurate solution of the integral equation a straightforward process.

4 Illustrative Results and Discussion

In view of the simplicity of the governing Fredholm integral equation, it suffices to employ ordinary quadrature methods for the numerical solution of (18), provided proper attention is given to the localized nature of the functions involved (Pak and Jennings, 1987). As illustrations, solutions for the shear-loading-only and moment-loading-only conditions are presented in Figs. 6 and 7, respectively. As can be observed from the figures, all solutions exhibit smooth variations throughout their intervals of definition. The bending moment $\bar{M}$ of the bar under shear loading condition (see Fig. 6(*a*)) typically reaches its peak value within the top half of the bar although the precise location of its occurrence varies with the bar-to-medium modulus ratio $\bar{E}$. In contrast, the maximum moment is found to occur consistently at the top of the bar for the moment loading condition as is evident from Fig. 7(*a*). While it is probably more apparent in the moment loading case because of scaling, one common feature between the bending moment profiles under both shear and moment loadings is a definite reversal of sign at some depth for bars that are not too rigid. This is particularly interesting in view of the conspicuous absence of such a characteristic in some existing numerical treatments of the problem (e.g., Poulos and Davis, 1980). The slopes of the bar for the two loading conditions are shown in Figs. 6(*b*) and 7(*b*), while the corresponding deflection profiles are illustrated in Figs. 6(*c*) and 7(*c*), respectively. In accord with the reciprocal theorem in linear elastostatics, the top rotation due to a unit horizontal force is found to be identical to the top displacement due to a unit applied moment for the whole range of modulus ratios.

To ascertain the possible existence of direct load transfers at the ends of the embedded bar as alluded to earlier, it is relevant to examine the limiting values of $V(z)$, the internal shear of the bar, as z tends to 0^+ and L^-, respectively. On the basis of the results that

$$\int_{\Pi_0^+} \hat{\sigma}_{31}(\mathbf{x};0)dA = -1, \tag{34}$$

$$\hat{\sigma}_{31}(\mathbf{x};s) = 0, \quad \mathbf{x}\in\Pi_0, \quad s>0, \tag{35}$$

it can be shown directly from (6) that $V(0^+)$ is equal to V_0. Thus, in contrast to the findings of Muki and Sternberg for plane problems, there is no concentrated load transfer occurring at $z = 0$ according to the present treatment. On the other hand, a portion of the applied load is often transmitted directly to the embedding medium through the terminal section, as $V(L^-)$ is found to be nonvanishing in general.

In this connection, it is also of interest to examine the

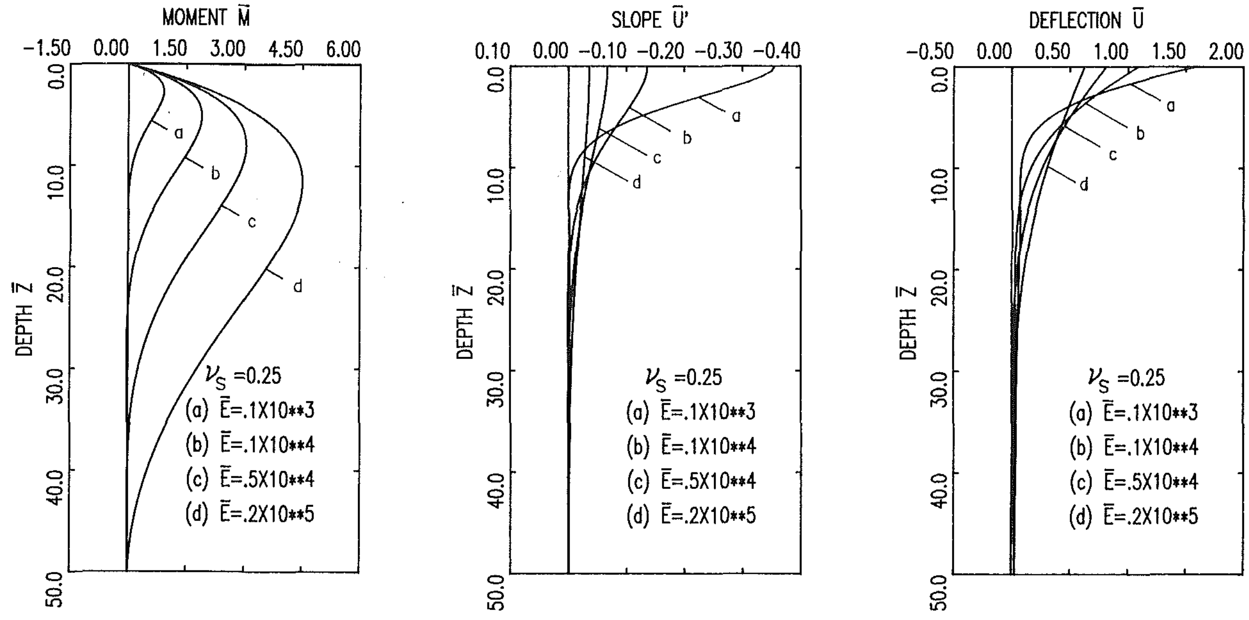

Fig. 6 Response under unit shear $\bar{V}_0(\bar{L}=50)$: (a) Bending moment profile, (b) Slope profile, (c) Displacement profile

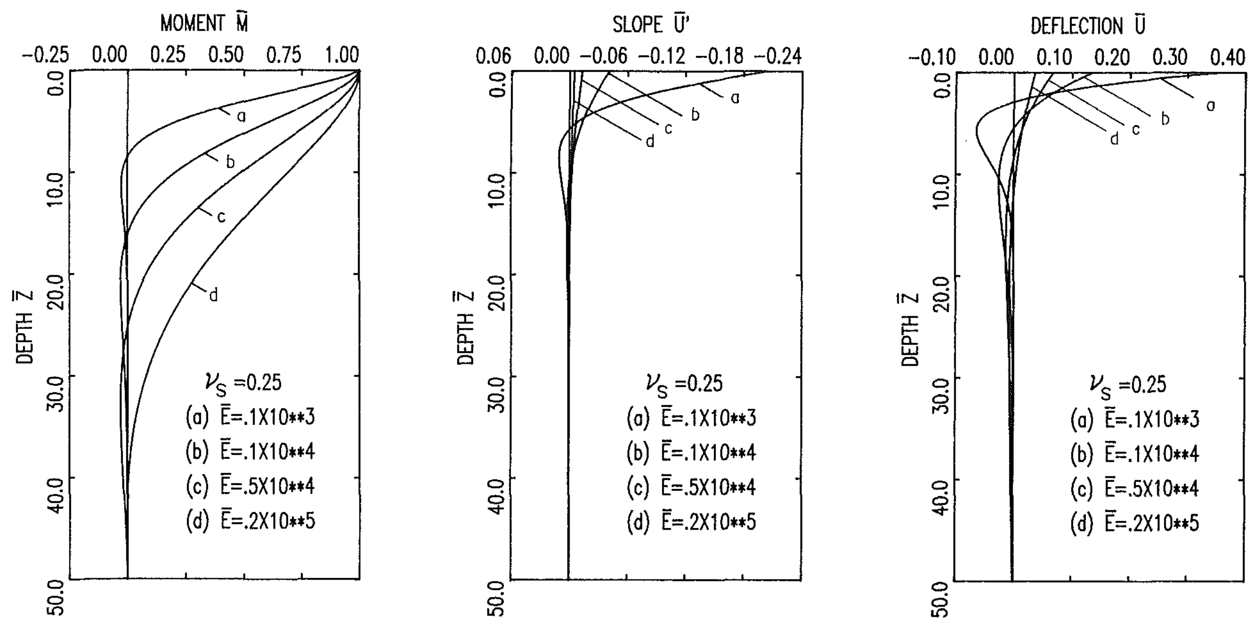

Fig. 7 Response under unit moment $\bar{M}_0(\bar{L}=50)$: (a) Bending moment profile, (b) Slope profile, (c) Displacement profile

behavior of B_* in a similar context because B_* is frequently regarded as the actual bar itself in numerous existing analyses. To facilitate the examination of the limit of $V_*(z)$ as $z-0^+$, it is useful to observe that (18) yields

$$\bar{V}(\bar{z}) = \frac{1}{A}\left\{\frac{(\bar{u}(\bar{L})-\bar{u}(0))}{\bar{L}} - \bar{V}_0\frac{\partial \hat{U}}{\partial \bar{z}}(\bar{z};0) + \bar{M}_0\frac{\partial^2 \hat{U}}{\partial \bar{z}\partial \bar{s}}(\bar{z};0) + \int_0^L \frac{\partial K}{\partial \bar{z}}(\bar{z};\bar{s})\bar{M}(\bar{s})d\bar{s}\right\} \tag{36}$$

where

$$\frac{\partial K}{\partial \bar{z}}(\bar{z};\bar{s}) = \frac{\partial^3 \hat{U}}{\partial \bar{z}\partial \bar{s}^2}(\bar{z};\bar{s}) - \kappa\frac{\partial G}{\partial \bar{z}}(\bar{z};\bar{s}), \tag{37}$$

$$\frac{\partial G}{\partial \bar{z}}(\bar{z};\bar{s}) = \left\{\begin{array}{ll} 1-\dfrac{\bar{s}}{\bar{L}}, & \bar{z}<\bar{s} \\ -\dfrac{\bar{s}}{\bar{L}}, & \bar{z}>\bar{s} \end{array}\right\}. \tag{38}$$

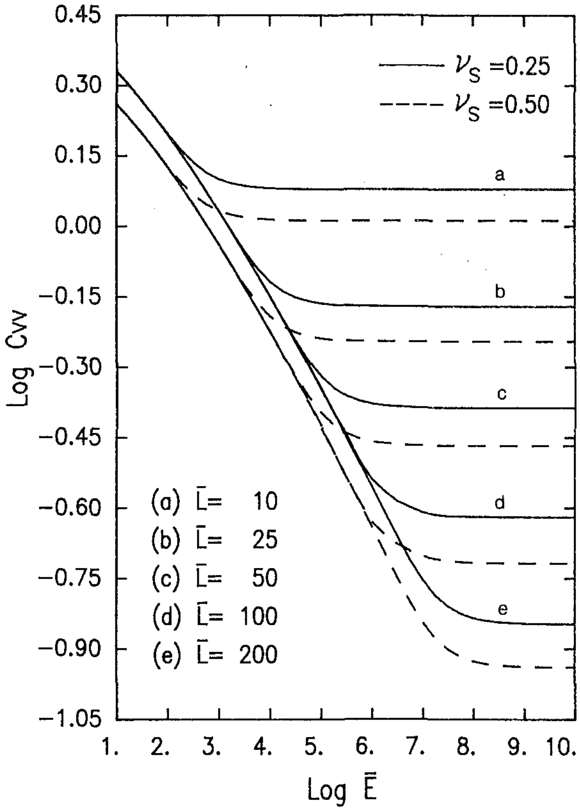

Fig. 8 Compliance function C_{vv}

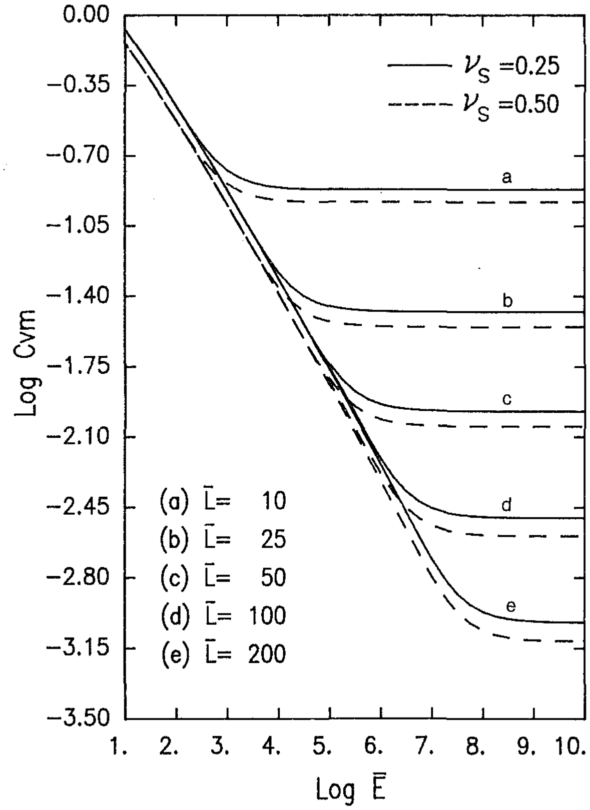

Fig. 9 Compliance function C_{vm}

On the basis of (36) and the solution of (18), it can be shown that $V_*(0)$ is in general not equal to V_0; moreover, their difference increases as $\bar{E}$ decreases. This is further supported by the direct deduction from (1), (2), (9), and (18) that the response of the reinforcement must vanish as $\bar{E}\to 1$ (i.e., the case where the moduli of elasticity of the bar and the surrounding solid are identical). On the latter occasion, the present formulation thus correctly indicates that the applied loads are to be transmitted directly to the embedding medium at the surface level. The implications of the general presence of such a direct load transfer at $z=0$ as a consequence of the simplistic assumption of B_* as B should warrant some attention.

In many engineering applications, the quantity of primary concern is the relationship between the top response of the bar and the applied loads. The desired correspondence can be expressed as

$$\begin{Bmatrix} \Delta \\ \Theta \end{Bmatrix} = \begin{bmatrix} C_{vv} & C_{vm} \\ C_{mv} & C_{mm} \end{bmatrix} \begin{Bmatrix} \bar{V}_0 \\ \bar{M}_0 \end{Bmatrix} \tag{39}$$

where

$$\Delta = \bar{u}(0), \quad \Theta = -\frac{d\bar{u}}{d\bar{z}}(0). \tag{40}$$

The compliance functions C_{vv}, C_{vm}, and C_{mm} are given for a range of physical parameters in Figs. 8 to 10 where the logarithm scales are to the base 10. The function C_{mv} is not presented because it is found to be identical to C_{vm} as alluded to earlier. To gain some perspective on the quality of the present result, it is useful to contrast it with some existing work on this structure-medium interaction problems, such as the one by Poulos (1971) and Poulos and Davis (1980). As is evident from Fig. 11 where the comparison is shown, there is a general departure of Poulos' result from the present solution except for a limited range of intermediate modulus ratios. The deviation is particularly serious at low values of $\bar{E}$ where the former analysis also fails to reveal the proper qualitative

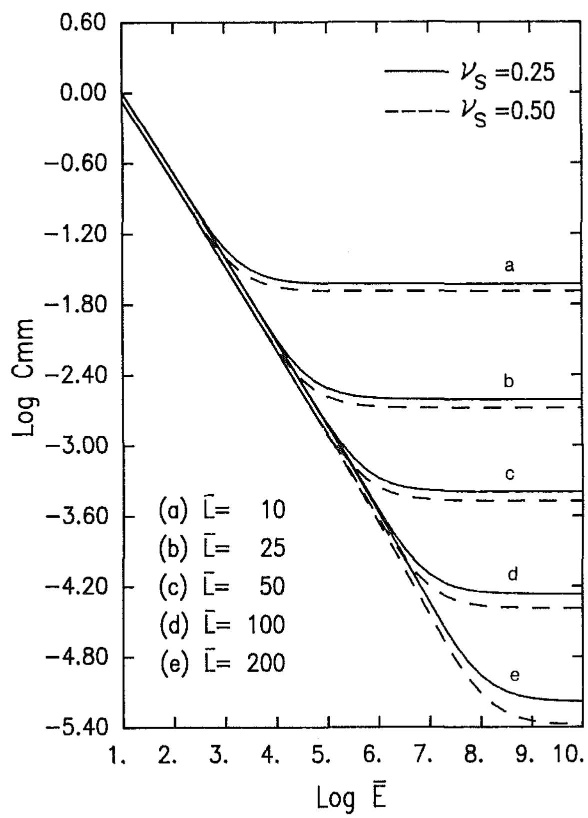

Fig. 10 Compliance function C_{mm}

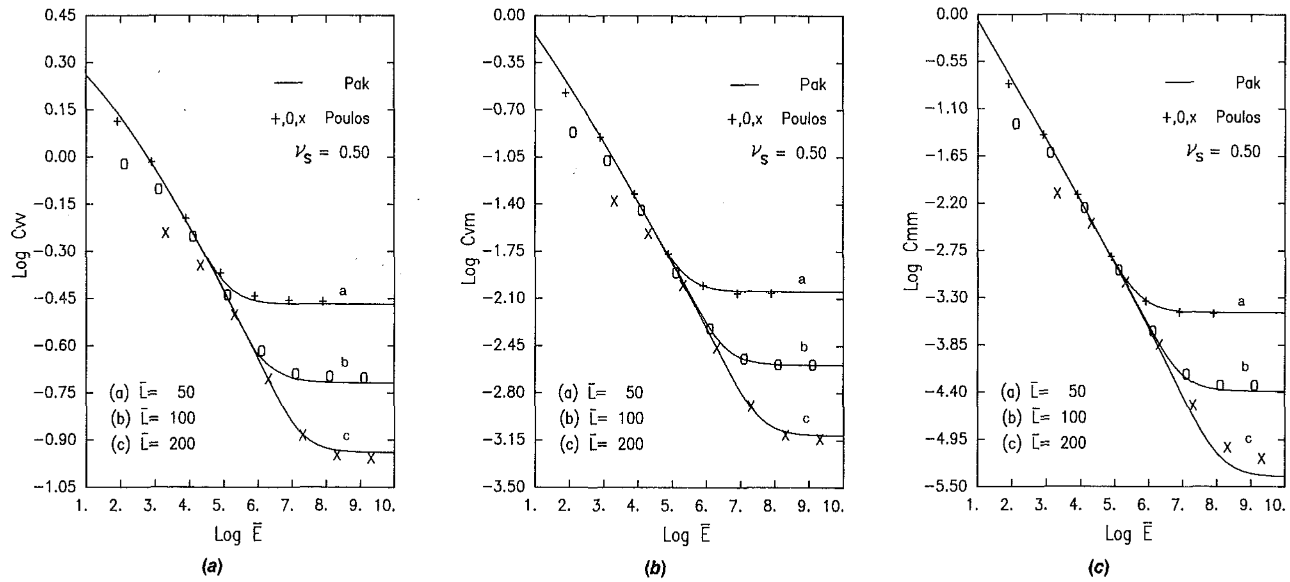

Fig. 11 Comparison with existing results

behavior expected of a rational solution. Here, reference is made to the divergence of Poulos' result for bars of different lengths as $\bar{E}\rightarrow 1$. To a lesser extent, a loss of accuracy in the solution under comparison is also observable as $\bar{E}\rightarrow\infty$. This can be due to the increasing significance in such an event of the terminal direct shear transfer at Π_L, which has not been properly accounted for in the aforementioned study.

5 Summary and Conclusions

A rigorous analysis is presented on the elastostatic response of a partially embedded bar under lateral loadings. By treating the bar as a one-dimensional continuum and the embedding half space as a three-dimensional elastic solid, the structure-medium interaction problem is formulated as a Fredholm integral equation of the second kind whose solution is then computed. In addition to furnishing a set of compliance functions which are directly useful in many applications, the present treatment is apt to be of value as a basis upon which approximate and numerical endeavors to this problem can be assessed.

Acknowledgment

The author is grateful to Prof. E. Sternberg for his constructive criticism on this work. The support provided by the National Science Foundation through Grant No. MSM-8611267 during the course of this investigation is gratefully acknowledged.

References

Luco, J. E., 1976, "Torsion of a Rigid Cylinder Embedded in an Elastic Half Space," ASME Journal of Applied Mechanics, Vol. 43, pp. 419–423.

Luk, V. K. and Keer, L. M., 1979, "Stress Analysis for an Elastic Half Space Containing an Axially-Loaded Rigid Cylindrical Rod," *International Journal of Solids and Structures*," Vol. 15, pp. 805–827.

Muki, R., 1960, "Asymmetric Problems of the Theory of Elasticity for a Semi-Infinite Solid and a Thick Plate," *Progress in Solid Mech.*, Vol. 1, North-Holland Publ. Co., Amsterdam.

Muki, R., and Sternberg, E., 1968, "On the Diffusion of Load from a Transverse Tension Bar into a Semi-Infinite Elastic Sheet," ASME Journal of Applied Mechanics, Vol. 35, pp. 737–746.

Muki, R., and Sternberg, E., 1969, "On the Diffusion of an Axial Load from an Infinite Cylindrical Bar Embedded in an Elastic Medium," *International Journal of Solids and Structures*, Vol. 5, pp. 587–605.

Muki, R., and Sternberg, E., 1970, "Elastostatic Load-Transfer to a Half-Space from a Partially Embedded Axially Loaded Rod," *International Journal of Solids and Structures*, Vol. 6, pp. 69–90.

Pak, R. Y. S., and Jennings, P. C., 1987, "Elastodynamic Response of Pile under Transverse Excitations," *Journal of Engineering Mechanics Division*, ASCE, Vol. 113, No. 7, pp. 1101–1116.

Poulos, H. G., 1971, "Behavior of Lateral Loaded Piles: I-Single Piles," *Journal of Soil Mechanics and Foundation Engineering*, ASCE, Vol. 97, SM5, pp. 711–731.

Poulos, H. G., and Davis, E. H., 1980, *Pile Foundation Analysis and Design*, John Wiley and Sons, New York, p. 188.

Reissner, E., 1940, "Note on the Problem of the Distribution of Stress in a Thin Stiffened Elastic Sheet," *Proceeding of the National Academy of Science*, Vol. 26, p. 300.

Kinking of a Crack Out of an Interface

Ming-Yuan He
Institute of Mechanics,
Chinese Academy of Sciences,
Beijing, China

John W. Hutchinson
Division of Applied Sciences,
Harvard University,
Cambridge, MA 02138
Fellow ASME

Kinking of a plane strain crack out of the interface between two dissimilar isotropic elastic solids is analyzed. The focus is on the initiation of kinking and thus the segment of the crack leaving the interface is imagined to be short compared to the segment in the interface. Accordingly, the analysis provides the stress intensity factors and energy release rate of the kinked crack in terms of the corresponding quantities for the interface crack prior to kinking. Roughly speaking, the energy release rate is enhanced if the crack heads into the more compliant material and is diminished if it kinks into the stiff material. The results suggest a tendency for a crack to be trapped in the interface irrespective of the loading when the compliant material is tough and the stiff material is at least as tough as the interface.

1 Introduction and Form of the Solution

A fracture mechanics of interfacial separation is beginning to emerge, although there are still conceptual difficulties to be overcome associated wtih the nonstandard oscillatory square root singularity of some interface cracks. In this paper an analysis of a crack kinking out of an interface is carried out with the aim of providing the crack mechanics needed to assess whether an interface crack will tend to propagate in the interface or whether it will advance by kinking out of the interface. The geometry analyzed is shown in Fig. 1. The parent interface crack lies on the interface between two semi-infinite blocks of isotropic elastic solids with differing elastic moduli. A straight crack segment of length a and angle ω (positive clockwise) kinks downward into material 2. The length a is assumed to be small compared to the length of the parent interface segment of the crack, and thus the asymptotic problem for the semi-infinite parent crack is analyzed. The stress field prior to kinking ($a \rightarrow 0$) is therefore the singularity field of an interface crack characterized by a complex intensity factor, $K = K_1 + iK_2$, to be specified precisely. The crack tip field at the end of the kinked crack is characterized by a combination of the standard mode I and mode II stress intensity factors, $K_{\rm I}$ and $K_{\rm II}$. The analysis provides the relationships among $K_{\rm I}$ and K_{II} for the kinked crack and K_1 and K_2 for the interface crack as dependent on the kink angle ω and the material moduli. The energy release rate of the kinked crack is also related to the energy release rate of the interface crack. Limiting results for the case when the moduli differences across the interface disappear are compared with previously published work on kinked cracks.

The remainder of this section is used to completely specify the functional form of the relationships sought. The numerical analysis is given in the next section and results and discussion are given in Sections 3 and 4. Section 2 containing the analysis may be skipped if one is primarily interested in the results.

Although there are three independent nondimensional material moduli parameters, Dundurs (1969) has shown that for problems of this class the solution depends on only two special parameters which in plane strain are

$$\alpha = [G_1(1-\nu_2) - G_2(1-\nu_1)]/[G_1(1-\nu_2) + G_2(1-\nu_1)] \quad (1)$$

$$\beta = \frac{1}{2}\,[G_1(1-2\nu_2) - G_2(1-2\nu_1)] \,/[G_1(1-\nu_2) + G_2(1-\nu_1)] \quad (2)$$

where G and ν are the shear modulus and Poisson's ratio and the subscript identifies the material as indicated in Fig. 1. Both α and β vanish when the dissimilarity between the elastic properties of the two materials vanishes and they change sign when the materials are interchanged.

The stress field for the semi-infinite interface crack ($a = 0$) has the form

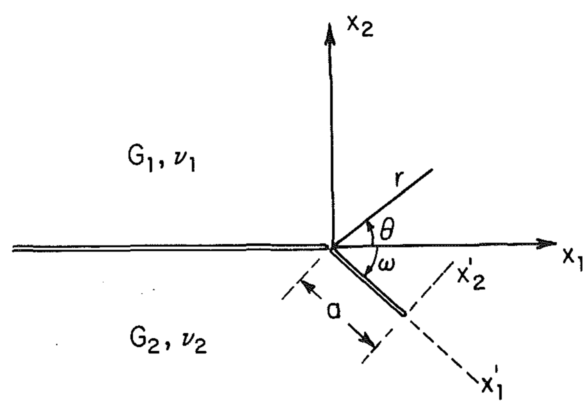

Fig. 1 Geometry of kinked crack

Contributed by the Applied Mechanics Division of THE AMERICAN SOCIETY OF MECHANICAL ENGINEERS for publication in the JOURNAL OF APPLIED MECHANICS.

Discussion on this paper should be addressed to the Editorial Department, ASME, United Engineering Center, 345 East 47th Street, New York, N.Y. 10017, and will be accepted until two months after final publication of the paper itself in the JOURNAL OF APPLIED MECHANICS. Manuscript received by ASME Applied Mechanics Division, March 7, 1988; final revision, September 1, 1988.

$$\sigma_{\alpha\beta} = Re\{K(2\pi r)^{-1/2} r^{i\epsilon}\tilde{\sigma}_{\alpha\beta}(\theta)\} \quad (3)$$

where $i = \sqrt{-1}$, r and θ are planar-polar coordinates centered at the origin, $K = K_1 + iK_2$ is the complex interface stress intensity factor, and

$$\epsilon = \frac{1}{2\pi} \ln\left(\frac{1-\beta}{1+\beta}\right). \quad (4)$$

The angular dependence $\tilde{\sigma}_{\alpha\beta}(\theta)$ is complex in general, but universal for a given material pair. On the interface ahead of the tip the tractions are

$$\sigma_{22} + i\sigma_{12} = K(2\pi r)^{-1/2} r^{i\epsilon}. \quad (5)$$

The notation and normalizations for the interface crack used here follow those introduced by Rice (1987) and Hutchinson, Mear, and Rice (1987) which, in turn, are based on the early papers on the subject by England (1965), Erdogan (1965), and Rice and Sih (1965). The interface intensity factors are defined so that $K_1 \rightarrow K_{\mathrm{I}}$ and $K_2 \rightarrow K_{\mathrm{II}}$ when the dissimilarity between the elasticity of the two materials vanishes. Note also that when $\beta = 0$ and thus $\epsilon = 0$, K_1 measures the normal component of the traction singularity acting on the interface while K_2 measures the shear component with the standard definitions for an intensity factor.

The complex interface factor $K = K_1 + iK_2$ is taken as the prescribed loading parameter in the present study. For a specific interface crack problem, K will necessarily have the dimensional form

$$K \equiv K_1 + iK_2 = (\text{applied stress}) \cdot L^{1/2} L^{-i\epsilon} F \quad (6)$$

which follows from its definition in equation (5), where L is a length quantity such as crack length or ligament length and F is a dimensionless function of the in-plane geometry and material moduli. Examples of specific solutions for K can be found in the aforementioned references.

The singular field at the tip of the kinked crack in material 2 is the classical field with conventional stress intensity factors K_{I} and K_{II} such that

$$\sigma_{2'2'} + i\sigma_{1'2'} = (K_{\mathrm{I}} + iK_{\mathrm{II}})(2\pi x_1')^{-1/2} \quad (7)$$

on the line ahead of the tip ($x_1' > 0$, $x_2' = 0$).

As already stated, the problem considered is the asymptotic one where a is small compared to all relevant in-plane length quantities (in particular, compared to L) so that the interface crack is taken as semi-infinite with stresses which remotely asymptote to (3). The relationship between the intensity factors of the kinked crack and the prescribed complex interface intensity K specifying the remote field can be written as

$$K_{\mathrm{I}} + iK_{\mathrm{II}} = c(\omega,\alpha,\beta) K a^{i\epsilon} + \bar{d}(\omega,\alpha,\beta)\bar{K} a^{-i\epsilon} \quad (8)$$

where ($\bar{\ }$) denotes complex conjugation and c and d are complex-valued functions of ω, α, and β.[1] The argument justifying (8) is as follows: The factors K_{I} and K_{II} have dimensions of stress • (length)$^{1/2}$ while K has the form (6). By dimensional considerations, a must combine with K as $Ka^{i\epsilon}$ or its conjugate, since in the asymptotic problem a is the only length quantity other than the length quantities implicit in K in (6). Equation (8) is a general representation of $K_{\mathrm{I}} + iK_{\mathrm{II}}$ consistent with this observation and with linearity. Use of $\bar{d}$ in (8) (rather than d) is purely for convenience. When $\epsilon = 0$, as when the material dissimilarity vanishes, or just when $\beta = 0$, the real and imaginary parts of (8) become

$$K_{\mathrm{I}} = (c_R + d_R)K_1 - (c_{\mathrm{I}} + d_{\mathrm{I}})K_2 \quad (9)$$

$$K_{\mathrm{II}} = (c_{\mathrm{I}} - d_{\mathrm{I}})K_1 + (c_R - d_R)K_2 \quad (10)$$

where $c = c_R + ic_{\mathrm{I}}$ and $d = d_R + id_{\mathrm{I}}$. This form is equivalent to

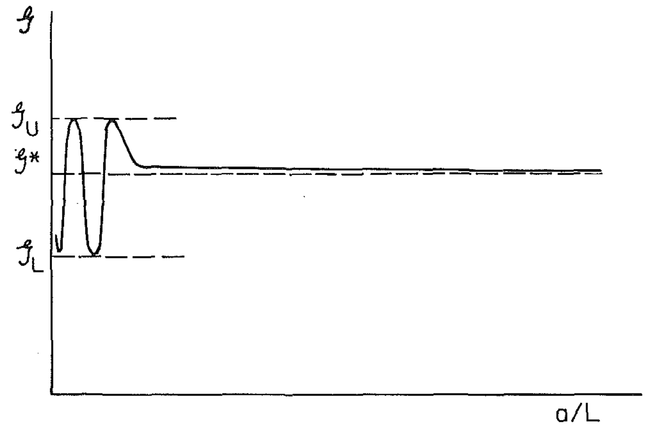

Fig. 2 Schemation variation of energy release rate with length of kinked segment of crack for $\beta \neq 0$

that employed by Bilby, Cardew, and Howard (1977) and Hayashi and Nemat-Nasser (1981) in reporting results for the homogeneous kinked crack problems which will be discussed in Section 2.

In plane strain, the energy release rate $\mathcal{G}_0$ of the interface crack advancing in the interface is related to K by (Malyshev and Salganik, 1965)

$$\mathcal{G}_0 = [(1-\nu_1)/G_1 + (1-\nu_2)/G_2] K\bar{K}/(4\cosh^2\pi\epsilon) \quad (11)$$

in the new normalization. The energy release rate $\mathcal{G}$ of the kinked crack ($a > 0$) is given by

$$\mathcal{G} = [(1-\nu_2)/(2G_2)](K_{\mathrm{I}}^2 + K_{\mathrm{II}}^2). \quad (12)$$

By (8),

$$\mathcal{G} = [(1-\nu_2)/(2G_2)]\{(|c|^2 + |d|^2)K\bar{K} + 2R_e(cdK^2a^{2i\epsilon})\}. \quad (13)$$

To reduce this expression further, write K as

$$K \equiv K_1 + iK_2 = |K| e^{i\gamma} L^{-i\epsilon} \quad (14)$$

where by (6), L is the in-plane length quantity characterizing the specific interface crack problem when $a = 0$. The real angular quantity γ will be used as the measure of the loading combination. Then by (11), (13), and (14),

$$\mathcal{G} = q^{-2}\mathcal{G}_0[|c|^2 + |d|^2 + 2R_e(cde^{2i\tilde{\gamma}})] \quad (15)$$

where

$$q = [(1-\beta^2)/(1+\alpha)]^{1/2} \quad (16)$$

and

$$\tilde{\gamma} = \gamma + \epsilon \ln(a/L). \quad (17)$$

When $\epsilon = 0$, the stress intensity factors, K_{I} and K_{II}, and $\mathcal{G}$ are *independent* of a. This is the case for similar moduli across the interface ($\alpha = \beta = 0$). By (4), ϵ is also zero whenever $\beta = 0$ regardless of the value of α. The oscillatory behavior of the interface crack fields and the a-dependence of $\mathcal{G}$ only appear when $\beta \neq 0$. A sensible approach to gaining insight into interfacial fracture behavior, while avoiding complications associated with the oscillatory singularity, would be to focus on material combinations with $\beta = 0$. Indeed, Hutchinson et al. (1987) tabulated strain values on α and β for six representative material combinations and found that β was quite small for most of the combinations. For example, $Mg0$ has a shear modulus more than four times that of A_u, yet this combination has $\alpha = .51$, $\beta = .011$, and $\epsilon = -.004$. In this paper, special attention is directed to material combinations with $\beta = 0$, but the role of β will also be examined.

When $\beta \neq 0$ and, therefore, $\epsilon \neq 0$, the interface crack with $a = 0$ suffers contact between the crack faces within some distance (usually exceedingly small) from the tip, as discussed recently by Rice (1987) and Anderson (1987), and as analyzed by Comninou (1977). Contact between crack faces is less likely

[1]In this paper the focus is on plane strain behavior. However, the results presented for the stress intensities are valid for plane stress as well when α and β are evaluated using plane stress formulas.

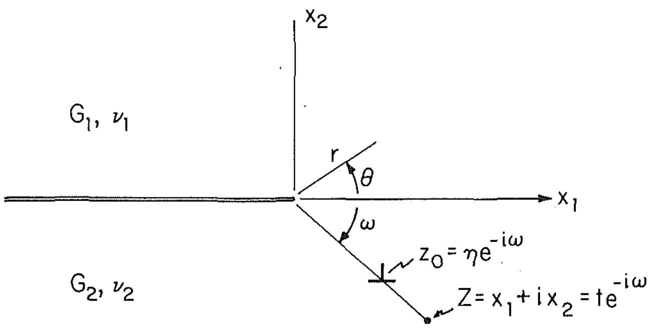

Fig. 3 Geometry and conventions for construction of integral equation

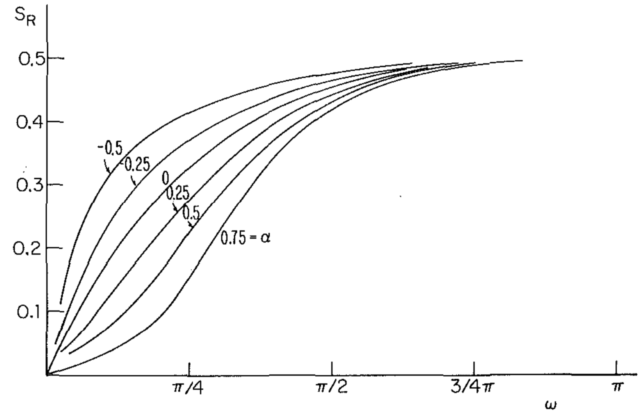

Fig. 4 Dependence of strength of singularity at kink, s, as a function of kink angle ω for various $\alpha(\beta = 0)$

for the kinked crack ($a>0$, $\omega>0$) loaded such that K_I and K_{II} are positive, since this will open up the crack at the kink. Nevertheless, contact will inevitably occur if $\epsilon \neq 0$ when a is sufficiently small compared to L.

The dependence of $\mathcal{G}$ on a for a given kink angle is sketched qualitatively in Fig. 2 as predicted by (15) when $\epsilon \neq 0$. When a/L becomes sufficiently small, $\mathcal{G}$ oscillates between a maximum $\mathcal{G}_U$ and a minimum $\mathcal{G}_L$, which are readily found to be

$$\mathcal{G}_U = q^{-2}\mathcal{G}_0[|c| + |d|]^2 \quad (18)$$

$$\mathcal{G}_L = q^{-2}\mathcal{G}_0[|c| - |d|]^2 \quad (19)$$

and which depend on K_1 and K_2 only through $\mathcal{G}_0$. For values of a/L outside the oscillatory range $\mathcal{G}$ approaches $\mathcal{G}^*$, given by (15), with $\tilde{\gamma} = \gamma$, i.e.,

$$\mathcal{G}^* = q^{-2}\mathcal{G}_0[|c|^2 + |d|^2 + 2R_e(cde^{2i\gamma})]. \quad (20)$$

Note that $\mathcal{G}^*$ coincides with $\mathcal{G}$ when $\epsilon = 0$. Contact between the crack faces will invalidate the prediction for $\mathcal{G}$ from (15) when a/L is in the range where oscillatory behavior occurs.

In presenting results for the energy release rate when $\epsilon \neq 0$, we will feature $\mathcal{G}^*$. From a physical standpoint, $\mathcal{G}^*$ should be relevant if there exist crack-like flaws emanating from the interface whose lengths are greater than the zone of contact. That is, $\mathcal{G}^*$ should be relevant for testing for kinking if the fracture process zone on the interface is large compared to the contact zone of the idealized elasticity solution. If it is not, then more attention must be paid to the a-dependence of $\mathcal{G}$ and to consideration of contact. In any case, $\mathcal{G}^*$ should play a prominent role in *necessary conditions* for a crack kinking out of an interface, because once nucleated, the kinked crack has an energy release rate which rapidly approaches $\mathcal{G}^*$ as it lengthens.

The final observation about the form of the solution concerns the behavior expected as $\omega \to 0$. When ω becomes small, the kinked segment parallels the interface and the solution approaches the solution obtained by Hutchinson et al. (1987) for a semi-infinite crack paralleling an interface a distance h below the interface. That solution has the property that $\mathcal{G} = \mathcal{G}_0$ and is given by

$$K_I + iK_{II} = qe^{i\phi}h^{i\epsilon}K \quad (21)$$

where ϕ is a real function of α and β which is tabulated by Hutchinson et al. (1987) and which is given approximately by $\phi = .158\alpha + .063\beta$ when α and β are small. In the present problem for small ω, h can be identified with $a \sin\omega \cong a\omega$ and (21) becomes

$$K_I + iK_{II} \cong qe^{i(\phi + \epsilon\ln\omega)}a^{i\epsilon}. \quad (22)$$

Thus, by comparing (8) and (22), one sees that for small ω

$$c \to qe^{i(\phi + \epsilon\ln\omega)}, \quad d \to 0, \quad \mathcal{G} \to \mathcal{G}_0. \quad (23)$$

2 Integral Equation and Solution Methods

The integral equation governing the solution to the kinked crack problem is constructed using a basic solution for an edge dislocation in material 2 interacting with a semi-infinite traction-free crack extending along the interface to the origin, as shown in Fig. 3. The dislocation is located at z_0 and its branch line extends parallel to the crack to $x_1 \to -\infty$. Its radial and circumferential components of the Burgers vector along $\theta = -\omega$ are b_r and b_θ. The traction at z on $\theta = -\omega$ can be written as

$$\sigma_{\theta\theta}(t) + i\sigma_{r\theta}(t) = 2\bar{B}e^{-i\omega}(t-\eta)^{-1} + BH_1(t,\eta) + \bar{B}H_2(t,\eta) \quad (24)$$

where

$$B = [G_2/(1-\nu_2)](b_r + ib_\theta)e^{-i\omega}/(4\pi i). \quad (25)$$

The functions H_1 and H_2 are specified in the Appendix. They are analytic at $t = \eta$, increase in proportion to $t^{-1/2}$ as $t \to 0$, and decrease in proportion to $\eta^{1/2}$ as $\eta \to 0$.

Denote the traction at z along $\theta = -\omega$ due to the interface crack tip field (3) by $\sigma^0_{\theta\theta}(t) + i\sigma^0_{r\theta}(t)$. This traction, which is also given in the Appendix, can be written as

$$\sigma^0_{\theta\theta}(t) + i\sigma^0_{r\theta}(t) = (Kh_1(t) + \bar{K}h_2(t))t^{-1/2}. \quad (26)$$

The functions h_1 and h_2 depend on ω and ϵ as well as t. When $\epsilon = 0$, h_1 and h_2 are independent of t.

The segment of the crack corresponding to $0 \le t \le a$ is represented by a distribution of dislocations $B(\eta)$ chosen such that the net tractions resulting from (24) and (26) are zero on this line segment. Since the a-dependence of the solution is already known from (8), a is taken to be unity. The integral equation is then

$$2e^{-i\omega}\int_0^1 \bar{B}(\eta)(t-\eta)^{-1}d\eta + \int_0^1 B(\eta)H_1(t,\eta)d\eta + \int_0^1 \bar{B}(\eta)H_2(t,\eta)d\eta = -(\sigma^0_{\theta\theta}(t) + i\sigma^0_{r\theta}(t)). \quad (27)$$

Similar formulations for other problems have been given by Bilby and Eshelby (1968), Rice (1968), and Hayashi and Nemat-Nasser (1968a,b).

Singularity at $t=1$. The dislocation density representing the kinked segment is proportional to $(1-t)^{-1/2}$ as $t \to 1$ and the stress intensity factors are given by

$$K_I + iK_{II} = (2\pi)^{3/2}e^{-i\omega}\lim_{t\to 1}\{(1-t)^{1/2}\bar{B}(t)\} \quad (28)$$

Singularity at $t=0$. A weaker singularity exists at the kink. The most singular stresses in the vicinity of the origin have the form $\sigma_{\alpha\beta} \sim r^{-s}\tilde{\sigma}_{ij}(\theta)$ where, in general, s is a complex number depending on ω, α, and β. Hein and Erdogan (1971) have derived the equation for s for the relevant bimaterial, wedge-shaped region. When $\beta = 0$, the imaginary part of s, s_I, is zero; the real part, s_R, is shown as a function of ω for several values

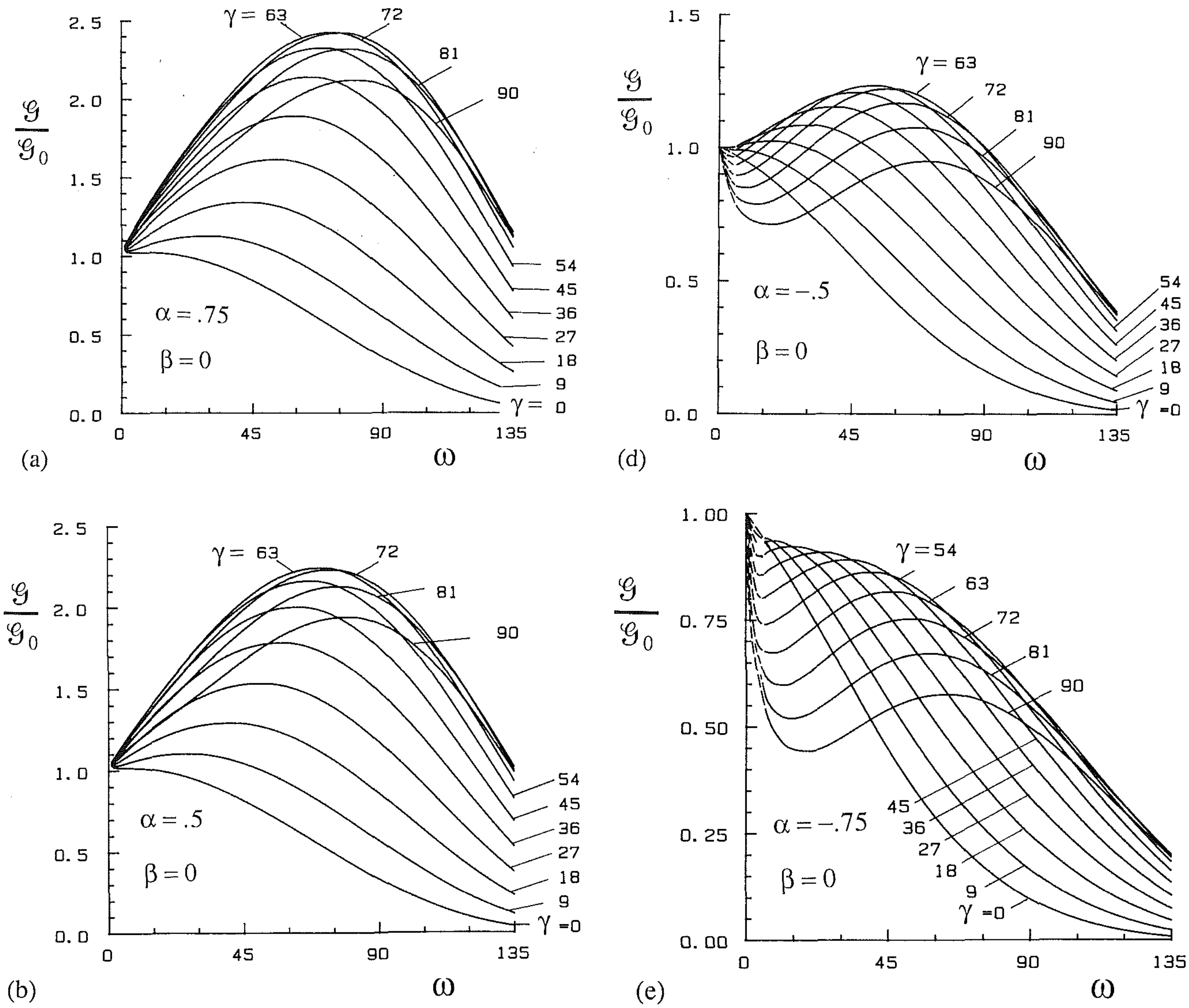

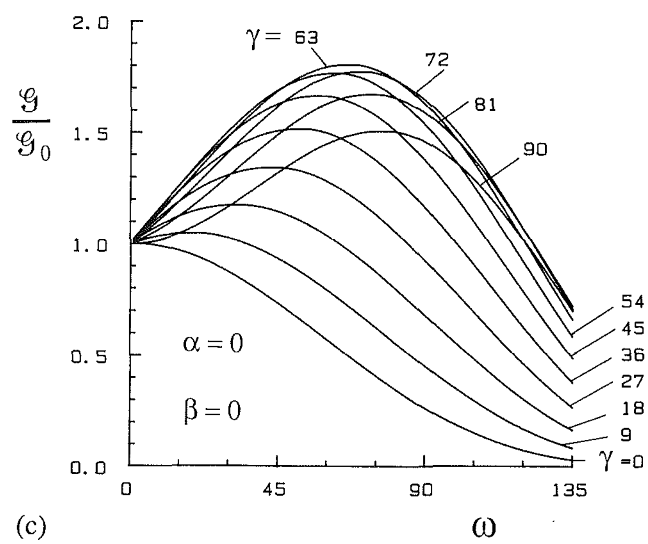

Fig. 5 Variation of $\mathcal{G}/\mathcal{G}_0$ with kink angle for loading combinations specified by $\gamma = \tan^{-1}(K_2/K_1)$ for various values of α, all with $\beta = 0$. The homogeneous case ($\alpha = \beta = 0$) is in (c).

of α in Fig. 4. When $\beta \neq 0$, s_1 is still zero over most of the range of ω except for ω greater than about $3\pi/4$ in most cases; the real part depends on ω in much the same way as displayed in Fig. 4. Thus, for essentially all cases of interest here, s is real and smaller than 1/2.

Solution Method #1. This method builds in the correct singularity of the dislocation distribution at each end of the interval with

$$B(\eta) = \eta^{-s}(1-\eta)^{-1/2}P(\eta) \tag{29}$$

where $P(\eta)$ is bounded on $0 \leq \eta \leq 1$. For an approximation with N unknown complex coefficients, C_j, P was represented by a polynomial of degree $N-1$ as

$$P(\eta) = \sum_{j=1}^{N} C_j \eta^{j-1}. \tag{30}$$

By substituting (29) and (30) in the integral equation (27) one obtains the equation

$$\sum_{j=1}^{N} \{C_j E_j(t) + \bar{C}_j F_j(t)\} = -(\sigma_{\theta\theta}^0(t) + i\sigma_{r\theta}^0(t)) \tag{31}$$

where the integral expressions for E_j and F_j are readily identified. To determine the N complex coefficients, (31) is satisfied at N points on the interval $0 < t < 1$; the set of Gauss-Legendre points were used once the interval had been mapped to $|t| \leq 1$. Some of the integrals making up the E_j and F_j must be evaluated numerically at each of the points t. Unusual care

Table 1 ($\omega = 45$ deg)

	Method #1		Method #2	
	$\alpha=0$		$\beta=0$	
N	$P_R(1)$	$P_m(1)$	$P_R(1)$	$P_m(1)$
4	0.05036	0.02135	0.04820	0.02046
8	0.05016	0.02113	0.04981	0.02112
10			0.04988	0.02112
12	0.05009	0.02106	0.04992	0.02111
16	0.05004	0.02104	0.04996	0.02109
20			0.04998	0.02107
40			0.05001	0.02103
	$\alpha=0.56$		$\beta=0.12$	
N	$P_R(1)$	$P_m(1)$	$P_R(1)$	$P_m(1)$
4	0.04268	0.01934	0.04279	0.01838
8	0.04207	0.01889	0.04216	0.01878
12	0.04204	0.01888	0.04208	0.01883
20			0.04204	0.01885
40			0.04202	0.01886
100			0.04201	0.01887

must be taken that these numerical integrations are performed accurately. It is this part of the computation which consumes the bulk of the computational effort. The polynomial representation (30) is equivalent to an expansion in any set of polynomials of degree $N-1$. The particular set (30) has certain advantages in reducing the computational effort involved in the numerical integrations.

Solution Method #2. This method is that used by Lo (1978) and Hayashi and Nemat-Nasser (1981a) which, in turn, follows the procedures developed by Erdogan and Gupta (1972). In our application of this method, s is taken to be 1/2 in (29) and the condition $P(0) = 0$ is imposed. The recipes developed by Erdogan and Gupta and used by Lo can then be taken over directly even though the singularity at $t=0$ is not strictly correct. At the Nth level of approximation, this method generates a system of algebraic equations for values of $P(\eta)$ at N Gauss-Chebychev points. The advantage of this method is that it requires far less numerical computation than Method #1 at the corresponding Nth level of approximation.

Table 1 compares results from the two methods for two examples at various levels of approximation. By (28) and (29), the stress intensity factors are given by

$$K_{\rm I} + iK_{\rm II} = (2\pi)^{3/2} e^{-i\omega} \overline{P(1)} \tag{32}$$

and Table 1 presents the real and imaginary parts of $P(1)$. The convergence of Method #1 is clearly faster than that of #2. Nevertheless, at corresponding levels of accuracy, Method #2 is still far more efficient than #1. The results presented in the following section were computed using Method #2 with $N=40$. A number of test calculations indicated that the difference in the values of $P(1)$ computed with $N=40$ and $N=100$ was less than .1 percent except at small values of ω, as will be discussed later.

3 Numerical Results

Homogeneous Limit ($\alpha=\beta=0$). The limiting case for crack kinking in a homogeneous material has been studied thoroughly in the literature, although considerable confusion has surrounded the problem because a number of early solutions were in error. Perhaps the most recent paper on the subject is that by Hayashi and Nemat-Nasser (1981a) which provides access to the literature. The results of Bilby, Cardew, and Howard (1977) derived using the method of Khrapkov (1971) and the results of Lo (1978) and Hayashi and Nemat-Nasser (1981a) are generally accepted to be correct, and our numerical results for this limit reproduced their results within the accuracy which could be inferred from their graphs and tables. All information can be derived from $c(\omega)$ and $d(\omega)$ in (8)–(10), and these coefficients are available in tabulated form in a limited-circulation companion report (He and Hutchinson, 1988). Our results agree within 1 percent with the equivalent set of tabulated coefficients included in the paper by Hayashi and Nemat-Nasser (1981a).

Plots of $\mathcal{G}/\mathcal{G}_0$ versus ω derived using (15) with the values of c and d are shown in Fig. 5(c) for a number of loading combinations as measured by $\gamma = \tan^{-1}(K_2/K_1)$. Since the crack has been taken to kink downward, the loading combinations which result in $K_{\rm I}>0$ (i.e., an opening at the tip) *and* an opening at the kink will generally require $K_1>0$ and $\gamma \geq 0$. Results for the maximum energy release rate and its associated direction, together with the direction in which $K_{\rm II} = 0$, will be presented later.

The approximation of Cotterell (1965), Vitek (1977), and Lawn and Wilshaw (1975) gives in the present notation

$$c = \frac{1}{2}\,(e^{-i\omega/2} + e^{-i3\omega/2}), \quad d = \frac{1}{4}\,(e^{-i\omega/2} - e^{i3\omega/2}). \tag{33}$$

Cotterell and Rice (1980) have shown that this approximation is asymptotically correct for small ω and is reasonably accurate for predicting $K_{\rm I}$ and $K_{\rm II}$ for ω as large as 45 deg or even 90 deg, depending on γ.

Bimaterial Problem With $\beta=0$. As discussed in Section 1, cases with $\beta=0$ and $\alpha \neq 0$ afford insight into interface problems without the added complication of oscillations, or contact, associated with nonzero ϵ. Roughly speaking, $\alpha>0$ implies that material 1 is stiffer than material 2, and conversely. In the present paper the crack is always taken to kink downward into material 2 so that the relevant range of loading is restricted to $K_1>0$ and $\gamma>0$ as mentioned earlier.

Values of $c(\omega)$ and $d(\omega)$ have been tabulated for various values of α and are available in He and Hutchinson (1988). Plots of $\mathcal{G}/\mathcal{G}_0$ versus ω for various γ are shown in Fig. 5 for $\alpha = .75, .5, 0, -.5$, and $-.75$. As noted in (23), $\mathcal{G} \rightarrow \mathcal{G}_0$ as $\omega \rightarrow 0$, and the numerical results for c and d were indeed in agreement with (23) for small ω. As long as α is positive the numerical method is accurate for ω as small as 1 deg. For negative values of α the numerical method became increasingly inaccurate as ω was decreased and results for ω less than about 5 deg could not be obtained accurately for the cases $\alpha = -.5$ and $-.75$. Thus, for $\omega<5$ deg the curves in Fig. 5(d, e) have been interpolated to the limit $\mathcal{G}=\mathcal{G}_0$ for $\omega=0$, and these sections of the curves have been dashed.

The qualitative features which emerge from the directional dependence of the energy release rate in Fig. 5 are the following: The more compliant is the material into which the crack kinks (i.e., the larger is α), the larger is the energy release rate, all other factors being equal. Conversely, if the lower material into which the crack kinks is relatively stiffer ($\alpha<0$), then the energy release rate is reduced. These features are consistent with the role of moduli differences across an interface when a crack approaches the interface from within one of the two materials. When the differences are relatively large, the energy release rate for a crack kinking into the stiff material can be less than the interface release rate $\mathcal{G}_0$ for all combinations of loading, as can be seen in Fig. 5(e) for $\alpha = -.75$. This suggests that under conditions when the compliant material is tough and the stiff material and the interface are each relatively brittle with comparable toughnesses (as measured by a critical value of energy release rate), the crack will tend to be trapped in the interface for all loading combinations. If the stiff material is even less tough than the interface, the crack may leave the interface but not necessarily by kinking. For example, when $\alpha = -.75$ in Fig. 5(e), the largest energy release rates occur when ω is small approaching zero, suggesting that the crack may smoothly curve out of the interface. Such a path, however, would not necessarily satisfy $K_{\rm II} \cong 0$. Some further discussion of these issues is given in the last section.

The direction $\hat{\omega}$ corresponding to the maximum energy release rate (i.e., where $d\mathcal{G}/d\omega = 0$ or at $\omega=0$, whichever gives the larger $\mathcal{G}$) is displayed as a function of the loading angle γ for various α in Fig. 6. For positive α, when the crack enters the more compliant material, $\hat{\omega}$ increases smoothly as γ increases from 0 deg to 90 deg. Note that even when $K_2 = 0$ (i.e., $\gamma = 0$), the direction of maximum energy release rate is a finite angle into material 2 when $\alpha>0$. For negative α there is a range of γ in the vicinity of $\gamma = 0$ for which the maximum occurs at $\omega=0$. In addition, for sufficiently negative α the maximum of $\mathcal{G}$ also occurs at $\omega=0$ when γ is in the vicinity of 90 deg, as can be seen in Fig. 5. For α, more negative than $-.67$, the maximum occurs at $\omega=0$ for all γ.

The direction $\tilde{\omega}$ corresponding to $K_{II} = 0$ is sometimes suggested as an alternative to $\hat{\omega}$ as the kink direction. A comparison between $\tilde{\omega}$ and $\hat{\omega}$ is shown in Fig. 7 for $\alpha=0$ and $\pm.5$. In the homogeneous case when $\alpha=0$, the difference between $\tilde{\omega}$ and $\hat{\omega}$ is less than 1 deg for nearly all γ except near $\gamma = \pi/2$ where it becomes about 2 deg. (Apparently, a numerical comparison between these two directions has not previously been reported for the homogeneous case.) The difference between the two directions is also very minor for $\alpha = \pm.5$. It would be virtually impossible to distinguish between these directions using experimental observation of kinked cracks. For more negative values of α than $-.5$, the range of γ in which $\mathcal{G}_{max}$ occurs at $\hat{\omega} = 0$ becomes significant, while $K_{II} = 0$ at values of ω near the local maximum of $\mathcal{G}$ (see Fig. 5(*e*)) which occurs for ω between about 45 deg and 60 deg depending on γ. In this range of γ, $\tilde{\omega}$ and $\hat{\omega}$ are significantly different.

Bimaterial Problem With $\beta\neq0$. Values of $c(\omega)$ and $d(\omega)$ have also been tabulated in He and Hutchinson (1988) for various pairs of α and β. The calculated values are in accord with the limits for small ω indicated in (23) although for values ω less than some value between 1 deg and 5 deg, depending on α and β, the computational procedure begins to become inaccurate.

As discussed in connection with (15), $\mathcal{G}$ is not independent of a when $\epsilon\neq0$, but $\mathcal{G}$ approaches $\mathcal{G}^*$ for all but very small a.

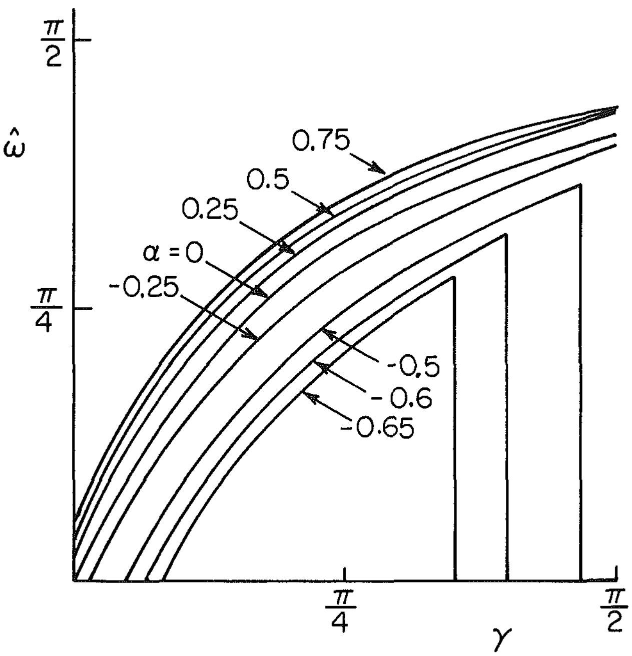

Fig. 6 Kinking angle $\hat{\omega}$ corresponding to maximum energy release rate as a function of the loading combination $\gamma = \tan^{-1}(K_2/K_1)$, in each case for $\beta = 0$

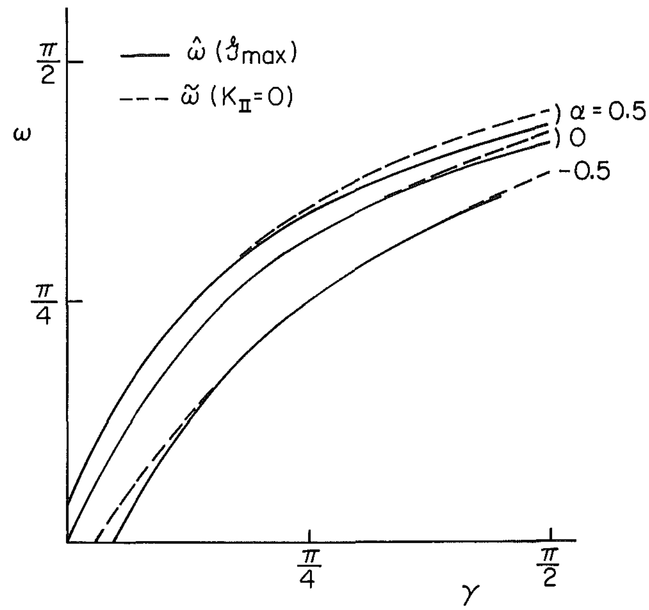

Fig. 7 Kinking angle associated with $K_{II} = 0$, $\tilde{\omega}$, as a function of γ compared with kinking angle associated with maximum energy release rate, $\hat{\omega}$, in each case for $\beta = 0$

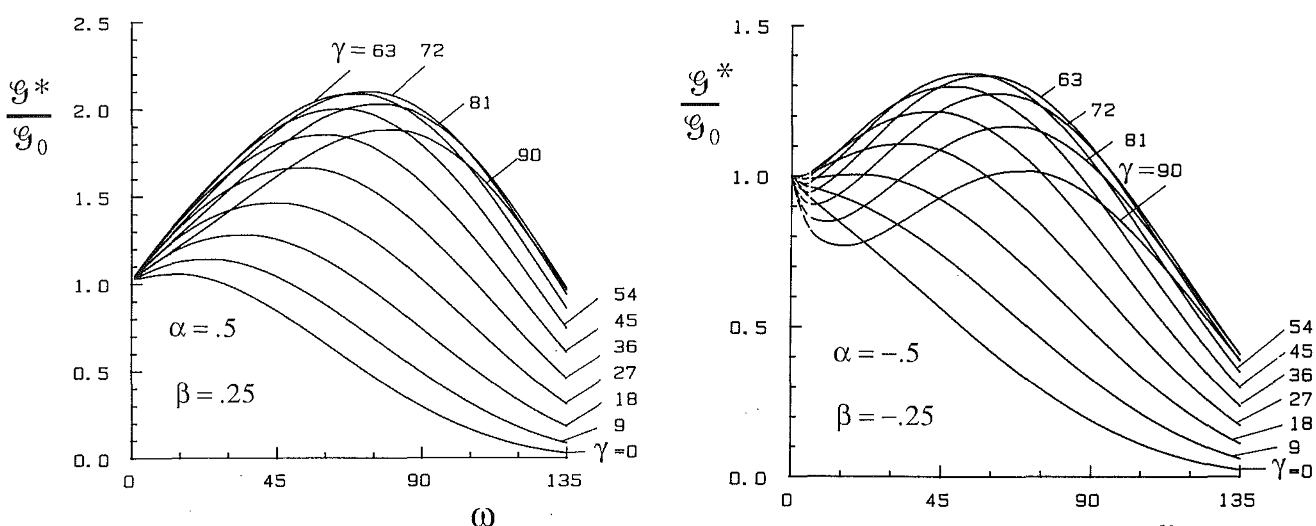

Fig. 8 $\mathcal{G}^*/\mathcal{G}_0$ versus ω for two cases in which $\beta \neq 0$

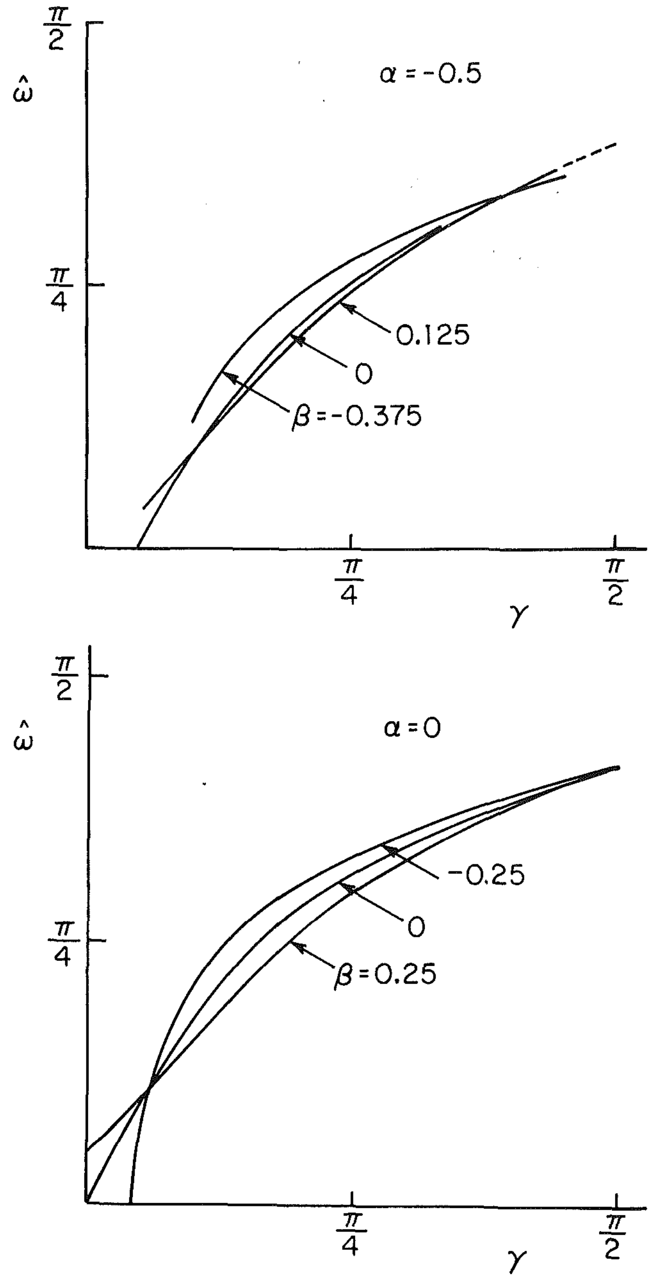

Fig. 9 Kinking angle $\hat{\omega}$ associated with maximum value of $\mathcal{G}^*$

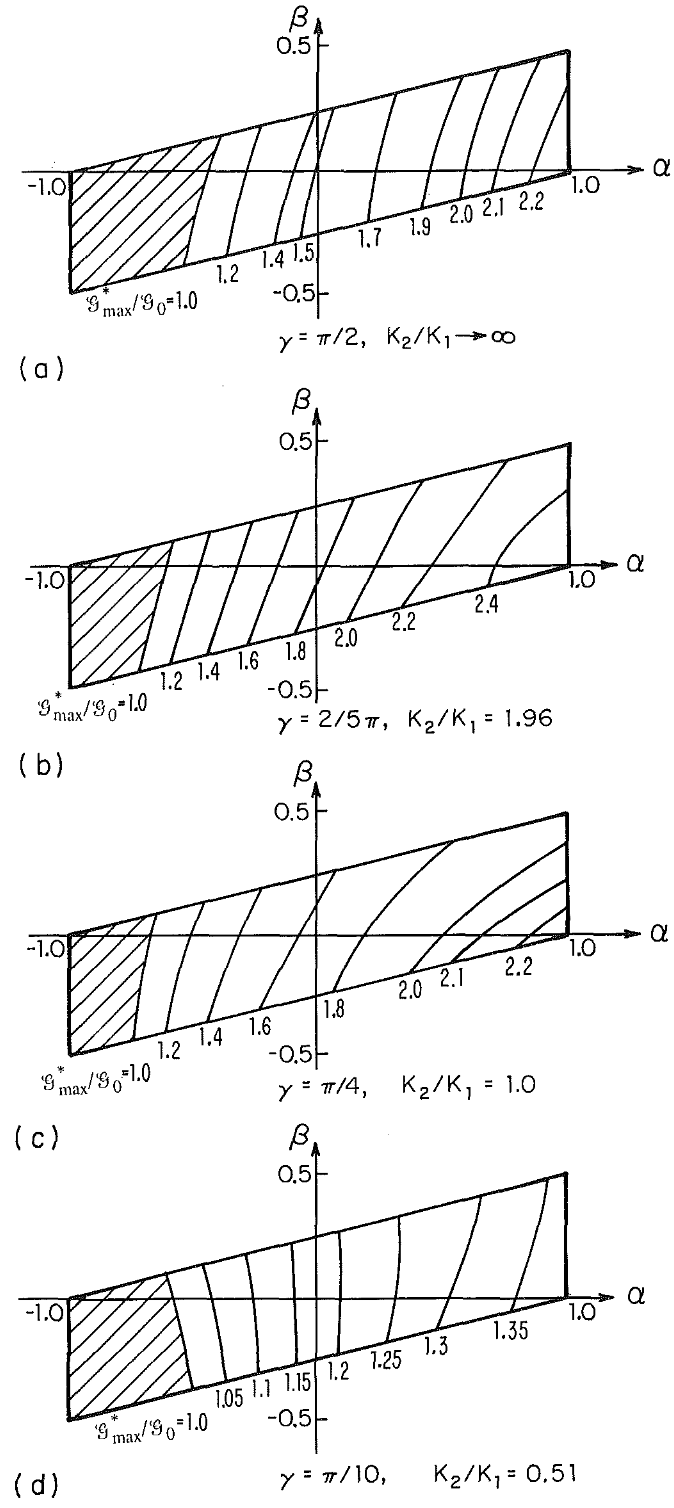

Fig. 10 Contour plots of the maximum value of $\mathcal{G}^*/\mathcal{G}_0$ as a function of α and β for four loading combinations specified by γ. The shaded regions correspond to $(\mathcal{G}^*/\mathcal{G}_0)_{max} = 1$ with $\hat{\omega} \to 0$.

Plots of $\mathcal{G}^*/\mathcal{G}_0$ as a function of ω are shown in Fig. 8 for ($\alpha = .5, \beta = .25$) and ($\alpha = -.5, \beta = -.25$). Although the β-values in these examples are quite large, the curves are quite similar to the curves in Fig. 5 with the same values of α and with $\beta = 0$. Curves of $\hat{\omega}$ associated with the maximum value of $\mathcal{G}^*$ are shown versus γ in Fig. 9. The effect of β on this variable appears to be relatively weak.

Contour plots of maximum values of $\mathcal{G}^*/\mathcal{G}_0$ are shown in Fig. 10 where α and β are coordinates whose range shown is restricted to non-negative values of the Poisson's ratios, ν_1 and ν_2. Each of the four plots is associated with a given loading combination measured by γ. The cross-hatched areas coincided with those pairs of α and β for which the maximum value of $\mathcal{G}^*$ is $\mathcal{G}_0$ with $\hat{\omega} = 0$. Note that $\mathcal{G}^*_{max}/\mathcal{G}_0$ varies by roughly a factor of 2 for α ranging from 1 to -1. These plots also reveal that the dependence of $\mathcal{G}^*_{max}$ on β is not particularly strong, especially in the range $|\beta| < .1$.

The only other paper on cracks kinking out of a bimaterial interface appears to be that of Hayashi and Nemat-Nasser (1981b). These authors consider a very special crack geometry and account for crack surface contact.

4 Concluding Remarks

The results for the kinked crack can be used to assess whether an interface crack will propagate in the interface or whether it will kink out of the interface. The simplest ap-

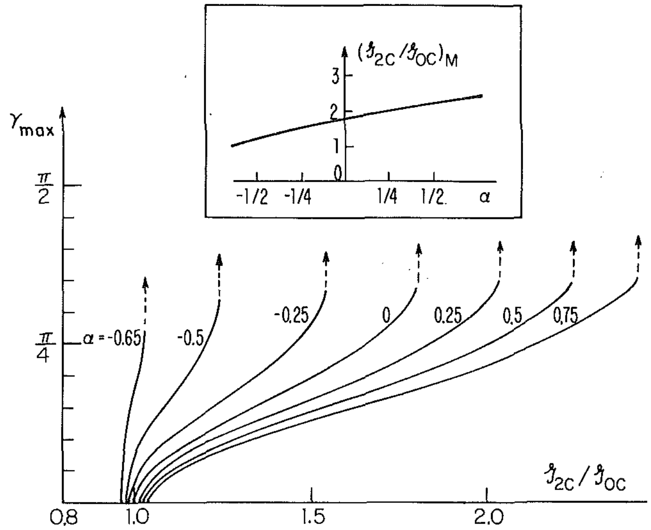

Fig. 11 For loading combinations $\gamma = \tan^{-1}(K_2/K_1)$ satisfying $0 \le \gamma \le \gamma_{max}$ the crack will not kink out of the interface into material 2. Assuming a propagation criterion based on maximum energy release rate, the dependence of γ_{max} on the ratio of material 2 toughness to interface toughness is shown for various α, all with $\beta = 0$. The insert figure shows the minimum value of this toughness ratio needed to ensure that the crack will not kink into material 2 for all loading combinations.

proach is to assume that the condition for propagation in the interface is $\mathcal{G}_0 = \mathcal{G}_{0c}$ and that for propagation in material 2 is $\mathcal{G} = \mathcal{G}_{2c}$. If $\mathcal{G}_{2c}$ is sufficiently large, compared to $\mathcal{G}_{0c}$, the crack will never kink into material 2. When $\mathcal{G}_{2c}$ is comparable to $\mathcal{G}_{0c}$ there will still be a loading range, i.e., $0 \le \gamma < \gamma_{max}$, such that the crack stays in the interface, while for $\gamma > \gamma_{max}$, the interface crack will kink into material 2. Figure 11 displays the dependence of γ_{max} on $\mathcal{G}_{2c}/\mathcal{G}_{0c}$ for various α-values, all with $\beta = 0$. When material 2 is the more compliant material $\mathcal{G}_{2c}$ must be greater than the interface toughness $\mathcal{G}_{0c}$ by as much as 2.5 (for $\alpha = .75$) if the crack is to stay in the interface for all γ. On the other hand, when material 2 is relatively stiff ($\alpha = -.65$), the crack will stay in the interface as long as $\mathcal{G}_{2c} \cong \mathcal{G}_{0c}$. The plot in the insert in Fig. 11 gives the *minimum value* of the toughness ratio, $(\mathcal{G}_{2c}/\mathcal{G}_{0c})_M$, needed to ensure that the crack will not leave the interface and propagate in material 2 for *all* combinations of loading.

A similar analysis can be carried out when $\mathcal{G}_{0c}$ depends on γ. This can be expected when the fractured interface has some roughness, with $\mathcal{G}_{0c}$ increasing with γ. Curves similar to those in Fig. 11 can be plotted from the basic results in Section 3. The important point is that the level of $\mathcal{G}_{2c}$ required to prevent kinking out of the interface will depend on the interface toughness $\mathcal{G}_{0c}$ at the loading angle γ applied.

When there is no dissimilarity in the elastic properties of the materials across the interface, the directions of kinking associated with the maximum energy release rate and with $K_{II} = 0$ are virtually the same (cf. Fig. 7). This is also true when the crack kinks into the more compliant material ($\alpha > 0$), at least when $\beta = 0$. However, when the crack kinks into a material 2 which is substantially stiffer than material 1, there exist ranges of loading where the maximum energy release rate occurs at small kink angles while the kink angle associated with $K_{II} = 0$ is around 45 deg or larger. When $\alpha < -.67$ (with $\beta = 0$) the direction $\tilde{\omega}$ associated with $K_{II} = 0$ is quite different from the direction of maximum energy release rate ($\hat{\omega} \cong 0$) for all loading combinations. It is an open question as to the criterion for crack kinking out of an interface when $\hat{\omega}$ and $\tilde{\omega}$ differ considerably. When the crack has penetrated well into material 2 a criterion based on $K_{II} = 0$ is expected to hold. A choice of criterion for the initial kinking step will have to be guided by experiment.

Pathological crack tip behavior associated with nonzero β (i.e., nonzero ϵ) has stood in the way of the development of an interfacial fracture mechanics for some years. This is in spite of the fact that there does not appear to be any compelling experimental evidence that the unusual behavior associated with nonzero β is essential to interfacial fracture phenomena. As a way to break the impasse, a tentative proposal put forward in the body of the paper is that the role of β be downplayed by arbitrarily taking $\beta = 0$ in the use of analytical results to interpret tests and make predictions, especially when β is small anyway. Such an approach seems sensible where the primary fracture variables of interest depend weakly on β, as is the case for most quantities examined in this paper. Obviously, a continual monitoring for any possible essential role of β should go on if this proposal is adopted.

Acknowledgments

This work was supported in part by DARPA University Research Initiative (Subagreement P.O. #VB38639-0 with the University of California, Santa Barbara, ONR Prime Contract N00014-86-K-0753) and by the Division of Applied Sciences, Harvard University.

References

Anderson, P. A., 1988, "Small Scale Contact Conditions for the Linear-Elastic Interface Crack," ASME JOURNAL OF APPLIED MECHANICS, Vol. 55, pp. 814-817.

Bilby, B. A., Cardew, G. E., and Howard, I. C., 1977, "Stress Intensity Factors at the Tip of a Kinked and Forked Cracks," *Fracture, 1977*, Vol. 3, University of Waterloo Press, p. 197.

Bilby, B., and Eshelby, J. D., 1968, "Dislocations and the Theory of Fracture," *Fracture, and Advanced Treatise*, Vol. I, H. Liebowitz, ed., Academic Press, New York, pp. 99-182.

Comninou, M., 1977, "The Interface Crack," ASME JOURNAL OF APPLIED MECHANICS, Vol. 44, pp. 631-636.

Cotterell, B., 1965, "On Brittle Fracture Paths," *Int. J. Fracture Mech.*, Vol. 1, pp. 96-103.

Cotterell, B., and Rice, J. R., 1980, "Slightly Curved or Kinked Cracks," *Int. J. Fracture*, Vol. 16, pp. 155-169.

Dundurs, J., 1969, "Edge-bonded Dissimilar Orthogonal Elastic Wedges," ASME JOURNAL OF APPLIED MECHANICS, Vol. 36, pp. 650-652.

England, A. H., 1965, "A Crack Between Dissimilar Media," ASME JOURNAL OF APPLIED MECHANICS, Vol. 32, pp. 400-402.

Erdogan, A. H., 1965, "Stress Distribution in Bonded Dissimilar Materials with Cracks," ASME JOURNAL OF APPLIED MECHANICS, Vol. 32, pp. 403-410.

Erdogan, F., and Gupta, G. D., 1972, "On the Numerical Solution of Singular Integral Equations," *Quarterly of Appl. Math.*, Vol. 29, pp. 525-534.

Hayashi, K., and Nemat-Nasser, S., 1981a, "Energy-Release Rate and Crack Kinking under Combined Loading," ASME JOURNAL OF APPLIED MECHANICS, Vol. 48, pp. 520-524.

Hayashi, K., and Nemat-Nasser, S., 1981b, "On Branched, Interface Cracks," ASME JOURNAL OF APPLIED MECHANICS, Vol. 48, pp. 529-533.

He, M-Y., and Hutchinson, J. W., 1988, "Kinking of a Crack Out of an Interface: Tabulated Solution Coefficients," Harvard University Report MECH-113A (available for a limited period from Marion Remillard, Pierce Hall 314, Division of Applied Sciences, Harvard University, Cambridge, MA 02138).

Hein, V. L., and Erdogan, F., 1971, "Stress Singularities in a Two-Material Wedge," *Int. J. Fracture Mech.*, Vol. 7, pp. 317-330.

Hutchinson, J. W., Mear, M., and Rice, J. R., 1987, "Crack Paralleling an Interface Between Dissimilar Materials," ASME JOURNAL OF APPLIED MECHANICS, Vol. 54, pp. 828-832.

Khrapkov, A. A., 1971, "The First Basic Problem for a Notch at the Apex of an Infinite Wedge," translated by I. Sneddon, *Int. J. Fracture Mech.*, pp. 373-382.

Lawn, B. R., and Wilshaw, T. R., 1975, *Fracture of Brittle Solids*, Cambridge University Press.

Lo, K. K., 1978, "Analysis of Branched Cracks," ASME JOURNAL OF APPLIED MECHANICS, Vol. 45, pp. 792-802.

Malyshev, B. M., and Salganik, R. L., 1965, "The Strength of Adhesive Joints Using the Theory of Cracks," *Int. J. Fracture Mech.*, Vol. 1, pp. 114-118.

Rice, J. R., 1968, "Mathematical Analysis in the Mechanics of Fracture," *Fracture, an Advanced Treatise*, Vol. II, H. Liebowitz, ed., Academic Press, New York, pp. 191-311.

Rice, J. R., 1988, "Elastic Fracture Mechanics concepts for Interfacial Cracks" ASME JOURNAL OF APPLIED MECHANICS, Vol. 55, pp. 98-103.

Rice, J. R., and Sih, G. C., 1965, "Plane Problems of Cracks in Dissimilar Media," ASME JOURNAL OF APPLIED MECHANICS, Vol. 32, pp. 418-423.

APPENDIX

The basic solution for an edge dislocation at z_0 ($z_0 = \eta e^{-i\omega}$) in material 2 interacting with a semi-infinite, traction-free crack extending along the interface to the origin (Fig. 3) was obtained by using complex variable methods. If the traction on the radial line through z ($z = te^{-i\omega}$) is written as (24), the functions H_1 and H_2 are given by

$$\begin{aligned} H_1(t,\eta) &= H_{10}(t,\eta) + H_{11}(t,\eta) \\ H_2(t,\eta) &= H_{20}(t,\eta) + H_{21}(t,\eta) \end{aligned} \qquad (A1)$$

where

$$H_{10} = -\delta\left(\frac{1}{z-\bar{z}_0} + \frac{(\bar{z}_0 - z_0)}{(z-z_0)^2} + e^{-2i\omega}\,\frac{(\bar{z}_0 - \bar{z})}{(z-\bar{z}_0)^2}\right)$$

$$H_{20} = -\delta\left(\frac{1}{\bar{z}-z_0} + \frac{(z_0 - \bar{z}_0)}{(z-\bar{z}_0)^2} + e^{-2i\omega}\frac{(z_0-\bar{z}_0)(z+\bar{z}_0-2\bar{z})}{(z-\bar{z}_0)^3}\right)$$

$$-\frac{\lambda}{z-\bar{z}_0}\,e^{-2i\omega} \qquad (A2)$$

and

$$H_{11} = -(1+\alpha)(1-\beta)\mathcal{L}\left[\frac{F(z,z_0)}{1-\beta} + \frac{F(z,\bar{z}_0)}{1+\beta}\right]$$

$$H_{21} = -(1+\alpha)(1-\beta)\mathcal{L}\left[\frac{z_0-\bar{z}_0}{1+\beta} + \frac{\partial}{\partial\bar{z}_0}\,F(z,\bar{z}_0)\right].$$

The functions H_{10} and H_{20} are for a dislocation below the bimaterial interface without the crack. The functions H_{11} and H_{21} are the additional terms to satisfy the traction-free condition on the semi-infinite crack. In the above

$$\delta = \frac{\beta-\alpha}{1+\beta}, \quad \lambda = \frac{\alpha+\beta}{\beta-1} \qquad (A3)$$

and

$$\mathcal{L}(\phi(z)) = \phi(z) + \overline{\phi(z)} + e^{-2i\omega}\left[(\bar{z}-z)\phi'(z) + \frac{(1-\beta)}{(1+\beta)}\,\bar{\phi}(z) - \phi(z)\right]$$

$$F(z,z_0) = \frac{1}{2}\left[1 - \left(\frac{z_0}{z}\right)^{1/2+i\epsilon}\right]/(z-z_0). \qquad (A4)$$

The formula for $\sigma^0_{\theta\theta}(t) + i\sigma^0_{r\theta}(t)$ in (26) is

$$\sigma^0_{\theta\theta} + i\sigma^0_{r\theta} = \phi_0'(z) + \overline{\phi_0'(z)} + e^{-2i\omega}[\bar{z}\phi_0''(z) + \chi_0'(z)] \qquad (A5)$$

where

$$\phi_0'(z) = \frac{1}{2\sqrt{2\pi}\,\cosh\,\pi\epsilon}\,e^{-\epsilon\pi}\bar{K}z^{-(1/2+i\epsilon)}$$

$$\chi_0'(z) = \frac{1}{2\sqrt{2\pi}\,\cosh\,\pi\epsilon}\left[e^{\epsilon\pi}Kz^{-1/2+i\epsilon} - e^{-\epsilon\pi}\left(\frac{1}{2} - i\epsilon\right)\bar{K}z^{-(1/2+i\epsilon)}\right]. \qquad (A6)$$

M. Ortiz

A. E. Giannakopoulos

Division of Engineering,
Brown University,
Providence, R.I. 02912

Maximal Crack Tip Shielding by Microcracking

It is shown here that the shielding effect of a distribution of microcracks, i.e., the extent to which they alleviate the severity of a near-tip singular field, is maximized when the microcracks develop normal to the direction of maximum tension. In passing, we derive mode I asymptotic solutions for a class of anisotropic damage models.

1 Introduction

Stable microcracking in ceramic materials has the beneficial effect of partially relieving the stress concentrations that arise at the tip of a crack, in effect shielding it from the action of remote loads. Extensive microcracking of this type has been observed in certain classes of ceramics (Hoagland et al., 1973; Claussen, 1976; Wu et al., 1978). Microcracks develop mainly at grain boundary facets as a result of residual stresses generated during cooling and of applied tensile stresses (Fu, 1983). Once the microcracks are formed they tend to remain confined to their facets with their tips pinned stably at grain junctures. As the number of microcrack nucleation sites is exhausted a saturation stage ensues during which the material sustains no further damage.

Interest in the shielding mechanism stems from its potential for enhancing the fracture toughness of ceramic materials (Evans, 1984). The shielding effect may be quantified by means of the *shielding ratio* K_t/K_∞, where K_t and K_∞ are the stress intensity factors of the near-tip singular fields and of the surrounding K-field. The value of K_∞ is a function of the applied loads and the geometry of the body. Thus, the shielding ratio provides a measure of the extent to which the remote loads are screened by the intervening effect of the microcracks. It bears emphasis, however, that the shielding ratio cannot be directly construed as giving the net toughness enhancement. In reality, the presence of microcracks ahead of the crack tip degrades the intrinsic resistance to fracture of the material, an effect which may partially or totally offset the toughness gains derived from shielding (Ortiz, 1988).

In recent years, shielding phenomena have been the subject of several studies. Some authors have based their analyses on approximate solutions to many-crack problems (Gong and Horii, 1987; Hoagland and Embury, 1980; Kachanov, 1986). Others have relied on models of distributed damage (Charalambides and McMeeking, 1987; Hutchinson, 1987; Ortiz, 1987; Rodin, 1987). Among the latter, Charalambides and McMeeking (1987) considered the case of isotropic damage and Ortiz (1987) the case of damage normal to the maximum tensile direction. Hutchinson (1987) based his analysis on both isotropic and anisotropic models of dilute microcracking. The available observational evidence (Hayhurst and Leckie, 1973; Leckie and Hayhurst, 1974) seems to support the notion that microcracks tend to develop normal to the direction of maximum tension. A comparison of the results of Ortiz and Charalambides and McMeeking, as well as the aforementioned work of Hutchinson, reveals that highly polarized microcracking provides a more effective shield than randomly-oriented isotropic damage.

In this paper we show that microcracking normal to the maximum tensile direction, or *normal microcracking* for short, does indeed maximize shielding. More precisely, among all possible arrangements of a fixed density of microcracks, the largest shielding effect is attained for normal microcracking. Our analysis relies on a model of damage to provide the necessary link between microcrack densities and the elastic moduli of the solid. In the interest of simplicity, we make the assumption that all points in the region of damage surrounding the crack tip undergo ostensibly proportional stressing. Under these conditions, the effective material behavior may be idealized as that of a nonlinear elastic solid. Within this constitutive framework, the singular mode I fields can be obtained in closed form for arbitrary microcrack orientations. Furthermore, the stress intensity factor at the crack tip may be related to the applied stress intensity factor by recourse to the J-integral of Rice (see, e.g., Rice, 1968). An analysis of the resulting shielding ratios shows that shielding is maximized when all microcracks are oriented at right angles to the maximum tensile direction.

2 Effective Constitutive Behavior

We first concern ourselves with the problem of characterizing the effective behavior of an elastic solid containing distributed microcracks. Of primary interest here is the anisotropy that results from the existence of preferred orientations in microcrack distribution. To gain some insight into the structure of the constitutive response, we resort to a simple dilute model. For the applications we pursue here, it suffices to consider plane-strain states of deformation of the body and

Contributed by the Applied Mechanics Division of THE AMERICAN SOCIETY OF MECHANICAL ENGINEERS for publication in the JOURNAL OF APPLIED MECHANICS.

Discussion on this paper should be addressed to the Editorial Department, ASME, United Engineering Center, 345 East 47th Street, New York, N.Y. 10017, and will be accepted until two months after final publication of the paper itself in the JOURNAL OF APPLIED MECHANICS. Manuscript received by ASME Applied Mechanics Division, March 7, 1988; final revision, August 2, 1988.

planar distributions of damage for which all microcracks are contained in planes normal to the plane of the analysis.

Let $P(\beta)$ denote the fraction of microcracks subtending an angle β to the direction of maximum tension. Note the normalization condition

$$\int_{-\pi/2}^{\pi/2} P(\beta)d\beta = 1 \tag{1}$$

to be satisfied by $P(\beta)$. If we assume that the concentration of microcracks is low enough that their interactions may be neglected, it is then possible to express the complementary energy of the body as

$$\chi(\sigma) = \frac{1}{2}\left[C^0_{ijkl} + C\int_{-\pi/2}^{\pi/2} n_i n_j n_k n_l P(\beta)d\beta\right]\sigma_{ij}\sigma_{kl} \tag{2}$$

where σ_{ij} are the components of the stress tensor, C^0_{ijkl} are the elastic compliances of the uncracked solid, $(n_1, n_2) = (\cos\beta, \sin\beta)$ are the microcrack normals, and C is a coefficient, which depends on the density of microcracks and the elastic constants of the matrix material. In equation (2) and henceforth, Latin indeces take values $\{1, 2\}$. In arriving at expression (2) it is assumed that the microcracks open primarily in mode I under the action of the resolved normal stress. The first term in (2) is simply the strain energy of the uncracked body, whereas the second term represents the strain energy introduced by the microcracks. A detailed derivation and discussion of (2) may be found in Kachanov (1980).

Equation (2) is expressed with reference to a cartesian frame $x_1 - x_2$ contained in the plane of the analysis. If, instead, we rephrase (2) in terms of the principal stress axes, we obtain the simpler form

$$\chi(\sigma) = \frac{1}{2} C^0_{ijkl}\sigma_{ij}\sigma_{kl} + \frac{1}{2} C_{\alpha\beta}\sigma_\alpha\sigma_\beta \tag{3}$$

where the indeces α and β range over $\{1, 2\}$, $\sigma_1 > 0$ and $\sigma_2 > 0$ are the in-plane principal stresses and

$$C_{11} = C\int_{-\pi/2}^{\pi/2} \cos^4\beta P(\beta)d\beta$$

$$C_{12} = C\int_{-\pi/2}^{\pi/2} \cos^2\beta \sin^2\beta\, P(\beta)d\beta = C_{21} \tag{4}$$

$$C_{22} = C\int_{-\pi/2}^{\pi/2} \sin^4(\beta)P(\beta)d\beta.$$

Some limiting cases of P are noteworthy. If, as assumed by Ortiz (1987), all microcracks are oriented normal to the direction of maximum tension, one has

$$P(\beta) = \delta(\beta) \tag{5}$$

where δ signifies Dirac's delta function. In this case, the coefficients (4) reduce to

$$C_{11} = C, \quad C_{12} = C_{21} = C_{22} = 0. \tag{6}$$

If, by way of contrast, we assume all microcrack orientations to be equally probable, one has

$$P(\beta) = \frac{1}{\pi} \tag{7}$$

and

$$C_{11} = C_{22} = \frac{3C}{8}, \quad C_{12} = C_{21} = \frac{C}{8}. \tag{8}$$

In subsequent developments, we shall confine our attention to proportional and monotonic stress paths. Under these conditions, the ceramic materials under consideration here are thought to exhibit a saturation stage in their constitutive response which ensues as the available microcrack nucleation sites are exhausted (Fu, 1983). Throughout this paper, we shall adopt the complementary energy potential defined in (3) and

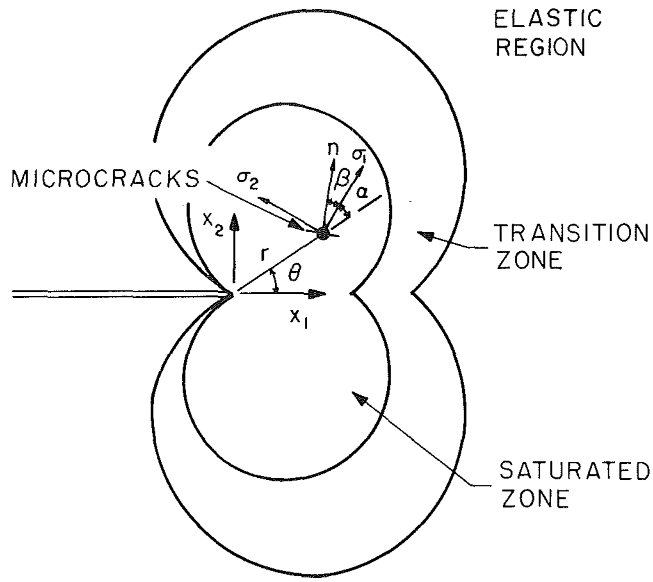

Fig. 1 Geometry of semi-infinite crack problem

(4) to describe the behavior of the material in the saturated range. The corresponding stress-strain relations follow as

$$\epsilon_{ij} = \partial\chi(\sigma)/\partial\sigma_{ij} \tag{9}$$

We note that the coefficient C bears a one-to-one relation to the microcrack density. Thus, keeping C constant while permitting $P(\beta)$ to vary arbitrarily yields all possible effective moduli attainable by a given microcrack density.

It is always possible to write down a uniformly valid, complementary energy potential $\chi(\sigma)$ which reduces to χ_0 and χ as limiting cases. To this end, it suffices to let

$$\chi(\sigma) = \chi_0(\sigma) + f(\sigma_1, \sigma_2) \tag{10}$$

where

$$\chi_0(\sigma) = \frac{1}{2} C^0_{ijkl}\sigma_{ij}\sigma_{kl} \tag{11}$$

is the complementary energy potential of the undamaged material and f is any function satisfying the conditions

$$\frac{\partial^2 f}{\partial\sigma_\alpha\partial\sigma_\beta}(0, 0) = 0,$$

$$\lim_{\sqrt{\sigma_1^2+\sigma_2^2}\to\infty} \frac{\partial^2 f}{\partial\sigma_\alpha\partial\sigma_\beta}(\sigma_1, \sigma_2) = C_{\alpha\beta}. \tag{12}$$

It will be assumed that one such complementary energy potential describes the response of the material under proportional and monotonic stress paths. The first conditions in equation (12) requires that the tangent moduli in the initial stress free configuration coincide with those of the uncracked material, whereas the second of (12) implies the existence of a saturation stage governed by potential (3). Although, in actual computations only the undamaged and saturated potentials will be explicitly employed, the existence of a uniformly-valid potential needs to be postulated for the J-integral formalism to apply.

Finally, we note for later reference that the saturated complementary energy potential (3), although strongly nonlinear, is homogeneous of degree two.

3 Asymptotic Fields for a Stationary Crack

Consider a semi-infinite crack in a body subjected to plane-strain mode I loading, Fig. 1. Assume that the conditions are met for the effect of microcracking to be describable within the framework of continuum damage models. Thus, all processes of interest are presumed to possess characteristic length scales much larger than the microcrack size and separation.

With reference to Fig. 1, we identify three regions surrounding the crack. In the innermost region, the material is assumed to have attained the saturation stage. By contrast, at sufficiently large distances from the crack tip, the material is presumed to be undamaged. These two regions are joined by a transition zone wherein the material, albeit damaged, is not as yet saturated. Within the region of saturation, we shall denote by α the angle subtended by the maximum tensile direction and the position vector measured from the crack tip. Furthermore, the orientation of the microcracks may be characterized by means of the angle β between the normal to the microcrack and the maximum tensile direction.

The loads applied to the body are assumed to result in a remote K-field of the form

$$\sigma_{ij}(r,\theta)=\frac{K_\infty}{\sqrt{2\pi r}}\,\tilde{\sigma}^0_{ij}(\theta) \tag{13}$$

where K_∞ is the remote stress-intensity factor and r, θ are polar coordinates centered at the crack tip with θ measured from the plane of the crack. The familiar linear elastic angular fields $\tilde{\sigma}^0_{ij}(\theta)$ are given by (see, e.g., Rice, 1968)

$$\begin{Bmatrix}\tilde{\sigma}^0_{rr}(\theta)\\ \tilde{\sigma}^0_{\theta\theta}(\theta)\\ \tilde{\sigma}^0_{r\theta}(\theta)\end{Bmatrix}=\begin{Bmatrix}(5/4)\cos(\theta/2)-(1/4)\cos(3\theta/2)\\ (3/4)\cos(\theta/2)+(1/4)\cos(3\theta/2)\\ (1/4)\sin(\theta/2)+(1/4)\sin(3\theta/2)\end{Bmatrix}. \tag{14}$$

The value of K_∞ depends upon the particular geometry of the body and provides a single-parameter characterization of the magnitude and distribution of the applied loads.

For montonic loading, the stress paths at all material points may be reasonably expected to remain nearly proportional. Under these conditions, the inelastic behavior of the solid may be described by means of a deformation theory of damage, such as that formulated in Section 2.

Since the adopted stress-strain relations derive from a complementary energy potential which is homogeneous of degree two, a classical argument (see, e.g., Rice, 1968) shows that the most singular term in the near-tip fields must be of the form

$$\sigma_{ij}(r,\theta)=\frac{K_t}{\sqrt{2\pi r}}\,\tilde{\sigma}_{ij}(\theta) \tag{15}$$

where K_t is the near-tip, stress-intensity factor and the angular distributions $\tilde{\sigma}_{ij}(\theta)$ are to be determined. In general K_t is different from K_∞, owing to the shielding effect of the microcracks surrounding the crack tip. As mentioned in the introduction, the ratio K_t/K_∞, or shielding ratio, may be taken as a measure of the extent of shielding.

Ortiz (1987) has noted that for damage normal to the maximum tensile direction, i.e., for the case $C_{11}=C$, $C_{12}=C_{21}=C_{22}=0$, the near-tip singular fields possess a structure identical to that of the elastic solution (14). Here, we show that the elastic fields also happen to furnish the solution for arbitrary choices of the moduli $C_{\alpha\beta}$. In this way, we are able to characterize the near-tip mode I fields for material behavior ranging continuously from isotropic to normal microcracking.

Start by noting that the stress field

$$\tilde{\sigma}_{ij}(\theta)=\tilde{\sigma}^0_{ij}(\theta) \tag{16}$$

satisfies equilibrium and traction-free boundary conditions on the crack faces. Thus, it suffices to show that the associated strain field is compatible. With reference to Fig. 1, the direction of maximum tensile stress is computed to be

$$\mathbf{e}_1=(\cos\alpha,\ \sin\alpha),\quad \alpha=\begin{cases}\pi/4-\theta/4, & 0<\theta\le\pi;\\ -\pi/4-\theta/4, & -\pi\le\theta<0;\end{cases} \tag{17}$$

Thus, the angle α subtended by the direction of maximum tension and the position vector measured from the crack tip varies linearly with θ, from a value of $\alpha=45$ deg at $\theta=0^+$ to $\alpha=0$ deg on the crack face $\theta=\pi$.

Let $\mathbf{e}_2=(-\sin\alpha,\ \cos\alpha)$ be the remaining principal stress direction. Thus, $(\mathbf{e}_1,\mathbf{e}_2)$ is the principal basis associated with the stress tensor. Then, the stress-strain relations in the saturated region take the form

$$\begin{aligned}\epsilon_{ij}=\partial\chi/\partial\sigma_{ij}=C^0_{ijkl}\sigma_{kl}&\\ +(C_{11}e_{1i}e_{1j}+C_{12}e_{2i}e_{2j})\sigma_1&\\ +(C_{21}e_{1i}e_{1j}+C_{22}e_{2i}e_{2j})\sigma_2&\end{aligned} \tag{18}$$

where the principal stresses σ_α may be expressed as

$$\sigma_\alpha(r,\theta)=\frac{K_t}{\sqrt{2\pi r}}\,\tilde{\sigma}_\alpha(\theta). \tag{19}$$

The angular fields $\tilde{\sigma}_\alpha$ are computed from (14) to be

$$\begin{aligned}\tilde{\sigma}_1&=\cos\frac{\theta}{2}+\left|\sin\frac{\theta}{2}\cos\frac{\theta}{2}\right|\\ \tilde{\sigma}_2&=\cos\frac{\theta}{2}-\left|\sin\frac{\theta}{2}\cos\frac{\theta}{2}\right|.\end{aligned} \tag{20}$$

Inserting (15) and (16) into (18), the asymptotic strain field is found to exhibit the additive structure

$$\epsilon_{ij}=\epsilon^e_{ij}+\epsilon^d_{ij} \tag{21}$$

where the elastic strain field ϵ^e_{ij} takes the familiar form

$$\begin{Bmatrix}\epsilon^e_{rr}(r,\theta)\\ \epsilon^e_{\theta\theta}(r,\theta)\\ \gamma^e_{r\theta}(r,\theta)\end{Bmatrix}=\frac{K_t}{\sqrt{2\pi r}}\frac{1}{2G_0}\begin{Bmatrix}(5/4-2\nu_0)\cos(\theta/2)-(1/4)\cos(3\theta/2)\\ (3/4-2\nu_0)\cos(\theta/2)+(1/4)\cos(3\theta/2)\\ (1/2)\sin(\theta/2)+(1/2)\sin(3\theta/2)\end{Bmatrix}. \tag{22}$$

Here, E_0, ν_0, and $G_0=E_0/2(1+\nu_0)$ are the initial Young's modulus, Poisson's ratio, and shear modulus of the uncracked material. The term contributed by damage may be expressed in separable form,

$$\epsilon^d_{ij}(r,\theta)=\frac{K_tC}{\sqrt{2\pi r}}\,\tilde{\epsilon}^d_{ij}(\theta) \tag{23}$$

where the angular fields $\tilde{\epsilon}^d_{ij}(\theta)$ read

$$\begin{aligned}\begin{Bmatrix}\tilde{\epsilon}^d_{rr}\\ \tilde{\epsilon}^d_{\theta\theta}\\ \tilde{\gamma}^d_{r\theta}\end{Bmatrix}&=\mu_{11}\begin{Bmatrix}\tilde{\sigma}_1\cos^2\alpha\\ \tilde{\sigma}_1\sin^2\alpha\\ 2\tilde{\sigma}_1\sin\alpha\cos\alpha\end{Bmatrix}+\mu_{12}\begin{Bmatrix}\tilde{\sigma}_1\sin^2\alpha\\ \tilde{\sigma}_1\cos^2\alpha\\ -2\tilde{\sigma}_1\sin\alpha\cos\alpha\end{Bmatrix}\\ &+\mu_{21}\begin{Bmatrix}\tilde{\sigma}_2\cos^2\alpha\\ \tilde{\sigma}_2\sin^2\alpha\\ 2\tilde{\sigma}_2\sin\alpha\cos\alpha\end{Bmatrix}+\mu_{22}\begin{Bmatrix}\tilde{\sigma}_2\sin^2\alpha\\ \tilde{\sigma}_2\cos^2\alpha\\ -2\tilde{\sigma}_2\sin\alpha\cos\alpha\end{Bmatrix},\\ &0<\theta\le\pi.\end{aligned} \tag{24}$$

Here, the dimensionless coefficients $\mu_{\alpha\beta}$ are defined to be

$$\mu_{\alpha\beta} = C_{\alpha\beta}/C. \tag{25}$$

The fields (24) may be extended by symmetry to the lower half of the plane.

Next, we seek to ascertain whether the strain field (21) satisfies the compatibility equation

$$\frac{1}{r}\frac{\partial^2\gamma_{r\theta}}{\partial r\partial\theta} - \frac{\partial^2\epsilon_{\theta\theta}}{\partial r^2} - \frac{1}{r^2}\frac{\partial^2\epsilon_{rr}}{\partial\theta^2} + \frac{1}{r}\frac{\partial\epsilon_{rr}}{\partial r} + \frac{1}{r^2}\frac{\partial\gamma_{r\theta}}{\partial\theta} - \frac{2}{r}\frac{\partial\epsilon_{\theta\theta}}{\partial r} = 0. \tag{26}$$

Since the elastic fields are compatible, it suffices to consider the strains contributed by microcracking. For separable fields such as (23), the compatibility equation reduces to the condition

$$\mathcal{L}(\bar\epsilon^d) = \frac{d^2\bar\epsilon^d_{rr}}{d\theta^2} - \frac{1}{2}\frac{d\bar\gamma^d_{r\theta}}{d\theta} + \frac{1}{2}\bar\epsilon^d_{rr} - \frac{1}{4}\bar\epsilon^d_{\theta\theta} = 0 \tag{27}$$

for the angular fields. A lengthy but straightforward computation yields the results

$$\mathcal{L}\left\{\begin{array}{c}\tilde\sigma_1\cos^2\alpha\\ \tilde\sigma_1\sin^2\alpha\\ 2\tilde\sigma_1\sin\alpha\cos\alpha\end{array}\right\} = \mathcal{L}\left\{\begin{array}{c}\tilde\sigma_2\sin^2\alpha\\ \tilde\sigma_2\cos^2\alpha\\ -2\tilde\sigma_2\sin\alpha\cos\alpha\end{array}\right\} = 0$$

$$\mathcal{L}\left\{\begin{array}{c}\tilde\sigma_1\sin^2\alpha\\ \tilde\sigma_1\cos^2\alpha\\ -2\tilde\sigma_1\sin\alpha\cos\alpha\end{array}\right\} = -\mathcal{L}\left\{\begin{array}{c}\tilde\sigma_2\cos^2\alpha\\ \tilde\sigma_2\sin^2\alpha\\ 2\tilde\sigma_2\sin\alpha\cos\alpha\end{array}\right\} = \frac{3}{8}\sin\theta. \tag{28}$$

Hence, in view of (28), we conclude that the strain field due to damage is compatible if and only if

$$C_{12} = C_{21}. \tag{29}$$

For the model adopted here, the satisfaction of this condition is assured by the choice (4) of coefficients $C_{\alpha\beta}$.

The displacements may now be computed from the strain field, which yields

$$\left\{\begin{array}{c}u_r(r,\theta)\\ u_\theta(r,\theta)\end{array}\right\} = \frac{K_t}{4G_0}\sqrt{\frac{r}{2\pi}}\left\{\begin{array}{c}(2\kappa_0-1)\cos(\theta/2)-\cos(3\theta/2)\\ -(2\kappa_0+1)\sin(\theta/2)+\sin(3\theta/2)\end{array}\right\} + K_t\sqrt{\frac{r}{2\pi}}$$
$$\left\{\begin{array}{c}C_{11}(1+\sin(\theta/2))^2\cos(\theta/2)+(C_{12}+C_{21})\cos^3(\theta/2)+C_{22}(1-\sin(\theta/2))^2\cos(\theta/2)\\ -C_{11}(1+\sin(\theta/2))^2\sin(\theta/2)+(C_{12}+C_{21})\cos^2(\theta/2)\sin(\theta/2)-C_{22}(1-\sin(\theta/2))^2\sin(\theta/2)\end{array}\right\} \tag{30}$$

where $\kappa_0 = 3-4\nu_0$. The displacements in the lower half plane follow by symmetry. Of particular interest is the crack opening profile

$$[[u_2]](r) = -u_\theta(r,\pi) + u_\theta(r,-\pi) = 8K_t\left(\frac{1-\nu_0^2}{E_0} + C_{11}\right)\sqrt{\frac{r}{2\pi}}. \tag{31}$$

As may be seen, the coefficients C_{12} and C_{22} do not contribute to the opening displacement.

4 Crack Tip Stress-Intensity Factor: Application of the J-Integral

Next, we endeavor to compute the crack tip stress-intensity factor K_t as a function of the remote K_∞. Assuming that the stress histories experienced by all material points remain nearly proportional and monotonic, the behavior of the material is indistinguishable from that of a nonlinear elastic body possessing a complementary energy potential of the form (10). Under these conditions, the sought relation between K_t and K_∞ may be obtained by recourse to the J-integral of Rice (Rice, 1968).

Start by recalling that the contour integral

$$J = \int_\Gamma [W(\epsilon)m_1 - \sigma_{ij}m_ju_{i,1}]ds \tag{32}$$

is path-independent under the assumptions stated above. Here, $\mathbf{m}$ signifies the outer normal to the contour Γ encircling the crack tip. If the contour is chosen to lie entirely within the remote field, J reduces to the well-known expression

$$J_\infty = \frac{1-\nu_0^2}{E_0}K_\infty^2. \tag{33}$$

For a contour shrunk down to the crack tip, the J-integral may be computed directly from the near-tip singular fields derived in the preceding section. A lengthy but straightforward calculation yields

$$J_t = \frac{1-\nu_0^2}{E_0}K_t^2 + (aC_{11}+bC_{22})K_t^2 \tag{34}$$

where

$$a = \frac{15\pi+56}{30\pi} \approx 1.0942, \quad b = \frac{15\pi-56}{30\pi} \approx -0.0942. \tag{36}$$

Finally, the path independence of the J-integral requires that

$$J_t = J_\infty \tag{37}$$

where upon one concludes

$$\frac{K_t}{K_\infty} = 1\Big/\sqrt{1+(aC_{11}+bC_{22})E_0/(1-\nu_0^2)}. \tag{38}$$

In view of (4) it is seen that the shielding ratio K_t/K_∞ depends on the microcrack orientation density $P(\beta)$ through the coefficients C_{11} and C_{22}. Furthermore, the shielding ratio is a decreasing function of

$$\mathcal{G}[P] = aC_{11} + bC_{22} = C\int_{\pi/2}^{\pi/2}(a\cos^4\beta + b\sin^4\beta)P(\beta)d\beta. \tag{39}$$

Thus, the distribution density $P(\beta)$ for which maximal shielding is attained follows as the solution of the linear optimization problem

$$\begin{array}{ll}\text{Maximize} & \mathcal{G}[P]\\ \text{subject to} & \int_{-\pi/2}^{\pi/2}P(\beta)d\beta = 1\end{array} \tag{40}$$

where C is regarded as a constant. It bears emphasis that, since C and the microcrack density are in one-to-one correspondence, the maximization implied in (40) is effected over all possible arrangements of a *fixed* population of microcracks.

We next claim that the only solution to problem (40) is given by (5), which corresponds to the case in which all microcracks are oriented normal to the direction of maximum tension. To prove this assertion, note that

$$\mathcal{G}[\delta]/C = a. \tag{41}$$

On the other hand, the following holds:

$$a \cos^4\beta + b \sin^4 \beta \leq a, \quad \beta \in [-\pi/2, \pi/2]. \tag{42}$$

From the inequality it follows that, for any distribution function $P(\beta) \geq 0$ satisfying the normalization condition (1),

$$\mathcal{G}[P]/C = \int_{\pi/2}^{\pi/2} (a \cos^4\beta + b \sin^4\beta) P(\beta) d\beta \leq a \int_{-\pi/2}^{\pi/2} P(\beta) d\beta = a \tag{43}$$

i.e., the value of the functional $\mathcal{G}[P]/C$ can be at most a. Hence, in view of (41), we conclude that $P = \delta$ is indeed a maximum. To see that this is the only solution to the problem, it suffices to note that, by virtue of inequality (42), any component of P whose domain lies in $[-\pi/2, \pi/2] - \{0\}$ necessarily reduces the value of $\mathcal{G}[P]$. Therefore, the domain of a maximum of the functional must reduce to $\{0\}$, which in conjunction with (1) necessitates $P = \delta$. Thus we have proved the main result of this section, namely, that *normal microcracking maximizes shielding*.

Acknowledgments

The support of the Office of Naval Research through grant N00014-85-K-0720 is gratefully acknowledged.

References

Charalambides, P., and McMeeking, R. M., 1987, "Near Tip Mechanics of Stress Induced Microcracking in Brittle Materials," *Mechanics of Materials*, Vol. 6, pp. 71–87.

Claussen, N., 1976, "Fracture Toughness of Al_2O_3 with an Unstabilized ZrO_2 Dispersed Phase," *J. Am. Ceram. Soc.*, Vol. 59, pp. 49–51.

Evans, A. G., 1984, "Aspects of the Reliability of Ceramics," *Defect Properties and Processing of High-Technology Nonmetallic Materials*, J. H. Crawford, Y. Chen, and W. A. Sibley, eds., North-Holland, pp. 63–80.

Fu, Y., 1983, "Mechanics of Microcrack Toughening in Ceramics," Ph.D. Thesis, University of California, Berkeley, California.

Gong, S., and Horii, H., "General Solution to the Problem of Microcracks near the Tip of a Main Crack," Report 87-12, Department of Civil Engineering, University of Tokyo, Dec. 1987.

Hayhurst, D. R., and Leckie, F. A., 1973, "The Effect of Creep Constitutive and Damage Relationships upon the Rupture Time of a Solid Circular Torsion Bar," *J. Mech. Phys. Solids*, Vol. 21, pp. 431–446.

Hoagland, R. G., Hahn, G. T., and Rosenfield, A. R., 1973, "Influence of Microstructure on the Fracture Propagation in Rock," *Roc. Mech.*, Vol. 5, pp. 77-106.

Hoagland, R. G., and Embury, J. D., 1980, "A Treatment of Inelastic Deformation around a Crack Tip Due to Microcracking," *J. Am. Ceram. Soc.*, Vol. 63, pp. 404–410.

Hutchinson, J. W., 1987, "Crack Tip Shielding by Micro-Cracking in Brittle Solids," *Acta Metall.*, Vol. 35, No. 7, pp. 1605–1619.

Kachanov, M., 1980, "Continuum Model of Medium with Cracks," *J. Engr. Mech. Div.*, ASCE, Vol. 106, pp. 1039–1051.

Kachanov, M., 1986, "On Crack-Microcrack Interactions," *Int. J. Fracture*, Vol. 30, pp. R65-R72.

Leckie, F. A., and Hayhurst, D. R., 1974, "Creep Rupture of Structures," *Proc. Roy. Soc. London*, Vol. A340, pp. 323–347.

Ortiz, M., 1987, "A Continuum Theory of Crack Shielding in Ceramics," ASME Journal of Applied Mechanics, Vol. 54, pp. 54–58.

Ortiz, M., 1988, "Microcrack Coalescence and Macroscopic Crack Growth Initiation in Brittle Solids," *Int. J. Solids Structures*, Vol. 24, pp. 231–250.

Rice, J. R., 1968, "Mathematical Analysis in the Mechanics of Fracture," *Fracture*, Vol. 2, H. Liebowitz, ed. Academic Press, pp. 191–311.

Rodin, G., 1987, "An Example of Crack Tip Analysis in Brittle Damaged Materials," *Int. J. Fracture*, Vol. 33, pp. R31-R35.

Wu, C. C., Freiman, S. W., Rice, R. W., and Mecholsky, J. J., 1978, "Microstructural Aspects of Crack Propagation in Ceramics," *J. Mater. Sci.*, Vol. 13, pp. 2659–2670.

A New Boundary Integral Equation Formulation for Elastodynamic and Elastostatic Crack Analysis

Ch. Zhang[1]

J. D. Achenbach
Fellow, ASME

The Technological Institute,
Northwestern University,
Evanston, IL 60208

An elastodynamic conservation integral, the $\tilde{J}_k$ integral, is employed to derive boundary integral equations for crack configurations in a direct and natural way. These equations immediately have lower-order singularities than the ones obtained in the conventional manner by the use of the Betti-Rayleigh reciprocity relation. This is an important advantage for the development of numerical procedures for solving the BIE's, and for an accurate calculation of the strains and stresses at internal points close to the crack faces. For curved cracks of arbitrary shape the BIE's presented here have simple forms, and they do not require integration by parts, as in the conventional formulation. For the dynamic case the unknown quantities are the crack opening displacements and their derivatives (dislocation densities), while for the static case only the dislocation densities appear in the formulation. For plane cracks the boundary integral equations reduce to the ones obtained by other investigators.

1 Introduction

Boundary integral equations, in conjunction with the boundary element method, provide an effective numerical technique for the solution of boundary value problems in solid mechanics. The boundary integral equation method (BIEM) has been successfully applied to a wide range of problems in linear and nonlinear elasticity. Recent developments of the boundary integral equation method have been concerned with applications to elastostatic and elastodynamic crack analysis. The method is attractive for crack analysis, because the semi-analytical nature of the BIEM makes it easy to take into account the singularities at the crack tips.

The conventional BIE formulation, due to Rizzo (1967) and Cruse (1969), is based on the Betti-Rayleigh reciprocity theorem for two independent elastostatic or elastodynamic states. By choosing one of the states as the unknown field and the other as the basic singular solution (the Green's function), a representation integral for the displacement components can be derived. The integral, which is over the surface of the crack, contains the crack opening displacements (the displacement jumps across the crack faces) and derivatives of the Green's function in its integrand. Unfortunately, a direct limiting process on the representation integral for the displacements as the observation point approaches a crack face, gives rise to a degenerate set of BIE's, as shown by Cruse (1975). This has motivated the use of representation integrals for the tractions, and their corresponding boundary integral equations, rather than displacement BIE's. Such traction BIE's are, however, highly singular, and they cannot be solved directly by numerical methods. To circumvent these difficulties several approaches have been proposed, see for example, the papers by Cruse (1975, 1987), Weaver (1977), Budiansky and Rice (1979), Schmerr (1982), Sládek and Sládek (1984), Nishimura and Kobayashi (1987), Zhang and Achenbach (1988), and Budreck and Achenbach (1988). Most of these studies first reduce the higher-order singularities to integrable ones, and then solve the modified BIE's numerically. The reduction is achieved by the use of partial integration. The required manipulations are reasonably easy for simple configurations such as three-dimensional planar or two-dimensional straight cracks, but they become cumbersome for curved cracks. Furthermore, different forms of the regularized BIE's are obtained through the nonunique integration-by-parts process, though they are equivalent (see Cruse, 1987).

In this paper we present a new BIE formulation for crack analysis. The motivation for this study is the paper by Hu (1987), who proposed a novel way to obtain a new type of BIE, to solve elastostatic boundary value problems. Hu's formulation is based on the conservation integral J_k. In the present paper it is shown that Hu's BIE's are especially suited for solving crack problems. For elastodynamic problems, the J_k integral of elastostatics is generalized to time-harmonic elastodynamics, and the result is denoted by $\tilde{J}_k$. Boundary integral equations are then derived from $\tilde{J}_k$ in a direct and natural manner, for arbitrary crack configurations. The BIE's that are obtained are immediately less singular than the ones of the conventional formulation, and they do not require additional manipulation in developing numerical solution procedures. The BIE's presented in this paper have relatively sim-

[1] Permanent Address: Department of Engineering Mechanics, Tongji University, Shanghai, People's Republic of China.

Contributed by the Applied Mechanics Division of THE AMERICAN SOCIETY OF MECHANICAL ENGINEERS for publication in the JOURNAL OF APPLIED MECHANICS.

Discussion on this paper should be addressed to the Editorial Department, ASME United Engineering Center, 345 East 47th Street, New York, N.Y. 10017, and will be accepted until two months after final publication of the paper itself in the JOURNAL OF APPLIED MECHANICS. Manuscript receied by the ASME Applied Mechanics Division, April 15, 1988; final revision, October 10, 1988.

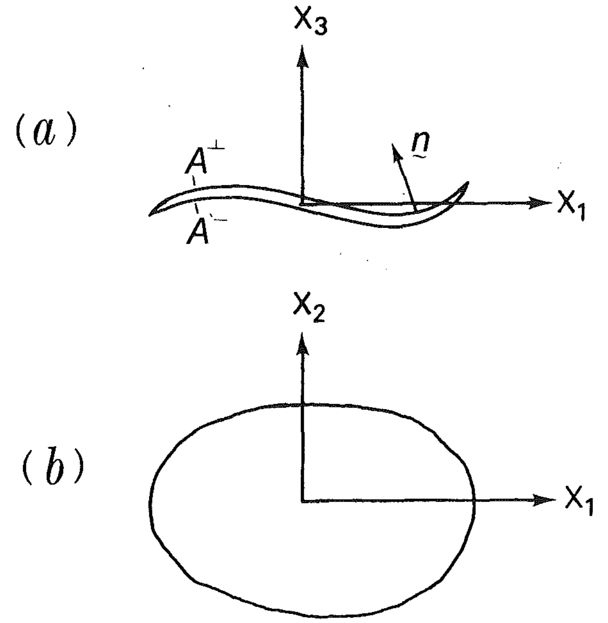

Fig. 1 Curved crack of arbitrary shape; (a) x_1x_3-plane, (b) top view

ple forms, and they reduce to those for elastostatics by letting the circular frequency, ω, approach zero, and by using the appropriate static Kelvin solutions. For planar and straight cracks the results agree with those obtained by other authors. New BIE's derived from the complementary conservation integral $\tilde{J}_k^c$ are also given, but these equations do not offer advantages over the conventional formulation.

The significance of J_k (or $\tilde{J}_k$) integral as a relevant crack-tip parameter in linear and nonlinear fracture mechanics has been well established (see Moran and Shih, 1987). The present paper presents a novel application of such path-independent or conservation integrals in elastodynamic and elastostatic crack analysis.

2 Problem Statement and Conventional BIE Formulation

A crack is a surface of displacement discontinuity when external loads are applied to the body. The faces of a mathematical crack are infinitesimally close prior to loading, and they do not interact when loads are applied. This is an acceptable approximation for real cracks whose faces are initially sufficiently separated so that the faces will not touch when the body is disturbed.

In this paper we consider a three-dimensional (curved) crack of arbitrary shape which is contained in an unbounded, homogenous, isotropic, linearly elastc solid. The geometry is shown in Fig. 1. The solid is subjected to time-harmonic motion, but the term exp $(-i\omega t)$ has been suppressed throughout the analysis.

The stress equations of motion are given by (see Achenbach, 1973)

$$\sigma_{ij,j}+\rho\omega^2 u_i=0, \tag{1}$$

where σ_{ij} defines the stress components, u_i denotes the displacement components, ρ is the mass density, and ω is the angular frequency. In equation (1) body forces are not considered and the summation convention is implied. In the linear theory, the strain components are defined as

$$\epsilon_{ij}=\frac{1}{2}(u_{i,j}+u_{j,i}). \tag{2}$$

The stress and strain components are related by Hooke's law

$$\sigma_{ij}=C_{ijkl}\epsilon_{kl}, \tag{3}$$

where C_{ijkl} are elastic constants which for isotropic materials can be written as

$$C_{ijkl}=\lambda\delta_{ij}\delta_{kl}+\mu(\delta_{ik}\delta_{jl}+\delta_{il}\delta_{jk}). \tag{4}$$

Here, λ and μ are Lamé's elastic constants and δ_{ij} is the Kronecker delta. The tractions vanish on the faces of the crack, i.e.,

$$f_i=\sigma_{ij}n_j=0,\ \mathbf{x}\epsilon A, \tag{5}$$

where $A=A^++A^-$. For a scattering problem A^+ is the insonified side of the crack and A^- is the shadow side. Also, n_j is the unit normal vector of A.

The total fields generated by the interaction of an incident wave with the crack can be written as

$$u_i=u_i^{in}+u_i^{sc},\ \sigma_{ij}=\sigma_{ij}^{in}+\sigma_{ij}^{sc}, \tag{6}$$

where u_i^{in} and σ_{ij}^{in} represent the incident field in the absence of the crack, and u_i^{sc}, σ_{ij}^{sc} define the scattered field. Both the total fields and the partial fields satisfy equations (1)–(3). For a given incident field the total field has to satisfy the boundary conditions on the faces of the crack, equation (5).

Following the procedure proposed by Rizzo (1967) and Cruse (1969), a representation integral for the scattered displacement can be obtained by using the Betti-Rayleigh reciprocal theorem and the fundamental solution due to a unit time-harmonic point force. For a three-dimensional crack, the representation integral can be written as

$$u_k^{sc}(\mathbf{x})=\int_{A^+}\sigma_{ijk}^G(\mathbf{x}-\mathbf{y})\Delta u_i(\mathbf{y})n_j dA(\mathbf{y}),\ \mathbf{x}\notin A^+. \tag{7}$$

Here, $\mathbf{x}$ is the position vector of the observation point, $\sigma_{ijk}^G(\mathbf{x}-\mathbf{y})$ is the stress Green's function (Appendix A), and $\Delta u_i(\mathbf{y})$ defines the displacement jumps (crack opening displacements) across the faces of the crack.

As shown by Cruse (1975) for the static case, equation (7) will lead to a degenerate BIE formulation as $\mathbf{x}\rightarrow A^+$. A natural remedy for this difficulty is to use the representation integral for the traction components, which can be obtained by substituting equation (7) into Hooke's law and by using $f_p^{sc}=\sigma_{pq}^{sc}n_q$. The result is

$$f_p^{sc}(\mathbf{x})=-C_{pqkl}n_q(\mathbf{x})\int_{A^+}\sigma_{ijk,l}^G(\mathbf{x}-\mathbf{y})\Delta u_i(\mathbf{y})n_j dA(\mathbf{y}),\ \mathbf{x}\notin A^+. \tag{8}$$

Boundary integral equations can be derived from equation (8) by letting $\mathbf{x}\rightarrow A^+$ and by applying the boundary conditions (5). The system of boundary integral equations that is obtained in this manner is, however, hypersingular when the observation point $\mathbf{x}$ and the source point $\mathbf{y}$ coincide, since the terms $\sigma_{ijk,l}^G(\mathbf{x}-\mathbf{y})$ behave as (Appendix A)

$$\sigma_{ijk,l}^G(\mathbf{x}-\mathbf{y})\sim\begin{cases}\dfrac{1}{r^2}, & \text{two-dimensional,}\\ & \qquad\qquad \text{as } r\rightarrow 0,\\ \dfrac{1}{r^3}, & \text{three-dimensional,}\end{cases} \tag{9}$$

where $r=|\mathbf{x}-\mathbf{y}|$. These higher-order singularities prevent a reliable direct numerical solution of equation (8).

To overcome these difficulties Budiansky and Rice (1979) used partial integration to reduce the higher-order singularities, and to derive a system of BIE's for a flat crack in the plane $x_3=0$ (see Fig. 1). Regularization procedures have also been proposed by Sládek and Sládek (1984), by

Nishimura and Kobayashi (1987), and by Budreck and Achenbach (1988).

For a two-dimensional crack configuration, analogous formulations have been proposed by Tan (1975), by Schmerr (1982), and by Zhang and Achenbach (1988). The corresponding elastostatic crack analysis using BIE methods has been presented by Cruse (1975) and Weaver (1977). A comprehensive discussion and an extensive list of references have been given by Cruse (1987).

All the studies mentioned previously have used partial integration to reduce the higher-order singularities (9). This procedure is easily implemented for flat or straight cracks, but it becomes quite cumbersome for curved cracks. In this paper, we will present a new BIE formulation which follows very naturally from a path-independent integral, and which has lower-order singularities than the ones obtained in the conventional BIE formulation.

3 The $\tilde{J}_k$ Integral and Related BIE's

In elastostatics the J_k integral has the form (Eshelby, 1951, Rice, 1968)

$$J_k = \int_S (W\delta_{jk} - \sigma_{ij}u_{i,k})n_j dS, \tag{10}$$

where S is the surface of a body with volume V, n_j is the outward normal vector, and W is the elastic strain energy density

$$W = \frac{1}{2}\sigma_{ij}\epsilon_{ij}. \tag{11}$$

The integral J_k, which vanishes if there are no body forces and singularities present in V, is usually referred to as a path-independent integral or a conservation law. The application of the J_1 component as a relevant crack-tip parameter in linear and nonlinear fracture mechanics has been well established (see Moran and Shih, 1987). It can easily be shown that $J_k = 0$, by applying the divergence theorem, by using

$$\sigma_{ij} = \frac{\partial W}{\partial \epsilon_{ij}}, \tag{12}$$

and by employing the equilibrium equations $\sigma_{ij,j} = 0$. The generalization of J_k to time-harmonic elastodynamics, which is denoted by $\tilde{J}_k$, can be written as

$$\tilde{J}_k = \int_S [(W+L)\delta_{jk} - \sigma_{ij}u_{i,k}]n_j dS, \tag{13}$$

where L is the kinetic energy density

$$L = \frac{1}{2}\rho\ddot{u}_i u_i = -\frac{1}{2}\rho\omega^2 u_i u_i. \tag{14}$$

Here also $\tilde{J}_k = 0$, under the same assumptions as for J_k. The proof is again very simple if we apply the divergence theorem, use equation (12) and employ the equations of motion (1). We note that $\tilde{J}_k = 0$ holds for any time-harmonic elastodynamic state which satisfies equations (1)–(3).

Now let us consider two independent time-harmonic elastodynamic states for the same body:

$$u_i^{(1)},\ \epsilon_{ij}^{(1)},\ \sigma_{ij}^{(1)} \tag{15}$$

$$u_i^{(2)},\ \epsilon_{ij}^{(2)},\ \sigma_{ij}^{(2)} \tag{16}$$

These states satisfy the equations of motion (1), the strain-displacement equation (2), and Hooke's law (3). By virtue of linear superposition, the sum of (15) and (16)

$$u_i = u_i^{(1)} + u_i^{(2)},\ \epsilon_{ij} = \epsilon_{ij}^{(1)} + \epsilon_{ij}^{(2)},\ \sigma_{ij} = \sigma_{ij}^{(1)} + \sigma_{ij}^{(2)}, \tag{17}$$

also satisfies equations (1)–(3). Substitution of (17) into (13) yields

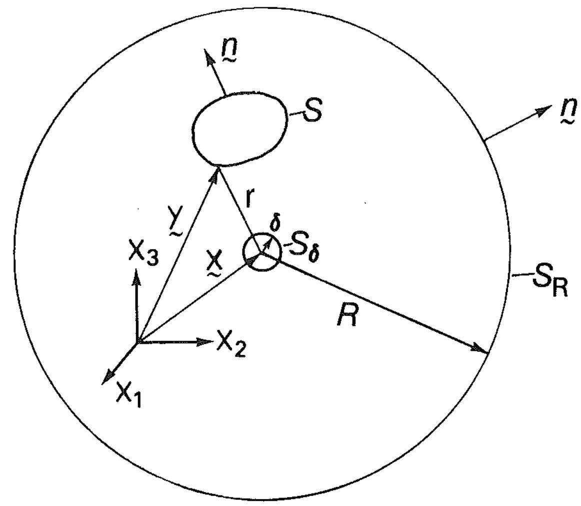

Fig. 2 A scatterer in an unbounded solid

$$\tilde{J}_k[u_i] = \tilde{J}_k[u_i^{(1)}] + \tilde{J}_k[u_i^{(2)}]$$

$$+ \int_S [(u^{(1)}_{m,n}\sigma^{(2)}_{mn} - \rho\omega^2 u_i^{(1)}u_i^{(2)})\delta_{jk} - u^{(1)}_{i,k}\sigma^{(2)}_{ij} - \sigma^{(1)}_{ij}u^{(2)}_{i,k}]n_j dS. \tag{18}$$

Clearly, the terms $\tilde{J}_k[u_i^{(1)}]$ and $\tilde{J}_k[u_i^{(2)}]$ must vanish because $u_i^{(1)}$ and $u_i^{(2)}$ are two independent elastodynamic states. Since $\tilde{J}_k\ [u_i] = 0$ we therefore conclude that

$$\int_S [cu^{(1)}_{m,n}\sigma^{(2)}_{mn} - \rho\omega^2 u_i^{(1)}u_i^{(2)})\delta_{jk} - u^{(1)}_{i,k}\sigma^{(2)}_{ij} - \sigma^{(1)}_{ij}u^{(2)}_{i,k}]n_j dS = 0. \tag{19}$$

Equation (19) is an extension of the two-state conservation integrals proposed by Chen and Shield (1977) for elastostatics ($\omega \to 0$). The first state is now taken to be the unknown field

$$\{u_i^{(1)},\ \sigma_{ij}^{(1)}\} = \{u_i^{sc},\ \sigma_{ij}^{sc}\}, \tag{20}$$

while the second state is selected as the fundamental solution due to a unit point force

$$\{u_i^{(2)},\ \sigma_{ij}^{(2)}\} = \{u^G_{il}a_l,\ \sigma^G_{ijl}\}, \tag{21}$$

where u^G_{il} and σ^G_{ijl} are three-dimensional time-harmonic elastodynamic Green's functions (see Appendix A), and a_l indicates the directions of the applied point force. Application of (19) to the surfaces S, S_δ, and S_R (Fig. 2), and use of the equations (20) and (21) results in

$$-\int_S I_{lk}(\mathbf{x};\mathbf{y})dS(\mathbf{y}) + \int_{S_\delta} I_{lk}(\mathbf{x};\mathbf{y})dS(\mathbf{y})$$

$$+ \int_{S_R} I_{lk}(\mathbf{x};\mathbf{y})dS(\mathbf{y}) = 0, \tag{22}$$

where S is the surface of the scatterer, S_δ is the surface of a sphere of radius δ, centered at $\mathbf{x}$, and S_R is the surface of a sphere with radius R, centered at $\mathbf{x}$, as shown in Fig. 2. The surface S is assumed to be closed, regular, and smooth. The small sphere (radius δ) is selected to exclude the singularities in the Green's functions, and the sphere with radius R must be sufficiently large so that the scatterer S and the sphere S_δ are included in it. The integrand I_{lk} in (22) is given by

$$I_{lk}(\mathbf{x};\mathbf{y}) = \{[u^{sc}_{m,n}(\mathbf{y})\sigma^G_{mnl}(\mathbf{x}-\mathbf{y}) - \rho\omega^2 u_i^{sc}(\mathbf{y})u^G_{il}(\mathbf{x}-\mathbf{y})]\delta_{jk}$$

$$- u^{sc}_{i,k}(\mathbf{y})\sigma^G_{ijl}(\mathbf{x}-\mathbf{y}) - \sigma^{sc}_{ij}(\mathbf{y})u^G_{il,k}(\mathbf{x}-\mathbf{y})\}n_j, \tag{23}$$

in which $\mathbf{x}$ represents the position vector of the observation point, and $\mathbf{y}$ represents the position vector of the source point, respectively.

After elementary calculations the second integral in equation (22) can be evaluated as

$$\int_{S_\delta} I_{lk}(\mathbf{x};\mathbf{y})dS(\mathbf{y}) = -u^{sc}_{l,k}(\mathbf{x}), \text{ as } \delta \to 0. \tag{24}$$

By using the asymptotic expansions of the Green's functions for large $|\mathbf{y}|$ (Appendix B), the last integral in equation (22) can be rewritten in the following form

$$\int_{S_R} I_{lk}(\mathbf{x};\mathbf{y})dS(\mathbf{y}) = -\frac{ik_L}{\lambda+2\mu}\frac{\exp(ik_LR)}{4\pi R}\int_{S_R}$$

$$\times\{[\sigma^{sc}_{ij}n_j - i(\lambda+2\mu)k_L u^{sc}_i]n_i\}$$

$$\times n_l n_k \exp(-ik_L\mathbf{n}\cdot\mathbf{x})dS(\mathbf{y}) -$$

$$-\frac{ik_T}{\mu}\frac{\exp(ik_TR)}{4\pi R}\int_{S_R}\{(\sigma^{sc}_{ij}n_j - i\mu k_T u^{sc}_i)$$

$$\times(\delta_{il} - n_i n_l)n_k\}\exp(-ik_T\mathbf{n}\cdot\mathbf{x})dS(\mathbf{y}). \tag{25}$$

Applying the Cauchy-Schwartz inequality

$$\left|\int_{S_R} f(\mathbf{y})dS(\mathbf{y})\right| \le \left(\int_{S_R} dS(\mathbf{y})\right)^{1/2}\left(\int_{S_R}\left|f(\mathbf{y})\right|^2 dS(\mathbf{y})\right)^{1/2}$$

$$= 2\sqrt{\pi}R\left(\int_{S_R}\left|f(\mathbf{y})\right|^2 dS(\mathbf{y})\right)^{1/2}, \tag{26}$$

and considering the following elastodynamic radiation conditions (see Tan, 1975; Achenbach, 1982),

$$\lim_{R\to\infty}\int_{S_R}\left|[\sigma^{sc}_{ij}n_j - i(\lambda+2\mu)k_L u^{sc}_i]n_i\right|^2 dS(\mathbf{y}) = 0, \tag{27}$$

$$\lim_{R\to\infty}\int_{S_R}\left|\sigma^{sc}_{ij}n_j - i\mu k_T u^{sc}_i)(\delta_{il} - n_i n_l)\right|^2 dS(\mathbf{y}) = 0, \tag{28}$$

we obtain

$$\int_{S_R} I_{lk}(\mathbf{x};\mathbf{y})dS(\mathbf{y}) = 0, \text{ as } R\to\infty. \tag{29}$$

Thus, equation (22) is reduced to

$$u^{sc}_{l,k}(\mathbf{x}) = -\int_S\{[u^{sc}_{m,n}(\mathbf{y})\sigma^G_{mnl}(\mathbf{x}-\mathbf{y}) - \rho\omega^2 u^{sc}_i(\mathbf{y})u^G_{il}(\mathbf{x}-\mathbf{y})]\delta_{jk} -$$

$$-u^{sc}_{i,k}(\mathbf{y})\sigma^G_{ijl}(\mathbf{x}-\mathbf{y}) - \sigma^{sc}_{ij}(\mathbf{y})u^G_{il,k}(\mathbf{x}-\mathbf{y})\}n_j dS(\mathbf{y}),$$

$$\mathbf{x}\notin S. \tag{30}$$

Substitution of equation (30) into Hooke's law leads to the following representation integral for the traction components at $\mathbf{x}$

$$f^{sc}_p(\mathbf{x}) = -C_{pqlk}n_q(\mathbf{x})\int_S\{[u^{sc}_{m,n}(\mathbf{y})\sigma^G_{mnl}(\mathbf{x}-\mathbf{y})$$

$$-\rho\omega^2 u^{sc}_i(\mathbf{y})u^G_{il}(\mathbf{x}-\mathbf{y})]\delta_{jk} -$$

$$-u^{sc}_{i,k}(\mathbf{y})\sigma^G_{ijl}(\mathbf{x}-\mathbf{y}) - \sigma^{sc}_{ij}(\mathbf{y})u^G_{il,k}(\mathbf{x}-\mathbf{y})\}n_j dS(\mathbf{y}), \ \mathbf{x}\notin S. \tag{31}$$

Equation (31) is a generalization of Hu's results for elastostatics (1987).

Application of equation (31) to a three-dimensional crack yields

$$f^{sc}_p(\mathbf{x}) = -C_{pqlk}n_q(\mathbf{x})\int_{A^+}\{[\Delta u_{m,n}(\mathbf{y})\sigma^g_{mnl}(\mathbf{x}-\mathbf{y})$$

$$-\rho\omega^2\Delta u_i(\mathbf{y})u^G_{il}(\mathbf{x}-\mathbf{y})]\cdot\delta_{jk}$$

$$-\Delta u_{i,k}(\mathbf{y})\sigma^G_{ijl}(\mathbf{x}-\mathbf{y})\}n_j dA(\mathbf{y}), \ \mathbf{x}\notin A^+ \tag{32}$$

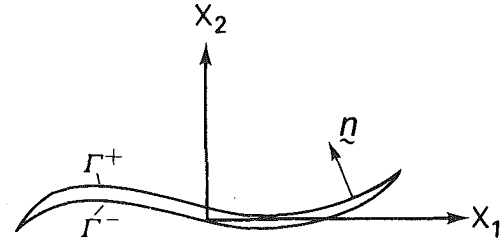

Fig. 3 A curved crack in a two-dimensional geometry

where Δu_i are the crack opening displacements and $\Delta u_{i,k}$ are their derivatives with respect to y_k. The last term of equation (31) disappears because of the continuity of $\sigma_{ij}n_j$ across the crack faces. BIE's are obtained by letting $\mathbf{x}\to A^+$ as

$$f^{in}_p(\mathbf{x}) = C_{pqlk}n_q(\mathbf{x})\int_{A^+}\{[\Delta u_{m,n}(\mathbf{y})\sigma^G_{mnl}(\mathbf{x}-\mathbf{y})$$

$$-\rho\omega^2\Delta u_i(\mathbf{y})u^G_{il}(\mathbf{x}-\mathbf{y})]\cdot\delta_{jk}$$

$$-\Delta u_{i,k}(\mathbf{y})\sigma^G_{ijl}(\mathbf{x}-\mathbf{y})\}n_j dA(\mathbf{y}), \ \mathbf{x}\epsilon A^+. \tag{33}$$

The integral of (33) is understood in the sense of Cauchy principal values. No extra discontinuity terms enter (33) as $\mathbf{x}\to A^+$. Equation (33) is valid for a three-dimensional crack of arbitrary shape. The corresponding BIE's for a two-dimensional crack in plane strain and antiplane strain can be derived directly from (33). For plane strain we obtain

$$f^{in}_\alpha(\mathbf{x}) = C_{\alpha\beta\gamma\epsilon}n_\beta(\mathbf{x})\int_{\Gamma^+}\{[\Delta u_{\xi,\eta}(\mathbf{y})\sigma^g_{\xi\eta\gamma}(\mathbf{x}-\mathbf{y}) - \rho\omega^2\Delta u_\delta(\mathbf{y}).$$

$$u^g_{\delta\gamma}(\mathbf{x}-\mathbf{y})]\delta_{\lambda\epsilon} - \Delta u_{\mu,\epsilon}(\mathbf{y})\sigma^g_{\mu\lambda\gamma}(\mathbf{x}-\mathbf{y})\}n_\lambda ds(\mathbf{y}), \ \mathbf{x}\epsilon\Gamma^+, \tag{34}$$

while for antiplane strain we find

$$f^{in}_3(\mathbf{x}) = \mu\int_{\Gamma^+}\{[\Delta u_{3,\alpha}(\mathbf{y})\sigma^g_{3\alpha3}(\mathbf{x}-\mathbf{y})$$

$$-\rho\omega^2\Delta u_3(\mathbf{y})u^g_{33}(\mathbf{x}-\mathbf{y})]\delta_{\beta\gamma}$$

$$-\Delta u_{3,\beta}(y)\sigma^g_{3\gamma3}(\mathbf{x}-\mathbf{y})\}n_\gamma ds(\mathbf{y}), \ \mathbf{x}\epsilon\Gamma^+. \tag{35}$$

Here Γ^+ denotes the insonified side of the two-dimensional crack (see Fig. 3) and the superscript "g" represents the two-dimensional Green's functions (Appendix A). All integrals of (34) and (35) are understood as Cauchy principal values.

The BIE's (33) (as well as (34) and (35)) have the advantage over the conventional BIE formulation, i.e., equation (8), that no higher-order singularities appear. The unknown boundary quantities in the new formulation are the crack opening displacements and their derivatives, where the latter have the physical meanings of dislocation densities. We note also that the procedure in deriving (33) is very natural, and no elaborate manipulations, such as integration by parts, have been used. The BIE's stated here apply also to elastostatic crack analysis by letting $\omega\to 0$, and by using the corresponding elastostatic fundamental solution (Kelvin solution). For the static case, the term containing Δu_i disappears in the BIE's, and the only unknown quantities are the dislocation densities. The new formulation allows an immediate numerical implementation. When Δu_i has been computed, equation (7) can be employed to calculate the displacement field.

As pointed out by Carlsson (1974), Bui (1977), and Moran and Shih (1987), there exists a complementary integral to J_k which is also path independent. For time-harmonic elastodynamics, the complementary integral may be stated as

$$\bar{J}^c_k = \int_S[(W^c + L^c)\delta_{jk} - \sigma_{ij,k}u_i]n_j dS = 0, \tag{36}$$

where W^c and L^c are defined by the Legendre transformation

$$W^c = \sigma_{ij}\epsilon_{ij} - W, \tag{37}$$

$$L^c = \rho\ddot{u}_i u_i - L. \tag{38}$$

The assumptions in deriving (36) are the same as for $\tilde{J}_k$. The proof of equation (36) can be performed directly by using the divergence theorem, by considering the relation

$$\epsilon_{ij} = \frac{\partial W^c}{\partial \sigma_{ij}}, \tag{39}$$

and by employing equation (1).

Following the same procedure as in deriving equation (31), a novel representation integral for the scattered traction components $f_p^{sc}(\mathbf{x})$ is obtained from (36) as

$$f_p^{sc}(\mathbf{x}) = -C_{pqlk}n_q(\mathbf{x})\int_S \{[u_{m,n}^{sc}(\mathbf{y})\sigma_{mnl}^G(\mathbf{x}-\mathbf{y}) - \rho\omega^2 u_i^{sc}(\mathbf{y})u_{il}^G(\mathbf{x}-\mathbf{y})]\delta_{jk} - \sigma_{ij,k}^{sc}(\mathbf{y})u_{il}^G(\mathbf{x}-\mathbf{y}) - u_i^{sc}(\mathbf{y})\sigma_{ijl,k}^G(\mathbf{x}-\mathbf{y})\}n_j dS(\mathbf{y}),\ \mathbf{x}\notin S. \tag{40}$$

Corresponding BIE's can be derived by applying equation (40) to the crack faces and by letting $\mathbf{x} \rightarrow A$, taking into account the boundary conditions (5). Such BIE's are, however, again highly singular due to the presence of the term $\sigma_{ijl,k}^G(\mathbf{x}-\mathbf{y})$. Hence, equation (40) has no advantages over the conventional formulation given by equation (8).

4 Examples

In this section we will apply the BIE's (33) (as well as (34) and (35)), which are valid for arbitrary shaped cracks, to some simple cases. We first consider three-dimensional analysis for a flat crack in an unbounded body subjected to an incident time-harmonic wave. The crack is located in the plane $x_3 = 0^{\pm}$. Hence, $n_1 = n_2 = 0$, and $n_3 = 1$. The BIE's (33) separate into two decoupled equations:

$$\sigma_{33}^{in}(x_1,x_2,0) = \int_{A^+} \{[(\lambda+2\mu)\sigma_{\alpha 33}^G(\mathbf{x}-\mathbf{y}) - \lambda\sigma_{33\alpha}^G(\mathbf{x}-\mathbf{y})]\Delta u_{3,\alpha}(\mathbf{y}) - \rho\omega^2(\lambda+2\mu)u_{33}^G(\mathbf{x}-\mathbf{y})\Delta u_3(\mathbf{y})\}dA(\mathbf{y}),\ \mathbf{x}\epsilon A^+, \tag{41}$$

$$\sigma_{\beta 3}^{in}(x_1,x_2,0) = \mu\int_{A^+} \{[\sigma_{\alpha\gamma\beta}^G(\mathbf{x}-\mathbf{y}) - \sigma_{\alpha 33}^G(\mathbf{x}-\mathbf{y})\delta_{\beta\gamma}]\Delta u_{\alpha,\gamma}(\mathbf{y}) - \rho\omega^2 u_{\alpha\beta}^G(\mathbf{x}-\mathbf{y})\Delta u_\alpha(\mathbf{y})\}dA(\mathbf{y}),\ \mathbf{x}\epsilon A^+, \alpha,\beta = 1,2, \tag{42}$$

where σ_{33}^{in} and $\sigma_{\beta 3}^{in}$ are stress components corresponding to the incident wave. We note that equation (41) is for the normal crack opening displacement Δu_3, while equation (42) is for the transverse crack opening displacements Δu_α. Equations (41) and (42) have exactly the same forms as those derived by Budiansky and Rice (1979), who used the conventional formulation in conjunction with partial integration.

BIE's for three-dimensional analysis of a flat crack under static surface loading $\sigma_{33}(x_1, x_2, 0)$ and $\sigma_{\beta 3}(x_1, x_2, 0)$ can be obtained from (41) and (42) by letting $\omega \rightarrow 0$ and by employing the corresponding static fundamental solutions. The result is

$$\sigma_{33}(x_1 x_2,0) = \frac{\mu}{4\pi(1-\nu)}\int_{A^+} \frac{r_{,\alpha}}{r^2}\Delta u_{3,\alpha}(\mathbf{y})dA(\mathbf{y}),\ \mathbf{x}\epsilon A^+, \tag{43}$$

$$\sigma_{\beta 3}(x_1 x_2,0) = \frac{\mu}{8\pi(1-\nu)}\int_{A^+} \frac{1}{r^2}\{(1-2\nu)[\delta_{\alpha\beta}r_{,\gamma} - \delta_{\alpha\gamma}r_{,\beta}] + 3r_{,\alpha}r_{,\beta}r_{,\gamma}\}\Delta u_{\alpha,\gamma}(\mathbf{y})dA(\mathbf{y}),\ \mathbf{x}\epsilon A^+. \tag{44}$$

Here $r = |\mathbf{x}-\mathbf{y}|$, and ν denotes Poisson's ratio. Equations (43) and (44) are identical to the equations stated by Weaver (1977).

Next, we consider two-dimensional analysis for a straight crack for states of deformation in plane strain and antiplane strain. The crack is defined by $x_2 = 0^{\pm}$, $|x_1| \le a$. For the case of plane strain, the BIE's (34) become

$$\sigma_{12}^{in}(x_1,0) = \mu\int_{-a}^{a} \{[\sigma_{111}^g(\mathbf{x}-\mathbf{y}) - \sigma_{122}^g(\mathbf{x}-\mathbf{y})]\Delta u_{1,1}(y_1) - \rho\omega^2 u_{11}^g(\mathbf{x}-\mathbf{y})\Delta u_1(y_1)\}dy_1,\ |x_1| \le a, \tag{45}$$

$$\sigma_{22}^{in}(x_1,0) = \int_{-a}^{a} \{[(\lambda+2\mu)\sigma_{112}^g(\mathbf{x}-\mathbf{y}) - \lambda\sigma_{221}^g(\mathbf{x}-\mathbf{y})]\Delta u_{2,1}(y_1) - \rho\omega^2(\lambda+2\mu)u_{22}^g(\mathbf{x}-\mathbf{y})\Delta u_2(y_1)\}dy_1,\ |x_1| \le a, \tag{46}$$

while for antiplane strain equation (35) takes the following form

$$\sigma_{32}^{in}(x_1,0) = \mu\int_{-a}^{a} \{[\sigma_{313}^g(\mathbf{x}-\mathbf{y})\Delta u_{3,1}(y_1) - \rho\omega^2 u_{33}^g(\mathbf{x}-\mathbf{y})\Delta u_3(y_1)\}dy_1,\ |x_1| \le a. \tag{47}$$

The BIE's (45) and (46) have been derived by Tan (1975) via the conventional formulation. For plane-strain deformation, the BIE for the normal crack opening displacement, Δu_2 (Mode I), decouples from the one for the transverse crack opening displacement, Δu_1 (Mode II). For a two-dimensional crack under static loading $\sigma_{12}(x_1,0)$, $\sigma_{22}(x_1,0)$, and $\sigma_{32}(x_1,0)$, we obtain from (45) and (46)

$$\sigma_{12}(x_1,0) = \frac{\mu}{2\pi(1-\nu)}\int_{-a}^{a} \frac{\Delta u_{1,1}}{x_1 - y_1}dy_1,\ |x_1| \le a, \tag{48}$$

$$\sigma_{22}(x_1,0) = \frac{\mu}{2\pi(1-\nu)}\int_{-a}^{a} \frac{\Delta u_{2,1}}{x_1 - y_1}dy_1,\ |x_1| \le a, \tag{49}$$

for plane strain, and from (47)

$$\sigma_{32}(x_1,0) = \frac{1}{2\pi}\int_{-a}^{a} \frac{\Delta u_{3,1}}{x_1 - y_1}dy_1,\ |x_1| \le a, \tag{50}$$

for antiplane strain. Equations (48)–(49) are integral equations for dislocation densities, and they are again well known (see Mura, 1987).

The BIE's presented here must, in general, be solved numerically. Special care must be taken in the numerical implementation to account for the local behavior of Δu_i and $\Delta u_{i,j}$ near the crack edges, and for the singularities of the Green's functions at $\mathbf{x} = \mathbf{y}$. For two-dimensional analysis of cracks subjected to static loading the method developed by Erdogan et al. (1973) has been frequently used, while Zhang and Achenbach (1988) solved the modified BIE's of (45) and (46) numerically for time-harmonic wave scattering problems. For three-dimensional analysis of a flat crack, numerical methods have been proposed by Polch et al. (1987) for the static case, and by Nishimura and Kobayashi (1987) for the dynamic case.

5 Concluding Comments

A novel application of an elastodynamic conservation integral, the $\tilde{J}_k$ integral, to elastodynamic and elastostatic crack analysis has been presented. Boundary integral equations follow from $\tilde{J}_k$ in a direct and natural way. These equations immediately have lower-order singularities than the ones obtained in the conventional manner by the use of the Betti-Rayleigh reciprocity integral. This is an important advantage for the development of a numerical procedure for solving the BIE's, and for an accurate calculation of the strains and stresses at internal points close to the crack faces. For three-dimensional or two-dimensional analysis of cracks of arbitrary shapes the BIE's presented here have simple forms, and they do not require integration by parts, as in the conventional formulation. In the dynamic case, the unknown quantities are the crack opening displacements and their derivatives (dislocation densities), while the static case only the dislocation densities appear in the formulation. Thus, higher-order shape functions for Δu_i are desirable in the dynamic case. The complementary conservation integral $\tilde{J}_k^c$ gives rise to more singular BIE's which offer no advantages over the conventional equations.

The representation integral for the traction components, equation (32), can be used to derive BIE's for general boundary value problems (not necessary cracks) of time-harmonic elastodynamic or elastostatics. The advantages and drawbacks of this approach compared to the conventional formulation have been discussed in the paper by Hu (1987).

As pointed out by Hu (1987), new BIE's can be derived from other conservation integrals. Following essentially the same procedure as described in Section 3, the present authors have obtained another set of representation formulas for combinations of $u_i(\mathbf{x})$ and $u_{i,j}(\mathbf{x})$ from the well-known M and L_k integrals (see Knowles and Sternberg (1972), Budiansky and Rice (1973)). The significance of these representation formulas and their associated BIE's for solving boundary value problems is under investigation.

Acknowledgment

This paper was prepared in the course of research sponsored by the Office of Naval Research under Contract N00014-85-K-0401 with Northwestern University.

References

Achenbach, J. D., 1973, *Wave Propagation in Elastic Solids*, North-Holland, Amsterdam/New York.

Achenbach, J. D., Gautesen, A. K., and McMaken, H., 1982, *Ray Methods for Waves in Elastic Solids*, Pitman, Boston.

Budiansky, B., and Rice, J. R., 1973, "Conservation Laws and Energy-Release Rates," ASME Journal of Applied Mechanics, Vol. 40, pp. 201–203.

Budiansky B., and Rice, J. R. 1979, "An Integral Equation for Dynamic Elastic Response of an Isolated 3-D Crack," *Wave Motion*, Vol. 1, pp. 187–192.

Budreck, D. E., and Achenbach, J. D., 1988, "Scattering From Three-Dimensional Planar Cracks by the Boundary Integral Equation Method," ASME Journal of Applied Mechanics, Vol. 55, pp. 405–412.

Bui, H. D., 1974, "Dual Path Independent Integrals in the Boundary-Value Problems of Cracks," *Engng. Fract. Mech.*, Vol. 6, pp. 287–296.

Carlsson, A. J., 1974, "Path Independent Integrals in Fracture Mechanics and Their Relation to Variational Principles," *Prospects in Fracture Mechanics*, G. C. Sih, et al. eds., Leyden, Noordhoff, pp. 139–158.

Chen, F. H. K., and Shield, R. T. 1977, "Conservation Laws in Elasticity of the J-Integral Type," *ZAMP*, Vol. 28, pp. 1–22.

Cruse T. A., 1969, "Numerical Solutions in Three-Dimensional Elastostatics," *Int. J. Solids Structures*, Vol. 5, pp. 1259–1274.

Cruse, T. A., 1975, "Boundary-Integral Equation Method for Three-Dimensional Elastic Fracture Mechanics Analysis," Report No. AFOSR-TR-75-0813, Accession No. ADA01160, pp. 13–20.

Cruse, T. A., 1987, "Fracture Mechanics," *Boundary Element Methods in Mechanics*, D. E. Beskos, ed., North Holland, pp. 333–365.

Erdogan, F., Gupta, G. D., and Cook, T. S. 1973, "Numerical Solution of Integral Equations," *Mechanics of Fracture, Methods of Analysis and Solutions of Crack Problems*, G. C. Sih, ed., Leyden, Noordhoff, pp. 368–425.

Eshelby, J. D., 1951, "The Force on an Elastic Singularity," *Phil. Trans. Roy. Soc.*, Vol. A244, pp. 87–112.

Hu, Haichang, 1987, "A New Type of Boundary Integral Equation in Elasticity," *Scientia Sinica* (Series A), Vol. 30, No. 4, pp. 385–390.

Knowles, J. K., and Sternberg, E., 1972, "On a Class of Conservation Laws in Linearized and Finite Elastostatics," *Arch. Rat. Mech. Anal.*, Vol. 44, pp. 187–211.

Moran, B., and Shih, C. F., 1987, "Crack Tip and Associated Domain Integrals from Momentum and Energy Balance," *Engng. Fract. Mech.*, Vol. 27, pp. 615–642.

Moran, B., and Shih, C. F., 1987, "A General Treatment of Crack Tip Contour Integrals," *Int. J. Fracture*, Vol. 35, pp. 295–310.

Mura, T., 1987, *Micromechanics of Defects in Solids*, 2nd rev. ed., Martinus Nijhoff Publishers.

Nishimura, N., and Kobayashi, S., 1987, "An Improved Boundary Integral Equation Method for Crack Problems," *Proc. IUTAM Symposium on Advanced Boundary Element Methods*, T. A. Cruse ed., Springer, 1987.

Polch, E. Z., Cruse, T. A., and Huang, C. F., 1987, "Traction BIE Solutions for Flat Cracks," *Comput. Mech.*, Vol. 2, pp. 253–267.

Rice, J. R., 1968, "A Path Independent Integral and the Approximate Analysis of Strain Concentration by Notches and Cracks," ASME Journal of Applied Mechanics, Vol. 35, pp. 379–386.

Rizzo, F. J., 1967, "An Integral Equation Approach to Boundary Value Problems of Classical Elastostatics," *Quart. Appl. Mathematics*, Vol. 25, pp. 83–95.

Schmerr, L. W., 1982, "The Scattering of Elastic Waves by Isolated Cracks Using a New Integral Equation Model," *Review of Progress in Quantitative Nondestructive Evaluation*, Vol. 1, D. O. Thompson and D. E. Chimenti, eds., Plenum Press, New York, pp. 511–515.

Sládek, V., and Sládek, J., 1984, "Transient Elastodynamic Three-Dimensional Problems in Cracked Bodies," *Appl. Math. Modelling*, Vol. 8, pp. 2–10.

Tan, T. H., 1975, *Diffraction Theory for Time-Harmonic Elastic Waves*, Doctoral Dissertation, Delft University of Technology.

Weaver, J., 1977, "Three-Dimensional Crack Analysis," *Int. J. Solids Structures*, Vol. 13, pp. 321–330.

Zhang, Ch., and Achenbach, J. D., 1988, "Scattering by Multiple Crack Configurations," ASME Journal of Applied Mechanics, Vol. 55, pp. 104–110.

APPENDIX A

Green's Functions

The Green's function for the three-dimensional elastodynamic state is given by (see Tan, 1975; Achenbach et al., 1982)

$$u_{ik}^G(\mathbf{x}-\mathbf{y}) = \frac{1}{4\pi\rho\omega^2}\left[\frac{\exp(ik_T r)}{r} - \frac{\exp(ik_L r)}{r}\right]_{,ik} + \frac{\exp(ik_T r)}{4\pi\mu r}\delta_{ik}, \quad (A1)$$

where

$$r = |\mathbf{x}-\mathbf{y}|. \quad (A2)$$

The function $u_{ik}^G(\mathbf{x}-\mathbf{y})$ denotes the displacement in the i-direction observed at position $\mathbf{x}$ due to a unit force in the k-direction, applied at position $\mathbf{y}$. The corresponding components of the stress tensor follow from Hooke's law

$$\sigma_{ijk}^G = C_{ijmn} u_{mk,n}^G. \quad (A3)$$

Similarly, the Green's functions for the two-dimensional plane strain and antiplane strain time-harmonic elastodynamic states are

$$u_{\alpha\gamma}^g(\mathbf{x}-\mathbf{y}) = \frac{i}{4\rho\omega^2}\Big\{[H_o^{(1)}(k_T r) - H_o^{(1)}(k_L r)]_{,\alpha\gamma} + k_T^2\delta_{\alpha\gamma}H_o^{(1)}(k_T r)\Big\}, \quad (A4)$$

$$u_{33}^g(\mathbf{x}-\mathbf{y}) = \frac{i}{4\mu}H_o^{(1)}(k_T r), \quad (A5)$$

respectively, where $H_o^{(1)}(\cdot)$ denotes the Hankel function of the first kind and zeroth order. Expressions for the stress components can be obtained by using

$$\sigma_{\alpha\beta\gamma}^g = C_{\alpha\beta\xi\eta}u_{\xi\gamma,\eta}^g, \quad \text{for plane strain}, \quad (A6)$$

$$\sigma_{3\alpha 3}^g = \mu u_{33,\alpha}^g, \quad \text{for antiplain strain}. \quad (A7)$$

The Kelvin solution for the three-dimensional elastostatics case may be written as

$$u_{ik}^G(\mathbf{x}-\mathbf{y}) = \frac{1}{16\pi\mu(1-\nu)r}[(3-4\nu)\delta_{ik} + r_{,i}r_{,k}], \quad (A8)$$

while for two-dimensional elastostatics we have

$$u^g_{\alpha\gamma}(\mathbf{x}-\mathbf{y}) = -\frac{1}{8\pi\mu(1-\nu)}[(3-4\nu)\delta_{\alpha\gamma}lnr - r_{,\alpha}r_{,\gamma}], \quad (A9)$$

$$u^g_{33}(\mathbf{x}-\mathbf{y}) = -\frac{1}{2\pi\mu}lnr, \quad (A10)$$

for plane strain and antiplane strain, respectively. The corresponding stress components for elastostatics follow from the equations ($A3$), ($A6$), and ($A7$).

We note that both the dynamic and the static Green's functions possess the same singularities at $r=0$, namely.

$$\left.\begin{array}{l} u^G_{ik} \sim \dfrac{1}{r} \\ \sigma^G_{ijk} \sim \dfrac{1}{r^2} \\ \sigma^G_{ijk,l} \sim \dfrac{1}{r^3} \end{array}\right\} \text{as } r \to 0, \quad (A11)$$

for the three-dimensional case, and

$$\left.\begin{array}{lll} u^g_{\alpha\beta}, & u^g_{33} & \sim lnr \\ \sigma^g_{\alpha\beta\gamma}, & \sigma^g_{3\alpha 3} & \sim \dfrac{1}{r} \\ \sigma^g_{\alpha\beta\gamma,\delta}, & \sigma^g_{3\alpha 3,\beta} & \sim \dfrac{1}{r^2} \end{array}\right\} \text{as } r \to 0, \quad (A12)$$

for two-dimensional plane strain and antiplane strain. All derivatives in the Green's functions are understood to be with respect to $\mathbf{y}$.

APPENDIX B

Asymptotic Expansions of the Elastodynamic Green's Functions

For $|\mathbf{y}| \gg |\mathbf{x}|$, the following approximation holds

$$r = |\mathbf{x}-\mathbf{y}| \simeq |\mathbf{y}| - \hat{\mathbf{y}} \cdot \mathbf{x}, \quad (B1)$$

where $\hat{\mathbf{y}}$ denotes the unit vector along $\mathbf{y}$. By using ($B1$), asymptotic expressions for the three-dimensional elastodynamic Green's functions are obtained as

$$u^G_{il}(\mathbf{x}-\mathbf{y}) \simeq \sum_{\xi=L,T} A^\xi_{il}(\hat{\mathbf{y}}) \frac{\exp(ik_\xi |\mathbf{y}|)}{4\pi |\mathbf{y}|} \exp(-ik_\xi \hat{\mathbf{y}} \cdot \mathbf{x}), \quad (B2)$$

$$u^G_{il,k} \simeq \sum_{\xi=L,T} ik_\xi B^\xi_{ilk}(\hat{\mathbf{y}}) \frac{\exp(ik_\xi |\mathbf{y}|)}{4\pi |\mathbf{y}|} \exp(-ik_\xi \hat{\mathbf{y}} \cdot \mathbf{x}), \quad (B3)$$

$$\sigma^G_{ijk}(\mathbf{x}-\mathbf{y}) \simeq \sum_{\xi=L,T} ik_\xi C^\xi_{ijk}(\hat{\mathbf{y}}) \frac{\exp(ik_\xi |\mathbf{y}|)}{4\pi |\mathbf{y}|} \exp(-ik_\xi \hat{\mathbf{y}} \cdot \mathbf{x}), \quad (B4)$$

in which

$$A^L_{il}(\hat{y}) = \hat{y}_i \hat{y}_l / (\lambda + 2\mu), \quad (B5)$$

$$A^T_{il}(\hat{\mathbf{y}}) = (\delta_{il} - \hat{y}_i \hat{y}_l)/\mu, \quad (B6)$$

$$B^L_{ilk}(\hat{\mathbf{y}}) = \hat{y}_i \hat{y}_l \hat{y}_k / (\lambda + 2\mu), \quad (B7)$$

$$B^T_{ilk}(\hat{\mathbf{y}}) = (\delta_{il} - \hat{y}_i \hat{y}_l) \hat{y}_k / \mu, \quad (B8)$$

$$C^L_{ijk}(\hat{\mathbf{y}}) = [2\kappa^{-2} \hat{y}_i \hat{y}_j + (1 - 2\kappa^{-2})\delta_{ij}] \hat{y}_k, \quad (B9)$$

$$C^T_{ijk}(\hat{\mathbf{y}}) = \delta_{ik} \hat{y}_j + \delta_{jk} \hat{y}_i - 2\hat{y}_i \hat{y}_j \hat{y}_k, \quad (B10)$$

$$\kappa = k_T / k_L. \quad (B11)$$

Also, k_L and k_T are the wave numbers of longitudinal and transverse waves, respectively.

For a large sphere of radius R (see Fig. 2), the following relations hold

$$|\mathbf{y}| \simeq R, \quad (B12)$$

$$r_{,k} = \hat{y}_k = n_k, \quad (B13)$$

where n_k is the components of the unit outward normal vector of the sphere. Substitution of equations ($B2$)–($B13$) into equations (22) and (23) yields equation (25).

A Tension Crack Impinging Upon Frictional Interfaces

Anna Dollar

Paul S. Steif
Assoc. Mem. ASME

Department of Mechanical Engineering,
Carnegie-Mellon University,
Pittsburgh, Pa. 15213

A crack impinging normally upon a frictional interface is studied theoretically. We employ a solution technique which superposes the solution of a crack in a perfectly-bonded elastic medium with a continuous distribution of dislocations which represent slippage at the frictional interface. This procedure reduces the problem to a singular integral equation which is solved numerically. Specifically, we consider the problem of an infinite sheet subjected to uniaxial tension containing a finite crack which lies normal to the tension axis and has both crack tips impinging normally on frictional interfaces. The limiting problem of a semi-infinite crack impinging on a frictional interface is considered as well. Posed as model problems for cracking in weakly bonded fiber composites, these studies reveal the effective blunting that can result when a weak interface serves to deflect a propagating crack.

Introduction

Fiber composites proposed for high-temperature applications are generally made of constituents that are relatively brittle. Futhermore, these constituents are often weakly bonded, though this depends sensitively on the fiber preparation and the processing. It has been suggested by some workers (Phillips, 1974; Prewo and Brennan, 1980) that coupling between fiber and matrix in poorly-bonded composites is by friction or mechanical interlocking. While this lack of a strong bond is detrimental to some properties such as compressive strength and transverse tensile strength, it is believed to be a significant contributor to the composite's toughness and resistance to flaws propagating normal to the fiber direction.

The following qualitative picture of the potential toughening effect has emerged. Let a crack be propagating normal to the fibers while the composite is subjected to tensile loading parallel to the fibers. At any instant, a portion of the crack front will be at a fiber-matrix interface. A weak interface offers a degree of toughening if it can deflect the crack onto the interface, instead of permitting it to propagate forwards. The potential to deflect the crack is generally couched in terms of the energy to fracture the interface relative to the energy to fracture the fiber.

In this paper we focus on composites in which the constituents are coupled by a friction-like mechanism, and we offer an explanation of the deflection process which is framed in terms of stresses, instead of energies. To do this we pose and solve a simple model problem in which a crack impinges normally upon a weak interface. The model problem shows that the frictional interface acts to eliminate the singular stresses at the crack tip. Depending on the interface characteristics, the effective blunting of the crack tip may be sufficient to entirely impede propagation of the crack. In particular, we consider a finite crack with both tips impinging on frictional interfaces, which is subjected to remote tension normal to the crack. In the limit of a very low remote load, this problem is equivalent to the crack being semi-infinite, and this case will be handled explicitly. Since the friction stress is likely to depend on the normal stress, we model the interface as characterized by a pointwise Coulomb friction law.

Finally, we mention that the problems studied here are also of interest in hydraulic fracturing. In that context, similar problems have been considered by Papadopoulous (1979), Keer (1981), and Lam and Cleary (1984), who correctly postulate blunting of the crack. The analytical treatment here goes beyond Lam and Cleary (1984) in a number of respects, including a careful treatment of the near-tip behavior, which explicitly reveals the nature of the blunting induced by frictional slip.

Problem Statement

The problem we are contemplating is shown schematically in Fig. 1. An infinite strip occupying $-2a<x<0$, is sandwiched between two half planes, occupying $x>0$ and $x<-2a$. The two half planes and the strip are homogeneous, isotropic, linear elastic solids, and all have identical moduli G and ν. A remote compression $\sigma_{xx}=-\sigma_o$ acts to press the regions together, and the interfaces at $x=-2a$ and $x=0$ are capable of slip according to a Coulomb friction law. A finite crack lies along $-2a<x<0, y=0$ and a remote tension $\sigma_{yy}=\sigma_\infty$ is acting normal to the crack. We wish to analyze the distribution of stress, and the amount and extent of slip at the interface. Note that the problem has two planes of symmetry: parallel and normal to the crack plane. Although we solve this model problem with the aim of understanding the behavior of a crack in one constituent impinging upon a second constituent, we have ignored any differences in the constituent elastic moduli. This assumption substantially simplifies the analysis presented here. Nevertheless, it should be pointed out that the consti-

Contributed by the Applied Mechanics Division of The American Society of Mechanical Engineers for publication in the Journal of Applied Mechanics.

Discussion on this paper should be addressed to the Editorial Department, ASME, United Engineering Center, 345 East 47th Street, New York, N.Y. 10017, and will be accepted until two months after final publication of the paper itself in the Journal of Applied Mechanics. Manuscript received by ASME Applied Mechanics Division, March 16, 1988; final revision, October 10, 1988.

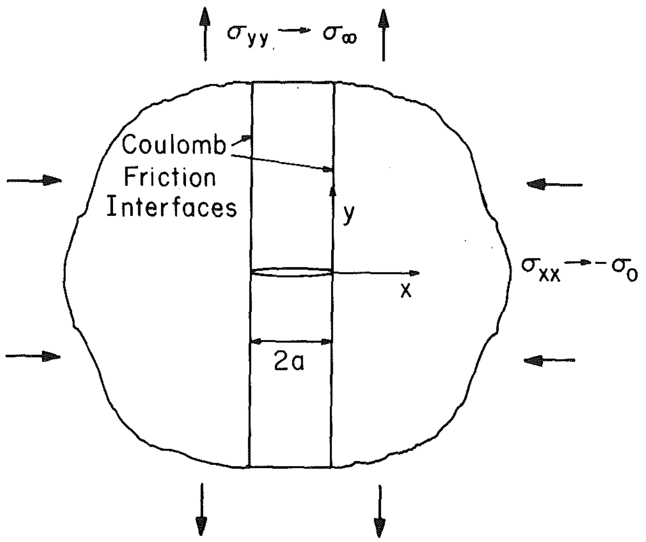

Fig. 1 Schematic of finite crack impinging on frictional interfaces

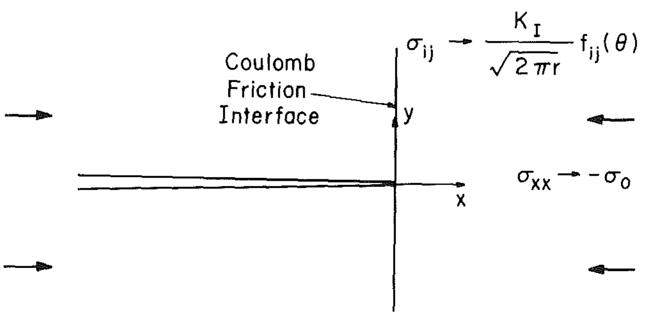

Fig. 2 Schematic of semi-infinite crack impinging on a frictional interface

tuent moduli of many composites intended for high temperature applications are not so different, at least as compared with resin-matrix composites. In addition, this allows us to focus on the effect of the interface.

As mentioned in the Introduction, a pointwise Coulomb friction interface law is employed. According to this friction law, at any instant in the loading history, either sticking, slipping, or opening occurs at a generic point along the interface. Conditions for these three states along the interface at $x=0$ are as follows:

stick condition

$$\sigma<0,\ |\tau|<\mu\,|\sigma|, \frac{dg}{dt}=0, h=\frac{dh}{dt}=0 \tag{1a}$$

slip condition

$$\sigma<0,\ |\tau|=\mu\,|\sigma|,\ \mathrm{sgn}\left(\frac{dg}{dt}\right)=\mathrm{sgn}(\tau),\ h=\frac{dh}{dt}=0 \tag{1b}$$

open condition

$$\sigma=\tau=0, h>0 \tag{1c}$$

with

$$\sigma=\sigma_{xx} \qquad \tau=\sigma_{xy}$$

$$g=\lim_{\epsilon\to 0^+}\left[v(\epsilon,y)-v(-\epsilon,y)\right]$$

$$h=\lim_{\epsilon\to 0^+}\left[u(\epsilon,y)-u(-\epsilon,y)\right].$$

In these equations u and v denote the x- and y-components of displacement, respectively, μ is the friction coefficient which is assumed to be constant along the interface, and $d(\ )/dt$ denotes the derivative with respect to a time-like parameter that increases monotonically as loading proceeds. The condition $\mathrm{sgn}(dg/dt)=\mathrm{sgn}(\tau)$ is the condition of positive energy dissipation which dictates that the instantaneous increment of slip be in the same direction as the shear stress. Note that we ignore the distinction between static and kinetic friction.

The limiting case of a semi-infinite crack is shown schematically in Fig. 2. We refer to this problem as the "small-scale slipping" problem, in analogy with elastic-plastic fracture mechanics, since it is an appropriate formulation of the problem when the slip length is small compared with the crack length. Again, a remote compressive stress $\sigma_{xx}=-\sigma_o$ is applied pressing the half planes together. Remote from the crack tip, the Mode I elastic singular field is applied with stress intensity factor K_I. (The legitimacy of this remote field in the presence of the interface is justified next.) This means that the remote stresses are of the form

$$\sigma_{ij}=\frac{K_I}{\sqrt{2\pi r}}f_{ij}(\theta)-\sigma_o\delta_{i1}\delta_{j1}$$

where r and θ denote radial and angular coordinates centered at the crack tip, subscripts i and j denote Cartesian components, and $f_{ij}(\theta)$ are the standard angular variations at a crack tip in a homogeneous, isotropic, linear elastic medium (see, for example, Rice (1968)).

Near-Tip Analysis

As will be seen below, there is a range of friction coefficients for which the interface in the vicinity of the crack tip undergoes slip, but does not open. (It is important to note that we will refer to the interface opening (or not opening), as well as the crack opening. The "interface" refers to the lines $x=-2a$ and $x=0$; the "crack" refers to $-2a<x<0, y=0$.) Thus, it is necessary to understand the effect of frictional slip on the stress fields in the neighborhood of the crack tip. The asymptotic behavior of the stresses at the crack tip is one example of the general problem of a composite wedge, which has been studied extensively by a number of authors (see Dempsey and Sinclair (1981) for a review and a list of references). In this instance, we have wedges of identical materials, one containing a crack, which share a frictional interface (see Fig. 3(a)).

We look for solutions to the biharmonic equation of two-dimensional elasticity, which feature an Airy's stress function χ of the form

$$\chi=r^{2-\lambda}p(\theta,\lambda).$$

The function χ is related to the polar components of stress and displacement according to

$$\sigma_{rr}=\frac{1}{r}\frac{\partial\chi}{\partial r}+\frac{1}{r^2}\frac{\partial^2\chi}{\partial\theta^2} \qquad \sigma_{\theta\theta}=\frac{\partial^2\chi}{\partial r^2}$$

$$\sigma_{r\theta}=\frac{1}{r^2}\frac{\partial\chi}{\partial\theta}-\frac{1}{r}\frac{\partial^2\chi}{\partial r\partial\theta}$$

$$2Gu_r=-\frac{\partial\chi}{\partial r}+\frac{1}{4}\gamma r\frac{\partial\Psi}{\partial\theta}$$

$$2Gu_\theta=-\frac{1}{r}\frac{\partial\chi}{\partial\theta}+\frac{1}{4}\gamma r^2\frac{\partial\Psi}{\partial r}$$

where $\gamma=4(1-\nu)$ in plane strain, and

$$\nabla^2\chi=\frac{\partial}{\partial r}\left[r\frac{\partial\Psi}{\partial\theta}\right].$$

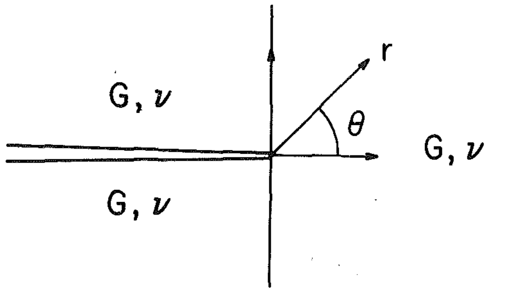

Fig. 3(*a*) Configuration for near-tip stress analysis

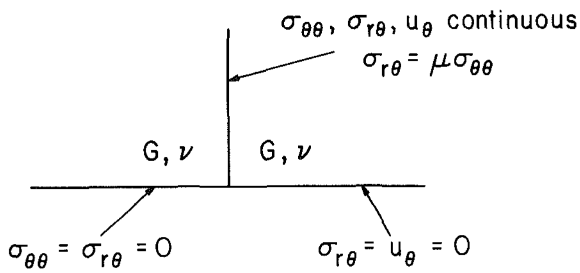

Fig. 3(*b*) Boundary conditions for near-tip stress analysis

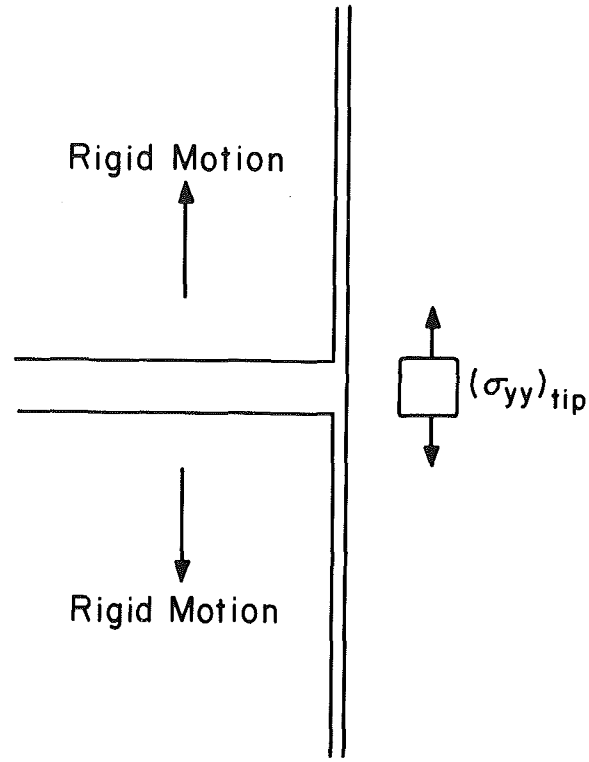

Fig. 4 Stresses associated with dominant eigenfunction

If we contemplate only fields which are symmetric about the x-axis (Mode I), then only the range $0<\theta<\pi$ need be considered (see Fig. 3(*b*)). The boundary conditions are

$$\sigma_{\theta\theta}(\pi) = \sigma_{r\theta}(\pi) = 0$$

$$\sigma_{r\theta}(0) = u_\theta(0) = 0$$

and the interface condition is $\sigma_{r\theta} = \mu\sigma_{\theta\theta}$. (Note that $\sigma_{r\theta} = -\sigma_{xy}$ on $\theta = \pi/2$.) The result is the following equation (Dempsey and Sinclair, 1981) for the eigenvalue λ (stress $\sim r^{-\lambda}$)

$$\cos\rho\,[\cos\rho(2\sin^2\rho-(1-\lambda)^2)-\mu(2-\lambda)(1-\lambda)\sin\rho]=0$$

where $\rho=(1-\lambda)\pi/2$. This implies two sets of eigenvalues, namely

$$\lambda = 0,2,4,6,\ldots$$

which leave the interface traction-free, and $\lambda_j (j=1,2,3,\ldots)$, where each λ_j satisfies

$$\mu = \frac{\cos\rho\,[2\sin^2\rho-(\sigma_{r\theta}-\lambda)^2]}{(2-\lambda)\ (1-\lambda)\sin\rho}. \tag{2}$$

Since the crack is opening in response to the load, we are looking for singular fields which satisfy $\sigma_{r\theta}>0$ and $\sigma_{\theta\theta}<0$ along the interface, implying that μ is negative. A search for solutions to equation (2) for various $\mu<0$ reveals all eigenvalues λ to be less than zero. Thus, there is *no* stress singularity in response to a remote tensile loading. On the other hand, for $\mu>0$, there can be eigenvalues greater than zero. This implies that remote compression tending to close the crack can give rise to singular stresses, provided the crack faces do not contact one another. Such a scenario may be relevant to the closing of the crack after opening and frictional slippage have occurred. We note that a similar effect was observed by Gdoutos and Theocaris (1975) and Comninou (1976) who studied the related problem of a wedge frictionally sliding on a half plane. They found that the existence of singular stresses was sensitively dependent on the direction in which the wedge slips. This discussion reveals the subtlety which underlies the assumption adopted without proof by Papadopoulos (1979) and Lam and Cleary (1984) that the crack is effectively blunted by the frictional slip.

More insight into the behavior at the crack tip can be gained by considering the dominant eigenfunction, namely $\lambda=0$. This corresponds to piecewise constant stress fields in $0<\theta<\pi/2$ and $\pi/2<\theta<\pi$. Since σ_{xy} and σ_{yy} are zero on $\theta=\pi$, they must be zero throughout $\pi/2<\theta<\pi$. Continuity of tractions implies that σ_{xy} is also zero in $0<\theta<\pi/2$. Since the interface is assumed to be in a state of slip and σ_{xy} is zero, σ_{xx} must be zero throughout $0<\theta<\pi$. This leaves only σ_{yy} nonzero in $0<\theta<\pi/2$. The fields are, thus, uniaxial tension (referred to as $(\sigma_{yy})_{\text{tip}}$) parallel to the interface ahead of the crack $(-\pi/2<\theta<\pi/2)$, with the two blocks $\pi/2<\theta<\pi$ and $-\pi<\theta<-\pi/2$ moving rigidly up and down, respectively (see Fig. 4).

The piecewise homogeneous stress state just discussed prevails right at the crack tip. It is a state, however, that could prevail whether or not there is contact at the interface in the vicinity of the crack tip. On the other hand, consider the eigenfunctions associated with the λ_j, implicitly given by equation (2). They yield stresses which behave as $r-\lambda_j$, where $-\lambda_j>0$; the tractions σ_{xx} and σ_{xy} are nonzero and their ratio equals the value μ, even as $r\to 0$. The point to emphasize is that it is *theoretically possible* for slipping contact to be maintained along the entire interface right up to the crack tip. Of course, opening of the interface at the crack tip is also a possible state; only an analysis of the complete problem—including far-field boundary conditions—will reveal whether contact or opening actually occurs. We contrast our conclusion with the tacit *assumption* of Papadopoulos (1979) and Lam and Cleary (1984) that opening at the interface ("lift-off" in their language) *must* occur. We return to this point below.

Finally, before discussing the solution method, we verify the appropriateness of the far-field boundary condition for the case of the semi-infinite crack. Assuming the usual elastic singular field to be valid at $r\to\infty$, one can compute the ratio

$$\frac{\sigma_{xy}}{\sigma_{xx}} = \frac{1}{4\sqrt{\pi r - 1}}.$$

Note that the interface is in a state of stick if this ratio is less than μ, and if $\sigma_{xx}<0$. If a portion of the interface is always in a state of stick, then it is like it is perfectly bonded. Hence, provided $\sigma_o > 0$, there is always some range of r including $r \to \infty$ which acts like it is perfectly bonded. This means that this "small-scale slipping problem" is legitimate if some nonzero residual compression exists at the interface (as simulated by σ_o).

Method of Solution

The solution method employed here is fashioned after the approach used previously by Dollar and Steif (1987) to study a pullout test with a Coulomb friction interface. We express the field quantities as a superposition of two solutions: (*i*) the elastic field associated with a crack in a single infinite, homogeneous sheet subjected to remote tension, plus (*ii*) a distribution of edge dislocations which represent the slip that occurs at the interface. We will assume that contact is maintained along the entire interface and that there are regions of slip near the crack tips. The validity of this assumption for a range of friction coefficients will be verified.

Since the crack must remain free of tractions and since the field (*i*) satisfies this traction-free condition, the distributed dislocations must also leave the crack faces free of traction. This is readily achieved by letting the kernel dislocation solution be that of an edge dislocation at the point (x_o, y_o) in the presence of a traction-free crack. Then, any distribution of such dislocations also leaves the crack free of tractions. A convenient solution to this problem has been given by Lo (1978). The solution is readily expressed in terms of the Muskhelishvili complex stress potentials $\phi(z)$ and $\psi(z)$, which are related to the stresses and displacements according to

$$\sigma_{xx} + \sigma_{yy} = 2(\phi' + \overline{\phi'}) \tag{3a}$$

$$\sigma_{yy} - \sigma_{xx} + 2i\sigma_{xy} = 2(\bar{z}\phi'' + \psi') \tag{3b}$$

$$2G(u + iv) = \kappa\phi - \bar{z}\overline{\phi'} - \bar{\psi} \tag{3c}$$

where $\kappa = \gamma - 1 = 3 - 4\nu$ in plane strain.

Lo's (1978) solution for a single dislocation at the point z_o can be written as

$$\phi' = \phi_\infty' + \phi_R' \qquad \psi' = \psi_\infty' + \psi_R'.$$

The functions ϕ_∞ and ψ_∞ represent the solution for a dislocation in an infinite medium, and the functions ϕ_R and ψ_R represent the solution associated with relieving the tractions induced by ϕ_∞ and ψ_∞ on the crack faces. These functions are given by

$$\phi_\infty'(z, z_o) = \alpha \frac{1}{z - z_o} \qquad \psi_\infty'(z, z_o) = \alpha \left[\frac{1}{z - z_o} - \frac{\bar{z}_o}{(z - z_o)^2} \right]$$

$$\phi_R'(z, z_o) = -\left[\alpha F(z, z_o) + \alpha F(z, \bar{z}_o) + \alpha(z_o - \bar{z}_o) H(z, \bar{z}_o) \right]$$

$$\psi_R'(z, z_o) = \bar{\phi}_R'(z, z_o) - \phi_R'(z, z_o) - z\phi_R''(z, z_o)$$

where

$$F(z, z_o) = \frac{1}{2} \frac{\left[1 - \dfrac{X(z_o)}{X(z)} \right]}{z - z_o}$$

$$H(z, z_o) = \frac{\partial}{\partial z_o} F(z, z_o)$$

and

$$X(z) = \sqrt{z(z + 2a)}.$$

The normalized Burger's vector, α, given by

$$\alpha = \frac{G b_y}{\pi(\kappa + 1)}$$

has been specialized to the case of interest here in which only the y-component of the Burger's vector, b_y, is nonzero. (Below, we will introduce a continuous distribution of dislocations; the derivative of b_y with respect to y—the dislocation density—will be denoted by b.) Note that ϕ_∞ and ψ_∞ have the usual dislocation singularity at $z = z_o$ (and eventually constitute the singular part of the integral equation). The terms ϕ_R and ψ_R have the characteristic square-root singularity at the crack tips since they represent the fields which relieve the traction on the crack faces.

Symmetry of the problem dictates that there are symmetric (above and below the crack plane) slip zones along both interfaces; that is $b(0, y_o) = b(0, -y_o) = -b(-2a, y_o) = -b(-2a, -y_o)$. Thus, the distribution of dislocations can be characterized by a single function $b(y_o)$ for $y_o > 0$. We now assume that there is a single region occupying $0 < y < L_s$ which undergoes slip. Then an integral equation governing $b(y_o)$ is derived by enforcing the slip condition

$$\sigma_{xy} = \mu\, \sigma_{xx}$$

along $0 < y < L_s$. This leads to the singular integral equation

$$\int_0^{L_s} b(y_o) \left[R_0(y, y_o) - R_1(y, y_o) - \mu R_2(y, y_o) \right] dy_o + f(y) = 0 \tag{4}$$

where the functions R_0 (the singular part), R_1, R_2, and f are given in the Appendix. Since $y = L_s$ represents the boundary between a slip zone and a stick zone, $b(L_s) = 0$ (see, for example, Dundurs and Comninou, 1979). The value of $b(0)$, which we show below to be proportional to the finite tensile stress at the crack tip, is determined as part of the solution.

The "small-scale slipping" problem is handled in an analogous manner. The solution of the traction-free, semi-infinite crack in a single homogeneous medium (the elastic singular field) is superposed with dislocations along $x = 0, 0 < |y| < L_s$. In this case, the kernel dislocation solution is that of a dislocation in the presence of a traction-free, semi-infinite crack. This solution (Lo, 1978) is of the same form as the first kernel solution; the only difference is that the limit of $a \to \infty$ converts $X(z)$ to $(z)^{1/2}$. The corresponding expressions for the functions appearing in equation (4) are simpler; they are also given in the Appendix.

A condition which can be used to determine the slip length is obtained by considering, once again, the near-tip stress field. As was previously shown, the stresses are not singular at the crack tip. However, our means of constructing the solution fails to account for this nonsingularity. We are superposing one field, that of a crack in a single homogeneous medium, which has a square-root singularity at the crack tip, with a second field associated with the dislocations, which is also square-root singular at the crack tip (through the terms ϕ_R and ψ_R). This can only be reconciled by insisting that the total magnitude of the singular term vanish. The condition of zero net stress intensity factor can be expressed in the form

$$\frac{4G}{\pi(\kappa+1)} \int_0^{L_s} b(y_o) \left[\frac{2z_0 + 3a}{X(z_0)(z_0 + 2a)} + \frac{2z_0 + 3a}{X(z_0)(\bar{z}_0 + 2a)} \right] dy_o = \sigma_\infty$$

for the finite crack, and in the form

$$\frac{6G}{\sqrt{\pi}(\kappa+1)} \int_0^{L_s} \frac{b(y_o)}{\sqrt{y_o}}\, dy_o = K_I$$

for the semi-infinite crack.

Our solution method serves to illuminate the difficulty with the tacit assumption of Papadopoulous (1979) and Lam and Cleary (1984) that the interface *must* open at the crack tip. (As will be shown, the interface will open if the friction coefficient is sufficiently high, which may be the case in the hydraulic fracturing problem.) Their assumption may have been motivated by the presence of the singular tensile stress σ_{xx}

which is usually associated with a crack tip. It must be borne in mind, however, that each slip dislocation contributes a negative stress intensity at the crack tip. In rendering the net stress intensity factor zero, not only do the dislocations blunt the crack (making σ_{yy} nonsingular), they also make σ_{xx} nonsingular. Hence, the interface is not forced to open; instead, it can be either open or closed, as seen next.

For both crack problems, we normalize the stress components by σ_o. The spatial variables and the slip length are normalized differently, however. For the finite crack problem, they are normalized by the crack half length a; for the semi-infinite crack problem, they are normalized by $(K/\sigma_o)^2$. The "small-scale slipping" problem may be solved once and for all (for a given μ) assuming the remote loading has a unit stress intensity factor. This derives from the fact that this problem has no inherent length scale, a feature it shares with the small-scale yielding problem in elastic-plastic fracture mechanics (see Rice, 1968). The stress at the crack tip is independent of the load; the loading serves only to rescale the spatial coordinates. Hence, the residual stress σ_o acts roughly as a yield stress to limit the level of stresses at the concentrator. On the other hand, in the case of a finite crack it will be seen that the residual stress no longer limits the level of stress at the crack tip.

A rather simple numerical discretization of the nondimensionalized version of equation (4) was used. Once $b(y_o)$ is determined, essentially all other field quantities may be computed. One result of great interest may be determined directly from $b(y_o)$. Since $b(y_o)$ is equal to the jump in the strain ϵ_{yy} along the slip length, and since σ_{xx} is continuous across the slip zone, $b(y_o)$ is proportional to the jump in σ_{yy} divided by $E/(1-\nu^2)$. Furthermore, since the stress σ_{yy} approaches 0 behind the tip, one can express the tensile stress ahead of the crack tip as

$$(\sigma_{yy})_{\text{tip}} = \frac{E}{1-\nu^2} b(0) \qquad (7)$$

for plane strain. This result is, of course, consistent with that obtained from applying the Plemelj formulae.

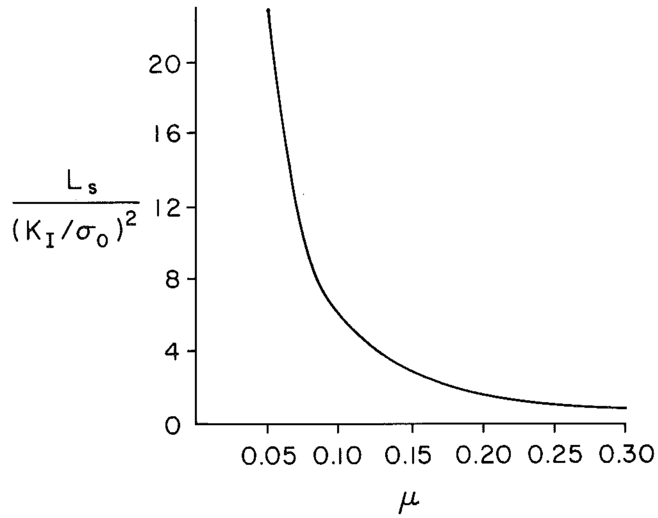

Fig. 5 Slip length as a function of friction coefficient for small-scale slipping problem

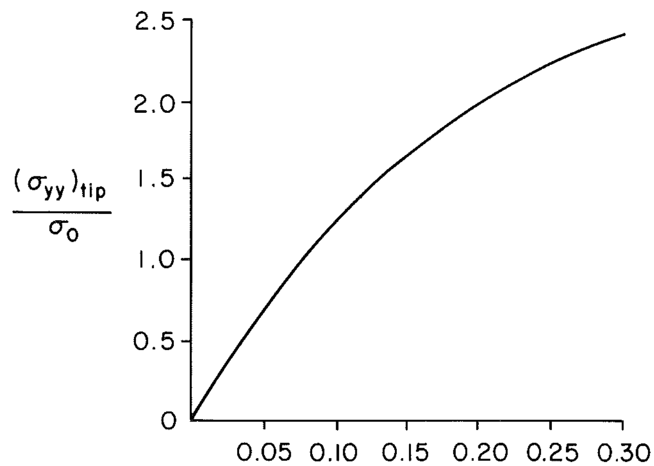

Fig. 6 Crack-tip stress as a function of friction coefficient for small-scale slipping problem

Results

As mentioned previously, the small-scale slipping problem depends only on the friction coefficient μ. Results for this limiting case are shown in Figs. 5 and 6, which depict the slip length and the tensile stress at the crack tip as functions of μ. As might be expected, lower friction coefficients translate into easier slip and, thus, longer slip lengths. Likewise, since frictional slippage at the interface relieves the stress singularity, lower friction coefficents lead to lower stress concentrations. A brief comment should be made regarding the vanishing of the tensile stress as μ approaches zero. Recall that the results shown in Figs. 5 and 6 presume that small-scale slipping conditions prevail; namely, that the slip length is short compared with the crack length. From Fig. 5, it can be seen that the slip length grows without bound as μ approaches zero. Hence, a vanishing friction coefficient makes no sense in the context of small scale slipping. As can be discerned from results to be presented, the stress at the tip is equal to the remotely applied stress for very small coefficents of friction.

In practice, the stress at the tip in Fig. 6 was not computed via (7). Instead, σ_{yy} was computed at several different points near (but ahead of) the crack tip by an integration over the whole distribution $b(y)$; the results were then extrapolating to the tip. The difference between this calculation and that based on (7) was approximately 4 percent. However, this difference is not representative of the accuracy of the solution as a whole. As mentioned above, the slip length, L_s, is adjusted until the net stress intensity factor is zero. Of course, this must be done numerically. It was found that varying L_s a slight amount had a correspondingly slight influence on all field quantities, except on $b(0)$, which depended sensitively on L_s. On the other hand, σ_{yy}, as computed from the whole distribution $b(y)$, was relatively insensitive to small variations in L_s. To assess the correctness of the assumption that there is no opening of the interface one must verify that the resulting normal stress at the interface is compressive ($\sigma_{xx}<0$). This was, in fact, found to be the case for the semi-infinite crack provided μ was less than roughly 0.3. For larger values of μ, a small region near the crack tip was found in which $\sigma_{xx}>0$; hence, such results are not shown. It was also verified that slip would not occur other than on the slip zones immediately adjacent to the crack tip.

Next, we turn to the results for the finite crack. Figure 7 shows the normalized slip length as a function of the dimensionless loading parameter σ_∞/σ_o. The slip length increases with the load and decreases with the friction coefficient μ. (Results for $\mu=0.4$ are not given for σ_∞/σ_o near zero, since opening of the interface occurs near the crack tip for very small remote loads.) For comparison, we show the slip length one would predict if the results for the semi-infinite crack were used, together with $K_I=\sigma_\infty(\pi a)^{1/2}$ (see Fig. 8). As expected, the results agree for small loads σ_∞/σ_o, since then the slip length is small compared with the crack length—the condition

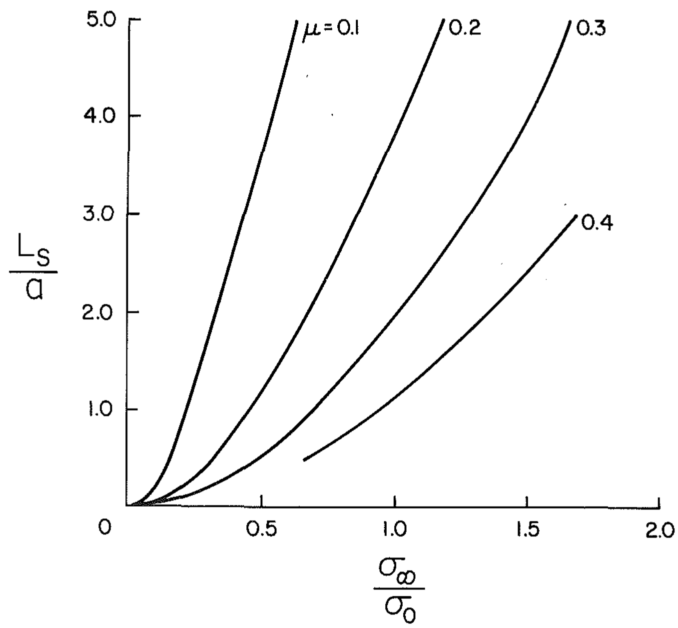

Fig. 7 Slip length as a function of remote load for finite crack

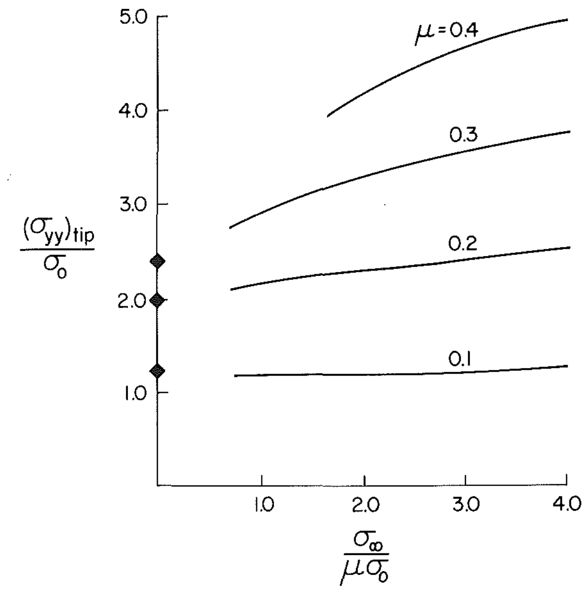

Fig. 9 Crack-tip stress as a function of remote load for finite crack

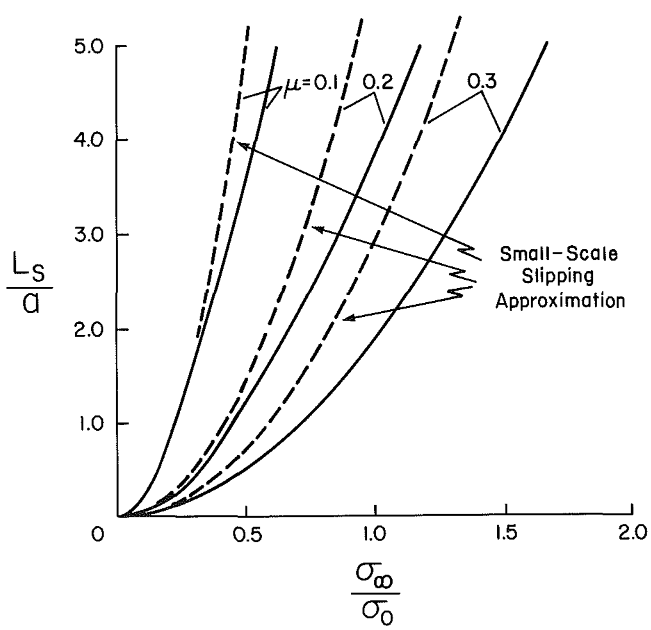

Fig. 8 Comparison of slip lengths for finite crack with small-scale slipping approximation

necessary to the small-scale slipping assumption. On the other hand, once the remote stess σ_∞ becomes on the order of the residual stress σ_o, the slip length deviates from the small-scale slipping prediction.

At this point it is useful to call attention to previous work by Dollar and Steif (1987), who studied a two-dimensional pullout test which features a Coulomb friction interface law identical to that considered here. They compared their results with the results one would obtain using a highly approximate style of analysis, which is quite common in the composites literature. Typically, these approximate analyses assume that a constant shear stress (the friction stress) prevails at the interface. To have a sensible comparison, Dollar and Steif (1987) equated the combination $\mu\sigma_o$, which is a nominal friction stress, with the interfacial shear stress of these approximate analyses. It was found that the slip length during the pullout test, as well as other quantities, depends on μ and σ_o *individually* and not just on their *product*. We attempted a similar comparison here by reconsidering L_s/a, now as a function of the renormalized load $\sigma_\infty/\mu\sigma_o$. The curves (not presented) for different μ were found to be nearly coincident, once the slip length was on the order of the crack length. This implies that, at least insofar as the slip length is concerned, the dependence is essentially on the product $\mu\sigma_o$. (In the case of the semi-infinite crack, however, the slip length did not depend exclusively on the product $\mu\sigma_o$; that is L_s is *not* equal to $(K_I/\mu\sigma_o)^2$ times a constant which is *independent* of μ.)

The normalized tensile stress at the crack tip is shown in Fig. 9. Though the remote loading has been normalized by $\mu\sigma_o$, the resulting crack-tip stress still depends on μ. (That is, the dependence is not purely on the nominal friction stress $\mu\sigma_o$, as it was for the slip length.) As can be surmised, the crack-tip stress increases as the remote load increases. Though results are only plotted for a limited range of $\sigma_\infty/\mu\sigma_o$, it was apparent from the numerical results that the stress at the crack tip approached σ_∞ as $\sigma_\infty/\mu\sigma_o\rightarrow\infty$. From this observation, there emerges the following interpretation of the effect of a frictional interface on an impinging crack. For vanishing small remote loads ($\sigma_\infty/\mu\sigma_o<<1$), the crack acts almost as a crack in a single homogeneous medium; though the stress at the crack tip is finite (on the order of σ_o), the stress concentration $(\sigma_{yy})_{\text{tip}}/\sigma_\infty$ is unbounded. As the load increases, the interface "blunts" the crack more and more in the sense that the stress concentration diminishes. In the limit of an infinitely large load, the stress concentration has been eliminated: slip would have traversed the entire fiber length, and the half plane $x>0$ would be subjected to a uniaxial tension σ_∞. As before, the curve for $\mu=0.4$ was not extended to values of the remote load at which the interface opened. In this regard, the following observation was made: the interface remains closed even for higher friction coefficients, provided the remote load is sufficiently high.

Finally, we turn to the load carried by the "fiber" ($-2a<x<0$) as a function of distance from the crack. This transfer of load from the matrix back to the fiber is an important aspect of micromechanical models of composite properties. Accordingly, we plot (in Fig. 10) the average stress σ_{yy} in the fiber (denoted by Σ), normalized by the remote stress σ_∞, as a function of normalized distance y/a. This is shown for several values of the friction coefficient, but with the normalized load held fixed at $\sigma_\infty/\mu\sigma_o=2.5$. For comparison, we

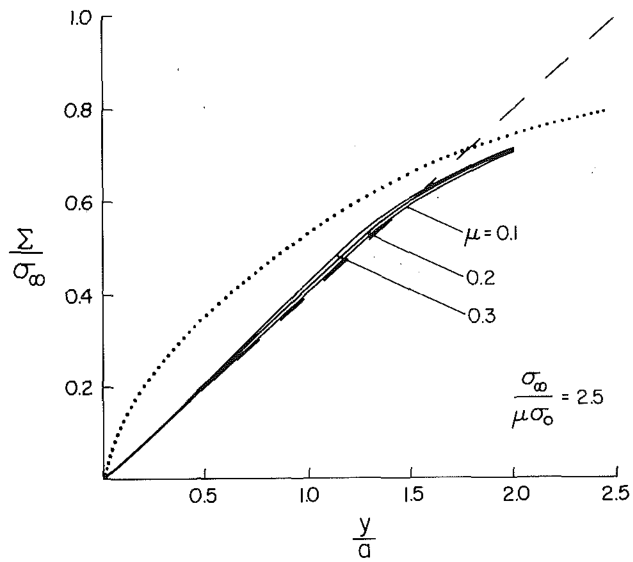

Fig. 10 Load transfer to fiber (. . . .perfect bonding;----constant shear-stress approximation

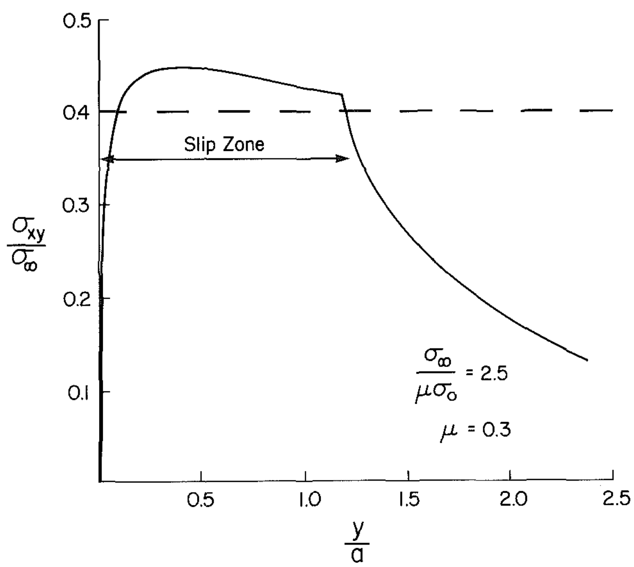

Fig. 11 Interfacial shear near crack tip

exhibit (dotted curve) the load transfer associated with a fiber and matrix that are perfectly bonded (the crack in a single homogeneous medium), as well as the highly approximate result which assumes that the shear stress at the interface is constant and equal to $\mu\sigma_o$ (dashed curve). Clearly, the load in the fiber is not so different from that predicted on the basis of the constant shear stress assumption.

Some understanding of this can be gained from considering the distribution of interfacial traction σ_{xy} (see Fig. 11). As was found from the near-tip analysis, the tractions at the interface are zero at the crack tip. However, these tractions increase rapidly with distance from the crack tip. For example, the shear stress quickly increases (in magnitude) to exceed $\mu\sigma_o$ and eventually returns to zero. This was reflected in the load transfer curves. Generally, the actual fiber load exceeds that of the constant shear stress approximation, except very near the crack tip (this is difficult to detect from Fig. 10). Hence, while the rapidly varying stress fields usually associated with a crack play a role in the stress concentration at the blunted crack tip, they do not serve to significantly alter the rate of load transfer back to the fiber.

Acknowledgments

The authors appreciate the assistance provided by H. Schwietert in carrying out the computations. In addition, we are indebted to J. M. Papadopoulos for bringing to our attention the related work done in the study of hydraulic fracturing. This research has been supported by the National Science Foundation under grant MSM-8451080, by the General Electric Engine Business Group and by the Department of Mechanical Engineering, Carnegie-Mellon University.

References

Comninou, M., 1976, "Stress Singularity at Sharp Edge in Contact Problems With Friction," *ZAMP*, Vol. 27, p. 493.

Dempsey, J. P., and Sinclair, G. B., 1981, "On the Singular Behavior at the Vertex of a Bi-material Wedge," *J. Elasticity*, Vol. 11, p. 317.

Dollar, A., and Steif, P. S., 1987, "Load Transfer in Composites With a Coulomb Friction Interface," *Int. J. Solid Structures*, Vol. 24, p. 789.

Dundurs, J., and Comninou, M., 1982," Some Consequences of the Inequality Conditions in Contact and Crack Problems," ASME JOURNAL OF APPLIED MECHANICS, Vol. 49, p. 47.

Gdoutos, E. E., and Theocaris, P. S., 1975, "Stress Concentrations at the Apex of a Plane Indenter Acting on an Elastic Half Plane," ASME JOURNAL OF APPLIED MECHANICS, Vol. 42, p. 688.

Keer, L. M., 1981, "The Intersection of a Pressurized Crack With a Joint," *J. Geophysical Res.*, Vol. 86, p. 1032.

Lo, K. K., 1978, "Analysis of Branched Cracks," ASME JOURNAL OF APPLIED MECHANICS, Vol. 45, p. 797.

Lam, K. Y., and Cleary, M. P., 1984, "Slippage and Re-initiation of (Hydraulic) Fractures at Frictional Interfaces," *Int. J. Num. Anal. Meth. in Geom.*, Vol. 8, p. 589.

Papadopoulos, J. M., 1979, "A Model for Crack Blunting a Frictional Interface," B. S. Thesis, Massachusetts Institute of Technology.

Phillips, D. C., 1974, "Interfacial Bonding and Toughness of Carbon Fibre Reinforced Glass and Glass Ceramics," *J. Mat Sci.*, Vol. 9, p. 1847

Prewo, K. W., and Brennan, J. J., 1980, "High-Strength Silicon Carbide Fibre-Reinforced Glass-Matrix Composites," *J. Mat. Sci.*, Vol. 15, p. 463.

Rice, J. R., 1968, *Mathematical Analysis in the Mechanics of Fracture, Fracture*, Vol. 2, H. Leibowitz, ed., Academic Press, New York.

APPENDIX

Herein, we give expressions for the terms appearing in the dimensional version of the integral equation (4). For the finite crack

$$R_0(y,y_0)=\frac{-2}{y-y_0}$$

$$R_1(y,y_0)=2Im[h_2]+Im\left[\frac{\bar{h}_3^2+h_3^2}{\bar{h}_3}+\frac{\bar{h}_4^2+h_4^2}{\bar{h}_4}\right]$$

$$+2yRe[G'(z,z_0)+G'(z,\bar{z}_0)$$

$$-G'(z,-z_0-2)G'(z,-\bar{z}_0-2)]$$

$$R_2(y,y_0)=-Re\left[\frac{\bar{h}_3^2+h_3^2}{\bar{h}_3}+\frac{\bar{h}_4^2+h_4^2}{\bar{h}_4}\right]$$

$$+2yIm[G'(z,z_0)+G'(z,\bar{z}_0)$$

$$-G'(z,-z_0-2)-G'(z,-\bar{z}_0-2)]$$

$$-2Re[G(z,z_0)+G(z,\bar{z}_0)$$

$$-G(z,-z_0-2)-G(z,-\bar{z}_0-2)]$$

where

$$h_2 = \frac{1}{z - \bar{z}_0} \qquad h_3 = \frac{1}{z + z_0 + 2} \qquad h_4 = \frac{1}{z + \bar{z}_0 + 2}$$

$$G(z,z_0) = \frac{1}{z - z_0} + \frac{1}{2}\,\frac{\bar{z}_0 - z_0}{(z - z_0)^2}$$

$$- \frac{X(z_0)}{X(z)}\left[\frac{1}{z - z_0} + \frac{1}{2}\,\frac{\bar{z}_0 - z_0}{(z - z_0)^2}\right.$$

$$\left. + \frac{1}{2}\,\frac{\bar{z}_0 - z_0}{z\text{-}z_0}\left(\frac{z_0 + 1}{[X(z_0)]^2}\right)\right]$$

and

$$G' = \frac{\partial G}{\partial z}$$

$$f(y) = f_1(y) - \mu f_2(y)$$

$$f_1(y) = -\frac{1}{2} Im\left[\frac{\bar{z} - 2}{[X(z)]^3}\right]\frac{\sigma_\infty}{\sigma_0}$$

$$f_2(y) = \left\{-1 + Re\left[\frac{z+1}{X(z)}\right] + \frac{1}{2}\, Re\left[\frac{\bar{z} - 2}{[X(z)]^3}\right]\right\}\frac{\sigma_\infty}{\sigma_0} - 1.$$

For the semi-infinite crack

$$R_0(y,y_0) = \frac{-2}{y - y_0}$$

$$R_1(y,y_0) = \frac{2y_0(y - y_0)}{(y + y_0)^3} + \frac{\sqrt{\dfrac{y_0}{y}}\,[14yy_0 - 3y^2 - 3y_0^2] + 4y(y - 3y_0)}{2(y - y_0)^3}$$

$$R_2(y,y_0) = \sqrt{\frac{y_0}{y}}\left[\frac{y^2 - 3y_0^2 + 6yy_0}{2(y + y_0)^3}\right]$$

$$f(y) = f_1(y) - \mu f_2(y)$$

$$f_1(y) = \frac{-1}{4\sqrt{\pi y}}$$

$$f_2(y) = \frac{1}{4\sqrt{\pi y}} - 1.$$

ERRATA

Errata on "An Historical Note on Finite Rotations" by Hui Cheng and K. C. Gupta and published in the March 1989 issue of the ASME Journal of Applied Mechanics, Vol. 56, pp. 139–145:

The second through fifth lines following equation (9) should read "angles, respectively. The aforementioned paper contains derivation details in Euler Angles, and related details can also be found in a 1770 paper in *L. E. Opera Omnia-Mathematica*, Vol. 1 (6), pp. 287–315, 1921; but not in Euler (1775a) which was erroneously"...

On page 144, equation ($B2$), replace the second occurrence of ϕ' by ϕ.

Also on page 144, equation ($C1$), replace the first occurrence of H'' by H' in the third line.

On page 145 replace F'' by F' in equation ($C4b$), G'' by G' in equation ($C5b$), and t'' by t' in the third line of equation ($C15$).

Jes Christoffersen
Department of Solid Mechanics,
The Technical University of Denmark,
Lyngby, Denmark

When is a Moment Conservative?

A simple, yet fully-general condition under which moment loading is conservative is presented. The condition is stated in terms of a Maxwell-type reciprocity relation between infinitesimal rotations and an appropriately defined differential of the moment. The usefulness of this concept is illustrated by examples concerning torsional instability of shafts.

1 The Problem

The work of a force $\mathbf{F}$ on an infinitesimal displacement $d\mathbf{r}$ of its point of action with position vector $\mathbf{r}$ is

$$dW = \mathbf{F} \cdot \mathbf{dr}, \tag{1}$$

a dot between vector or matrix symbols signifying a contracted product.

Assuming that the force is determined by $\mathbf{r}$, it is conservative whenever infinitesimal changes of $\mathbf{F}$, $d_1\mathbf{F}$, and $d_2\mathbf{F}$, bear to the infinitesimal displacements that cause them, respectively, $d_1\mathbf{r}$ and $d_2\mathbf{r}$, the relation

$$d_1\mathbf{F} \cdot d_2\mathbf{r} = d_2\mathbf{F} \cdot d_1\mathbf{r}. \tag{2}$$

A moment $\mathbf{M}$ acting on a body performs the work

$$dW = \mathbf{M} \cdot \delta\omega, \tag{3}$$

where $\delta\omega$ is an infinitesimal rotation of the body. However, a Maxwell reciprocity relation like equation (2) does not apply. In general,

$$d_1\mathbf{M} \cdot \delta_2\omega \neq d_2\mathbf{M} \cdot \delta_1\omega$$

if $\mathbf{M}$ represents a conservative loading. The reason for this discrepancy is that, as emphasized by the notation, while $d\mathbf{r}$ is a total differential, the rotation $\delta\omega$ is not.

It is an intriguing question whether a differential operator d^* can be defined such that

$$d_1^*\mathbf{M} \cdot \delta_2\omega = d_2^*\mathbf{M} \cdot \delta_1\omega \tag{4}$$

when $\mathbf{M}$ is conservative. As shown in the next section, such a differential does indeed exist.

2 The Solution

As a necessary prerequisite for a moment $\mathbf{M}$ to be conservative, its value must be given by the orientation of the body on which it acts. This orientation may be described by an ortho-normal matrix $\mathbf{Q}$ that transforms reference state directions to their current values. If an infinitesimal rotation $\delta\omega$ is performed, away from the current state, then $\mathbf{Q}$ changes by

$$d\mathbf{Q} = \delta\omega \times \mathbf{Q}. \tag{5}$$

The symbol $\times$ denotes a vector product. The vector product of $\delta\omega$ and a matrix $\mathbf{Q}$ is defined by the identity

$$(\delta\omega \times \mathbf{Q}) \cdot \mathbf{a} = \delta\omega \times (\mathbf{Q} \cdot \mathbf{a}) \tag{6}$$

to hold for arbitrary vectors $\mathbf{a}$.

Now, introduce through the Hodge duality skew matrices $\delta\hat{\omega}$ and $\hat{\mathbf{M}}$ such that

$$\delta\hat{\omega} \cdot \mathbf{a} = \delta\omega \times \mathbf{a}, \ \hat{\mathbf{M}} \cdot \mathbf{b} = \mathbf{M} \times \mathbf{b}, \tag{7}$$

identical in $\mathbf{a}$ and $\mathbf{b}$. The work of $\mathbf{M}$ on $\delta\omega$ may then be written as

$$\mathbf{M} \cdot \delta\omega = -\frac{1}{2}\hat{\mathbf{M}} : \delta\hat{\omega}.$$

The symbol ":" denotes a double contraction, so that $\mathbf{A}:\mathbf{B}$ is the trace of $\mathbf{A}.\mathbf{B}$, the product of matrices $\mathbf{A}$ and $\mathbf{B}$. From (5) and (7), observing that the inverse of $\mathbf{Q}$ is equal to its transpose $\mathbf{Q}^T$,

$$\delta\hat{\omega} = d\mathbf{Q} \cdot \mathbf{Q}^T.$$

Hence,

$$\mathbf{M} \cdot \delta\omega = \left[-\frac{1}{2}\mathbf{Q}^T \cdot \hat{\mathbf{M}}\right] : d\mathbf{Q}. \tag{8}$$

With $\mathbf{M}$ given by $\mathbf{Q}$, this is a total differential whenever differentials d_1 and d_2 of matrices $\mathbf{Q}$ and $[-1/2\mathbf{Q}^T \cdot \hat{\mathbf{M}}]$ are related through the Maxwell-type reciprocity relation

$$d_1\left[-\frac{1}{2}\mathbf{Q}^T \cdot \hat{\mathbf{M}}\right] : d_2\mathbf{Q} = d_2\left[-\frac{1}{2}\mathbf{Q}^T \cdot \hat{\mathbf{M}}\right] : d_1\mathbf{Q}. \tag{9}$$

Now, according to (5) and (7),

$$d_1\left[-\frac{1}{2}\mathbf{Q}^T \cdot \hat{\mathbf{M}}\right] : d_2\mathbf{Q} = \left[-\frac{1}{2}\mathbf{Q}^T \cdot d_1\hat{\mathbf{M}} + \frac{1}{2}\mathbf{Q}^T \cdot \delta_1\hat{\omega} \cdot \hat{\mathbf{M}}\right] : (\delta_2\hat{\omega} \cdot \mathbf{Q})$$

or

$$d_1\left[-\frac{1}{2}\mathbf{Q}^T \cdot \hat{\mathbf{M}}\right] : d_2\mathbf{Q} = -\frac{1}{2}d_1\hat{\mathbf{M}} : \delta_2\hat{\omega} + \left[\frac{1}{2}\hat{\omega}_1 \cdot \hat{\mathbf{M}}\right] : \delta_2\hat{\omega},$$

which in view of (7) is further reducible to

Contributed by the Applied Mechanics Division of THE AMERICAN SOCIETY OF MECHANICAL ENGINEERS for presentation at the Joint ASCE/ASME Applied Mechanics, Biomechanics, and Fluids Engineering Conference, San Diego, CA, July 9 to 12, 1989.

Discussion of this paper should be addressed to the Editorial Department, ASME, United Engineering Center, 345 East 47 Street, New York, N.Y. 10017, and will be accepted until two months after final publication of the paper itself in the JOURNAL OF APPLIED MECHANICS. Manuscript received by ASME Applied Mechanics Division, May 4, 1988; final revision, September 1, 1988.

Paper No. 89-APM-34.

$$d_1\left[-\frac{1}{2}\mathbf{Q}^T\bullet\hat{\mathbf{M}}\right]:d_2\mathbf{Q}=d_1\mathbf{M}\bullet\delta_2\omega-\frac{1}{2}|\delta_1\omega\mathbf{M}\delta_2\omega|,$$

where $|\mathbf{a}\ \mathbf{b}\ \mathbf{c}|$ is the determinant with the columns indicated. Thus, conservative loading implies, and is implied by,

$$d_1\mathbf{M}\bullet\delta_2\omega-\frac{1}{2}|\delta_1\omega\mathbf{M}\delta_2\omega|=d_2\mathbf{M}\bullet\delta_1\omega-\frac{1}{2}|\delta_2\omega\mathbf{M}\delta_1\omega|, \quad (10)$$

and this has the required form (4) if we set

$$d^*\mathbf{M}=d\mathbf{M}-\frac{1}{2}\delta\omega\times\mathbf{M}. \quad (11)$$

The differential $d^*\mathbf{M}$ is related to the Jaumann differential

$$\mathfrak{D}\mathbf{M}=d\mathbf{M}-\delta\omega\times\mathbf{M}, \quad (12)$$

but unlike this, $d^*\mathbf{M}$ is influenced by rotations of the reference frame, hence, nonobjective.

3 An Example: Moments of Constant Forces

Modeling a moment through conservative, e.g, constant, forces acting on rigid members serves well to illustrate the significance of the rotational term in (11). Referring the moment to the origo of the reference system, a number of forces $\mathbf{F}_i$. $i=1, 2, \ldots$, acting at points with position vectors $\mathbf{r}_i$, produce a moment

$$\mathbf{M}=\sum_i \mathbf{r}_i\times\mathbf{F}_i. \quad (13)$$

Assuming that the forces are constant,

$$d\mathbf{M}=\sum_i d\mathbf{r}_i\times\mathbf{F}_i \quad (14)$$

represents an infinitesimal change of the moment. Let the $\mathbf{r}_i$ be rigid arms that are further rigidly attached to the body on which the forces act, so

$$d\mathbf{r}_i=\delta\omega\times\mathbf{r}_i, \quad (15)$$

where $\delta\omega$ is the infinitesimal rotation of the body. Hence,

$$d\mathbf{M}=\sum_i(\delta\omega\times\mathbf{r}_i)\times\mathbf{F}_i,$$

and this may be rewritten as

$$d\mathbf{M}=\sum_i[\mathbf{r}_i\otimes\mathbf{F}_i-(\mathbf{r}_i\bullet\mathbf{F}_i)\mathbf{1}]\bullet\delta\omega \quad (16)$$

where "$\otimes$" denotes a dyadic product, and $\mathbf{1}$ is the unit matrix. Clearly, the matrix relating vector $d\mathbf{M}$ to vector $\delta\omega$ is nonsymmetric. However,

$$\delta\omega\times\mathbf{M}=\sum_i\delta\omega\times(\mathbf{r}_i\times\mathbf{F}_i),$$

or

$$\delta\omega\times\mathbf{M}=\sum_i(\mathbf{r}_i\otimes\mathbf{F}_i-\mathbf{F}_i\otimes\mathbf{r}_i)\bullet\delta\omega. \quad (17)$$

So, according to (11),

$$d^*\mathbf{M}=\mathbf{K}\bullet\delta\omega, \quad (18)$$

where

$$\mathbf{K}=\sum_i\left[\frac{1}{2}\mathbf{r}_i\otimes\mathbf{F}_i+\frac{1}{2}\mathbf{F}_i\otimes\mathbf{r}_i-(\mathbf{r}_i\bullet\mathbf{F}_i)\mathbf{1}\right]. \quad (19)$$

This is a symmetric matrix,

$$\mathbf{K}^T=\mathbf{K}, \quad (20)$$

and so the reciprocity relation (4) is satisfied.

4 Torsional Stability of Beams

Following early investigations by Greenhill (1883), Ziegler (1952) emphasized the importance of specifying in stability problems for beams under torsion the rules according to which the torsional moment introduces infinitesimal bending moments as the beam deflects infinitesimally (see also Ziegler (1968)). In particular it has been pointed out that, unlike a constant force, a constant moment does not possess a potential and, hence, is nonconservative. This is apparent also from equation (10) with $d_1\mathbf{M}=d_2\mathbf{M}=0$: The two determinants appearing in the expression are numerically equal but of opposite signs.

Ziegler solves a number of stability problems including problems of beams subject to conservative, as well as nonconservative, torsional loading. As to the former, he derives rules for the change with deflections of bending moments on the basis of simple mechanical models. These imply that the torsional moment is introduced via forces acting on rigid members attached to the beam in various fashions, as described in the previous section.

For a brief and incomplete survey of the problems, consider an elastic beam with isotropic cross-section. Let α be its bending rigidity. In a fixed Cartesian frame, the beam extends along the z-axis from $z=0$, where it is clamped, to $z=l$, which is a free (i.e, unconstrained) end. This is loaded by a torsional moment M.

For small deflections from the straight configuration, the governing equations may be expressed in terms of rotations $(\delta\omega_x, \delta\omega_y)$ as

$$\begin{aligned}\alpha\delta\omega_x'(z)+M\delta\omega_y(z)&=dM_x(l),\\ \alpha\delta\omega_y'(z)-M\delta\omega_x(z)&=dM_y(l).\end{aligned} \quad (21)$$

A prime denotes differention with respect to z. The solution, respecting the boundary conditions $\delta\omega_x(0)=\delta\omega_y(0)=0$, is

$$\begin{aligned}\delta\omega_x(z)&=\frac{1}{M}\left[dM_x(l)\sin\frac{Mz}{\alpha}-dM_y(l)\left(1-\cos\frac{Mz}{\alpha}\right)\right]\\ \delta\omega_y(z)&=\frac{1}{M}\left[dM_x(l)\left(1-\cos\frac{Mz}{\alpha}\right)+dM_y(l)\sin\frac{Mz}{\alpha}\right].\end{aligned} \quad (22)$$

We stipulate

$$\begin{pmatrix}d^*M_x(l)\\ d^*M_y(l)\end{pmatrix}=M\begin{pmatrix}k_{xx} & k_{xy}\\ k_{yx} & k_{yy}\end{pmatrix}\begin{pmatrix}\delta\omega_x(l)\\ \delta\omega_y(l)\end{pmatrix}. \quad (23)$$

With (11)

$$\begin{pmatrix}dM_x(l)\\ dM_y(l)\end{pmatrix}=M\begin{pmatrix}k_{xx} & k_{xy}+½\\ k_{yx}-½ & k_{yy}\end{pmatrix}\begin{pmatrix}\delta\omega_x(l)\\ \delta\omega_y(l)\end{pmatrix}. \quad (24)$$

The loading is conservative if, as we assume,

$$k_{yx}-k_{xy}. \quad (25)$$

This condition was established by Beck (1955). Introducing (24) in (22) with $z=l$,

$$\frac{1}{1+t^2}\begin{pmatrix}-k_{xy}t^2+k_{xx}t-½ & -k_{yy}t^2+k_{xy}t+½t\\ k_{xx}t^2+k_{xy}t-½t & k_{xy}t^2+k_{yy}t-½\end{pmatrix}\begin{pmatrix}\delta\omega_x(l)\\ \delta\omega_x(l)\end{pmatrix}=\begin{pmatrix}0\\ 0\end{pmatrix} \quad (26)$$

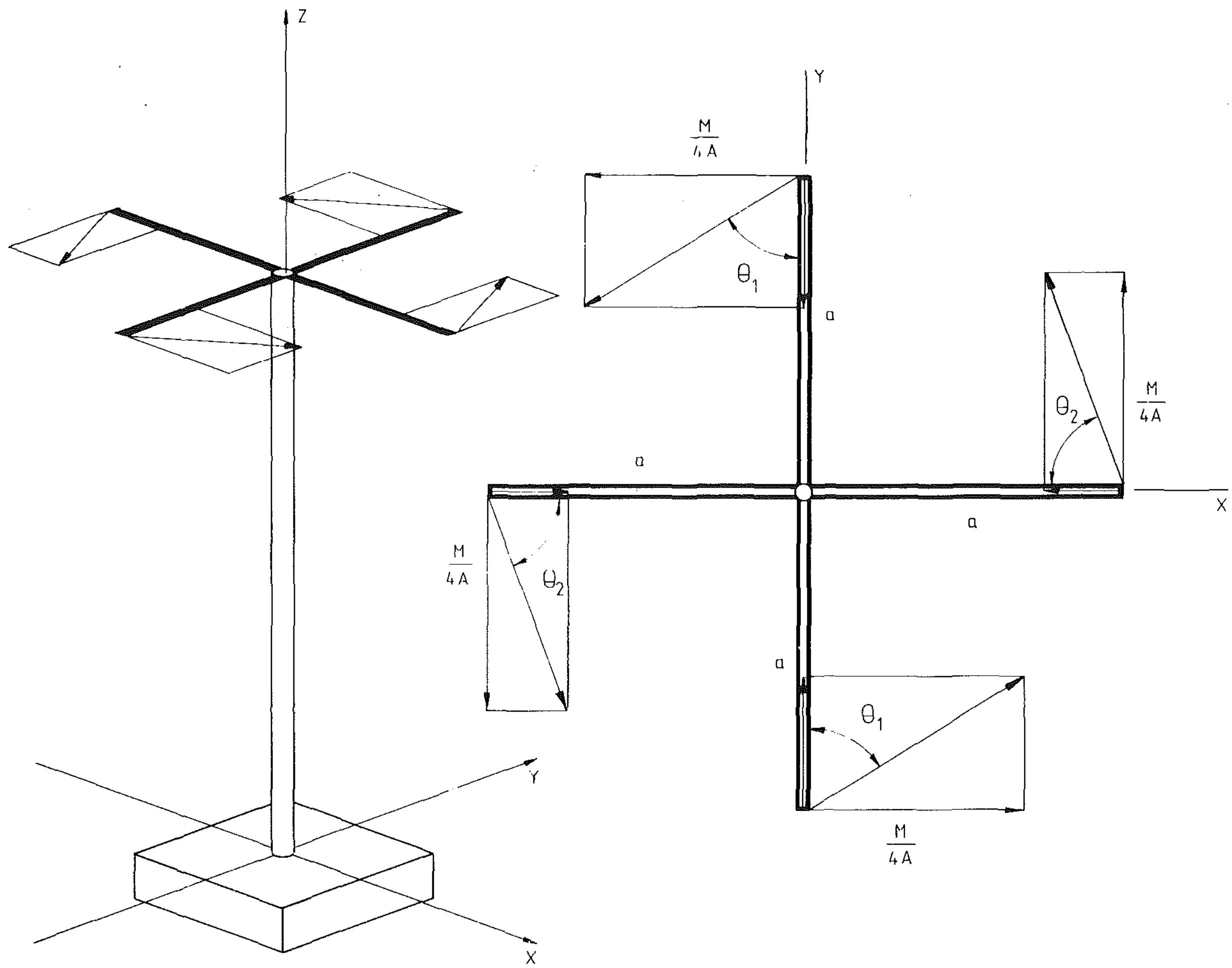

Fig. 1 Torisional moment applied through four constant forces

where

$$t = \tan \frac{Ml}{2\alpha}. \tag{27}$$

A nontrivial solution of (26) exists if the determinant of the system vanishes,

$$\frac{1}{4} - \frac{1}{2}(k_{xx} + k_{yy})t + (k_{xx}k_{yy} - k_{xy}^2)t^2 = 0. \tag{28}$$

The roots are given by

$$(2t)^{-1} = \begin{pmatrix} k_1 \\ k_2 \end{pmatrix} = \frac{1}{2}(k_{xx} + k_{yy}) \pm \sqrt{\left[\frac{1}{4}(k_{xx} - k_{yy})^2 + k_{xy}^2\right]}, \tag{29}$$

so they are related to the principal values of matrix **k** in a simple fashion.

Ziegler has specifically considered the following cases,

semitangential case, $k_1 = 0, k_2 = 0$,

quasitangential case, $k_1 = \frac{1}{2}, k_2 = -\frac{1}{2}$,

pseudotangential case, $0 < k_1 < \frac{1}{2}, k_1 k_2 = -\frac{1}{4}$.

This is, of course, not a complete classification (neither was it intended to be). Koiter (1980) has investigated the case in which the torsional moment is applied via a Cardan joint (Hooke's joint) from a rigid shaft aligned with the flexible shaft. It turns out that this case is identical with Ziegler's quasi-tangential case.

We finally present a force model consisting of four forces acting on rigid members in the x-y plane and covering the full range of eigenvalues k_1 and k_2. The critical values of the torsional moment, M_1 and M_2 may, for the boundary conditions here considered (one end clamped, the other free), be read off Fig. 1. Indeed,

$$\theta_1 = \frac{M_1 l}{2\alpha}, \ \theta_2 = \frac{M_2 l}{2\alpha} \tag{30}$$

as is readily derived from equation (19) together with (27) and (29).

References

Beck, M., 1955, "Knickung gerader Stäbe durch Druck und konservative Torsion" *Ingenieur-Archiv*, Vol. 23, pp. 231–253.

Greenhill, A. G., 1883, "On the Strength of Shafting when Exposed Both to Torsion and to End Thrust," *Proceedings of the Institution of Mechanical Engineers*, April, pp. 182–209 (discussion: pp. 210–225).

Koiter, W. T., 1980, "Buckling of a Flexible Shaft Under Torque Loads Transmitted by Cardan Joints," *Ingenieur-Archiv*, Vol. 49, pp. 369–373.

Ziegler, H., 1952, "Knickung gerader Stäbe unter Torsion," *Zeitschrift für angewandte Mathematik und Physik*, Vol. 3, pp. 96–119.

Ziegler, H., 1968, *Principles of Structural Stability*, Chapter 5, Section 3, Blaisdell, Waltham, Mass., Toronto, London.

Cavity Formation at the Center of a Composite Incompressible Nonlinearly Elastic Sphere

C. O. Horgan
Department of Applied Mathematics,
School of Engineering and Applied Science,
University of Virginia,
Charlottesville, Va. 22903
Mem. ASME

T. J. Pence
College of Engineering,
Michigan State University,
East Lansing, Mich. 48824
Assoc. Mem. ASME

In this paper, the effect of material inhomogeneity on void formation and growth in incompressible nonlinearly elastic solids is examined. A bifurcation problem is considered for a solid composite sphere composed of two arbitrary homogeneous isotropic incompressible elastic materials perfectly bonded across a spherical interface. Under a uniform radial tensile dead load, a branch of radially symmetric configurations involving a traction-free internal cavity centered at the origin bifurcates from the undeformed configuration. In contrast to the situation for a homogeneous neo-Hookean sphere, bifurcation here may occur either locally to the right or to the left. *In the latter case, the cavity has finite radius on first appearance. This discontinuous change in stable equilibrium configurations is reminiscent of the snap-through buckling phenomenon observed in certain structural mechanics problems. Explicit conditions determining the type of bifurcation are established for the general composite sphere. An analysis of the stress distribution is carried out and the effect of cavitation at the center on possible interface debonding is explored for the special case when the constituent materials are both neo-Hookean. It is shown that, in a quasi-static loading process, cavitation has the effect of preventing debonding at the interface.*

1 Introduction

The phenomenon of void nucleation and growth in solids has long been of concern in view of its fundamental role in fracture and other failure mechanisms (see, e.g., Goods and Brown (1979) for a discussion of cavity nucleation in metals). Sudden void formation ("cavitation") in vulcanized rubber has also been observed experimentally by Gent and Lindley (1958). Nonlinear theories of solid mechanics have been used recently to account for such phenomena. The impetus for much of the recent theoretical developments has been supplied by the work of Ball (1982). Ball has studied a class of bifurcation problems for the equations of nonlinear elasticity which model the appearance of a cavity in the interior of an apparently solid homogeneous isotropic elastic body once a critical load has been attained. An alternative interpretation for such problems in terms of the growth of a *pre-existing* microvoid has been given by Horgan and Abeyaratne (1986). Further investigations of such bifurcation problems have been carried out by Stuart (1985), Podio-Guidugli et al. (1986), Sivaloganathan (1986 a,b), Chung et al. (1987), and Antman and Negron-Marrero (1987). It is worth noting that cavitation can be shown to occur only when *finite* strain measures are taken into account. The corresponding problems in linearized elasticity or in the infinitesimal strain theory of plasticity do *not* exhibit such bifurcations.

In a recent paper (Horgan and Pence, 1989) the authors have examined some aspects of the effect of *material inhomogeneity* on void formation and growth in incompressible nonlinearly elastic solids. A bifurcation problem is considered for a solid composite sphere composed of two neo-Hookean materials perfectly bonded across a spherical interface. Under a uniform radial tensile dead load, p_o, a branch of radially symmetric configurations involving a traction-free internal cavity bifurcates from the undeformed configuration. Although there is the possibility that nonradially symmetric deformations may occur, this is not addressed in Horgan and Pence (1989). Within the class of radially symmetric deformations, it is shown that a configuration with an internal cavity is the only stable solution for sufficiently large loads. In contrast to the situation for a homogeneous neo-Hookean sphere, bifurcation may occur either locally to the right (supercritical) or *to the left* (subcritical). A detailed stability analysis based on energy minimization within the class of radially symmetric solutions was carried out. In the subcritical case, this analysis predicts that the cavity has finite radius on first appearance. This discontinuous change in stable equilibrium configurations is reminiscent of the snap-through buckling phenomenon observed in certain structural mechanics problems (see, e.g.,

Contributed by the Applied Mechanics Division of The American Society of Mechanical Engineers for presentation at the Joint ASCE/ASME Applied Mechanics, Biomechanics, and Fluids Engineering Conference, San Diego, CA, July 9 to 12, 1989.

Discussion of this paper should be addressed to the Editorial Department, ASME, United Engineering Center, 345 East 47th Street, New York, N.Y. 10017, and will be accepted until two months after final publication of the paper itself in the Journal of Applied Mechanics. Manuscript received by ASME Applied Mechanics Division, October 19, 1987; final revision, September 6, 1988.

Paper No. 80-APM-28.

Budiansky, 1974), and was referred to by Horgan and Pence (1989) as "snap cavitation." Criteria for determination of the transition loads at which this occurs were developed and found to be sensitive to the precise notion of stability employed. A snap cavitation phenomenon has also been encountered recently by Antman and Negron-Marrero (1987) in the study of radially symmetric equilibrium states of *homogeneous anisotropic* compressible nonlinearly elastic bodies.

The purpose of the present paper is to provide further elaboration of these striking material instabilities in composite materials. Our main developments are twofold: We establish conditions which can lead to snap cavitation for tensile dead loading of composite spheres composed of two *arbitrary* homogeneous incompressible elastic materials perfectly bonded at a spherical interface. Secondly, an analysis of the stress distribution in such spheres is carried out and the effect of cavitation at the center on possible interface debonding is explored. The latter considerations are developed for the special case when the constituent materials are both neo-Hookean.

In Section 2, we formulate the basic boundary value problem that arises. One obtains, in addition to the trivial homogeneous state in which the sphere remains undeformed but stressed, other solutions for sufficiently large values of the applied dead load p_o, which involve an internal traction-free spherical cavity. In Section 3, the relationship between applied load and cavity radius is examined in detail. The critical load p_{cr} at which bifurcation takes place is obtained (equation (16)) and *is found to depend only on the material properties of the inner core*. The notation p_{cr} is reserved for the value of the applied load at which an equilibrium solution path involving an internal cavity intersects the equilibrium solution path corresponding to the undeformed configuration. It is important to note that this value of the load need *not* coincide with the load at which cavitation takes place. Continuous or smooth cavitation at $p_o = p_{cr}$ can only occur when bifurcation is locally to the right. However, when bifurcation at $p_o = p_{cr}$ is locally to the left, a cavity of finite radius appears at a transition load $\tilde{p}$ which may be less than p_{cr}. Characterization of $\tilde{p}$ is discussed in Section 3. We establish a criterion (see equation (23)) which differentiates between bifurcation to the right and to the left. This criterion depends only on p_{cr}, the shear moduli for infinitesimal deformations of *both* materials, and the volume fractions of the two materials. It is shown that if the volume fraction of the core material is sufficiently large, then bifurcation is to the right irrespective of material properties. Bifurcation is also to the right if the material in the surrounding shell is stronger in infinitesimal shear than the core material. Bifurcation to the left occurs only if the core is sufficiently smaller than the shell and is composed of a material which is sufficiently strong in infinitesimal shear. In Section 4, an analysis of the stress distribution is carried out for the particular case when the constituent materials are both neo-Hookean. When the cavity is nucleated, in the case of smooth cavitation, it is shown that the predominant stress variation is confined to a narrow boundary layer near the cavity wall. Finally, the effect of cavitation at the center on possible interface debonding is considered. It is assumed that debonding occurs uniformly whenever the normal stress at the interface reaches a threshold value. It is then shown that, in a quasi-static loading process, cavitation relieves the interfacial normal stress so that subsequent interface debonding is precluded.

It should be emphasized that our attention is confined to radially symmetric deformations. The possibility for bifurcations to nonradially symmetric configurations exists (see, e.g., the discussions in Needleman (1977) and in Ogden (1982, 1984) concerning such bifurcations in the problem of inflation of an initially spherical balloon) but we shall not pursue this possibility here.

2 Boundary Value Problem for a Composite Sphere: Formulation and Solution

We are concerned in what follows with a sphere composed of an incompressible isotropic elastic material. Let $D_o = \{(r, \theta, \phi) | 0 \le r < b,\ 0 < \theta \le 2\pi,\ 0 \le \phi \le \pi\}$ denote the interior of the sphere in its undeformed configuration. The sphere is subjected to a prescribed uniform radial tensile dead load of magnitude p_o on its boundary. The resulting deformation is a mapping which takes the point with spherical polar coordinates (r, θ, ϕ) to the point (R, Θ, Φ) in the deformed region D. We assume that the deformation is radially symmetric so that $R = R(r) \ge 0$, $\Theta = \theta$, $\Phi = \phi$ on D_o, where $R(r)$ is to be determined. Incompressibility then requires that

$$R(r) = (r^3 + c^3)^{1/3}, \tag{1}$$

where $c \ge 0$ is a constant to be determined. If it is found that $c = 0$, (1) *implies that the body remains a solid sphere in the* current configuration. On the other hand, if c is found to be positive, then $R(0) = c > 0$ and so there is a cavity of radius c centered at the origin in the current configuration. In this event, the cavity surface is assumed to be traction-free.

We shall be concerned in what follows with the case of a composite sphere composed of two different homogeneous isotropic incompressible materials perfectly bonded across the interface $r = a (< b)$. The strain-energy density per unit undeformed volume for such a material is denoted by $W(\lambda_1, \lambda_2, \lambda_3; r)$, where $\lambda_i (i = 1, 2, 3)$ are the principal stretches. We use the notation

$$W(\lambda_1, \lambda_2, \lambda_3; r) = \left.\begin{array}{ll} W^1(\lambda_1, \lambda_2, \lambda_3), & 0 \le r < a \\ W^2(\lambda_1, \lambda_2, \lambda_3), & a < r < b \end{array}\right\} \tag{2}$$

where W^i $(i = 1, 2)$ denotes the strain-energy density per unit undeformed volume of the respective phases. By virtue of isotropy, these expressions are invariant with respect to interchange of the λ_i.

The principal stretches associated with the radially symmetric deformation at hand are $\lambda_r = \dot{R}(r)$, $\lambda_\theta = \lambda_\phi = R(r)/r$, where the dot denotes differentiation with respect to r. Thus, in view of (1) we have

$$\lambda_r = (R/r)^{-2},\ \lambda_\theta = \lambda_\phi = R/r. \tag{3}$$

The principal components of the Cauchy stress tensor τ yield force per unit deformed area and are given by

$$\tau_{ii} = \lambda_i \frac{\partial W}{\partial \lambda_i} - p, \text{ (no sum on } i) \tag{4}$$

where p is the hydrostatic pressure associated with the incompressibility constraint $\lambda_1 \lambda_2 \lambda_3 = 1$. For the radially symmetric deformation with principal stretches given by (3), these principal stress components are

$$\begin{aligned} \tau_{RR}(r) &= v^{-2} W_1(v^{-2}, v, v; r) - p(r), \\ \tau_{\Theta\Theta} &= \tau_{\Phi\Phi} = v W_2(v^{-2}, v, v; r) - p(r), \end{aligned} \tag{5}$$

where we have used the notation (cf., Ball, 1982)

$$v = v(r) = R/r = (1 + \frac{c^3}{r^3})^{1/3}. \tag{6}$$

Notice that in (5) we consider $\tau(r)$ rather than the more conventional $\tau(R)$. Standard notation is used in (5) where the subscripts denote differentiation with respect to the appropriate argument. In (5) we have also used $W_2(v^{-2}, v, v; r) = W_3(v^{-2}, v, v; r)$ which follows from the invariance of W with respect to interchange of its first three entries. In (5) the derivatives are understood to be one-sided derivatives at the material interface $r=a$. The pressure $p(r)$ is allowed to have a jump discontinuity at $r=a$ and is assumed smooth elsewhere.

The boundary of the sphere is subjected to a uniform tensile dead load normal traction of magnitude $p_o>0$ and so yields the boundary condition

$$\tau_{RR}(b)=p_o\left(\frac{b}{R(b)}\right)^2=p_o\,[v(b)]^{-2}. \tag{7}$$

We note that the boundary conditions of vanishing shear tractions are satisfied identically.

In the absence of body forces, the composite sphere will be in equilibrium provided that div $\tau=0$, which will be true provided that

$$\frac{\partial}{\partial r}\tau_{RR}+\frac{2\dot{R}}{R}(\tau_{RR}-\tau_{\Theta\Theta})=0 \tag{8}$$

holds in each individual phase and that the normal traction component is continuous at the material interface, i.e.,

$$\tau_{RR}(a-)=\tau_{RR}(a+). \tag{9}$$

Thus, the problem to be solved is the following: *For a prescribed value of the dead load traction $p_o>0$, we seek a pressure field $p(r)$ and a constant $c\geq 0$ such that* (8), (9), *and* (7) *are satisfied where τ_{RR}, $\tau_{\Theta\Theta}$, $\tau_{\Phi\Phi}$ are given by* (5), (6). *In addition, if $c>0$, then the condition for a traction-free cavity surface*

$$\tau_{RR}(0)=0 \tag{10}$$

must also hold.

It may be readily shown that one solution to the foregoing problem, for all values of p_o, is

$$p(r)=W_1(1,1,1;r)-p_o,\; c=0. \tag{11}$$

This corresponds to the trivial homogeneous state of deformation $R(r)=r$ with corresponding stresses $\tau_{RR}=\tau_{\Theta\Theta}=\tau_{\Phi\Phi}=p_o$. Thus, even though the pressure p given in (11) is, in general, discontinuous across the interface $r=a$, the corresponding stresses are continuous.

Solutions for which $c>0$, corresponding to the presence of a traction-free cavity at the origin, have been obtained by Horgan and Pence (1989). The applied load p_o necessary to sustain a cavity of radius c is found to be

$$p_o=\left(1+\frac{c^3}{b^3}\right)^{2/3}\left[\int_{(1+c^3/b^3)^{1/3}}^{(1+c^3/a^3)^{1/3}}(v^3-1)^{-1}\frac{d\hat{W}^2}{dv}(v)dv\right.$$
$$\left.+\int_{(1+c^3/a^3)^{1/3}}^{\infty}(v^3-1)^{-1}\frac{d\hat{W}^1}{dv}(v)dv\right], \tag{12}$$

where, following Ball (1982), the notation

$$\hat{W}^i(x)=W^i(x^{-2},x,x)\quad (i=1,2) \tag{13}$$

is used. *Thus, for a given p_o, solutions involving* a *traction-free internal cavity exist only for those values of radius c* (*if any*) *that are positive roots of* (12). The associated radial stress component τ_{RR} given by (5) can then be written in the form

$$\left.\begin{aligned}\tau_{RR}(r)&=\int_{(1+c^3/r^3)^{1/3}}^{\infty}(v^3-1)^{-1}\frac{d\hat{W}^1}{dv}(v)dv, && 0\leq r\leq a\\ &=p_o(1+c^3/b^3)^{-2/3}+\int_{(1+c^3/r^3)^{1/3}}^{(1+c^3/b^3)^{1/3}}(v^3-1)^{-1}\frac{d\hat{W}^2}{dv}(v)dv, && a\leq r\leq b\end{aligned}\right\}. \tag{14}$$

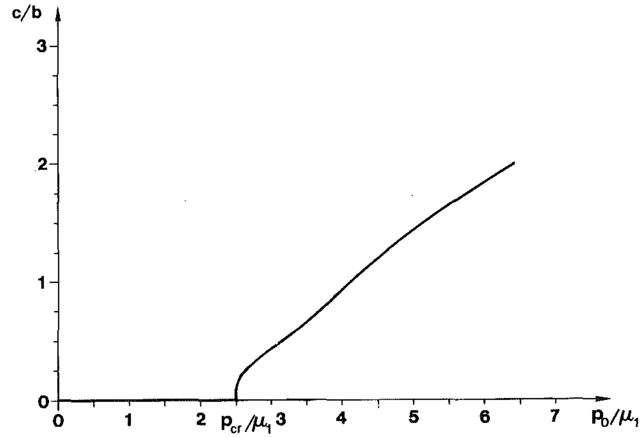

Fig. 1 Variation of the deformed cavity radius c/b with applied dead load traction p_o/μ_1 for a composite neo-Hookean sphere with strain-energy density given by (29) where $a=b/2$, $\mu_2=2\mu_1$, $p_{cr}/\mu_1=5/2$

Note that the continuity of τ_{RR} at the interface $r=a$ is ensured by (12). The remaining normal stresses $\tau_{\Theta\Theta}$, $\tau_{\Phi\Phi}$ follow from (5) as

$$\tau_{\Theta\Theta}=\tau_{\Phi\Phi}=vW_2^i(v^{-2},v,v)-v^{-2}W_1^i(v^{-2},v,v)+\tau_{RR}\qquad (i=1,2), \tag{15}$$

where $v=v(r)$ is given in (6) and the superscript i refers to the appropriate phase. Unlike the radial stress, these stresses are discontinuous across the interface $r=a$.

3 Bifurcation and Cavitation

Consider a quasi-static loading program in which the composite sphere is subjected to a dead load p_o that increases slowly from zero. Cavity formation and growth is described by the relationship $p_o=p_o(c)$ given in (12). This relationship was examined in detail by Horgan and Pence (1989) for the special case in which both constituent materials are neo-Hookean. One of the main results obtained shows that this process can occur in two distinct ways. On the one hand, smooth cavitation can take place, by which we mean that a cavity of zero radius is formed at the critical load p_{cr} with the cavity radius subsequently increasing continuously as p_o is further increased. The critical load p_{cr} is the value at which the curve $p_o=p_o(c)$ bifurcates from the straight line $c=0$ corresponding to the trivial homogeneous solution. It is shown in Horgan and Pence (1989), using an energy minimization treatment within the class of radially symmetric solutions, that this trivial homogeneous solution is unstable for $p>p_{cr}$. Smooth cavitation will occur only if the function $p_o(c)$ is monotonically increasing in c so that the curve $p_o=p_o(c)$ must bifurcate to the right at $p_o=p_{cr}$ (see, e.g., Fig. 1). On the other hand, a snap cavitation phenomenon may instead occur. By this we mean that a cavity of finite radius forms abruptly at a value of dead load $\tilde{p}$ less than or equal to p_{cr}. One situation that leads to this circumstance is the case in which the function $p_o(c)$ is monotonically decreasing for small values of c but is monotonically increasing thereafter (see, e.g., Fig. 2). The value of the transition load $\tilde{p}$ can be taken either as the value at which the trivial homogeneous solution loses absolute stability (i.e., ceases to furnish an absolute energy minimum) or, alternatively, as the value at which this trivial solution loses metastability (i.e., ceases to furnish a relative energy minimum). In the former case, $\tilde{p}<p_{cr}$ (as shown in Fig. 2), whereas in the latter case $\tilde{p}=p_{cr}$. A detailed stability analysis establishing the foregoing assertions for the neo-Hookean composite sphere is carried out in Horgan and Pence (1989).

Our purpose in this section is to establish explicit conditions which determine whether bifurcation at $p_o=p_{cr}$ is locally to the right or to the left for the case where the two constituent

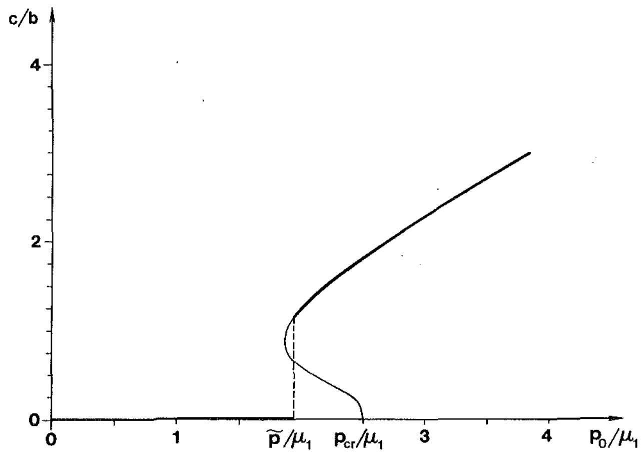

Fig. 2 Variation of the deformed cavity radius c/b with applied dead load traction p_o/μ_1 for a composite neo-Hookean sphere with strain-energy density given by (29) where $a=b/2$, $\mu_2=\mu_1/4$, $\tilde{p}/\mu_1=1.95$, $p_{cr}/\mu_1=5/2$

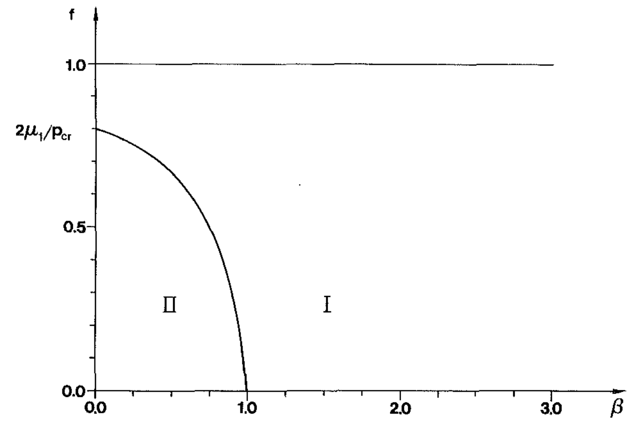

Fig. 3 Semi-infinite strip $0<f=a^3/b^3<1$, $\beta=\mu_2/\mu_1>0$. For parameter pairs (β, f) in region I, bifurcation occurs to the right while in region II, bifurcation occurs to the left. For the curve shown, $p_{cr}=5\mu_1/2$.

materials are general homogeneous, incompressible isotropic elastic materials. The critical load at which bifurcation occurs is found by letting $c\rightarrow 0+$ in (12) and so

$$p_{cr}=\int_1^\infty (v^3-1)^{-1}\frac{d\hat{W}^1}{dv}dv. \tag{16}$$

It is important to observe from (16) that *the material dependence of p_{cr} rests solely on the strain-energy density W^1 of the material occupying the inner core $0\le r<a$.* For the case of a *homogeneous* incompressible sphere, the value of p_{cr} is also given by (16) with $\hat{W}^1$ replaced by the strain-energy $\hat{W}$ of the homogeneous material (Ball, 1982).

Since the integral in (16) is improper, p_{cr} may or may not be finite, and so cavitation may or may not be possible. *Clearly, cavitation can occur in composite spheres only when a homogeneous sphere composed of the inner material alone allows for cavitation.* Henceforth we assume that this is the case, so that the integral in (16) is assumed to be finite. As regards the lower limit in (16), it is shown in the Appendix that

$$\frac{d\hat{W}^1}{dv}(1)=0,\ \frac{d^2\hat{W}^1}{dv^2}(1)=12\mu_1, \tag{17}$$

where μ_1 denotes the shear modulus for infinitesimal deformations of the inner material. Thus, by l'Hôpital's rule, the limit of the integrand in (16) is finite as $v\rightarrow 1$. Consequently, the question of whether or not p_{cr} is finite depends on the behavior of $\hat{W}^1(v)$ for *large values* of the stretch v. For a discussion of the analogous issue for the case of a *homogeneous* incompressible sphere, we refer to Ball (1982).

We turn now to the development of a criterion which determines whether the bifurcation at p_{cr} is to the right or to the left. Assume, for the moment, that Figs. 1, 2 are typical. In this case, bifurcation to the right corresponds to smooth cavitation while bifurcation to the left corresponds to snap cavitation. In general, snap cavitation must occur if bifurcation is to the left. Whether or not bifurcation to the right implies smooth cavitation depends on whether or not the curve $p_o=p_o(c)$ remains monotonic.

To determine the local character of the bifurcation at $p_o=p_{cr}$, we examine the curve $p_o=p_o(c)$ as given in (12) for small values of c. One easily finds that

$$p_o=p_{cr}+K(c/b)^3+o(c^3),\ \text{as } c\rightarrow 0 \tag{18}$$

where

$$K\equiv\lim_{c\rightarrow o} dp_o/dc^3. \tag{19}$$

This expression for K becomes

$$K=\frac{2}{3}p_{cr}-\frac{1}{3}\left(\frac{b}{a}\right)^3\lim_{v\rightarrow 1}(v^3-1)^{-1}\frac{d\hat{W}^1}{dv}$$
$$+\frac{1}{3}\left[\left(\frac{b}{a}\right)^3-1\right]\lim_{v\rightarrow 1}(v^3-1)^{-1}\frac{d\hat{W}^2}{dv}. \tag{20}$$

It is shown in the Appendix that

$$\lim_{v\rightarrow 1}(v^3-1)^{-1}\frac{d\hat{W}^i}{dv}=4\mu_i (i=1,\ 2), \tag{21}$$

where the $\mu_i>0 (i=1, 2)$ are the shear moduli for infinitesimal deformations of the inner and outer materials, respectively. Using the notation

$$f=\frac{a^3}{b^3},\ 0<f<1, \tag{22}$$

for the volume fraction of the core material to the total material, K in (20) can now be written

$$K=2/3\left[p_{cr}-2\mu_1 f^{-1}+2\mu_2(f^{-1}-1)\right]. \tag{23}$$

We see from (18) *that if $K>0$, bifurcation is to the right while if $K<0$, bifurcation is to the left.* Although our primary interest in this work concerns the *composite* sphere, it is of interest to observe that as $f\rightarrow 1$ in (23), one obtains the value of K appropriate to the homogeneous sphere composed of the inner material, namely

$$K_h\equiv 2/3(p_{cr}-2\mu_1). \tag{24}$$

Henceforth, we shall assume

$$p_{cr}-2\mu_1>0, \tag{25}$$

so that bifurcation for the *homogeneous* sphere is always assumed to be to the right.

Returning to (23), we discuss the circumstances which determine whether the bifurcation is to the right or to the left. It is convenient to treat these two cases with reference to the schematic diagram in Fig. 3. In this figure, the semi-infinite strip $0<f<1$, $0<\beta<\infty (\beta\equiv\mu_2/\mu_1)$, is divided into two regions I, II by the monotone decreasing curve

$$f=(\beta-1)/[\beta-p_{cr}/(2\mu_1)] \tag{26}$$

on which $K=0$. If (β, f) lies in region I, then $K>0$ and so bifurcation is to the right while if (β, f) lies in region II, then $K<0$ and so bifurcation is to the left. One can discuss this diagram with reference to a composite sphere of either fixed geometric properties together with varying material properties or vice versa. Taking the former view we see that, for $f>(2\mu_1/p_{cr})$, bifurcation is always to the right. *Thus, if the*

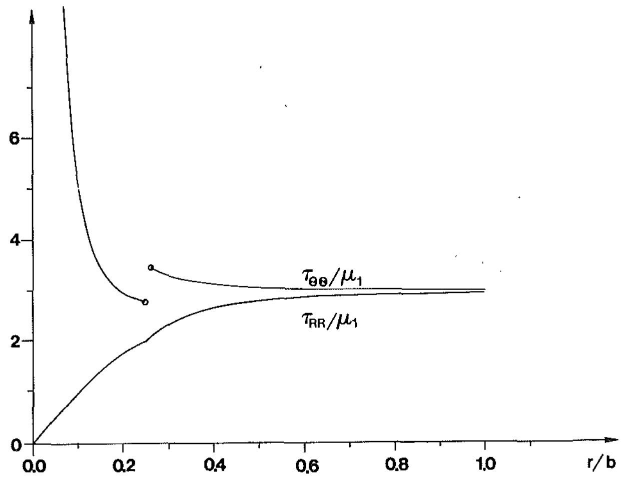

Fig. 4 Variation of the stresses $\tau_{RR}(r)$, $\tau_{\Theta\Theta}(r)=\tau_{\Phi\Phi}(r)$ with undeformed radius r subsequent to cavitation for a composite neo-Hookean sphere. Here, $\mu_2=2\mu_1$, $a=b/4$, $p_o=2.96\mu_1$.

volume fraction of the core to the total volume exceeds $2\mu_1/p_{cr}$, bifurcation is to the right regardless of the material properties of the outer material. Taking the latter view, we also see that, for $\beta\geq 1$, bifurcation is again always to the right. This corresponds to $\mu_2\geq\mu_1$. *Thus, if the material in the surrounding shell is stronger in infinitesimal shear than the core material, bifurcation is to the right irrespective of geometry.*

On the other hand, the condition for bifurcation to the left requires *both* geometric and material restrictions. These restrictions may be written as

$$f<(2\mu_1/p_{cr}) \tag{27}$$

and

$$\mu_2<\frac{\mu_1-p_{cr}f/2}{1-f}. \tag{28}$$

Thus, the occurrence of bifurcation to the left in a composite sphere requires a sufficiently small core surrounded by a shell of sufficiently weak material.

For the special case of a composite sphere composed of two neo-Hookean materials perfectly bonded at the interface $r=a$, one has

$$\left.\begin{aligned} W^1(\lambda_1,\lambda_2,\lambda_3)&=\frac{\mu_1}{2}(\lambda_1^2+\lambda_2^2+\lambda_3^2-3)\\ W^2(\lambda_1,\lambda_2,\lambda_3)&=\frac{\mu_2}{2}(\lambda_1^2+\lambda_2^2+\lambda_3^2-3)\end{aligned}\right\}. \tag{29}$$

In this case,

$$p_{cr}=5\mu_1/2 \tag{30}$$

and the preceding considerations regarding bifurcation to the right or left can be simplified (see, Horgan and Pence, 1989[1]). In fact, Figs. 1 and 2 exhibiting both smooth and snap cavitation pertain to the composite neo-Hookean sphere.

4 Stress Distribution

We proceed now to discuss the stress distribution in the composite sphere. Of particular interest is the influence of cavitation at the center on the possibility of debonding at the interface $r=a$ for sufficiently large applied loads p_o.

The stresses $\tau_{RR}(r)$, $\tau_{\Theta\Theta}(r)$, $\tau_{\Phi\Phi}(r)$, subsequent to cavitation, are given in (14), (15). Prior to that, one has only the constant stress distribution $\tau_{RR}=\tau_{\Theta\Theta}=\tau_{\Phi\Phi}=p_o$. For simplicity in what follows, we confine our subsequent discussion to the case of the composite neo-Hookean sphere (29). Thus, in this case, (14) becomes

$$\left.\begin{aligned}\tau_{RR}(r)&=\frac{\mu_1}{2}\left[\left(1+\frac{c^3}{r^3}\right)^{-4/3}+4\left(1+\frac{c^3}{r^3}\right)^{-1/3}\right],\ 0\leq r\leq a,\\ \tau_{RR}(r)&=p_o\left(1+\frac{c^3}{b^3}\right)^{-2/3}+\frac{\mu_2}{2}\left[\left(1+\frac{c^3}{r^3}\right)^{-4/3}\right.\\ &\quad-\left(1+\frac{c^3}{b^3}\right)^{-4/3}\\ &\quad\left.+4\left(1+\frac{c^3}{r^3}\right)^{-1/3}-4\left(1+\frac{c^3}{b^3}\right)^{-1/3}\right],\ a\leq r\leq b,\end{aligned}\right\} \tag{31}$$

while (15) reads

$$\tau_{\Theta\Theta}=\tau_{\Phi\Phi}=\mu_i\left[(1+c^3/r^3)^{2/3}-(1+c^3/r^3)^{-4/3}\right]+\tau_{RR}\qquad (i=1,2). \tag{32}$$

The $p_o=p_o(c)$ relation (12) now becomes

$$p_o=\frac{1}{2}\left(1+\frac{c^3}{b^3}\right)^{2/3}\Big[(\mu_1-\mu_2)\{(1+\frac{c^3}{a^3})^{-4/3}+4(1+\frac{c^3}{a^3})^{-1/3}\}+\mu_2\Big\{(1+\frac{c^3}{b^3})^{-4/3}+4(1+\frac{c^3}{b^3})^{-1/3}\Big\}\Big]. \tag{33}$$

It is readily verified that τ_{RR} is a continuous monotone increasing function of r in $0\leq r\leq b$, with a discontinuity in slope at the interface $r=a$. Similarly, $\tau_{\Theta\Theta}=\tau_{\Phi\Phi}$ are easily shown to be monotone decreasing functions of r in the respective ranges $0\leq r\leq a$, $a\leq r\leq b$, with a jump discontinuity at the interface $r=a$. Since $\tau_{RR}(0)=0$, it is clear from (32) that $\tau_{\Theta\Theta}=\tau_{\Phi\Phi}\rightarrow\infty$ as $r\rightarrow 0$. In Fig. 4, all these stresses are plotted for a case with $\mu_1<\mu_2$. When $\mu_1>\mu_2$, the jump in $\tau_{\Theta\Theta}=\tau_{\Phi\Phi}$ is in the opposite direction to that in Fig. 4, while the slope discontinuity in τ_{RR} has opposite character. Observe from (32), that $\tau_{\Theta\Theta}(r)=\tau_{\Phi\Phi}(r)>\tau_{RR}(r)$ for $c>0$.

Another feature of interest concerning the stresses $\tau_{RR}(r)$, $\tau_{\Theta\Theta}(r)$, $\tau_{\Phi\Phi}(r)$ immediately after cavitation is the presence of a boundary layer near the cavity wall when smooth cavitation taken place. To see this, consider the limit as $c\rightarrow 0+$ in (31), (32), and (33) for fixed $r>0$. Thus, from (33), we find $\lim_{c\rightarrow 0+} p_o(c)=5\mu_1/2\equiv p_{cr}$ and so $(31)_2$ yields, for fixed r in $[a,b]$,

$$\lim_{c\rightarrow 0+}\tau_{RR}(r)=p_{cr},\ (a\leq r\leq b), \tag{34}$$

whereas $(31)_1$ yields, for fixed r in $(0,a]$,

$$\lim_{c\rightarrow 0+}\tau_{RR}(r)=p_{cr},\ (0<r\leq a). \tag{35}$$

Since $\tau_{RR}(0)=0$, (34) and (35) show that the radial stress suffers a rapid growth near the cavity wall for applied dead loads p_o slightly larger than p_{cr}. The boundary layer is illustrated in Fig. 5, for different values of p_o. From (32), it is clear that a similar boundary layer exists in the stress components $\tau_{\Theta\Theta}$, $\tau_{\Phi\Phi}$. Observe that such severe boundary layers for the stresses do *not* occur in the case of snap cavitation since in this case the deformed cavity radius c jumps to a finite value upon cavity formation.

Observe also, from Fig. 5, that the values of the radial stress

[1]The shear moduli employed in Horgan and Pence (1989) are one-half the actual infinitesimal shear moduli used here.

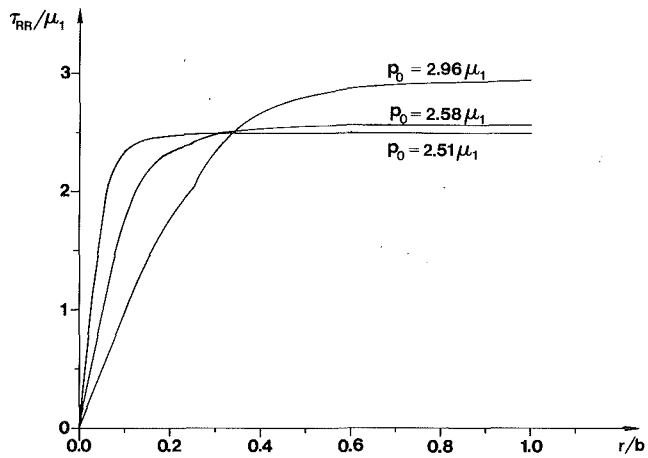

Fig. 5 Variation of the radial stress $\tau_{RR}(r)$ with undeformed radius subsequent to cavitation for a composite neo-Hookean sphere. Here, $\mu_2 = 2\mu_1$, $a = b/4$.

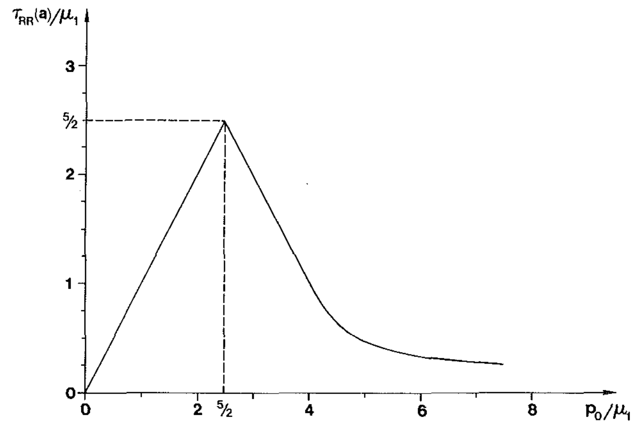

Fig. 6 Variation of radial stress at the interface $\tau_{RR}(a)/\mu_1$ with applied dead load traction p_o/μ_1 for a composite neo-Hookean sphere with $\mu_2 = 2\mu_1$, $a = b/4$

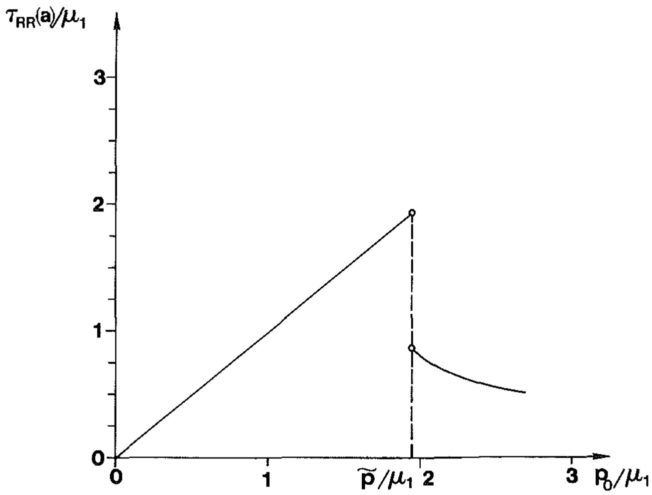

Fig. 7 Variation of radial stress at the interface $\tau_{RR}(a)/\mu_1$ with applied dead load traction p_o/μ_1 for a composite neo-Hookean sphere with $\mu_2 = \mu_1/4$, $a = b/2$, $\tilde{p}/\mu_1 = 1.95$

τ_{RR}, for fixed values of r in $0<r<a$, decrease as the dead load p_o increases beyond the value p_{cr}. In fact this monotone property may be verified directly from $(31)_1$, since this equation shows that $d\tau_{RR}/dc<0$ (for fixed r in $0<r\leq a$). In Fig. 6, we plot the values of the radial stress at the interface $r=a$ versus the applied dead load traction p_o for a sphere of the same material and geometric configuration as used in Fig. 5. The straight line portion of the graph corresponds to the constant stress field that occurs prior to cavitation. Figure 6 is typical when smooth cavitation taken place. In the event of snap cavitation, the corresponding figure exhibits a jump discontinuity in $\tau_{RR}(a)$ at the value of $p_o=\tilde{p}$ at which cavitation occurs (Fig. 7).

The foregoing considerations have immediate implications relating to the issue of possible debonding at the material interface $r=a$. Suppose that the interface bond is sustained only so long as the normal stress at the interface remains less than a threshold value. Thus, debonding would occur if

$$\tau_{RR}(a)=\tau_d \tag{36}$$

where τ_d is an independently determined measure for the strength of the interface bond. Consider again a quasi-static loading process in which p_o increases slowly from zero. In the absence of cavitation, interface debonding would occur when p_o reaches the value τ_d. If $\tau_d<p_{cr}$ for smooth cavitation ($\tau_d<\tilde{p}$ for snap cavitation), then in the quasi-static process just envisioned, debonding occurs when $p_o=\tau_d$ and cavitation is no longer relevant. On the other hand, if $\tau_d>p_{cr}(\tau_d>\tilde{p})$, then cavitation occurs when $p_o=p_{cr}(p_o=\tilde{p})$. The resulting stress relief at the interface then precludes the criterion (36) from being met and thus eliminates the possibility of interface debonding.

Acknowledgments

The work of one of the authors (C.O.H.) was supported, in part, by the U.S. National Science Foundation under Grant MSM 85-12825, and by the Composite Materials and Structures Center, Michigan State University under the REED program. We are grateful to the reviewers and the Associate Editor for their comments on an earlier version of the paper.

References

Antman, S. S., and Negron-Marrero, P. V., 1987, "The remarkable nature of radially symmetric equilibrium states of aeolotropic nonlinearly elastic bodies," *J. Elasticity*, Vol. 18, pp. 131–164.

Ball, J. M., 1982, "Discontinuous equilibrium solutions and cavitation in nonlinear elasticity," *Phil. Trans. R. Soc. Lond.*, Vol. A 306, pp. 557–610.

Budiansky, B., 1974, "Theory of buckling and post-buckling behavior of elastic structures," *Advances in Applied Mechanics*, Vol. 14, C. -S. Yih, ed., Academic Press, New York, pp. 1–65.

Chung, D. -T., Horgan, C. O., and Abeyaratne, R., 1987, "A note on a bifurcation problem in finite plasticity related to void nucleation," *Int. J. Solids Structures*, Vol. 23, pp. 983–988.

Gent, A. N., and Lindley, P. B., 1958, "Internal rupture of bonded rubber cylinders in tension," *Proc. R. Soc. Lond.*, Vol. A 249, pp. 195–205.

Goods, S. H., and Brown, L. M., 1979, "The nucleation of cavities by plastic deformation," *Acta Met.*, Vol. 27, pp. 1–15.

Horgan, C. O., and Abeyaratne, R., 1986, "A bifurcation problem for a compressible nonlinearly elastic medium: Growth of a micro-void," *J. Elasticity*, Vol. 16, pp. 189–200.

Horgan, C. O., and Pence, T. J., 1989, "Void nucleation in tensile dead-loading of a composite incompressible nonlinearly elastic sphere," *J. Elasticity*, Vol. 21, in press.

Needleman, A., 1977, "Inflation of spherical rubber balloons," *Int. J. Solids Structures*, Vol. 13, pp. 409–421.

Ogden, R. W., 1982, "Elastic deformations of rubberlike solids," *Mechanics of Solids* (R. Hill 60th Anniversary Volume), H. G. Hopkins and M. J. Sewell, eds., Pergamon Press, New York, pp. 499–537.

Ogden, R. W., 1984, *Non-Linear Elastic Deformations*, Halsted Press, New York.

Podio-Guidugli, P., Vergara Caffarelli, G., and Virga, E. G., 1986, "Discontinuous energy minimizers in nonlinear elastostatics; An example of J. Ball revisited," *J. Elasticity*, Vol. 16, pp. 75–96.

Sivaloganathan, J., 1986a, "Uniqueness of regular and singular equilibria for spherically symmetric problems of nonlinear elasticity," *Arch. Ration. Mech. Analysis*, Vol. 96, pp. 97–136.

Sivaloganathan, J., 1986b, "A field theory approach to stability of radial equilibria in nonlinear elasticity," *Math. Proc. Camb. Phil. Soc.*, Vol. 99, pp. 589–604.

Stuart, C. A., 1985, "Radially symmetric cavitation for hyperelastic materials," *Ann. Inst. Henri Poincaré–Analyse non linéaire*, Vol. 2, pp. 33–66.

APPENDIX

Verification of (17), (21)

For our purposes here, it is convenient to drop the superscript notation on W introduced in (2). To establish (17), we recall from (13) that

$$\hat{W}(v) = W(v^{-2}, v, v) \tag{A1}$$

and so

$$\frac{d\hat{W}(v)}{dv} = -2v^{-3}W_1(v^{-2}, v, v) + 2W_2(v^{-2}, v, v) \tag{A2}$$

on using the chain rule and the fact that $W_2(v,^{-2} v, v) = W_3(v^{-2}, v, v)$. Thus,

$$\frac{d\hat{W}}{dv}(1) = 2[W_2(1, 1, 1) - W_1(1, 1, 1)] = 0, \tag{A3}$$

which establishes $(17)_1$ as desired.

To verify $(17)_2$, we recall from finite elasticity theory (see, e.g., Ogden, 1984) that the shear modulus for infinitesimal deformations of an incompressible homogeneous isotropic material with strain-energy density $\bar{W}(I_1, I_2)$ is given by

$$\mu = 2\left(\frac{\partial \bar{W}}{\partial I_1} + \frac{\partial \bar{W}}{\partial I_2}\right)\Big|_{I_1 = I_2 = 3.} \tag{A4}$$

Here, $I_1 = \lambda_1^2 + \lambda_2^2 + \lambda_3^2$, $I_2 = \lambda_1^2\lambda_2^2 + \lambda_2^2\lambda_3^2 + \lambda_3^2\lambda_1^2$ are the usual first and second invariants. Thus, from $(A1)$ we have

$$\hat{W}(v) = \bar{W}(\tilde{I}_1(v), \tilde{I}_2(v)) \tag{A5}$$

where

$$\tilde{I}_1(v) = v^{-4} + 2v^2,\ \tilde{I}_2(v) = 2v^{-2} + v^4. \tag{A6}$$

Using the chain rule, and observing that

$$\frac{d\tilde{I}_1}{dv} = \frac{d\tilde{I}_2}{dv} = 0 \text{ at } v = 1, \tag{A7}$$

it is readily verified that

$$\frac{d^2\hat{W}(1)}{dv^2} = \left(\frac{\partial \bar{W}}{\partial I_1}\frac{d^2\tilde{I}_1}{dv^2} + \frac{\partial \bar{W}}{\partial I_2}\frac{d^2\tilde{I}_2}{dv^2}\right)\Big|_{\substack{I_1 = I_2 = 3 \\ v = 1}} \tag{A8}$$

and so it follows from $(A4)$ on using $(A6)$, that

$$\frac{d^2\hat{W}(1)}{dv^2} = 12\mu, \tag{A9}$$

which establishes $(17)_2$ as desired.

Finally, (21) may be verified by using $(A3)$, l'Hôpital's rule, and $(A9)$.

Void Growth in Elastic-Plastic Materials

C. L. Hom

R. M. McMeeking
Mem. ASME

Department of Materials and Department of Mechanical Engineering,
University of California,
Santa Barbara, Calif. 93106

Three-dimensional finite element computations have been done to study the growth of initially spherical voids in periodic cubic arrays. The numerical method is based on finite strain theory and the computations account for the interaction between neighboring voids. The void arrays are subjected to macroscopically uniform fields of uniaxial tension, pure shear, and high triaxial stress. The macroscopic stress-strain behavior and the change in void volume were obtained for two initial void volume fractions. The calculations show that void shape, void interaction, and loss of load carrying capacity depend strongly on the triaxiality of the stress field. The results of the finite element computation were compared with several dilatant plasticity continuum models for porous materials. None of the models agrees completely with the finite element calculations. Agreement of the finite element results with any particular constitutive model depended on the level of macroscopic strain and the triaxiality of the remote uniform stress field.

Introduction

The nucleation, growth, and eventual coalescence of voids by plastic deformation is an important failure mechanism in ductile metals (Rogers, 1960; Bluhm and Morrisey, 1966). In ductile fracture, voids are nucleated under tension at hard particles which crack or tear loose. The voids grow due to plasticity and eventually coalesce to form a microcrack or cause the propagation of an existing crack. In addition, the collapse of voids due to plasticity occurs in the pressing of metal powders at certain rates and temperatures (Helle, Easterling, and Ashby, 1985). In the pressing of powder metals, particles are forced together and bonding across necks develops between the powders at which stage the porosity is interconnected. At a later stage, however, the pores become isolated. Rate-independent plasticity can dominate pore contraction, although the final closure occurs by creep if the temperature is sufficiently high.

For progress in understanding both the phenomenon of ductile fracture and the process of nonisostatic pressing, it is desirable to have models for the growth/collapse of voids in arbitrary states of stress. McClintock (1968) developed growth predictions for isolated cylindrical voids, while later Rice and Tracey (1969) obtained results for spherical holes by minimizing a functional of the velocity field. The model for spherical holes was later improved by Budiansky, Hutchinson, and Slutsky (1982). The solutions show the strong effect of stress triaxiality on the rate of growth. In all cases, the analysis was carried out for a single void in an infinite matrix and so the results are valid only for a porosity which is a small fraction of the whole. On the other hand, Needleman (1972a) and Tvergaard (1981) treated cylindrical holes in a square array subject to a macroscopically uniform state of stress. They used the finite element method to obtain the solutions. Interactions between voids are apparent in the velocity fields and the local stress distributions. The coupling is probably stronger in these two-dimensional problems than in the interactions between initially spherical voids. In an attempt to understand such three-dimensional effects, Andersson (1977) and Tvergaard (1982) used the finite element method to analyze the growth of a spherical void in a high triaxial stress state constrained to axially symmetric deformation in a cylinder. Because of the constraint, the implied interaction between neighboring voids is still strong. Hancock (1986) has used similar calculations of axisymmetric deformations to study void-void interactions and observed that there are strong couplings between voids on the 45 deg planes.

Another approach to modeling void growth extends the Rice and Tracey approach by using the same method applied to spherical cells containing spherical holes. This technique was used by Gurson (1977a,b) to study the behavior of voids in high volume fractions for a variety of states of stress. At low volume fractions, the results agree with those of Rice and Tracey (1969). The rate of dilatation of the voids was determined by Gurson (1977a,b) and presented in indirect form because the main purpose was to obtain a yield condition and associated flow law for a macroscopic composite containing a volume fraction of spherical voids. The stress-strain laws that resulted are presented in the Appendix to this paper. Modifications of these laws were developed by Tvergaard (1981,1982) (see Appendix) to improve their agreement with

Contributed by the Applied Mechanics Division of The American Society of Mechanical Engineers for presentation at the Joint ASCE/ASME Applied Mechanics, Biomechanics, and Fluids Engineering Conference, San Diego, Calif., July 9 to 12, 1989.

Discussion of this paper should be addressed to the Editorial Department, ASME, United Engineering Center, 345 East 47th Street, New York, NY 10017, and will be accepted until two months after final publication of the paper itself in the Journal of Applied Mechanics. Manuscript received by ASME Applied Mechanics Division, December 23, 1987; final revision, September 9, 1988.

Paper No. 89-APM-32.

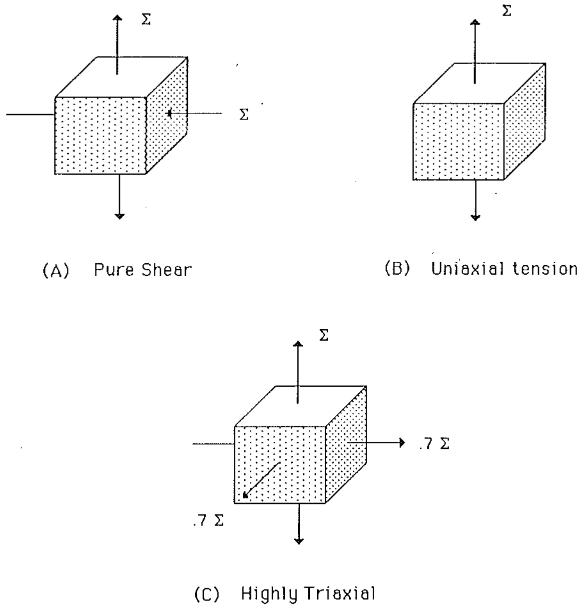

Fig. 1 The three stress states

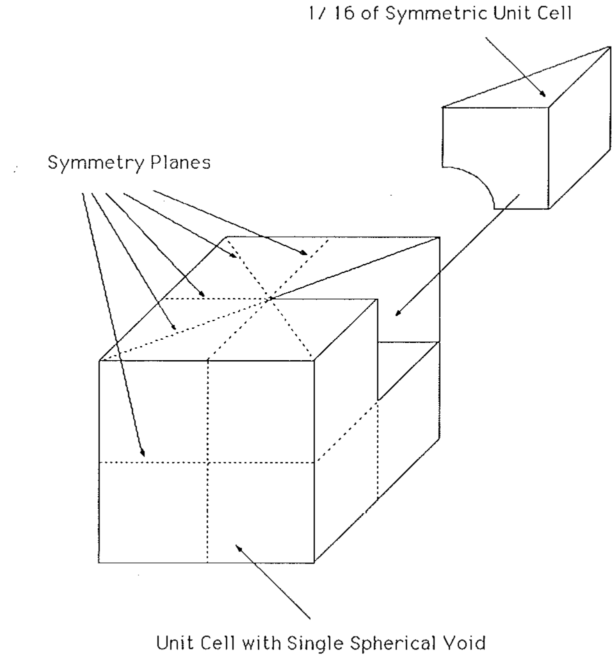

Fig. 2 Symmetry of unit cell and the one-sixteenth cell used for the finite element calculations

calculations of bifurcation into shear banding in square arrays of cylindrical holes and axisymmetric spherical holes.

There is little work on comparing these constitutive laws for porous ductile materials with experimental data. Bourcier, Koss, Smelser, and Richmond (1986) have shown that partially densified powder metallurgy specimens of Ti and Ti-6A1-4V have lower flow stresses than predicted by the models of Gurson (1977a,b) and Tvergaard (1981,1982). Similarly, Richmond (1987) has data for iron confirming this overprediction. Based on these data for Ti, Ti-6A1-4V and iron, and on considerations of yielding in shear of a material containing a cubic array of spherical voids, Richmond and Smelser (1985) have devised an alternative yield function and a corresponding flow law which agrees with the experimental data. This constitutive law is described also in the Appendix.

In this paper, the behavior of initially spherical holes in cubic arrays is analyzed by a large deformation finite element technique and thus follows on from the initial work of Harren (1983). A representative fraction of a unit cell is treated with appropriate symmetry and periodic conditions to produce macroscopically homogeneous deformation. The full, three-dimensional interactions between voids are accounted for, and a moderate and high volume fraction of the voids are studied. Simple shear, uniaxial tension, and a state of high triaxiality are applied in the calculations. The results are compared with the models of Gurson (1977a,b), Tvergaard (1981,1982), and Richmond and Smelser (1985) in an attempt to assess which conforms most closely to the finite element calculations.

Problem Formulation

A cubic array of initially spherical voids in an infinite elastic-plastic body was considered. The void sizes and spacings were chosen to give two initial porosities of 6.5 percent and 0.82 percent. The material was originally stress-free, and monotonically changing principal stresses were applied to the infinite body in such a manner that they were aligned with the axes of the cubic array. The states of stress were macroscopically homogeneous and accounted for pure shear, uniaxial tension, and an axisymmetric state of high triaxiality as shown in Fig. 1.

The matrix material surrounding the voids was elastically isotropic subject to yielding governed by the Von Mises criterion with σ_f taken as the true flow stress in uniaxial tension. Isotropic strain hardening was used with a power law form given by

$$\left(\frac{\sigma_f}{\sigma_0}\right)^{1/N} - \left(\frac{\sigma_f}{\sigma_0}\right) = \frac{3G\bar{\epsilon}^p}{\sigma_0} \qquad (1)$$

where σ_0 is the initial yield stress, G is the elastic shear modulus, and $\bar{\epsilon}^p$ is the tensile equivalent plastic strain.

Large strains and rotations were allowed for through the finite deformation formulation of McMeeking and Rice (1975) as modified and implemented in the ABAQUS finite element code (Hibbitt, Karlsson, and Sorensen (1984)). As such, the method is similar to that developed by Needleman (1972b) and Osias and Swedlow (1974).

Because of the periodic arrangement of the voids, it was sufficient to consider only a single unit cell consisting of a cube containing one void. Each cell deforms into a right parallelopiped due to imposed velocities on the boundary. The evolving shape was determined by the state of stress. The technique of Needleman (1972a) was used to ensure the correct rect state of stress. This technique consists of adjusting the uniform normal displacement increments of each face of the unit cells to ensure that the average true stress on each face maintains the desired level as shown in Fig. 1. However, a reduction of the size of the problem was possible due to the symmetries illustrated in Fig. 2. Those shown in the figure pertain to the axisymmetric states of uniaxial stress and high triaxiality, in which case it is necessary to solve the problem in only on sixteenth of the unit cell as shown. In pure shear, the one-sixteenth segment and its neighbor across the diagonal plane must be used.

Relative to the one-sixteenth segment shown in Fig. 2, the boundary conditions are as follows for the axisymmetric stress states. All faces are free of shear traction. The void surface is also free of normal traction. The bottom, front, and diagonal faces are constrained to have zero-normal velocity. The top surface is given a uniform-specified normal velocity. As previously discussed, the remaining face on the right is given a uniform, normal velocity sufficient to induce the desired average true stress, either zero (uniaxial stress case) or 70 percent of the average tensile true stress (high triaxiality case). In

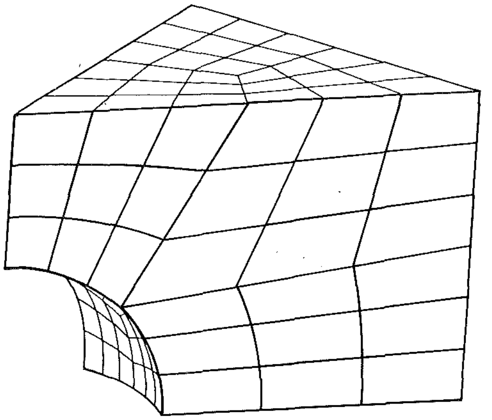

Fig. 3 Typical finite element mesh used to model the one-sixteenth cell of the void-matrix aggregate

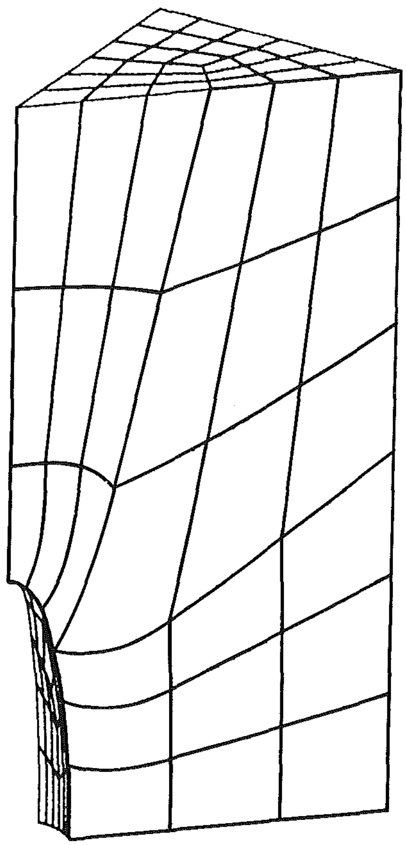

Fig. 4 The deformed mesh for uniaxial tension with an initial void volume fraction $f_i = 0.82$ percent and hardening exponent $N = 0.1$ at a true strain $E_3 = 0.70$

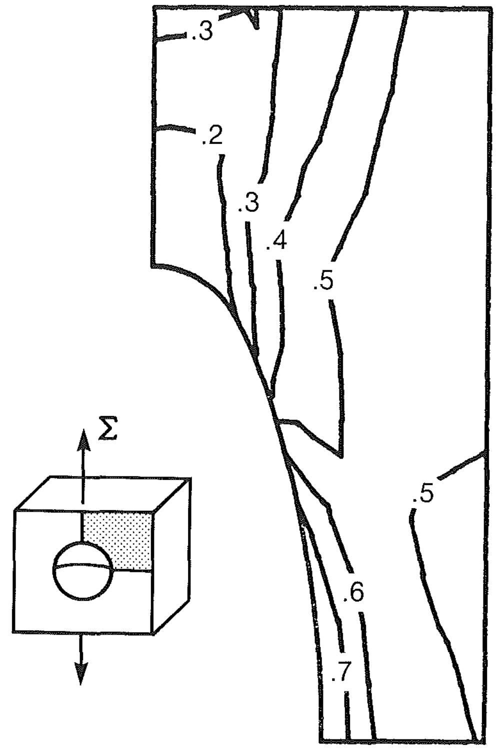

Fig. 5 A contour plot of the equivalent plastic strain $\bar{\epsilon}^p$ for uniaxial tension at a true strain $E_3 = 0.70$ with $f_i = 6.5$ percent and $N = .1$

the case of pure shear, again, all surfaces are free of shear traction and the void is completely traction-free. Relative to the one-eighth segment, the bottom, front, rear, and left faces are constrained to have zero-normal velocity. The top surface is given a specified uniform normal velocity and the face on the right is required to have a uniform normal velocity such that the average true stress there is the negative of the true stress on the top.

Finite Element Solutions

The ABAQUS finite element program developed by Hibbitt, Karlsson, and Sorensen (1984) was used to solve the problems described in the previous section. The large deformation updated Lagrangian feature was used with the modified Riks algorithm described by Powell and Simons (1981) for incrementing the load. This iteration scheme was useful since an unstable load-displacement response was obtained in the calculations.

The finite element mesh used for the axisymmetric problems is shown in Fig. 3, whereas the mesh for pure shear was simply double that shown. The illustrated mesh has 135 twenty-noded isoparametric brick elements and 1084 nodes. The dilatation in the element was represented by extra degrees-of-freedom. The model was freed from locking overconstraint by the feature of ABAQUS based on the method of Nagtegaal, Parks, and Rice (1974).

The calculations were carried out incrementally up to macroscopic true strains of the order 0.7 for the uniaxial tension state and 0.3 for the pure shear state and the high triaxial stress state. The macroscopic true strain is defined to be $E_3 = \ln(l/l_0)$ where l_0 is the undeformed length of the edge of the unit cell shown in Fig. 2 and l is the current length of the unit cell in the x_3 direction which is vertical in Fig. 1. Typically, 50 increments were necessary to obtain macroscopic true strains of the order 0.7 for the uniaxial tension state and 0.3 for the pure shear state and the high triaxial stress state. In each increment, iterations were performed to achieve equilibrium at the end of the step. In a typical case, there were four iterations which were carried out in ABAQUS using a Newton method with a Jacobian formed from the tangent elastic-plastic stiffness.

The calculations were carried out on supercomputers in various locations. The Cray 1A at the University of Minnesota and the Cray X-MP/48 at the San Diego Supercomputer Center were both used. A calculation with 135 elements, 3252 degrees-of-freedom, 50 increments, and 4 iterations per increment took about 700 minutes on the Cray 1A at the University of Minnesota.

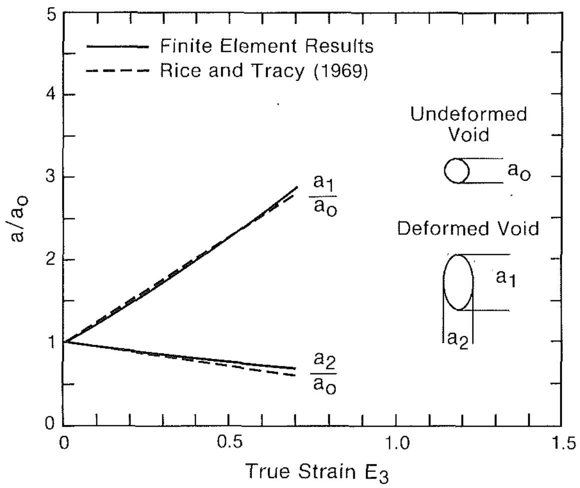

Fig. 6 Comparison of change in void shape for uniaxial tension predicted by the finite element analysis and the Rice and Tracey solution for an isolated void

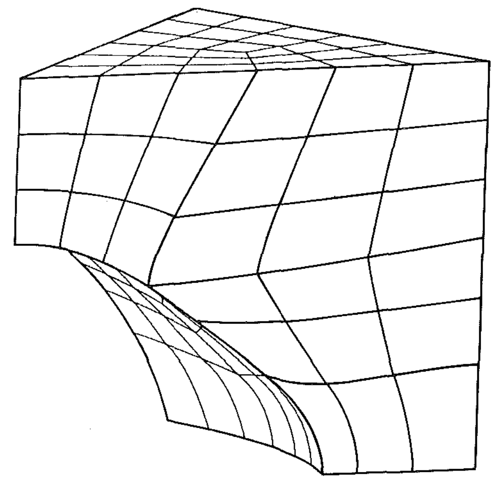

Fig. 8 The deformed mesh for the high triaxial stress state, with an initial void volume fraction $f_i = 6.5$ percent and hardening exponent $N = 0.1$ at a true strain $E_3 = 0.25$

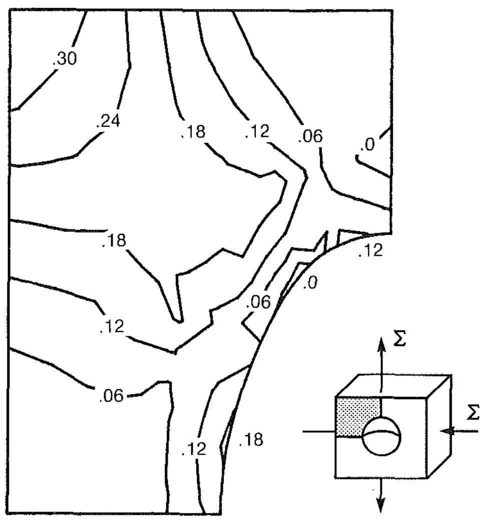

Fig. 7 A contour plot of the equivalent plastic strain $\bar{\epsilon}^p$ for pure shear at a true strain $E_3 = 0.25$ with $f_i = 6.5$ percent and $N = .1$

Results for Growth of Voids in Cubic Cells

The finite element calculations were carried out for a power-law hardening matrix material with $E/\sigma_0 = 200$ and $\nu = 0.3$. The uniaxial true stress/logarithmic tensile strain law given by equation (1) was used with $N = 0.1$. In this section, the results for initial void volume fractions f_i of 6.5 percent and 0.82 percent are presented for three different loadings: uniaxial tension, pure shear, and highly triaxial stress.

***(i)* Change in Void Shape.** In the case of uniaxial tension, the initially spherical void elongates in the tensile direction with increasing strain. Figure 4 shows the deformed finite element mesh for $f_i = 0.82$ percent at a tensile true strain of 0.7. The holes are long and narrow and the ligaments between neighboring voids are like columns with a curvilinear cross-shape for the section. Figure 5, a contour plot of the equivalent plastic strain for $f_i = 6.5$ percent, shows that the plastic deformation is concentrated in these ligaments. In Fig. 6, the change in the void's major and minor axes predicted by the finite element calculations is compared with the results of Rice and Tracey (1969) for isolated spherical voids. The almost identical behavior of the two solutions indicates that little or no void interaction occurs between neighboring voids in the cubic array under uniaxial tension. In this way, behavior of the initially spherical voids differs greatly from that predicted by Needleman (1972a) for cylindrical voids in square cells under uniaxial tension. Needleman found that after a stage of transverse contraction, cylindrical holes start to grow laterally with high strains in the ligaments. The change in behavior occurs at moderate strains of 0.3. Therefore, it seems that the interaction of transverse neighbors is stronger for cylindrical voids than for spherical voids.

In the case of pure shear, the voids elongate in the tensile direction and contract in the compressive direction, but the void volume fraction remains almost exactly constant throughout the whole load history. Figure 7 is a contour plot of $\bar{\epsilon}^p$ for $f_i = 6.5$ percent. In this case, the maximum effective plastic strain occurs between neighboring voids in the principal shear plane. Unlike uniaxial tension, this maximum does not occur at the void's surface or in the ligament between transverse neighboring voids. Instead, the maximum occurs at the intersection of shear, band-like features extending from void to void.

In contrast to the low triaxial stress states, when there is high triaxiality, the voids dilate substantially and strong neighbor interaction occurs. For $f_i = 0.82$ percent the void's volume increases steadily and the hole remains roughly spherical in shape. For the higher initial void volume fraction $f_i = 6.5$ percent, the strength of void interaction is more apparent. In Fig. 8, the deformed mesh at a tensile strain of 0.25 shows that the void has started to bulge out towards its transverse neighbor. Figure 9, a contour plot of $\bar{\epsilon}^p$ for $f_i = 6.5$ percent, shows that the plastic strains are concentrated in the ligament and are significantly larger than for the low triaxial cases at the same nominal strain. The ligament between voids transverse to the maximum principal stress exhibits necking behavior, which indicates that the voids are beginning to coalesce.

***(ii)* Initial Yield Predictions.** The results of the finite element calculation can be used also to evaluate the accuracy of the existing continuum models for dilatant plastic behavior caused by the presence of voids. The Gurson, Tvergaard, and Richmond yield conditions of such models have been discussed earlier and are described in detail in the Appendix. One method of comparison is to examine the yield point predicted by the finite element calculations and the continuum models for the three loading conditions. The yield point in the finite element calculations is estimated to be at the region of rapid reduction of the tangent stiffness in the load deflection curves.

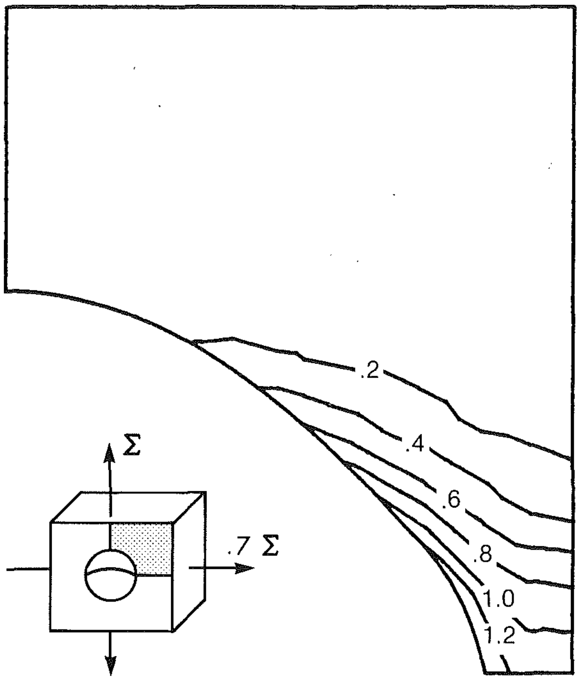

Fig. 9 A contour plot of the equivalent plastic strain $\bar{\epsilon}^p$ for the high triaxial stress state at true strain $E_3 = 0.20$ with $f_i = 6.5$ percent and $N = 0.1$

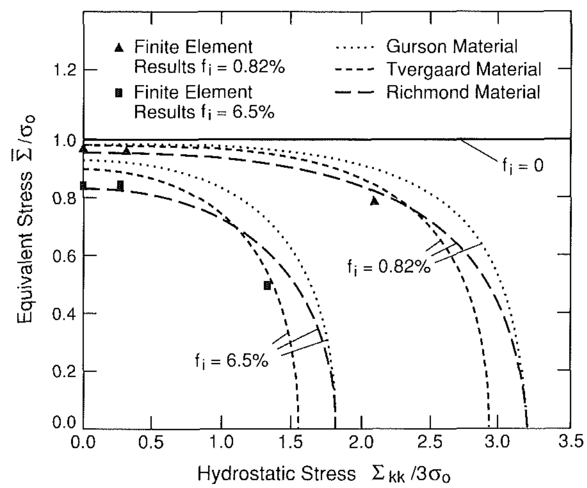

Fig. 10 Yield stresses predicted by finite element analysis and yield surfaces of the Gurson, Tvergaard, and Richmond models

In Fig. 10, the yield surfaces of the continuum models and the yield points predicted by the finite element analysis are plotted in the plane of tensile equivalent stress versus hydrostatic stress. For the low triaxial stress states of pure shear and uniaxial tension, the yield points of the finite element calculations agree best with the Richmond model. This result is interesting since the Richmond model is based on the concept of yielding being concentrated on shear bands at 45 deg to the principal stress directions and is more persuasive in the case of pure shear. For pure shear with an initial void volume fraction of 6.5 percent, the finite element results predict yield at $\Sigma = 0.49\ \sigma_0$ when the pure material yields at $\Sigma = 0.58\ \sigma_0$. By comparison, initial yield occurs at $\Sigma = 0.54\ \sigma_0$, $0.52\ \sigma_0$, and $0.48\ \sigma_0$ for the Gurson, Tvergaard, and Richmond models, respectively. In the uniaxial tension case, the finite element calculation predicts yield at $\Sigma = 0.85\ \sigma_0$ for an initial void

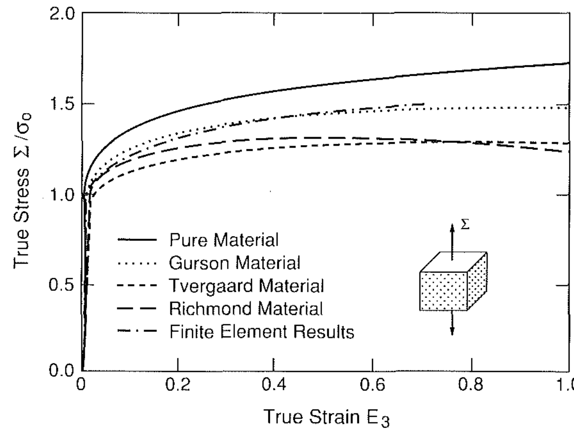

Fig. 11 Comparison of the stress-strain behavior of the finite element analysis and the continuum models for uniaxial tension, with an initial void volume fraction $f_i = 6.5$ percent and a hardening coefficient $N = 0.1$

volume fraction of 6.5 percent where the Gurson, Tvergaard, and Richmond models predict yield at $\Sigma = 0.93\ \sigma_0$, $0.89\ \sigma_0$ and $0.84\ \sigma_0$, respectively.

For the high triaxial stress state, the finite element calculations agree better with the Tvergaard and Richmond models. For an initial void volume fraction of 6.5 percent, the finite element results predict yield at $\Sigma = 1.66\ \sigma_0$ compared with $\Sigma = 3.33\ \sigma_0$ for the material without voids. By comparison, yield occurred at $\Sigma = 1.93\ \sigma_0$, $1.69\ \sigma_0$, and $1.83\ \sigma_0$ for the Gurson, Tvergaard, and Richmond models, respectively. This behavior is not surprising, since Tvergaard's modification of Gurson's equation is based partially on axisymmetric finite element results for a high triaxial stress state. Richmond's modification of Gurson's equation is based on kinematic shearing modes at low triaxiality, but retains the behavior of the solution by Torre (1948) for a hydrostatic tension in a rigid-plastic material containing spherical voids.

***(iii)* Plastic Flow Behavior.** In addition to the yield point calculation, the stress-strain curves of the finite element computations have been used for comparison with the plastic flow characteristics of the continuum models. The results of this comparison depend strongly on the macroscopic stress state. In the low triaxiality cases, where the void volume remains roughly constant, the stress-strain curves of the finite element calculation become relatively stiff at high strains compared to the behavior at low strain and further loss in the material's load carrying capacity due to void growth is negligible. However, for the high triaxiality case, rapid void growth causes a substantial decay in the load-deflection curve of the finite element calculation. It was found that this type of behavior was not completely described by any particular continuum model.

Figure 11 shows the stress-strain curves predicted by the finite element analysis and the three continuum models for uniaxial tension with $f_i = 6.5$ percent and $N = 0.1$. The finite element computation rapidly diverges from the initial yield prediction of the Richmond model and conforms to the Tvergaard prediction up to about 0.1 true strain. From a strain of 0.2 to about 0.4 strain, the numerical results stiffen toward the Gurson prediction. However, for true strains above 0.4, the finite element model maintains a higher load carrying capacity than for all three continuum models. The behavior of the finite element computation for $f_i = 0.82$ percent is similar to the higher porosity case. The results agree with the Tvergaard prediction at low strain, and diverge to the Gurson result with increasing strain. At high strains, a stiff response compared with the continuum models is observed. For uniaxial tension, the voids of the finite element analysis grow at a slower rate than the voids of the continuum models.

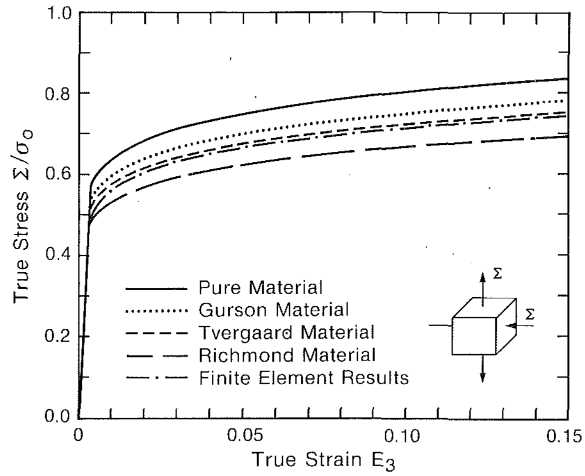

Fig. 12 Comparison of the stress-strain behavior of the finite element analysis and the continuum models for pure shear, with an initial void volume fraction $f_i = 6.5$ percent and a hardening coefficient $N = 0.1$

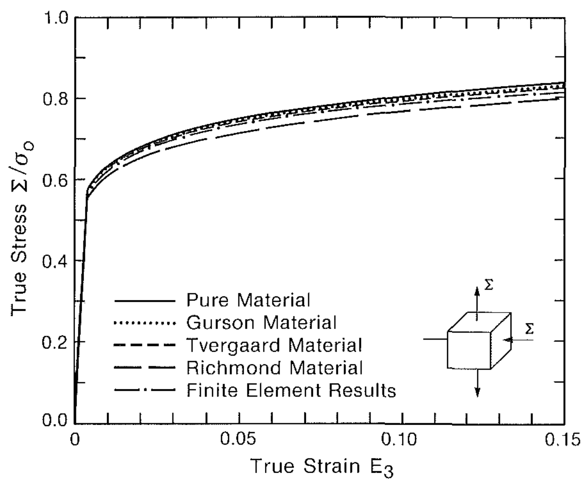

Fig. 13 Comparison of the stress-strain behavior of the finite element analysis and the continuum models for pure shear, with an initial void volume fraction $f_i = 0.82$ percent and a hardening coefficient $N = 0.1$

At high strains, the void volume fraction predicted by the continuum models increases at an accelerating rate while the rate of increase of the void volume fraction predicted by the finite element method seems to be tending towards a low asymptotic value. Since they are idealized to remain spherical, the voids of the continuum models are modeled as growing in the transverse directions and thus interact strongly with neighboring voids. However, the voids of the finite element solution grow as ellipsoids and give rise to ligaments which only change their cross-sectional area slowly. These ligaments have a larger cross-sectional area and are capable of carrying more load than the ligaments surrounding spherical voids of the same current volume fraction. This determines the difference between the flow stress predictions of the continuum models and the finite element predictions, as summarized in Fig. 11. The dominance of void shape change in the finite element results at high strains results in lower void growth rates which, in turn, results in higher load carrying capacity. This explains why the finite element model does not lose load carrying capacity at high strains like the continuum models. This result indicates that, in addition to the void volume fraction, internal variables are required in the continuum models to account for the effect of void shape changes.

Figure 12 shows the true stress-strain behavior of the finite

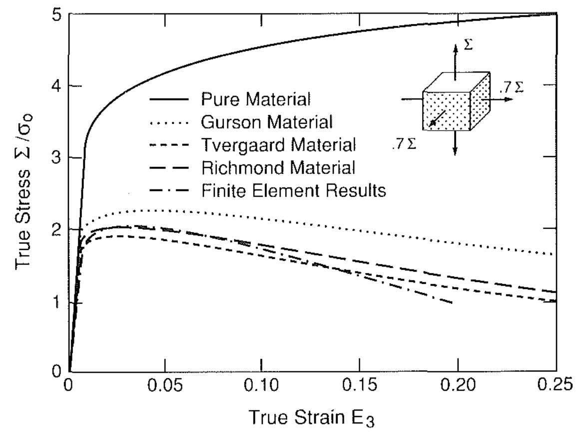

Fig. 14 Comparison of the stress-strain behavior of the finite element analysis and the continuum models for the high triaxial stress state, with an initial void volume fraction $f_i = 6.5$ percent and a hardening coefficient $N = 0.1$

element model and the continuum models for pure shear loading with an initial void volume fraction of 6.5 percent and a hardening exponent of 0.1. As in the uniaxial stress case, the finite element prediction diverges rapidly from the initial agreement with the Richmond model. At strains larger than 0.01, the agreement between the Tvergaard model and the finite element results is good. At this stage, the finite element results predict a loss of load carrying capacity of 11 percent compared to the material without voids. The loss of load carrying capacity predicted by the Gurson, Tvergaard, and Richmond materials are 7, 10, and 17 percent, respectively. Figure 13 shows the true stress-strain behavior for the finite element analysis and the continuum models for the lower initial porosity of 0.82 percent. Even though the finite element prediction of initial yield agrees best with the Richmond model, continued straining increases the macroscopic flow stress of the cubic cell until at 0.05 strain the effective value is only slightly lower than the prediction of the Tvergaard model. However, thereafter, the trend is for the finite element results to move gradually away from the Tvergaard prediction and back down towards the Richmond model. Overall, though, the Tvergaard model is in best agreement with the finite element calculations.

Unlike the low triaxial stress states, the character of the finite element calculation for the high triaxial stress state depends more on the initial void volume fraction. Figures 14 and 15 show the true stress-strain behavior of the finite element and continuum models with initial porosities of 6.5 percent and 0.82 percent, respectively, both with a strain-hardening exponent of 0.1. In each case the finite element calculation reaches a maximum in load in the early stages of straining. For an initial void volume fraction of 6.5 percent, this maximum is followed by a rapid drop in the load carrying capacity compared with the continuum models. However, this sharp drop is not observed in the lower initial porosity material. As noted earlier, in the finite element calculations, the voids for the 0.82 percent initial porosity remain spherical, while the voids for the 6.5 percent initial porosity bulge out towards their neighbors. It is clear that there is a strong void-void interaction in the high void volume fraction case and this gives rise to the rapid decay of the flow stress for the finite element calculations in Fig. 14. By comparison, the Richmond model agrees very well with the finite element results up to strains of 0.1. However, at higher strains, all the continuum models overestimate the load carrying capacity at high porosities because they underestimate the void-void interaction. It is of some interest that the Gurson model predicts quite well the void volume fraction in the finite element

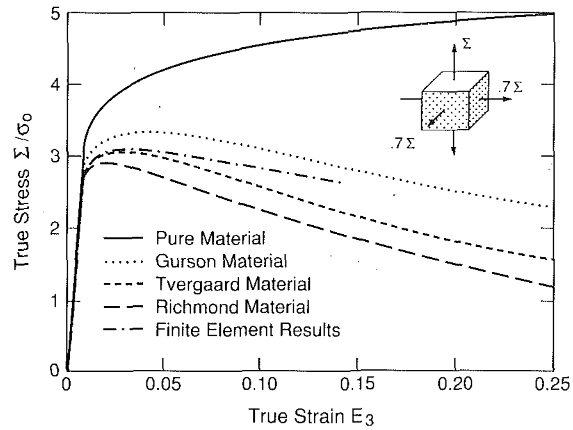

Fig. 15 Comparison of the stress-strain behavior of the finite element analysis and the continuum models for the high triaxial stress state, with an initial void volume fraction $f_i = 0.82$ percent and a hardening exponent $N = 0.1$

calculations above strains of about 0.05 in the high initial porosity case. However, this agreement does not lead, in turn, to a good agreement between the macroscopic flow stress. By contrast, all of the continuum models overpredict the void volume fraction of the finite element calculations when the initial porosity is 0.82 percent, although the Gurson predictions are the best of the three models. In Fig. 15, it can be seen that, at first, the Tvergaard model agrees best with the finite element calculations. After a strain of about 0.05, the finite element results seem to be converging on the Gurson predictions, although, as just noted, the Gurson model does not predict the void volume fraction very well. At the largest strain attained in the finite element calculation for $f_i = 0.82$ percent (nearly 0.15), the void volume fraction is about 4 percent. Extrapolation of the void growth trend in this finite element calculation indicates that at a strain of 0.25, the void volume fraction would be about 6.5 percent. Thus, the strong void-void interaction observed in the case $f_i = 6.5$ percent should set in and soften the response of the cubic cell model when the strain is around 0.25, if not earlier.

Discussion

The results of the finite element calculations indicate that, depending on the level of strain, void shape change and void-void interaction influence the macroscopic stress-strain relationship of an elastic-plastic material containing a cubic array of initially spherical voids of equal size. It is to be expected that the same phenomena will influence the overall stress-strain behavior of materials containing more random distributions of voids of various sizes and shapes. The simplifications used in the calculations presented in this paper do not allow us to address the features of the behavior arising from the random nature of void size, shape, and distribution. However, we assume that the special arrangement of a cubic array of initially spherical voids of equal size behaves under plastic straining in a manner which reflects the basic features of the more general case when somewhat equi-axed cavities are involved. This can also be said of calculations based on spherical or ellipsoidal voids in circular cylinders (Andersson, 1977; Tvergaard, 1982; and Hancock, 1986) or spherical voids in spherical cells (Gurson (1977a,b)) which have been used by others to generate models for the ductile behavior of a material containing voids. However, the cubic cell used here has the advantage that it fills space. In addition, nonaxisymmetric stress states, such as pure shear, can be studied easily using the cubic array. In consequence, we believe that our calculations provide a reliable basis for the assessment of continuum elastic-plastic constitutive laws (Tvergaard, 1981,1982; Gurson, 1977a,b; and Richmond and Smelser, 1985) developed to describe materials containing voids, especially in the case where the voids are of uniform size and initially spherical.

None of the three continuum models (Gurson, 1977a,b; Tvergaard, 1981,1982; Richmond and Smelser, 1985) reproduce all aspects of the stress-strain behavior of the cubic array. It is interesting that even in the high triaxiality case, which all three are designed for, the continuum models are not precise. It should be said that for low void volume fractions and substantial strains greater than 0.1, the Gurson model is reasonably good in the high stress triaxiality situation. However, the slope of the stress-strain curve in this case is modeled less accurately by the Gurson equations (a deficiency of all the models). Thus, material behavior sensitive to the slope of the stress-strain curve, such as shear banding, may still not be reproduced well by this model. In other situations, void shape change or void-void interactions lead to different continuum models being valid at different strain levels. The simplest situation is pure shear, where initial yielding takes place at the level predicted by the Richmond model, but as strain increases, the flow stress rises to the Tvergaard level. Enhanced continuum models with additional internal variables, such as those proposed by Becker, Smelser, and Richmond (1985) and Hancock (1986), are necessary to allow for the macroscopic behavior influenced by void shape change and void-void interaction.

The comparisons made so far relate continuum models to cubic cell calculations carried out by the finite element method. We have made no attempt to compare the finite element calculations with experimental measurements. However, the data for partially densified powder metallurgy specimens of Ti-6A1-4V (Bourcier et al., 1986) and iron (Richmond, 1987) indicate that the flow stresses are lower than those predicted by the Gurson model and also by the softer Tvergaard model. Indeed, Richmond (1987) favors the Richmond model, softer still, to simulate the stress-strain curves of the powder metallurgy specimens. In this sense, the finite element cubic cell calculations presented here predict a flow stress for porous materials which is too high. It is possible that features not present in the cubic cell calculations, such as inhomogeneity of particle size, shape and distribution, are responsible for the softness of the response of the stress-strain behavior in the experiments. Indeed, Bourcier et al. (1986) and Thomson and Hancock (1985) have postulated that, with random distribution of particles, there are large colonies of voids surrounded by nearly incompressible voidless material. This situation would create higher triaxial stresses in the regions of high void concentration and, consequently, a larger loss in the material's load carrying capacity.

Acknowledgments

This work was carried out while both authors were supported by Grant MSM85-04411 from the National Science Foundation. We are also grateful to Dr. J. W. Hancock of the University of Glasgow and Dr. O. Richmond of the Alcoa Technical Center for helpful comments and discussion. We gratefully acknowledge the provision of the ABAQUS program by Hibbitt, Karlsson, and Sorensen, Inc. of Providence, R.I.

References

Andersson, H., 1977, *J. Mech. Phys. Solids*, Vol. 25, p. 217.

Becker, R. C., Smelser, R. E., and Richmond, O., 1985, unpublished research.

Bluhm, J. I., and Morrisey, J. R., 1966, *Proc. 3rd Int. Conf. Fracture*, T. Yokobori, T. Kawasaki, and J. L. Swedlow, eds., Vol. III, Japanese Soc. for Strength and Fracture of Materials, Sendai, p. 1739.

Bourcier, R. J., Koss, D. A., Smelser, R. E., and Richmond, O., 1986, *Acta Metall.*, Vol. 34, p. 2443.

Budiansky, B., Hutchinson, J. W., and Slutsky, S., 1982, *Mechanics of Solids*, The Rodney Hill 60th Anniversary Volume, H. G. Hopkins, and M. J. Sewell, eds., Pergamon Press, Oxford, p. 13.

Gurson, A. L., 1977a, *J. Engng Matl. Tech., Trans. ASME*, Series H, Vol. 99, p. 2.

Gurson, A. L., 1977b, *Proc. 4th Int. Conf. Fracture*, Taplin, D. M. R., ed., Vol. 2, Pergamon Press, Oxford, p. 357.

Hancock, J. W., 1986, *Chemistry and Physics of Fracture*, R. M. Latanison and R. H. Jones, eds., Martinus Nijhoff, Dordrecht, p. 148.

Harren, S. V., 1983, "The Effects of Spherical Voids in an Isotropic Strain-Hardening Elastic-Plastic Medium," M. S. Thesis, University of Illinois at Urbana-Champaign.

Helle, A. S., Easterling, K. E., and Ashby, M. F., 1985, *Acta Metall.*, Vol. 33, p. 2163.

Hibbitt, H. D., Karlsson, B. I., and Sorensen, E. P., 1984, ABAQUS, User Manual, Version 4, Providence, RI.

McClintock, F. A., 1968, ASME JOURNAL OF APPLIED MECHANICS, Vol. 35, p. 363.

McMeeking, R. M., and Rice, J. R., 1975, *Int. J. Solids Struct.*, Vol. 11, p. 601.

Nagtegaal, J. C., Parks, D. M., and Rice, J. R., 1974, *Comp. Meth. Appl. Mech. Engng.*, Vol. 4, p. 153.

Needleman, A., 1972a, ASME JOURNAL OF APPLIED MECHANICS, Vol. 39, p. 964.

Needleman, A., 1972b, *J. Mech. Phys. Solids*, Vol. 20, p. 111.

Osias, J. R., and Swedlow, J. L., 1974, *Int. J. Solids Struct.*, Vol. 10, p. 321.

Powell, G., and Simons, J., 1981, *Int. J. Nonlinear Struct.*, Vol. 17, p. 1455.

Rice, J. R., and Tracey, D. M., 1969, *J. Mech. Phys. Solids*, Vol. 17, p. 201.

Richmond, O., 1987, private communication.

Richmond, O., and Smelser, R. E., 1985, Alcoa Technical Center Memorandum.

Rogers, H. C., 1960, *Trans. Metall. Soc.*, A.I.M.E., Vol. 218, p. 498.

Thomson, R. D., and Hancock, J. W., 1985, *Res Mechanica*, Vol. 16, p. 135.

Torre, C., 1948, *Berg-und Huttenleute der Hochschule Loben*, Vol. 93, p. 62.

Tvergaard, V., 1981, *Int. J. Fracture*, Vol. 17, p. 389.

Tvergaard, V., 1982, *Int. J. Fracture*, Vol. 18, p. 237.

APPENDIX

Elastic-Plastic Continuum Models For Materials With Voids

The macroscopic stress $\boldsymbol{\Sigma}$ in a representative element of the composite material composed of solid and voids is the volume average of the local stress $\boldsymbol{\sigma}$. The average is taken over the solid and the void space. Macroscopic yielding of an isotropic composite can be phrased in terms of a function of macroscopic stress, uniaxial flow or yield stress σ_f of the matrix material, and internal variables representing the void volume fraction f. Gurson (1977a,b) developed an isotropic yield function by considering spherical voids contained within spherical cells. Flow fields were considered for a variety of stress states and an upper-bound technique was used to determine the yield function. Gurson approximated his numerical results with

$$\Phi = \frac{\bar{\Sigma}^2}{\sigma_f^2} + 2f\, q_1 \cosh\left(\frac{\Sigma_{kk}}{2\sigma_f}\right) - (1 + q_2 f^2) = 0 \qquad (A1)$$

with $q_1 = q_2 = 1$. The macroscopic tensile equivalent stress is defined, as usual, by

$$\bar{\Sigma}^2 = \frac{3}{2}\Sigma'_{ij}\Sigma'_{ij} \qquad (A2)$$

where $\boldsymbol{\Sigma}'$ is the macroscopic stress deviator. The form stated in equation ($A1$) was intended primarily for conditions of high triaxiality. For values of $\Phi < 0$, the material responds elastically and $\Phi > 0$ is forbidden. It should be noted that when $f = 0$, the yield condition ($A1$) reduces to the standard Von Mises form.

Tvergaard (1981,1982) modified the original Gurson function by introducing the parameters q_1 and q_2. Tvergaard suggested the values $q_1 = 1.5$ and $q_2 = q_1^2$ based on considerations of bifurcation in shear of a square array of cylindrical holes. These values and form ($A1$) are used in this paper when the "Tvergaard material" is referred to. The form ($A1$), with $q_1 = q_2 = 1$, is used as the "Gurson material."

Richmond and Smelser (1985) have also proposed a modified form of Gurson's yield surface. One reason for this modification was the possibility that shear bands could dominate the yielding process, or that shear bands could easily develop after yielding. It was noted that a cubic array of spherical voids may yield in shear at a lower stress than predicted by the laws of Gurson or Tvergaard. Richmond and Smelser (1985) argued that an effective volume fraction of voids could be calculated on a two-dimensional surface giving the maximum porosity. For cubic arrays of voids, this gives an effective volume fraction proportional to $f^{2/3}$. However, for high triaxial stress states, a yield function based solely on this effective volume fraction results in yielding at very low stresses. For this reason Richmond and Smelser (1985) also weighted the effect of the mean stress on the yield surface to obtain better agreement with calculations by Torre (1948) for voids in a rigid-perfectly plastic material under a pure hydrostatic load. These considerations just discussed lead to a modified Gurson law stated as

$$\Phi = \frac{\bar{\Sigma}^2}{\sigma_f^2} + 2f^{\,m} \cosh\left(\frac{m\Sigma_{kk}}{2\sigma_f}\right) - (1 + f^{\,2m}) = 0 \qquad (A3)$$

where m is a material constant between 2/3 and 1. Based on experimental data, Richmond and Smelser (1985) suggested $m = (2+N)/3$ where N is the exponent for the power hardening law $\sigma_f = k(\bar{\epsilon}^p)^N$. In this paper, "Richmond material" refers to equation ($A3$) with m equal to 2/3.

In all cases, the macroscopic material has an associated flow law given by

$$D_{ij}^p = \frac{1}{H}\eta_{ij}\eta_{kl}\dot{\Sigma}_{kl} \qquad (A4)$$

where $\mathbf{D}$ is the macroscopic rate of deformation which is the volume average of $\mathbf{d}$ and $\dot{\boldsymbol{\Sigma}}$ is the stress rate. The tensor $\boldsymbol{\eta}$ is such that

$$\eta_{ij} = \frac{3}{2}\,\frac{\Sigma'_{ij}}{\sigma_f} + \alpha\delta_{ij} \qquad (A5)$$

where δ_{ij} is the Kronecker delta. H is defined as

$$H = h\left(\omega + \frac{\alpha\Sigma_{kk}}{\sigma_f}\right)^2 - 3\sigma_f\,(1-f)\alpha\gamma \qquad (A6)$$

where $h = d\sigma_f/d\bar{\epsilon}^p$ is the hardening rate of the matrix material and

$$\omega = \frac{\bar{\Sigma}^2}{\sigma_f^2}. \qquad (A7)$$

For the Gurson and Tvergaard material

$$\alpha = \frac{1}{2}q_1 f \sinh\left(\frac{\Sigma_{kk}}{2\sigma_f}\right). \qquad (A8)$$

and

$$\gamma = q_1 \cosh\left(\frac{\Sigma_{kk}}{2\sigma_f}\right) - q_1^2 f. \qquad (A9)$$

For the Richmond material, equations ($A8$) and ($A9$) for α and γ should be replaced by

$$\alpha = \frac{m}{2} f^{\,m} \sinh\left(\frac{m\Sigma_{kk}}{2\sigma_f}\right) \qquad (A10)$$

$$\gamma = m\left(f^{\,m-1}\cosh\left(\frac{m\Sigma_{kk}}{2\sigma_f}\right) - f^{\,2m-1}\right). \qquad (A11)$$

The rate of increase of the equivalent plastic strain in the matrix is chosen to ensure equivalency of the plastic work. This leads to

$$\dot{\bar{\epsilon}}^p = \frac{\left(\omega + \frac{\alpha\Sigma_{kk}}{\sigma_f}\right)\left(\frac{\dot{\omega}}{2} + \frac{\alpha\dot{\Sigma}_{kk}}{\sigma_f}\right)}{(1-f)H} \qquad (A12)$$

which is used to determine the value of h since it can be regarded as a function of $\bar{\epsilon}^p$.

It is worth noting that the Kronecker delta in equation ($A5$) ensures that the plastic dilatation of the material occurs by growth of holes only. Consequently, the rate of change of f is given by

$$\dot{f} = (1-f)D^p_{kk}. \qquad (A13)$$

In these continuum models, any tendency for the voids to change shape is ignored and the constitutive laws remain isotropic. This is suitable for states of high triaxiality where rapid dilatation of the holes takes place. At lower triaxialities, such as in uniaxial stress, the shape change of the holes is important, although ignored in the continuum models discussed in this Appendix.

The laws described here for the Gurson, Tvergaard, and Richmond materials were integrated for the states of stress depicted in Fig. 1. The initial values of f and the matrix-hardening laws were chosen to correspond to equivalent finite element calculations. The results are discussed in the text along with those of the finite element solutions.

Obtaining Residual Stresses in Metal Forming After Neglecting Elasticity on Loading

Yong-Shin Lee

Paul R. Dawson
Assoc. Mem., ASME

Sibley School of Mechanical and Aerospace Engineering,
Cornell University,
Ithaca, NY 14853

A methodology for computing residual stresses in forming operations is examined in which the elasticity is neglected during the loading phase of the operation. The elastic response is recovered on unloading through the analysis of an initially-stressed body. Two examples are presented which provide a quantitative assessment of the accuracy of the approach. The first is the axisymmetric expansion of a thick-walled tube. In this case the residual stresses are compared to those computed with an elastic-plastic analysis for both the loading and unloading phases. The second example is a ring upsetting application that has been analyzed using a finite element formulation and for which there are experimental data available for comparison.

Introduction

Deformation processes, by their nature, typically induce significant inelastic strains to alter the workpiece geometry. This is particularly true in many bulk-forming operations, such as extrusion or rolling, where inelastic strains are large throughout the workpiece. In many other types of processes the zones within the workpiece where the strains are large are restricted to a few critical locations. However, it is these zones of large inelastic strains that accommodate most of the desired shape changes. For example, in sheet bending the strains are large where the changes in curvature are large, while in the rest of the workpiece the deformations remain small.

Numerical techniques have assumed an important role in the analysis of forming operations because of their ability to deal with many complexities inherent to forming. Historically, the development of numerical models for deformation processes has followed two paths. One is an extension of elastic-plastic analyses of small strain applications where the deformations are a combination of elastic and inelastic strains, but the governing equations are amended for large strains (Hibbitt et al., 1970; McMeeking and Rice, 1975; Argyris and Kleiber, 1977). The second approach is to assume that the inelastic behavior is dominant and to neglect the concurrent elastic response (Thompson et al., 1969; Kobayashi, 1977; Dawson, 1978). This approach is motivated by the fact that where the shape changes are significant the magnitude of the inelastic strains far exceeds that of the elastic strains. Considerable computational advantages may stem from the simplifying assumption of neglecting the elastic response, but at the expense of not capturing some (possibly important) aspects of the total response. For instance, thermal expansion of a workpiece due to heating during a forming process may alter the stress field and cause yielding to occur earlier (or later) than in a corresponding viscoplastic approximation. Residual stresses cannot be predicted unless elasticity is included at some stage in the simulation.

In this article, we examine a specific method for computing residual stresses wherein the loading phase is strictly inelastic and the unloading is strictly elastic. Such an approach, if accurate, could give an estimate of the residual stresses due to forming without the computational expense of including elasticity throughout the simulation. This notion is not new in metal forming (Crandal and Dahl, 1959), and in fact was applied for the analysis of springback in several forming processes (Zienkiewicz et al., 1978; Monfort and Bragard, 1985). However, as pointed out in the previously mentioned work (Zienkiewicz et al., 1978), its application has not been explored adequately in terms of quantitative comparisons to experiment or to solutions with both elastic and inelastic behaviors throughout the simulation. In the context of using finite element methods, obtaining sufficiently accurate residual stresses is complicated by the use of displacement based formulations for incompressible motions. In such formulations, the stresses are (usually) discontinuous derivative quantities of lower order. Special techniques often are required to evaluate them accurately.

To help assess the accuracy of this approach we compare the residual stress state predicted using the strictly inelastic loading approximation to that obtained by analyzing the entire process with an elastic-plastic formulation. One set of comparisons is given for the deformation of a thick-walled tube subjected to internal pressure. As a second example the residual elastic strains in an upset ring are computed with this approximate approach and then are compared to those computed with a full elastic-plastic simulation and those measured experimentally (Flower et al., 1987). The second example has

Contributed by the Applied Mechanics Division of THE AMERICAN SOCIETY OF MECHANICAL ENGINEERS for publication in the JOURNAL OF APPLIED MECHANICS.

Discussion on this paper should be addressed to the Editorial Department, ASME, United Engineering Center, 345 East 47th Street, New York, N.Y. 10017, and will be accepted until two months after final publication of the paper itself in the JOURNAL OF APPLIED MECHANICS. Manuscript received by ASME Applied Mechanics Division, April 4, 1988; final revision, June 10, 1988.

Table 1 Material parameters for the simplified Hart's model for annealed 304 stainless steel

a_0 (s^{-1})	f_0 (s^{-1})	G (GPa)	σ_0^* (MPa)
$1.36 \cdot 10^{35}$	$8.03 \cdot 10^{26}$	73.1	150.0

Q_0 (kcal/mole)	Q_0' (kcal/mole)	c_0	γ
98	21.7	$3.01 \cdot 10^{-9}$	0.15

M	m	n	m'
7.8	5.0	7.5	4.0

been analyzed using a finite element formulation, and requirements to obtain accurate stresses are addressed.

Governing Equations

The workpiece will be assumed to be isothermal and fully dense. Further, it is assumed that it is deforming slowly so that inertia may be neglected. For this case the balance of linear momentum (equilibrium) is written as:

$$\operatorname{div} \boldsymbol{\sigma} = 0 \tag{1}$$

where $\boldsymbol{\sigma}$ is the Cauchy stress tensor and the body forces are neglected.

The rate of deformation ($\mathbf{d}$) at points within the body is defined as the symmetric portion of the velocity gradient ($\mathbf{L}$):

$$\mathbf{d} = \frac{1}{2}(\mathbf{L} + \mathbf{L}^T). \tag{2}$$

In general, the material response may be written as a combination of elastic and inelastic motions. In this work, the rate of deformation is decomposed into elastic and inelastic components:

$$\mathbf{d} = \mathbf{d}_e + \mathbf{d}_n, \tag{3}$$

for which constitutive relations may be written separately. Hereafter, subscripts e and n indicate elastic and inelastic components, respectively. The forming processes discussed herein have been divided into two distinct phases: loading and unloading. The loading phase is dominated by the inelastic deformations, while during unloading the elasticity is assumed to dominate. In the simulations presented later, the complete response is approximated with the dominant mode of behavior so that the following relationships apply:

$$\mathbf{d} = \mathbf{d}_n \quad \text{during loading, and} \tag{4}$$

$$\mathbf{d} = \mathbf{d}_e \quad \text{during unloading.} \tag{5}$$

The elastic unloading behavior obeys a linear, isotropic relationship of the form:

$$\boldsymbol{\sigma} = 2G\boldsymbol{\epsilon}_e + \eta \operatorname{tr}(\boldsymbol{\epsilon}_e)\mathbf{I}. \tag{6}$$

Here, G and η are the Lame's constants, $\mathbf{I}$ is the identity tensor, and $\boldsymbol{\epsilon}_e$ is a small strain measure that is linear in the displacement gradients and is measured from the configuration of the body just prior to unloading.

The inelastic behavior is assumed to be isotropic and isochoric. The deviatoric response is described by a viscoplastic state variable model that consists of three parts. The first is the yield condition wherein the magnitude of the deviatoric stress necessary to induce inelastic straining is a function of the rate of deformation, the temperature, and the current state. The second part is the flow law which states that the direction of inelastic straining is in the direction of the deviatoric stress. Finally, the evolution equation defines the rate of change of the state variable in terms of the rate of inelastic deformation, temperature, and the current state. For our purpose here we consider only changes to the state variable caused by strain hardening, which can include both athermal hardening and dynamic recovery; static recovery is neglected. The use of isotropic state variable models with these features for forming simulations is discussed in detail in separate articles (Dewhurst and Dawson, 1984; Dawson, 1987; Eggert and Dawson, 1987).

The specific model used in both applications presented later is a single transient version of Hart's model (Hart, 1976) that captures the change in flow stress with straining over large strains. In this version of Hart's model, the flow stress (yield condition) for a material point is the sum of two contributions:

$$\sigma' = \tau'^{v} + \tau'^{p}, \tag{7}$$

where σ' is the effective deviatoric Cauchy stress.[1] A prime indicates a deviatoric quantity and superscripts v and p denote the viscous and plastic contributions, respectively. The viscous contribution is from the frictional resistance to dislocation glide along slip planes:

$$\tau'^{v} = G\left(\frac{d_n'}{a}\right)^{1/M}; \qquad a = a_0 \exp\left(\frac{-Q_0'}{R\theta}\right), \tag{8}$$

where d_n' is the effective rate of deformation,[2] R is the universal gas constant. The plastic contribution represents the resistance to inelastic flow as controlled by dislocation motion past strong barriers:

$$\tau'^{p} = \sigma^* \exp\left[-\left(\frac{d^*}{d_n'}\right)^{\gamma}\right];$$

$$d^* = f_0\left(\frac{\sigma^*}{G}\right)^{m} \exp\left(\frac{-Q_0}{R\theta}\right). \tag{9}$$

This resistance increases with straining due to an increase in the dislocation density since the dislocations themselves act as barriers to continued dislocation motion. The scalar state variable, σ^*, quantifies the barrier strength in an average (isotropic) sense. The contribution from the frictional mechanism is usually much smaller than that from the plastic mechanism except at high strain rates or low temperatures. The parameters a and d^* depend on the temperature (θ) and state variable as shown. The flow law is a Levy-Mises relation:

$$\mathbf{d}_n' = \frac{3d_n'}{2\sigma'}\boldsymbol{\sigma}'. \tag{10}$$

The evolution equation for the state variable predicts a decreasing rate of evolution as the state measure increases or the stress associated with dislocation motion past strong barriers (the plastic contribution) decreases. So long as deformation is occurring the evolution rate is never identically zero. However, the rate of change eventually does become very small. The evolution for the state variable is given by:

$$\frac{D}{Dt}(\sigma^*) = c_0\sigma^*\left(\frac{G}{\sigma^*}\right)^{m'}\left(\frac{\tau'^{p}}{\sigma^*}\right)^{n} d_n', \tag{11}$$

where D/Dt denotes a material derivative. In equations (8) to (11), Q_0, Q_0', a_0, c_0, n, M, m, γ, m', and f_0 are material parameters which must be determined from experimental data. The initial value of the state variable, σ_0^*, also must be known for the workpiece material. The above parameters have been evaluated for 304 stainless steel based primarily on stress relaxation and constant deformation rate compression tests (Eggert and Dawson, 1987; Cook, 1957; McQueen et al., 1975; Kumar et al., 1979). The parameters used in the examples discussed herein are listed in Table 1.

The formulation is completed with specification of the

[1]$(\sigma' = \sqrt{3/2 \operatorname{tr}(\boldsymbol{\sigma}'\boldsymbol{\sigma}')})$

[2]$(d_n' = \sqrt{2/3 \operatorname{tr}(\mathbf{d}_n'\mathbf{d}_n')})$

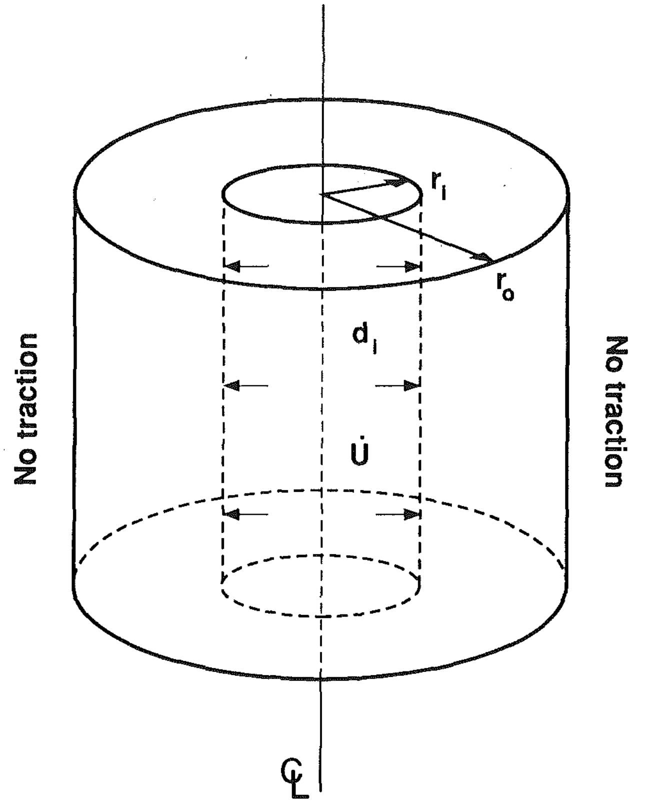

Fig. 1 Schematic diagram for the tube expansion application. $\dot{U}$ and r_i are the velocity and the deformation rate at inside radius, respectively.

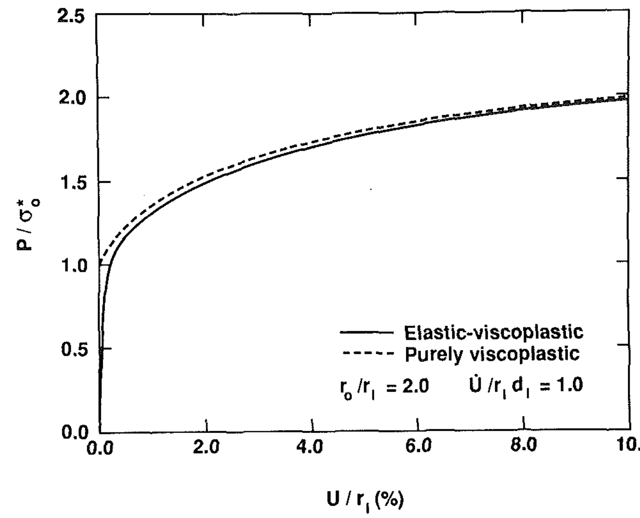

Fig. 2 Pressure as a function of inner wall displacement

boundary conditions and initial conditions. Over the surface of the body either known velocities or tractions are imposed throughout the deformation. At the time corresponding to the start of the process, the temperature and state everywhere within the body are specified.

The methodology examined here for solving the system of equations consists of analyzing the loading phase of a deformation process with an inelastic (viscoplastic) approximation that neglects any contributions to the deformation from elasticity. Once the loading phase is completed, the body is unloaded elastically using the final stress state from the loading phase as an initial condition for the unloading analysis. Because the loading and unloading phases are assumed to be dominated by the inelastic and elastic behaviors, respectively, and the inelastic deformations are rate dependent, the transition between the phases must occur quickly. This requirement is more critical at high temperatures or low strain rates where significant inelastic deformations continue following reductions in the level of stress. This point is discussed in more detail later.

Applications

Two applications are presented to illustrate the computation of residual stresses after simulating the loading phase using a purely inelastic analysis. The first is the expansion of a thick-walled tube under an imposed internal pressure. Because of the relatively simple kinematics of this problem, numerical solutions, which include the elastic response during the loading phase, are easily computed using the equations outlined in the previous section and are similar to the well-known autofrettage solutions for the rate-independent plastic case (Calladine, 1969). Direct comparisons between the full elastic-viscoplastic and the viscoplastic models are possible for this case because the only difference between two analyses is the treatment of elasticity during loading. The second example is the deformation of a thick ring subjected to diametrically opposing forces. This problem is analyzed with a three-dimensional viscoplastic formulation that has been modified to perform elastic unloading analyses. Experimental data of the residual elastic strains following a fixed amount of upset are available for this application.

Expansion of a Thick-Walled Tube. A thick-walled tube is expanded radially by an imposed velocity at the inside radius. As shown in Fig. 1, the tube has an inside radius of r_i and an outside radius of r_o. The problem is one of plane strain and axisymmetry, with a one-dimensional flow field. For this case, assuming incompressible flow, the equilibrium equations reduce to:

$$\frac{\partial \sigma_r}{\partial r} = \frac{\sigma_\theta - \sigma_r}{r} = 2\,\frac{\sigma_\theta'}{r}. \tag{12}$$

Here, σ_r and σ_θ are the stress components in the radial and circumferential directions, respectively. The deviatoric component of the circumferential stress was evaluated using a simplified version of Hart's model and integration of the equation (12) was performed numerically. For an elastic-viscoplastic analysis, elasticity was included by imposing the consistency:

$$\sigma' = 2\mu \mathbf{d}_n' = 2G\epsilon_e', \tag{13}$$

where ϵ_e' is a deviatoric elastic strain tensor. A more general treatment for including elasticity is discussed in another article (Eggert and Dawson, 1988).

Two different initial configurations were examined: $r_o/r_i = 2$ and $r_o/r_i = 10$. The stresses computed by the elastic-viscoplastic and by the viscoplastic approximation have been compared throughout the loading phase. The internal pressure has been plotted in Fig. 2 as a function of the radial displacement (U) at the tube inside radius for the case of $r_o/r_i = 2$. Early in the deformation the two analyses are qualitatively different. In the elastic-viscoplastic analysis the internal pressure starts at zero and builds toward a level where inelastic deformations become significant. In the viscoplastic analysis the internal pressure immediately assumes a value that enables the stresses to satisfy the yield criterion everywhere. As the deformation increases and the inelastic deformations begin to dominate in the elastic-viscoplastic solution, the internal pressure computed by the two methods approach the same magnitude.

The variation of stress with radius (Fig. 3) shows more vividly the difference between the solutions with and without elasticity during loading. A low stress levels (Fig. 3(a)), the material responds almost entirely by elastic straining in the elastic-viscoplastic analysis. The circumferential stress decreases from the inside to outside radii. However, for a displacement having

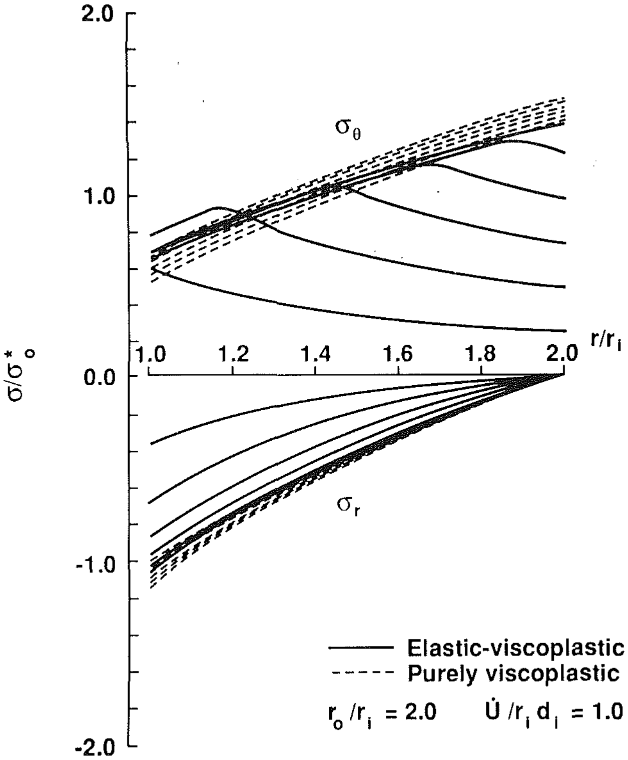

Fig. 3(*a*) Stress as a function of radius for $\epsilon_n(r_i) \le 0.003$

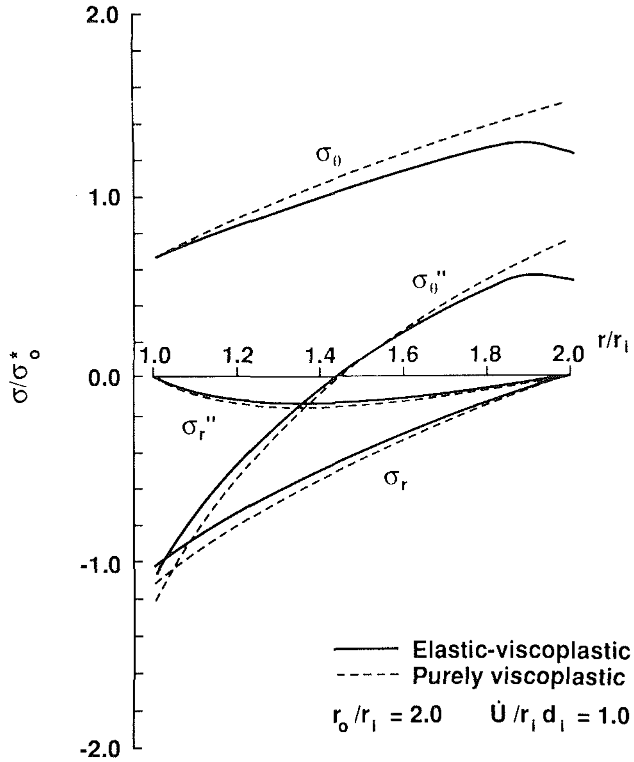

Fig. 4(*a*) Stress distribution at $\epsilon_n(r_i) = 0.0025$. Here, double prime denotes residual stresses.

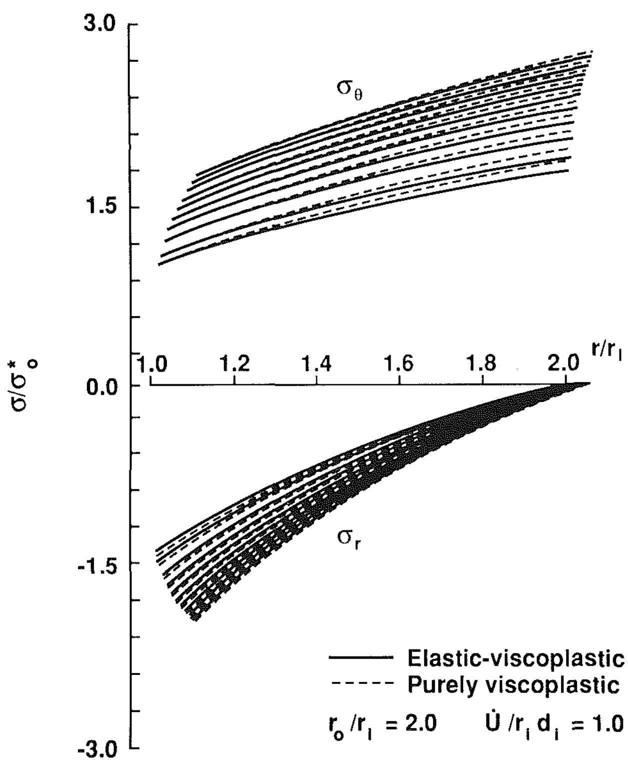

Fig. 3(*b*) Stress as a function of radius for $0.01 \le \epsilon_n(r_i) \le 0.1$

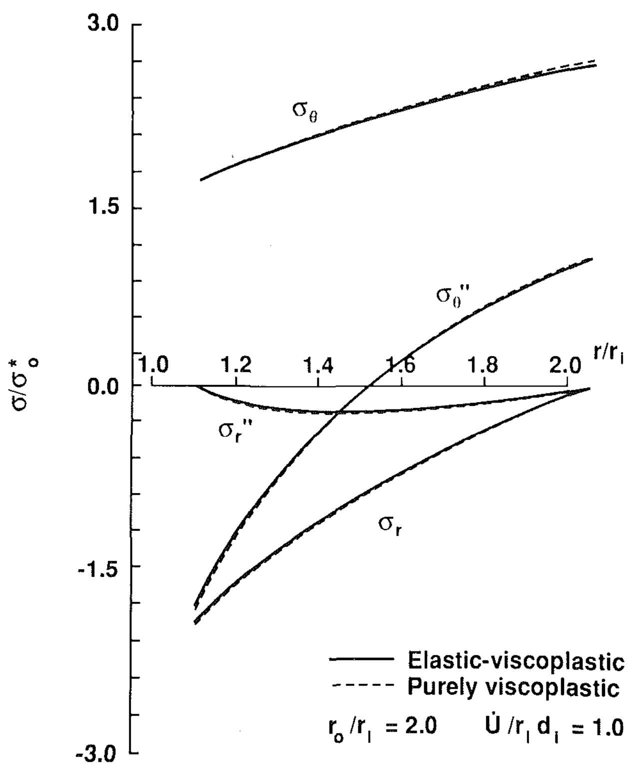

Fig. 4(*b*) Stress distribution at $\epsilon_n(r_i) = 0.1$. Here, double prime denotes residual stresses.

the same strain at the inside radius, the viscoplastic solution shows an increasing circumferential stress component. This is due to the deformations being entirely inelastic from the onset of loading with the viscoplastic approximation. The compliance offered by the elasticity which dominates at the onset of loading in the elastic-viscoplastic solution is neglected. As the deformation proceeds, more of the cross-section reaches the stress level at which significant inelastic straining occurs in the elastic-viscoplastic solution. The circumferential stress increases with the radius through the elastic-plastic zone nearer

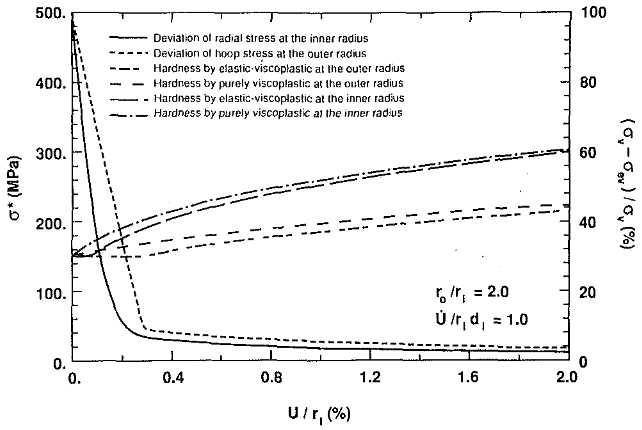

Fig. 5(*a*) State variable and stress error as a function of inner wall displacement for a tube with initial $r_o/r_i = 2.0$

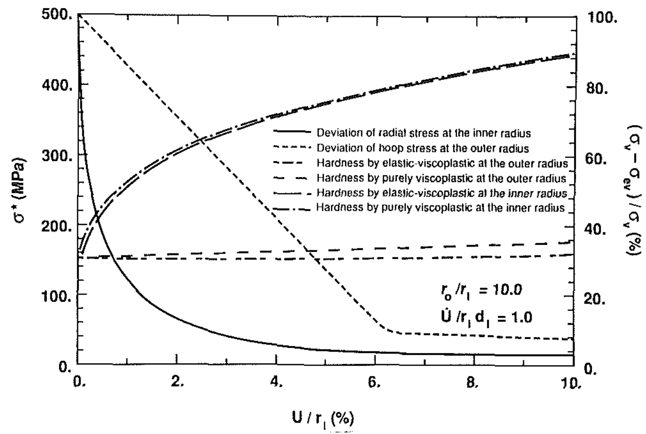

Fig. 5(*b*) State variable and stress error as a function of inner wall displacement for a tube with initial $r_o/r_i = 10.0$

the inside radius and then decreases again after reaching the elastic zone nearer the outside radius. After the strain at the inside radius reaches approximately 0.003, the entire cross-section exhibits inelastic straining and the stress patterns are comparable both qualitatively and quantitatively. The stress distributions corresponding to inside radius strains ranging from 0.01 to 0.10 are shown in Fig. 3(*b*). Here the entire body is experiencing inelastic deformations and the tube is visibly expanded. The stresses are increasing due to an increase in the flow stress associated with strain hardening. As is evident from the figure, the stresses obtained from the viscoplastic loading approximation are in good agreement with those computed from an elastic-viscoplastic model.

The residual stresses obtained by unloading after reaching a prescribed amount of straining at the inside radius are shown in Fig. 4. In Fig. 4(*c*) the stresses just before and after unloading are plotted for the case where the ring is unloaded after reaching an inside radius strain of 0.0025. At this point material near the outside radius is still essentially elastic according to the elastic-viscoplastic solution. The residual stresses computed with the simplified viscoplastic loading simulation are least accurate in the region where the error was greatest before unloading. This is the region where the elastic strains were still dominant. However, over the remainder of the body the residual stresses from the viscoplastic loading approximation are in qualitatively good agreement with the elastic-viscoplastic solution. At larger strains, the stresses before unloading as computed with the viscoplastic approximation are accurate throughout the region and, as a consequence, the residual stresses are captured well. This is shown in Fig. 4(*b*) for the case where the inside radius strain was 0.10 before unloading initiated.

Table 2 Springback normalized with respect to the displacement during loading at the inner wall for the thick-walled tube ($r_o/r_i = 2$)

$\epsilon_{rr}(r_i)$ (percent)	Viscoplastic Loading	Elastic-Viscoplastic Loading	Error (percent)
0.05	2.7616	1.0	176.2
0.1	1.4270	0.9492	50.34
0.2	0.7527	0.6693	12.46
0.25	0.6159	0.5677	8.49
1.0	0.1874	0.1806	3.76
10.0	0.0300	0.0298	0.67

The stress error (normalized difference between the elastic-viscoplastic stress and the viscoplastic approximation) is shown in Figs. 5(*a*) and (*b*) together with the predicted changes in state variable as a function of the inside radius displacement for both solutions. The error in the computed stress is large just as loading begins since the elastic-viscoplastic solution builds up from zero stress but the viscoplastic approximation starts at the stress required for inelastic straining. Evolution of the state variable occurs immediately for the viscoplastic approximation but is delayed for the elastic-viscoplastic case. It is evident from these figures that when the full cross-section becomes inelastic and hardening starts at the outside radius, the error in the stress becomes small.

The displacements recovered during the elastic unloading phase can be interpreted as the elastic springback of the workpiece. The displacements computed following an analysis using the viscoplastic loading approximation have been computed for various amounts of displacement at the inside radius during loading (see Table 2). When the strains are small $\epsilon_{rr}(r_i) \leq 0.05$ percent) and the deformations are elastic throughout the cross-section, the springback computed with the approximate method is seriously in error (176 percent). However, once the inside radius strain becomes larger, and most or all of the cross-section exhibits inelastic deformations, the error decreases substantially. After 1 percent of inside radius strain, the difference between computed values of springback at the inside radius is less than 4 percent; once the inside radius strain reaches 10 percent, the error in springback displacement is less than 1 percent.

Similar results have been obtained for the case of r_o/r_i equal to 10. However, in this case because of the relatively larger outside radius, the inside radius displacement required to produce inelastic deformations that extend throughout the cross-section is larger. Again, when the outside radius begins to experience significant inelastic strains (as is apparent from the state variable beginning to change), the magnitude of the error in the computed stresses drops to less than 5 percent. Unloading from this point produces essentially equivalent residual stresses with both formulations.

Compression of a Thick Ring. The second example is geometrically more complicated than the first example and presently requires numerical methods to obtain solutions. A metal ring is loaded with diametrically opposing forces applied on small flat landings. These landings facilitated positioning in the experiment and act to distribute idealized point loads. The deformations of the ring were computed with the intention of comparing the computed residual strains to values measured experimentally for a ring of the same geometry and subjected to the same loading (Flower et al., 1987). For this purpose, a three-dimensional finite element program for viscoplastic flow, ISAIAH (Dewhurst and Dawson, 1985), was modified so that at the end of a loading sequence a body could be unloaded using an elastic analysis.

This type of viscoplastic formulation for the loading phase

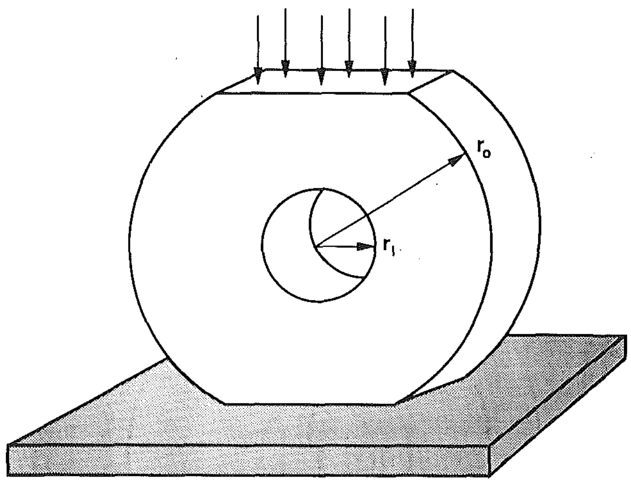

Fig. 6 Schematic diagram of the ring upset application. The ring is initially 13 mm thick, r_i = 76 mm and r_o = 127 mm.

is fully inelastic and has been used extensively for simulating large strain bulk-forming operations (Kobayashi, 1977; Zienkiewicz et al., 1981; Rebelo and Kobayashi, 1980; Li and Kobayashi, 1981; Dawson, 1984; Eggert and Dawson, 1986; Smelser et al., 1986; Beaudoin Woodbury, 1986; Surdon and Chenot, 1986; Thompson, 1986). The solution involves computing the velocity field for a fixed state (the geometry and the temperature and state distributions) and then advancing the state over a time step. The approximate solution for the velocity field is obtained from a finite element discretization based on a virtual rate of work statement[3].

$$\delta J = -\int_V \mathrm{tr}(\sigma \cdot \delta \mathbf{d}) dV + \int_S \mathbf{T} \cdot \delta \mathbf{u} dS, \tag{14}$$

where $\mathbf{T}$ is the surface traction, $\mathbf{u}$ is the velocity vector, V is the workpiece volume, and S is its surface in the current configuration. The yield condition and the flow rule are used to eliminate the deviatoric portion of the stress that appears in the first integral. The incompressibility constraint may be treated by various methods. For example, equation (10) may be modified to permit volumetric deformations in a viscous material using a relation of the form:

$$\sigma = 2\mu \mathbf{d} + \lambda \mathbf{I}\mathrm{tr}(\mathbf{d}), \tag{15}$$

where μ is the effective viscosity defined by the yield condition $(=\sigma'/3d_n')$, which may be a function of the rate of deformation, state variables, and temperature. The material parameter λ is defined in terms of μ and Poisson's ratio, ν, as:

$$\lambda = \frac{2\nu\mu}{1-2\nu}. \tag{16}$$

Incompressibility then is enforced by using ν close to 0.5, while allowing compressible motions as legitimate modes. A value of ν of 0.499995 has been used successfully such that λ plays a role of penalty parameter. However, the use of this conventional penalty method can result in spurious pressure modes and, consequently, unreliable stress fields. To avoid such behaviors, several techniques have been proposed (Zienkiewicz et al., 1971; Oden, 1982; Reddy, 1982; Engelman et al., 1982; Kheshi and Scriven, 1985; Dhatt and Hubert, 1986). It has been found that consistent penalty techniques give more accurate pressure and velocity fields with less computation time. The approach suggested by Engelman and co-workers uses a linear, discontinuous interpolation function for pressure to avoid spurious pressure modes with quadratic velocity approximation. With this approach, the stress in equation (14) is approximated as:

$$\sigma + p\mathbf{I} = 2\mu \mathbf{d}'. \tag{17}$$

$$p = -\lambda \mathrm{tr}(\mathbf{d}). \tag{18}$$

Here, the pressure, p, is externally penalized. To increase the accuracy of the consistent penalty method, Kheshgi and Scriven (1985) have allowed the penalty parameter, λ, to vary from element to element. This variable penalty parameter approach was effective for incompressible, linear viscous flow problems especially when the variations in element size were large. In the work presented here, a variable penalty parameter is used that is defined as a weighted average of the moduli evaluated at quadrature points with equation (16). Following standard finite element procedures, the resulting matrix equations from equations (14) and (18), respectively, then are:

$$[K_\mu]\{u\} + [G]\{-\hat{p}\} = \{F\} \tag{19}$$

and

$$[M_p]\{\hat{p}\} = -\Lambda [G]^T \{u\} \tag{20}$$

where

$$\Lambda = \sum_{i=1}^{NQP} \lambda_i \times W_i. \tag{21}$$

Here, W_i are the standard Gauss weights and NQP indicates the number of quadrature points per element. Detail expressions for $[K_\mu]$, $[G]$, $[M_p]$, and $\{F\}$ are available in other papers (Engelman et al., 1982; Dawson, 1984). The pressure can be eliminated at an element level, thereby reducing the problem to one involving only nodal point velocities. Thus, we obtain:

$$[K_\mu + K_\lambda]\{u\} = \{F\} \tag{22}$$

where

$$[K_\lambda] = \Lambda [G][M_P]^{-1}[G]^T. \tag{23}$$

Because the accuracy of the residual stresses is strongly influenced by the accuracy of the stresses computed at the end of the loading phase, predicting accurate pressures is a critical aspect in the successful use of this approximate approach for obtaining residual stresses. The additional effort of the consistent penalty technique was not only warranted, but was actually found to be necessary.

The state of the workpiece is updated over a time increment. This consists of updating the geometry according to the velocity field and the state variable according to its evolution equation. The geometry advances merely by updating the mesh coordinates with an Euler integration of the nodal point velocities. The evolution equation for the change of the state variable with deformation is integrated with a combination of Galerkin weighted residual and Crank-Nicholson methods. The weighted residual for the evolution equation of the simplified Hart's model can be written as:

$$W_{\sigma^*} = \int_V \left(\frac{D}{Dt}(\sigma^*) - c_0 \sigma^* \left(\frac{G}{\sigma^*}\right)^{m'} \left(\frac{\tau'^p}{\sigma^*}\right)^n d_n' \right) N_{\sigma^*} dV \tag{24}$$

where N_{σ^*} is the weighting function. After approximating the temporal derivative of the state variable with a finite difference expression and linearizing the remaining term in σ^*, a matrix equation for the state variable values at the end of a time step is obtained. Because terms in the coefficient matrix depend on the state variable, the equation is solved iteratively. This procedure of finding a velocity field at fixed state and then updating the state over a time increment is repeated as often as necessary to accrue the imposed deformation of the forming operation. Details are available in other references (Dewhurst and Dawson, 1984; Dawson, 1987; Eggert and Dawson, 1987).

The elastic unloading is analyzed with a finite element dis-

[3]The Euler equations are equation (1) and the traction boundary conditions.

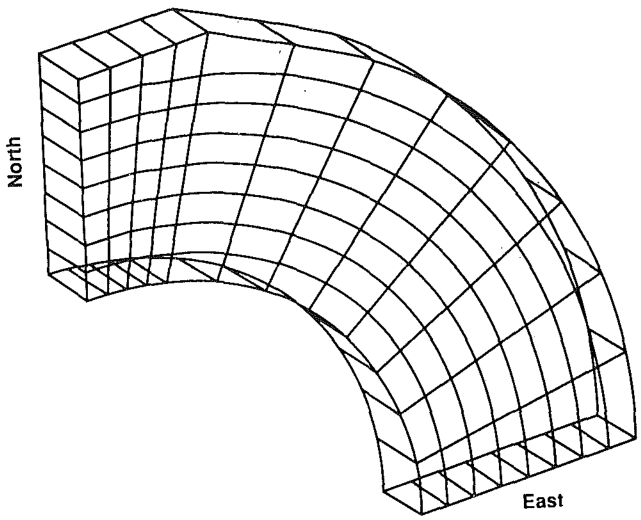

Fig. 7 Finite element mesh for the ring upset application

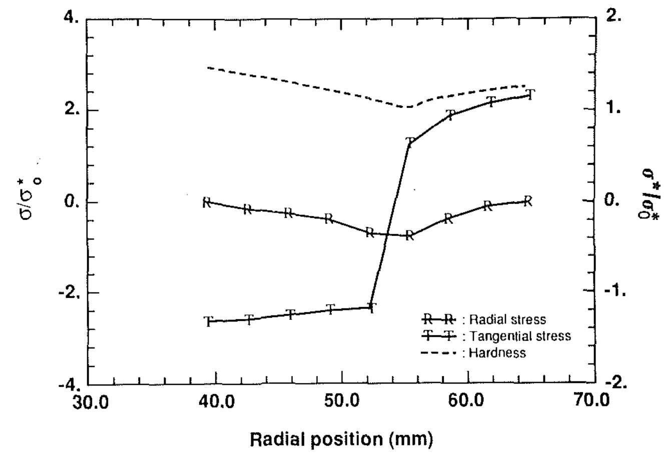

Fig. 8(*a*) State variable and stresses at the east location before unloading

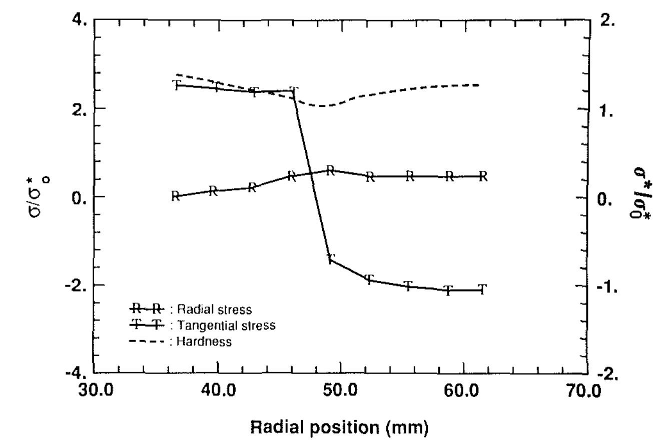

Fig. 8(*b*) State variable and stresses at the north location before unloading

cretization of a virtual work formulation (Bathe, 1982) in which a matrix equation is obtained after eliminating the stress with the elasticity relationship (equation (6)) and writing the strains in terms of the displacements using kinematics for small strain deformations.[4] Here, the deformation is only the change in shape between the start and the end of the unloading phase of the operation. Loads are applied which, by superposition, remove the boundary tractions on the surface. By noting that under small strain-small displacement kinematics the velocities of the viscoplastic formulation are analogous to displacements of the elasticity formulation, it is possible to use the same finite element program for both loading and unloading phases. The material moduli that appear as viscosities in the viscoplastic formulation are the Lame's constants for the elastic solution.

During the loading phase, fixed velocities are imposed on the landings that compress the ring. The velocities were applied until approximately 2.5 percent upset was obtained. At that point the velocities were removed and an elastic unloading analysis was performed, as described previously. The finite element mesh for the symmetric upper quadrant is shown in Fig. 7. The material properties of 304 stainless steel were assigned to the ring as specified in Table 1.

The computed changes in state variable on a cross-section defined by a horizontal plane that cuts through the ring center (hereafter referred to as the east position) are shown first in Fig. 8(*a*). The distribution indicates that greater straining has occurred at the inside and outside radii than at an intermediate radius. This is expected as a plastic hinge develops during the deformation. Where the normalized state variable remains close to unity the inelastic deformations are small. Conversely, where the changes in the state variable are large the inelastic deformations are significant and the normalized state variable exceeds unity. The stresses through the ring thickness at the east position also are shown in Fig. 8(*a*) at the instant prior to unloading. The distributions show that the tangential component of the stress is larger than the radial component. The tangential component is compressive at the inside radius and tensile at the outside radius, as expected from elementary curved beam theory.

The residual elastic strains are shown in Figs. 9 and 10. The features of the distributions are dominated by the bending behavior and the formation of plastic hinges prior to unloading. The residual elastic strains (hereafter called just strains) at the east position are compared to measured values reported by Flower et al. (1987) and to values from a plane stress, elastic-plastic simulation (Flower et al., 1987) using the finite element code NIKE2D (Hallquist, 1986) with a rate-independent model for plasticity (both for loading and unloading) in Fig. 9. The tangential component of the strain is larger than the radial (the latter being a consequence principally of the Poisson effect). The predicted distribution of the tangential component compares well both in form and magnitude to the data and to the elastic-plastic simulation. The experimental data has been measured for two crystal directions, one of which, the (0,0,2) direction, consistently shows greater strains. As pointed out by Flower et al., this direction is more compliant than the other. In the simulations, average (macroscopic) values of the elastic moduli have been used, with the result being that the computed strains lie between the two sets of experimental data. The discrepancy between the two simulations is not large, but might be reduced further with greater resolution in our simulations. The difference between computed and measured strains, as well as the scatter of the data itself, appears to be larger for the radial component, but this is due principally to the smaller overall magnitudes associated with this component. Again, the form of the distribution is consistent with unloading from a plastic hinge distribution. Both the ISAIAH results reported here and the NIKE2D results reported earlier by Flower et al. appear to show larger residual strains at the inside diameter than is apparent from the experimental data. Flower et al. address this point, but do not reach a conclusion regarding

[4] While we have restricted our attention to small strain-small displacement unloading behavior, this part of the formulation could be generalized to large deformation (and rotation) kinematics as long as the small strain condition is preserved.

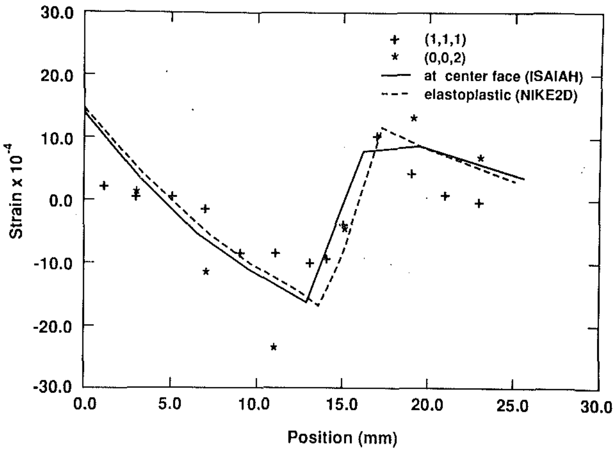

Fig. 9(*a*) Residual tangential strains at the east location

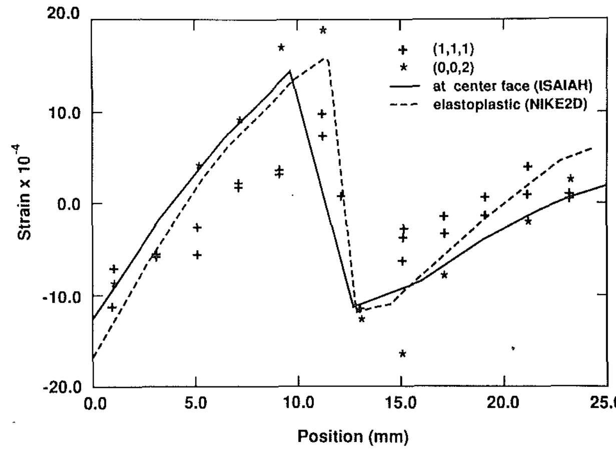

Fig. 10(*a*) Residual tangential strains at the north location

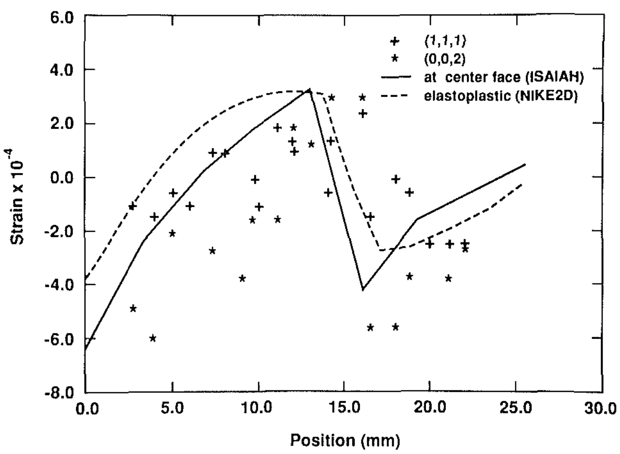

Fig. 9(*b*) Residual radial strains at the east location

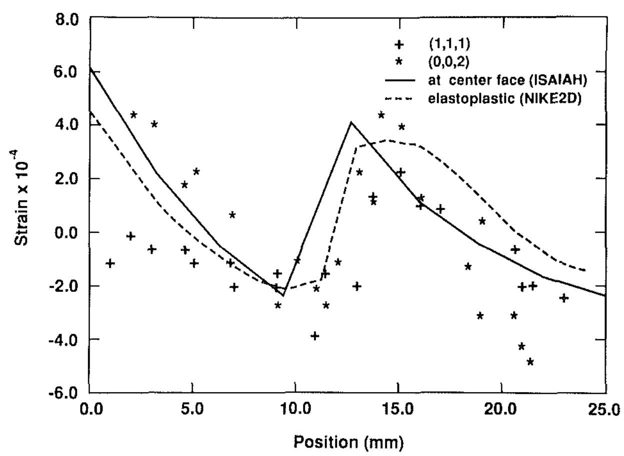

Fig. 10(*b*) Residual radial strains at the north location

the source of the discrepancy. Beyond their discussion the following point is relevant: The isotropic hardening plasticity model used in these calculations overpredicts the initial flow stress on reloading (using a microstrain definition). Since the inside radius is the farthest point from the neutral axis of bending, the stress there will be the highest and that point would be the first point to yield on reverse loading. In reality, a very small amount of plasticity diminishes the stress at the inside radius. In this respect, one expects that the computational and experimental results will differ the most at this point.

Similar results for the stresses (Fig. 8(*b*)) and the strains (Fig. 10) as functions of radial position were obtained for a cross-section revealed by passing a vertical plane through the ring center (hereafter called the north location). Again, the tangential component of the strain after unloading is larger than the radial component, the latter being essentially a Poisson effect. The sense of the strains is opposite to that of the east location because the moment induced by the loading is opposite in sign to that at the east location. Comparing the two computed distributions it is evident that the NIKE2D simulations predict a sharper transition from tension to compression across the neutral axis, but otherwise are very similar.

As with the first example, the displacements of the elastic unloading give the springback. For this example, the springback computed at the landing was approximately 0.24 mm, or about 15 percent of the displacement during loading. No values are available for comparison of this prediction, however.

Discussion

Based on the experiences obtained in examining the two previous examples, a few statements can be made regarding the accuracy of estimating residual stresses using a viscoplastic analysis for loading. These statements are made in the context of modeling deformation response in materials processing where the objective is to alter the workpiece geometry, rather than for design applications involving, at most, limited deformations of a part. The statements are not meant to be completely general since the experience in applying the technique is limited and a formal proof of accuracy has not been derived.

It appears reasonable to expect accurate computation of residual stresses in cases where the stresses are well known prior to unloading. Strictly, this should be true everywhere in the workpiece, but actually may not be required. Where the deformations are large the magnitude of the stresses is limited by the yield condition and probably is sufficiently well known from the viscoplastic loading approximation. One measure of the degree of plastic deformation is the change in the state variable that characterizes the change in flow stress with straining. If the state variable is evolving everywhere, then the stresses are limited by the yield condition for the inelastic deformations. However, since with a viscoplastic approximation all of the deformation is inelastic, that portion of the deformation that occurs without a state change is neglected. The change in state thus can be overestimated and the fact that the state has changed in a viscoplastic simulation does not imply that any change would have taken place in an elastic-plastic simulation of the same process. This is evident from the first example. It is possible, however, to estimate the maximum change in state that would be observed in a viscoplastic simulation for deformations of the magnitude of the elastic deformations at yield. For example, over a monotonic path in strain space, the maximum change in the state variable (σ^*) for an effective strain of 0.2 percent is around 27 percent of the initial value of the state variable. When the changes in state exceed this value the magnitude of the deformation is sufficiently large to ensure inelastic deformation (and stresses limited by the yield criterion) in an elastic-plastic simulation. This approach is, in essence, just an examination of the magnitude of the state variables beyond which the inelastic deformations really are the dominant mode of deformation during loading. The basic requirement for accurate results using a viscoplastic formulation is that the inelastic deformation rate is considerably larger than the elastic deformation rate. This usually isn't true as the body is loaded up to the yield stresses, but often can be the case for the deformations once the loads are sufficiently high to induce inelastic deformations. Thus a minimum requirement for accurate residual stress predictions is that the deformations extend past the initial loading phase where the deformation can be accommodated by the elasticity and where the elastic deformation rate may be comparable to, or larger than, the inelastic deformation rate. The examples presented here suggest that once the conditions for accurate simulations using a viscoplastic loading approximation are met, the residual stress predictions using the decoupled approach will in turn be accurate.

A second point that is important in the computation of residual stresses by the technique presented here is that during unloading the elasticity must dominate. This places a restriction on the time frame over which the unloading must occur. Referring to equation (3), the elastic contribution must be large compared to the inelastic one. By substituting constitutive relations for the elastic and inelastic deformation rates it can be shown that for rate-dependent plasticity the unloading time must be small in comparison to the effective relaxation time of the material. If this condition is not satisfied there could be continued inelastic straining during unloading that could relax the stresses in comparison to the purely elastic case. In the rate-insensitive (or rate-independent) regime, relaxation time is long (or infinite) so that this condition is easily satisfied. In the rate-sensitive regime (e.g., high temperatures), this condition will be more restrictive. For both examples presented here the unloading phase was assumed to occur instantaneously, so that this condition was satisfied.

Enforcement of the incompressibility constraint in the finite element formulation requires special attention. A standard penalty approach gave pressures that were too noisy to define the initial stress state satisfactorily for unloading. That is, using only the penalty method the form of the residual strain distribution was masked by large fluctuations coming from the mean component of the stress. Using a consistent penalty method, which is somewhat more costly, the pressures were smoother and more accurate. Consequently, the residual stresses demonstrated the correct distribution.

Summary

Two applications have been presented that demonstrate a technique for computing residual stresses subsequent to forming processes using a viscoplastic approximation for the loading phase. It was observed in the thick-walled tube example that residual stresses were obtained only after the deformations were sufficiently large to induce inelastic strains throughout the cross-section. In the thick ring application the degree of upset was adequate to form a plastic hinge during loading. The stresses throughout the cross-section thus were limited by the yield criterion and a viscoplastic approximation was able to capture them well. As a consequence the residual elastic strains compared well to experimental measurements and to the results of an elastic-plastic simulation. We suggest that the key element to predicting residual stresses accurately by this approach is the accurate calculation of the stresses prior to unloading. Physically, this means that the stresses should be limited by the flow stress (inelastic deformations are occurring); numerically, special care must be exercised to obtain accurate pressures in the finite element discretization of the viscoplastic formulation for the loading phase. The criteria for viscoplastic approximations to be accurate are that the inelastic deformation rate dominates and the strains are well in excess of the elastic strains that would exist in the workpiece.

Acknowledgments

This research was supported by the National Science Foundation under Grant DMC-8352275 with matching support from Alcoa, General Electric, and the Xerox Foundation. Computations were performed on a facility supported by the Mathematical Sciences Institute at Cornell University under sponsorship of the U.S. Army Office of Basic Research. We wish to thank Elane Flower for her cooperation in providing the residual stress data for the ring upsetting application. We also thank Anand Jagota and Vincent Prantil for their many helpful comments in preparing the paper.

References

Argyris, J. H., and Kleiber, M., 1977, "Incremental Formulation in Nonlinear Mechanics and Large Strain Elasto-Plasticity—Natural Approach, Part 1," *Computer Methods in Applied Mechanics and Engineering*, Vol. 11, pp. 215–247.

Bathe, K.-J., 1982, *Finite Element Procedures in Engineering Analysis*, Prentice-Hall, Englewood Cliffs, N.J.

Beaudoin, A. J., Jr., and Woodbury, K. A., 1986, "Mathematical Modelling of Hot Rolling of Aluminum," *Aluminum Technology '86*, The Institute of Metals, pp. 110.1–110.7.

Calladine, C. R., 1969, *Engineering Plasticity*, Pergamon Press.

Cook, P. M., 1957, "True Stress-Strain Curves for Steel in Compression at High Temperatures and Strain Rates, for Application to the Calculation of Load and Torque in Hot Rolling," *Proceedings of the Conference on Properties of Materials at High Rate of Strain*, IME, pp. 86–97.

Crancall, S. H., and Dahl, N. C., ed., 1959, *An Introduction to the Mechanics of Solids*, McGraw-Hill, New York, pp. 334–336.

Dawson, P. R., 1978, "Viscoplastic Finite Element Analysis of Steady-State Forming Processes Including Strain History and Stress Flux Dependence," *Applications of Numerical Methods to Forming Processes*, H. Armen and R. F. Jones, eds., ASME, New York, pp. 55–66.

Dawson, P. R., 1984, "A Model for the Hot or Warm Forming of Metals With Special Use of Deformation Mechanism Maps," *International Journal of Mechanical Sciences*, Vol. 26, pp. 227–244.

Dawson, P. R., 1987, "On Modeling Mechanical Property Changes During Flat Rolling of Aluminum," *International Journal of Solids and Structures*, Vol. 23, No. 7, pp. 947–968.

Dewhurst, T. B., and Dawson, P. R., 1984, "Analysis of Large Plastic Deformations at Elevated Temperatures Using State Variable Models," In K. J. William, editor, *Constitutive Equations: Macro and Computational Aspects*, K. J. William, ed., ASME, New York, pp. 149–164.

Dewhurst, T. B., and Dawson, P. R., 1985, ISAIAH—"A Finite Element Program for Viscoplastic Flow and Heat Transfer in Three Dimensions," Technical Report No. *MM-85-01*, Sibley School of Mechanical and Aerospace Engineering, Cornell University.

Dhatt, G., and Hubert, G., 1986, "A Study of Penalty Elements for Incompressible Laminar Flows," *International Journal for Numerical Methods in Fluids*, Vol. 6, pp. 1–19.

Eggert, G. M., and Dawson, P. R., 1986, "Assessment of a Thermoviscoplastic Model of Upset Welding by Comparison to Experiment," *International Journal of Mechanical Sciences*, Vol. 28, No. 9, pp. 563–589.

Eggert, G. M., and Dawson, P. R., 1987, "On the Use of Internal Variable Constitutive Equations in Transient Forming Processes," *International Journal of Mechanical Sciences*, Vol. 29, No. 2, pp. 95–113.

Eggert, G. M., and Dawson, P. R., 1988, "A Viscoplastic Formulation With Elasticity for Transient Metal Forming," *Computer Methods in Applied Mechanics and Engineering*, Vol. 70, No. 2, pp. 165–190.

Engelman, M. S., Sani, R. L., Gresho, P. M., and Bercovier, M., 1982, "Consistent Versus Reduced Integration Penalty Methods for Incompressible Media Using Several Old and New Elements," *International Journal for Numerical Methods in Fluids*, Vol. 2, pp. 25–42.

Flower, E., MacEwen, S. R., and Holden, T. M., 1987, "FEA Predictions of Residual Stress in Stainless Steel Compared to Neutron and X-Ray Diffraction Measurements," *Proceeding of Advances in Numerical Methods in Engineering Theory and Application*, to appear.

Hallquist, J. O., 1986, "NIKE2D—A Vectorized Implicit, Finite Deformation, Finite Element Code for Analyzing the Static and Dynamic Response of 2-D Solids With Interactive Rezoning and Graphics," Report No. UCID 19677, Lawrence Livermore National Laboratory.

Hart, E. W., 1976, "Constitutive Relations for Inelastic Deformation of Metals," *Journal of Engineering Materials and Technology*, Vol. 98, pp. 193–202.

Hibbitt, H. D., Marcal, P. V., and Rice, J. R., 1970, "A Finite Element Formulation for Problems of Large Strain and Large Displacement," *International Journal of Solids and Structures*, Vol. 6, pp. 1069–1086.

Kheshgi, H. S., and Scriven, L. E., 1985, "Variable Penalty Method for Finite Element Analysis of Incompressible Flow," *International Journal for Numerical Methods in Fluids*, Vol. 5, pp. 785–803.

Kobayashi, S., 1977, "Rigid Plastic Finite Element Analysis of Axisymmetric Metal Forming Processes," *Numerical Modeling of Manufacturing Processes*, R. F. Jones, Jr., H. Armen, and J. T. Fong, eds., ASME, New York, pp. 49–66.

Kumar, V., Mukherjee, S., Huang, F. H., and Li, C. Y., 1979, "Deformation in Type 304 Austenitic Stainless Steel," Technical Report NP-1276, Electric Power Research Institute, Palo Alto, Calif.

Li, J. L., and Kobayashi, S. 1981, "Rigid Plastic Finite Element Analysis of Plane Strain Rolling," ASME Paper No. 81-WA/Prod-13.

McMeeking, R. M., and Rice, J. R., 1975, "Finite Element Formulations for Problems of Large Elastic-Plastic Deformation," *International Journal of Solids and Structures*, Vol. 11, pp. 601–616.

McQueen, H. J., Petkovic, R., Weiss, H., and Hinton, L. G., 1975, "Flow Stress and Microstructural Changes in Austenitic Stainless Steel During Hot Deformation," *AIME Seminar on Hot Deformation of Austenite*, Cincinnati, Ohio.

Monfort, G., and Bragard, A., 1985, "A Simple Model of Shape Errors in Forming and its Application to Reduction of Springback," *Computer Modeling of Sheet Metal Forming Processes; Theory, Verification and Application*, N.-M. Wang and S. C. Tang, eds., pp. 273–287.

Oden, J. T., 1982, "Penalty Method and Reduced Integration for the Analysis of Fluids," *Penalty Finite Element Method in Mechanics*, J. N. Reddy, ed., ASME, New York, pp. 21–32.

Rebelo, N., and Kobayashi, S., 1980, "A Coupled Analysis of Viscoplastic Deformation and Heat Transfer—Theoretical Considerations," *International Journal of Mechanical Sciences*, Vol. 22, pp. 699–705.

Reddy, J. N., 1982, "On Penalty Function Methods in the Finite Element Analysis of Flow Problems," *International Journal for Numerical Methods in Fluids*, Vol. 2, pp. 151–171.

Smelser, R. E., Richmond, O., and Thompson, E. G., 1986, "A Numerical Study of the Effects of Die Profile on Extrusion," *Proceedings of the NUMIFORM '86 Conference*, Gothenberg, pp. 305–312.

Surdon, G., and Chenot, J. L., 1986, "Finite Element Calculation of Three-Dimensional Hot Forging," *Proceedings of the NUMIFORM '86 Conference*, Gothenberg, pp. 287–292.

Thompson, E. G., 1986, "Transient Analysis of Metal Forming Operations Using Pseudo-Concentrations," *Proceedings of the NUMIFORM '86 Conference*, Gothenberg, pp. 65–69.

Thompson, E. G., Mack, L. R. and Lin, F. S., 1969, "Finite Element Method for Incompressible Slow Viscous Flow With a Free Surface," *Developments in Mechanics*, Vol. 5, pp. 93–111.

Zienkiewicz, O. C., and Godbole, P. N., 1974, "Flow of Plastic and Visco-Plastic Solids With Special Reference to Extrusion and Forming Processes," *International Journal for Numerical Methods in Engineering*, Vol 8, pp. 3–16.

Zienkiewicz, O. C., Jain, P. C., and Oñate, E., 1978, "Flow of Solids During Forming and Extrusion: Some Aspects of Numerical Solutions," *International Journal of Solids and Structures*, Vol. 14, pp. 15–38.

Zienkiewicz, O. C., Oñate, E., and Heinrich, J. C., 1981, "A General Formulation for Coupled Thermal Flow of Metals Using Finite Elements," *International Journal for Numerical Methods in Engineering*, Vol. 17, pp. 1497–1514.

Zienkiewicz, O. C., Taylor, R. L., and Too, J. M., 1971, "Reduced Integration Technique in General Analysis of Plates and Shells," *International Journal for Numerical Methods in Engineering*, Vol. 3, pp. 275–290.

Axisymmetric Elastic Deformations of a Finite Circular Cylinder With Application to Low Temperature Strains and Stresses in Solder Joints

E. Suhir
AT&T Bell Laboratories,
Murray Hill, N.J. 07974
Mem. ASME

We consider an axially symmetric elastic problem for a finite circular cylinder whose end planes are subjected to identical radial deformations. The obtained solution is used to evaluate low temperature strains and stresses for solder joints in assemblies having matched thermal expansion coefficients of the components. The thermomechanical behavior of solder joints is determined in this case by the mismatch between the solder and the soldered materials. It is shown that the arising strains and stresses, especially in the axial direction, can be rather great and could possibly result in the failure of the joint. They can be brought down by increasing its height-to-diameter ratio. The stresses can also be reduced if low modulus solder materials, such as 95 percent Pb/5 percent Sn solders or indium-based alloys, are used.

1 Introduction

In this analysis we consider an axially symmetric elastic problem for a circular cylinder with small height-to-diameter ratio. The end planes of the cylinder are subjected to identical radial displacements, and remain flat during deformation. The obtained solution is used to evaluate low temperature mechanical behavior of solder joints in assemblies with thermally-matched components. In this case the arising strains and stresses are due to the thermal expansion (contraction) mismatch between the solder and the soldered materials. The major objective of our study is to assess the role of the main factors affecting the magnitude and the distribution of strains and stresses. In particular, we intend to determine whether an increase in the height-to-diameter ratio can result in essential reduction in the strain/stress level.

Structural response of solder joints in surface-mounted assemblies was studied experimentally and on the basis of finite element technique by many investigators (Engelmaier, 1983, 1988; Lau and Rice, 1985; Hall and Sherry, 1986; and others). The problem of finite solid cylinders with given end displacements was addressed by Swan (1986) and Bentham and Minderhaud (1972). Thermomechanical strains in solder joints with consideration of their expansion (contraction) mismatch at the package and substrate interfaces were addressed by Clech (1987) on the basis of the finite element method, and by Robert (1987) who utilized an eigenfunction expansion technique.

Contributed by the Applied Mechanics Division of THE AMERICAN SOCIETY OF MECHANICAL ENGINEERS for presentation at the Winter Annual Meeting, San Francisco, Calif., December 10–15, 1989.

Discussion on this paper should be addressed to the Editorial Department, ASME, United Engineering Center, 345 East 47th Street, New York, N.Y. 10017, and will be accepted until two months after final publication on the paper itself in the JOURNAL OF APPLIED MECHANICS. Manuscript received by the ASME Applied Mechanics Division, June 27, 1988; final revision, September 9, 1988.

Paper No. 89-WA/APM-3.

2 Analysis

2.1 Assumptions. The following basic assumptions are used in our study:

- The thermomechanical strains and stresses can be evaluated on the basis of an elastic approach.
- The free contraction of the soldered materials is not affected by the interfacial stresses and, therefore, the maximum radial displacements are given ("prescribed") values, which can be determined by the formula (Fig. 1):

$$u_{\max} = u\left(a, \pm\frac{h}{2}\right) = \Delta\alpha\Delta t a. \tag{1}$$

Here $u(r, z)$ are radial displacements, a is the radius of the cylinder, h is its height, $\Delta\alpha = \alpha_s - \alpha_p$ is the difference between the coefficients of thermal expansion of the solder and the soldered materials, and Δt is the change in temperature. The origin O of the cylindrical coordinates r, z is in the middle of the cylinder of its axis.

- Not only the in-plane, but also the flexural rigidity of the soldered components is so great, that the end planes of the cylinder remain flat during its deformation, so that the follow-

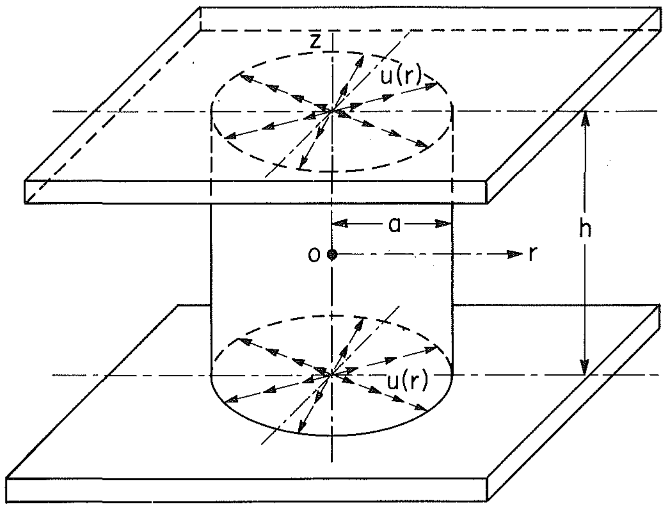

Fig. 1 Circular cylinder clamped at its end planes

ing boundary condition for the axial displacement $w(r, z)$ takes place:

$$\frac{\partial w}{\partial r}=0 \qquad \text{for } z\pm\frac{h}{2}. \tag{2}$$

• Since the height-to-diameter ratio of the cylinder is small, the displacements in the cylinder are strongly affected by the boundary conditions at both the end planes, and can be sought in the form:

$$u(r,z)=-f(r)\cos\gamma z+Ar,\ w(r,z)=\phi(r)\sin\gamma z+Bz, \tag{3}$$

where, in order to satisfy the condition (2), the parameter γ is chosen as follows:

$$\gamma=\frac{2\pi}{h}. \tag{4}$$

Note that if the height-to-diameter ratio is not small, the trigonometric functions in (3) would have to be replaced by an exponential function, to account for the fact that in such a case the displacements should fade with an increase in the distance from the end planes. Elastic deformations in cylinders with large height-to-diameter ratios were examined in numerous publications (see, for instance, Filon, 1902; Love, 1944; Timoshenko and Goodier, 1970).

2.2 Approximate Solution to the Elastic Problem. With the formulas (3) we have the following equations for the strains:

$$\left.\begin{aligned}
\epsilon_r &= \frac{\partial u}{\partial r}=-f'(r)\cos\gamma z+A,\\
\epsilon_t &= \frac{u}{r}=-\frac{f(r)}{r}\cos\gamma z+A,\\
\epsilon_z &= \frac{\partial w}{\partial z}=\gamma\phi(r)\cos\gamma z+B,\\
\gamma_{rz} &= \frac{\partial u}{\partial z}+\frac{\partial w}{\partial r}=[\gamma f(r)+\phi'(r)]\sin\gamma z
\end{aligned}\right\} \tag{5}$$

We use the Hooke's law equations in the form (see, for instance, Love, 1944):

$$\sigma_r=\lambda\theta+2G\epsilon_r,\ \sigma_t=\lambda\theta+2G\epsilon_t,\ \sigma_z=\lambda\theta+2G\epsilon_z,\ \tau_{rz}=G\gamma_{rz}, \tag{6}$$

where

$$\theta=\epsilon_r+\epsilon_t+\epsilon_z \tag{7}$$

is the strain invariant,

$$\lambda=\frac{E\nu}{(1+\nu)(1-2\nu)}=2G\frac{\nu}{1-2\nu},\ G=\frac{E}{2(1+\nu)} \tag{8}$$

are the Lamé constants, E is Young's modulus and ν is Poisson's ratio. In the above relationships ϵ_r, ϵ_t and ϵ_z are linear strains in the radial, tangential (circumferential), and axial directions, respectively, σ_r, σ_t, and σ_z are normal stresses in these directions, and γ_{rz} and τ_{rz} are shearing strain and stress. Introducing (5) into (6) we obtain:

$$\left.\begin{aligned}
\sigma_r &= -[(\lambda+2G)f'(r)+\lambda\frac{f(r)}{r}-\gamma\lambda\phi(r)]\cos\gamma z\\
&\quad+\lambda\left[\frac{A}{\nu}+B\right]\\
\sigma_t &= -[(\lambda f'(r)+(\lambda+2G)\frac{f(r)}{r}-\gamma\lambda\phi(r)]\cos\gamma z\\
&\quad+\lambda\left[\frac{A}{\nu}+B\right]\\
\sigma_z &= -[(\lambda f'(r)+\lambda\frac{f(r)}{r}-\gamma(\lambda+2G)\phi(r)]\cos\gamma z\\
&\quad+\lambda\left[2A+\frac{1-\nu}{\nu}B\right]\\
\tau_{rz} &= G[\gamma f(r)+\phi'(r)]\sin\gamma z
\end{aligned}\right\}. \tag{9}$$

Substitution of these expressions into the equations of equilibrium

$$\frac{\partial\sigma_r}{\partial r}+\frac{\partial\tau_{rz}}{\partial z}+\frac{\sigma_r-\sigma_z}{r}=0,\ \frac{\partial}{\partial r}(r\tau_{rz})+r\frac{\partial\sigma_z}{\partial z}=0 \tag{10}$$

results in the following system of ordinary linear differential equations for the unknown functions $f(r)$ and $\phi(r)$:

$$\left.\begin{aligned}
&(\lambda+2G)\left[f''(r)+\frac{f'(r)}{r}-\frac{f(r)}{r^2}\right]-\gamma^2Gf(r)\\
&\quad-\gamma\lambda(\lambda+G)\phi'(r)=0\\
&\gamma(\lambda+G)\left[f'(r)+\frac{f(r)}{r}\right]+G\left[\phi''(r)+\frac{\phi'(r)}{r}\right]\\
&\quad-\gamma^2(\lambda+2G)\phi(r)=0
\end{aligned}\right\}. \tag{11}$$

The equations (11) have the following solutions:

$$f(r)=C_0rI_0(\gamma r)+C_1aI_1(\gamma r),\quad \phi(r)=D_0aI_0(\gamma r)+D_1rI_1(\gamma r), \tag{12}$$

where $I_0(x)$ and $I_1(x)$ are modified Bessel functions of the first kind of zero and first order, respectively. These functions obey the following rules of differentiation (see, for instance, Watson, 1952; Sneddon, 1956; or Spanier and Oldham, 1987):

$$I_0'(\gamma r)=\gamma I_1(\gamma r),\ I_1'(\gamma r)=\gamma I_0(\gamma r)-\frac{I_1(\gamma r)}{r}. \tag{13}$$

The relationships between the constants of integration in (12) can be obtained by introducing these formulas, with consideration of (13) in (11):

$$D_0=\frac{4(1-\nu)}{\xi}C_0+C_1,\qquad D_1=C_0. \tag{14}$$

Here

$$\xi=\gamma a=2\pi\frac{a}{h} \tag{15}$$

is the parameter of the radius-to-height ratio.

The constants A, B, C_0 and C_1 can be determined on the basis of the condition (1) for the maximum radial displacements, the condition

$$\int_0^a \sigma_z\left(r, \pm\frac{h}{2}\right)dr = 0 \tag{16}$$

of self-equilibrium for the interfacial axial stress, and the stress-free boundary condition

$$\sigma_r(a, z) = 0 \tag{17}$$

for the radial stress. Note, that a similar condition for the shearing stress is not fulfilled in our analysis. This is supposed to result in a reasonable overestimation of the maximum shearing stress. A similar approach has been taken in the analyses of adhesively-bonded joints (see, for instance, Goland and Reissner, 1944), and in some engineering theories of thermally-induced stresses in bimaterial assemblies (Chen and Nelson, 1979, Suhir, 1986).

After introducing the formula for the displacement $u(r,z)$ from (3), and the formula for the function $f(r)$ from (12) into the condition (1), we have

$$A = \Delta\alpha\Delta t - C_0 I_0(\xi) - C_1 I_1(\xi). \tag{18}$$

Substitution of (12) into the formula for the axial stress in (9) yields:

$$\sigma_z\left(r, \pm\frac{h}{2}\right) = -2G\{[2(2-\nu)C_0 + \xi C_1]I_0(\gamma r) + C_0\gamma r I_1(\gamma r)\} - \frac{E}{\nu}A. \tag{19}$$

Then the condition (16) results in the equation:

$$[2(2-\nu)S_0 + 2S_1]C_0 + \xi S_0 C_1 = -\frac{1+\nu}{\nu}A, \tag{20}$$

where

$$S_0 = \frac{1}{a}\int_0^a I_0(\gamma r)dr = \frac{1}{\xi}\int_0^\xi I_0(x)dx, \tag{21}$$

$$S_1 = \frac{1}{a}\int_0^a r I_1(\gamma r)dr = \frac{1}{\gamma}[I_0(\xi) - S_0(\xi)]. \tag{22}$$

The latter formula was obtained on the basis of integration by parts. Using (22) we rewrite (20) as follows:

$$[(3-2\nu)S_0(\xi) + I_0(\xi)]C_0 + \xi S_0(\xi)C_1 = -\frac{1+\nu}{\nu}A. \tag{23}$$

The condition (17), the expression for the radial stress in (9), and the solutions (12) result in the following equations for the constants A, B, C_0 and C_1:

$$A + \nu B = 0, \tag{24}$$

$$[(1-2\nu)I_0(\xi) + \xi I_1(\xi)]C_0 + [\xi I_0(\xi) - I_1(\xi)]C_1 = 0. \tag{25}$$

From (23) and (25), we obtain the formulas for the constants C_0 and C_1 in the form:

$$C_0 = \chi_0(\xi)A, \qquad C_1 = \chi_1(\xi)A, \tag{26}$$

where

$$\left.\begin{aligned}\chi_0(\xi) &= -\frac{1+\nu}{\nu}\,\frac{\xi I_0(\xi) - I_1(\xi)}{D(\xi)} \\ \chi_1(\xi) &= \frac{1+\nu}{\nu}\,\frac{(1-2\nu)I_0(\xi) + \xi I_1(\xi)}{D(\xi)}\end{aligned}\right\}, \tag{27}$$

and

$$D(\xi) = [2\xi I_0(\xi) - (3 - 2\nu + \xi^2)I_1(\xi)]S_0(\xi) + I_0(\xi)[\xi I_0(\xi) - I_1(\xi)] \tag{28}$$

is the determinant of the system of equations (23) and (25).

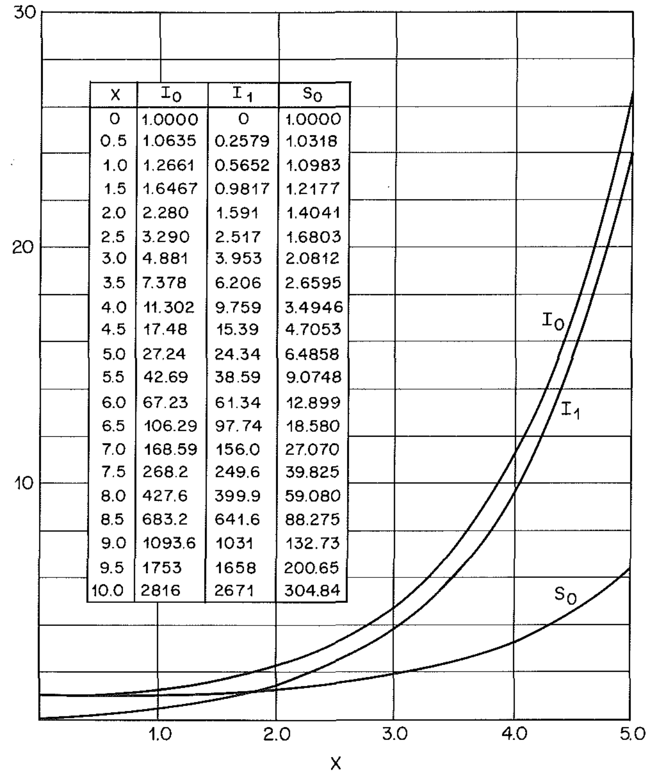

X	I_0	I_1	S_0
0	1.0000	0	1.0000
0.5	1.0635	0.2579	1.0318
1.0	1.2661	0.5652	1.0983
1.5	1.6467	0.9817	1.2177
2.0	2.280	1.591	1.4041
2.5	3.290	2.517	1.6803
3.0	4.881	3.953	2.0812
3.5	7.378	6.206	2.6595
4.0	11.302	9.759	3.4946
4.5	17.48	15.39	4.7053
5.0	27.24	24.34	6.4858
5.5	42.69	38.59	9.0748
6.0	67.23	61.34	12.899
6.5	106.29	97.74	18.580
7.0	168.59	156.0	27.070
7.5	268.2	249.6	39.825
8.0	427.6	399.9	59.080
8.5	683.2	641.6	88.275
9.0	1093.6	1031	132.73
9.5	1753	1658	200.65
10.0	2816	2671	304.84

Fig. 2

Introducing (26) into (18), we obtain the formula for the constant A in the form:

$$A = \bar{A}(\xi)\Delta\alpha\Delta t, \tag{29}$$

where

$$\bar{A}(\xi) = [1 + \chi_0(\xi)I_0(\xi) + \chi_1(\xi)I_1(\xi)]^{-1} = \left[1 + \frac{1+\nu}{\nu}\,\frac{2(1-\nu)I_0(\xi)I_1(\xi)I_1(\xi) - \xi[I_0^2(\xi) - I_1^2(\xi)]}{D(\xi)}\right]^{-1}. \tag{30}$$

After the constant A is found, the B value can be determined from (24).

This concludes the solution to the elastic problem. We would like to emphasize that this solution is intended to be used primarily for the purpose of evaluation of the interfacial stresses. The modified Bessel functions entering the above formulas can be taken from the tables given in handbooks on special functions (see references). The functions $I_0(x)$, $I_1(x)$ and $S_0(x)$ are plotted in Fig. 2.

The function $S_0(x)$ can be evaluated either numerically or on the basis of one of the following formulas (Gradshteyn and Ryzhik, 1980):

$$S_0(x) = \frac{2}{x}\sum_{m=0}^{\infty}(-1)^m I_{2m+1}(x),$$

$$S_0(x) = I_0(x) - \frac{\pi}{2}[I_1(x)L_0(x) - I_0(x)L_1(x)]. \tag{31}$$

In the latter formula, $L_n(x)$ is the modified Struve function of the order n, defined by the expansion

$$L_n(x) = \sum_{m=0}^{\infty}\frac{\left(\frac{x}{2}\right)^{2m+n+1}}{\Gamma\left(m+\frac{3}{2}\right)\Gamma\left(\frac{3}{2}\right)} =$$

$$= \frac{2}{\sqrt{\pi}} \frac{\left(\frac{x}{2}\right)^{n+1}}{\Gamma\left(n+\frac{3}{2}\right)} \left[1 + \frac{x^2}{3(2n+3)} + \frac{x^4}{(3)(5)(2n+3)(2n+5)} + \ldots\right]. \tag{32}$$

For large x values the following asymptotic formulas can be obtained

$$L_0(x) \cong I_0(x) - \frac{2}{\pi x},\ L_1(x) \cong I_1(x) - \frac{2}{\pi},$$
$$S_0(x) \cong \frac{I_1(x)}{x},\ x > 25. \tag{33}$$

2.3 Strains and Stresses. The formulas for the maximum strains can be obtained from the equations (5), (12), (14), and (26), and are as follows:

$$\left.\begin{aligned}
\epsilon_r &= A\Big\{1 + [\chi_0(\xi) + \xi\chi_1(\xi)]I_0(\gamma r) \\
&\quad + \left[\chi_0(\xi)\gamma r - \chi_1(\xi)\frac{\xi}{\gamma r}\right]I_1(\gamma r)\Big\} \\
\epsilon_t &= A\left\{1 + \left[\chi_0(\xi)I_0(\gamma r) + \chi_1(\xi)\frac{\xi}{\gamma r}I_1(\gamma r)\right]\right\} \\
\epsilon_z &= -A\Big\{\frac{1}{\nu} + \Big[(4(1-\nu)\chi_0(\xi) + \xi\chi_1(\xi))I_0(\gamma r) \\
&\quad + \chi_0(\xi)\gamma r I_1(\gamma r)\Big]\Big\} \\
\gamma_{rz} &= 2A\Big\{\chi_0(\xi)\gamma r I_0(\gamma r) + [2(1-\nu)\chi_0(\xi) \\
&\quad + \xi\chi_1(\xi)]I_1(\gamma r)\Big\}
\end{aligned}\right\}. \tag{34}$$

The factor A in these formulas is expressed by the equation (29). The maximum linear strains take place in the end planes, while the maximum shearing strains occur in the cross-sections located at the distances of one-quarter of the cylinder's height.

The strain invariant, expressed by the formula (7), can be presented for the interfacial strains as follows:

$$\theta = -(1-2\nu)A\left[\frac{1}{\nu} + 2\chi_0(\xi)I_0(\gamma r)\right]. \tag{35}$$

Then the equations (6) result in the following formulas for the normal stresses, acting in the end planes:

$$\left.\begin{aligned}
\sigma_r &= 2GA\Big\{[(1-2\nu)\chi_0(\xi) + \xi\chi_1(\xi)]I_0(\gamma r) \\
&\quad + \left[\chi_0(\xi)\gamma r - \chi_1(\xi)\frac{\xi}{\gamma r}\right]I_1(\gamma r) \\
\sigma_t &= 2GA\left[(1-2\nu)\chi_0(\xi)I_0(\gamma r) - \gamma_1(\xi)\frac{\xi}{\gamma r}I_1(\gamma r)\right] \\
\sigma_z &= -2GA\Big\{1 + \frac{1}{\nu} + [2(2-\nu)\chi_0(\xi) + \xi\chi_1(\xi)]I_0(\gamma r) \\
&\quad + \chi_0(\xi)\gamma r I_1(\gamma r)\Big\}
\end{aligned}\right\}. \tag{36}$$

The shearing stresses in the $z = \pm h/2$ cross-sections are as follows:

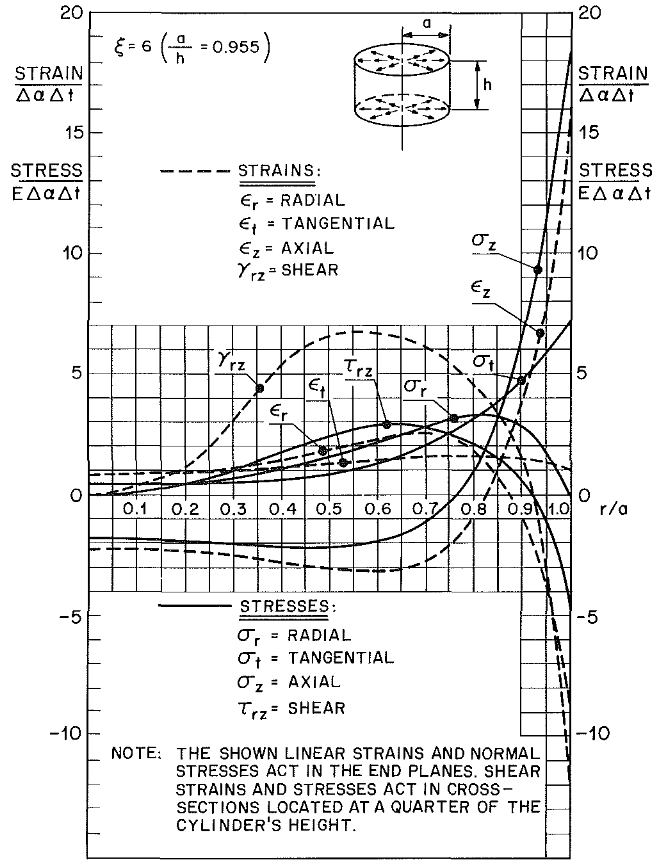

Fig. 3 Distribution of strains and stresses along the radius of the cylinder

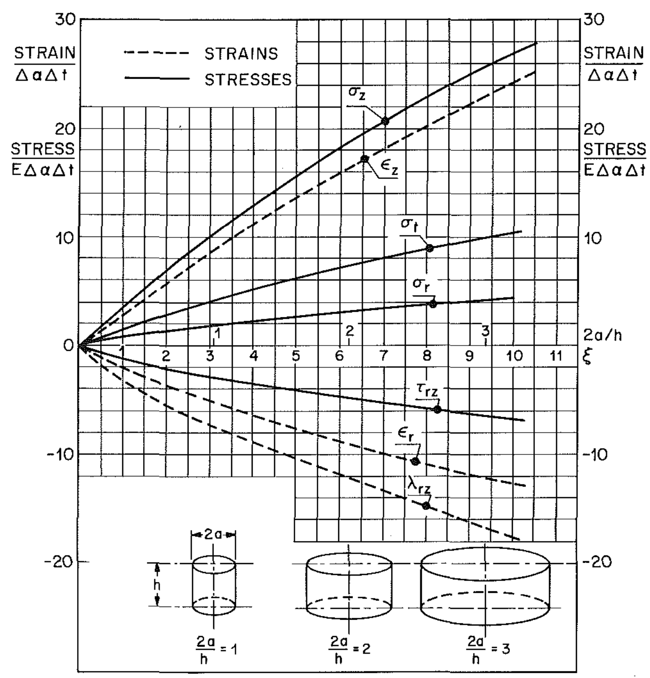

Fig. 4 Maximum strains and stresses versus diameter-to-height ratio

$$\tau_{rz} = 2GA\{\chi_0(\xi)\gamma r I_0(\gamma r) + [2(1-\nu)\chi_0(\xi) + \xi\chi_1(\xi)]I_1(\gamma r)\}. \tag{37}$$

Note, that for the points close to the cylinder axis (small γr

Table 1

r/α	0	0.2	0.5	0.7	0.9	0.95	1.0
				$\xi=3.0$			
$\epsilon_r/\Delta\alpha\Delta t$	2.377	2.345	1.930	0.818	−2.114	−3.365	−4.885
$\epsilon_t/\Delta\alpha\Delta t$	2.377	2.367	2.268	2.038	1.490	1.271	1.000
$\epsilon_z/\Delta\alpha\Delta t$	−4.402	−4.252	−3.090	−0.815	4.296	6.334	8.769
$\gamma_{rz}/\Delta\alpha\Delta t$	0	2.034	3.271	2.147	−2.628	−4.828	−7.598
$\sigma_r/E\Delta\alpha\Delta t$	2.048	2.104	2.279	2.145	1.168	0.658	0
$\sigma_t/E\Delta\alpha\Delta t$	2.048	2.121	2.532	3.060	3.871	4.134	4.413
$\sigma_z/E\Delta\alpha\Delta t$	−3.047	−2.844	−1.486	−0.920	5.975	7.931	10.240
$\tau_{rz}/E\Delta\alpha\Delta t$	0	0.763	1.227	0.805	−0.985	−1.811	−2.849
				$\xi=6.0$			
$\epsilon_r/\Delta\alpha\Delta t$	0.927	1.005	1.968	2.499	−0.824	−3.757	−8.444
$\epsilon_t/\Delta\alpha\Delta t$	0.927	0.992	1.269	1.569	1.561	1.367	1.000
$\epsilon_z/\Delta\alpha\Delta t$	−2.168	−2.268	−3.036	−2.735	3.978	8.716	15.892
$\gamma_{rz}/\Delta\alpha\Delta t$	0	1.225	6.624	6.121	1.695	−3.298	−11.770
$\sigma_r/E\Delta\alpha\Delta t$	0.460	0.551	1.626	2.874	2.917	1.927	0
$\sigma_t/E\Delta\alpha\Delta t$	0.460	0.542	0.801	2.176	4.706	5.770	7.083
$\sigma_z/E\Delta\alpha\Delta t$	−1.861	−1.904	−2.127	−1.052	6.519	11.281	18.252
$\tau_{rz}/E\Delta\alpha\Delta t$	0	0.459	2.484	2.295	0.636	−1.237	−4.414
				$\xi=10.0$			
$\epsilon_r/\Delta\alpha\Delta t$	0.420	0.464	1.053	2.709	2.267	−2.085	−12.490
$\epsilon_t/\Delta\alpha\Delta t$	0.420	0.434	0.570	0.908	1.456	1.401	1.000
$\epsilon_z/\Delta\alpha\Delta t$	−1.226	−1.277	−1.884	−3.240	1.035	8.544	24.353
$\gamma_{rz}/\Delta\alpha\Delta t$	0	0.169	1.556	5.575	7.786	0.839	−17.469
$\sigma_r/E\Delta\alpha\Delta t$	0.0269	0.0645	0.594	2.315	5.268	4.332	0
$\sigma_t/E\Delta\alpha\Delta t$	0.0269	0.0417	0.232	0.964	4.660	6.947	10.406
$\sigma_z/E\Delta\alpha\Delta t$	−1.208	−1.242	−1.609	−2.147	4.345	12.304	27.921
$\tau_{rz}/E\Delta\alpha\Delta t$	0	0.0634	0.583	2.091	2.920	0.315	−6.551

ϵ_r, σ_r = radial strain and stress
ϵ_t, σ_t = tangential (circumferential) strain and stress
ϵ_z, σ_z = axial strain and stress
γ_{rz}, τ_{rz} = shear strain and stresses

values) the ratio $I_1(\gamma r)/\gamma r$ in the aforementioned formulas is equal to 0.5.

2.4 Calculated Data. The results of the computations performed for the cases $\xi=3$, 6, and 10 ($d/h=0.995$, 1.910, 3.183), with $\nu=1/3$, are shown in Table 1. The distributions of stresses and strains along the radius are plotted in Fig. 3 for the case $\xi=6$. The maximum strains and stresses occurring in the interfaces (in the case of linear strains and normal stresses), and in the cross-section $z=\pm h/4$ (in the case of shearing strains and stresses), are plotted in Fig. 4 versus ξ values.

2.5 Numerical Example. The numerical example is carried out for a 5 percent Sn/95 percent Pb solder joint interconnection ($E=0.2\times10^6$ kg/cm$^2\cong2.84\times10^6$ psi, $\nu=1/3$, $\alpha=28\times10^{-6}$°C) between a silicon chip and a silicon substrate ($\alpha\cong3.0\times10^{-6}$°C). The soldering temperature is 320°C. The calculations are performed for the temperature −50°C, so that $\Delta\alpha\Delta t=0.00925$, and $E\Delta\alpha\Delta t=1850$ kg/cm^2 (26270 psi). The joint's height is $h=60$ μm and its diameter is $d=115$ μm. Hence, $\xi=\pi d/h=6$. The distributions of the strains and stresses along the radius coincide with those shown in Table 1 for the case $\xi=6$ (see also Fig. 4).

The calculated stresses are very high, and, if the strains were not restricted (obviously, as long as the "generating" radial strains in the end planes cannot exceed $\Delta\alpha\Delta t$, all the resulting strains are always finite, though can be, of course, very large) would inevitably result in an ultimate failure of the joint. The maximum linear strains occurring on the contours of the interfaces, are tensile and directed upwards. In accordance with the Table 1 data, these strains are 15.892 $\times0.00925=0.147=14.7$ percent. The ultimate elongations ϵ_u for the solder in question vary from 30 to 60 percent and, therefore, the margin of safety in this case is at least about two. The ultimate shearing strain can be assessed by the formula

$$\gamma_u=\frac{2(1+\nu)}{\sqrt{3}}\epsilon_u.$$

With the ϵ_u value varying in the above range, we have $\gamma_u=40\rightarrow93$ percent, for $\nu=1/3$. The maximum shearing strain for the solder joint in question is −11.77 $\times0.00925=0.1089=-10.9$ percent, i.e., essentially smaller than the ultimate strain. From the standpoint of the fatigue strength, however, the calculated strain level could turn out too high. If the aspect ratio of the solder joint is reduced by the factor of two, then the maximum axial strain becomes about 8.1 percent, which is supposed to result in a significantly greater fatigue life. If, for instance, the Manson-Coffin formula (as modified by W. Englemaier, 1983) is used to evaluate the number of cycles till failure, then the expected increase in the fatigue life, because of smaller maximum strains, can be assessed by the formula:

$$\frac{N_2}{N_1}=\left(\frac{\epsilon_1}{\epsilon_2}\right)^m,$$

where the calculated value of the exponent m is between 2.5 and 3.0 (Englemaier, 1983). Then the twofold reduction in the maximum strain will result in about 5.7→8.0 times longer fatigue life of the interconnection.

3 Conclusions

The following major conclusions can be drawn from the above analysis:

- All the calculated strains and stresses are the greatest either on the lateral surface itself or in the vicinity of this surface. Hence, it is the peripheral part of the joint, which is primarily responsible for its mechanical performance.

- The maximum linear strains and the maximum normal stresses occur in the interfaces, while the maximum shearing strains and stresses take place in the cross-sections located at one-quarter of the joint's height.
- The maximum strains act in the axial direction and concentrate near the lateral surface, then follow the radial and the shearing strains. These are also the greatest at the lateral surface. The tangential (circumferential) strains are relatively small.
- The maximum stresses also act in the axial direction and concentrate at the lateral surface. These stresses are significantly greater than all the other stress categories. When the coefficient of thermal expansion of the soldered materials is smaller than the coefficient of thermal expansion of the solder, then the low temperature axial stresses at the lateral surface are tensile. This could possibly result in an ultimate failure or in the crack initiation during thermal cycling. The adverse effect of the concentrated axial stresses is aggravated in such a case by tensile tangential stresses, which, unlike tangential strains, are rather great, and, in combination with significant axial stresses, result in a three-dimensional stress condition. This could lead to fracture initiation in the "corners" of the joint, especially at low temperatures, when materials are more prone to fracture formation. The radial and shearing stresses are essentially smaller than the stresses of the first two categories.
- The diameter-to-height ratio is the only geometrical parameter, affecting the strains and stresses. Therefore, joints with identical diameter-to-height ratios are expected to experience the same strains and stresses, as long as they are manufactured of the same material and are subjected to the same external thermal mismatch strain $\Delta\alpha\Delta t$.
- In the range of diameter-to-height ratios of practical interest ($d/h = 0.5 \rightarrow 3.0$), the strains and stresses essentially increase with an increase in these ratios. As a "rule of thumb," one may assume that the strains and stresses are approximately proportional to the diameter-to-height ratio. When the diameter-to-height ratio decreases, for instance, from two (solder joints of this aspect ratio were employed in the advanced packaging technology described by Bartlett et al., 1987) to unity, then the strains and stresses decrease by about two times (Fig. 4). Such a reduction in the diameter-to-height ratio, can increase the fatigue life of a solder joint interconnection by about 6 to 8 times.
- Materials with smaller Young's moduli experience smaller stresses. From this standpoint a 5 percent Sn/95 percent Pb solder, whose Young's modulus is about 4.6 times smaller than that of a 60 percent Sn/40 percent Pb solder, is expected to result in smaller stresses at low temperature conditions, even despite the fact that its melting point is higher. Indium and some indium-based alloys seem to be even more attractive in this respect.

Note that the above conclusions, at least those concerning strains, seem to be true not only for elastic, but also for elastoplastic deformations, both at low and elevated temperatures.

4 Acknowledgment

The author acknowledges, with thanks, the comments made by the members of the Bell Laboratories Leaded Packages Subcommittee (LEAP) of the Surface Mount Attachment Reliability Taskgroup (SMART), J. A. Augis, J.-P. M. Clech, W. Englemaier, R. W. Kotlowitz, and R. M. Richman.

References

Bartlett, C. J., Segelken, J. M., and Teneketges, N. A., 1987, "Multi-chip Packaging Design for VLSI-based Systems," Proceedings of the 37th Electronic Component Conference, Boston, Mass., pp. 518–525.

Benthem, J. P., and Minderhaud, P., 1972, "The Problem of the Solid Cylinder Compressed Between Rigid Stamps," *Int. J. of Solids and Structures*, Vol. 8, pp. 1027–1042.

Chen, W. T., and Nelson, C. W., 1979, "Thermal Stresses in Bonded Joints," *IBM J. Res. Develop.*, Vol. 23, No. 2, pp. 179–187.

Clech, J.-P. M., 1987, "Analysis of Thermomechanical Strains in Solder Joints of Surface Mount Assemblies," presented at the 1987 IEEE International Electronic Manufacturing Technology Symp., Anaheim, Calif.

Englemaier, W., 1983, "Fatigue Life of Leadless Chip Carrier Solder Joint During Power Cycling," *IEEE Trans.*, Vol. CHMT-6, No. 3, pp. 232–237.

Engelmaier, W., 1988, "Surface Mount Attachment Reliability of Clip-Leaded Ceramic Chip Carriers on FR-4 Circuit-Boards," *NEPCON EAST '88 Conference*, Boston, Mass., June 13–16, 1988, pp. 121–137.

Filon, L., 1902, "On the Elastic Equilibrium of Circular Cylinders Under Certain Practical Systems of Loads," *Phil. Trans. of the Royal Soc., London*, Ser. A, p. 198.

Goland, M., and Reissner, E., 1944, "The Stresses in Cemented Joints," ASME Journal of Applied Mechanics, Vol. 11, pp. 17–27.

Gradshteyn, I. S., and Ryzhik, 1980, *Tables of Integrals, Series and Products*, 2nd English ed., Academic Press, New York.

Hall, P. M., and Sherry, W. M., 1986, "Materials, Structures and Mechanics of Solder Joints for Surface-Mount Microelectronics Technology," *Proc. of the 3rd Int. Conf. on Interconnection Technology in Electronics*," Fellbach, Fed. Republic of Germany, pp. 47–61.

Lau, J. H., and Rice, D. W., 1985, "Solder Joint Fatigue in Surface Mount Technology: State of the Art," *Solid State Technology*, Vol. 28, pp. 91–104.

Love, A. E. H., 1944, *A Treatise on the Theory of Elasticity*, Dover Publications, New York.

Robert, M. P., 1987, "Mechanical Modeling Problems Associated with Microelectronic Components," Ph.D. Dissertation, Northwestern Univ., Evanston, Ill.

Sneddon, I. N., 1956, *Special Functions of Mathematical Physics and Chemistry*, Oliver and Boyd, Edinburgh.

Spanier, J., and Oldham, K. B., 1987, *An Atlas of Functions*, Hemisphere Publishing Corp., New York.

Suhir, E., 1986, "Stresses in Bi-Metal Thermostats," ASME Journal of Applied Mechanics, Vol. 53, pp. 657–660.

Swan, G. N., 1968, "The Semi-Infinite Cylinder with Prescribed End Displacements," *SIAM J. of Appl. Math.*, Vol. 16, pp. 860–881.

Timoshenko, S. P., and Goodier, J. N., 1970, *Theory of Elasticity*, 3rd ed., McGraw-Hill, New York.

Watson, G. N., 1952, *A Treatise on the Theory of Bessel Functions*, 2nd ed., Cambridge, Cambridge University Press.

End Effects and Time-Harmonic Longitudinal Wave Propagation in a Semi-Infinite Solid Cylinder

Yoon Young Kim
Research Associate.

Charles R. Steele
Professor.
Fellow, ASME

Division of Applied Mechanics
Stanford University,
Stanford, Calif. 94305

Axisymmetric end problems of longitudinal wave propagation are studied in a semi-infinite isotropic solid circular cylinder which is free of traction on its cylindrical surface. An accurate and computationally efficient method of solution is presented which can exploit the asymptotic behavior for high harmonics in the radial direction. The stresses and displacements are expanded in terms of the eigenfunctions of the case of a lubricated-rigid cylindrical surface condition. The expansions are used to construct a stiffness matrix relating the harmonics of stress and displacement for the traction-free case, which is shown to approach asymptotically that of the case of the mixed condition. Unlike other approaches such as finite element or boundary integral methods, which typically require the solution of large systems of equations for rapidly varying end conditions, the present formulation can lead to a coupled system of equations for lower spatial harmonics and a weakly coupled system for higher spatial harmonics. Due to the small number of equations in the coupled system, the present approach is very effective in handling general boundary conditions, and is particularly efficient for end conditions with rapid spatial variation.

1 Introduction

The study of wave propagation in a solid cylinder has many applications, such as nondestructive evaluation of material properties, flaw detection, and the determination of resonances. The analgous problem is that of a fluid contained in a cylindrical vessel. A motivation for the present work was the extension of the analysis of the cochlear model calculation procedure of Miller (1985). Another motivation was the need for an efficient dynamic analysis of the cylindrical stem of a hemispherical resonator gyroscope (see Loper and Lynch (1983) and Lynch (1987)). A specific concern is the effect of imperfection in the cylindrical stem attachment on the dynamic behavior of the gyro. In this paper, end effects and time-harmonic longitudinal wave propagation in a solid circular cylinder without an imperfection are studied. The computational technique which is developed should provide a crucial building block for the treatment of the general problem.

The first aspect treated is the end "stiffness" which is the relation between the stress and displacement quantities that can be prescribed at the end. The second aspect concerns the relation of the end quantities and the amplitudes of both propagating and evanescent modes at distances near and far from the end. End distributions of stress and/or displacement which are either slowly or rapidly varying with the radial coordinate must be considered. Since localized or rapidly varying end distributions can contribute significantly to all propagating modes, the correct relation between slowly and rapidly varying distributions must be preserved. To capture these effects with finite elements or boundary elements would require very large arrays. On the other hand, typical analytical solution techniques, which use modal expansions, also require a large number of modes and usually converge very slowly. The difficulties of the analytic method are due to the coupled wave nature of dilation and shear.

The present approach, based on analytical solutions, utilizes the asymptotic behavior of a stiffness matrix which relates the spatial harmonics of stress and displacement and leads to two systems of equations: a small coupled system for lower harmonics and a weakly coupled system for higher harmonics. The weakly coupled system can be made as large as desired, so that the inclusion of higher harmonics does not result in poor conditioning or significantly increase computational effort. Although the method can be generalized to nonaxisymmetric wave propagation problems, the present work is limited to axisymmetric problems.

The exact solution for wave propagation in an infinite cylinder was obtained by Pochhammer (1876) and Chree (1886), who also developed an approximate theory by replacing the Bessel functions in the frequency equation by the first two terms of the series expansions. Rayleigh (1945) derived an almost identical approximate equation by including the effect of the inertia of lateral motion.

Contributed by the Applied Mechanics Division of The American Society of Mechanical Engineers for presentation at the Joint ASCE/ASME Applied Mechanics, Biomechanics, and Fluids Engineering Conference, San Diego, Calif., July 9 to 12, 1989.

Discussion of this paper should be addressed to the Editorial Department, ASME, United Engineering Center, 345 East 47th Street, New York, N.Y. 10017, and will be accepted until two months after final publication of the paper itself in the Journal of Applied Mechanics. Manuscript received by the ASME Applied Mechanics Division, December 9, 1987; final revision, September 21, 1988.

Paper No. 89-APM-29.

Mindlin and Herrmann (1951) obtained an approximate equation to take into account the coupling between longitudinal and radial modes. Later, Mindlin and McNiven (1960) derived a three-mode approximate equation in which they expanded the displacements in terms of the Jacobi polynomials in the radial directions. Ulitko and Bobyleva (1986) generalized the results of Mindlin and McNiven (1960) for a piezoceramic medium. Achenbach and Fang (1970) and Vasudeva et al. (1986) used perturbation techniques to derive approximate equations for small wave numbers. The history of the analysis of elastic wave propagation is described by Green (1960), Miklowitz (1966), McNiven and McCoy (1974), and Pao (1983).

Most work to date has been concerned with the establishment and physical understanding of dispersion relations. The work by Zemanek (1962, 1972), based on the exact solution, gives a through understanding of the dispersion relations for real, imaginary, and complex wave numbers. Zemanek uses a collocation method to study reflection and end resonance. McNiven (1961) uses the Mindlin-McNiven approximate theory for the analysis of reflection and end resonance. Folk et al. (1958) studies an impact problem such that a constant pressure is suddenly applied with a constraint in the radial motion (a mixed end condition). To study reflection in semi-infinite plates, Torvik (1967) employs the variational form of the equations of motion, and uses the well-known modes of vibration for the infinite plate as elements of expansion applicable to semi-infinite plates.

The collocation and variational approaches lead to a coupled system of linear equations because the eigenfunctions are not orthogonal. When either the normal stress and radial displacement or the shear stress and axial displacement is prescribed at the end of the cylinder, *bi-orthogonality* can be employed. When stresses alone or displacements alone are prescribed at the end, bi-orthogonality is not directly applicable. The bi-orthogonality property of solutions to static problems in semi-infinite circular cylindrical bodies established by Fama (1972) is extended to dynamic problems by Frazer (1975). Later, Gregory (1983) rederives the bi-orthogonality relation by means of the elastic reciprocal theorem and the elastic symmetry of the cylinder in planes perpendicular to its generators. Fama suggests the use of bi-orthongonality to solve problems with general boundary conditions, but this also requires a system of equations.

The existing methods for the problems with stress or displacement end conditions, such as collocation or the methods suggested by Torvik and Fama, are most useful when the end conditions are smooth. For rapidly varying end conditions in which higher modes must be included, these methods typically encounter computational difficulties due the large number of equations to be solved and slow convergence.

In the present work, solutions are obtained to the axisymmetric problems with the traction-free cylindrical surface, where either stresses alone or displacements alone are prescribed at the end of the cylinder. Stresses and displacements are expanded in terms of the Fourier-Bessel series, which satisify a mixed condition on the cylindrical surface. We then construct the stiffness matrix which relates the coefficients of the Fourier-Bessel series for the stress quantities to those of the displacement quantities at the end of the cylinder. For higher harmonics, it is shown that the stiffness matrix corresponding to the traction-free cylindrical surface condition is asymptotically equivalent to the stiffness matrix for the mixed cylindrical surface condition, for which the harmonics are decoupled. This asymptotic behavior allows the system of equations partitioned into a coupled system and a weakly coupled system, where only the coupled system, which corresponds to the stiffness matrix for lower harmonics, needs to be solved explicitly. The weakly coupled system, which corresponds to the stiffness matrix for higher harmonics, may have as many equations as necessary in order to capture any rapid variation of the end conditions.

The stiffness matrix approach is applied to several numerical examples and compared with the collocation method. The advantage of the present work is that even very rapidly varying end conditions can be handled effectively. It is observed that the present stiffness approach, even without incorporating the asymptotic behavior, is much more efficient than the collocation method.

2 Axisymmetric Solutions for Cylindrical Problems

An axisymmetric solution to the wave equation for an isotropic elastic solid cylinder (see, e.g., Miklowitz (1978) or Achenbach (1975)) can be expressed

$$u_i(r,z,t)=\tilde{u}_i(r)\exp[i(\lambda z-\Omega t)]$$
$$\sigma_{ij}(r,z,t)=\tilde{\sigma}_{ij}(r)\exp[i(\lambda z-\Omega t)] \tag{1}$$

where

$$\tilde{u}_r(r) = A\frac{dJ_0(hr)}{dr}+Bi\lambda\frac{dJ_0(kr)}{dr} \tag{2a}$$

$$\tilde{u}_z(r) = Ai\lambda J_0(hr)+Bk^2J_0(kr) \tag{2b}$$

and

$$\tilde{\sigma}_{rr}(r) = A\left\{-\frac{1}{r}\frac{dJ_0(hr)}{dr}-\left(\frac{\Omega^2}{2}-\lambda^2\right)J_0(hr)\right\} + Bi\lambda\left\{-\frac{1}{r}\frac{dJ_0(hr)}{dr}-k^2J_0(kr)\right\} \tag{3a}$$

$$\tilde{\sigma}_{\theta\theta}(r) = A\left\{-\left(\frac{1}{2}-\alpha^2\right)\Omega^2J_0(hr)+\frac{1}{r}\frac{dJ_0(hr)}{dr}\right\} + Bi\lambda\frac{1}{r}\frac{dJ_0(kr)}{dr} \tag{3b}$$

$$\tilde{\sigma}_{zz}(r) = A\left(h^2-\frac{\Omega^2}{2}\right)J_0(hr)+B(i\lambda)k^2J_0(kr) \tag{3c}$$

$$\tilde{\sigma}_{rz}(r) = A(i\lambda)\frac{dJ_0(hr)}{dr}+B\left(\frac{\Omega^2}{2}-\lambda^2\right)\frac{dJ_0(kr)}{dr}. \tag{3d}$$

In (1), dimensionless quantities are used by referring the displacement u_i and stress σ_{ij} to the radius a of the cylinder, and 2μ, twice the shear radius, respectively. The radial and axial coordinates r and z are referred to a and the time t is referred to a/c_s, where c_s is the shear wave velocity in an infinite medium. The dimensionless frequency Ω is referred to c_s/a and the parameters h and k are defined as

$$h^2=\alpha^2\Omega^2-\lambda^2;\quad k^2=\Omega^2-\lambda^2. \tag{4}$$

The dimensionless wave number λ is referred to $1/a$, the constant α^2 is given by

$$\alpha^2=\left(\frac{c_s}{c_d}\right)^2=\frac{1-2\nu}{2(1-\nu)} \tag{5}$$

where c_d is the dilatational wave velocity, and ν is Poisson's ratio. The unknowns A and B are to be determined from boundary conditions.

3 Mixed Boundary Condition on the Cylindrical Surface

In the present work, the solutions which satisfy a mixed cylindrical surface condition are used to construct a stiffness matrix, and serve as an expansion set to solve problems with a traction-free condition on the cylindrical surface.

The mixed, or lubricated-rigid condition is defined by (see, e.g., Auld, 1973)

$$u_r|_{r=1}=0; \quad \sigma_{rz}|_{r=1}=0 \tag{6}$$

and the corresponding frequency equation is

$$J_0'(h)J_0'(k)=0. \tag{7}$$

From (7), we have the solutions

$$J_0'(h)=0, \quad A\neq 0 \ (B=0),$$

$$h=\xi_m, \quad \lambda^2=\alpha^2\Omega^2-\xi_m^2\equiv\lambda_{dm}^2 \ (m=0,1,2,\ldots) \tag{8a}$$

$$J_0'(k)=0, \quad B\neq 0 \ (A=0),$$

$$k=\xi_m, \quad \lambda^2=\Omega^2-\xi_m^2\equiv\lambda_{sm}^2 \ (m=1,2,\ldots) \tag{8b}$$

where ξ denotes the zero of $J_0'(r)$. The subscripts d and s are used to denote the dilatational and shear waves, respectively. The solutions of (8) show that dilational and shear waves are uncoupled.

The solutions for waves propagating along the $+z$ axis can, therefore, be written for a given frequency Ω

$$u_r(r,z,t)=-\sum_{m=1}^{n_h}A_m\xi_mJ_1(\xi_mr)e^{i(\lambda_{dm}z-\Omega t)} - \sum_{m=1}^{n_h}B_mi\lambda_{sm}\xi_mJ_1(\xi_mr)e^{i(\lambda_{sm}z-\Omega t)} \tag{9a}$$

$$u_z(r,z,t)=\sum_{m=0}^{n_h}A_mi\lambda_{dm}J_0(\xi_mr)e^{i(\lambda_{dm}z-\Omega t)} + \sum_{m=1}^{n_h}B_m\xi_m^2J_0(\xi_mr)e^{i(\lambda_{sm}z-\Omega t)} \tag{9b}$$

$$\sigma_{rz}(r,z,t)=-\sum_{m=1}^{n_h}A_mi\lambda_{dm}\xi_mJ_1(\xi_mr)e^{i(\lambda_{dm}z-\Omega t)} - \sum_{m=1}^{n_h}B_m\left(\xi_m^2-\frac{\Omega^2}{2}\right)\xi_mJ_1(\xi_mr)e^{i(\lambda_{sm}z-\Omega t)} \tag{9c}$$

$$\sigma_{zz}(r,z,t)=\sum_{m=0}^{n_h}A_m\left(\xi_m^2-\frac{\Omega^2}{2}\right)J_0(\xi_mr)e^{i(\lambda_{dm}z-\Omega t)} + \sum_{m=1}^{n_h}B_m\xi_m^2i\lambda_{sm}J_0(\xi_mr)e^{i(\lambda_{sm}z-\Omega t)}. \tag{9d}$$

Note that (8) can be used to determine whether a particular term in (9) corresponds to a propagating wave (λ real) or decaying end effect (λ imaginary in $z>0$).

Equations (9) show that the eigenfunctions for u_r and σ_{rz} are simply the Bessel functions of the first kind of order 1, and the eigenfunctions for u_z and σ_{zz} are the Bessel functions of the first kind of order 0 in the r direction. One can, therefore, expand the quantities which can be prescribed at $z=0$ as

$$u_r(r,0,t) = U_r(r)e^{-i\Omega t} \tag{10a}$$

$$u_z(r,0,t) = U_z(r)e^{-i\Omega t} \tag{10b}$$

$$\sigma_{rz}(r,0,t) = S_r(r)e^{-i\Omega t} \tag{10c}$$

$$\sigma_{zz}(r,0,t) = S_z(r)e^{-i\Omega t} \tag{10d}$$

where

$$U_r(r) = \sum_{m=1}^{n_h}U_mJ_1(\xi_mr) \tag{11a}$$

$$U_z(r) = W_0+\sum_{m=1}^{n_h}W_mJ_0(\xi_mr) \tag{11b}$$

$$S_r(r) = \sum_{m=1}^{n_h}S_mJ_1(\xi_mr) \tag{11c}$$

$$S_z(r) = Z_0+\sum_{m=1}^{n_h}Z_mJ_0(\xi_mr). \tag{11d}$$

Note that the physical quantities are real parts of the above quantities.

The coefficients U_m, and W_m can be computed by using the orthogonality property of Bessel functions (see, e.g., Churchill and Brown, 1978).

$$U_m=\frac{2}{[J_2(\xi_m)]^2}\int_0^1U_r(r)J_1(\xi_mr)rdr \quad \text{for } m=1,2,\ldots \tag{12a}$$

$$W_m=\begin{cases}\dfrac{2}{[J_0(\xi_m)]^2}\displaystyle\int_0^1U_z(r)J_0(\xi_mr)rdr & \text{for } m=1,2,\ldots\\ 2\displaystyle\int_0^1U_z(r)rdr & \text{for } m=0.\end{cases} \tag{12b}$$

To compute S_m, and Z_m, we replace U_m by S_m, $U_r(r)$ by $S_r(r)$ and W_m by Z_m and $U_z(r)$ by $S_z(r)$ in (12).

From (9)–(11), the following stiffness relation can be obtained for $m\neq 0$:

$$\begin{Bmatrix}Z_m\\S_m\end{Bmatrix}=\mathbf{K}_m\begin{Bmatrix}W_m\\U_m\end{Bmatrix} = \begin{bmatrix}(\mathbf{K}_m)_{1,1} & (\mathbf{K}_m)_{1,2}\\(\mathbf{K}_m)_{2,1} & (\mathbf{K}_m)_{2,2}\end{bmatrix}\begin{Bmatrix}W_m\\U_m\end{Bmatrix} \tag{13}$$

where

$$\begin{aligned}\Delta_m(\mathbf{K}_m)_{1,1} &= \frac{\Omega^2}{2}(i\lambda_{sm})\\ \Delta_m(\mathbf{K}_m)_{1,2} &= \xi_m\left[(i\lambda_{dm})(i\lambda_{sm})-\xi_m^2+\frac{\Omega^2}{2}\right]\\ \Delta_m(\mathbf{K}_m)_{2,2} &= \frac{\Omega^2}{2}(i\lambda_{dm})\\ (\mathbf{K}_m)_{2,1} &= (\mathbf{K}_m)_{1,2}\end{aligned} \tag{14}$$

in which

$$\Delta_m=\xi_m^2-(i\lambda_{dm})(i\lambda_{sm}). \tag{15}$$

Note that the real parts of $i\lambda_{sm}$ and $i\lambda_{dm}$ must be negative in (14) and (15). For $m=0$, we obtain

$$Z_0=\left(\frac{i\Omega}{2\alpha}\right)W_0. \tag{16}$$

Thus,

$$(\mathbf{K}_0)_{i,j} = \begin{cases} \dfrac{i\Omega}{2\alpha} & \text{if } i=j=1 \\ 0 & \text{otherwise} \end{cases} \tag{17}$$

For large wave numbers ($|\lambda| \gg 1$), the asymptotic form of (13) is

$$\mathbf{K}_m \approx \left(\frac{-\xi_m}{1+\alpha^2}\right) \begin{bmatrix} 1-\dfrac{\Omega^2}{2\xi_m^2} & \alpha^2 \\ \alpha^2 & 1-\dfrac{\alpha^2\Omega^2}{2\xi_m^2} \end{bmatrix} \tag{18}$$

The stiffness relation for the mixed boundary condition can, therefore, be expressed:

$$\begin{Bmatrix} \mathbf{Z} \\ \mathbf{S} \end{Bmatrix} = \mathbf{K} \begin{Bmatrix} \mathbf{W} \\ \mathbf{U} \end{Bmatrix} = \begin{bmatrix} \mathbf{K11} & \mathbf{K12} \\ \mathbf{K21} & \mathbf{K22} \end{bmatrix} \begin{Bmatrix} \mathbf{W} \\ \mathbf{U} \end{Bmatrix} \tag{19}$$

where

$$\mathbf{Z} = \begin{Bmatrix} Z_0 \\ Z_1 \\ Z_2 \\ \bullet \\ \bullet \\ \bullet \\ Z_{n_h} \end{Bmatrix}; \quad \mathbf{S} = \begin{Bmatrix} S_1 \\ S_2 \\ S_3 \\ \bullet \\ \bullet \\ \bullet \\ S_{n_h} \end{Bmatrix}$$

$$\mathbf{W} = \begin{Bmatrix} W_0 \\ W_1 \\ W_2 \\ \bullet \\ \bullet \\ \bullet \\ W_{n_h} \end{Bmatrix}; \quad \mathbf{U} = \begin{Bmatrix} U_1, \\ U_2 \\ U_3 \\ \bullet \\ \bullet \\ \bullet \\ U_{n_h} \end{Bmatrix} \tag{20}$$

where n_h is the number of the highest term in the Fourier-Bessel series. Due to the orthogonality of the Bessel functions, the components of the submatrices **KIJ** are given by

$$(\mathbf{KIJ})_{l,m} = \delta_{lm}(\mathbf{K}_m)_{\mathbf{I},\mathbf{J}} \tag{21}$$

where **I** and **J** are 1 or 2 and δ_{lm} is the Kronecker delta.

For the mixed condition, the solutions can be easily obtained since dilatational and shear waves are decoupled; for stress end conditions, 2×2 stiffness matrix $\mathbf{K}_m$ can be used to compute the corresponding displacements, and for displacement end conditions, the inverse of $\mathbf{K}_m$ can be utilized.

4 Traction-Free Boundary Condition on the Cylindrical Surface

For a cylinder with the traction-free cylindrical surface, the dilational and shear waves are coupled. Due to the coupling, it is much more difficult to get a solution for this case. We repeat the well-known facts concerning axisymmetric wave propagation.

The traction-free condition on the cylindrical surface $r=1$ is expressed

$$\sigma_{rr}|_{r=1} = 0; \quad \sigma_{rz}|_{r=1} = 0 \tag{22}$$

and the corresponding frequency equations are given by

$$kJ_0(k) - 2J_1(k) = 0 \tag{23}$$

$$(\Omega^2 - 2\lambda^2)^2 J_0(h)J_1(k) + 4\lambda^2 hkJ_0(k)J_1(h) - 2\Omega^2 hJ_1(h)J_1(k) = 0. \tag{24}$$

Equation (23) is the frequency equation for torsional waves and (24) is the frequency equation for longitudinal (axisymmetric) waves or the Pochhammer-Chree frequency equation. Note that the solution of (24) indicates that for the traction-free boundary condition, dilatational, and shear waves are coupled for a given excitation frequency.

The cutoff frequencies for wave propagation are the roots of

$$J_1(\Omega)[\Omega J_0(\alpha\Omega) - 2\alpha J_1(\alpha\Omega)] = 0 \tag{25}$$

which is obtained from (24) be letting λ approach zero while Ω remains finite. Similarly, if Ω is allowed to approach zero while λ remains finite, the equation for zero-frequency intercepts is obtained:

$$\lambda^2(1-\alpha^2)[J_0^2(i\lambda) + J_1^2(i\lambda)] + J_1^2(i\lambda) = 0. \tag{26}$$

For $|\lambda| \gg 1$, the roots of (26) can be approximated by the asymptotic result

$$\lambda \approx \pm\frac{1}{2}\ln(4m\pi) \pm im\pi \tag{27}$$

where m is an integer.

With the knowledge of cutoff frequencies and zero-frequency intercepts, complete dispersion curves for a given Poisson's ratio ν can be obtained (see Zemanek (1962, 1972) for details). For example, the wave numbers for a given frequency Ω can be determined by assuming the zero-frequency intercepts as initial guesses and solving (24) numerically.

With wave numbers for a given frequency Ω, we can write

$$\Psi(r,z,t) = \sum_{p=1}^{\infty} E^p \Phi^p(r) e^{i(\lambda^p z - \Omega t)} \tag{28}$$

where

$$[\Psi, \Phi^p(r)] \in \{[u_r, \tilde{u}_r^p(r)], [u_z, \tilde{u}_z^p(r)], [\sigma_{rz}, \tilde{\sigma}_{rz}^p(r)], [\sigma_{zz}, \tilde{\sigma}_{zz}^p(r)], [\sigma_{rr}, \tilde{\sigma}_{rr}^p(r)], [\sigma_{\theta\theta}, \tilde{\sigma}_{\theta\theta}^p(r)]\} \tag{29}$$

and E^p is the pth expansion coefficient to be determined by application of the condition at the ends of the cylinder. For example, $\tilde{u}_r^p(r)$ can be obtained from (2*a*) by replacing λ, h, k by λ^p, h^p, k^p and A, B by A^p, B^p, where one can choose

$$A^p = -\frac{k^p[\Omega^2 - 2(\lambda^p)^2]J_1(k^p)}{2(i\lambda^p)} \tag{30a}$$

$$B^p = h^p J_1(h^p). \tag{30b}$$

Note that the pth wave number λ^p is the solution of (24) and that A^p and B^p are chosen to satisfy (22). The radial displacement at $z=0$ can be written from (10*a*), (28), and (29)

$$U_r(r) = \sum_{p=1}^{\infty} E^p \tilde{u}_r^p(r). \tag{31}$$

Similarly, the expressions for $U_z(r)$, $S_r(r)$ and $S_z(r)$ can be obtained. For waves propagating along the $+z$ axis, we should include real wave numbers with positive group velocities, and purely imaginary or complex wave numbers whose imaginary parts are positive. Purely imaginary and complex wave numbers correspond to end effects, which are evanescent along the $+z$ axis.

Unlike in the mixed case, there exists no orthogonality condition for the eigenfunctions, $\tilde{u}_r^p(r)$, $\tilde{u}_z^p(r)$, $\tilde{\sigma}_{rz}^p(r)$, and $\tilde{\sigma}_{zz}^p(r)$ in the traction-free case. However, the bi-orthogonality relation derived by Frazer (1975) and Gregory (1983) exists such that

$$\int_0^1 [\bar{\sigma}^p_{zz}(r)\tilde{u}^q_z(r) - \tilde{u}^p_r(r)\bar{\sigma}^q_{rz}(r)]rdr = 0 \tag{32}$$

$$\text{for } p \neq q.$$

For $p=q$, the integration in the above expression can be carried out in a closed form by making use of (see, e.g, Tranter, 1968)

$$(a^2-b^2)\int zJ_\nu(az)J_\nu(bz)dz = z[aJ_\nu(bz)J_{\nu+1}(az) - bJ_\nu(az)J_{\nu+1}(bz)]. \tag{33}$$

From (32) we can see that this bi-orthogonality property can be directly utilized only when (σ_{zz}, u_r) or (σ_{rz}, u_z) is prescribed at $z=0$, but not when $(\sigma_{zz}, \sigma_{rz})$ or (u_r, u_z) is specified.

5 Solution Procedure: Mixed End Conditions

When (σ_{zz}, u_r) or (σ_{rz}, u_z) is prescribed at $z=0$, stress and displacement quantities everywhere in the cylinder can be obtained by using (32) directly. For example, if (σ_{zz}, u_r) is prescribed at $z=0$ for a given Ω (a time-harmonic end condition), we can compute the expansion coefficients

$$E^p = \frac{\int_0^1 [S_z(r)\tilde{u}^p_z(r) - U_r(r)\bar{\sigma}^p_{rz}(r)]rdr}{\int_0^1 \bar{\sigma}^p_{zz}(r)\tilde{u}^p_r(r) - \tilde{u}^p_r(r)\bar{\sigma}^p_{rz}(r)]rdr} \equiv \frac{N^p}{D^p} \tag{34}$$

and thus we can compute the stress and displacements by means of (28) and (29).

Our solution procedure employs the solutions of the mixed case as an orthogonal expansion set for all harmonics of stress and displacement. The following matrices **A** and **B** are thus constructed, which are defined by

$$\begin{Bmatrix} \mathbf{W} \\ \mathbf{S} \end{Bmatrix} = \mathbf{A} \begin{Bmatrix} \mathbf{Z} \\ \mathbf{U} \end{Bmatrix} = \begin{bmatrix} \mathbf{A11} & \mathbf{A12} \\ \mathbf{A21} & \mathbf{A22} \end{bmatrix} \begin{Bmatrix} \mathbf{Z} \\ \mathbf{U} \end{Bmatrix} \tag{35}$$

$$\begin{Bmatrix} \mathbf{Z} \\ \mathbf{U} \end{Bmatrix} = \mathbf{B} \begin{Bmatrix} \mathbf{W} \\ \mathbf{S} \end{Bmatrix} = \begin{bmatrix} \mathbf{B11} & \mathbf{B12} \\ \mathbf{B21} & \mathbf{B22} \end{bmatrix} \begin{Bmatrix} \mathbf{W} \\ \mathbf{S} \end{Bmatrix} \tag{36}$$

where **Z**, **S**, **W** and **U** are defined by (20). Note that **A11**, and **B11** are of order $(n_h+1)\times(n_h+1)$, **A12**, and **B12**, of order $(n_h+1)\times n_h$, **A21**, **B21**, of order $n_h \times (n_h+1)$, and **A22**, and **B22**, of order $n_h \times n_h$.

The matrices **A** and **B** are constructed as follows. First, we expand the eigenfunctions of the traction-free case in terms of the eigenfunctions of the mixed case.

$$\begin{aligned} \tilde{u}^p_r(r) &= \sum_{m=1}^{n_h} U^p_m J_1(\xi_m r);\ \tilde{u}^p_z(r) = \sum_{m=0}^{n_h} W^p_m J_0(\xi_m r) \\ \bar{\sigma}^p_{rz}(r) &= \sum_{m=1}^{n_h} S^p_m J_1(\xi_m r);\ \bar{\sigma}^p_{zz}(r) = \sum_{m=0}^{n_h} Z^p_m J_0(\xi_m r). \end{aligned} \tag{37}$$

The coefficients U^p_m, W^p_m, S^p_m, and Z^p_m may be obtained using (12) and it can be observed that no numerical integration is required in (37).

Now equation (34) will be employed to compute **A** and **B**. In order to compute **A11** and **A21**, we consider the following *time-harmonic end condition at $z=0$ when*

$$\begin{cases} S_z(r) = J_0(\xi_m r) \\ U_r(r) = 0 \end{cases} \tag{38}$$

for a given frequency Ω. First, we compute E^p_m, which is the pth expansion coefficient in (34) for the end condition (38), and given by

$$E^p_m = \frac{1}{D^p}\left[\frac{J_0^2(\xi_m)}{2}\right] W^p_m. \tag{39}$$

Recall that no numerical integration is required in order to compute the denominator of (39). The corresponding axial displacement $[U_z(r)]_m$ at $z=0$ can therefore be calculated:

$$\begin{aligned} [U_z(r)]_m &= \sum_{p=1}^{n_e} E^p_m u^p_z(r) \\ &= \sum_{p=1}^{n_e} E^p_m \sum_{l=0}^{n_h} W^p_l J_0(\xi_l r) \\ &= \sum_{l=0}^{n_h} J_0(\xi_l)\left[\sum_{p=1}^{n_e} E^p_m W^p_l\right]. \end{aligned} \tag{40}$$

Similarly, the shear stress can be determined

$$[S_r(r)]_m = \sum_{l=1}^{n_h} J_1(\xi_l)\left[\sum_{p=1}^{n_e} E^p_m S^p_l\right]. \tag{41}$$

The components of **A11** and **A21** are thus given as

$$(\mathbf{A11})_{l,m} = \sum_{p=1}^{n_e} E^p_m W^p_l \quad \text{for } l=0,1,2,\ldots,n_h \tag{42a}$$

$$(\mathbf{A21})_{l,m} = \sum_{p=1}^{n_e} E^p_m S^p_l \quad \text{for } l=1,2,\ldots,n_h \tag{42b}$$

for $m=0, 1, 2, \ldots, n_h$.

By considering an end condition at $z=0$,

$$\begin{cases} U_z(r) = 0 \\ S_r(r) = J_1(\xi_m r), \end{cases} \tag{43}$$

the components of **B12** and **B22** can be obtained

$$(\mathbf{B12})_{l,m} = \sum_{p=1}^{n_e} E^p_m Z^p_l \quad \text{for } l=0,1,2,\ldots,n_h \tag{44a}$$

$$(\mathbf{B22})_{l,m} = \sum_{p=1}^{n_e} E^p_m U^p_l \quad \text{for } l=1,2,\ldots,n_h \tag{44a}$$

for $m=1, 2, \ldots, n_h$ where

$$E^p_m = -\frac{1}{D^p}\left[\frac{J_0^2(\xi_m)}{2}\right] U^p_m. \tag{45}$$

The matrices (**A12**, **A22**), and (**B11**, **B21**) can be computed similarly by considering $[S_z(r)=0,\ U_r(r)=J_1(\xi_m r)]$, and $[U_z(r)=J_0(\xi_m r),\ S_r(r)=0]$, respectively.

Though the solution procedure based on the expansion of stress and displacement for the mixed end conditions is presented, one may directly use equation (34); however, the expansion discussed in the present section will be utilized in the subsequent analysis for general end conditions.

6 Solution Procedure: Traction and Displacement End Conditions

For problems for which either $(\sigma_{zz}, \sigma_{rz})$ or (u_r, u_z) is prescribed at $z=0$, the bi-orthogonality property (32) is not *directly applicable. The solution procedure presented here is* applicable to problems when either stresses alone or displacements alone are specified at the end, but unlike conventional numerical approaches, the procedure is useful for end conditions with both slow and rapid variation in the radial direction.

Our procedure is based on the construction of the stiffness matrix **S** such that

$$\begin{Bmatrix} \mathbf{Z} \\ \mathbf{S} \end{Bmatrix} = \mathbf{S} \begin{Bmatrix} \mathbf{W} \\ \mathbf{U} \end{Bmatrix} = \begin{bmatrix} \mathbf{S11} & \mathbf{S12} \\ \mathbf{S21} & \mathbf{S22} \end{bmatrix} \begin{Bmatrix} \mathbf{W} \\ \mathbf{U} \end{Bmatrix} \tag{46}$$

From (35), (36), and (46), the submatrices of S can be determined:

$$\mathbf{S11} = \mathbf{A11}^{-1} \qquad \mathbf{S12} = \mathbf{B12} \cdot \mathbf{B22}^{-1},$$
$$\mathbf{S21} = \mathbf{A21} \cdot \mathbf{A11}^{-1}, \qquad \mathbf{S22} = \mathbf{B22}^{-1}, \tag{47}$$

Following the procedure used to determine **S**, we may also construct the flexibility matrix **F** such that

$$\begin{Bmatrix} \mathbf{W} \\ \mathbf{U} \end{Bmatrix} = \mathbf{F} \begin{Bmatrix} \mathbf{Z} \\ \mathbf{S} \end{Bmatrix} = \begin{bmatrix} \mathbf{F11} & \mathbf{F12} \\ \mathbf{F21} & \mathbf{F22} \end{bmatrix} \begin{Bmatrix} \mathbf{Z} \\ \mathbf{S} \end{Bmatrix} \tag{48}$$

where

$$\mathbf{F11} = \mathbf{B11}^{-1} \qquad \mathbf{F12} = \mathbf{A12} \cdot \mathbf{A22}^{-1},$$
$$\mathbf{F21} = \mathbf{B21} \cdot \mathbf{B11}^{-1}, \qquad \mathbf{A22} = \mathbf{A22}^{-1}, \tag{49}$$

By using the end stiffness and flexibility matrices, we can also compute the stresses and displacements at z other than $z=0$. To this end, the expansion coefficient in (28) for the traction-free case should be determined first. For example, if nonzero $U_z(r)$ zero $U_r(r)$ is given at the end, we first compute $S_z(r)$, and $S_r(r)$, which will be given as (11c) and (11d). Then any combinations of the stresses and displacements are known at the end so that the expression (34), the statement of the bi-orthogonality condition, can be employed:

$$E^p = \frac{1}{D^p} \int_0^1 [S_z(r)\tilde{u}_z^p(r) - U_r(r)\tilde{\sigma}_{rz}^p(r)] r dr = \frac{1}{D^p} \sum_{m=0}^{n_h} \left[\frac{J_0^2(\xi_m)}{2} \right] Z_m W_m^p. \tag{50}$$

It can be also written more explicitly as

$$E^p = \frac{1}{D^p} \sum_{j=0}^{n_h} \left[\sum_{m=0}^{n_h} \frac{J_0^2(\xi_m)}{2} W_m^p (\mathbf{S11})_{m,j} \right] W_j. \tag{51}$$

The combination $[U_z(r),\ S_r(r)]$ may be used for E^p in (50), but there is no advantage. For general displacement end conditions, the expansion coefficient E^p becomes

$$E^p = \frac{1}{D^p} \sum_{j=0}^{n_h} \left[\sum_{m=0}^{n_h} \frac{J_0^2(\xi_m)}{2} W_m^p (\mathbf{S11})_{m,j} \right] W_j - \frac{1}{D^p} \sum_{j=1}^{n_h} \left[\sum_{m=1}^{n_h} \frac{J_1^2(\xi_m)}{2} U_m^p (\mathbf{S22})_{m,j} \right] U_j. \tag{52}$$

Note that only **S11** and **S22** are used in (52) so that accurate determination of **S11** and **S22** is important for E^p. Similar analysis can be carried out for stress end conditions.

For high harmonics of stresses and displacements, characterized by wavelengths in the radial direction which are much smaller than the cylindrical radius, the boundary conditions at the cylindrical surface $r=1$ will have no signficant effect on the solution, except near the cylindrical surface. This implies that as the wavelength of the end condition becomes shorter, the solution of the traction-free case must approach asymptotically that of the mixed case; this asymptotic behavior is studied numerically in the following sections. For the lower harmonics, the solutions of the traction-free case are retained and their bi-orthogonality property is utilized.

By means of numerical studies, it will be shown in the next section that for higher harmonics, the components of the stiffness matrix **S** for the traction-free case approaches asymptotically the components of **K** for the mixed case. Due to this asymptotic behavior, the computation of **S** for n_h larger than a certain number of n_u is not needed; instead the solutions of the traction-free case are replaced by the solutions of the mixed case.

7 Asymptotic Behavior of the Stiffness Matrix

The stiffness matrix under consideration relates the radial harmonics of stress and displacement, as opposed to nodal values. The advantage of working with these quantities lies in the asymptotic behavior of **K** and **S** for high harmonics. In addition to the comparison of **K** and **S**, the stiffness matrix for a strip with a lubricated-rigid condition on its lateral faces will also be considered. The stiffness matrix **M** for the strip is given by (see the appendix)

$$\begin{aligned}
(\mathbf{M11})_{l,m} &= -\delta_{lm}\Omega^2 i\zeta_{sm}/2\Delta_m \\
(\mathbf{M12})_{l,m} &= \delta_{lm}\beta_m\left(\beta_m^2 - \frac{\Omega^2}{2} + \zeta_{dm}\zeta_{sm}\right)/\Delta_m \\
(\mathbf{M21})_{l,m} &= (\mathbf{M12})_{m,l} \\
(\mathbf{M22})_{l,m} &= -\delta_{lm}\Omega^2 i\zeta_{dm}/2\Delta_m
\end{aligned} \tag{53}$$

where

$$\Delta_m = -\zeta_{dm}\zeta_{sm} - \beta_m^2; \quad \beta_m = m\pi (m \text{ is an integer})$$
$$\zeta_{dm} = (\alpha^2\Omega^2 - \beta_m^2)^{1/2}; \quad \zeta_{sm} = (\Omega^2 - \beta_m^2)^{1/2}. \tag{54}$$

The stiffness matrices were evaluated for a Poisson's ration of 0.3317 and Ω equal to 2.0. The frequency under consideration is below the first cutoff frequency (3.8317) (also, below the end resonance, see Zemanek, 1972). In the region below the first cutoff frequency, we have one real wave number and an infinite number of complex wave numbers. A real wave number with its group velocity positive and complex wave numbers with their imaginary parts positive should be included since we are looking for waves traveling along the $+z$ axis.

To study the asymptotic behaviors of the stiffness matrices, we choose $n_h = 20$ ($n_e = 101$)[1]. For $n_e = 101$, we have one real number and 50 pairs of complex wave numbers. Note that if a complex number λ_k is included, $-\lambda_k^*$ is also included, where * represents the complex conjugate (see Zemanek, 1972).

For the present choice of ν and Ω all elements of **K** are real-valued, except $(\mathbf{K11})_{0,0}$, which corresponds to a mode which propagates along the $+z$ axis. Recall that the submatrices of **K** are diagonal matrices and that those of **S** are not.

The asymptotic behavior of **S** can be studied by considering

[1]The number n_e of wave numbers here should be sufficiently large so that the end conditions such as (38), and (43) for $m=0$ ($m=1$) to $m=20$ can be well represented by n_e eigenfunctions of the traction-free case. With $n_e \approx 5n_h$, in general, good results were obtained.

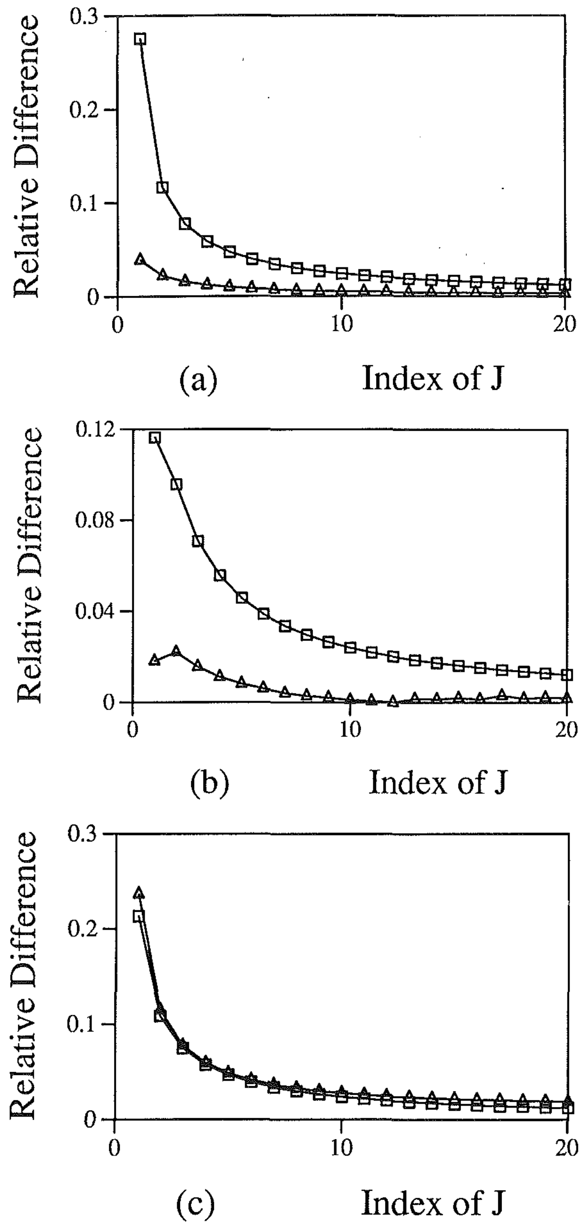

Fig. 1 Comparison of the diagonal elements of the end stiffness matrix. The magnitudes of the diagonal elements of S, the stiffness matrix for the cylinder with traction-free cylindrical conditions, and M, the stiffness matrix for a semi-infinite plate strip with mixed face conditions, are compared with those of K, the stiffness matrix for the cylinder with mixed cylindrical conditions. ($\Omega = 2$) The relative difference is represented by $|C_{j,j} - K_{j,j}|/|K_{j,j}|$, where C = S for —△— and C = M for —□— in (a) submatrices 11, (b) submatrices 12, and (c) submatrices 22. $S_{j,j}$ asymptotically approaches $K_{j,j}$.

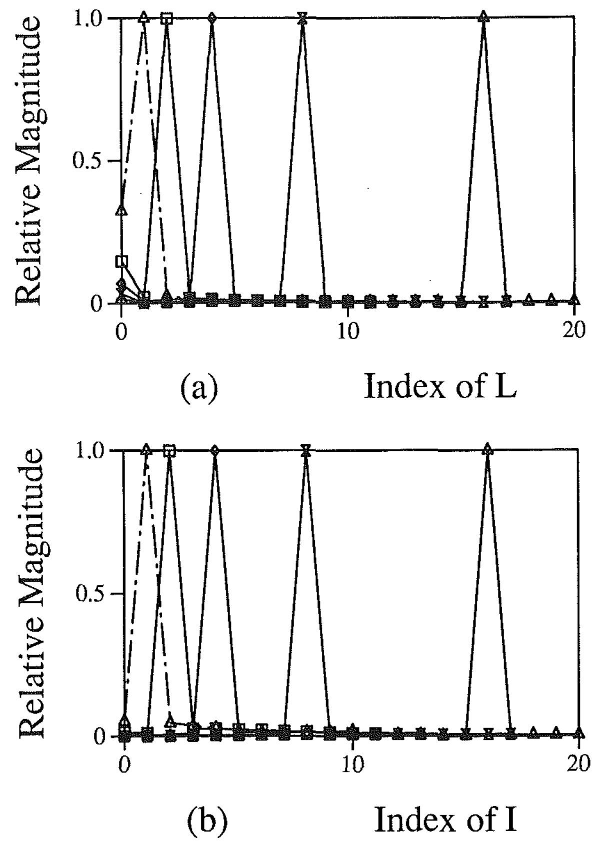

Fig. 2 Diagonal dominance in S11, a submatrix of the stiffness matrix of the cylinder with traction-free cylindrical conditions. ($\Omega = 2$) (a) $|S11_{j,l}|/|S11_{j,j}|$: Row-wise dominance of the diagonal elements over off-diagonal elements in each row; (b) $|S11_{i,j}/S11_{j,j}|$: Column-wise dominance of the diagonal elements over off-diagonal elements in each column. —·△—·—: $j=1$, —□—: $j=2$, —◇—: $j=4$, —⧖—: $j=8$, —△—: $j=16$. Strong diagonal dominance in S11 is shown.

the magnitudes of the diagonal elements, the real-valuedness, and the diagonal dominance of **S**. First, the magnitudes of the diagonal elements of **S11**, **S12**, and **S22** are considered. These elements are compared with the counterparts for the cylinder with a mixed condition on its cylindrical surface. Figure 1 shows that the magnitudes of the diagonal elements of the stiffness matrix of the cylinder with a traction-free cylindrical surface asymptotically approach those of the mixed case (**K11**, **K12**, and **K22**).

The diagonal elements of the submatrices of **K** can also be compared with those of **M**, the stiffness matrix for a strip with a lubricated-rigid condition on its lateral faces. Figure 1 shows the relative difference in magnitude between $(\mathbf{M11})_{j,j}$ and $(\mathbf{K11})_{j,j}$. Though based on different eigenfunctions, the stiffness matrix **M** asymptotically approaches the matrix **K**. Note that **S** approaches **K** faster than **M** does. The stiffness matrix for the strip, with a different geometry but similar boundary condition is, therefore, a poorer approximation to **S** than the stiffness matrix **K**, based on the same geometry but different boundary conditions.

The relative magnitude of the imaginary parts of $(\mathbf{S11})_{j,j}$ $(\mathbf{S12})_{j,j}$ and $(\mathbf{S22})_{j,j}$ is studied, too. It can also be shown that the real parts of the diagonal elements are asymptotically predominant over the imaginary parts. Figures 2 and 3 show the diagonal dominance of **S11** and **S22**, respectively. From these figures, it is seen that as j becomes larger, $(\mathbf{S11})_{j,j}$ becomes larger relative to its off-diagonal elements. Of interest is that even for a small j, the diagonal element $(\mathbf{S22})_{j,j}$ is much bigger than the off-diagonal elements in the same row (see Fig. 3(*a*)) but not in the same column (see Fig. 3(*b*)). As shown in Figs. 2 and 3, **S22** is diagonally less dominant than **S11**. This is because the expansion set for $U_r(r)$ imposes $U_r|_{r=1} \equiv 0$ whereas $\tilde{u}_r^p(r)$ is not zero at $r=1$.

No attempt has been made to prove analytically the asymptotic behavior of the stiffness matrix. However, the numerical results show all the asymptotic behaviors such as the diagonal dominance, real-valuedness, and vanishing relative differences of $S_{j,j}$ with respect to $K_{j,j}$. Thus, the solutions of the cylinder with the mixed lateral condition (6) are good approximations for the solutions of the cylinder with the traction-free lateral condition for rapidly varying end conditions. It should be again noted that this is valid only for solutions at the end of the cylinder; E^p must be computed (from (52)).

From the foregoing analysis, one can put the stiffness submatrix **S11** in the following form:

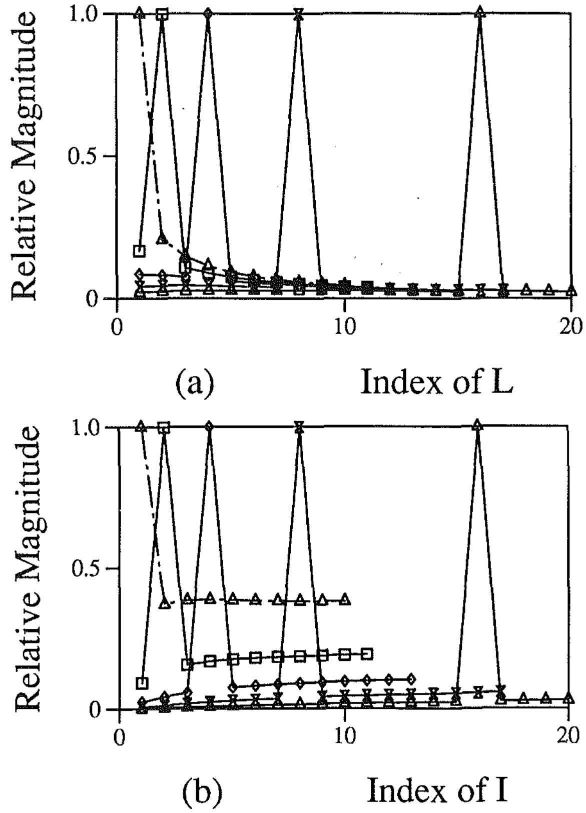

Fig. 3 Diagonal dominance in **S22**, a submatrix of the stiffness matrix of the cylinder with traction-free cylindrical conditions. ($\Omega=2$) (*a*) $|\mathbf{S22}_{j,l}/\mathbf{S22}_{j,j}|$: Row-wise dominance of the diagonal elements over off-diagonal elements in each row; (*b*) $|\mathbf{S22}_{i,j}/\mathbf{S22}_{j,j}|$: Column-wise dominance of the diagonal elements over off-diagonal elements in each column. —• Δ—•—: $j=1$, — □ —: $j=2$, — ◇ —: $j=4$, — ⧖ —: $j=8$, —Δ—: $j=16$. Stronger row-wise diagonal dominance is observed than column-wise diagonal dominance in **S22**.

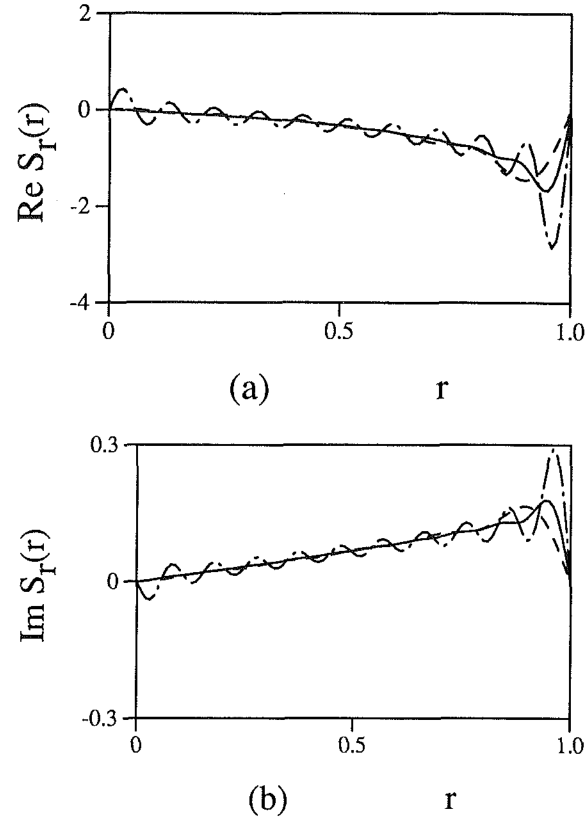

Fig. 4 Convergence of stress distributions at $z=0$ for the smooth prescribed displacements $U_r(r)=r$, $U_z(r)=0$ at $z=0$. ($\Omega=2$) the results are (*a*) real part and (*b*) imaginary part of the shear stress $S_r(r)$ obtained by 10 terms with Cesaro sum (dashed lines), 20 terms without Cesaro (dot-dashed lines), and 20 terms with Cesaro sums (solid lines). Solutions by the present approach appear to converge, and the Cesaro sum effectively suppresses the local oscillatory behaviors.

$$\mathbf{S11} = \begin{bmatrix} \mathbf{S11U} & \mathbf{S11R} \\ \mathbf{S11L} & \mathbf{S11D} \end{bmatrix} \tag{55}$$

$$\mathbf{S11D} \approx \mathbf{K11D}$$

where the magnitudes of the elements of **S11L** and **S11R** are much smaller than those of **S11D** and **S11U**. The replacement of **S11D** by **K11D** can be justified by the observations that the diagonal elements of **S11** are dominant and their magnitudes approach those of **K11**. Similarly, **S22** has the same form as **S11**, but the size n_u of **S22U** must be larger than that of **S11U**. (See Figs. 2 and 3). Similar structures can apply to other submatrices of **S**, **F**, **A**, and **B**.

It appears that the fact that the submatrices of **A** and **B** are of the structure (55) is not of great advantage to the construction of **S**; we may have to invert **A11** and **B22** in (47) as if they were full matrices. However, the fact that **PD** can be replaced by a diagonal submatrix can be incorporated, where **P** stands for any of the stiffness/flexibility matrices. Consider the inversion of the matrix **P** such that

$$\mathbf{P} = \begin{bmatrix} \mathbf{PU} & \mathbf{PR} \\ \mathbf{PL} & \mathbf{PD} \end{bmatrix} \tag{56}$$

where **PD** is a diagonal submatrix and **PU** is a square submatrix. The inverse of **P**, which will be denoted by **Q**, will be written

$$\mathbf{Q} = \mathbf{P}^{-1} = \begin{bmatrix} \mathbf{QU} & \mathbf{QR} \\ \mathbf{QL} & \mathbf{QD} \end{bmatrix} \tag{57}$$

where

$$\begin{aligned} \mathbf{QU} &= \mathbf{PU}^{-1} - \mathbf{PR}\cdot\mathbf{PD}^{-1}\cdot\mathbf{PL} \\ \mathbf{QR} &= -\mathbf{QU}\cdot\mathbf{PR}\cdot\mathbf{PD}^{-1} \\ \mathbf{QL} &= -\mathbf{PD}^{-1}\cdot\mathbf{PL}\cdot\mathbf{QU} \\ \mathbf{QD} &= \mathbf{PD}^{-1}\cdot(\mathbf{I} + \mathbf{PR}\cdot\mathbf{QU}\cdot\mathbf{PL}\cdot\mathbf{PD}^{-1}). \end{aligned} \tag{58}$$

Note that for $\mathbf{P}^{-1}$, the inversion of a full matrix is only limited to **PU**; the inversion of **PD** is trivial. Since the stiffness matrices **S** and **F** can be put in the form of (57) where **PU** is a small matrix, and **PD** is a large matrix, the inversion of such a matrix can be performed extremely efficiently.

Note that $\mathbf{S12} \neq \mathbf{S21}^T$ in general, because the expansion set for **S** does not consist of the eigenfunctions of the traction-free case. However, **S12** asymptotically approaches $\mathbf{S21}^T$.

8 Numerical Examples

Case 1. Slowly Varying End Condition: $[U_r(r)=r, U_z(r)=0]$.

First, we consider a smooth displacement distribution prescribed at $z=0$ and determine stress distributions at the end. The computation of **U**, the coefficients of the Fourier-Bessel series for $U_r(r)$, can be performed efficiently by the modified Clenshaw-Curtis method by Piessens and Branders (1983, 1984). Then the stiffness submatrices **SIJ** in (46) is constructed. **S** and **Z** can be computed by applying (46), from which we determine the stress distribution at $z=0$ by summing up the series in (11*c*), (11*d*). With $n_h = n_u$ equal to 10 ($n_e=51$) and 20 ($n_e=101$), the results for stresses at $z=0$ are shown in

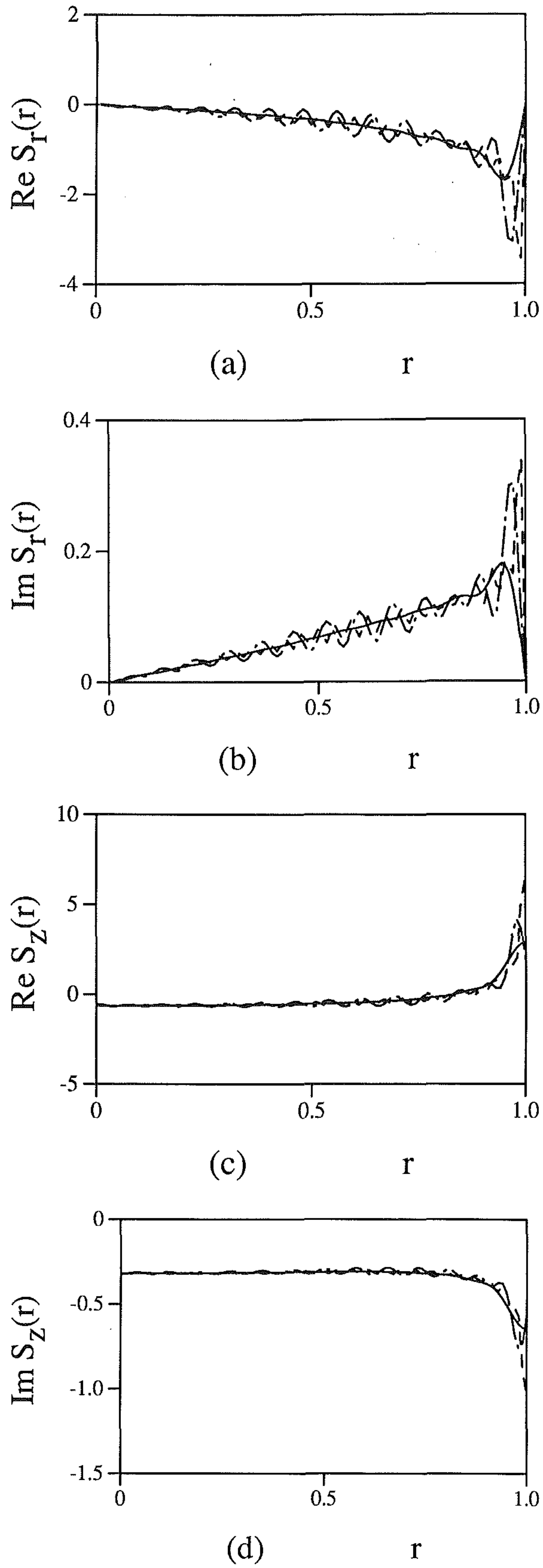

Fig. 5 Comparison of the present method to collocation for the smooth prescribed displacements $U_r(r)=r$, $U_z(r)=0$ at $z=0$ ($\Omega=2$). Real part (a), and imginary part (b) of the shear stress $S_r(r)$, and real part (c), and imaginary part (d) of the normal stress $S_z(r)$. Results shown for 20 terms with Cesaro sum (solid), and collocation with 51 unkowns (dot-dashed) and 101 unknowns (dashed). Good agreement between the results by the present approach and collocation is observed.

Figs. 4 and 5. (The structure (55) needs not be used for this smooth end condition.)

We present solutions which are computed by means of Cesaro sums (see, e.g., Edwards, 1979). The Cesao sums in a weighted sum of the terms in a Fourier (or Fourier-Bessel) series, and is computed as the arithmetic mean of partial sums. This technique improves the convergence of a finite Fourier series which would otherwise converge slowly. Because the low-order terms are weighted more heavily, the Cesaro sum works most effectively when applied to the slowly convergent "tail" of the series, for which the coefficients decrease monotonically. Figure 4 shows the distribution of the shear stress at $z=0$ as a function of r with $n_h=20$. The present solutions appear to converge expect at $r=1$, where the shear stress is expected to be singular and the series grows accordingly. It is also seen in Fig. 4 that the Cesaro sum effectively suppresses the local oscillatory behaviors.

In Fig. 5, the present solutions ($n_h=20$) with the Cesaro sums are compared with the results obtained by the collocation method with $n_e=51$ and $n_e=101$. (Zemanek (1972) used the collocation method to determine the end resonance.) The comparison shows good agreement between the present results ($n_h=20$) and the results by collocation with $n_e=101$ except near $r=1$. Table 1 shows the CPU times in obtaining the stresses at $z=0$. It may be seen that the collocation method is not very efficient even for slowly varying end condition.

Case 2. Rapidly Varying End Condition: $[U_r(r)=0, U_z(r)=\cos(25\pi r)]$.

As a second example, a prescribed displacement distribution with rapid spatial variation is treated. The present solutions with $n_h=40$ ($n_e=201$) are obtained with and without employing the structure (55). They are compared with the results obtained by the collocation method with $n_e=301$ and $n_e=501$. When the form (55) is employed in the present approach, n_u is chosen to be 20; the relative differences of $\mathbf{S11}_{j,j}$ and $\mathbf{S21}_{j,j}$ with respect to $\mathbf{K11}_{j,j}$ and $\mathbf{K21}_{j,j}$ for $j>20$ are insignificant.

The results for the stresses at $z=0$ are shown in Fig. 6, and the axial stresses at z other than $z=0$, namely at $z=0.5$ and $z=1.0$, are shown in Fig. 7.

Before examining the detailed stress distributions, we show in Table 2 the first few expansion coefficients E^p determined by the two methods. Note that the first few terms are important for far-field solutions. In Table 3 we also present the CPU times required in obtaining all the results shown in Figs. 6 and 7.

Table 2 shows that the expansion coefficients estimated by the present approach agree very well with those by the collocation method with 501 terms. The results for E^p by the present solutions with the structure (55) incorporated are almost as good as those obtained by collocation with $n_e=301$. One can see that the collocation method requires very many unknowns for accurate solutions and converges very slowly. A comparison of the CPU times in Table 3 shows that the collocation method requires a great deal of computation. The present solution approach is very efficient especially for rapidly varying end conditions.

Examining the detailed stress distributions in Figs. 6 and 7, we see good agreement between the two methods. Figure 7 shows how rapidly the first mode is reached as z becomes larger. The large real parts of the stresses at $z=0$ (Figs. 6(b), (d)) imply that the rapidly varying end condition results in so-called *end effects*. The small imaginary parts of the stresses

Table 1 CPU time for Case 1 in Convex C-1

Collocation ($n_e=51$)	Collocation ($n_e=101$)	Present ($n_h=10$)	Present ($n_h=20$)
69 Sec.	239 Sec.	8 Sec.	28 Sec.

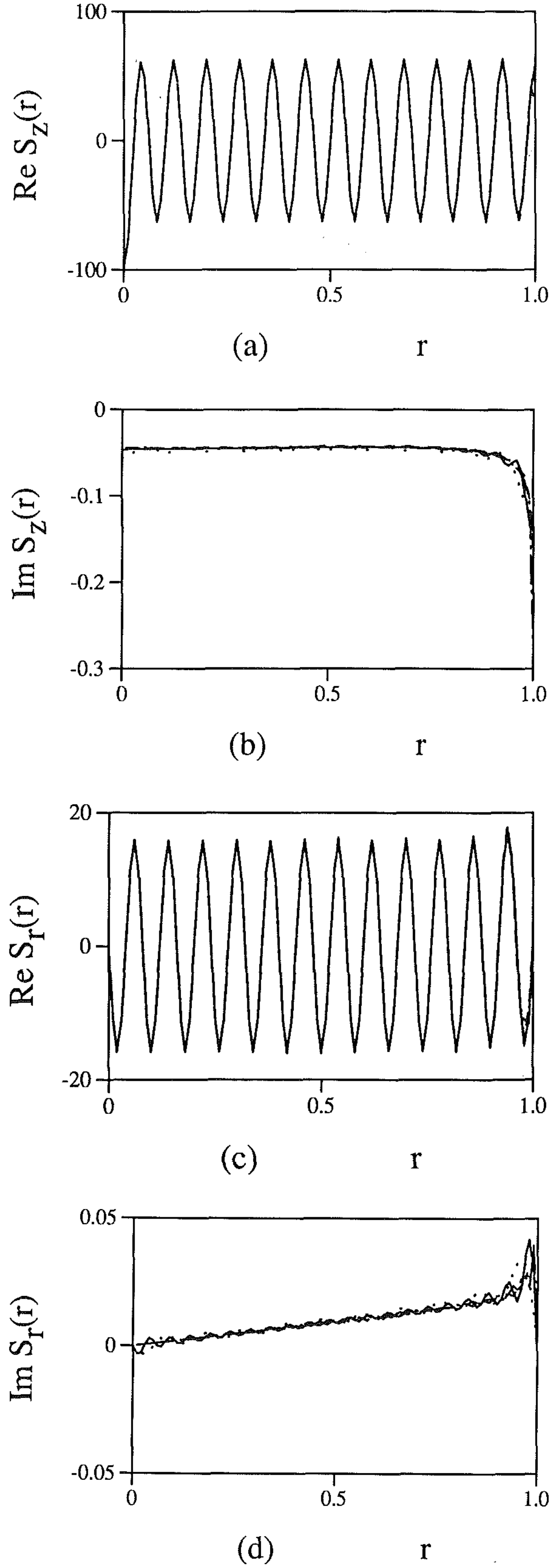

Fig. 6 End stresses due to rapidly varying prescribed displacement $U_z(r) = \cos(25\pi r)$, $U_r(r) = 0$ ($\Omega = 2$). Real part (*a*), and imaginary part (*b*) of the normal stress $S_z(r)$; and real part (*c*) and imaginary part (*d*) of the shear stress $S_r(r)$. Results shown for 40 terms with (dotted) and without (solid) asymptotic forms, and collocation with 301 unknowns (dashed) and 501 unknowns (dot-dashed). With much smaller numbers of the unknowns, the present solutions agree very well with those by collocation.

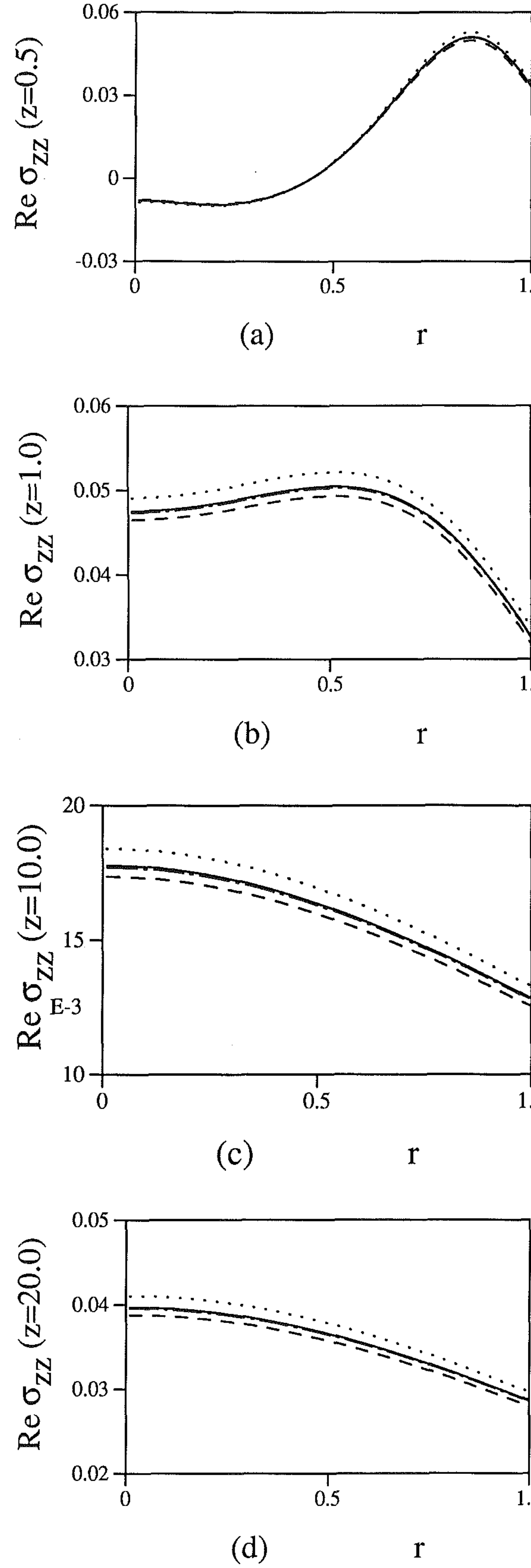

Fig. 7 Real part of normal stress as a function of r subject to the end condition $U_z(r) = \cos(25\pi r)$, $U_r(r) = 0$ at various z ($\Omega = 2$); (*a*) $z = 0.5$, (*b*) $z = 1.0$, (*c*) $z = 10.0$, and (*d*) $z = 20.0$. Results shown for 40 terms with (dotted) and without (solid) asymptotic forms, and collocation with 301 unknowns (dashed) and 501 unknowns (dot-dashed). Both for near- and far-field solutions, the present results are in good agreement with those by collocation.

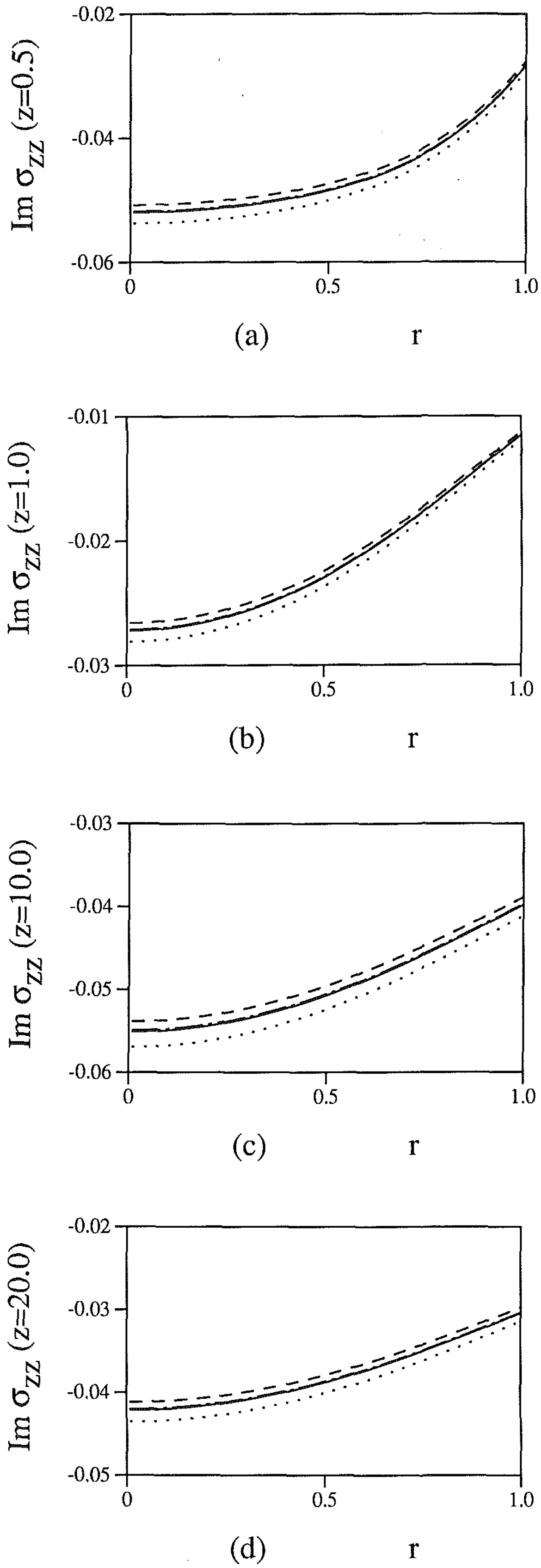

Fig. 8 Imaginary part of normal stress as a function of r subject to the end condition $U_z(r) = \cos(25\pi r)$, $U_r(r) = 0$ at various z ($\Omega = 2$); (a) $z = 0.5$, (b) $z = 1.0$, (c) $z = 10.0$, and (d) $z = 20.0$. Results shown for 40 terms with (dotted) and without (solid) asymptotic forms, and collocation with 301 unknowns (dashed) and 501 unkowns (dot-dashed); Both for near- and far-field solutions, the present results are in good agreement with those by collocation.

correspond to the power input. To see this, one can consider the time-averaged power input at $z = 0$, which can be expressed by

$$\begin{aligned} \langle \dot{W} \rangle &= -\frac{1}{(2\pi/\Omega)}\int_0^{\frac{2\pi}{\Omega}} dt \int_0^1 r dr \Big[\sigma_{zz}(r,0,t)\frac{\partial u_z(r,0,t)}{\partial t} \\ &\qquad + \sigma_{rz}(r,0,t)\frac{\partial u_r(r,0,t)}{\partial t}\Big] \\ &= \frac{1}{2}\int_0^1 \{\Im[S_z(r)]\Re[U_z(r)] - \Im[S_z(r)]\Im[U_z(r)]\} r dr \\ &= \frac{1}{2}\int_0^1 \{\Im[S_r(r)]\Re[U_r(r)] - \Im[S_r(r)]\Im[U_r(r)]\} r dr. \end{aligned} \tag{59}$$

The negative sign is required in the first line of (59) because the r and z components of the traction at $z = 0$ are $-\sigma_{rz}$ and $-\sigma_{rz}$, respectively.

For the end condition under consideration,

$$\langle \dot{W} \rangle = \frac{1}{2}\int_0^1 \Im[S_z(r)]\Re[U_z(r)] r dr. \tag{60}$$

From (60), one can observe that the imaginary part of the normal stress in the present case carries energy away from the end. Thus, the big real part of the shear stress in comparison with the imaginary part produces a very localized stress and displacement distribution near the end. We may also see that the average power input is positive, which confirms the solutions are meaningful.

We have also studied some stress end conditions and obtained good results in comparison with collocation. Generally, the observations made here are applicable to the stress end conditions.

9 Conclusions

End effects and wave propagation have been studied in a semi-infinite circular cylinder which is free of traction on its cylindrical surface. An efficient analysis procedure was presented, which is based on a stiffness matrix which relates the radial harmonics of stresses and displacements. In forming this stiffness matrix, solutions for the cylinder with a lubricated-rigid condition on its cylindrical surface provide an expansion set for the traction-free case. For high-order harmonics, the stiffness matrices for the traction-free and lubricated-rigid conditions are asymptotically equivalent.

Unlike other numerical methods such as finite element or boundary integral methods which typically require the solution of large systems of equations, the present method can lead to a small coupled system for lower harmonics and a weakly coupled system for higher harmonics. Due to the small number of equations in the coupled system, the present method is very efficient for end conditions wih rapid variation. The effectiveness of the present method was demonstrated by means of numerical examples. The technique of Cesaro sums proved effective in enhancing the convergence of the solutions, especially for slowly varying results, and good agreement with the conventional collocation method was observed.

Acknowledgments

This work was partially supported by Grant 2R01-NS12086 from the National Institute of Neurological and Communicative Disorders and Strokes. Additional support was provided by Delco Electronics Division, Santa Barbara. We also thank C.D. Balch and the reviewers for their comments on the earlier version of the manuscript.

Table 2 Magnitudes of the expansion coefficients for Case 2

$\lvert E^p \rvert$	Collocation ($n_e=301$)	Collocation ($n_e=501$)	Present ($n_h=40$; $n_u=40$)	Present with (55) ($n_h=40$; $n_u=20$)
$\lvert E^1 \rvert$	0.341E-1	0.348E-1	0.349E-1	0.361E-1
$\lvert E^2 \rvert$	0.680E-2	0.694E-2	0.696E-2	0.719E-2
$\lvert E^3 \rvert$	0.430E-2	0.439E-2	0.440E-2	0.454E-2
$\lvert E^4 \rvert$	0.144E-2	0.149E-2	0.147E-2	0.152E-2

Table 3 CPU time for Case 2 in Convex C-1

Collocation ($n_e=301$)	Collocation ($n_e=501$)	Present ($n_h=40$; $n_u=40$)	Present with (55) ($n_h=40$; $n_u=20$)
2599 Sec.	9122 Sec.	191 Sec.	77 Sec.

References

Achenbach, J. D., 1975, *Wave Propagation in Elastic Solids*, North-Holland Publishing Co., Amsterdam.

Achenbach, J. D., Fang, S. J., 1970, "Asymptotic Analysis of the Modes of Wave Propagation in a Solid Cylinder," *J. Acoust. Soc. Am.*, Vol. 47, pp. 1282–1289.

Auld, B. A., 1973, *Acoustical Fields and Waves in Solids*, Vol. 2, John Wiley and Sons, New York.

Chree, C., 1886, "Longitudinal Vibrations of a Circular Bar," *Quart. J. Pure and Appl. Math.*, Vol. 21, pp. 287–298.

Churchill, R. V., and Brown, J. W., 1978, *Fourier Series and Boundary Value Problems*, 3rd ed., McGraw-Hill, New York.

Edwards, R. E., 1979, *Fourier Series: A Modern Introduction*, Vol. 1, 2nd ed., Springer-Verlag, New York.

Fama, M. E. D., 1972, "Radial Eigenfunctions for the Elastic Circular Cylinder," *Quart. J. Mech. Appl. Mech.*, Vol. 15, pp. 479–495.

Folk, R., Fox, G., Shook, C. A., and Curtis, C. W., 1958, "Elastic Strain Produced by Sudden Application of Pressure to One End of Cylindrical Bar. I. Theory," *J. Acoust. Soc. Am*, Vol. 30, pp. 552–558.

Frazer, W. B., 1975, "An Orthogonality Relation for the Modes of Wave Propagation in an Elastic Circular Cylinder," *J. Sound Vibration*, Vol. 43, pp. 568–571.

Gregory, R. D., 1983, "A Note on Bi-Orthogonality Relations for Elastic Cylinders of General Cross Section," *J. Elasticity*, Vol. 13, pp. 351–355.

Green, W. A., 1960, "Dispersion Relations for Elastic Waves in Bars," *Progress in Solid Mechanics*, I.N. Sneddon and R. Hill, eds., North-Holland Publishing, Amsterdam, pp. 223–261.

Loper, E. J., and Lynch, D. D., 1983, "Projected System Performance Based on Recent HRG Test Results," *1983 IEEE/AIAA Fifth Digital Avionics Systems Conference*, pp. 18.1.1–18.1.6.

Lynch, D. D., 1987, "Vibration-Induced Drift in Hemispherical Resonator Gyro," Proc. *Annual Meeting, Institute of Navigation*, Dayton, OH, June 23–25, 1987.

McNiven, H. D., 1961, "Extensional Waves in a Semi-Infinite Elastic Rod," *J. Acoust. Soc. Am.*, Vol. 33, pp. 23–27.

Miklowitz, J., 1966, "Elastic Wave Propagation," *Applied Mechanics Survey*, H. N. Abramson, H. Liebowitz, J. N. Crowley, and S. Juhasz, eds., Spartan Books, Washington, pp. 809–839.

Milkowitz, J., 1978, *The Theory of Elastic Waves and Waveguides*, North Holland Publishing Co., Amsterdam.

Miller, C. E., 1985, "VLFEM Analysis of a Two-Dimensional Cochlear Model," ASME JOURNAL OF APPLIED MECHANICS, Vol. 52, pp. 743–751.

Mindlin, R. D., and Herrmann, G., 1951, "A One-Dimensional Theory of Compressional Waves in an Elastic Rod," *Proceedings of the First National Congress of Applied Mechanics*, pp. 203–208.

Mindlin, R. D., and McNiven, H. D., 1960, "Axially Symmetric Waves in Elastic Rods," ASME JOURNAL OF APPLIED MECHANICS, Vol. 27, pp. 145–151.

Pao, Y.-H., 1983, "Elastic Waves in Solids," ASME JOURNAL OF APPLIED MECHANICS, Vol. 50, pp. 1152–1164.

Piessens, R., and Branders, M., 1983, "Modified Clenshaw-Curtis Method for the Computation of Bessel Function Integrals," *BIT*, Vol. 23, pp. 370–381.

Piessens, R., and Branders, M., 1984, "Algorithm for the Computation of Bessel Functions Integrals," *J. Comp. Appl. Math.*, Vol. 11, pp. 119–137.

Pochhammer, L., 1876, "Ueber die Fortpflanzungsgeschwindigkeiten kleiner Schwingungen in einem unbegrenzten isotropen Kreiscylinder," *J. für reine und angewandte Mathematik*, Vol. 81, pp. 324–336.

Rayleigh, L., 1945, *Theory of Sound*, Dover Publications, New York, pp. 251–252.

Torvik, P. J., 1967, "Reflection of Wave Trains in Semi-Infinite Plates," *J. Acoust. Soc. Am.*, Vol. 41, pp. 346–353.

Tranter, C. J., 1968, *Bessel Functions with some Physical Applications*, The English Universities Press Ltd., St. Paul's House.

Ulitko, A. F., and Bobyleva, T. N., 1986, "Refined Theory of Mindlin-McNiven Type for Axisymmetric Waves in Piezoceramic Cylinders," *Soviet Appl. Mech.*, Vol. 22, pp. 803–807.

Vasudeva, R. Y., Bhaskara, P., and Rao, G., and Avadhani, B. V. S., 1986, "On Higher-Order Elastodynamic Rod Theories," *J. Acoust. Soc. Amer.*, Vol. 80, pp. 1777–1781.

Zemanek, J., 1962, "An Experimental and Theoretical Investigation of Elastic Wave Propagation in a Cylinder," Ph.D. thesis, University of California, Los Angeles, Calif.

Zemanek, J., 1972, "An Experimental and Theoretical Investigation of Elastic Wave Propagation in a Cylinder," *J. Acoust. Soc. Am.*, Vol. 51, pp. 265–283.

APPENDIX

Consider a strip with a lubricated-rigid condition on its lateral faces, assuming a plane strain condition in the x-z plane. The boundary condition can be expressed

$$u_x|_{x=\pm 1}=0, \quad \sigma_{xz}|_{x=\pm 1}=0. \tag{A1}$$

Note that the coordinates x, z and the displacements $u_x(x, z, t)$, $u_z(x, z, t)$ are referred to the strip half-width a, and all the stress quantities are referred to 2μ. Otherwise, we use the same dimensionless quantities introduced in Section 2. The solutions for symmetric waves propagating along the $+z$ axis can be rendered in the following form (see Miklowitz (1978))[2]:

$$\begin{aligned} u_x(x,z,t) &= -\sum_{m=0}^{\infty} A_m\beta_m(\sin\beta_m x)e^{i(\zeta_{dm}z-\Omega t)} \\ &\quad + \sum_{m=1}^{\infty} B_m i\zeta_{sm}(\sin\beta_m x)e^{i(\zeta_{sm}z-\Omega t)} \end{aligned} \tag{A2}$$

$$\begin{aligned} u_z(x,z,t) &= \sum_{m=0}^{\infty} A_m i\zeta_{dm}(\cos\beta_m x)e^{i(\zeta_{dm}z-\Omega t)} \\ &\quad - \sum_{m=1}^{\infty} B_m\beta_m(\cos\beta_m x)e^{i(\zeta_{sm}z-\Omega t)} \end{aligned} \tag{A3}$$

$$\begin{aligned} \sigma_{xz}(x,z,t) &= -\sum_{m=0}^{\infty} A_m i\beta_m\zeta_{dm}(\sin\beta_m x)e^{i(\zeta_{dm}z-\Omega t)} \\ &\quad + \sum_{m=1}^{\infty}\left[B_m\left(\beta_m^2-\frac{\Omega^2}{2}\right)\right](\sin\beta_m x)e^{i(\zeta_{sm}z-\Omega t)} \end{aligned} \tag{A4}$$

$$\begin{aligned} \sigma_{zz}(x,z,t) &= \sum_{m=0}^{\infty} A_m\left(\beta_m^2-\frac{\Omega^2}{2}\right)(\cos\beta_m x)e^{i(\zeta_{dm}z-\Omega t)} \\ &\quad - \sum_{m=1}^{\infty} B_m\beta_m i\zeta_{sm}(\cos\beta_m x)e^{i(\zeta_{sm}z-\Omega t)} \end{aligned} \tag{A5}$$

where $\zeta_{dm}^2=\alpha^2\Omega^2-\beta_m^2$, $\zeta_{sm}^2=\Omega^2-\beta_m^2$, and $\beta_m=m\pi$ (m is an integer). One can expand the quantities, which can be prescribed at $z=0$ in terms of the sine and cosine series, as

$$U_x(x)=\sum_{m=1}^{\infty} U_m(\sin\beta_m x) \tag{A8}$$

$$U_z(x)=W_0+\sum_{m=1}^{\infty} W_m(\cos\beta_m x) \tag{A9}$$

[2]The coordinate system used here is different from the system used by Miklowitz; interchanging x and z will produce the solutions given by Miklowitz.

$$S_{xz}(x) = \sum_{m=1}^{\infty} S_m (\sin\beta_m x) \tag{A10}$$

$$S_{zz}(x) = Z_0 + \sum_{m=1}^{\infty} Z_m (\cos\beta_m x) \tag{A11}$$

where $U_x(x)$ and $U_z(x)$ denote the tangential and normal displacements, and $S_r(x)$ and $S_z(x)$ are the shear and normal stresses at $z=0$. Note that the time dependence of the end conditions is omitted. The coefficients U_m, W_m, S_m, and Z_m can be determined using the orthogonality property of the Fourier series. Following the procedure used to derive **K**, we obtain the stiffness matrix **M** for the strip with the mixed wall condition:

$$\begin{Bmatrix} \mathbf{Z} \\ \mathbf{S} \end{Bmatrix} = \mathbf{M} \begin{Bmatrix} \mathbf{W} \\ \mathbf{U} \end{Bmatrix} = \begin{bmatrix} \mathbf{M11} & \mathbf{M12} \\ \mathbf{M21} & \mathbf{M22} \end{bmatrix} \begin{Bmatrix} \mathbf{W} \\ \mathbf{U} \end{Bmatrix} \tag{A12}$$

where **Z**, **S**, **W**, and **U** are defined in (20).

The components of the submatrices are

$$\begin{aligned} (\mathbf{M11})_{l,m} &= -\delta_{lm}\frac{\Omega^2}{2} i\zeta_{lm}/2\Delta_m \\ (\mathbf{M12})_{l,m} &= \delta_{lm}\beta_m\left(\beta_m^2 - \frac{\Omega^2}{2} + \zeta_{dm}\zeta_{sm}\right)/\Delta_m \\ (\mathbf{M21})_{l,m} &= (\mathbf{M12})_{m,l} \\ (\mathbf{M22})_{l,m} &= -\delta_{lm}\left(\frac{\Omega^2}{2} i\zeta_{dm}\right)/\Delta_m \end{aligned} \tag{A13}$$

where

$$\Delta_m = -\zeta_{dm}\zeta_{sm} - \beta_m^2. \tag{A14}$$

Uncoupled Wave Systems and Dispersion in an Infinite Solid Cylinder

Yoon Young Kim
Graduate Student,
Division of Applied Mechanics,
Stanford University,
Stanford, Calif. 94305

In this study, it is shown that there exist uncoupled wave systems for general nonaxisymmetric wave propagation in an infinite isotropic cylinder. Two cylindrical surface conditions corresponding to the uncoupled wave systems are discussed. The solutions of the uncoupled wave systems are shown to provide proper bounds of Pochhammer's equation for a free cylindrical surface. The bounds, which are easy to construct for any Fourier number in the circumferential direction, can be used to trace the branches of Pochhammer's equation. They also give insight into the modal composition of the branches of Pochhammer's equation at and between the intersections of the bounds. More refined dispersion relations of Pochhammer's equation are possible through an asymptotic analysis of the itersections of the branches of Pochhammer's equation with one family of the bounds. The asymptotic nature of wave motion corresponding to large wave numbers, imaginary or complex, for Pochhammer's equation is studied. The wave motion is asymptotically equivoluminal for large imaginary wave numbers, and is characterized by coupled dilatation and shear for large complex wave numbers.

1 Introduction

Pochhammer (1876) studied wave propagation in a solid circular cylinder with a traction-free cylindrical surface. Numerous subsequent investigations, both analytical and numerical, have shown that the traction-free condition leads to an intricate dispersion relation, and wave systems with coupled shear and dilatational behavior. Establishing the dispersion relation has therefore been a major concern.

Many attempts to construct the dispersion relation have been made. Perhaps the most noteworthy of those has been by Mindlin and his colleagues, who have used the ideas of bounds—grids of intersecting curves—to construct approximately the branches of Pochhammer's equation. Onoe, McNiven, and Mindlin (1962) present a technique for determining approximately the dispersion relation for axially symmetric wave propagation. By means of bounds, the branches of Pochhammer's equation are approximated for both real and imaginary wave numbers. The bounds are chosen in such a way that the exact equation for the cutoff frequencies is satisfied.

Pao and Mindlin (1960) also apply bounds in constructing the dispersion relation of flexural waves for real wave numbers. For the flexural wave motion, other families of curves, called barriers and intersectors, are introduced in addition to the two families of bounds which satisfy the exact equation for cutoff frequencies. One family of the bounds is easy to construct, but the other family is difficult to construct directly, and is constructed approximately through auxiliary barriers and bounds. Some of the auxiliary curves are determined approximately because the corresponding governing equations are not simple to solve. These families of curves are all employed in order to trace the branches of Pochhammer's equation approximately.

Pao (1962) extends the technique used for flexural wave motion with real wave numbers to the case of imaginary wave numbers. Kumar (1972) also discusses the dispersion relation for flexural wave motion with imaginary wave numbers. Due to the complicated nature of Pochhammer's equation, there are no simple bounds which satisfy Pochhammer's equation, either exactly or approximately at some intersections of the bounds, and the equation for the cutoff frequencies.

The application of bounds has not been extended to general nonaxisymmetric wave propagation in the cylinder. The bound technique of Pao and Mindlin (1960) is not very simple to use; thus, it appears that a substantial amount of work would be required to extend the technique to nonaxisymmetric wave propagation.

Rather than constructing an approximate dispersion relation of Pochhammer's equation, Armenàkas, et al. (1969), and Zemanek (1972) solve the exact dispersion relation numerically for several Fourier numbers in the circumferential direction. A CDC 6400 machine was utilized to construct the branches of Pochhammer's equation for real, imaginary, and complex wave numbers. Nelson, et al. (1971) employ a semi-analytic finite element formulation to obtain dispersion rela-

Contributed by the Applied Mechanics Division of THE AMERICAN SOCIETY OF MECHANICAL ENGINEERS for presentation at the Joint ASCE/ASME Applied Mechanics, Biomechanics, and Fluids Engineering Conference, San Diego, Calif., July 9 to 12, 1989.

Discussion of this paper should be addressed to the Editorial Department, ASME, United Engineering Center, 345 East 47th Street, New York, N.Y. 10017, and will be accepted until two months after final publication of the paper itself in the JOURNAL OF APPLIED MECHANICS. Manuscript received by the ASME Applied Mechanics Division, May 26, 1988; final revision, October 28, 1988.

Paper No. 89-APM-25.

tions for real wave numbers in orthotropic hollow cylinders, and Huang and Dong (1984) extend the approach to anisotropic cylinders to construct dispersion relations for real, imaginary, and complex wave numbers.

The idea of establishing bounds goes back to Holden (1951) and Mindlin (1951), who identified bounds by simple algebraic equations with roots which coincide with those of the frequency equations for rods and plates. Mindlin (1960) shows that for wave propagation in an infinite plate, the solutions for rigid-lubricated lateral surfaces can be used as bounds for the branches of the Rayleigh-Lamb frequency equation. Note that for plates, the proper bounds are the solutions corresponding to a lateral surface condition different from the traction-free boundary condition. The solutions for the plate with the rigid-lubricated condition give an uncoupled wave system, and at the intersections of the bounds, the solutions can be used to characterize the nature of wave motion governed by the Rayleigh-Lamb equation.

Unlike wave propagation in the plate, the bounds for the branches of Pochhammer's equation discussed so far have not been related to solutions of a cylinder with any other physical boundary conditions than the traction-free condition. In addition, uncoupled wave systems for general nonaxisymmetric wave propagation in a cylinder have not been studied. Due to the fact that no completely uncoupled wave motion can be found for Pochhammer's equation at the cutoff frequencies, it has been assumed that completely uncoupled wave motions corresponding to physical boundary conditions are not possible. (See Pao and Mindlin (1960).)

In the present study, it is shown that there exist uncoupled wave systems for general nonaxisymmetric wave propagation. Two cylindrical surface conditions corresponding to the uncoupled wave systems are discussed. It is shown that the solutions of the uncoupled wave systems provide proper, easily constructed bounds for Pochhammer's equation. The bounds defined by Pao and Mindlin (1960) are such that Pochhammer's branches must not cross them except a set of predetermined points (Pao, 1988). However, the present bounds simply refer to auxiliary curves from which Pochhammer's branches may be traced approximately. Only one of the two families of cutoff frequencies for the traction-free case is satisfied exactly by one set of the present bounds, and the branches emanating from them can be traced systematically. The other family of cutoff frequencies is not obtained exactly by the present bounds, but the branches starting from these can still be traced systematically.

An important aspect of the present approach is that the present bounds well approximate the points corresponding to local maximum and minimum group velocities in the frequency-wave number plane. This aspect may become useful in transient wave propagation. Shen (1988) points out that the wave modes of frequencies centered around the local maximum and minimum group velocities contribute most to the response in transient wave propagation.

From the numerical point of view, the present bounds can alleviate the computational efforts substantially, especially where the branches of Pochhammer's equation are close. (See, e.g., Fig. 2) It was difficult to obtain the correct dispersion relation numerically without knowing the behavior of Pochhammer's branches, which can be predicted by the present bounds.

2 Pochhammer's Equation and Its Asymptotic Forms

A solution to the wave equation for an isotropic elastic solid cylinder (see, e.g., Miklowitz (1978) or Achenbach (1975)) can be expressed

$$u_i(r,\theta,z,t)=\tilde{u}_i(r)\begin{Bmatrix}\cos n\theta\\ \sin n\theta\end{Bmatrix}\exp[i(\lambda z-\Omega t)]$$

$$\sigma_{ij}(r,\theta,z,t)=\tilde{\sigma}_{ij}(r)\begin{Bmatrix}\cos n\theta\\ \sin n\theta\end{Bmatrix}\exp[i(\lambda z-\Omega t)] \tag{1}$$

where

$$\tilde{u}_r(r)=A\,\frac{dJ_n(hr)}{dr}+B(i\lambda)\,\frac{dJ_n(kr)}{dr}-C\,\frac{n}{r}\,J_n(kr) \tag{2a}$$

$$\tilde{u}_\theta(r)=-A\,\frac{n}{r}\,J_n(hr)-B(i\lambda)\,\frac{n}{r}\,J_n(kr)+C\,\frac{dJ_n(kr)}{dr} \tag{2b}$$

$$\tilde{u}_z(r)=A(i\lambda)J_n(hr)+Bk^2J_n(kr) \tag{2c}$$

and

$$\begin{aligned}\tilde{\sigma}_{rr}(r)=&A\left\{-\frac{1}{r}\,\frac{dJ_n(hr)}{dr}+\left[\frac{n^2}{r^2}-\left(\frac{\Omega^2}{2}-\lambda^2\right)\right]J_n(hr)\right\}\\&+B(i\lambda)\left\{-\frac{1}{r}\,\frac{dJ_n(kr)}{dr}+\left(\frac{n^2}{r^2}-k^2\right)J_n(kr)\right\}\\&-C_n\,\frac{d}{dr}\left[\frac{J_n(kr)}{r}\right]\end{aligned} \tag{3a}$$

$$\begin{aligned}\tilde{\sigma}_{\theta\theta}(r)=&A\left\{-\left[\frac{n^2}{r^2}+\left(\frac{1}{2}-\alpha^2\right)\Omega^2\right]J_n(hr)+\frac{1}{r}\,\frac{dJ_n(hr)}{dr}\right\}\\&+B(i\lambda)\left[-\frac{n^2}{r^2}\,J_n(kr)+\frac{1}{r}\,\frac{dJ_n(kr)}{dr}\right]\\&+Cn\,\frac{d}{dr}\left[\frac{J_n(kr)}{r}\right]\end{aligned} \tag{3b}$$

$$\tilde{\sigma}_{zz}(r)=A\left(h^2-\frac{\Omega^2}{2}\right)J_n(hr)+B(i\lambda)k^2J_n(kr) \tag{3c}$$

$$\begin{aligned}\tilde{\sigma}_{r\theta}(r)=&A\left[-\frac{n}{r}\,\frac{dJ_n(hr)}{dr}+\frac{n}{r^2}\,J_n(hr)\right]\\&+B(i\lambda)\left[-\frac{n}{r}\,\frac{dJ_n(kr)}{dr}+\frac{n}{r^2}\,J_n(kr)\right]\\&+C\left[-\frac{1}{r}\,\frac{dJ_n(kr)}{dr}+\left(\frac{n^2}{r^2}-\frac{k^2}{2}\right)J_n(kr)\right]\end{aligned} \tag{3d}$$

$$\begin{aligned}\tilde{\sigma}_{rz}(r)=&A(i\lambda)\,\frac{dJ_n(hr)}{dr}+B\left(\frac{\Omega^2}{2}-\lambda^2\right)\frac{dJ_n(kr)}{dr}\\&-C\left(\frac{i\lambda}{2}\right)\frac{n}{r}\,J_n(kr)\end{aligned} \tag{3e}$$

$$\begin{aligned}\tilde{\sigma}_{\theta z}(r)=&-A(i\lambda)\,\frac{n}{r}\,J_n(hr)-B\left(\frac{\Omega^2}{2}-\lambda^2\right)\frac{n}{r}\,J_n(kr)\\&+C\left(\frac{i\lambda}{2}\right)\frac{dJ_n(kr)}{dr}\,.\end{aligned} \tag{3f}$$

In equation (1), u_θ, $\sigma_{r\theta}$, and $\sigma_{\theta z}$ take $\sin n\theta$ and the other quantities take $\cos n\theta$. Dimensionless quantities are employed; the displacement u_i and stress σ_{ij}, are referred to the radius a of the cylinder, and 2μ, twice the shear modulus, respectively. The radial and axial coordinates denoted by r and z are referred to a and the time t is referred to a/c_s. The velocities of dilatational and shear waves in infinite isotropic media will be denoted by c_d and c_s, respectively. The dimensionless frequency Ω is referred to c_s/a and n is the Fourier number in the circumferential direction θ. The parameters h and k are defined as

$$h^2=\alpha^2\Omega^2-\lambda^2;\quad k^2=\Omega^2-\lambda^2 \tag{4}$$

where λ is the dimensionless wave number referred to $1/a$, and the material property α is given by

$$\alpha^2 = \left(\frac{c_s}{c_d}\right)^2 = \frac{1-2\nu}{2(1-\nu)} \tag{5}$$

where ν is Poisson's ratio. J_n is the Bessel function of the first kind of order n. The parameters h and k are associated with dilatational and shear waves, respectively, and the unknown constants A, B, and C are to be determined from boundary conditions.

For future reference, we first repeat some of the well-known facts concerning Pochhammer's frequency equation. Pochhammer's equation can be obtained by applying the traction-free cylindrical surface condition, namely,

$$\sigma_{rr}|_{r=1} = 0; \quad \sigma_{r\theta}|_{r=1} = 0; \quad \sigma_{rz}|_{r=1} = 0. \tag{6}$$

For $n \neq 0$, the traction-free boundary condition gives

$$\begin{bmatrix} M_{11} & M_{12} & M_{13} \\ M_{21} & M_{22} & M_{23} \\ M_{31} & M_{32} & M_{33} \end{bmatrix} \begin{Bmatrix} A \\ B \\ C \end{Bmatrix} = \begin{Bmatrix} 0 \\ 0 \\ 0 \end{Bmatrix} \tag{7a}$$

where

$$\begin{aligned}
M_{11} &= \left(n^2 - 1 - \frac{\Omega^2}{2} + \lambda^2\right) J_n(h) \\
M_{21} &= -hJ_n'(h) + J_n(h) \\
M_{31} &= (i\lambda) hJ_n'(h) \\
M_{12} &= (i\lambda)(n^2 - 1 - k^2) J_n(k) \\
M_{22} &= (i\lambda)[-kJ_n'(k) + K_n(k)] \\
M_{32} &= \left(\frac{\Omega^2}{2} - \lambda^2\right) kJ_n'(k) \\
M_{13} &= \left(-n + \frac{1}{n}\right) kJ_n'(k) + \left(\frac{k^2}{2n}\right) J_n(k) \\
M_{23} &= -\frac{k}{n} J_n'(k) + \left(n - \frac{k^2}{2n}\right) J_n(k) \\
M_{33} &= -\left(\frac{i\lambda}{2}\right) nJ_n(k).
\end{aligned} \tag{7b}$$

In (7b), the superscript $'$ denotes differentiation with respect to the following argument. By requiring that $|M_{ij}| = 0$, Pochhammer's frequency equation is obtained.

For $n = 0$, (7) degenerates to two sets of equations:

$$\begin{bmatrix} M_{11}^0 & M_{12}^0 \\ M_{21}^0 & M_{22}^0 \end{bmatrix} \begin{Bmatrix} A \\ B \end{Bmatrix} = \begin{Bmatrix} 0 \\ 0 \end{Bmatrix} \tag{8a}$$

where

$$\begin{aligned}
M_{11}^0 &= -hJ_0'(h) + \left(\lambda^2 - \frac{\Omega^2}{2}\right) J_0(h) \\
M_{21}^0 &= (i\lambda) hJ_0'(h) \\
M_{12}^0 &= (i\lambda)[-kJ_0'(k) - k^2 J_0(k)] \\
M_{22}^0 &= \left(\frac{\Omega^2}{2} - \lambda^2\right) kJ_0'(k)
\end{aligned} \tag{8b}$$

and

$$\left[kJ_0'(k) + \left(\frac{k^2}{2}\right) J_0(k)\right] C = 0. \tag{9}$$

By imposing $|M_{ij}^0| = 0$, the frequency equation for symmetric longitudinal waves is obtained. Equation (9) corresponds to the frequency equation for torsional waves.

It is known that for a given Ω, there are a finite number of real wave numbers and an infinite number of imaginary and complex wave numbers, where the imaginary and complex wave numbers are associated with end effects. Note that dilational and shear waves do not propagate at distinct phase velocities, but at the same phase velocity since Pochhammer's equation gives a coupled wave system.

For $n \neq 0$, the cutoff frequencies are obtained by letting $\lambda = 0$ in (7)

$$J_n'(\Omega) = 0 \tag{10a}$$

$$\begin{aligned}
&[2(n^2-1)\Omega J_n'(\Omega) - \Omega^2 J_n(\Omega)][\alpha\Omega J_n'(\alpha\Omega) - J_n(\alpha\Omega)] \\
&\quad - \left(n^2 - 1 - \frac{\Omega^2}{2}\right) J_n(\alpha\Omega)[(2n^2 - \Omega^2) J_n(\Omega) \\
&\quad - 2\Omega J_n'(\Omega)] = 0.
\end{aligned} \tag{10b}$$

Corresponding to (10a), A, C, and λ are identically zero and, thus, from (2) the displacement is purely axial and equivoluminal. Corresponding to (10b),

$$\begin{aligned}
&B = 0 \\
&\frac{A}{C} = \frac{2(1-n^2)\Omega J_n'(\Omega) + \Omega^2 J_n(\Omega)}{n(2n^2 - 2 - \Omega^2) J_n(\alpha\Omega)}
\end{aligned} \tag{11}$$

where the particle motion is restricted in the cross-sectional plane ($u_z = 0$).

For the longitudinal waves, the cutoff frequencies are determined by

$$J_1(\Omega) = 0 \tag{12a}$$

$$\Omega J_0(\alpha\Omega) - 2\alpha J_1(\alpha\Omega) = 0. \tag{12b}$$

For (12a), $A = 0$ and the motion is entirely axial and equivoluminal. For (12b), $B = 0$ and only the radial motion remains.

When $\nu = 1/2$ (incompressible materials), (12b) disappears for $n = 0$, and (10b) must be replaced by

$$\begin{aligned}
&(n-1)[2(n^2-1)\Omega J_n'(\Omega) - \Omega^2 J_n(\Omega)] \\
&\quad - \left(n^2 - 1 - \frac{\Omega^2}{2}\right)[(2n^2 - \Omega^2) J_n(\Omega) - 2\Omega J_n'(\Omega)] = 0.
\end{aligned}$$

For short real-wave lengths, it is known that the phase velocity of the lowest branch approaches the Rayleigh surface wave velocity and the phase velocities of higher branches approach the shear wave velocity in an infinite medium (See, e.g., Bancroft (1941), and Hudson (1943)). The discussion to this point roughly covers the well-known aspects of Pochhammer's equation.

The equation for the zero-frequency intercepts of Pochhammer's equations can be written

$$\begin{aligned}
&(1-\alpha^2)\{2\mu^3 J_n'(\mu) + [(\mu^2 - n^2)^2 - n^2] J_n(\mu)\} \\
&\quad \bullet \{\mu^2 [J_n'(\mu)]^2 + (\mu^2 - n^2) J_n^2(\mu)\} \\
&\quad + 2(n^2-1)\mu^3 [J_n'(\mu)]^3 - \mu^4 [J_n'(\mu)]^2 J_n(\mu) \\
&\quad + (2n^2\mu^2 + 2n^2 - 2n^4)\mu J_n'(\mu) J_n^2(\mu) - \mu^2 n^2 J_n^3(\mu) = 0
\end{aligned} \tag{13}$$

where $\mu = i\lambda$. For moderate n's, (13) can be approximated by

$$\{\mu^2 [J_n'(\mu)]^2 + (\mu^2 - n^2) J_n^2(\mu)\} J_n(\mu) \approx 0. \tag{14}$$

The asymptotic solution of the first factor of (14) is

$$\mu = i\lambda \approx \pm \left(m + \frac{n}{2}\right)\pi \pm \frac{1}{2} \ln 4 \left[\left(m + \frac{n}{2}\right)\pi\right] i \tag{15}$$

where m is an integer. Similarly, the approximate solution of the second factor of (14) is given by

$$\mu = i\lambda \approx \pm \left(m + \frac{n}{2} - \frac{1}{4}\right)\pi. \tag{16}$$

The equation (15) for the zero-intercepts is also given by Zemanek (1972), which can be obtained by dividing (13) by $J_n^3(\mu)$. Since $J_n^3(\mu)$ is assumed to be nonzero in Zemanek's analysis, the asymptotic solution (15) is obtained, but not the asymptotic solution (16).

For a given Ω and n, the asymptotic solutions (15) and (16) remain valid as λ approaches infinity. Through the asymptotic analysis, it can be shown that for (15), $C \approx 0$, but the solutions related to A and B remain where the dilatational wave and one of the shear waves are coupled. For (16), $A \approx 0$, $B \approx 0$, and the only nonvanishing solution in the asymptotic analysis corresponds to the coefficent C. In this case, the motion is asymptotically equivoluminal. Thus, in characterizing the wave motion for certain limits, this analysis for large imaginary and complex wave numbers will be useful, just like the known results for the wave behavior for small wave numbers, and for large, real wave numbers.

From (4) it may be seen that the plane of Ω and positive real λ is divided into three sectors in which Pochhammer's equation has different behaviors, depending on whether the arguments h and k of the Bessel functions are real or imaginary:

Sector $1 (0 < \Omega/\lambda < 1)$: h and k imaginary
Sector $2 (1 < \Omega/\lambda < 1/\alpha)$: h imaginary, k real
Sector $3 (1/\alpha < \Omega/\lambda < \infty)$: h and k real.

When $k=0$, the displacements corresponding to the B and C parts must be replaced:

$$\tilde{u}_r(r) = A\,\frac{dJ_n(hr)}{dr} + Br^{n-1} + Cr^{n+1} \tag{17a}$$

$$\tilde{u}_\theta(r) = -A\,\frac{n}{r}\,J_n(hr) - Br^{n-1} + Cr^{n+1} \tag{17b}$$

$$\tilde{u}_z(r) = A(i\lambda)J_n(hr) - C\,\frac{2(n+1)}{i\lambda}\,r^n. \tag{17c}$$

Then M_{ij} will be given by

$$\begin{aligned} M_{12} &= n - \frac{1}{n} \\ M_{22} &= -1 + \frac{1}{n} \\ M_{32} &= \frac{i\lambda}{2} \\ M_{13} &= n+1 \\ M_{23} &= 0 \\ M_{33} &= \frac{1}{2}\left[i\lambda - \frac{2n(n+1)}{i\lambda}\right] \end{aligned} \tag{18}$$

and M_{11}, M_{21}, and M_{31} are unchanged. For $n=0$,

$$\tilde{u}_r(r) = A\,\frac{dJ_0(hr)}{dr} - B(i\lambda)r \tag{19a}$$

$$\tilde{u}_z(r) = A(i\lambda)J_0(hr) + 2B \tag{19b}$$

and M_{12}^0 and M_{22}^0 in (8) are replaced by

$$M_{12}^0 = -i\lambda; \quad M_{22}^0 = \frac{\lambda^2}{2}. \tag{20}$$

Similarly for $h=0$, one must replace the following elements in (7) by

$$\begin{aligned} M_{11} &= (n^2+n-2) - \left(\frac{\nu}{1-2\nu}\right)\lambda^2 \\ M_{21} &= -n+1 \\ M_{31} &= n(i\lambda) \end{aligned} \tag{21}$$

where the appropriate displacements corresponding to the coefficient A are Anr^{n-1}, $-Anr^{n-1}$, and $A(i\lambda)r^n$ for $\tilde{u}_r(r)$, $\tilde{u}_\theta(r)$, and $\tilde{u}_z(r)$, respectively. For $n=0$, no replacement is necessary. The analysis for $k=0$ and $h=0$ is an extension to general n of Pao and Mindlin's work (1960) for the flexural wave propagation.

3 Uncoupled Wave Systems

In the preceding section, we have considered the traction-free boundary condition and have noted some aspects of the intricate nature of Pochhammer's equation. Due to the intricacy which is associated with the coupling of the dilational and shear waves, Pochhammer's equation is not easy to solve. One way to construct the dispersion relation of Pochhammer's equation is to use the bounds suggested by Mindlin and his colleagues. As pointed out in Section 1, their analysis is limited to longitudinal and flexural wave motions. The technique may produce good approximate solutions, but it requires a considerable amount of work even in constructing the bounds themselves. It also appears that generalization of their technique to n other than 0 or 1 would require much effort. The difficulties arise because the bounds must satisfy the exact cutoff frequency equations as well as Pochhammer's equation either exactly or approximately at the intersections of the bounds. Furthermore, as pointed out by McNiven and McCoy (1974), it is difficult to use the bounds in identifying the nature of the branches of Pochhammer's equation.

In the present study, a different approach is taken in order to study Pochhammer's equation. Instead of examining Pochhammer's equation at certain special points, solutions of general cylindrical boundary conditions are studied. It is shown that there exist uncoupled wave systems for two sets of boundary conditions. These uncoupled systems correspond to purely dilatational or equivoluminal deformations. The solutions of the uncoupled wave systems are shown to provide appropriate, easily constructed bounds for any n.

The general conditions on the cylindrical surface $r=1$ can be written

$$\begin{aligned} \sigma_{rr} + e_1 u_r &= 0 \\ \sigma_{rz} + e_2 u_z &= 0 \\ \sigma_{r\theta} + e_3 u_\theta &= 0 \end{aligned} \tag{22}$$

where e_i can be any number. The traction-free and rigidly fixed surface conditions are obtained by taking $e_1 = e_2 = e_3 = 0$ and ∞, respectively.

First, consider the following cylindrical surface condition, which can be obtained by setting $e_1 = \infty$, $e_2 = 0$ and $e_3 = 1$ in (22)

$$u_r = 0 \tag{23a}$$

$$\sigma_{rz} = 0 \tag{23b}$$

$$\sigma_{r\theta} + u_\theta = 0. \tag{23c}$$

Equations (23a, b) state that the cylindrical surface is rigidly constrained radially, but free to move axially (or lubricated). Equation (23c) is an elastic spring constraint in the circumferential direction.

Substituting equations (1)–(3) into equations (23) leads to the following frequency equation

$$J_n'(h)J_n'(k)J_n(k) = 0. \tag{24}$$

The solutions are

$J_n'(h) = 0, A \neq 0 (B = C = 0),$

$$h = \xi_j,\ \lambda^2 = (\alpha^2\Omega^2 - \xi_j^2) \equiv \lambda_{dj}^2 \tag{25a}$$

$$J_n'(k)=0, B\neq 0(A=C=0),$$

$$k=\xi_l, \lambda^2=(\Omega^2-\xi_l^2)\equiv\lambda_{sl}^2 \tag{25b}$$

$$J_n(k)=0, C\neq 0(A=B=0),$$

$$k=\rho_m, \lambda^2=(\Omega^2-\rho_m^2)\equiv\lambda_{tm}^2 \tag{25c}$$

where ξ and ρ denote the zeros of $J_n'(r)$ and $J_n(r)$, respectively, and j, l, and m are integers. The subscript d is used to denote the dilatational wave and s and t are used for the two shear waves. From (25), it is easily seen that the corresponding wave systems are uncoupled.

Secondly, consider the conditions obtained by taking $e_1=1$, $e_2=e_3=0$ in (22), which are

$$\sigma_{rr}+u_r=0 \tag{26a}$$

$$u_z=0 \tag{26b}$$

$$u_\theta=0. \tag{26c}$$

Equation (26*a*) represents an elastic constraint in the radial direction, and equations (26*b*, *c*) are rigid cylindrical surface conditions in the axial and circumferential directions.

Substitution of equations (1–3) into equations (26) gives

$$J_n(h)J_n(k)J_n'(k)=0. \tag{27}$$

Corresponding to (27), we have another uncoupled wave system, with

$$J_n(h)=0, A\neq 0(B=C=0),$$

$$h=\rho_p, \lambda^2=(\alpha^2\Omega^2-\rho_p^2)\equiv\mu_{dp}^2 \tag{28a}$$

$$J_n(k)=0, B\neq 0(A=C=0),$$

$$k=\rho_q, \lambda^2=(\Omega^2-\rho_q^2)\equiv\mu_{sq}^2 \tag{28b}$$

$$J_n'(k)=0, C\neq 0(A=B=0),$$

$$k=\xi_r, \lambda^2=(\Omega^2-\xi_r^2)\equiv\mu_{tr}^2 \tag{28c}$$

where p, q, and r are integers.

It is interesting that the surface condition

$$u_r=0;\quad \sigma_{rz}+u_z=0;\quad \sigma_{r\theta}=0 \tag{29}$$

gives the same equation as (27), but a completely uncoupled wave system cannot be obtained from this condition. In general, when $e_i=0$ or ∞, which includes the cases $u_r=\sigma_{rz}=\sigma_{\theta z}=0$ and $\sigma_{rr}=u_z=u_\theta=0$, no uncoupled wave system can be found.

When $n=0$, it is seen that (23) and (26) degenerate to

$$\begin{cases} u_r=0 \\ \sigma_{rz}=0 \end{cases} \tag{30}$$

$$\begin{cases} \sigma_{rr}+u_r=0 \\ u_z=0 \end{cases} \tag{31}$$

and

$$\begin{cases} u_\theta=0 \\ \sigma_{r\theta}+u_\theta=0. \end{cases} \tag{32}$$

Equations (30) and (31) are the cylindrical conditions for the uncoupled wave systems for axisymmetric longitudinal wave propagation, whereas (32) is the condition for torsional motion. The solution of the uncoupled wave system (30) is

$$J_0'(h)=0;\quad h=\xi_j$$
$$\lambda^2=\alpha^2\Omega^2-\xi_j^2 \tag{33a}$$

$$J_1(k)=0;\quad k=\xi_l$$
$$\lambda^2=\Omega^2-\xi_l^2 \tag{33b}$$

where ξ is the solution of $J_0'(r)=0$. Similarly for (31),

$$J_0(h)=0;\quad h=\rho_p$$
$$\lambda^2=\alpha^2\Omega^2-\rho_p^2 \tag{34a}$$

$$J_0(k)=0;\quad k=\rho_q$$
$$\lambda^2=\Omega^2-\rho_q^2 \tag{34b}$$

where ρ is the solution of $J_0(r)=0$.

Kim and Steele (1987) use the solution of (30) to solve the axisymmetric end problems of longitudinal wave propagation. Except for the wave system corresponding to (30), it appears that the wave systems explored here, including (31), have not been discussed previously and it has been believed that there exist no uncoupled wave systems for general nonaxisymmetric wave propagation. The usefulness of the uncoupled wave systems presented in the present work is not just that the solutions of the uncoupled systems provide the proper bounds of Pochhammer's equation and can be used to study the nature of Pochhammer's equation (as shall be discussed later); but that these solutions may be used as an expansion set for displacement and stress for end problems of general nonaxisymmetric wave propagation as done by Kim and Steele (1987) for longitudinal wave propagation in a semi-infinite cylinder.

In the subsequent discussion, the families of curves which correspond to (25*a*) and (28*a*) will be called *P* and *PP* curves. The curves represented by either (25*b*) or (28*c*) and either (25*c*) or (28*b*) will be called *S* and *T* curves.

4 The Dispersion Curves of Pochhammer's Equation and Bounds

Though the dispersion curves for longitudinal wave propagation can be constructed from the present bounds, nonaxisymmetric wave propagation, which is more difficult to deal with, is focused on here.

The dispersion relation for $n=2$ is considered first. In Fig. 1, the dispersion curves of the traction-free case and of the uncoupled wave systems are shown. Here $\nu=0.3317$ is used for the purpose of comparison with Zemanek's work (1972). The branches of Pochhammer's equation are denoted by thick solid lines which are the numerical solutions of Pochhammer's equation. The *P*, *PP*, *S*, and *T* curves are denoted by solid, long dot-dashed, dotted, and dashed lines, respectively. The thick dashed line corresponds to $h=0$, where the phase velocity is the velocity of the dilational wave in an infinite medium. First consider the dispersion curves for real wave numbers. As shown in Fig. 1, the branches of Pochhammer's equation pass through the intersections of the *P* and *S* curves, namely, the intersections of the solid and dotted lines approximately. Similarly, the branches of Pochhammer's equation are very close to the intersections of the *PP* and *T* curves (the intersections of the long dot-dashed and dashed lines).

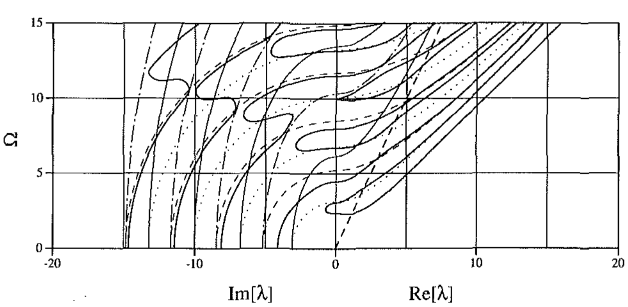

Fig. 1 The branches of Pochhammer's equation (thick solid lines) and the dispersion curves of the uncoupled wave systems for real and imaginary wave numbers for $n=2$, $\nu=0.3317$. The $h=0$ line is represented by the thick, dashed line. The dispersion curves of the uncoupled systems are denoted by solid lines ($J_n'(h)=0$), long dot-dashed lines ($J_n(h)=0$), dotted lines ($J_n'(k)=0$), and dashed lines ($J_n(k)=0$).

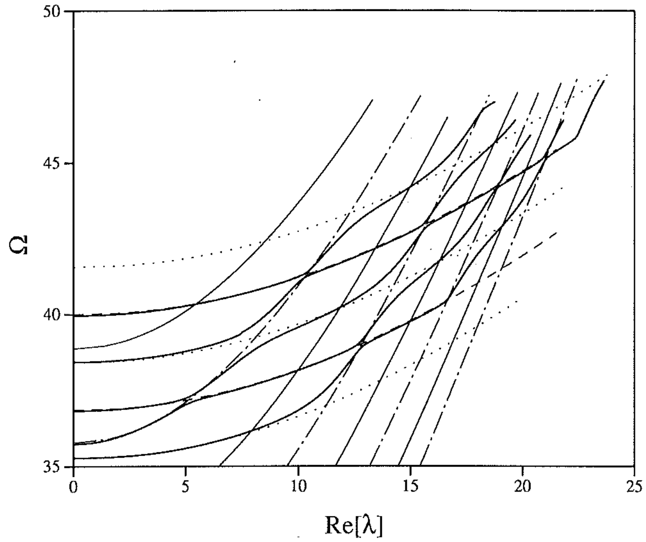

Fig. 2 Intricate nature of the branches of Pochhammer's equation for a relatively high frequency range for $n=2$, $\nu=0.3317$. The intersections of the dispersion curves of the uncoupled wave systems are accurate asymptotic solutions of the branches of Pochhammer's equations (thick solid lines). (Namely, the intersections of solid ($J_n'(h)=0$) and dotted ($J_n'(k)=0$) lines and the intersections of long dot-dashed ($J_n(h)=0$) and dashed ($J_n(k)=0$) lines.)

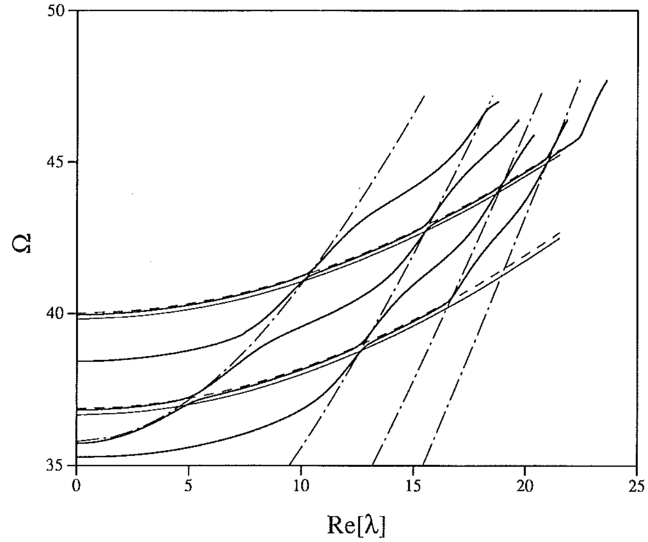

Fig. 3 The asymptotic solutions of the branches of Pochhammer's equation (thick solid lines) at some special points for $n=2$, $\nu=0.3317$. There are two sets of solutions of Pochhammer's equation which pass through the long dot-dashed lines ($J_n(h)=0$). They are the intersections of the long dot-dashed lines with the dashed ($J_n(k)=0$) and solid lines ($J_n(k)+[5+(1-\alpha^2)/\alpha^2]J_{n-1}(k)/k \approx 0$).

In order to see the more intricate nature of Pochhammer's equation, the dispersion curves for a relatively high frequency range must be considered. Figure 2 shows the complicated nature of Pochhammer's equation for a relatively high frequency range and the dispersion curves of the uncoupled wave systems. The branches of Pochhammer's equation pass through the intersections of the P and S curves (solid and dotted lines) approximately, and they are asymptotically tangent to the S curves (dotted) at these intersections. It is seen that the intersections are points of inflection of the branches.

An asymptotic analysis can be carried out in order to see how good the intersections of the P and S curves are as the solutions of Pochhammer's equation. If the equation $J_n'(k)=0$ for the S curves is substituted into Pochhammer's equation, the result is

$$\Theta_n(h)-n-\frac{\lambda^2+k^2}{2(n^4-n^2-2n^2k^2+k^4)}=0 \tag{35}$$

where $\Theta_n(h)=J_{n-1}(h)/J_n(h)$. For large k, the asymptotic form of (35) is

$$\Theta_n(h)\approx n \ \Leftrightarrow\ J_n'(h)\approx 0. \tag{36}$$

This asymptotic form, which is the equation for the P curves, is $O(1/\lambda^2)$ accurate. Thus the intersections of the P and S curves (solid and dotted) are the solutions of Pochhammer's equation to $O(1/\lambda^2)$.

From Fig. 2, it is also seen that at each intersection of the PP and T curves (long dot-dashed and dashed), there are two nearby branches which are very close to each other and change their slopes abruptly. Note that they never cross each other, though it might appear that they do. The higher branch remains on the T curves (dashed) before the intersection. The slope of the higher branch is asymptotic to the slope of the T curve (dashed) just before the intersection, but is asymptotic to the slope of the PP curve (long dot-dashed) just after the intersection. After the intersection, the branch has a negative curvature, and is "ready" to cross the intersection of the P and S curves (solid and dotted). In contrast, the lower branch approaches the $PP-T$ intersection from the intersections of P and S curves, which is located below and to the left. It is seen that the segment of the branch between the two intersections has a positive curvature and a slope which is asymptotic to the S curve (dotted) near the $P-S$ intersection and asymptotic to the PP curve (long dot-dashed) near the $PP-T$ intersection. After the lower branch passes through the intersection of the PP and T curves, its slope becomes asymptotic to the slope of T curve (dashed), until it approaches the next $PP-T$ intersection.

Even though the intersections of the PP and T curves predict the behavior of the branches of Pochhammer's equation and provide approximate solutions to Pochhammer's equation, the asymptotic study near such intersections proves useful for the further refinement of the approximate solutions. For this purpose, $J_n(h)=0$, which is the equation for the PP curves, is imposed to Pochhammer's equation. We then obtain two forms of asymptotic solutions for large k:

$$J_n(k)\approx 0 \tag{37a}$$

$$J_n(k)+[5+(1-\alpha^2)/\alpha^2]J_{n-1}(k)/k\approx 0. \tag{37b}$$

For $n=1$, (37a) is the exact solution, and this equation is the equation characterizing the T curves (dashed lines). For $n=2$ and $\nu=0.3317$, the solutions of (37a) are

5.136, 8.417, 11.61, . . . , 33.72, 36.86, 40.01, . . .

and the solutions of (37b) are

4.255, 7.699, 11.04, . . . , 33.49, 36.65, 39.81, ...

As k becomes larger, the solutions of (37a) and (37b) approach each other. Thus if one attempted to determine numerically the dispersion relation near the intersections of the PP and T curves for large wave numbers, one set of the two sets of solutions would be missing. For convenience, TA is used to denote the curves given by $k_v^2=\Omega^2-\lambda^2$ where k_v is the solutions of (37b).

In Fig. 3, in conjunction with the PP (long dot-dashed), T and TA curves (dashed and solid, respectively), the branches of Pochhammer's equations are plotted. This figure shows that the T and TA curves determine very accurately the intersections of the branches of Pochhammer's equation with the PP curves. Thus in addition to the T curves, the TA curves turn out to be useful bounds for accurate tracing of Pochhammer's equation.

One can observe that the present bounds well approximate the points corresponding to local maximum and minimum

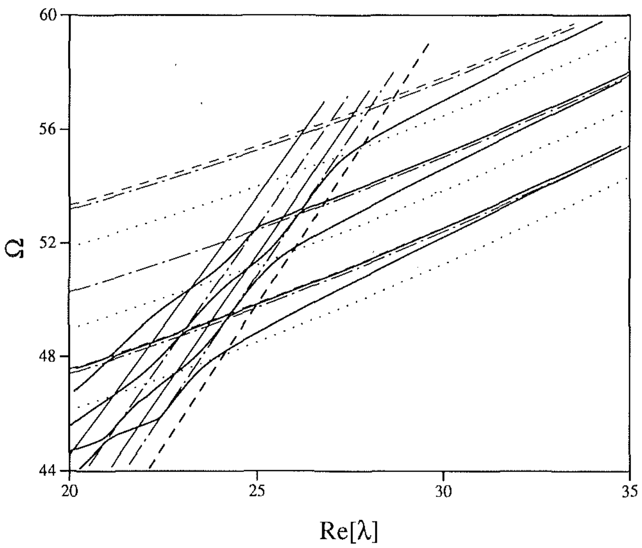

Fig. 4 The branches of Pochhammer's equation (thick solid lines) near the $h=0$ line (thick dashed) for $n=2$, $\nu=0.3317$. The solid lines ($J_n'(h)=0$), long dot-dashed lines (nearly parallel to the solid lines) ($J_n(h)=0$), dotted lines ($J_n'(k)=0$) and dashed lines ($J_n(k)=0$) are the dispersion curves of the uncoupled wave systems.

group velocities in the $\Omega-\lambda$ plane. This observation may prove useful for transient wave propagation, since the main contribution to the response comes from the wave modes corresponding to the local maximum and minimum group velocities (Shen, 1988).

So far, the portion of Sector 3 away from the $h=0$ line has been considered. Figure 4 illustrates the behavior of the branches of Pochhammer's equation near $h=0$. The $h=0$ line, which can be regarded as a nominal solution of (25*a*)[1] or (28*a*) is designated by the thick dashed line. As shown in Fig. 4, the intersections of the branches of Pochhammer's equations with $h=0$ approach asymptotically the intersections of the $h=0$ line and the S and T curves. The behavior of the branches at these intersections are similar to those in the portion of Sector 3 away from the $h=0$ line. The major difference is that unlike the intersections of the P and S curves, the curvatures of the branches do not change at the intersections of $h=0$ and the S curves (dotted). After passing through these intersections, the branches asymptotically approach the T curves (dashed), more accurately, the TA curves (long dot-dashed), whose asymptotes are the $k=0$ line. Note that at the $k=0$ line, the phase velocity is the velocity of shear waves in an infinite medium. The branches of Pochhammer's equation that pass through the intersections of the $h=0$ line and the T curves (dashed) approach the T curves after they pass the $h=0$ line.

The foregoing analysis has shown that the solutions of the uncoupled systems provide proper bounds for the branches of Pochhammer's equation. Moreover, these bounds also provide an insight into the modal composition corresponding to points on the branches both at and between the intersections of the bounds. If the branch segments of Pochhammer's equation are asymptotic to the S curves, for instance, the nature of wave motion will be asymptotically equivoluminal. Such examples include the segments between the intersections of the S curves with the P and PP curves which are next to each other (see Fig. 2).

To compare the present bounds, which are obtained from the solutions of the uncoupled wave systems with the existing bounds by Pao and Mindlin (1960), the dispersion curves for flexural wave propagation are considered. Figures 5 through 8

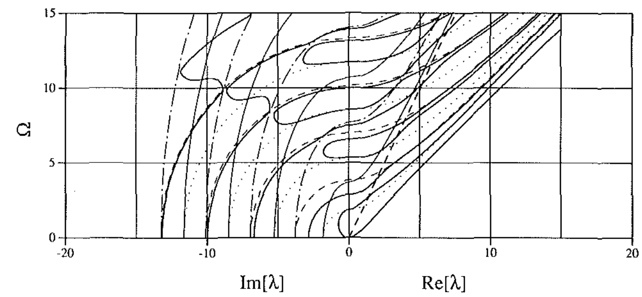

Fig. 5 The branches of Pochhammer's equation (thick solid lines) and the dispersion curves of the uncoupled wave systems for real and imaginary wave numbers for $n=1$, $\nu=1/3$. (See caption of Fig. 1 for meanings of lines.)

show the branches of Pochhammer's equation and the dispersion curves corresponding to the uncoupled wave system for $\nu=1/3$[2]. Especially for $n=1$, the intersections of the PP and T curves are the exact solutions of Pochhammer's equation. Other than this, the discussion for $n=2$ is also valid for any n, including $n=1$.

Pao and Mindlin (1960) study Pochhammer's equation directly. Since Pochhammer's equation does not have uncoupled motion at $\lambda=0$, it was difficult to generate simple bounds which satisfy the cutoff frequency equation and Pochhammer's equation at some points. Since there are no such simple bounds, the auxiliary barriers and intersectors had to be introduced to construct the bounds themselves. The equations for some of the auxiliary curves are not easy to solve, though aymptotic solutions may be used. The present bounds, however, are relatively easy to compute and can be extended in a straightforward manner to general n.

With the present bounds, the branches of Pochhammer's equations can be traced for real wave numbers. The only information required is the cutoff frequencies. The branches emanating from the cutoff frequencies that are solutions of (10*a*) can be easily traced near $\lambda=0$, because the solutions corresponding to the T curves have the same cutoff frequencies and the branches of Pochhammer's equation are asymptotic to the T curves. For the construction of the branches emanating from the cutoff frequencies which are the solutions of (10*b*), it can be noted that the slope $d\Omega/d\lambda$ at $\lambda=0$ is equal to zero, unless the cutoff frequencies governed by (10*a*) and (10*b*) coincide. Therefore, these branches can be traced by using the fact that $d\Omega/d\lambda=0$ at $\lambda=0$ and by making use of the nature of Pochhammer's equation at the intersections of the present bounds (which is explained along with Figs. 2 and 3). In addition, the fact that the branches of Pochhammer's equation do not pass through the intersections of the PP and S curves is also helpful in the construction.

Though the present discussion has been rather limited to real wave numbers, a similar analysis can be carried out for imaginary wave numbers. For instance, the points of inflections for imaginary wave numbers are also located approximately at the intersections of the P and S curves (solid and dotted lines in Fig. 1 and Fig. 5). At the intersections of the PP and T curves (long dot-dashed and dashed lines in Figs. 1, 6), two branches of Pochhammer's equation are close to each other.

The dispersion relations for other Poisson's ratios including $\nu=1/2$ have been studied, and similar results as in the previous examples are obtained. For $\nu=1/2$ and $n=1$, the dispersion relations for large real wave numbers are shown in Fig. 9. In this case, the $h=0$ line becomes the Ω axis so that the disper-

[1]For $n=1$, the line $h=0$ can be interpreted as a solution of $dJ_n(kr)/dr|_{r=1}=0$.

[2]The lines used in Figs. 5, 6, 7, and 8 have the same meanings as in Figs. 8. 1, 2, 3, and 4, respectively.

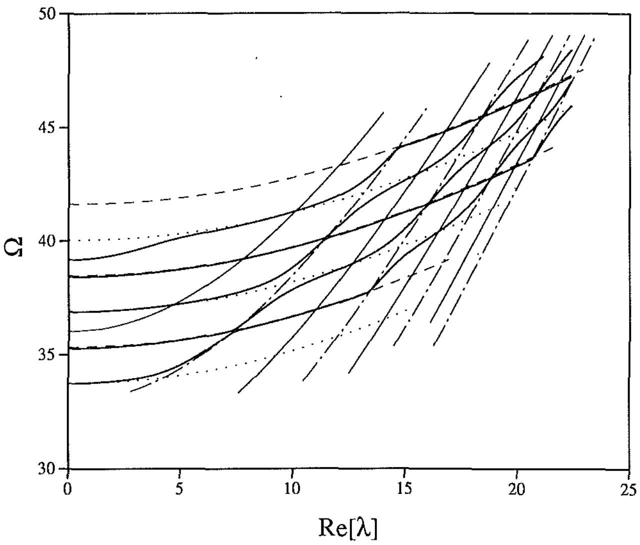

Fig. 6 Intricate nature of the branches of Pochhammer's equation for a relatively high frequency range for $n = 1$, $\nu = 1/3$. See caption of Fig. 2 for meanings of lines.

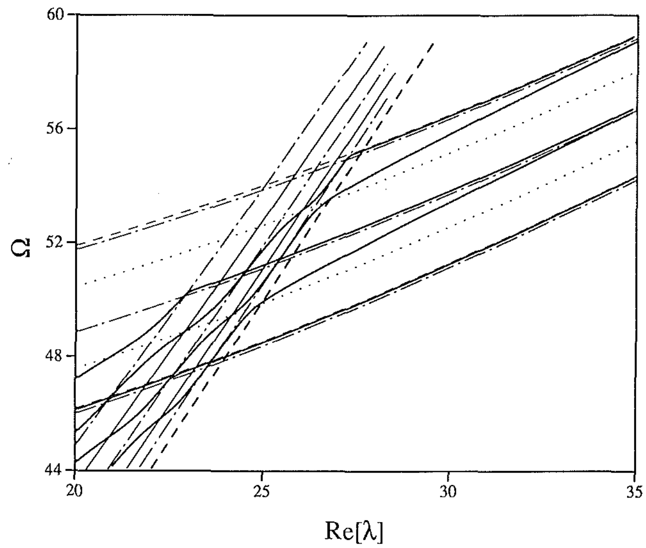

Fig. 8 The branches of Pochhammer's equation (thick solid lines) near the $h = 0$ line (thick dashed) for $n = 1$, $\nu = 1/3$. See caption of Fig. 4 for meanings of lines.

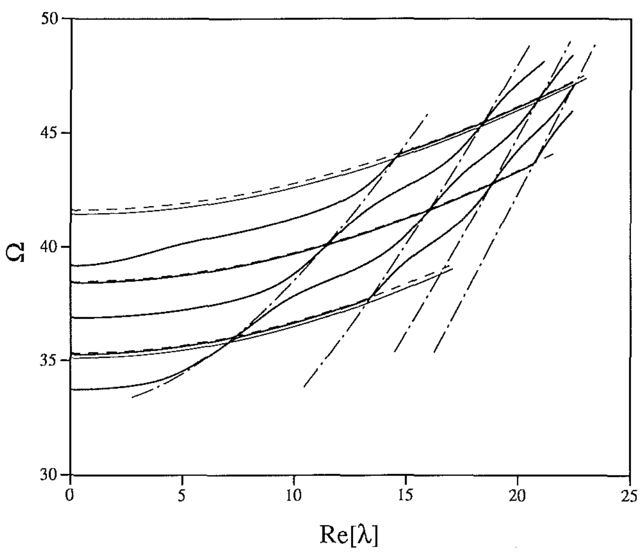

Fig. 7 The asymptotic solutions of the branches of Pochhammer's equation (thick solid lines) at some special points for $n = 1$, $\nu = 1/3$. See caption of Fig. 3 for meanings of lines.

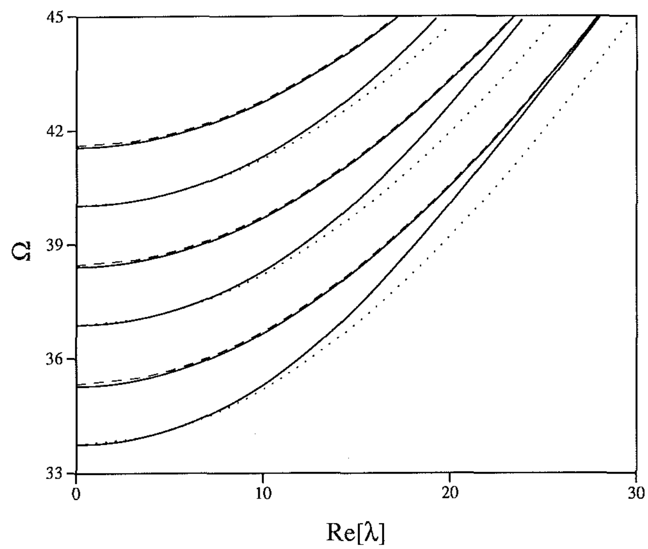

Fig. 9 The branches of Pochhammer's equation (thick solid lines) for $n = 1$ and $\nu = 1/2$ (incompressible materials). The dotted lines ($J_n'(k) = 0$) and dashed lines ($J_n(k) = 0$) are the dispersion curves of the uncoupled wave systems.

sion relations in Fig. 9 look like those in Sectors 1 and 2 of Fig. 4, and Fig. 8.

5 Conclusions

Wave propagation in an isotropic solid circular cylinder has been investigated. The asymptotic analysis of Pochhammer's frequency equation for a traction-free cylindrical surface condition is carried out. The wave motion is asymptotically equivoluminal for large imaginary wave numbers, and is characterized by coupled dilatation and shear.

The present study shows that there exist uncoupled wave systems for two sets of appropriate boundary conditions. These uncoupled wave systems correspond to purely dilatational or equivoluminal deformations, and the solutions of the uncoupled system provide proper, easily constructed bounds for Pochhammer's equation. The bounds can be used to trace the branches of Pochhammer's equation for any n, which may be otherwise difficult to obtain numerically in general.

Acknowledgment

This work was partially supported by Grant 2R01-NS12086 from the National Institute of Neurological and Communicative Disorders and Strokes. The author is very grateful to Prof. C. R. Steele for his encouragement and advice throughout the investigation. He also wishes to thank Dr. C. D. Balch, Prof. Y.-H. Pao, and the reviewers for their comments on the earlier version of the manuscript.

References

Achenbach, J. D., 1975, *Wave Propagation in Elastic Solids*, North-Holland Publishing Co., Amsterdam.

Armenenàkas, A. E., Gazis, D. C., and Herrmann, G., 1969, *Free Vibrations of Circular Cylindrical Shells*, Pergamon Press, Oxford.

Bancroft, D., 1941, "The Velocity of Longitudinal Waves in Cylindrical Bars," *Physical Review*, Vol. 59, pp. 588–593.

Holden, A. N., 1951, "Longitudinal Modes of Elastic Waves in Isotropic Cylinders and Slabs," *Bell System Technical Journal*, Vol. 30, pp. 956–969.

Huang, K. H., and Dong, S. B., 1984, "Propagating Waves and Edge Vibrations in Anisotropic Composite Cylinders," *J. Sound Vibration*, Vol. 96, pp. 8–19.

Hudson, G. E., 1943, "Dispersion of Elastic Waves in Solid Circular Cylinders," *Physical Review*, Vol. 63, pp. 46–51.

Kim, Y. Y., and Steele, C. R., 1989, "End Effects and Time-Harmonic Wave Propagation in a Semi-Infinite Solid Cylinder," ASME JOURNAL OF APPLIED MECHANICS, Vol. 56, pp. 334–346.

Kumar, R., 1972, "The Dispersion Relation of Flexural Waves in an Elastic Circular Cylinder," ASME JOURNAL OF APPLIED MECHANICS, Vol. 39, pp. 817–819.

McNiven, H. D., and McCoy, J. J., 1974, "Vibrations and Wave Propagation in Rods," *R. D. Mindlin and Applied Mechanics*, G. Herrmann, ed., Pergamon Press, New York, pp. 197–226.

Miklowitz, J., 1978, *The Theory of Elastic Waves and Waveguides*, North-Holland Publishing Co., Amsterdam.

Mindlin, R. D., 1951, "Thickness-Shear and Flexural Vibrations of Crystal Plates," *Journal of Applied Physics*, Vol. 22, pp. 316–323.

Mindlin, R. D., 1960, "Waves and Vibrations in Isotropic, Elastic Plates," *Structural Mechanics*, J. Goodier, and N. Hoff, eds., Pergamon Press, New York, pp. 199–232.

Nelson, R. B., Dong, S. B., and Kalra, R. D., 1971, "Vibrations and Waves in Laminated Orthotropic Circular Cylinders," *J. Sound Vibration*, Vol. 18, pp. 429–444.

Onoe, M., McNiven, H. D., and Mindlin, R. D., 1962, "Dispersion of Axially Symmetric Waves in Elastic Rods," ASME JOURNAL OF APPLIED MECHANICS, Vol. 29, pp. 729–734.

Pao, Y.-H., 1962, "The Dispersion of Flexural Waves in an Elastic, Circular Cylinder—Part 2," ASME JOURNAL OF APPLIED MECHANICS, Vol. 29, pp. 61–64.

Pao, Y.-H., 1988, private communication.

Pao, Y.-H., and Mindlin, R. D., 1960, "Dispersion of Flexural Waves in an Elastic, Circular Cylinder," ASME JOURNAL OF APPLIED MECHANICS, Vol. 27, pp. 513–520.

Pochhammer, L., 1876, "Ueber die Fortpflanzungsgeschwindigkeiten kleinder Schwingungen in einem unbegrenzten isotropen Kreiscylinder," *J. für reine und angewandte Mathmatik*, Vol. 81, pp. 324–336.

Shen, S.-Q., 1988, "Transient Elastic Waves in a Circular Cylinder," Ph.D. Thesis, Cornell University, Ithaca, New York.

Zemanek, J., 1972, "An Experimental and Theoretical Investigation of Elastic Wave Propagation in a Cylinder," *J. Acoust. Soc. Am.*, Vol. 51, pp. 265–283.

Bending of Simply-Supported Elliptic Plates: B.P.M. Solutions With Second-Order Derivative Boundary Conditions[1]

R. Parnes[2]
Laboratoire de Mécanique des Solides,
Ecole Polytechnique,
91128 Palaiseau, France
Mem. ASME

A higher-order boundary perturbation method (B.P.M.) is formulated to treat a class of problems defined in an elliptic domain with associated boundary conditions expressed in terms of second-order derivatives. The method is applied to study a simply-supported elliptic plate subjected to a central lateral point load. The accuracy is investigated and the B.P.M. solution is found to yield highly accurate results for moderately elliptic domains.

1 Introduction

In this study, we obtain by means of a Boundary Perturbation Method, the bending solution to the problem of a simply-supported elliptic plate subjected to a lateral point load.

Although the Boundary Perturbation Method (B.P.M.) has existed in the literature for some time, a higher-order B.P.M. was only recently developed, in general, for the treatment of a variety of problems encountered in solid mechanics. Parnes and Beltzer (1986a) formulated the method to treat problems defined within an elliptic domain, as well as those in a circular domain, which contain an eccentric source; general expressions required to study these classes of problems were derived. The method was applied by Parnes and Beltzer (1986b) to problems which do not yield tractable solutions by standard analytic methods. The accuracy of the B.P.M. was investigated by Parnes (1987) where it was found that the method yields upper bounds to the stiffness of elastostatic system. In all of the aforementioned works, *the boundary conditions considered were of the Dirichlet or Neumann type.*

In this paper, we first extend the method to permit the treatment of problems defined in an elliptic domain with associated boundary conditions expressed in terms of second-order derivatives. Using the methodology of Parnes and Beltzer (1986a) we derive, in Section 2, the general expressions necessary to treat this class of problems.

The resulting relations are applied in Section 3 to investigate a simply-supported elliptic plate subjected to a transverse point force at the center, a classical problem which appears not to have been solved heretofore. The corresponding simpler problem of the plate subjected to a uniformly distributed load was treated by Galerkin (1923) who, making use of elliptic coordinates, derived an exact solution. However, while exact, the solution possesses the disadvantage of masking the effects of ellipticity: Such effects can only be seen from a numerical evaluation of the final relations expressed in terms of the elliptic coordinates. On the other hand, the B.P.M. solution to the present problem has the distinct advantage of yielding simple analytic expressions in terms of the given ellipticity. These are readily evaluated in Section 4 where displacement and moments are presented as a function of the ellipticity.

Estimates of the accuracy and domain of validity of the B.P.M. solutions are established in Section 5 based on a comparison of the B.P.M. solution for a simply-supported ellipitic plate under uniform load (as derived in the Appendix) with the exact solution given by Galerkin (1923). The B.P.M. is seen to yield very accurate results even for domains defined by moderate ellipticities. Finally, a comparison of the two solutions confirms that the B.P.M. yields an upper bound to the stiffness of elastostatic system.

2 General Expressions

***(a)* The Perturbation Scheme.** Consider a body defined within an ellipse C_e having semi-major and minor radii, a and b, respectively. The ellipticity ϵ is given by the relation

$$\epsilon = a/b - 1, \quad b < a. \tag{1}$$

The governing field equation is then

$$L[f(r,\psi)] = \phi(r,\psi), \tag{2}$$

[1]Part of this work was performed while the author was Visiting Professor at the Laboratoire de Mécanique Théorique, Université Pierre et Marie Curie, Paris VI.

[2]Permanent Address: Department of Solid Mechanics, Materials and Structures, Faculty of Engineering, Tel Aviv University, 69978 Ramat-Aviv, Israel.

Contributed by the Applied Mechanics Division of The American Society of Mechanical Engineers for presentation at the Joint ASCE/ASME Applied Mechanics, Biomechanics, and Fluids Engineering Conference, San Diego, Calif., July 9 to 12, 1989.

Discussion of this paper should be addressed to the Editorial Department, ASME, United Engineering Center, 345 East 47th Street, New York, N.Y. 10017, and will be accepted until two months after final publication of the paper itself in the Journal of Applied Mechanics. Manuscript received by ASME Applied Mechanics Divisions, February 3, 1987; final revision, November 19, 1987.

Paper No. 89-APM-39.

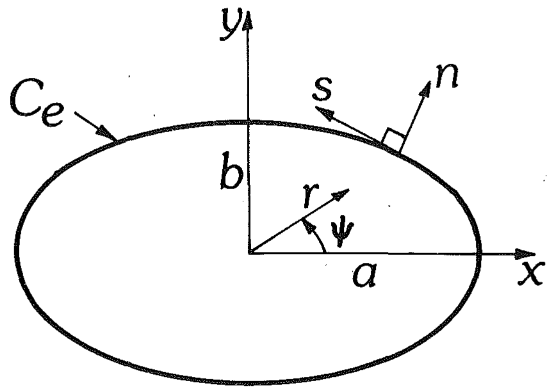

Fig. 1 Geometry of problem

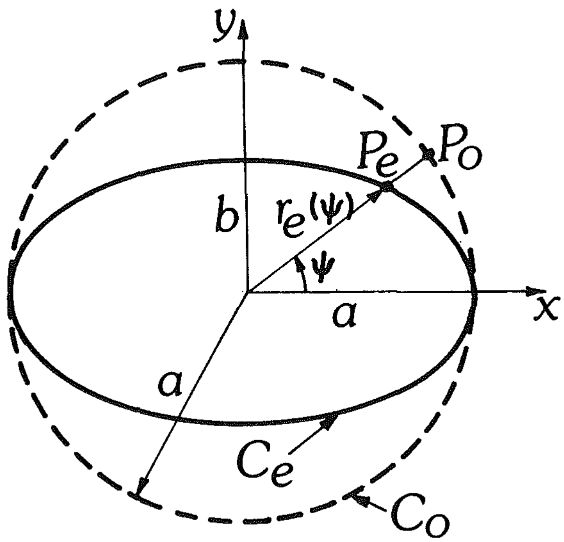

Fig. 2 Perturbed geometry

(where r,ψ is a polar coordinate system, L a linear differential operator, and $\phi(r,\psi)$ a given function), to which there corresponds a set of boundary conditions on C_e,

$$f(r,\psi)\,|_{C_e} = f_e(r,\psi), \tag{3a}$$

and

$$B_2[f(r,\psi)]\,|_{C_e} = 0. \tag{3b}$$

In the aforementioned equation, $f_e(r,\psi)$ is a given function on C_e and B_2 represents linear boundary conditions containing combinations of derivatives of second order, i.e.,

$$B_2[f(r,\psi)]\,|_{C_e} = B_2\left[\frac{\partial^2 f}{\partial n^2}, \frac{\partial^2 f}{\partial s^2}\right], \tag{4}$$

where n and s denote normal and tangential directions, respectively, along C_e (Fig. 1).

If ϵ is not large, then C_e can be considered as the perturbed curve of a circumscribing circle of radius a with points P_e on C_e the mapping of P_0 on C_0 (Fig. 2). The ellipse is thus represented as a curve with varying radial distance from 0, $r_e = r_e(\psi)$; symbolically, the perturbed relation $C_0 \to C_e$ may be written as

$$a \to r_e = r_e(a,\psi,\epsilon), \tag{5}$$

with $r_e|_{\epsilon=0} = a$.

In applying the B.P.M., we assume that all functions are analytic within the domain defined by C_0. For a second-order scheme, we let

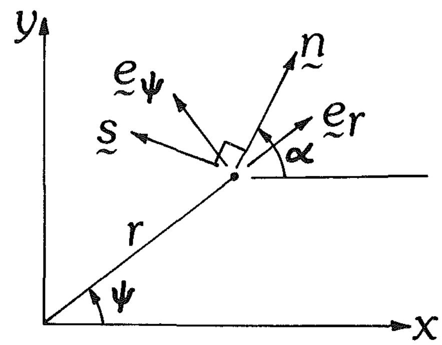

Fig. 3

$$f(r,\psi) = \sum_{j=0}^{2} \epsilon^j \overset{(j)}{f}(r,\psi). \tag{6}$$

Using the linearity property of L, equation (2) is satisified if

$$L[\overset{(0)}{f}(r,\psi)] = \phi(r,\psi) \tag{7a}$$

$$L[\overset{(j)}{f}(r,\psi)] = 0, \quad j = 1,2. \tag{7b}$$

We now consider the boundary condition, (3). Since the points P_0 and P_e possess the same ψ coordinate, the original boundary conditions on $f(r,\psi)|_{C_e}$ and $B_2[f]|_{C_e}$ at P_e can be expressed in terms of combinations of $f(r,\psi)|_{C_0}$ and $B_2[f]|_{C_0}$ on the fictitious curve C_0 by means of a Taylor series expansion in powers of $(a - r_e)$ which, in turn, are expressed as powers of ϵ for any ψ. Thus

$$f|_{C_e} = f|_{C_0} + \epsilon B_0^{(1)}[f]|_{C_0} + \epsilon^2 B_0^{(2)}[f]|_{C_0} \tag{8a}$$

and

$$B_2[f]\,|_{C_e} = B_2^{(0)}|_{C_0} + \epsilon B_2^{(1)}|_{C_0} + \epsilon^2 B_2^{(2)}|_{C_0}, \tag{8b}$$

where

$$B_i^{(j)}|_{C_0} = B_i^{(j)}[f^{(k)}(a,\psi)];\ i = 0,2;\ j = 1,2;\ k = 0,1 \tag{9}$$

are, in general, ψ-dependent coefficients evaluated on C_0, i.e., at $r = a$.

Since (8a) is valid for arbitrary ϵ, the boundary conditions, (3), are satisfied by letting

$$f|_{C_0} = f_e, \quad B_2^{(0)}|_{C_0} = 0 \tag{10}$$

and by setting

$$\left.\begin{aligned} B_0^{(j)}[\overset{(k)}{f}(a,\psi)] = 0 \\ B_2^{(j)}[\overset{(k)}{f}(a,\psi)] = 0 \end{aligned}\right\} j > 0. \tag{11}$$

We turn now to the derivation of the explicit expressions required for the evaluation of the $B_i^{(j)}$ coefficients.

(b) Geometric Relations and Perturbation Expressions. We denote by **n** and **s** the respective unit vectors in two arbitrary orthogonal directions (n, s). Furthermore, let $\mathbf{e}_r$ and $\mathbf{e}_\psi$ denote the radial and circumferential unit vectors in the polar coordinate system (r, ψ) at any point (Fig. 3). Then clearly

$$\mathbf{n} = \cos(\alpha - \psi)\mathbf{e}_r + \sin(\alpha - \psi)\mathbf{e}_\psi \tag{12a}$$

$$\mathbf{s} = -\sin(\alpha - \psi)\mathbf{e}_r + \cos(\alpha - \psi)\mathbf{e}_\psi \tag{12b}$$

where α represents the inclination of **n** with respect to the x-axis. For the polar coordinate system, with

$$\nabla = \mathbf{e}_r \frac{\partial}{\partial r} + \mathbf{e}_\psi \frac{1}{r}\frac{\partial}{\partial \psi}, \tag{13}$$

the dyadic $\nabla\nabla f$ is given by

$$\nabla\nabla f = \mathbf{e}_r\mathbf{e}_r f_{,rr} + \left(\frac{1}{r} f_{,r\psi} - \frac{1}{r^2} f_{,\psi}\right)(\mathbf{e}_r\mathbf{e}_\psi + \mathbf{e}_\psi\mathbf{e}_r) + \left(\frac{1}{r} f_{,r} + \frac{1}{r^2} f_{,\psi\psi}\right)\mathbf{e}_\psi\mathbf{e}_\psi. \qquad (14)^3$$

Noting that

$$\frac{\partial^2 f}{\partial n^2} = \mathbf{n}\cdot(\nabla\nabla f)\cdot\mathbf{n}, \quad \frac{\partial^2 f}{\partial s^2} = \mathbf{s}\cdot(\nabla\nabla f)\cdot\mathbf{s}, \qquad (15a\text{-}b)$$

and substituting (12)–(14) in (15), we obtain

$$\frac{\partial^2 f}{\partial n^2} = \cos^2(\alpha-\psi) f_{,rr} + 2\cos(\alpha-\psi)\sin(\alpha-\psi) \times \left(\frac{1}{r} f_{,r\psi} - \frac{1}{r^2} f_{,\psi}\right) + \sin^2(\alpha-\psi)\left(\frac{1}{r} f_{,r} + \frac{1}{r^2} f_{,\psi\psi}\right) \qquad (16a)$$

$$\frac{\partial^2 f}{\partial s^2} = \sin^2(\alpha-\psi) f_{,rr} - 2\cos(\alpha-\psi)\sin(\alpha-\psi) \times \left(\frac{1}{r} f_{,r\psi} - \frac{1}{r^2} f_{,\psi}\right) + \cos^2(\alpha-\psi)\left(\frac{1}{r} f_{,r} + \frac{1}{r^2} f_{,\psi\psi}\right). \qquad (16b)$$

Now, it was shown by Parnes and Beltzer (1986a) that the radial distance $r_e(\psi)$ to any point P_e on the ellipse C_e is given exactly by

$$r_e^2 = a^2[1 + (2\epsilon + \epsilon^2)\sin^2\psi]^{-1} \qquad (17a)$$

and that, upon expanding in powers of ϵ and retaining terms up to $0(\epsilon^2)$,

$$r_e = a\left[1 - \epsilon\sin^2\psi + \frac{\epsilon^2}{2}\sin^2\psi(2\sin^2\psi - \cos^2\psi)\right] + 0(\epsilon^3) \qquad (17b)$$

so that

$$(r_e - a)^2 = a^2\sin^4\psi + 0(\epsilon^3) \qquad (17c)$$

and

$$\frac{1}{r_e} = \frac{1}{a}\left(1 + \epsilon\sin^2\psi + \frac{\epsilon^2}{8}\sin^2 2\psi\right) + 0(\epsilon^3). \qquad (17d)$$

Further, with n the normal to C_e, we have for a given point on C_e,

$$\cos(\alpha-\psi) = 1 - \frac{1}{2}(\sin 2\psi)^2\epsilon^2 + 0(\epsilon^3) \qquad (18a)$$

$$\sin(\alpha-\psi) = \sin\psi\cos\psi[2\epsilon + (\cos^2\psi - 3\sin^2\psi)\epsilon^2] + 0(\epsilon^3). \qquad (18b)$$

Substituting the appropriate equations, (17)–(18) in (15), performing the expansions and again retaining terms up to power ϵ^2, yields

$$\left.\frac{\partial^2 f}{\partial n^2}\right|_{C_e} = f_{,rr} + \frac{2\sin 2\psi}{a}\left[f_{,\psi r} - \frac{f_{,\psi}}{a}\right]\epsilon + \left\{(\sin 2\psi)^2\left[-f_{,rr} + \frac{1}{a} f_{,r} + \frac{f_{,\psi\psi}}{a}\right] + \frac{\sin 4\psi}{2a} f_{,\psi r} - \frac{\sin 2\psi}{a^2} f_{,\psi}\right\}\epsilon^2 \qquad (19a)$$

$$\left.\frac{\partial^2 f}{\partial s^2}\right|_{C_e} = \frac{1}{a} f_{,r} + \frac{f_{,\psi\psi}}{a^2} + \left\{\frac{\sin^2\psi}{a}\left[\frac{2}{a} f_{,\psi\psi} + f_{,r}\right] + \frac{2}{a}\sin 2\psi\left[\frac{f_{,\psi}}{a} - f_{,\psi r}\right]\right\}\epsilon + \left\{\frac{\sin^2\psi}{a^2}(1 - 4\cos^2\psi) f_{,\psi\psi} + \frac{\sin 2\psi}{a}\left[\frac{1}{a} f_{,\psi} - \cos 2\psi f_{,r\psi}\right] + (\sin 2\psi)^2\left[f_{,rr} - \frac{7}{8a} f_{,r}\right]\right\}\epsilon^2. \qquad (19b)$$

It is noted that the aforementioned expressions are evaluated at points along the curve C_e. Now, as discussed previously, all quantities on C_e can be expressed in terms of corresponding quantities at the mapped points P_0 and C_0 by means of a Taylor expansion in powers of $(r-a)$. For any given function g (representing f, $f_{,r}$, $f_{,\psi}$, etc. . .) we have, from Parnes and Beltzer (1986a):

$$g(r_e,\psi) = g_a - (a\sin^2\psi g_{a,r})\epsilon + \frac{a}{2}\sin^2\psi[(2\sin^2\psi - \cos^2\psi)g_{a,r} + a\sin^2\psi g_{a,rr}]\epsilon^2 + 0(\epsilon^3) \qquad (20)$$

where $g_a \equiv g(a,\psi)$, etc. . .

Expressing $f(r,\psi)$ in terms of the perturbation functions $\overset{(j)}{f}(r,\psi)$ [6] and expanding the right-hand side of (19) according to (20), upon collecting in powers of ϵ and retaining terms up to order ϵ^2, the following expressions are obtained:

$$\left.\frac{\partial^2 f}{\partial n^2}\right|_{C_e} = \left.f^{(0)}_{,rr}\right|_{C_0} + \left\{\left.f^{(1)}_{,rr}\right|_{C_0} + {}_{nn}\Psi_1^{(0)}\right\}\epsilon + \left\{\left.f^{(2)}_{,rr}\right|_{C_0} + {}_{nn}\Psi_1^{(1)} + {}_{nn}\Psi_2^{(0)}\right\}\epsilon^2 \qquad (21)$$

$$\left.\frac{\partial^2 f}{\partial s^2}\right|_{C_e} = \left.\Delta^{(0)}\right|_{C_0} + \left\{\left.\Delta^{(1)}\right|_{C_0} + {}_{ss}\Psi_1^{(0)}\right\}\epsilon + \left\{\left.\Delta^{(2)}\right|_{C_0} + {}_{ss}\Psi_1^{(1)} + {}_{ss}\Psi_2^{(0)}\right\}\epsilon^2. \qquad (22)$$

In equations (21) and (22)

$$\Delta^{(j)} = \frac{1}{a}\left[f_{,r} + \frac{1}{a} f_{,\psi\psi}\right]^{(j)} \qquad (23)$$

$${}_{nn}\Psi_1^{(j)} = \left[-a\sin^2\psi f_{,rrr} + \frac{2\sin 2\psi}{a}\left(f_{,\psi r} - \frac{f_{,\psi}}{a}\right)\right]^{(j)} \qquad (24a)$$

$${}_{nn}\Psi_2^{(j)} = \left[\sin^2\psi\left\{a\left(\sin^2\psi - \frac{1}{2}\cos^2\psi\right) f_{,rrr} + \frac{a^2}{2}\sin^2\psi f_{,rrrr} - 2\sin 2\psi f_{,\psi rr}\right\} + (\sin 2\psi)^2\left(-f_{,rr} + \frac{1}{a} f_{,r} + \frac{1}{a^2} f_{,\psi\psi}\right) + \frac{\sin 2\psi}{a}\left(f_{,\psi r} - \frac{f_{,\psi}}{a}\right)\right]^{(j)} \qquad (24b)$$

$${}_{ss}\Psi_1^{(j)} = \frac{1}{a^2}\left[\sin^2\psi(af_{,r} + 2f_{,\psi\psi} - af_{,r\psi\psi} - a^2 f_{,rr}) + 2\sin 2\psi(f_{,\psi} - af_{,r\psi})\right]^{(j)} \qquad (25a)$$

$${}_{ss}\Psi_2^{(j)} = \left[\sin^2\psi\left\{2\sin 2\psi f_{,rr\psi} - \frac{1}{2a}(1 + \sin^2\psi) f_{,r\psi\psi} + \frac{\sin^2\psi}{2}(f_{,rr\psi\psi} + af_{,rrr}) + \frac{1}{a^2}(1 - 4\cos^2\psi) f_{,\psi\psi}\right\} + \frac{\sin 2\psi}{2a^2}\left\{2f_{,\psi} + \frac{7a}{4}\sin 2\psi(af_{,rr} - f_{,r}) - 2af_{,r\psi}\right\}\right]^{(j)}. \qquad (25b)$$

Bracketed terms, $[\ldots]^{(j)}$, denote that the combination of

[3]Here, and in all subsequent expressions, derivatives with respect to a variable are denoted by a subscript preceded by a comma.

functions and derivatives contained within refer to the function $\overset{(j)}{f}(a,\psi)$.

For the boundary conditions on f, expressed in the form of (3a), equivalent expressions for the functions in terms of $f^{(j)}$ were derived by Parnes and Beltzer (1986a). For completeness, they are repeated here; viz

$$f|_{C_e} = f|_{C_0} + \left\{ f^{(1)}\Big|_{C_0} + {}_0\Psi_1^{(0)} \right\}\epsilon + \left\{ f^{(2)}\Big|_{C_0} + {}_0\Psi_1^{(1)} + {}_0\Psi_2^{(0)} \right\}\epsilon^2 \tag{26}$$

where

$${}_0\Psi_1^{(j)} = -a\sin^2\psi f_{,r}^{(j)} \tag{27a}$$

$${}_0\Psi_2^{(j)} = \frac{a}{2}\sin^2\psi\left[(2\sin^2\psi - \cos^2\psi)f_{,r} + a\sin^2\psi f_{,rr}\right]^{(j)}. \tag{27b}$$

We observe finally that all quantities appearing on the right-hand side of (23)–(27) are evaluated at points $P_0(a,\psi)$ of the circle C_0.

Using (21) and (26) one may treat, by the B.P.M., any problem in an elliptic domain which is subject to boundary conditions up to second order.

In the following section we apply the relations developed above to obtain the B.P.M. solution for a simply-supported elliptic plate subjected to a concentrated force at the center.

3 B.P.M. Solution for a Simply-Supported Elliptic Plate Subjected to a Lateral Force at the Center

(a) Formulation of the Perturbation Solution. We consider an elastic elliptic plate of thickness h with semi-major and minor radii a and b, respectively, and simply-supported along the boundary C_e. The material constants of the plate are E, the modulus of elasticity and ν, Poisson's ratio. The plate is subjected at point 0 to a lateral force P acting normal to the plane of the plate.

Denoting the transverse displacement by $W(r,\psi)$, the governing equation is

$$\nabla^4 W(r,\psi) = \frac{\phi(r)}{D} \tag{28}$$

where

$$\phi(r) = P\,\delta(r) \tag{29a}$$

$$D = \frac{E\,h^3}{12(1-\nu^2)} \tag{29b}$$

and where ∇^4 is the biharmonic operator and $\delta(r)$ the Dirac-delta function.

The appropriate boundary conditions are then

$$W|_{C_e} = 0 \tag{30a}$$

$$\frac{\partial^2 W}{\partial n^2} + \nu\frac{\partial^2 W}{\partial s^2}\Big|_{C_e} = 0 \tag{30b}$$

where n and s denote the normal and tangential directions, respectively, to C_e.

Following the development of the previous section, we postulate $W(r,\psi)$ to be of the form given by (6) where $W \equiv f$ here and following and also note that $L \equiv D\nabla^4$ of the previous section.

Using (26), the boundary condition corresponding to (30a) becomes

$$W^{(0)} + \{W^{(1)} + {}_0\Psi_1^{(0)}\}\epsilon + \{W^{(2)} + {}_0\Psi_1^{(1)} + {}_0\Psi_2^{(0)}\}\epsilon^2 = 0. \tag{31a}$$

Similarly, the boundary condition given by (30b) becomes, upon using (21)–(22),

$$\left\{W_{,rr}^{(0)} + \nu\Delta^{(0)}\right\} + \left\{\left[W_{,rr}^{(1)} + \nu\Delta^{(1)}\right] + \left[{}_{nn}\Psi_1^{(0)} + \nu_{ss}\Psi_1^{(0)}\right]\right\}\epsilon$$
$$+ \left\{\left[W_{,rr}^{(2)} + \nu\Delta^{(2)}\right] + \left[{}_{nn}\Psi_1^{(1)} + \nu_{ss}\Psi_1^{(1)}\right]\right.$$
$$\left. + \left[{}_{nn}\Psi_2^{(0)} + \nu_{ss}\Psi_2^{(0)}\right]\right\}\epsilon^2 = 0. \tag{31b}$$

We observe, in passing, that the quantities in brackets, $\{\ldots\}$, corresponding to the coefficients $B_0^{(j)}$ and $B_2^{(j)}$ given in (9), must vanish for all ϵ.

(b) The $j=0$ Case

Following the previous section, $W^{(0)}$ must satisfy the equation

$$\nabla^4 \overset{(0)}{W}(r) = \frac{P\,\delta(r)}{D} \tag{32}$$

subject to the boundary conditions

$$W_0^{(0)}|_{C_0} = 0, \quad W_{,rr}^{(0)} + \frac{\nu}{a}W_{,r}^{(0)}\Big|_{C_0} = 0, \tag{33a–b}$$

which, recognized as the axisymmetric case of a simply-supported circular plate subjected to a central load, has the known solutions (Timoshenko and Woinowsky-Krieger, 1959):

$$\overset{(0)}{W}(r) = A\left[\frac{3+\nu}{1+\nu}(a^2-r^2) + 2r^2\log\left(\frac{r}{a}\right)\right], \tag{34a}$$

where

$$A = P/16\pi D. \tag{34b}$$

(c) The Perturbed Solutions, $j>0$. According to (7b), $\overset{(j)}{W}(r,\psi)$ must satisfy the governing equation

$$\nabla^4 W^{(j)} = 0, \quad j=1,2 \tag{35}$$

subject to the corresponding boundary conditions expressed as the vanishing of the coefficients of ϵ^j ($j=1$ and 2) in (31).

Appropriate solutions to the biharmonic equation are (Prescott, 1961):

$$W^{(j)} = C_0 + C_1 r^2 + (\alpha_n r^n + \beta_n r^{n+2})\cos n\psi \tag{36}$$

where C_0, C_1, α_n, and β_n ($n=1,2,3,\ldots$) are constants to be evaluated from the boundary conditions.

We now proceed to solve sequentially the set of equations using the given boundary conditions.

Case j = *1.* Substituting $W^{(0)}$, given by (34), in the boundary conditions,

$$W^{(1)}|_{C_0} = -{}_0\Psi_1^{(0)} \tag{37a}$$

$$W^{(1)} + \nu\Delta^{(1)}|_{C_0} = -({}_{nn}\Psi_1^{(0)} + {}_{ss}\Psi_1^{(0)}) \tag{37b}$$

and performing the required operations, we obtain explicitly

$$W_{,rr}^{(1)}(a,\psi) = -\frac{2Aa^2}{1+\nu}(1-\cos 2\psi) \tag{38a}$$

$$W_{,rr}^{(1)}(a,\psi) + \nu\Delta^{(1)}(a,\psi) = 2A(1+\nu)(1-\cos 2\psi). \tag{38b}$$

From (38), it is clear that the constants of (36), $\alpha_n = \beta_n = 0$ for $n \neq 2$; the remaining set, (C_0, C_1) and (α_2, β_2) are immediately determined and lead to the following expression for $W^{(1)}$:

$$\overset{(1)}{W}(r,\psi) = Aa^2\left\{-\frac{3+\nu}{1+\nu} + \rho^2 + \frac{1}{(1+\nu)(5+\nu)}\right.$$
$$\left.\times[(\nu^2+2\nu+13)\rho^2 - (\nu^2+3)\rho^4]\cos 2\psi\right\} \tag{39a}$$

where

$$\rho = \frac{r}{a} \tag{39b}$$

is the nondimensional radial coordinate.

Case j = 2. The appropriate boundary conditions on $W^{(2)}$,

$$W^{(2)}|_{C_0} = -({}_0\Psi_1^{(1)} + {}_0\Psi_2^{(0)}) \tag{40a}$$

$$W_{,rr}^{(2)} + \nu\Delta^{(2)}|_{C_0} = -({}_{nn}\Psi_1^{(1)} + \nu_{ss}\Psi_1^{(1)}) - ({}_{nn}\Psi_2^{(0)} + \nu_{ss}\Psi_2^{(0)}), \tag{40b}$$

obtained similarly by substituting the known solutions for $W^{(0)}$ and $W^{(1)}$, yield the explicit conditions

$$\overset{(2)}{W}(a,\psi) = \Gamma\{(3\nu^2 + 10\nu + 15) - 4(\nu^2 + \nu + 4)\cos 2\psi + (\nu^2 - 6\nu + 1)\cos 4\psi\} \tag{41a}$$

$$W_{,rr}^{(2)}(a,\psi) + \nu\Delta^{(2)}(a,\psi) = \Gamma\{-(28\nu^3 + 2\nu^2 + 55\nu - 78) + 2(18\nu^3 - 42\nu^2 + 72\nu - 62)\cos 2\psi - (8\nu^3 - 86\nu^2 + 99\nu - 46)\cos 4\psi\} \tag{41b}$$

where

$$\Gamma = A[4(1-\nu)(5+\nu)]^{-1}. \tag{41c}$$

The constants of (36), upon setting $\alpha_n = \beta_n = 0$, $n \neq 2$ or 4, are then readily evaluated. Omitting all algebraic details, the expression for $W^{(2)}$ becomes

$$W^{(2)}(r,\psi) = \frac{Aa^2}{4(1+\nu)(5+\nu)}\left\{\frac{1}{2(1+\nu)}(\gamma_0 + \bar{\gamma}_0\rho^2) + \frac{\rho^2}{5+\nu}(\gamma_1 + \bar{\gamma}_1\rho^2)\cos 2\psi + \frac{\rho^4}{2(9+\nu)}(\gamma_2 + \bar{\gamma}_2\rho^2)\cos 4\psi\right\} \tag{42}$$

where

$$\gamma_0 = 34\,\nu^3 + 28\,\nu^2 + 105\,\nu - 48 \tag{43a}$$

$$\bar{\gamma}_0 = -(28\,\nu^3 + 2\,\nu^2 + 55\,\nu - 78) \tag{43b}$$

$$\gamma_1 = -(18\,\nu^3 - 18\,\nu^2 + 101\,\nu + 34) \tag{43c}$$

$$\bar{\gamma}_1 = 14\,\nu^3 - 42\,\nu^2 + 65\,\nu - 46 \tag{43d}$$

$$\gamma_2 = -(2\,\nu^3 - 4\,\nu^2 + 91\,\nu + 16) \tag{43e}$$

$$\bar{\gamma}_2 = 4\,\nu^3 + 2\,\nu^2 - 15\,\nu + 34 \tag{43f}$$

The total displacement of the plate is then, by (6),

$$W(r,\psi) = W^{(0)} + \epsilon W^{(1)} + \epsilon^2 W^{(2)} \tag{44}$$

where $W^{(j)}$ are given by (34), (37), and (42).

4 Displacements and Moments Along Principal Axes: Numerical Results

Along the principal axes, the expressions for $W^{(j)}$, $j = 1,2$, reduce to

$$\frac{DW^{(1)}}{Pa^2}\bigg|_{\psi=0,\frac{\pi}{2}} = C\{-(3+\nu)(5+\nu) + (1+\nu)(5+\nu)\rho^2 \pm [(\nu^2 + 2\nu + 13)\rho^2 - (\nu^2+3)\rho^4]\} \tag{45a}$$

$$\frac{DW^{(2)}}{Pa^2}\bigg|_{\psi=0,\frac{\pi}{2}} = \frac{C}{8}\left\{\frac{\gamma_0}{1+\nu} + \left(\frac{\bar{\gamma}_0}{1+\nu} \pm \frac{2\gamma_1}{5+\nu}\right)\rho^2 + \left(\frac{\gamma_2}{9+\nu} \pm \frac{2\bar{\gamma}_1}{5+\nu}\right)\rho^4 + \frac{\bar{\gamma}_2}{9+\nu}\rho^6\right\} \tag{45b}$$

where γ_i, $\bar{\gamma}_i$ are defined by (43) and where

$$C = [16\pi(1+\nu)(5+\nu)]^{-1}. \tag{45c}$$

The moments M_r along the principal axes, obtained from the relation,

$$M_{x,y} \equiv M_r\bigg|_{\psi=0,\frac{\pi}{2}} = -D\left[W_{,rr} + \frac{\nu}{r}\left(W_{,r} + \frac{1}{r}W_{,\psi\psi}\right)\right]\bigg|_{\psi=0,\frac{\pi}{2}} \tag{46}$$

are given by

$$M_{x,y}\bigg|_{\psi=0,\frac{\pi}{2}} = M_r^{(0)} + \epsilon M_r^{(1)} + \epsilon^2 M_r^{(2)}\bigg|_{\psi=0,\frac{\pi}{2}} \tag{47}$$

where

$$\frac{M_r^{(0)}}{P} = -\frac{1}{4\pi}(1+\nu)\log\rho \tag{48a}$$

$$M_r^{(1)}\bigg|_{\psi=0,\frac{\pi}{2}} = -\frac{1}{8\pi}\left\{(1+\nu) \pm [(1+\nu)(5+\nu)]^{-1} \times [(1-\nu)(\nu^2 + 2\nu + 13) - 6(\nu^2+3)\rho^2]\right\} \tag{48b}$$

$$\frac{M_r^{(2)}}{P}\bigg|_{\psi=0,\frac{\pi}{2}} = -\frac{1}{64\pi}(1-\nu)^{-1}(5+\nu)^{-1}\left\{\bar{\gamma}_0 \pm \frac{2(1-\nu)}{5+\nu}\gamma_1 + 6\left[\frac{(1-\nu)}{9+\nu}\gamma_2 \pm \frac{2\bar{\gamma}_1}{5+\nu}\right]\rho^2 + \frac{5(3-\nu)}{9+\nu}\bar{\gamma}_2\rho^4\right\}. \tag{48c}$$

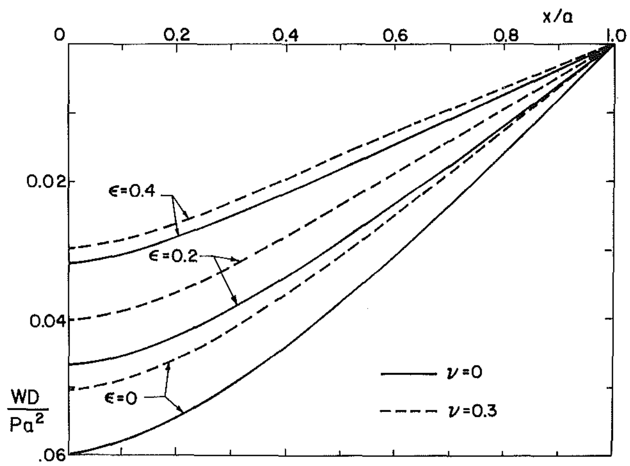

Fig. 4 Displacement distribution along x-axis

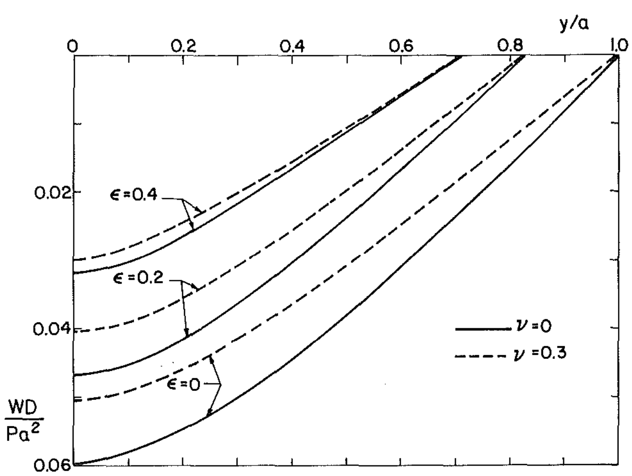

Fig. 5 Displacement distribution along y-axis

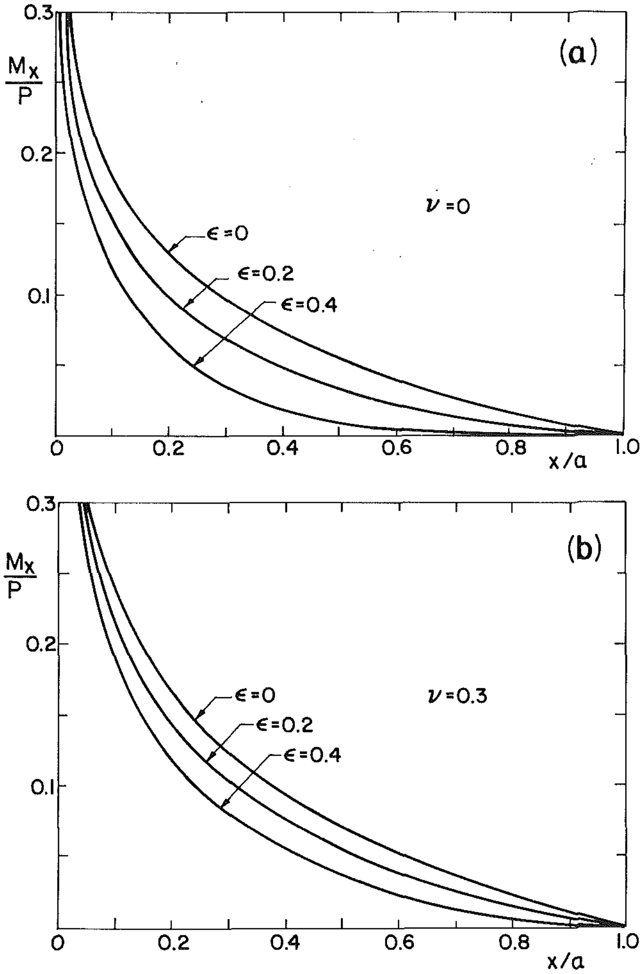

Fig. 6 Moment $M_x \equiv M_r(\psi = 0)$ along x-axis

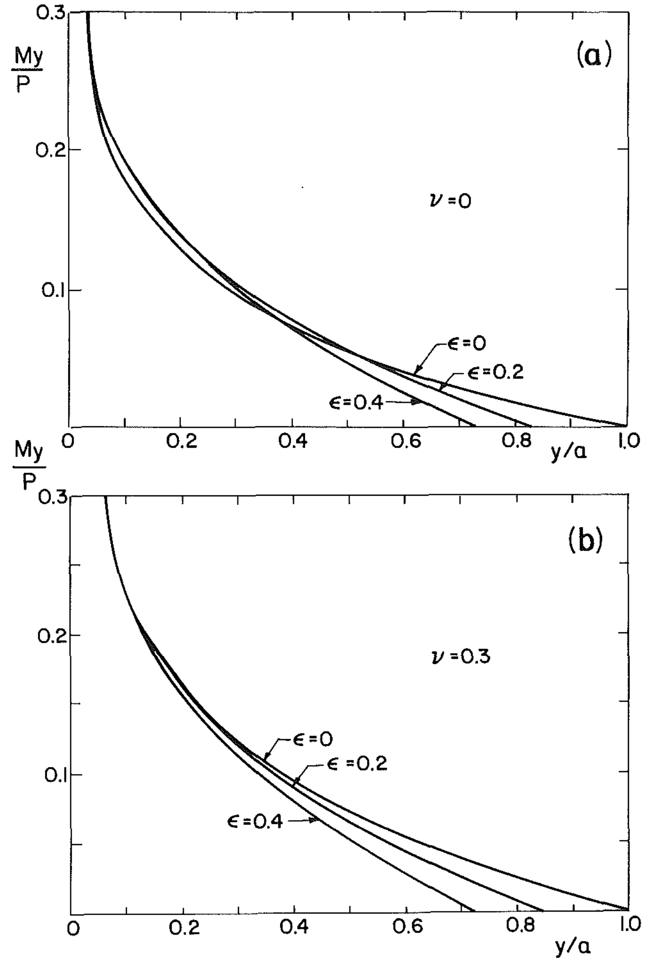

Fig. 7 Moment $M_y \equiv M_r(\psi = \pi/2)$ along y-axis

At the center point 0 ($\rho = 0$), the displacement becomes

$$\frac{DW_0}{Pa^2} = C(5+\nu)\left[(3+\nu)(1-\epsilon) + \frac{1}{2}(34\nu^3 + 28\nu^2 + 105\nu - 48)\epsilon^2\right]. \tag{49}$$

Numerical results for the nondimensional displacement distribution WD/Pa^2 along the principal axes are presented in Figs. 4 and 5 for two values of Poisson ratio, $\nu = 0$ and $\nu = 0.3$, and for several ellipticity parameters ϵ: $\epsilon = 0$, 0.2 and 0.4. We observe, in Fig. 4, that with increasing ellipticity the displacements along the x-axis are considerably reduced. Moreover, as expected, for all values of ϵ the displacements for a plate material with $\nu = 0.3$ are smaller than for $\nu = 0$. Similar behavior is observed for the displacements along the y-axis as shown in Fig. 5.

The variation of moments M_r along the x-axis is presented in Fig. 6 (a and b) as a family of curves representing several ellipticities. We observe that for larger values of ν, the moments are greater and that in all cases, for increasing ellipticity, the moments are reduced. It is noted that in the region of load application, $|x/a| \ll 1$, the moment tends to infinity as a logarithmic singularity, reflecting as in the classical case of circular plates, the representation of a point load. Similar results for the moment M_r along the y-axis are shown in Fig. 7.

The effect of ellipticity is most readily seen in Fig. 8 where the ratio $W_{0,\text{ellip.}}/W_{0,\text{circ.}}$ (representing the displacement of the center point of an elliptic plate of semi-major radius a, normalized with respect to the corresponding displacement of a circular plate of the same radius) is shown as a function of ϵ for several values of ν. We observe that the ellipticity reduces substantially the displacements. Moreover, it is seen that a given ellipticity has a greater effect upon the plate displacement for lower values of ν; e.g., for $\epsilon = 0.5$, the displacement of a plate with $\nu = 0$ is reduced by over 60 percent, while for a similar plate with $\nu = 0.5$, the reduction is 47 percent.

5 Investigation of Accuracy and Domain of Validity of BPM Solution

In order to investigate the accuracy of the B.P.M., solution, we compare the B.P.M. solution for the case of an elliptic plate subjected to a uniformly distributed load q (obtained in the Appendix) with numerical results presented by Galerkin (1923) based on his exact analytic solution.

The displacements at the center, W_0, calculated from ($A8$) using $\nu = 0.3$, as well as those given by Galerkin, (expressed in terms of parameters used in this paper) are shown in Table 1.

Table 1

ϵ	$\frac{a}{b}$	$W/\frac{qa^2}{D}$ Galerkin	$W/\frac{qa^2}{D}$ B.P.M.	Percent Error
0	1	0.0641	0.0641	0
0.1	1.1	0.0519	0.0518	0.01
0.2	1.2	0.0424	0.0414	0.10
0.3	1.3	0.0343	0.0327	4.7
0.4	1.4	0.0279	0.0255	8.6
0.5	1.5	0.0228	0.0199	12.7

Table 2

ϵ	$\frac{a}{b}$	M_x/qa^2			M_y/qa^2		
		Galerkin	B.P.M.	Δ Percent	Galerkin	B.P.M.	Δ Percent
0	1	0.2063	0.2063	0	0.2063	0.2063	0
0.1	1.1	0.1777	0.1763	0.8	0.1942	0.1950	0.4
0.2	1.2	0.1521	0.1484	2.4	0.1813	0.1820	0.4
0.3	1.3	0.1320	0.1225	7.2	0.1669	0.1671	0.1
0.4	1.4	0.1138	0.0987	13.3	0.1546	0.1503	2.9
0.5	1.5	0.09867	0.0768	22.2	0.1427	0.1317	7.7

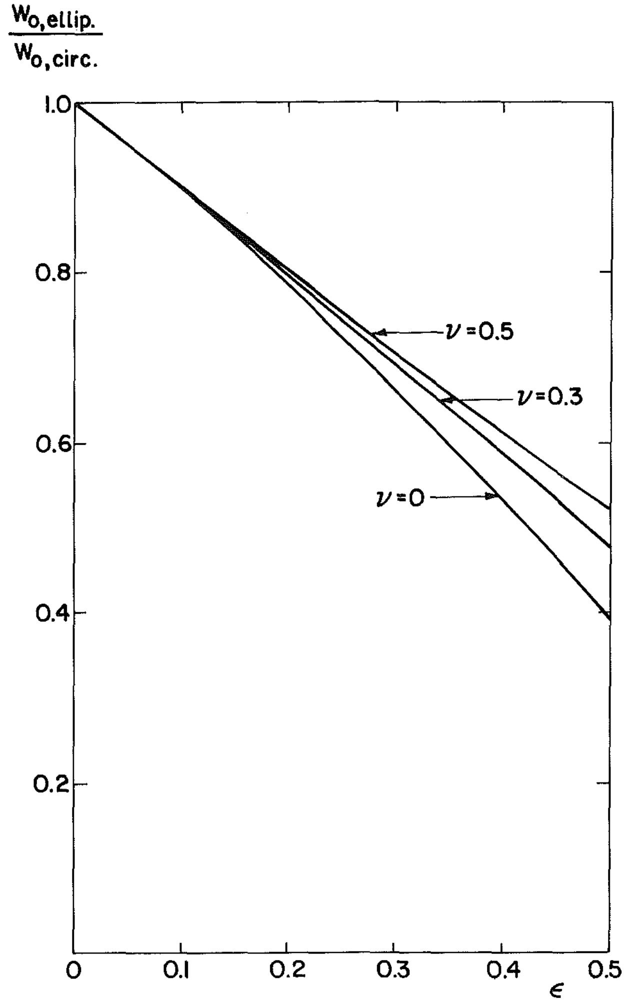

Fig. 8 Center displacement: effect of ellipticity

A comparison of the results reveals that the B.P.M. solution always yields lower bounds for the displacements. Furthermore, it is possible to conclude that for small ellipticities, $\epsilon \leq 0.25$, the results are accurate to within an order of 1 percent. Moreover, for relatively moderate ellipticities, $\epsilon = 0.5$, one observes that the second-order B.P.M. yields quite good results, the accuracy being 12.7 percent.

The moment M_x and M_y at the center $(x=y=0)$, calculated from equations $(A9)$, as well as those given by Galerkin $(\nu=0.3)$, are shown in Table 2.[4]

A comparison of the B.P.M. results with Galerkin's exact solution shows that the B.P.M. moments for M_y are more accurate than the displacements, while the M_x results are of a considerably lesser accuracy. Nevertheless, from both Tables 1 and 2, we may conclude that for ellipticities $\epsilon < 0.3$ the B.P.M. solution yields an accuracy better than 8 percent.

Finally, upon comparing the resulting displacements, the assertions of the previous study by Parnes (1987) are confirmed; namely, that the B.P.M. solution always yields lower bounds to the true displacements.

[4] Results from Galerkin (1923), are presented using the notation of this paper. It is noted that, as opposed to this referenced work, $M_x \equiv M_r(\psi=0)$, $M_y \equiv M_r(\psi=\pi/2)$.

References

Galerkin, B. G., 1923, "Berechnung der frei galagerten elliptischen Platte auf Biegung," *Zeitschrift für amgewandte Mathematik und Mechanik*, Vol. 3, pp. 113–117.

Parnes, R., Beltzer, A. I., 1986a, "A Higher-Order Boundary Perturbation Method for Asymmetric Dynamic Problems in Solids—Part I: General Formulation," *International Journal of Solids and Structures*, Vol. 22, No. 11, pp. 1177–1187.

Parnes, R., Beltzer, A. I., 1986b, "A Higher-Order Boundary Perturbation Method for Asymmetric Dynamic Problems in Soilds—Part II: Application to Dislocation Radiation," *International Journal of Solids and Structures*, Vol. 22, No. 11, pp. 1189–1199.

Parnes, R., 1987, "The Boundary Perturbation Method in Elastostatics: Investigation of Higher Order Effects and Accuracy of Solutions," *Journal de Mécanique Théorique et Appliquée*, Vol. 6, No. 2, pp. 293–314.

Prescott, J., 1961, *Applied Elasticity*, Dover, New York.

Timoshenko, S., and Woinowsky-Krieger, S., 1959, *Theory of Plates and Shells*, McGraw-Hill, New York.

APPENDIX

B.P.M. Solution for a Simply-Supported Elliptic Plate Subjected to a Uniform Load

We treat here the case of an elliptic plate subject to a uniform load q in order to provide a comparison with the exact analytic solution given by Galerkin (1923). The development is parallel to that of Section 3.

For this problem, (28) to (33) remain the same with the exception that here $\phi(r)=q$ so that (32) becomes

$$\nabla^4 \overset{(0)}{W}(r) = \frac{q}{D} . \qquad (A1)$$

The $j=0$ case, again recognized as that of a simply-supported circular plate of radius a, possesses the known solution (Timoshenko and Woinowsky-Krieger, 1959)

$$\overset{(0)}{W}(r) = \frac{\kappa}{64}\left[\rho^4 - \frac{2(3+\nu)}{1+\nu}\,\rho^2 + \frac{5+\nu}{1+\nu}\right] \qquad (A2a)$$

where

$$\kappa = q\,\frac{a^4}{D} \qquad (A2b)$$

and where $\rho = \dfrac{r}{a}$.

The $j>0$ must then satisfy the biharmonic equations, (35), whose solution is given by (36).

Case $j=1$. Substituting $(A2)$ in the boundary conditions, (37), the explicit boundary conditions become

$$\overset{(1)}{W}(a,\psi) = -\frac{\kappa}{16(1+\nu)}\,(1-\cos 2\psi) \qquad (A3a)$$

$$W^{(1)}_{,rr}(a,\psi)+\nu\Delta^{(1)}(a,\psi)=\frac{(3+\nu)\kappa}{16\ a^2}(1-\cos 2\psi). \qquad (A3b)$$

Substituting (36), and setting $C_2=0$, $\alpha_n=\beta_n=0$, $n\neq 2$, by a simple matching procedure, the nonvanishing constants, C_0, C_1, α_2, β_2 are determined, from which

$$\overset{(1)}{W}(r,\psi)=\frac{\kappa}{32(1+\nu)}\Big\{-(5+\nu)+(3+\nu)\rho^2 + \frac{1}{5+\nu}\Big[(\nu^2+4\nu+15)\rho^2-(\nu^2+2\nu+5)\rho^4\Big]\cos 2\psi\Big\} \qquad (A4)$$

Case $j=2$. In a similar manner, substitution of ($A4$) in (40) yields the explicit boundary conditions

$$\overset{(2)}{W}(a,\psi)=\frac{\kappa(5+\nu)^{-1}}{128(1+\nu)}\Big\{(3\nu^2+22\nu+75)-4(\nu^2+5\nu+20) \times\cos 2\psi+(\nu^2-2\nu+5)\cos 4\psi\Big\} \qquad (A5a)$$

$$W^{(2)}_{,rr}(a,\psi)+\nu\Delta^{(2)}(a,\psi)=-\frac{\kappa(5+\nu)^{-1}}{128(1+\nu)a^2}\{2(39\nu^2+22\nu-25) +4(-3\nu^2-12\nu^2+13\nu+30)\cos 2\psi +2(6\nu^3-15\nu^2-48\nu-35)\cos 4\psi\} \qquad (A5b)$$

which permit evaluation of the nonzero constants, C_0, C_1, α_n, β_n, $n=2$ and 4; the resulting expression for $W^{(2)}$ becomes

$$\overset{(2)}{W}(r,\psi)=\frac{\kappa(5+\nu)^{-1}}{128(1+\nu)}\Big\{\frac{1}{1+\nu}[(3\nu^3+64\nu^2+119\nu+50) -(39\nu^2+22\nu-25)\rho^2]+\frac{2}{5+\nu}[-(3\nu^3+24\nu^2+47\nu+210)\rho^2 +(\nu^3+4\nu^2-43\nu+10)\rho^4]\cos 2\psi+\frac{1}{9+\nu}[(\nu^3+10\nu^2 -103\nu+40)\rho^4-(3\nu^2-90\nu-5)\rho^6]\cos 4\psi\Big\}. \qquad (A6)$$

The final expression then is

$$W(r,\psi)=W^{(0)}+W^{(1)}\epsilon+W^{(2)}\epsilon^2+0(\epsilon^3), \qquad (A7)$$

where $W^{(j)}$, given by ($A2$), ($A4$), and ($A6$), reveals a solution dependent on $\cos 2\,n\psi$ ($n=0$, 1, 2) having coefficients which are functions of r and ν. The displacement at the center point, under the load, yields the simple expression

$$W_0=\frac{\kappa(5+\nu)^{-1}}{128(1+\nu)^2}[2(5+\nu)^2(1+\nu)-4(5+\nu)^2(1+\nu)\epsilon +(3\nu^3+64\nu^2+119+50)\epsilon^2]+0(\epsilon^3). \qquad (A8)$$

The moments M_x and M_y at the center point ($r=0$), obtained by substituting ($A2$), ($A4$), and ($A6$) in (46), are the following:

$$M_{x,y}\Big|_{\rho=0}=\frac{qa^2}{16}[3+\nu+M_r^{(1)}\epsilon+M_r^{(2)}\epsilon^2] \qquad (A9)$$

where

$$M_r^{(1)}=-[(3+\nu)\pm(1-\nu)(5+\nu)^{-1}(1+\nu)^{-1}(\nu^2+4\nu+15)] \qquad (A10a)$$

$$M_r^{(2)}=\frac{1}{4}(1+\nu)^{-1}(5+\nu)^{-1}[39\nu^2+22\nu -25\pm 2(1-\nu)(5+\nu)^{-1}(3\nu^3+24\nu^2+47\nu+210)]. \qquad (A10b)$$

J. T. Katsikadelis
Assoc. Professor of Structural Analysis,
Department of Civil Engineering,
National Technical University of Athens,
Athens, Greece

A. E. Armenàkas
Professor of Aerospace Engineering,
Polytechnic University,
New York, N.Y.
Mem. ASME

A New Boundary Equation Solution to the Plate Problem

A new boundary equation method is presented for analyzing plates of arbitrary geometry. The plates may have holes and may be subjected to any type of boundary conditions. The boundary value problem for the plate is formulated in terms of two differential and two integral coupled boundary equations which are solved numerically by discretizing the boundary. The differential equations are solved using the finite difference method while the integral equations are solved using the boundary element method. The main advantages of this new method are that the kernels of the boundary integral equations are simple and do not have hypersingularities. Moreover, the same set of equations is employed for all types of boundary conditions. Furthermore, the use of intrinsic coordinates facilitates the modeling of plates with curvilinear boundaries. The numerical results demonstrate the accuracy and the efficiency of the method.

1 Introduction

The bending problem of thin elastic plates of arbitrary geometry using the boundary integral equation method with numerical integration of the boundary integral equations has been treated by several investigators. Some of them, (e.g., Segedin and Brickell, 1968; Jaswon and Maiti, 1968; Maiti and Chakrabarty, 1974; Irschik and Ziegler, 1981) have developed boundary integral equation methods suitable for plates of certain geometries and certain boundary conditions. Others (e.g., Niwa et al., 1974; Bezine, 1978; Stern, 1979; Costa and Brebbia, 1984; Guoshu and Mukherjee, 1986) have developed general integral formulations and obtained numerical results by solving two coupled integral equations involving boundary quantities having direct geometrical and physical significance (displacement, slope, bending moment, and effective shear force on the boundary). These approaches allow the treatment of plates whose boundary has corners and whose boundary conditions are mixed. However, they lead to boundary integral equations with complicated kernels which exhibit higher-order singularities (hypersingularities) and for this reason their numerical solution requires a special cumbersome treatment.

In this investigation a new boundary equation method is presented for analyzing plates subjected to transverse forces and having any type of boundary conditions uniform or mixed (i.e., clamped, simply-supported, free, guided, elastically restrained). The plate may have holes and its boundary may have corners. In this method the deflection and the stress resultants of the plate are established from four boundary quantities, i.e., the deflection, its Laplacian and their normal derivatives. These quantities are established by solving on the boundary four coupled equations, two differential and two singular integral.

The coupled boundary equations are solved numerically using the finite difference method for the differential equations and the boundary element method for the integral equations. The method is easily programmed and is well suited for computer-aided analysis. The computation time is reduced considerably by converting the domain integrals which appear in the integral equations into boundary line integrals. Numerical results are presented for several plates (rectangular, circular, semicircular, triangular, elliptical) having various boundary conditions (uniform or mixed). The numerical results are compared with those obtained from analytical and other BEM solutions. Moreover, results are presented for a plate of composite geometry with mixed boundary conditions.

One of the main advantages of this new boundary equation method is that only four different kernels appear in the integral equations which are simple in form, and those which are singular have either a logarithmic or a Cauchy-type singularity i.e., the singular line integrals are single- or double-layer potentials which are readily integrated. Moreover, the use of intrinsic coordinates facilitates the modeling of plates with curvilinear boundary.

2 Formulation of the Boundary Value Problem

Consider a thin elastic plate of thickness h, occupying a two-dimensional region R in the x-y plane, bounded by a curve C_o. The region may be multiply connected, i.e., it may have M holes bounded by the curves $C_1, C_2, \ldots C_M$ (see Fig. 1). Moreover, the curves C_i $(i=0, 1, \ldots M)$ may be piecewise smooth, i.e., they may have a finite number of corners.

When the plate is subjected to a transverse loading $f(P)$, its

Contributed by the Applied Mechanics Division of THE AMERICAN SOCIETY OF MECHANICAL ENGINEERS, for presentation at the Joint ASCE/ASME Applied Mechanics, Biomechanics, and Fluids Engineering Conference, San Diego, Calif., July 9, to 12, 1989.

Discussion of this paper should be addressed to the Editorial Department, ASME, United Engineering Center, 345 East 47th Street, New York, N.Y. 10017, and will be accepted until two months after final publication of the paper itself in the JOURNAL OF APPLIED MECHANICS. Manuscript received by ASME Applied Mechanics Division, October 15, 1987; final revision, July 12, 1988.

Paper No. 89-APM-9.

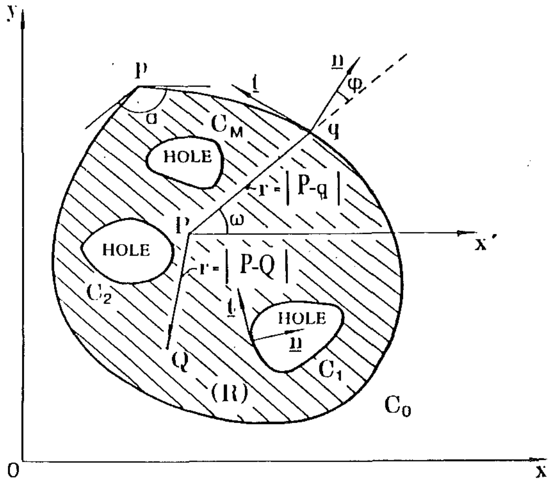

Fig. 1 Two-dimensional region R occupied by the plate

deflection $w(P)$ must satisfy the following differential equation (Timoshenko and Woinowsky-Krieger, 1959)

$$\nabla^4 w = f(P)/D, \qquad P \in R \tag{1}$$

where $D = Eh^3/12(1-\nu^2)$ is the flexural rigidity of the plate and ∇^4 is the biharmonic operator defined as

$$\nabla^4 = \frac{\partial^4}{\partial x^4} + 2\,\frac{\partial^4}{\partial x^2 \partial y^2} + \frac{\partial^4}{\partial y^4}. \tag{2}$$

Moreover, the deflection w of the plate must satisfy the following boundary conditions (Katsikadelis, 1982) on the boundary $C = \cup_{i=0}^{M} C_i$.

$$\alpha_1(p)w + \alpha_2(p)Vw = \alpha_3(p) \tag{3a}$$

$$\beta_1(p)\,\frac{\partial w}{\partial n} + \beta_2\,(p)Mw = \beta_3(p) \tag{3b}$$

where the functions α_k and β_k ($k=1, 2, 3$) are defined on the boundary C as $\alpha_k\,(p) = \alpha_k^i\,(p)$, $\beta_k\,(p) = \beta_k^i(p)$ when $p \in C_i$; α_k^i (p), $\beta_k^i\,(p)$ are specified functions on C_i. The operators M and V are defined as

$$M = -D\left[\nabla^2 + (\nu-1)\,\frac{\partial^2}{\partial t^2}\right] \tag{4a}$$

$$V = -D\left[\frac{\partial}{\partial n}\nabla^2 - (\nu-1)\,\frac{\partial}{\partial s}\,\left(\frac{\partial^2}{\partial n \partial t}\right)\right]. \tag{4b}$$

In the preceding relations $\partial/\partial n$ and $\partial/\partial t$ denote differentiation along the outward normal and the tangential direction, respectively, while $\partial/\partial s$ denotes differentiation with respect to the arc length of the boundary. Notice that the bending moment M_n and the effective shear force V_n acting on the boundary of the plate are given as

$$M_n = Mw \tag{5a}$$

$$V_n = Vw. \tag{5b}$$

Equations (3) express the most general case of linear boundary conditions for a plate. The conventional boundary conditions are obtained from equations (3) by specifying appropriately the functions α_k and β_k. Thus, a portion $\tilde{C}$ of the boundary C is

(*a*) clamped if

$$\alpha_1 = 1,\ \alpha_2 = 0,\ \alpha_3 = 0,\ \beta_1 = 1,\ \beta_2 = 0,\ \beta_3 = 0 \tag{6a}$$

(*b*) simply-supported if

$$\alpha_1 = 1,\ \alpha_2 = 0,\ \alpha_3 = 0,\ \beta_1 = 0,\ \beta_2 = 1,\ \beta_3 = 0 \tag{6b}$$

(*c*) free if

$$\alpha_1 = 0,\ \alpha_2 = 1,\ \alpha_3 = 0,\ \beta_1 = 0,\ \beta_2 = 1,\ \beta_3 = 0 \tag{6c}$$

(*d*) guided if

$$\alpha_1 = 0,\ \alpha_2 = 1,\ \alpha_3 = 0,\ \beta_1 = 1,\ \beta_2 = 0,\ \beta_3 = 0. \tag{6d}$$

Notice that at points where the boundary conditions change, the functions α_k, β_k may be discontinuous.

Using intrinsic coordinates (Katsikadelis, 1982) the operators (4) may be written as

$$M = -D\left[\nabla^2 + (\nu-1)\,\left(\frac{\partial^2}{\partial s^2} + K\frac{\partial}{\partial n}\right)\right] \tag{7a}$$

$$V = -D\left[\frac{\partial}{\partial n}\nabla^2 - (\nu-1)\,\frac{\partial}{\partial s}\,\left(\frac{\partial^2}{\partial s \partial n} - K\frac{\partial}{\partial s}\right)\right] \tag{7b}$$

where $K = K(s)$ is the curvature of the boundary. For rectilinear boundary ($K=0$, $t \equiv s$) equations (7) become identical in form to equations (4).

Using relations (7) the boundary conditions (3) can be written as

$$\alpha_1(s)\Omega - D\alpha_2(s)\left[\Psi - (\nu-1)\frac{\partial}{\partial s}\,\left(\frac{\partial X}{\partial s} - K\,\frac{\partial \Omega}{\partial s}\right)\right] = \alpha_3(s) \tag{8}$$

$$\beta_1(s)X - D\beta_2(s)\,\left[\Phi + (\nu-1)\,\left(\frac{\partial^2 \Omega}{\partial s^2} + KX\right)\right] = \beta_3(s) \tag{9}$$

where the following notation has been introduced

$$\Omega = w(s),\ X = \frac{\partial w(s)}{\partial n},\ \Phi = \nabla^2 w(s),\ \Psi = \frac{\partial}{\partial n}\nabla^2 w(s). \tag{10}$$

Equations (8) and (9) constitute two coupled differential equations on the boundary C of the plate with respect to the unknown boundary functions Ω, X, Φ, and Ψ.

3 Integral Representation of the Solution

The integral representation of the solution $w(P)$ of equation (1) is readily obtained using the Rayleigh-Green identity for the biharmonic operator (Katsikadelis and Armenàkas, 1984b) as

$$\begin{aligned} w(P) = \iint_R v(P,Q)f(Q)d\sigma_Q - D\int_C [v(P,q)\,\frac{\partial}{\partial n_q}\nabla^2 w(q) \\ - w(q)\,\frac{\partial}{\partial n_q}\nabla^2 v(P,q) - \frac{\partial v(P,q)}{\partial n_q}\nabla^2 w(q) \\ + \frac{\partial w(q)}{\partial n_q}\nabla^2 v(P,q)]ds_q \end{aligned} \tag{11}$$

where

$$v(P,Q) = \frac{1}{8\pi D}r^2 \ln r, \qquad r = |P-Q| \tag{12}$$

is the fundamental solution to equation (1), i.e., a partial singular solution of equation

$$\nabla^4 v = \delta(P-Q)/D \tag{13}$$

where $\delta(P-Q)$ is the Dirac Delta function; Q is the field point and P is the source point. Note that the two-point function $v(P,Q)$ is symmetric with respect to the points P and Q and, thus, their role can be interchanged, $v(P,Q) = v(Q,P)$.

In the aforementioned equations, points inside the region R are denoted by capital letters (P or Q), while points on the boundary C are denoted by small letters (p or q). Moreover, the subscript in the differentials ds_q or $d\sigma_Q$ and in the normal derivative $\partial/\partial n_q$ indicates the point which varies during integration or differentiation.

Substituting equation (12) into equation (11), carrying out the differentiations and using notation (10), the integral respresentation of the solution of equation (1) can be written in the following form

$$w(P)=\frac{1}{2\pi D}\iint_R \Lambda_4(r)fd\sigma$$

$$-\frac{1}{2\pi}\int_C [\Lambda_1(r)\Omega+\Lambda_2(r)X+\Lambda_3(r)\Phi+\Lambda_4(r)\Psi]ds \quad (14)$$

where the kernels Λ_i (r) $(i=1,2,3,4)$ are given as

$$\Lambda_1(r)=-\frac{\cos\varphi}{r} \qquad \Lambda_2(r)=\ln r+1 \quad (15a,b)$$

$$\Lambda_3(r)=-\frac{1}{4}\ (2r\ln r+r)\cos\varphi \quad \Lambda_4(r)=\frac{1}{4}r^2\ln r. \quad (15c,d)$$

Notice that for the line integral $r=|P-q|$, while for the domain integral $r=|P-Q|$, P, $Q\epsilon R$, $q\epsilon C$; $\varphi=\mathbf{r},\hat{}\mathbf{n}$ is the angle between the direction of r and the normal $\mathbf{n}$ to the boundary at point q.

The kernels Λ_i (r) $(i=1,2,3,4)$ are known functions. Hence, if the boundary quantities Ω, X, Φ, and Ψ are established, the deflection of the plate $w(P)$ can be computed from equation (14).

4 Boundary Integral Equations

The boundary quantities Ω, X, Φ, and Ψ are related by the two differential equations (8) and (9). Consequently, two more equations are required in order to be able to establish them. In this section two boundary integral equations, relating the boundary quantities, are derived from the integral representation (11) by employing the procedure presented in (Katsikadelis and Armenàkas, 1984b).

The first boundary integral equation is obtained by letting point P in equation (11) approach a point p on C and by taking into account that in the limit as $P\rightarrow p\epsilon C$, the line integral with kernel $\partial/\partial n\ \nabla^2 v$ exhibits a discontinuity jump equal to

$$\lim_{P\rightarrow p}\int_C \frac{\partial}{\partial n_q}\nabla^2 v(P,q)w(q)ds_q$$

$$-\int_C \frac{\partial}{\partial n_q}\nabla^2\ v(p,q)w(q)ds_q=\frac{2\pi-\alpha}{2\pi D}w(p). \quad (16)$$

Thus, the first boundary integral equation is

$$\alpha\Omega=\frac{1}{D}\iint_R \Lambda_4(r)fd\sigma$$

$$-\int_C [\Lambda_1(r)\Omega+\Lambda_2(r)X+\Lambda_3(r)\Phi+\Lambda_4(r)\Psi]ds \quad (17)$$

where $r=|p-q|$, p, $q\epsilon C$ and α is the angle between the tangents at point p (see Fig. 1). For a point p where the boundary is smooth $\alpha=\pi$.

The second boundary integral equation is obtained by applying the operator ∇^2 on both sides of equation (11) and, subsequently, letting point P approach a point p on C. Thus, by taking into account that $\nabla^4\ v(P,\ q)\ =\ \partial/\partial n\nabla^4 v\ (P,q)=0$ and using equation (16) the second boundary integral equation is

$$\alpha\Phi=\frac{1}{D}\iint\Lambda_2(r)fd\sigma-\int_C\ [\Lambda_1(r)\Phi+\Lambda_2(r)\Psi]ds. \quad (18)$$

The boundary differential equations (8) and (9), together with the boundary integral equations (17) and (18), constitute a set of four simultaneous equations for the unknown boundary quantities Ω, X, Φ, Ψ. Notice, that the boundary conditions affect only the boundary differential equations through

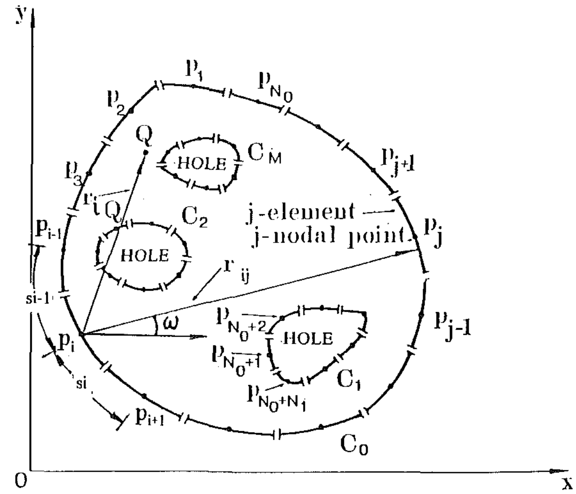

Fig. 2 Discretization of the boundary

the parameters α_i and b_i $(i=1,2,3)$ which, in general, could be functions of the arc length s. The two boundary integral equations are not affected by the boundary conditions. Thus, any type of boundary conditions (uniform, mixed, elastic support) can be treated in a unified manner by solving the same set of boundary equations. For clamped or simply-supported plates it is possible to reduce equations (8), (9), (17), (18) to two boundary integral equations by eliminating two of the unknown boundary quantities (Katsikadelis and Armenàkas 1984a, 1984b). However, this can not be done for plates with free or guided boundaries. In these cases elimination of the boundary quantities yields two boundary integrodifferential equations whose solution involves considerable difficulties.

5 Numerical Solution of the Boundary Equations

The boundary integral equations (17) and (18) are solved numerically using the boundary element method, while the boundary differential equations (8) and (9) are solved numerically using the finite difference method.

In the boundary element method, the boundary C of the plate is divided into a finite number of segments referred to as boundary elements. On each element two approximations are made. The geometry of the element is approximated by a straight line, or by a parabolic arc, and the unknown boundary quantities are assumed either to be constant or to vary linearly or parabolically on the element. In this investigation, each element is approximated by a parabolic arc and the boundary quantities are assumed to be constant on the element. This approximation of the boundary reduces considerably the error induced by the geometry of the curved boundary (Katsikadelis and Sapountzakis, 1985; Katsikadelis and Kallivokas, 1986).

In the finite difference method the derivatives in the boundary differential equations (8) and (9) are approximated by unevenly-spaced, central finite difference schemes, that is

$$\left(\frac{\partial g}{\partial s}\right)_i=\frac{-s_i^2g_{i-1}+(s_i^2-s_{i-1}^2)g_i+s_{i-1}^2g_{i+1}}{s_{i-1}s_i(s_{i-1}+s_i)} \quad (19a)$$

$$\left(\frac{\partial^2 g}{\partial s^2}\right)_i=2\,\frac{s_ig_{i-1}-(s_{i-1}+s_i)g_i+s_{i-1}g_{i+1}}{s_{i-1}s_i(s_{i-1}+s_i)} \quad (19b)$$

where g_i stands for a boundary quantity at the nodal point i and s_{i-1}, s_i are the distances along the boundary between the nodal points p_{i-1}, p_i and p_i, p_{i+1}, respectively, (see Fig. 2).

Discretization of the boundary C into N elements and application of the aforementioned technique yields the following set of $4N$ linear algebraic equations in $4N$ unknowns

$$\sum_{j=i-1}^{i+1} (A_{11})_{ij}\Omega_j + \sum_{j=i-1}^{i+1} (A_{12})_{ij}X_j + (A_{14})_{ii}\Psi_i = (B_1)_i \qquad (20a)$$

$$\sum_{j=i-1}^{i+1} (A_{21})_{ij}\Omega_j + (A_{22})_{ii}X_i + (A_{23})_{ii}\Phi_i = (B_2)_i \qquad (20b)$$

$$\sum_{j=1}^{N} [(A_{31})_{ij}\Omega_j + (A_{32})_{ij}X_j + (A_{33})_{ij}\Phi_j + (A_{34})_{ij}\Psi_j] = (B_3)_i \qquad (20c)$$

$$\sum_{j=1}^{N} (A_{43})_{ij}\Phi_j + (A_{44})_{ij}\Psi_j = (B_4)_i \quad (i=1,2, \ldots N). \qquad (20d)$$

Notice that in equations (20a) and (20b) the subscript j may take the values $j=0$ or $j=N+1$. Hence, these values must be replaced by $j=N$ and $j=1$, respectively.

The coefficients $(A_{kl})_{ij}$, and the constant terms $(B_k)_i$ ($k,l=1, 2, 3, 4$ and $i, j = 1, 2, \ldots N$) are given by the following relations

$$(A_{11})_{i,i-1} = -(\alpha_2)_i s_i \left(-\frac{\partial K_i}{\partial s} s_i + 2K_i\right) \qquad (21a)$$

$$(A_{11})_{ii} = (\alpha_1)_i/[(\nu-1)De_i] + (\alpha_2)_i (s_{i-1}+s_i) \times \left[(s_{i-1}-s_i)\frac{\partial K_i}{\partial s} + 2K_i\right] \qquad (21b)$$

$$(A_{11})_{i,i+1} = -(\alpha_2)_i s_{i-1} \left(\frac{\partial K_i}{\partial s} s_{i-1} + 2K_i\right) \qquad (21c)$$

$$(A_{12})_{i,i-1} = 2(\alpha_2)_i s_i \qquad (21d)$$

$$(A_{12})_{ii} = -2(\alpha_2)_i (s_{i-1}+s_i) \qquad (21e)$$

$$(A_{12})_{i,i+1} = 2(\alpha_2)_i s_{i-1} \qquad (21f)$$

$$(A_{14})_{ii} = -(\alpha_2)_i/[(\nu-1)e_i] \qquad (21g)$$

$$(A_{21})_{i,i-1} = -2(\beta_2)_i s_i \qquad (21h)$$

$$(A_{21})_{ii} = 2(\beta_2)_i (s_{i-1}+s_i) \qquad (21i)$$

$$(A_{21})_{i,i+1} = -2(\beta_2)_i s_{i-1} \qquad (21j)$$

$$(A_{22})_{ii} = (\beta_1)_i/[(\nu-1)De_i] - (\beta_2)_i K_i/e_i \qquad (21k)$$

$$(A_{23})_{ii} = -(\beta_2)_i/[(\nu-1)e_i] \qquad (21l)$$

$$(A_{31})_{ij} = -\int_j d\omega_{iq} + \alpha\delta_{ij} \qquad (21m)$$

$$(A_{32})_{ij} = \int_j (\ln r_{iq}+1)ds_q \qquad (21n)$$

$$(A_{33})_{ij} = -\frac{1}{4}\int_j r_{iq}^2 (2\ln r_{iq}+1)d\omega_{iq} \qquad (21o)$$

$$(A_{34})_{ij} = \frac{1}{4}\int_j r_{iq}^2 \ln r_{iq} ds_q \qquad (21p)$$

$$(A_{43})_{ij} = (A_{31})_{ij} \qquad (21q)$$

$$(A_{44})_{ij} = (A_{32})_{ij} \qquad (21r)$$

$$(B_1)_i = (\alpha_3)_i/[De_i(\nu-1)] \qquad (21s)$$

$$(B_2)_i = (\beta_3)_i/[De_i(\nu-1)] \qquad (21t)$$

$$(B_3)_i = \frac{1}{4D}\iint_R r_{iQ}^2 \ln r_{iQ} f(Q)d\sigma_Q \qquad (21u)$$

$$(B_4)_i = \frac{1}{D}\iint_R (\ln r_{iQ}+1)f(Q)d\sigma_Q \qquad (21v)$$

where $e_i = 1/[s_{i-1}s_i(s_{i-1}+s_i)]$; $r_{iQ} = [p_i - Q]$; $Q \epsilon R$; $r_{iq} = |p_i - q|$, $q \epsilon j$-element; ω_{iq} = is the angle between the x-axis and the line r_{ij} (see Fig. 2); $(\alpha_k)_i$ and $(\beta_k)_i$ are values of the functions α_k (s) and β_k (s), respectively, at point p_i; the symbol $\int_j$ indicates integration over the j-element. The integrals in the expressions for the coefficients $(A_{31})_{ij}$ $(A_{31})_{ij}$ and $(A_{32})_{ij}$ have been obtained using the relation $\cos\varphi ds = r d\omega$ (Katsikadelis and Armenàkas, 1984b).

In matrix form, equations (20) are written as

$$\begin{bmatrix} \mathbf{A}_{11} & \mathbf{A}_{12} & \mathbf{0} & \mathbf{A}_{14} \\ \mathbf{A}_{21} & \mathbf{A}_{22} & \mathbf{A}_{23} & \mathbf{0} \\ \mathbf{A}_{31} & \mathbf{A}_{32} & \mathbf{A}_{33} & \mathbf{A}_{34} \\ \mathbf{0} & \mathbf{0} & \mathbf{A}_{43} & \mathbf{A}_{44} \end{bmatrix} \begin{bmatrix} \mathbf{\Omega} \\ \mathbf{X} \\ \mathbf{\Phi} \\ \mathbf{\Psi} \end{bmatrix} = \begin{bmatrix} \mathbf{B}_1 \\ \mathbf{B}_2 \\ \mathbf{B}_3 \\ \mathbf{B}_4 \end{bmatrix} \qquad (22)$$

where

$$\begin{aligned} \mathbf{\Omega}^T &= [\Omega_1\ \Omega_2 \ldots \Omega_N] \\ \mathbf{X}^T &= [X_1\ X_2 \ldots X_N] \\ \mathbf{\Phi}^T &= [\Phi_1 \Phi_2 \ldots \Phi_N] \\ \mathbf{\Psi}^T &= [\Psi_1 \Psi_2 \ldots \Psi_N] \\ \mathbf{B}_k^T &= [(B_k)_1 (B_k)_2 \ldots (B_k)_N],\ k=1,2,3,4. \end{aligned} \qquad (23)$$

In deriving equations (20a) and (20b), the derivatives at the nodal points have been approximated by unevenly-spaced central differences. However, the function $X = \partial w/\partial n$ is discontinuous at corner points and, thus, the derivatives at the nodal points before (after) the corner are approximated by backward (forward) differences. In this case equation (20a) is replaced by

$$\sum_{j=i-1}^{i+1} (A_{11})_{ij}\Omega_j + (A_{12})_{i,i\pm3}X_{i\pm3} + (A_{12})_{i,i\pm2}X_{i\pm2} + (A_{12})_{i,i\pm1}X_{i\pm1} + (A_{12})_{ii}X_i + (A_{14})_{ii}\Psi_i = 0 \qquad (24)$$

where

$$(A_{12})_{ii} = 2(\alpha_2)_i h_2 h_3 (h_2+h_3)(3h_1+2h_2+h_3)e_i^*/e_i \qquad (25a)$$

$$(A_{12})_{i,i\pm1} = -2(\alpha_2)_i h_3 (h_1+h_2)(h_1+h_2+h_3) \times (2h_1+2h_2+h_3)e_i^*/e_i \qquad (25b)$$

$$(A_{12})_{i,i\pm2} = 2(\alpha_2)_i h_1 (h_2+h_3)(h_1+h_2+h_3) \times (2h_1+h_2+h_3)e_i^*/e_i \qquad (25c)$$

$$(A_{12})_{i,i\pm3} = -2(\alpha_2)_i h_1 h_2 (h_1+h_2)(2h_1+h_2)e_i^*/e_i \qquad (25d)$$

$$e_i^* = 1/[h_1 h_2 h_3 (h_1+h_2)(h_2+h_3)(h_1+h_2+h_3)].$$

In equations (25) $h_1 = s_{i-1}$, $h_2 = s_{i-2}$, $h_3 = s_{i-3}$ or $h_1 = s_i$, $h_2 = s_{i+1}$, $h_3 = s_{i+2}$ depending on whether backward or forward differences are used, respectively.

Special care must be taken at the corner points of the boundary when the deflections are not prevented (free corner). In this case the replacement of the twisting moments along the boundary by a distribution of equivalent couples of vertical forces gives rise to fictitious concentrated corner forces which affect greatly the deflections and the stress resultants. This shortcoming of Kirchoff's plate theory is overcome by imposing the additional corner condition

$$(Tw)^+ - (Tw)^- = 0 \qquad (26)$$

where Tw is the twisting moment along the boundary which, using intrinsic coordinates and notation (10), can be expressed as

$$Tw = D(1-\nu)\left(\frac{\partial^2 w}{\partial s \partial n} - K\frac{\partial w}{\partial s}\right) = D(1-\nu)\left(\frac{\partial X}{\partial n} - K\frac{\partial \Omega}{\partial s}\right). \tag{27}$$

Substituting relation (27) into (26), the corner condition may be written as

$$\left(\frac{\partial X}{\partial s}\right)^{(+)} - \left(\frac{\partial X}{\partial s}\right)^{(-)} = \left(K^{(+)} - K^{(-)}\right)\frac{\partial \Omega}{\partial s}. \tag{28}$$

Denoting by p_i and p_{i+1} the nodal points adjacent to the corner, and approximating the derivatives of X by forward and backward differences and the derivatives of Ω by central differences, condition (28) is expressed as

$$\sum_{j=i-1}^{j=i+2} c_j \Omega_j + \sum_{j=i-2}^{j=i+3} d_j X_j = 0 \tag{29}$$

where

$$\begin{aligned}
c_{i-1} &= K_i s_i/[s_{i-1}(s_{i-1}+s_i)]\\
c_i &= -K_i(s_i - s_{i-1})/(s_{i-1}s_i) - K_{i+1}/[s_i(s_i+s_{i+1})]\\
c_{i+1} &= -K_i s_{i-1}/[s_i(s_{i-1}+s_i)] + K_{i+1}(s_{i+1}-s_i)/(s_i s_{i+1})\\
c_{i+2} &= K_{i+1}s_i/[s_{i+1}(s_i+s_{i+1})]\\
d_{i-2} &= -s_{i-1}/[s_{i-2}(s_{i-2}+s_{i-1})]\\
d_{i-1} &= (s_{i-1}+s_{i-2})/(s_{i-2}s_{i-1})\\
d_i &= -(s_{i-2}+2s_{i-1})/[s_{i-1}(s_{i-2}+s_{i-1})]\\
d_{i+1} &= -(2s_{i+1}+s_{i+2})/[s_{i+1}(s_{i+1}+s_{i+2})]\\
d_{i+2} &= (s_{i+1}+s_{i+2})/(s_{i+1}s_{i+2})\\
d_{i+3} &= -s_{i+1}/[s_{i+2}(s_{i+1}+s_{i+2})].
\end{aligned} \tag{30}$$

Condition (29) represents an additional equation which must be satisfied simultaneously with equations (22). Thus, the number of equations which must be solved exceeds the number of unknowns. To overcome this difficulty, it is assumed that an unknown concentrated force acts at each free corner of the plate. These forces are evaluated by requiring that the results satisfy the additional equation (29) at each corner.

For plates with clamped or simply-supported boundaries, equation (22) can be simplified as follows:

(*a*) **Clamped Plate**. In this case $\alpha_1 = \beta_1 = 1$, $\alpha_2 = \alpha_3 = \beta_2 = \beta_3 = 0$. Consequently, $\mathbf{A}_{12} = \mathbf{A}_{14} = \mathbf{A}_{21} = \mathbf{A}_{22} = \mathbf{B}_1 = \mathbf{B}_2 = \mathbf{0}$ and equations (22) reduce to

$$\boldsymbol{\Omega} = \mathbf{0},\ \ \mathbf{X} = \mathbf{0},\ \ \begin{bmatrix} \mathbf{A}_{33} & \mathbf{A}_{34} \\ \mathbf{A}_{43} & \mathbf{A}_{44} \end{bmatrix} \begin{bmatrix} \boldsymbol{\Phi} \\ \boldsymbol{\Psi} \end{bmatrix} = \begin{bmatrix} \mathbf{B}_3 \\ \mathbf{B}_4 \end{bmatrix} \tag{31a,b,c}$$

(*b*) **Simply-Supported Plate**. In this case $\alpha_1 = \beta_2 = 1$, $\alpha_2 = \alpha_3 = \beta_1 = \beta_3 = 0$. Consequently, $\mathbf{A}_{12} = \mathbf{A}_{14} = \mathbf{B}_1 = \mathbf{B}_2 = \mathbf{0}$ and equations (22) reduce to

$$\boldsymbol{\Omega} = \mathbf{0},\ \ \begin{bmatrix} \mathbf{A}_{22} & \mathbf{A}_{23} & \mathbf{0} \\ \mathbf{A}_{32} & \mathbf{A}_{33} & \mathbf{A}_{34} \\ \mathbf{A}_{42} & \mathbf{A}_{43} & \mathbf{A}_{44} \end{bmatrix} \begin{bmatrix} \mathbf{X} \\ \boldsymbol{\Phi} \\ \boldsymbol{\Psi} \end{bmatrix} = \begin{bmatrix} \mathbf{0} \\ \mathbf{B}_3 \\ \mathbf{B}_4 \end{bmatrix} \tag{32a,b}$$

In all other cases a $4N \times 4N$ system of simultaneous linear algebraic equations must be solved. However, it is apparent from equations (21) that the matrices $\mathbf{A}_{kl}$ ($k=1,2$ $l=1,2,3,4$) are very sparsely populated and, thus, the solution of the system can be drastically simplified.

6 Evaluation of the Boundary and Domain Integrals

With the exception of the line integral (21n) when $i=j$, all line integrals (21m,o,p) are regular and can be evaluated using any of the known numerical techniques for the evaluation of line integrals. In this investigation the curved boundary is approximated by a parabolic arc passing through its nodal and extreme points and its value is computed using eight-point Gauss quadrature. However, when $i=j$ the argument r vanishes for $q=p_i$ and, consequently, the line integral (21n) exhibits a logarithmic singularity. In this case it is evaluated using the technique presented in (Katsikadelis and Armenàkas, 1985).

In evaluating the domain integrals (21u, v) we distinguish the following four cases of loading:

(a) The plate is subjected to a concentrated load P at a point Q_o. In this case, the loading function $f(Q)$ can be represented as

$$f(Q) = P\delta(Q - Q_o). \tag{33}$$

Using relation (33) the values of the integrals (21u, v) are

$$(B_3)_i = \frac{P}{4D} r_{iQ_o}^2 \ln r_{iQ_o}, \qquad (B_4)_i = \frac{P}{D}(\ln r_{iQ_o} + 1) \tag{34a,b}$$

where $r_{iQ_o} = |p_i - Q_o|$.

(b) The plate is subjected to a line load $p(s)$ distributed along a curve L^* in R. In this case, the domain integrals can be computed using equations (34a, b) from the following line integrals along the curve L^*

$$(B_3)_i = \frac{1}{4D}\int_{L^*} p(Q) r_{iQ}^2 \ln r_{iQ} ds_Q \tag{35a}$$

$$(B_4)_i = \frac{1}{D}\int_{L^*} p(Q)(\ln r_{iQ} + 1) ds_Q \tag{35b}$$

where $r_{iQ} = |p_i - Q|$, $Q \epsilon L^*$.

(c) The plate is subjected to a uniform or a linearly varying load distributed over an area $R^* \subseteq R$ of the plate bounded by a curve C^*. In this case, which is very usual in engineering practice, it is $\nabla^2 f = 0$ and the domain integrals can be readily converted into the following line integrals on the boundary C^* (see Appendix)

$$(B_3)_i = \frac{1}{4D}\int_{C^*}\left[f(q)\frac{\partial\, u_1(r_{iq})}{\partial n_q} - u_1(r_{iq})\frac{\partial f(q)}{\partial n_q}\right] ds_q \tag{36a}$$

$$(B_4)_i = \frac{1}{D}\int_{C^*}\left[f(q)\frac{\partial u_2(r_{iq})}{\partial n_q} - u_2(r_{iq})\frac{\partial f(q)}{\partial n_q}\right] ds_q \tag{36b}$$

where $r_{iq} = |p_i - q|$, $q \epsilon C^*$. The functions u_1 (r), u_2 (r) are given in the Appendix.

The substitution of the domain integrals by line integrals drastically reduces the required computer time.

The curves L^* or C^* are discretized into a finite number of parabolic elements and the line integrals (35a, b) or (36a, b) are evaluated on each element. The results are added to yield the values of the integrals on L^* or C^*.

(d) In the general case where the loading is given by an arbitrary function $f(Q)$ over R^*, the conversion of the domain integrals into boundary line integrals is also feasible using the Rayleigh-Green identity (see Appendix). In this case

$$(B_3)_i = \epsilon u_i + \frac{1}{4D}\int_{C^*}[\Lambda_1(r_{iq})u(q) + \Lambda_2(r_{iq})\frac{\partial u(q)}{\partial n_q} + \Lambda_3(r_{iq})\nabla^2 u(q) + \Lambda_4(r_{iq})\frac{\partial}{\partial n_q}\nabla^2 u(q)] ds_q \tag{37a}$$

$$(B_4)_i = \epsilon(\nabla^2 u)_i + \frac{1}{D}\int_{C^*}[\Lambda_1(r_{iq})\nabla^2 u(q) + \Lambda_2(r_{iq})\frac{\partial}{\partial n_q}\nabla^2 u(q)] ds_q \tag{37b}$$

where $r_{iq} = |p_i - q|$, $q \epsilon C^*$ and u is a particular solution of equation $\nabla^4 u = f$; ϵ = is given by equations (A9) of the Appendix. A shortcoming of this approach is the need to establish the function u. A procedure of doing so is given in the Appendix. Moreover, the function u for certain loading functions f is tabulated in the Appendix.

For an arbitrary function $f(Q)$ the domain integrals can be also evaluated using the equally efficient technique developed in (Katsikadelis, 1989).

7 Evaluation of the Deflections, the Reactions, and the Stress Resultants

When the matrices $\mathbf{A}_{lm}$, $\mathbf{B}_k$ $(kl=1,2,3,4)$ are established, the system of simultaneous algebraic equations (22) is solved, and the values Ω_j, X_j, Φ_j, and Ψ_j of the boundary functions $\Omega(s)$, $X(s)$, $\Phi(s)$, and $\Psi(s)$ are obtained at the nodal points p_j. These values can be substituted in the discretized form of equation (14) to yield the deflection $w(P)$ at any point P of the plate, and in equations (5) to yield the reacting force V_n, and the bending moment M_n along the boundary of the plate. The derivatives involved in equations (5) are computed using numerical differentiation.

The bending moments M_x, M_y, the twisting moment M_{xy} and the shearing forces Q_x and Q_y at any point of the plate are given (Timoshenko and Woinowsky-Krieger, 1959) in terms of the deflections as

$$M_x = -D\left(\frac{\partial^2 w}{\partial x^2} + \nu\frac{\partial^2 w}{\partial y^2}\right) \quad M_y = -D\left(\frac{\partial^2 w}{\partial y^2} + \nu\frac{\partial^2 w}{\partial x^2}\right) \tag{38a,b}$$

$$M_{xy} = -M_{yx} = D(1-\nu)\frac{\partial^2 w}{\partial x \partial y} \tag{38c}$$

$$Q_x = -D\frac{\partial}{\partial x}\nabla^2 w \quad Q_y = -D\frac{\partial}{\partial y}\nabla^2 w. \tag{38d,e}$$

The second- and third-order derivatives of the deflections in equations (38) may be evaluated from the computed values of the deflections using numerical differentiation. However, the accuracy of the results improves and the computer time is considerably reduced when the following combinations of derivatives in equations (38) are evaluated by direct differentiation of relation (14):

$$d_i = \frac{1}{2\pi D}\iint_R B_i(r) f d\sigma - \frac{1}{2\pi}\int_C [C_i(r)\Omega + D_i(r)X + E_i(r)\Phi + B_i(r)\Psi] ds \quad (i=1,2,3,4,5) \tag{39}$$

where

$$d_1 = \frac{\partial^2 w}{\partial x^2} + \frac{\partial^2 w}{\partial y^2}, \quad d_2 = \frac{\partial^2 w}{\partial x^2} - \frac{\partial^2 w}{\partial y^2}, \quad d_3 = \frac{\partial^2 w}{\partial x \partial y}$$
$$d_4 = \frac{\partial}{\partial x}\nabla^2 w, \quad d_5 = \frac{\partial}{\partial y}\nabla^2 w \tag{40}$$

and

$$B_1(r) = \ln r + 1, \; B_2(r) = \frac{1}{2}\cos 2\omega, \; B_3(r) = \frac{1}{4}\sin 2\omega$$

$$B_4(r) = -\frac{\cos\omega}{r}, \; B_5(r) = -\frac{\sin\omega}{r}$$

$$C_1(r) = 0, \; C_2(r) = \frac{4\cos(2\omega-\varphi)}{r^3}, \; C_3(r) = \frac{2\sin(2\omega-\varphi)}{r^3}$$

$$C_4(r) = 0, \; C_5(r) = 0$$

$$D_1(r) = 0, \; D_2(r) = \frac{2\cos 2\omega}{r^2}, \; D_3(r) = \frac{\sin 2\omega}{r^2}$$

$$D_4(r) = 0, \; D_5(r) = 0$$

$$E_1(r) = \frac{\cos\varphi}{r}, \; E_2(r) = \frac{\sin 2\omega \sin\varphi}{r}, \; E_3(r) = -\frac{2\cos 2\omega \sin\varphi}{r}$$

$$E_4(r) = \frac{\cos(\omega-\varphi)}{r^2}, \; E_5(r) = \frac{\sin(\omega-\varphi)}{r^2}. \tag{41}$$

When the loading is due to a concentrated force P, at some point Q_o or to a line load $p(s)$ along a curve L^* the domain integrals in equation (39) can be computed as described in Section 6.

When the plate is loaded by a load $f(Q)$ distributed over a region $R^* \subseteq R$ bounded by a curve C^* the domain integral in equation (39) can be converted into a line integral on C^*. Thus, using integration by parts and taking into account that the kernels $\Lambda_2(r)$ and $\Lambda_4(r)$ are symmetric, we obtain

$$\iint_{R^*}\left(\frac{\partial^2}{\partial x^2} - \frac{\partial^2}{\partial y^2}\right)\Lambda_4(r) f d\xi d\eta$$
$$= \iint_{R^*}\Lambda_4(r)\left(\frac{\partial^2 f}{\partial \xi^2} - \frac{\partial^2 f}{\partial \eta^2}\right) d\xi d\eta - \int_{C^*}\Lambda_4(r)\left(\frac{\partial f}{\partial \xi}\cos\alpha - \frac{\partial f}{\partial \eta}\sin\alpha\right) ds + \int_{C^*}\left(\frac{\partial}{\partial \xi}\cos\alpha - \frac{\partial}{\partial \eta}\sin\alpha\right)\Lambda_4(r) f ds \tag{42a}$$

$$\iint_{R^*}\frac{\partial^2}{\partial x \partial y}\Lambda_4(r) f d\xi d\eta = \iint_{R^*}\Lambda_4(r)\frac{\partial^2 f}{\partial \xi \partial \eta} d\xi d\eta + \int_{C^*}\left[\frac{\partial \Lambda_4(r)}{\partial \eta} f\cos\alpha - \Lambda_4(r)\frac{\partial f}{\partial \xi}\sin\alpha\right] ds \tag{42b}$$

$$\iint_{R^*}\frac{\partial}{\partial x}\nabla^2\Lambda_4(r) f d\xi d\eta = \iint_{R^*}\Lambda_4(r)\frac{\partial}{\partial \xi}\nabla^2 f d\xi d\eta + \int_{C^*}\left[\frac{\partial f}{\partial \xi}\frac{\partial \Lambda_4(r)}{\partial n} - \Lambda_4(r)\frac{\partial^2 f}{\partial n \partial \xi}\right] ds - \int_{C^*}\Lambda_2(r) f\cos\alpha ds \tag{42c}$$

$$\iint_{R^*}\frac{\partial}{\partial y}\nabla^2\Lambda_4(r) f d\xi d\eta$$
$$= \iint_{R^*}\Lambda_4(r)\frac{\partial}{\partial \eta}\nabla^2 f d\xi d\eta + \int_{C^*}\left[\frac{\partial f}{\partial \eta}\frac{\partial \Lambda_4(r)}{\partial n} - \Lambda_4(r)\frac{\partial^2 f}{\partial n \partial \eta}\right] ds - \int_{C^*}\Lambda_2(r) f\sin\alpha ds \tag{42d}$$

where $r = |P-Q|$, $P \epsilon R$, $Q \epsilon R^*$ in the domain integrals, while $r = |P-q|$, $P \in R$, $q \epsilon C^*$ in the line integrals; $\alpha = \widehat{\mathbf{x},\mathbf{n}}$.

Notice that if the loading is constant or varies linearly on R^*, the domain integrals in the right-hand side of equations (42) vanish. However, if f is an arbitrary function, these domain integrals can be converted into line integrals using equation (A7) of the Appendix.

8 Internal Supports

Due to functional requirements, it is often necessary to support a plate not only on its boundary but also on columns (point supports) and on load bearing walls (line supports). At these interior supports the deflection is prescribed while the corresponding reaction is unknown. In order to treat this problem, equations (17) and (18) must be supplemented by loading terms of the form given by equations (34a, b) and (35a, b) for point and line supports, respectively. In this case,

Table 1 Deflections of plates of various shapes and boundary conditions subjected to a uniform load q as compared with those obtained from existing solutions (analytical or numerical)

	Shape and boundary conditions	$w_o/(qa^4/D)$ Computed	Existing
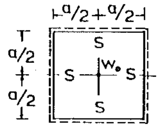	Square plate; all edges simply-supported ($\nu=0.30$)	0.00406 (60 B.E.)	0.00406 (Timoshenko and Woinowsky-Krieger, 1959)
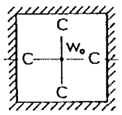	Square plate; all edges clamped	0.00126 (60 B.E.)	0.00126 (Roark and Young, 1975)
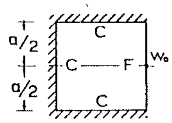	Square plate; three edges clamped and one edge free ($\nu=0.15$)	0.00273 (76 B.E.)	0.00276 (Bareš, 1979)
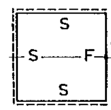	Square plate; three edges simply-supported and one edge free ($\nu=0.30$)	0.0124 (76 B.E.)	0.0129 (Timoshenko and Woinowsky-Krieger, 1959)
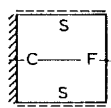	Square plate; two opposite edges simply-supported, one edge clamped and one edge free ($\nu=0.30$)	0.0109 (76 B.E.)	0.0112 (Timoshenko and Woinowsky-Krieger, 1959)
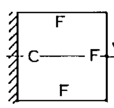	Square plate; three edges free, one edge clamped (cantilever plate) ($\nu=0.30$)	0.131 (60 B.E.)	0.131,0.129,0.127 (Lee and Lam, 1983)
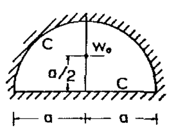	Semicircular clamped plate	0.00202 (60 B.E.)	0.00202 (Szilard, 1974)
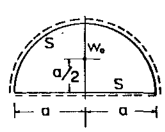	Semicircular simply-supported plate ($\nu=0.30$)	0.00812 (60 B.E.)	0.00811 (Timoshenko and Woinowsky-Krieger, 1959)
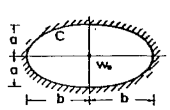	Elliptic clamped plate; Semi-axes ratio $a/b=0.625$	0.0295 (60 B.E.)	0.0295 (Timoshenko and Woinowsky-Krieger, 1959)
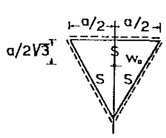	Equilateral triangular plate; all edges simply-supported	0.000579 (60 B.E.)	0.000579 (Timoshenko and Woinowsky-Krieger, 1959)
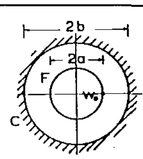	Annular plate. Outer edge clamped, inner edge free. Ratio of radii $b/a=2$ ($\nu=0.30$)	0.0843 (60 B.E.)	0.0843 (Timoshenko and Woinowsky-Krieger, 1959)

Table 2 **Deflections and stress resultants of simply-supported square plate with side length a and Poisson's ratio $\nu = 0.2$ subjected to a uniform load q. Upper numbers: computed; lower numbers: exact)**

$y = x$	$w/(qa^4/D)$	M_x/qa^2	M_{xy}/qa^2	Q_x/qa	V_x/qa $x = a/2$
	.4063E−02	.4421E−01	0	0	−.2162E+01
0	.4063E−02	.4420E−01	0	0	−.2160E+01
	.3704E−02	.4125E−01	.2728E−02	−.4854E−01	−.2102E+01
0.1a	.3704E−02	.4125E−01	.2728E−02	−.4854E−01	−.2107E+01
	.2744E−02	.3291E−01	.1025E−01	−.8827E−01	−.1955E+01
0.2a	.2744E−02	.3290E−01	.1025E−01	−.8827E−01	−.1950E+01
	.1503E−02	.2079E−01	.2069E−01	−.1097E+00	−.1647E+01
0.3a	.1503E−02	.2079E−01	.2069E−01	−.1097E+00	−.1651E+01
	.4349E−03	.7852E−02	.3119E−01	−.9881E−01	−.1260E+01
0.4a	.4346E−03	.7843E−02	.3119E−01	−.9888E−01	−.1129E+01

Table 3 Deflections and reactions of a clamped circular plate loaded by a concentrated load P at its center

	$w/(Pa^2/D)$				M_r/P	V_ra/P
	$r/a = 0$	$r/a = 0.25$	$r/a = 0.50$	$r/a = 0.75$	at $r = a$	at $r = a$
Kats. & Arm.	0.01989	0.01520	0.00803	0.00227	−0.07957	−0.15915
BEM (Guoshu & Mukh. 1986)	0.01989	0.01523	0.00804	0.00227	−0.07959	−0.15924
Exact (Timosh. & Woin.-Kr., 1959)	0.01989	0.01520	0.00803	0.00227	−0.07957	−0.15915

Table 4 Deflections $\bar{w} = w/(qa^4/Eh^3)$ at the inner free edge ($r = a$) and bending stress $\bar{\sigma}_r = 6M_r/qa^2$ at the outer clamped edge ($r = b$) of an annular plate ($\nu = 0.30$) subjected to a uniform load

	$b/a = 1.25$		$b/a = 1.5$		$b/a = 2$		$b/a = 3$		$b/a = 4$	
	$\bar{w}$	$\bar{\sigma}_r$	$\bar{w}$	$\bar{\sigma}_r$	$\bar{w}$	$\bar{\sigma}_r$	$\bar{w}$	$\bar{\sigma}_r$	$\bar{w}$	$\bar{\sigma}_r$
Kats. & Arm.	0.00199	0.1050	0.01390	0.2592	0.05753	0.4800	0.1296	0.6567	0.1621	0.7099
BEM (Guoshu & Mukh. 1986)	0.00201	0.1050	0.01391	0.2587	0.05758	0.4795	0.1301	0.6560	0.1629	0.7099
Exact (Timosh. & Woin.-Kr., 1959)	0.00199	0.1050	0.01390	0.2590	0.05750	0.4800	0.1300	0.6570	0.1620	0.7100

the forces P and $p(s)$ in equations (34a, b) and (35a, b) denote the unknown point and line support reactions. The application of the boundary element technique to approximate the line integrals (35a, b) results in a sum of terms involving the unknown values of the line reaction at the nodal points in the right-hand side of equations (20c, d). To evaluate these unknown reactions additional equations are required. These equations can be established by collocation at the support nodes (i.e., point supports and nodal points of the discretized line supports) using equation (14) (see Hartmann and Zotemantel (1986) and Katsikadelis et al. (1988)). Thus, the additional equations are

$$w_i = \iint_R v(r_{iQ}) f d\sigma_Q + \sum_{j=1}^{K} \Lambda_4(r_{ij}) P_j + \sum_{j=1}^{L} \Lambda_4(r_{ij}) p_j$$

$$+ \sum_{j=1}^{N} [\Lambda_1(r_{ij})\Omega_j + \Lambda_2(r_{ij})X_j + \Lambda_3(r_{ij})\Phi_j + \Lambda_4(r_{ij})\Psi_j] \qquad (43)$$

where w_i ($i = 1, 2, \ldots, (K+L)$) are the deflections at the $K+L$ internal support nodes; P_j ($j = 1, 2, \ldots K$) are the unknown reactions at the K-point supports; p_j ($j = 1, 2, \ldots, L$) are the unknown values of the line reaction at the L nodal points of the discretized line support; and Ω_j, X_j, Φ_j, Ψ_j are the $4N$ unknown nodal values of the boundary quantities defined by equations (10).

Equations (43) should be incorporated in equations (20a, b, c, d).

9 Numerical Results

In the past fifteen years, a number of papers have been published wherein various schemes are presented for analyzing elastic plates subjected to transverse forces by the BEM method (e.g., Maiti and Chakrabarty, 1974; Bezine, 1978; Stern, 1979; Costa and Brebbia, 1984). However, with few exceptions (e.g., Hartmann and Zotemantel, 1986; Guoshu and Mukherjee, 1986), these papers contain only a sampling of numerical results which are limited to plates of simple geometry (rectilinear boundary) and uniform boundary conditions. Curvilinear boundaries are avoided because they produce certain difficulties in the numerical analysis. Some results for plates with curvilinear boundaries are given by Guoshu and Mukherjee (1986).

In this investigation a computer program has been written for analyzing plates with arbitrary geometry using the numerical procedure described in the previous sections. Numerical results have been obtained for rectangular, triangular, circular, and ellliptical plates as well as for plates of arbitrary geometry having various boundary conditions (clamped, simply-supported, free, or mixed). Constant element with parabolic approximation of its curved boundary has been used. The results are compared with those available from analytical or other numerical solutions. In the tables and figures the results obtained in this investigation are referred to as Kats. & Arm.

In Table 1 values of the deflection at characteristic points of a variety of plates subjected to a uniform load are given. They are compared with those available from analytical or other numerical solutions. From this table it can be deduced that the method presented in this investigation is suitable for analyzing plates of any geometry (rectilinear or curvilinear boundary) and any boundary conditions (uniform or mixed).

In Table 2 values of the deflection and stress resultants for a simply-supported square plate subjected to a uniform load are given. They are compared with those obtained from the Navier series solution (Timoshenko and Woinowsky-Krieger, 1959). The results given in this table illustrate the efficiency and accuracy of the method presented in this investigation.

Table 5 Corner reaction $R = [Tw]/qa^3$ in a uniformly-loaded simply-supported square plate ($\nu = 0.30$) compared with the exact and other BEM solutions

	Number of Nodes	R
Kats. & Arm.	32	0.0723 (0.068)
	60	0.0726 (0.067)
BEM (Stern, 1979)	32	0.0651
	64	0.0648
BEM (Costa and Brebbia, 1984)	36	0.0648
Exact (Timosh. & Woin.-Kr., 1959)		0.065

Table 6 Deflection and bending moment at the center of a uniformly-loaded simply-supported equilateral triangular plate with side length a and $\nu = 0.30$

	$w/(qa^4/D) \times 10^3$	$M_x/qa^2 \times 10^2$	$M_y/qa^2 \times 10^2$
Kats. & Arm. 24 B.E.	0.580	1.807	1.807
Maiti and Chakr. (1974) 24 const. B.E.	0.582	1.816	1.807
Costa and Brebbia (1984) 27 const. B.E.	0.568	1.830	1.830
Exact (Timosh. & Woin.-Kr., 1959)	0.579	1.805	1.805

In Table 3 values of the deflection and stress resultants for a circular clamped plate loaded by a concentrated load P at its center are presented. They are compared with those obtained from the exact analysis and by Guoshu and Mukherjee (1986).

In Table 4 values of the deflections and stress resultants for a uniformly-loaded annular plate with free inner edge and clamped outer edge are given. They are compared with those obtained from the exact analysis and by Guoshu and Mukherjee (1986).

In Table 5 values of the corner reactions of a simply-supported square plate, subjected to a uniform load, are given. Moreover, in Figs. 3 and 4, values for the slope $\partial w/\partial n$ and the effective shearing force V_n are plotted. They are compared with those obtained by using the conventional BEM solutions (Stern, 1977; Costa and Brebbia, 1984) and by the Navier series solution (Timoshenko and Woinowsky-Krieger, 1959). In the approach presented in this investigation the effective shearing forces, the twisting moments and, consequently, the corner reactions, are established by differentiating numerically, along the boundary – the normal slope of the elastic surface of the plate (see equations (7b), (26), and (27)). Thus, small error in the values of the slope may result in greater error in the values of the twisting moments, the effective shearing forces, and the corner reactions. This occurs at the nodal points in the neighborhood of the corners of the plate. The results may improve either by using graded elements of varying size near the corner or by using more refined techniques (Mitra and Ingber, 1987) which, however, are applied at the expense of the simplicity afforded by the constant element approximation. A simple remedy is to replace the computed values of the slope at the nodal points adjacent to the corners by those obtained by parabolic extrapolation of the neighboring nodal values (see values in parentheses in Table 5).

In Figs. 5 and 6 values of the bending moment M_n and the effective shearing force V_n of a clamped square plate subjected to a uniform load are plotted. They are compared with those obtained from another BEM solution (Stern, 1979) and by Moody (1960).

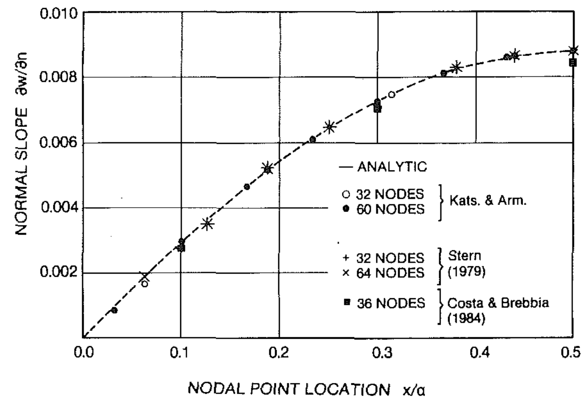

Fig. 3 Normal slope on an edge of a uniformly-loaded simply-supported square plate

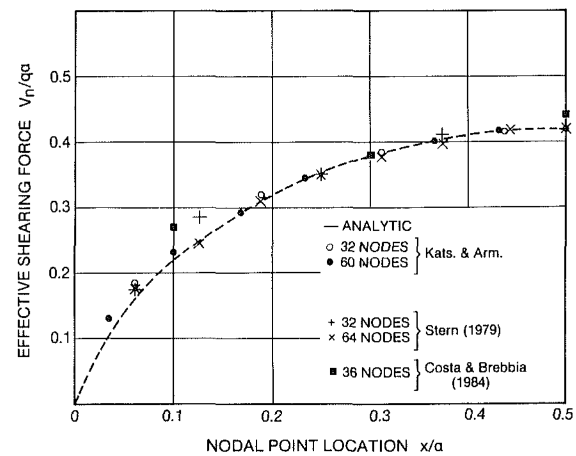

Fig. 4 Effective shearing force on an edge of a uniformly-loaded simply-supported square plate

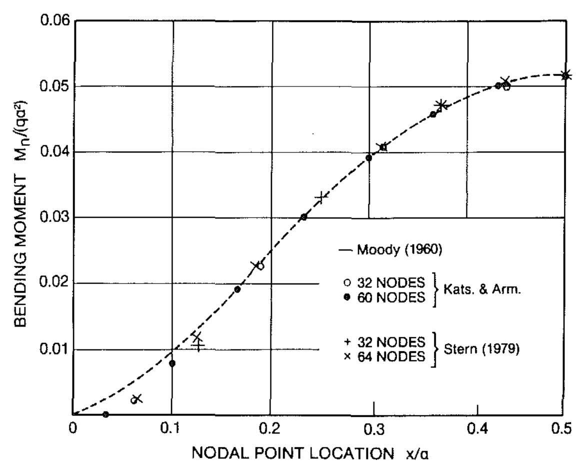

Fig. 5 Bending moment on an edge of a uniformly-loaded clamped square plate

In Table 6 results for a simply-supported equilateral triangular plate subjected to a uniform load are presented. They are compared with those obtained from the exact analysis and by other BEM solutions (Maiti and Chakrabarty, 1974; Costa and Brebbia, 1984).

In Fig. 7 values of the bending moment M_x along the cross-sections $y = 0$ and $y = 2$ of a simply-supported rectangular plate with four internal columns are plotted. They are compared with those obtained by Hartmann and Zotemantel (1988). The plate is subjected to a uniformly distributed load.

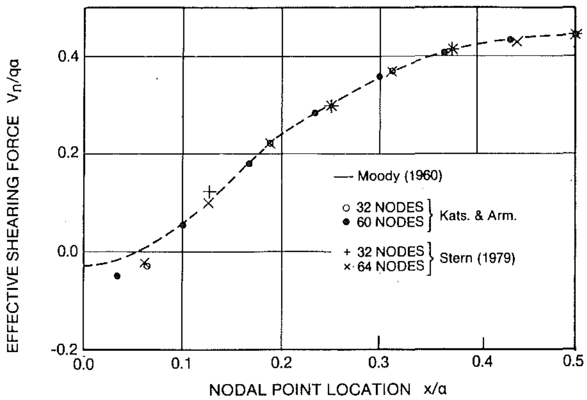

Fig. 6 Effective shearing force on an edge of a uniformly-loaded clamped square plate

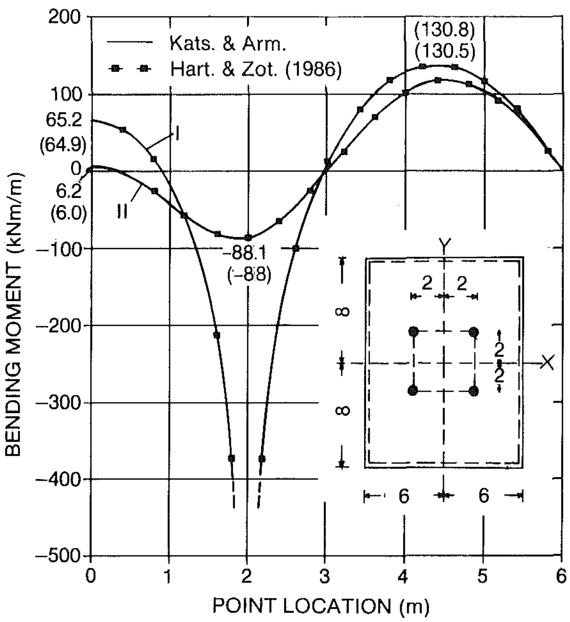

Fig. 7 Distribution of the bending moment M_x at $y = 2$ (curve I) and $y = 0$ (curve II) in a rectangular simply-supported plate with four internal supports ($\nu = 0.3$, $D = 2700$kNm, $q = 100$kN/m^2). The values in the parentheses are taken from Hartmann and Zotemantel (1986).

Finally, in Fig. 8 the contours for the deflection of a plate with a circular hole having an external boundary of composite geometry and mixed boundary conditions are plotted. This illustrates the applicability of the method presented in this investigation to the analysis of plates of any specified geometry and boundary conditions.

10 Concluding Remarks

In this paper a new boundary equation method for the analysis of thin elastic plates subjected to transverse forces is presented. The main conclusions drawn from this investigation can be summarized as follows:

(a) The method is very well suited for computer-aided analysis.

(b) The method is very well suited for analyzing plates, with or without holes, having a complex geometry with rectilinear or curvilinear boundary and subjected to any kind of loading.

(c) The method is very well suited for analyzing plates of arbitrary shape with mixed boundary conditions, including internal supports.

(d) The method can be extended to solve other boundary value problems with complex boundary conditions.

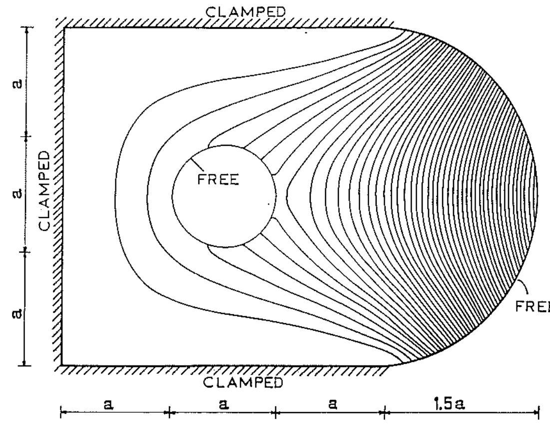

Fig. 8 Deflections $\bar{w} = w/(qa^4/D)$ of a plate with composite shape ($\nu = 0.30$) subjected to a uniform load q. The contour lines are drawn $\bar{w} = 0.035$ apart.

(e) The conversion of the domain integrals into line integrals reduces drastically the computer time and renders the BEM a powerful tool for analyzing plates with complex geometry and loading.

(f) Only four different kernels appear in the boundary integral equations which have simple expressions. Those of the kernels which are singular involve only logarithmic or Cauchy-type singularities. Thus, hypersingularities which lead to divergent integrals are avoided and, consequently, the computational task is reduced and the numerical solution of the integral equations is highly simplified.

References

Bareš, R., 1979, *Tables for the Analysis of Plates, Slabs, and Diaphragms*, 3rd ed., Bauverlag GmbH, Wiesbaden and Berlin.

Bezine, G. P., 1978, "Boundary Integral Formulation for Plate Flexure with Arbitrary Boundary Conditions," *Mech. Res. Commun.*, Vol. 5, pp. 197-206.

Costa, Jr., J. A., and Brebbia, C. A., 1984, "Plate Bending Problems Using BEM," *Proc. 6th Int. Conf. on Board the Liner the Queen Elisabeth 2*, Southampton to New York, 3/43-3/63, Springer-Verlag.

Guoshu, S., and Mukherjee, S., 1986, "Boundary Element Method of Bending of Elastic Plates of Arbitrary Shape with General Boundary Conditions," *Engineering Analysis*, Vol. 3, pp. 36-44.

Hartmann, F., and Zotemantel, R., 1986, "The Direct Boundary Element Method in Plate Bending," *Int. J. Num. Meth. Eng.*, Vol. 23, pp. 3049-3069.

Irschik, H., and Ziegler, F., 1981, "Application of the Green's Function Method to Thin Elastic Plates," *Acta Mech.*, Vol. 39, pp. 155-169.

Jaswon, M. A., and Maiti, M., 1968, "An Integral Equation Formulation of Plate Bending Problems," *J. Eng. Math.*, Vol. 2, pp. 83-89.

Katsikadelis, J. T., 1982, "The Analysis of Plates on Elastic Foundation by the Boundary Integral Equations Method," PhD. Thesis, Polytechnic Institute of New York, Brooklyn, N.Y.

Katsikadelis, J. T., 1989, "A Gaussian Quadrature Technique for Two-Dimensional Regions with Arbitrary Shape," to be published.

Katsikadelis, J. T., and Armenàkas, A. E., 1984a, "Plates on Elastic Foundation by the BIE Method," *ASCE, J. Eng. Mech.*, Vol. 110, pp. 1086-1105.

Katsikadelis, J. T., and Armenàkas, A. E., 1984b, "Analysis of Clamped Plates on Elastic Foundation by the Boundary Integral Equation Method," ASME Journal of Applied Mechanics, Vol. 51, pp. 574-580.

Katsikadelis, J. T., and Armenàkas, A. E., 1985, "Numerical Evaluation of Line Integrals with a Logarithmic Singularity," *AIAA Journal*, Vol. 23, pp. 1135-1137.

Katsikadelis, J. T., and Kallivokas, L. F., 1986, "Clamped Plates on Pasternak-Type Elastic Foundation by the Boundary Element Method," ASME Journal of Applied Mechanics, Vol. 53, pp. 909-917.

Katsikadelis, J. T., and Sapountzakis, E. J., 1985, "Torsion of Composite Bars by the Boundary Element Method," *ASCE J. Eng. Mech.*, Vol. 111, pp. 1197-1210.

Katsikadelis, J. T., Sapountzakis, E. J., and Zorba, E. G., 1988, "A BEM Approach to Static and Dynamic Analysis of Plates with Internal Supports," *Proc., 10th Int. Conf. on Boundary Element Methods in Engineering*, Southampton, Sept. 6-9, 1988, Vol. 4, Springer-Verlag, Berlin, pp. 431-444.

Lee, P. C. Y., and Lam, C. S., 1983, "Stresses in Rectangular Crystal Plates Under Transverse Loading," *Int. J. Solids Structures*, Vol. 19, pp. 55-66.

Maiti, M., and Chakrabarty, S. K., 1974, "Integral Equation Solutions for Simply Supported Polygonal Plates," *Int. J. Engrng. Sci.*, Vol. 12, pp. 793-806.

Mitra, A. K., and Ingber, M. S., 1987, "Resolving Difficulties in the BIEM

Caused by Geometric Corners and Discontinuous Boundary Conditions," *Proc. of 9th Int. Conf. on Boundary Element Methods in Engineering*, Vol. 1, Stuttgart, Springer-Verlag, Berlin, pp. 519–532.

Moody, W. T., 1960, "Moments and Reactions for Rectangular Plates, U.S. Department of Interior Bureau of Reclamations, Engineering Monograph 27.

Niwa, Y., Kobayashi, S., and Fukui, T., 1974, "An Application of the Integral Equation Method to Plate Bending Problems," *Memo*, Vol. 36, Pt. 2, Faculty of Civil Engineering, Kyoto University, Japan, pp. 140–158.

Roark, R. J., and Young, W. C., 1975, *Formulas for Stress and Strain*, 5th ed., McGraw-Hill Kogakusha Ltd., Tokyo.

Segedin, C. M., and Brickell, D. G. A., 1968, "Integral Equation Method for a Corner Plate," *ASCE, J. ST. 1*, Vol. 94, pp. 41–52.

Stern, M., 1979, "A General Boundary Integral Formulation for the Numerical Solution of Plate Bending Problems," *Int. J. Solids and Structures*, Vol. 15, pp. 769–782.

Szilard, R., 1974, *Theory and Analysis of Plates*, Prentice-Hall, Englewood Cliffs, N.J.

Timoshenko, S., and Woinowsky-Krieger, S., 1959, *Theory of Plates and Shells*, McGraw-Hill, New York.

APPENDIX

In this Appendix techniques for the conversion of the domain integrals ($21u$) and ($21v$) into line integrals are presented. Two cases are distinguished.

(*a*) Consider a function $f(Q)$, Q: (ξ, η) which is harmonic in a subregion R^* of R bounded by the curve C^*, i.e., $\nabla^2 f = 0$ in $R^* \subseteq R$. Moreover, consider a function $v(r)$, $r = |P-Q|$, $P \epsilon R$, $Q \epsilon R^*$, as well as a function $u(r)$, which is a particular solution of the following equation

$$\nabla^2 u = v. \tag{A1}$$

Applying Green's identity to the functions f and $u(r)$, we obtain

$$\iint_{R^*} vf d\sigma = \int_{C^*} \left(f\frac{\partial u}{\partial n} - u\frac{\partial f}{\partial n} \right) ds. \tag{A2}$$

In order to establish the function u, equation ($A1$) is written as

$$\frac{1}{r}\frac{d}{dr}\left(r\frac{du}{dr}\right) = v(r). \tag{A3}$$

Integration of equation ($A3$) yields

$$\text{for } v = r^2 \ln r/4 \quad u_1 = (2r^4 \ln r - r^4)/128 \tag{A4}$$

$$\text{for } v = \ln r + 1 \quad u_2 = r^2 \ln r/4. \tag{A5}$$

Note that, for $u = u_1$ or $u = u_2$, the line integral in equation ($A2$) varies continuously as the point P crosses the boundary C^*.

(b) Consider an arbitrary function $f(Q)$ defined in a subregion R^* of R bounded by a curve C^*. Moreover, consider the function $v = (1/8\pi)r^2 \ln r$, $r = |P-Q|$, $P \epsilon R$, $Q \epsilon R^*$ as well as a function $u(r)$, which is a particular solution of the following equation:

$$\nabla^4 u = f. \tag{A6}$$

Applying the Rayleigh-Green identity to the functions v and u, we obtain

Table $A1$ Particular integrals of equation $\nabla^4 u = f$

$f(x,y)$	$u(x,y)$		
1	$x^4/24$	$y^4/24$	$x^2y^2/8$
x	$x^5/120$	$xy^4/24$	$x^3y^2/24$
y	$x^4y/24$	$y^5/120$	$x^2y^3/24$
x^2	$x^6/360$		
y^2	$y^6/360$		
xy	$x^5y/120$	$xy^5/120$	$x^3y^3/72$
x^3	$x^7/440$		
y^3	$y^7/440$		
x^2y	$x^6y/360$		
xy^2	$xy^6/360$		
e^x	e^x		
e^y	e^y		
$\cos x$	$\cos x$		
$\cos y$	$\cos y$		
$\sin x$	$\sin x$		
$\sin y$	$\sin y$		

$$\iint_{R^*} vf d\sigma = \epsilon u(P) + \int_{C^*} \left(v\frac{\partial}{\partial n}\nabla^2 u - u\frac{\partial}{\partial n}\nabla^2 v + \nabla^2 v\frac{\partial u}{\partial n} - \nabla^2 u\,\frac{\partial v}{\partial n} \right) ds \tag{A7}$$

and

$$\iint_{R^*} \nabla^2 v f d\sigma = \epsilon \nabla^2 u(P) + \int_{C^*} \left(\nabla^2 v\frac{\partial}{\partial n}\nabla^2 u - \nabla^2 u\frac{\partial}{\partial n}\nabla^2 v \right) ds \tag{A8}$$

where

$$\begin{array}{lll} \epsilon = 1 & \text{when} & P \epsilon R^* \\ \epsilon = 1/2 & \text{when} & P \epsilon C^* \\ \epsilon = 0 & \text{when} & P \epsilon R \backslash \bar{R}^* \end{array} \tag{A9}$$

$\bar{R}^*$ is the closure of R^*.

The discontinuity in relations ($A7$) and ($A8$) is due to the fact that the line integral with kernel $\partial \nabla^2 v/\partial n$ behaves like a double layer potential.

In order to establish the function u, equation ($A6$) is written as

$$16\frac{\partial^4 u}{\partial z^2 \partial \bar{z}^2} = f(z, \bar{z}) \tag{A10}$$

where

$$z = x + iy, \quad \bar{z} = x - iy, \quad i = \sqrt{-1}$$

The function u is obtained by consecutive integrations of equation ($A10$).

For simple functions f, the function u can be readily established as a particular solution to equation ($A6$) by inspection. In Table $A1$ particular integrals for certain simple functions $f(x,y)$ are given.

Dynamic Stability of Nonlinear Antisymmetrically-Laminated Cross-Ply Rectangular Plates

Andrzej Tylikowski

Professor,
Warsaw University of Technology,
Institute of Machine Design Fundamentals,
Warsaw 02-524, Poland

The dynamic stability problem is solved for rectangular plates that are laminated antisymmetrically about their middle plane and compressed by time-dependent deterministic or stochastic membrane forces. Moderately large deflection equations taking into account a coupling of in-plane and transverse motions are used. The asymptotic stability and almost-sure asymptotic stability criteria involving a damping coefficient and loading parameters are derived using Liapunov's direct method. A relation between the stability of nonlinear equations and linearized ones is analyzed. An influence on the number of orthotropic layers, material properties for different classes of parametric excitation on stability domains is shown.

Introduction

The problem of laminated composites has been an object of considerable attention over the past two decades. Numerous papers are available on laminated plates and shells under static and periodic loadings. The investigation of static buckling and free vibrations of laminated plates was initiated by Ashton (1969), Bert and Mayberry (1969), and Whitney and Leissa (1969). An exact theory and numerical results for buckling and free vibrations of unsymmetrically-laminated cross-ply rectangular plates were presented by Jones (1973). On the other hand, attempts were also made to investigate forced deterministic vibration of large aspect ratio laminated plates (Sun and Whitney, 1974). Free large amplitude vibrations of laminated plates described by nonlinear differential equations have also received much attention (Chandra and Basawa Raju, 1975; Bert, 1973; Hui, 1985). The first analysis of the parametric instability of simply-supported laminated plates subjected to sinusoidal deterministic in-plane forces with a constant frequency is due to Bennett (1971). In 1985 Birman published a study on the dynamic stability of unsymmetrically-laminated rectangular plates subjected to in-plane harmonic forces using a single model approach of transverse displacement. The result was obtained under the additional assumption that the governing linear partial differential equations of motion can be approximated by an ordinary differential equation. Instability regions as functions of the load amplitude and frequency were obtained analyzing the Mathieu differential equation. All mentioned papers have applied finite dimensional or model approximations in analysis of vibrations and stability. The Liapunov direct method is a quite different approach and can be successfully used to analyze continuous systems described by partial differential equations. A significant advantage is offered by the method in that the equations of motion do not have to be solved in order to examine stability. The method can be applied not only to a simple elastic column in a linearized approach, but also to plates and shells governed by nonlinear partial differential equations (Tylikowski 1978, 1984). The dynamics of layered plates subjected to harmonic in-plane loads was also examined by Srinivasan and Chellapandi (1986), who reduced the stability problem to that with finite number of degrees-of-freedom. The paper mentioned above does not include geometric nonlinear effects which can occur in the case of thin layered plates. Up to now, the stability problem of such plates due to time-varying excitations has not been investigated extensively enough. Contrary to the stability analysis of sandwich plates (Salama and Cheng, 1973), an influence of damping on stability regions was neglected. This omission causes that near the resonance of the plate, an infinitesimal magnitude of the time-dependent component of in-plane load produces loss of the plate stability (Birman, 1985).

In recent years the theory of random vibrations has been finding more and more applications in engineering. Numerous excitations acting on structures have a random nature and should be described by means of the probability theory. At the present time there exists a number of papers calculating response characteristics of randomly-excited sandwich and laminated plates (Kulkarni, Banerjee, and Sinha, 1975; Witt and Sobczyk, 1980).

The present paper is believed to be the first analysis of dynamic stability of geometrically nonlinear motion of a cross-ply antisymmetrically-laminated plate including a dissipation of energy and treating the plate as an infinite-dimensional continuous system. As it was mentioned previously, the stability analysis strongly depends on the dissipation of energy. One of the first studies on the dynamics of laminated plates including a material damping is due to Dong (1967) who modeled viscoelastic plies as standard linear solids. A more so-

Contributed by the Applied Mechanics Division of THE AMERICAN SOCIETY OF MECHANICAL ENGINEERS for publication in the JOURNAL OF APPLIED MECHANICS.

Discussion on this paper should be addressed to the Editorial Department, ASME, United Engineering Center, 345 East 47th Street, New York, N.Y. 10017, and will be accepted until two months after final publication of the paper itself in the JOURNAL OF APPLIED MECHANICS. Manuscript received by ASME Applied Mechanics Division, December 1, 1987; final revision, July 5, 1988.

phisticated model of material damping was introduced by Siu and Bert (1974) who used a whole matrix of damping coefficients to describe the damping in laminated plates excited by the sinusoidal with respect to time force. The proposed damping ratio varies with frequency, temperature, and strain. But its value even in recently published works is arbitrarily assumed and its variation with frequency, temperature, and strain is ignored (Alam and Asnani, 1986). In order to avoid these doubts and to simplify analyses, the simplest model of viscous damping is taken into account in the same way as the model is used in forced random vibrations analysis of composite structures (Witt and Sobczyk, 1980).

In the present paper the applicability of the Liapunov method is extended to antisymmetrically-laminated cross-ply rectangular plates compressed by time-dependent random in-plane forces. Using the appropriate energy-like Liapunov functional, sufficient conditions for the asymptotic stability and the almost-sure asymptotic stability of undeflected form of the plate are derived. Stability domains obtained by applying the linearized equations of motion are compared with those employing the dynamic Kármán-type plate theory.

Problem Formulation

Let us consider a thin, cross-ply laminated rectangular plate consisting of an even number of elastic orthotropic layers antisymmetrically laminated about its middle surface from both a geometric and a material property standpoint. The Kirchhoff hypothesis on nondeformable normal element and Kármán-type geometric nonlinearity are taken into account. Neglecting in-plane, rotatory, and coupling inertias, the governing partial differential equations are given as (Chia, 1980)

$$N_{x,x} + N_{xy,y} = 0 \quad (1)$$

$$N_{xy,x} + N_{y,y} = 0 \quad (2)$$

$$\rho h w_{,tt} + 2\beta\rho h w_{,t} - \bar{N}_x w_{,xx} - \bar{N}_y w_{,yy} - M_{x,xx} - 2M_{xy,xy} - M_{y,yy} - N_x w_{,xx} - N_y w_{,yy} - 2N_{xy} w_{,xy} = 0.$$
$$(x,y) \in \Omega \equiv (0,a) \times (0,b). \quad (3)$$

In-plane and transverse displacements are denoted u, v, and w, respectively. ρ is the density of plate material, h is the total thickness, a and b denote in-plane dimensions of the plate, β is a damping coefficient, and $\bar{N}_x$ and $\bar{N}_y$ are time-dependent membrane forces. In-plane forces and moments are expressed by displacements as follows

$$N_x = A_{11}u_{,x} + A_{12}v_{,y} - B_{11}w_{,xx} + \frac{1}{2}(A_{11}w_{,x}^2 + A_{12}w_{,y}^2)$$
$$N_y = A_{12}u_{,x} + A_{22}v_{,y} + B_{11}w_{,yy} + \frac{1}{2}(A_{12}w_{,x}^2 + A_{22}w_{,y}^2) \quad (4)$$
$$N_{xy} = A_{66}(u_{,y} + v_{,x} + w_{,x}w_{,y})$$

$$M_x = B_{11}u_{,x} - D_{11}w_{,xx} - D_{12}w_{,yy} + \frac{1}{2}B_{11}w_{,x}^2$$
$$M_Y = -B_{11}v_{,y} - D_{12}w_{,xx} - D_{22}w_{,yy} - \frac{1}{2}B_{11}w_{,y}^2 \quad (5)$$
$$M_{xy} = -2D_{66}w_{,xy}$$

in which the plate extensional, coupling, and bending stiffnesses are

$$(A_{ij}, \beta_{ij}, D_{ij}) = \int_{-h/2}^{h/2} Q_{ij}(1, z, z^2)dz.$$

The reduced in-plane stiffnesses of an individual lamina are expressed in terms of the lamina principal material properties as

$$Q_{11} = E_1/(1 - \nu_{12}\nu_{21})$$
$$Q_{12} = E_2\nu_{12}/(1 - \nu_{12}\nu_{21})$$
$$Q_{22} = E_2/(1 - \nu_{12}\nu_{21})$$
$$Q_{66} = G_{12}$$
$$\nu_{21} = \nu_{12}E_2/E_1$$

where E_1, E_2, G_{12}, and ν_{12} are major Young's modulus, minor Young's modulus, and shear modulus, and major Poisson's ratio, respectively.

The plate is assumed to be simply supported along each edge. The conditions imposed on displacements and internal forces and moments, called according to Almroth's (1966) classification S2, can be written down as

$$w=0 \quad M_x=0 \quad N_x=0 \quad v=0 \quad \text{at} \quad x=0,a$$
$$w=0 \quad M_y=0 \quad N_y=0 \quad u=0 \quad \text{at} \quad y=0,b. \quad (6)$$

Dividing equations (1), (2), and (3) by ρh and denoting $n_x = N_x/\rho h$, $n_y = N_y/\rho h$, $n_{xy} = N_{xy}/\rho h$, $m_x = M_x/\rho h$, $m_y = M_y/\rho h$, $m_{xy} = M_{xy}/\rho h$, $f_x = N_x/\rho h$, $f_y = N_y/\rho h$ leads to the basic equations of motion

$$n_{x,x} + n_{xy,y} = 0 \quad (7)$$

$$n_{xy,x} + n_{y,y} = 0 \quad (8)$$

$$w_{,tt} + 2\beta w_{,t} - f_x w_{,xx} - f_y w_{,yy} - m_{x,xx} - 2m_{xy,xy} - m_{y,yy} - n_x w_{,xx} - n_y w_{,yy} - 2n_{xy} w_{,xy} = 0, \quad (x,y)\in\Omega \quad (9)$$

due to the bending-extension coupling the equations (7), (8), and (9) are coupled even in a linearized case.

Let us assume that the solution of equations (7), (8), and (9) exists and belongs to the Hilbert space $\dot{W}_{2,2}(\Omega)$.

The purpose of the present paper is to derive criteria for solving the following problem: Will the deviation of plate surface from the unperturbed state (trivial solution) be sufficiently small, in some stochastic sense, in the case when membrane forces are time dependent. The plate dynamically buckles when the membrane forces get so large that the plate does not oscillate about the unperturbed plane state and a new increasing mode of oscillations occurs. To estimate a perturbed plate surface, we introduce a measure $\|\cdot\|$ of distance of the solution of equations (7), (8), and (9) with nontrivial initial conditions from the trivial solution. Throughout the paper the meaning of the term measure is slightly different from that used in analysis. The introducing of a measure is necessary in order to define neighborhoods on $\dot{W}_{2,2}(\Omega)$ and to estimate motion perturbation. It should also be emphasized that there is a difference of meaning of the term stability in continuous (infinite-dimensional) systems from that in discrete systems. As, in general, norms, measures of distance, and metrics defined on infinite-dimensional spaces are not equivalent, it is possible to have stability for some measures, while giving instability with respect to others.

We are going to analyze the asymptotic and almost-sure asymptotic stability of unperturbed solution. Following Caughey and Gray (1965), we will say that the trivial solution of equations (7), (8), and (9) is almost-sure asymptotically stable, is a measure of distance between the perturbed solution with arbitrary initial conditions and the trivial one tends to zero with probability one as time tends to infinity

$$P(\lim_{t\to\infty} \|w\| = 0) = 1. \quad (10)$$

In the deterministic case, the trivial solution is called asymptotically stable if, for all solutions of equations (7), (8), and (9) with arbitrary initial conditions, a measure of distance between the perturbed solution and the trivial one tends to zero as time tends to infinity

$$\lim_{t\to\infty} \|w\| = 0. \quad (11)$$

From the mathematical point of view the feature common to all parametric vibrations is that they are described by differential equations with coefficients depending explicitly on time. In deterministic parametric vibration it is well known that the stability properties are determined from the Mathieu equation together with the corresponding Ince-Strutt diagram. If the parametric excitation becomes random the stability criteria depend on the statistical characteristics of the excitation and the system parameters. Specifically, if the excitation is sufficiently narrow-bounded or it has one latent periodicity, a series of wedges on the amplitude-frequency plane can be expected analogously to the deterministic parametric resonance. The task is not so simple when the stochastic excitation is wide-band and continuous systems with the infinite number of natural frequencies are analyzed. Difficulties especially arise when information concerning the power spectral density of the excitation is not available and the excitation is described by the probability distribution only. In the present analysis the direct Liapunov method is proposed to overcome these difficulties and to establish criteria for the almost-sure asymptotic stability of laminated plate treated as the infinite-dimensional system subjected to the in-plane stochastic forces with the known probability distribution.

Stability of Linearized Equations

We start from a linearized problem, i.e., omitting the nonlinear terms in formulae (4) and (5). Using Kozin's method derived for linear problems (Kozin, 1972), we construct the functional as a sum of modified kinetic energy T and potential energy of the plate

$$V = T + \frac{1}{2}\int_\Omega [-m_x w_{,xx} - m_y w_{,yy} - 2m_{xy}w_{,xy} + n_x u_{,x} + n_y v_{,y} + n_{xy}(u_{,y} + v_{,x})]d\Omega, \tag{12}$$

where

$$T = \frac{1}{2}\int_\Omega (w_{,t}^2 + 2\beta w w_{,t} + 2\beta^2 w^2)d\Omega.$$

The functional is positive definite as the terms of the integrand in T can be rearranged as a sum of squares. Under the previous assumptions imposed on in-plane forces, the classic differentiation rule can be applied to calculate the time-derivative of functional (12)

$$\frac{dV}{dt} = \int_\Omega \left\{(w_{,t} + \beta w)w_{,tt} + \beta w_{,t}^2 + 2\beta^2 w w_{,t} + \frac{1}{2} \times \left[-m_{x,t}w_{,xx} - m_x w_{,xxt} - m_{y,t}w_{,yy} - m_y w_{,yyt} - 2m_{xy,t}w_{,xy} - 2m_{xy}w_{,xyt} + n_{x,t}u_{,x} + n_x u_{,xt} + n_{y,t}v_{,y} + n_y v_{,yt} + n_{xy,t}(u_{,y} + v_{,x}) + n_{xy}(u_{,yt} + v_{,xt})\right]\right\}d\Omega. \tag{13}$$

Upon substituting the linearized version of equation (9), we rewrite expression (13) in the form

$$\frac{dV}{dt} = -2\beta V + 2U, \tag{14}$$

where an auxiliary functional U is defined as follows:

$$U = \frac{1}{2}\int_\Omega \Big[2\beta^2 w w_{,t} + 2\beta^3 w^2 + (w_{,t} + \beta w)(f_x w_{,xx} + f_y w_{,yy}) + m_{x,xx}w_{,t} + 2m_{xy,xy}w_{,t} + m_{y,yy}w_{,t} + \beta m_{x,xx}w + 2\beta m_{xy,xy}w + \beta m_{y,yy}w - \beta m_x w_{,xx} - \beta m_y w_{,yy} - 2\beta m_{xy}w_{,xy} - \frac{1}{2}(m_{x,t}w_{,xx} + m_x w_{,xxt} + m_{y,t}w_{,yy} + m_y w_{,yyt} + 2m_{xy,t}w_{,xy} + 2m_{xy}w_{,xyt})\Big]d\Omega + \frac{1}{2}I_1 + \frac{1}{2}I_2. \tag{15}$$

In equation (15), the last two terms are given by the relations

$$I_1 = \int_\Omega (n_{x,t}u_{,x} + n_{y,t}v_{,y} + n_{xy,t}(u_{,y} + v_{,x}))d\Omega,$$

$$I_2 = \int_\Omega (n_x u_{,xt} + n_y v_{,yt} + n_{xy}(u_{,yt} + v_{,xt}))d\Omega.$$

Upon integrating by parts, we obtain

$$I_1 = \int_0^b n_{x,t}\, u \Big|_0^a dy - \int_\Omega n_{x,xt}u d\Omega + \int_0^a n_{y,t}\, v \Big|_0^b dx - \int_\Omega n_{y,yt}v d\Omega + \int_0^a n_{xy,t}u \Big|_0^b dx - \int_\Omega n_{xy,yt}u d\Omega + \int_0^b n_{xy,t}v \Big|_0^a dy - \int_\Omega n_{xy,xt}v d\Omega.$$

Taking into account boundary conditions (6) imposed on n_x and $n_{,y}$, and substituting equations (7) and (8), we have

$$I_1 = -\int_\Omega \Big[(n_{x,x} + n_{xy,y})_{,t}u + (n_{y,y} + n_{xy,x})_{,t}v\Big]d\Omega = 0. \tag{16}$$

We can prove in the same fashion that

$$I_2 = 0. \tag{17}$$

Upon integrating by parts and using boundary conditions (6) imposed on transverse displacement w, transverse velocity $w_{,t}$, and moments, we arrive at the following formulae

$$\int_\Omega m_{x,xx}g d\Omega = \int_\Omega m_x g_{,xx}d\Omega$$
$$\int_\Omega m_{y,yy}g d\Omega = \int_\Omega m_y g_{,yy}d\Omega$$
$$\int_\Omega m_{xy,xy}g d\Omega = \int_\Omega m_{xy}g_{,xy}d\Omega, \tag{18}$$

where $g = (w,\ w_{,t})$.

The first two equations of motion (7) and (8), written explicitly in displacement, can be treated as a second-order system of partial differential equations with respect to functions u and v. Solving the system by means of Fourier series, we can check that the following equalities are satisfied

$$\int_\Omega m_{x,t}w_{,xx}d\Omega = \int_\Omega m_x w_{,xxt}d\Omega$$
$$\int_\Omega m_{y,t}w_{,yy}d\Omega = \int_\Omega m_y w_{,yyt}d\Omega. \tag{19}$$

Upon using equalities (16), (17), (18), and (19) it is possible to convert the functional U into the simple form

$$U = \frac{1}{2}\int_\Omega \Big[2\beta^2 w w_{,t} + 2\beta^3 w^2 + (w_{,t} + \beta w)(f_x w_{,xx} + f_y w_{,yy})\Big]d\Omega. \tag{20}$$

Now we attempt to construct a bound

$$U \le \lambda V, \tag{21}$$

where the function λ is to be determined. From equation (14) and inequality (21) we have

$$V(t) \le V(0)\exp\left\{-2t\left[\beta - \frac{1}{t}\int_0^t \lambda(s)ds\right]\right\}. \tag{22}$$

Thus, it immediately follows that the sufficient stability condition for the asymptotic stability, with respect to the measure $\|\bullet\| = V^{1/2}$, is

$$\beta \ge \lim_{t\to\infty}\frac{1}{t}\int_0^t \lambda(s)ds \tag{23}$$

or, for the almost-sure asymptotic stability, if the processes f_x and f_y are stationary and satisfy an ergodic property guaranteeing the equality of time averages and ensemble averages with probability, one is

$$E\lambda \leq \beta \tag{24}$$

where E denotes the operator of the mathematical expectation.

Our object now is to obtain a function λ satisfying inequality (21). It means that the function λ is defined as a maximum of ratio U/V over all admissible functions w and $w_{,t}$ satisfying boundary conditions. As the maximum is a particular case of a stationary point of the ratio, we apply the variational calculus and solve the problem $\delta(U/V) = 0$. Upon writing and solving the associated Euler equations, which are linear in the case of second-order functionals, we find the function

$$\hat{\beta} \geq E\left\{ \max_{i,j=1,2,\ldots} \left| \hat{\beta}^2 + (\hat{f}_x r^2 i^2 + \hat{f}_y j^2)/2 \right| (\hat{\beta}^2 + \Gamma_{ij} + \kappa_{ij})^{-1/2} \right\}, \tag{25}$$

where

$$\Gamma_{ij} = i^4 r^4 + 4 i^2 j^2 r^2 (p + 2q)/(F+1) + j^4,$$
$$\kappa_{ij} = -[3(F-1)^2/2(F+1)N^2][2(p+q) r^4 i^4 j^4 + ((F+1) r^2 i^2/2 + q j^2) j^6 + (q i^2 r^2 + (F+1) j^2/2) r^6 i^6] / \times [((F+1) r^2 i^2/2 + q j^2)(q r^2 i^2 + (F+1) j^2/2) - (p+q)^2 r^2 i^2 j^2], \quad \hat{\beta} = \beta b^2 (h\delta/D_{11}\pi^4)^{1/2},$$
$$\hat{f} = f b^2 \rho h / D_{11}\pi^2, \quad r = b/a,$$

$p = Q_{12}/Q_{11}$, $q = Q_{66}/Q_{11}$, $F = Q_{22}/Q_{11}$ and N denotes the number of layers. Inequality (25) provides a sufficient condition guaranteeing the almost-sure asymptotic stability of the undeflected form of plate subjected to time-dependent membrane forces. It should be mentioned that in view of equality (17), written for functions $u_{,x}$, $u_{,y}$, $v_{,x}$, $v_{,y}$ instead of $u_{,xt}$, $u_{,yt}$, $v_{,xt}$, and $v_{,yt}$, respectively, the Liapunov functional (12) can be simplified since the integral of the last three components of the integrand is equal to zero

$$\int_\Omega [n_x u_{,x} + n_y v_{,y} + n_{xy}(u_{,y} + v_{,x})] d\Omega = 0. \tag{26}$$

Stability of Nonlinear Equations

The auxiliary linearized problem being solved, we can direct our attention to equations (7), (8), and (9) governing the moderately large vibrations of plate. In order to construct a suitable Liapunov function, we change the second part of potential energy in expression (12), taking into account the strain components dependence on transverse displacement

$$V_N = T + \frac{1}{2} \int_\Omega \left[-m_x w_{,xx} - m_y w_{,yy} - 2m_{xy} w_{,xy} + n_x\left(u_{,x} + \frac{1}{2} w_{,x}^2\right) + n_y\left(v_{,y} + \frac{1}{2} w_{,y}^2\right) + n_{xy}(u_{,y} + v_{,x} + w_{,x} w_{,y}) \right] d\Omega, \tag{27}$$

where forces and moments are defined in formulae (4) and (5).

Upon differentiating, we convert the derivative of functional to the form (14), where U should be replaced by U_N

$$U_N = U + \frac{1}{4} \int_\Omega \left[\frac{1}{2} n_{x,t} w_{,x}^2 + \frac{1}{2} n_{y,t} w_{,y}^2 + n_{xy,t} w_{,x} + n_x w_{,x} w_{,xt} + n_y w_{,y} w_{,yt} + n_{xy}(w_{,xt} w_{,y} + w_{,x} w_{,yt}) + \beta(n_x w_{,x} + n_y w_{,y} + 2n_{xy} w_{,x} w_{,y}) \right] d\Omega. \tag{28}$$

Upon integrating by parts and using nonlinear boundary conditions (6), one can significantly simplify functional U_N

$$U_N = U - \frac{\beta}{2} \int_\Omega \left[n_x\left(u_{,x} + \frac{1}{2} w_{,x}^2\right) - n_y\left(v_{,y} + \frac{1}{2} w_{,y}^2\right) - n_{xy}(u_{,y} + v_{,x} + w_{,x} w_{,y}) \right] d\Omega. \tag{29}$$

It may be observed that contrary to the linearized case both V_N and U_N are fourth-order functionals. It complicates a stability analysis and the problem is to find a function λ satisfying inequality

$$U_N \leq \lambda V_N. \tag{30}$$

The associated Euler equations are nonlinear in the case of the fourth-order functionals. Therefore, our object now is to find such second-order functionals V^* and U^* that the inequality

$$U^* \leq \lambda V^*$$

will make inequality (30) to be true. In order to do this we introduce the following notations $(a_{ij}, b_{11}, d_{ij}) = (A_{ij}, B_{11}, D_{ij})/\rho h$ and express functional (27) in terms of displacements

$$V_N = T + \frac{1}{2} \int_\Omega \left[a_{11}\left(u_{,x} + \frac{1}{2} w_{,x}\right)^2 + a_{22}\left[v_{,y} + \frac{1}{2} w_{,y}\right]^2 + 2a_{12}\left(u_{,x} + \frac{1}{2} w_{,x}^2\right)\left(v_{,y} + \frac{1}{2} w_{,y}^2\right) + a_{66}(u_{,y} + v_{,x} + w_{,x} w_{,y})^2 - 2b_{11}\left(u_{,x} + \frac{1}{2} w_{,x}^2\right) w_{,xx} + 2b_{11}\left(v_{,y} + \frac{1}{2} w_{,y}^2\right) w_{,yy} + d_{11} w_{,xx}^2 + 2d_{12} w_{,xx} w_{,yy} + d_{22} w_{,yy}^2 + 4d_{66} w_{,xy}^2 \right] d\Omega. \tag{31}$$

Using the identity $V_N = V_N + V_b/4k^2 - V_b/4k^2$, where V_b is a bending energy of orthotropic plate with the same bending stiffnesses

$$V_b = \frac{1}{2} \int_\Omega (d_{11} w_{,xx}^2 + 2d_{12} w_{,xx} w_{,yy} + d_{22} w_{,yy}^2 + 4d_{66} w_{,xy}^2) d\Omega$$

and k is a number greater than 1, chosen so that we will obtain the greatest stability region, we regroup functional (31) in the following way:

$$V_N = V + \frac{1}{2} \int_\Omega \left[a_{11}\left(u_{,x} + \frac{1}{2} w_{,x}^2\right)^2 + 2a_{12}\left(u_{,x} + \frac{1}{2} w_{,x}^2\right) \times \left(v_{,y} + \frac{1}{2} w_{,y}^2\right) + a_{22}\left(v_{,y} + \frac{1}{2} w_{,y}^2\right)^2 + a_{66}(u_{,y} + v_{,x} + w_{,x} w_{,y})^2 - 4b_{11}k\left(u_{,x} + \frac{1}{2} w_{,x}^2\right) w_{,xx}/2k + 4b_{11}k\left(v_{,y} + \frac{1}{2} w_{,y}^2\right) w_{,yy}/2k + d_{11}(w_{,xx}/2k)^2 + 2d_{12}(w_{,xx}/2k)(w_{,yy}/2k) + d_{22}(w_{,yy}/2k)^2 + 4d_{66}(w_{,xy}/2k)^2 \right] d\Omega - \frac{1}{2} \int_\Omega [a_{11} u_{,x}^2 + 2a_{12} u_{,x} v_{,y} + a_{22} v_{,y}^2 - 4b_{11} k u_{,x} w_{,xx}/2k + 4b_{11} k v_{,y} w_{,yy}/2k] d\Omega - V_b/4k^2. \tag{32}$$

The second functional in equation (32) is positive definite for sufficiently small k. The functional can be interpreted as a modified potential energy of plate and can be written down as the integral of quadratic form

$$V_p = \frac{1}{2} \int_\Omega \mathbf{z}^T \mathbf{C} \mathbf{z} d, \tag{33}$$

where $(\bullet)^T$ denotes a transposition of matrix and $\mathbf{z}$ is a modified state of strain defined by a column matrix

$$
\mathbf{z} = \begin{bmatrix} u_{,x} + \frac{1}{2} w_{,x}^2 \\ v_{,y} + \frac{1}{2} w_{,y}^2 \\ u_{,y} + v_{,x} + w_{,x} w_{,y} \\ -\frac{1}{2k} w_{,xx} \\ -\frac{1}{2k} w_{,yy} \\ -\frac{1}{k} w_{,xy} \end{bmatrix}.
$$

The matrix **C** is given as follows:

$$
\mathbf{C} = \begin{bmatrix} a_{11} & a_{12} & 0 & -2kb_{11} & 0 & 0 \\ a_{12} & a_{22} & 0 & 0 & 2kb_{11} & 0 \\ 0 & 0 & a_{66} & 0 & 0 & 0 \\ -2kb_{11} & 0 & 0 & d_{11} & d_{12} & 0 \\ 0 & 2kb_{11} & 0 & d_{12} & d_{22} & 0 \\ 0 & 0 & 0 & 0 & 0 & d_{66} \end{bmatrix}. \tag{34}
$$

The functional V_p is positive definite if the Sylvester conditions of positive definiteness for matrix **C** are satisfied (Gantmacher, 1960)

$$
\begin{aligned}
& d_{11}^2 - d_{12}^2 > 0 \\
& a_{11}(d_{11}^2 - d_{12}^2) - 4k^2 b_{11}^2 d_{11} > 0 \\
& (d_{11}^2 - d_{12}^2)(a_{11}^2 - a_{12}^2) + 16k^4 b_{11}^4 \\
& \quad - 8k_{11}^2(a_{11}d_{11} - a_{12}d_{12}) > 0.
\end{aligned} \tag{35}
$$

We can solve inequalities (35) and obtain the number k as a function of material properties and the number of layers N. Omitting the fourth-order functional V_p and taking into account formula (26), we obtain the lower estimation of functional V_N by the second-order functional $V_N \geq V^* = T + (1 - 1/4k^2)V_b$. In a similar way we have the upper estimation of functional U_N $U_N \leq U^* = U + \beta V_b/16k^2$. Now we see that if a function λ satisfies the following condition for the second-order functionals

$$
U + \beta V_b/16k^2 \leq \lambda\,[T + (1 - 1/4k^2)V_b], \tag{36}
$$

then the same function λ will fulfill inequality (30).

We mention that condition (36) differs significantly from inequality (21) relating to the linearized case. Similar to the stability of uniform elastic shells (Tylikowski, 1984) described by Kármán's equations, it is found that the sufficient stability condition (24) can not be sufficient to ensure the stability of trivial solution of nonlinear equations for laminated plates.

Solving the associated Euler problem we find the function as follows:

$$
\begin{aligned}
\lambda = \max_{i,j=1,2,\ldots} \Big\{ & \hat{\beta}\Gamma_{ij}^2/4k^2 + \Big[\beta^2\Gamma_{ij}^4/16k^4 \\
& + 4\left(4\hat{\beta}^2 + (4 - 1/k^2)\Gamma_{ij}^2\right)(2\hat{\beta}^2 + \hat{f}_x r^2 i^2 \\
& + \hat{f}_y j^2)\Big]^{1/2}\Big\} \Big/ \left[2\left(4\hat{\beta}^2 + (4 - 1/k^2)\Gamma_{ij}^2\right)\right].
\end{aligned} \tag{37}
$$

Numerical Results and Discussion

Formulae (25) and (40) give us the possibility to calculate minimal damping coefficients guaranteeing the almost-sure asymptotic stability for given values of excitation intensity. The almost-sure asymptotic stability region is defined as the set where the damping coefficient $\hat{\beta}$ is greater than this critical value. Two groups of composite materials, namely glass epoxy and graphite epoxy, have been examined. The mechanical properties of these materials taken from the paper by Bert (1976) are given in Table 1. The number k^2 maximizing stability regions calculated from inequalities (35) depends on the number of layers. In the case of two-layered plates, when the bending-extension coupling is greatest, we have $k^2 = 1.31$ and $k^2 = 1.2$ for the glass epoxy and the graphite epoxy plate, respectively.

Table 1 Mechanical properties of the considered composite materials

Property	glass epoxy	graphite epoxy
Major Young's modulus E_1 (GPa)	53.8	172.4
Minor Young's modulus E_2 (GPa)	17.93	7.79
Shear modulus G_{12} (GPa)	8.96	5.3
Major Poisson's ratio ν_{12}	0.25	0.35
Density (kg m^{-3})	2004	1530

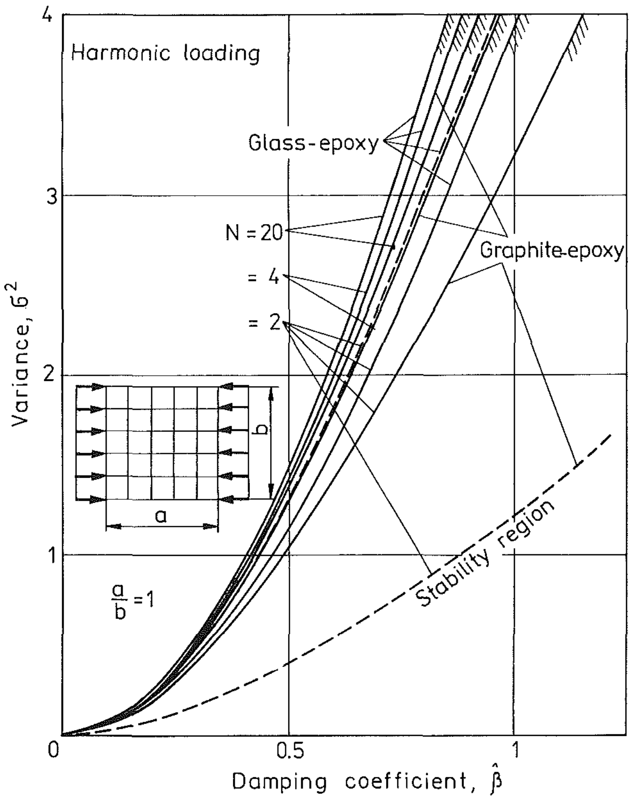

Fig. 1 Stability regions under the harmonic loading

The stability regions are calculated for two different classes of parametric excitation. First, under assumption that the excitation is harmonic with amplitude A, arbitrary frequency and random phase, the in-plane loading has the form $f = A \sin(\omega t + \varphi)$. If the random phase has a uniform distribution on $(0, 2\pi)$, the process f is zero-mean, stationary, and ergodic, and its probability density function is given as follows: $g(z) = [\pi A(1 - (z/A)^2)^{1/2}]^{-1}$ for $|z| < A$. The second class of parametric excitation is a Gaussian zero-mean process with variance σ^2. In order to compare the stability regions for both excitations, we introduce also the variance of the harmonic process related to the amplitude by means of the formula $\sigma^2 = A^2/2$.

The stability regions as functions of σ, $\hat{\beta}$, N, and r are calculated numerically in the case of unidirectional loading

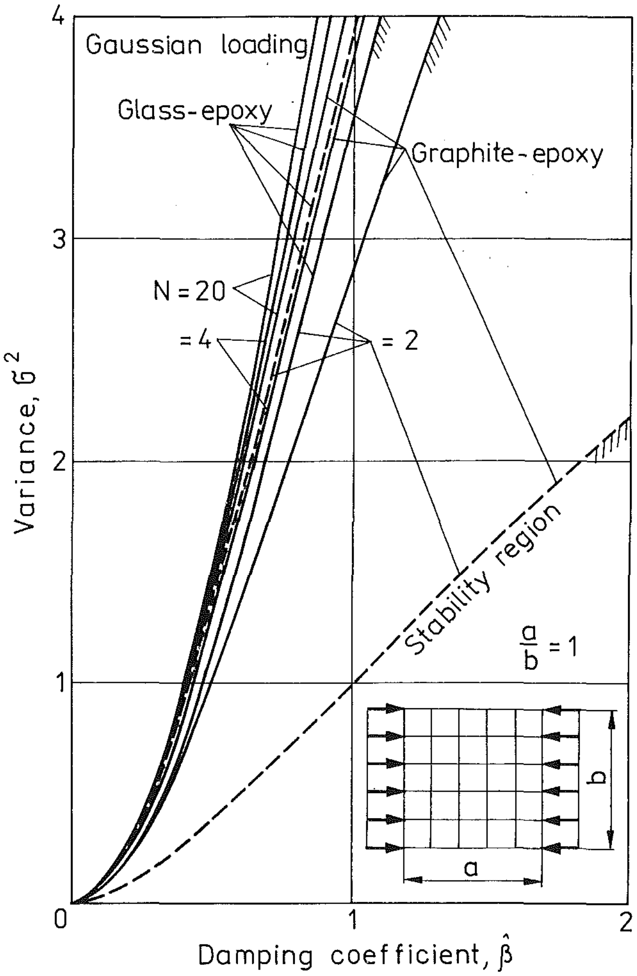

Fig. 2 Stability regions under the Gaussian loading

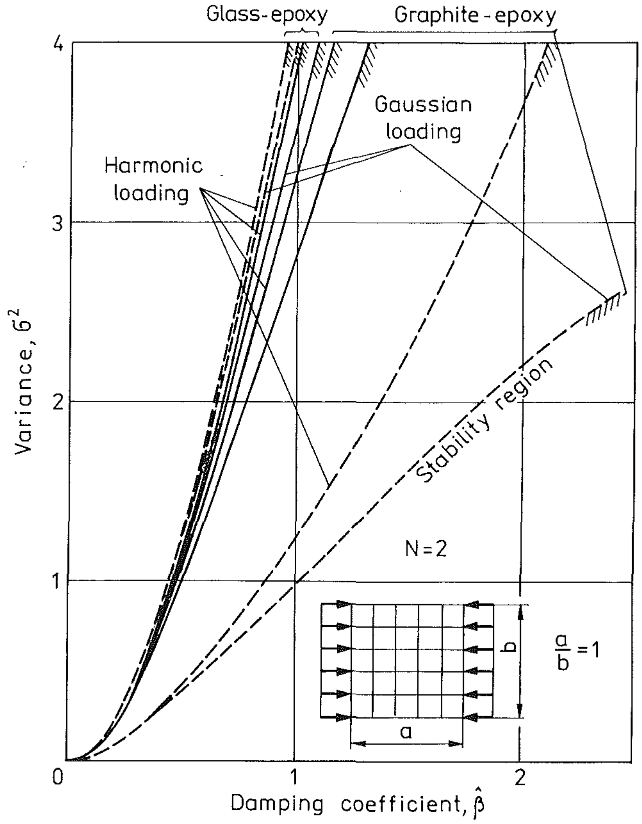

Fig. 3 Comparison of stability regions under the Gaussian and the harmonic loading

only. Boundaries of stability regions calculated from the nonlinear theory and the linearized one are drawn using the solid and broken line, respectively. The almost-sure asymptotic stability regions of a square plate harmonically loaded are shown in Fig. 1. It is seen that if N is increased $\hat{\beta}_{cr}$ decreases. The graphite epoxy plate is much more sensitive to increasing of N as compared with the glass epoxy plate. In order to test the influence of geometric nonlinearity, the stability regions for the linearized equations of the two-layered plate are also calculated. As observed, the stability regions for the glass-epoxy plate slightly depend on the approach applied. On the contrary, when the graphite epoxy plate is analyzed, β_{cr} calculated from the linearized theory is approximately two times more than that obtained from the nonlinear approach. The results obtained in the present paper can not be directly compared with those published by Birman (1985) in the form of wedges in the amplitude-frequency plane as they neglect the effect of damping. The present analysis applied to the deterministic harmonic loading enables one to calculate the bottom points of wedgelike stability regions embedded in the corresponding wedges obtained by Birman for undamped systems.

The boundaries of stability regions for a square plate loaded by the Gaussian process are plotted in Fig. 2. Their behavior is similar to that presented in Fig. 1. A comparison of stability regions of two-layered plate for the Gaussian loading and the harmonic one is shown in Fig. 3. Like before, β_{cr} of graphite epoxy plate is more sensitive to the change of loading class. It is seen that β_{cr} for the Gaussian loading is greater than for the harmonic loading. This increase can be attributed to the fact that the probability of event that the harmonic force is greater than $A = \sigma\sqrt{2}$ is equal to zero and the corresponding probability for the Gaussian process is positive. Moreover, the dependence is more articulated for the linearized theory, when the change from the glass epoxy plate to the graphite epoxy one rapidly increases β_{cr}. Figures 4 and 5 display increasing of stability regions with increasing of the plate aspect ratio r. The critical damping coefficients of the graphite epoxy plate change more rapidly as the plate aspect ratio increases in comparison with the glass epoxy plate. It should be noted that there is a significant difference in the dependence of stability regions on the linearized and the nonlinear approaches in relation to the glass epoxy and the graphite epoxy plate. The linearized approach in the case of glass epoxy plate gives more conservative results. On the other hand, when the graphite epoxy plate is analyzed, results do not belong to the stability region.

The Liapunov method used in the paper is general in nature. Although the present study is limited to the antisymmetrical configuration and the simply-supported boundary conditions S2, this can be extended without much effort to the symmetric configuration and the clamped boundary conditions C3. In both problems the Liapunov functional V and the auxiliary functional U have the same form and the final stability condition (24) can be derived, provided that the function λ in estimation (30) is known. The calculation of the function λ is more complicated as the presence of new coupling coefficients in dynamic equations and modified boundary conditions make a closed-form solution of associated Euler equations impossible. The approximate Rayleigh-Ritz technique or the Galerkin method should be used to solve the auxiliary variational problem.

Conclusions

The applicability of the direct Liapunov method has been extended to geometrically nonlinear laminated plates subjected

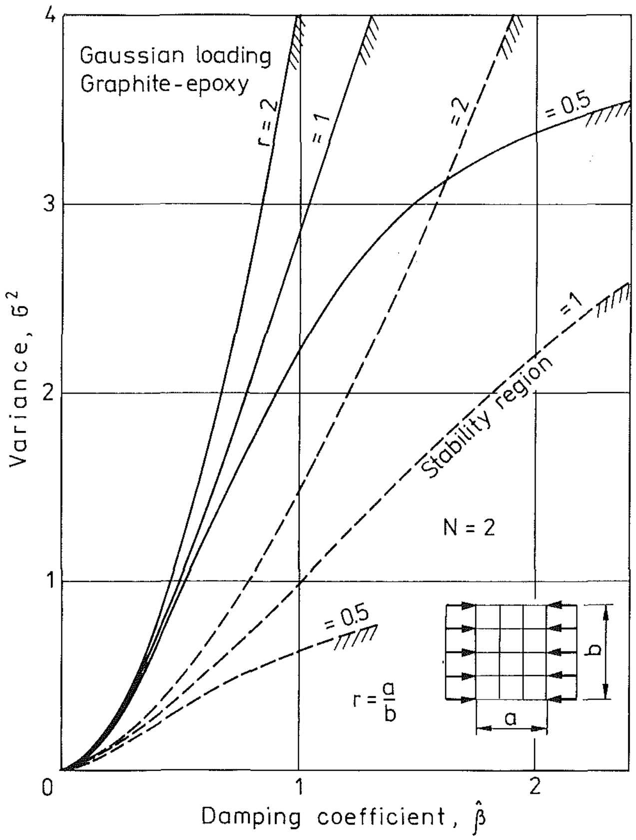

Fig. 4 Influence of plate aspect ratio on stability regions of the graphite epoxy laminated plate under the Gaussian loading

to time-dependent, in-plane forces. The major conclusion is that the linearized problem should be modified to ensure the stability of nonlinear plates. The criteria developed in the paper define stability regions in terms of the loading variance, the linear damping coefficient, the properties of plates, and the plate aspect ratio.

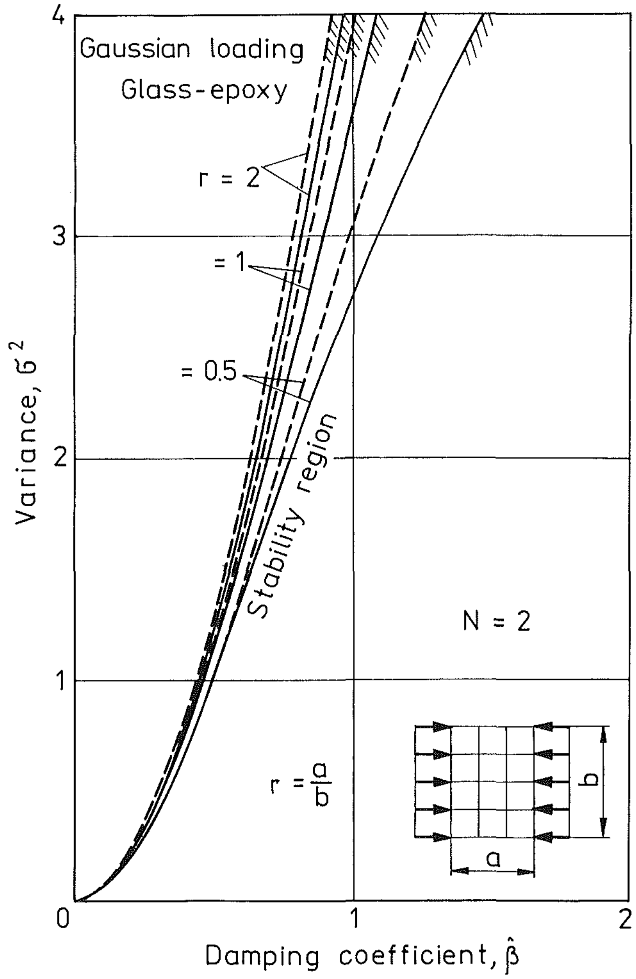

Fig. 5 Influence of plate aspect ratio on stability regions of the glass epoxy laminated plate under the Gaussian loading

References

Alam, N., and Asnani, N. T., 1986, "Vibration and Damping Analysis of Fibre Reinforced Composite Material Plates," *Journal of Composite Materials*, Vol. 20, pp. 2–18.

Almroth, B. O., 1966, "Influence of Edge Conditions on the Stability of Axially Compressed Cylindrical Shells," *Journal of American Institute of Aeronautics and Astronautics*, Vol. 4, pp. 134–140.

Ashton, J. E., 1969, "Approximate Solutions for Unsymmetrically Laminated Plates," *Journal of Composite Materials*, Vol. 3, pp. 189–191.

Bennett, J. A., 1971, "Nonlinear Vibration of Simply Supported Angle-Ply Laminated Plates," *Journal of American Institute of Aeronautics and Astronautics*, Vol. 9, pp. 1997–2003.

Bert, C. W., 1973, "Nonlinear Vibration of a Rectangular Plate Arbitrarily Laminated of Anisotropic Material," ASME Journal of Applied Mechanics, Vol. 40, pp. 452–458.

Bert, C. W., 1976, "Damping of Composite and Sandwich Panels, Part I," *The Shock and Vibration Digest*, Vol. 8, No. 10, pp. 37–48.

Bert, C. W., and Mayberry, B. L., 1969, "Free Vibration of Unsymmetrically Laminated Anisotropic Plates with Clamped Edges," *Journal of Composite Materials*, Vol. 3, pp. 282–293.

Birman, V., 1985, "Dynamic Stability of Unsymmetrically Laminated Rectangular Plates," *Mechanics Research Communications*, Vol. 12, pp. 81–86.

Caughey, T. K., and Gray, Jr., A. H., 1965, "On the Almost-Sure Stability of Linear Dynamic Systems with Stochastic Coefficients," ASME Journal of Applied Mechanics, Vol. 32, pp. 365–372.

Chandra, R., and Basawa Raju, B., 1975, "Large Deflection Vibration of Angle-Ply Laminated Plates," *Journal of Sound and Vibration*, Vol. 40, pp. 393–407.

Chia, C., 1980, *Nonlinear Analysis of Plates*, McGraw-Hill, New York, pp. 13–21.

Dong, S. B., 1967, "Behaviour of Laminated Orthotropic Viscoelastic Plates," *Journal of Spacecraft and Rockets*, Vol. 4, pp. 1385–1388.

Gantmacher, F. R., 1960, *The Theory of Matrices*, Vol. 1, Chelsea Publishing Co., New York.

Hui, D., 1985, "Soft-Spring Nonlinear Vibrations of Antisymmetrically Laminated Rectangular Plates," *International Journal of Mechanical Sciences*, Vol. 27, pp. 397–408.

Jones, R. M., 1973, "Buckling and Vibration of Unsymmetrically Laminated Cross-Ply Rectangular Plates," *Journal of American Institute of Aeronautics and Astronautics*, Vol. 11, pp. 1626–1632.

Kozin, F., 1972, "Stability of the Linear Stochastic Systems," *Lecture Notes in Mathematics*, Vol. 294, pp. 186–229.

Kulkarni, A. M., Banerjee, J. R., and Sinha, P. K., 1975, "Response of Randomly Excited Orthotropic Sandwich Plates," *Journal of Sound and Vibration*, Vol. 41, pp. 197–205.

Salama, A. M., and Chen, J. C., 1973, "On the Dynamic Stability of Multilayer Sandwich Plates," *Journal of Structure Mechanics*, Vol. 2, pp. 325–341.

Siu, C. C., and Bert, C. W., 1974, "Sinusoidal Response of Composite-Material Plates with Material Damping," ASME *Journal of Engineering for Industry*, Vol. 96, pp. 603–610.

Srinivasan, R. S., and Chellapandi, P., 1986, "Dynamic Stability of Rectangular Laminated Composite Plates," *Computers and Structures*, Vol. 24, pp. 233–238.

Sun, C. T., and Whitney, J. M., 1974, "Forced Vibrations of Laminated Composite Plates in Cylindrical Bending," *Journal of the Acoustical Society of America*, Vol. 55, pp. 1003–1008.

Tylikowski, A., 1978, "Stability of a Nonlinear Plate," ASME Journal of Applied Mechanics, Vol. 45, pp. 583–585.

Tylikowski, A., 1984, "Dynamic Stability of a Nonlinear Cylindrical Shell," ASME Journal of Applied Mechanics, Vol. 51, pp. 852–856.

Whitney, J. M., and Leissa, A. W., 1969, "Analysis of Heterogeneous Anisotropic Plates," ASME Journal of Applied Mechanics, Vol. 36, pp. 261–266.

Witt, M., and Sobczyk, K., 1980, "Dynamic Response of Laminated Plates to Random Loading," *International Journal of Solids and Structures*, Vol. 16, pp. 251–238.

D. A. Dillard
Engineering Science and
Mechanics Department,
Virginia Polytechnic Institute and
State University,
Blacksburg, VA 24061

Bending of Plates on Thin Elastomeric Foundations

Closed-form and series solutions are presented for the bending of plates bonded to a thin elastomeric foundation which is in turn bonded to a rigid substrate. The standard fourth-order governing differential equation of a classical Winkler elastic foundation becomes a sixth-order equation for the case of an incompressible foundation. Oscillation decay rates are shown to be significantly different from those of the Winkler solution due to the incompressibility of the elastomer.

Introduction

Elastomeric materials are commonly used as supports between machine or structural elements to give desired flexibility and damping characteristics. Because of the extremely low extensional and shear moduli compared to the bulk modulus, these materials often require different analysis techniques from other engineering materials. For example, when an elastomeric block is bonded between rigid platens and compressed (or extended), the pressure distribution is far from being uniform. Instead the pressures are almost parabolically distributed, being very high at the center and nearly zero at the edges. As has been pointed out by Gent and Meinecke (1970), the dominant stress distribution obeys Poisson's equation and is, therefore, equivalent to the torsion stress function or the deflection of a pressurized soap film.

When plates are supported on elastomeric foundations, special techniques must be employed to calculate the deflected shapes. This paper provides a solution for the case of an elastic plate bonded to a relatively thin elastomeric foundation which is in turn bonded to a rigid substrate. Plate solutions based on a Winkler foundation are shown to be inadequate for these configurations. An alternate solution is proposed which utilizes a modified plate theory approach to correctly account for the special nature of an incompressible foundation.

Background

The original solution for the bending of beams on an elastic foundation has been attributed to Winkler (1867). This solution assumes that the restoring force exerted on the beam by the foundation is proportional to the deflection. The implication is that the restoring force at a point is dependent only on the deflection at that point, not on neighboring deflections. Although this assumption is accurate for the case of closely-spaced independent springs, it breaks down when the foundation is a continuum. This is particularly true when the foundation material has a high Poisson's ratio. In an attempt to reduce the errors, Biot (1937) considered the cases of a beam on a narrow semi-infinite wall and a beam on a three-dimensional semi-infinite continuum. Only with proper adjustment of the foundation stiffness, k, could the Winkler solution be brought into even approximate agreement with Biot's solutions. Despite inaccuracies, the Winkler approach has remained a widely used and relatively simple solution for these beam problems.

When a Winkler-type continuum foundation is utilized for plate solutions even greater inaccuracies arise, because the constraint occurs in two directions. If Poisson's ratio is zero, the Winkler assumption that restoring pressure at a point is proportional to the deflection at that point is valid. If Poisson's ratio is greater than zero, the restoring pressure is actually a function of the entire plate deformation field. The kernel is heavily weighted towards the localized region around the point of interest. Since slopes and displacements are continuous, the Winkler assumption remains reasonably accurate if the proportionality constant is chosen to reflect Poisson's ratio (Timoshenko and Woinowski-Krieger, 1959). As expected, however, the accuracy of this approximation becomes worse as Poisson's ratio increases. Of interest in the current study is the case where the foundation is an elastomer and Poisson's ratio is a maximum, $\nu \sim 0.5$.

Although three-dimensional elasticity could be used to solve this problem, the technique would be very cumbersome, especially with the two materials required. In the spirit of classical plate studies, this work proposes an alternate governing differential equation which is valid for certain geometries involving elastomeric foundations. It provides a simple closed-form approach to accurately accommodate the restoring force distribution.

Problem Formulation

Figure 1 illustrates the problem being addressed. The thickness of the elastomer will be assumed to be small compared with the oscillation spacing of the deflected plate. The requirement for bonding between the surfaces ensures no slipping, although as shown by Thornton et al. (1988), very little slipping actually occurs between unbounded elastomer and substrate for the high coefficients of friction typical of elastomers. Bonding also implies that negative pressures at the

Contributed by the Applied Mechanics Division of the American Society of Mechanical Engineers for publication in the Journal of Applied Mechanics.

Discussion on this paper should be addressed to the Editorial Department, ASME, United Engineering Center, 345 East 47th Street, New York, N.Y. 10017, and will be accepted until two months after final publication of the paper itself in the Journal of Applied Mechanics. Manuscript received by ASME Applied Mechanics Division, October 29, 1987; final revision, July 30, 1988.

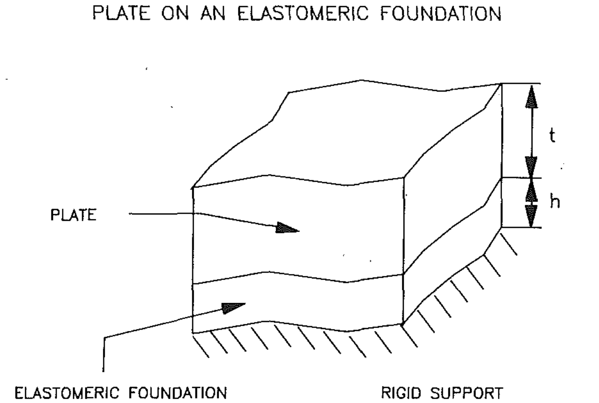

Fig. 1 Representative element of a plate on a thin elastomeric foundation

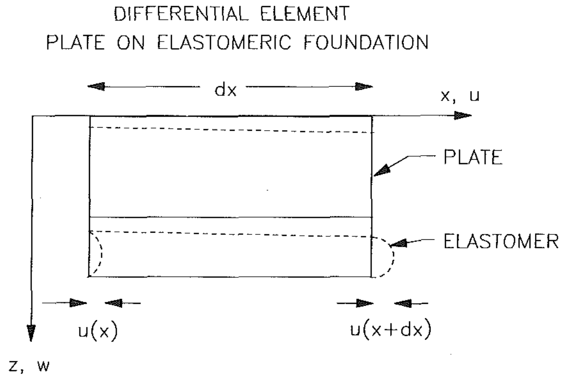

Fig. 2 Differential element in xz plane prior to and following deflection

surface can be maintained. The elastomer is treated as incompressible, although Dillard et al. (TBP) have provided a simple correction technique which could be applied to account for compressibility. The assumption of incompessibility, however, is believed to be quite valid unless the elastomeric foundation is extremely thin. The assumption of a rigid substrate is quite acceptable if the substrate has a high modulus compared to the elastomer, and if the elastomer is not extremely thin. We also require that the deflection of the plate be small according to plate theory definitions, and in comparison to the thickness of the elastomer.

Classical plate theory yields the governing differential equation as:

$$\frac{\partial^4 w}{\partial x^4} + 2\frac{\partial^4 w}{\partial x^2 \partial y^2} + \frac{\partial^4 w}{\partial y^4} = \frac{(p-q)}{D} \tag{1}$$

where w is the plate deflection, p is the applied loading distribution, q is the restoring pressure exerted by the foundation, and D is the plate bending stiffness given by

$$D = \frac{Et^3}{12(1-\nu^2)}.$$

For the Winkler foundation, $q = kw$, where k is the spring constant of the support.

When a bonded elastomeric block is compressed, the total force exerted may be thought of as the superposition of the force required to deform a perfectly lubricated block, and the force generated when the surfaces of the freely expanded block are forced back to their actual bonded location (Gent and Meinecke (1970)). For blocks with large shape factors, the pressure due to the former case is completely negligible. (The shape factor is defined as the ratio of the area of one loaded surface to the total exposed area.) Because of the assumption that the elastomeric foundation is thin compared with the oscillation spacing of the plate, we also may assume that the former term, which is given by $f_1 = E_e \epsilon$, is negligible, as will be substantiated later in the paper. Here, E_e is Young's modulus of the elastomer and ϵ is the strain given by $\epsilon = w/h$, where w is the deflection of the plate and h is the thickness of the elastomer. In essence, we have discarded the term which is equivalent to the Winkler foundation and will retain the pressure term which arises from the shearing stresses in the displaced elastomer.

Figure 2 shows a differential element of the plate and foundation prior to and after deflection. Assuming that the pressure is constant throughout the thickness of the elastomer, normals through the elastomer are deflected into parabolas. The demonstration of this is analogous to the parabolic velocity profiles arising in laminar flow. The displacements of the vertexes of the parabolas in the x and y directions are given by $u(x, y)$ and $v(x, y)$, respectively. Because the elastomer is assumed incompressible, the volume displayed by vertical motion of the plate leads to spatial variations in u and v defined by:

$$\frac{\partial u}{\partial x} + \frac{\partial v}{\partial y} = \frac{3w}{2h}. \tag{2}$$

These changes in u and v give rise to changes in shear strains and stresses and, hence, changes in pressure within the elastomer. These may be expressed by:

$$\frac{\partial \sigma_x}{\partial x} = \frac{8G}{h^2} u \tag{3a}$$

$$\frac{\partial \sigma_y}{\partial y} = \frac{8G}{h^2} v \tag{3b}$$

where σ_x and σ_y are normal stresses, and G is the shear modulus of the elastomer. Because the elastomer is thin compared to plate oscillation spacing, we further find that the stresses within the elastomer are approximately equal: $\sigma_x \approx \sigma_y \approx \sigma_z \approx -q$, where q is the hydrostatic restoring pressure. The validity of this step is justified by considering the high degree of constraint imposed by our requirements on elastomer thickness (Gent and Meinecke, 1970).

Differentiating equations (3a) and (3b) with respect to x and y, respectively, and substituting into equation 2, we obtain:

$$\frac{\partial^2 q}{\partial x^2} + \frac{\partial^2 q}{\partial y^2} = -\frac{12Gw}{h^3}. \tag{4}$$

Taking the Laplacian of the biharmonic equation (1), and substituting in equation (4), we obtain

$$\frac{\partial^6 w}{\partial x^6} + 3\frac{\partial^6 w}{\partial x^4 \partial y^2} + 3\frac{\partial^6 w}{\partial x^2 \partial y^4} + \frac{\partial^6 w}{\partial y^6} - \lambda^6 w = \frac{1}{D}\left[\frac{\partial^2 p}{\partial x^2} + \frac{\partial^2 p}{\partial y^2}\right] \tag{5}$$

or

$$\nabla^6 w - \lambda^6 w = \frac{1}{D}\nabla^2 p$$

where

$$\lambda^6 = \frac{12G}{Dh^3}. \tag{6}$$

Before solving this equation, we shall first examine the special case where the solution is only a function x.

Solution Independent of Y

If the loading and boundary conditions are independent of y for a plate which is infinitely wide in the y direction, equation (5) simplifies to

$$\frac{d^6 w}{dx^6} - \lambda^6 w = \frac{1}{D}\frac{d^2 p}{dx^2}. \tag{7}$$

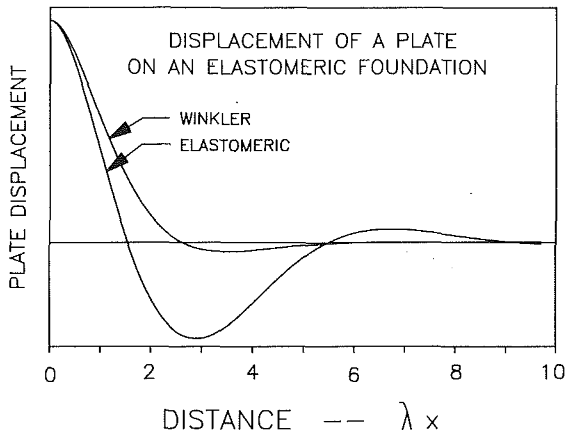

Fig. 3 Comparison of Winkler and elastomeric foundation solutions for plate deflection under a line load

In operator form, the homogeneous equation becomes

$$(\mathbf{D}^6 - \lambda^6)w = 0$$

where the boldface **D** represents the differential operator. Factoring this, we obtain the following roots

$$\mathbf{D}_1 = -\lambda \qquad \mathbf{D}_2 = \lambda \qquad \mathbf{D}_3 = -\frac{\lambda}{2}\sqrt{-1+i\sqrt{3}}$$

$$\mathbf{D}_4 = \frac{\lambda}{2}\sqrt{-1+i\sqrt{3}} \qquad \mathbf{D}_5 = -\frac{\lambda}{2}\sqrt{-1-i\sqrt{3}}$$

$$\mathbf{D}_6 = \frac{\lambda}{2}\sqrt{-1-i\sqrt{3}}.$$

Making use of De Moivre's Theorem, we can obtain

$$\mathbf{D}_3 = -\lambda\left(\frac{1}{2} + \frac{i\sqrt{3}}{2}\right) \qquad \mathbf{D}_4 = \lambda\left(\frac{1}{2} + \frac{i\sqrt{3}}{2}\right)$$

$$\mathbf{D}_5 = -\lambda\left(\frac{1}{2} - \frac{i\sqrt{3}}{2}\right) \qquad \mathbf{D}_6 = \lambda\left(\frac{1}{2} - \frac{i\sqrt{3}}{2}\right).$$

The homogeneous solution takes the form

$$w(x) = A_1 e^{\lambda x} + A_2 e^{-\lambda x} + e^{-\lambda/2\,x}\left(A_3 \cos\frac{\sqrt{3}}{2}\lambda x + A_4 \sin\frac{\sqrt{3}}{2}\lambda x\right) + e^{\lambda/2 x}\left(A_5 \cos\frac{\sqrt{3}}{2}\lambda x + A_6 \sin\frac{\sqrt{3}}{2}\lambda x\right). \quad (9)$$

Let us consider two loading cases.

Case I: Concentrated Line Load

We will apply the solution for all $x \geq 0$ for a concentrated line load of magnitude p at $x=0$. Since the deflection must vanish at large values of x, we conclude that $A_1 = A_5 = A_6 = 0$. The remaining constants may be evaluated by requiring that $u(0) = \theta(0) = 0$, where θ is the slope of the plate, and by enforcing equilibrium such that

$$\frac{p}{2} = \int_o^\infty q(x)\,dx.$$

The resulting solution for the plate deflection is given by

$$w(x) = \frac{p\lambda^3 h^3}{72G}\left\{-e^{-\lambda x} + 2e^{-\lambda/2\,x}\cos\frac{\sqrt{3}}{2}\lambda x\right\}$$

for all $x \geq 0$.

We now compare this with the Winkler solution for an equivalently loaded plate (Seely and Smith, 1952):

$$\tilde{w}(x) = \frac{P\beta}{2k}e^{-\beta x}[\cos\beta x + \sin\beta x] \quad (13)$$

where the tilde will represent the corresponding Winkler solution and

$$\beta = \sqrt[4]{\frac{k}{4D}}$$

where k is the spring constant given as stress/unit displacement.

We immediately note several differences in these two solutions. The decay exponent for the periodic term of the elastomeric foundation solution is smaller than the periodic argument, implying that the oscillations will decay more slowly than the Winkler solution. Furthermore, the $e^{-\lambda x}$ term represents a net shift of the deflection in the vicinity of $x=0$. This results in

$$\int_o^\infty w(x)\,dx = 0 \quad (14)$$

so that

$$\lim_{x\to\infty} u(x) = 0,$$

a requirement stemming from the incompressibility of the elastomer and the need for pressures to be finite.

If k for the elastomer is taken as

$$k = \frac{E_e}{h} = \frac{3G}{h}$$

as would be measured experimentally with a small shape factor specimen, totally unreasonable values for the elastic curve are obtained. A more realistic k value can be chosen such that the deflection under this line load is equivalent to the plate on the elastomeric foundation by letting:

$$k = \left(25.46\frac{G}{\lambda^3 h^3 D^{1/4}}\right)^{4/3}. \quad (15)$$

By setting $\tilde{w}(0) = w(0)$, we note that the maximum moments and restoring pressures for the elastomeric case may be related to the Winkler case according to:

$$M(0) = 1.2114\ \tilde{M}(0) \quad (16a)$$

and

$$q(0) = 0.7338\ \tilde{q}(0). \quad (16b)$$

Figure 3 illustrates the elastic curves for the two foundations normalized according to equation (15). As would be expected from equation (14), the displacements of the plate on the elastomeric foundation must average to zero, resulting in a large negative displacement adjacent to the applied load which is much more pronounced than the Winkler solution. As noted earlier, the decay rate for the Winkler solution is much faster than for the elastomeric founation. It is interesting to note that while the zero crossings for the Winkler solution occur at regular intervals, the elastomeric solution does not because of the leading exponential term.

Figure 4 gives the diagrams for plate shear, plate bending moment, slope, deflection, elastomer displacement, and elastomer pressure. Sign conventions are based on those given by Timoshenko and Woinowski-Krieger (1959). The equations for these parameters are given by:

$$V(x) = \frac{p}{6}\left\{-e^{-\lambda x} - 2e^{-\lambda/2\,x}\cos\frac{\sqrt{3}}{2}\lambda x\right\} \quad (17a)$$

$$M(x) = \frac{p}{6\lambda}\left\{e^{-\lambda x} + e^{-\lambda/2\,x}\left[\cos\frac{\sqrt{3}}{2}\lambda x - \sqrt{3}\sin\frac{\sqrt{3}}{2}\lambda x\right]\right\} \quad (17b)$$

$$\theta(x) = \frac{p\lambda^4 h^3}{72G}\left\{e^{-\lambda x} - e^{-\lambda/2\,x}\left[\cos\frac{\sqrt{3}}{2}\lambda x + \sqrt{3}\sin\frac{\sqrt{3}}{2}\lambda x\right]\right\} \quad (17c)$$

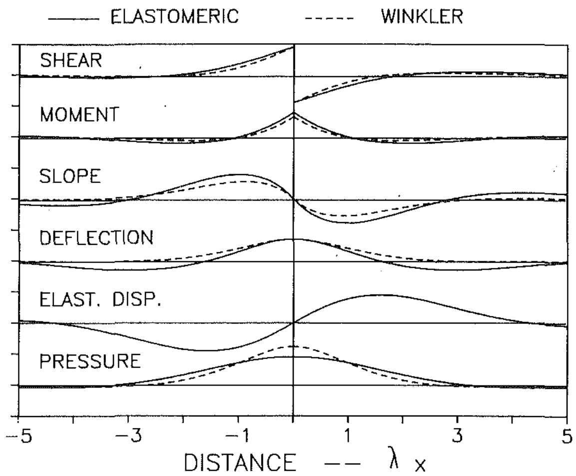

Fig. 4 Comparison of Winkler and elastomeric foundation solutions for plate bending functions

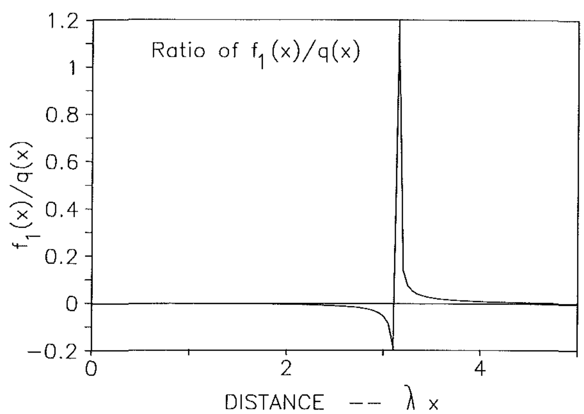

Fig. 5 Ratio of $f_1(x)/q(x)$ for $\lambda^2h^2/8=.0036$ showing f_1 is negligible except at singularity where $q(x)$ vanishes

$$w(x)=\frac{p\lambda^3h^3}{72G}\left\{-e^{-\lambda x}+2e^{-\lambda/2\,x}\cos\frac{\sqrt{3}}{2}\lambda x\right\} \tag{17d}$$

$$u(x)=\frac{p\lambda^2h^2}{48G}\left\{e^{-\lambda x}-e^{-\lambda/2\,x}\left[\cos\frac{\sqrt{3}}{2}\lambda x-\sqrt{3}\sin\frac{\sqrt{3}}{2}\lambda x\right]\right\} \tag{17e}$$

$$q(x)=\frac{p\lambda}{6}\left\{e^{-\lambda x}+e^{-\lambda/2\,x}\left[\cos\frac{\sqrt{3}}{2}\lambda x+\sqrt{3}\sin\frac{\sqrt{3}}{2}\lambda x\right]\right\} \tag{17f}$$

for all $x\geq 0$ except $V(x)$ which is valid for all $x>0$. We note that $u(0)=\theta(0)=0$ as required and that $V(0^+)=p/2$, as would be expected.

To evaluate our assumption that the f_1 is small compared to q, we use $f_1=E_e w/h$, and equations (17d) and (17f) to obtain the ratio of f_1 and q at $x=0$:

$$\frac{f_{1\,\max}}{q_{\max}}=\frac{f_1(0)}{q(0)}=\frac{\lambda^2h^2}{8}$$

concluding that as long as $\lambda^2h^2/8$ is small, the contributions from f_1 are negligible. The ratio of $f_1(x)/q(x)$ remains very small except for very localized regions where $q(x)\rightarrow 0$ and the ratio is unbounded. This is illustrated in Fig. 5 for a case of $\lambda^2h^2/8=.0036$ using the same data as for Fig. 4. Since $f_1(x)/q(x)$ is negligible except at localized singularity points, the f_1 contribution may be disregarded. We may express

$$\frac{\lambda^2h^2}{8}=\sqrt[3]{\frac{9G(1-\nu^2)h^3}{32\,Et^3}}$$

and note that for typical values of G for rubber and E and ν for steel, the quantity

$$0.012\,\frac{h}{t}$$

gives the approximate contribution of f_1 at the point of load application, implying that reasonable values of h and t may be accommodated by the model.

Case II: Concentrated Line Moment

If a uniform concentrated moment is distributed along $x=0$, solutions may be obtained simply by differentiating the solutions to Case I. Thus, the following are valid for $x\geq 0$; except $M(x)$ which is valid for $x>0$:

$$V(x)=\frac{M_o\lambda}{6}\left\{e^{-\lambda x}+e^{-\lambda/2\,x}\left[\cos\frac{\sqrt{3}}{2}\lambda x+\sqrt{3}\sin\frac{\sqrt{3}}{2}\lambda x\right]\right\} \tag{18a}$$

$$M(x)=\frac{M_o}{6}\left\{-e^{-\lambda x}-2e^{-\lambda/2\,x}\cos\frac{\sqrt{3}}{2}\lambda x\right\} \tag{18b}$$

$$\theta(x)=\frac{M_o\lambda^5h^3}{72G}\left\{-e^{-\lambda x}-e^{-\lambda/2\,x}\left[\cos\frac{\sqrt{3}}{2}\lambda x-\sqrt{3}\sin\frac{\sqrt{3}}{2}\lambda x\right]\right\} \tag{18c}$$

$$w(x)=\frac{M_o\lambda^4h^3}{72G}\left\{e^{-\lambda x}-e^{-\lambda/2\,x}\left[\cos\frac{\sqrt{3}}{2}\lambda x+\sqrt{3}\sin\frac{\sqrt{3}}{2}\lambda x\right]\right\} \tag{18d}$$

$$u(x)=\frac{M_o\lambda^3h^2}{48G}\left\{-e^{-\lambda x}+2e^{-\lambda/2\,x}\cos\frac{\sqrt{3}}{2}\lambda x\right\} \tag{18e}$$

$$q(x)=\frac{M_o\lambda^2}{6}\left\{-e^{-\lambda x}+e^{-\lambda/2\,x}\left[\cos\frac{\sqrt{3}}{2}\lambda x-\sqrt{3}\sin\frac{\sqrt{3}}{2}\lambda x\right]\right\}. \tag{18f}$$

These solutions for concentrated line forces and moments can be superposed to give results for arbitrary loading functions within the limitations set forth for plates independent of y.

General Solution

Returning to the governing differential equation (5), we now seek the general solution when the loading and/or boundary conditions may be functions of y, or when the plate is not infinite in the y direction. To illustrate the solution technique, we will turn our attention to a simply-supported plate with no constraint imposed on the exposed rubber surface, i.e., $q=0$ along the edges. The Navier solution for the deflection of the plate takes on the form

$$w(x,y)=\sum_{m=1}^{\infty}\sum_{n=1}^{\infty}W_{mn}\sin\frac{m\pi x}{a}\sin\frac{n\pi y}{b}. \tag{19}$$

If we assume the applied load to be of the form

$$p(x,y)=\sum_{m=1}^{\infty}\sum_{n=1}^{\infty}P_{mn}\sin\frac{m\pi x}{a}\sin\frac{n\pi y}{b}, \tag{20}$$

where

$$P_{mn}=\frac{4}{ab}\int_o^a\int_o^b p(x,y)\sin\frac{m\pi x}{a}\sin\frac{n\pi y}{b}\,dy\,dx, \tag{21}$$

we obtain

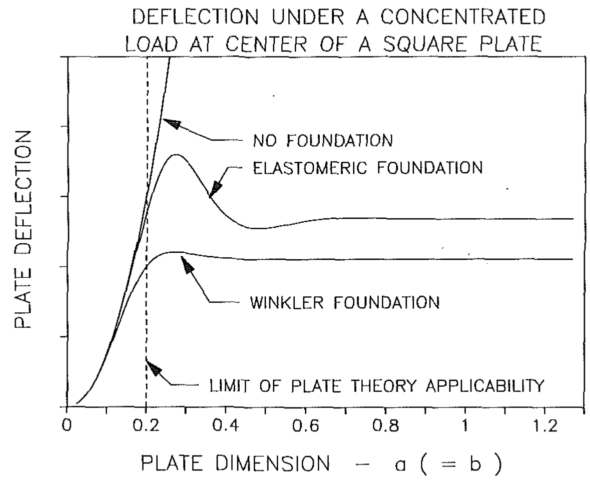

Fig. 6 Deflection of a square plate loaded at the center with a concentrated load as a function of plate length

$$W_{mn} = \frac{P_{mn}\left[\left(\frac{m\pi}{a}\right)^2 + \left(\frac{n\pi}{b}\right)^2\right]}{D\left\{\left[\left(\frac{m\pi}{a}\right)^2 + \left(\frac{n\pi}{b}\right)^2\right]^3 + \lambda^6\right\}}. \tag{22}$$

This is in contrast to the equivalent solution from a Winkler foundation which would be given by

$$\tilde{W}_{mn} = \frac{P_{mn}}{D\left[\left(\frac{m\pi}{a}\right)^2 + \left(\frac{n\pi}{b}\right)^2\right]^2 + k}. \tag{23}$$

It is convenient to define the influence coefficient $K(x,y;\ \zeta, \eta)$ as being the deflection at (x,y) due to a unit load applied at (ζ,η). We find that for the elastomeric foundation, the influence coefficient may be written as:

$$K(x,y;\ \zeta,\eta) = \sum_{m=1}^{\infty}\sum_{n=1}^{\infty} \frac{4\left[\left(\frac{m\pi}{a}\right)^2 + \left(\frac{n\pi}{b}\right)^2\right]\sin\frac{m\pi\zeta}{a}\sin\frac{n\pi\eta}{b}}{abD\left\{\left[\left(\frac{m\pi}{a}\right)^2 + \left(\frac{n\pi}{b}\right)^2\right]^3 + \lambda^6\right\}} \times \sin\frac{m\pi x}{a}\sin\frac{n\pi y}{b} \tag{24}$$

versus

$$\tilde{K}(x,y;\ \zeta,\eta) = \sum_{m=1}^{\infty}\sum_{n=1}^{\infty} \frac{4\sin\frac{m\pi\zeta}{a}\sin\frac{n\pi\eta}{b}}{ab\,D\left[\left(\frac{m\pi}{a}\right)^2 + \left(\frac{n\pi}{b}\right)^2\right]^2 + k} \times \sin\frac{m\pi x}{a}\sin\frac{n\pi y}{b} \tag{25}$$

for the Winkler foundation.

For illustration purposes, we consider a steel plate ($E=210$ GPa, $\nu=0.3$, $t=0.02$ m) on a thin elastomeric foundation ($G=1.3$ MPa, $h=0.02$ m). By varying the size of the plate, we can plot $K(a/2, a/2; a/2, a/2,)$ and $\tilde{K}(a/2, a/2; a/2, a/2)$. We have used the normalization scheme of equation (15) for plotting the results in Fig. 6. We do see a pronounced peak in the elastomeric foundation solution which coincides with the simply-supported boundaries being in register with the natural oscillation spacing of the plate. This is much more pronounced than for the Winkler solution. Comparison with the solution for no foundation shows good agreement for very small plate dimensions, as would be expected.

Conclusions

It has been shown that a Winkler foundation is inadequate to accurately model a thin elastomeric foundation bonded to a flexible plate and rigid substrate. Closed form and series solutions are presented for several cases, and it is seen that the deflection oscillations on an elastomeric foundation decay much slower than on a Winkler foundation. Also, by matching the k of the Winkler foundation to that of the elastomer for maximum deflection, the oscillation periods are significantly different.

The solution technique does depend on the assumption that the oscillation periods are large in comparison to the thickness of the elastomer. For extremely accurate predictions, this requires that the elastomer be several times thinner than the plate for typical engineering materials. On the other hand, reasonably accurate results are expected even if the elastomer is somewhat thicker than the plate. The elastomer has been assumed to be incompressible in the current analysis.

Acknowledgments

The author would like to acknowledge Virginia's Center for Innovative Technology and Texas Research Institute in Austin for their support of this work, the helpful conversations with J. S. Thornton of TRI, and Shelia Lucas for typing the manuscript.

References

Biot, M. A., 1937, "Bending of an Infinite Beam on an Elastic Foundation," ASME Journal of Applied Mechanics, Vol. 4, pp. 1–7.

Dillard, D. A., Lai, Y. H., Thornton, J. S., "The Effect of Compressibility on the Stress Distributions in Thin Elastomeric Blocks and Annular Bushings," ASME Journal of Applied Mechanics, in review.

Gent, A. N., and Meinecke, E. A., 1970, "Compression, Bending, and Shear of Bonded Rubber Blocks," *Polymer Engineering and Science*, Vol. 10, No. 1, pp. 48–53.

Seely, F. B., and Smith, J. O., 1952, *Advanced Mechanics of Materials*, 2nd ed., John Wiley and Sons, New York.

Thornton, J. S., Montgomery, R. E., Thompson, C. M., and Dillard, D. A., 1988, "Analysis of Interfacial Stresses for Elastomeric Gaskets in Compression," *Polymer Science and Engineering*, Vol. 28, No. 10, pp. 655–659.

Timoshenko, S., and Woinowski-Krieger, S., 1959, *Theory of Plates and Shells*, 2nd ed., McGraw-Hill, New York.

Winkler, E., 1867, "Die Lehre von der Elastizit ät und Festigkeit," Prag, p. 182.

E. N. Kuznetsov
Department of General Engineering,
University of Illinois
at Urbana-Champaign,
Urbana, Ill. 61801-2996
Mem. ASME

The Membrane Shell as an Underconstrained Structural System

Statical-kinematic analysis is employed to provide a new perspective on the structural behavior of membrane shells and the related limitations of the linear membrane theory. The obtained results include a resolution of an apparent paradox in the statics of membranes, a description and explanation of the peculiar behavior of toroidal membranes with an arbitrary cross-section, and a stronger version of a central theorem in the membrane theory.

Introduction

Underconstrained structural systems have fewer independent constraints (structural members) than necessary to be geometrically invariant. Nevertheless, such systems are widely used in engineering practice including many conventional applications. In particular, this is the case with exceptional underconstrained systems which lack kinematic mobility and possess a unique geometric configuration (multifreedom infinitesimal mechanisms).

The basic properties of underconstrained systems are studied by means of statical-kinematic analysis, both generic and system-specific. This analysis deals with structural topology and geometric invariance; relations between external loads, internal forces, and equilibrium configurations; infinitesimal or finite kinematic mobility; statical and kinematic indeterminacy; and other local or global features of structural behavior not related to the material properties (constitutive relations).

For the purposes of statical-kinematic analysis, a structural system can be modeled as an assembly of material points linked by ideal positional constraints representing the structural members. Then the kinematic properties of the system are fully determined by a compatible set of constraint equations

$$F_i(X_1, \ldots X_n, \ldots X_N) = 0, \quad i = 1, 2, \ldots I \tag{1}$$

relating the N generalized coordinates X_n of the system. The linearized equations derived by differentiating equation (1) at the solution point $X_n = X_n^o$ involve infinitesimal virtual displacements x_n:

$$F_{in}^o x_n = 0 \quad (F_{in} \equiv \partial F_i / \partial X_n). \tag{2}$$

(Here and in the following equations a repeated subscript denotes summation.) If the rank r of the Jacobian F_{in}^o is $r<N$, the system generally allows finite kinematic displacements and can acquire a variety of geometric configurations. However, there exist exceptional systems where $X_n = X_n^o$ is an isolated solution of equations (1) in spite of $r<N$ (Kuznetsov, 1988). Then the system lacks kinematic mobility and possesses a unique configuration. Such exceptional systems are infinitesimal mechanisms (like, for example, a rectilinear pin-bar chain with both ends fixed) and belong to two fundamentally different types. The first one is a degeneration of a geometrically invariant system resulting from improper (rather than insufficient) constraints, whereas the second is a singular case of a variant, underconstrained system. In both cases, a change in the system geometry may lead to an increase in the rank r, but the complete rank restoration ($r=N$) is possible only for the first type. Thus, upon exiting from the singular configuration (as a result of constraint variation), an infinitesimal mechanism becomes an ordinary system of the respective generic type. On this basis, the two singular types can be classified respectively as quasi-invariant and quasi-variant.

By employing the principle of virtual work, equilibrium equations in the unknown generalized constraint reactions, Λ_i, are obtained from (2):

$$F_{in}^o \Lambda_i = P_n \tag{3}$$

where an N-dimensional load vector P_n is called an equilibrium load if it is representable as a linear combination of the matrix columns. Thus, for a system in a given geometric configuration there exist r linearly-independent equilibrium loads. For a geometrically invariant system, $r=N$ and any load is an equilibrium load – a statical criterion of invariance.

Under an equilibrium load, the response of all types of systems is the same: Equilibrium is attained without kinematic deformations. This contrasts with the behavior of an ill-constrained (i.e., improperly or insufficiently constrained) system subjected to a general load. Because of $r<N$, equilibrium in the initial configuration is impossible, which makes the problem not only geometrically nonlinear but, in a

Contributed by the Applied Mechanics Division of THE AMERICAN SOCIETY OF MECHANICAL ENGINEERS for presentation at the Joint ASCE/ASME Applied Mechanics, Biomechanics, and Fluids Engineering Conference, San Diego, CA, July 9 to 12, 1989.

Discussion of this paper should be addressed to the Editorial Department, ASME, United Engineering Center, 345 East 47th Street, New York, N.Y. 10017, and will be accepted until two months after final publication of the paper itself in the JOURNAL OF APPLIED MECHANICS. Manuscript received by ASME Applied Mechanics Division, June 6, 1988; final revision, September 27, 1988.

Paper No. 89-APM-35.

certain sense, nonlinearizable. Specifically, the load increment method commonly used for nonlinear problems is, as a rule, inapplicable in this case. Indeed, solving (2) in terms of $(N-r)$ displacements x_p designated as independent enables all displacements to be expressed as

$$x_m = a_{mp} x_p \quad (a_{mp} = 1 \text{ at } m = p). \tag{4}$$

After introducing

$$b_{np} = F^o_{imn} \Lambda_i a_{mp} \quad (F_{imn} = \partial^2 F_i / \partial X_m \partial X_n) \tag{5}$$

an incremented version of equilibrium equations (3) can be written as

$$b_{np} x_p + F_{in} \lambda_i = p_n \tag{6}$$

where λ_i and p_n denote small increments of the corresponding quantities in (3). When the system is initially force-free, i.e., $\Lambda_i = 0$, the first term in (6) vanishes and, since $r < N$, a solution in terms of λ_i, in general, does not exist regardless of how small is the load increment. Like the original system of equations, the incremented one allows a solution only for equilibrium loads. This feature underlies the complex behavior of initially stress-free ill-constrained systems. In statics, small perturbations may cause large displacements (instability); in dynamics, a chaotic behavior may ensue.

The situation is quite different when initial forces Λ_i are present, due to either prestress (possible in singular systems) or an already existing equilibrium load. Although under a general load increment the system still must change its configuration before coming to equilibrium, equations (6) can be solved yielding all $(N-r)$ independent displacements x_p and r force increments λ_i. For a sufficiently small p_n the solution is accurate; otherwise it requires iterative refinements. An efficient iterative procedure[1] is based on a decomposition of a given external load P_n into equilibrium, P^*_n, and non-equilibrium, p_n, components

$$P_n = P^*_n + p_n \tag{7}$$

such that P^*_n is the projection of P_n onto the column space of the equilibrium matrix F_{in}, thereby minimizing the magnitude of p_n. This leads to the uncoupling of equation (6) so that the internal forces and the independent displacements are evaluated separately in alternating iterative steps. Moreover, there is no need to calculate P^*_n explicitly since the corresponding internal forces are found immediately by solving the overdetermined system (3) using the least squares method.

Although the foregoing statical-kinematic analysis deals with discrete underconstrained systems, it provides a useful insight and a conceptual framework for an analysis of continuous underconstrained systems as well. Among these, the membrane shell is the most interesting.

A Membrane as an Underconstrained System

A membrane shell is modeled analytically as a material surface devoid of bending stiffness and resisting only tangential (in-surface) forces – normal and shearing. Constraint idealization, whereby the membrane is assumed inextensible, reduces membrane deformations to isometric bending, smooth or piecewise smooth. The latter is characterized by curvature singularities over isolated lines or a network of lines; it occurs, for example, in a snap-through or buckling of rigid shells and as wrinkling in "soft" membranes. Since piecewise smooth bending cannot be prevented by any contour supports, a membrane always possesses this form of kinematic mobility. Thus, a membrane is an underconstrained structural system, either geometrically variant or quasi-variant.

In this context, the ability of an adequately supported membrane to equilibrate smooth surfaces loads in its original configuration demonstrates only that these are equilibrium loads for this underconstrained system. Furthermore, even within this class of loads, a membrane generally cannot be considered geometrically invariant. The fact is that, in order to completely immobilize a membrane, smooth bending must be precluded as well. This can be achieved by attaching a rigid bar to the membrane or by constraining its edge. However, a rigid bar or edge supports generally produce a line reaction with a normal component which cannot be equilibrated by the membrane without a change in geometry. Hence, the membrane still does not satisfy the statical criterion of invariance.

The above observations are analytically reflected in the inherent nonlinearity and nonlinearizability of the pertinent equations, a characteristic feature of underconstrained systems. Indeed, in the simplest, von Karman-type nonlinear formulation (small strains, finite rotations), the equilibrium equations for a membrane are

$$\begin{aligned}
&(BT_1)_\alpha - B_\alpha T_2 + (AS)_\beta + A_\beta S = 0 \\
&(AT_2)_\beta - A_\beta T_1 + (BS)_\alpha + B_\alpha S = 0 \\
&(BT_1)_\alpha W_\alpha / A + (AT_2)_\beta W_\beta / B + (SW_\beta)_\alpha + (SW_\alpha)_\beta \\
&\quad + BT_1[A\sigma_1 + (W_\alpha/A)_\alpha] + AT_2[B\sigma_2 + (W_\beta/A)_\beta] = PAB.
\end{aligned} \tag{8}$$

Here, T_1, T_2, and S are the membrane forces, A and B are the Lamé parameters (metric coefficients), σ_1 and σ_2 are the principal curvatures, W is the normal displacement, P is the normal surface load, and the subscripts α and β denote partial derivatives. The first two of equations (8) are linear and the third one can be linearized as follows:

$$\begin{aligned}
&[(t_{1\alpha} W_\alpha + T_{1\alpha} w_\alpha) B + (t_1 W_\alpha + T_1 w_\alpha) B_\alpha]/A \\
&\quad + [(t_{2\beta} W_\beta + T_{2\beta} w_\beta) A + (t_2 W_\beta + T_2 w_\beta) A_\beta]/B \\
&\quad + s_\alpha W_\beta + S_\alpha w_\beta + s_\beta W_\alpha + S_\beta w_\alpha + 2s W_{\alpha\beta} + 2S w_{\alpha\beta} \\
&\quad + \underline{AB\sigma_1 t_1} + BT_1 (w_\alpha/A)_\alpha + \underline{AB\sigma_2 t_2} + AT_2 (w_\beta/B)_\beta = pAB
\end{aligned} \tag{9}$$

where, as before, small letters designate small increments of the corresponding forces and displacements.

For an initially stress-free membrane, only the two underscored terms survive linearization and appear in the corresponding algebraic equation of the linear membrane theory. Without the highest derivative terms in the last equation, the system of equations degenerates and fails to produce the number of arbitrary elements needed to satisfy all boundary conditions. In terms of the general statical-kinematic analysis, this known failure of the linear membrane theory means that the latter is confined to the class of problems where the surface and edge loads, including the support reactions, constitute equilibrium load combinations. On the other hand, there is no such limitation for a membrane with pre-existing internal forces. The entire situation closely parallels the one previously discussed regarding the generic linearized equations (6) for discrete underconstrained systems.

The degeneration of the tangent operator in the statics and dynamics of membranes might be accompanied by a change in the equations type (Stoker, 1964; Zak, 1982). In statics, the outcome is an ill-posed boundary value problem with a nonelliptic operator (for membranes with Gaussian curvature $K \leq 0$). This prompted Marsden and Hughes (1983) to call membrane theory "linearization-unstable," which is yet another manifestation of the membrane being an underconstrained structural system.

Implications for the Linear Membrane Theory

One of the cornerstones of the linear membrane theory is the following theorem (Gol'denveizer, 1953; Vekua, 1959).

If the homogeneous geometric problem has J linearly-

[1] S. A. Burns, Computer program CHAIN, Department of General Engineering, University of Illinois at Urbana.

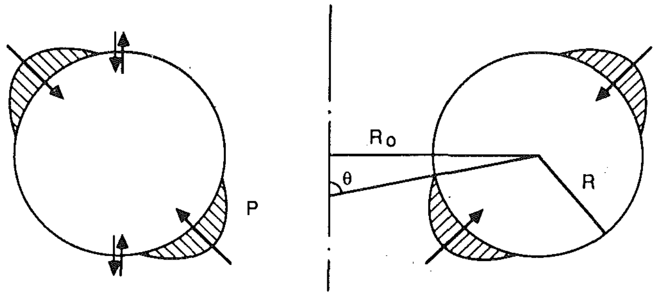

Fig. 1 Toroidal membrane under smooth self-balanced surface load

independent nontrivial solutions U_j, V_j, W_j ($j = 1, 2, \ldots J$), the conjugate statical problem of the membrane theory can have a solution only if J integral conditions

$$\int_G \int (XU_j + YV_j + ZW_j) AB d\alpha d\beta - \int_g LM_j ds = 0 \tag{10}$$

are satisfied. (X, Y, and Z are surface loads, L is a tangential load applied along the edge in a given direction l, and M_j is the projection of the edge displacements on the direction l.)

According to the theorem, for membranes satisfying its condition, the statical problem only can (but not always does) have a solution. Specifically, for membranes of positive Gaussian curvature, a solution (perhaps, nonunique) was shown to exist, while in a general case the question remains open. An example (or, rather, a counterexample) of a toroidal membrane was used to illustrate the general case. In differential geometry a torus is shown to be infinitesimally[2] rigid: It does not allow even infinitesimal smooth bending. By implication, the number of nontrivial solutions to the homogeneous geometric problem is zero so that conditions (10) are assuredly met and the membrane should be able to support any smooth self-balanced surface load. Yet, it is easily seen (Fig. 1) that equilibrium in the original configuration is impossible for an axisymmetric load with equal and opposite axial resultants for the inner and outer segments of the torus. (Such a load would produce a transverse shearing force along the parallel circles separating the two segments.)

However, a closer look at the conditions (10) shows these to be nothing but the implementation for an inextensible membrane of the principle of virtual work which is known to be both necessary *and sufficient* for equilibrium. Then how could it be possible that the statical problem does not *always* have a solution, if conditions (10) are satisfied?

The resolution of this apparent paradox lies in a subtle point concerning the nature of nontrivial solutions to the homogeneous geometric problem premised in the theorem. The fact is that a toroidal membrane is rigid only within the class of smooth bending; outside of this class its behavior is like that of a rectilinear pin-bar chain. For example, for a two-bar chain (Fig. 2), deflection Y is related to the bar strain, ϵ, by

$$l^2 + Y^2 = [l(1+\epsilon)]^2 \tag{11}$$

wherefrom

$$Y \simeq l\sqrt{2\epsilon}. \tag{12}$$

Thus, the system allows infinitesimal transverse displacements at the expense of second-order bar elongations; it displays the enhanced deformability of a singular system compared to an invariant system where displacements are related to the strains linearly. Nevertheless, when the bars are perfectly rigid ($\epsilon = 0$) the resulting homogeneous geometric problem still has only a trivial solution.

On the other hand, when equation (11) is linearized,

[2]This geometric term might appear controversial to a mechanician.

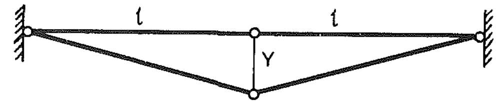

Fig. 2 Infinitesimal displacement in pin-bar chain

$$2Yy = 2\epsilon l^2 \tag{13}$$

a solution for the incremental displacement, y, is

$$y = \epsilon l^2 / Y. \tag{14}$$

At $\epsilon = 0$, $Y = 0$, the solution is indeterminate indicating that the system is singular (quasi-invariant).

As it happens, a torus also possesses this type of mobility but, since the corresponding infinitesimal displacement is not smooth, it escapes the test (10). It is not difficult to identify *smooth* surface loads which perform work over this virtual displacement and, therefore, cannot be equilibrated by the membrane. (Obviously, this is the case with the axisymmetric load shown in Fig. 1). In other words, even in the absence of line constraints (e.g., supports) smooth surface loads can give rise to nonsmooth infinitesimal bending.

Infinitesimal Mobility of Toroidal Membrane

The infinitesimal mobility of an inextensible toroidal membrane can be detected by a linear analysis establishing either (*i*) the existence of a nontrivial (although indeterminate) solution to the linear homogeneous geometric (strain-displacement) equations or (*ii*) the possibility of unbounded displacements at the expense of small strains. These two equivalent signs of a degenerate tangent operator exhibit the inadequacy of the linear model. The linear strain-displacement equations for an axisymmetric membrane are

$$\epsilon_1 = u_\alpha / A - \sigma_1 w, \quad \epsilon_2 = B_\alpha u / AB - \sigma_2 w \tag{15}$$

where ϵ_1 and ϵ_2 are, respectively, the meridional and hoop strains.

Choosing as an independent variable the angle θ between the normal to the surface and the axis of revolution (Fig. 1) enables the metric coefficients and the principal curvatures of the torus to be taken as

$$A = R, B = r = R_o + R\sin\theta, \sigma_1 = R, \sigma_2 = r/\sin\theta. \tag{16}$$

Exploring first the alternative (*i*), a nontrivial solution to equations (15) with $\epsilon_1 = \epsilon_2 = 0$ is obtained:

$$u = \pm\Delta\sin\theta, \ w = \pm\Delta\cos\theta \qquad \begin{matrix} \text{``+'' for } 0 \le \theta < \pi \\ \text{``}-\text{'' for } \pi \le 0 < 2\pi \end{matrix} \tag{17}$$

where Δ is arbitrary. Being physically inconsistent because of discontinuous w, solution (17), nevertheless, formally satisfies the homogeneous geometric equations (note that $\sigma_2 = 0$ at the crowns, where $\theta = 0, \pi$).

The alternative check (*ii*) confirms the outcome. Assuming, for example, constant strains and symmetry, with respect to the equatorial plane, yields the following solution to equations (15):

$$\begin{aligned} u/R &= (\epsilon_1 - \epsilon_2)\sin\theta \ln\tan\theta/2 + \epsilon_2 (R_o/R)\cos\theta \\ w/R &= (\epsilon_1 - \epsilon_2)\cos\theta \ln\tan\theta/2 - \epsilon_2 [1 + (R_o/R)\sin\theta] \end{aligned} \tag{18}$$

Almost everywhere in the membrane, the normalized displacements are of the same order as the strains but in the vicinity of the crown, w/R can exceed the strains by an arbitrarily large factor if $\epsilon_1 \neq \epsilon_2$.

Solutions (17) and (18) to the linearized geometric equations indicate infinitesimal first-order mobility requiring only second-order strains. Moreover, the solutions provide enough clues to the actual character of the corresponding displacement field so that its geometric possibility can be

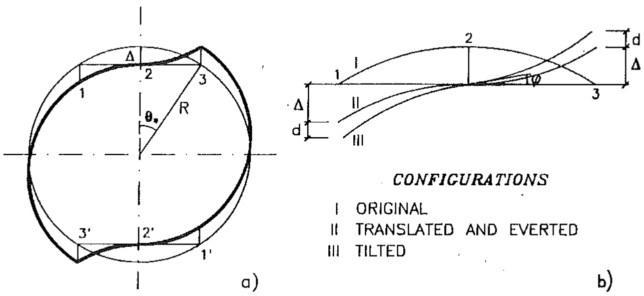

Fig. 3 Nonsmooth infinitesimal bending of torus; (a) Overall deformation pattern, and (b) Deformation stages

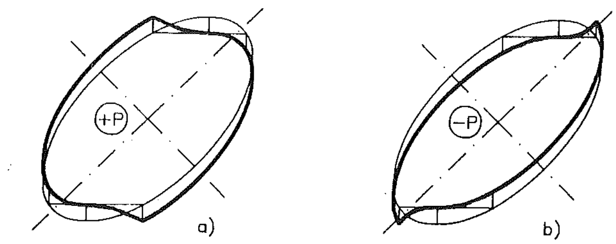

Fig. 4 Infinitesimal bending of torus with noncircular section; (a) Internal pressure and (b) External pressure

demonstrated explicitly (Fig. 3). First, the inner and outer segments of the torus undergo an infinitesimal, rigid-body mutual axial shift 2Δ accompanied by an eversion of the narrow annuluses 2–3 and 2′–3′ (Fig. 3(*a*)). So far, the deformation is a nonsmooth, strain-free bending with $\theta=\theta_*$ being the line of angular discontinuity. However, in the obtained configuration, the membrane still cannot support the load shown in Fig. 1. This requires an infinitesimal tilt, ϕ, of the horizontal tangents at points 2 and 2′ resulting in an additional axial displacement (Fig. 3(*b*))

$$2d/R \simeq 2\phi\theta_*. \tag{19}$$

The displacement d is possible at the expense of strains of the order ϕ^2 whereas the total normalized axial shift

$$2(\Delta+d)/R \simeq \theta_*(\theta_*+2\phi) \tag{20}$$

is still of the first order, since

$$\theta_* \simeq \sqrt{2\Delta/R}. \tag{21}$$

The magnitude of the angular discontinuity at points 3 and 3′ is

$$2\theta_*+\phi \simeq 2\theta_*. \tag{22}$$

The foregoing analysis demonstrates the possibility of nonsmooth infinitesimal bending in a torus subjected to smooth surface loads. It is the presence of asymptotic lines that facilitates this deformation with the very inception of loading. Consistent with the behavior of discrete quasi-invariant systems (Fig. 2), the deformed configuration of the torus (with two annular cusps) is geometrically invariant within the class of smooth loads.

It is interesting to compare the described behavior of an ideal membrane to that of a toroidal shell with bending stiffness. For an elastic shell, Steel (1964) found an almost stepwise jump in the displacement near the crowns. It seems logical to expect, that beyond the elastic limit, the displacement field should even closer approach the pattern of Fig. 3.

Quite recently Libai and Simmonds (1988) have raised a question: "What happens in a very thin, pressurized toroidal shell whose undeformed cross-section does *not* have points of horizontal tangency lying on the same vertical line? . . . We conjecture that wrinkling must occur." The deformed configurations shown in Fig. 4 represent nonsmooth infinitesimal bending of such a shell subjected, respectively, to an internal and external pressure. Curiously, to ensure the required geometric invariance of the final configuration, the points of horizontal tangency vanished altogether. Note that the proposed solution, based on the foregoing statical-kinematic analysis, is in line with the conjecture on wrinkling with just one qualification. Wrinkling is usually taken to mean the formation of a uniaxial stress zone (also called a tension field) in a membrane not resisting compression. In the presence of only a normal surface load, a tension field is known to be geodesic. However, this is not the case with the two circular ridges representing the key feature of the above deformation pattern. These are neither geodesic nor necessarily in tension; therefore, a connotation with wrinkling is undesirable. Obviously, in a pressurized "soft" toroidal membrane, meridional wrinkling is a possibility.

Conclusions

(1) A membrane is an underconstrained structural system, either variant or quasi-variant. For an initially stress-free membrane, the linear theory is consistent only within the class of problems involving equilibrium loads and reactions.

(2) Infinitesimal rigidity, with respect to smooth bending, is not synonymous with geometric invariance of a membrane, even within the class of smooth surface loads. Membrane invariance within this class of loads requires meeting one of the two equivalent criteria: (*a*) ability to support any such load in the original configuration; or (*b*) impossibility of infinitesimal smooth or nonsmooth displacements.

(3) Linear analysis detects both smooth and nonsmooth infinitesimal bending. Accordingly, an analytical implementation of the aforementioned criterion (*b*) is the absence of nontrivial solutions to the *linearized* homogeneous geometric problem.

(4) A stronger version of Gol'denveizer's theorem reads: "If the *linearized* homogeneous geometric problem has J linearly-independent nontrivial solutions, the conjugate statical problem of the membrane theory *has* a solution (perhaps nonunique) if *and only if* J conditions (10) are satisfied." (Italicized words are those inserted into the original formulation.)

Acknowledgment

The author expresses his gratitude to Prof. W. Brent Hall for discussions and to the reviewers of this paper for their constructive remarks and suggestions.

References

Gol'denveizer, A. L., 1953, *Theory of Elastic Thin Shells*, Moscow, (English translation by Pergamon Press, New York, 1961).

Kuznetsov, E. N., 1988, "Underconstrained Structural Systems," *Int. J. Solids Structures*, Vol. 24, pp. 153–63.

Libai, A., and Simmonds, J. G., 1988, *The Nonlinear Theory of Elastic Shells*, Academic Press.

Marsden, J. E., and Hughes, T. J. R., 1983, *Mathematical Foundations of Nonlinear Elasticity*, Prentice-Hall, New York.

Steele, C. R., 1964, "Orthotropic Pressure Vessels with Axial Constraint," *AIAA J.*, Vol. 2, pp. 703–709.

Stoker, J. J., 1964, *Topics in Nonlinear Elasticity*, Courant Institute, New York.

Vekua, I. N., 1959, *Generalized Analytic Functions*, Moscow (English translation by Pergamon Press, New York, 1962).

Zak, M., 1982, "On the Failure of Hyperbolicity in Elasticity," *J. Elasticity*, Vol. 12, pp. 219–29.

Lloyd H. Donnell
656 Lytton Avenue,
Palo Alto, Calif. 94301
Fellow, ASME

Thick General Shells Under General Loading

Three equilibrium equations in terms of three displacements are derived in scalar mathematics form, by linear, small-strain elasticity principles, for the case of general thick-walled shells under general loading. These reduce to well-known forms for the particular cases of flat-plates and thick circular cylindrical shells.

Note from the Editor: Lloyd Hamilton Donnell was born at Kents Hill, Maine in 1895. He has served the field of applied mechanics with distinction, providing leadership both through his outstanding contributions to the permanent engineering literature and through his service to the applied mechanics community. Among his awards have been the Worcester Reed Warner Medal (1960), von Karman Medal (1968), and the ASME Medal (1969). As evidenced by this paper, he is still active.

Introduction

"Thick-walled" means that the thickness of the shell is so large, compared to other dimensions, such as the radii of curvature and of twist, that the Kirchhoff-Love approximation of thin-shell theory is not applicable. One way of studying such shells is by starting with thin-shell theory and adding corrections. Another way, which is followed here, is to use the more exact methods of three-dimensional, linear small-strain elasticity. In doing this it will not be possible to include the nonlinear effects of large deflections of the order of the thickness. Such large deflections are hardly possible in thick shells made of metals or hard plastics in the elastic range; they *are* possible if the material is rubber-like, but study of such cases would require not only more complex nonlinear finite-strain elasticity relations but also more complex stress-strain relations. For simplicity, this discussion will be limited to shells of uniform thickness, t, made of elastic, homogeneous, isotropic material.

We will use lines of curvature of the undisplaced middle surface as two coordinate lines. Defined as lines along which there is no twist of the surface, it is known that there are always two orthogonal systems of such lines; in cases of symmetry they are intersections of planes of symmetry with the surface, and lines in the surface perpendicular to these. Figure 1 shows a general point O of the middle surface, with orthogonal lines of curvature of this surface, labeled α, β, passing through O and through neighboring points P, Q. We assume α, β to be independent, continuously-varying parameters having constant values along the β, α lines, respectively, taking the values of these parameters at a point as the coordinates of that point.

As third coordinate lines of the right-handed, three-dimensional coordinate system, we use straight lines perpendicular to the surface and therefore to the α, β lines; these are labeled γ, where γ is the distance from the middle surface. The positive directions of the α, β coordinates are in the directions of increase of α, β, and the right-handedness of the system defines the positive direction of the γ coordinate.

Shown also in Fig. 1 is a general point o in the shell wall, with coordinates α, β, γ. If we move a straight line of length γ, beginning with the line Oo, over the middle surface and perpendicular to it, with the upper end of it in the middle surface, the lower end generates a general surface of the shell wall, which includes the points o and neighboring points p, q. This general surface will also be perpendicular to the generating line; this follows from the fact that any motion of the generating line near a point such as O can be divided into a rotation about O and a movement parallel to its original position through O, and since either component would generate a line perpendicular to the generating line any combination of the components will also do so.

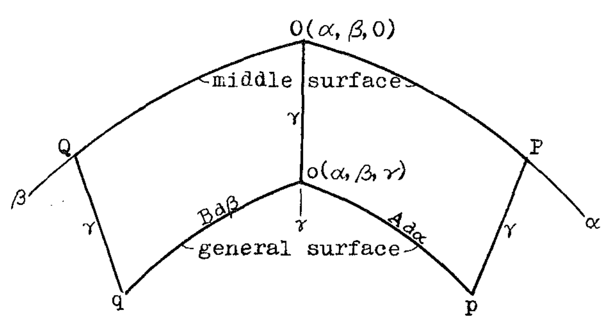

Fig. 1

Contributed by the Applied Mechanics Division of THE AMERICAN SOCIETY OF MECHANICAL ENGINEERS for presentation at the Joint ASCE/ASME Applied Mechanics, Biomechanics, and Fluids Engineering Conference, San Diego, California, July 9, to 12, 1989.

Discussion of this paper should be addressed to the Editorial Department, ASME, United Engineering Center, 345 East 47th Street, New York, N.Y. 10017, and will be accepted until two months after final publication of the paper itself in the JOURNAL OF APPLIED MECHANICS. Manuscript received by the ASME Applied Mechanics Division, May 18, 1988; final revision, December 1, 1988.

Paper No. 89-APM-40.

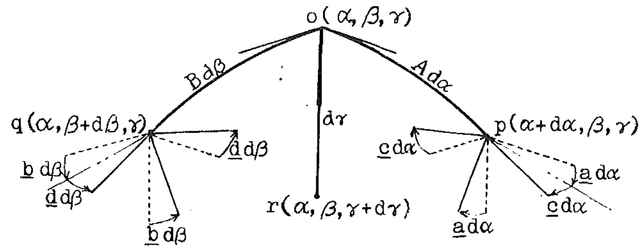

Fig. 2

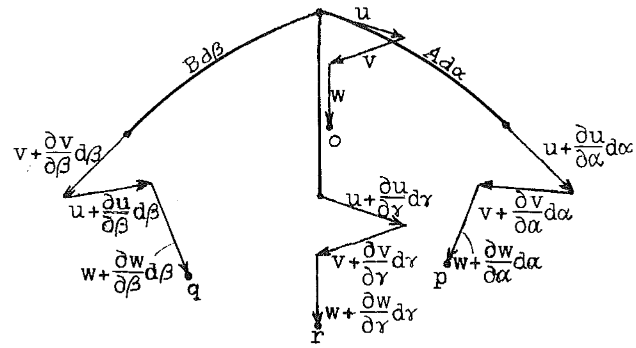

Fig. 3

The lines *op* and *oq* in the general surface, traced by the generating line as it moves along the *OP*, *OQ* lines, are also lines of curvature of the general surface. This follows from the fact that tangents to the *OP* line at *O* and to the *op* line at *o* are obviously parallel to each other because there is no twist along the *OP* line, and similarly for tangents at *P* and *p*. Then, since the generating line does not rotate about these tangents in going from *O* to *P*, it does not rotate about the same directions in going from *o* to *p*, and similarly for line *oq*.

Figure 2 shows the general surface with point *o*, having coordinates α, β, γ, and the neighboring points *p*, *q*, *r*, which have coordinates $\alpha+d\alpha$, β, γ, and α, $\beta+d\beta$, γ, and α, β, $\gamma+d\gamma$, respectively. Since coordinates such as α, β need not have the same scale everywhere, we introduce variable scale factors A, B defined so that $Ad\alpha$ and $Bd\beta$ are the distances measured along the curves between *o* and *p* and between *o* and *q*. We assume that A and B and their first derivatives are continuous functions of α, β, γ.

Due to the curvature of the α line, the α, β, γ directions at *p* (shown by the short tangent and perpendicular full lines at this point) are rotated relative to the α, β, γ directions at *o* (shown by similar short full lines at that point). We assume that these angles of rotation relative to the lines at *o* (or to the dotted lines at *p* parallel to the full lines at *o*) are continuous function of $d\alpha$. They can be expressed as power series in $d\alpha$, in which the constant term is absent (because the angle is zero when $d\alpha$ is zero) and terms of higher power than one can be ignored as small quantities of higher order. We can therefore take the angle about the β-direction as $a\,d\alpha$ and about the γ-direction as $c\,d\alpha$, as shown, assuming *a*, *c*, and their first derivatives to be continous functions of α, β, γ. There is no rotation about the α-direction because *op* is a line of curvature. Similarly for *b* and *d* at point *q*.

We designate by u, v, w the displacements of the general point *o* in the α, β, γ directions, as shown in Fig. 3, and assume that u, v, w and their first and second derivatives are continuous functions of α, β, γ. Since *p* differs from *o* only in the small change $d\alpha$ in α, the displacement of *p* in the α, β, γ directions (which are rotated relative to α, β, γ directions at *o* as shown in Fig. 2) must be $u+(\partial u/\partial\alpha)d\alpha$, $v+(\partial v/\partial\alpha)d\alpha$, $w+(\partial w/\partial\alpha)d\alpha$, as shown, and similarly for points *q* and *r*.

We now have the displaced and undisplaced positions of the general point *o* and of its neighboring points *p*, *q*, and *r* fully described, and can readily calculate the tensile and shear "engineering" strains ϵ_α, ϵ_β, ϵ_γ, $\epsilon_{\alpha\beta}$, $\epsilon_{\beta\gamma}$, $\epsilon_{\gamma\alpha}$ at *o*. The original length of the segment *op*, for instance, is $Ad\alpha$, and its change in length, using the angles of rotation at *p* in Fig. 2 and taking the cosines of these angles as unity and their sines as the angles themselves (ignoring small quantities of higher order) is:

$$\frac{\partial u}{\partial \alpha}d\alpha-\left(v+\frac{\partial v}{\partial \alpha}d\alpha\right)c\,d\alpha-\left(w+\frac{\partial w}{\partial \alpha}d\alpha\right)a\,d\alpha=\left(\frac{\partial u}{\partial \alpha}-cv-aw\right)d\alpha.$$

Dividing the change in length by the original length, the tensile strain in the α-direction at *o* is:

$$\epsilon_\alpha=\left(\frac{\partial u}{\partial \alpha}-cv-aw\right)/A.$$

Calculating the other strain-displacement relations at *o* in the same way, and introducing single-letter symbols f . . . k for compactness, where $\epsilon_\alpha=f$, $\epsilon_\beta=g$, $\epsilon_\gamma=h$, $\epsilon_{\alpha\beta}=i$, $\epsilon_{\beta\gamma}=j$, $\epsilon_{\gamma\alpha}=k$, we obtain:

$$\begin{aligned}
&e=f+g+h,\ f=\left(\frac{\partial u}{\partial \alpha}-cv-aw\right)/A,\\
&g=\left(\frac{\partial v}{\partial \beta}-du-bw\right)/B,\ h=\frac{\partial w}{\partial \gamma},\ i=\left(\frac{\partial v}{\partial \alpha}+cu\right)/A\\
&\quad+\left(\frac{\partial u}{\partial \beta}+dv\right)/B,\ j=\left(\frac{\partial w}{\partial \beta}+bv\right)/B\\
&\quad+\frac{\partial v}{\partial \gamma},\ k=\left(\frac{\partial w}{\partial \alpha}+au\right)/A+\frac{\partial u}{\partial \gamma}.
\end{aligned}\tag{1}$$

The quantity e, equal to the sum of the tensile strains is, of course, the unit increase in volume, or "dilatation."

The stress-strain relations are given by Hooke's Law, and, using equations (1), we find the stress-displacement relations:

$$\begin{aligned}
\sigma_\alpha&=\frac{E}{(1+\nu)(1-2\nu)}[(1-\nu)f+\nu g+\nu h]\\
&=\frac{E}{1+\nu}\left(f+\frac{\nu}{1-2\nu}e\right),\ \sigma_{\alpha\beta}=\frac{E}{2(1+\nu)}i\\
\sigma_\beta&=\frac{E}{(1+\nu)(1-2\nu)}[(1-\nu)g+\nu h+\nu f]\\
&=\frac{E}{1+\nu}\left(g+\frac{\nu}{1-2\nu}e\right),\ \sigma_{\beta\gamma}=\frac{E}{2(1+\nu)}j\\
\sigma_\gamma&=\frac{E}{(1+\nu)(1-2\nu)}[(1-\nu)h+\nu f+\nu g]\\
&=\frac{E}{1+\nu}\left(h+\frac{\nu}{1-2\nu}e\right),\ \sigma_{\gamma\alpha}=\frac{E}{2(1+\nu)}k.
\end{aligned}\tag{2}$$

We can now set up the equations of equilibrium of the forces in the α, β, γ directions on a general element of the shell wall at *o*, which is shown in Fig. 4. The angles between the sides of the element due to curvature are, of course, exaggerated in this figure to make clear their effect, which is very important even though the angles approach zero in the actual element. The figure shows the unit stresses on each face of the element, and the lengths of all the edges, from which the areas of the sides and, hence, the forces on each side can readily be calculated. Thus, the area of the top side could be approximated as the product of the average edge length in each direction, or $(A-Bc d\beta/2)d\alpha(B-Ad d\alpha/2)d\beta$; however, even this much refinement is unnecessary and the area can be taken as

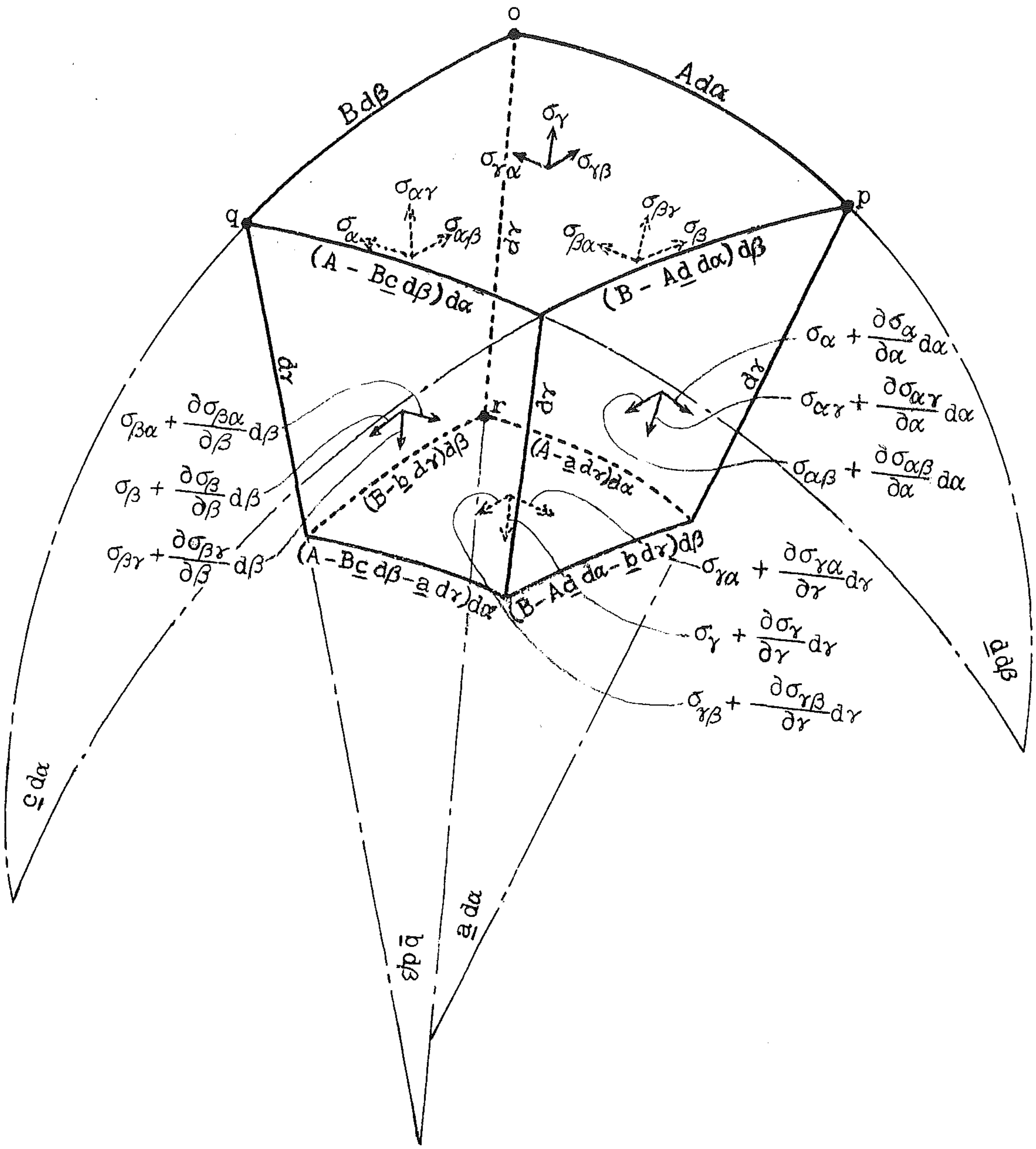

Fig. 4

$ABd\alpha d\beta$ since, if we retain other terms, we find that they cancel or are of higher order than the significant terms. In the final expressions only terms containing $d\alpha d\beta d\gamma$ are significant, those containing more differentials being small quantities of higher order and those containing less canceling.

The terms which must be included in each equilibrium equations are of three kinds: (1) differences between forces on opposite sides due to changes in the stresses and the areas on which they act, (2) resultants of the main forces on opposite sides due to the angle between these sides, and (3) body forces B_α, B_β, B_γ per unit volume in the α, β, γ directions, which may be functions of α, β, γ. Ignoring higher order terms, including the order of the subscripts in the expressions for shear stresses, the complete equilibrium equation in the α-direction is:

$$\left(\sigma_\alpha + \frac{\partial \sigma_\alpha}{\partial \alpha} d\alpha\right)(B - Ad\,d\alpha)d\beta d\gamma - \sigma_\alpha (Bd\beta)d\gamma$$

$$+ \left(\sigma_{\alpha\beta} + \frac{\partial \sigma_{\alpha\beta}}{\partial \beta} d\beta\right)(A - Bc\,d\beta)d\alpha d\gamma - \sigma_{\alpha\beta}(Ad\alpha)d\gamma$$

$$+ \left(\sigma_{\gamma\alpha} + \frac{\partial \sigma_{\gamma\alpha}}{\partial \gamma} d\gamma\right)(A - a\,d\gamma)d\alpha(B - b\,d\gamma)d\beta - \sigma_{\gamma\alpha}(Ad\alpha)(Bd\beta)$$

$$+ \sigma_\beta (Ad\alpha)d\gamma(d\,d\beta) - \sigma_{\alpha\beta}(Bd\beta)d\gamma(c\,d\alpha) - \sigma_{\gamma\alpha}(Bd\beta)d\gamma(a\,d\alpha)$$

$$+ B_\alpha (Ad\alpha)(Bd\beta)d\gamma = 0.$$

The first three lines are type (1) terms, the fourth line type (2), and the last line type (3). Expanding and simplifying as discussed, and dividing by $d\alpha d\beta d\gamma$, and similarly for the β, γ directions we find:

$$Ad(\sigma_\beta - \sigma_\alpha) - 2Bc\sigma_{\alpha\beta} - (Ab + 2Ba)\sigma_{\gamma\alpha}$$

$$+ B\frac{\partial \sigma_\alpha}{\partial \alpha} + A\frac{\partial \sigma_{\alpha\beta}}{\partial \beta} + AB\frac{\partial \sigma_{\gamma\alpha}}{\partial \gamma} + ABB_\alpha = 0$$

$$B c(\sigma_\alpha - \sigma_\beta) - 2Ad\sigma_{\alpha\beta} - (Ba + 2Ab)\sigma_{\beta\gamma}$$

$$+ A\frac{\partial \sigma_\beta}{\partial \beta} + B\frac{\partial \sigma_{\alpha\beta}}{\partial \alpha} + AB\frac{\partial \sigma_{\beta\gamma}}{\partial \gamma} + ABB_\beta = 0 \qquad (3)$$

$$Ba(\sigma_\alpha - \sigma_\gamma) + Ab(\sigma_\beta - \sigma_\gamma) - Ad\sigma_{\gamma\alpha} - Bc\sigma_{\beta\gamma}$$

$$+ AB\frac{\partial \sigma_{\beta\gamma}}{\partial \gamma} + A\frac{\partial \sigma_{\gamma\alpha}}{\partial \alpha} + ABB_\gamma = 0.$$

Substituting expressions (2) for the stresses, and multiplying by $(1+\nu)/E$, these equlibrium equations become:

$$Ad(g-f) - Bci - \left(\frac{Ab}{2} + Ba\right)k + \frac{\nu}{1-2\nu}B\frac{\partial e}{\partial \alpha}$$

$$+ B\frac{\partial f}{\partial \alpha} + \frac{A}{2}\frac{\partial i}{\partial \beta} + \frac{AB}{2}\frac{\partial k}{\partial \gamma} + \frac{1+\nu}{E}ABB_\alpha = 0$$

$$Bc(f-g) - Adi - \left(\frac{Ba}{2} + Ab\right)j + \frac{\nu}{1-2\nu}A\frac{\partial e}{\partial \beta}$$

$$+ A\frac{\partial g}{\partial \beta} + \frac{B}{2}\frac{\partial i}{\partial \alpha} + \frac{AB}{2}\frac{\partial j}{\partial \gamma} + \frac{1+\nu}{E}ABB_\beta = 0 \qquad (4)$$

$$Ab(g-h) + Ba(f-h) - \frac{Ad}{2}k - \frac{Bc}{2}j + \frac{\nu}{1-2\nu}AB\frac{\partial e}{\partial \gamma}$$

$$+ AB\frac{\partial h}{\partial \gamma} + \frac{A}{2}\frac{\partial j}{\partial \beta} + \frac{B}{2}\frac{\partial k}{\partial \alpha} + \frac{1+\nu}{E}ABB_\gamma = 0.$$

Equations (4) give three reasonably simple relations involving three unknowns u, v, w, using definitions (1) for the symbols e . . . k. To these must be added any edge boundary condition which may apply, or corresponding condition of cyclical continuity around any circumference, as well as surface boundary conditions such as:

$$\gamma = \frac{t}{2},\ -\frac{t}{2}:\ \sigma_\gamma = -p_i,\ -p_o;\ \sigma_{\beta\gamma},\ \sigma_{\gamma\alpha} = 0 \qquad (5)$$

where p_i and p_o are pressures on inside and outside surfaces, respectively, which may be functions of α, β. Physical problems in which $\sigma_{\beta\gamma}$ and $\sigma_{\gamma\alpha}$ are not zero at the inner and outer surfaces are possible but would be unusual. The aforementioned relations (4), with accompanying boundary conditions, form a complete solution which is applicable directly to numerical problems involving any mathematically definable elastic shell of any uniform thickness under any loading.

Table 1 gives suitable definitions for coordinate parameters α, β and corresponding values of the geometric functions A, B, a, b, c, d for some common types of shells; these may be deduced by simple geometric considerations or by application of mathematical theory.

Table 1

	α	β	γ	A	B	a	b	c	d
flate plate	x	y	z	1	1	0	0	0	0
right circular cylinder	x	θ	R-r	1	r	0	1	0	0
sphere	ϕ	θ	R-r	r	r$\sin\phi$	1	$\sin\phi$	0	$-\cos\phi$

For the cylinder and sphere, R is the middle surface radius and r the general point radius; for the cylinder x is the distance along the axis and θ the angle about the axis, clockwise looking in the x-direction; for the sphere θ is the angle of longitude, clockwise as seen from the north pole, and ϕ the angle of latitude measured from the north pole.

As an example of the application of this general theory, for a flat-plate relations (1) become:

$$f = \frac{\partial u}{\partial x},\ g = \frac{\partial v}{\partial y},\ h = \frac{\partial w}{\partial z},\ i = \frac{\partial v}{\partial x} + \frac{\partial u}{\partial y},$$

$$j = \frac{\partial w}{\partial y} + \frac{\partial v}{\partial z},\ k = \frac{\partial w}{\partial x} + \frac{\partial u}{\partial z}.$$

Equations (4) then reduce to the familiar equations of three-dimensional elasticity in terms of displacement: $\nabla^2 u + (1/1-2\nu)\partial e/\partial x = -2(1+\nu)B_x/E$, etc.

As another example, for a right circular cylinder the relations (1) become:

$$f = \frac{\partial u}{\partial x},\ g = \frac{1}{r}\left(\frac{\partial v}{\partial \theta} - w\right),\ h = -\frac{\partial w}{\partial r},$$

$$i = \frac{\partial v}{\partial x} + \frac{1}{r}\frac{\partial u}{\partial \theta},\ j = \frac{1}{r}\left(\frac{\partial w}{\partial \theta} + v\right) - \frac{\partial v}{\partial r},$$

$$k = \frac{\partial w}{\partial x} - \frac{\partial u}{\partial r}.$$

The first equilibrium equation (4) for the α-direction is then the same as for a flat plate given above (but, of course, with a different meaning of e and the operator ∇^2). The other two are also well known:

$$\nabla^2 v + \frac{1}{1-2\nu}\frac{1}{r}\frac{\partial e}{\partial \theta} - \frac{1}{r^2}\left(v + 2\frac{\partial w}{\partial \theta}\right) = -2(1+\nu)\frac{B_\theta}{E}$$

$$-\nabla^2 w + \frac{1}{1-2\nu}\frac{\partial e}{\partial r} + \frac{1}{r^2}\left(w - 2\frac{\partial v}{\partial \theta}\right) = -2(1+\nu)\frac{B_r}{E}$$

It should perhaps be noted that the thick-wall shell solution presented above does not contain as a special case the conventional thin-wall solution based on the Kirchhoff-Love approximation, or even its linear, small-deflection part. This is because these solutions are basically different. Exact solutions should convert to the same thing, but this is not necessarily true for approximate solutions. Such thin-wall solutions can not, in general, satisfy elasticity conditions or surface boundary conditions, in spite of being good approximations for the purposes for which they are designed.

Work-Conjugate Boundary Conditions in the Nonlinear Theory of Thin Shells

J. Makowski[1]
Assistant Professor.

W. Pietraszkiewicz[2]
Professor.

Ruhr Universität,
Lehrstuhl für Mechanik II,
D-4630 Bochum 1,
Federal Republic of Germany

Work-conjugate boundary conditions for a class of nonlinear theories of thin shells formulated in terms of displacements of the reference surface are discussed. Applying theorems of the theory of differential forms it is shown that many of the sets of static boundary conditions which have been proposed in the literature do not possess work-conjugate geometric counterparts. The general form of four geometric boundary conditions and their work-conjugate static boundary conditions is constructed and three particular cases are analyzed. The boundary conditions given here are valid for unrestricted displacements, rotations, strains and/or changes of curvatures of the reference surface.

Introduction

Within the nonlinear Kirchhoff-Love theory of shells, Galimov (1950) reduced the external forces applied to the lateral boundary surface of the deformed shell to three statically equivalent effective force resultants and one bending couple resultant. In particular, he replaced the torsional couple resultant by additional force resultants by applying the same procedure which had earlier been used by Love (1927) in the classical linear theory of shells and by Thompson and Tait (1883) in the linear theory of plates. The rigorous validity of those four reduced static boundary quantities was later confirmed by Koiter (1964) on the basis of purely static arguments.

From variational considerations it follows that each effective force resultant should perform work on an appropriate translation of the boundary while the bending couple resultant should perform work on a scalar parameter which describes the rotational deformation of the boundary. Such work-conjugate sets of static and geometric quantities and their related static and geometric boundary conditions have been established for the classical linear theory of shells as well as for various versions of the first-approximation geometrically nonlinear theory of shells undergoing moderate rotations (cf., Schmidt and Pietraszkiewicz, 1981, and the references given there). When strains and/or rotations of the shell material elements are not restricted, however, the effective force and couple resultants derived by means of purely static considerations do not necessarily possess work-conjugate geometric counterparts.

[1]On leave from the Technical University, ul. ZSP 5, 45-223 Opole, Poland.
[2]On leave from the Institute of Fluid Flow Machinery of the Polish Academy of Sciences, ul. Fiszera 14, 80-952 Gdańsk, Poland.

Contributed by the Applied Mechanics Division of THE AMERICAN SOCIETY OF MECHANICAL ENGINEERS for publication in the JOURNAL OF APPLIED MECHANICS.

Discussion on this paper should be addressed to the Editorial Department, ASME, United Engineering Center, 345 East 47th Street, New York, N.Y. 10017, and will be accepted until two months after final publication of the paper itself in the JOURNAL OF APPLIED MECHANICS. Manuscript received by ASME Applied Mechanics Division, April 26, 1988; final revision, August 17, 1988.

On the other hand, Novozhilov and Shamina (1975) performed a purely geometric analysis of an arbitrary deformation of the shell lateral boundary surface subject to the Kirchhoff-Love constraints. They were able to show, in particular, that three translations and one scalar parameter ϑ_ν completely describe an arbitrary deformation of the shell boundary. Unfortunately, the corresponding work-conjugate static boundary conditions have not been given in the literature.

A similar geometric analysis performed by Pietraszkiewicz and Szwabowicz (1981) led to the conclusion that three translations and an additional scalar function n_ν of the displacement derivatives may also be used to describe an arbitrary deformation of the shell boundary. The four work-conjugate static boundary conditions were then constructed in terms of n_ν as the natural boundary conditions generated by the two-dimensional principle of virtual displacements.

In most other works on the nonlinear theory of thin shells, the four static boundary conditions have also been obtained as the natural boundary conditions of the two-dimensional principle of virtual displacements, but this has been done without explicit reference to the corresponding geometric boundary conditions. Instead, it is usually assumed that the *virtual* displacements and rotations should be kinematically admissible. As a result, in the transformed boundary line integral, the bending couple resultant performs virtual work on some variational expression that describes the *virtual* rotation of the boundary but not the *variation* of a scalar parameter describing the rotation itself. Various forms of the variational expression associated with different natural definitions of the bending couple have been proposed in the literature. In each case the question arises whether the variational expression, possibly multiplied by a scalar function, can be represented as the variation of some scalar function φ of displacement derivatives. Only if such a representation is possible, the four natural static boundary quantities possess work-conjugate geometric counterparts.

The aim of this paper is to investigate the problem of existence and to derive the general form of the work-conjugate sets of static and geometric boundary conditions for the nonlinear theory of thin shells expressed in terms of displacements as basic independent field variables. In the analysis it is only assumed that the deformation of the shell as a three-dimensional body is completely determined by the stretching and bending of its reference surface. This assumption is far less restrictive than the usual Kirchhoff-Love constraints. In particular, the deformation of the shell in the direction of the normal to the reference surface is not restricted by this assumption.

A new and entirely general approach to the problem of work-conjugate boundary conditions is developed here. It is shown that at any point of the boundary, each of the variational expressions associated with the bending couple resultant may be regarded as a differential 1-form ω on a suitably defined six-dimensional manifold of displacement derivatives. Then the theorem of Poincaré provides the necessary condition for ω to be exact, i.e., of the form $\omega = \delta\varphi$, and the theorem of Frobenius provides the necessary condition for ω to be integrable, i.e., of the form $\mu\omega = \delta\varphi$, where μ is an integrating factor. Applying those theorems to various variational expressions proposed in the literature, their exactness and integrability is established. In particular, it is proved that the variational expression used originally by Galimov (1951) and in various different but equivalent forms in many subsequent papers, is *not integrable*. In such formulations of the nonlinear theory of shells the four natural static boundary quantities do not possess work-conjugate geometric counterparts.

The general procedure is worked out for the transformation of a nonintegrable 1-form into an integrable 1-form for which the primitive is obtained using a method of integration of total differential equations. This primitive is an *arbitrary* scalar function φ of the displacement derivatives. Associated general expressions for the natural force resultants and bending couple resultant, which perform virtual work on variations of the respective displacement components and of the function φ, are derived. Three particular definitions of φ are discussed, and the work-conjugate static boundary and corner conditions corresponding to the geometric boundary conditions of Novozhilov and Shamina (1975) are established.

Notation and Basic Relations

In this paper we largely rely on notation used by Koiter (1966) and Pietraszkiewicz (1977, 1979).

The position vectors of the undeformed and deformed reference surface M and $\bar{M}$ of the shell are denoted by $\mathbf{r}(\Theta^\alpha)$ and $\bar{\mathbf{r}}(\Theta^\alpha)$, respectively, where Θ^α, $\alpha=1, 2$, are convected (material) surface coordinates. At each point $M \epsilon M$ we have the natural base vectors $\mathbf{a}_\alpha = \partial\mathbf{r}/\partial\Theta^\alpha \equiv \mathbf{r},_\alpha$, the unit normal vector $\mathbf{n} = 1/2\epsilon^{\alpha\beta}\mathbf{a}_\alpha \times \mathbf{a}_\beta$, the covariant metric tensor $a_{\alpha\beta} = \mathbf{a}_\alpha \bullet \mathbf{a}_\beta$ with its determinant $a = \det a_{\alpha\beta} > 0$, the curvature tensor $b_{\alpha\beta} = - \mathbf{a}_\alpha \bullet \mathbf{n},_\beta$, and the permutation tensor $\epsilon_{\alpha\beta} = (\mathbf{a}_\alpha \times \mathbf{a}_\beta)\bullet\mathbf{n}$. The reciprocal base vectors $\mathbf{a}^\alpha$ and the contravariant metric tensor $a^{\alpha\beta}$ are then defined by $\mathbf{a}^\alpha \bullet \mathbf{a}_\beta = \delta^\alpha_\beta$ and $a^{\alpha\beta} = \mathbf{a}^\alpha \bullet \mathbf{a}^\beta$, where δ^α_β denotes the Kronecker symbol. In what follows Greek indices always refer to the coordinates Θ^α, and for a diagonally repeated index the summation convention will be invoked.

The boundary C of M is assumed to consist of a finite set of piecewise smooth curves with the position vector $\mathbf{r}(s) = \mathbf{r}[\Theta^\alpha(s)]$, where s is the arc length along C. At each regular point $M \epsilon C$ we denote the unit tangent vector by $\mathbf{t} = \mathbf{r}' = \mathbf{a}_\alpha t^\alpha$ and the outward unit normal vector by $\boldsymbol{\nu} = \mathbf{r},_\nu = \mathbf{a}_\alpha \nu^\alpha = \mathbf{t} \times \mathbf{n}$, $\nu^\alpha = \epsilon^{\alpha\beta} t_\beta$. Here, $(.)'$ indicates differentiation with respect to the arc length s and $(.),_\nu$ denotes the outward normal derivative at C.

Consider now an arbitrary smooth deformation $M \rightarrow \bar{M}$ of the shell reference surface and let $\mathbf{u}(\Theta^\alpha) = u^\lambda \mathbf{a}_\lambda + w\mathbf{n}$ be the associated displacement field such that $\bar{\mathbf{r}} = \mathbf{r} + \mathbf{u}$. To distinguish all geometric quantities defined on $\bar{M}$ and on its boundary $\bar{C}$ from those on M and C we use an overbar, e.g., $\bar{\mathbf{a}}_\alpha$, $\bar{\mathbf{n}}$, $\bar{a}_{\alpha\beta}$, $\bar{b}_{\alpha\beta}$, $\bar{\boldsymbol{\nu}}$, $\bar{\mathbf{t}}$, etc. The deformation of the shell reference surface may then be expressed in terms of the geometry of M and the displacement field $\mathbf{u}$. In particular, we obtain (cf., Pietraszkiewicz, 1980, 1984a)

$$\bar{\mathbf{a}}_\alpha = \bar{\mathbf{r}},_\alpha = \mathbf{a}_\alpha + \mathbf{u},_\alpha \bar{\mathbf{n}} = \frac{1}{2} j^{-1} \epsilon^{\alpha\beta} \bar{\mathbf{r}},_\alpha \times \bar{\mathbf{r}},_\beta, \tag{1a}$$

$$\gamma_{\alpha\beta} = \frac{1}{2}(\bar{a}_{\alpha\beta} - a_{\alpha\beta}) = \frac{1}{2}(\bar{\mathbf{r}},_\alpha \bullet \bar{\mathbf{r}},_\beta - a_{\alpha\beta}), \tag{1b}$$

$$\kappa_{\alpha\beta} = -(\bar{b}_{\alpha\beta} - b_{\alpha\beta}) = \bar{\mathbf{r}},_\alpha \bullet \bar{\mathbf{n}},_\beta + b_{\alpha\beta}, \tag{1c}$$

$$j^2 = \frac{\bar{a}}{a} = \frac{1}{2}\epsilon^{\alpha\lambda}\epsilon^{\beta\kappa}(\bar{\mathbf{r}},_\alpha \bullet \bar{\mathbf{r}},_\beta)(\bar{\mathbf{r}},_\lambda \bullet \bar{\mathbf{r}},_\kappa). \tag{1d}$$

Similarly, along the boundary we have

$$\bar{\mathbf{r}}' = \bar{\mathbf{a}}_\beta t^\beta = \mathbf{t} + \mathbf{u}' = c_\nu \boldsymbol{\nu} + c_t \mathbf{t} + c\mathbf{n}, \tag{2a}$$

$$\bar{\mathbf{r}},_\nu = \bar{\mathbf{a}}_\beta \nu^\beta = \boldsymbol{\nu} + \mathbf{u},_\nu, \tag{2b}$$

$$\bar{\mathbf{n}} = j^{-1}\bar{\mathbf{r}},_\nu \times \bar{\mathbf{r}}' = n_\nu \boldsymbol{\nu} + n_t \mathbf{t} + n\mathbf{n}, \tag{2c}$$

$$j = |\bar{\mathbf{r}},_\nu \times \bar{\mathbf{r}}'|,\ j^2 = |\bar{\mathbf{r}},_\nu|^2 |\bar{\mathbf{r}}'|^2 - (\bar{\mathbf{r}},_\nu \bar{\mathbf{r}}')^2. \tag{2d}$$

For future reference we also note the following relationships

$$\bar{\mathbf{a}}_t \equiv \bar{\mathbf{r}}' = \bar{a}_t \bar{\mathbf{t}},\ \bar{\mathbf{a}}_\nu = \bar{\mathbf{a}}_t \times \bar{\mathbf{n}} = \bar{a}_t \bar{\boldsymbol{\nu}}, \tag{3a}$$

$$\bar{a}_t = |\bar{\mathbf{r}}'| = \sqrt{1 + 2\gamma_{tt}},\ a_\nu = \boldsymbol{\nu} \bullet \bar{\mathbf{a}}_\nu, \tag{3b}$$

$$\bar{\mathbf{r}},_\nu = \bar{a}_t^{-1}(j\bar{\boldsymbol{\nu}} + 2\gamma_{\nu t}\bar{\mathbf{t}}), \tag{3c}$$

$$\bar{\mathbf{a}}^\beta = j^{-1}(\bar{a}_t \nu^\beta - 2\gamma_{\nu t}\bar{a}_t^{-1} t^\beta)\bar{\boldsymbol{\nu}} + \bar{a}_t^{-1} t^\beta \bar{\mathbf{t}}, \tag{3d}$$

$$2\gamma_{\nu t} = 2\gamma_{\alpha\beta}\nu^\alpha t^\beta = \bar{\mathbf{r}},_\nu \bullet \bar{\mathbf{r}}',\ 2\gamma_{tt} = 2\gamma_{\alpha\beta} t^\alpha t^\beta = |\bar{\mathbf{r}}'|^2 - 1. \tag{3e}$$

Statement of the Problem

We are concerned here with the class of nonlinear theories of thin shells for which the deformation of the shell as a three-dimensional body is completely determined by the stretching and bending of its reference surface. A common feature of various shell theories within this class is that their equilibrium conditions may be expressed by the following principle of virtual displacements

$$\iint_M (N^{\alpha\beta}\delta\gamma_{\alpha\beta} + M^{\alpha\beta}\delta\kappa_{\alpha\beta})dA = \iint_M (\mathbf{p}\bullet\delta\bar{\mathbf{r}} + \mathbf{h}\bullet\delta\bar{\mathbf{n}})dA$$

$$+ \int_{C_f} (\mathbf{T}\bullet\delta\bar{\mathbf{r}} + \mathbf{H}\bullet\delta\bar{\mathbf{n}})ds. \tag{4}$$

In (4) all quantities are defined with respect to undeformed reference surface M (Lagrangian description) and C_f is the part of C where the external boundary force and moment resultants $\mathbf{T}$ and $\mathbf{H}$ are prescribed. The Lagrangian surface strain measures $\gamma_{\alpha\beta}$ and $\kappa_{\alpha\beta}$ are defined by (1*b*, *c*) while $\bar{\mathbf{n}}$ on C is given by (2*c*, *d*). The mechanical variables $N^{\alpha\beta}$ and $M^{\alpha\beta}$ in (4) are two-dimensional symmetric second Piola-Kirchhoff type stress resultant and stress couple tensors while $\mathbf{p}$ and $\mathbf{h}$ are the external surface force and moment resultants on M. Explicit expressions for $N^{\alpha\beta}$ $M^{\alpha\beta}$ and $\mathbf{p}$, $\mathbf{h}$, $\mathbf{T}$, $\mathbf{H}$ in terms of three-dimensional surface and body forces and of the reference surface deformation depend on the particular type of nonlinear shell theory employed.

In view of (1*b*, *c*), the only independent variable undergoing variations in M is the position vector $\bar{\mathbf{r}}$ (or, equivalently, the displacement vector $\mathbf{u}$). Therefore, applying the standard variational procedure, the principle (4) may also be rewritten in the form

$$-\iint_M (\mathbf{T}^{\beta}{}_{|\beta}+\mathbf{p})\cdot\delta\bar{\mathbf{r}}dA+\int_{C_u} [(\mathbf{T}^{\beta}\nu_{\beta})\cdot\delta\bar{\mathbf{r}}+(M^{\alpha\beta}\bar{\mathbf{a}}_{\alpha}\nu_{\beta})\cdot\delta\bar{\mathbf{n}}]ds$$

$$+\int_{C_f}[(\mathbf{T}^{\beta}\nu_{\beta}-\mathbf{T})\cdot\delta\bar{\mathbf{r}}+(M^{\alpha\beta}\bar{\mathbf{a}}_{\alpha}\nu_{\beta}-\mathbf{H})\cdot\delta\bar{\mathbf{n}}]ds=0, \quad (5)$$

where

$$\mathbf{T}^{\beta}=N^{\alpha\beta}\bar{\mathbf{a}}_{\alpha}+M^{\alpha\beta}\bar{\mathbf{n}},_{\alpha}+\{[(M^{\lambda\kappa}\bar{\mathbf{a}}_{\lambda})|_{\kappa}+\mathbf{h}]\cdot\bar{\mathbf{a}}^{\beta}\}\bar{\mathbf{n}}, \quad (6)$$

and C_u, $C=C_u\cup C_f$, denotes the part of C where the geometric boundary conditions are prescribed. Also, $(.)_{|\beta}$ indicates covariant differentiation in the metric of M. From (5) we directly obtain the familiar equilibrium equations

$$\mathbf{T}^{\beta}{}_{|\beta}+\mathbf{p}=\mathbf{0} \text{ in } M. \quad (7)$$

The derivation of static and geometric boundary conditions which are consistent with (4) and (5) is, unfortunately, not straightforward and unique and has up until now never been performed in complete generality. Note that $\bar{\mathbf{n}}$ is not an independent variable on C, since by virtue of (2c, d) it is the function of $\bar{\mathbf{r}},_{\nu}$ and $\bar{\mathbf{r}}'$. Rather, the independent variables undergoing the variation on C are the position vector $\bar{\mathbf{r}}$ (and, hence, $\bar{\mathbf{r}}'$) and its outward normal derivative $\bar{\mathbf{r}},_{\nu}$. Those variables, however, have to satisfy two identities

$$\bar{\mathbf{r}}'\cdot\bar{\mathbf{n}}=0, \quad \bar{\mathbf{n}}\cdot\bar{\mathbf{n}}=1 \quad \text{along } C. \quad (8)$$

These identities imply that three components of $\bar{\mathbf{r}}$ (or $\mathbf{u}$) and one additional scalar function of position (or displacement) derivatives, say, $\varphi(\bar{\mathbf{r}},_{\nu},\bar{\mathbf{r}}')$, are necessary and sufficient to describe the shell deformation along its boundary uniquely. Consequently, the number of corresponding static boundary conditions can also be reduced to four.

The static boundary and corner conditions may be obtained from (4) as the natural boundary conditions. Indeed, performing the variation of (2c) directly or varying the identities (8), $\delta\bar{\mathbf{n}}$ may be written in the form

$$\delta\bar{\mathbf{n}}=-\nu_{\beta}\bar{\mathbf{a}}^{\beta}\ \{\bar{\mathbf{n}}\cdot\delta\bar{\mathbf{r}},_{\nu}\}-t_{\beta}\bar{\mathbf{a}}^{\beta}\ (\bar{\mathbf{n}}\cdot\delta\bar{\mathbf{r}}'). \quad (9a)$$

The expression (9a) may now be substituted into the second line integral of (5) and, subsequently, all terms containing $\delta\bar{\mathbf{r}}'$ may be eliminated by integration by parts. This leads to a reduced form of the line integral along C_f and some additional terms at each corner point $M_n\in C_f$, $n=1, 2, \ldots, N$. For arbitrary $\delta\bar{\mathbf{r}}$ and $\bar{\mathbf{n}}\cdot\delta\bar{\mathbf{r}},_{\nu}$ along C_f and $\delta\bar{\mathbf{r}}_n$ at each $M_n\in C_f$ their multipliers should vanish identically, which then gives four natural static boundary conditions along C_f and three natural static conditions at each corner $M_n\in C_f$.

The derivation of static boundary and corner conditions in the way just outlined is not unique, however, since using (8), $\delta\bar{\mathbf{n}}$ may also be expressed in several other, though essentially equivalent, forms such as, for example,

$$\delta\bar{\mathbf{n}}\ =\ \bar{\nu}\ \{\bar{\nu}\cdot\delta\bar{\mathbf{n}}\}-\frac{1}{\bar{a}_t^2}\ \bar{\mathbf{r}}'\ (\bar{\mathbf{n}}\cdot\delta\bar{\mathbf{r}}'), \quad (9b)$$

$$=\ \frac{1}{a_{\nu}}\ [\bar{\mathbf{a}}_{\nu}\ \{\nu\cdot\delta\bar{\mathbf{n}}\}+\nu\times\bar{\mathbf{n}}\ (\bar{\mathbf{n}}\cdot\delta\bar{\mathbf{r}}')]. \quad (9c)$$

Still other forms will be discussed subsequently. Each of the possible forms of $\delta\bar{\mathbf{n}}$ may be used for the derivation of a different set of natural static boundary and corner conditions, and each set of conditions will be consistent with the principle of virtual displacements (4). In particular, the corresponding bending couple resultant, which in each of the cases of (9) is defined by a different expression, performs virtual work on the respective variational expression $\bar{\mathbf{n}}\cdot\delta\bar{\mathbf{r}},_{\nu}$, $\bar{\nu}\cdot\delta\bar{\mathbf{n}}$ or $\nu\cdot\delta\bar{\mathbf{n}}$.

In the variational principle (4) all virtual displacements are assumed to be kinematically admissible, so that the first line integral over C_u in (5) must vanish identically. It will be shown in Chapter 5 that for any *given* set of the four geometric parameters $\bar{\mathbf{r}}$, φ, which describe an arbitrary deformation of the shell boundary, the kinematically admissible virtual displacement field indeed satisfies the kinematic constraints $\delta\bar{\mathbf{r}}=\mathbf{0}$ and $\delta\bar{\mathbf{n}}=\mathbf{0}$ along C_u. In view of expressions (9), the vanishing of the line integral over C_u in (5) is also assured by the fulfillment of only four kinematic constraints, that is by $\delta\bar{\mathbf{r}}=\mathbf{0}$ and $\bar{\mathbf{n}}\cdot\delta\bar{\mathbf{r}},_{\nu}=0$, $\bar{\nu}\cdot\delta\bar{\mathbf{n}}=0$ or $\nu\cdot\delta\bar{\mathbf{n}}=0$, respectively, along C_u, and $\delta\bar{\mathbf{r}}_m=\mathbf{0}$ at each corner $M_m\in C_u$, $m=1, 2, \ldots$, M. It is apparent that the constraint $\delta\bar{\mathbf{r}}=\mathbf{0}$ is equivalent to the geometric boundary conditions $\bar{\mathbf{r}}=\bar{\mathbf{r}}^*$ along C_u, and that $\delta\bar{\mathbf{r}}_m=\mathbf{0}$ corresponds to the geometric corner condition $\bar{\mathbf{r}}_m=\bar{\mathbf{r}}_m^*$ at each $M_m\in C_u$, where $(.)^*$ denotes the prescribed value. It is not immediately obvious, however, what kind of scalar parameter should be prescribed on C_u in order to satisfy the fourth kinematic constraint $\bar{\mathbf{n}}\cdot\delta\bar{\mathbf{r}},_{\nu}=0$, $\bar{\nu}\cdot\delta\bar{\mathbf{n}}=0$ or $\nu\cdot\delta\bar{\mathbf{n}}=0$, respectively. The question thus arises whether there exists a scalar function $\varphi(\bar{\mathbf{r}},_{\nu},\bar{\mathbf{r}}')$ such that its variation will coincide with $\bar{\mathbf{n}}\cdot\delta\bar{\mathbf{r}},_{\nu}$, $\bar{\nu}\cdot\delta\bar{\mathbf{n}}$ or $\nu\cdot\delta\bar{\mathbf{n}}$, possibly multiplied by some other nonvanishing scalar function $\mu(\bar{\mathbf{r}},_{\nu},\bar{\mathbf{r}}')$. When such a φ does exist, the fourth geometric boundary condition takes the form $\varphi=\varphi^*$ along C_u. Only in such a case are the four natural static boundary conditions generated from (5) and (9) work-conjugate to the geometric ones.

In the particular case of a pure rotation of the shell boundary, i.e., when three translations are prescribed, Zubov (1982) showed that such a scalar parameter $\varphi(\bar{\mathbf{r}},_{\nu})$ is the solution of an integrable Pfaffian equation. Later particular definitions of the parameter φ were discussed by Zubov (1984). In this paper we develop an alternative and entirely general approach to the problem of existence and of the form of the parameter φ. This approach is valid for an arbitrary deformation of the shell boundary.

Integrability Conditions

Let ω denotes any variational expression of the type enclosed in braces in (9). Its general form is

$$\omega=\mathbf{A}(\bar{\mathbf{r}},_{\nu},\bar{\mathbf{r}}')\cdot\delta\bar{\mathbf{r}},_{\nu}+\mathbf{B}(\bar{\mathbf{r}},_{\nu},\bar{\mathbf{r}}')\cdot\delta\bar{\mathbf{r}}', \quad (10)$$

where vector-valued functions $\mathbf{A}$ and $\mathbf{B}$ must be specified for each particular case.

The ω defined by (10) may be considered as a differential 1-form on the infinite-dimensional space consisting of the ordered pairs $(\bar{\mathbf{r}},_{\nu}(s), \bar{\mathbf{r}}'(s))$ of vector-valued functions defined along C (cf., Cartan, 1970). However, for our present purposes it is sufficient to consider ω at an arbitrary fixed point M $\in C$. Then ω, as defined by (10), may be regarded as a differential 1-form on the six-dimensional manifold X with local coordinates ξ_i, $i=1, 2, \ldots, 6$ (in a neighborhood of $x_o\in X$), which may be identified with components of $(\bar{\mathbf{r}},_{\nu}, \bar{\mathbf{r}}')$ in the orthonormal base $\{\nu, \mathbf{t}, \mathbf{n}\}$, i.e.,

$$(\xi_i)=(\nu\cdot\bar{\mathbf{r}},_{\nu},\ \mathbf{t}\cdot\bar{\mathbf{r}},_{\nu},\ \mathbf{n}\cdot\bar{\mathbf{r}},_{\nu},\ \nu\cdot\bar{\mathbf{r}}',\ \mathbf{t}\cdot\bar{\mathbf{r}}',\ \mathbf{n}\cdot\bar{\mathbf{r}}'). \quad (11)$$

Here x_o with local coordinates (1, 0, 0, 0, 1, 0) signifies the undeformed state of the shell boundary. Thus, the 1-form ω may be rewritten as

$$\omega=\sum_{i=1}^{6}A_i(\xi_j)\ \delta\xi_i, \quad (12)$$

where $\delta\xi_i$ are understood to be differentials in the usual sense and A_i, $i=1, 2, \ldots, 6$, are defined as components of $(\mathbf{A}, \mathbf{B})$ in the base $\{\nu, \mathbf{t}, \mathbf{n}\}$, that is

$$(A_i)=(\nu\cdot\mathbf{A},\ \mathbf{t}\cdot\mathbf{A},\ \mathbf{n}\cdot\mathbf{A},\ \nu\cdot\mathbf{B},\ \mathbf{t}\cdot\mathbf{B},\ \mathbf{n}\cdot\mathbf{B}). \quad (13)$$

The interpretation of ω as a differential 1-form makes it possible to apply some basic definitions and theorems of the theory of differential forms (cf., Cartan, 1970, Westenholz, 1981). For convenience they are briefly summarized below in our notation.

The 1-form (10) is said to be *exact* on X if there exists a scalar-valued function $\varphi(\bar{\mathbf{r}},_\nu,\bar{\mathbf{r}}')$, called the *primitive* of ω, such that $\omega = \delta\varphi$, i.e., $\partial\varphi/\partial\bar{\mathbf{r}},_\nu = \mathbf{A}$ and $\partial\varphi/\partial\bar{\mathbf{r}}' = \mathbf{B}$. According to the lemma of Poincaré, the necessary condition for ω, to be exact, is $d\omega = 0$, where $d\omega$ denotes the exterior derivative of ω. In the notation of (12), the condition $d\omega = 0$ reads

$$A_{i,j} - A_{j,i} = 0 \text{ for } i,j = 1,2,\ldots,6, \tag{14}$$

which implies that the matrix $\partial A_i/\partial\xi_j \equiv A_{i,j}$ has to be symmetric. In a sufficiently small neighborhood of $x_o \in X$ the conditions (14) are also sufficient for ω to be exact.

The 1-form (10) is said to be *integrable* on X if there exist scalar-valued functions $\mu(\bar{\mathbf{r}},_\nu,\bar{\mathbf{r}}')$, called the *integrating factor*, and $\varphi(\bar{\mathbf{r}},_\nu,\bar{\mathbf{r}}')$ such that $\mu\omega = \delta\varphi$, i.e., $\mu^{-1}(\partial\varphi/\partial\bar{\mathbf{r}},_\nu) = \mathbf{A}$ and $\mu^{-1}(\partial\varphi/\partial\bar{\mathbf{r}}') = \mathbf{B}$. According to the theorem of Frobenius, the necessary condition for ω to be integrable is $\omega\wedge d\omega = 0$, where $\wedge$ denotes the exterior product. In a sufficiently small neighborhood of $x_o \in X$ this condition is also sufficient for ω to be integrable. In the notation of (12) the integrability condition $\omega\wedge d\omega = 0$ takes the form (cf., Ince, 1956)

$$A_i(A_{k,j} - A_{j,k}) + A_j(A_{i,k} - A_{k,i}) + A_k(A_{j,i} - A_{i,j}) = 0 \tag{15}$$

for $i, j, k = 1, 2, \ldots, 6$. There are twenty such equations of which only ten are independent. It is obvious that the exact 1-form is integrable and that $\mu\omega$ is exact if ω is integrable.

Now we are in a position to discuss the problem of existence of the fourth geometric boundary condition corresponding to various variational expressions enclosed in braces in (9). Consider the case (9*b*) for which the natural static boundary conditions were given first by Galimov (1951) and were rederived in different but equivalent forms in many subsequent papers. In this case $\omega = \bar{\nu}\cdot\delta\bar{\mathbf{n}}$, and the corresponding vector-valued functions $\mathbf{A}$ and $\mathbf{B}$, calculated with the help of (9*a*) and (3*d*), take the form

$$\mathbf{A} = -\bar{a}_t j^{-1}\bar{\mathbf{n}}, \quad \mathbf{B} = 2\bar{a}_t^{-1} j^{-1}\gamma_{\nu t}\bar{\mathbf{n}}, \tag{16}$$

where all quantities on the right-hand sides are functions of $\bar{\mathbf{r}},_\nu$ and $\bar{\mathbf{r}}'$ given by (2*c,d*) and (3*e*). Differentiation of (16), with respect to $\bar{\mathbf{r}},_\nu$ and $\bar{\mathbf{r}}'$, gives

$$\frac{\partial\mathbf{A}}{\partial\bar{\mathbf{r}},_\nu} = \bar{a}_t^2 j^{-2}\,(\bar{\nu}\otimes\bar{\mathbf{n}} + \bar{\mathbf{n}}\otimes\bar{\nu}), \tag{17a}$$

$$\frac{\partial\mathbf{A}}{\partial\bar{\mathbf{r}}'} = j^{-1}\,\bar{\mathbf{t}}\otimes\bar{\mathbf{n}} - 2j^{-2}\gamma_{\nu t}\,(\bar{\nu}\otimes\bar{\mathbf{n}} + \bar{\mathbf{n}}\otimes\bar{\nu}) = \left(\frac{\partial\mathbf{B}}{\partial\bar{\mathbf{r}},_\nu}\right)^T, \tag{17b}$$

$$\frac{\partial\mathbf{B}}{\partial\bar{\mathbf{r}}'} = \bar{a}_t^{-2}\,[\bar{\mathbf{n}}\otimes\bar{\nu} + 4j^{-2}\gamma_{\nu t}^2\,(\bar{\nu}\otimes\bar{\mathbf{n}} + \bar{\mathbf{n}}\otimes\bar{\nu}) - 2j^{-1}\gamma_{\nu t} - (\bar{\mathbf{t}}\otimes\bar{\mathbf{n}} + \bar{\mathbf{n}}\otimes\bar{\mathbf{t}})]. \tag{17c}$$

Since (17*a*) is symmetric and (17*b*) holds, (17*c*) leads to the only nonvanishing expression

$$\frac{\partial\mathbf{B}}{\partial\bar{\mathbf{r}}'} - \left(\frac{\partial\mathbf{B}}{\partial\bar{\mathbf{r}}'}\right)^T = \bar{a}_t^{-2}\,(\bar{\mathbf{n}}\otimes\bar{\nu} - \bar{\nu}\otimes\bar{\mathbf{n}}). \tag{18}$$

Therefore, conditions (14) are identically satisfied for any combination of $i, j \in (1, 2, \ldots, 6)$ except for $(i, j) = (4, 5)$, $(4, 6)$, and $(5, 6)$. As a result, the 1-form $\omega = \bar{\nu}\cdot\delta\bar{\mathbf{n}}$ is not exact on X.

If components of (17) are introduced into (15), the integrability conditions are satisfied identically for any combination of $i, j, k \in (1, 2, \ldots, 6)$, except for such combinations in which any two of three indices i, j, k assume the values (4, 5), (4, 6) or (5, 6) while the remaining third index assumes the value 1, 2 or 3. For example, it is easy to see that for $(i, j, k) = (1, 4, 5)$ the left-hand side of (15) is $\bar{a}_t^{-1} j^{-1}(\nu\cdot\bar{\mathbf{n}})(n\cdot\bar{\mathbf{t}})$, which does not vanish identically. As a result, the 1-form $\omega = \bar{\nu}\cdot\delta\bar{\mathbf{n}}$ is not integrable on X.

The variational expression $\bar{\nu}\cdot\delta\bar{\mathbf{n}}$ may itself be represented in several different but equivalent forms. If $\boldsymbol{\beta} = \bar{\mathbf{n}} - \mathbf{n}$ is the difference vector, then $\delta\bar{\mathbf{n}} = \delta\boldsymbol{\beta}$ and $\bar{\nu}\cdot\delta\bar{\mathbf{n}} = \bar{\nu}\cdot\delta\boldsymbol{\beta} \equiv \delta\bar{\beta}_\nu$, which was used by Pietraszkiewicz (1977). However, in the expression $\delta\bar{\beta}_\nu$ the symbol δ should not be understood as the symbol of variation, since so defined $\delta\bar{\beta}_\nu \neq \delta(\bar{\nu}\cdot\boldsymbol{\beta})$.

The total rotation of the shell boundary is described by the total rotation tensor $\mathbf{R}_t = \bar{\nu}\otimes\nu + \bar{\mathbf{t}}\otimes\mathbf{t} + \bar{\mathbf{n}}\otimes\mathbf{n}$ such that $\bar{\mathbf{n}} = \mathbf{R}_t\mathbf{n}$ (cf., Pietraszkiewicz, 1979). The skew-symmetric tensors $\delta\mathbf{R}_t\mathbf{R}_t^T$ and $\mathbf{R}_t^T\delta\mathbf{R}_t$ can be associated with the respective axial vectors of virtual rotation $\delta\boldsymbol{\omega}_t$ and $\delta\mathbf{w}_t$ such that

$$\delta\mathbf{R}_t\mathbf{R}_t^T = \delta\boldsymbol{\omega}_t \times \mathbf{1}, \; \mathbf{R}_t^T\delta\mathbf{R}_t = \delta\mathbf{w}_t \times \mathbf{1}, \tag{19a}$$

$$\delta\boldsymbol{\omega}_t = \mathbf{R}_t\delta\mathbf{w}_t, \tag{19b}$$

where $\mathbf{1}$ is the metric tensor of the three-dimensional Euclidean space. Since $\delta\bar{\mathbf{n}} = \delta\boldsymbol{\omega}_t \times \bar{\mathbf{n}} = \mathbf{R}_t(\delta\mathbf{w}_t \times \mathbf{n})$, it follows that $\bar{\nu}\cdot\delta\bar{\mathbf{n}} = \delta\boldsymbol{\omega}_t\cdot\bar{\mathbf{t}} = \delta\mathbf{w}_t\cdot\mathbf{t}$. An expression analogous to $\delta\boldsymbol{\omega}_t\cdot\bar{\mathbf{t}}$ was used in a number of papers, for example, by Wempner (1981), Sakurai et al. (1983), and Axelrad (1987) while $\delta\mathbf{w}_t\cdot\mathbf{t}$ may be found in the recent paper of Szwabowicz (1986). Likewise, in the definitions of $\delta\boldsymbol{\omega}_t$ and $\delta\mathbf{w}_t$ the symbol δ should not be understood as the symbol of variation, since the symbols $\boldsymbol{\omega}_t$ or $\mathbf{w}_t$ alone have no geometric meaning.

The variational expression $\bar{\nu}\cdot\delta\bar{\mathbf{n}}$ may also be transformed as follows:

$$\bar{\nu}\cdot\delta\bar{\mathbf{n}} = -\bar{\mathbf{n}}\cdot\delta\bar{\nu} = -\bar{\mathbf{n}}\cdot\delta\bar{\mathbf{r}},_{\bar{\nu}} = \tag{20a}$$

$$= -(\bar{\mathbf{n}}\cdot\delta\bar{\mathbf{r}}),_{\bar{\nu}} + \bar{b}_\alpha^\beta\bar{\nu}^\alpha\bar{\mathbf{a}}_\beta\cdot\delta\bar{\mathbf{r}}. \tag{20b}$$

The expression $(\bar{\mathbf{n}}\cdot\delta\bar{\mathbf{r}}),_{\bar{\nu}}$ was used by Koiter (1966), Danielson (1970), and Zubov (1982).

From the discussion just presented it is seen that, as far as their representations in terms of derivatives $\bar{\mathbf{r}},_\nu$ and $\bar{\mathbf{r}}'$ are concerned, all differential 1-forms $\delta\bar{\beta}_\nu$, $\delta\boldsymbol{\omega}_t\cdot\bar{\mathbf{t}}$, $\delta\mathbf{w}_t\cdot\mathbf{t}$, $-\bar{\mathbf{n}}\cdot\delta\bar{\nu}$ and $-\bar{\mathbf{n}}\cdot\delta\bar{\mathbf{r}},_{\bar{\nu}}$ are equivalent to the 1-form $\bar{\nu}\cdot\delta\bar{\mathbf{n}}$, i.e., all 1-forms are defined by the same expression (10) with (16). As a result, neither of those 1-forms is exact or integrable as well. In all cases there exists no function φ such that $\mu\bar{\nu}\cdot\delta\bar{\mathbf{n}} = \delta\varphi$, and the natural bending couple generated by (5) with (9*b*) does not possess a work-conjugate geometric counterpart. In the language of analytic mechanics, this means that all kinematic constraints which are equivalent to $\bar{\nu}\cdot\delta\bar{\mathbf{n}} = 0$ are nonholonomic constraints. As a result, all those versions of the nonlinear theory of thin shells, in which the natural static boundary conditions are constructed with the help of (5) and (9*b*), can not be presented in a variational form which requires a functional to be stationary. In particular, it immediately follows from this discussion that several variational principles, which have been proposed in the literature for such versions of geometrically nonlinear first-approximation theories of elastic shells, must be incorrect.

The discussion of the exactness and integrability of two other differential 1-forms appearing in braces in (9*a*) and (9*c*) is given in the Appendix. There is proved that $\omega = \bar{\mathbf{n}}\cdot\delta\bar{\mathbf{r}},_\nu$ also is not integrable on X, while at the same time it is confirmed that $\omega = \nu\cdot\delta\bar{\mathbf{n}}$ is indeed exact on X.

It is quite obvious that $\nu\cdot\delta\bar{\mathbf{n}}$ is exact because ν is not varied and, therefore, $\omega = \nu\cdot\delta\bar{\mathbf{n}} = \delta(\nu\cdot\bar{\mathbf{n}}) \equiv \delta n_\nu$. As a result, the specification of $\bar{\mathbf{r}}$ and n_ν along C_u establishes those geometric boundary conditions which are work-conjugate to the corresponding static ones following from (5) and (9*c*). Such a complete set of the work-conjugate boundary conditions was originally derived by Pietraszkiewicz and Szwabowicz (1981) with the help of a modified tensor of change of curvature and rederived by Pietraszkiewicz (1984a,b) using $\kappa_{\alpha\beta}$ defined by (1*c*). Within the geometrically nonlinear first-approximation theory of elastic shells, this led to a number of results on variational principles, consistently approximated relations for shells undergoing restricted rotations, stability equations, and superposed deformations, which have been summarized by Szwabowicz (1982), Pietraszkiewicz (1984a), Schmidt (1985), and Stumpf (1986) where further references are given.

General Form of Boundary Conditions

The differential 1-forms previously discussed are only examples of the variety of 1-forms which may appear in the boundary line integral of the principle of virtual displacements. Each particular 1-form generates a different set of the natural static boundary and corner conditions on C_f. Indeed, each of the 1-forms enclosed in braces in (9) may be multiplied by a nonvanishing scalar function $\eta(\bar{\mathbf{r}},_\nu,\bar{\mathbf{r}}')$. This leads to a modification of the corresponding natural boundary condition for the bending couple resultant which essentially consists of a division by η. Furthermore, an additional term of the type $\mathbf{c}(\bar{\mathbf{r}},_\nu,\bar{\mathbf{r}}')\cdot\delta\bar{\mathbf{r}}'$ may also be added to each of the 1-forms. If, then, the same term is substracted from the 1-form one obtains, upon substituting (9) into (5) and integrating by parts, appropriate modifications of the corresponding force boundary and corner conditions. Among the variety of the 1-forms, which may be obtained by such transformations, the most important are the exact, or even only integrable 1-forms, since only those 1-forms generate the proper natural static boundary and corner conditions which are work-conjugate to the geometric ones.

Let the expression (9*a*) be rewritten as

$$\delta\bar{\mathbf{n}} = -\nu_\beta j^{-1}\bar{\mathbf{a}}^\beta \,\{\mathbf{d}\cdot\delta\bar{\mathbf{r}},_\nu\} - t_\beta\bar{\mathbf{a}}^\beta\,(\bar{\mathbf{n}}\cdot\delta\bar{\mathbf{r}}'), \tag{21}$$

$$\mathbf{d} = \bar{\mathbf{r}},_\nu \times \bar{\mathbf{r}}'. \tag{22}$$

The simple variational expression appearing in (21),

$$\vartheta = \mathbf{d}\cdot\delta\bar{\mathbf{r}},_\nu = A_1\delta\xi_1 + A_2\delta\xi_2 + A_3\delta\xi_3, \tag{23}$$

$$A_1 = \xi_2\xi_6 - \xi_3\xi_5,\; A_2 = \xi_3\xi_4 - \xi_1\xi_6,\; A_3 = \xi_1\xi_5 - \xi_2\xi_4, \tag{24}$$

may also be regarded as a differential 1-form of the type (10) on the six-dimensional manifold X, only in this case $\mathbf{B} \equiv \mathbf{0}$. It is easy to verify that the 1-form (23) is not integrable on X, for the conditions (15) are not identically satisfied when, for example, $(i, j, k) = (1, 2, 4)$. Our aim is to transform the expression (23) in such a way as to represent it in terms of an exact 1-form.

Suppose, for a moment, that $\bar{\mathbf{r}}$ is prescribed along C. Then so is $\bar{\mathbf{r}}'$ and, hence, the coordinates ξ_4, ξ_5, ξ_6 are not varied but rather play the role of parameters in (23). Thus, (23) may now be regarded as a differential 1-form on the three-dimensional submanifold $Y \subset X$ with local coordinates ξ_1, ξ_2, ξ_3. It then follows from (23) that for different $i, j \in (1, 2, 3)$ $A_{i,j} \neq A_{j,i}$, and the 1-form ϑ is not exact on Y. There is only one integrability condition (15) for $(i, j, k) = (1, 2, 3)$. Using (24), it is easy to verify that this condition is identically satisfied. Therefore, the 1-form ϑ is integrable on Y. In order to find its integrating factor and its primitive on Y, we follow the method of integration of total differential equations (see Ince, 1956, Section 2.8).

Let, for a moment, one of the coordinates ξ_i be constant. Since in the undeformed configuration $A_3 = 1$, $\xi_5 = 1$, it is convenient to assume this to be ξ_2. Then the 1-form $\vartheta = A_1(\xi_3)d\xi_1 + A_3(\xi_1)d\xi_3$, given on the two-dimensional submanifold $Z \subset Y$ with local coordinates ξ_1, ξ_3, is always integrable on Z. Its integrating factor then is $\lambda = -\xi_5/A_1A_3$ and its primitive is given by $\kappa = \ln|A_1/A_3|$. If now ξ_2 is again allowed to vary, that is, the 1-form ϑ is again supposed to be given on Y, then the functions $\lambda(\xi_i)$ and $\kappa(\xi_i)$, $i = 1, 2, 3$, previously calculated allow one to evaluate the function $S(\chi, \xi_2) = \lambda A_2 - \kappa,_2$. In the present case it vanishes, so that $S = 0$. As a result, $\lambda(\xi_i)$ is the respective integrating factor and $\kappa(\xi_i)$ is the primitive of the 1-form ϑ on Y, such that $\lambda\vartheta = \delta\kappa$ holds. This can easily be confirmed by a direct analysis. Moreover, $\beta(\kappa)$ is also the primitive of ϑ for any differentiable scalar function β so that, as a result, the general form of the primitive of ϑ on Y is given by $\beta\,\{\ln[\,|\,|\,(A_1/A_3)]\} \equiv h(A_1/A_3)$, where h is an arbitrary differentiable function (cf., Zubov, 1984).

If one follows the same procedure keeping ξ_1 or ξ_3 temporarily constant, one finds that $k(A_2/A_3)$ or $l(A_1/A_2)$ are also primitives of ϑ for arbitrary differentiable functions k and l. But from the identities (8), the fact that $\bar{\mathbf{r}}$ is prescribed along C and the arbitrariness of h, it is seen that primitives k and l are different but equivalent forms of the primitive h.

Now we remove the initial constraint that $\bar{\mathbf{r}}$ is prescribed along C and allow it to vary again. Thus, we return to the 1-form ϑ given on X, according to (23) and (24). Let $\varphi(\bar{\mathbf{r}}',\alpha)$, $\alpha = A_1/A_3 = n_\nu/n$ be an arbitrary differentiable scalar-valued function of its arguments. The variation of α then leads to

$$\delta\alpha = -A_3^{-2}\,(\xi_5\mathbf{d}\cdot\delta\bar{\mathbf{r}},_\nu - \xi_2\mathbf{d}\cdot\delta\bar{\mathbf{r}}'), \tag{25}$$

which allows one to derive the expression for the variation of φ in the form

$$\delta\varphi = \eta\mathbf{d}\cdot\delta\bar{\mathbf{r}},_\nu + \mathbf{c}\cdot\delta\bar{\mathbf{r}}' \tag{26}$$

$$\eta = -A_3^{-2}\xi_5\chi, \quad \mathbf{c} = \boldsymbol{\lambda} + A_3^{-2}\xi_2\chi\mathbf{d}, \tag{27a}$$

$$\boldsymbol{\lambda} = \frac{\partial\varphi}{\partial\bar{\mathbf{r}}'}, \quad \chi = \frac{\partial\varphi}{\partial\alpha}. \tag{27b}$$

It follows from (26) that we have, in fact, constructed the scalar-valued function $\eta(\bar{\mathbf{r}},_\nu,\bar{\mathbf{r}}')$ and the vector-valued function $\mathbf{c}(\bar{\mathbf{r}},_\nu,\bar{\mathbf{r}}')$ which have allowed us to transform the nonintegrable 1-form (23) into the exact 1-form ψ defined by the right-hand side of (26), such that $\psi = \delta\varphi$. If now (26) is solved for $\mathbf{d}\cdot\delta\bar{\mathbf{r}},_\nu$ and the result is introduced into (21) we obtain

$$\delta\bar{\mathbf{n}} = \bar{\mathbf{a}}^\alpha\nu_\alpha f\,\{\delta\varphi\} - \bar{\mathbf{a}}^\alpha\,([\nu_\alpha f\boldsymbol{\lambda} + (\nu_\alpha g + t_\alpha)\bar{\mathbf{n}}]\cdot\delta\bar{\mathbf{r}}'), \tag{28}$$

$$f = \frac{jn^2}{c_t\chi}, \quad g = \frac{\xi_2}{\xi_5} = \frac{1}{\bar{a}_t^2}\left(\frac{c_\nu n - cn_\nu}{jc_t} + 2\gamma_{\nu t}\right). \tag{29}$$

This is yet another expression for $\delta\bar{\mathbf{n}}$. It differs qualitatively from (9*a*, *b*) and (21), since it is given directly in terms of the exact 1-form $\delta\varphi$.

If now (28) is substituted into the boundary integral of (5) and the term containing $\delta\bar{\mathbf{r}}'$ is eliminated by integration by parts, the integral takes the final form

$$\int_{C_f} [(\mathbf{P} - \mathbf{P}^*)\cdot\delta\bar{\mathbf{r}} + (M - M^*)\delta\varphi]ds + \sum_n (\mathbf{F}_n - \mathbf{F}_n^*)\cdot\delta\bar{\mathbf{r}}_n, \tag{30}$$

where the effective force resultants and the bending couple resultant are defined by

$$\mathbf{P} = \mathbf{T}^\beta\nu_\beta + \mathbf{F}', \quad \mathbf{F} = fM_{\nu\nu}\boldsymbol{\lambda} + (gM_{\nu\nu} + M_{\nu t})\bar{\mathbf{n}}, \tag{31a}$$

$$\mathbf{P}^* = \mathbf{T} + \mathbf{F}^{*\prime}, \quad \mathbf{F}^* = (\mathbf{H}\cdot\bar{\mathbf{a}}^\beta)\,[\nu_\beta f\boldsymbol{\lambda} + (\nu_\beta g + t_\beta)\bar{\mathbf{n}}], \tag{31b}$$

$$M = fM_{\nu\nu}, \; M^* = f(\mathbf{H}\cdot\bar{\mathbf{a}}^\beta\nu_\beta), \tag{31c}$$

$$\mathbf{F}_n = \mathbf{F}(s_n + 0) - \mathbf{F}(s_n - 0), \; \mathbf{F}_n^* = \mathbf{F}^*(s_n + 0) - \mathbf{F}^*(s_n - 0), \tag{31d}$$

$$\bar{\mathbf{r}}_n = \bar{\mathbf{r}}(s_n), \tag{31e}$$

$$M_{\nu\nu} = M^{\alpha\beta}\nu_\alpha\nu_\beta, \quad M_{\nu t} = M^{\alpha\beta}\nu_\alpha t_\beta. \tag{31f}$$

From (5) and (30) it follows that the static boundary and corner conditions take the form

$$\mathbf{P}(s) = \mathbf{P}^*(s), \; M(s) = M^*(s) \text{ on } C_f, \tag{32a}$$

$$\mathbf{F}_n = \mathbf{F}_n^* \text{ at each corner } M_n \in C_f. \tag{32b}$$

Furthermore, it is seen from (5) and (30) that the geometric boundary conditions which are work-conjugate to the static ones (32) are given by

$$\bar{\mathbf{r}}(s) = \bar{\mathbf{r}}^*(s), \; \varphi[\bar{\mathbf{r}}'(s), \alpha(s)] = \varphi^*(s) \text{ on } C_u, \tag{33}$$

where, by definition, $\alpha(s) = \alpha\,[\bar{\mathbf{r}},_\nu(s), \bar{\mathbf{r}}'(s)]$. It also follows from (30) and (28) that $\bar{\mathbf{r}}$ is kinematically admissible if $\delta\bar{\mathbf{r}} = \mathbf{0}$ and $\delta\varphi = 0$ on C_u. Hence, $\delta\bar{\mathbf{n}} = \mathbf{0}$ on C_u as well.

The general forms (32) and (33) of four work-conjugate static and geometric boundary conditions are derived here in terms of the function $\varphi(\bar{\mathbf{r}}',\alpha)$ in which $\alpha = n_\nu/n$ is an intermediate variable. The analysis clearly indicates that the choice of α by no means is the only possible choice of such an intermediate variable. Other scalar functions of $\bar{\mathbf{r}},_\nu$, $\bar{\mathbf{r}}'$ may also be chosen instead of α. However, since φ is an arbitrary function of its arguments, this would lead to formally different, though essentially equivalent representations of the boundary conditions.

It follows from the analysis that $\varphi(\bar{\mathbf{r}}', \alpha)$ should be differentiable with respect to both arguments. The definition of f in (29) indicates also that $\partial\varphi/\partial\alpha$ should not vanish identically in some neighborhood of the undeformed shell boundary. However, in order to be physically meaningful, φ has to satisfy a number of additional requirements based on mathematical and mechanical considerations. This allows one to arrive at a more restricted class of admissible scalar functions for the description of rotational deformation of the shell boundary. In particular, φ must vanish in the undeformed state, that is $\varphi(\mathbf{t}, 0) = 0$, and upon linearization it should coincide with the linearized rotation of the shell boundary $\varphi_\nu = \mathbf{n}\cdot\mathbf{u},_\nu$ which is used in the classical linear theory of shells. It is also reasonable to require φ to be a monotonous function of α, at least in some neighborhood of the undeformed state.

Some Special Cases

We close our considerations with a brief discussion of some particular definitions of φ which may be used in the nonlinear theory of thin shells. For any choice of φ, the corresponding work-conjugate static boundary conditions may be derived directly from (32), (31), (29), and (27*b*).

It follows from (2*a*) and (2*b*) that the identities (8) imply that

$$\frac{n_t}{n} = -c_t^{-1}\,(c_\nu\alpha + c), \tag{34}$$

$$n^2 = [1 + \alpha^2 + c_t^{-2}\,(c_\nu\alpha + c)^2]^{-1}. \tag{35}$$

Therefore, $\bar{\mathbf{n}}$ may be expressed as the function of $\bar{\mathbf{r}}'$ and α,

$$\bar{\mathbf{n}}(\bar{\mathbf{r}}',\alpha) = n[\alpha\boldsymbol{\nu} - c_t^{-1}\,(c_\nu\alpha + c)\mathbf{t} + \mathbf{n}], \tag{36}$$

where n is to be determined from (35). For an arbitrary deformation of the boundary the sign of n, following from (35), is not unique. However, it follows from (2*c*) and (2*d*) that in some neighborhood of the undeformed state, n must be positive.

It immediately follows from (36) that $n_\nu = \boldsymbol{\nu}\cdot\bar{\mathbf{n}}$ is a particular case of φ indeed. The corresponding work-conjugate static boundary and corner conditions were given by Pietraszkiewicz (1984a, b).

Novozhilov and Shamina (1975) used the fourth geometric boundary parameter ϑ_ν defined by

$$\vartheta_\nu = \bar{a}_t^{-2}\,(\bar{\mathbf{n}} - \mathbf{n})\cdot\bar{\mathbf{a}}_\nu. \tag{37}$$

From (3*a*) and (36) it is seen that

$$\bar{\mathbf{a}}_\nu = n[(c_t - c\frac{n_t}{n})\boldsymbol{\nu} + (c\alpha - c_\nu)\mathbf{t} + (c_\nu\frac{n_t}{n} - c_t\alpha)\mathbf{n}], \tag{38}$$

and, according to (36) and (37),

$$\vartheta_\nu = n\bar{a}_t^{-2}\,[c_t\alpha + c_t^{-1}c_\nu(c_\nu\alpha + c)]. \tag{39}$$

Therefore, $\vartheta_\nu = \vartheta_\nu\,(\bar{\mathbf{r}}', \alpha)$ is also a particular case of φ. Let us derive the corresponding work-conjugate static boundary conditions.

Taking the variation of (37), and introducing it into the expression (9*a*) multiplied by $\bar{\mathbf{a}}_t \times \bar{\mathbf{n}}$, we obtain after some transformations

$$\delta\bar{\mathbf{n}} = n^{-1}\bar{a}_t\bar{\boldsymbol{\nu}}\delta\vartheta_\nu + \{n^{-1}\,[2\vartheta_\nu\bar{\boldsymbol{\nu}}\otimes\bar{\mathbf{t}} + \bar{a}_t^{-1}\bar{\boldsymbol{\nu}}\otimes(\bar{\mathbf{n}}\times\mathbf{n})] - \bar{a}_t^{-1}\bar{\mathbf{t}}\otimes\bar{\mathbf{n}}\}\cdot\delta\bar{\mathbf{r}}'. \tag{40}$$

Note that the expression (40) has the same structure as the general expression (28). Introducing (40) into the line integral of (5), we finally obtain the following definitions for the natural static parameters on the boundary which are work-conjugate to the geometric parameters $\bar{\mathbf{r}}$ and ϑ_ν,

$$\mathbf{F} = (M_{\nu t} + 2\bar{a}_t^{-2}\gamma_{\nu t}M_{\nu\nu})\bar{\mathbf{n}} - jn^{-1}\bar{a}_t^{-1}M_{\nu\nu}\,(2\vartheta_\nu\bar{\mathbf{t}} + \bar{a}_t^{-1}\bar{\mathbf{n}}\times\mathbf{n}), \tag{41a}$$

$$\mathbf{F}^* = \bar{a}_t^{-1}\,(\mathbf{H}\cdot\bar{\mathbf{t}})\bar{\mathbf{n}} - n^{-1}\,(\mathbf{H}\cdot\bar{\boldsymbol{\nu}})(2\vartheta_\nu\bar{\mathbf{t}} - \bar{a}_t^{-1}\bar{\mathbf{n}}\times\mathbf{n}), \tag{41b}$$

$$M = jn^{-1}M_{\nu\nu},\; M^* = n^{-1}\bar{a}_t\,(\mathbf{H}\cdot\bar{\boldsymbol{\nu}}). \tag{41c}$$

Thus, the set of work-conjugate boundary conditions takes the general form (32) and (33), except that $\vartheta_\nu\,[\bar{\mathbf{r}},_\nu(s), \bar{\mathbf{r}}'(s)]$ stands for φ in (33), and definitions (41) are used in (32).

Finally, the rotational deformation of the shell boundary may also be described by the total rotation tensor $\mathbf{R}_t$. Noting (3*a*), (2*a*), and (36) it is seen that the tensor $\mathbf{R}_t$ referred to the undeformed base vectors takes the form

$$\begin{aligned}\mathbf{R}_t = \bar{a}_t^{-1}n\,(\{[c_t + c_t^{-1}c(c_\nu\alpha + c)]\boldsymbol{\nu} + (c\alpha - c_\nu)\mathbf{t} -\\ - [c_\nu c_t^{-1}\,(c_\nu\alpha + c) + c_t\alpha]\mathbf{n}\}\otimes\boldsymbol{\nu} + n^{-1}(c_\nu\boldsymbol{\nu} + c_t\mathbf{t} + c\mathbf{n})\otimes\mathbf{t}\\ + [\alpha\boldsymbol{\nu} - c_t^{-1}\,(c_\nu\alpha + c)\mathbf{t} + \mathbf{n}]\otimes\mathbf{n}).\end{aligned} \tag{42}$$

It follows from (42) and (2*a*) that $\mathbf{R}_t = \mathbf{R}_t(\bar{\mathbf{r}}',\alpha)$ and the parameter φ may be defined as some scalar function of $\mathbf{R}_t$, that is $\varphi = \varphi(\mathbf{R}_t)$. In particular, the angle of total rotation ω_t corresponding to $\mathbf{R}_t$ is given by $\omega_t = \arccos\,(1/2 - 1/2\; tr\mathbf{R}_t)$, where it follows from (42) and (34) that

$$tr\mathbf{R}_t = n^2\,[1 + \bar{a}_t^2\,(c_\nu c\alpha - c_\nu^2)]. \tag{43}$$

Therefore, the angle of total rotation ω_t may also be chosen as the fourth geometric parameter of the boundary deformation. This choice has been found by Simmonds (1985b) to be the most natural one in the displacement form of nonlinear equations which govern an axisymmetric deformation of shells of revolution.

The work-conjugate static boundary conditions corresponding to the particular cases of φ discussed above, are obviously quite complex. More suitable particular forms of φ may be obtained under additional, more restrictive, mathematical and mechanical requirements.

Concluding Remarks

In this paper an entirely general approach to the derivation of the work-conjugate static and geometric boundary conditions has been developed for a class of nonlinear theories of thin shells. In this approach, basic theorems of the theory of differential forms have been applied to various variational expressions which may appear in the boundary line integral of the principle of virtual displacements. It has been shown that the majority of static boundary conditions, which have been proposed in the literature, do not possess work-conjugate geometric counterparts, because the corresponding differential forms are not integrable. Such static boundary conditions are, however, hardly acceptable in the consistent formulation of the nonlinear theory of shells.

The general forms of the four geometric boundary conditions and of the corresponding work-conjugate static boundary conditions have been derived for the first time in the literature. They have been expressed in terms of an arbitrary scalar function φ of displacement derivatives which describes the rotational deformation of the shell boundary. Since φ is arbitrary, one has a wide range of possibilities to choose the form of boundary conditions to be used in the nonlinear theory of thin shells. This freedom of choice enables one to select φ in such a way that it best suits the particular version of the shell theory or the particular shell problem at hand. As an example, three particular definitions of φ have been discussed.

In the analysis it has been assumed that the deformation of the shell as a three-dimensional body is entirely determined by the stretching and bending of its reference surface. No restrictions have, however, been imposed on the magnitudes of the displacements, rotations, strains and/or changes of curvatures of the reference surface. There is not even a need to specify the material behavior of the shell, since the principle (4) itself does not require $N^{\alpha\beta}$ and $M^{\alpha\beta}$ to be derivable from a strain energy function. Therefore, the boundary conditions derived here are valid for a large class of three-dimensionally different (even inelastic) shell theories which have the same two-dimensional mathematical structure implied by the principle of virtual displacements (4). This generalizes considerably the results available in the literature for some simple versions of nonlinear theory of thin shells.

For any shell theory it is necessary to specify on M and C_f how the fields $N^{\alpha\beta}$, $M^{\alpha\beta}$, $\mathbf{p}$, $\mathbf{h}$, $\mathbf{T}$, $\mathbf{H}$ are related to the corresponding three-dimensional external surface and body forces and to the deformation of the reference surface. For the geometrically nonlinear first-approximation theory of thin elastic shells such definitions have been given, for example, by Pietraszkiewicz and Szwabowicz (1981) and Pietraszkiewicz (1984b). In simple versions of the finite-strain bending theory of elastic rubberlike shells developed by Chernykh (1980) and Simmonds (1985a), the corresponding definitions should also explicitly take into account the appropriate approximate form of the shell deformation in the transverse normal direction. As was noted by Stumpf and Makowski (1986) and Makowski and Stumpf (1986), the finite strain theory of elastic shells may have a richer mathematical structure than the one discussed here, if the transverse normal strains are fully accounted for. However, in the majority of cases it is usually sufficient to express the transverse normal strains in terms of the stretching and bending of the reference surface.

The work-conjugate boundary conditions derived here allow for a thin shell to formulate properly the nonlinear boundary value problem in terms of displacements as basic independent field variables. Such displacement form of nonlinear shell equations is used most often to analyze problems of flexible shells. In the case of conservative loads the work-conjugate boundary conditions allow to construct various functionals, whose stationarity conditions are equivalent to the proper field equations and boundary conditions.

References

Axelrad, E. L., 1987, *Theory of Flexible Shells*, North-Holland Pub. Co., Amsterdam, Chapter 1, Section 7.

Cartan, H., 1970, *Differential Forms*, Kershaw Publishing Company Ltd., Chapter 1, Section 2.1.

Chernykh, K. F., 1980, "Nonlinear Theory of Isotropically Elastic Shells," *Mechanics of Solids*, (Izvestiia AN SSSR, MTT), Vol. 15, pp. 118–127.

Galimov, K. Z., 1950, "General Theory of Elastic Shells with Finite Displacements," *Izvestiia Kazanskogo Filiala AN SSSR, Seriia Fiz.-Mat. i Tekhn. Nauk*, (in Russian), No. 2, pp. 3–38.

Galimov, K. Z., 1951, "On the General Theory of Plates and Shells with Finite Displacements and Deformations," *Prikladnaia Matematika i Mekhanika*, (in Russian), Vol. 15, pp. 723–742.

Ince, E. L., 1956, *Ordinary Differential Equations*, Dover Publications, Inc., Chapter 2.

Koiter, W. T., 1964, "On the Dynamic Boundary Conditions in the Theory of Thin Shells," *Proceedings, Koninkl. Nederl. Akademie van Wetenschappen-Amsterdam*, Series B, Vol. 67, pp. 117–126.

Koiter, W. T., 1966, "On the Non-Linear Theory of Thin Elastic Shells," *Proceedings, Koninkl. Nederl. Akademie van Wetenschappen – Amsterdam*, Series B, Vol. 69, pp. 1–54.

Love, A. E. H., 1927, *A Treatise on the Mathematical Theory of Elasticity*, 4th Ed., Dover Publications, Chapter 24, Articles 329 and 332.

Makowski, J., and Stumpf, H., 1986, "Finite Strains and Rotations in Shells," *Finite Rotations in Structural Mechanics*, W. Pietraszkiewicz, ed., Springer-Verlag, Berlin, pp. 175–194.

Novozhilov, V. V., and Shamina, V. A., 1975, "On Kinematic Boundary Conditions in Non-Linear Elasticity Problems," *Mechanics of Solids*, (Izvestiia AN SSSR, MTT), Vol. 5, pp. 63–74.

Pietraszkiewicz, W., 1977, "Introduction to the Non-Linear Theory of Shells," *Ruhr-Universität Bochum, Mitteilungen aus dem Institut für Mechanik*, No. 10, pp. 1–154.

Pietraszkiewicz, W., 1979, *Finite Rotations and Lagrangian Description in the Non-Linear Theory of Shells*, Polish Scientific Publishers, Warszawa, Poznań.

Pietraszkiewicz, W., 1980, "Finite Rotations in the Non-Linear Theory of Thin Shells," *Thin Shell Theory, New Trends and Applications*, W. Olszak, ed., Springer-Verlag, Wien, pp. 153–208.

Pietraszkiewicz, W., 1984a, "Lagrangian Description and Incremental Formulation in the Non-Linear Theory of Thin Shells," *International Journal of Non-Linear Mechanics*, Vol. 19, pp. 115–140.

Pietraszkiewicz, W., 1984b, "On Entirely Lagrangian Displacement Form of Non-Linear Shell Equations," *Flexible Shells*, E. L. Axelrad and F. A. Emmerling, eds., Springer-Verlag, Berlin, pp. 106–123.

Pietraszkiewicz, W., and Szwabowicz, M. L., 1981, "Entirely Lagrangian Nonlinear Theory of Thin Shells," *Archives of Mechanics*, Vol. 33, pp. 273–288.

Sakurai, T., Hasegawa, A., and Nishino, F., 1983, "A Finite Displacement Formulation of Elastic Shells," *Proceedings of the Japan Society of Civil Engineers*, No. 330, pp. 151–159.

Schmidt, R., and Pietraszkiewicz, W., 1981, "Variational Principles in the Geometrically Non-Linear Theory of Shells Undergoing Moderate Rotations," *Ingenieur-Archiv*, Vol. 50, pp. 187–201.

Schmidt, R., 1985, "A Current Trend in Shell Theory: Constrained Geometrically Non-Linear Kirchhoff - Love Type Theories Based on Polar Decomposition of Strains and Rotations," *Computers and Structures*, Vol. 20, pp. 265–275.

Simmonds, J. G., 1985a, "The Strain - Energy Density of Rubber-Like Shells," *International Journal of Solids and Structures*, Vol. 21, pp. 67–77.

Simmonds, J. G., 1985b, "A New Displacement Form for the Nonlinear Equations of Motion of Shells of Revolution," ASME JOURNAL OF APPLIED MECHANICS, Vol. 52, pp. 507–509.

Stumpf, H., 1986, "General Concept of the Analysis of Thin Elastic Shells," *Zeitschrift für Angewandte Matematik und Mechanik*, Vol. 66, pp. 337–350.

Stumpf, H., and Makowski, J., 1986, "On Large Strain Deformations of Shells," *Acta Mechanica*, Vol. 65, pp. 153–168.

Szwabowicz, M. L., 1982, "Geometrically Non-Linear Theory of Thin Elastic Shells in the Lagrangian Description," Ph.D. Dissertation, (in Polish), Institute of Fluid-Flow Machinery, PASci, Gdańsk, Poland.

Szwabowicz, M. L., 1986, "Variational Formulation in the Geometrically Non-Linear Thin Elastic Shell Theory," *International Journal of Solids and Structures*, Vol. 22, pp. 1161–1175.

Thomson, W., and Tait, P. G., 1883, *Treatise on Natural Philosophy*, 2nd Ed., Vol. 1, Part 2, Cambridge, U.K.

Von Westenholz, C., 1981, *Differential Forms in Mathematical Physics*, 2nd Ed., North-Holland Pub. Co., Amsterdam, Chapter 8.

Wempner, G., 1981, *Mechanics of Solids with Applications to Thin Bodies*, Sijthoff and Noordhoff, Alphen aan den Rijn, Chapter 12.

Zubov, L. M., 1982, *Methods of Non-Linear Elasticity in Shell Theory*, (in Russian), Rostov University Press, Chapter 4, Section 5.

Zubov, L. M., 1984, "On Boundary Condition for Rotation Angle of the Edge in Non-Linear Shell Theory," *Voprosy Dinamiki i Prochnosti*, (in Russian), Vol. 44, pp. 22–28.

APPENDIX

Let us verify the exactness and integrability of the 1-form $\omega = \bar{\mathbf{n}} \cdot \delta\bar{\mathbf{r}},_\nu$ appearing in (9*a*). In this case $\mathbf{A} = \bar{\mathbf{n}}$, $\mathbf{B} = \mathbf{0}$ so that the differentiation of (2*c*) gives

$$\frac{\partial \mathbf{A}}{\partial \bar{\mathbf{r}},_\nu} = -\bar{a}_t j^{-1} \bar{\nu} \otimes \bar{\mathbf{n}}, \quad \frac{\partial \mathbf{B}}{\partial \bar{\mathbf{r}},_\nu} = \frac{\partial \mathbf{B}}{\partial \bar{\mathbf{r}}'} = \mathbf{0}, \qquad (A1a)$$

$$\frac{\partial \mathbf{A}}{\partial \bar{\mathbf{r}}'} = 2(\bar{a}_t j)^{-1} \gamma_{\nu t} \bar{\nu} \otimes \bar{\mathbf{n}} - \bar{a}_t^{\,-1} \bar{\mathbf{t}} \otimes \bar{\mathbf{n}}, \qquad (A1b)$$

what implies that the conditions (14) are not satisfied and the 1-form $\bar{\mathbf{n}} \cdot \delta\bar{\mathbf{r}},_\nu$ is not exact on X. If we introduce (A1) into (15), eleven conditions of (15) are identically satisfied while nine are not satisfied. For example, the left-hand side of (15) for $(i, j, k) = (1, 3, 4)$ is $j^{-1}(\boldsymbol{\nu} \cdot \bar{\mathbf{n}})\xi_2$ what does not identically vanish. As a result, the 1-form $\bar{\mathbf{n}} \cdot \delta\bar{\mathbf{r}},_\nu$ is also not integrable on X.

In the case of the 1-form $\boldsymbol{\nu} \cdot \delta\bar{\mathbf{n}}$ it follows from (9*a*) and (3*d*) that

$$\mathbf{A} = -\bar{a}_t j^{-1} (\boldsymbol{\nu} \cdot \bar{\nu}) \bar{\mathbf{n}}, \quad \mathbf{B} = \bar{a}_t^{\,-1} (2 j^{-1} \gamma_{\nu t} \boldsymbol{\nu} \cdot \bar{\nu} - \boldsymbol{\nu} \cdot \bar{\mathbf{t}}) \bar{\mathbf{n}}. \quad (A2)$$

Differentiation of (A2) with (2) and (3) gives

$$\frac{\partial \mathbf{A}}{\partial \bar{\mathbf{r}},_\nu} = \bar{a}_t^2 j^{-2}\ [(\nu \cdot \bar{\nu})(\bar{\nu} \otimes \bar{\mathbf{n}} + \bar{\mathbf{n}} \otimes \bar{\nu}) - (\nu \cdot \bar{\mathbf{n}})\bar{\mathbf{n}} \otimes \bar{\mathbf{n}}], \tag{A3a}$$

$$\frac{\partial \mathbf{A}}{\partial \bar{\mathbf{r}}'} = -2j^{-2}\gamma_{\nu t}\ (\nu \cdot \bar{\nu})(\bar{\nu} \otimes \bar{\mathbf{n}} + \bar{\mathbf{n}} \otimes \bar{\nu}) + j^{-1}(\nu \cdot \bar{\mathbf{t}})\bar{\mathbf{n}} \otimes \bar{\nu}$$

$$+ j^{-1}(\nu \cdot \bar{\nu})\bar{\mathbf{t}} \otimes \bar{\mathbf{n}} + 2j^{-2}\gamma_{\nu t}(\nu \cdot \bar{\mathbf{n}})\bar{\mathbf{n}} \otimes \bar{\mathbf{n}} = \left(\frac{\partial \mathbf{B}}{\partial \bar{\mathbf{r}},_\nu}\right)^T \tag{A3b}$$

$$\frac{\partial \mathbf{B}}{\partial \bar{\mathbf{r}}'} = 2\bar{a}_t^{\,-2} j^{-1}\gamma_{\nu t}\,(2j^{-1}\gamma_{\nu t}\nu \cdot \bar{\nu} - \nu \cdot \bar{\mathbf{t}})(\bar{\nu} \otimes \bar{\mathbf{n}} + \bar{\mathbf{n}} \otimes \bar{\nu}) +$$
$$+ \bar{a}_t^{-2}(\nu \cdot \bar{\mathbf{t}} - 2j^{-1}\gamma_{\nu t}\nu \cdot \bar{\nu})(\bar{\mathbf{t}} \otimes \bar{\mathbf{n}} + \bar{\mathbf{n}} \otimes \bar{\mathbf{t}}) - \tag{A3c}$$
$$- \bar{a}_t^{-2}(1 + 4j^{-2}\gamma_{\nu t}^2)(\nu \cdot \bar{\mathbf{n}})\bar{\mathbf{n}} \otimes \bar{\mathbf{n}}.$$

Since ($A3a$) and ($A3c$) are symmetric and ($A3b$) holds, the component matrix $A_{i,j}$ is also symmetric and all the conditions (14) are identically satisfied. Therefore, the 1-form $\nu \cdot \delta\bar{\mathbf{n}}$ is exact on X.

Non-Probabilistic Models of Uncertainty in the Nonlinear Buckling of Shells With General Imperfections: Theoretical Estimates of the Knockdown Factor

Yakov Ben-Haim
Department of Nuclear Engineering.

Isaac Elishakoff
Faculty of Aerospace Engineering.

Technion—Israel Institute of Technology,
Haifa 32000, Israel

A non-probabilistic, set-theoretical treatment of the buckling of shells with uncertain initial geometrical imperfections is presented. The minimum buckling load is determined as a function of the parameters which describe the (generally infinite) range of possible initial imperfection profiles of the shell. The central finding of this paper is a theoretical estimate of the knockdown factor as a function of the characteristics of the uncertainty in the initial imperfections. Two classes of set-theoretical models are employed. The first class represents the range of variation of the most significant N *Fourier coefficients by an ellipsoidal set in* N*-dimensional Euclidean space. The minimum buckling load is then explicitly evaluated in terms of the shape of the ellipsoid. In the second class of models, the uncertainty in the initial imperfection profile is expressed by an envelope of functions. The bounding functions of this envelope can be viewed as a radial tolerance on the shape. It is demonstrated that a non-probabilistic model of uncertainty in the initial imperfections of shells is successful in determining the minimum attainable buckling load of an ensemble of shells and that such an approach is computationally feasible.*

1 Introduction

Thin-walled shells, which are among the most utilized structural elements in engineering, possess the unfortunate property of being sensitive to initial geometrical imperfections (Koiter, 1945; Budiansky and Hutchinson, 1979). This means that the buckling load may be significantly reduced due to deviations of the real shell from its ideal, nominal counterpart. The experimental buckling load sometimes amounts to no more than one-tenth of the buckling load of a perfect shell. Existing computer codes are able to predict the buckling load of a structure with specified initial imperfections. However, due to the very nature of the manufacturing process, it is hard to imagine that two identical shells are ever produced, even by the same manufacturing process. Consequently, it is imperative to consider the effect on the buckling load of uncertainty in the imperfections of the shell.

Engineers are accustomed to using empirical "knockdown factors" (NASA, 1979) in order to accommodate the large discrepancy between theoretical and experimental values of the buckling load. The knockdown factor, when multiplied by the classical buckling load for the perfect structure, yields an estimated lower bound of the buckling load for the imperfect structure. Knockdown factors are often adopted as the lower bound of the buckling loads obtained experimentally for a range of distinct structures, materials, and manufacturing processes. Such an approach has several drawbacks. It would seem that the estimates should constantly be updated to include new experimental results. Furthermore, this approach mixes shells produced by rough manufacturing procedures (and therefore associated with a greater reduction of the buckling load) with those produced by more refined techniques (and, hence, buckling at greater load). This implies that the design of shells with low initial imperfections will be overly conservative.

A natural way to deal with uncertainty in the initial imperfections is to employ a stochastic approach. Apparently the first probabilistic analysis of initial imperfections, treated as random variables with given joint distribution, was given by Bolotin (1958). The next step was treatment by Fraser and Budiansky (1969) of initial imperfections as random field with given mean and autocorrelation function. These approaches have been bridged by Elishakoff (1979, 1980) in the context of the Monte Carlo method. For acquaintance with pertinent

Contributed by the Applied Mechanics Division of The American Society of Mechanical Engineers for publication in the Journal of Applied Mechanics.

Discussion on this paper should be addressed to the Editorial Department, ASME, United Engineering Center, 345 East 47th Street, New York, N.Y. 10017, and will be accepted until two months after final publication of the paper itself in the Journal of Applied Mechanics. Manuscript received by ASME Applied Mechanics Division, April 21, 1988; final revison, August 28, 1988.

results one may consult the review paper by Amazigo (1976) and the monographs by Elishakoff (1983) and Roorda (1980).

Probabilistic analysis treats the initial imperfections as random functions of the shape coordinates y, z of the shell. Let $\eta(y, z)$ represent the deviation of the shell from its nominal shape at point y, z. If one knows an analytic relation between the buckling load Λ and the initial imperfection function $\eta(y, z)$

$$\Lambda = \Psi(\eta(y,z)) \tag{1}$$

then one can relate the probabilistic characteristics of Λ with those of η, resulting in an expression for the probability density of the buckling load. Except for the simplest cases, there is no analytical relation of type (1) available in the literature. Usually, the initial imperfection function is expanded in a Fourier series:

$$\eta(y,z) = \sum_{i,j} A_{ij}\phi_{ij}(y,z) \tag{2}$$

where A_{ij} are the Fourier coefficients and $\{\phi_{ij}\}$ is a complete set of functions. Then, available computer codes (Arbocz and Babcock, 1974) yield relations of the type:

$$\Lambda = \Psi(\{A_{ij}\}). \tag{3}$$

For probabilistic methods of dealing with equation (3), with appropriate bibliography, one can consult Elishakoff and Arbocz (1985) and Elishakoff et al. (1987).

Despite the success of stochastic analysis, one may recognize that uncertainty can be modeled on the basis of alternative, non-probabilistic conceptual frameworks. One such approach, based on a set-theoretic formulation, has been pioneered in the field of state estimation by Schweppe (1968), Witsenhausen (1968b), Bertekas and Rhodes (1971), and Schlaepfer and Schweppe (1972). Set theoretic models of uncertainty have also been applied in designing optimal controllers for linear systems by Witsenhausen (1968a), Delfour and Mittler (1969), Glover and Schweppe (1971, 1972), and Schweppe (1973). Independent of these developments, Drenick (1970) used set models of uncertainty in the study of earthquake excitation. Set models of uncertainty have been applied by Ben-Haim in the optimization of multihypothesis algorithms for malfunction isolation in linear dynamic systems (1986), by Ben-Haim and Elias (1987) in optimizing inverse measurements of two-phase flow, and by Ben-Haim (1985) in a wide range of material assay problems.

The aim of the present analysis is to exploit fragmentary information (which is usually all that is available) about the initial imperfection of thin shells, in order to determine the buckling loads which may be expected. Explicitly, the minimum buckling load will be determined as a function of parameters which characterize the range of possible initial imperfection profiles of the shell. Non-probabilistic models of uncertainty in the initial imperfection will be employed. This means that an infinite set of initial profiles will be adopted on the basis of available data, and then the minimum of the buckling load on this set will be sought. A significant result of this analysis is a theoretical estimate of the knockdown factor. In addition, the knockdown factor will be expressed as a function of simple manufacturing specifications. It will be seen that the set-theoretic approach to modeling uncertainty in the initial imperfections of the shell is quite flexible and allows one to examine imperfection sensitivity from various perspectives.

The range of variation of the initial imperfection profiles will be modeled in several distinct ways. In Sections 2 and 3 the uncertainty in the initial imperfection profiles will be quantified in terms of the variability of the Fourier coefficients of those profiles. The most significant N Fourier coefficients are assumed to fall in an ellipsoidal set in N-dimensional Euclidean space. The minimum buckling load is then evaluated as a function of the shape of the ellipsoid. In Section 4, the uncertainty in the initial imperfection profile is expressed as a uniform bound on the deviation of the surface from its nominal value. Thus the initial imperfection profiles are integrable functions, which satisfy a uniform bound. The minimum buckling load will be determined as a function of the uniform bound on the initial imperfection. This uniform bound on the initial imperfections can be viewed as a shape tolerance, so that the buckling load is related to a manufacturing specification of the shell. In Section 5 the initial imperfection profiles are allowed to vary within an envelope. This enables the designer to study the buckling sensitivity of the shell as a function of requiring the manufacture of the shell to adhere to different tolerances in different areas of the shell.

Following Elishakoff et al. (1987), the change of the buckling load with the initial imperfection profile will be studied as a perturbation problem. Both first- and second-order variations from a mean or typical initial imperfection will be considered. The buckling load of the mean initial imperfection will be evaluated on the basis of a numerical, nonlinear buckling code.

2 Bounded Fourier Coefficients: First-Order Analysis

Let x be a vector whose components are the N dominant Fourier coefficients of the initial imperfection profile of a thin shell. Furthermore, let $\Psi(x)$ represent the buckling load for a shell whose initial imperfection profile has x as its Fourier spectrum. Let x^o be a nominal Fourier imperfection spectrum. For example, x^o may correspond to the average imperfection spectrum. The buckling limit for an initial imperfection spectrum $x^o + \zeta$, to first order in ζ, is:

$$\Psi(x^o + \zeta) = \Psi(x^o) + \sum_{n=1}^{N} \frac{\partial \Psi(x^o)}{\partial x_n} \zeta_n. \tag{4}$$

We will evaluate the lower limit of the buckling load as ζ varies on an ellipsoidal set of initial imperfection spectra. For convenience of notation let us define:

$$\phi^T = \left(\frac{\partial \Psi(x^o)}{\partial x_1}, \ldots, \frac{\partial \Psi(x^o)}{\partial x_N}\right) \tag{5}$$

where the superscript T means matrix transposition.

The deviation ζ from the nominal initial imperfection spectrum is assumed to vary on the following ellipsoidal set:

$$Z(\alpha,\omega) = \left\{\zeta : \sum_{n=1}^{N} \frac{\zeta_n^2}{\omega_n^2} \le \alpha^2\right\} \tag{6}$$

where the size parameter α and the semi-axes $\omega_1, \ldots, \omega_N$ are based on experimental data, obtainable from initial imperfection data banks. Thus, $Z(\alpha,\omega)$ represents a realistic ensemble of shells. The lowest buckling load which can be obtained from any of the shells in this ensemble is expressed formally as the minimum of expression (4) on the set $\mathbf{Z}$:

$$\mu(\alpha,\omega) = \min_{\zeta \in \mathbf{Z}(\alpha,\omega)} [\Psi(x^o) + \phi^T \zeta]. \tag{7}$$

$\mu(\alpha, \omega)$ is the buckling load of the "weakest" shell in the ensemble $\mathbf{Z}$ which is constructed to represent a realistic range of shells. It will be recognized, from the discussion in the Introduction, that the ratio of μ to the classical buckling load will correspond to the empirical knockdown factor. This will be discussed further in Section 6.

Equation (7) calls for finding the mimimum of the linear functional $\phi^T\zeta$ on the convex set $\mathbf{Z}(\alpha,\omega)$. This extreme value will occur on the set of extreme points[1] of $\mathbf{Z}$, which is the col-

[1] An extreme point of a set A is an element of A, which does not lie between any two other elements of A. A compact convex set is the convex hull of its extreme points (Balakrishnan, 1981). Also, the extrema of a linear functional on a convex set occur on the extreme points of the set (Kelly and Weiss, 1979).

Table 1

Fourier Coefficient*	B − 1**	B − 2**	B − 3**	B − 4**	ω_n	$\partial\Psi/\partial x_i$**
a_2	−0.010809	−0.027238	−0.089906	−0.017560	0.0315	0.09668
a_4	0.022578	−0.007836	−0.025508	−0.009239	0.0174	0.00340
$b_{1,2}$	0.417400	0.392870	0.741280	0.222900	0.187	−0.01854
$b_{1,6}$	−0.077872	−0.143490	0.017483	0.077668	0.0853	−0.05687
$b_{1,8}$	−0.263690	−0.009405	0.112470	0.101510	0.152	−0.24686
$b_{1,10}$	0.036568	0.043628	−0.245610	−0.008853	0.119	−0.08183
$b_{2,3}$	−0.101290	0.034018	−0.064766	−0.001887	0.0526	−0.01314
$b_{2,11}$	0.009732	−0.008685	−0.028261	0.013545	0.0166	−0.07173

*Notation of equation (42)
**From Elishakoff et al. (1987)

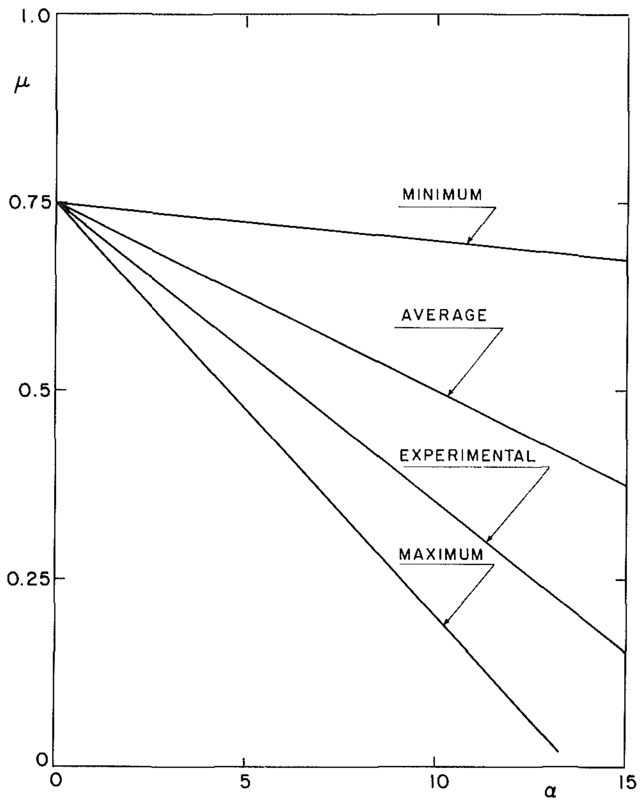

Fig. 1 Minimum buckling load, equation (17), as a function of the size of the imperfection ellipsoid, for four different sets of semi-axes

lection of vectors $c=(c_1, \ldots, c_N)$ in the following set:

$$C(\alpha,\omega)=\left\{c\colon \sum_{n=1}^{N}\frac{c_n^2}{\omega_n^2}=\alpha^2\right\}. \tag{8}$$

Thus, the minimum buckling load, equation (7), becomes:

$$\mu(\alpha,\omega)=\min_{c\in C(\alpha,\omega)}\left[\Psi(x^o)+\phi^T c\right]. \tag{9}$$

Define Ω as an $N\times N$ diagonal matrix whose nth diagonal element is $1/\omega_n^2$. Then, as seen from equation (8), we must minimize $\phi^T c$ subject to the constraint:

$$f(c)\equiv c^T\Omega c-\alpha^2=0 \tag{10}$$

We will proceed by the method of Lagrange multipliers (Bryson and Ho, 1975). Define the Hamiltonian as:

$$H(c)=\phi^T c+\gamma f(c) \tag{11}$$

where γ is a constant multiplier whose value must be determined, and ϕ is defined in equation (5). For an extremum, we require that the derivative of the Hamiltonian vanish:

$$0=\frac{\partial H}{\partial c}=\phi+2\gamma\Omega c \tag{12}$$

which implies:

$$c=-\frac{1}{2\gamma}\,\Omega^{-1}\phi. \tag{13}$$

Substituting this into the constraint, equation (10) yields the following expression for the multiplier:

$$\gamma^2=\frac{1}{4\alpha^2}\,\phi^T\Omega^{-1}\phi \tag{14}$$

from which we find that the extremal values of the vector c are:

$$c=\pm\frac{\alpha}{\sqrt{\phi^T\Omega^{-1}\phi}}\,\Omega^{-1}\phi. \tag{15}$$

We now find that the minimum buckling load, given in equation (9), becomes:

$$\mu(\alpha,\omega)=\Psi(x^o)-\alpha\sqrt{\phi^T\Omega^{-1}\phi}. \tag{16}$$

It is significant that this analysis yields an explicit relationship between the minimum buckling load and the characteristics of the initial imperfections, as represented in the parameters α and $\omega_1, \ldots, \omega_N$. Since Ω is a diagonal matrix, equation (16) can be written explicitly as:

$$\mu(\alpha,\omega)=\Psi(x^o)-\alpha\left(\sum_{n=1}^{N}\left(\omega_n\,\frac{\partial\Psi(x^o)}{\partial x_n}\right)^2\right)^{1/2}. \tag{17}$$

From this relation one recognizes that significant reduction in the buckling load results from large sensitivity of the nominal buckling load to Fourier ceofficients, whose semi-axes in the imperfection ellipsoid are large. Furthermore, one notices that the mimimum buckling load depends linearly on the overall size, α, of the imperfection ellipsoid, and nonlinearly on its shape, $\omega_1, \ldots, \omega_N$ and on the partial derivatives $\partial\Psi(x^o)/\partial x_n$.

Let us consider the numerical evaluation of equation (17), based on partial derivatives of Ψ with respect to eight significant Fourier coefficients (from Eliskhakoff et al. 1987). The buckling load with the nominal imperfection profile is 0.746 (in units of the classical buckling load), for the shells in question. The diagonal elements of the matrix Ω are chosen as the mean squared deviations from the average of the corresponding Fourier coefficients of the four B-shells studied by Elishakoff et al. (1987). These measured values of the Fourier coefficients for these four shells, the values of $\omega_1, \ldots, \omega_8$ and the derivatives of Ψ are presented here in Table 1.

The linear variation of the minimum buckling load with the size parameter α is shown in Fig. 1. The four lines are based on different choices of the semi-axes of the imperfection ellipsoid. The curve labeled "experimental" employs the empirical values of $\omega_1, \ldots, \omega_8$ in Table 1; for the other three curves the imperfection sets are spheroids whose radii equal the minimum, the maximum, and the average of the semi-axes in Table 1. Equation (17) indicates that the mimimum buckling load is sensitive to the size and shape of the imperfection ellip-

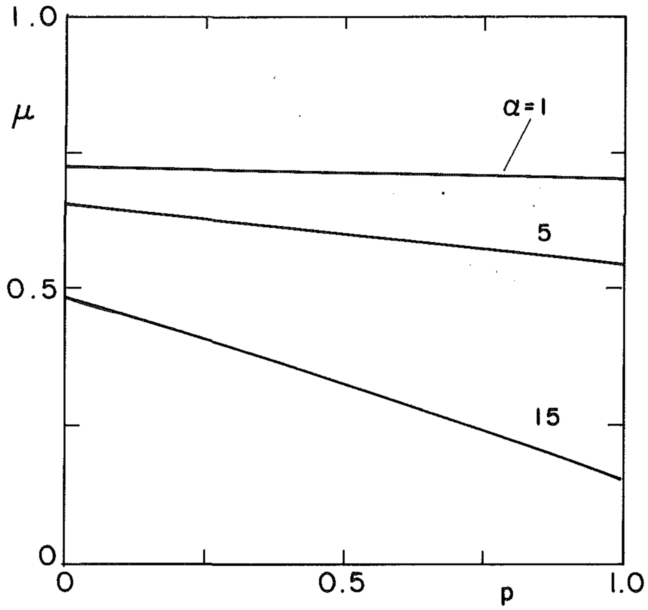

Fig. 2 Minimum buckling load as a function of the shape of the imperfection ellipsoid, for three values of α

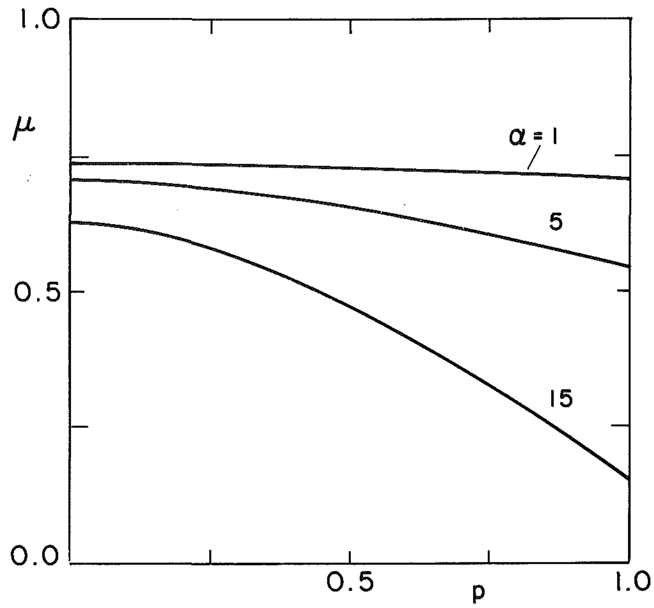

Fig. 3 Minimum buckling load as a function of the shape of the imperfection ellipsoid and of the derivatives of Ψ, for three values of α

soid. To demonstrate this we evaluate μ as the imperfection ellipsoid varies from the ellipsoid of Table 1 to a spheroid of equal volume. The radius of the equivalent spheroid is $\omega_s = 0.0585$. The semi-axes vary parametrically with a control parameter p as $p\omega_n + (1-p)\omega_s$ for $n = 1, \ldots, 8$. The minimum buckling load, μ, is displayed in Fig. 2 versus the parameter p, for three values of the ellipsoid size, α.

Equation (17) indicates that the minimum buckling load is sensitive to the values of the derivatives of Ψ as well as to the size and shape of the imperfection ellipsoid. In Fig. 3 we evaluate μ as the imperfection ellipsoid varies from the ellipsoid of Table 1 to a spheroid of equal volume, and as the derivative of Ψ vary from the values in Table 1 to the average of those derivatives. The radius of the equivalent spheroid is 0.0585 as before, and the average of the eight derivatives of Ψ listed in Table 1 is $\bar{d} = -0.04861$. The semi-axes vary parametrically with the parameter p as in Fig. 2, while the derivatives vary parametrically as $p(\partial\Psi/\partial x_n) + (1-p)\bar{d}$ for $n = 1, \ldots, 8$. The minimum buckling load, μ, is displayed in Fig. 3 versus the parameter p, for three values of the ellipsoid size, α.

It should be noted that, although equations (16) and (17) are written in closed form, $\Psi(x^o)$ as well as $\partial\Psi(x^o)/\partial x_n$ must be determined numerically from existing nonlinear computer codes. Thus, the latest numerical sophistications can be directly incorporated in this analysis.

3 Bounded Fourier Coefficients: Second-Order Analysis

In the previous section a first-order expansion of the nonlinear buckling load was studied. In this section a second-order expansion is considered. Let $\mathbf{Z}(\alpha,\omega)$ and ϕ be defined as in Section 2, and define the $N \times N$ matrix Ξ whose elements are:

$$\xi_{mn} = \frac{\partial^2 \Psi(x^o)}{\partial x_m \partial x_n}. \tag{18}$$

Let x^o be a nominal initial imperfection spectrum. The buckling limit for an initial imperfection $x^o + \zeta$, to second order in ζ, is:

$$\Psi(x^o + \zeta) = \Psi(x^o) + \phi^T\zeta + \frac{1}{2}\zeta^T\Xi\zeta. \tag{19}$$

As before, we are interested in the minimum buckling load on the ensemble $\mathbf{Z}$ of shells. This minimum may be expressed formally as:

$$\mu(\alpha,\omega) = \min_{\zeta\epsilon Z(\alpha,\omega)} \left[\Psi(x^o) + \phi^T\zeta + \frac{1}{2}\zeta^T\Xi\zeta\right]. \tag{20}$$

This is a nonlinear optimization problem with an inequality constraint. Define $\mathbf{\Omega}$ as in Section 2. The inequality constraint on the deviations ζ from the nominal initial imperfection profile, embodied in the set $Z(\alpha,\omega)$, becomes:

$$f(\zeta) \equiv \zeta^T\mathbf{\Omega}\zeta - \alpha^2 \leq 0. \tag{21}$$

Again, the method of Lagrange multipliers will be adopted to solve this problem. Under the new circumstances the Hamiltonian will be defined as:

$$H(\zeta) = \Psi(x^o + \zeta) + \gamma f(\zeta). \tag{22}$$

Necessary conditions for a minimum of Ψ are that the derivative of the Hamiltonian vanish:

$$0 = \frac{\partial H}{\partial\zeta} = \phi + \Xi\zeta + 2\gamma\mathbf{\Omega}\zeta. \tag{23}$$

and that the constraint be satisfied:

$$\zeta^T\mathbf{\Omega}\zeta \leq \alpha^2. \tag{24}$$

Because the constraint is an inequality, the Lagrange multiplier must satisfy one of the following relations:

$$\gamma \geq 0 \quad \text{if} \quad \xi^T\mathbf{\Omega}\zeta = \alpha^2 \tag{25}$$

$$\gamma = 0 \quad \text{if} \quad \zeta^T\mathbf{\Omega}\zeta < \alpha^2. \tag{26}$$

Equation (23) implies that:

$$\zeta = -[\Xi + 2\gamma\mathbf{\Omega}]^{-1}\phi. \tag{27}$$

We must now consider the determination of γ, whose value depends on whether the minimizing value of ζ occurs on the boundary of $\mathbf{Z}(\alpha,\omega)$ (equation (25)) or in the interior (equation (26)). From equations (26) and (27) we see that the minimum occurs for a value of ζ in the interior of $\mathbf{Z}(\alpha,\omega)$ and, thus, $\gamma = 0$ if the following inequality holds:

$$\phi^T\Xi^{-1}\mathbf{\Omega}\Xi^{-1}\phi < \alpha^2. \tag{28}$$

If this relation holds, then the minimum buckling load is obtained from equation (20) as:

$$\mu(\alpha,\omega)=\Psi(x^o)-\frac{1}{2}\phi^T\Xi^{-1}\phi. \tag{29}$$

On the other hand, if relation (28) is not satisfied, then the minimum occurs for a value of ζ on the boundary of $\mathbf{Z}(\alpha,\omega)$, and $\gamma\geq 0$. In order to find the value of γ, note that equation (25) requires the following equality to hold:

$$\alpha^2=\zeta^T\Omega\zeta \tag{30}$$

which, together with equation (27), determines γ. Then, substituting equation (27) into equation (20), one finds the minimum buckling load to be:

$$\mu(\alpha,\omega)=\Psi(x^o)-\phi^T[\Xi+2\gamma\Omega]^{-1}\phi$$
$$+\frac{1}{2}\phi^T[\Xi+2\gamma\Omega]^{-1}\Xi[\Xi+2\gamma\Omega]^{-1}\phi. \tag{31}$$

As in the previous section, a closed-form expression is obtained for the minimum buckling load. Note that if $\Xi\equiv 0$, then this relation reduces to the first-order expression, equation (16). However, when the second-order variation of the buckling with the Fourier coefficients is known, equation (31) enables a more realistic assessment of the minimum buckling than is provided by equation (16).

It should be stressed that the first and second derivatives in equations (4) and (19) may strongly depend on the magnitude of x^o. Moreover, the validity of a truncated Taylor series approximation appears to us as a challenge both to the numerical analysts and to the experimentalists.

4 Uniform Bound on the Imperfection Profiles

In the previous sections we have represented the initial imperfection profile and its variations exclusively in terms of Fourier coefficients. It appears interesting to define the variations of the imperfections in terms of a radial tolerance on the shape of the shell. In this section this tolerance is uniform over the shell, while in the next section the tolerance varies from point to point on the shell.

Let us consider a perfect right, circular cylindrical shell of length L and circumference $2\pi R$. A point on the surface is specified by the coordinates y, z where y is the length from one end of the cylinder and z is the distance around the shell from a reference position. Let $\xi=\pi y/L$ and $\theta=z/R$ be normalized positional coordinates. Let $\eta(\xi,\theta)$ be the deviation of a real shell from the perfect cylinder at point (ξ,θ). Let $\eta_o(\xi,\theta)$ be the nominal imperfection profile; it can be chosen as any typical (e.g., average) initial imperfection profile. Let x^o be the significant Fourier coefficients of the nominal spectrum η_o.

In these new circumstances, the allowed variations around η_o are the elements of the following set of functions:

$$\mathbf{H}(\hat{\eta})=\{\eta:\ |\eta(\xi,\theta)|\leq\hat{\eta}\} \tag{32}$$

Thus, the deviations from the nominal initial imperfection profile are uniformly bounded by the maximum deviation $\hat{\eta}$. In other words, $\mathbf{H}(\hat{\eta})$ represents an ensemble of shells for which $\hat{\eta}$ is the (uniform) tolerance in the radial dimension of the shell.

For any initial imperfection profile $\eta_o(\xi,\theta)+\eta(\xi,\theta)$, the corresponding vector of significant Fourier coefficients is denoted $x(\eta_o+\eta)$. Let $X(\hat{\eta})$ represent the collection of all Fourier vectors corresponding to shells in the ensemble $\mathbf{H}(\hat{\eta})$:

$$X(\hat{\eta})=\{x: x=x(\eta)\quad\text{for}\quad \eta\in\mathbf{H}(\hat{\eta})\}. \tag{33}$$

Also let us define the transposed vector $\phi^T=\partial\Psi(x^o)/\partial x$.

With these definitions we can express the nonlinear buckling load for the first-order deviations from the nominal initial imperfection profiles as:

$$\Psi(x^o+x(\eta))=\Psi(x^o)+\phi^T[x(\eta_o+\eta)-x(\eta_o)]. \tag{34}$$

The Fourier coefficients are linear homogeneous functions of the imperfection profile. This means that:

$$x(\eta_o+\eta)-x(\eta_o)=x(\eta). \tag{35}$$

Consequently, equation (34) becomes:

$$\Psi(x^o+x(\eta))=\Psi(x^o)+\phi^Tx(\eta). \tag{36}$$

Now we can determine the lowest buckling load obtainable for any uniformly-bounded deviation $\eta(\xi,\theta)$ from the initial nominal imperfection profile η_o:

$$\mu(\hat{\eta})=\min_{x(\eta)\in X(\hat{\eta})}[\Psi(x^o)+\phi^Tx(\eta)] \tag{37}$$

$$=\Psi(x^o)+\min_{\eta\in\mathbf{H}(\hat{\eta})}\phi^Tx(\eta) \tag{38}$$

$\mu(\hat{\eta})$ is the lowest buckling load of any shell in the ensemble of shells defined by the set $\mathbf{H}(\hat{\eta})$. Equation (38) calls for the minimum of the linear functional $\phi^Tx(\eta)$ on the convex set $\mathbf{H}(\hat{\eta})$. This extremum can be sought on the set $T(\hat{\eta})$ of extreme-point functions[2] of $\mathbf{H}(\hat{\eta})$. Thus:

$$\mu(\hat{\eta})=\Psi(x^o)+\min_{\eta\in T(\hat{\eta})}\phi^Tx(\eta). \tag{39}$$

Let D represent the domain of the surface of the cylinder:

$$D=\{(\xi,\theta): 0\leq\xi\leq\pi,\ 0\leq\theta\leq 2\pi\}. \tag{40}$$

The set of extreme-point functions is:

$$T(\hat{\eta})=\{\eta:\eta(\xi,\theta)=\hat{\eta}[K_P(\xi,\theta)-K_Q(\xi,\theta)],$$
$$P\cap Q=\emptyset,\ P\cup Q=D\} \tag{41}$$

where $K_V(\xi,\theta)$ is a characteristic function, defined as follows: For any set V of points on the surface of the shell, $K_V(\xi,\theta)=1$ if the point (ξ,θ) belongs to the set V, and equals zero otherwise. Thus, $T(\hat{\eta})$ is the set of all functions which switch arbitrarily back and forth between $+\hat{\eta}$ and $-\hat{\eta}$.

We will now proceed to evaluate the minimum in equation (39). Before doing so we need to evaluate the Fourier coefficients of an arbitrary element of $T(\hat{\eta})$. We can approximate the initial imperfection function in a truncated two-dimensional Fourier series as follows:

$$\eta(\xi,\theta)=\sum_{i=0}^{N_1}a_i\cos i\xi+\sum_{j=1}^{N_2}\sum_{k=1}^{N_3}[b_{jk}\sin j\xi\cos k\theta$$
$$+c_{jk}\sin j\xi\sin k\theta]. \tag{42}$$

The coefficients in this expansion are evaluated as:

$$a_i(\eta)=\frac{1}{(1+\delta_{i0})\pi^2}\int_0^{2\pi}\int_0^{\pi}\eta(\xi,\theta)\cos i\xi\,d\xi d\theta\quad i=0,1,2,\ldots \tag{43}$$

$$b_{jk}(\eta)=\frac{2}{\pi^2}\int_0^{2\pi}\int_0^{\pi}\eta(\xi,\theta)\sin j\xi\cos k\theta\,d\xi d\theta\quad j,k>0 \tag{44}$$

$$c_{jk}(\eta)=\frac{2}{\pi^2}\int_0^{2\pi}\int_0^{\pi}\eta(\xi,\theta)\sin j\xi\sin k\theta\,d\xi d\theta\quad j,k>0 \tag{45}$$

where δ_{i0} is the Kronecker delta function.

To develop an explicit expression for the minimum buckling load, let us adopt the following nomenclature for the elements of the vector ϕ:

$$\alpha_i=\frac{\partial\Psi(x^o)}{\partial a_i},\quad i=0,1,2,\ldots \tag{46}$$

[2] Since $\mathbf{H}(\hat{\eta})$ is a compact convex set, it is the convex hull of its extreme points. These extreme points are themselves functions, like the elements of $\mathbf{H}(\hat{\eta})$.

$$\beta_{jk} = \frac{\partial \Psi(x^o)}{\partial b_{jk}}, \quad j,k>0 \tag{47}$$

$$\gamma_{jk} = \frac{\partial \Psi(x^o)}{\partial c_{jk}}, \quad j,k>0. \tag{48}$$

Expanding the inner product $\phi^T x(\eta)$ which appears in equation (36), explicitly in terms of the quantities α_i, β_{jk}, γ_{jk}, $a_i(\eta)$, $b_{jk}(\eta)$ and $c_{jk}(\eta)$, one obtains the following expression for the buckling load, to first order in the imperfection profile:

$$\Psi(x^o + x(\eta)) = \Psi(x^o) + \sum_{i=0}^{N_1} \alpha_i a_i(\eta) + \sum_{j=1}^{N_2} \sum_{k=1}^{N_3} [\beta_{jk} b_{jk}(\eta) + \gamma_{jk} c_{jk}(\eta)]. \tag{49}$$

Let us define the following function:

$$S(\xi,\theta) = \frac{1}{\pi^2} \sum_{i=0}^{N_1} \frac{1}{1+\delta_{i0}} \alpha_i \cos i\xi + \frac{2}{\pi^2} \sum_{j=1}^{N_2} \sin j\xi \sum_{k=1}^{N_3} [\beta_{jk} \cos k\theta + \gamma_{jk} \sin k\theta]. \tag{50}$$

Combining equations (43)–(45) with equation (49) one finds that the buckling load for an initial imperfection spectrum η is given by:

$$\Psi(x^0 + x(\eta)) = \Psi(x^o) + \int_0^{2\pi} \int_0^{\pi} \eta(\xi,\theta) S(\xi,\theta) d\xi d\theta. \tag{51}$$

We now wish to determine the lowest value of this buckling load for the ensemble $\mathbf{H}(\hat{\eta})$ of shells. Thus, we seek the minimum of $\Psi(x^o + x(\eta))$ as η varies on $\mathbf{H}(\hat{\eta})$. As we mentioned in connection with equation (38), this minimization may be sought as η varies on the set $T(\hat{\eta})$ of extreme-point functions. Examination of equation (41) shows that each extreme-point function $\eta(\xi,\theta)$ switches between $+\hat{\eta}$ and $-\hat{\eta}$ as (ξ,θ) moves over the domain D. Thus, equation (51) is minimized by choosing $\eta = +\hat{\eta}$ for those values of (ξ,θ) for which $S(\xi,\theta)$ is negative, and by choosing $\eta = -\hat{\eta}$ for those values of (ξ,θ) for which $S(\xi,\theta)$ is positive. Equivalently, the minimum buckling load is obtained from that function $\eta(\xi,\theta) \epsilon T(\hat{\eta})$ whose sign is always the opposite of the sign of $S(\xi,\theta)$. Thus, for the minimum buckling load we arrive at:

$$\mu(\hat{\eta}) = \Psi(x^o) - \hat{\eta} \int_0^{2\pi} \int_0^{\pi} |S(\xi,\theta)| d\xi d\theta. \tag{52}$$

As anticipated, this formula indicates that the minimum buckling load of the ensemble of shells with uncertain but uniformly-bounded imperfections is lower than for the nominal shell. The decrease of the buckling load can be readily estimated by equation (52). Using data from Elishakoff et al. (1987) one finds the integral equal to 0.4555. Thus, the minimum buckling load for an ensemble whose imperfections are uniformly bounded by $\hat{\eta}$ is $\mu = 0.746 - 0.4555\hat{\eta}$. For example, $\mu = 0.70045$ for $\hat{\eta} = 0.1$. That is, if the uniform bound on the initial imperfections constitutes one-tenth thickness, then the buckling load of the weakest shell in the ensemble is 70 percent of the classical buckling load. These numerical results should be viewed with caution, as they are based on an incomplete set of partial derivatives of the Ψ function. Derivatives of Ψ, with respect to additional imperfection modes, may significantly alter the numerical value of the minimum buckling load. The calculations presented here demonstrate the feasibility of this analysis.

5 Envelope Bound on the Imperfection Profiles

The derivation of equation (51) depends on the convexity of the set of initial imperfection functions, and on the Taylor expansion in equation (36) being to first order, but not on the specific structure of the initial imperfection set. We are thus free to employ equation (51) for a first-order analysis when the function $\eta(\xi,\theta)$ is an extreme-point function of *any* convex set of initial imperfection functions. A useful generalization of the uniform bound model of initial imperfections is to consider imperfection profiles which are contained in an envelope. Let us consider the following set of initial imperfection functions:

$$\mathbf{H}(\eta_l,\eta_u) = \{\eta: \eta_l(\xi,\theta) \le \eta(\xi,\theta) \le \eta_u(\xi,\theta)\}. \tag{53}$$

The set $\mathbf{H}(\eta_l,\eta_u)$ represents an ensemble of shells for which the radial tolerance varies over the surface of the shell; $\eta_l(\xi,\theta)$ is the lower envelope function and $\eta_u(\xi,\theta)$ is the upper envelope function. The extreme-point functions of $\mathbf{H}(\eta_l,\eta_u)$ are the functions belonging to the set:

$$T(\eta_l,\eta_u) = \{\eta: \eta(\xi,\theta) = \eta_u(\xi,\theta) K_P(\xi,\theta) + \eta_l(\xi,\theta) K_Q(\xi,\theta), P \cap Q = \emptyset, P \cup Q = D\} \tag{54}$$

where D is defined in equation (40). The value of a function in $T(\eta_l,\eta_u)$ switches between $\eta_l(\xi,\theta)$ and $\eta_u(\xi,\theta)$ as (ξ,θ) moves over the domain D. The minimum buckling load is obtained for that function which takes the lower value, $\eta_l(\xi,\theta)$, when $S(\xi,\theta)$ is positive and takes the upper value, $\eta_u(\xi,\theta)$, when $S(\xi,\theta)$ is negative. To conveniently formulate the minimum buckling load, let us define the following two subsets of D:

$$\Delta_+ = \{(\xi,\theta): S(\xi,\theta) \ge 0\} \tag{55}$$

$$\Delta_- = \{(\xi,\theta): S(\xi,\theta) < 0\}. \tag{56}$$

The lowest buckling load, to first order in the imperfection profile, obtainable from any initial imperfection profile bounded within the envelope defined in equation (53) is:

$$\mu(\eta_l,\eta_u) = \Psi(x^o) + \int_{\Delta_-} \eta_u(\xi,\theta) S(\xi,\theta) d\xi d\theta + \int_{\Delta_+} \eta_l(\xi,\theta) S(\xi,\theta) d\xi d\theta. \tag{57}$$

This relation has several practical implications. First of all, one realizes that the upper bound, η_u, on the ensemble of initial imperfection profiles influences the value of the minimum buckling load only in the domain Δ_-. That is, η_u can assume any values whatsoever[3] in Δ_+ without altering the buckling load of the weakest shell in the ensemble $\mathbf{H}(\eta_l,\eta_u)$. Similarly, the lower bound, η_l, effects the buckling load only at points in Δ_+, and can be freely chosen[4] in Δ_-.

Following this line of thought, it is convenient to characterize the ensemble $\mathbf{H}(u_l,\eta_u)$ of shells with a single tolerance function, $\tau(\xi,\theta)$, rather than with two envelope functions η_l and η_u. Let $\tau(\xi,\theta)$ be the function:

$$\tau(\xi,\theta) = \begin{cases} \eta_l(\xi,\theta) & \text{for} \quad (\xi,\theta) \epsilon \Delta_+ \\ \eta_u(\xi,\theta) & \text{for} \quad (\xi,\theta) \epsilon \Delta_-. \end{cases} \tag{58}$$

Let $\mathbf{H}'(\tau)$ be the set of initial imperfection profiles, η, which satisfy:

$$\eta(\xi,\theta) \ge \tau(\xi,\theta) \quad \text{for} \quad (\xi,\theta) \epsilon \Delta_+ \tag{59}$$

$$\eta(\xi,\theta) \le \tau(\xi,\theta) \quad \text{for} \quad (\xi,\theta) \epsilon \Delta_-. \tag{60}$$

[3] Subject to two important restrictions: That $\eta_u \ge \eta_l$ throughout D, and that the magnitude of η_u not become so large as to invalidate the use of a first-order expansion of $\Psi(x^o)$.

[4] Subject to the same two constraints, applied to η_l.

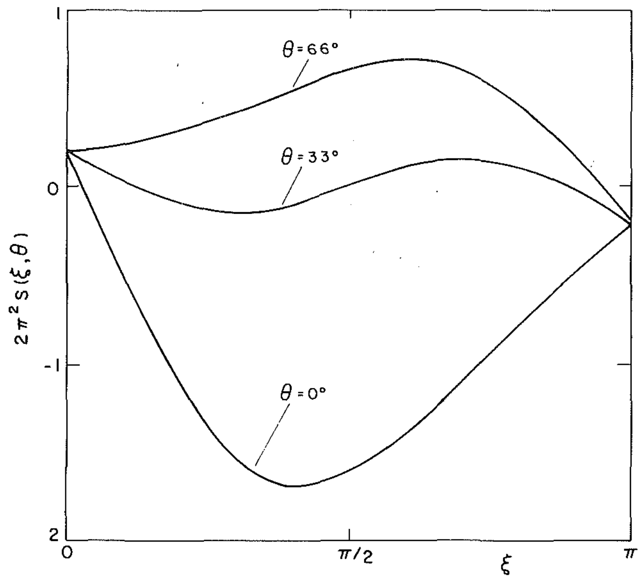

Fig. 4 Axial variation of the local sensitivity to imperfection, for three different azimuthal angles

The sets $\mathbf{H}(\eta_l,\eta_u)$ and $\mathbf{H}'(\tau)$ are not identical. However, the buckling loads of the weakest shell in each of these ensembles are the same. In other words, τ (and equations (59) and (60)) is equivalent to η_l and η_u (and equation (53)) as far as the minimum buckling load is concerned.

The tolerance function is defined in terms of the sign of $S(\xi,\theta)$. The magnitude of S also carries a physical significance, and can be thought of as a measure of the sensitivity to imperfection in the infinitestimal portion $d\xi d\theta$ of the shell at point ξ,θ. The magnitude of S at each point on the surface of the shell serves to weight the local contribution to the buckling load of an initial imperfection at that point. As indicated by equations (51) and (57), if the magnitude of S is small over a region of the surface, then the initial imperfections in that region can be comparatively large without excessively enlarging the buckling load. Conversely, the buckling load is very sensitive to imperfections in those regions of the shell for which $|S|$ is large. The axial variation of S is demonstrated in Fig. 4, based on data from Elishakoff et al. (1987). This figure illustrates that the contribution to imperfection sensitivity of the top and bottom portions of the shell is invariably near zero, while around the midplane the sensitivity achieves its maximum values. Figures such as this provide useful insight to the spatially varying sensitivity of the shell to initial imperfections.

A tolerance function defines an ensemble of shells, as in equations (59) and (60). Suppose that one wishes to construct a radial tolerance function for which the minimum buckling load on the corresponding ensemble assumes the value M. That is, one wishes to choose τ so that:

$$M = \Psi(x^o) + \int_0^{2\pi} \int_0^{\pi} \tau(\xi,\theta) S(\xi,\theta) d\xi d\theta. \tag{61}$$

Furthermore, suppose one desires the tolerance in each region to be as large as possible, consistent with equation (61). One way to do this is to choose the tolerance so that the local contribution to the minimum buckling load is uniform over the surface of the shell. This requires that:

$$\tau(\xi,\theta) S(\xi,\theta) = \text{constant}. \tag{62}$$

Combining these two equations yields the following expression for the desired radial tolerance function:

$$\tau(\xi,\theta) = \frac{M - \Psi(x^o)}{2\pi^2 S(\xi,\theta)} . \tag{63}$$

Note that the sign of τ is always the opposite of the sign of S, because the nominal buckling load, $\Psi(x^o)$, exceeds the ensemble minimum M. This is consistent with the use of equation (63) as a tolerance function, as defined in equations (59) and (60).

To summarize, envelope-bound models allow one to study the effect (on the minimum buckling load) of relaxing the radial tolerance selectivity in different areas of the shell. The function $S(\xi,\theta)$ enables one to assess the contribution to imperfection sensitivity of various portions of the shell, and makes it possible to design a spatially-varying tolerance function accordingly.

6 Theoretical Estimates of the Knockdown Factor

The knockdown factor κ is an engineering parameter whose product with the classical buckling load, P_{cl}, yields a lower bound for the buckling load of the structure. The knockdown factor can be viewed as a property of an ensemble of shells, and the lower bound is the buckling load of the weakest shell in the ensemble. In the previous sections we have obtained explicit expressions for the minimum buckling load μ of an ensemble of shells. The ratio μ/P_{cl} provides an estimate of the knockdown factor. This estimate can be evaluated for each of the models which has been discussed, thereby relating the knockdown factor to different characterizations of the uncertainty in the initial imperfections.

It will be noted that μ depends on the choice of a nominal, initial imperfection spectrum, x^o. If the initial imperfection spectra of the ensemble tend to cluster around an average spectrum, $\bar{x}$, then a reasonable estimate of the knockdown factor would be:

$$\kappa = \frac{\mu(\bar{x})}{P_{cl}} . \tag{64}$$

A noteworthy characteristic of this relation is that it enables estimation of the knockdown factor based on limited empirical knowledge of the ensemble at hand: the mean imperfection of the ensemble and the tolerance to which the ensemble was produced.

7 Conclusions

In this study we considered the buckling of shells with general, geometrical imperfections. Instead of assuming extensive knowledge of the probabilistic characteristics of the initial imperfections, we adopted a non-probabilistic, set-theoretical approach to modeling uncertainty in the initial imperfections. In particular, we assumed that the initial imperfections are uncertain but bounded. Three different set-models of uncertainty were studied. The set $\mathbf{Z}(\alpha,\omega)$ (equation (6)) represents an ensemble of shells whose Fourier coefficients are contained in an ellipsoid. The set $\mathbf{H}(\hat{\eta})$ (equation (32)) defines an ensemble for which $\hat{\eta}$ is a uniform bound on the tolerance in the radial dimension of the shell. Finally, $\mathbf{H}(\eta_l,\eta_u)$ (equation (53)) represents an ensemble of shells whose manufacture is subject to a radial tolerance which varies over the surface of the shell. For each of these ensembles we have obtained an explicit expression for the buckling load of the weakest shell in the ensemble, and we have related this to the knockdown factor. We have shown that the function $S(\xi,\theta)$ can be used to define a spatially-varying radial tolerance. Finally, we have demonstrated that numerical results from sophisticated, nonlinear buckling codes can be readily incorporated in the evaluation of these quantities.

Acknowledgment

The authors appreciate the constructive criticism of Prof.

T. Koiter of the Delft University of Technology, as well as the comments and suggestions of Prof. Donald Olander of the University of California at Berkeley and of the reviewer.

References

Amazigo, J. C., 1976, "Buckling of Stochastically Imperfect Structures," *Buckling of Structures*, B. Budiansky, ed., Springer, Berlin, pp. 172–182.

Arbocz, J., and Babcock, Jr., C. D., 1974, "Multi-Mode Analysis for Calculating Buckling Loads of Imperfect Cylindrical Shells," CALCIT Report SM-74-4, California Institute of Technology, Pasadena, California.

Balakrishnan, A. V., 1981, *Applied Functional Analysis*, 2nd ed., Springer-Verlag, New York, p. 40.

Ben-Haim, Y., 1985, *The Assay of Spatially Random Material*, D. Reidel Publishing Co., Dordrecht, The Netherlands.

Ben-Haim, Y., 1986, "Convexity Analysis: A Tool for Optimization of Malfunction Isolation," *25th IEEE Conference on Decision and Control*, Athens, Greece, pp. 1570–1575.

Ben-Haim, Y., and Elias, E., 1987, "Indirect Measurement of Surface Temperature and Heat Flux: Optimal Design Using Convexity Analysis," *International Journal of Heat and Mass Transfer*, Vol. 30, pp. 1673–1683.

Bertsekas, D. P., and Rhodes, I. B., 1971, "Recursive State Estimation for a Set-Membership Description of Uncertainty," *IEEE Transactions*, Vol. AC-16, pp. 117–128.

Bolotin, V. V., 1962, "Statistical Methods in the Nonlinear Theory of Elastic Shells," *Izvestiya Akademii Nauk SSSR, Otdelenie Tekhnicheskikh Nauk*, No. 3 (English Translation: NASA TTF-85, pp. 1–16).

Bryson, A. E., and Ho, Y.-C., 1975, *Applied Optimal Control*, John Wiley and Sons, New York.

Budiansky, B., and Hutchinson, J. W., 1979, "Buckling: Progress and Challenge," *Trends in Solid Mechanics*, J. F. Besseling and A.M.A. ver der Heijden, eds., Sijthoff and Noordhoff Int'l. Publishers, Alphen a/d Rijn, The Netherlands, pp. 93–116.

Delfour, M. C., and Mittler, S. K., 1969, "Reachability of Perturbed Systems and Min Sup Problems," *SIAM of Journal of Control*, Vol. 7, pp. 521–533.

Drenick, R. F., 1970, "Model-Free Design of Aseismic Structures," *Journal of Engineering*, Mechanics Division, Proceedings of the ASCE, Vol. 96, No. EM4, pp. 483–493.

Elishakoff, I., 1979, "Buckling of a Stochastically Imperfect Finite Column on a Nonlinear Elastic Foundation—A Reliability Study," ASME JOURNAL OF APPLIED MECHANICS, Vol. 46, pp. 411–416.

Elishakoff, I., 1980, "Hoff's Problem in a Probabilistic Setting," ASME JOURNAL OF APPLIED MECHANICS, Vol. 47, pp. 403–408.

Elishakoff, I., 1983, *Probabilistic Methods in the Theory of Structures*, Wiley-Interscience, New York.

Elishakoff, I., and Arbocz, J., 1985, "Reliability of Axially Compressed Cylindrical Shells with General Nonsymmetric Imperfections," ASME JOURNAL OF APPLIED MECHANICS, Vol. 52, pp. 122–128.

Elishakoff, I., van Manen, S., Vermeulen, P. G., and Arbocz, J., 1987, "First-Order Second-Moment Analysis of the Buckling of Shells With Random Imperfections," *AIAA Journal*, Vol. 25, pp. 1113–1117.

Fraser, W. B., and Budiansky, B., 1969, "The Buckling of a Column With Random Initial Deflections," ASME JOURNAL OF APPLIED MECHANICS, Vol. 36, pp. 232–240.

Glover, J. D., and Schweppe, F. C., 1971, "Control of Linear Dynamic Systems With Set Constrained Disturbances," *IEEE Transactions*, Vol. AC-16, pp. 411–423.

Glover, J. D., and Schweppe, F. C., 1972, "Advanced Load Frequency Control," *IEEE Transactions*, Vol. PAS-91, pp. 2095–2103.

Kelly, P. J., and Weiss, M. L., 1979, *Geometry and Convexity*, John Wiley and Sons, New York, p. 209.

Koiter, W. T., 1945, "On the Stability of Elastic Equilibrium," Doctoral Thesis, Delft University of Technology, English translations, (a) TTF-10, 1967, and (b) AFFDL, TF 70-25, 1970.

NASA, 1968, "Buckling of Thin-Walled Circular Cylinders," NASA SP-8007.

Roorda, J., 1980, *Buckling of Elastic Structures*, Waterloo University Press, Waterloo.

Schaepfer, F. M., and Schweppe, F. C., 1972, "Continuous-Time State Estimation Under Disturbances Bounded by Convex Sets," *IEEE Transactions*, Vol. AC-17, pp. 197–205.

Schweppe, F. C., 1968, "Recursive State Estimation: Unknown but Bounded Errors and System Inputs," *IEEE Transactions*, Vol. AC-13, pp. 22–28.

Schweppe, F. C., 1973, *Uncertain Dynamic Systems*, Prentice-Hall, Eaglewood Cliffs, N.J.

Witsenhausen, H. S., 1968a, "A Minimax Control Problem for Sampled Linear Systems," *IEEE Transactions*, Vol. AC-13, pp. 5–21.

Witsenhausen, H. S., 1968b, "Sets of Possible States of Linear Systems Given Perturbed Observations," *IEEE Transactions*, Vol. AC-13, pp. 556–558.

G. A. Kardomateas[1]
Engineering Mechanics Department,
General Motors Research Laboratories,
Warren, Mich. 48090-9055

Transient Thermal Stresses in Cylindrically Orthotropic Composite Tubes

A solution is given for the stresses and displacements in an orthotropic, hollow circular cylinder, due to an imposed constant temperature on the one surface and heat convection into a medium of a different constant temperature at the other surface. Temperature-independent material properties are assumed and a displacement approach is used. Results for the variation of stresses with time and through the thickness are presented.

Introduction

An understanding of thermally-induced stresses in anisotropic bodies is essential for a comprehensive study of their response due to an exposure to a temperature field, which may in turn occur in service or during the manufacturing stages. For example, during the curing stages of filament wound bodies, thermal stresses may be induced from the heat buildup and cooling process. The level of these stresses may well exceed the ultimate strength.

Composite tubes, which can be produced by filament winding on a cylindrical mandrel, have useful applications in such parts as automotive suspension components, landing gears, and launch tubes. Considerable work has been done on the stress field due to mechanical loading (e.g., Lehknitskii, 1963; Sherrer, 1967; Pagano, 1972). Less literature is devoted to studies of thermally-induced stresses. To this extent, formulations and solutions for the thermal stresses in orthotropic cylinders have been presented, for example, by Kalam and Tauchert (1978) due to a steady-state plane temperature distribution, and Hyer and Cooper (1986) due to a steady-state circumferential temperature gradient. The plane thermal-stress problem of a thin circular disc of orthotropic material was considered by Parida and Das (1972). Thermal effects on the microstructure level were analyzed by Avery and Herakovich (1986), by considering an orthotropic fiber in an isotropic matrix under a uniform temperature change.

In this work the problem of transient (time-dependent) thermal stresses in a hollow orthotropic circular cylinder is treated. It is assumed that one surface of the cylinder is at a constant temperature T_0, and at the other there is heat convection into a medium at the reference temperature. The insight provided by this analysis may prove helpful in such instances as choosing curing cycle conditions. The material properties are assumed temperature-independent and a displacement approach is used. It is also assumed that the stresses act on the planes normal to the cylinder axis and do not vary along the generator and that there are no body forces. Numerical results are presented for the variation of the stresses and displacements with time and through the thickness.

[1]Currently at the School of Aerospace Engineering, Georgia Institute of Technology, Atlanta, GA 30332-0150.

Contributed by the Applied Mechanics Division of THE AMERICAN SOCIETY OF MECHANICAL ENGINEERS for publication in the JOURNAL OF APPLIED MECHANICS.

Discussion on this paper should be addressed to the Editorial Department, ASME, United Engineering Center, 345 East 47th Street, New York, N.Y. 10017, and will be accepted until two months after final publication of the paper itself in the JOURNAL OF APPLIED MECHANICS. Manuscript received by ASME Applied Mechanics Division, October 29, 1987; final revision, July 1, 1988.

Mathematical Formulation

Consider a hollow cylinder of inner and outer radius r_1 and r_2, respectively. We denote by r the radial, θ the circumferential, and z the axial coordinate (Fig. 1). The cylinder is assumed to have zero initial temperature. For $t>0$, the boundary $r=r_1$ is kept at temperature T_0 and at $r=r_2$ there is convection into a medium at the reference (zero) temperature. Although the reference temperature is taken as zero, the analysis would be valid for any nonzero value (this is discussed further in the results section).

The thermal problem consists of the heat conduction equation

$$K\left(\frac{\partial^2 T(r,t)}{\partial r^2}+\frac{1}{r}\,\frac{\partial T(r,t)}{\partial r}\right)=\frac{\partial T(r,t)}{\partial t}(r_1<r<r_2,t>0), \tag{1a}$$

and the initial and boundary conditions

$$T(r,t=0)=0 \quad \text{at} \quad r_1 \le r \le r_2, \tag{1b}$$

$$T(r_1,t)=T_0(t>0), \tag{1c}$$

$$\left.\frac{\partial T(r,t)}{\partial r}\right|_{r=r_2}+hT(r_2,t)=0(t>0), \tag{1d}$$

where K is the thermal diffusivity of the composite in the r direction, and h is the ratio of the convective heat-transfer coefficient of the composite tube and the surrounding medium, and the thermal conductivity of the composite in the r direction. The temperature distribution $T(r,t)$ can be found in Carslaw and Jaeger (1959) in terms of the Bessel functions of the first and second kind J_n and Y_n (note that as the range r

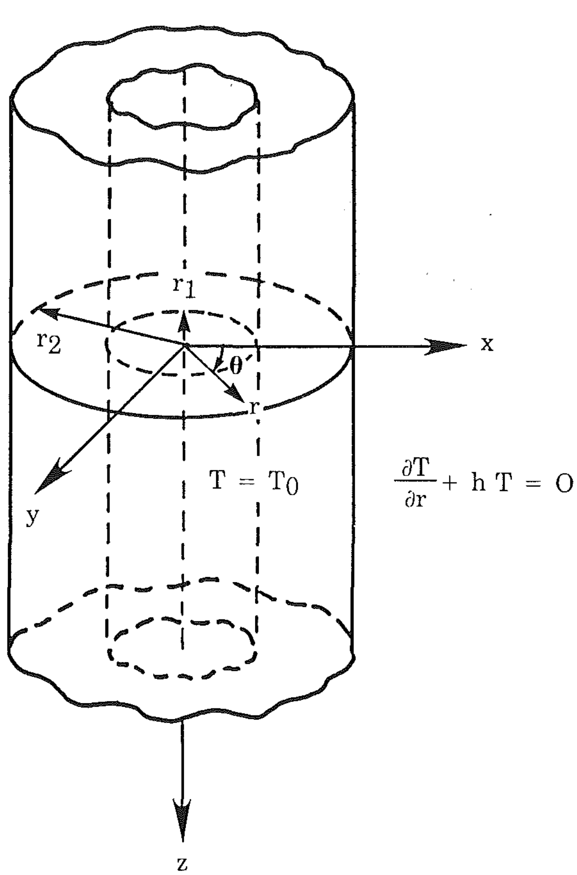

Fig. 1 Definition of the geometry

does not extend to the origin, Bessel functions of the second kind are not excluded, as opposed to the solid cylinder case). It is given in the form

$$T(r,t) = d_1 + d_2 \ln(r/r_2)$$
$$+ \sum_{n=1}^{\infty} e^{-Ka_n^2 t}[d_{4n}J_0(ra_n) + d_{5n}Y_0(ra_n)], \tag{2}$$

where $\pm a_n$ are the roots (all real and simple) of:

$$[xY_1(r_2x) - hY_0(r_2x)]J_0(r_1x) - [xJ_1(r_2x) - hJ_0(r_2x)]Y_0(r_1x) = 0. \tag{3}$$

The constants d_i are given in Appendix I. Since there is only radial dependence of the temperature field, the hoop displacements are zero and the stresses and strains are independent of θ. Therefore, for the orthotropic body, the thermoelastic stress-strain relations are

$$\begin{bmatrix} \sigma_{rr} \\ \sigma_{\theta\theta} \\ \sigma_{zz} \\ \tau_{\theta z} \\ \tau_{rz} \\ \tau_{r\theta} \end{bmatrix} = \begin{bmatrix} C_{11} & C_{12} & C_{13} & 0 & 0 & 0 \\ C_{12} & C_{22} & C_{23} & 0 & 0 & 0 \\ C_{13} & C_{23} & C_{33} & 0 & 0 & 0 \\ 0 & 0 & 0 & C_{44} & 0 & 0 \\ 0 & 0 & 0 & 0 & C_{55} & 0 \\ 0 & 0 & 0 & 0 & 0 & C_{66} \end{bmatrix} \begin{bmatrix} \epsilon_{rr} - \alpha_r \Delta T \\ \epsilon_{\theta\theta} - \alpha_\theta \Delta T \\ \epsilon_{zz} - \alpha_z \Delta T \\ \gamma_{\theta z} \\ \gamma_{rz} \\ \gamma_{r\theta} \end{bmatrix}, \tag{4}$$

where C_{ij} are the elastic constants and α_i the thermal expansion coefficients (we have used the notation $1 \equiv r$, $2 \equiv \theta$, $3 \equiv z$).

Since the temperature does not depend on the axial coordinate, we can assume that the stresses are independent of z. In addition to the constitutive equations (4), the elastic response of the cylinder must satisfy the equilibrium equations:

$$\sigma_{rr,r} + (\sigma_{rr} - \sigma_{\theta\theta})/r = 0, \tag{5a}$$

$$\tau_{r\theta,r} + 2\tau_{r\theta}/r = 0; \quad r^{-1}(r\tau_{rz})_{,r} = 0. \tag{5b}$$

For the problem without the thermal effects the expressions for the displacement field were derived by Lehknitskii (1963). A similar procedure was followed and lead to the general solution for the displacements in this thermoelastic problem (see also Hyer and Cooper, 1986). Due to the symmetry of the problem, only rigid body translation and rotation contribute to the θ component of the displacement field and the strains and stresses do not depend on θ. Furthermore, there are no twisting strains. Therefore, the displacements have the form:

$$u_r = U(r,t) + z(\omega_y \cos\theta - \omega_x \sin\theta) + v_{0x}\cos\theta + v_{0y}\sin\theta, \tag{6a}$$

$$u_\theta = -z(\omega_x r\cos\theta + \omega_y r\sin\theta) - v_{0x}\sin\theta + v_{0y}\cos\theta + \omega_z r, \tag{6b}$$

$$u_z = zC(t) + \omega_x r\sin\theta - \omega_y r\cos\theta + v_{0z}. \tag{6c}$$

In the above expressions, the function $U(r,t)$ represents the radial displacements accompanied by deformation, and the constants v_{0x}, v_{0y}, v_{0z}, ω_x, ω_y, ω_z characterize the rigid body translation and rotation about the cartesian coordinate system. The parameter C is time-dependent and is found from the boundary conditions, as discussed later.

The strains are now expressed in terms of the displacement U:

$$\epsilon_{rr} = \frac{\partial U(r,t)}{\partial r}; \; \epsilon_{\theta\theta} = \frac{U(r,t)}{r}; \; \epsilon_{zz} = C(t). \tag{7a}$$

$$\gamma_{\theta z} = \gamma_{rz} = \gamma_{r\theta} = 0 \tag{7b}$$

Substituting (4) and (7) into (5a) yields the following differential equation for the displacement field $U(r,t)$:

$$C_{11}\left(\frac{\partial^2 U(r,t)}{\partial r^2} + \frac{1}{r}\,\frac{\partial U(r,t)}{\partial r}\right) - \frac{C_{22}}{r^2}U(r,t)$$
$$= q_1 \frac{\partial T(r,t)}{\partial r} + q_2 \frac{T(r,t)}{r} + (C_{23} - C_{13})\frac{C(t)}{r}, \tag{8}$$

where

$$q_1 = C_{11}\alpha_r + C_{12}\alpha_\theta + C_{13}\alpha_z, \tag{9a}$$

$$q_2 = (C_{11} - C_{12})\alpha_r + (C_{12} - C_{22})\alpha_\theta + (C_{13} - C_{23})\alpha_z. \tag{9b}$$

The parameter $C(t)$ is now written in the form

$$C(t) = c_0 + \sum_{n=1}^{\infty} c_n e^{-Ka_n^2 t}. \tag{10}$$

To solve equation (8), set

$$U(r,t) = U_0(r) + \sum_{n=1}^{\infty} e^{-Ka_n^2 t} R_n(r). \tag{11}$$

Substituting (2), (10), and (11) in (8) gives the following equations for U_0 and R_n:

$$C_{11}\left(U_0''(r) + \frac{U_0'(r)}{r}\right) - \frac{C_{22}}{r^2}U_0(r)$$
$$= \frac{q_1 d_2 + q_2 d_1 + (C_{23} - C_{13})c_0}{r} + q_2 d_2 \frac{\ln(r/r_2)}{r}, \tag{12}$$

$$C_{11}\left(R_n''(r) + \frac{R_n'(r)}{r}\right) - \frac{C_{22}}{r^2}R_n(r)$$
$$= \frac{(C_{23} - C_{13})c_n}{r} + d_{4n}\left[\frac{J_0(ra_n)}{r} - q_1\alpha_n J_1(ra_n)\right]$$
$$+ d_{5n}\left[\frac{Y_0(ra_n)}{r} - q_1 a_n Y_1(ra_n)\right] \quad n = 1, \ldots, \infty. \tag{14}$$

The solution to these equations is the sum of the solution of the homogeneous equation and a particular solution. The solution of the homogeneous equation (8) is

$$U_g(r,t)=G_1(t)r^{\lambda_1}+G_2(t)r^{\lambda_2};\quad \lambda_{1,2}=\pm\sqrt{C_{22}/C_{11}}. \tag{15a}$$

In a similar fashion to the parameter $C(t)$, set $G_i(t)$ in the form:

$$G_i(t)=G_{i0}+\sum_{n=0}^{\infty}G_{in}e^{-Ka_n^2 t};\quad i=1,2. \tag{15b}$$

Since the constants c_j and G_{ij} are yet unknown, we shall indicate the places where they enter in the expressions that follow (these constants are found later from the boundary conditions). For $C_{11}\neq C_{22}$ the solution of (12) for $U_0(r)$ is

$$U_0(r)=G_{10}r^{\lambda_1}+G_{20}r^{\lambda_2}+\frac{C_{23}-C_{13}}{C_{11}-C_{22}}c_0 r+U_0^*(r), \tag{16a}$$

$$U_0^*(r)=\frac{q_2}{C_{11}-C_{22}}d_2 r\ln(r/r_2)+\left[\frac{q_1d_2+q_2d_1}{C_{11}-C_{22}}-\frac{2C_{11}q_2d_2}{(C_{11}-C_{22})^2}\right]r. \tag{16b}$$

For $C_{11}=C_{22}$ the corresponding solution of (12) is

$$U_0(r)=G_{10}r+\frac{G_{20}}{r}+\frac{(C_{23}-C_{13})}{2C_{11}}c_0 r\ln(r/r_2)+U_0^*(r), \tag{17a}$$

$$U_0^*(r)=\frac{q_2}{4C_{11}}d_2 r\ln^2(r/r_2)+\frac{(2q_1-q_2)d_2+2q_2d_1}{4C_{11}}r\ln(r/r_2). \tag{17b}$$

To solve (14), we use the series expansions of the Bessel functions to obtain a series expansion of the right-hand side (see Appendix II). In the following, γ stands for the Euler's constant ($\simeq 0.577215\ldots$).

For $C_{11}\neq C_{22}$, the solution of (14) for R_n, $n=1,\ldots\infty$, is

$$R_n(r)=G_{1n}r^{\lambda_1}+G_{2n}r^{\lambda_2}+\frac{C_{23}-C_{13}}{C_{11}-C_{22}}c_n r+R_n^*(r), \tag{18a}$$

$$R_n^*(r)=B_{0n}r+\frac{2}{\pi}\frac{d_{5n}}{(C_{11}-C_{22})}r\ln(ra_n/2)+\sum_{k=0}^{\infty}B_{1nk}r^{2k+3}\ln(ra_n/2)+B_{2nk}r^{2k+3}, \tag{18b}$$

where

$$B_{0n}=\frac{d_{4n}+(2/\pi)(q_1+\gamma)d_{5n}}{C_{11}-C_{22}}-\frac{4C_{11}d_{5n}}{\pi(C_{11}-C_{22})^2}. \tag{18c}$$

The coefficients in the sum over k are given in terms of

$$f_{kn}=\left[d_{4n}-\frac{2d_{5n}}{\pi}\left(1+\frac{1}{2}+\ldots+\frac{1}{k+1}-\gamma\right)\right][1+2q_1(k+1)]+\frac{2d_{5n}q_1}{\pi}, \tag{18d}$$

as follows:

$$B_{1nk}=\frac{2d_{5n}(-1)^{k+1}a_n^{2k+2}[1+2q_1(k+1)]}{\pi 2^{2k+2}[(k+1)!]^2[C_{11}(2k+3)^2-C_{22}]}, \tag{18e}$$

$$B_{2nk}=\frac{(-1)^{k+1}a_n^{2k+2}}{2^{2k+2}[(k+1)!]^2[C_{11}(2k+3)^2-C_{22}]}\times\left\{f_{kn}-\frac{(4C_{11}/\pi)(2k+3)d_{5n}[1+2q_1(k+1)]}{C_{11}(2_k+3)^2-C_{22}}\right\}. \tag{18f}$$

In the (unlikely) event that for a certain k, $C_{11}(2k+3)^2=C_{22}$, the term in the sum for this k is replaced by the one in Appendix III.

For $C_{11}=C_{22}$ the solution of (14) for R_n is

$$R_n(r)=G_{1n}r+\frac{G_{2n}}{r}+\frac{C_{23}-C_{13}}{2C_{11}}c_n r\ln(r/r_2)+R_n^*(r), \tag{19a}$$

$$R_n^*(r)=B_{0n}r\ln(ra_n/2)+\frac{d_{5n}}{2\pi C_{11}}r\ln^2(ra_n/2)+\sum_{k=0}^{\infty}B_{1nk}r^{2k+3}\ln(ra_n/2)+B_{2nk}r^{2k+3}, \tag{19b}$$

where

$$B_{0n}=\frac{\pi d_{4n}+d_{5n}(2q_1+2\gamma-1)}{2\pi C_{11}}. \tag{19c}$$

It should be noted that although the sum over the roots a_n is extended from $n=1$ to ∞, only the first few terms are dominant and it usually suffices to include a small number of roots. This issue is discussed in detail in the Results section.

Next, turn to the boundary conditions. We assume that no external tractions exist. Then the conditions on the contour bounding the cross-section (at $r=r_1$ and $r=r_2$) can be written in the following form:

$$\sigma_{rr}(r_i,t)=\tau_{r\theta}(r_i,t)=\tau_{rz}(r_i,t)=0,\qquad i=1,2. \tag{20}$$

Only the condition for the stress σ_{rr} is not satisfied identically and it is written in terms of the displacement field:

$$C_{11}U_{,r}(r_i,t)+C_{12}\frac{U(r_i,t)}{r}+C_{13}C(t)-q_1T(r_i,t)=0;\quad i=1,2. \tag{21}$$

By substituting (2), (10), and (11) in (21) and the expressions (17) for $U_0(r)$, gives, in turn, the following two linear equations in G_{10}, G_{20}, c_0:

$$(C_{11}\lambda_1+C_{12})r_i^{\lambda_1-1}G_{10}+(C_{11}\lambda_2+C_{12})r_i^{\lambda_2-1}G_{20}+A_0c_0=-C_{11}U_0^{*\prime}(r_i)-C_{12}\frac{U_0^*(r_i)}{r_i}+q_1[d_1+d_2\ln(r_i/r_2)]\quad i=1,2, \tag{22a}$$

where

$$A_0=\frac{C_{11}+C_{12}}{C_{11}-C_{22}}(C_{23}-C_{13})+C_{13}\quad\text{for}\quad C_{11}\neq C_{22}$$
$$=\frac{C_{23}-C_{13}}{2C_{11}}[C_{11}+(C_{11}+C_{12})\ln(r_i/r_2)]+C_{13}\quad\text{for}\quad C_{11}=C_{22}. \tag{22b}$$

In a similar fashion, by substituting the expressions (18) for $R_n(r)$, there correspond two linear equations for G_{1n}, G_{2n}, c_n for each n, $n=1,\ldots\infty$, as follows,

$$(C_{11}\lambda_1+C_{12})r_i^{\lambda_1-1}G_{1n}+(C_{11}\lambda_2+C_{12})r_i^{\lambda_2-1}G_{2n}+A_0c_n=-C_{11}R_n^{*\prime}(r_i)-C_{12}\frac{R_n^*(r_i)}{r_i}+q_1[d_{4n}J_0(r_ia_n)+d_{5n}Y_0(r_ia_n)];\quad i=1,2. \tag{23}$$

Now, let us consider the conditions of resultant forces and moments. Since the stresses do not depend on z, these conditions exist in any cross-section. It can be proved (e.g., Lehnkitskii, 1963, although thermal effects are not included), that the conditions of zero-resultant forces along the x- and y-

Table 1 Convergence of the series solution. Values of the nth term (at $r=r_2$) of the temperature, displacement, and stress quantities.

	$n=1$	$n=2$	$n=3$
$a_n(\mathrm{m}^{-1})$	87.1	291.0	488.8
$\tilde{t}=\mathbf{0.25}$			
$T(°\mathrm{C})$	-0.743×10^{2}	0.144×10^{0}	-0.426×10^{-5}
$U(\mathrm{m})$	-0.910×10^{-5}	0.142×10^{-7}	0.687×10^{-11}
$\sigma_{\theta\theta}(\mathrm{MN/m^2})$	0.297×10^{2}	-0.870×10^{-1}	0.133×10^{-4}
$\sigma_{zz}(\mathrm{MN/m^2})$	0.818×10^{1}	-0.104×10^{0}	0.948×10^{-6}
$\tilde{t}=\mathbf{0.5}$			
$T(°\mathrm{C})$	-0.457×10^{2}	0.635×10^{-3}	-0.976×10^{-12}
$U(\mathrm{m})$	-0.560×10^{-5}	0.629×10^{-10}	0.157×10^{-17}
$\sigma_{\theta\theta}(\mathrm{MN/m^2})$	0.183×10^{2}	-0.385×10^{-3}	0.305×10^{-11}
$\sigma_{zz}(\mathrm{MN/m^2})$	0.503×10^{1}	-0.460×10^{-3}	0.217×10^{-12}

axes are satisfied identically. The conditions of zero-resultant moment along x- and y-axes (and that of zero twisting moment) are also satisfied by the symmetry of the problem. Therefore, it remains only a condition of zero resultant-axial force, P_z:

$$\int_{r_1}^{r_2} \sigma_{zz}(r,t)2\pi r dr = P_z(t) = 0. \tag{24}$$

This gives the last set of equations that are needed to determine the constants G_{ij}, c_j. In terms of

$$q_3 = C_{13}\alpha_r + C_{23}\alpha_\theta + C_{33}\alpha_z, \tag{25}$$

(24) gives

$$\left(C_{13}+\frac{C_{23}-C_{13}}{\lambda_1+1}\right)(r_2^{\lambda_1+1}-r_1^{\lambda_1+1})G_{10}+A_1G_{20}+A_2c_0$$
$$= -E_0(r_1,r_2)+\frac{q_3}{2}\left[\frac{r_2^2-r_1^2}{2}(2d_1-d_2)+d_2r_1^2\ln(r_2/r_1)\right], \tag{26}$$

and for $n=1,\ldots\infty$,

$$\left(C_{13}+\frac{C_{23}-C_{13}}{\lambda_1+1}\right)(r_2^{\lambda_1+1}-r_1^{\lambda_1+1})G_{1n}+A_1G_{2n}+A_2c_n$$
$$= -E_n(r_1,r_2)+(q_3/a_n)\sum_{i=1}^{2}(-1)^i[d_{4n}r_iJ_1(r_ia_n)$$
$$+d_{5n}r_iY_1(r_ia_n)], \tag{27}$$

where $E_0(r_2,r_1)$ and $E_n(r_1, r_2)$ are given in Appendix IV. The coefficients A_1, A_2 are defined as:

$$A_1 = \left(C_{13}+\frac{C_{23}-C_{13}}{\lambda_2+1}\right)(r_2^{\lambda_2+1}-r_1^{\lambda_2+1}) \quad \text{for} \quad C_{11}\neq C_{22}$$
$$= C_{13}+(C_{23}-C_{13})\ln(r_2/r_1) \quad \text{for} \quad C_{11}=C_{22} \tag{28a}$$

$$A_2 = \frac{r_2^2-r_1^2}{2}\left(C_{33}+\frac{C_{23}^2-C_{13}^2}{C_{11}-C_{22}}\right) \quad \text{for} \quad C_{11}\neq C_{22}$$
$$= \frac{(r_2^2-r_1^2)}{8C_{11}}[4C_{33}C_{11}-(C_{23}-C_{13})^2] \tag{28b}$$
$$+\frac{C_{23}^2-C_{13}^2}{4C_{11}}r_1^2\ln(r_2/r_1) \text{ for } C_{11}=C_{22}.$$

Therefore the constants c_j, G_{ij} and, hence, the displacement U, can be found by solving (21), (26) and (22), (27). After obtaining the displacement field, the stresses can be found by substituting in (7) and (4).

Results and Discussion

Before presenting specific results we shall address several issues that were previously raised. First, in the aforementioned formulation, the reference temperature was assumed to be zero. Since, however, thermal stresses are produced by temperature differentials, the analysis remains the same for any initial temperature other than zero, at which the body is assumed to be stress free. In this case, T_0 is the applied temperature above this initial value.

Second, in producing numerical results, the series expansion for the Bessel's functions (see Appendix II) cannot be used for large arguments. This means that there is a limit to the number of roots a_n of the characteristic equation (3), over which the summation in (11) is performed. Except for very small values of the time t, this does not limit the accuracy of the results. This is because only the first few terms of the series over n are dominant and there is rapid convergence as can be seen from Table 1, which shows the nth term of some quantities for the example case that was considered (the specifics of the example case are described in detail next), and for time values $\tilde{t}=Kt/(r_2-r_1)^2=0.25$ and 0.5. In view of the almost-zero values for the third term, there is no need to consider more than the first three roots. For very small values of time it becomes, however, necessary to include more terms.

As an illustrative example, the distribution of thermal stresses was determined for a glass/epoxy circular cylinder of inner radius $r_1=20$ mm and outer radius $r_2=36$ mm. It is supposed to be made, for example, by filament winding, with the fibers oriented around the circumference. The moduli in $\mathrm{GN/m^2}$ and Poisson's ratio for this material are listed next, where 1 is the radial (r), 2 is the circumferential (θ), and 3 the axial (z) direction:

$$E_1=13.7, E_2=55.9, E_3=13.7, G_{12}=5.6, G_{23}=5.6,$$
$$G_{31}=4.9, \nu_{12}=0.068, \nu_{23}=0.277, \nu_{31}=0.4.$$

The thermal expansion coefficients are: $\alpha_r=40\times10^{-6}/°\mathrm{C}$, $\alpha_\theta=10\times10^{-6}/°\mathrm{C}$, $\alpha_z=40\times10^{-6}/°\mathrm{C}$. For this material, the thermal diffusivity in the radial direction is $K=0.112\times10^{-5}\mathrm{m^2/s}$. Let us assume that the ratio of the convective heat-transfer coefficient between the composite tube and the surrounding medium at $r=r_2$ and the thermal conductivity of the tube in the radial direction is $h=0.15\ \mathrm{m^{-1}}$ (which is a typical value for heat convection to the air). A temperature of $T_0=100$ °C above the reference one is applied at $r=r_1$.

To illustrate the results, the nondimensional radial distance (through the thickness) $\tilde{r}=(r-r_1)/(r_2-r_1)$ is used. Figure 2 shows the temperature and Fig. 3 the displacement distribution for time values $\tilde{t}=0.25$, 0.5, 1.0, and 10 (the last one is a nearly steady, constant temperature state). The corresponding distribution of stresses σ_{rr}, $\sigma_{\theta\theta}$, and σ_{zz} are shown in Figs. 4, 5, and 6. The biggest of those is the hoop stress $\sigma_{\theta\theta}$ and its value at the outer surface $\tilde{r}=1$ is seen to be larger for $\tilde{t}=0.25$ than the steady-state value (for $\tilde{t}=10$) by a factor of about 1.5. At the inner surface $\tilde{r}=0$, the steady-state ($\tilde{t}=10$) stress is compressive and it becomes smaller in magnitude (tending to be tensile) for smaller time values. The radial stress σ_{rr}, is initially mostly tensile and becomes compressive at the final steady state. The axial stress σ_{zz} is compressive closer to the inner surface (small values of $\tilde{r}$) but tensile closer to the outer surface; its maximum absolute value is about eight times higher at

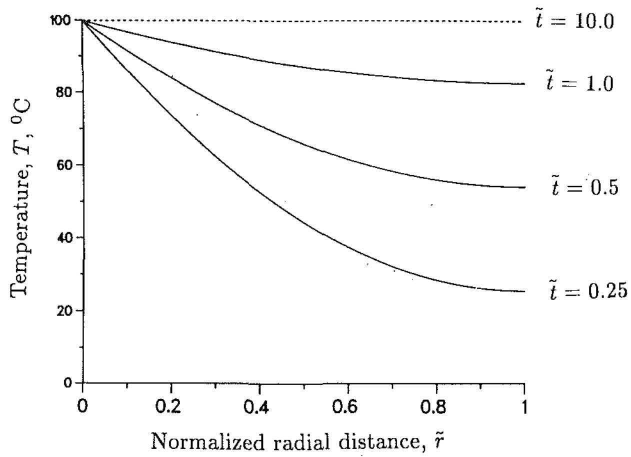

Fig. 2 Radial distribution of the temperature T at different times. The nondimensional time is defined by $\tilde{t} = Kt/(r_2 - r_1)^2$. The dashed line is the nearly steady, constant temperature state.

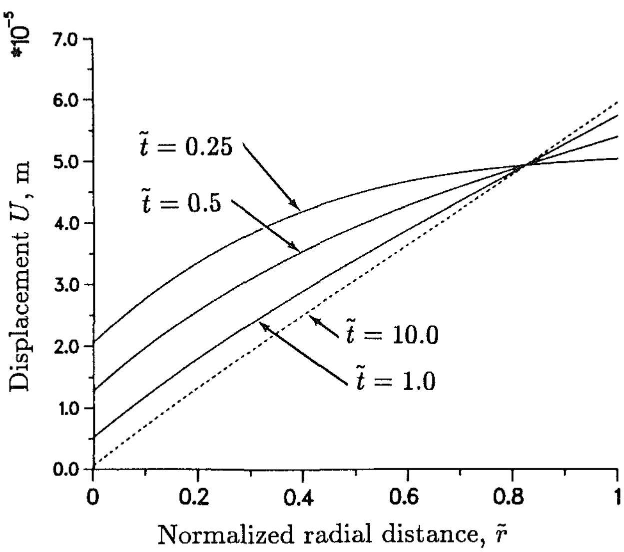

Fig. 3 Radial distribution of the displacement U

$\tilde{t} = 0.25$ than at $\tilde{t} = 10$. It should be pointed out that, although the axial and radial stresses are smaller than the hoop, they may be more critical because the material is weaker in the directions normal to the fibers (typically the ultimate strength of glass/epoxy in the directions normal to the fibers may be less than that in the direction of the fibers by a factor ranging from seven to ten). These results are specific for the example we consider and trends may be different, depending on the mechanical and thermal constants of the material. They show, however, that transient thermal stresses may be of considerable magnitude, the level of which can be determined from the above solution.

Summary

In summary, we have presented a solution for the thermal stresses of a homogeneous, orthotropic hollow cylinder subjected to a constant temperature on the one surface and heat convection into a medium of a different constant temperature at the other surface. Temperature-independent material properties were assumed and a series solution for the displacement was found. Numerical examples were presented for the distribution of the transient thermal stresses, which turned out to be of significant magnitude.

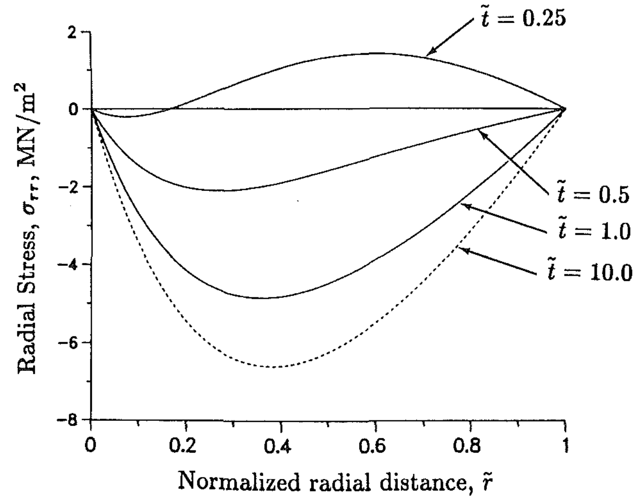

Fig. 4 Distribution of the radial stress σ_{rr}

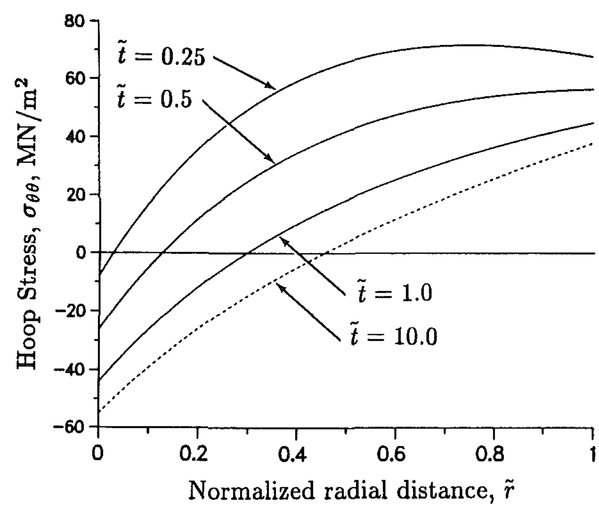

Fig. 5 Distribution of the hoop stress $\sigma_{\theta\theta}$

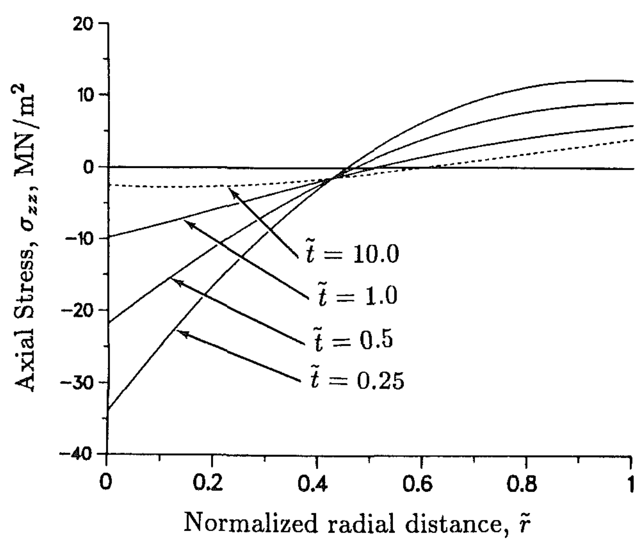

Fig. 6 Distribution of the axial stress σ_{zz}

References

Avery, W. B., and Herakovich, C. T., 1986, "Effect of Fiber Anisotropy on Thermal Stresses in Fibrous Composites," ASME Journal of Applied Mechanics, Vol. 53, pp. 751–756.

Carslaw, H. S., and Jaeger, J. C., 1959, "Conduction of Heat in Solids," 2nd ed., Clarendon Press.
Kalam, M. A., and Tauchert, T. R., 1978, "Stresses in an Orthotropic Elastic Cylinder due to a Plane Temperature Distribution $T(r,\theta)$," *Journal of Thermal Stresses*, Vol. 1, pp. 13–24.
Hyer, M. W., and Cooper, D. E., 1986, "Stresses and Deformations in Composite Tubes Due to a Circumferential Temperature Gradient," ASME JOURNAL OF APPLIED MECHANICS, Vol. 53, pp. 757–764.
Lekhnitskii, S. G., 1963, "Theory of Elasticity of an Anisotropic Elastic Body," Holden Day, also Mir Publishers, 1981.
Pagano, N. J., 1972, "The Stress Field in a Cylindrically Anisotropic Body Under Two-Dimensional Surface Tractions," ASME JOURNAL OF APPLIED MECHANICS, Vol. 39, pp. 791–796.
Parida, J., and Das, A. K., 1972, "Thermal Stresses in a Thin Circular Disc of Orthotropic Material Due to an Instantaneous Point Heat Source," *Acta Mechanica*, Vol. 13, pp. 205–214.
Sherrer, R. E., 1967, "Filament Wound Cylinder with Axial Symmetric Loads," *Journal of Composite Materials*, Vol. 1, pp. 344–355.
Wylie, C. Ray, 1975, "Advanced Engineering Mathematics," 4th ed., McGraw-Hill Book Company, New York.

APPENDIX I

The constants d_i in the expression for the temperature (3) are given in terms of

$$F(a_n) = (a_n^2 + h^2)J_0^2(r_1 a_n) - [a_n J_1(r_2 a_n) - hJ_0(r_2 a_n)]^2, \quad (A1)$$

as follows:

$$d_1 = \frac{T_0}{1 + r_2 h \ln(r_2/r_1)}; \qquad d_2 = -\frac{r_2 T_0 h}{1 + r_2 h \ln r_2/r_1)}, \quad (A2)$$

$$d_{4n} = \frac{\pi T_0 Y_0(r_1 a_n)}{F(a_n)}[a_n J_1(r_2 a_n) - hJ_0(r_2 a_n)]^2, \quad (A3a)$$

$$d_{5n} = -\frac{\pi T_0 J_0(r_1 a_n)}{F(a_n)}[a_n J_1(r_2 a_n) - hJ_0(r_2 a_n)]^2, \quad (A3b)$$

APPENDIX II

The Bessel functions of first- and second-kind of order zero and one have a series of expansion of the form (see e.g., Wylie, 1975)

$$J_0(x) = \sum_{k=0}^{\infty} \frac{(-1)^k x^{2k}}{2^{2k}(k!)^2}; \quad J_1(x) = \sum_{k=0}^{\infty} \frac{(-1)^k x^{2k+1}}{2^{2k+1}k!(k+1)}, \quad (A4)$$

$$Y_0(x) = \frac{2}{\pi}\left(\ln\frac{x}{2} + \gamma\right)J_0(x) - \frac{2}{\pi}\sum_{k=1}^{\infty}\frac{(-1)^k x^{2k}}{2^{2k}(k!)^2}\psi(k), \quad (A5a)$$

$$Y_1(x) = \frac{2}{\pi}\left(\ln\frac{x}{2} + \gamma\right)J_1(x) - \frac{2}{\pi}\frac{1}{x} - \frac{1}{\pi}\sum_{k=0}^{\infty}\frac{(-1)^k x^{2k+1}}{2^{2k+1}(k!)(k+1)!}\left(2\psi(k+1) - \frac{1}{k+1}\right). \quad (A5b)$$

In the above expressions $\gamma = 0.577215\ldots$ is the Euler's constant and $\psi(k)$ is defined as

$$\psi(k) = 1 + \frac{1}{2} + \ldots + \frac{1}{k}. \quad (A6)$$

The above series expansions can be used to calculate the Bessel's functions up to a value of the argument of about $x = 18$. They are rapidly convergent, especially for small values of the argument (adopting a smallest number limit of $10 \times^{-71}$ would require, at most, 72 terms at $x = 18$).

Using the series expansion, we obtain the following equation in place of (14):

$$C_{11}\left(R_n''(r) + \frac{R_n'(r)}{r}\right) - \frac{C_{22}}{r^2}R_n(r) = \frac{d_{4n} + (2/\pi)(q_1 + \gamma)d_{5n} + (C_{23} - C_{13})c_n}{r} + \frac{2d_5}{\pi}\frac{\ln(ra_n/2)}{r} + \frac{2d_5}{\pi}\sum_{k=0}^{\infty}\frac{(-1)^{k+1}a_n^{2k+2}r^{2k+1}\ln(ra_n/2)}{2^{2k+2}[(k+1)!]^2}[1 + 2q_1(k+1)] + \sum_{k=0}^{\infty}\frac{(-1)^{k+1}a_n^{2k+2}r^{2k+1}}{2^{2k+2}[(k+1)!]^2}f_{kn}, \quad (A7)$$

where f_{kn} is defined in (18d).

APPENDIX III

In the event that for a certain k, $C_{11}(2k+3)^2 = C_{22}$, the term in the sum in (18b) and (19b) for this k is

$$B_{1nk}r^{2k+3}\ln^2(ra_n/2) + B_{2nk}r^{2k+3}\ln(ra_n/2), \quad (A8)$$

where now

$$B_{1nk} = \frac{2d_{5n}(-1)^{k+1}a_n^{2k+2}[1 + 2q_1(k+1)]}{\pi 2^{2k+2}[(k+1)!]^2 4C_{11}(2k+3)}, \quad (A9a)$$

$$B_{2nk} = \frac{(-1)^{k+1}a_n^{2k+2}}{2^{2k+2}[(k+1)!]^2 2C_{11}(2k+3)}\left\{f_{kn} - \frac{2d_{5n}[1 + 2q_1(k+1)]}{2\pi(2k+3)}\right\}. \quad (A9b)$$

APPENDIX IV

For $C_{11} \neq C_{22}$, the expression for E_0 in (26), is:

$$E_0(r_1, r_2) = \frac{q_2 r_1^2 d_2}{2(C_{11} - C_{22})}(C_{23} + C_{13})\ln(r_2/r_1) + \frac{(r_2^2 - r_1^2)}{4(C_{11} - C_{22})} \times \left\{(C_{13} - C_{23})q_2 d_2 + 2(C_{13} + C_{23})\left[q_1 d_2 + q_2 d_1 - \frac{2C_{11}q_2 d_2}{C_{11} - C_{22}}\right]\right\}, \quad (A10a)$$

and the expressions for E_n, $n = 1, \ldots \infty$, in (27), are

$$E_n(r_1, r_2) = \frac{(r_2^2 - r_1^2)}{2}\left[(C_{23} + C_{13})B_{0n} + \frac{1}{\pi}\frac{d_{5n}}{(C_{11} - C_{22})}(C_{13} - C_{23})\right] + \frac{1}{\pi}\frac{d_{5n}(C_{13} + C_{23})}{(C_{11} - C_{22})}\sum_{i=1}^{2}(-1)^i r_i^2 \ln(r_i a_n/2) + S_n, \quad (A10b)$$

where

$$S_n = \sum_{k=0}^{\infty}\sum_{i=1}^{2}(-1)^i\frac{r_i^{2k+4}\ln(r_i a_n/2)}{2k+4}B_{1nk}[(C_{23} + (2k+3)C_{13}] + \sum_{k=0}^{\infty}\sum_{i=1}^{2}(-1)^i\frac{r_i^{2k+4}}{2k+4}\left\{B_{2nk}[C_{23} + (2k+3)C_{13}] + B_{1nk}\frac{C_{13} - C_{23}}{2k+4}\right\}. \quad (A11)$$

For $C_{11} = C_{22}$, the expression for E_0 is

$$E_0(r_1,r_2)=\frac{-q_2r_1^2d_2}{8C_{11}}(C_{23}+C_{13})\ln^2(r_2/r_1)$$

$$+\frac{\ln(r_2/r_1)}{8C_{11}}\{r_1^2d_2(C_{13}-C_{23})q_2+r_1^2(C_{13}+C_{23})[(2q_1-q_2)d_2$$

$$+2q_2d_1]\}+\frac{(r_2^2-r_1^2)}{8C_{11}}(C_{23}-C_{13})[(q_2-q_1)d_2-q_2d_1], \qquad (A12a)$$

and the expressions for E_n, $n=1, \ldots \infty$, are

$$E_n(r_1,r_2)=\frac{(r_2^2-r_1^2)}{4}(C_{23}-C_{13})\left(\frac{d_{5n}}{2\pi C_{11}}-B_{0n}\right)$$

$$+\sum_{i=1}^{2}\frac{d_{5n}}{4\pi C_{11}}(C_{13}+C_{23})(-1)^i r_i^2\ln^2(r_ia_n/2)$$

$$+\frac{1}{2}\sum_{i=1}^{2}\left[\frac{d_{5n}(C_{13}-C_{23})}{2\pi C_{11}}+(C_{13}+C_{23})B_{0n}\right]$$

$$\times(-1)^i r_i^2\ln(r_ia_n/2)+S_n. \qquad (A12b)$$

In the event that $C_{11}(2k+3)^2=C_{22}$, the corresponding k term in the sum S_n in equation $(A11)$ is

$$\sum_{i=1}^{2}(-1)^i\frac{r_i^{2k+4}\ln^2(r_ia_n/2)}{2k+4}[C_{23}+(2k+3)C_{13}]B_{1nk}$$

$$+\sum_{i=1}^{2}(-1)^i\frac{r_i^{2k+4}\ln(r_ia_n/2)}{2k+4}\Big\{[C_{23}$$

$$+(2k+3)C_{13}]B_{2nk}+(C_{13}-C_{23})\frac{2B_{1nk}}{2k+4}\Big\}$$

$$+\sum_{i=1}^{2}(-1)^i\frac{r_i^{2k+4}}{(2k+4)^2}(C_{23}-C_{13})\left(\frac{2B_{1nk}}{2k+4}-B_{2nk}\right). \qquad (A13)$$

Thermal Expansion of Three-Phase Composite Materials

George J. Dvorak
Fellow, ASME

Tungyang Chen
Graduate Research Assistant.

Department of Civil Engineering,
Rensselaer Polytechnic Institute,
Troy, N.Y. 12180

Exact expressions are found for overall thermal expansion coefficients of a composite medium consisting of three perfectly-bonded transversely isotropic phases of cylindrical shape and arbitrary transverse geometry. The results show that macroscopic thermal expansion coefficients depend only on the thermoelastic constants and volume fractions of the phases, and on the overall compliance. The derivation is based on a decomposition procedure which indicates that spatially uniform elastic strain fields can be created in certain heterogeneous media by superposition of uniform phase thermal strains with local strains caused by piecewise uniform stress fields, which are in equilibrium with prescribed surface tractions. The procedure also allows evaluation of thermal stress fields in the aggregate in terms of known local fields caused by axisymmetric overall stresses. Finally, averages of local fields are found with the help of known mechanical stress and strain concentration factors.

1 Introduction

In his 1967 paper, Levin found that macroscopic thermal expansion coefficients of an elastic heterogeneous composite medium, consisting of two distinct, perfectly-bonded isotropic phases of arbitrary shape, depend in a unique way on the overall elastic moduli of the aggregate and on the thermoelastic constants of the phases. Such coefficients are the average overall strains caused by a uniform thermal change of unit magnitude in a traction-free composite. Levin's results, and their extension to binary systems with anisotropic constituents (Rosen and Hashin 1970), permit a direct evaluation of these coefficients in terms of the known overall elastic moduli and local thermoelastic constants. However, the approach cannot be applied to composites of three or more constituents without additional information about local stress concentration factors. Thermoelastic constants of such multiphase media can be bounded with the help of thermoelastic extremum principles (Schapery 1968, Rosen and Hashin 1970), or evaluated in terms of estimated values of phase stress concentration factors which are indicated by certain averaging techniques (Christensen, 1979), but their direct evaluation appears possible only in a few special cases. For example, Hashin (1984) recently found an exact relation between the thermal expansion coefficients and the bulk moduli of certain statistically isotropic polycrystalline aggregates.

Contributed by the Applied Mechanics Division of THE AMERICAN SOCIETY OF MECHANICAL ENGINEERS for presentation at the Joint ASCE/ASME Applied Mechanics, Biomechanics, and Fluids Engineering Conference, San Diego, CA, July 9 to 12, 1989.

Discussion of this paper should be addressed to the Editorial Department, ASME, United Engineering Center, 345 East 47th Street, New York, N.Y. 10017, and will be accepted until two months after final publication of the paper itself in the JOURNAL OF APPLIED MECHANICS. Manuscript received by ASME Applied Mechanics Division, April 28, 1988; final revision, September 14, 1988. Paper No. 89-APM-30.

This work is concerned with the macroscopic response of three-phase fibrous composite materials which are subjected to simultaneous increments of uniform thermal change and uniform overall stress or strain. In particular, we derive relationships between overall thermal expansion coefficients and the overall elastic moduli of a composite medium which consists of three perfectly-bonded cylindrical phases of arbitrary cross-section. Similar connections are found between mechanical and thermal microstress fields. Each of the phases can be transversely isotropic or isotropic; phase properties are assumed to be temperature independent within the applied increment. Unidirectional hybrid fiber composites, or binary systems reinforced by coated aligned fibers, can be regarded as particular examples of such three-phase media.

2 Governing Equations

The composite material under consideration consists of three perfectly-bonded homogeneous phases. Each of the phases is of cylindrical shape and is, at most, transversely isotropic about the "fiber" direction x_3 of a Cartesian coordinate system. In the transverse x_1x_2-plane, the cross-sections and the distributions of the phases can be arbitrary, providing that all such transverse sections are identical and the composite can be regarded as statistically homogeneous and free of voids. Overall isotropy in the transverse plane is permissible but not required; thus, the composite medium may have only one plane of elastic symmetry. The thermoelastic constants of the phases are known. Also, the overall elastic stiffness tensor **L** and the compliance tensor **M** of the aggregate are assumed to be known; they can be determined experimentally or estimated by various averaging methods. For example, the self-consistent method (Hershey, 1954; Budiansky, 1965; Hill, 1965), the Mori-Tanaka (1973) procedure, and the differential scheme (McLaughlin, 1977; Norris, 1985) lead to such

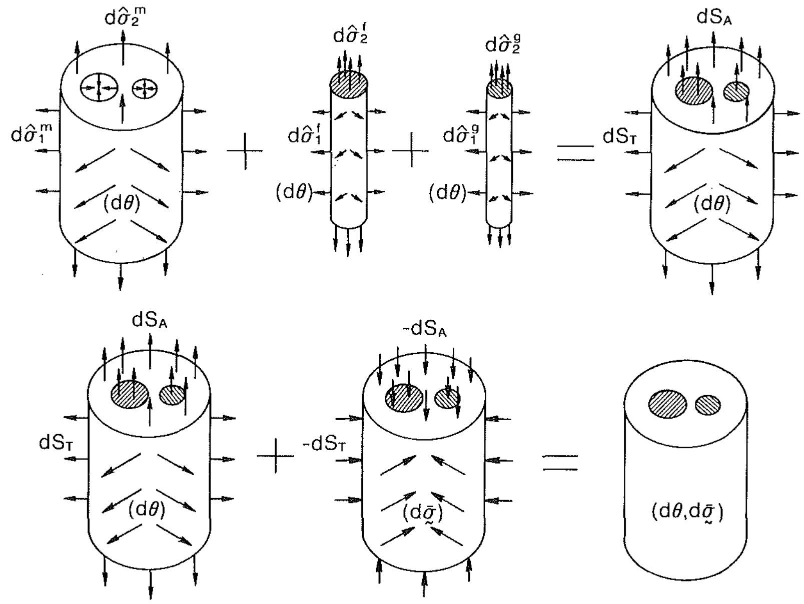

Fig. 1 Scheme of decomposition procedure

estimates. Also, Walpole (1984) gives bounds on overall mechanical properties of some of the multiphase materials considered herein.

A representative volume element V of the composite is selected and subjected to certain uniform overall stress $\bar{\sigma}_o$ or strains $\bar{\epsilon}_o$ which are imposed by prescribed surface tractions or displacements applied at the surface S of volume V. Also, a certain uniform thermal change has been applied such that θ_o is the current uniform temperature in V. Suppose that at this particular point of the loading sequence, the aggregate is subjected to simultaneous, uniform, infinitesimal increments of $d\theta$ and $d\bar{\sigma}$, or of $d\theta$ and $d\bar{\epsilon}$. The response of the aggregate to these load increments is described by the constitutive equations

$$d\bar{\epsilon} = \mathbf{M} d\bar{\sigma} + \mathbf{m} d\theta, \quad d\bar{\sigma} = \mathbf{L} d\bar{\epsilon} - \mathbf{l} d\theta, \tag{1}$$

where $\mathbf{L}$, $\mathbf{M}$ are the known (6×6) overall stiffness and compliance matrices, and $\mathbf{l}$, $\mathbf{m}$ are (6×1) overall thermal stress and strain vectors which are to be found in terms of $\mathbf{L}$ or $\mathbf{M}$, and the thermoelastic constants and volume fractions of the phases.

The thermoelastic properties and response of the transversely isotropic phases can be described by phase variants of equation (1). A particular form, which will be useful in the sequel, relates the axisymmetric stress and strain invariants of the transversely isotropic medium (Dvorak, 1986):

$$\begin{Bmatrix} d\epsilon_1 \\ d\epsilon_2 \end{Bmatrix} = \frac{1}{kE} \begin{bmatrix} n & -l \\ -l & k \end{bmatrix} \begin{Bmatrix} d\sigma_1 \\ d\sigma_2 \end{Bmatrix} + \begin{Bmatrix} \alpha \\ \beta \end{Bmatrix} d\theta \tag{2}$$

$$\begin{Bmatrix} d\sigma_1 \\ d\sigma_2 \end{Bmatrix} = \begin{bmatrix} k & l \\ l & n \end{bmatrix} \begin{Bmatrix} d\epsilon_1 \\ d\epsilon_2 \end{Bmatrix} - \begin{bmatrix} k\alpha + l\beta \\ l\alpha + n\beta \end{bmatrix} d\theta \tag{3}$$

where k, l, n are Hill's (1964) elastic moduli, $E = n - l^2/k$, $\alpha = 2\alpha_T$, $\beta = \alpha_L$, and α_T, α_L are the linear coefficients of thermal expansion in the transverse plane and in the longitudinal direction, respectively. For an isotropic phase with the usual elastic constants K, G, and ν, one finds that $k = G/(1-2\nu)$, $l = K - 2G/3$, and $n = K + 4G/3$. The strain and stress invariants are defined as:

$$d\epsilon_1 = d\epsilon_{11} + d\epsilon_{22}, \quad d\epsilon_2 = d\epsilon_{33},$$
$$d\sigma_1 = \tfrac{1}{2}(d\sigma_{11} + d\sigma_{22}), \; d\sigma_2 = d\sigma_{33}. \tag{4}$$

In the sequel, the three phases will be denoted by letters f, g, and m, or by a single letter $r = f, g, m$. For example, the phase volume fractions $c_f + c_g + c_m = 1$. Equations (2), (3), with appropriate values of thermoelastic constants, will describe the response of each phase to the respective axisymmetric invariants (4).

3 Decomposition Procedure

The unknown thermal stress and strain vectors $\mathbf{l}$, $\mathbf{m}$ of the three-phase composite medium will be found with a special form of the decomposition procedure of Dvorak (1983, 1986, 1987). In the first step of the procedure which is illustrated in Fig. 1, the three phases are separated and surface tractions or displacements which preserve the current local stresses $\boldsymbol{\sigma}_o^r$ and strains $\boldsymbol{\epsilon}_o^r$ are applied to each phase $r = f, g, m$. Then, a uniform thermal change $d\theta$ is applied to each phase. This causes uniform, but dissimilar thermal strains or stresses (2), (3), in the phases, so that the phases are no longer compatible and cannot be reassembled. To make the phases compatible, auxiliary uniform stress increments of as yet unknown magnitude are applied to each phase simultaneously with $d\theta$. These stress increments are limited to the components which appear in (4), and are axisymmetric, i.e., $d\sigma_{11} = d\sigma_{22}$. Therefore, the corresponding strains are also limited to those in (4), with $d\epsilon_{11} = d\epsilon_{22}$, and follow from (2). The auxiliary uniform fields in the separated phases, which are denoted in the sequel by top hats, are thus given by:

$$d\hat{\epsilon}_1^f = (n_f d\hat{\sigma}_1^f - l_f d\hat{\sigma}_2^f)/k_f E_f + \alpha_f d\theta, \tag{5}$$

$$d\hat{\epsilon}_1^g = (n_g d\hat{\sigma}_1^g - l_g d\hat{\sigma}_2^g)/k_g E_g + \alpha_g d\theta, \tag{6}$$

$$d\hat{\epsilon}_1^m = (n_m d\hat{\sigma}_1^m - l_m d\hat{\sigma}_2^m)/k_m E_m + \alpha_m d\theta, \tag{7}$$

$$d\hat{\epsilon}_2^f = (-l_f d\hat{\sigma}_1^f + k_f d\hat{\sigma}_2^f)/k_f E_f + \beta_f d\theta \tag{8}$$

$$d\hat{\epsilon}_2^g = (-l_g d\hat{\sigma}_1^g + k_g d\hat{\sigma}_2^g)/k_g E_g + \beta_g d\theta \tag{9}$$

$$d\hat{\epsilon}_2^m = (-l_m d\hat{\sigma}_1^m + k_m d\hat{\sigma}_2^m)/k_m E_m + \beta_m d\theta. \tag{10}$$

We recall that each of the contributing fields in (5) to (10) is axisymmetric and spatially uniform. Therefore, internal equilibrium and compatibility of the phases can be assured by the following conditions which relate the total uniform fields:

$$d\hat{\epsilon}_1^f = d\hat{\epsilon}_1^g = d\hat{\epsilon}_1^m \tag{11}$$

$$d\hat{\sigma}_1^f = d\hat{\sigma}_1^g = d\hat{\sigma}_1^m = dQ_T \tag{12}$$

$$d\hat{\epsilon}_2^f = d\hat{\epsilon}_2^g = d\hat{\epsilon}_2^m \tag{13}$$

$$c_f d\hat{\sigma}_2^f + c_g d\hat{\sigma}_2^g + c_m d\hat{\sigma}_2^m = dQ_A. \tag{14}$$

Here, dQ_A, dQ_T are the overall stress components which must be applied to the surface S of V while $d\hat{\sigma}_1^r$ and $d\hat{\sigma}_2^r$ are applied to the phases. They are defined by the overall forms of $(4_3, 4_4)$, but unless the composite medium has an axis of rotational symmetry x_3 they are not necessarily invariant in the overall stress space.

The fourteen equations (5) to (14) can be solved for the twelve stresses and strains $d\hat{\sigma}_1^r$, $d\hat{\sigma}_2^r$, $d\hat{\epsilon}_1^r$, $d\hat{\epsilon}_2^r$, and for dQ_A, dQ_T. The solution gives the magnitudes of the overall stress components dQ_A, and dQ_T, which, if applied together with the uniform thermal change $d\theta$, would create a spatially uniform incremental strain field in the heterogeneous medium. In reality, such overall stresses are not prescribed. Therefore, they must be eventually removed by application of $-dQ_A$, and $-dQ_T$ to the surface S of V.

The existence of the solution of the system of equations should be verified in each case, but if there are no special relationships between phase properties, the solution exists and can be found as follows: Equations (5) to (7) are substituted into (11), and (8) to (10) into (12). These, together with (13) and (14) are then solved in terms of $d\theta$. The result is:

$$dQ_A = s_A d\theta \tag{15}$$

$$dQ_T = s_T d\theta \tag{16}$$

where,

$$s_A = [(a_2 b_1 - a_1 b_2)s_T + a_3 b_1 - a_1 b_3]/(b_1 - a_1) \tag{17}$$

$$s_T = (B_{fm} C_{gf} - B_{fg} C_{mf})/(A_{gf} B_{fm} - B_{fg} A_{mf}) \tag{18}$$

with scalar quantities

$$A_{pq} = \left[\left(\frac{n_p}{k_p E_p} - \frac{n_q}{k_q E_q}\right) - \frac{l_p}{k_p}\left(\frac{l_p}{k_p E_p} - \frac{l_q}{k_q E_q}\right)\right] \tag{19}$$

$$B_{pq} = (l_p/k_p - l_q/k_q)/E_p \tag{20}$$

$$C_{pq} = l_p(\beta_q - \beta_p)/k_p + (\alpha_q - \alpha_p) \tag{21}$$

where the subscripts p, q, assume the phase designations f, g, m for the phase moduli k_r, l_r, n_r, and E_r; $p \neq q$.

The remaining terms in (17) are:

$$a_1 = c_f + c_g \frac{l_f}{k_f E_f} \cdot \frac{k_g E_g}{l_g} + c_m \frac{l_f}{k_f E_f} \cdot \frac{k_m E_m}{l_m} \tag{22}$$

$$a_2 = c_g \frac{k_g E_g}{l_g}\left(\frac{n_g}{k_g E_g} - \frac{n_f}{k_f E_f}\right) + c_m \frac{k_m E_m}{l_m}\left(\frac{n_m}{k_m E_m} - \frac{n_f}{k_f E_f}\right) \tag{23}$$

$$a_3 = c_g k_g E_g(\alpha_g - \alpha_f)/l_g + c_m k_m E_m(\alpha_m - \alpha_f)/l_m \tag{24}$$

$$b_1 = c_f + c_g E_g/E_f + c_m E_m/E_f \tag{25}$$

$$b_2 = c_g E_g\left(\frac{l_g}{k_g E_g} - \frac{l_f}{k_f E_f}\right) + c_m E_m\left(\frac{l_m}{k_m E_m} - \frac{l_f}{k_f E_f}\right) \tag{26}$$

$$b_3 = c_g E_g(\beta_f - \beta_g) + c_m E_m(\beta_f - \beta_m). \tag{27}$$

The solution of the system (5) to (14) can be written in the following form which reflects a change from the invariants (4) to the (6×1) vectors. The local auxiliary strain fields are:

$$\begin{aligned}
d\hat{\epsilon}_{11}^f &= d\hat{\epsilon}_{22}^f = \frac{1}{2}\, d\hat{\epsilon}_1^f = h_1 d\theta \\
d\hat{\epsilon}_{33}^f &= d\hat{\epsilon}_2^f = h_2 d\theta \\
d\hat{\epsilon}_{11}^g &= d\hat{\epsilon}_{22}^g = \frac{1}{2}\, d\hat{\epsilon}_1^g = h_1 d\theta \\
d\hat{\epsilon}_{33}^g &= d\hat{\epsilon}_2^g = h_2 d\theta \\
d\hat{\epsilon}_{11}^m &= d\hat{\epsilon}_{22}^m = \frac{1}{2}\, d\hat{\epsilon}_1^m = h_1 d\theta \\
d\hat{\epsilon}_{33}^m &= d\hat{\epsilon}_2^m = h_2 d\theta
\end{aligned} \tag{28}$$

where

$$h_1 = \frac{1}{2}\left(n_f s_T - l_f \frac{A_{gf} C_{mf} - A_{mf} C_{gf}}{A_{gf} B_{fm} - A_{mf} B_{fg}}\right)/(k_f E_f) + \frac{1}{2}\alpha_f \tag{29}$$

$$h_2 = \left(k_f \frac{A_{gf} C_{mf} - A_{mf} C_{gf}}{A_{gf} B_{fm} - A_{mf} B_{fg}} - l_f s_T\right)/(k_f E_f) + \beta_f. \tag{30}$$

The local auxiliary stress fields are:

$$\begin{aligned}
d\hat{\sigma}_{11}^f &= d\hat{\sigma}_{22}^f = d\hat{\sigma}_1^f = s_T d\theta \\
d\hat{\sigma}_{33}^f &= d\hat{\sigma}_2^f = \gamma s_T d\theta \\
d\hat{\sigma}_{11}^g &= d\hat{\sigma}_{22}^g = d\hat{\sigma}_1^g = s_T d\theta \\
d\hat{\sigma}_{33}^g &= d\hat{\sigma}_2^g = \rho s_T d\theta \\
d\hat{\sigma}_{11}^m &= d\hat{\sigma}_{22}^m = d\hat{\sigma}_1^m = s_T d\theta \\
d\hat{\sigma}_{33}^m &= d\hat{\sigma}_2^m = \psi s_T d\theta
\end{aligned} \tag{31}$$

where

$$\gamma = (A_{gf} C_{mf} - A_{mf} C_{gf})/(B_{fm} C_{gf} - B_{fg} C_{mf}) \tag{32}$$

$$\rho = D_{gf}/B_{gf} + C_{fg}/(s_T B_{gf}) \tag{33}$$

$$\psi = D_{mf}/B_{mf} + C_{fm}/(s_T B_{mf}) \tag{34}$$

and, with reference to the notation used in (19) to (21):

$$D_{pg} = \left[\left(\frac{n_p}{k_p E_p} - \frac{n_g}{k_g E_g}\right) - \frac{l_g}{k_g}\left(\frac{l_p}{k_p E_p} - \frac{l_g}{k_g E_g}\right)\right]. \tag{35}$$

The final results that appear in the sequel assume a more concise form with the definitions:

$$\begin{aligned}
\mathbf{h} &= [h_1,\ h_1,\ h_2,\ 0,\ 0,\ 0]^T \\
\mathbf{s} &= [s_T,\ s_T,\ s_A,\ 0,\ 0,\ 0]^T \\
\boldsymbol{\gamma} &= [1,\ 1,\ \gamma,\ 0,\ 0,\ 0]^T \\
\boldsymbol{\rho} &= [1,\ 1,\ \rho,\ 0,\ 0,\ 0]^T \\
\boldsymbol{\psi} &= [1,\ 1,\ \psi,\ 0,\ 0,\ 0]^T
\end{aligned} \tag{36}$$

where $[\ ]^T$ denotes a transpose and the coefficients appear in (17), (18), and (32) to (34).

In the final step of the decomposition procedure, the phases are reassembled and the auxiliary surface tractions are removed by application of overall stresses $-dQ_A$, $-dQ_T$. This leads to the results described in the next section.

4 Overall Properties and Local Fields

The aforementioned results make it possible to write directly the expression for the overall strain increment caused in the composite by superposition of simultaneous increments of $d\theta$ and $d\bar{\sigma}$, and also the expression for the overall stress increment in a composite subjected to simultaneous changes $d\theta$ and $d\bar{\epsilon}$:

$$d\bar{\epsilon} = \mathbf{h}\, d\theta + \mathbf{M}(d\bar{\sigma} - \mathbf{s}\, d\theta) \tag{37}$$

$$d\bar{\sigma} = \mathbf{s}\, d\theta + \mathbf{L}(d\bar{\epsilon} - \mathbf{h}\, d\theta). \tag{38}$$

A comparison with (1) yields the unknown overall thermal strain and stress vectors, which contain the desired overall thermal expansion coefficients:

$$\mathbf{m} = \mathbf{h} - \mathbf{M}\ \mathbf{s} \tag{39}$$

$$\mathbf{l} = -\mathbf{s} + \mathbf{L}\ \mathbf{h}. \tag{40}$$

To facilitate applications we note that the overall thermal strain vector

$$\mathbf{m} = [\alpha_1,\ \alpha_2,\ \alpha_3,\ \alpha_4,\ \alpha_5,\ \alpha_6]^T \tag{41}$$

and

$$\mathbf{l} = \mathbf{L}\ \mathbf{m}. \tag{42}$$

If the medium has only one plane of elastic symmetry perpendicular to x_3, then the overall compliance $\mathbf{M}$ in (39) depends on 13 independent elastic coefficients. Examples in Section 5 show that, in this case, $\alpha_4 = \alpha_5 = 0$. On the other hand, if the medium is transversely isotropic, then $\mathbf{m}$ can be written in the form

$$\mathbf{m} = [\alpha_T,\ \alpha_T,\ \alpha_A,\ 0,\ 0,\ 0]^T \tag{43}$$

where α_T, α_A are the overall linear coefficients of thermal expansion in the transverse plane and in the longitudinal directions, respectively. Then, using (39), one can find these coefficients in the explicit form:

$$\alpha_T = h_1 - \frac{1}{2(nk - l^2)}\ (ns_T - ls_A) \tag{44}$$

$$\alpha_A = h_2 - \frac{1}{nk - l^2}\ (ks_A - ls_T). \tag{45}$$

If the volume fraction of one of the phases is reduced to zero, then one recovers from these formulae the results for binary composites given by Dvorak (1986).

Note also that the decomposition procedure suggests the following connection between thermal microstress fields in the composite and mechanical microstress fields under axisymmetric uniform overall stresses. In particular, suppose that latter are written in the form

$$d\sigma(x_i) = \mathbf{B}(x_i)\ d\bar{\sigma} \tag{46}$$

where $\mathbf{B}(x_i)$ describes the spatial distribution of the local stresses under any overall stress $d\bar{\sigma}$. As a minimum, $\mathbf{B}(x_i)$ must describe the response to axisymmetric uniform stresses $d\bar{\sigma}_{11} = d\bar{\sigma}_{22} = d\bar{\sigma}_1$, and $d\bar{\sigma}_{33} = d\bar{\sigma}_2$. According to the decomposition sequence, the local thermal stresses after the reassembly of the aggregate are given by (31). In the final step, one must remove the axisymmetric surface stresses dQ_A, dQ_T, represented by $\mathbf{s}$ in (36). Of course, that can be done using (46) to yield:

$$\begin{aligned}
&\text{In phase } f\text{:}\ d\sigma(x_i) = s_T\ \gamma + \mathbf{B}(x_i)(d\bar{\sigma} - \mathbf{s}d\theta)\\
&\text{In phase } g\text{:}\ d\sigma(x_i) = s_T\ \rho + \mathbf{B}(x_i)(d\bar{\sigma} - \mathbf{s}d\theta)\\
&\text{In phase } m\text{:}\ d\sigma(x_i) = s_T\ \psi + \mathbf{B}(x_i)(d\bar{\sigma} - \mathbf{s}d\theta)
\end{aligned} \tag{47}$$

where $d\theta$ and $d\bar{\sigma}$ are the prescribed uniform thermal change and overall stress vector, respectively.

Similarly, if instead of (46), there is a known connection between local and overall strains in the form:

$$d\epsilon(x_i) = \mathbf{A}(x_i)d\bar{\epsilon} \tag{48}$$

then one finds from (28) and (36) the local strain field in the aggregate loaded by a uniform thermal change $d\theta$ and an arbitrary overall strain $d\bar{\epsilon}$:

$$d\epsilon(x_i) = \mathbf{h}d\theta + \mathbf{A}(x_i)(d\bar{\epsilon} - \mathbf{h}\ d\theta). \tag{49}$$

These results can be readily reduced to those for average stresses and strains in the phases. If the mechanical stress and strain concentration factors $\mathbf{B}_r$ and $\mathbf{A}_r$ of the phases are known, then the local averages can be written in the form

$$\begin{aligned}
d\sigma_r &= \mathbf{B}_r d\bar{\sigma} + \mathbf{b}_r d\theta\\
d\epsilon_r &= \mathbf{A}_r d\bar{\epsilon} - \mathbf{a}_r d\theta \qquad (r = f,g,m)
\end{aligned} \tag{50}$$

where the phase thermal stress concentration factors are:

$$\begin{aligned}
\mathbf{b}_f &= s_T\gamma - \mathbf{B}_f\mathbf{s}\\
\mathbf{b}_g &= s_T\rho - \mathbf{B}_g\mathbf{s}\\
\mathbf{b}_m &= s_T\psi - \mathbf{B}_m\mathbf{s}\\
\mathbf{a}_r &= (\mathbf{A}_r - \mathbf{I})\mathbf{h}, \qquad r = (f,g,m).
\end{aligned} \tag{51}$$

5 Examples

To illustrate the results (39) to (42) we consider first a three-phase composite with transversely isotropic phases. Overall material symmetry elements are limited to a single plane of elastic symmetry with the normal x_3. The overall compliance matrix $\mathbf{M}$ has the following form:

$$\mathbf{M} = \begin{bmatrix} M_{11} & M_{12} & M_{13} & 0 & 0 & M_{16}\\ M_{12} & M_{22} & M_{23} & 0 & 0 & M_{26}\\ M_{13} & M_{23} & M_{33} & 0 & 0 & M_{36}\\ 0 & 0 & 0 & M_{44} & M_{45} & 0\\ 0 & 0 & 0 & M_{45} & M_{55} & 0\\ M_{16} & M_{26} & M_{36} & 0 & 0 & M_{66} \end{bmatrix}. \tag{52}$$

The stiffness matrix $\mathbf{L}$ is formally similar to $\mathbf{M}$. Now, $\mathbf{h}$ is taken from (36) and substituted, together with $\mathbf{M}$, into (39). That leads to an explicit form of (41):

$$\mathbf{m} = \begin{bmatrix} h_1 - M_{11}s_T - M_{12}s_T - M_{13}s_A\\ h_1 - M_{12}s_T - M_{22}s_T - M_{23}s_A\\ h_2 - M_{13}s_T - M_{23}s_T - M_{33}s_A\\ 0\\ 0\\ -M_{16}s_T - M_{26}s_T - M_{36}s_A \end{bmatrix}. \tag{53}$$

One also finds from (40) that

$$\mathbf{l} = \begin{bmatrix} -s_T + L_{11}h_1 + L_{12}h_1 + L_{13}h_2\\ -s_T + L_{12}h_1 + L_{22}h_1 + L_{23}h_2\\ -s_A + L_{13}h_1 + L_{23}h_1 + L_{33}h_2\\ 0\\ 0\\ L_{16}h_1 + L_{26}h_1 + L_{36}h_2 \end{bmatrix}. \tag{54}$$

If the arrangement of the three transversely isotropic phases is such that the composite medium is transversely isotropic, then the coefficients $M_{16} = M_{26} = M_{36} = M_{45} = 0$ in (50) and also, $L_{16} = L_{26} = L_{36} = L_{45} = 0$. The specific forms of (41) and (42) then follow in an obvious manner from (53) and (54).

6 Conclusion

The results represent exact connections between overall elastic thermal stress and strain vectors, overall stiffness $\mathbf{L}$ or compliance $\mathbf{M}$, and phase thermoelastic properties of a three-phase composite medium consisting of perfectly-bonded cylindrical phases of arbitrary transverse geometry. They remain formally unchanged, except for $\mathbf{L}$ and $\mathbf{M}$, if the overall elastic symmetry properties of the composite are modified within the indicated constraints. Application of the decomposition procedure is limited to such combinations of phase properties for which the governing equations can be solved. The exceptional cases can be established by examination of (17) and (18). For example, one such exception would arise if all three phases were isotropic and if any two of them had the same Poisson's ratio. Another such exception occurs when the three phases have identical mechanical properties but different thermal expansion coefficients. Furthermore, in an n-phase fibrous medium the decomposition leads to $5n - 1$ equations for $4n + 2$ unknowns. Hence, the system can be solved for $n = 3$, and it allows a choice of an additional constraint if $n = 2$. This last property was utilized by Dvorak (1986) in an application of this procedure to binary fibrous systems with an elastic-plastic matrix.

A particularly useful result is given by (47) and (49) which show that not only the overall response (37) and (38), but also the local thermal fields can be evaluated from known mechanical fields by a modification of the overall stress or strain increment, and by an addition of a piecewise uniform stress field or a uniform strain field.

Acknowledgments

The authors wish to acknowledge useful discussions with Prof. Yakov Benveniste. Funding for this work was provided in part, by the DARPA-HiTASC program at RPI, and by the Mechanics Division of the Office of Naval Research.

References

Budiansky, B., 1965, "On the Elastic Moduli of Some Heterogeneous Materials," *Journal of the Mechanics and Physics of Solids*, Vol. 13, p. 223.

Christensen, R. M., 1979, *Mechanics of Composite Materials*, John Wiley and Sons, New York.

Dvorak, G. J., 1983, "Metal Matrix Composites: Plasticity and Fatigue," *Mechanics of Composite Materials: Recent Advances*, Z. Hashin and C. T. Herakovich, eds., Pergamon Press, pp. 73-91.

Dvorak, G. J., 1986, "Thermal Expansion of Elastic-Plastic Composite Materials," ASME JOURNAL OF APPLIED MECHANICS, Vol. 53, pp. 737-743.

Dvorak, G. J., 1987, "Thermomechanical Deformation and Coupling in Elastic-Plastic Composite Materials," *Thermomechanical Couplings in Solids*, H. D. Bin, and Q. S. Nguyen, eds., North-Holland, pp. 43-54.

Hashin, Z., 1984, "Thermal Expansion of Polycrystalling Aggregates. I. Exact Analysis," *Journal of the Mechanics and Physics of Solids*, Vol. 32, pp. 149-158.

Hershey, A. V., 1954, "The Elasticity of an Isotropic Aggregate of Anisotropic Cubic Crystals," ASME JOURNAL OF APPLIED MECHANICS, Vol. 21, pp. 236-240.

Hill, R., 1964, "Theory of Mechanical Properties of Fiber-Strengthened Materials: I. Elastic Behaviour," *Journal of the Mechanics and Physics of Solids*, Vol. 12, pp. 199-212.

Hill, R., 1965, "A Self-Consistent Mechanics of Composite Materials," *Journal of the Mechanics and Physics of Solids*, Vol. 13, pp. 213-222.

Levin, V. M., 1967, "Thermal Expansion Coefficients of Heterogeneous Materials," *Mekhanika Tverdogo Tela*, Vol. 2, pp. 88-94.

McLaughlin, R., 1977, "A Study of the Differential Scheme for Composite Materials," *International Journal of Engineering Science*, Vol. 15, pp. 237-244.

Mori, T., and Tanaka, K., 1973, "Average Stress in Matrix and Average Elastic Energy of Materials with Misfitting Inclusions," *Acta Metal*, Vol. 21, p. 571.

Norris, A. N., 1985, "A Differential Scheme for the Effective Moduli of Composites," *Mechanics of Materials*, Vol. 4, pp. 1-16.

Rosen, B. W., and Hashin, Z., 1970, "Effective Thermal Expansion Coefficients and Specific Heats of Composite Materials," *International Journal of Engineering Science*, Vol. 8, pp. 157-173.

Schapery, R. A., 1968, "Thermal Expansion Coefficients of Composite Materials Based on Energy Principles," *Journal of Composite Materials*, Vol. 2, pp. 380-404.

Walpole, L. J., 1984, "The Analysis of the Overall Elastic Properties of Composite Materials," *Fundamentals of Deformation and Fracture*, B. A. Bilby, K. J. Miller, J. R. Willis, eds., pp. 91-107.

Andrei Smirnov
Department of Mathematics and Mechanics,
Leningrad University,
Leningrad, U.S.S.R.

Free Vibrations of the Rotating Shells of Revolution[1]

1 Introduction

This paper is devoted to the problems of free vibrations of thin rotating shells. The theory of vibration of rotating shells is part of the theory of an arbitrary rotating body and the results which are valid for an arbitrary body are also valid for the shells. Though numerical methods are the main approach to the investigation of the dynamics of rotating bodies, some analytical results have been obtained for some simple bodies like rotating beams and discs. The mathematical theory of nonrotating thin shells is well developed. Several of the most successful are two-dimensional theories of the Kirckhoff-Love type. Using the Novozhilov shell theory, which is of this type, A. L. Goldenveiser, V. B. Lidsky, and P. E. Tovstik have developed the theory of asymptotic integration of the equation of vibration of shells. This theory allows one to estimate and, in some cases, to find analytical solutions for the eigenvalues. The main results of this theory are presented by Goldenveiser et al. (1979).

The aim of this paper is to apply asymptotic methods to the solution of the eigenvalue problem for a rotating shell. We will use Novozhilov's two-dimensional shell theory to obtain the equations for the vibration of the shell and the theory of asymptotic integration of the differential equation to solve the eigenvalue problem for these equations.

For the last few years the analytical approach to the solution of the eigenvalue problem for a rotating shell has become popular. In the list of references we only mention research which deals with the application of two-dimensional theories for obtaining the equation of vibration and papers devoted to the mathematical consideration of these equations. Unfortunately, space does not permit a detailed description of these works.

2 Geometry of a Shell

Consider the thin shell of revolution of constant thickness h. To describe the shell geometry we introduce an orthogonal curvilinear coordinate system, connected with the meridans and parallels of a shell. A position of a point on the neutral surface of a shell is defined by a longitudinal angle $\alpha(0 \leq \alpha < 2\pi)$ and the length of the arc of meridan $s(s_1 \leq s \leq s_2)$. The shell is limited to two parallels $s = s_1$ and $s = s_2$. As a particular case, a shell may be closed at the top (sphere, cupola).

The geometry of the shell is characterized by the function $B(s)$, which is the distance between the axis of symmetry and the neutral surface (see Fig. 1). We will also use functions R_1 and R_2, which are the main radii of a curvature and function $\theta(s)$, which is the angle between the initial normal to the neutral surface and the axis of symmetry. These functions are expressed through the function B:

$$\frac{1}{R_1} = \frac{d\theta}{ds} = -\frac{B''}{\sqrt{1-B'^2}}\,,\ \frac{1}{R_2} = \frac{\sin\theta}{B} = \frac{\sqrt{1-B'^2}}{B},$$

$$\cos\theta = B',\ 0 \leq \theta < \pi.$$

At each point of the neutral surface we introduce a local system of cartesian coordinates, the axes of which are the tangent to the meridan, the tangent to the parallel, and the initial normal. **U** is a displacement vector with components u, v, w in the local coordinate system.

The shell rotates with the constant angular velocity Ω around the axis of symmetry.

We use the following notation:

E = Young's modulus
σ = Poisson's ratio
ρ = density of the shell material
l = the length of the cylindric shell
ϵ_k, ω = components of the tangential deformation and the angle of the elastic rotations
T,Π = kinetic and potential energies
t = time

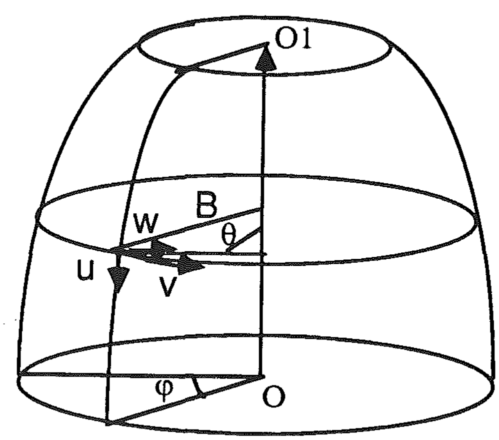

Fig. 1 The geometry of the shell of revolution

[1]This paper was prepared by Dr. Smirnov during his participation in the official exchange between Carleton University, Ottawa, Ontario, Canada and the State University of Leningrad.

Contributed by the Applied Mechanics Division of The American Society of Mechanical Engineers for presentation at the Joint ASCE/ASME Applied Mechanics, Biomechanics, and Fluids Engineering Conference, San Diego, Calif., July 9 to 12, 1989.

Discussion of this paper should be addressed to the Editorial Department, ASME, United Engineering Center, 345 East 47th Street, New York, N.Y. 10017, and will be accepted until two months after final publication of the paper itself in the Journal of Applied Mechanics. Manuscript received by ASME Applied Mechanics Division, January 13, 1988; final revision, May 1, 1988.

Paper No. 89-APM-23.

We will nondimensionalize the variables as follows:

$$(\mathbf{U},u,v,w,R_k,B,s,l)=R^{-1}(\mathbf{U}^*,u^*,v^*,w^*,R_k^*,B^*,s^*,l^*),$$

$$(\epsilon_k,\omega)=(\epsilon_k^*,\omega^*),\ t=k^{-1}t^*,\ k=R\sqrt{\frac{\rho(1-\nu^2)}{E}},$$

$$h=(R\sqrt{12})^{-1}h^*,\ (\omega,\Omega)=k(\omega^*,\Omega^*),$$

$$(T,\Pi)=(1-\nu^2)(Eh^*)^{-1}(T^*,\Pi^*),$$

where R is a characteristic radius of a shell. For example, if $B(s_1)\neq 0$ we can assume $R=B(s_1)$.

3 The Equation of a Motion

There are various ways to get the equations of vibration of a rotating shell. We will use Hamilton's principle. The mathematical formulation of this principle is

$$\delta(T-\Pi)=0, \tag{1}$$

where T is the kinetic energy of the shell and Π is the potential energy of the shell. δ is a symbol of variation. If $\mathbf{V}$ is the velocity of a shell element, the kinetic energy of the shell will be

$$T=\frac{1}{2}\int_0^{2\pi}\int_{s_1}^{s_2}\mathbf{V}^2Bdsd\varphi,\ \mathbf{V}=\mathbf{\Omega}\times(\mathbf{r}+\mathbf{U})+\dot{\mathbf{U}}, \tag{2}$$

where $\mathbf{r}$ is a radius vector to a point on the neutral surface. Here we take only the linear displacements terms. In the work by Vorobiov and Detistov (1981a) some nonlinear terms were retained.

The potential energy Π may be expressed as

$$\Pi=\frac{1}{2}\int_0^{2\pi}\int_{s_1}^{s_2}\Pi Bdsd\varphi, \tag{3}$$

Here the second Π is a strain energy density. We will consider it as a function of the displacements and their first derivatives.

If we substitute expressions (2) and (3) into (1) we obtain the equation of vibration

$$\int_0^{2\pi}\int_{s_1}^{s_2}(\rho\ddot{\mathbf{U}}+\rho\mathbf{\Omega}\times[\mathbf{\Omega}\times(\mathbf{r}+\mathbf{U})]+2\rho\mathbf{\Omega}\times\dot{\mathbf{U}}$$
$$+\nabla\Pi[\mathbf{U}])\delta\mathbf{U}Bdsd\varphi=0, \tag{4}$$

where

$$\nabla\Pi=\frac{\partial\Pi}{\partial\mathbf{U}}-\frac{1}{B}\frac{\partial}{\partial s}\left(B\frac{\partial\Pi}{\partial\mathbf{U}_s'}\right)-\frac{\partial}{\partial\varphi}\frac{\partial\Pi}{\partial\mathbf{U}_\varphi'}.$$

For arbitrary elastic bodies this equation has been obtained by Vilke (1986), using the Lagrange-D'Alembert's principle. The precise form of the density Π depends on the type of shell theory used. We will discuss this problem next. The only condition, which the shell theory must satisfy, is that the reciprocity principle of Betti is valid. More details about the application of Betti's principle in the theory of shells can be found in Goldenveizer's monograph (1961).

Equation (4) is valid for all theories of shells in which the strain energy density is only a function of the displacements and their derivatives, for example, theories of the Kirchoff-Love type. Theories of other types may include additional independent variables. For example, in Reisner's shell theory, the two angles of rotation of the normal to shell element are independent quantities. Using this theory of shells the equation for the vibrations of a cone was obtained by Vorobiov and Detistov (1981a).

We will investigate small vibrations of shells about the axisymmetric equilibrium state generated by centrifugal forces. We represent the displacement $\mathbf{U}(s,\varphi,t)$ as a combination of an initial axisymmetrical displacement $\mathbf{U}^0(s)$ and an additional displacement $\mathbf{U}^1(s,\varphi,t)$

$$\mathbf{U}(s,\varphi,t)=\mathbf{U}^0(s)+\mathbf{U}^1(s,\varphi,t). \tag{5}$$

The expressions for the vectors $\mathbf{r}$ and $\mathbf{\Omega}$ in a local system of coordinates will be

$$\mathbf{r}=(B\cos\theta,0,-B\sin\theta),\ \mathbf{\Omega}=(-\Omega\sin\theta,0,-\Omega\cos\theta). \tag{6}$$

Since strain energy density Π is positive and we are only considering small deformations, we may assume that this density is a quadratic form of the deformations and the angles of rotations. The actual expressions for the deformations and angles of rotation will be introduced next. For now, we write them in the form

$$x_i=\sum_j a_{ij}y_i+\sum_j b_{ij}y_i^2$$

Here x is any deformation or angle of rotation and y is a displacement or its derivative. Geometrical linear shell theory assumes $b_{ij}=0$.

Now we represent the strain energy density in the next form

$$\Pi[\mathbf{U}^1,\mathbf{U}^0]=\Pi[\mathbf{U}^1]+\Pi_F[\mathbf{U}^1,U^0]+\Pi_0[\mathbf{U}^0]$$
$$+\Pi_\Omega[\mathbf{U}^1,\mathbf{U}^0]+\Pi_*[\mathbf{U}^1,\mathbf{U}^0]. \tag{7}$$

Here $\Pi[\mathbf{U}^1]$ is the quadratic form of the displacements $\mathbf{U}$. $\Pi_F[\mathbf{U}^1,\mathbf{U}^0]$ is the linear form with respect to both $\mathbf{U}^1$ and $\mathbf{U}^0$. $\Pi_0[\mathbf{U}^0]$ is a term depending only on $\mathbf{U}^0$. $\Pi_\Omega[\mathbf{U}^1,\mathbf{U}^0]$ is the quadratic form with respect to $\mathbf{U}^1$ and the linear form with respect to $\mathbf{U}^0$, in $\Pi_*[\mathbf{U}^1,\mathbf{U}^0]$ we include all other items. In our consideration we will neglect the last item. We will also omit the index "1" for the displacement.

Substituting expressions (5–7) into equation (4), and taking into account the independence of the coordinates, we get two vector equations:

$$L_F(\mathbf{U}^0)=\mathbf{F}, \tag{8}$$

$$L(\mathbf{U})+\Omega^2L_\Omega[\mathbf{U}^0,\mathbf{U}]=\ddot{\mathbf{U}}+2\Omega L_C\dot{\mathbf{U}}+\Omega^2L_e\mathbf{U}, \tag{9}$$

where

$$L_C=\begin{pmatrix}0 & \cos\theta & 0\\ -\cos\theta & 0 & \sin\theta\\ 0 & -\sin\theta & 0\end{pmatrix},$$

$$L_e=\begin{pmatrix}-\cos^2\theta & 0 & \sin\theta\cos\theta\\ 0 & -1 & 0\\ \sin\theta\cos\theta & 0 & -\sin^2\theta\end{pmatrix},$$

$$L_F(\mathbf{U}^0)=-\nabla\Pi_F[\mathbf{U}^0,\mathbf{U}],\quad L_\Omega(\mathbf{U}^0,\mathbf{U})=-\frac{1}{\Omega^2}\nabla\Pi_\Omega[\mathbf{U}^0,\mathbf{U}],$$
$$L(\mathbf{U})=-\nabla\Pi[\mathbf{U}],\quad \mathbf{F}=\Omega^2\mathbf{r}=\Omega^2(B\cos\theta,0,-B\sin\theta). \tag{10}$$

From equation (8) we can find the initial displacements and stresses in a shell, which we will substitute into the equation of free vibration of a shell (9). Operator L corresponds to the nonrotating shell. Operator L_Ω describes the change of the geometry of shell and the existence of the initial stresses. The equation of vibration of rotating shells was obtained in a number of papers for different kinds of shell geometry (most often for cylinders) under different assumptions for different types of shell theories. Some of these papers are listed in the references. In these papers the equation of vibration has the different operators L and L_Ω and depend on the type of shell theory and assumptions about the initial equilibrium. However, for all theories of the Kirckhoff-Love type, the differences in operators L will be only in terms of order h^2 and higher.

The scalar product of the vectors $\mathbf{U}_k$ and $\mathbf{U}_l$ are determined by the formula

$$(\mathbf{U}_k, \mathbf{U}_l) = \int_{s_1}^{s_2} (u_k u_l + v_k v_l + w_k w_l) B ds.$$

For a large class of boundary conditions all operators included in equation (9) are self-adjoint, i.e.,

$$(L\mathbf{U}_k, \mathbf{U}_l) = (L\mathbf{U}_l, \mathbf{U}_k). \tag{11}$$

For that it is only necessary for the principle of Betti to be valid. We will use only those boundary conditions, which are usually called "idealized." For example, the boundary conditions of free, clamped, and freely-supported edges are of that kind. All idealized boundary conditions are linear, hence,

$$\Gamma(\mathbf{U}) = 0, \quad \Gamma(\mathbf{U}^0) = 0$$

are boundary conditions for the initial and additional displacements.

4 The Form of Solution

For linear and homogeneous boundary conditions we can search the solution of equation (9) in a form of "running waves," that is

$$u(s,\varphi,t) = \sum_{m=0}^{\infty} \sum_{k=-\infty}^{\infty} \sum_{l=1}^{2} u_{mk}(s) C_{mk}^{l} \cos(m\varphi + \omega_{mk} t - \alpha^l)$$

$$v(s,\varphi,t) = \sum_{m=0}^{\infty} \sum_{k=-\infty}^{\infty} \sum_{l=1}^{2} v_{mk}(s) C_{mk}^{l} \sin(m\varphi + \omega_{mk} t - \alpha^l),$$

$$w(s,\varphi,t) = \sum_{m=0}^{\infty} \sum_{k=-\infty}^{\infty} \sum_{l=1}^{2} w_{mk}(s) C_{mk}^{l} \cos(m\varphi + \omega_{mk} t - \alpha^l),$$

$$\alpha^1 = 0, \quad \alpha^2 = \frac{\pi}{2}. \tag{12}$$

where α^l is the phase, m is the wave number along a parallel, and ω_{mk} is the frequency of the free vibrations. Since the boundary conditions and equations of vibrations are linear, we can consider the vibrations separately for each wave number m. The equation of vibration of a shell for fixed m is

$$L_m(\mathbf{U}_m) + \Omega^2 L_{\Omega m}(\mathbf{U}_m) + \omega_m^2 \mathbf{U}_m + 2\omega_m \Omega L_{Cm} \mathbf{U}_m + \Omega^2 L_{em} \mathbf{U}_m = 0, \quad \Gamma(\mathbf{U}_m) = 0, \tag{13}$$

where

$$L_{Cm} = \begin{pmatrix} 0 & -\cos\theta & 0 \\ -\cos\theta & 0 & \sin\theta \\ 0 & \sin\theta & 0 \end{pmatrix},$$

$$L_{em} = \begin{pmatrix} \cos^2\theta & 0 & -\sin\theta\cos\theta \\ 0 & 1 & 0 \\ -\sin\theta\cos\theta & 0 & \sin^2\theta \end{pmatrix}.$$

The operators L_m and $L_{\Omega m}$ are operators L and L_Ω for fixed m. Further, we will consider the problem for fixed m and omit the index "m" for both variables and operators.

It is useful to write the energy equation corresponding to vector equation (9). Multiplying it by $\mathbf{U}$, we obtain:

$$\omega^2 T + 2\omega\Omega T_C + \Omega^2 T_e = \Pi + \Pi_\Omega, \tag{14}$$

where

$$(\mathbf{U},\mathbf{U}) = \int_{s_1}^{s_2} (u^2 + v^2 + w^2) B ds = 2T,$$

$$(L(\mathbf{U}),\mathbf{U}) = -(\nabla\Pi[\mathbf{U}],\mathbf{U}) = -2\int_{s_1}^{s_2} \Pi B ds = -2\Pi,$$

$$(L_\Omega(\mathbf{U}),\mathbf{U}) = = -(\nabla\Pi_\Omega[\mathbf{U}_0,\mathbf{U}],\mathbf{U})$$

$$= -\frac{2}{\Omega^2}\int_{s_1}^{s_2} \Pi_\Omega B ds = -2\Pi_\Omega,$$

$$(L_C(\mathbf{U}),\mathbf{U}) = -2\int_{s_1}^{s_2} (\cos\theta u - \sin\theta w) v B ds = 2T_C,$$

$$(L_e(\mathbf{U}),\mathbf{U}) = \int_{s_1}^{s_2} ((\cos\theta u - \sin\theta w)^2 + v^2) B ds = 2T_e.$$

Here Π is the potential energy of the additional displacements, Π_Ω is the potential energy of the initial stresses and displacements, and T is the kinetic energy of the relative motion. All energies are computed for the fixed mode.

It is known that the nonrotating shell of revolution has a series of frequencies of free vibrations and modes, for which

$$\omega_k = \omega_{-k}, \quad \mathbf{U}_k = \mathbf{U}_{-k}. \tag{15}$$

That is, two running waves propagate in opposite directions along the parallel with equal angular speeds. The relations (15) can be used to transform expressions (12). We consider the sum of two waves, running in opposite directions for fixed k, with the arbitrary constant in a form

$$C_k^1 = C_{-k}^1, \quad C_k^2 = C_{-k}^2 = 0. \tag{16}$$

Thus, for the displacement u, we get

$$u = C u_k \cos m\varphi \sin\omega_k t. \tag{17}$$

This is a standing wave, oscillating with a frequency ω_k.

Now consider the case of a rotating shell. For the rotating shell the expressions (15) are not valid. We introduce the parameters α and β as

$$\alpha = \frac{1}{2}(\omega_k - \omega_{-k}), \quad \beta = \frac{1}{2}(\omega_k + \omega_{-k})$$

and amplitude vectors as

$$\mathbf{U}_k^1 = \mathbf{U}_k + \mathbf{U}_{-k}, \mathbf{U}_k^2 = \mathbf{U}_k - \mathbf{U}_{-k}.$$

The arbitrary constants are determined by expression (16). Making the same transformations we get

$$u = C(u_k^1 \cos(m\varphi + \beta t)\cos\alpha t + u_k^2 \sin(m\varphi + \beta t)\sin\alpha t). \tag{18}$$

This is a superposition of the two standing waves, oscillating with a frequency α and precessing with the angular velocity β/m. It is clear that for nonrotating shell $\alpha = \omega_k$, $\beta = 0$, $\mathbf{U}^2 = 0$, and expression (18) transforms into expression (17). The reader has to pay attention that the rotation generates both precession of the modes and shift of the frequency of oscillation.

5 Application of a Small Disturbance Method

Let Ω be the small parameter. The correctness of such an assumption has been discussed by Smirnov and Tovstik (1981) and Lidsky and Tovstik (1984). We expand frequencies ω_k and amplitude vectors $\mathbf{U}_k$ in a series of the parameter Ω, that is

$$\omega_k = \alpha(\Omega) + \beta(\Omega), \ \omega_{-k} = -\alpha(\Omega) + \beta(\Omega)$$

$$\alpha(\Omega) = \omega_0 + \sum_{i=1}^{\infty} \Omega^{2i}\alpha_{2i}, \beta(\Omega) = \sum_{i=0}^{\infty} \Omega^{2i+1}\beta_{2i+1},$$

$$\mathbf{U}_k(\Omega) = \sum_{i=0}^{\infty} (-1)^i \mathbf{U}_i \Omega^i. \tag{19}$$

The frequency ω_0 is the corresponding frequency of the nonrotating shell. It is obvious that $\alpha(0) = \omega_0$ and $\beta(0) = 0$. Substituting these expressions (19) into equation (13), and equating the coefficients for equal powers of Ω, we get

$$L\mathbf{U}_0 + \omega_0^2\mathbf{U}_0 = 0, \quad \Gamma(\mathbf{U}_0) = 0$$
$$L\mathbf{U}_1 + \omega_0^2\mathbf{U}_1 = -2\omega_0(L_C\mathbf{U}_0 + \beta_1\mathbf{U}_0), \quad \Gamma(\mathbf{U}_1) = 0$$
$$L\mathbf{U}_2 + \omega_0^2\mathbf{U}_2 = -2\omega_0(L_C\mathbf{U}_1 + \beta_1\mathbf{U}_1) - (2\omega_0\alpha_2 + \beta_1^2)\mathbf{U}_0 - $$
$$- 2\beta_1 L_C\mathbf{U}_0 - L_e\mathbf{U}_0 - L_\Omega\mathbf{U}_0, \quad \Gamma(\mathbf{U}_2) = 0. \tag{20}$$

These equations determine the amplitude vectors $\mathbf{U}$ and free frequencies ω. The first equation gives the free frequencies and modes of the nonrotating shell. To obtain the coefficient β_1, we scalar multiply the second equation by $\mathbf{U}_0$ and apply the property of self-adjoint operators (11). Hence,

$$\beta = \beta_1\Omega + O(\Omega^3), \quad \beta_1 = -\frac{T_C(\mathbf{U}_0)}{T(\mathbf{U}_0)}. \tag{21}$$

The speed of precession is determined by β/m.

Applying the same method we can find all the coefficients in the series α and β. We write only the second term for α.

$$\alpha_2 = \frac{\beta_1^2}{2\omega_0} - \frac{(L_C\mathbf{U}_1, \mathbf{U}_0) + \beta_1(\mathbf{U}_1, \mathbf{U}_0)}{2T(\mathbf{U}_0)} + \frac{T_e(\mathbf{U}_0) + \Pi_\Omega(\mathbf{U}_0)}{2\omega_0 T(\mathbf{U}_0)}. \tag{22}$$

Later we will call β_1 the coefficient of bifurcation and α_2 the coefficient of shift. We will assume that it is possible to neglect the second term in formula (22). This assumption has been verified by Smirnov and Tovstik (1982) for some special cases, for example, the low frequency vibrations of shells of zero curvature. However, in the general case, the error of this assumption has not yet been established. With this assumption, the formula for α may be rewritten in the form

$$\alpha = \alpha_2\Omega^2(1 + O(\Omega^2)), \ \alpha_2 = \frac{1}{2\omega_0}\left(\beta_1^2 + \frac{T_e(\mathbf{U}_0) + \Pi_\Omega(\mathbf{U}_0)}{T(\mathbf{U}_0)}\right). \tag{23}$$

Estimating the coefficients of bifurcation and shift requires the amplitude vectors of the nonrotating shell $\mathbf{U}_0$. This is possible only if we know the operator L or the density Π. The form of this density depends on the type of the shell theory. In the next section we will apply Novozhilov's shell theory, which is of the Kirkhoff-Love type.

It is possible to make some conclusions about the coefficient of bifurcation. Vilke (1986) has shown that $-1 \le \beta \le 0$. Egarmin (1986) has shown that $\beta = -1$ only for $m = 1$ and only for rings or cylinders where axial displacements are zero; i.e., $u = 0$.

It is clear now why the effect of precession of modes of the rotating solid body was ignored for many years. First, this effect is rather small for low speeds of rotation and, secondly, it could not be discovered using a one-dimensional model. This effect only appears in two- or three-dimensional models. Finally, this phenomenon does not appear in axisymmetric vibrations. Indeed, it is known that axisymmetric vibrations may be separated into twisting modes with amplitude vector $\mathbf{U}_1 = (0, v, 0)$ and longitudinal-bending modes with amplitude vector $\mathbf{U}_2 = (u, 0, w)$. It is clear that the scalar products $(L_C\mathbf{U}_1, \mathbf{U}_1)$ and $(L_C\mathbf{U}_2, \mathbf{U}_2)$ and the coefficient of bifurcation $\beta = 0$ are all equal to zero.

The effect of precession is well known in physics and is a consequence of the theorem of conservation of angular momentum. In all cases, when an arbitrary body oscillates in a field of gyroscopic forces $\mathbf{F}$, such that

$$\mathbf{F} = \mathbf{a} \times \mathbf{V},$$

where $\mathbf{a}$ is a field vector and $\mathbf{V}$ is the speed of a body element, we have the precession of a mode. The effect of bifuration of the frequencies for an oscillation of a particle in a field of magnetic forces is known as Larmore precession. Another example of this effect is the vibration of the Foucault pendulum.

To determine the strain energy density Π we have to choose the shell theory. We will use the Novozhilov's theory. Smirnov and Tovstik (1981) and Smirnov (1981a, 1981b) have shown that for Novozhilov's shell theory the expresssions for items proportional to Ω^2 in equation (14) have the next form

$$\Pi_0(\mathbf{U}_0) + P\Pi_P(\mathbf{U}_0) = \Pi_\Omega(\mathbf{U}_0) - \Omega^2 T_e(\mathbf{U}_0), \quad \Pi_0 = m^2 T - 2mT_C. \tag{24}$$

Constant P depends on the boundary conditions and not equal to zero only when both edges are clamped, i.e., $u(s_1) = u(s_2) = 0$. We will not consider this case.

If P is equal to zero, the formulas for the shift coefficients will be rewritten as:

$$\alpha = \frac{1}{2\omega_0}\ (m + \beta_1)^2\Omega^2(1 + O(\Omega^2)), \tag{25}$$

If we assume $\mathbf{U} = \mathbf{U}_0$, and submit the expression (24) into (14), we immediately obtain

$$\omega_\pm = \beta_1\Omega \pm (\omega_0 + (m + \beta_1)^2\Omega^2)^{1/2}. \tag{26}$$

The last expression is more precise for lower eigenvalues, but from an asymptotic point of view the relative error will be the same as in formula (25), that is $O(\Omega^2)$.

6 Partition Method

Most of the results of Sections 3, 4, and 5 are valid for an arbitrary elastic body, rotating around an axis of symmetry. For example, for any elastic body

$$\beta = \frac{T_C(\mathbf{U}_0)}{T(\mathbf{U}_0)}\ \Omega(1 + O(\Omega^2)),$$

describes the gyroscopic effect, where $\mathbf{U}_0$ is the vector of displacements for a nonrotating body. We will omit the index $_0$.

Now we will use the specific property of the shell, small thickness h, to find the approximate analytical expression for the modes of a nonrotating shell. For the quantities of the same order as h, we will use the symbol $\sim$. If we manage to construct the modes in the form

$$\mathbf{U} = \mathbf{U}^0 + \mathbf{U}^1, \ \|\mathbf{U}^1\| \sim h^\alpha \|\mathbf{U}^0\|, \ \alpha > 0,$$

we then get an approximation for the coefficient β in a form

$$\beta = \frac{T(\mathbf{U}^0)}{T_C(\mathbf{U}^0)}\ \Omega(1 + O(\Omega^2) + O(h^\alpha)).$$

The solution $\mathbf{U}^0$ is usually called the general solution and $\mathbf{U}^1$ is called the additional solution. If h is a small parameter, it is possible to represent the modes as a power series in h. The character of both the general and additional solutions and, hence, the actual form of the series depends on the frequency, geometry of the shell, boundary conditions, and value of the wave number m. For example, the general solution of the equations of vibration with lower frequency is often the bending mode and the additional solution has the character of a boundary effect. The main results of the theory of asymptotic integration of the equations of vibration of shells can be found in a monograph (Goldenveiser et al., 1979). In the next sections we will use the results of this work.

7 Rayleigh's Vibrations

From a technical point of view, the quality of a structure is often determined by the lower eigenvalues. In this paper we are interested in the lower part of the spectrum of the frequencies of free vibration. Among the lower frequencies we are mostly interested in superlow frequencies. These frequencies are of the order of h^α, where $\alpha > 0$ and, hence, decrease as the thickness decreases. If the thickness is small enough, all lower frequencies are superlow, if they exist. In a paper by Smirnov and Tovstik (1982), it was shown that the maximum effect of the rotation is on these frequencies. The results of numerical investigations proving this conclusion can be found in a paper by Shih-sen Wang and Chen Yu (1974).

Let us consider the Rayleigh formula for frequencies

$$\omega^2 = \frac{\Pi_\epsilon(\mathbf{U}) + h^2 \Pi_\chi(\mathbf{U})}{T(\mathbf{U})}.$$

Here Π_ϵ is the elongation-shear energy and Π_χ is the bending-twisting energy.

It is clear that the eigenvalues are superlow if we consider the modes for which the potential energy of the elongation (membrane energy) is small, i.e.,

$$\Pi_\epsilon \sim h^\beta, \quad \beta > 0.$$

The limiting case $\Pi_\epsilon = 0$, represents pure bending modes. These modes have been investigated by Lord Rayleigh.

The condition $\Pi_\epsilon = 0$ is equivalent to the system of equations

$$\epsilon_1 = \epsilon_2 = \omega = 0,$$

or, using the definition for the tangential deformations (Goldenveizer, 1961), to a system of differential equations

$$u' - \frac{w}{R_1} = 0,$$

$$\frac{B'u}{B} + \frac{mv}{B} - \frac{w}{R_2} = 0,$$

$$B\left(\frac{v}{B}\right)' - \frac{mu}{B} = 0. \tag{27}$$

This system has two solutions which may be found for any given shell type.

8 Shells of Zero Curvature

In this section we will consider shells of zero curvature, i.e., cones and cylinders. For cones the radii of curvature and function B can be determined from:

$$\frac{1}{R_1} = 0, \quad \frac{1}{R_2} = \frac{\cos\alpha}{B}, \quad B = s \sin\alpha, \quad B' = \sin\alpha,$$

where α is the cone semi-angle. The case $\alpha = 0$ represents cylinder.

For a cone, the system of equations (27) has the solutions

$$\mathbf{U}_1 = \left(0, s, \frac{ms}{\cos\alpha}\right), \ \mathbf{U}_2 = \left(\sin\alpha, -m, \frac{\sin^2\alpha - m^2}{\cos\alpha}\right), \tag{28}$$

and for a cylinder the system of equations (27) has the solution

$$\mathbf{U}_1 = (0, 1, m), \quad \mathbf{U}_2 = (1, ms, m^2 s). \tag{29}$$

It is possible to show that the first mode is symmetric to the middle of the shell and the second mode is in an antisymmetric mode. The frequency corresponding to the first mode is always lower than the frequency corresponding to the second mode.

Now, if we have a boundary condition, which allows the existence of pure bending, the formulas (28) and (29) give us an approximation for the exact modes. The error of this approximation is proportional to the influence of boundary effects, that is, $O(\sqrt{h})$.

We substitute the modes (28) and (29) into (21) and (26). For the cone we get

$$\omega_\pm = \beta_1 \Omega \pm (\Omega_0^2 + (m - \beta_1{}^2)^{1/2}, \tag{30}$$

where, for the first mode

$$\beta_1 = -\frac{2m\cos^2\alpha}{\cos^2\alpha + m^2},$$

and for the second mode

$$\beta_1 = -\frac{2m^3}{A_m}, \quad A_m = \sin^2\alpha + m^2 + \left(\frac{\sin^2\alpha - m^2}{\cos\alpha}\right)^2.$$

Here, ω_0 is the eigenvalue of the nonrotating shell.

For the first mode of the cylinder we get

$$\beta_1 = -\frac{2m}{1+m^2}, \quad \omega_\pm = \beta_1 \omega \pm \left(\Omega_0^2 + m^2\left(\frac{m^2-1}{m^2+1}\right)^2 \Omega^2\right)^{1/2}. \tag{31}$$

For the second mode we may use the same expression, but with an error of the order $O(m^{-2} l^{-2})$.

If m is a large parameter, the formulas for the first and second modes converge and we obtain the next approximation

$$\beta_1 = -\frac{2\cos^2\alpha}{m}(1 + O(m^{-2})), \quad \omega_\pm = \beta_1 \Omega \pm (\omega_0^2 + m^2 \Omega^2)^{1/2}. \tag{32}$$

All these results are valid for pure bending vibration, but not all shells and boundary conditions produce pure bending. For some cases, the shell has modes very similar to bending modes. These modes are called pseudobending modes. The reader can find theoretical results about pseudobending modes in a monograph by Goldenveiser et al. (1979).

We will consider only two cases of vibration of shells with zero curvature, where pseudobending modes exist. The first is the vibration of a shell of medium length, i.e., $l \sim R$. It was shown (Goldenveiser et al., 1979) that for the medium length shells of zero curvature, pseudobending modes exist for any type of the boundary condition. For these modes the wave number is large ($m \sim h^{-1/4}$) and the lowest frequency is of the order of $h^{1/2}$. To determine the frequencies of vibrations of these modes, we can use the formula (32). The error of this formula increases when we consider large or small values of m. The error will rise if we consider a rigid boundary condition. For example, this formula gives better results for simply-supported edges than for clamped edges. Nevertheless, (32) gives a good approximation for low frequencies. Figure 2 compare the eigenvalues of a cylindrical shell determined by numerical method (points on the graph) by using (32) (lines on the graph) for $m = 5$, $l = 2$, $h = 0.01$. Endo et al. (1984) and Saito and Endo (1986) obtained good agreement between numerical, experimental, and theoretical results for a wide range of parameters of thickness and wave number, and various boundary conditions.

The influence of rotation on the eigenvalues, determined with formula (32), does not depend on the boundary condition. Using the asymptotic representation found by Goldenveiser et al. (1979), it is possible to get the next term in the series for the eigenvalue, taking into account the effect of the boundary condition. For a cylinder, Goldenveiser et al. (1979) have found that the first term for the displacement has the form

$$\mathbf{U}^0 = \left(\frac{1}{m^2}(w^0)', \frac{1}{m} w^0, w^0\right)(1 + O(\sqrt{h})), \tag{33}$$

where w^0 is a solution of the equation

$$(1-\nu^2)(w^0)^{iv} + (m^8 h^2 - \omega_0^2 m^4) w^0 = 0.$$

For the simply-supported edges, the corresponding boundary conditions are

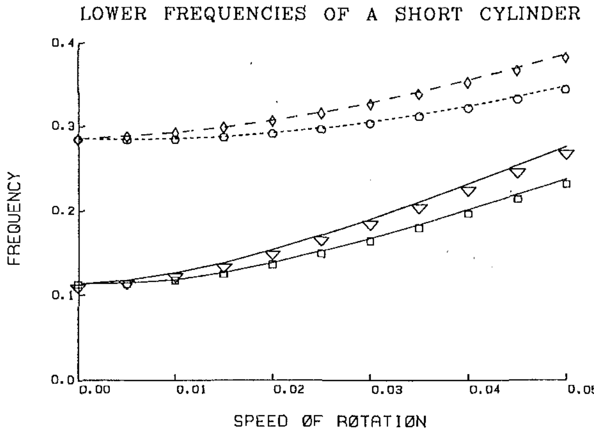

Fig. 2 The lower eigenvalues versus speed of rotation for a short cylindrical shell

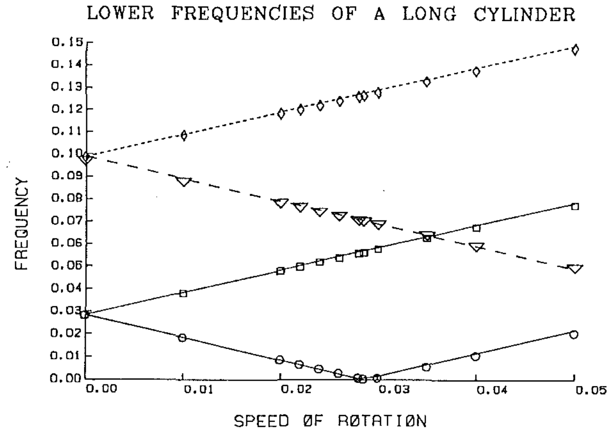

Fig. 3 The lower eigenvalues versus speed of rotation for a long shell

$$(w^0)''(0) = w^0(0) = (w^0)''(l) = w^0(l) = 0.$$

It is clear that if m is a large parameter, for example, $(m \sim h^{-1/4})$, equation (32) is still valid. The error due to neglecting terms of the order of m^{-2}, is of the same order as that due to neglecting the boundary effect. If m is not large; we must use the more precise formula.

The second case we will consider is long cylindrical shells. It was shown that for the sufficiently long shells for each wave number, m pseudobending modes exist. In this case, the error in frequency due to (32) is proportional to $m^{-2}l^{-2}$. Egarmin (1986), did not require the assumption $\epsilon_1 = 0$. It allowed him to obtain the next term in the expression for the coefficient of bifurcation

$$\beta_1 = -\frac{2m}{m^2 + 1 + D^k \dfrac{1}{m^2 l^2}}, \tag{34}$$

where coefficient D^k depends on the boundary conditions and the wave number (k) in the direction of the meridian. D^k increases with k, so the influence of the boundary condition increases for higher modes. The coefficient D^k is larger for more rigid boundary conditions.

The same result can be obtained using (33). For example, for a simply-supported shell,

$$\mathbf{U}^0 = \left(\frac{\pi k}{l m^2} \cos \frac{\pi k s}{l}, \frac{1}{m} \sin \frac{\pi k s}{l}, \sin \frac{\pi k s}{l} \right)$$

and the coefficient of bifurcation is equal to:

$$\beta_1 = -\frac{2m}{m^2 + 1 + \dfrac{\pi^2 k^2}{m^2 l^2}}.$$

In this case, $D^k = \pi^2 k^2$. For higher modes we must use (34), but for the case $k = 1$ and for long shells, (32) provides adequate results.

The influence of rotation is maximum for $m = 1$. This is the only case when the eigenvalue may be equal to zero for some rotation speed. For a long cylinder with $m = 1$, (34) transforms into

$$\omega_+ = \omega_0 - \Omega, \quad \omega_- = -\omega_0 - \Omega_0. \tag{35}$$

The comparison of the numerical (points on the graph) and asymptotic (lines on the graph) results for the lower frequencies of the long cylinder can be seen in Fig. 3 for the following parameters $m = 1$, $h = 0.01$, and $l = 15$.

We see that for certain specific values of the speed of rotation, the eigenvalue is equal to zero and the shell becomes unstable. The behavior of a long shell is thus similar to the behavior of a long beam, which also becomes unstable at critical speeds of rotation.

9 Vibrations of Spherical Shells

In this section we will consider the vibration of spherical cupolas, which were first examined by Zhuravliev and Klimov (1985). The geometry of these shells is described by function $B = \sin\theta$, $0 \le \theta \le \theta_2$, $R_1 = R_2 = 1$. We start by investigating pure bending modes of vibration. Rayleigh has solved the system (27) for a spherical shell. There are two solutions. We consider the one which is limited in the top of the cupola:

$$\mathbf{U} = \left(\sin\theta \left(\tan\frac{\theta}{2}\right)^m, \ \sin\theta \left(\tan\frac{\theta}{2}\right)^m, \right.$$
$$\left. (m + \cos\theta)\left(\tan\frac{\theta}{2}\right)^m \right), \ 0 \le \theta \le \theta_2. \tag{36}$$

Now if we substitute this solution into (21) and (26), we get the formulas for the coefficients of bifurcation and shift

$$\omega \pm = \beta_1 \Omega \pm (\omega_0 + (m + \beta_1)^2 \Omega^2)^{1/2}, \ \beta_1 = -2m \frac{I_m^1}{I_m^2 + I_m^3 + I_m^4}, \tag{37}$$

where

$$q = \cos^2 \frac{\theta_2}{2},$$

$$I_m^1 = 4\int_q^1 (1-t)^{m+1} t^{1-m} dt, \ I_m^2 = (m-1)^2 \int_q^1 (1-t)^m t^{-m} dt,$$

$$I_m^2 = 4(m+1)\int_q^1 (1-t)^m t^{1-m} dt, \ I_m^3 = -4\int_q^1 (1-t)^m t^{2-m} dt.$$

For each value of m we can compute these integrals. For $m = 2$, the value of the coefficient of bifurcation has been determined by Egarmin (1986). In our notation

$$\beta_1 = -2 \frac{24 \ln q - 72q + 36q^2 - 8q^3 + 44}{3q^{-1} - 30 \ln q + 81q - 30q^2 + 4q^3 - 58}. \tag{38}$$

It is interesting to investigate the value of the coefficient of bifurcation as a function of the angle θ_2, which is a coordinate of the free edge of the spherical shell. In Fig. 4 we can see the value of the modulus of the coefficient of bifurcation as a function of the angle θ_2. The maximum $(\beta_1 = 0.76)$ corresponds to a cupola with an angle of 135 deg. It is interesting

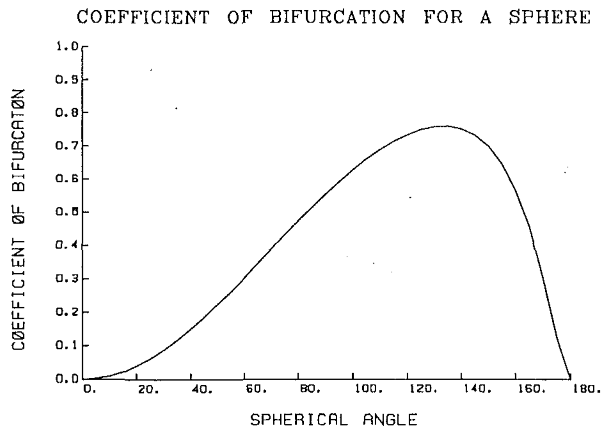

Fig. 4 The relationship between the coefficient of bifurcation and the spherical angle for a spherical shell

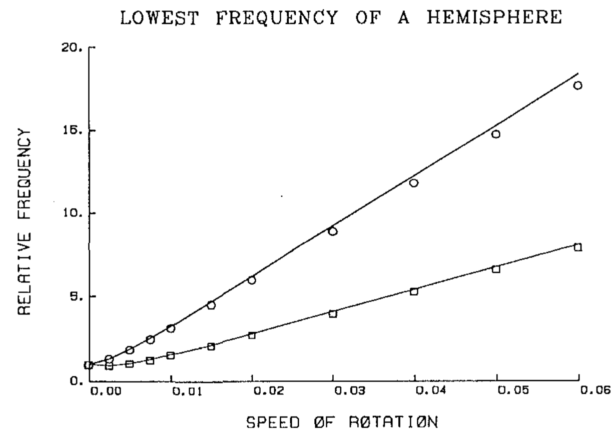

Fig. 5 The lowest eigenvalue versus speed of rotation for a hemisphere

to compare the results for the sphere with the results for the cylinder. For $m=2$, the maximum value of the modulus of the coefficient of bifurcation for cylindrical shell, according to (34), is 0.8. Since the influence of rotation on the shells of different geometry is maximal for cylinders, the last number is an upper limit for the coefficient of bifurication of a spherical shell. In the case of a spherical shell, the bifurcation will be more for the shell, which is more "similar" to the cylinder.

For a hemisphere ($\theta_2=\pi/2$) with $m=2$, we obtain $\beta_1=-0.554$ and the speed of precession $\beta/m=-0.227$. This result was first obtained by Zhuravliev and Klimov (1985). Evaluating the limit of expression (38) for θ_2 converging to 0 and to π, it is not difficult to show that β_1 converges to zero.

The comparison of the numerical (points on the graph) and asymptotic (lines on the graph) results for the lowest frequency of the hemisphere with free edge can be seen in Fig. 5 for the following parameters $m=2$, $h=0.01$. The frequency for the nonrotational shell is assumed to be equal to 1.

These results are valid for spheres with a clamped top and free edge. The error in the mode and, hence, for frequencies is determined by the boundary effect and is $O(\sqrt{h})$. For other boundary conditions at the top, or if $\theta_1>0$, the error in using (36) increases. Egarmin (1986) estimated the influence of the boundary conditions on the eigenvalues. He has shown that this effect is much less important than the effect of the influence of the free edge. This seems reasonable since the main vibration for these shells is concentrated at the free edge.

Acknowledgment

The opportunity for the appearance of this paper is provided by the program of scientific exchange between Carleton University and Leningrad University. The author expresses special gratitude to Prof. J. Goldak, for very fruitful discussions and help. I also thank my friends who helped me with advice and support.

References

DiTaranto, R. A., and Lessen, M., 1964, "Coriolis acceleration effect on the vibration of a rotating thin-walled circular cylinder," ASME Journal of Applied Mechanics, Vol. 31, pp. 700–701.

Egarmin, N. E., 1986, "O precessii stoiachikh voln kolebanii vrashchaiushcheisia osesimmetrichnoi obolochki," *Mekhanika tverdogo tela*, Vol. 21, pp. 142–148.

Endo, M., et al., 1984, "Flexural vibration of a thin rotating ring," *Journal of Sound and Vibration*, Vol. 92, pp. 261–272.

Goldenveizer, A. L., 1961, *Theory of Elastic Thin Shell*, Pergamon Press, London.

Goldenveizer, A. L., Lidsky, V. B., and Tovstik, P. E., 1979, *Svobodnye kolebania tonkikh uprugikh obolochek*, Nauka, Moscow.

Lidsky, V. B., and Tovstik, P. E., 1984, "Spektry v teorii obolochek," *Advances in Mechanics*, Vol. 7, pp. 25–54.

Padovan, J., 1973, "Natural frequencies of rotating prestressed cylinders," *Journal of Sound and Vibration*, Vol. 31, pp. 469–482.

Padovan, J., 1974, "Orthogonality principle for the vibrational modes of anisotropic composite domain problem," ASME Journal of Applied Mechanics, Vol. 41, pp. 832–834.

Padovan, J., 1975a, "Numerical analysis of asymmetric frequency and buckling eigenvalues of prestressed rotating anisotropic shells of revolution," *Computers and Structures*, Vol. 5, pp. 145–154.

Padovan, J., 1975b, "Travelling wave vibrations and buckling of rotating anisotropic shells of revolution by finite elements," *International Journal of Solids and Structures*, Vol. 11, pp. 1367–1380.

Padovan, J., 1978, "On gyroscopic problems in elasticity," *International Journal of Engineering Science*, Vol. 16, pp. 1061–1073.

Saito, T., and Endo, M., 1986, "Vibration of finite length rotating cylindrical shells," *Journal of Sound and Vibration*, Vol. 107, pp. 17–28.

Shih-sen Wang, and Chen Yu, 1974, "Effect of rotation on vibrations of circular cylindrical shells," *Journal of the Acoustic Society of America*, Vol. 55, pp. 1340–1342.

Smirnov, A. L., 1981a, "Kolebania vrashchaiushchikhsia obolochek vrashchenia," *Pricladnaia mekhanica*, vyp. 5, Leningrad University Publishers, pp. 176–186.

Smirnov, A. L., 1981b, "Kolebania vrashchaiushchikhsia obolochek vrashchenia," Ph.D. Thesis, Leningrad University, Leningrad.

Smirnov, A. L., 1981c, "Integraly uravnenii kolebanii vrashchaiushchikhsia obolochek vrashchenia," *Vestnik Leningradskogo Universiteta*, No. 13, pp. 114–117.

Smirnov, A. L., and Tovstik, P. E., 1982, "Kachestvennoe issledovanie dinamiki vrashchaiushchikhsia obolochek vrashchenia," *Sovremennye problemy mekhaniki i aviacii*, Mashinostroenie, Moscow, pp. 280–290.

Srinivasan, A. V., and Lauterbach, G. F., 1971, "Travelling waves in rotating cylindrical shell," ASME *Journal of Engineering for Industry*, Vol. 93, pp. 1229–1232.

Vilke, V. G., 1986, "Ob inercialnykh svoistvakh sobstvennykh form osesymmetrichnogo uprugogo tela," *Vestnik Moscovskogo universiteta*, ser. 1, No. 2, pp. 66–72.

Vorobiev, Yu.S., and Detistov, S. I., 1981a, "K vyvodu uravnenii kolebanii vrashchaiushcheisia ortotropnoi konicheskoi obolochki," *Problemy mashinostroenia*, No. 13, pp. 12–17.

Vorobiev, Yu.S., and Detistov, S. I., 1981b, "O vliianii centrobezhnykh sil na sobstvennye chastoty krugovykh konicheskikh obolochek," *Problemy mashinostroenia*, No. 14, pp. 27–29.

Zhuravliev, V. F., and Klimov, A. L., 1985, "O precessii sobstvennoi formy kolebanii sfericheskoi obolochki pri eie vrashchenii," *Mechanica tverdogo tela*, Vol. 20, pp. 147–151.

Zohar, A., and Aboudi, J., 1973, "The free vibrations of a thin circular finite rotating cylinder," *International Journal of Mechanical Science*, Vol. 15, pp. 269–278.

G. Borino[1]
Visiting Research Associate.

U. Perego[2]
Visiting Research Associate.

P. S. Symonds
Professor of Engineering (Research),
Fellow, ASME

Division of Engineering,
Brown University,
Providence, R.I. 02912

An Energy Approach to Anomalous Damped Elastic-Plastic Response to Short Pulse Loading

In beams with full-end constraints, loaded transversely by short pressure pulses, the effect of extensional plastic deformation is to make possible instabilities related to snap buckling in the elastic-plastic recovery after the first peak displacement (Symonds and Yu, 1985). In the present paper we make use of a damped, Shanley-type model to study the calculation of the final displacement, reached asymptotically. We show that plots of the elastic strain energy and of the total energy as functions of the displacement help to guide thinking. They provide clarification of previously observed phenomena (Genna and Symonds, 1988) that appear complex at small damping, and lead to lower and upper bounds on the load parameter such that anomalous responses are observed. The response is calculable with the usual accuracy in problems where bifurcations are concerned.

1 Introduction

A single degree-of-freedom beam model of Shanley type is used here for further study of the nonlinear elastic-plastic response of a structure to a short pulse of transverse loading. The model (Fig. 1) consists of two rigid bars connected to each other by a deformable *cell*, and to rigid supports by smooth pins. This model has been shown to capture the essential features of the elastic-plastic response of pulse-loaded fully-constrained beams (Symonds and Yu, 1985; Symonds et al., 1986; Genna and Symonds, 1987). It serves as an efficient device for studying the instabilities that may occur because of the transformation of the beam into a shallow arch by the plastic deformations in the first deflection swing. The response following the first peak may thus involve anomalous behaviors and difficulties in numerical computation.

The present work is a continuation of work relating to the damped system by Genna and Symonds (1988) in which it was shown, that in certain ranges of the parameters, the final displacement alternates in a discontinuous manner between positive and negative values, when plotted as function of the pulse strength.

The loss of energy in plastic deformation and damping, together with the associated changes in geometry of the structure, are basic features in these phenomena. Considerable insight is provided by a new type of energy plot, involving both the total energy of the system and the elastic strain energy, as functions of the displacement. These help in understanding the interplay between energy and geometry changes, and their dependence on the pulse-loading magnitude.

A main purpose of the paper is to discuss how these energetic quantities control the approach to the final state. Damping, of course, is an essential property in these considerations. The final response is critically altered by the introduction of damping. As mentioned in appropriate circumstances, as the load parameter is increased, the final displacement has alternately positive and negative signs in successive intervals. For moderately small values of the damping ratio, the final displacement is calculable to any desired accuracy *inside* each such interval of the load parameter.

According to Poddar et al. (1988), chaotic behavior is observed when the model is subjected to periodic loading. This is *not* foreshadowed by a fractal dimension of the boundary between attracting *basins* in the present case, where the structure is free of external excitation following the short pulse of loading. However, if the damping ratio is taken vanishingly small (but nonzero), the situation becomes one where the final state is unpredictable mathematically (this is apart from the obvious difficulty or impossibility of predicting the final state of a physical system).

The present energy approach provides a guide in studies now being pursued of the more complex responses of the prototype beams with fixed pin or fully-fixed end conditions (Symonds and Yu, 1985; Symonds et al., 1986; Segev, 1986; Yankelevsky, 1987).

Basic Relations

The system is illustrated in Fig. 1. The deformable cell of negligible length that connects the two rigid rods is conceived

[1]On leave from Universita di Palermo, Dipartimento di Ingegneria Strutturale e Geotecnica, Viale Delle Scienze, 90128 Palermo, Italy.

[2]On leave from Politecnico di Milano, Dipartimento di Ingegneria Strutturale, Piazza L. Da Vinci 32, 21033 Milano, Italy.

Contributed by the Applied Mechanics Division of THE AMERICAN SOCIETY OF MECHANICAL ENGINEERS for presentation at the Joint ASCE/ASME Applied Mechanics, Biomechanics, and Fluids Engineering Conference, San Diego, Calif., July 9 to 12, 1989.

Discussion of this paper should be addressed to the Editorial Department, ASME United Engineering Center, 345 East 47th Street, New York, N.Y. 10017, and will be accepted until two months after final publication of the paper itself in the JOURNAL OF APPLIED MECHANICS. Manuscript received by the ASME Applied Mechanics Division, April 29, 1988; final revision, October 26, 1988.

Paper No. 89-APM-36.

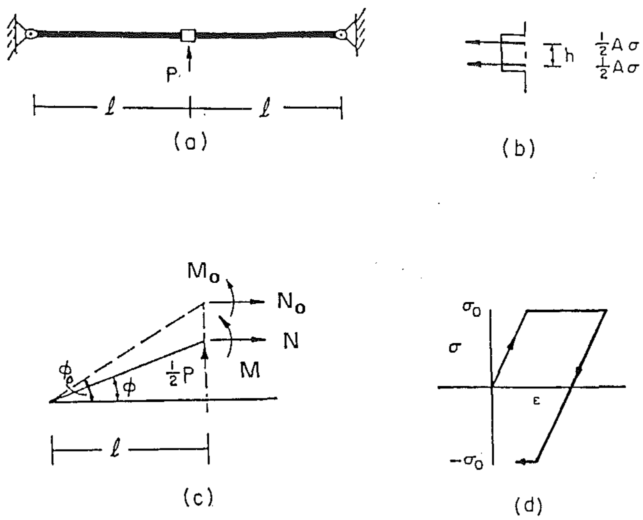

Fig. 1 The Shanley model. (a) indicates rigid bars attached by pins to rigid supports. (b) shows deformable *cell* with notation for stresses; M, N are bending moment and axial force exerted by cell. (c) shows notation for displacement angle ϕ; peak displacement due to short pulse load is ϕ_0, taken as loading parameter. (d) shows elastic-perfectly plastic behavior assumed for each bar.

as consisting of two equal elastic-perfectly-plastic bars at distances $\pm h/2$ from the centerline. The angle of rotation ϕ serves as measure of displacement. The strain in each bar is defined as the ratio of its elongation to the length l of the rigid rods. Accordingly, for small rotations, ϕ, the strain increments $d\epsilon_1$ and $d\epsilon_2$ due to an increment $d\phi$ are

$$d\epsilon_1 = \left(\phi + \frac{\eta}{2}\right) d\phi; \quad d\epsilon_2 = \left(\phi - \frac{\eta}{2}\right) d\phi, \tag{1}$$

where $\eta = h/l$ and the subscripts 1 and 2 refer to the upper and lower bar, respectively. We can express the strain increments in terms of elastic and plastic increments as follows:

$$d\epsilon_1 = d\epsilon_1^e + d\epsilon_1^p = \frac{ds_1}{\mu} + d\epsilon_1^p; \quad d\epsilon_2 = d\epsilon_2^e + d\epsilon_2^p = \frac{ds_2}{\mu} + d\epsilon_2^p, \tag{2}$$

where $s_1 = \sigma_1/\sigma_0$, $s_2 = \sigma_2/\sigma_0$; σ_1 and σ_2 are stresses in the upper and lower bars, respectively, σ_0 is the yield limit and $\mu = E/\sigma_0$, E being a Young's modulus. Integrating, the plastic strains may be computed as the difference between total and elastic strains, as follows:

$$\epsilon_1^p = \frac{1}{2}(\phi^2 + \eta\phi) - \frac{s_1}{\mu}; \quad \epsilon_2^p = \frac{1}{2}(\phi^2 - \eta\phi) - \frac{s_2}{\mu}. \tag{3}$$

Alternatively, the stresses may be expressed as

$$s_1 = \mu\left(\frac{1}{2}\phi^2 + \frac{1}{2}\eta\phi - \epsilon_1^p\right); \quad s_2 = \mu\left(\frac{1}{2}\phi^2 - \frac{1}{2}\eta\phi - \epsilon_2^p\right), \tag{4}$$

(both forms will be used). Finally, the yield and consistency conditions are

$$\begin{gathered} |s_i| \le 1; \qquad i = 1,2 \\ (s_i \pm 1)\dot\epsilon_i^p \ge 0; \\ \dot s_i \dot\epsilon_i^p = 0, \end{gathered} \tag{5}$$

(no summation over i); an overhead dot denotes the time derivative.

The basic equation of motion is the equation for the angular acceleration of each bar. In terms of nondimensional stresses this takes the form

$$J\ddot\phi + s_1\left(\phi + \frac{\eta}{2}\right) + s_2\left(\phi - \frac{\eta}{2}\right) + c\dot\phi = f, \tag{6}$$

where $f = P/A\sigma_0$, $P(t)$ being the external force acting on the model; $J = 2ml/3A\sigma_0$, m is the mass of each rigid rod, $A/2$ is the area of each bar of the cell, and c is a coefficient of viscous damping. Taking the expressions for s_1 and s_2 from equation (4), the equation of motion in terms of ϕ and the plastic strains is

$$J\ddot\phi + \zeta c_c\dot\phi + \mu\phi^3 + \frac{1}{2}\eta^2\mu\phi = f + \mu\left(\phi + \frac{\eta}{2}\right)\epsilon_1^p + \mu\left(\phi - \frac{\eta}{2}\right)\epsilon_2^p. \tag{7}$$

This expresses the damping in terms of the ratio $\zeta = c/c_c$, $c_c = (2J\mu\eta^2)^{1/2}$ being the critical damping coefficient for small deflections of the elastic system.

From equation (7) it appears that four parameters must be specified in order to define the problem, namely J, μ, η, and ζ. (Yu and Xu (1988) have recently considered the undamped case, and showed that in addition to J, there is then only one independent structural parameter, which is proportional to $\mu\eta^2$). For consistency with earlier work, we adopt the following values:

$$J = 6 \times 10^{-8}\,\text{sec}^2; \quad \eta = 0.0271; \quad \mu = 400. \tag{8}$$

The model permits the simplification for short pulses of taking the peak deflection due to the pulse as a measure of the pulse strength. The motion can be assumed to start from a configuration specified by an initial rotation ϕ_0 and zero velocity. The system is assumed to have attained this initial state along a monotonic deformation path so that the stresses (s_{1_0}, s_{2_0}) and plastic strains $(\epsilon_{1_0}^p, \epsilon_{2_0}^p)$ are unambiguously associated with each value of ϕ_0.

When the system is released from the initial position, its recovery behavior is initially elastic. However, in the following motion either one or both bars may undergo further plastic deformation. It is helpful to write work-energy integrals. We start by multiplying equation (6) by $d\phi$. The incremental form can be written as

$$d(J\dot\phi^2/2) + s_1\left(\phi + \frac{\eta}{2}\right)d\phi + s_2\left(\phi - \frac{\eta}{2}\right)d\phi + \zeta c_c\dot\phi\, d\phi = 0, \tag{9}$$

the right-hand side being zero in the recovery motion. In view of equations (1) and (2), this can be written as

$$d(J\dot\phi^2/2) + s_1\left(\frac{ds_1}{\mu} + d\epsilon_1^p\right) + s_2\left(\frac{ds_2}{\mu} + d\epsilon_2^p\right) + \zeta c_c\dot\phi\, d\phi = 0. \tag{10}$$

Integrating between limits ϕ_0 and ϕ and rearranging, we obtain

$$\frac{1}{2}J\dot\phi^2 + \frac{1}{2\mu}(s_1^2 + s_2^2) = \frac{1}{2\mu}(s_{1_0}^2 + s_{2_0}^2) - \int_{\phi_0}^{\phi}(s_1 d\epsilon_1^p + s_2 d\epsilon_2^p) - \zeta c_c\int_{\phi_0}^{\phi}\dot\phi\, d\phi, \tag{11}$$

where s_{1_0}, s_{2_0} are the stresses at the start of the recovery (i.e., those associated with monotonic loading to the initial angle ϕ_0). We rewrite this as

$$T + V = U = V_0 - D_p\Big|_{\phi_0}^{\phi} - D_v\Big|_{\phi_0}^{\phi} \tag{12}$$

where:

$$T = \frac{1}{2}J\dot\phi^2; \tag{13a}$$

$$V = \frac{1}{2\mu}(s_1^2 + s_2^2) = \frac{1}{4}\mu\phi^4 + \frac{1}{4}\mu(\eta^2 - 2\epsilon_1^p - 2\epsilon_2^p)\phi^2 - \frac{1}{2}\mu\eta(\epsilon_1^p - \epsilon_2^p)\phi + \frac{1}{2}\mu(\epsilon_1^{p2} + \epsilon_2^{p2}); \tag{13b}$$

$$V_0 = \frac{1}{2\mu}(s_{1_0}^2 + s_{2_0}^2) = V(\phi_0); \tag{13c}$$

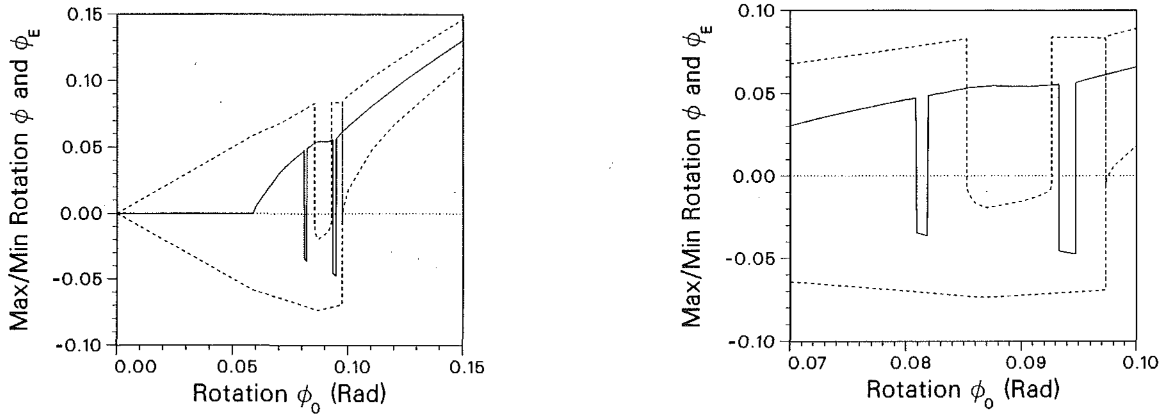

Fig. 2(a)

Fig. 2(b)

Fig. 2 ***Characteristic diagram*** **for damping ratio $\zeta = 0.1$. (b) shows central portion to enlarged scale. Solid line is final rest displacement; dashed curves show envelope of continuing elastic vibration for the undamped case ($\zeta = 0$).**

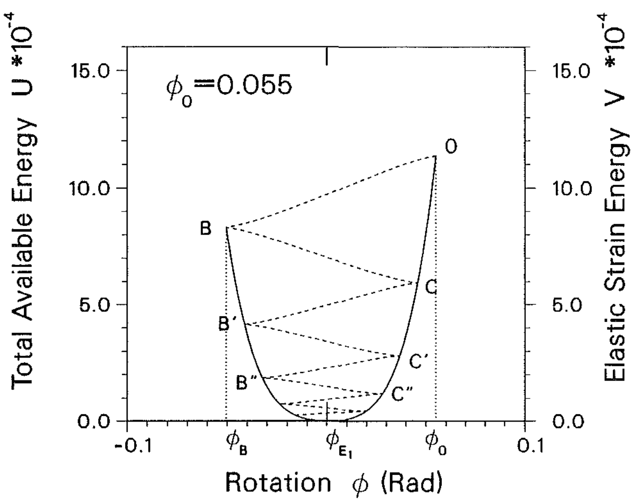

Fig. 3 Energy curves for wholly-elastic case with $\phi_0 = 0.055$, damping ratio $\zeta = 0.1$. Solid line is elastic strain energy V; dashed line is total available energy U. Kinetic energy at any displacement is $U - V$.

$$D_p \Big|_{\phi_0}^{\phi} = \int_{\phi_0}^{\phi} (s_1 d\epsilon_1^p + s_2 d\epsilon_2^p) = \int_0^t (\, |\dot{\epsilon}_1^p| + |\dot{\epsilon}_2^p|)dt; \tag{13d}$$

$$D_v \Big|_{\phi_0}^{\phi} = \zeta c_c \int_{\phi_0}^{\phi} \dot{\phi} d\phi = \zeta c_c \int_0^t \dot{\phi}^2 dt. \tag{13e}$$

T is the kinetic energy, V and V_0 are the current and initial elastic strain (or complementary) energies, respectively, computed from the stresses, and U is the total energy of the system (kinetic energy plus strain energy). V is a function of ϕ and the history-dependent plastic strains ϵ_1^p, ϵ_2^p. For brevity we shall usually write $V(\phi)$ in place of $V(\phi;\, \epsilon_1^p,\, \epsilon_2^p)$. Similarly, we omit explicit expression of the history-dependent parameters of $U(\phi)$. U decreases by the amount of the plastic dissipation $D_p|_{\phi_0}^{\phi}$ plus the energy lost in viscous damping $D_v|_{\phi_0}^{\phi}$. We shall refer to U as the *total available energy*. Its initial value is V_0, strain energy of the system assumed initially at rest. For constant ϵ_1^p, ϵ_2^p, equation (7) is a form of Duffing equation.

In the damped system, the terms in equation (11) can be evaluated only by a numerical integration furnishing the time histories $\phi(t)$, $\dot{\epsilon}_1^p(t)$, etc. When damping is omitted and the external loads are independent of time, they are obtainable directly from the first integral with respect to displacement angle. We are here interested especially in the effects of damping, and the energy plots discussed in what follows were computed by a step-by-step integration scheme based on central differences.

3 Energy Plots and Their Interpretation

Previous calculations for the undamped model (Symonds and Yu, 1985; Genna and Symonds, 1987; Yu and Xu, 1988) have led to plots of *characteristic diagrams* (CD's) which show the envelope of the final elastic vibration as a function of the initial angle ϕ_0. Calculations with damping furnish the final asymptotic displacement angle, and the CD's showing this as a function of ϕ_0, reveal striking differences from the undamped case (Genna and Symonds, 1988). Figures 2 and 5 present examples for damping ratio $\zeta = 0.1$ and 0.01, respectively; the envelope curves for the undamped model (dashed lines) are also shown for comparison.

Referring to Fig. 2, there are seen to be two *slots*—i.e., regions of ϕ_0 in which the final angle is negative—bounded by discontinuous jumps from a positive to negative value or vice versa. But for the smaller value $\zeta = 0.01$, Fig. 5 shows a more complex diagram, with 25 slots. In both cases, in the central region of the diagram the final angle computed for the damped model appears to be virtually unrelated to the envelope curves of the undamped system. Thus, the response calculations for the undamped case are incapable of predicting even the *sign* of the final displacement of the damped system, in the central region of the diagram. The energy diagrams discussed in this paper do help greatly in understanding this rather surprising situation. We will focus attention first on the somewhat simpler case of $\zeta = 0.1$, and then treat more briefly the case of $\zeta = 0.01$.

To begin with, suppose that ϕ_0 is so small that no plastic strains develop during the loading phase. Then the recovery motion is that of an elastic beam subjected to a small initial displacement. The recovery process is illustrated in Fig. 3. The dashed curve represents the variation of U with ϕ while the solid line refers to the elastic strain energy V. Since part of the energy is dissipated because of the damping effect, the energy balance (12) implies that the total available energy decreases. For each value of ϕ, the difference between the dashed and the solid curves gives the kinetic energy. Since the recovery in this example is completely elastic, the shape of the elastic strain energy curve does not change as the motion progresses. The upper and lower limits of successive cycles are marked as C, B', C', B'', etc. The final asymptotic configuration of static equilibrium (ϕ_{E_1}) coincides with the minimum of V.

Turning now to the case of elastic-plastic recovery, the energy plots of the type of Fig. 3 are, of course, somewhat

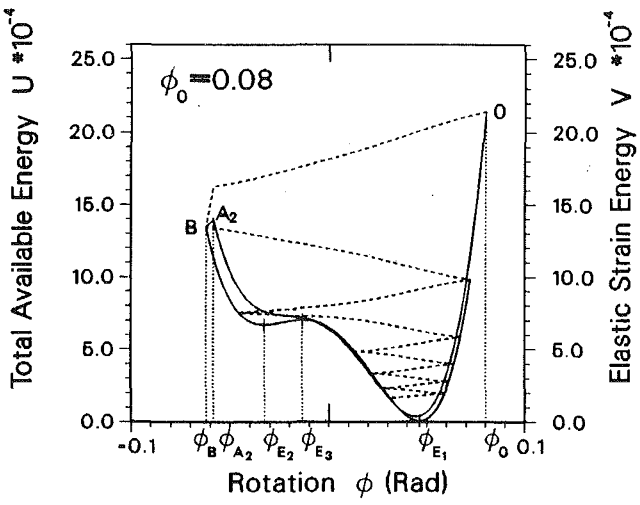

Fig. 4(a)

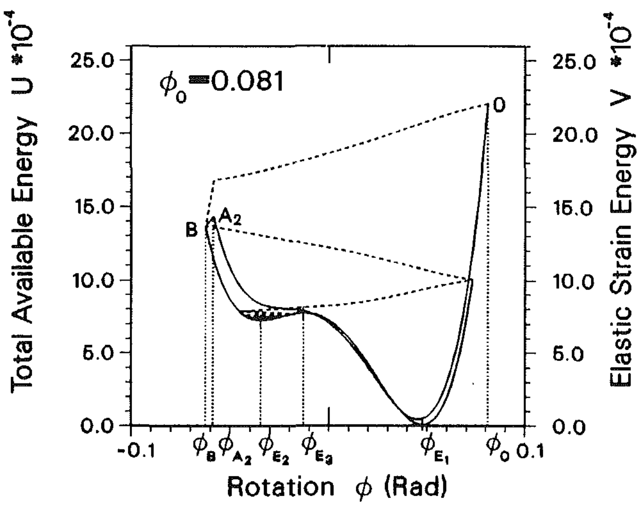

Fig. 4(b)

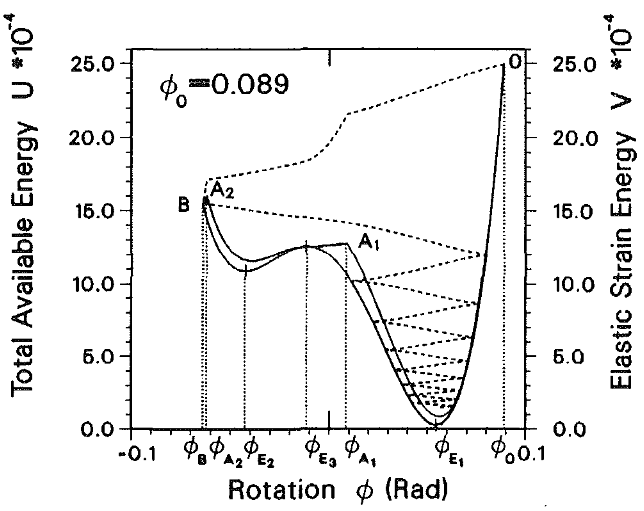

Fig. 4(c)

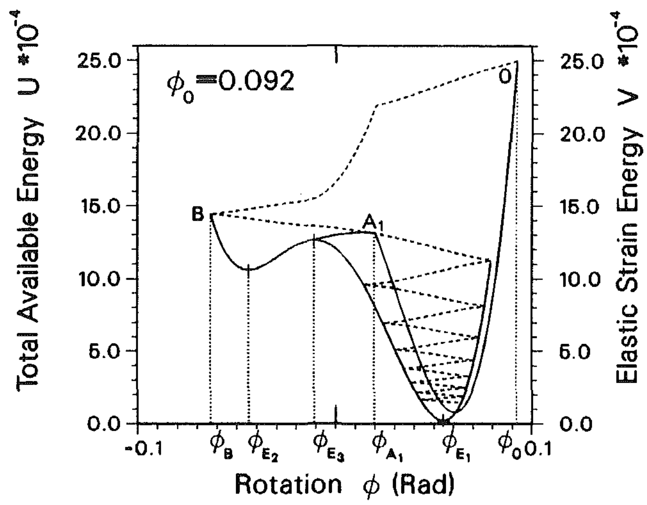

Fig. 4(d)

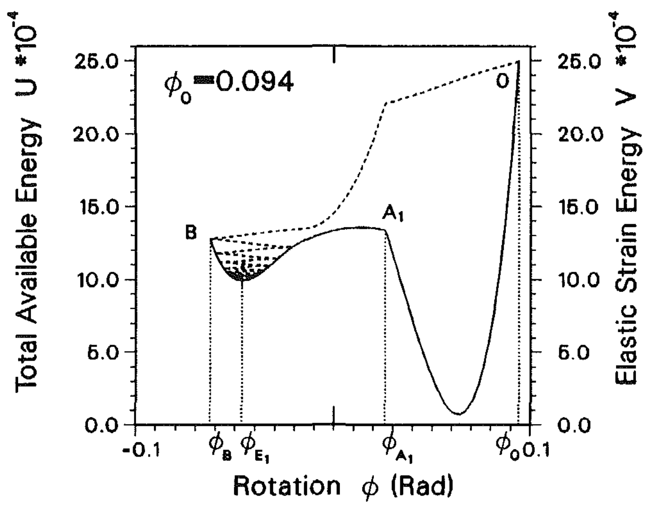

Fig. 4(e)

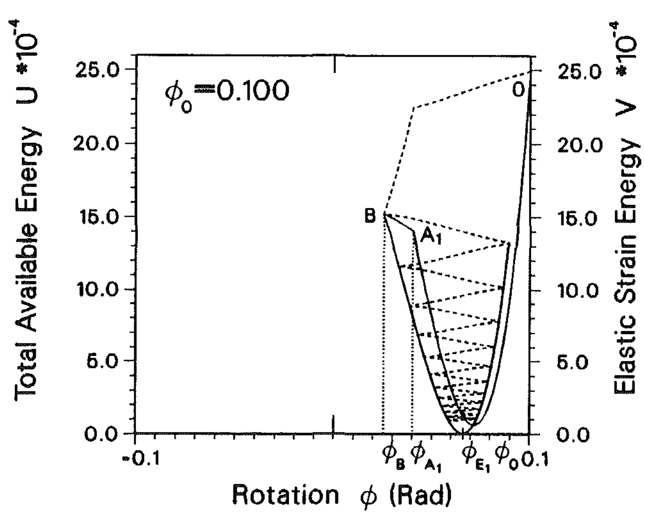

Fig. 4(f)

more complicated. First of all, U decreases now because of plastic dissipation as well as damping. Secondly, the development of plastic strains during the recovery changes the shape of V in the V-ϕ diagram. A sequence of energy plots corresponding to different values of ϕ_0 and to a damping ratio

Fig. 4 Energy diagrams for damping ratio $\zeta = 0.1$ for range of values of pulse load parameter ϕ_0 such that plastic deformation occurs in the first half-cycle of the *recovery* motion following the peak displacement due to the load pulse. Full lines show elastic energy *V*. Dashed lines show total available energy *U*. Kinetic energy $T = U - V$.

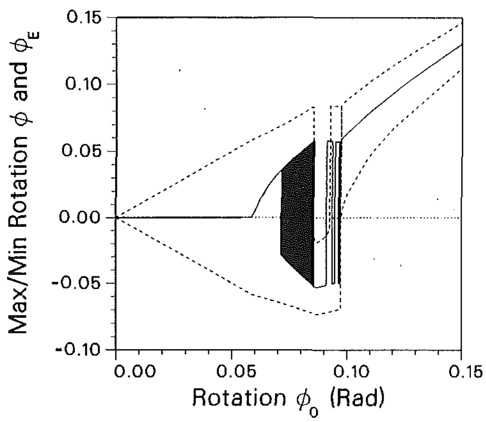

Fig. 5(a)

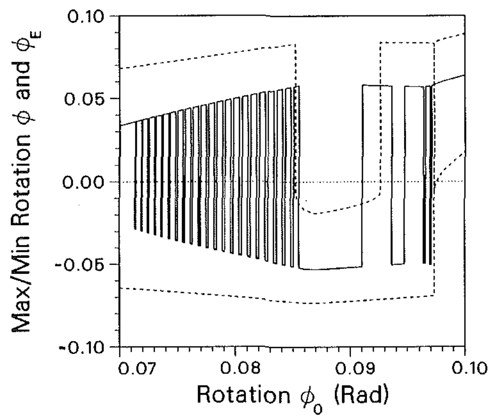

Fig. 5(b)

Fig. 5 ***Characteristic diagram*** **for damping ratio $\zeta=0.01$. (b) shows central portion to enlarged scale. Solid line is final rest displacement; dashed curves show envelope of continuing elastic vibration of undamped system ($\zeta=0$).**

$\zeta=0.1$, is shown in Figs. 4(*a*)-(*f*). Before discussing these separately, it is worth pointing out some common features. All the diagrams of Fig. 4 refer to an initial situation where at least one of the two bars has yielded in tension. When the minimum peak is reached at the end of the first semicycle of recovery ($\phi=\phi_B$), at most one bar is yielding plastically, namely either the lower bar in tension, Figs. 4(*a*), (*b*), (*c*), or the upper bar in compression Fig. 4(*f*). Finally, in the recovery phase energy is dissipated plastically only during the first semicycle; this is found in all our calculations, but not proved in general terms.

Let us focus now on Figs. 4(*a*) and 4(*b*). As always, the dashed line represents U and the solid line V; their difference is the kinetic energy T. When the system is released, the motion proceeds from ϕ_0 to ϕ_{A_2}. At $\phi=\phi_{A_2}$, the stress in the lower bar reaches its tensile yield value; and from ϕ_{A_2} to ϕ_B, U undergoes a brusque decrease due to the plastic dissipation. As far as V is concerned, the development of new plastic strains can be interpreted as a change in the geometry of the structure. In other words, if the plastic strains are considered as dislocations imposed on the structure, it can be regarded as an elastic system changing its shape under the effect of these dislocations. We can associate to each pair of plastic strains a particular elastic system endowed with its proper elastic strain energy function. Thus, the two curves from ϕ_0 to ϕ_{A_2} and from ϕ_B to ϕ_C can be considered as relevant to two elastic systems with different morphology. The curve between ϕ_{A_2} and ϕ_B represents the transition from the first system to the second one. V has two local minima between ϕ_B and ϕ_C, so that two possible final equilibrium configurations exist. At this point it is impossible to foresee, on the basis only of the shape of V, whether the final displacement will be on the positive or on the negative side. An example of this is given in Figs. 4(*a*) and 4(*b*) where a relatively small change in ϕ_0 produces a dramatic change in the final state.

By following the same path of reasoning, the interpretation of the remaining diagrams is rather straightforward. While in Figs. 4(*a*) and 4(*b*) the plastic dissipation during the recovery occurred near the end of the first semicycle (from ϕ_{A_2} to ϕ_B), in Fig. 4(*c*) the plastic dissipation occurs partly near the flat position when the upper bar yields in compression and partly at the end of the first semicycle when the lower bar yields in tension. Figures 4(*d*), (*e*) refer to a case where all the plastic dissipation is due to the compression of the upper bar. The first of these diagrams represents a case where the asymptotic configuration is positive whereas the second one gives another example of final counter-intuitive behavior.

It is worth observing that the unstable stationary point of V in the second semicycle (point ϕ_{E_3} in Fig. 4(*a*)) rises as ϕ_0 increases due to a greater initial plastic deformation in tension. This trend reverses as the upper bar starts to become plastic in compression during the recovery phase, e.g., as indicated in Figs. 4(*d*),(*e*). If the initial angle ϕ_0 is such that both bars are plastic in tension in the initial configuration, the initial value V_0 cannot increase further, while the energy dissipated during the recovery does continue to grow. This leads to a situation where no bifurcation is possible, as illustrated in Fig. 4(*f*). This remark, among other considerations of the just described energy diagrams, suggests how to define necessary conditions for the occurrence of bifurcations and, consequently, to bound the range of initial values ϕ_0 such that a counter-intuitive behavior is possible; see Section 4.

We turn first to discuss the effects of changing the damping coefficient. The situation for relatively small damping is especially interesting, and we shall give illustrations for the case of $\zeta=0.01$. However, let us begin by reviewing the role of damping in general, in the light of the energetic diagrams previously discussed.

These make it clear that there are two distinct consequences of damping. One is merely to provide a means of reducing the total energy so as to bring the system to an equilibrium state. When the final curve of the elastic strain energy $V(\phi)$ has a *hump* (i.e., an unstable equilibrium point between two stable ones) as in Figs. 4(*a*)-(*b*), the energy loss due to damping causes the total energy $U(\phi)$ to zig-zag down, initially between alternately (+) and (−) limits and, finally, between either (+)-(+) or (−)-(−) limits, depending on whether its intersection with the $V(\phi)$ curve is on the right or on the left side of the hump. As the load parameter ϕ_0 is increased, the hump is raised and the intersection of the two curves changes from one side to the other. Thus, the final equilibrium state alternates between positive and negative values.

The second role of damping is to change the shape of the final $V(\phi)$ curve. This curve represents the quartic function of ϕ whose coefficients depend on ϵ_1^p and ϵ_2^p, as shown explicitly in equation (13*b*); for the *final* $V(\phi)$ curve, of course, these plastic strains are both constant. Now, as already mentioned, plastic flow may be occurring in either the upper bar or the lower bar, as the minimum displacement is approached in the first half-cycle of the recovery. In either case, if damping is present the plastic strain is reduced below what it would be in its absence—a consequence of the loss of energy in damping as well as in plastic flow.

With these preliminaries in mind, the effect of changing the damping ratio ζ can be easily understood. When ζ is relatively small, the effect of damping on the plastic strains is reduced, and the shape of the $V(\phi)$ curve in the limit approaches that of the undamped system. The presence of damping, of course, always brings the structure to rest at a stable equilibrium point, i.e., at a point where the $V(\phi)$ curve has a local minimum. In the range of loading where there are two distinct minima, the decrease in the available energy due to damping leads to a change from an initial vibration with (+)-(−) limits to one with either (+)-(+) or a (−)-(−) limits. As the damping coefficient decreases, so does the damping loss per cycle, and many cycles may be necessary to reach the bifurcation point. Thus the final displacement, plotted as function of the load parameter, correspondingly will alternate in sign with increasing rapidity as ζ is reduced.

In Fig. 6 we give examples of energy diagrams for $\zeta=0.01$. These show why the characteristic diagram changes as it does from Fig. 2 to Fig. 5. Figures 6(*a*), (*b*) illustrate the reason for the proliferation of narrow slots as ζ is decreased. Figures 6(*c*), (*d*) illustrate why, when ζ becomes sufficiently small, the features of the CD of the undamped system reappear in the damped final response curve of Fig. 5. Note that in the undamped case there is a wide interval of ϕ_0 (between about 0.085 and 0.093), within which the motion is trapped on the negative side. Here, small changes in ϕ_0 produce only small changes in the response. Such a wide slot is seen in the solid curve of Fig. 5 for $\zeta=0.01$. To have it in a damped system requires a quite small value of the damping ratio; thus, there is no trace of the slot in Fig. 2 for $\zeta=0.1$, nor is there in the curve for $\zeta=0.05$ (see Genna and Symonds, (1988)).

These results are of practical significance. They indicate that to observe the anomalous negative final displacements in real physical beams, where damping losses may be of several kinds and unlikely to be equivalent to as small a value as $\zeta=0.01$, calculations for the undamped system may be worthless as a guide.

4 Upper and Lower Bounds for the Occurrence of Counter-Intuitive Behavior

In the presence of damping, values of ϕ_0 at which discontinuities occur in the CD cannot be computed except by a step-by-step numerical procedure. However, by defining the necessary conditions for a counter-intuitive behavior to occur in the undamped system, it is possible to bound from above and below the interval on the ϕ_0 axis where these discontinuities may arise.

For small values of ϕ_0 (Fig. 3), the recovery is completely elastic and V is described by a convex function in the V-ϕ plane. The minimum, at ϕ_{E_1}, represents the only possible

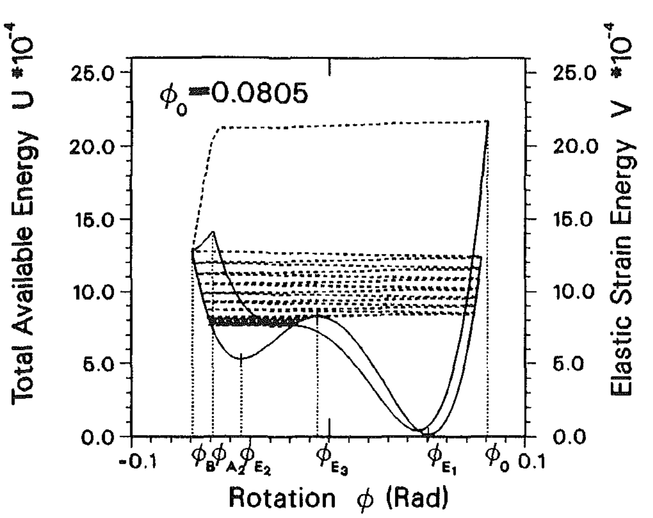

Fig. 6(*a*)

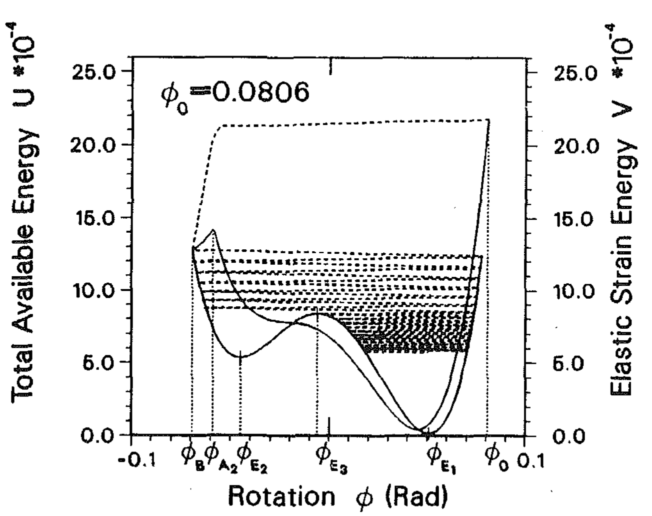

Fig. 6(*b*)

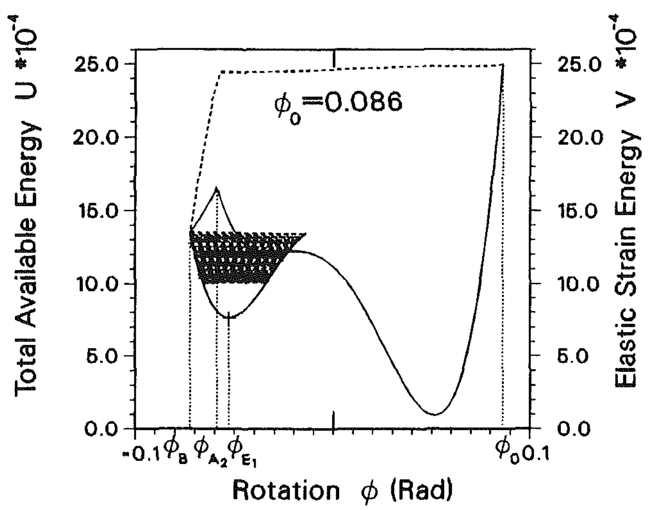

Fig. 6(*c*)

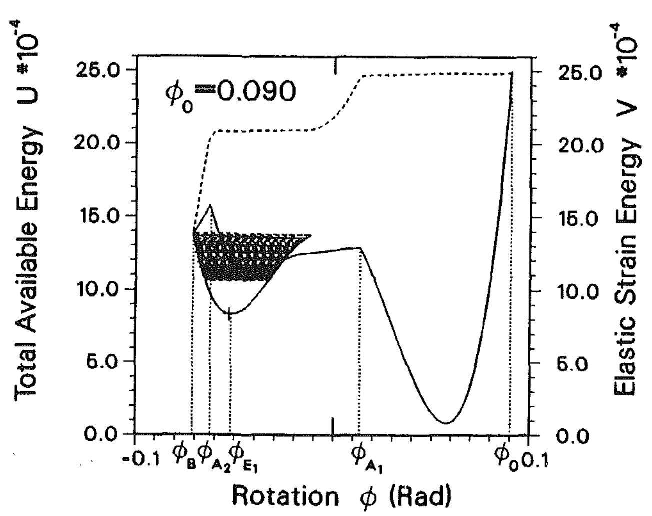

Fig. 6(*d*)

Fig. 6 Energy diagrams for damping ratio $\zeta=0.01$. Solid lines show *V*, dashed curves *U*.

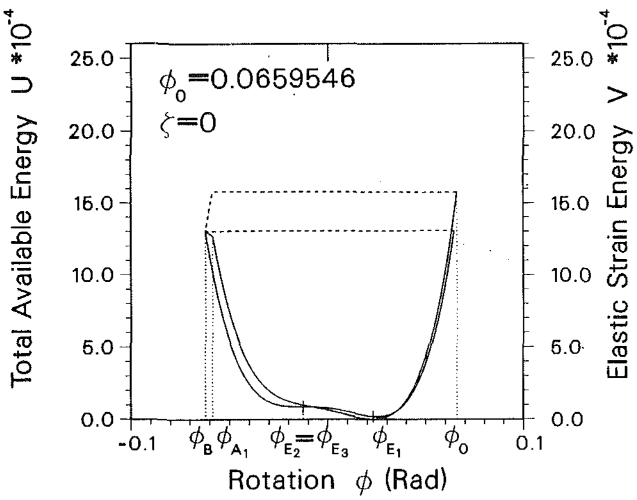

Fig. 7(a)

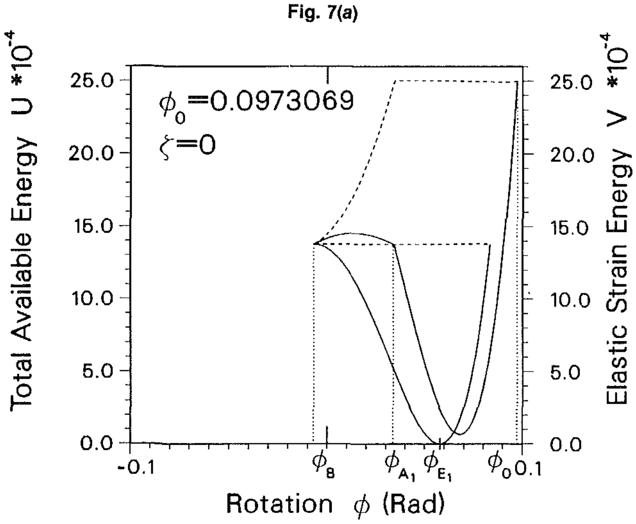

Fig. 7(b)

Fig. 7 Energy diagrams for values of ϕ_0 bounding regions where anomalous behavior may occur. (a) lower bound; (b) upper bound.

equilibrium configuration, and is attained asymptotically by the damped system. For a larger value of ϕ_0 (e.g., Fig. 4(*a*)), there are three possible asymptotic equilibrium states: two stable and one unstable, at least one of which is on the negative side. In this case there are always combinations of ϕ_0 and ζ such that the final configuration is counter-intuitive. The lower bound for the possible occurrence of counter-intuitive behavior is, therefore, given by that value of ϕ_0 such that for the first time more than one equilibrium state is possible (Fig. 7(*a*)). Equilibrium configurations can be obtained from the equation of motion (7) when $\ddot{\phi}$ is set equal to zero. Let $\epsilon^p_{1_B}$ and $\epsilon^p_{2_B}$ be the plastic strains in the two bars at the end of the first swing ($\phi = \phi_B$). Since no plastic dissipation takes place in the subsequent motion, the equilibrium configurations are solutions to

$$\frac{1}{2}\mu\eta^2\phi + \mu\phi^3 = \mu\left(\phi + \frac{\eta}{2}\right)\epsilon^p_{1_B} + \mu\left(\phi - \frac{\eta}{2}\right)\epsilon^p_{2_B}, \qquad (14)$$

where $\epsilon^p_{1_B}$ and $\epsilon^p_{2_B}$ play the role of assigned parameters. We assume that the sought lower bound belongs to a range of initial values ϕ_0 such that only the upper bar becomes plastic in tension during the loading phase, and such that neither bar becomes plastic in compression during the recovery motion. This assumption turns out to be valid for the values of η and μ used here, but might not hold true for other systems, characterized by different choices. If the just described history of deformation is considered, the plastic strains accumulated in the two bars at the end of the first swing can be expressed as

$$\epsilon^p_{1_B} = \frac{1}{2}(\phi_0^2 + \eta\phi_0) - \frac{1}{\mu};$$
$$\epsilon^p_{2_B} = \frac{1}{2}(\phi_B^2 - \eta\phi_B) - \frac{1}{\mu}. \qquad (15)$$

Substituting these expressions in (14) and rearranging, yields

$$\phi^3 + \frac{1}{2}\left(\eta^2 - \phi_0^2 - \eta\phi_0 - \phi_B^2 - \eta\phi_B + \frac{4}{\mu}\right)\phi$$
$$+ \frac{1}{4}\eta(-\phi_0^2 - \eta\phi_0 + \phi_B^2 - \eta\phi_B) = 0. \qquad (16)$$

This is a cubic equation in ϕ of the type

$$x^3 + a_1 x + a_2 = 0. \qquad (17)$$

The condition for the existence of three real roots, at least two of which are coincident, is given by

$$\frac{1}{27}a_1^3 + \frac{1}{4}a_2^2 = 0. \qquad (18)$$

Equation (18), when applied to (16), leads to the following condition on ϕ_0 and ϕ_B

$$\frac{1}{27}\left[\eta^2 - (\phi_0^2 + \eta\phi_0) - (\phi_B^2 - \eta\phi_B) + \frac{4}{\mu}\right]^3$$
$$+ \frac{\eta^2}{8}[(\phi_B^2 - \eta\phi_B) - (\phi_0^2 + \eta\phi_0)]^2 = 0. \qquad (19)$$

The two variables ϕ_0 and ϕ_B in (19) are not independent: ϕ_B is a function of ϕ_0 through the elastic-plastic history of the motion, and for the undamped system it can be determined by noticing that, at $\phi = \phi_B$, the kinetic energy vanishes. Hence, the sum of V at ϕ_B and of the energy plastically dissipated along the path between ϕ_0 and ϕ_B must be equal to V_0, i.e.,

$$V(\phi;\epsilon^p_{1_B},\epsilon^p_{2_B}) + D_p\Big|_{\phi_0}^{\phi_B} = V_0(\phi_0). \qquad (20)$$

The fact that equation (20) refers to the undamped case is here acceptable, inasmuch as we are interested only in finding a lower bound. It is easy to verify that the lower bound for the undamped case is also a lower bound for the damped one. If the history of plastic deformation is as decribed, and the plastic strains given by equations (15) are substituted in the expressions (13*b*), (13*d*), (13*c*) for V, D_p, and V_0, respectively, equation (20) can be written explicitly as

$$\left\{\frac{\mu}{8}\left[(\phi_B^2 + \eta\phi_B) - (\phi_0^2 + \eta\phi_0) + \frac{2}{\mu}\right]^2 + \frac{1}{2\mu}\right\}$$
$$+ \left\{\frac{1}{2}(\phi_B^2 - \eta\phi_B) - \frac{1}{\mu}\right\} = \left\{\frac{\mu}{8}(\phi_0^2 - \eta\phi_0)^2 + \frac{1}{2\mu}\right\}. \qquad (21)$$

Equations (19) and (21) are a system of two nonlinear equations in the unknowns ϕ_0 and ϕ_B. The value of ϕ_0, which is a solution to this system, is the lower bound we are seeking. Taking η and μ as in equation (8), the following solution is obtained by applying a Newton-Raphson iterative procedure:

$$\phi_0 = 0.0659546; \quad \phi_B = -0.0621585. \qquad (22)$$

To obtain an upper bound, let us now focus on Fig. 4(*f*). This figure refers to a case where both bars become plastic in tension during the loading phase and the upper bar becomes plastic in compression during the first recovery swing. The energy dissipated plastically in this second instance is such that the system does not have enough energy left to reach a stable equilibrium configuration on the negative side. As a result, again, there exists only one possible equilibrium configuration. If the system is damped, the further dissipation makes this situation arise at a value of ϕ_0, which is necessarily smaller than the value for the undamped case. Therefore, we define as upper bound for the occurrence of counter-intuitive behavior that value of ϕ_0 such that for the first time, the second minimum cannot be attained by the undamped system (Fig. 7(*b*)). This value of ϕ_0 is expressed by the condition that the point ϕ_B, where the kinetic energy vanishes at the end of the first swing, also corresponds to an equilibrium configuration. This condition requires that equations (20) and (14) be satisfied simultaneously for the history of plastic deformation previously described. In this case, the plastic strains at ϕ_B are given by

$$\epsilon^p_{1B} = \frac{1}{2}(\phi_B^2 + \eta\phi_B) + \frac{1}{\mu};$$
$$\epsilon^p_{2B} = \frac{1}{2}(\phi_0^2 - \eta\phi_0) - \frac{1}{\mu}. \quad (23)$$

Substituting these expressions in (20) and (14) leads to the following set of two nonlinear equations:

$$\frac{\mu}{4}\left[(\phi_B^2 - \eta\phi_B) - (\phi_0^2 - \eta\phi_0) + \frac{2}{\mu}\right](2\phi_B - \eta) - \frac{1}{2}(2\phi_B + \eta) = 0;$$

$$\left\{\frac{\mu}{8}\left[(\phi_B^2 - \eta\phi_B) - (\phi_0^2 - \eta\phi_0) + \frac{2}{\mu}\right]^2 + \frac{1}{2\mu}\right\} + \left\{-\frac{1}{2}(\phi_B^2 + \eta\phi_B) + \frac{1}{2}(\phi_0^2 + \eta\phi_0) - \frac{2}{\mu}\right\} = \frac{1}{\mu}. \quad (24)$$

For η, μ as in equation (8), solving this system by a Newton-Raphson iterative procedure, gives:

$$\phi_0 = 0.0973066; \quad \phi_B = -0.0070029. \quad (25)$$

With reference to the CD of Fig. 2, this value of ϕ_0 coincides with the last discontinuity in the undamped case (dashed lines), i.e., the one where the final steady oscillations jump from positive-negative to positive-positive. This seems to be a general result not affected by the characteristic parameters chosen for the system (Yu and Xu, 1988).

5 Generalized Initial Conditions

In the foregoing discussion we have taken the initial displacement angle ϕ_0 as a convenient parameter of loading. This is valid for short pulses such that ϕ_0 is the peak deflection, reached after the pulse force has decreased to zero. The precise form of the pulse is then of no significance, our interest being in the response history of the *recovery* following the first displacement maximum, not in the peak itself.

The analysis presented in Section 3 explains why, for any finite damping coefficient, the final rest displacement has a value that changes sign in successive intervals of ϕ_0. Within each of these intervals the value is calculable without difficulty. With damping present, a step-by-step numerical procedure is required. However, numerical schemes of different types, namely a standard Newmark implicit method (Genna and Symonds, 1988), and the central difference scheme used for the present results, have been found to give very close agreement, not only for the final displacement but even for the values of ϕ_0 at which the bifurcation occurs. Solutions that are essentially exact within the usual limitations of numerical analysis are obtainable throughout the load range of interest, in which anomalous (counter-intuitive) final displacements are concerned.

This conclusion can be generalized to a somewhat wider class of loading, namely that in which the load parameters are an initial velocity together with an initial displacement. As always, we assume that the displacement angle and the strains increase monotonically to their maxima. Any chosen value ϕ_0

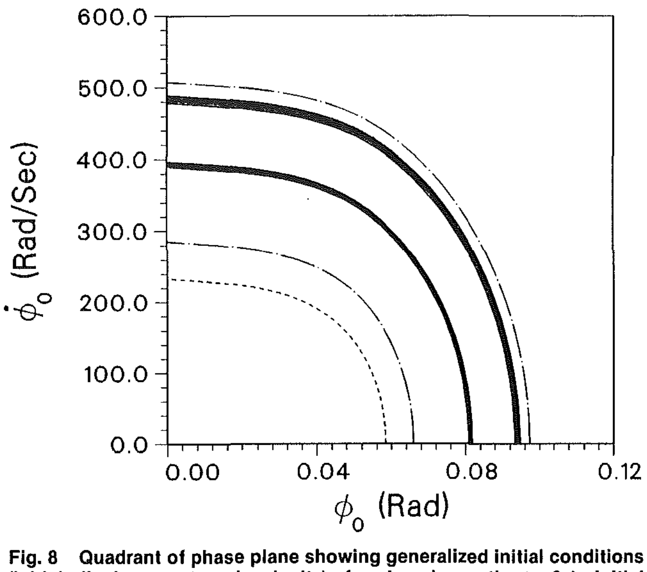

Fig. 8 Quadrant of phase plane showing generalized initial conditions (initial displacement and velocity), for damping ratio $\zeta = 0.1$. Initial values in shaded zones lead to negative final displacement. Dot-dash lines show lower and upper bounds. Dashed curve shows boundary between wholly-elastic and elastic-plastic response.

can be regarded as the peak displacement attained by the system when loaded by a *pure impulse* applied to the undeflected structure; thus, the pair of initial values $(\phi, \dot{\phi}) = (0, \dot{\phi}_1)$ leads to the pair $(\phi, \dot{\phi}) = (\phi_0, 0)$. Moreover, in the time history of the response from the initial values $(0, \dot{\phi}_1)$ to the final values $(\phi_0, 0)$, at every instant t_i there is a pair of values $(\phi_i, \dot{\phi}_i)$ that provide *equivalent* initial conditions in the sense that the eventual response is identical for all of them. It is reemphasized that to each such pair, by assumption, we associate the total and plastic strains that result from monotonic increase of deflection from the undeflected and unstrained configuration.

The time history of response from the initial values $(0, \dot{\phi}_1)$ to the state $(\phi_0, 0)$ provides a sequence of values of displacement and velocity which define a contour in the first quadrant of the $(\phi, \dot{\phi})$ phase plane. Both the time history and the contour in the phase plane depend upon the damping coefficient ζ, of course, but each contour is uniquely defined and calculable to an accuracy limited only by the precision of the computational device and algorithm being used. Contours defined for any fixed ζ and a range of values of ϕ_0 do not touch or intersect one another.

Regarding the ϕ-axis as the locus of values of the peak deflection ϕ_0, the successive intervals, in which the sign of the final asymptotic deflection takes alternately plus and minus values, correspond to zones in the first quadrant of the phase plane. These are illustrated in Fig. 8 for damping ratio $\zeta = 0.1$. Here, the shaded areas represent initial conditions leading to negative final displacements, the unshaded areas to positive ones. The boundary curves correspond to bifurcation points (they are, in fact, singular points in the phase plane diagrams which would correspond to complete time histories). They are well-defined calculable curves, as previously noted; they can be computed analytically for the undamped case. There is no fine structure or independence of scale, such as observed in the fractal boundaries between attracting basins that characterize chaotic behavior (Thompson and Stewart, 1986).

When ζ is made smaller, the zones of Fig. 8 become narrower and more numerous (as do the slots of the characteristic diagrams). If we consider ζ arbitrarily small, the separation of the boundary curves eventually becomes less than the precision of the calculation. The boundaries then cannot be drawn, and the final state cannot be predicted. This limiting situation, while of theoretical and some practical interest, has nothing to do with deterministic chaos.

For the sake of completeness, Fig. 8 displays also the upper and lower bounds defined in the previous section (dot-dashed curves) as well as the elastic limit (dashed curve).

6 Conclusion

Curves showing the elastic strain energy V and the total available energy U as functions of displacement display clearly the combined roles of plastic deformation and damping in determining the final rest position of the Shanley beam model under short pulse excitation. The apparently complex alternation of positive and negative final states, as the load parameter is increased, is seen to depend on the changes of shape of the $V(\phi)$ curve due to plastic deformation in the first half cycle of the recovery motion following the first peak displacement. Lower and upper bounds on the load parameters such that anomalous final response may occur have been computed for the system under consideration.

Except when damping is taken arbitrarily small, the final response can be calculated accurately by standard methods with the special care normally required when bifurcation may occur. The presence of moderate damping does not introduce essential new difficulties. There is no fine structure within the zones illustrated in Fig. 8; the approach to the boundary contours is smooth.

Acknowledgment

Support from the U.S. Army Research Office under Contract DAAL03-87-K-0038 is gratefully acknowledged.

References

Genna, F., and Symonds, P. S., 1987, "Induced Vibrations and Dynamic Plastic Instabilities of a Nonlinear Structural Model Due to Pulse Loading," *Meccanica*, Vol. 22, pp. 144–149.

Genna, F., and Symonds, P. S., 1988, "Dynamic Plastic Instabilities in Response to Short Pulse Excitation—Effects of Slenderness Ratio and Damping," *Proc. Royal Society of London*, Vol. A417, pp. 31–44.

Poddar, B., Moon, F. C., and Mukherjee, S., 1988, "Chaotic Motion of an Elastic-Plastic Beam," ASME JOURNAL OF APPLIED MECHANICS, Vol. 55, pp. 185–189.

Segev, E., 1986, "Reverse Snap Through of Beam Under Transverse Loading," Master's Thesis in Mechanics, Technion-Israel Institute of Technology, Haifa.

Symonds, P. S., and Yu, T. X., 1985, "Counter-Intuitive Behavior in a Problem of Elastic-Plastic Beam Dynamics," ASME JOURNAL OF APPLIED MECHANICS, Vol. 52, pp. 517–522.

Symonds, P. S., McNamara, J. F., and Genna, F., 1986, "Vibrations and Permanent Displacements of a Pin-Ended Beam Deformed Plastically By Short Pulse Excitation," *International Journal of Impact Engineering*, Vol. 4, pp. 72–82.

Thompson, J. M. T., and Stewart, H. B., 1986, *Nonlinear Dynamics and Chaos*, John Wiley and Sons, Chichester, U.K.

Yankelevsky, D. Z., 1988, "Vibrations of a Pin-Ended Beam Loaded by a Short Pulse," *International Journal of Impact Engineering*, Vol. 7, pp. 345–356.

Yu, T. X., and Xu, Y., 1988, "The Anomalous Response of an Elastic-Plastic Structural Model to Impulsive Loading," submitted to ASME JOURNAL OF APPLIED MECHANICS.

The Extensible Cable as a Limiting Case of a Very Flexible Rod

J. V. Huddleston
State University of New York at Buffalo,
Buffalo, N.Y. 14260
Mem. ASME

For an extensible cable with a free end, the exact nonlinear differential equations that describe the final shape of the cable present difficulties when one tries to integrate them to find the angle of inclination in the vicinity of that free end. To circumvent these difficulties, a method is proposed wherein the cable is replaced by a flexible rod. The moment of inertia of the cross-section of the rod is then allowed to approach zero while the cross-sectional area and the length of the rod remain finite. In that process, the rod approaches the cable as a limiting case, but since the rod has a proper differential equation on the inclination, no singularity occurs. To establish the validity of the method, two cases without a free end are considered first. For these, cable solutions previously obtained by the author are used for comparison. After that, the method is used to solve two cases involving a cable with a free end. In each of these two cases, the cable is suspended in a moving fluid, but they differ in the assumptions made about the drag force. The results obtained appear reasonable and suggest that this method, tantamount to removing the idealization of perfect flexibility from the cable, shows promise as a method of analyzing cables with a free end.

Introduction

Recently, the author has exhibited a method for analyzing extensible cables by numerically integrating the system of exact nonlinear differential equations that describe a cable in its final state (Huddleston, 1981). Consider the cable in Fig. 1. With the adoption of an engineering definition of strain, the differential equations become:

$$\frac{dN_x}{dx} = -p_x \tag{1a}$$

$$\frac{dN_y}{dx} = -p_y \tag{1b}$$

$$N = \sqrt{N_x{}^2 + N_y{}^2} \tag{1c}$$

$$\sigma = \frac{N}{A} \tag{1d}$$

$$\epsilon = g(\sigma) \tag{1e}$$

$$\theta = \arctan\left(\frac{N_y}{N_x}\right) \tag{1f}$$

$$\frac{d\xi}{dx} = (1+\epsilon)\frac{N_x}{N} \tag{1g}$$

$$\frac{d\eta}{dx} = (1+\epsilon)\frac{N_y}{N} \tag{1h}$$

$$\frac{ds}{dx} = 1+\epsilon \tag{1i}$$

in which x is the original coordinate of the general point P when the cable is in an unstretched state, N_x and N_y are the components of the normal force N in the cable, σ is the stress, ϵ the strain, θ the final inclination of the centerline, ξ the final x-coordinate, η the final y-coordinate, s the distance along the centerline in the stretched state, and p_x and p_y the distributed forces per unit length of original centerline. The quantity A is the effective cross-sectional area. To obtain a differential equation on θ, equation (1f) can be differentiated with respect to x to obtain:

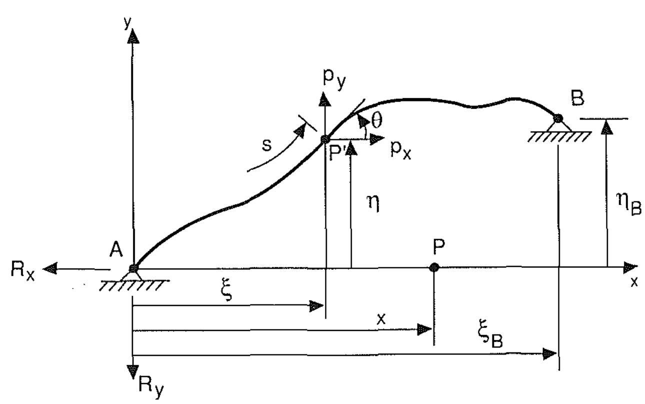

Fig. 1 Extensible cable

Contributed by the Applied Mechanics Division of The American Society of Mechanical Engineers for presentation at the Joint ASCE/ASME Applied Mechanics, Biomechanics, and Fluids Engineering Conference, San Diego, CA, July 9 to 12, 1989.
Discussion of this paper should be addressed to the Editorial Department, ASME, United Engineering Center, 345 East 47th Street, New York, N.Y. 10017, and will be accepted until two months after final publication of the paper itself in the Journal of Applied Mechanics. Manuscript received and accepted by ASME Applied Mechanics Division, May 10, 1988.
Paper No. 89-APM-31.

$$\frac{d\theta}{dx}=\frac{N_x\dfrac{dN_y}{dx}-N_y\dfrac{dN_x}{dx}}{N_x{}^2+N_y{}^2}. \tag{2}$$

To achieve a linear stress-strain relation, let equation (1e) be written as:

$$\epsilon=\frac{\sigma}{E} \tag{3}$$

where E is the effective modulus.

If forces q_x, q_y per unit length of deformed centerline are specified, then p_x, p_y can be computed from:

$$p_x=q_x\,\frac{ds}{dx} \tag{4a}$$

$$p_y=q_y\,\frac{ds}{dx}\,. \tag{4b}$$

A number of cases in which the cable is fixed at both ends have been solved (Huddleston, 1981). In the analysis of a cable with a free end, however, a difficulty arises in establishing a value for the inclination θ at that free end, inasmuch as the only differential equation available for θ in this theory is equation (2), and that one presents problems when an attempt is made to integrate it in the vicinity of the free end, where N and thus both of its components are zero. This difficulty also manifests itself in the indeterminate forms that occur in equations (1f), (1g), and (1h) at the free end.

The purpose of the present paper is to show a way to circumvent such difficulties by treating the extensible cable as a limiting case of a very flexible rod. This picks up on a suggestion made by Huddleston and Dowd (1979), which is to let the moment of inertia I_o of the cross-section of the rod approach zero while its area A_o and its original length L remain finite. In this process, the extensibility parameter C defined as

$$C=\frac{I_o}{A_oL^2} \tag{5}$$

approaches zero.

The exact differential equations of an extensible rod are as follows (Huddleston and Dowd, 1979, and Nicolau and Huddleston, 1982):

$$\frac{d\theta}{dx}=\frac{M}{EI} \tag{6a}$$

$$\frac{du_y}{dx}=\left(1+\frac{N}{EA}\right)\sin\theta \tag{6b}$$

$$\frac{d\xi}{dx}=\left(1+\frac{N}{EA}\right)\cos\theta \tag{6c}$$

$$\frac{ds}{dx}=1+\frac{N}{EA} \tag{6d}$$

$$\frac{du_x}{dx}=\frac{d\xi}{dx}-1 \tag{6e}$$

$$\frac{dN}{dx}=-Q\,\frac{d\theta}{dx}-p_x\cos\theta-p_y\sin\theta \tag{6f}$$

$$\frac{dQ}{dx}=N\,\frac{d\theta}{dx}-p_x\sin\theta+p_y\cos\theta \tag{6g}$$

$$\frac{dM}{dx}=Q\left(1+\frac{N}{EA}\right) \tag{6h}$$

in which, in addition to the notation defined for equations (1), u_x and u_y are the displacements of the general point P from its original position, I is the moment of inertia of the cross-section about its centroidal axis, Q is the shear force, and M is the bending moment. For the case of a prismatic rod, $A=A_o$ and $I=I_o$.

For the prismatic rod, equations (6) can be reformulated in a dimensionless way as follows:

$$\frac{d\theta}{d\left(\frac{x}{L}\right)}=\frac{1}{C}\,\frac{M}{EA_oL} \tag{7a}$$

$$\frac{d\left(\frac{u_y}{L}\right)}{d\left(\frac{x}{L}\right)}=\left(1+\frac{N}{EA_o}\right)\sin\theta \tag{7b}$$

$$\frac{d\left(\frac{\xi}{L}\right)}{d\left(\frac{x}{L}\right)}=\left(1+\frac{N}{EA_o}\right)\cos\theta \tag{7c}$$

$$\frac{d\left(\frac{s}{L}\right)}{d\left(\frac{x}{L}\right)}=1+\frac{N}{EA_o} \tag{7d}$$

$$\frac{d\left(\frac{u_x}{L}\right)}{d\left(\frac{x}{L}\right)}=\frac{d\left(\frac{\xi}{L}\right)}{d\left(\frac{x}{L}\right)}-1 \tag{7e}$$

$$\frac{d\left(\frac{N}{EA_o}\right)}{d\left(\frac{x}{L}\right)}=-\frac{Q}{EA_o}\,\frac{d\theta}{d\left(\frac{x}{L}\right)}-\frac{p_xL}{EA_o}\cos\theta-\frac{p_yL}{EA_o}\sin\theta \tag{7f}$$

$$\frac{d\left(\frac{Q}{EA_o}\right)}{d\left(\frac{x}{L}\right)}=\frac{N}{EA_o}\,\frac{d\theta}{d\left(\frac{x}{L}\right)}-\frac{p_xL}{EA_o}\sin\theta+\frac{p_yL}{EA_o}\cos\theta \tag{7g}$$

$$\frac{d\left(\frac{M}{EA_oL}\right)}{d\left(\frac{x}{L}\right)}=\frac{Q}{EA_o}\left(1+\frac{N}{EA_o}\right). \tag{7h}$$

Now there is a proper differential equation on θ, equation (7a), that gives $d\theta/dx=0$ at a free end as long as C is nonzero. The method of this paper is to solve the rod problem with progressively smaller values of C to determine if there is a limiting shape that could be considered the solution to the corresponding cable problem. An integrating package for nonlinear two-point boundary value problems, similar to that used by Huddleston and Dowd (1979), is used for this purpose.

Four cases are considered:

(A) cable under a midspan concentrated force,
(B) cable under its own weight,
(C) cable with free end, suspended in a moving fluid, drag a function of inclination only, and

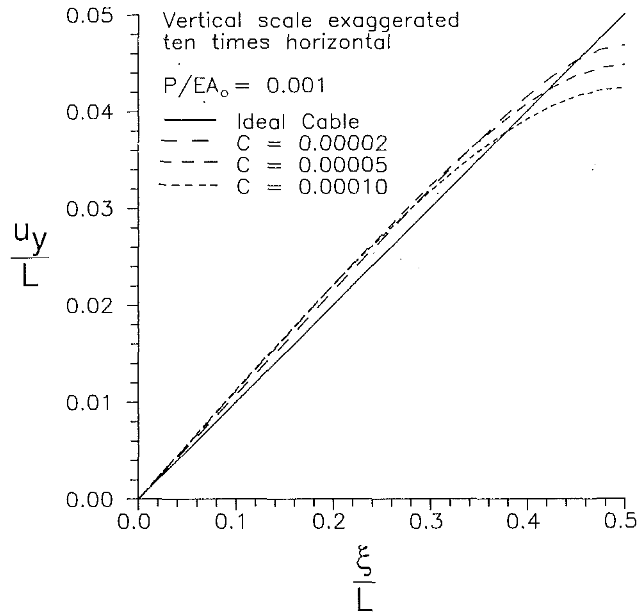

Fig. 2 Tie rod under midspan concentrated force

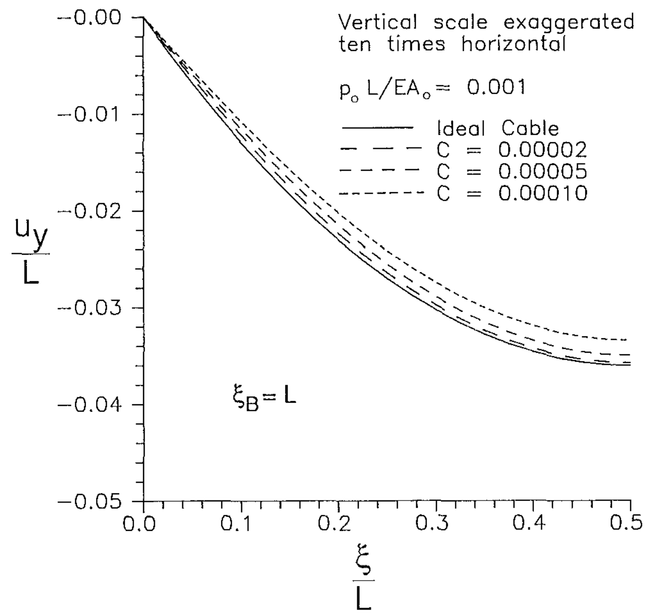

Fig. 3 Tie rod under own weight

(D) cable with free end, suspended in a moving fluid, drag a function of inclination and depth.

Cases (A) and (B) are used to compare the rod solutions with known cable solutions given by Huddleston (1981). Cases (C) and (D) are posed as problems for which the cable solution is not readily apparent, but some information about it can be obtained by the method of this paper. For all of the problems solved, the computer package can be used in a form consisting of a main program and eight subroutines. The main program and two of the subroutines are problem dependent. The rest are problem independent.

One advantage of the method is that a small amount of flexural stiffness can be left in the rod to represent the small amount of moment-carrying capacity of a cable that is an important effect in some practical problems.

Cable Under a Midspan Concentrated Force

Figure 2 shows profiles of a pinned-pinned tie rod carrying a midspan concentrated force given in dimensionless form as:

$$\frac{P}{EA_o} = 0.001. \tag{8}$$

The parameter C starts at the smallest value considered by Huddleston and Dowd (1979) and is then reduced two more times to still smaller values. Also plotted is the shape of the ideal cable obtained from equations (7) of the paper by Huddleston and Dowd (1979). The abrupt slope change at the midpoint of the ideal cable, of course, cannot be replicated by the tie rod, so this problem makes excessive demands on the proposed method.

Cable Under Its Own Weight

Figure 3 shows profiles of a pinned-pinned tie rod under its own weight, with

$$p_x = 0,\ p_y = -p_o \tag{9}$$

and with

$$\frac{p_o L}{EA_o} = 0.001. \tag{10}$$

Three curves are shown using the same three values of C as in Fig. 2, and the result for the ideal cable obtained by the method of Huddleston (1981) is also shown.

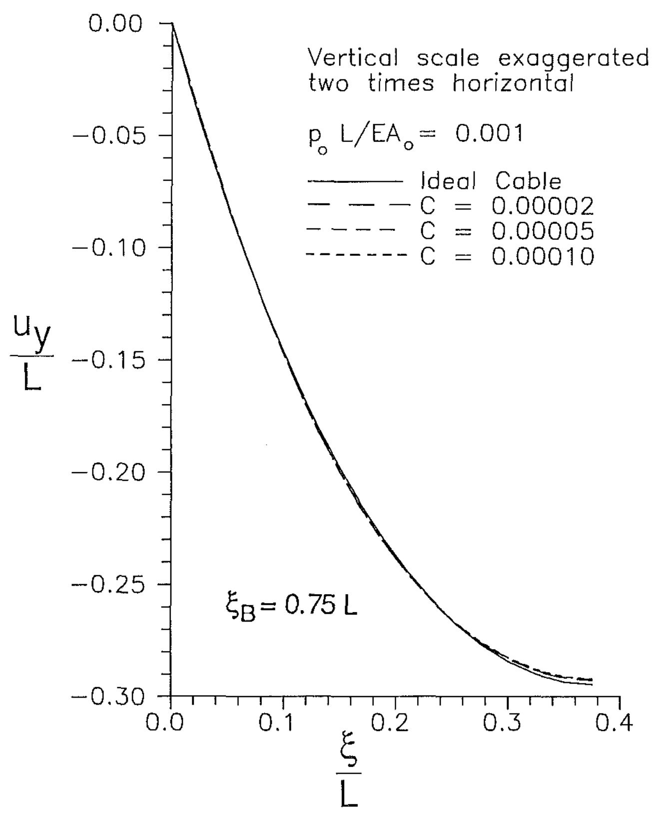

Fig. 4 Tie rod with right support displaced inwardly

Figure 4 shows similar results for the configuration considered by Huddleston (1981) of the right-end support at a distance of $0.75L$ from the left-end one.

Finally for this problem, Fig. 5 shows how the tie rod quantities

$$\theta_A \text{ and } R_A/EA_o$$

at the left end, where R_A is the horizontal reaction, vary with the position of the right-end support for a single value of C, namely, 0.00005.

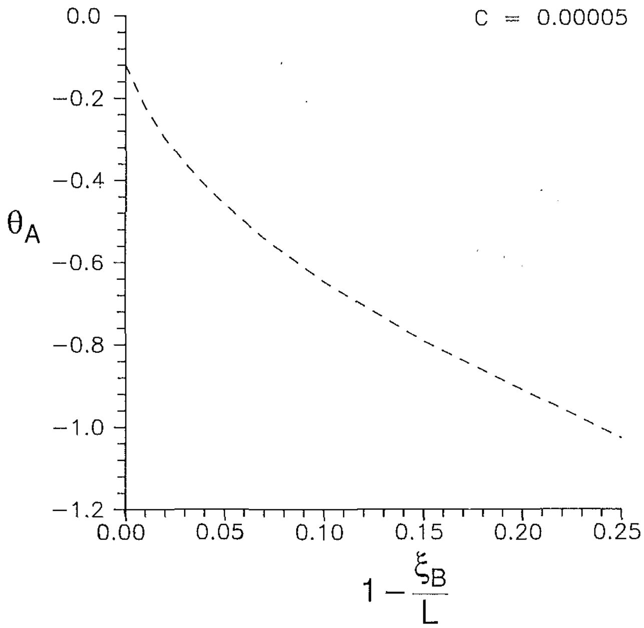

Fig. 5(*a*) Variation of θ_A with right-end position

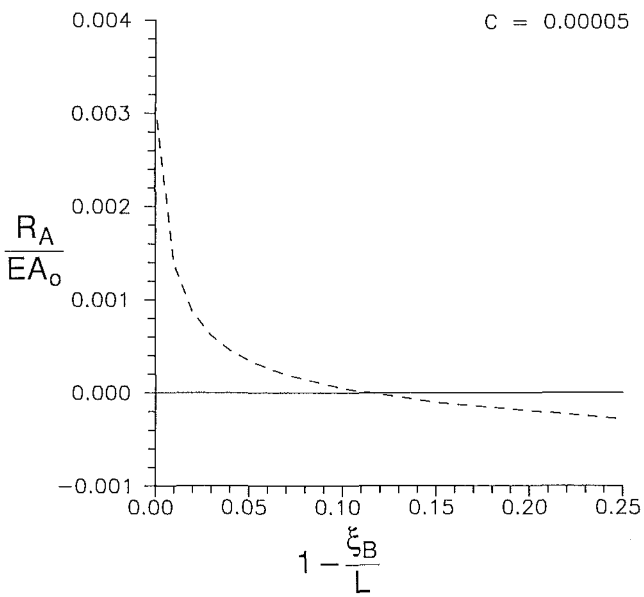

Fig. 5(*b*) Variation of R_A/EA_o with right-end position

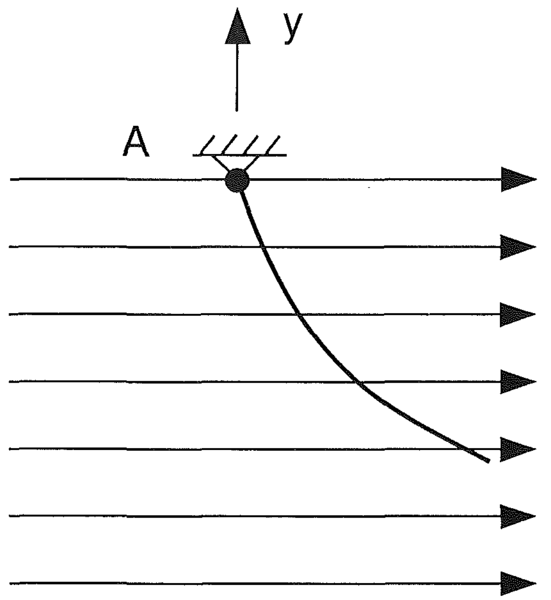

Fig. 6 Cable in moving fluid

Cable With Free End, Suspended in a Moving Fluid, Drag a Function of Inclination Only

To test the method on a cable with a free end, the problem of a cable suspended in a moving fluid, as in Fig. 6, is considered. In this case, it is assumed that the drag force is horizontal and is a linear function of $|\theta|$, i.e.,

$$q_x = \frac{2}{\pi} q_o |\theta| \tag{11}$$

but that again

$$p_y = -p_o. \tag{12}$$

From equation (4*a*), therefore,

$$p_x = \frac{2}{\pi} q_o |\theta| \frac{ds}{dx}. \tag{13}$$

More realistic drag forces, with normal and tangential components determined separately, could be incorporated into the method.

Cases with

$$q_o = \alpha p_o \tag{14}$$

for various values of α have been solved, and results are shown in Fig. 7 for $\alpha = 0.5$. The rod profiles come out very close to straight lines, thus suggesting the possibility that the cable possesses an equilibrium state with θ equal to a constant in this case. To investigate that possibility, consider the following boundary value problem taken from equations (1*a*), (1*b*), and (1*f*):

$$\frac{d\left(\frac{N_x}{EA_o}\right)}{d\left(\frac{x}{L}\right)} = -\frac{p_x L}{EA_o} \tag{15a}$$

$$\frac{d\left(\frac{N_y}{EA_o}\right)}{d\left(\frac{x}{L}\right)} = -\frac{p_y L}{EA_o} \tag{15b}$$

$$\tan\theta = \frac{N_y}{N_x}. \tag{15c}$$

If the cable is *inextensible*, then

$$\frac{ds}{dx} = 1 \tag{16}$$

and the applied forces are:

$$\frac{p_x L}{EA_o} = \frac{2}{\pi}\alpha \frac{p_o L}{EA_o} |\theta| \tag{17a}$$

$$\frac{p_y L}{EA_o} = -\frac{p_o L}{EA_o}. \tag{17b}$$

Thus, equations (15*a*) and (15*b*) become:

$$\frac{d\left(\frac{N_x}{EA_o}\right)}{d\left(\frac{x}{L}\right)} = -\frac{2}{\pi}\alpha \frac{p_o L}{EA_o} |\theta| \tag{18a}$$

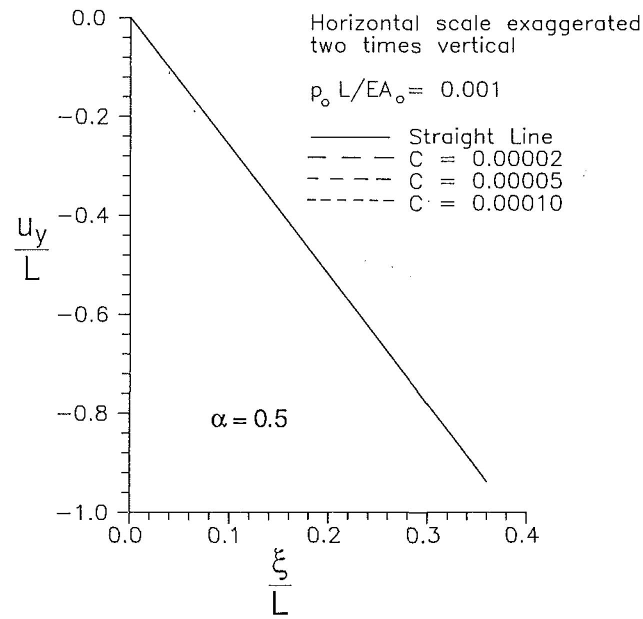

Fig. 7 Rod suspended in moving fluid

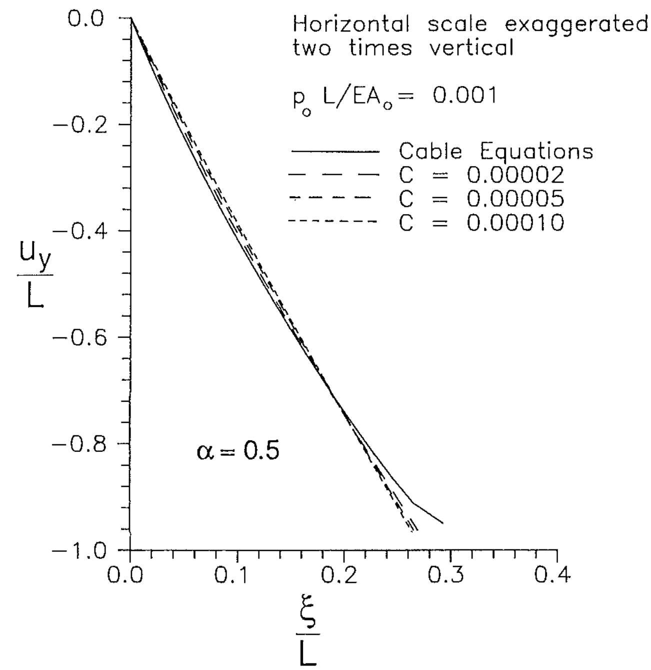

Fig. 8 Drag also a function of depth

$$\frac{d\left(\frac{N_y}{EA_o}\right)}{d\left(\frac{x}{L}\right)} = \frac{p_o L}{EA_o}. \tag{18b}$$

Now search for a solution with constant $|\theta|$. With that assumption, equations (18) can be integrated to obtain:

$$\frac{N_x}{EA_o} = -\frac{2}{\pi}\alpha\frac{p_o L}{EA_o}|\theta|\left(\frac{x}{L}\right) + \frac{2}{\pi}\alpha\frac{p_o L}{EA_o}|\theta| \tag{19a}$$

$$\frac{N_y}{EA_o} = \frac{p_o L}{EA_o}\left(\frac{x}{L}\right) - \frac{p_o L}{EA_o}. \tag{19b}$$

At $x/L = 0$:

$$\frac{N_x}{EA_o} = \frac{2}{\pi}\alpha\frac{p_o L}{EA_o}|\theta| \tag{20a}$$

$$\frac{N_y}{EA_o} = -\frac{p_o L}{EA_o}. \tag{20b}$$

Therefore, from equation (15c):

$$\tan|\theta| = \frac{\pi}{2\alpha}\frac{1}{|\theta|}. \tag{21}$$

For the cases displayed in Fig. 7:

$$\tan|\theta| = \frac{\pi}{|\theta|}. \tag{22}$$

A value of $\theta = -1.2046$ satisfies this equation, and a straight line with this inclination is also plotted in Fig. 7.

It is obvious that the rod solutions approximate the inextensible-cable solution very well in this case.

Cable With Free End, Suspended in a Moving Fluid, Drag a Function of Inclination and Depth

To ensure that the cable profile is not a straight line, a final case is considered in which the drag is a function of depth as well as inclination. Equation (11) is now replaced by:

$$q_x = \frac{2}{\pi}q_o|\theta|\left|\frac{u_y}{L}\right|. \tag{23}$$

Figure 8 shows the rod profiles for the three values of C again. These, like the results in Fig. 7, were obtained by solving a two-point boundary value problem with shear and bending moment specified as zero at the free end. Among the results yielded by the package of computer programs are the inclination and horizontal reaction at the pinned end. These are more easily found from the rod package than from the cable package because of the aforementioned difficulty experienced in dealing with the free end of the cable. Now, however, the missing initial conditions found in the rod solution can be used to solve the cable problem in the form of an initial-value problem. The result so obtained, using values from the case $C = 0.00002$, is also plotted in Fig. 8. The validity of this curve is questionable, however, since the singularity still exists at the terminal point of the integration process.

Conclusions

For an extensible cable with a free end, the idealization of perfect flexibility leads to difficulties in solving the mathematical problem, much in the same way that the idealization of inextensibility in a tie rod, fixed at both ends, leads to physically meaningless results. By removing some of the idealizations and approaching reality more closely, one can obtain more meaningful results. Then the idealized state can be looked upon as a limiting case.

In this paper, the extensible cable is treated as a rod with a small amount of flexural stiffness, and the perfect cable is then regarded as a limiting case.

References

Huddleston, J. V., 1981, "Computer Analysis of Extensible Cables," *Journal of the Engineering Mechanics Division*, ASCE., New York, Vol. 107, No. EM1, pp. 27–37.

Huddleston, J. V., and Dowd, J. P., 1979, "A Nonlinear Analysis of Extensible Tie-Rods," *Journal of the Structural Division*, ASCE, Vol. 105, No. ST11, pp. 2456-2460.

Nicolau, A. M., and Huddleston, J. V., 1982, "The Compressible Elastica on an Elastic Foundation," ASME Journal of Applied Mechanics, Vol. 49, No. 3, pp. 577–583.

Nonlinear Modeling of Flexible Multibody Systems Dynamics Subjected to Variable Constraints

S. K. Ider
Mem. ASME

F. M. L. Amirouche
Assistant Professor.
Mem. ASME

Department of Mechanical Engineering,
University of Illinois at Chicago,
Chicago, Ill. 60680

This paper presents the geometric stiffening effects and the complete nonlinear interaction between elastic and rigid body motion in the study of constrained multibody dynamics. A recursive formulation (or direct path approach) of the equations of motion based on Kane's equations, finite element method and modal analysis techniques is presented. An extended matrix formulation of the partial angular velocities and partial velocities for flexible (elastic) bodies is also developed and forms the basis for our analysis. Closed loops and kinematical constraints (specified motions) are allowed and their corresponding Jacobian matrices are fully developed. The constraint equations are appended onto the governing equations of motion by representing them in a minimum dimension form using an innovative method called the Pseudo-Uptriangular Decomposition method. Examples are presented to illustrate the method and procedures proposed.

1 Introduction

With the advent of computer hardware and software, it is becoming apparent that much is needed to be investigated before the new technology of faster robots, more efficient, and intelligent systems is to be developed. Algorithms for simulation of complex mechanical systems require the understanding of the application in question. The deployment of space satellites, the assembly of space structures, mechanisms, intelligent teleoperators, advanced robot systems, walking machines, among others, share a common kinematical, dynamical, and control problem. A number of researchers are developing theories and methodologies in the study of multibody dynamics where the effects of geometric nonlinearities, coriolis effects, nonuniform cross-section areas, and body structure composition are considered and, hence, automatically included in the equations of motion. The need in modeling with accuracy the dynamics of mechanical systems requires the automatic inclusion of geometric stiffening and complete nonlinear interaction between elastic and rigid body motion. The equations of motion must also be expressed in a minimum dimension form.

Earlier models of multibody systems by finite element or assumed mode methods were based on the assumption that small deformations of the bodies do not affect the nominal rigid body motion significantly (Imam and Sandor, 1975; Baghat and Willmert, 1976; Turcic and Midha, 1984; Naganathan and Soni, 1986; Sunada and Dubowsky, 1981; Ho, 1977). In their analysis, the inertia and reaction forces were evaluated from rigid motion and introduced to the linear elasticity problem as external forces for computing the corresponding deflections. The elastic deformation is then superimposed on the nominal rigid body motion. This procedure, however, does not yield accurate results when high speed systems are concerned, since it does not provide for the dynamic coupling of both the rigid and elastic motion.

Analysis procedures developed by Yoo and Haug (1985) and Agarwal and Shabana (1985) involve formulation of the equations of motion of each elastic body in terms of its "absolute" rigid body and elastic degrees-of-freedom. Then the rigid body motion and elastic deformations are solved simultaneously. However, the interconnections of the bodies are described by a large set of constraint equations formulated for each type of joints. This procedure increases the dimension of the problem considerably and the coordinate reduction by the elimination of the Lagrange multipliers associated with the constraint forces from the system equations of motion require the costly computations of updated transformations.

Singh et al. (1984) used a recursive formulation based on Kane's equations for multi-flexible body systems using assumed modes method where the assumed modes are obtained by a prior finite element analysis of each body. However, the formulation was restricted to clamped-free mode shapes and to the analysis of open tree configurations.

Recently Kane et al. (1986) showed that the geometrical nonlinearities in beam-like bodies arising from the coupling of longitudinal and transverse deformations have a considerable effect on the deformation of beams in high speed systems. These coupling effects were considered in the generalized inertia forces where a constraint equation is used to express the

Contributed by the Applied Mechanics Division of THE AMERICAN SOCIETY OF MECHANICAL ENGINEERS for presentation at the Joint ASCE/ASME Applied Mechanics, Biomechanics, and Fluids Engineering Conference, San Diego, CA, July 9 to 12, 1989.

Discussion of this paper should be addressed to the Editorial Department, ASME, United Engineering Center, 345 East 47th Street, New York, N.Y. 10017, and will be accepted until two months after final publication of the paper itself in the JOURNAL OF APPLIED MECHANICS. Manuscript received by ASME Applied Mechanics Division, May 2, 1988; final revision, October 21, 1988.

Paper No. 89-APM-38.

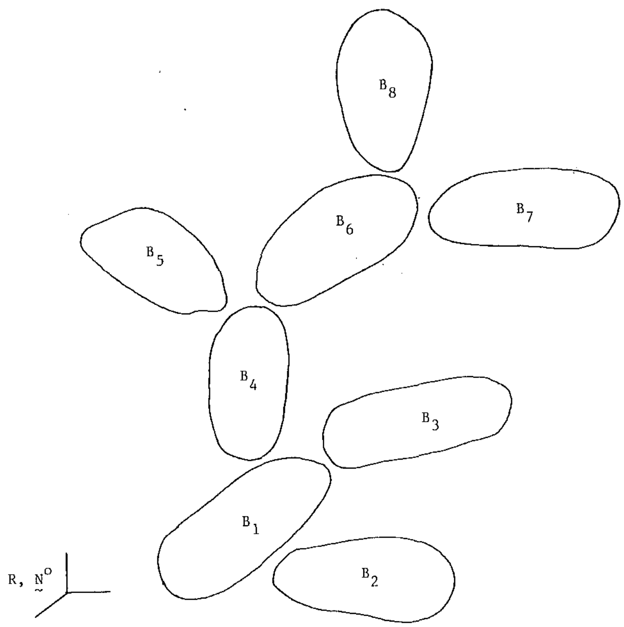

Fig. 1 A multibody structure

relationship between the deformation displacement components.

This paper's motivation stems from the purpose of overcoming the shortcomings of the various approaches undertaken and the algorithms developed in the past. A general recursive formulation utilizing relative coordinates and an algorithm ready for programming will be developed using Kane's equations and the convenience of partial velocity vectors. The equations of motion developed will incorporate arbitrary-shaped flexible bodies, will contain the complete interations of the rigid body motion and elastic deformations, and will be applicable to both open and closed configurations with prescribed motions. For these purposes, flexible body reference frames whose orientations depend on both the rigid body motion and the specified boundary conditions, consistent mass finite element approach together with component mode reduction, and a stable and efficient method for the elimination of the undetermined multipliers will be utilized.

2 Analytical Development

2.1 Notation and Preliminary Considerations. Consider a multibody system consisting of N rigid and flexible bodies as depicted by Fig. 1. The bodies in the system are interconnected by joints allowing, in general, six degrees-of-freedom. The system may be an open tree-like system, it may contain one or more closed loops, and any selected points may have prescribed motions.

In the notation, bold characters will be used to denote vectors whose components are described along unit vectors in a Cartesian reference frame. Matrices and vectors in the form of column matrices will be represented by omitting the subscripts. In the equations, the summation sign will be omitted, such that repeated index in a term implies summation over the range of the index. Superscripts are generally part of the labeling and do not imply summation unless otherwise specified.

A typical flexible body of the system is defined as a body B_k that undergoes relative rigid body motion, with respect to the lower body B_j, and small deformations at the same time. For this purpose the bodies in the mechanical systems are numbered in ascending order like a tree configuration starting from an arbitrary body.

The topology of the structure will be described by means of a tree array $\Gamma^h(k)$, $k=1, \ldots, N$. Let $\Gamma^1(k)$ denote the adjacent lower body connected to B_k. Then one can generate $\Gamma^h(k) h \geq 2$. Let $H(k)$ represent the maximum order h for which $\Gamma^h(k)$ is nonzero for B_k. Then the tree array $\Gamma^h(k) h = 1, \ldots, H$ indicates the chain of bodies which are on the path from B_k to the reference frame (Huston et al., 1978).

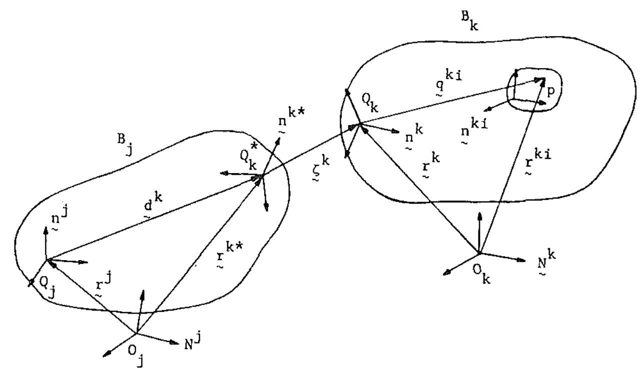

Fig. 2 Labeling position vectors in adjacent bodies ($\mathbf{N}^k$ represents an axis frame whose mutually-perpendicular unit vectors are $\mathbf{N}_1^k, \mathbf{N}_2^k, \mathbf{N}_3^k$. Similar representation is used for the other axis frames $\mathbf{n}^k$, $\mathbf{n}^{k^*}$, $\mathbf{n}^{ki}$).

Two connecting bodies R_k and B_j are shown in Fig. 2. The connection points are Q_k and Q_k^* on B_k and B_j, respectively. The rigid body degrees-of-freedom of B_k are characterized by the relative translation and the relative rotation of the $\mathbf{n}^k$ axes fixed (to an infinitesimal element) at Q_k, with respect to the $\mathbf{n}^{k^*}$ axes fixed at Q_k^*. (See Fig. 2 for the representation of the unit vectors.)

Let $\mathbf{N}^k$ be the body reference axes of B_k relative to which the deformation of the body is defined. $\mathbf{N}^k$, in general, is not fixed to a point on the body. Its orientation during the rigid body motion and the deformation is defined such that the boundary conditions specified at the connection points are satisfied. By this way any set of boundary conditions at the joints can be specified corresponding to the mode shapes, which best describe the deformation of the body. Consider an axis frame denoted by $\overline{\mathbf{n}}^{ki}$ which is located at O_k and parallel to the initial orientation of the element axes $\mathbf{n}^{ki}$. Then the position vector from O_k to an arbitrary point P in the element, $\mathbf{r}^{ki}$ can be written in $\mathbf{N}^k$ as

$$\mathbf{r}^{ki} = \phi_l^{ki} e_l^{ki} \quad l = 1, \ldots, n^{ki} \tag{1}$$

where ϕ^{ki} is the shape function matrix containing the necessary transformations from $\overline{\mathbf{n}}^{ki}$ to $\mathbf{N}^k$, and e_l^{ki} is given by

$$e_l^{ki} = e_{ol}^{ki} + \alpha_l^{ki} \tag{2}$$

where e_{ol}^{ki} are the initial nodal coordinates of element i, yielding the undeformed position vector, and α_l^{ki} are the nodal deformation displacement coordinates of element i. In equation (1), n^{ki} is the number of the nodal coordinates of element i. The total number of the nodal coordinates of B_k, after assemblage, will be denoted by n^k. And the summation of n^k, from $k=1$ to N, will then be denoted by n.

Expressing $\mathbf{r}^k$ in a similar manner, $\mathbf{q}^{ki}$ can be written as

$$\mathbf{q}^{ki} = (\phi_l^{ki} B_{lp}^{ki} - \phi_l^k B_{lp}^k) e_p^k \quad p = 1, \ldots, n^k; l = 1, \ldots, n^{ki} \tag{3}$$

where ϕ^k is the shape function matrix of the element in which Q_k lies, evaluated at the coordinates of Q_k, e_p^k are the nodal coordinates of B_k and B^{ki} and B^k are boolean matrices indicating the indices of nodal coordinates of the respective elements in e_p^k. These boolen matrices describe the connectivity between the elements.

Similarly, we also express $\mathbf{d}^k$ in $\mathbf{N}^j$ as

$$\mathbf{d}^k = (\phi_l^{k^*} B_{lp}^{k^*} - \phi_l^j B_{lp}^j) e_p^j \tag{4}$$

where ϕ^{k^*} and ϕ^j are the corresponding shape function matrices at the coordinates of Q_k^* and Q_j in $\mathbf{N}^j$, and B^{k^*} and B^j are the corresponding boolean matrices.

By utilizing the rotation displacement relations of elasticity (Dym and Shames, 1973), the rotations θ_r^{ki}, $= r = 1, 2, 3$ of an infinitesimal element at element i, with respect to $\mathbf{N}^k$, can be expressed in terms of the nodal coordinates, in the form

$$\theta_r^{ki} = \psi_{rl}^{ki} e_l^{ki} \quad r = 1, 2, 3;\ l = 1, \ldots, n^{ki} \tag{5}$$

where ψ^{ki} are functions of the undeformed position coordinates.

2.2 The Generalized Coordinates and Generalized Speeds. To reduce the large number of elastic coordinates, the standard component mode technique will be utilized (Hurty, 1965). This involves using a small number of mode shapes for each flexible body. The modal coordinates η_l are given by the modal transformation X obtained for the system from the free-vibration eigenvalue problems of each flexible body,

$$\alpha_l = X_{lp}\eta_p \quad l = 1, \ldots, n;\ p = 1, \ldots, m. \tag{6}$$

The eigenvalue problem for B_k can be expressed as (Przemieniecki, 1968)

$$M_{rl}^k \ddot{\alpha}_l^k + K_{rl}^k \alpha_l^k = 0 \tag{7}$$

where M^k and K^k are the structural mass and stiffness matrices obtained by imposing the selected boundary conditions at the connection points. The approximate solution to equation (7) is

$$\alpha_l^k = X_{lp}^k \eta_p^k \quad l = 1, \ldots, n^k;\ p = l, \ldots, m^k \tag{8}$$

where X^k is the matrix with eigenvectors (mode shapes) as columns, η_p^k are the modal coordinates of B_k and m^k is the number of the eigenvectors retained. Then X in equation (6) is obtained as a block diagonal matrix whose diagonal submatrices are X^k, $k = 1, \ldots, N$.

The relative rigid body translation vector ζ^k can be expressed as

$$\zeta^k = \zeta_l^k \mathbf{n}_l^{k^*} \quad l = 1, 2, 3. \tag{9}$$

For the relative rigid body rotation degrees-of-freedom, the successive Euler angles (in transforming $\mathbf{n}^{k^*}$ to $\mathbf{n}^k$) can be used. Hence, the position of the system can be described by $3N$ Euler angles, $3N$ relative translation components, and m modal coordinates.

The angular velocity of $\mathbf{n}^k$, with respect to $\mathbf{n}^{k^*}$, can be expressed as

$$^{\mathbf{n}^{k^*}}\boldsymbol{\omega}^{\mathbf{n}^k} = \hat{\omega}_p^k \mathbf{n}_p^{k^*} \quad p = 1, 2, 3 \tag{10}$$

where $\hat{\omega}_p^k$ denotes the relative angular velocity components.

Then the generalized speeds y_l of the system could be conveniently selected as the $3N$ relative angular velocity components $\hat{\omega}_l$, the $3N$ relative translational velocity components $\dot{\zeta}_l$, and m modal coordinate dervatives $\dot{\eta}_l$,

$$\hat{\omega} = [\hat{\omega}_1^1, \hat{\omega}_2^1, \hat{\omega}_3^1, \ldots, \hat{\omega}_1^N, \hat{\omega}_2^N, \hat{\omega}_3^N]^T \tag{11}$$

$$\dot{\zeta} = [\dot{\zeta}_1^1, \dot{\zeta}_2^1, \dot{\zeta}_3^1, \ldots, \dot{\zeta}_1^N, \dot{\zeta}_2^N, \dot{\zeta}_3^N]^T \tag{12}$$

$$\dot{\eta} = [\dot{\eta}_1^1, \ldots, \eta_{n^1}^1, \ldots, \dot{\eta}_1^N, \ldots, \dot{\eta}_{m^N}^N]^T \tag{13}$$

and

$$y = [\hat{\omega}^T, \dot{\zeta}^T, \dot{\eta}^T]^T. \tag{14}$$

2.3 Angular Velocities. For obtaining the velocity of point P in the stationary reference $\mathbf{N}^o$, we need the angular velocity of $\mathbf{N}^k$ in $\mathbf{N}^o$, ω^k, and the angular velocity of $\mathbf{n}^{k^*}$ in $\mathbf{N}^o$, ω^{k^*}. ω^k can be written as

$$\omega^k = {}^{\mathbf{N}^o}\boldsymbol{\omega}^{\mathbf{n}^1} + {}^{\mathbf{n}^1}\boldsymbol{\omega}^{\mathbf{n}^{2^*}} + \ldots + {}^{\mathbf{n}^j}\boldsymbol{\omega}^{\mathbf{n}^{k^*}} + {}^{\mathbf{n}^{k^*}}\boldsymbol{\omega}^{\mathbf{n}^k} + {}^{\mathbf{n}^k}\boldsymbol{\omega}^{\mathbf{N}^k}. \tag{15}$$

Using equation (5), ${}^{\mathbf{n}^j}\boldsymbol{\omega}^{\mathbf{n}^{k^*}}$ and ${}^{\mathbf{n}^k}\boldsymbol{\omega}^{\mathbf{N}^k}$ can be expressed as

$${}^{\mathbf{n}^j}\boldsymbol{\omega}^{\mathbf{n}^{k^*}} = (\psi_l^{k^*} B_{lq}^{k^*} - \psi_l^j B_{lq}^j)\dot{\alpha}_q^j \tag{16}$$

and

$${}^{\mathbf{n}^k}\boldsymbol{\omega}^{\mathbf{N}^k} = -\psi_l^k B_{lq}^k \dot{\alpha}_q^k \tag{17}$$

where the matrices ψ^{k^*}, ψ^j and ψ^k of respective elements are evaluated at the coordinates of Q_k^*, Q_j, and Q_k, respectively. Using equations (10), (16), and (17), considering the topological information of the multibody system and making use of the transformation matrices between axis systems, ω^k can be compactly expressed as

$$\omega^k = \nu_l^k \hat{\omega}_l + \mu_p^k \dot{\alpha}_p \quad l = 1, \ldots, 3N;\ p = 1, \ldots, n \tag{18}$$

where ν_l^k and μ_p^k are the partial angular velocity vectors composed of the coefficients of $\hat{\omega}_l$ and $\dot{\alpha}_p$, respectively,

$$\nu_l^k = \sum_{h=o}^{H(k)} S_{mu}^{os^*} a_{ul}^s \mathbf{N}_m^o \quad s = \Gamma^h(k);\ r = \Gamma(s) \tag{19}$$

and

$$\mu_p^k = \left\{ \sum_{h=o}^{H(k)} S_{mu}^{or}(\psi_{ut}^{s^*} B_{tq}^{s^*} - \psi_{ut}^r B_{tq}^r) b_{qp}^r - S_{mu}^{ok}\psi_{ut}^k B_{tq}^k b_{qp}^k \right\} \mathbf{N}_m^o \tag{20}$$

where the boolean matrices a^k and b^k are defined such that $\hat{\omega}_u^k = a_{ul}^k \hat{\omega}_l$ and $e_q^k = b_{qp}^k e_p$. ω^{k^*} is obtained by deleting the last two terms in equation (15),

$$\omega^{k^*} = \nu_l^j \hat{\omega}_l + \mu_p^{k^*} \dot{\alpha}_p \quad j = \Gamma(k) \tag{21}$$

where for μ^{k^*} the last term in equation (20) is deleted.

2.4 Velocity and Acceleration of an Arbitrary Point. The position vector to P in R is

$$\mathbf{p}^{ki} = \sum_s \zeta^s + \sum_s \mathbf{d}^s + \mathbf{q}^{ki} \tag{22}$$

where the summations are carried for the bodies along path from $\mathbf{N}^o$ to B_k.

Differentiating equation (22), utilizing equations (3), (4), (9), (18), and (21), and making use of the coordinate transformation matrices and boolean matrices, the velocity vector $\mathbf{v}^{ki}$ can be expressed as

$$\mathbf{v}^{ki} = \gamma_l^{ki}\hat{\omega}_l + \nu_l^k \dot{\zeta}_l + \beta_p^{ki}\dot{\eta}_p \tag{23}$$
$$l = 1, \ldots, 3n; \quad p = 1, \ldots, m$$

where γ_l^{ki}, ν_l^k, and β_p^{ki} are the partial velocity vectors containing the coefficients of the generalized speeds $\hat{\omega}_l$, $\dot{\zeta}_l$ and $\dot{\eta}_p$. Again, the partial velocity arrays can be expressed in a form ready for coding,

$$\gamma_l^{ki} = \left\{ \sum_{z=o}^{H(k)} [S_{hq}^{os^*}\zeta_q^s \nu_{tl}^r e_{mth} + S_{hq}^{or} d_q^s \nu_{tl}^r e_{mth}] + S_{hq}^{ok} q_q^{ki} \nu_{tl}^k e_{mth} \right\} \mathbf{N}_m^o \tag{24}$$

and

$$\beta_p^{ki} = \left\{ \sum_{z=o}^{H(k)} [S_{hq}^{os^*}\zeta_q^s \mu_{tj}^{s^*} e_{mth} + S_{hq}^{or} d_q^s \mu_{tj}^r e_{mth} + S_{mt}^{or}(\phi_{tv}^{s^*} B_{vu}^{s^*} - \phi_{tv}^r B_{vu}^r) b_{uj}^r] + S_{mt}^{ok}(\phi_{tv}^{ki} B_{vu}^{ki} - \phi_{tv}^k B_{vu}^{ki}) b_{uj}^k + S_{hq}^{ok} q_q^{ki} \mu_{tj}^k e_{mth} \right\} X_{jp} \mathbf{N}_m{}^o. \tag{25}$$

The acceleration of point P is then obtained by differentiating equation (23)

$$\mathbf{a}^{ki} = \gamma_l^{ki}\dot{\omega}_l + \nu_l^k\ddot{\zeta}_l + \beta_p^{ki}\ddot{\eta}_p + \dot{\gamma}_l^{ki}\omega_l + \dot{\nu}_l^k\dot{\zeta}_l + \dot{\beta}_p^{ki}\dot{\eta}_p. \tag{26}$$

2.5 Equations of Motion for Tree Topology. Kane's equations for the multibody system can be written as

$$F_l^* + F_l - F_l^s = 0 \quad l = 1, \ldots, 6N+m \tag{27}$$

where F_l^* are the generalized inertia forces, F_l the generalized external forces and F_l^s the generalized internal forces due to the strain energy of the bodies.

The generalized inertia forces due to the inertias of the particles in each body for the entire system are

$$F_l^* = -\sum_{k=1}^{N}\sum_{i=1}^{E_k}\int_{V_{ki}}\rho^{ki}\frac{\partial \mathbf{v}^{ki}}{\partial y_l}\cdot\mathbf{a}^{ki}dV \quad l = 1, \ldots, 6N+m \tag{28}$$

where ρ^{ki} is the mass density and V_{ki} is the volume of the element.

For the generalized external forces, let the element i be subject to external surface tractions $\mathbf{f}^{ki}$ and body forces $\mathbf{b}^{ki}$, expressed in terms of the axis $\mathbf{N}^o$. Then

$$F_l = \sum_{k=1}^{N}\sum_{i=1}^{E_k}\left[\int_{S_{ki}}\frac{\partial \mathbf{v}^{ki}}{\partial y_l}\cdot\mathbf{f}^{ki}dS + \int_{V_{ki}}\frac{\partial \mathbf{v}^{ki}}{\partial y_l}\cdot\mathbf{b}^{ki}dV\right]$$
$$l = 1, \ldots, 6N+m \tag{29}$$

where S_{ki} denotes the part of the element surface which lies in the global boundary.

The equations of motion for the multibody system can then be written as

$$M\dot{y} + S + Q = F \tag{30}$$

or

$$\begin{bmatrix} M^{11} & M^{12} & M^{13} \\ M^{21} & M^{22} & M^{23} \\ M^{31} & M^{32} & M^{33} \end{bmatrix}\begin{bmatrix}\dot{\omega}\\ \ddot{\zeta}\\ \ddot{\eta}\end{bmatrix} + \begin{bmatrix}0\\0\\S^3\end{bmatrix} + \begin{bmatrix}Q^1\\Q^2\\Q^3\end{bmatrix} = \begin{bmatrix}F^1\\F^2\\F^3\end{bmatrix} \tag{31}$$

where

$$M_{rl}^{11} = \sum_k\sum_i\int_{V_{ki}}\rho\gamma_{mr}^{ki}\gamma_{ml}^{ki}dV \quad m = 1,2,3;\ r,l = 1, \ldots, 3N \tag{32a}$$

$$M_{rl}^{22} = \sum_k\sum_i\int_{V_{ki}}\rho\nu_{mr}^{k}\nu_{ml}^{k}dV \tag{32b}$$

$$M_{st}^{33} = \sum_k\sum_i\int_{V_{ki}}\rho\beta_{ms}^{ki}\beta_{mt}^{ki}dV \quad s,t = 1, \ldots, m \tag{32c}$$

$$M_{rl}^{12} = \sum_k\sum_i\int_{V_{ki}}\rho\gamma_{mr}^{ki}\nu_{ml}^{k}dV \tag{32d}$$

$$M_{rs}^{13} = \sum_k\sum_i\int_{V_{ki}}\rho\gamma_{mr}^{ki}\beta_{ms}^{ki}dV \tag{32e}$$

$$M_{rs}^{23} = \sum_k\sum_i\int_{V_{ki}}\rho\nu_{mr}^{k}\beta_{ms}^{ki}dV \tag{32f}$$

$$Q_r^1 = \sum_k\sum_i\int_{V_{ki}}\rho\gamma_{mr}^{ki}(\dot{\gamma}_{ml}^{ki}\omega_l + \dot{\nu}_{ml}^{k}\dot{\zeta}_l + \dot{\beta}_{mp}^{ki}\dot{\eta}_p)dV \tag{32g}$$

$$Q_r^2 = \sum_k\sum_i\int_{V_{ki}}\rho\nu_{mr}^{k}(\dot{\gamma}_{ml}^{ki}\omega_l + \dot{\nu}_{ml}^{k}\dot{\zeta}_l + \dot{\beta}_{mp}^{ki}\dot{\eta}_p)dV \tag{32h}$$

$$Q_s^3 = \sum_k\sum_i\int_{V_{ki}}\rho\beta_{mr}^{ki}(\dot{\gamma}_{ml}^{ki}\omega_l + \dot{\gamma}_{ml}^{k}\dot{\zeta}_l + \dot{\beta}_{mp}^{ki}\dot{\eta}_p)dV \tag{32i}$$

$$F_r^1 = \sum_k\sum_i\left[\int_{S_{ki}}\gamma_{mr}^{ki}f_m^{ki}dS + \int_{V_{ki}}\gamma_{mr}^{ki}b_m^{ki}dV\right] \tag{32j}$$

$$F_r^2 = \sum_k\sum_i\left[\int_{S_{ki}}\nu_{mr}^{k}f_m^{ki}dS + \int_{V_{ki}}\nu_{mr}^{k}b_m^{ki}dV\right] \tag{32k}$$

$$F_r^3 = \sum_k\sum_i\left[\int_{S_{ki}}\beta_{ms}^{ki}f_m^{ki}dS + \int_{V_{ki}}\beta_{ms}^{ki}b_m^{ki}dV\right] \tag{32l}$$

and

$$S_s^3 = X_{sp}^T(K_{pq} + G_{pq})\alpha_q \quad p,q = 1, \ldots, n,\ s = 1, \ldots, m. \tag{33}$$

In equation (33), G represents nonlinear stiffening terms due to structural geometrical constraints of the deformable body, and needs to be updated. K and G are block diagonal matrices expressed as

$$K = \text{diag}[K^1, \ldots, K^k, \ldots, K^N] \tag{34}$$

and

$$G = \text{diag}[G^1, \ldots, G^k, \ldots, G^N] \tag{35}$$

where K^k and G^k are, respectively, the structural and geometric stiffness matrices of B_k.

By manipulation in equations (32), the time-dependent and space-dependent terms are separated reducing the spatial integrals to

$$\int_{V_{ki}}\phi_{uv}^{ki}dV,\ \int_{V_{ki}}\phi_{uv}^{ki}\phi_{st}^{ki}dV, \quad u,s = 1, 2, 3;\ v,t = 1, \ldots, n^{ki}$$

which are evaluated only once in the analysis.

2.6 Geometrical Stiffness for Beams in Three-Dimensional Motion. The linear strain energy theory assumes that the deformation components are independent. But in high speed systems, high axial forces occur and the coupling between the axial and transverse deflections become significant, causing geometrical stiffening of the transverse deformations. For this reason, higher-order terms in the strain energy need to be considered.

Consider a beam element where the element reference axis frame $\mathbf{n}$ is located at the centroidal line. Let $\mathbf{x}_1$ be tangent to the centroidal line and the other two axes be the principle axes of the cross-section. Let $\nu_i(x, t)$ and $\theta_i(x, t)$ represent the deformation displacement and rotation components of axis frames located along the centroidal line x distance away from the element axis in the undeformed state. Then the displacement field for arbitrary points in the beam element, $u_i(x, y, z, t)$ can be expressed for small bending and torsion in terms of the undeformed state coordinates

$$\begin{aligned} u_1 &= v_1 + z\theta_2 - y\theta_3 \\ u_2 &= v_2 - z\theta_1 \\ u_3 &= v_3 + y\theta_1. \end{aligned} \tag{36}$$

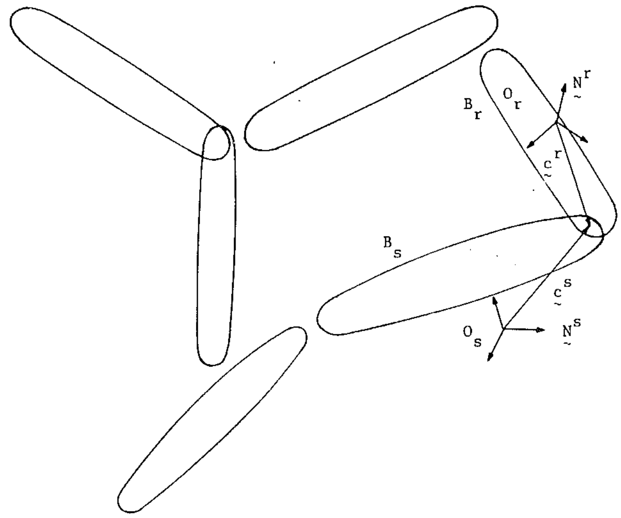

Fig. 3 A multibody structure with closed loop

If the volume change of an infinitesimal element in the deformed body is negligible, the strain energy is given by (Dym and Shames, 1973)

$$U = \int_V \epsilon^T \sigma dV \tag{37}$$

where ϵ and σ are, respectively, the vectors of strain and stress components.

ϵ_p, $p = 1, \ldots, 6$ are determined using nonlinear strain displacement relations where the displacements are given by equation (36). Utilizing generalized Hook's law, the strain energy is obtained from equation (37).

Considering that the beam is not subject to lateral tension or compression, σ_2 and σ_3 can be taken to be zero. Our aim is to retain the significant nonlinear terms in the strain energy related to high axial stresses, which is not ruled out by the assumed deformation field given by equations (36). Hence, fourth-order terms in $\partial v_2/\partial x$ and $\partial v_3/\partial x$; third-order terms in $\partial\theta_p/\partial x$, $p = 1, 2, 3$; and second-order terms in $\partial\theta_p/\partial x$ multiplied by $\partial v_2/\partial x$ or $\partial v_3/\partial x$ are neglected. Furthermore, the shear deformation is assumed small so that third-order terms involving $(\partial v_2/\partial x - \theta_3)$ and $(\partial v_3/\partial x + \theta_2)$ are neglected. This yields the following additional terms in the strain energy

$$U^G = \frac{EA}{2}\int_L \frac{\partial v_1^{ki}}{\partial x}\left(\frac{\partial v_2^{ki}}{\partial x}\right)^2 dx + \frac{EA}{2}\int_L \frac{\partial v_1^{ki}}{\partial x}\left(\frac{\partial v_2^{ki}}{\partial x}\right)^2 dx \tag{38}$$

where E is modulus of elasticity and A is cross-sectional area.

The element geometrical stiffness matrix can be determined by making use of Castigliano's theorem, then the matrix G^k in equation (35) can be obtained by the standard finite element assembly procedure.

3 Constrained Systems

3.1 Constraint Equations. Let us suppose that in the multibody system there are closed loops, and some bodies have a given prescribed motion, then the system becomes subjected to these constraints.

For a closed loop, let B_r and B_s connect with each other to form the closed loop as in Fig. 3. Also, let $\mathbf{c}^r$ be the undeformed position vector in $\mathbf{N}^r$ from O_r to the connection point, and $\mathbf{c}^s$ the undeformed position vector in $\mathbf{N}^s$ from O_s to the connection point. Then the associated three constraint equations are

$$(\gamma_l^{ri} - \gamma_l^{si})\hat{\omega}_l + (\nu_l^r - \nu_l^s)\dot{\zeta}_l + (\beta_p^{ri} - \beta_p^{ri})\dot{\eta}_p^{si} = 0 \tag{39}$$

where γ_l^{ri} and β_p^{ri} correspond to the spatial coordinates (c_1^r, c_2^r, c_3^r) and γ_l^{si} and β_p^{si} to (c_1^s, c_2^s, c_3^s).

In the case where a point has prescribed motion, let the prescribed velocity of a point A in B_r be $\mathbf{g}(t)$ with respect to $\mathbf{N}^o$, and let $\mathbf{c}^r$ be the undeformed position vector in $\mathbf{N}^r$ from O_r to A. The three constraint equations become

$$\gamma_l^{ri}\hat{\omega}_l + \nu_l^r\dot{\zeta}_l + \beta_p^{ri}\eta_p = \mathbf{g}(t) \tag{40}$$

where the spatial coordinates in γ_l^{ri} and β_p^{ri} are (c_1^r, c_2^r, c_3^r).

Finally, consider a body B_r whose reference axis $\mathbf{N}^r$ has a prescribed angular velocity $\mathbf{h}(t)$. In this case the constraint equations are

$$\nu_l^r\hat{\omega}_l + \mu_j^r X_{jp}\dot{\eta}_p = \mathbf{h}(t). \tag{41}$$

The holonomic and nonholonomic constraint equations can be compactly written as

$$B_{il}y_l = g_i \quad i = 1, \ldots, c; \; l = 1, \ldots, 6N+m \tag{42}$$

where c is the number of the constraint equations.

Kane's equations for the constrained system are given by

$$F_l^* + F_l - F_l^s + F_l^c = 0 \quad l = 1, \ldots, 6N+m \tag{43}$$

where

$$F_l^c = \lambda_i B_{li}^T \quad i = 1, \ldots, c. \tag{44}$$

F_l^c are the generalized constraint forces and λ_i are the undetermined multipliers.

It is rather obvious, from a computational point of view, that the equations of motion must be reduced. If the system has $6N+m$ degrees-of-freedom and is subjected to c constraints, then the degrees-of-freedom reduces to $6N+m-c$. The representation of the generalized constraint forces, as depicted by equation (44), makes the reduction of the equations of motion more attractive. To eliminate the undetermined multipliers, one needs to find an orthogonal complement matrix to the Jacobian matrix B.

There are a number of methods available for eliminating the undetermined multipliers in equation (43) which reduce the governing equations to $6N+m-c$. These include the zero eigenvalue theorem (Kamman and Huston, 1984) and singular value decomposition (Singh and Likins, 1985) – which require solving $6N+m$ dimensional eigenvalue problems – and coordinate partitioning methods (Wehage and Haug, 1982; Wampler et al., 1985) – which may lead to singularities depending on the selection of the independent coordinates.

Recently new computationally-efficient methods have been introduced, based on uptriangular decomposition of the constraint Jacobian matrix B, by successive Householder transformations (Amirouche and Jia, 1988); or by generating a row equivalence transformation matrix using Gauss-elimination row operations (Ider and Amirouche, 1988). Then a matrix orthogonal complement to the uptriangular matrix is identified. This leads to the generation of a transformation matrix C which is orthogonal complement to B. These methods also provide the capability of avoiding singularities that occur when the constraint equations become instantaneously linearly-dependent.

3.2 Solution Procedure. Premultiplying equations (43) by C^T, we obtain

$$C_{pl}^T(F_l^* + F_l - F_l^s) = 0 \tag{45}$$

$$p = 1, \ldots, 6N+m-r; \quad l = 1, \ldots, 6N+m$$

where $r \le c$ is the number of the linearly-independent constraint equations.

Using the results of the previous section, equation (45) becomes

$$C^T M\dot{y} = C^T(F - S - G). \tag{46}$$

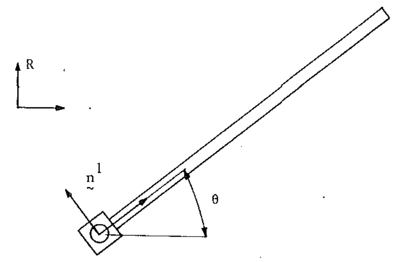

Fig. 4 Cantilever beam with rotating base

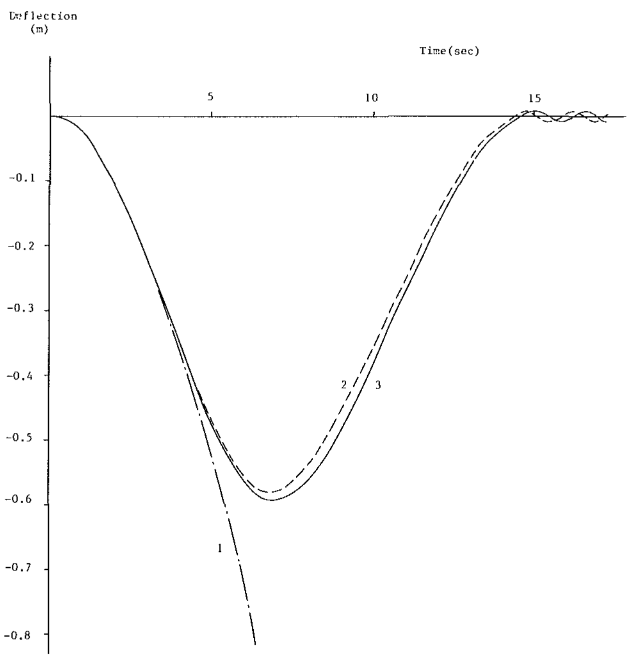

Fig. 5 Tip deflection: (1) without geometric stiffening, (2) with geometric stiffening (Ryan, 1987), and (3) with geometric stiffening (this paper)

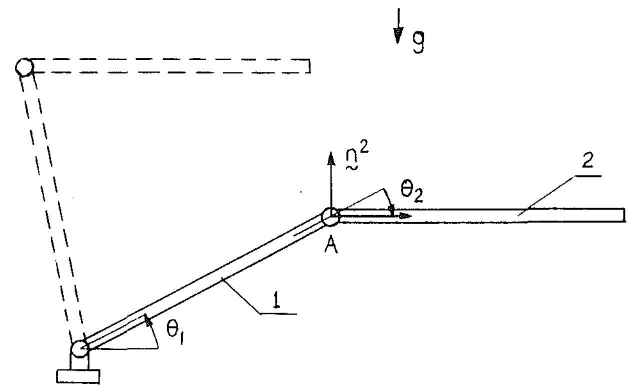

Fig. 6 Planar manipulator with link 2 constrained to remain horizontal

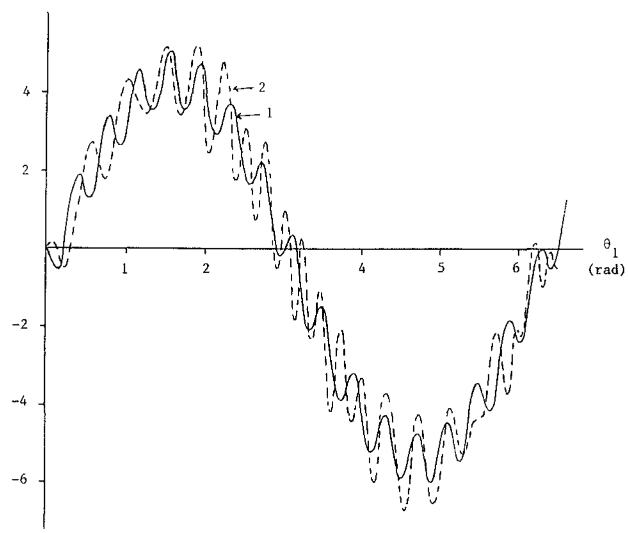

Fig. 7 Tip deflection of link 2: (1) link 1 rigid and (2) both links flexible

Let r-independent constraint equations be written as

$$D_{il}y_l = h_i \quad i=1, \ldots, r; \, l=1, \ldots, 6N+m \tag{47}$$

where the selection of the independent equations are done automatically during the formulation of C (Amirouche and Ider, 1988). Differentiating equations (47), we have

$$D_{il}\dot{y}_l + \dot{D}_{il}y_l - \dot{h}_l = 0 \quad i=1, \ldots, r. \tag{48}$$

Combining equations (46) and (48) we obtain

$$H_{lp}\dot{y}_p = R_l \quad p,l=1, \ldots, 6N+m \tag{49}$$

where

$$H = \begin{bmatrix} C_{pl}M_{lq} \\ D_{iq} \end{bmatrix} \quad p=1, \ldots, 6N+m-r, \; i=1, \ldots, r$$
$$l,q=1, \ldots, 6N+m \tag{50}$$

and

$$R = \begin{bmatrix} C_{pl}(-S_l - G_l + F_l) \\ -\dot{D}_{il}y_l + \dot{h}_i \end{bmatrix}. \tag{51}$$

The $6N+m$ equations (49) together with the $6N+m$ equations (14) form a set of first-order differential equations which can be numerically integrated, e.g., with a variable step predictor-corrector algorithm, to yield the time history of the $6N+m$ generalized speeds $\hat{\omega}_l$, $\dot{\zeta}_l$, and $\dot{\eta}_p$, the relative orientation angles (through the usage of transformations between the orientation angle derivatives and $\hat{\omega}_l^k$ (Kane et al., 1983)), the relative translation components ζ, and the modal coordinates η. To avoid singularities, Euler parameters can be used in place of the orientation angles.

4 Numerical Results

A general purpose computer program for constrained multibody systems has been developed utilizing the procedures presented in this paper. The program automatically eliminates the constrained joint degrees-of-freedom by deleting the corresponding rows in the partial velocity vectors, hence eliminating constraint equations for the joint connections.

To illustrate the effects of the geometrical nonlinearities and effects of the elastic deformations on other bodies, simulations of a cantilever beam with rotating base and a planar manipulator will be presented.

4.1 Cantilever Beam With Base Motion. The system shown in Fig. 4 was simulated as a spin-up benchmark problem by Ryan (1987). In this reference, an explicit relation between the axial and transverse deformations was used in the derivation of the generalized inertia forces to obtain the related geometric stiffening terms. The data used for the simulation as given by Ryan (1987) are: length $L = 10$ m, cross-sectional area $A = 0.0004$ m^2, mass $m = 12$ kg, area moment of inertia $I = 2 \times 10^{-7}$ m^4, the modulus of elasticity $E = 7 \times 10^{10}$ N/m^2 and the shear modulus $G = 3 \times 10^{10}$ N/m^2.

The simulation was performed by using four elements and by including the first three transverse, and the first longitudinal modes, using standard beam, element shape functions as given by Przemieniecki (1968).

The generalized coordinates of the system are the base rotation θ and the four modal coordinates. The fact that base motion is prescribed is represented as a constraint equation, hence equation (49) is used for numerical integration. The cantilever beam undergoes a rotational acceleration period, where initially $\dot{\theta} = 0$, and the base acceleration ($\dot{h}$ in equation (48)) is given by

$$\ddot{\theta} = \begin{cases} \dfrac{2}{5}\left(1 - \cos\dfrac{\pi t}{7.5}\right)\text{rad/sec} & 0 \leq t \leq 15 \text{ sec} \\ 0 & t \geq 15 \text{ sec} \end{cases} \tag{52}$$

Figure 5 shows the tip deflections in the local beam axis for 20 seconds and, as expected, the results agree with those of Ryan (1987). This simulation shows clearly that without the proper stiffening expressions, the simulations of spin-up motions may lead to completely incorrect results.

4.2 Planar Manipulator. In the planar manipulator shown in Fig. 6, link 1 rotates with a constant angular velocity $\dot{\theta}_1 = 10$ rad/sec, while the motion of link 2 is such that it remains always in the horizontal position. This is assumed to be achieved by the joint moments. Weights of the bodies act in the downward direction.

The generalized coordinates of the system are the joint rotation coordinates θ_1 and θ_2 and the elastic coordinates of the flexible bodies. The prescribed motions are expressed by two constraint equations – first representing the constant angular velocity of link 1 local axis and the second the zero-absolute angular velocity of link 2 local axis – whose general expressions are given by equation (41). Hence, the second constraint involves also the elastic coordinates of link 1 in addition to the joint rotation coordinates.

The properties of the links are: $L_1 = 0.8$ m, $A_1 = 0.0004$ m^2, $m_1 = 2.512$ kg, $I_1 = 5.333 \times 10^{-8}$ m^4, $L_2 = 0.8$ m, $A_2 = 0.0004$ m^2, $m_2 = 2.512$ kg, $I_2 = 1.333 \times 10^{-8}$m^4.

Initially, $\theta_1 = \theta_2 = 0$. The system is simulated for one complete revolution of link 1, for the cases when link 1 is considered rigid and when both links are considered flexible. Four elements and two modes were used. The tip deflections of link 2 in the local axis $\mathbf{n}^2$ are given in Fig. 7.

5 Discussions and Conclusion

The new procedures outlined in this paper contained the following features: An extended form for the partial velocity arrays to include the kinematics of the flexible bodies. They are strictly composed of submatrices and, hence, they are suitable for computer implementation. From searching in the literature, only Huston et al. (1978) have been successful in developing the partial velocity arrays in a consistent form, but those were only for rigid body dynamics. One of the most attractive features of these arrays is the role that they play in the formulation of the equations of motion. They form the basis of our analysis.

The nonlinear geometric stiffening is automatically incorporated through the proper formulation of the strain energy.

A recursive (direct path) approach with relative rigid body generalized coordinates has been adopted to eliminate the need for specifying separate constraint equations describing the joint connections. In addition to the computational advantages, this is especially useful for robotics and space mechanism applications. Selection of joint types, and specifying the joint forces and moments or determining the joint forces and moments arising from other external effects, can be done easily without additional effort.

Body reference frames relative to which the deformation of the body is defined and which, in general, are not permanently attached to any point in the body are used. This allows selection of any boundary conditions at the connection points to be imposed by physical considerations.

Closed loops and prescribed motions are included via the constraint equations. The pseudo-uptriangular method automatically generates the orthogonal complement array required for reduction, even when the constraint equations become instantaneously linearly-dependent.

A consistent mass approach is used for exact consideration of the inertia forces. The flexible bodies may have arbitrary shapes. For this purpose the corresponding shape functions and structural stiffness matrices need to be used.

References

Agarwal, O. P., and Shabana, A. A., 1985, "Dynamic Analysis of Multibody Systems Using Component Modes," *Computers and Structures*, Vol. 21, No. 6, pp. 1303–1312.

Amirouche, F. M. L., and Ider, S. K., 1988, "Stability Analysis of Multibody Systems with Variable Kinematical Constraints," *International Conference on Computational Engineering Science*, Atlanta, Ga.

Amirouche, F. M. L., and Jia, T., 1988, "A Pseudo-Uptriangular Decomposition Method for Constrained Multibody Systems Using Kane's Equations," *Journal of Guidance, Control, and Dynamics*, Vol. 10, No. 7.

Baghat, B. M., and Willmert, K. D., 1976, "Finite Element Vibrational Analysis of Planar Mechanisms," *Mechanism and Machine Theory*, Vol. 11, pp. 47–71.

Dym, C. L., and Shames, I. H., 1973, *Solid Mechanics, A Variational Approach*, McGraw-Hill, New York.

Ho, J. Y. L., 1977, "Direct Path Method for Flexible Multibody Spacecraft Dynamics," *Journal of Spacecraft and Rockets*, Vol. 14, No. 2, pp. 102–110.

Hurty, W. C., 1965, "Dynamic Analysis of Structural Systems Using Component Modes," *AIAA Journal*, Vol. 3, No. 4, pp. 678–685.

Huston, R. L., and Passarello, C. E., 1979, "On Multi-rigid-body System Dynamics," *Computers and Structures*, Vol. 10, pp. 439–446.

Ider, S. K., and Amirouche, F. M. L., 1988, "Coordinate Reduction in Constrained Spatial Dynamic Systems – A New Approach," ASME JOURNAL OF APPLIED MECHANICS, Vol. 55, No. 4, pp. 899–904.

Imam, I., and Sandor, G. N., 1975, "High Speed Mechanism Design – A General Analytical Approach," ASME *Journal of Engineering for Industry*, Vol. 97, No. 2, pp. 609–628.

Kamman, J. W., and Huston, R. L., 1984, "Dynamics of Constrained Multibody Systems," ASME JOURNAL OF APPLIED MECHANICS, Vol. 51, No. 4, pp. 899–903.

Kane, T. R., Likins, P. W., and Levinson, D. A., 1983, *Spacecraft Dynamics*, McGraw-Hill, New York.

Kane, T. R., Ryan, R. R., and Banerjee, A. K., 1987, "Dynamics of a Cantilever Beam Attached to a Moving Base," *Journal of Guidance, Control and Dynamics*, Vol. 10, No. 2, pp. 139–151.

Naganathan, G., and Soni, A. H., 1986, "Nonlinear Modeling of Kinematic and Flexibility Effects in Manipulator Design," ASME Paper, 86-DET-88.

Przemieniecki, J. S., 1968, *Theory of Matrix Structural Analysis*, McGraw-Hill, New York.

Ryan, R. R., 1987, "Flexible Multibody Dynamics: Problems and Solutions," *SDIO/NASA Workshop on Multibody Dynamics*, Jet Propulsion Laboratory, California.

Singh, R. P., and Likins, P. W., 1985, "Singular Value Decomposition for Constrained Dynamical Systems," ASME JOURNAL OF APPLIED MECHANICS, Vol. 52, pp. 943–948.

Singh, R. P., VanderVoort, R. J., and Likins, P. W., 1984, "Dynamics of Flexible Bodies in Tree Topology – A Computer Oriented Approach," AIAA Paper, 84-1024.

Sunada, W., and Dubowsky, S., 1981, "The Application of Finite Element Methods to the Dynamic Analysis of Flexible Spatial and Co-Planar Linkage Systems," ASME *Journal of Mechanical Design*, Vol. 103, pp. 643–651.

Turcic, D. A., and Midha, A., 1984, "Generalized Equations of Motion for the Dynamic Analysis of Elastic Mechanism Systems," ASME *Journal of Dynamic Systems, Measurement, and Control*, Vol. 106, pp. 243–248.

Wampler, C., Buffington, K., and Shu-hui, J., 1985, "Formulation of Equations of Motion for Systems Subject to Constraints," ASME JOURNAL OF APPLIED MECHANICS, Vol. 52, No. 2, pp. 465–470.

Wehage, R. A., and Haug, E. J., 1982, "Generalized Coordinate Partitioning for Dimension Reduction in Analysis of Constrained Dynamical Systems," ASME *Journal of Mechanical Design*, Vol. 104, No. 1, pp. 247–255.

Yoo, W. S., and Haug, E. J., "Dynamics of Flexible Mechanical Systems Using Vibration and Static Correction Modes," ASME *Design Engineering Technical Conference*, Cincinnati, Ohio.

Formulation of a Basic Building Block Model for Interaction of High Speed Vehicles on Flexible Structures

L. Vu-Quoc
Department of Aerospace Engineering,
Mechanics, and Engineering Science,
University of Florida,
Gainesville, Fla. 32611
Member ASME

M. Olsson
Division of Structural Mechanics,
Lund University,
S-221 00 Lund, Sweden

In traditional analyses of vehicle/structure interaction, especially when there are constraints between vehicle masses and the structure, vehicle nominal motion is prescribed a priori, *and therefore unaffected by the structure flexibility. In this paper, a concept of* nominal *motion is defined, and a methodology is proposed in which the above restriction is removed, allowing the vehicle nominal motion to become unknown, and encompassing the traditional approach as a particular case. General nonlinear equations of motion of a building block model, applicable to both wheel-on-rail and magnetically levitated vehicles, are derived. These equations are simplified to a set of mildly nonlinear equations upon introducing additional assumptions – essentially on small structural deformation. An example is given to illustrate the present formulation.*

1 Introduction

In recent years considerable interest has been developed in implementing energy-efficient, high-speed, low-noise systems for airport-city or intercity transportation – in particular, the magnetically levitated (Maglev) vehicle systems (cf. Eastham and Hayes (1987)). Currently, to ensure success of Maglev systems, guideway structures must be designed to be stiff so that deflections remain within narrow margins of tolerance. The cost of a stiff guideway structure can easily exceed 70 percent of the total cost of a system (Zicha (1986)). More flexible guideways are less expensive, but present complex vehicle/structure interaction.[1] The interaction between high speed moving vehicles and flexible supporting structures is the focus of the present paper. Even though the impetus behind this work is geared toward high speed vehicles, the problem of moving loads does find applications in various fields of engineering (cf. Frýba (1972), Blejwas et al. (1979)). Extensive lists of references on the subject of moving loads over elastic structures are contained in the classical monograph by Frýba (1972), and in several review papers, e.g., Kortüm and Wormley (1981), Ting and Yener (1983), report of Subcommittee on Vibration Problems (1985) and Kortüm (1986).

Formulation of vehicle/structure interaction for wheel-on-rail vehicles, or for electromagnetic Maglev vehicles with tight gap control, leads to a complex system of equations of motion. This complexity stems mainly from the constraints between moving masses and the flexible structure, and from the existence of convective terms, which are important for high speed regimes. Such problem does not arise for vehicle models connected to the structure via suspension systems where there are no constraints between moving masses and the structure. In addition, efficient numerical algorithms must be developed to deal with the resulting complex system of equations of motion; analytical solution (for simple cases) is possible only when convective terms are neglected (e.g., Stanisic (1985)). So far, research effort has been based on the assumption that vehicle nominal motion is known *a priori* (e.g., Ting, Genin and Ginsberg (1974), Venancio-Filho (1978), Olsson (1985–1986), and Wallrapp (1986)). Since mathematical models in these work require prescribed vehicle nominal motion and do not admit driving forces, there is no possibility to study effects of structure flexibility on vehicle nominal motion, or effects of applied accelerating or braking forces on the vehicle/structure system. We have not come across any reference where the assumption of known vehicle nominal motion is not used.

We propose herein a methodology to analyze the complete vehicle/structure interaction, valid for high speed regime, without resorting to the usual assumption of known nominal motion. This general setting clearly includes the case where nominal motion is prescribed *a priori*. The scope of this paper is restricted to a basic model of planar motion of a rigid wheel, or a Maglev magnet unit with tight gap control, moving over a flexible beam. Energy dissipative mechanisms are not considered here. The present prototype model serves as a basic building block for more complex vehicle/structure models.

[1] Progress in suspension control technology will make possible the use of flexible guideways, and the efficiency of Maglev systems will increase with advance in superconductor research.

Contributed by The Applied Mechanics Division of THE AMERICAN SOCIETY OF MECHANICAL ENGINEERS for presentation at the Joint ASCE/ASME Applied Mechanics, Biomechanics, and Fluids Engineering Conference, San Diego, Calif., July 9 to 12, 1989.

Discussion of this paper should be addressed to the Editorial Department, ASME, United Engineering Center, 345 East 47th Street, New York, N.Y. 10017, and will be accepted until two months after final publication of the paper itself in the JOURNAL OF APPLIED MECHANICS. Manuscript received by ASME Applied Mechanics Division, January 27, 1988; final revision, August 23, 1988.

Paper No. 89-APM-37.

We note that the wheel model also finds application in electrodynamic (repulsive) Maglev vehicles since these vehicles move on wheels up to a maximum lift-off speed of about 80 km/h (Alscher et al. (1983)). Further, both high speed Maglev vehicles and wheel-on-rail vehicles may possibly run on the same bivalent guideway structure.

Nonlinear equations of motion of the basic model, valid for large deformation of the beam, are derived for a class of general (nonlinear) contact constraints via Hamilton's principle of stationary action.[2] In the present work, structural response in the small deformation range is, however, our main interest. With assumptions of small deformation, the nonlinear equations of motion are then reduced, in a consistent manner, to a system of mildly nonlinear equations. This consistency is an important feature that distinguishes the present approach from traditional practice of complete linearization: Nonlinear terms of physical relevance, essential for high speed regime, are retained in the equation for nominal motion of the basic model. Finally, an example of vehicle/structure interaction at different initial velocities is given to illustrate the present formulation.

Note that the study of dynamic motion of the complete system, driven by external forces, as done here, is the only way to explain the Timoshenko paradox: Consider a constant vertical force traversing, with some prescribed motion, a simply-supported beam. Since the net work done by the force is zero, where does the energy which leaves the beam in a vibratory state after the traversing come from? The same question can be asked for a moving mass with prescribed motion. In fact, the "excess" of energy comes precisely from the work done by (unmodeled) external forces needed for the vehicle to follow the motion prescribed (cf. Maunder (1960)).

2 Description of Basic Problem

In this section, we describe the basic problem of planar motion of a high speed moving load – a single rigid wheel or a suspended magnet with tight gap control – over a flexible beam. Attention is focused, however, to the dynamics of the more complex case of a rolling wheel. Several possible models of a Magleve magnet ("magnetic wheel") can be obtained from this basic model. Recall that the present basic model serves as a building-block for more complex vehicle/structure models.

2.1. Basic Assumptions. Let $\{\mathbf{E}_1, \mathbf{E}_2\}$ be orthonormal basis vectors, and (X^1, X^2) the coordinates along these axes. These objects define a coordinate system for the material (undeformed) configuration of a beam. The line of centroids of the beam, of length L and initially straight, is assumed to lie along the axis $\mathbf{E}_1$; the coordinate of a material point on the line of centroids is denoted by $S \equiv X^1 \in [0, L]$. Let $\{\mathbf{e}_1, \mathbf{e}_2\}$ be the set of orthonormal vectors spanning the spatial (deformed) configuration, and conveniently chosen such that $\mathbf{E}_i \equiv \mathbf{e}_i$, for $i = 1, 2$. The displacement of a material point S is denoted by $\mathbf{u}(S,t) = u^\alpha(S,t)\mathbf{e}_\alpha$,[3] where $t \in [0, +\infty)$ is the time parameter.

Consider a rigid wheel with mass M, radius R, and rotatory inertia about its center of mass I_w. Let $\mathbf{Y}(t) = Y^\alpha(t)\,\mathbf{E}_\alpha$ be the position of the wheel center of mass in the material configuration of the beam; its position in the spatial configuration is denoted by $\mathbf{y}(t) = y^\alpha(t)\mathbf{e}_\alpha$. We consider the following general form of constraint

$$y^\alpha(t) = Y^\alpha(t) + g^\alpha(\mathbf{u}(Y^1(t),t), \mathbf{u},_S\,(Y^1(t),t)), \tag{1}$$

for $\alpha = 1,2$, where $g^\alpha(\bullet,\bullet)$ are some functions of the structural displacement $\mathbf{u}$ and its spatial derivative $\mathbf{u},_S \equiv \partial\mathbf{u}/\partial S = (\partial u^\beta/\partial S)\mathbf{e}_\beta$, such that $g^\alpha(0, 0) \equiv 0$. We call $\mathbf{Y}(t)$, the motion of the wheel in the material configuration of the beam, the *nominal motion* of the wheel. Thus, for $\mathbf{u}(S,t) \equiv 0$, we have $y^\alpha(t) \equiv Y^\alpha(t)$. Given the functions $y^1(t)$, $\mathbf{u}(S,t)$, and $g^1(\mathbf{u}, \mathbf{u}_S)$, relation (1) with $\alpha = 1$ could be taken as a definition of the (unknown) nominal motion $Y^1(t)$, i.e., $Y^1(t)$ is defined to be a solution of (1). In this formulation, we consider only the case where $Y^2 \equiv \bar{R}$, for some constant $\bar{R}$. Let θ denote the angle of revolution of the wheel, which is considered to be a function of the nominal position Y^1 and the structural deformation $(\mathbf{u}, \mathbf{u},_S)$. We will often employ the shorthand notation $g^\alpha(Y^1,t) \equiv \hat{g}^\alpha(\mathbf{u}(Y^1,t), \mathbf{u},_S(Y^1,t))$, and similarly with $\theta(Y^1,t) \equiv \hat{\theta}(Y^1,\mathbf{u}(Y^1,t), \mathbf{u},_S(Y^1,t))$. Thus,

$$\frac{\partial g^\alpha}{\partial S} \equiv \frac{\partial \hat{g}^\alpha}{\partial u^\beta}\frac{\partial u^\beta}{\partial S} + \frac{\partial \hat{g}^\alpha}{\partial u^\beta,_S}\frac{\partial^2 u^\beta}{\partial S^2}, \tag{2a}$$

$$\frac{\partial \theta}{\partial S} \equiv \frac{\partial \hat{\theta}}{\partial S} + \frac{\partial \hat{\theta}}{\partial u^\beta}\frac{\partial u^\beta}{\partial S} + \frac{\partial \hat{\theta}}{\partial u^\beta,_S}\frac{\partial^2 u^\beta}{\partial S^2}. \tag{2b}$$

2.2 Kinetic Energy and Potential Energy. The kinetic energy $I\!K$ of the basic system (wheel and flexible beam) is given by

$$I\!K := \frac{1}{2}M\Big\{[\dot{Y}^1 + \dot{g}^1(Y^1,t)^2 + [\dot{g}^2(Y^1,t)]^2\Big\} + \frac{1}{2}I_w[\dot{\theta}(Y^1,t)]^2 + \frac{1}{2}\int_{[0,L]} A_\rho\Big\{[u^1,_t(S,t)]^2 + [u^2,_t(S,t)]^2\Big\}dS, \tag{3}$$

where the superposed "$\bullet$" denotes the total time derivative (i.e., $(\dot{\ }) \equiv d/dt\,(\bullet)$); $u^\alpha,_t \equiv \partial u^\alpha/\partial t$ denotes the partial derivative of u^α in time, and A_ρ the mass per unit length of the beam.[4] Now, consider a function f: $[0, L] \times [0, \infty) \to I\!R$, smooth enough in both arguments. The first and second total time derivatives of $f(S,t)$, evaluated at $S = Y^1(t)$, are obtained as follows

$$\dot{f}(Y^1, \dot{Y}^1, t) = \frac{\partial f(Y^1,t)}{\partial S}\dot{Y}^1 + \frac{\partial f(Y^1,t)}{\partial t}, \tag{4a}$$

$$\ddot{f}(Y^1, \dot{Y}^1, \ddot{Y}^1, t) = \frac{\partial f(Y^1,t)}{\partial S}\ddot{Y}^1 + \frac{\partial^2 f(Y^1,t)}{\partial S^2}(\dot{Y}^1)^2 + 2\frac{\partial^2 f(Y^1,t)}{\partial S\partial t}\dot{Y}^1 + \frac{\partial^2 f(Y^1,t)}{\partial t^2}. \tag{4b}$$

We will often omit to specify $(\dot{Y}^1, \ddot{Y}^1)$ in the argument lists of quantities such as $\dot{f}$ and $\ddot{f}$, and simply write $\dot{f}(Y^1,t)$ and $\ddot{f}(Y^1,t)$.[5] Thus, employing (2) and (4) with $f \equiv g^\alpha$ to evaluate $\dot{g}^\alpha(Y^1,t)$ and $\dot{\theta}(Y^1,t)$, one obtains an expanded form of the kinetic energy (3). The convective terms in (4) – i.e., the first term in (4a), and the first three terms in (4b) – play an important role in the interaction between high speed moving vehicles and the supporting flexible structures, as shown in Blejwas, Feng, and Ayre (1979), where numerical results corroborated experimental findings (see also Ting, Genin, and Ginsberg (1974)). Further, by the assumed smoothness of the function f in (4), total time derivatives and spatial derivatives are interchangeable,

$$\frac{d^i}{dt^i}\left[\frac{\partial^j f(Y^1,t)}{\partial S^j}\right] = \frac{\partial^j}{\partial S^j}\left[\frac{d^i f(Y^1,t)}{dt^i}\right], \tag{5}$$

[2] The term "contact" is also used here for Maglev magnets with tight gap control.

[3] Throughout the paper, summation convention is implied on repeated indices, which take values in {1, 2}.

[4] It should be noted that in (3) we do not consider the rotatory inertia of the beam cross-section; however, an analysis including this term could be carried out following the same methodology presented in this paper.

[5] This shorthand notation had been used in (3).

and thus notation such as $\dot{f}_{,S}(Y^1,t)$ can be used without confusion.

The wheel is subjected to an applied force $\mathbf{F} = F^\alpha \mathbf{e}_\alpha$, and a torque T about its center of mass. Without loss of generality, for the moment, the applied force and torque can be considered constant in time for the purpose of deriving the equations of motion. The work done by the external forces is then given by $W := \mathbf{F}\cdot\mathbf{y} + T\theta$. Further, let $\psi(\mathbf{u})$ denote the elastic strain energy stored in the beam. The formulation is so far valid for large deformation in the beam, and we have not yet introduced assumptions of small deformation at this stage. Explicit expression of $\psi(\mathbf{u})$ for finite deformation of a beam in plane motion can be found in Simo and Vu-Quoc (1986).

3 Derivation of Equations of Motion

In this section, we derive the equations of motion for the basic problem, valid for large structural deformation, by employing Hamilton's principle of stationary action. Additional assumptions of small deformation in the structure are subsequently introduced to further simplify the equations of motion. This simplification process is carefully carried out in a manner that is consistent with the assumptions. It should be indicated that even though particularized to small structural deformation the resulting equations of motion do retain some crucial nonlinear terms, for an adequate description of the dynamics at high speed regime.

3.1 The General Nonlinear Equations of Motion. The Lagrangian of the system can be written as

$$\mathbb{L}(Y^1,\mathbf{u}) := \mathbb{K}(Y^1,\mathbf{u}) - \psi(\mathbf{u}) + W(Y^1,\mathbf{u}),^{6} \tag{6}$$

Consider the time interval $[t_1,t_2]$. Let $(\psi(t),\eta^1(S,t),\eta^2(S,t))$ be the admissible variations corresponding to the functions (Y^1,u^1,u^2), and vanishing at time $t=t_1$ and $t=t_2$. The equations of motion are obtained from the stationary condition of the action integral, i.e., the Euler-Lagrange equations corresponding to (6):

$$\frac{d}{d\epsilon}\int_{[t_1,t_2]} \mathbb{L}(Y^1+\epsilon\psi,\mathbf{u}+\epsilon\eta)dt\,\Big|_{\epsilon=0} = 0, \tag{7}$$

for all admissible variations (ψ,η), where $\eta = \eta^\beta \mathbf{e}_\beta$. It follows that the equations for nominal motion Y^1 and for structural displacement $\mathbf{u}$ are, respectively, given by

$$\begin{aligned}&\frac{d}{d\epsilon}\int_{[t_1,t_2]} \mathbb{L}(Y^1+\epsilon\psi,\mathbf{u})dt\,\Big|_{\epsilon=0} = 0,\\ &\frac{d}{d\epsilon}\int_{[t_1,t_2]} \mathbb{L}(Y^1,\mathbf{u}+\epsilon\eta)dt\,\Big|_{\epsilon=0} = 0,\ \forall \text{ admissible } (\psi,\eta)\end{aligned} \tag{8}$$

Nominal Motion $\mathbf{Y}^1$. We first note that from (4*a*) one has

$$\frac{\partial \dot{f}(Y^1,\dot{Y}^1,t)}{\partial} \equiv \frac{\partial f(Y^1,t)}{\partial S}. \tag{9a}$$

Then, it follows from (9*a*) and (5) that

$$\frac{d}{dt}\left(\frac{\partial \dot{f}(Y^1,t)}{\partial}\right) = \frac{d}{dt}\left(\frac{\partial f(Y^1,t)}{\partial S}\right) \equiv \frac{\partial \dot{f}(Y^1,t)}{\partial S}. \tag{9b}$$

Further, the variation of f with respect to Y^1 is given by

$$\frac{d}{d\epsilon}\dot{f}(Y^1+\epsilon\psi,t)\Big|_{\epsilon=0} = \frac{\partial \dot{f}(Y^1,t)}{\partial S}\psi + \frac{\partial f(Y^1,t)}{\partial S}\dot{\psi}, \tag{10}$$

where we have made use of (4*a*).[7] Next, after evaluation of the directional derivative $(8)_1$, and applying integration by parts with the boundary conditions $\psi(t_1) = \psi(t_2) \equiv 0$, we obtain

$$\begin{aligned}-\frac{d}{d\epsilon}\int_{[t_1,t_2]} \mathbb{K}(Y^1+\epsilon\psi,\mathbf{u})dt\,\Big|_{\epsilon=0} &= \int_{[t_1,t_2]}\Big\{M\Big(1+\frac{\partial g^1(Y^1,t)}{\partial S}\Big)[\ddot{Y}^1+\ddot{g}^1(Y^1,t)]\\ &+M\frac{\partial g^2(Y^1,t)}{\partial S}\ddot{g}^2(Y^1,t)+I_w\frac{\partial\theta(Y^1,t)}{\partial S}\ddot{\theta}(Y^1,t)\Big\}\psi\,dt,\end{aligned} \tag{11a}$$

$$\begin{aligned}\frac{d}{d\epsilon}\int_{[t_1,t_2]} W(Y^1+\epsilon\psi,\mathbf{u})dt\,\Big|_{\epsilon=0} &= \int_{[t_1,t_2]}\Big\{F^1\Big(1+\frac{\partial g^1(Y^1,t)}{\partial S}\Big)\\ &+F^2\frac{\partial g^2(Y^1,t)}{\partial S}+T\frac{\partial\theta(Y^1,t)}{\partial S}\Big\}\psi\,dt,\end{aligned} \tag{11b}$$

where use has been made of (9) and (10) with $f \equiv g^\alpha$ to allow cancellation of certain terms. The stationary condition $(8)_1$ and relations (11) yield the equation for the nominal motion Y^1:

$$\begin{aligned}&M\Big(1+\frac{\partial g^1(Y^1,t)}{\partial S}\Big)[\ddot{Y}^1+\ddot{g}^1(Y^1,t)]\\ &\quad+M\frac{\partial g^2(Y^1,t)}{\partial S}\ddot{g}^2(Y^1,t)+I_w\frac{\partial\theta(Y^1,t)}{\partial S}\ddot{\theta}(Y^1,t)\\ &=F^1\Big(1+\frac{\partial g^1(Y^1,t)}{\partial S}\Big)+F^2\frac{\partial g^2(Y^1,t)}{\partial S}+T\frac{\partial\theta(Y^1,t)}{\partial S}.\end{aligned} \tag{12}$$

Structural Motion (u^1,u^2). Similar to relations (9), one can prove that the following identifies hold

$$\frac{\partial \dot{g}^\alpha(\mathbf{u},\mathbf{u}_{,S})}{\partial \dot{u}^\beta} \equiv \frac{\partial g^\alpha(\mathbf{u},\mathbf{u}_{,S})}{\partial u^\beta}, \tag{13a}$$

$$\frac{d}{dt}\left(\frac{\partial \dot{g}^\alpha(\mathbf{u},\mathbf{u}_{,S})}{\partial \dot{u}^\beta}\right) \equiv \frac{\partial \dot{g}^\alpha(\mathbf{u},\mathbf{u}_{,S})}{\partial u^\beta}, \tag{13b}$$

$$\frac{\partial \dot{g}^\alpha(\mathbf{u},\mathbf{u}_{,S})}{\partial \dot{u}^\beta{}_{,S}} \equiv \frac{\partial g^\alpha(\mathbf{u},\mathbf{u}_{,S})}{\partial u^\beta{}_{,S}}, \tag{13c}$$

$$\frac{d}{dt}\left(\frac{\partial \dot{g}^\alpha(\mathbf{u},\mathbf{u}_{,S})}{\partial \dot{u}^\beta{}_{,S}}\right) \equiv \frac{\partial \dot{g}^\alpha(\mathbf{u},\mathbf{u}_{,S})}{\partial u^\beta{}_{,S}}. \tag{13d}$$

Now, computation of the directional derivative in $(8)_2$, and integration by parts with respect to time yield the following results

$$\begin{aligned}&-\frac{d}{d\epsilon}\int_{[t_1,t_2]} \mathbb{K}(Y^1,\mathbf{u}+\epsilon\eta)dt\,\Big|_{\epsilon=0}\\ &=\int_{[t_1,t_2]}\Big\{M\ddot{y}^\alpha\Big(\eta^\beta(Y^1,t)\frac{\partial g^\alpha(Y^1,t)}{\partial u^\beta}\\ &+\eta^\beta{}_{,S}(Y^1,t)\frac{\partial g^\alpha(Y^1,t)}{\partial u^\beta{}_{,S}}\Big)+I_w\ddot{\theta}(Y^1,t)\Big(\eta^\beta(Y^1,t)\frac{\partial\theta(Y^1,t)}{\partial u^\beta}\\ &+\eta^\beta{}_{,S}(Y^1,t)\frac{\partial\theta(Y^1,t)}{\partial u^\beta{}_{,S}}\Big)+\int_{[0,L]}A_\rho\eta^\beta u^\beta{}_{,tt}\,dS\Big\}dt,\end{aligned} \tag{14a}$$

$$\begin{aligned}&\frac{d}{d\epsilon}\int_{[t_1,t_2]} W(Y^1,\mathbf{u}+\epsilon\eta)dt\,\Big|_{\epsilon=0}\\ &=\int_{[t_1,t_2]}\Big\{F^\alpha\Big(\eta^\beta(Y^1,t)\frac{\partial g^\alpha(Y^1,t)}{\partial u^\beta}+\eta^\beta{}_{,S}(Y^1,t)\frac{\partial g^\alpha(Y^1,t)}{\partial u^\beta{}_{,S}}\Big)\end{aligned}$$

[6]We omit the time derivatives of $(Y^1,\mathbf{u})$ in the argument lists of $\mathbb{L}$ and $\mathbb{K}$ to alleviate the notation.

[7]Another way to obtain (10) is by interchanging $d/d\epsilon$ and d/dt, and then using (5).

$$+T\left(\eta^\beta(Y^1,t)\frac{\partial\theta(Y^1,t)}{\partial u^\beta}+\eta^\beta{}_{,S}(Y^1,t)\frac{\partial\theta(Y^1,t)}{\partial u^\beta{}_{,S}}\right)\Big\}dt, \tag{14b}$$

where we have made use of the (homogeneous) boundary conditions of (η^1, η^2) at $t=t_1$ and $t=t_2$, relation (4*a*), and the identities (13)[8]. Next, let the weak form of the stiffness operator be denoted by $G(\cdot,\cdot)$, and

$$G(\mathbf{u},\eta)=\frac{d}{d\epsilon}\psi(\mathbf{u}+\epsilon\eta)\Big|_{\epsilon=0}, \tag{15a}$$

where we recall that $\psi(\mathbf{u})$ designates the strain energy of the beam – see Vu-Quoc (1986) and Simo and Vu-Quoc (1986) for an expression of $G(\mathbf{u},\eta)$. Therefore, using $(8)_2$, (14) and (15*a*), the weak form of the structural equations of motion is then given by

$$\begin{aligned}&[-F^1+M[\ddot{Y}^1+\ddot{g}^1(Y^1,t)]]\left[\eta^\beta(Y^1,t)\frac{\partial g^1(Y^1,t)}{\partial u^\beta}\right.\\ &\qquad\left.+\eta^\beta{}_{,S}(Y^1,t)\frac{\partial g^1(Y^1,t)}{\partial u^\beta{}_{,S}}\right]+[-F^2+M\ddot{g}^2(Y^1,t)]\\ &\qquad\times\left[\eta^\beta(Y^1,t)\frac{\partial g^2(Y^1,t)}{\partial u^\beta}+\eta^\beta{}_{,S}(Y^1,t)\frac{\partial g^2(Y^1,t)}{\partial u^\beta{}_{,S}}\right]\\ &+[-T+I_w\ddot{\theta}(Y^1,t)]\left[\eta^\beta(Y^1,t)\frac{\partial\theta(Y^1,t)}{\partial u^\beta}+\eta^\beta{}_{,S}(Y^1,t)\frac{\partial\theta(Y^1,t)}{\partial u^\beta{}_{,S}}\right]\\ &+\int_{[0,L]}A_\rho\eta^\beta(S,t)u^\beta{}_{,tt}(S,t)dS+G(\mathbf{u},\eta)=0,\ \forall\text{ admissible }\eta.\end{aligned} \tag{15b}$$

The corresponding partial differential equations of motion can be easily obtained from (15) by integrating by parts in S, and by invoking the fundamental lemma of calculus of variations.[9] We prefer, however, to retain the structural equations of motion in its weak form for numerical work.

Remark 3.1. Energy Balance. The balance of system energy at time t can be written as follows

$$I\!K_t+\psi_t-\int_0^t[F^\alpha(\tau)\dot{y}^\alpha(\tau)+T(\tau)\dot{\theta}(\tau)]d\tau=I\!K_0+\psi_0, \tag{16}$$

where $I\!K_t$ is as given in (3), ψ_t as given in Simo and Vu-Quoc (1986); the integral term is the work done by (time-varying) external forces. On the right-hand side of (16) are, respectively, the initial kinetic energy $I\!K_0$ and the initial potential energy ψ_0. The discrete form of the system energy balance (16) has proved to be a very useful criterion in the design of reliable numerical integration algorithms for the equations of motion; see Vu-Quoc and Olsson (1987, 1988a) for the details. ■

3.2 Contact Constraints and Contact Forces. The wheel is assumed to be in permanent contact with, and rolling without slipping on, the beam.[10] Clearly, without structural deformation ($\mathbf{u}(S,t)\equiv 0$), the revolution of the wheel is related to its nominal motion by $\theta = Y^1/R$. Let $\bar{R}\ (=Y^2)$ denote the distance from the beam centroidal line to the center of mass of the wheel (Fig. 1). For $\bar{R}=R$, the wheel is moving with its circumference tangent to the beam centroidal line. An explicit form of the function g^α in the general constraint equations (1) for wheel/beam contact, or magnet/beam with constant gap,

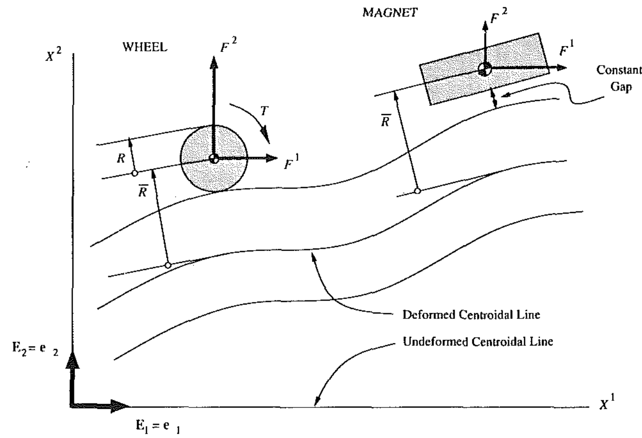

Fig. 1 ***Basic problem*****: Building block models for wheel-on-rail and Maglev vehicles.**

can be written exactly as follows

$$g^1(\mathbf{u},\mathbf{u}_{,S})=u^1-\bar{R}\sin\chi(\mathbf{u}_{,S}), \tag{17a}$$

$$g^2(\mathbf{u},\mathbf{u}_{,S})=u^2-\bar{R}[1-\cos\chi(\mathbf{u}_{,S})], \tag{17b}$$

$$\text{where }\chi(\mathbf{u}_{,S}):=\tan^{-1}\left(\frac{u^2{}_{,S}}{1+u^1{}_{,S}}\right), \tag{17c}$$

represents the slope angle of the deformed beam (cf. Fig. 1). It should be noted that the expressions in (17) are written for beam theory without shear deformation, and are valid for a finitely deformed beam.

Remark 3.2 "Magnetic Wheel." The above formulation encompasses several possible models for a Maglev vehicle using electromagnetic suspension (attractive system) with tight gap control.[11] By letting $I_w\equiv 0$ (or $\theta\equiv 0$) in the kinetic energy (3), we have a model (A) of a moving magnet, where $\bar{R}$ represents the distance from the beam centroidal line to the magnet center of mass (Fig. 1). Next, by letting $I_w=\bar{R}\equiv 0$, in which case the constraints (1) becomes $y^1(t) = Y^1(t) + u^1(Y^1,t)$ and $y^2(t) = u^2(Y^1,t)$, we obtain yet another model (B) of a moving magnet. In practice, often even simpler constraints are chosen (model C) so that $y^1(t)\equiv Y^1(t)$ and $y^2(t) = u^2(Y^1,t)$ (cf., e.g., Wallrapp (1986)). Thus, there is no direct coupling between vehicle nominal motion and structural axial deformation. In this case, the equations of motion (12) and (15) (in weak form) simplify to

$$M\left[\ddot{Y}^1+\frac{\partial u^2(Y^1,t)}{\partial S}\ddot{u}^2(Y^1,t)\right]=F^1+F^2\frac{\partial u^2(Y^1,t)}{\partial S}, \tag{18a}$$

$$\begin{aligned}&\eta^2(Y^1,t)[-F^2+M\ddot{u}^2(Y^1,t)]\\ &\qquad+\int_{[0,L]}A_\rho\eta^\beta(S,t)\,u^\beta{}_{,tt}(S,t)dS+G(\mathbf{u},\eta)=0,\end{aligned} \tag{18b}$$

which are also valid for a finitely deformed beam. In (18), the equation for axial displacement and the equation for transverse displacement are coupled through the nonlinear nature of $G(\mathbf{u},\eta)$ for the finite deformation case. ■

In the design of flexible structures under moving vehicles, it is important to quantify the (dynamic) contact forces. In particular, these forces are crucial in studying structural response to emergency braking of a vehicle. For the basic problem considered herein, let $\mathbf{F}_c = F_c^\alpha\mathbf{e}_\alpha$ be the contact force acting on the beam. Once Y^1 and u^α have been solved for, the contact force can be evaluated by $\mathbf{F}_c = \mathbf{F}-M\ddot{\mathbf{y}}$, obtained from considering the equilibrium of forces acting on the wheel. Recall that $\ddot{\mathbf{y}}$ is

[8]We could also obtain these results by making use of the interchangeability of $d/d\epsilon$ and d/dt.

[9]The containing space of the variations (η^1,η^2) should be suitably chosen and should include the essential boundary conditions at $S=0$ and $S=L$ (see, e.g., Rektorys (1980)).

[10]The velocity of the contact point on the wheel is only about one thousandth of the velocity of the wheel center of mass (rigid slip); see Kalker (1979).

[11]The gap between a magnet and the guideway is in the range of 10–15 mm, independently of vehicle speed (Eastham and Hayes (1987)). See also the review paper by Kortüm and Wormley (1981).

evaluated using (1), (17), and with the aid of (4b). In the case of a moving magnet, the contact force $\mathbf{F}_c$ is the required active control force that should be exerted on the magnet to maintain a constant gap.

3.3 Assumptions on Small Structural Deformation. Equations (12) and (15) form the complete set of coupled, fully nonlinear equations describing the motion of a rigid wheel moving over a flexible beam. In the present work, we consider the following additional assumptions to reduce the equations (12) and (15) to a mildly nonlinear form: **(A1)** $|u^\alpha,_S| << 1$, for $\alpha = 1,2$; **(A2)** The Bernoulli-Euler hypothesis is adopted for beam response,

$$\psi(\mathbf{u}) = \frac{1}{2}\int_{[0,L]}\left\{EA\,[u^1,_S]^2 + EI\,[u^2,_{SS}]^2\right\}dS, \qquad (19a)$$

where EA is the axial stiffness, and EI the bending stiffness; **(A3)** All nonlinear terms in the displacement u^α are neglected in the equations for structural motion; **(A4)** The wheel rolls without slipping and with little influence from structural deformation,

$$\theta(Y^1,t) \approx \frac{Y^1}{R},\ \frac{\partial\theta(Y^1,t)}{\partial S} \approx \frac{1}{R},\ \dot\theta(Y^1,t) \approx \frac{\dot Y^1}{R},\ \ddot\theta(Y^1,t) \approx \frac{\ddot Y^1}{R},$$

$$\frac{\partial\theta}{\partial u^\beta} \approx 0, \quad \text{and} \quad \frac{\partial\theta}{\partial u^\beta,_S} \approx 0. \qquad (19b)$$

Note that the aforementioned assumptions are not only physically relevant in real operational conditions of the system, but carry important implications on the numerical treatment as well (see Vu-Quoc and Olsson (1988a)).

3.4 The Mildly Nonlinear Equations of Motion. Considering the structural equations of motion (15b), assumption **(A3)** implies that we neglect nonlinear terms in u^1 and u^2 in the fully-expanded expressions of $\ddot g^1$ and of $\ddot g^2$ obtained from using (2a) and (4b) in (17). Thus, together with assumption **(A1)**, we arrive at the approximations

$$\ddot g^1 \approx \ddot u^1 - \bar R\ddot u^2,_S, \quad \ddot g^2 \approx \ddot u^2. \qquad (20)$$

Note that approximations (20) together with relations (4) when applied to g^1 and g^2 imply

$$\frac{\partial^{i+j}g^1}{\partial S^i\partial t^j} \approx \frac{\partial^{i+j}u^1}{\partial S^i\partial t^j} - \bar R\,\frac{\partial^{i+j+1}u^2}{\partial S^{i+1}\partial t^j},\quad \frac{\partial^{i+j}g^2}{\partial S^i\partial t^j} \approx \frac{\partial^{i+j}u^2}{\partial S^i\partial t^j}, \quad (21)$$

for (i,j) = (1,0), (2,0), (1,1), (0,2). Further, assumptions **(A1)** and **(A3)** lead to the following approximations

$$\frac{\partial g^1}{\partial u^1,_S} \approx \bar R u^2,_S, \quad \frac{\partial g^1}{\partial u^2,_S} \approx -\bar R, \qquad (22a)$$

$$\frac{\partial g^2}{\partial u^1,_S} \approx 0, \quad \frac{\partial g^2}{\partial u^2,_S} \approx -\bar R u^2,_S, \qquad (22b)$$

$$1 + \frac{\partial g^1}{\partial S} \approx 1 - \bar R u^2,_{SS}, \quad \frac{\partial g^2}{\partial S} \approx u^2,_S, \qquad (22c)$$

where (22c) are obtained with the additional aid of (21) (or (2a)). As a result of (4b), (20), (22), together with assumption **(A4)** (i.e., (19b)), the equation for nominal motion (12) can be approximated by

$$c_3(Y^1,t)\ \ddot Y^1 + c_2(Y^1,t)(\dot Y^1)^2 + c_1(Y^1,t)\dot Y^1 + c_0(Y^1,t) = 0, \qquad (23a)$$

where

$$c_0(Y^1,t) \approx -F^1[1-\bar R u^2,_{SS}(Y^1,t)] - F^2u^2,_S(Y^1,t) - \frac{T}{R}$$

$$+ M\Big[[1-\bar R u^2,_{SS}(Y^1,t)]\ [u^1,_{tt}(Y^1,t) - \bar R u^2,_{Stt}(Y^1,t)]$$

$$+ u^2,_S(Y^1,t)u^2,_{tt}(Y^1,t)\Big], \qquad (23b)$$

$$c_1(Y^1,t) \approx 2M\Big[[1-\bar R u^2,_{SS}(Y^1,t)]\ [u^1,_{St}(Y^1,t)$$

$$-\bar R u^2,_{SSt}(Y^1,t)] + u^2,_S(Y^1,t)u^2,_{St}(Y^1,t)\Big], \qquad (23c)$$

$$c_2(Y^1,t) \approx M\Big[[1-\bar R u^2,_{SS}(Y^1,t)]\ [u^1,_{SS}(Y^1,t)$$

$$-\bar R u^2,_{SSS}(Y^1,t)] + u^2,_S(Y^1,t)u^2,_{SS}(Y^1,t)\Big], \qquad (23d)$$

$$c_3(Y^1,t) \approx M[1-\bar R u^2,_{SS}(Y^1,t)]^2 + \frac{I_w}{R^2}. \qquad (23e)$$

Remark 3.3. Consistency in the Formulation. The nonlinear term in g^2 in the equation for the nominal motion (12) is, according to (20) and (22), approximated by

$$\frac{\partial g^2(Y^1,t)}{\partial S}\ddot g^2(Y^1,t) \approx u^2,_S(Y^1,t)\ddot u^2(Y^1,t), \qquad (24a)$$

which is also nonlinear in u^2. Using (4b), we obtain the term (24a) in expanded form as given in (23). This term plays an important role in representing the influence of transverse structural displacement on vehicle nominal motion at high speed. To see this, we rewrite the equation for nominal motion (18a) of Maglev model C, for $F^1 = 0$, as follows

$$M\ddot Y^1 = u^2,_S(Y^1,t)\ [F^2 - M\ddot u^2(Y^1,t)] \equiv u^2,_S(Y^1,t)\ F_c^2(t). \qquad (24b)$$

At high speed, the amplitude of the vertical contact force F_c^2 may significantly exceed that of the vertical force F^2. We will present next an example with high speed vehicle motion where one has $|F_c^2(t)| > 1.5\ |F^2|$, for some time t. In other words, the inertia force $M\ddot u^2$ could be of the same order of magnitude as that of F^2, and should be retained in equation (23). Hence, it is shown that the formulation would not be appropriate for high speed regime, had we systematically removed all nonlinear terms in u^α from the equations of motion. This is a variance with the usual practice of complete linearization (see discussion in Kortüm (1986)), which is therefore inconsistent in the present situation. ■

Now, applying assumptions **(A1-A4)**, the weak form of the equations for structural motion, which is linear in the displacement u^α, is given by

$$\eta^1(Y^1,t)\ \Big(-F^1 + M[\ddot Y^1 + \ddot u^1(Y^1,t) - \bar R\ddot u^2,_S(Y^1,t)]\Big)$$

$$-\bar R[F^1 - M\ddot Y^1]\eta^1,_S(Y^1,t)u^2,_S(Y^1,t)$$

$$+\int_{[0,L]} A_\rho\eta^1(S,t)u^1,_{tt}(S,t)dS$$

$$+\int_{[0,L]} EA\ \eta^1,_S(S,t)u^1,_S(S,t)dS = 0, \qquad (25a)$$

and

$$-\bar R\eta^2,_S(Y^1,t)\Big(-F^1 + M[\ddot Y^1 + \ddot u^1(Y^1,t) - \bar R\ddot u^2,_S(Y^1,t)]\Big)$$

$$+\eta^2(Y^1,t)\Big(-F^2 + M\ddot u^2(Y^1,t)\Big)$$

$$+\bar R F^2\eta^2,_S(Y^1,t)u^2,_S(Y^1,t) + \int_{[0,L]} A_\rho\eta^2(S,t)u^2,_{tt}(S,t)dS$$

$$+\int_{[0,L]} EI\ \eta^2,_{SS}(S,t)u^2,_{SS}(S,t)dS = 0, \qquad (25b)$$

for all admissible variations (η^1, η^2). Next, using the relations (4), we can recast equations (25a), (25b) to the following expanded form

$$\Big[M\eta^1(Y^1,t)\Big(u^1,_{tt}(Y^1,t)-\bar{R}u^2,_{Stt}(Y^1,t)\Big)$$

$$+\int_{[0,L]} A_\rho \eta^1(S,t)u^1,_{tt}(S,t)dS\Big]+2M\dot{Y}^1\eta^1(Y^1,t)\Big[u^1,_{St}(Y^1,t)$$

$$-\bar{R}u^2,_{SSt}(Y^1,t)\Big]+\Big[M\eta^1(Y^1,t)\Big(\ddot{Y}^1[u^1,_S(Y^1,t)-\bar{R}u^2,_{SS}(Y^1,t)]$$

$$+(\dot{Y}^1)^2\,[u^1,_{SS}(Y^1,t)-\bar{R}u^2,_{SSS}(Y^1,t)\Big)$$

$$-\bar{R}[F^1-M\ddot{Y}^1]\eta^1,_S(Y^1,t)u^2,_S(Y^1,t)$$

$$+\int_{[0,L]} EA\eta^1,_S(S,t)u^1,_S(S,t)dS\Big]=\eta^1(Y^1,t)[F^1-M\ddot{Y}^1], \tag{26a}$$

and

$$\Big[-\bar{R}M\eta^2,_S(Y^1,t)\Big(u^1,_{tt}(Y^1,t)-\bar{R}u^2,_{Stt}(Y^1,t)\Big)$$

$$+M\eta^2(Y^1,t)u^2{}_{tt}(Y^1,t)+\int_{[0,L]} A_\rho\eta^2(S,t)u^2,_{tt}(S,t)dS\Big]$$

$$+2M\dot{Y}^1\Big[-\bar{R}\eta^2,_S(Y^1,t)\Big(u^1,_{St}(Y^1,t)-\bar{R}u^2,_{SSt}(Y^1,t)\Big)$$

$$+\eta^2(Y^1,t)u^2,_{St}(Y^1,t)\Big]+\Big[M\ddot{Y}^1\Big\{-\bar{R}\eta^2,_S(Y^1,t)\Big(u^1,_S(Y^1,t)$$

$$-\bar{R}u^2,_{SS}(Y^1,t)\Big)+\eta^2(Y^1,t)u^2,_S(Y^1,t)\Big\}$$

$$+M(\dot{Y}^1)^2\Big\{-\bar{R}\eta^2,_S(Y^1,t)\Big(u^1,_{SS}(Y^1,t)$$

$$-\bar{R}u^2,_{SSS}(Y^1,t)\Big)+\eta^2(Y^1,t)u^2,_{SS}(Y^1,t)\Big\}$$

$$+\bar{R}F^2\eta^2,_S(Y^1,t)u^2,_S(Y^1,t)+\int_{[0,L]} EI\eta^2,_{SS}(S,t)u^2,_{SS}(S,t)dS\Big]$$

$$=-\bar{R}\eta^2,_S(Y^1,t)[F^1-M\ddot{Y}^1]+\eta^2(Y^1,t)F^2, \tag{26b}$$

for all admissible variations (η^1, η^2), where terms are grouped in square brackets according to their nature (mass, velocity-convection, and stiffness terms on the left-hand side, and applied forces on the right-hand side). Note the geometric stiffness character of the term with factor $\bar{R}[F^1-M\ddot{Y}^1]$, and of the term with factor $\bar{R}F^2$ in the stiffness operators of (26a) and (26b), respectively. Even though equations (23) and (26) are the simplified versions of the fully nonlinear equations (12) and (15), according to assumptions **(A1)** to **(A4)**, they remain nonlinear and coupled. Moreover, these equations in spatially discrete form are not explicit ordinary differential equations, and special algorithms must be designed for numerical computation. The system is driven by the initial conditions $\{Y^1(0); \dot{Y}^1(0), \mathbf{u}(S,0), \mathbf{u},_t(S,0)\}$ and the forces $\{F^1, F^2, T\}$ applied on the wheel.

Remark 3.4. In connection with Remark 3.3, we note that the linearized structural equations of motion (26b) contains the (low order) effect of the contact force $F_c^2 = F^2 - M\ddot{u}^2$ (the term $M\ddot{u}^2$ appears in (26b) in expanded form using (4b). Thus, the contact force F_c^2 is consistently accounted for in both equations (23) and (26). ■

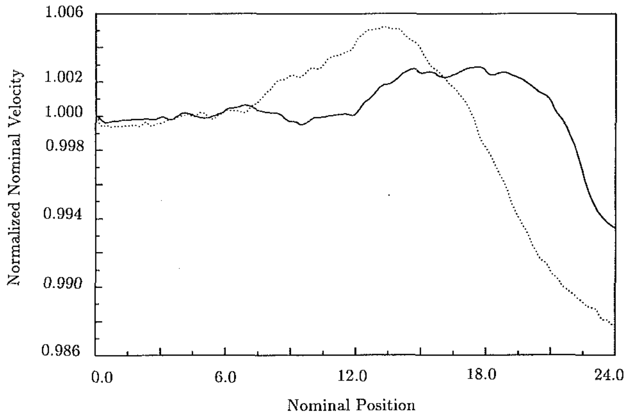

Fig. 2 ***Vehicle/structure interaction at different initial velocities:*** **Nominal velocity (normalized wrt initial values) versus Nominal position. Solid line: $\dot{Y}^1(0)$ = 100 m/s. Dotted line: $\dot{Y}^1(0)$ = 50 m/s. Beam length L = 24 m**

Remark 3.5. With assumptions **(A1-A3)**, equation (18b) is decoupled into an equation of motion for axial vibration and an equation of motion for the transverse vibration. But this means that the Maglev model C, unlike models A and B (see Remark 3.2), cannot be used to study effects of vehicle accelerating or braking on the axial structural response. ■

4 An Illustrative Example

In this section, an example is given to illustrate the above basic model for interaction between a vehicle, starting with different initial velocities, and a flexible supporting structure. Emphasis is focused on results which are not achievable using formulations based on the traditional assumption of known vehicle nominal motion. The results, obtained by numerical methods, correspond to the set of mildly nonlinear, coupled equations (23) and (26). We refer to Vu-Quoc and Olsson (1987, 1988a) for details and discussions on the numerical algorithms employed in solving these equations.

Consider a basic model with parameters M = 3000 kg, I_w = 135 kgm^2, R = 0.3 m, $\bar{R}$ = 0.9 m, L = 24 m, A_ρ = 1250 kg/m, $EA = 5\times10^9 N$, and $EI = 10^9 N\text{m}^2$. The beam has simple supports at its ends. The wheel is subjected to a constant vertical force $F^2 = -600{,}000\,N$ (with $F^1 = T \equiv 0$), whose magnitude is about 20 times that of the weight of the wheel (acceleration of gravity 9.81 m/s^2), creating a maximum midspan static deflection of 0.1728 m or about $L/140$. The lowest flexural frequency of the beam is 2.44 Hz; its lowest axial frequency is 20.8 Hz. Initial conditions are set to: $Y^1(0) = 0$, $\mathbf{u}(S,0) = \mathbf{u},_t(S,0) \equiv 0$ with the origin of S being coincident with the left support. The vehicle moves mainly due to its own initial velocity $\dot{Y}^1(0)$.

Nominal Velocity. Figure 2 shows the variation of the nominal velocities, normalized with respect to their respective initial values (at the entry of the beam) of $\dot{Y}^1(0)$ = 50 m/s and 100 m/s, as functions of the nominal position Y^1. From this figure, one can clearly observe a loss in nominal velocity at the end of the traversing: An entry velocity of 50 m/s drops by 1.2 percent at the exit, while an entry velocity of 100 m/s drops by 0.7 percent at the exit. The peak-to-peak variations in nominal velocity for these two cases are, respectively, 1.7 percent and 1.0 percent of their initial velocities. These variations stand in contrast to traditional analyses where the velocity $\dot{Y}^1$ is prescribed to its initial value throughout the traversing.

The drop in velocity is related to a drop in vehicle kinetic

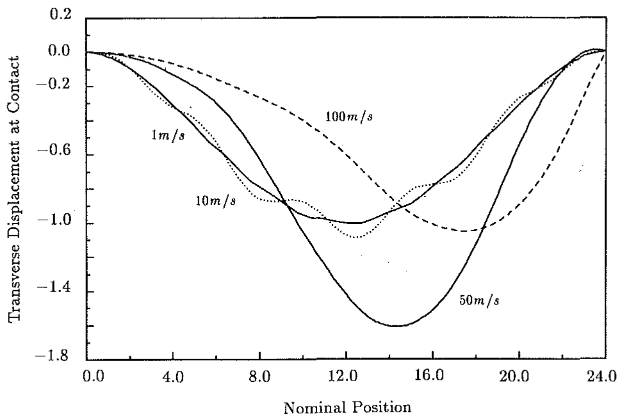

Fig. 3 ***Vehicle/structure interaction at different initial velocities:*** **Vertical displacement at contact point (normalized wrt 0.1728 m) versus Nominal position. $\dot{Y}^1(0)$ = 1 m/s, 10 m/s, 50 m/s, 100 m/s. L = 24 m.**

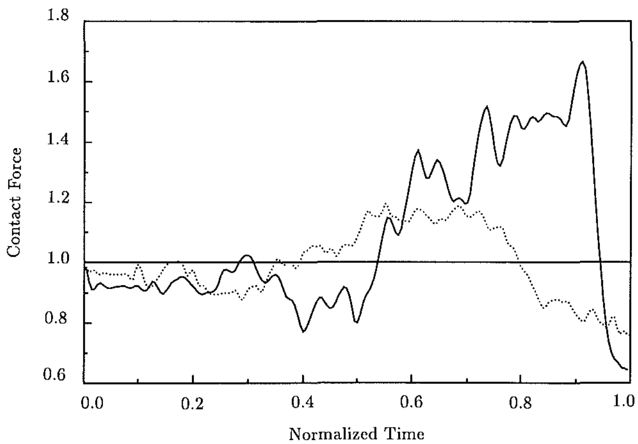

Fig. 4 ***Vehicle/structure interaction at different initial velocities:*** **Vertical contact force F_c^2 (normalized wrt vertical force F^2) versus Time (normalized wrt traversing time on rigid structure). Solid line: $\dot{Y}^1(0)$ = 100 m/s. Dotted line: $\dot{Y}^1(0)$ = 50 m/s.**

energy, as part of this initial kinetic energy is transferred to the beam; we refer to Vu-Quoc and Olsson (1987) for the details. This energy transfer, which keeps the beam in free vibration after the passage of the vehicle, effectively explains the Timoshenko paradox. We note that for a sufficiently long multiple-span structure, a vehicle moving under its initial velocity, without the aid of any other external force than a vertical one, and even in the absence of all energy-dissipative force, will experience a continuous drop in velocity as a result of this type of energy transfer (examples are given in Vu-Quoc and Olsson (1988a,b).

It is also interesting to note that at very low speed, one has a large relative increase in velocity during the traversing. For instance, for $\dot{Y}^1(0)$ = 1 m/s, the increase in nominal velocity is about 400 percent, i.e., the maximum velocity is about 5 m/s. As a result, the traversing time ($\approx$ 9s) is only about one-third of the traversing time on a rigid structure (24s). This increase in velocity is, however, drastically reduced to about 10 percent for $\dot{Y}^1(0)$ = 10 m/s (see Vu-Quoc and Olsson (1988a)).

Structural Deflection. The greater relative loss of velocity for $\dot{Y}^1(0)$ = 50 m/s is due to larger vertical displacement at contact point, compared to the same displacement for $\dot{Y}^1(0)$ = 100 m/s, as recorded in Fig. 3. Also plotted on this figure are displacement at contact point for $\dot{Y}^1(0)$ = 1 m/s (close to a static curve) and for $\dot{Y}^1(0)$ = 10 m/s. We note the shift of the location of maximum displacement closer to the exit as entry velocity increases.

Contact Force. Recorded in Fig. 4 are time histories of the vertical contact force F_c^2, for initial velocities of 50 m/s and 100 m/s. As noted in Remark 3.2, the inertia force $M\ddot{u}^2$ is non-negligible at high speed: For $\dot{Y}^1(0)$ = 100 m/s, this inertia force could reach 60 percent of the vertical force F^2 (Fig. 4). Again, this points to the consistency of the present formulation, which is crucial for a high speed regime.

5 Closure

We have presented a basic building block model for analyzing the interaction between high speed vehicles and supporting flexible structures. The present formulation departs completely from traditional practice of assuming known vehicle nominal motion. Nonlinear equations of motion for the basic model, with a general form of constraints and valid for large structural deformation, are derived using Hamilton's principle. Additional assumptions, essentially on small structural deformation, are introduced to simplify these equations to a mildly nonlinear form. The applicability of the present model is demonstrated through an example. In subsequent publications, we will present efficient algorithms to integrate the nonlinear equations of motion of the complete vehicle/structure interaction problem, and further results.

Acknowledgments

The kind encouragement of Prof. R. L. Taylor and Dr. J. E. Higgins as well as the support from The Sweden-America Foundation to Dr. M. Olsson, are gratefully acknowledged.

References

Alscher, H., Iguchi, M., Eastham, A. R., and Boldea, I., 1983, "Non-Contact Suspension and Propulsion Technology," *Vehicle System Dynamics*, Vol. 12, pp. 259–289.

Blejwas, T. E., Feng, C. C., and Ayre, R. S., 1979, "Dynamic Interaction of Moving Vehicles and Structures," *J. Sound and Vibration*, Vol. 67, No. 4, pp. 513–521.

Eastham, A. R., and Hayes, W. F., 1987, "The Status of Development of Maglev Systems," *Proc. of the 37th IEEE Vehicular Technology Conference*, Tampa, Florida, June, pp. 231–239.

Frýba, L., 1972, *Vibration of Solids and Structures under Moving Loads*, Noordhoff International Publishing, Groningen.

Kalker, J. J., 1979, "Survey of Wheel-Rail Rolling Contact Theory," *Vehicle System Dynamics*, Vol. 5, pp. 317–358.

Kortüm, W., and Wormley, D. N. 1981, "Dynamic Interaction Between Travelling Vehicles and Guideway Systems," *Vehicle System Dynamics*, No. 10, pp. 285–317.

Kortüm, W., 1986, "Introduction to System-Dynamics of Ground Vehicles," *Proc. of the 3rd ICTS Course and Seminar on Advanced Vehicle System Dynamics*, Amalfi, Italy, May, pp. 1–36.

Maunder, L., 1960, "On the Work of a Force Crossing a Beam," *Quart. of Applied Mathematics*, Vol. 17, pp. 437–440.

Olsson, M., 1985, "Finite Element, Modal Co-ordinate Analysis of Structures Subjected to Moving Loads," *J. Sound and Vibration*, Vol. 99, No. 1, pp. 1–12.

Olsson, M., 1986, "Analysis of Structures Subjected to Moving Loads," Doctoral Dissertation, Report TVSM-1003, Division of Structural Mechanics, Lund University, Sweden.

Rektorys, K., 1980, *Variational Methods in Mathematics, Science, and Engineering*, D. Reidel Pub. Co., Dortrecht, Holland.

Simo, J. C., and Vu-Quoc, L., 1986, "On the Dynamics of Flexible Beams Under Large Overall Motions – The Plane Case: Parts I and II," ASME Journal of Applied Mechanics, Vol. 53, No. 4, pp. 849–863.

Stanisic, M. M., 1985, "On a New Theory of the Dynamic Behavior of the Structures Carrying Moving Masses," *Ingenieur-Archiv*, Vol. 55, pp. 176–185.

Subcommitee on Vibration Problems Associated with Flexural Members on Transit Systems, Structural Division 1985, "Dynamics of Steel Elevated Guideways – An Overview," *J. Structural Engineering*, Vol. 111, No. 9, pp. 1873–1898.

Ting, E. C., Genin, J., and Ginsberg, J. H., 1974, "A General Algorithm for Moving Mass Problems," *J. Sound and Vibration*, Vol. 33, No. 1, pp. 49–58.

Ting, E. C., and Yener, M., 1983, "Vehicle-Structure Interactions in Bridge Dynamics," *Shock and Vibration Digest*, Vol. 15, No. 12, pp. 3–9.

Venancio-Filho, F., 1979, "Finite Element Analysis of Structures Under Moving Loads, *Shock and Vibration Digest*, Vol. 10, No. 8, pp. 27–35.

Vu-Quoc, L., 1986, "Dynamics of Flexible Structures Performing Large

Overall Motions: A Geometrically-Nonlinear Approach," Doctoral Dissertation, Electronics Research Laboratory Memorandum UCB/ERL M86/36, University of California, Berkeley.

Vu-Quoc, L., and Olsson, M., 1987, "Interaction Between High-Speed Moving Vehicles and Flexible Structures: An Analysis Without Assumption of Known Vehicle Nominal Motion," Structural Engineering, Mechanics, and Materials, Report No. UCB/SEMM-87/10, NISEE Center, University of California, Berkeley, December.

Vu-Quoc, L., and Olsson, M., 1988a, "A Computational Procedure for Interaction of High-Speed Vehicles on Flexible Structures Without Assuming Known Vehicle Nominal Motion," to appear in *Computer Methods in Applied Mechanics and Engineering*.

Vu-Quoc, L., and Olsson, M. 1988b, "Some Aspects of Vehicle/Structure Interaction at High Vehicle Speed on Multiple-Span Elevated Guideways," in preparation.

Wallrapp, O., 1986, "Elastic Vehicle Guideway Structures," *Proc. of the 3rd ICTS Course and Seminar on Advanced Vehicle System Dynamics*, Amalfi, Italy, May, pp. 215–232.

Zicha, J. H., 1986, "Civil Aspects of Maglev Design," *Proc. of the IEEE Int. Conf. on Maglev and Linear Drives*, Vancouver, Canada, May, pp. 69–87.

J. L. Wegner
Assoc. Mem. ASME

J. B. Haddow
Mem. ASME

Department of Mechanical Engineering,
University of Victoria,
Victoria, B.C. V8W 2Y2, Canada

R. J. Tait
Department of Mathematics,
University of Alberta,
Edmonton, AB T6G 2G8, Canada

Unloading Waves in a Plucked Hyperelastic String

The governing equations for the finite deformation plane motion of a hyperelastic string are obtained in conservation form. These equations and the corresponding jump relations are used to investigate the response of a symmetrically-plucked string when it is suddenly released. Similarity solutions, which are valid until the first reflection occurs at a fixed end, are obtained for two strain energy functions. Justification is given for the use of isothermal strain energy functions.

1 Introduction

In a recent paper (Beatty and Haddow, 1985), governing equations for the finite deformation plane motion of a stretched hyperelastic string are derived and used to obtain similarity solutions for a neo-Hookean or Mooney-Rivlin string, subjected to a suddenly applied force at one end. In the present paper the governing equations are derived in conservation form and a corresponding hyperbolic system of first-order partial differential equations is obtained. This system may be simpler to apply, for certain problems, than the equivalent system given by Beatty and Haddow (1985) and we use it to investigate the wave propagation which results when a symmetrically-plucked string is suddenly released. Similarity solutions, which are valid until the first reflection occurs at a fixed end, are obtained for two realistic strain energy functions, a particular case of the Mooney-Rivlin and a three-term function proposed by Ogden (1972), which gives an "S" shaped nominal stress-stretch curve for simple tension.

Numerical schemes such as those proposed by Godunov or Glimm (Sod, 1985) can be used to extend the solutions beyond the time of the first reflection, and a system of governing equations in conservation form is essential for application of these schemes.

The adiabatic approximation is implied in the derivation of the system of governing equations. That is, the effect of heat conduction is neglected. This is reasonable for rubberlike materials, which are poor heat conductors. It is evident that some justification for the use of an isothermal strain energy function is required, since the adiabatic approximation implies that the deformation is piecewise isentropic. In order to investigate the errors which arise from the use of an isothermal strain energy function in the plucked-string problem, simple tension of an incompressible hyperelastic solid with strictly entropic elasticity (Chadwick and Creasy, 1984) is considered. For realistic values of the material properties for rubberlike materials the thermal effects, due to strictly entropic elasticity, are not significant in the present problem, provided the maximum stretch which occurs is not too large, say less than six. The effect on the stress-stretch relation of the jump in entropy, which occurs across a shock, is neglected if the isentropic approximation is used in addition to the adiabatic approximation.

Contributed by the Applied Mechanics Division of THE AMERICAN SOCIETY OF MECHANICAL ENGINEERS for presentation at the Joint ASME/ASCE Applied Mechanics, Biomechanics, and Fluids Engineering Conference, San Diego, Calif., July 9 to 12, 1989.

Discussion of this paper should be addressed to the Editorial Department, ASME, United Engineering Center, 345 East 47th Street, New York, N.Y. 10017, and will be accepted until two months after final publication of the paper itself in the JOURNAL OF APPLIED MECHANICS. Manuscript received by ASME Applied Mechanics Division, March 23, 1988; final revision, August 3, 1988.

Paper No. 89-APM-4.

2 Formulation of Problem

We consider a perfectly flexible, uniform hyperelastic string fixed at points $x_1 = \pm l_0$ of the x_1 axis of a rectangular Cartesian coordinate system. The reference configuration is taken as the unstressed configuration, at temperature T_o, which occupies the interval $[-L,L]$ of the x_1 axis. The x_1 coordinate of a particle in the reference configuration is $X\epsilon[-L,L]$, and at time t the particle is at place $\mathbf{x}=\mathbf{x}(X,t)$.

We consider plane motion in the Ox_1x_2 plane and at time $t=0$; the string is released from the symmetrically-deformed configuration given by

$$x_1(X,0)=\frac{l_0}{L}X, \quad x_2(X,0)=-l_o\left(\frac{L-X}{L}\right)\tan\theta_1, \tag{1}$$

for $X\epsilon[0,L]$, where θ_1 is the angle the string makes with the x_1 axis as shown in Fig. 1. The stretch λ_1 at $t=0$ is given by

$$\lambda_1=\lambda_o/\cos\theta_1>1 \tag{2}$$

where $\lambda_o=l_o/L$. If $0<\lambda_o<1$, the string is slack before the deformation (1) is applied, and $\theta_1>\cos^{-1}(l_o/L)$. After the string is suddenly released it is assumed that the subsequent deformed shape of the string is symmetrical about the x_2 axis, consequently only the part $X\epsilon[0,L]$ is considered.

3 Governing Equations

We obtain the conservation form of the system of Lagrangian governing equations and the corresponding form with dependent variables u, v, λ, and θ, where u and v are the x_1 and x_2 components, respectively, of the particle velocity,

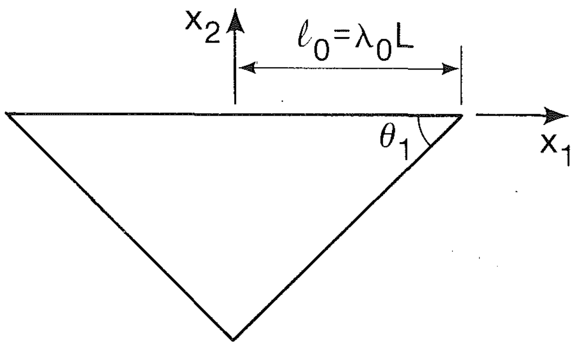

Fig. 1 Deformed configuration at $t=0$

and θ is the angle the tangent to the string makes with the x_1 axis. The dependent variables for the system of equations derived by Beatty and Haddow (1985) are τ, ν, λ and θ, where τ and ν are the tangential and normal components, respectively, of the particle velocity. However, these dependent variables, or combinations of them, are not convenient for determination of a system in conservation form.

If $s(X,t)$ denotes the arc length, measured from $\mathbf{x}=\mathbf{x}(0,t)$ in the deformed configuration, the stretch is given by

$$\lambda(X,t)=\frac{\partial s}{\partial X}, \tag{3}$$

and it follows that

$$\frac{\partial(\lambda\cos\theta)}{\partial t}=\frac{\partial u}{\partial X},\ \frac{\partial(\lambda\sin\theta)}{\partial t}=\frac{\partial v}{\partial X}. \tag{4}$$

The string is assumed to be perfectly flexible, consequently, the direction of the tensile force P per unit cross-sectional area of the string in the reference configuration, is tangential to the string. For the present we assume P can be expressed as a function of λ only. The nonzero components S_{11} and S_{12} of the nominal stress tensor are given by

$$S_{11}=P(\lambda)\cos\theta \text{ and } S_{12}=P(\lambda)\sin\theta,$$

consequently, the Lagrangian equations of motion are,

$$\frac{\partial(P(\lambda)\cos\theta/\rho_o)}{\partial X}=\frac{\partial u}{\partial t},\ \frac{\partial(P(\lambda)\sin\theta/\rho_o)}{\partial X}=\frac{\partial v}{\partial t}, \tag{5}$$

where ρ_o is the density.

The system of equations (4) and (5) is in conservation form and may be expressed as

$$\frac{\partial \mathbf{G}}{\partial t}+\frac{\partial \mathbf{H}(\mathbf{G})}{\partial X}=\mathbf{0}, \tag{6}$$

where $\mathbf{G}=(\lambda\cos\theta,\ \lambda\sin\theta,\ u,\ v)^T$, $\mathbf{H}=-(u,v,P\cos\theta/\rho_o,P\sin\theta/\rho_o)^T$ and a superposed T denotes the transpose. A convenient nonconservation form obtained from (6) is

$$\frac{\partial \mathbf{Q}}{\partial t}+\mathbf{A}\frac{\partial \mathbf{Q}}{\partial X}=0 \tag{7}$$

where $\mathbf{Q}=(\lambda,\theta,u,v)^T$, (8)

$$\mathbf{A}=\left[\begin{array}{cc|cc} 0 & 0 & -\cos\theta & -\sin\theta \\ 0 & 0 & \lambda^{-1}\sin\theta & -\lambda^{-1}\cos\theta \\ \hline -C_L^2\cos\theta & \lambda C_T^2\sin\theta & 0 & 0 \\ -C_L^2\sin\theta & -\lambda C_T^2\cos\theta & 0 & 0 \end{array}\right], \tag{9}$$

$$C_L^2=\frac{1}{\rho_o}\frac{dP}{d\lambda},\qquad C_T^2=\frac{P}{\rho_{o\lambda}}. \tag{10}$$

System (7) is strictly hyperbolic if $C_L^2>0$, $C_T^2>0$, and $C_L\neq C_T$. The eigenvalues of $\mathbf{A}$ are $\pm C_T$ and $\pm C_L$ and if the system is strictly hyperbolic, there are four distinct families of characteristics with slopes $\pm C_L$ and $\pm C_T$ in the X,t plane, so that λ and θ are propagated with Lagrangian wave speeds C_L and C_T, respectively, along these characteristics. We use the terms longitudinal and transverse wave speeds to describe C_L and C_T, respectively. For the strain energy functions considered in this paper, $C_L^2>0$ and $C_T^2>0$ for all $\lambda>1$, however, $C_L=C_T$ for isolated values of $\lambda>1$.

Relations along the characteristics are obtained from

$$\mathbf{l}^T\frac{d\mathbf{Q}}{dt}=0 \quad\text{on}\quad \frac{dX}{dt}=\alpha,$$

where $\alpha=\pm C_L,\ \pm C_T$ and $\mathbf{l}$ is the corresponding left eigenvector of $\mathbf{A}$. These relations are not required for what follows and we do not obtain them.

A further conservation equation, the equation of conservation of energy, can be obtained from (4) and (5) and the relation

$$P(\lambda,S)=\rho_o\frac{\partial U}{\partial\lambda},$$

where $U(\lambda,S)$ is the internal energy per unit mass and S is the specific entropy. With the adiabatic approximation this equation becomes,

$$\frac{\partial}{\partial t}\left\{\rho_o\frac{(u^2+v^2)}{2}+\rho_o U\right\}-\frac{\partial}{\partial X}\{P(u\cos\theta+v\sin\theta)\}=0. \tag{11}$$

If we adopt the isentropic approximation, (11) is not required.

4 Discontinuity Relations

Jump relations for discontinuities are given by Beatty and Haddow (1985). In this section these jump relations are considered in a different way and in more detail. We use the term shock to denote a discontinuity of either λ or θ.

Since system (6) is in conservation form, the jump relations across a shock are given by,

$$V[\mathbf{G}]=[\mathbf{H}] \tag{12}$$

where the square brackets indicate the jump across the shock of the enclosed quantity, and V is the Lagrangian shock velocity. Two expressions for V^2,

$$V^2=[C_T^2\lambda\cos\theta]/[\lambda\cos\theta],\ \ V^2=[C_T^2\lambda\sin\theta]/[\lambda\sin\theta],$$

can be obtained from (12). These are compatible if and only if, either,

$$\frac{(\lambda\sin\theta)^+}{(\lambda\cos\theta)^+}=\frac{(\lambda\sin\theta)^-}{(\lambda\cos\theta)^-}\quad\text{or}\quad [C_T^2]=0, \tag{13}$$

where the superscripts + and − indicate values ahead of, and behind the shock, respectively. It may be deduced from (13) that, across a shock, there are three possibilities $\theta^+=\theta^-$ and $[C_T^2]\neq 0$, $\theta^+=\theta^-\pm\pi$ and $[C_T^2]\neq 0$, $\theta^+\neq\theta^-$ and $[C_T^2]=0$. For the present problem, the possibility $\theta^+=\theta^-\pm\pi$ is not physically admissible, so that a discontinuity with both C_T^2 and θ discontinuous is not possible. In general $[C_T^2]=0$ implies that $[\lambda]=0$, however, if $C_L(\lambda_c)=C_T(\lambda_c)$ for $\lambda=\lambda_c$, there is a set, Ω, of pairs of values of λ, where

$$\Omega=\{(\lambda',\lambda'')\,|\,1\le\lambda'<\lambda_c<\lambda'',\ C_T(\lambda')=C_T(\lambda'')\}.$$

If there is a jump in λ and $(\lambda^+,\lambda^-)\epsilon\Omega$, a jump in θ is possible across the jump in λ. Otherwise, a jump in θ cannot occur across a jump in λ and vice versa. If $[C_T^2]\neq 0$, there are two possible shock velocities: V_L and V_T, the velocities of propagation of discontinuities of λ and θ, respectively. It then follows from (12) that there are two sets of discontinuity relationships,

$$V_L[\lambda]\cos\theta = -[u], \quad V_L[\lambda]\sin\theta = -[v], \tag{14}$$

$$V_L[u] = -[P]\cos\theta/\rho_o, \quad V_L[v] = -[P]\sin\theta/\rho_o, \tag{15}$$

and

$$V_T\lambda[\cos\theta] = -[u], \quad V_T\lambda[\sin\theta] = -[v], \tag{16}$$

$$V_T[u] = -P[\cos\theta]/\rho_o, \quad V_T[v] = -P[\sin\theta]/\rho_o. \tag{17}$$

It follows from (14) and (15) that

$$V_L = \pm\left\{\frac{[P]}{\rho_o[\lambda]}\right\}^{1/2} \tag{18}$$

and from (16) and (17) that

$$V_T \pm \left\{\frac{P}{\rho_o\lambda}\right\}^{1/2}. \tag{19}$$

Comparison of (10) and (19) shows that $V_T = \pm C_T$, consequently a discontinuity of θ, is propagated along a characteristic.

A further jump relation,

$$V\left[\rho_o\,\frac{(u^2+v^2)}{2} + \rho_o\,U\right] = -[P(u\cos\theta + v\sin\theta] \tag{20}$$

is obtained from (11). Since U does not depend explicitly on θ, (20) gives

$$V_T\left[\rho_o\,\frac{(u^2+v^2)}{2}\right] = -[P(u\cos\theta + v\sin\theta], \tag{21}$$

across a jump in θ, and with V replaced by V_L, holds across a jump in λ. If the isentropic approximation is adopted, (20) with $\rho_o U$ replaced by W is not satisfied across a jump in λ.

When $[C_T{}^2] = 0$ and $[\lambda] \neq 0$, $[\theta] \neq 0$, then $V_L = V_T = V$ and there is only one set of discontinuity relations,

$$V[\lambda\cos\theta] = -[u], \quad V[\lambda\sin\theta] = -[v], \tag{22}$$

$$V[u] = -[P\cos\theta]/\rho_o, \quad V[v] = -[P\sin\theta]/\rho_o, \tag{23}$$

where
$$V = \pm\left(\frac{P^+}{\rho_o\lambda^+}\right)^{1/2} = \pm\left(\frac{P^-}{\rho_o\lambda^-}\right)^{1/2}.$$

5 Constitutive Relations

We obtain results for special cases of the Mooney-Rivlin and three-term Ogden (1972) strain energy functions. The simple tension forms of these strain energy functions are:

$$W = \frac{\mu}{2}\left\{\alpha\left(\lambda^2 + \frac{2}{\lambda} - 3\right) + (1-\alpha)(\lambda^{-2} + 2\lambda - 3)\right\} \tag{24}$$

and
$$W = \sum_{i=1}^{3} \frac{\mu_i}{a_i}\,(\lambda^{a_i} + 2\lambda^{-a_i/2} - 3), \tag{25}$$

respectively, where μ is the infinitesimal shear modulus, $0 \le \alpha \le 1$, and

$$\sum_{i=1}^{3} \mu_i a_i = 2\mu.$$

Ogden (1972) has shown that the relation, (26)

obtained from

$$P = \frac{dW}{d\lambda} \tag{27}$$

and (25) gives a close fit with experimental data for simple tension of certain rubbers up to stretches of about 7, when the μ_i and a_i take the values,

$$\mu_1/\mu = 1.491, \quad \mu_2/\mu = 0.003, \quad \mu_3/\mu = -0.0237,$$
$$a_1 = 1.3, \quad a_2 = 5.0, \quad a_3 = -2.0. \tag{28}$$

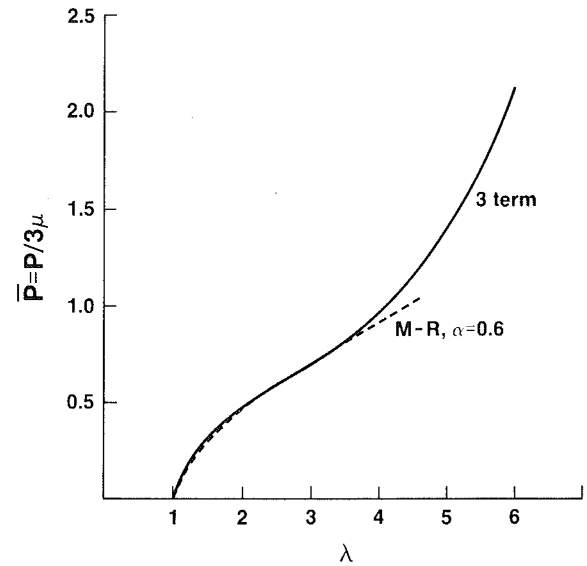

Fig. 2 Nominal stress-stretch relations

The corresponding relation for (24) is

$$P = \mu(\alpha + (1-\alpha)/\lambda)(\lambda - 1/\lambda^2), \tag{29}$$

which, with $\alpha = 0.6$, gives a close fit with simple tension experimental data for λ up to about 3.5. Relation (26) with (28) and relation (29) with $\alpha = 0.6$ are shown graphically in Fig. 2.

The strain energy functions (24) and (25) give the stored elastic energy per unit volume for isothermal simple tension at the reference temperature T_o. Since we are adopting the isentropic approximation, an isentropic stress-stretch relation should be used and, if (26) and (29) are used, some justification if required. In order to investigate this point we assumed the string is incompressible and its elastic behavior is strictly entropic, as predicted by the Gaussian theory of rubber elasticity. Strictly entropic elasticity is a limiting case of modified entropic elasticity, which has been shown by Chadwick and Creasy (1984) to be a realistic model for rubberlike solids. If a solid possesses strictly entropic elasticity, stresses arise entirely from changes of entropy and the internal energy can be expressed as a function of temperature only. The other limiting case of modified entropic elasticity is piezotropic elasticity. In this case mechanical and thermal effects are completely uncoupled and the use of an isothermal stress-stretch relation is exact even for a heat conducting material, since an isothermal deformation is also isentropic.

When nonisothermal simple tension of an incompressible solid which exhibits strictly entropic elasticity is considered, (27) should be replaced by

$$\tilde{P}(\lambda,T) = \frac{T}{T_o}\,\frac{dW}{d\lambda}, \tag{30}$$

or equivalently by

$$\tilde{P}(\lambda,S) = \frac{dW}{d\lambda}\exp\left(\frac{S}{C} + \beta\,\frac{W}{\mu}\right), \tag{31}$$

where $\beta = \eta/\rho C T_o$, S is the entropy, and C, which is assumed to be constant, is the specific heat at constant deformation. For strictly entropic or modified entropic elasticity, C depends only on T, but if $|T - T_o|/T_o \ll 1$, the temperature dependence can be neglected. A typical value of the nondimensional quantity β for rubberlike solids is $\beta = 10^{-3}$. In obtaining (31) the entropy is taken as zero in the reference state, so that for isentropic deformation from the reference state,

$$\tilde{P}(\lambda,0) = \frac{dW}{d\lambda}\exp\left(\beta\,\frac{W}{\mu}\right). \tag{32}$$

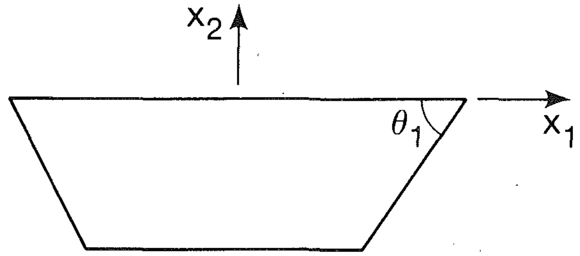

Fig. 3 Form of deformed configuration for $t>0$ and before first reflection

If the string is deformed isothermally to stretch λ_1 before being released then, for the isentropic deformation, which is assumed to occur after release

$$\tilde{P}(\lambda,S_1) = \frac{dW}{d\lambda} \exp\left(\frac{S_1}{C} + \beta \frac{W}{\mu}\right), \tag{33}$$

where

$$\frac{S_1}{C} = -\beta W(\lambda W(\lambda_1)/\mu,$$

and if $|S_1/C - \beta W/\mu| \ll 1$, the isothermal relation is a good approximation. With $\beta = 10^{-3}$ it can be shown that the maximum error that results from the use of (27), rather than (31), is less than 1.5 percent for stretches up to about 6. There is no difficulty in using (31), rather than (27), but this is not done since the additional complication is not justified for the range of λ considered. When a jump in λ occurs the deformation is piecewise isentropic with a jump in entropy across the shock, if the adiabatic approximation is adopted. According to (31) this results in a change in the isentropic P, λ relation as the shock passes. We have verified that for the values of $[\lambda]$ which occur across the unloading shocks in the problems considered, the error, resulting from neglect of the effect of the entropy jump on the P, λ relation, is less than 0.5 percent. This justifies the use of the isentropic approximation.

6 Similarity Solutions

Similarity solutions can be obtained for the motion of the string after it is suddenly released from the deformed configuration (1). These solutions are valid until the first reflection occurs at $X = \pm L$. For certain values of λ_0 and θ_1 no reflected wave is possible, since the string cannot sustain compression. We have already noted that a discontinuity of θ is propagated along characteristics with slopes $\pm C_T$ in the (X,t) plane. Since there is no such characteristic parallel to the t axis of the (X,t) plane for $\lambda \neq 1$, we seek similarity solutions for which the deformed shape is as indicated in Fig. 3, and the dependent variables are functions of $Z = X/t$. A system of ordinary differential equations,

$$(\mathbf{A} - Z\mathbf{I}) \frac{d\mathbf{Q}}{dZ} = 0, \tag{34}$$

where $\mathbf{Q}$ and $\mathbf{A}$ are given by (8) and (9), respectively, and $\mathbf{I}$ is the identity matrix, is then obtained. A nontrivial solution to system (34) exists, if the only if $Z = \pm C_L$ or $Z = \pm C_T$, and since we are seeking solutions which are symmetric about $X=0$, we only consider $Z = C_L$ and $Z = C_T$.

Solutions satisfying (34) and the jump relations consist of centered simple waves and/or shocks. Since $V_T = C_T$ and a discontinuity of θ propagates along a characteristic, it may be deduced that the initial discontinuity of θ at $X=0$ does not result in a centered simple wave, but propagates as a discontinuity as indicated in Fig. 3.

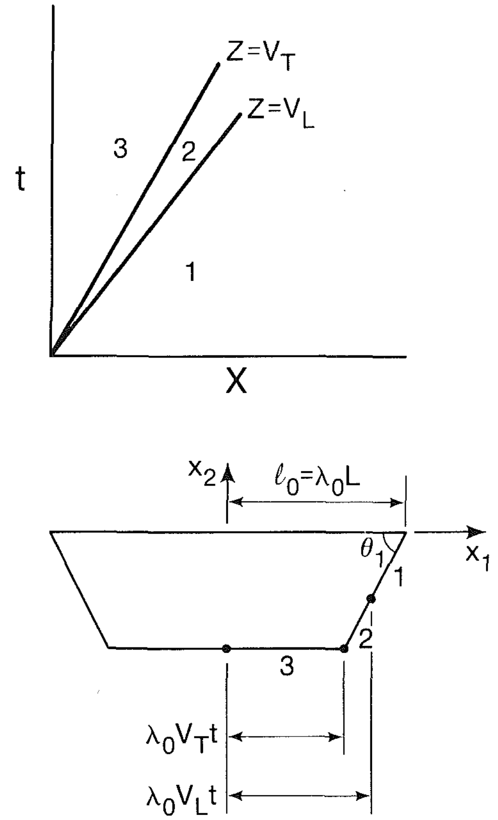

Fig. 4 Form of solution for Mooney-Rivlin Material, $\alpha=0.6$, $\lambda_1<\lambda_c$ or $\lambda_1>\lambda_c$ and $\lambda_3<\lambda_*$

7 Solutions

It is convenient to introduce the following nondimensionalization scheme,

$$\bar{P} = \frac{P}{3\mu}, \quad \bar{\mathbf{q}} = \frac{\mathbf{q}}{C_o}, \quad \bar{X} = \frac{X}{L}, \quad \bar{t} = \frac{C_o t}{L},$$

$$\bar{Z} = \frac{\bar{X}}{\bar{t}} = \frac{X}{C_o t}, \tag{35}$$

where $\mathbf{q} = (u,v,C_L,V_L,V_T)^T$ and $C_o = C_L(1) = (3\mu/\rho_o)^{1/2}$ is the wave speed for infinitesimal amplitude longitudinal waves propagating into an undeformed region. Henceforth, we use nondimensional variables given by (35) but omit the bars.

(*a*) Mooney-Rivlin String with $\alpha = 0.6$. The nondimensional wave speeds obtained from (10) and (27) are

$$C_L = \left\{\frac{1}{3}\left[\alpha\left(1 + \frac{2}{\lambda^3}\right) + 3(1-\alpha)\lambda^{-4}\right]\right\}^{1/2}, \tag{36}$$

$$C_T = \left\{\frac{1}{3}\left[\alpha + \frac{(1-\alpha)}{\lambda}\right]\left(1 - \frac{1}{\lambda^3}\right)\right\}^{1/2}. \tag{37}$$

It is easily shown that $C_L \gtreqless C_T$ when $\lambda \lesseqgtr \lambda_c$ where $\lambda_c = 2.473$ for $\alpha = 0.6$. We obtain similarity solutions which consist of three constant state regions in the (X,t) plane, separated by shocks $Z = V_T$ and $Z = V_L$, where V_T and V_L are determined by λ_1 and θ_1. Equations (34) are trivially satisfied in the constant state regions and the jump relations and entropy conditions are satisfied across the shocks. The initial values θ_1 and λ_o determine whether $V_L > V_T$ or $V_T > V_L$. First we consider the case with $V_L > V_T$, as indicated by the X,t plane shown in Fig. 4 for $X \epsilon [0,L]$. The following solution is valid if $\lambda_1 < \lambda_c$ or if $\lambda_1 > \lambda_c$ and $\lambda_3 = \lambda_2 < \lambda_*$ where $\lambda_* < \lambda_c$ and

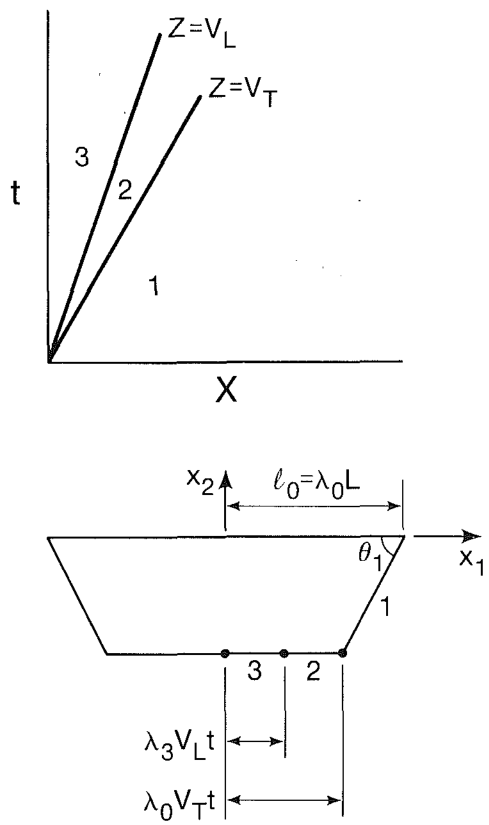

Fig. 5 Form of solution for Mooney-Rivlin Material, $\alpha=0.6$, $\lambda_1>\lambda_c$ and $\lambda_3>\lambda_*$

$C_T(\lambda_*)=C_L(\lambda_1)$, and the subscripts, 1,2,3 refer to the corresponding regions indicated in Fig. 4.

Region 1: $X/t>V_L$;

$$u=v=0,\quad \lambda=\lambda_1,\ \theta=\theta_1.$$

Region 2: $V_L>X/t>V_T$;

$$u=u_2,\ v=v_2,\ \lambda=\lambda_2,\ \theta=\theta_2=\theta_1,$$
$$v_2=u_2\tan\theta_1,$$

where the nondimensional longitudinal shock speed,

$$V_L=\left\{\frac{P(\lambda_2)-P(\lambda_1)}{(\lambda_2-\lambda_1)}\right\}^{1/2} \tag{38}$$

is obtained from (18) and (29), and

$$u_2=-V_L(\lambda_2-\lambda_1)\cos\theta_1,\ v_2=-V_L(\lambda_2-\lambda_1)\sin\theta_1 \tag{39}$$

are obtained from (14).

Region 3: $V_T>X/t>0$;

$$v=v_3,\ u=0,\ \lambda=\lambda_3=\lambda_2,\ \theta=0,$$

where the nondimensional transverse shock speed,

$$V_T=\left\{\frac{P(\lambda_2)}{\lambda_2}\right\}^{1/2} \tag{40}$$

is obtained from (19) and (29), and

$$u_2=V_T\lambda_2(1-\cos\theta_1),\ v_3=V_T\lambda_2\sin\theta_1+v_2, \tag{41}$$

and are obtained from (16).

All the unknowns can be determined from (38) to (41) and (2) if λ_o and θ_1 are given.

Next, we consider the case $V_T>V_L$, as indicated in Fig. 5, for $X\epsilon[0,L]$. The solution given is valid if $\lambda_1>\lambda_c$ and $\lambda_3=\lambda_2>\lambda_*$.

Region 1: $X/t>V_T$;

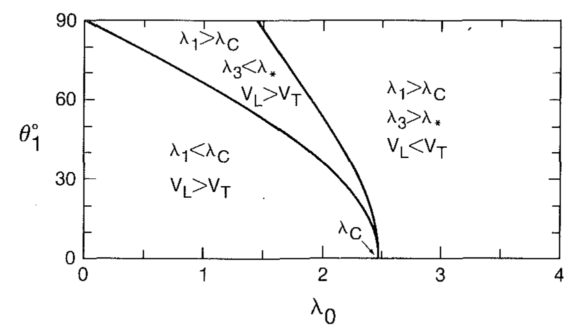

Fig. 6 Regions of validity of solutions for Mooney-Rivlin Material with $\alpha=0.6$

$$u=v=0,\ \lambda=\lambda_1,\ \theta=\theta_1,$$

where

$$V_T=\left\{\frac{P(\lambda_1)}{\lambda_1}\right\}^{1/2}. \tag{42}$$

Region 2: $V_T>X/t>V_L$;

$$u=u_2,\ v=v_2,\ \lambda=\lambda_1,\ \theta=0,$$
$$u_2=-V_T\lambda_1(1-\cos\theta_1),\ v_2=V_T\lambda_1\sin\theta_1 \tag{43}$$

are obtained from (16).

Region 3: $V_L>X/t>0$;

$$u=0,\ v=v_2=v_3,\ \lambda=\lambda_3,\ \theta=0,$$

where

$$V_L=\left\{\frac{P(\lambda_3)-P(\lambda_1)}{(\lambda_3-\lambda_1)}\right\}^{1/2}, \tag{44}$$

is obtained from (18) and (29) and

$$u_2=V_L(\lambda_3-\lambda_1), \tag{45}$$

is obtained from (14).

All the unknowns can be determined from (42)–(45) and (2) if λ_o and θ_1 are given.

The regions of validity in the (λ_o,θ_1) plane of the aforementioned solutions are shown in Fig. 6.

For the limiting cases of these solutions as $\lambda\rightarrow\lambda_*$ so that $V_L\rightarrow V_T$ and Region 2 in Figs. 4 and 5 becomes vanishingly small, a solution is readily obtained from jump relations (22) and (23). This solution is particularly simple since $\lambda_3=\lambda_*=\lambda_o$.

(b) Three-Term S.E.F. String. The non-dimensional wave speeds obtained from (10) and (26) are

$$C_L=\left\{\sum_{i=1}^{3}\frac{\mu_i}{3\mu}\left[(a_i-1)\lambda^{a_i-2}+\left(\frac{a_i}{2}+1\right)\lambda^{-a_i/2-2}\right]\right\}^{1/2},$$

$$C_T=\left\{\sum_{i=2}^{3}\frac{\mu_i}{3\mu}\ (\lambda^{a_i-2}-\lambda^{-a_i/2-2},\right\}^{1/2}$$

where the a_i and η_i are given by (28). Referring to Fig. 7, $C_L>C_T$, if $\lambda<\lambda_{c1}$ or $\lambda>\lambda_{c2}$, and $C_L<C_T$ if $\lambda_{c1}<\lambda<\lambda_{c2}$, where $\lambda_{c1}=2.1674$ and $\lambda_{c2}=3.1674$. In Fig. 7, $\lambda_i=2.6404$ is the stretch corresponding to the inflection point of the (P,λ) curve. Solutions for $\lambda_1<\lambda_i$ are of the same form as those for the Mooney-Rivlin string. We present two solutions, one which is valid if $\lambda_1>\lambda_4>\lambda_{c2}$ and one which is valid if $\lambda_1>\lambda_{c2}>\lambda_4>\lambda_i$, where λ_4 is the unloaded stretch. The first solution consists of constant state regions 1, 3, and 4 and a centered, simple wave Region 2, as indicated in Fig. 8, and is as follows:

Region 1: $X/t\geq C_L(\lambda_1)$;

$$u=v=0,\ \lambda=\lambda_1,\ \theta=\theta_1.$$

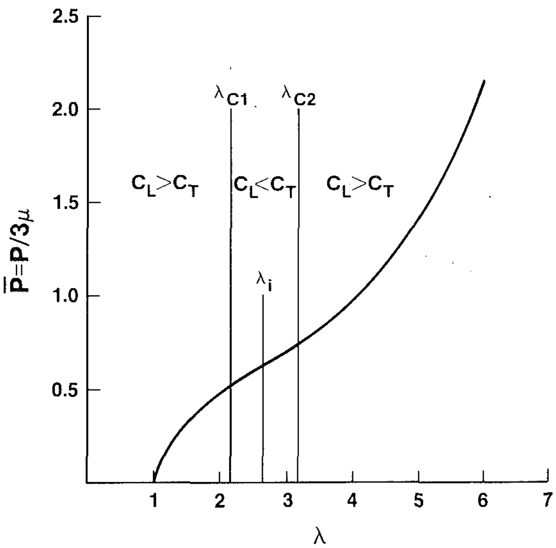

Fig. 7 Nominal stress stretch curve for three-term strain energy functions

Region 2: $C_L(\lambda_1) \geq X/t \geq C_L(\lambda_3)$;

$$u = u_2 = -\int_{\lambda_1}^{\lambda} C_L(\eta) d\eta \cos\theta_1,$$

$$v = v_2 = -\int_{\lambda_1}^{\lambda} C_L(\eta)\, d\eta \sin\theta_1, \tag{46}$$

$$\frac{X}{t} = C_L(\lambda),\ \theta = \theta_1. \tag{47}$$

Region 3: $C_L(\lambda_3) \geq X/t > V_T(\lambda_3)$;

$$u = u_3 = -\int_{\lambda_1}^{\lambda_3} C_L(\lambda)\, d\lambda \cos\theta_1,$$

$$v = v_3 = -\int_{\lambda_1}^{\lambda_3} C_L(\lambda) d\lambda \sin\theta_1, \tag{48}$$

$$\lambda = \lambda_3,\ \theta = \theta_1.$$

Region 4: $V_T(\lambda_3) > X/t$;

$$u = 0,\ v = v_4,\ \lambda = \lambda_4 = \lambda_3,\ \theta = 0,$$

where

$$v_4 = v_3 + V_T \lambda_4 \sin\theta_1, \tag{49}$$

is obtained from (16). If λ_o and θ_1 are given, the unknowns can be obtained from (46)-(49) and (2). As λ_4 approaches λ_{c2} Region 3 shrinks, and for $\lambda_4 = \lambda_{c2}$ the characteristics bounding Region 3 coincide. A small modification to the above solution is required. When $\lambda_1 > \lambda_{c2} > \lambda_4 > \lambda_i$ the solution consists of constant state Regions 1 and 4 and centered, simple wave Regions 2 and 3, as shown in Fig. 9, and is as follows:

Region 1: $X/t \geq C_L(\lambda_1)$;

$$u = v = 0,\ \lambda = \lambda_1,\ \theta = \theta_1.$$

Region 2: $C_L(\lambda_1) \geq X/t > V_T(\lambda_{c2})$;

$$u = u_2 = -\int_{\lambda_1}^{\lambda} C_L(\eta) d\eta \cos\theta_1,$$

$$v = v_2 = -\int_{\lambda_1}^{\lambda} C_L(\eta) d\eta \sin\theta_1, \tag{50}$$

$$\frac{X}{t} = C_L(\lambda),\ \theta = \theta_1$$

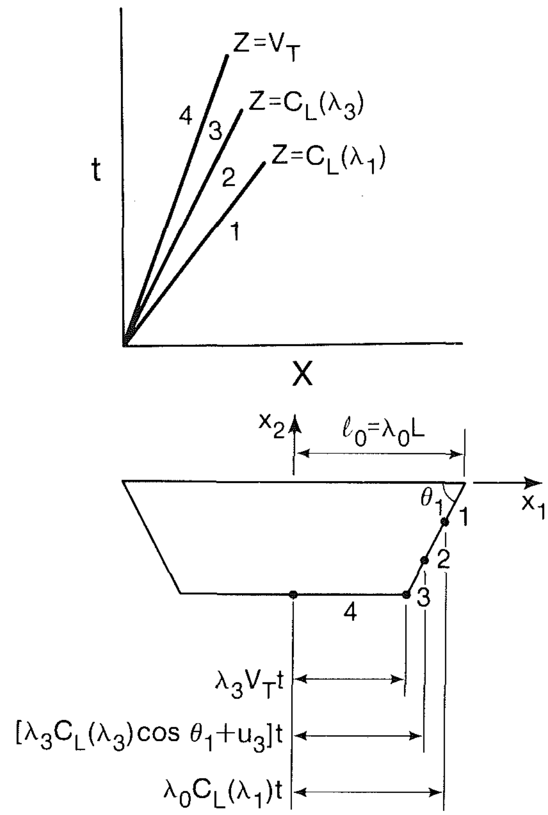

Fig. 8 Form of solution for material with three-term strain energy function $\lambda_4 > \lambda_{c2}$

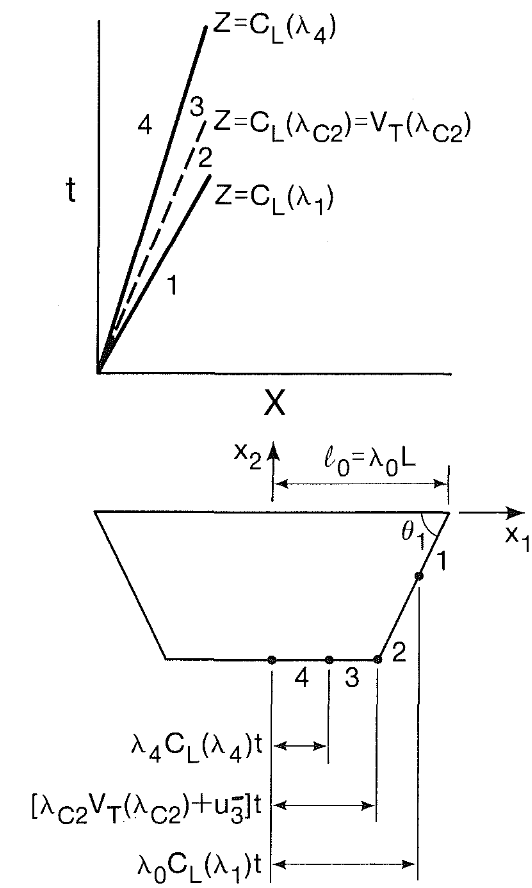

Fig. 9 Form of solution for material with three-term strain energy function $\lambda_1 > \lambda_{c2}$, $\lambda_i < \lambda_4 < \lambda_{c2}$

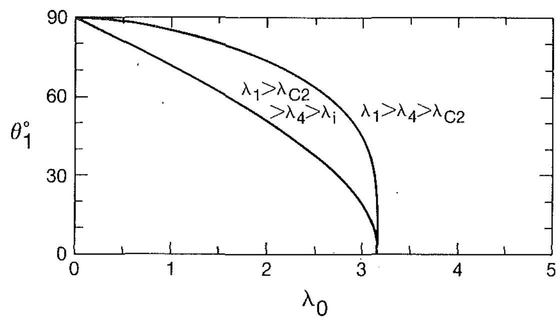

Fig. 10 Regions of validity of solutions for the three-term strain energy function.

Region 3: $V_T(\lambda_{c2}) > X/t \geq C_L(\lambda_4)$;

$$u = u_3 = u_3^- - \int_{\lambda_2}^{\lambda} C_L(\eta) d_\eta, \quad v = v_3^- \tag{51}$$

$$\frac{X}{t} = C_L(\lambda), \quad \theta = 0$$

where

$$u_3^- = -\int_{\lambda_1}^{\lambda_{c2}} C_L(\eta) d\eta \cos\theta_1 - V_T(\lambda_{c2})\lambda_{c2}(1 - \cos\theta_1), \tag{52}$$

$$v_3^- = -\int_{\lambda_1} C_L(\eta) d\eta \sin\theta_1 + V_T(\lambda_{c2})\lambda_{c2} \sin\theta_1, \tag{53}$$

are obtained from the jump relations (16).

Region 4: $C_L(\lambda_4) \geq X/t \geq 0$;

$$u = 0, \quad v = v_3 = v_4, \quad \theta = 0,$$

$$u_3^- = \int_{\lambda_{c2}}^{\lambda_4} C_L(\lambda) d\lambda. \tag{54}$$

If λ_0 and θ_1 are given, the unknowns can be obtained from (50)–(54) and (2). The region of validity in the (λ_0, θ_1) plane is shown in Fig. 10.

Solutions can be obtained in a similar manner when λ_1 and λ_4 are in other regions of the nominal stress-stretch curve shown in Fig. 7. The determination of these solutions is simplified if it is noted that the solution for λ, for the plucked string problem, is the same as that for the sudden unloading of a string in unaxial simple tension from stretch λ_1 to the final unloaded stretch.

A simple way to obtain solutions is to specify λ_1 and λ_3 for the Mooney-Rivlin string or λ_1 and λ_4 for the three-term strain energy function, then θ_1 is easily obtained along with the other unknowns.

8 Analogy With Propagation of Waves in Incompressible Elastic Half Space

Collins (1966) has considered the problem of propagation of waves in an incompressible elastic half space, when the surface is given a uniform motion by the sudden application of shearing stress, and has shown that, if the material is isotropic, a pair of transverse simple waves or shocks and a pair of circular waves can propagate. The transverse simple waves and circular waves are analogous to the longitudinal and transverse waves, respectively, of the string problem. The quantities, λ, P, θ, u, v, in the string problem are analogous to the resultant simple shear, shearing stress, polarization angle, and components of particle velocity, respectively, in the shear problem. Governing equations (6) are of the same form as those given by Collins for the shear problem, however, the analogy is not complete, since the relationship between the resultant simple shear and the shearing stress is an odd function unlike the relationship between P and λ. Furthermore, Collins considered a strain energy function, which resulted in a strictly hyperbolic system with distinct eigenvalues for the whole range of simple shear, except for propagation into an undeformed region.

9 Concluding Remarks

The validity of the deformed configuration shown in Fig. 2 has been verified experimentally. Experiments were conducted on rubber cords with a simple tension relation accurately modeled by that for the three-term strain energy function with parameters given by (28). Good agreement with the solutions given by (38)–(41) was obtained.

In order to continue the solutions, after the first reflection occurs at a fixed end, the Godunov finite difference method (Sod, 1985) was used by the authors. This method is based on the solution of a sequence of Riemann problem and requires a system of governing equations in conservation form.

References

Beatty, M. F., and Haddow, J. B., 1985, "Transverse Impact of a Stretched String," ASME Journal of Applied Mechanics, Vol. 52, pp. 137–143.

Chadwick, P., and Creasy, C. F. M., 1984, "Modified Entropic Elasticity of Rubberlike Materials," *Journal of Mechanics and Physics of Solids*, Vol. 32, pp. 337–357.

Collins, W. D., 1966, "One-Dimensional Non-Linear Wave Propagation in Incompressible Elastic Materials," *Quarterly Journal of Applied Mathematics and Mechanics*, Vol. 14, pp. 259–328.

Ogden, R. W., 1972, "Large Deformation Isotropic Elasticity: On the Correlation of Theory and Experiment for Incompressible Rubberlike Solids," *Proceedings of the Royal Society of London*, Series A, Vol. 326, pp. 565–584.

Sod, G., 1985, *Numerical Methods in Fluid Dynamics*, Cambridge Univ. Press.

Pseudodissipative Systems II: Stability of Reduced Equilibria

J. A. Walker
Department of Mechanical Engineering,
Northwestern University,
Evanston, Ill. 60208

In terms of the Lagrange formulation of dynamics, ignorable coordinates are defined for the class of "pseudodissipative" mechanical systems. Reduced equilibria (steady motions) of such systems are defined and studied with regard to their stability properties. We obtain broad results and results readily applicable to specific technical problems.

1 Introduction

The study of stability of steady motions of mechanical systems seems to have begun with (Routh, 1860). Utilizing Lagrange's formulation, E. J. Routh noticed that certain generalized coordinates may be "ignorable" and steady motions often correspond to equilibrium values of a "reduced state." This work has been continued by many others, and considerable recent interest has centered on the difference between the stability properties of "free systems" and those of related "restrained systems" driven by constant-speed motors (Hagedorn, 1979; Pascal, 1975; Rumiantsev, 1975). In most of this work, friction has been either ignored or treated as an afterthought; the general effects of friction and the properties of real motors have been given little consideration.

Our objective is to improve on this situation and provide more general stability results. By considering systems which are "pseudodissipative" (Walker, 1988), we find that frictional effects influence not only the stability properties of "reduced equilibria" but even their number and identities (compare examples 4.1–4.2).

Employing the concepts and definitions of Section 2, we obtain in Section 3 both broad results (Theorems 3.1–3.3) and simple results (Corollaries 3.1–3.3) regarding the stability properties of reduced equilibria. The theory developed in Sections 2–3 enables us to study not only the free system of example 4.2, but also the related "real system" of example 4.1, which is of much greater significance. In Section 5 we compare our stability conclusions for these systems to stability conclusions obtained earlier for the related restrained system (Walker, 1988).

2 Notation and Terminology

Consider a collection of particles observed by some inertial observer, and choose n "generalized coordinates" $(q_1,q_2,\ldots,q_n)\equiv q\in\mathcal{O}\subset\mathcal{R}^n$, where $\mathcal{O}$ is some open subset of $\mathcal{R}^n$; the dimension n of the *generalized position* $q\in\mathcal{R}^n$ need not be minimal. We denote by $u\in\mathcal{R}^n$ the corresponding *generalized speed*; i.e., $u(t)=\dot q(t)$ along motions $q(\cdot):\mathcal{R}\to\mathcal{R}^n$. The resulting *generalized kinetic energy* T: $\mathcal{R}\times\mathcal{O}\times\mathcal{R}^n\to\mathcal{R}$ and *generalized force* Q: $\mathcal{R}\times\mathcal{O}\times\mathcal{R}^n\to\mathcal{R}^n$ depend upon the *generalized state* $(q,u)\in\mathcal{O}\times\mathcal{R}^n$ and possibly the current time $t\in\mathcal{R}$. Any and all kinematic constraints on (q,u) may be accounted for by defining a *kinematically possible set* $\mathcal{C}(t)\subset\mathcal{O}\times\mathcal{R}^n$, consisting of all generalized states (q,u) kinematically possible at time $t\in\mathcal{R}$. A C^1-smooth function $q(\cdot):\mathcal{R}\to\mathcal{R}^n$ is kinematically possible on $[t_1,t_2)$ if $(q(t),\dot q(t))\in\mathcal{C}(t)$ for all $t\in[t_1,t_2)$.

Apart from some of the foregoing notation, we depart from the classical Lagrange formulation only by assuming that Q is explicitly known, continuous, and "pseudodissipative" in the following sense:

Definition 2.1. The generalized force Q will be called *pseudodissipative* if there exists a C^1-smooth function U:$\mathcal{R}\times\mathcal{O}\times\mathcal{R}^n\to\mathcal{R}$, affine with respect to its third argument $u\in\mathcal{R}^n$, and another function D:$\mathcal{R}\times\mathcal{O}\times\mathcal{R}^n\to\mathcal{R}^n$ such that

$$\sum_{l=1}^{n}(u_l-v_l)[D_l(t,q,u)-D_l(t,q,v)]\le 0 \tag{1}$$

for all $(t,q,u,v)\in\mathcal{R}\times\mathcal{O}\times\mathcal{R}^n\times\mathcal{R}^n$, and along every kinematically possible $q(\cdot)$,

$$\sum_{l=1}^{n}\delta_l(t)Q_l(t,q(t),\dot q(t))=\sum_{l=1}^{n}\delta_l(t)D_l(t,q,(t),\dot q(t))$$

$$+\sum_{l=1}^{n}\delta_l(t)\left[\frac{d}{dt}\frac{\partial}{\partial u_l}U(t,q(t),\dot q(t))-\frac{\partial}{\partial q_l}U(t,q(t),\dot q(t))\right] \tag{2}$$

for all C^1-smooth $\delta(\cdot)$: $\mathcal{R}\to\mathcal{R}^n$ such that $(q(t),\dot q(t)+\delta(t))\in\mathcal{C}(t)$ for all $t\in\mathcal{R}$.

U will be called a *pseudopotential* and the function $L\equiv T-U$ will be called the *Lagrangian*. Due to property (1), D will be called the *dissipative part* of Q.

The generalized force Q will be called *strongly* pseudodissipative if equality occurs in condition (1) *only* when $u=v$. Q will be called *pseudoconservative* if $D\equiv 0$.

Contributed by the Applied Mechanics Division of THE AMERICAN SOCIETY OF MECHANICAL ENGINEERS for publication in the JOURNAL OF APPLIED MECHANICS.

Discussion on this paper should be addressed to the Editorial Department, ASME, United Engineering Center, 345 47th Street, New York, N.Y. 100017, and will be accepted until two months after final publication of the paper itself in the JOURNAL OF APPLIED MECHANICS. Manuscript received by ASME Applied Mechanics Division, March 1988; final revision, July 27, 1988.

Definition 2.1 was made and discussed earlier (Walker, 1988). Our presentation here is based on four assumptions, of which the first three are as follows:

(i) A particular initial instant t_o has been chosen, and the time interval of interest is $[t_o,\infty)$.

(ii) Q is known, continuous, and pseudodissipative on $[t_o,\infty)$.

(iii) For some $r<n$, the last $n-r$ generalized coordinates $q_{r+1}, q_{r+2}, \ldots, q_n$ are "ignorable" in the sense of the following definition.

Definition 2.2. If Q is pseudodissipative, then the last $n-r$ generalized coordinates $(q_{r+1},q_{r+2},\ldots,q_n)\equiv w\in\mathbb{R}^{n-r}$ are said to be *ignorable* if the following conditions are met with $q\equiv(\tilde{q},w)\in\mathbb{R}^r\times\mathbb{R}^{n-r}$, $\tilde{q}\equiv(q_1,q_2,\ldots,q_r)$:

(a) There exist selections for U and D such that D and $L\equiv T-U$ are independent of $w\in\mathbb{R}^{n-r}$; in particular, there exist an open set $\tilde{\mathcal{O}}\subset\mathbb{R}^r$ and functions $\tilde{L}$: $\mathbb{R}\times\tilde{\mathcal{O}}\times\mathbb{R}^n\to\mathbb{R}$, $\tilde{D}$: $\mathbb{R}\times\tilde{\mathcal{O}}\times\mathbb{R}^n\to\mathbb{R}^n$, such that $\mathcal{O}\subset\tilde{\mathcal{O}}\times\mathbb{R}^{n-r}$ and

$$L(t,q,u)=\tilde{L}(t,\tilde{q},u),\ D(t,q,u)=\tilde{D}(t,\tilde{q},u),$$

for all $(t,q,u)\in\mathbb{R}\times\mathcal{O}\times\mathbb{R}^n$.

(b) There exist sets $\tilde{\mathcal{C}}(t)\subset\tilde{\mathcal{O}}\times\mathbb{R}^n$ and $\mathcal{S}(t,\tilde{q})\subset\mathbb{R}^{n-r}$ such that $\mathcal{C}(t)=\{(q,u)\subset\mathcal{O}\times\mathbb{R}^n\ |(\tilde{q},u)\in\tilde{\mathcal{C}}(t),\ w\in\mathcal{S}(t,\tilde{q})\}$, $t\in\mathbb{R}$.

We say $w\in\mathbb{R}^{n-r}$ is an *ignorable part* of $q\in\mathbb{R}^n$, $\tilde{q}\in\mathbb{R}^r$ is the corresponding *reduced position*, $(\tilde{q},u)\in\mathbb{R}^r\times\mathbb{R}^n$ is the corresponding *reduced state*, and $\tilde{\mathcal{C}}(t)\subset\mathbb{R}^r\times\mathbb{R}_n$ is the corresponding *reduced kinematically possible set*.

Since our ordering of the generalized coordinates is of no physical significance, Definition 2.2 serves to determine whether or not any particular generalized coordinate q_l is ignorable. It is possible that $r=0$, since the entire generalized position q may happen to be ignorable: $w\equiv q$. In this case, there is no reduced position $\tilde{q}$ and the reduced state is merely the generalized speed $u\in\mathbb{R}^n$.

Definition 2.2 is more general than others stated elsewhere in the literature (Routh, 1860), which seem to assume that $\mathcal{C}(t)\equiv\mathcal{O}\times\mathbb{R}^n$ and $D\equiv 0$. Definition 2.2 makes the following theory applicable to a larger class of problems. Under assumptions (ii)-(iii), Lagrange's formulation produces the following consequence of Newton's second law, which defines the dynamically possible motions of our collection of particles.

Theorem 2.1. If a continuous function $(\tilde{q}(\cdot),u(\cdot))$: $\mathbb{R}\to\mathbb{R}^r\times\mathbb{R}^n$ is dynamically possible on $[t_o,t_f)$, then for all $t\in[t_o,t_f)$,

$$(\tilde{q}(t),u(t))\in\tilde{\mathcal{C}}(t),\ u_l(t)=\dot{q}_l(t)\ \text{ for } l\le r, \tag{3}$$

and

$$0=\sum_{l=1}^{n}\delta_l(t)\left[\frac{d^+}{dt}\frac{\partial}{\partial u_l}\tilde{L}(t,\tilde{q}(t),u(t))\right.$$
$$\left.-\frac{\partial}{\partial q_l}\tilde{L}(t,\tilde{q}(t),u(t))-\tilde{D}_l(t,\tilde{q}(t),u(t))\right] \tag{4}$$

for all C^1-smooth $\delta(\cdot)$: $\mathbb{R}\to\mathbb{R}^n$ such that $(\tilde{q}(t), u(t)+\delta(t))\in\tilde{\mathcal{C}}(t)$, $t_o\le t<t_f$.

Our fourth and last general assumption is as follows:

(iv) For each $(\tilde{q}^o,u^o)\in\tilde{\mathcal{C}}(t_o)$, there exists a continuous solution $(\tilde{q}(\cdot),u(\cdot))$:$[t_o,\infty)\to\mathbb{R}^r\times\mathbb{R}^n$ of (3)-(4) such that $\tilde{q}(t_o)=\tilde{q}^o$, $u(t_o)=u^o$. Moreover, at each $t>t_o$, $(\tilde{q}(t),u(t))$ depends continuously on $(\tilde{q}^o,u^o)$.

Assumptions (i)-(iv) are very mild and will be maintained henceforth without further comment.

Obviously, the simplest type of solution of the reduced motion equations (3)-(4) would be a constant solution, $(\tilde{q}(t),u(t))\equiv(\tilde{q}^e,u^e)$ for some fixed $(\tilde{q}^e,u^e)\in\mathbb{R}^r\times\mathbb{R}^n$; the corresponding initial reduced state $(\tilde{q}^e,u^e)\in\tilde{\mathcal{C}}(t_o)$ is called a *reduced equilibrium*. Since $r<n$ by assumption (iii), each reduced equilibrium corresponds to a family of steady motions $q(\cdot)$:$[t_o,\infty)\to\mathbb{R}^n$ parameterized by the initial values of the $n-r$ ignorable coordinates.

Corollary 2.1. If $\tilde{L}$ is time-invariant, then $(\tilde{q}^e,u^e)\in\mathbb{R}^r\times\mathbb{R}^n$ is a reduced equilibrium if and only if $u^e_l=0$ for each $l\le r$ and, for all $t\ge t_o$, $(\tilde{q}^e,u^e)\in\tilde{\mathcal{C}}(t)$ and

$$0=\sum_{l=1}^{n}\delta_l(t)\left[\frac{\partial}{\partial q_l}\tilde{L}(t_o,\tilde{q}^e,u^e)+\tilde{D}_l(t,\tilde{q}^e,u^e)\right] \tag{5}$$

for all C^1-smooth $\delta_l(\cdot)$: $\mathbb{R}\to\mathbb{R}^n$ such that $(\tilde{q}^e,u^e+\delta(t))\in\tilde{\mathcal{C}}(t)$, $t\ge t_o$.

If a reduced equilibrium $(\tilde{q}^e,u^e)$ does exist, we may be interested in its "stability properties." In terms of some norm $|\cdot|_m$: $\mathbb{R}^m\to\mathbb{R}$ for $\mathbb{R}^m$, we define the open set

$$\eta_h\equiv\{(\tilde{q},u)\in\mathbb{R}^r\times\mathbb{R}^n\ |0<|\tilde{q}-\tilde{q}^e|_r+|u-u^e|_n<h\}, \tag{6}$$

and its closure

$$\bar{\eta}_h\equiv\{(\tilde{q},u)\in\mathbb{R}^r\times\mathbb{R}^n\ ||\tilde{q}-\tilde{q}^e|_r+|u-u^e|_n\le h\}, \tag{7}$$

both of which are related to $(\tilde{q}^e,u^e)$ and parameterized by $h>0$.

Definition 2.3. Let $(\tilde{q}(\cdot),u(\cdot))$: $[t_o,\infty)\to\mathbb{R}^r\times\mathbb{R}^n$ denote the unique solution of the reduced equations (3)-(4) that corresponds to a given but arbitrary initial reduced state $(\tilde{q}^o,u^o)\in\tilde{\mathcal{C}}(t_o)$, and let a particular reduced equilibrium $(\tilde{q}^e,u^e)$ be considered. The reduced equilibrium $(\tilde{q}^e,u^e)$ is said to be *stable* if to each $\epsilon>0$ there corresponds some $h>0$ such that the statement $(\tilde{q}^o,u^o)\in\tilde{\mathcal{C}}(t_o)\cap\eta_h$ implies that $(\tilde{q}(t),u(t))\in\bar{\eta}_\epsilon$ for all $t\ge t_o$. The reduced equilibrium $(\tilde{q}^e,u^e)$ is *unstable* if it is not stable.

If $(\tilde{q}^e,u^e)$ *is* stable and there exists some $h>0$ such that the statement $(\tilde{q}^o,u^o)\in\tilde{\mathcal{C}}(t_o)\cap\eta_h$ implies that

$$|\tilde{q}(t)-\tilde{q}^e|_r+|u(t)-u^e|_n\to 0\text{ as }t\to\infty,$$

then $(\tilde{q}^e,u^e)$ is said to be *asymptotically stable*.

In all of the stability results of Section 3, we shall assume that $\tilde{L}$ is time-invariant. At each reduced equilibrium $(\tilde{q}^e,u^e)$ we shall employ four $(\tilde{q}^e,u^e)$-related functions defined on $\tilde{\mathcal{O}}\times\mathbb{R}^n$:

$$G(\tilde{q},u)\equiv-\tilde{L}(t_o,\tilde{q},u)+\sum_{l=1}^{n}(u_l-u^e_l)\frac{\partial}{\partial u_l}\tilde{L}(t_o,\tilde{q},u)$$
$$+\sum_{l=1}^{n}(q_l-q^e_l)\frac{\partial}{\partial q_l}\tilde{L}(t_o,\tilde{q}^e,u^e), \tag{8}$$

$$J(\tilde{q},u;\tilde{\Gamma})\equiv\sum_{i=1}^{r}\sum_{j=1}^{r}\gamma_{ij}(q^e_i-q_i)\left[\frac{\partial}{\partial u_j}\tilde{L}(t_o,\tilde{q},u)\right.$$
$$\left.-\frac{\partial}{\partial u_j}\tilde{L}(t_o,\tilde{q}^e,u^e)\right], \tag{9}$$

$$R(\tilde{q},u;\tilde{\Gamma})\equiv\sum_{i=1}^{r}\sum_{j=1}^{r}\gamma_{ij}(u_i-u^e_i)\left[\frac{\partial}{\partial u_j}\tilde{L}(t_o,\tilde{q},u)\right.$$
$$\left.-\frac{\partial}{\partial u_j}\tilde{L}(t_o,\tilde{q}^e,u^e)\right]$$
$$+\sum_{i=1}^{r}\sum_{j=1}^{n}\gamma_{ij}(q_i-q^e_i)\left[\frac{\partial}{\partial q_j}\tilde{L}(t_o,\tilde{q},u)+\tilde{D}_j(t_o,\tilde{q},u)\right], \tag{10}$$

$$H(\tilde{q},u;A) \equiv \sum_{i=1}^{n-r} \left| \sum_{j=1}^{n-r} a_{ij} \left[\frac{\partial}{\partial u_{r+j}} \tilde{L}(t_o,\tilde{q},u) - \frac{\partial}{\partial u_{r+j}} \tilde{L}(t_o,\tilde{q}^e,u^e) \right] \right|, \tag{11}$$

where $\tilde{\Gamma} \equiv [\tilde{\gamma}_{ij}]$ is an arbitrary real $r \times r$ matrix and $A = [a_{ij}]$ is some real $(n-r) \times (n-r)$ matrix such that

$$\sum_{j=1}^{n-r} a_{ij} \tilde{D}_{r+j}(t,\tilde{q},u) = 0, \quad \text{each } i > 0, \tag{12}$$

for all $(\tilde{q},u) \in \tilde{\mathcal{O}} \times \mathbb{R}^n$, $t \geq t_o$. We define $n \times n$ matrices

$$\Gamma \equiv \left[\begin{array}{c|c} \tilde{\Gamma} & 0 \\ \hline 0 & A \end{array} \right], \quad \Lambda \equiv \left[\begin{array}{c|c} 0 & 0 \\ \hline 0 & A \end{array} \right]. \tag{13}$$

We shall also employ the $(\tilde{q}^e,u^e)$-related set η_h of (6), the subset

$$\Omega_h \equiv \{ (\tilde{q},u) \in \eta_h \mid G(\tilde{q},u) < G(\tilde{q}^e,u^e) \}, \tag{14}$$

and another $(\tilde{q}^e,u^e)$-related set

$$\mathcal{H}(A) \equiv \{ (\tilde{q},u) \in \tilde{\mathcal{O}} \times \mathbb{R}^n \mid H(\tilde{q},u;A) = 0 \} \tag{15}$$

parameterized by the $(n-r) \times (n-r)$ matrix A.

3 Stability Results for Reduced Equilibria

The following Theorems 3.1–3.3 are based upon Definitions 2.1–2.2 and assumptions (i)–(iv) of the foregoing Section 2. Although quite complicated, Theorems 3.1–3.3 lead to the much simpler (and more restricted) Corollaries 3.1–3.3.

Theorem 3.1. Suppose that $(\tilde{q}^e,u^e)$ is a reduced equilibrium and the following conditions hold for some $h > 0$:

(a) $\eta_h \cap \tilde{\mathcal{C}}(t)$ is time-invariant and the statement $(\tilde{q},u) \in \eta_h \cap \tilde{\mathcal{C}}(t_o)$ implies that both $(\tilde{q},u^e) \in \tilde{\mathcal{C}}\{t_o\}$ and (5) holds with $\delta(t) \equiv u - u^e$.

(b) $\tilde{L}$ is time-invariant and $\tilde{D}(t,\tilde{q},u^e) = \tilde{D}(t,\tilde{q}^e,u^e)$ for all $(t,\tilde{q})$ with $\|\tilde{q}-\tilde{q}^e\|_r < h$, $t \geq t_o$.

(c) $G(\tilde{q},u) > G(\tilde{q}^e,u^e)$ for all $(\tilde{q},u) \in \eta_h \cap \bar{\tilde{\mathcal{C}}}(t_o)$, where $\bar{\tilde{\mathcal{C}}}(t_o)$ denotes the closure of $\tilde{\mathcal{C}}(t_o)$.

Then $(\tilde{q}^e,u^e)$ is *stable*. If Q is pseudoconservative ($\tilde{D} \equiv 0$), then $(\tilde{q}^e,u^e)$ is *not* asymptotically stable.

Suppose that the following condition also holds:

(d) $\tilde{D}$ is time-invariant and there does *not* exist a solution $(\tilde{q}(\cdot),u(\cdot)):[t_o,\infty) \to \mathbb{R}^r \times \mathbb{R}^n$ of (3)–(4) along which $(\tilde{q}(t),u(t)) \in \eta_h$, $G(\tilde{q}(t),u(t))$ is constant, and

$$\sum_{l=1}^{n} [u_l(t) - u^e][\tilde{D}_l(t_o,\tilde{q}(t),u(t)) - \tilde{D}_l(t_o,\tilde{q}^e,u^e)] = 0.$$

Then $(\tilde{q}^e,u^e)$ is *asymptotically* stable.

If the foregoing conditions (a) and (b) hold, (d) holds with η_h replaced by Ω_h, but in place of (c), we have its strong contradiction (e).

The set $\Omega_\epsilon \cap \tilde{\mathcal{C}}(t_o)$ is nonempty for every $\epsilon > 0$, then $(\tilde{q}^e,u^e)$ is *unstable*.

Sketch of proof. Under assumptions (a)–(b), we consider some solution $(\tilde{q}(\cdot), u(\cdot)):[t_o,\infty) \to \mathbb{R}^r \times \mathbb{R}^n$ of (3)–(4) such that $(\tilde{q}(t),u(t)) \in \eta_h$ on some interval $[t_o,t_1)$. Supposing for simplicity that $u(\cdot)$ is C^1-smooth, and choosing $\delta(t) = u^e - u(t)$ in (4)–(5) for $t \in [t_o,t_1)$, we compute that $(d^+/dt)G(\tilde{q}(t),u(t)) =$

$$\sum_{l=1}^{n} [u_l(t) - u_l^e][\tilde{D}(t,\tilde{q}(t),u(t)) - \tilde{D}_l(t,\tilde{q}(t),u^e)] \leq 0$$

for all $t \in [t_o,t_1)$. Hence, G is a Liapunov function (Walker, 1980) on $\eta_h \cap \tilde{\mathcal{C}}(t_o)$.

Condition (c) and a basic Liaponov stability argument now imply that $(\tilde{q}^e,u^e)$ is stable but, if Q is pseudoconservative, $(\tilde{q}^e,u^e)$ is not asymptotically stable. If Q is not pseudoconservative, then LaSalle's invariance principle (Walker, 1980) leads to the remaining asymptotic stability and instability conclusions.

We note that condition (c) of Theorem 3.1 requires that $(\tilde{q}^e,u^e)$ provide a strict local minimum of G over $\bar{\tilde{\mathcal{C}}}(t_o)$, while condition (e) requires that $(\tilde{q}^e,u^e)$ *not* provide a weak local minimum of G over $\tilde{\mathcal{C}}(t_o)$.

Often condition (d) is not difficult to check. For instance, if Q is strongly pseudodissipative and $\tilde{D}$ is time-invariant, then condition (d) is satisfied provided that some η_h contains no other reduced equilibrium $(\tilde{q}^o,u^o)$ with $u^o = u^e$.

A phenomenon called "gyroscopic stabilization," where $\tilde{\Omega}_\epsilon \cap \tilde{\mathcal{C}}(t_o)$ is nonempty for every $\epsilon > 0$ and yet $(\tilde{q}^e,u^e)$ is stable, is *not* predicted by Theorem 3.1. The following Theorem 3.2 addresses the possibility of gyroscopic stabilization of $(\tilde{q}^e,u^e)$ by further restricting $\tilde{\mathcal{C}}(t)$ and $\tilde{D}$. In Theorems 3.2–3.3, $\tilde{q}$ and u are identified with column matrices when this is appropriate.

Theorem 3.2. Suppose that $(\tilde{q}^e,u^e)$ is a reduced equilibrium and the following conditions hold for some $h > 0$ and some real $(n-r) \times (n-r)$ matrix A which meets condition (12):

(a) $\eta_h \cap \tilde{\mathcal{C}}(t)$ is time-invariant and the statement $(\tilde{q},u) \in \eta_h \cap \tilde{\mathcal{C}}(t_o)$ implies that $(\tilde{q},u^e) \in \tilde{\mathcal{C}}(t_o)$, $(\tilde{q},u + \Lambda^T v) \in \tilde{\mathcal{C}}(t_o)$ for all $v \in \mathbb{R}^n$, and (5) holds with $\delta(t) \equiv u - u^e$.

(b) $\tilde{L}$: is time-invariant and $\tilde{D}(t,\tilde{q},u^e) = \tilde{D}(t,\tilde{q}^e,u^e)$ for all $\tilde{q}$ with $\|\tilde{q}-\tilde{q}^e\|_r < h$, $t \geq t_o$.

(c) $G(\tilde{q},u) > G(\tilde{q}^e,u^e)$ for all $(\tilde{q},u) \in \eta_h \cap \mathcal{H}(A) \cap \tilde{\mathcal{C}}(t_o)$.

Then $(\tilde{q}^e,u^e)$ is *stable* but, if $A \neq 0$, it is *not* asymptotically stable.

If the foregoing conditions (a)–(b) hold, but instead of (c), we have both its strong contradiction

(d) The set $\Omega_\epsilon \cap \mathcal{H}(A) \cap \tilde{\mathcal{C}}(t_o)$ is nonempty for every $\epsilon > 0$, and

(e) $\tilde{D}$ is time-invariant and there does *not* exist a solution $(\tilde{q}(\cdot),u(\cdot)):[t_o,\infty) \to \mathbb{R}^r \times \mathbb{R}^n$ of (3)–(4) along which $(\tilde{q}(t),u(t)) \in \Omega_h \cap \mathcal{H}(A)$, $G(\tilde{q}(t),u(t))$ is constant, and

$$\sum_{l=1}^{n} [u_l(t) - u^e][\tilde{D}_l(t_o,\tilde{q}(t),u(t)) - \tilde{D}_l(t_o,\tilde{q}^e,u^e)] = 0,$$

then $(\tilde{q}^e,u^e)$ is *instable.*

Sketch of Proof. Consider some solution of (3)–(4) such that $(\tilde{q}(t),u(t)) \in \eta_h$ on some interval $[t_o,t_1)$. Due to conditions (a)–(b) we find that $H(\tilde{q}(t),u(t);A) = H(\tilde{q}^o,u^o;A)$ for all $t \in [t_o,t_1)$. If $A \neq 0$, $H(\tilde{q}^o,u^o;A) \neq H(\tilde{q}^e,u^e;A)$ for some $(\tilde{q}^o,u^o) \in \eta_\epsilon$, every $\epsilon > 0$, and it follows from continuity of H that $(\tilde{q}^e,u^e)$ cannot be asymptotically stable.

The computation made for $(d^+/dt)G(\tilde{q}(t),u(t))$ in the proof of Theorem 3.1 remains valid on $[t_o,t_1)$, so G, H, and $F_\lambda \equiv G + \lambda H$ are Liapunov functions (Walker, 1980) on $\eta_h \cap \tilde{\mathcal{C}}(t_o)$, for every $\lambda \in \mathbb{R}$. Due to the structures of G and H, condition (c) implies that we may choose $\lambda > 0$ so that $F_\lambda(\tilde{q},u) > F_\lambda(\tilde{q}^e,u^e)$ for all $(\tilde{q},u) \in \eta_h \cap \tilde{\mathcal{C}}(t_o)$. Hence, F_λ and a basic Liapunov stability argument imply that $(\tilde{q}^e,u^e)$ is stable under conditions (a)–(c).

If condition (c) is violated but conditions (a)–(b) and (d)–(e) are met, then G, H, and LaSalle's invariance principle (Walker, 1980) imply instability of $(\tilde{q}^e,u^e)$.

There is no reason to apply Theorem 3.2 with $A = 0$. Although the choice $A \equiv 0$ is always possible in (12), Theorem 3.2 becomes a special case of Theorem 3.1. If $A \neq 0$, Theorem

3.2 may serve to demonstrate that gyroscopic stabilization occurs. Condition (c) of Theorem 3.2 requires only that $(\tilde{q}^e,u^e)$ provide a strict local minimum of G over $\tilde{\mathcal{C}}(t_o)\cap\mathcal{K}(A)$ rather than the larger set $\tilde{\mathcal{C}}(t_o)$; hence, $\tilde{\Omega}_\epsilon\cap\tilde{\mathcal{C}}(t_o)$ might be nonempty for every $\epsilon>0$ and yet $(\tilde{q}^e,u^e)$ might be gyroscopically stabilized.

Theorems 3.1–3.2 provide conditions sufficient to ensure that $(\tilde{q}^e,u^e)$ is stable, asymptotically stable, or unstable. If the dissipative part $\tilde{D}$ is too weak for us to easily check condition (d) of Theorem 3.1 or condition (e) of Theorem 3.2, then the following instability result may be useful.

Theorem 3.3 Suppose that $(\tilde{q}^e,u^e)$ is a reduced equilibrium and the following conditions hold for some $h>0$, some real $r\times r$ matrix $\tilde{\Gamma}$, and some real $(n-r)\times(n-r)$ matrix A which meets condition (12):

(a) $\Omega_h\cap\tilde{\mathcal{C}}(t)$ is time-invariant and the statement $(\tilde{q},u)\in\Omega_h\cap\tilde{\mathcal{C}}(t_o)$ implies that $(\tilde{q},u^e)\in\tilde{\mathcal{C}}(t_o)$, $(\tilde{q},u+[\tilde{\Gamma}\,|0]^T(\tilde{q}-\tilde{q}^e))\in\tilde{\mathcal{C}}(t_o)$, $(\tilde{q},u+\Lambda^T v)\in\tilde{\mathcal{C}}(t_o)$ for all $v\in\mathbb{R}^n$, and (5) holds with $\delta(t)\equiv u-u^e$.

(b) $\tilde{D}$ and $\tilde{L}$ are time-invariant, and $\tilde{D}(t_o,\tilde{q},u^e)=\tilde{D}(t_o,\tilde{q}^e,u^e)$ for all $\tilde{q}$ with $\|\tilde{q}-\tilde{q}^e\|_r<h$,

(c) The set $\Omega_\epsilon\cap\mathcal{K}(A)\cap\tilde{\mathcal{C}}(t_o)$ is nonempty for every $\epsilon>0$.

(d) There exists a real number $\mu\geq 0$ such that

$$R(\tilde{q},u;\tilde{\Gamma})-\mu\sum_{l=1}^{n}(u_l-u_l^e)[\tilde{D}_l(t_o,\tilde{q},u)-\tilde{D}_l(t_o,\tilde{q}^e,u^e)]\geq 0$$

for all $(\tilde{q},u)\in\Omega_h\cap\mathcal{K}(A)\cap\tilde{\mathcal{C}}(t_o)$.

(e) There does *not* exist a solution $(\tilde{q}(\cdot),u(\cdot)):[t_o,\infty)\to\mathbb{R}^r\times\mathbb{R}^n$ of (3)–(4) along which $(\tilde{q}(t),u(t))\in\Omega_h\cap\mathcal{K}(A)$, $G(\tilde{q}(t),u(t))$ and $J(\tilde{q}(t),u(t);\tilde{\Gamma})$ are constant, and

$$R(\tilde{q}(t),u(t);\tilde{\Gamma})=0$$
$$=\sum_{l=1}^{r}[u_l(t)-u_l^e][\tilde{D}_l(t_o,\tilde{q}(t),u(t))-\tilde{D}_l(t_o,\tilde{q}^e,u^e)].$$

Then $(\tilde{q}^e,u^e)$ is *unstable.*

Sketch of proof. Consider some solution of (3)–(4) such that $(\tilde{q}^o,u^o)\in\Omega_h\cap\mathcal{K}(A)$ and $(\tilde{q}(t),u(t))\in\Omega_h$ on some interval $[t_o,t_1)$, and suppose for simplicity that $u(\cdot)$ is C^1-smooth on $[t_o,t_1)$. Due to conditions (a)–(b), the foregoing computations of $H(\tilde{q}(t),u(t);A)$ and $(d^+/dt)G(\tilde{q}(t),u(t))$ remain valid on $[t_o,t_1)$; moreover, the choice $\delta(t)\equiv[\tilde{\Gamma}\,|0]^T(\tilde{q}(t)-\tilde{q}^e)$ in (4) leads to $(d^+/dt)J(\tilde{q}(t),u(t);\tilde{\Gamma})=-\tilde{R}(q(t),u(t);\tilde{\Gamma})$ for all $t\in[t_o,t_1)$. It follows that $(\tilde{q}(t),u(t))\in\Omega_h\cap\mathcal{K}(A)$ for all $t\in[t_o,t_1)$. Moreover, G and H are Liapunov functions (Walker, 1980) on $\Omega_h\cap\mathcal{K}(A)\cap\tilde{\mathcal{C}}(t_o)$ and, due to condition (d), so is $J+\mu G$. Under conditions (c) and (e), LaSalle's invariance principle (Walker, 1980) now implies that $(\tilde{q}^e,u^e)$ is unstable.

Often condition (e) of Theorem 3.3 is not difficult to check. If condition (d) is strongly satisfied (>0 replaces ≥ 0, then condition (e) is met.

Condition (d) of Theorem 3.3 may be weakened somewhat. Nonuniqueness of U and Din Definition 2.1 leads to nonuniqueness of R in (10), and R may be replaced in conditions (d)–(e) by many other function $\hat{R}$ of the form

$$\hat{R}(\tilde{q},u;\tilde{\Gamma})\equiv R(\tilde{q},u;\Gamma)-\sum_{i=1}^{r}\sum_{j=1}^{r}\gamma_{ij}u_i\Big[\frac{\partial}{\partial q_j}F(\tilde{q})-\frac{\partial}{\partial q_i}F(\tilde{q}^e)$$
$$+\sum_{l=1}^{r}(\tilde{q}_l-\tilde{q}_l^e)\frac{\partial^2}{\partial q_l\partial q_j}F(\tilde{q})\Big]\qquad(16)$$

where $F:\tilde{\mathcal{O}}\to\mathbb{R}^n$ is any C^2-smooth function[1]. Moreover, the open set Ω_h may consist of two or more disjoint open components, and Theorem 3.3 remains valid if Ω_h is replaced by any such component which meets conditions (a) and (c).

Although of more restricted applicability, the following Corollaries 3.1–3.3 are much simpler than our basic stability theorems. We utilize a number of matrices related to (q^e,u^e): $n\times n$ matrices $M=[m_{ij}]$, $C=[c_{ij}]$, $\bar{C}\equiv(C+C^T)/2$, an $r\times r$ matrix $\tilde{K}=[k_{ij}]$, and an $r\times r$ matrix $\tilde{B}=[b_{ij}]$, which are defined as follows:

$$m_{ij}\equiv\partial^2\tilde{L}(t_o,\tilde{q}^e,u^e)/\partial u_i\partial u_j,\qquad c_{ij}\equiv-\partial D_i(t_o,\tilde{q}^e,u^e)/\partial u_j,\qquad(17)$$

$$k_{ij}\equiv-\partial^2\tilde{L}(t_o,\tilde{q}^e;u^e)/\partial q_i\partial q_j\qquad\text{for } i\leq r,\ j\leq r,\qquad(18)$$

$$b_{ij}\equiv\partial^2\tilde{L}(t_o,\tilde{q}^e,u^e)/\partial q_i\partial u_j\qquad\text{for } i\leq r,\ j\leq n.\qquad(19)$$

We note that M, $\bar{C}$, and $\tilde{K}$ are symmetric, while $\tilde{B}$ is not square $(r<n)$; moreover, M and $\bar{C}$ are at least positive semidefinite. We define $\tilde{C}$ to be the $r\times n$ matrix consisting of the first r rows of C.

In terms of the foregoing matrices, the matrices $\tilde{\Gamma}$, A, Γ and Λ of Section 2, some $r\times r$ matrix $\tilde{S}=\tilde{S}^T$, and some real numbers ρ, ν, μ, we also define an $r\times n$ matrix $\Sigma\equiv[\tilde{S}\,|0]$ and two $(r+n)\times(r+n)$ symmetric matrices

$$W(\rho,A)\equiv\left[\begin{array}{c|c}\tilde{K}&0\\\hline 0&M\end{array}\right]+\rho\begin{bmatrix}\tilde{B}\Lambda\tilde{B}^T&\tilde{B}\Lambda M\\(\tilde{B}\Lambda M)^T&M\Lambda M\end{bmatrix},\qquad(20)$$

$$P(\mu,\nu,\rho,\tilde{\Gamma},\tilde{S},A)\equiv\nu W(\rho,A)$$
$$+\begin{bmatrix}-\tilde{\Gamma}\tilde{K}-\tilde{K}\tilde{\Gamma}^T&\tilde{\Gamma}(\tilde{B}-\Sigma-\tilde{C})+(\tilde{B}-\Sigma)\Gamma^T\\{}[\tilde{\Gamma}(\tilde{B}-\Sigma-\tilde{C})+(\tilde{B}-\Sigma)\Gamma^T]^T&\Gamma M+M\Gamma^T+2\mu\bar{C}\end{bmatrix}.\qquad(21)$$

Proofs of Corollaries 3.1–3.2 are based on estimates of the functions appearing in Theorems 3.1–3.3, and have been relegated to the Appendix.

Corollary 3.1. Suppose that $(\tilde{q}^e,u^e)$ is a reduced equilibrium and the following conditions hold:

(a) $\tilde{\mathcal{C}}(t)\supset\eta_h$ for all $t\geq t_o$, some $h>0$.

(b) $\tilde{L}$: is time-invariant and C^2-smooth, and $\tilde{D}(t,\tilde{q},u^e)=\tilde{D}(t,\tilde{q}^e,u^e)$ for all $(t,\tilde{q})\in\mathbb{R}\times\tilde{\mathcal{O}}$.

(c) Both the $n\times n$ matrix M and the $r\times r$ matrix $\tilde{K}$ are positive definite.

Then $(\tilde{q}^e,u^e)$ is *stable.* If Q is pseudoconservative $(\tilde{D}\equiv 0)$, then $(\tilde{q}^e,u^e)$ is *not* asymptotically stable.

If, in addition to (a)–(c),

(d) $\tilde{D}$ is time-invariant and C^1-smooth, and the $n\times n$ matrix $\bar{C}$ is positive definite,

then $(\tilde{q}^e,u^e)$ is *asymptotically* stable.

If the foregoing conditions (a), (b), and (d) hold, but in place of (c) we have its strong contradiction,

(e) $r\geq 1$ and $\det(\tilde{K})\neq 0$, but $\tilde{K}$ is *not* positive definite, then $(\tilde{q}^e,u^e)$ is *unstable.*

Corollary 3.2. Suppose that $(\tilde{q}^e,u^e)$ is a reduced equilibrium and the following conditions hold for some real $(n-r)\times(n-r)$ positive semidefinite symmetric matrix A which meets condition (12):

[1]In Definition 2.1, notice that the pair (U,D) can be replaced by $(\hat{U},D)$ with $\hat{U}\equiv U+\sum_{l=1}^{r}u_l\frac{\partial}{\partial q_l}F(\tilde{q})$.

(*a*) $\tilde{\mathcal{C}}(t) \supset \eta_h$ for all $t \geq t_o$, some $h > 0$.

(*b*) $\tilde{L}$ is time-invariant and C^2-smooth and $(\tilde{D}(t,\tilde{q},u^e) = \tilde{D}(t,\tilde{q}^e,u^e)$ for all $\tilde{q} \in \tilde{\mathcal{O}}$, $t \geq t_o$.

(*c*) There exists a real number $\rho \geq 0$ such that $W(\rho,A)$ is positive definite.

Then, $(\tilde{q}^e,u^e)$ is *stable* but, if $A \neq 0$, it is *not* asymptotically stable.

Corollary 3.3. Suppose that $(\tilde{q}^e,u^e)$ is a reduced equilibrium and the following conditions hold for some real $(n-r) \times (n-r)$ positive semidefinite symmetric matrix A which meets condition (12):

(*a*) $\tilde{\mathcal{C}}(t) \supset \eta_h$ for all $t \geq t_o$, some $h > 0$.

(*b*) $\tilde{L}$ is time-invariant and C^2-smooth, $\tilde{D}$ is time-invariant and C^1-smooth, and $\tilde{D}(t_o,\tilde{q},u^e) = \tilde{D}(t_o,\tilde{q}^e,u^e)$ for all $\tilde{q} \in \tilde{\mathcal{O}}$.

(*c*) $W(\rho,A)$ is indefinite for all real numbers $\rho \geq 0$.

(*d*) There exist real numbers $\mu \geq 0$, $\nu \geq 0$, $\rho \geq 0$, and real $r \times r$ matrices $\tilde{\Gamma}, \tilde{S} = \tilde{S}^T$, such that $P(\mu,\nu,\rho,\tilde{\Gamma},\tilde{S},A)$ is positive definite.

Then $(\tilde{q}^e,u^e)$ is *unstable*.

If $r \equiv 0$ and the reduced state is only $u \in \mathbb{R}^n$, then $\tilde{\mathcal{K}}$ and $\tilde{B}$ are simply ignored in Corollaries 3.1–3.2, Corollary 3.3 is inapplicable, and Corollary 3.2 differs from Corollary 3.1 only by its claim that u^e is not asymptotically stable for $A \neq 0$.

Since $\Lambda = \Lambda^T \geq 0$ in Corollaries 3.2–3.3, condition (*c*) of Corollary 3.2 is met if and only if $\tilde{q}^T\tilde{K}\tilde{q} + u^T M u > 0$ for all nonzero $(\tilde{q},u) \in \mathbb{R}^r \times \mathbb{R}^n$ such that $\Lambda\tilde{B}^T\tilde{q} + \Lambda M u = 0$; condition (*c*) of Corollary 3.3 is met if and only if $\tilde{q}^T\tilde{K}\tilde{q} + u^T M u < 0$ for some $(\tilde{q},u)$ such that $\Lambda B^T\tilde{q} + \Lambda M u = 0$. There is no reason to apply Corollary 3.2 with $A \equiv 0$, a choice which is always possible[2]; then $\Lambda = 0$ and the simpler Corollary 3.1 will do at least as well. However, Corollary 3.3 may be useful whether or not $A = 0$.

Corollary 3.3 is made complicated by its generality. The following comments bear on the problem of making useful parameter selections during applications. Comments 3.1 and 3.3 also are helpful when applying Corollary 3.2.

Comment 3.1. If Q is pseudoconservative ($\tilde{D} \equiv 0 \in \mathbb{R}^n$), it seems best to choose $A \equiv I$ in (12). If $\tilde{D} \neq 0$, it seems best to choose diagonal $(n-r) \times (n-r)$ $A = A^T \geq 0$ with $a_{ii} \equiv 1$ if $\tilde{D}_{r+i} \equiv 0$, and $a_{ii} \equiv 0$, otherwise.

Comment 3.2. Whether or not $A = 0$, condition (*c*) of Corollary 3.3 cannot be met unless $r \geq 1$ and $\tilde{K}$ is not positive semidefinite.

Comment 3.3. Since $\tilde{C} \geq 0$, it is often best to choose very large $\mu > 0$ when attempting to satisfy condition (*d*) of Corollary 3.3. If $\tilde{C} > 0$, then $A = 0$ in (12) and Corollaries 3.2–3.3 should not be employed, since they say no more than the simpler Corollary 3.1.

Comment 3.4. Our choice of $\tilde{S} = \tilde{S}^T$ affects $P(\mu,\nu,\rho,\tilde{\Gamma},\tilde{S},A)$ only through the off-diagonal submatrices in P. Partitioning M, $\tilde{B}$, and C as

$$M \equiv \left[\begin{array}{c|c} M_1 & M_2 \\ \hline M_2^T & M_4 \end{array}\right], \quad \tilde{B} \equiv [B_1 | B_2], \quad C \equiv \left[\begin{array}{c|c} C_1 & C_2 \\ \hline C_3 & C_4 \end{array}\right], \tag{22}$$

where M_1, B_1, and C_1 are $r \times r$ matrices, we usually find the choice

$$\tilde{S} \equiv \frac{1}{2}(B_1 + B_1^T) - \frac{1}{4}(C_1 + C_1^T) \tag{23}$$

to be best, and it can be proved to be best for $r = 1$.

[2]Note that condition (12) *requires* $A = 0$ if Q is strongly pseudodissipative.

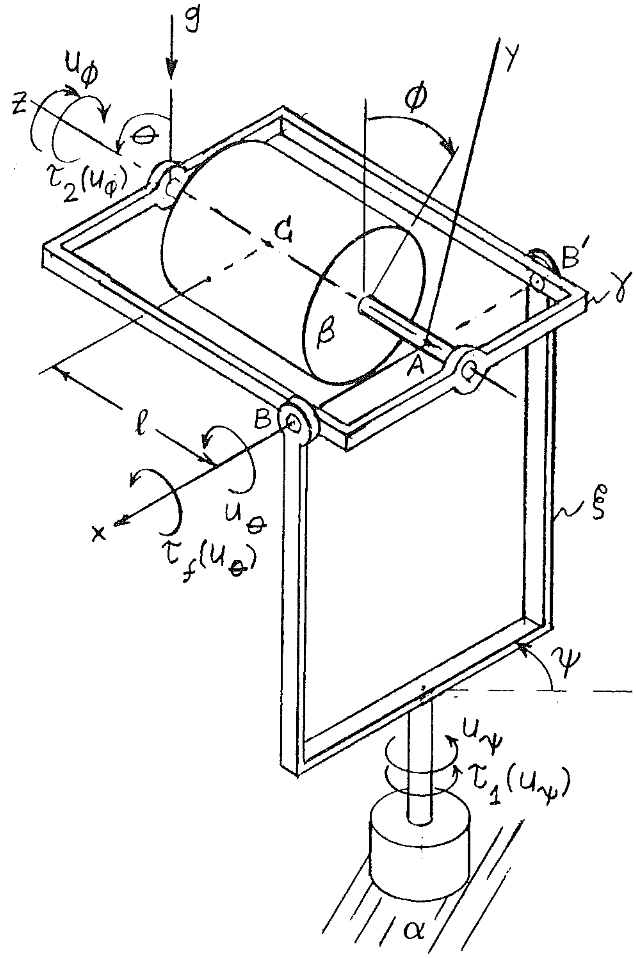

Fig. 1 Mechanism of Examples 4.1–4.2

Comment 3.5. Unless $\tilde{K}$ is indefinite, it seems best to choose $\tilde{\Gamma} = I$ in condition (*d*) of Corollary 3.3.

Comment 3.6. Suppose that $r > 1$ and $\tilde{K}$ is indefinite. In terms of the partitions (22), it seems best to choose $\tilde{\Gamma}$ such that $\nu\tilde{K} - \tilde{\Gamma}\tilde{K} - \tilde{K}\tilde{\Gamma}^T > 0$ and $\nu M_1 + \tilde{\Gamma}M_1 + M_1\tilde{\Gamma}^T > 0$ for some $\nu \geq 0$. This always can be done[3] if $M_1 > 0$ and $\det(\tilde{K}) \neq 0$.

Comparing Corollaries 3.1–3.3, we see that Corollary 3.1 is the simplest and the only one providing sufficient conditions for asymptotic stability. Corollary 3.2 provides a more general means of assuring nonasymptotic stability, and Corollary 3.3 provides the most general means of assuring instability. If $\tilde{\mathcal{C}}(t) \supset \eta_h$ for all $t \geq t_o$, some $h > 0$, this comparison is also valid for Theorems 3.1–3.3, respectively.

Corollaries 3.1–3.3 are much simpler than Theorems 3.1–3.3, and are employed in the following examples. These examples are closely related to, and may be compared with, a simpler example in (Walker, 1987).

4 Examples

Example 4.1. The housing γ of a motor with armature β is hinged to a clevis ξ which is driven about a vertical axis by another motor attached to the floor α, assumed to be inertial.

[3]Suitable $\tilde{\Gamma}$ can be explicitly constructed in terms of the solutions (λ,g) of the eigenvalue problem $(\lambda M_1 + \tilde{K})g = 0$.

(See Fig. 1.) Along motions, bearing friction at B and B' creates a torque $\tau_f(\dot{\theta}(t))$ on γ about the horizontal bearing axis Ax, where $\tau_f:\mathbb{R}\rightarrow\mathbb{R}$ is C^1-smooth, $\tau_f(0)=0$, and $\tau_f'(u_\theta)\leq 0$ for all $u_\theta\in\mathbb{R}$. Both motors have strictly declining delivered-torque/speed relations. In particular, the C^1-smooth torques $\tau_1(u_\psi)$ and $\tau_2(u_\phi)$ (delivered to ξ and β by the lower and upper motors, respectively) have strictly negative derivatives, include the effects of motor-bearing friction, and become zero at known angular rates ω_1 and ω_2, respectively. $Axyz$ is a principal coordinate system for both the armature β and the housing γ of the upper motor, and C is the mass center of this motor. I_A will denote the moment of inertial (about a vertical axis through A) of the clevis ξ (including the lower motor armature).

Choosing $\gamma+\beta+\xi$ to be our collection and defining $q\equiv(\theta,\psi,\phi)\in\mathbb{R}^3\equiv\mathcal{O}$, we see that $u=(u_\theta,u_\psi,u_\phi)\in\mathbb{R}^3$, $\mathcal{C}(t)=\mathbb{R}^3\times\mathbb{R}^3$ for all $t\in\mathbb{R}$,

$$T(t,q,u)=\frac{1}{2}\,[\bar{J}_1u_\theta^2+\bar{J}_2u_\psi^2\sin^2\theta+J_3(u_\phi^2+2u_\phi u_\psi\cos\theta)+(I_A+\bar{J}_3\cos^2\theta)u_\psi^2] \tag{24}$$

with $\bar{J}_1=J_1+I_1,\ \bar{J}_2=J_1+I_2,\ \bar{J}_3=J_3+I_3,$

$$J_{Axyz}^{(\beta)}=\begin{bmatrix}J_1&0&0\\0&J_1&0\\0&0&J_3\end{bmatrix},\qquad J_{Axyz}^{(\gamma)}=\begin{bmatrix}I_1&0&0\\0&I_2&0\\0&0&I_3\end{bmatrix}, \tag{25}$$

and Q is pseudodissipative with

$$U(t,q,u)=mgl\cos\theta, \tag{26}$$

$$D(t,q,u)=[\tau_f(u_\theta),\ \tau_1(u_\psi),\ \tau_2(u_\phi)]\in\mathbb{R}^3. \tag{27}$$

Both ψ and ϕ are ignorable and we define $\tilde{q}\equiv\theta\in\mathbb{R}^1\equiv\tilde{\mathcal{O}}$, $\tilde{\mathcal{C}}(t)\equiv\mathbb{R}^1\times\mathbb{R}^3$, $S(t,\theta)\equiv\mathbb{R}^2$, $\tilde{L}\equiv T-U$, and $\tilde{D}\equiv D$. For convenience, we also define two new parameters

$$\sigma\equiv\omega_1^2(\bar{J}_3-\bar{J}_2),\ \ \zeta\equiv J_3\omega_1\omega_2-mgl, \tag{28}$$

and note that

$$\frac{\partial}{\partial\theta}\,\tilde{L}(t,\theta,u)=[(\bar{J}_2-\bar{J}_3)u_\psi^2\cos\theta-J_3u_\psi u_\phi+mgl]\sin\theta. \tag{29}$$

Since $0=\tau_f(0)=\tau_1(\omega_1)=\tau_2(\omega_2)$ and $\tilde{L}$ is time-invariant, Corollary 2.1 shows that there exist at least two physically distinct, reduced equilibria

$(\theta^e,u^e)\in\mathbb{R}^1\times\mathbb{R}^3$,

$$(\theta^e,u^e)_1=(0,0,\omega_1,\omega_2),\quad(\theta^e,u^e)_2=(\pi,0,\omega_1,\omega_2),$$

and if $|\sigma|>|\zeta|$ there exist two more:

$$(\theta^e,u^e)_3\ \text{with}\ \sin\theta^e>0,\quad\zeta=-\sigma\cos\theta^e,$$
$$(\theta^e,u^e)_4\ \text{with}\ \sin\theta^e<0,\quad\zeta=-\sigma\cos\theta^e,$$

where $u^e=(0,\ \omega_1,\ \omega_2)$.

At every (θ^e,u^e) we find the matrices of (17)–(19) to be

$$M=\begin{bmatrix}\bar{J}_1&0&0\\0&\bar{J}_2\sin^2\theta^e+\bar{J}_3\cos^2\theta^e+I_A&J_3\cos\theta^e\\0&J_3\cos\theta^e&J_3\end{bmatrix}>0, \tag{30}$$

$$\bar{C}=C=\begin{bmatrix}-\tau_f'(0)&0&0\\0&-\tau_1'(\omega_1)&0\\0&0&-\tau_2'(\omega_2)\end{bmatrix}\geq0,\ \tilde{C}=[-\tau_f'(0),\ 0\ 0], \tag{31}$$

	$\sigma<-\lvert\zeta\rvert$	$\sigma>\lvert\zeta\rvert$	$\zeta<-\lvert\sigma\rvert$	$\zeta>\lvert\sigma\rvert$
$(\theta^e,u^e)_1$	UNSTABLE	STABLE	UNSTABLE	STABLE
$(\theta^e,u^e)_2$	UNSTABLE	STABLE	STABLE	UNSTABLE
$(\theta^e,u^e)_{3,4}$	STABLE	UNSTABLE	IMPOSSIBLE	

Fig. 2 Stability table for Example 4.1

$$\tilde{B}=[0,(2(\bar{J}_2-\bar{J}_3)\omega_1\cos\theta^e-J_3\omega_2)\sin\theta^e,\ -J_3\omega_1\sin\theta^e], \tag{32}$$

$$\tilde{K}=k_{11}=(\zeta+\sigma\cos\theta^e)\cos\theta^e-\sigma\sin^2\theta^e. \tag{33}$$

By condition (12) we must choose the 2×2 matrix $A=0$, and following the suggestions of Comments 3.4–3.5 we choose $\tilde{S}=s_{11}=b_{11}-c_{11}/2=\tau_f'(0)/2$, $\tilde{\Gamma}=\gamma_{11}=1$; hence, at every (θ^e,u^e) we have $\Lambda=0$, $\Sigma=[\tau_f'(0)/2,\ 0,\ 0]$,

$$W(\rho,A)=\left[\begin{array}{c|c}\dfrac{k_{11}}{0}&\dfrac{0}{M}\end{array}\right],\qquad\Gamma=\begin{bmatrix}1&0&0\\0&0&0\\0&0&0\end{bmatrix},$$

$$P(\mu,\nu,\rho,\tilde{\Gamma},\tilde{S},A)=\left[\begin{array}{c|c}\dfrac{(\nu-2)k_{11}}{0}&\dfrac{0\quad b_{12}\quad b_{13}}{\nu M+\Gamma M+M\Gamma^T+2\mu\bar{C}}\\ \begin{matrix}b_{12}\\b_{13}\end{matrix}&\end{array}\right].$$

We note that W and P are independent of ρ. If $k_{11}<0$, then W is indefinite and P is positive definite for $\nu=1$ and sufficiently large $\mu>0$, since $\tau_1'(\omega_1)$ and $\tau'_2(\omega_2)$ are negative numbers.

At $(\theta^e,u^e)_1$ we have $\theta^e=0$ and $k_{11}=\sigma+\zeta$, so Corollary 3.1 implies stability for $\sigma+\zeta>0$, while Corollary 3.3 implies instability for $\sigma+\zeta<0$.

At $(\theta^e,u^e)_2$ we have $\theta^e=\pi$ and $k_{11}=\sigma-\zeta$, so Corollary 3.1 implies stability for $\sigma>\zeta$ and Corollary 3.3 implies instability for $\sigma<\zeta$.

At both $(\theta^e,u^e)_3$ and $(\theta^e,u^e)_4$ we have $\sin\theta^e\neq0$, $\zeta+\sigma\cos\theta^e=0$, and $k_{11}=-\sigma\sin^2\theta^e$. Hence, Corollary 3.1 implies stability for $\sigma<0$ while Corollary 3.3 implies instability for $\sigma>0$.

The foregoing results are summarized in the table of Fig. 2, but more can be said if more is known about the frictional torque at the bearings $B-B'$. If $\tau_f'(0)<0$, then $\bar{C}>0$, each claim of "stability" is strengthened to "asymptotic stability," and all conclusions can be obtained from Corollary 3.1; Corollary 3.3 is not needed.

Example 4.2. We modify Example 4.1 by supposing that both motors always deliver exactly zero torque: $\tau_1(x)=0=\tau_2(x)$ for all $x\in\mathbb{R}$. Now Corollary 2.1 yields four distinct *families* of reduced equilibria *parameterized* by $(u_\psi^e,u_\phi^e)\in\mathbb{R}^2$ but all having $u_\theta^e=0$:

$$(\theta^e,u^e)_1\ \text{with}\ \theta^e=0,\ (\theta^e,u^e)_2\ \text{with}\ \theta^e=\pi,$$
$$(\theta^e,u^e)_{3,4}\ \text{with}\ \sin\theta^e\neq0,\ \zeta^e=-\sigma^e\cos\theta^e,$$

where $\sin\theta^e>0$ for $(\theta^e,u^e)_3$, $\sin\theta^e<0$ for $(\theta^e,u^e)_4$, and

$$\sigma^e\equiv|u_\psi^e|^2(\bar{J}_3-\bar{J}_2),\ \ \zeta^e\equiv J_3u_\psi^eu_\phi^e-mgl. \tag{35}$$

At every reduced equilibrium (θ^e,u^e), the matrices (30)–(33) of Example 4.1 are valid when modified by the substitutions $(\sigma,\zeta,\omega_1,\omega_2,\tau_1'(\omega_1),\ \tau_2'(\omega_2))\rightarrow(\sigma^e,\zeta^e,u_\psi^e,u_\phi^e,0,0)$. However, condition (12) now allows us to choose the 2×2 matrix $A\equiv I$. Choosing $\tilde{S}$ and $\tilde{\Gamma}$ as before, we have $\Gamma=I$, $\Sigma=[\tau_f'(0)/2,\ 0,\ 0]$,

$$\Lambda = \begin{bmatrix} 0 & 0 & 0 \\ 0 & 1 & 0 \\ 0 & 1 & 0 \end{bmatrix},$$

$$W(\rho,A) = \left[\begin{array}{c|c} \dfrac{k_{11} + \rho(b_{12}^2 + b_{13}^2)}{(\rho\tilde{B}M)^T} & \dfrac{\rho\tilde{B}M}{M + \rho M\Lambda M} \end{array}\right],$$

$$P(\mu,\nu,\rho,\tilde{\Gamma},\tilde{S},A) = \nu W(\rho,A) + 2 \left[\begin{array}{c|c} \dfrac{-k_{11}}{\tilde{B}^T} & \dfrac{\tilde{B}}{M + \mu\bar{C}} \end{array}\right].$$

Defining another (θ^e,u^e)-related parameter

$$\lambda^e \equiv k_{11} + (m_{33}b_{12}^2 - 2m_{23}b_{12}b_{13} + m_{22}b_{13}^2)/(m_{22}m_{33} - m_{23}^2), \quad (36)$$

we find[4] that $W(\rho,A) > 0$ (for sufficiently large $\rho > 0$) if and only if $\lambda^e > 0$. If $\lambda^e < 0$, then not only is $W(\rho,A)$ indefinite for all $\rho \geq 0$, but also $P(0,0,0,\tilde{\Gamma},\tilde{S},A) > 0$. Note that $\lambda^e \geq k_{11}$.

At any reduced equilibrium in the family $(\theta^e,u^e)_1$ we have $\theta^e = 0$, $b_{12} = 0 = b_{13}$, and $k_{11} = \sigma^e + \zeta^e = \lambda^e$. Hence, Corollary 3.1 implies stability for $\sigma^e + \zeta^e > 0$ and Corollary 3.3 implies instability for $\sigma^e + \zeta^e < 0$.

At any reduced equilibrium in the family $(\theta^e,u^e)_2$ we have $\theta^e = \pi$, $b_{12} = 0 = b_{13}$, and $k_{11} = \sigma^e - \zeta^e = \lambda^e$. Hence, Corollary 3.1 implies stability for $\sigma^e > \zeta^e$ and Corollary 3.3 implies instability for $\sigma^e < \zeta^e$.

At any reduced equilibrium in the families $(\theta^e,u^e)_3$ and $(\theta^e,u^e)_4$ we have $\sin\theta^e \neq 0$, $\zeta^e + \sigma^e\cos\theta^e = 0$, and $k_{11} = -\sigma^e\sin^2\theta^e < \lambda^e$. Hence, Corollary 3.1 implies stability for $\sigma^e < 0$, Corollary 3.2 implies stability for $\lambda^e > 0$ (*even if* $\sigma^e > 0$)[5], and Corollary 3.3 implies instability for $\lambda^e < 0$.

Our results are summarized by the table of Fig. 2 with the substitution $(\sigma,\zeta) \rightarrow (\sigma^e,\zeta^e)$ and the following exception: If $\sigma^e > |\zeta^e|$, then a reduced equilibrium in the families $(\theta^e,u^e)_{3,4}$ if *stable* if $\lambda^e > 0$ (and unstable if $\lambda^e < 0$). Since $A \neq 0$, Corollary 3.2 implies that no claim of "stability" can be strengthened to "asymptotic stability," even if $\tau_f'(0) < 0$.

5 Concluding Remarks

Despite the complexity of Theorems 3.1–3.3, the simpler Corollaries 3.1–3.3 have been found to be both teachable and worthwhile in a graduate course on advanced dynamics.

Example 4.1 employs a pair of realistic motors, whereas the zero-torque motors of Example 4.2 cannot be built (due to friction). For the "free system" of Example 4.2, gyroscopic stabilization occurs for reduced equilibria in the families $(\theta^e,u^e)_{3,4}$ if $\sigma^e > |\zeta^e|$ and $\lambda^e > 0$; it does not occur for the "real system" of Example 4.1, where the torque/speed relations are strictly declining.

Another idealization of Example 4.1 was considered in (Walker, 1988); there both motors were assumed to be constant speed ($u_\psi \equiv \omega_1$, $u_\phi \equiv \omega_2$), the generalized state was $(q,u) \equiv (\theta,u_\theta) \in \mathbb{R}^2$, and stability of generalized equilibria $(\theta^e,0) \in \mathbb{R}^2$ was studied in $\mathbb{R}^2$. Although stability of reduced equilibria is studied with respect to $(\theta,u_\theta,u_\psi,u_\phi) \in \mathbb{R}^4$ in Example 4.1, our stability conclusions for Example 4.1 are otherwise identical to those obtained in (Walker, 1988) for the "restrained system". We note that true constant-speed motors do not exist.

[4]See the second paragraph following Corollary 3.3.

[5]Although (36) is very complicated for $(\theta^e,u^e)_{3,4}$, it can be shown that $\lambda^e > 0$ for every member of these families if $\bar{J}_2 > I_3$.

These results suggest that constant-speed approximations of real motors with sharply declining delivered torques may be less misleading than zero-torque approximations of real motors with slowly declining delivered torques. However, Example 4.1 demonstrates that neither type of approximation is necessary or desirable. The realistic Example 4.1 is much easier than the free Example 4.2, which has many more reduced equilibria and somewhat different stability properties, and Example 4.1 is only slightly more difficult than the restrained example of (Walker, 1988).

References

Hagedorn, P., 1979, "On the Stability of Steady Motions in Free and Restrained Dynamical Systems," ASME JOURNAL OF APPLIED MECHANICS, Vol. 46, pp. 427–432.

Pascal, M., 1975, "Sur la recherche des mouvements stationaires dans les systemes ayant des variables cycliques," *Celestial Mechanics*, Vol. 2, pp. 337–358.

Rumiantsev, V. V., 1975, "On the Influence of Gyroscopic Forces on the Stability of Steady-State Motion," *Journal of Applied Mathematics and Mechanics*, (PMM), Vol. 39, pp. 929–938.

Routh, E. J., 1860, *Advanced Dynamics of a System of Rigid Bodies*; 6th ed., (1905), Dover Publications, New York, 1955.

Walker, J. A., 1980, *Dynamical Systems and Evolution Equations*, Plenum Press, New York.

Walker, J. A., 1988, "Pseudodissipative Systems I: Stability of Generalized Equilibria," ASME JOURNAL OF APPLIED MECHANICS, Vol. 55, pp. 681–686.

APPENDIX

Proof of Corollary 3.1

Condition (b) implies that

$$\left| G(\tilde{q},u) - G(\tilde{q}^e,u^e) - \frac{1}{2}(u-u^e)^T M(u-u^e) - \frac{1}{2}(\tilde{q}-\tilde{q}^e)^T \tilde{K}(\tilde{q}-\tilde{q}^e) \right| \leq o(\|\tilde{q}-\tilde{q}^e\|_r^2 + \|u-u^e\|_n^2). \quad (37)$$

If M and $\tilde{K}$ are positive definite, this estimate implies that $G(\tilde{q},u) > G(\tilde{q}^e,u^e)$ for all $(\tilde{q},u) \in \eta_h$ with sufficiently small $h > 0$. Hence, our current conditions (a)–(c) assure the satisfaction of conditions (a)–(c) of Theorem 3.1. On the other hand, if $r \geq 1$ and $\tilde{K}$ is not even positive semidefinite, (37) implies that the set Ω_ϵ is nonempty for every $\epsilon > 0$.

If $\tilde{D}$ is time-invariant and C^1-smooth, it follows from condition (b) that

$$\left| \sum_{l=1}^{n} (u_l - u_l^e)[\tilde{D}_l(t_o,\tilde{q},u) - \tilde{D}_l(t_o,\tilde{q}^e,u^e)] + (u-u^e)^T C(u-u^e) \right| \leq o(\|u-u^e\|_n^2) \quad (38)$$

for all $(\tilde{q},u) \in \eta_h$, some $h > 0$. If $\bar{C} > 0$, this estimate implies

$$\sum_{l=1}^{n} (u_l - u_l^e)[\tilde{D}_l(t_o,\tilde{q},u) - \tilde{D}_l(t_o,\tilde{q}^e,u^e)] < 0$$

for all $(\tilde{q},u) \in \eta_h$ with h sufficiently small and $u \neq u^e$. We also find that if $\det(\tilde{K}) \neq 0$, then conditions (a)–(b) and result (5) imply that $(\tilde{q}^e, u^e)$ is isolated from all other reduced equilibria $(\tilde{q}^o,u^o)$ with $u^o = u^e$.

We see that our current conditions (a)–(b) imply satisfaction of the corresponding conditions (a)–(d) of Theorem 3.1. Alternatively, under our current conditions (a), (b), (d), and (e), our estimates imply that the corresponding conditions of Theorem 3.1 are met.

Proof of Corollary 3.2

Since $A = A^T \geq 0$, (13) implies $\Lambda = \Lambda^T \geq 0$; hence (11) and (15) imply

$$0 \leq [M(u-u^e) + \tilde{B}^T(\tilde{q}-\tilde{q}^e)]^T \Lambda [M(u-u^e) + \tilde{B}^T(\tilde{q}-\tilde{q}^e)] \leq o(\|\tilde{q}-\tilde{q}^e\|_r^2 + \|u-u^e\|_n^2) \tag{39}$$

for all $(\tilde{q},u) \in \mathcal{K}(A)$. Combining this estimate with (37), we find that our current conditions (a)–(c) imply that conditions (a)–(c) of Theorem 3.2 are met.

Proof of Corollary 3.3

Clearly, we need only show that our current conditions (a)–(d) imply the satisfaction of conditions (c)–(e) of Theorem 3.3. Combining (37) and (39), our current condition (c) implies that $\Omega_\epsilon \cap \mathcal{K}(A)$ is nonempty for every $\epsilon > 0$. Moreover, our definition (13) of Γ implies

$$|2R(\tilde{q},u;\tilde{\Gamma}) - (u-u^e)^T[(\Gamma M + M\Gamma^T](u-u^e) + 2(\tilde{\Gamma}\tilde{B} + \tilde{B}\Gamma^T - \tilde{\Gamma}C)(\tilde{q}-\tilde{q}^e)] + (\tilde{q}-\tilde{q}^e)^T(\tilde{\Gamma}\tilde{K} + \tilde{K}\tilde{\Gamma}^T)(\tilde{q}-\tilde{q}^e)| \leq o(\|\tilde{q}-\tilde{q}^e\|_r^2 + \|u-u^e\|_n^2) \tag{40}$$

for all $(\tilde{q},u) \in \mathcal{K}(A)$. $\tilde{B}$ may be replaced by $\tilde{B} - \Sigma$ in this estimate, for arbitrary $r \times r$ $\tilde{S} = \tilde{S}^T$, if R is replaced by some "equivalent" $\hat{R}$ (see equation (16) with $F(\tilde{q}) \equiv \tilde{q}^T\tilde{S}\tilde{q}/2$).

Combining all estimates (37)–(40), we find that our current condition (d) implies

$$\nu[G(\tilde{q},u) - G(\tilde{q}^e,u^e)] + R(\tilde{q},u;\tilde{\Gamma}) - \mu \sum_{l=1}^{n} (u_l - u_l^e)[\tilde{D}_l(t_o,\tilde{q},u) - \tilde{D}_l(t_o,\tilde{q}^e,u^e)] > 0$$

for all $(\tilde{q},u) \in \eta_h \cap \mathcal{K}(A)$, some $h > 0$. Since $\nu \geq 0$ and $G(\tilde{q},u) < G(\tilde{q}^e,u^e)$ for all $(\tilde{q},u) \in \Omega_h$, it follows that conditions (d)–(e) of Theorem 3.3 are met.

ERRATA

Errata on "On the Certain Refined Theories for Plate Bending," by K. P. Soldatos and published in the December 1988 issue of the ASME Journal of Applied Mechanics, Vol. 55, pp. 994–995:

On page 995 in the second set of equations (8), the printed fraction "17/24" should read "17/21". Also, in the first of equations (10), "P" should be "p".

Journal of Applied Mechanics

Brief Notes

A Brief Note is a short paper that presents a specific solution of technical interest in mechanics but which does not necessarily contain new general methods or results. A Brief Note should not exceed 1500 words *or equivalent* (a typical one-column figure or table is equivalent to 250 words; a one line equation to 30 words). Brief Notes will be subject to the usual review procedures prior to publication. After approval such Notes will be published as soon as possible. The Notes should be submitted to the Technical Editor of the JOURNAL OF APPLIED MECHANICS. Discussions on the Brief Notes should be addressed to the Editorial Department, ASME, United Engineering Center, 345 East 47th Street, New York, N. Y. 10017, or to the Technical Editor of the JOURNAL OF APPLIED MECHANICS. Discussions on Brief Notes appearing in this issue will be accepted until two months after publication. Readers who need more time to prepare a Discussion should request an extension of the deadline from the Editorial Department.

On Symmetrizability of Asymmetric Nonconservative Systems

Shahram M. Shahruz[1] **and Fai Ma**[2]

1 Introduction

Several researchers have studied nonconservative systems whose (linearized) equation of motion is given by

$$\mathbf{M}\ddot{x}(t) + \mathbf{C}\dot{x}(t) + \mathbf{K}x(t) = f(t),\ t \geq 0, \qquad (1.1)$$

where for all $t \geq 0$, $x(t)$ is the n-dimensional vector of generalized coordinates, $f(t)$ is the n-dimensional vector of generalized forces, and the coefficient matrices $\mathbf{M}$, $\mathbf{C}$, and $\mathbf{K}$ are $n \times n$ real constant matrices with no specific symmetry or definiteness property. For instance, Wahed and Bishop (1976), Fawzy and Bishop (1977), and Bishop and Price (1979) have studied nonconservative systems represented by (1.1).

The system (1.1) is said to be *symmetrizable* if and only if there exists a linear change of coordinates

$$x(t) = Tq(t),\ t \geq 0, \qquad (1.2)$$

such that when (1.2) is applied to (1.1), the system can be represented by

$$\ddot{q}(t) + C_s\dot{q}(t) + K_s q(t) = g(t),\ t \geq 0, \qquad (1.3)$$

where C_s and K_s are $n \times n$ *real symmetric* matrices. In (1.2), T is an $n \times n$ real matrix and $q(t)$ is an n-dimensional vector for all $t \geq 0$. The symmetrized system represented by (1.3) can be studied more conveniently. Symmetrizable systems have been studied by several researchers; for instance, Inman (1983) and Ahmadian and Chou (1987) have given conditions under which the system (1.1) is symmetrizable.

In this note, we give a sufficient condition as well as a necessary and sufficient condition for symmetrizability of the system (1.1). Furthermore, we specify the appropriate change of coordinates (1.2) for the symmetrizable systems by giving a formula for T.

[1]Department of Electrical Engineering and Computer Sciences and the Electronic Research Laboratory, University of California, Berkeley, CA 94720.

[2]Department of Mechanical Engineering, University of California, Berkeley, CA 94720.

Manuscript received by the ASME Applied Mechanics Division, August 25, 1987; final revision, October 19, 1988.

2 Symmetrizable Matrices

It is well known that any real square matrix can be factored as the product of two symmetric matrices, one of which is nonsingular (see, e.g., Taussky, 1968; Parlett, 1980). Hence, any real square matrix F can be represented by

$$F = F_l F_r, \qquad (2.1)$$

where $F_l = F_l^T$ and $F_r = F_r^T$ are real square matrices (F_l^T denotes the transpose of the matrix F_l). The choice of F_l and F_r is not unique. Having one of the factors positive definite leads us to the following definition (see, e.g., Taussky, 1968): A real square matrix F is said to be *symmetrizable* if and only if it can be factored as the product of two symmetric matrices such that one of them is positive definite. Characterization of symmetrizable matrices has been given by Taussky (1968): A real square matrix F is symmetrizable if and only if F has real eigenvalues and a full set of eigenvectors.

For a symmetrizable matrix F, we adopt the factorization by Parlett (1980, p. 304); hence, F can be represented by (2.1) with either

$$F_l = SS^T,\quad F_r = S^{-T}\Lambda S^{-1}, \qquad (2.2)$$

or

$$F_l = S\Lambda S^T,\quad F_r = (SS^T)^{-1}, \qquad (2.3)$$

where S is a nonsingular matrix whose columns are the eigenvectors of F, and Λ is the diagonal Jordan form of F. By S^{-1}, we denote the inverse of the matrix S, and by S^{-T}, the transpose of the inverse of S. By $F > 0$, we denote the positive definite matrix F.

3 Criteria for Symmetrizability of Systems

Throughout this note we assume that:

($A1$) $\mathbf{M}$ is invertible;

($A2$) $\mathbf{M}^{-1}\mathbf{C}$ and $\mathbf{M}^{-1}\mathbf{K}$ are symmetrizable, i.e.,

$$\mathbf{M}^{-1}\mathbf{C} = B = B_l B_r,\quad \mathbf{M}^{-1}\mathbf{K} = C = C_l C_r, \qquad (3.1)$$

where B_l, B_r, C_l, and C_r are real symmetric matrices, and at least one of the factors of both B and C is positive definite.

Having B and C defined by (3.1), we may write (1.1) as

$$\ddot{x}(t) + B\dot{x}(t) + Cx(t) = \mathbf{M}^{-1}f(t),\ t \geq 0. \qquad (3.2)$$

Inman (1983) has shown that: If $\mathbf{C} = r\,\mathbf{M} + s\,\mathbf{K}$ for some real numbers r and s, then the system (1.1) is symmetrizable; the following theorem generalizes this result.

Theorem 3.1. If $BC = CB$, where B and C are given by (3.1), then the system (1.1) is symmetrizable.

Proof. The matrices B and C are symmetrizable, hence, are diagonalizable. Two diagonalizable matrices B and C can be diagonalized simultaneously by a single transformation if and only if $BC = CB$ (see, e.g., Horn and Johnson, 1985). Suppose that $BC = CB$, and let V denote the matrix whose columns are the eigenvectors of C. Applying the change of coordinates $x(t) = Vq(t)$, $t \geq 0$, to (3.2) and multiplying the resulting equation by V^{-1}, from the left, we obtain an equation such as (1.3), in which the coefficient matrices are diagonal.

It is easy to see that Theorem 3.1 generalizes the earlier result by Inman (1983). For, if $\mathbf{C} = r\,\mathbf{M} + s\,\mathbf{K}$, or $B = rI_n + sC$, (I_n denotes the $n \times n$ identity matrix) for some real numbers r and s, then $BC = CB$. However, $BC = CB$ does not necessarily imply $\mathbf{C} = r\,\mathbf{M} + s\,\mathbf{K}$, for some real numbers r and s (for an example see Shahruz, 1987).

When $BC = CB$, the (symmetrizable) system (1.1) can actually be decoupled. In general, however, symmetrizable systems need not be decouplable. For this reason, the condition for symmetrizability in Theorem 3.1 is rather strong. In fact, there are symmetrizable systems for which $BC \neq CB$; an example is given later. The following result, which perhaps represents the most general condition for symmetrizability, is due to Inman (1983).

Theorem 3.2. (Inman, 1983). The system (1.1) is symmetrizable if and only if there exists a factorization of B and C such as (3.1) with $B_l = C_l > 0$.

When the above theorem is applicable the change of coordinates (1.2) is identified as $x(t) = B_l^{1/2}\, q(t)$, $t \geq 0$. It is easy to see that Theorem 3.2 remains valid if the right factors of B and C in (3.1) satisfy $B_r = C_r > 0$. In this case, the change of coordinates which transforms (1.1) to an equation with symmetric coefficients is $x(t) = B_r^{-1/2}\, q(t)$, $t \geq 0$.

Now, we seek a necessary and sufficient condition under which the symmetrizable matrices B and C, when factored as (3.1), have left (right) symmetric positive-definite common factor. We make an additional assumption:

($A3$) B and C have distinct eigenvalues.

By ($A2$), B and C are symmetrizable, thus we can factor (i) both matrices B and C according to (2.2), (ii) both matrices B and C according to (2.3), and (iii) one of the matrices B or C according to (2.2) and the other one according to (2.3). We examine Case (i) in detail.

Case (i). In this case both matrices B and C are factored according to (2.2), i.e.,

$$B = (UU^T)(U^{-T}\Lambda_B U^{-1}), \tag{3.3a}$$

$$C = (VV^T)(V^{-T}\Lambda_C V^{-1}), \tag{3.3b}$$

where U, (V, respectively) is the matrix whose columns are the eigenvectors of B, (C) and Λ_B, (Λ_C) is the diagonal Jordan form of B, (C). We look for nonsingular matrices P and Q, so that when they are introduced into (3.3) in the following way

$$B = (UU^TP)(P^{-1}U^{-T}\Lambda_B U^{-1}), \tag{3.4a}$$

$$C = (VV^TQ)(Q^{-1}V^{-T}\Lambda_C V^{-1}), \tag{3.4b}$$

the factors of B and C become symmetric, i.e.,

$$UU^TP = P^TUU^T, \tag{3.5a}$$

$$P^{-1}U^{-T}\Lambda_B U^{-1} = U^{-T}\Lambda_B U^{-1}P^{-T}, \tag{3.5b}$$

$$VV^TQ = Q^TVV^T, \tag{3.5c}$$

$$Q^{-1}V^{-T}\Lambda_C V^{-1} = V^{-T}\Lambda_C V^{-1}Q^{-T}. \tag{3.5d}$$

It can be shown that (Shahruz, 1987), P satisfies (3.5a) and (3.5b) if and only if

$$P^TB = BP^T. \tag{3.6}$$

The matrix equation (3.6) always has a solution for P^T (see, e.g., Gantmacher, 1959). Since by ($A3$), the matrix B has distinct eigenvalues, (3.6) has a solution for P^T (and hence P) which depends on n arbitrary parameters; this solution is of the following form:

$$P = U^{-T}DU^T, \tag{3.7}$$

where $D = \text{diag}\,(d_1, \ldots, d_n)$ is a diagonal matrix with n arbitrary real parameters d_i, $i = 1, \ldots, n$, on its diagonal. Similarly, it can be shown that Q satisfies (3.5c) and (3.5d) if and only if

$$Q = V^{-T}\Delta V^T, \tag{3.8}$$

where $\Delta = \text{diag}\,(\delta_1, \ldots, \delta_n)$ is a diagonal matrix with n arbitrary parameters δ_i, $i = 1, \ldots, n$, on its diagonal. Substituting P, (Q, respectively) from (3.7), ((3.8)) into (3.4a), ((3.4b)), we obtain

$$B = (UDU^T)(U^{-T}D^{-1}\Lambda_B U^{-1}), \tag{3.9a}$$

$$C = (V\Delta V^T)(V^{-T}\Delta^{-1}\Lambda_C V^{-1}). \tag{3.9b}$$

In (3.9), the left factors of B and C are identified as $B_l = UDU^T$, and $C_l = V\Delta V^T$. The factors B_l and C_l satisfy the condition of Theorem 3.2, when $UDU^T = V\Delta V^T > 0$; since U and V are nonsingular matrices, this condition holds if and only if

$$\Delta = WDW^T > 0, \tag{3.10}$$

where

$$W = V^{-1}U. \tag{3.11}$$

We denote the rows of W by $\rho_i = [w_{i1} \ldots w_{in}]$, $i = 1, \ldots, n$, and define the row vector $\rho_i \odot \rho_j = [w_{i1}w_{j1} \ldots w_{in}w_{jn}]$. We substitute $W = [w_{ij}]$ and $D = \text{diag}\,(d_1, \ldots, d_n)$ into the right-hand side of (3.10), multiply the matrices, and denote the resulting symmetric matrix by $M = [m_{ij}]$. Equating Δ and M, we obtain

$$\delta_i = m_{ii} = \sum_{j=1}^{n} w_{ij}^2\, d_j, \quad i = 1, \ldots, n, \tag{3.12a}$$

$$m_{ij} = \sum_{k=1}^{n} w_{ik}\, w_{jk}\, d_k = 0, \quad i, j = 1, \ldots, n,\ i \neq j. \tag{3.12b}$$

Therefore the off-diagonal elements of m are zero if and only if

$$Rd = 0, \tag{3.13}$$

where R is an $n(n-1)/2 \times n$ real matrix, and d is an n-dimensional vector given by

$$R = \begin{bmatrix} \rho_1 \odot \rho_2 \\ \vdots \\ \rho_1 \odot \rho_n \\ \text{---------} \\ \rho_2 \odot \rho_3 \\ \vdots \\ \rho_2 \odot \rho_n \\ \text{---------} \\ \vdots \\ \text{---------} \\ \rho_{n-1} \odot \rho_n \end{bmatrix}, \quad d = \begin{bmatrix} d_1 \\ \vdots \\ d_n \end{bmatrix}. \tag{3.14}$$

Now, we give an easy-to-check necessary and sufficient condition for symmetrizability of the system (1.1); this condition is similar to that given by Ahmadian and Chou (1987), however, we have arrived at this result by an entirely different approach. In the following, a positive vector means a vector whose elements are all positive.

Theorem 4.1. The system (1.1) is symmetrizable if and only if there exists a positive vector in the null space of the matrix R given in (3.14).

Proof. Two nonzero diagonal matrices $D = \mathrm{diag}(d_1, \ldots, d_n)$ and Δ satisfy (3.10) if and only if d in (3.13) is a nonzero vector. A nonzero vector satisfies (3.13) if and only if rank $R<n$. Suppose that rank $R<n$, then a nonzero d is in the null space of R. Since W is nonsingular, $WDW^T>0$ if and only if $D>0$. The matrix $D>0$, if and only if d is a positive vector. Having $WDW^T>0$, then $UDU^T>0$ and $V\Delta V^T>0$. Therefore, B and C when factored as (3.9) have symmetric positive-definite left common factor, and by Theorem 3.2 the system (1.1) is symmetrizable.

By Theorem 4.1, in order to check symmetrizability of the system (1.1), we first compute $W = V^{-1}U$, and then R in (3.14). Then we determine the null space of R. The system (1.1) is symmetrizable if and only if the null space of R contains a positive vector. The null space of a matrix can be obtained conveniently by using the singular value decomposition (SVD) (see, e.g., Noble and Daniel, 1977) of the matrix.

When the system (1.1) is symmetrizable, $UDU^T = V\Delta V^T>0$, and we can apply the change of coordinates $x(t) = Tq(t)$, $t\geq 0$, with

$$T = (V\Delta V^T)^{1/2}, \tag{3.15}$$

to (3.2), in order to have a system equation such as (1.3) with symmetric coefficient matrices.

So far we have only considered Case (*i*), with B and C possessing positive-definite left common factor. Of course, B and C may have positive-definite right common factor instead, and there are also Cases (*ii*) and (*iii*); all these possibilities are studied by Shahruz (1987). Considering all the possible cases we conclude that, so long as symmetrizability of the system (1.1) is concerned, we only need to check if the matrix R satisfies the condition in Theorem 4.1.

4 Example

Let the matrices B and C for the system (1.1) be

$$B = \begin{bmatrix} 9 & -7 & 6 \\ 16 & -12 & 8.5 \\ 16 & -12 & 8 \end{bmatrix}, \quad C = \begin{bmatrix} 1 & 1 & 0 \\ 0 & 2 & 1 \\ 0 & 0 & 3 \end{bmatrix}. \tag{4.1}$$

The matrices B and C have distinct eigenvalues and, hence, are symmetrizable. For this example $BC \neq CB$. We compute Λ_B, Λ_C, U, V, $W = V^{-1}U$, and

$$R = \begin{bmatrix} 0.4344 & 0.0551 & -26.8421 \\ 3.0275 & -0.1159 & -3.6610 \\ 1.2963 & -0.0855 & 11.5903 \end{bmatrix}, \tag{4.2}$$

where R is computed using (3.14). We determine the singular value decomposition of R. It turns out that one singular value of R, namely $\sigma_{33} = 0$. Therefore, the null space of R is one-dimensional, and the singular vector $y_3 = [0.2971 \quad 7.1448 \quad 0.0195]^T$. Since y_3 is a positive vector, by Theorem 4.1, the system (1.1) is symmetrizable. We have $D = \mathrm{diag}\,(0.2971, 7.1448, 0.0195)$ and $\Delta = \mathrm{diag}\,(1, 2, 4)$, where Δ is obtained via (3.12*a*). Using D and Δ in (3.9), we obtain the left common factor of B and C,

$$B_l = C_l = \begin{bmatrix} 7 & 10 & 8 \\ 10 & 18 & 16 \\ 8 & 16 & 16 \end{bmatrix}, \tag{4.3}$$

which is symmetric and positive definite; the right factors of B and C are symmetric.

5 Conclusions

In this note, we considered second-order systems with asymmetric coefficient matrices. We gave conditions for symmetrizability of these systems. Furthermore, we determined the appropriate change of coordinates by which the system can be transformed to a symmetric representation. We comment that asymmetric systems are seldom symmetrizable. However, it is important to have criteria for determining symmetrizability of such systems and an effective procedure for symmetrizing symmetrizable systems.

Acknowledgment

This research has been supported in part by the National Science Foundation under Grant No. MSM-8657619. Opinions, findings, and conclusions expressed in this paper are those of the authors and do not reflect the views of the National Science Foundation.

References

Ahmadian, M., and Chou, S.-H., 1987, "A New Method for Finding Symmetric Form of Asymmetric Finite-Dimensional Dynamic Systems," ASME Journal of Applied Mechanics, Vol. 54, pp. 700–750.

Bishop, R. E. D., and Price, W. G., 1979, "An Investigation into the Linear Theory of Ship Response to Waves," *J. of Sound and Vibration*, Vol. 62, pp. 353–363.

Fawzy, I., and Bishop, R. E. D., 1977, "On the Nature of Resonance in Non-Conservative Systems," *J. of Sound and Vibration*, Vol. 55, pp. 475–485.

Gantmacher, F. R., 1959, *The Theory of Matrices*, Vol. 1, Chelsea, New York.

Horn, R. A., and Johnson, C. R., 1985, *Matrix Analysis*, Cambridge University Press, Cambridge.

Inman, D. J., 1983, "Dynamics of Asymmetric Nonconservative Systems," ASME Journal of Applied Mechanics, Vol. 50, pp. 199–203.

Noble, B., and Daniel, J. W., 1977, *Applied Linear Algebra*, 2nd ed., Prentice-Hall, Inc., New Jersey.

Parlett, B. N., 1980, *The Symmetric Eigenvalue Problem*, Prentice-Hall, New Jersey.

Shahruz, S. M., 1987, "Symmetrizability of Asymmetric Nonconservative Systems," Master's Thesis, University of California, Berkeley.

Taussky, O., 1968, "Positive Definite Matrices and Their Role in the Study of the Characteristic Roots of General Matrices," *Advances in Mathematics*, Vol. 2, pp. 175–186.

Wahed, I. F. A., and Bishop, R. E. D., 1976, "On the Equations Governing the Free and Forced Vibrations of a General Non-Conservative System," *J. Mech. Engr. Science*, Vol. 18, pp. 6–10.

Remarks on the Potential Cross Flow Over Tube Banks

Y. B. Suh[3], S. Somasundaram[3], and N. K. Anand[3]

Nomenclature

d = diameter of tube
f = function appearing in equation (2)
β = semimajor axis of oval
N = number of rows
Nu = Nusselt number
k,l,m,n = summation indices
Re,Im = real and imaginary parts
Pr = Prandtl number
$S(z)$ = function defined in equation (3)
s = spacing between tubes
s_L = longitudinal spacing

[3]Mechanical Engineering Department, Texas A&M University, College Station, Tex. 77843.

Manuscript received by the ASME Applied Mechanics Division, March 25, 1988; final revision, September 26, 1988.

is similar to that given by Ahmadian and Chou (1987), however, we have arrived at this result by an entirely different approach. In the following, a positive vector means a vector whose elements are all positive.

Theorem 4.1. The system (1.1) is symmetrizable if and only if there exists a positive vector in the null space of the matrix R given in (3.14).

Proof. Two nonzero diagonal matrices $D = \text{diag}(d_1, \ldots, d_n)$ and Δ satisfy (3.10) if and only if d in (3.13) is a nonzero vector. A nonzero vector satisfies (3.13) if and only if rank $R<n$. Suppose that rank $R<n$, then a nonzero d is in the null space of R. Since W is nonsingular, $WDW^T>0$ if and only if $D>0$. The matrix $D>0$, if and only if d is a positive vector. Having $WDW^T>0$, then $UDU^T>0$ and $V\Delta V^T>0$. Therefore, B and C when factored as (3.9) have symmetric positive-definite left common factor, and by Theorem 3.2 the system (1.1) is symmetrizable.

By Theorem 4.1, in order to check symmetrizability of the system (1.1), we first compute $W = V^{-1}U$, and then R in (3.14). Then we determine the null space of R. The system (1.1) is symmetrizable if and only if the null space of R contains a positive vector. The null space of a matrix can be obtained conveniently by using the singular value decomposition (SVD) (see, e.g., Noble and Daniel, 1977) of the matrix.

When the system (1.1) is symmetrizable, $UDU^T = V\Delta V^T>0$, and we can apply the change of coordinates $x(t) = Tq(t)$, $t \geq 0$, with

$$T = (V\Delta V^T)^{1/2}, \tag{3.15}$$

to (3.2), in order to have a system equation such as (1.3) with symmetric coefficient matrices.

So far we have only considered Case (*i*), with B and C possessing positive-definite left common factor. Of course, B and C may have positive-definite right common factor instead, and there are also Cases (*ii*) and (*iii*); all these possibilities are studied by Shahruz (1987). Considering all the possible cases we conclude that, so long as symmetrizability of the system (1.1) is concerned, we only need to check if the matrix R satisfies the condition in Theorem 4.1.

4 Example

Let the matrices B and C for the system (1.1) be

$$B = \begin{bmatrix} 9 & -7 & 6 \\ 16 & -12 & 8.5 \\ 16 & -12 & 8 \end{bmatrix}, \quad C = \begin{bmatrix} 1 & 1 & 0 \\ 0 & 2 & 1 \\ 0 & 0 & 3 \end{bmatrix}. \tag{4.1}$$

The matrices B and C have distinct eigenvalues and, hence, are symmetrizable. For this example $BC \neq CB$. We compute Λ_B, Λ_C, U, V, $W = V^{-1}U$, and

$$R = \begin{bmatrix} 0.4344 & 0.0551 & -26.8421 \\ 3.0275 & -0.1159 & -3.6610 \\ 1.2963 & -0.0855 & 11.5903 \end{bmatrix}, \tag{4.2}$$

where R is computed using (3.14). We determine the singular value decomposition of R. It turns out that one singular value of R, namely $\sigma_{33} = 0$. Therefore, the null space of R is one-dimensional, and the singular vector $y_3 = [0.2971 \quad 7.1448 \quad 0.0195]^T$. Since y_3 is a positive vector, by Theorem 4.1, the system (1.1) is symmetrizable. We have $D = \text{diag}(0.2971, 7.1448, 0.0195)$ and $\Delta = \text{diag}(1, 2, 4)$, where Δ is obtained via (3.12*a*). Using D and Δ in (3.9), we obtain the left common factor of B and C,

$$B_l = C_l = \begin{bmatrix} 7 & 10 & 8 \\ 10 & 18 & 16 \\ 8 & 16 & 16 \end{bmatrix}, \tag{4.3}$$

which is symmetric and positive definite; the right factors of B and C are symmetric.

5 Conclusions

In this note, we considered second-order systems with asymmetric coefficient matrices. We gave conditions for symmetrizability of these systems. Furthermore, we determined the appropriate change of coordinates by which the system can be transformed to a symmetric representation. We comment that asymmetric systems are seldom symmetrizable. However, it is important to have criteria for determining symmetrizability of such systems and an effective procedure for symmetrizing symmetrizable systems.

Acknowledgment

This research has been supported in part by the National Science Foundation under Grant No. MSM-8657619. Opinions, findings, and conclusions expressed in this paper are those of the authors and do not reflect the views of the National Science Foundation.

References

Ahmadian, M., and Chou, S.-H., 1987, "A New Method for Finding Symmetric Form of Asymmetric Finite-Dimensional Dynamic Systems," ASME Journal of Applied Mechanics, Vol. 54, pp. 700–750.

Bishop, R. E. D., and Price, W. G., 1979, "An Investigation into the Linear Theory of Ship Response to Waves," *J. of Sound and Vibration*, Vol. 62, pp. 353–363.

Fawzy, I., and Bishop, R. E. D., 1977, "On the Nature of Resonance in Non-Conservative Systems," *J. of Sound and Vibration*, Vol. 55, pp. 475–485.

Gantmacher, F. R., 1959, *The Theory of Matrices*, Vol. 1, Chelsea, New York.

Horn, R. A., and Johnson, C. R., 1985, *Matrix Analysis*, Cambridge University Press, Cambridge.

Inman, D. J., 1983, "Dynamics of Asymmetric Nonconservative Systems," ASME Journal of Applied Mechanics, Vol. 50, pp. 199–203.

Noble, B., and Daniel, J. W., 1977, *Applied Linear Algebra*, 2nd ed., Prentice-Hall, Inc., New Jersey.

Parlett, B. N., 1980, *The Symmetric Eigenvalue Problem*, Prentice-Hall, New Jersey.

Shahruz, S. M., 1987, "Symmetrizability of Asymmetric Nonconservative Systems," Master's Thesis, University of California, Berkeley.

Taussky, O., 1968, "Positive Definite Matrices and Their Role in the Study of the Characteristic Roots of General Matrices," *Advances in Mathematics*, Vol. 2, pp. 175–186.

Wahed, I. F. A., and Bishop, R. E. D., 1976, "On the Equations Governing the Free and Forced Vibrations of a General Non-Conservative System," *J. Mech. Engr. Science*, Vol. 18, pp. 6–10.

Remarks on the Potential Cross Flow Over Tube Banks

Y. B. Suh[3], S. Somasundaram[3], and N. K. Anand[3]

Nomenclature

d = diameter of tube
f = function appearing in equation (2)
β = semimajor axis of oval
N = number of rows
Nu = Nusselt number
k,l,m,n = summation indices
Re,Im = real and imaginary parts
Pr = Prandtl number
$S(z)$ = function defined in equation (3)
s = spacing between tubes
s_L = longitudinal spacing

[3]Mechanical Engineering Department, Texas A&M University, College Station, Tex. 77843.

Manuscript received by the ASME Applied Mechanics Division, March 25, 1988; final revision, September 26, 1988.

s_T = transverse spacing
$T(z)$ = function defined in equation (8)
U_∞ = onset flow
q = magnitude of velocity
x,y = cartesian coordinates
z,ζ = complex variables
μ = doublet strength
ν = kinematic viscosity
u,v = velocity components in x and y directions
W = complex potential
W' = complex velocity

Introduction

The cross flow over tube banks is important in numerous industrial applications, such as steam generation in a boiler, or air cooling in the coil of an air conditioner, especially in conjunction with heat transfer (Zhukauskas, 1972). In this note, analytical expressions have been derived for velocity fields in an incompressible flow over an array of tube banks. The dependence of the potential flow field (or equivalently, the pressure field) on the transverse and longitudinal spacings of aligned and staggered tube banks is also demonstrated. We first consider a row of ovals. The situation is depicted in Fig. 1(a), which shows the semimajor axis of the oval to be β. The potential flow field for this can be easily generated by a row of doublets with strength, μ, aligned with the free stream, U_∞ (Fig. 1(b)). The complex potential for this combination is given by:

$$W(z) = -\sum_{n=-\infty}^{\infty} \frac{\mu}{2\pi(z-ins_T)} + U_\infty z, \text{ where } z = x+iy \qquad (1)$$

Reviewing the long established formula from the complex variable theory (for instance, Morse and Feshbach 1953), we have

$$\sum_{-\infty}^{\infty} f(n) = -\sum_{\text{poles}} \text{Res}[\pi\cot\pi\zeta f(\zeta)],$$

$$\zeta = \text{complex variable.} \qquad (2)$$

Equation (1) may be rewritten as:

$$W(z) = -\frac{\mu}{2\pi} S(z) + U_\infty z,$$

$$\text{where } S(z) \equiv \sum_{-\infty}^{\infty} \frac{1}{z - is_T n}. \qquad (3)$$

The formula (2) is utilized to obtain the series $S(z)$ as follows:

$$S(z) \equiv \sum_{n=-\infty}^{\infty} \frac{1}{z-is_T n} = -\sum_{\text{poles}} \text{Res}\left[\pi \cot\pi\zeta \frac{1}{z - is_T\zeta}\right]$$

$$= -\left(\frac{\pi}{s_T}\coth\frac{\pi}{s_T}z + \sum_{-\infty}^{\infty}\frac{1}{z-is_T k}\right).$$

Here the poles are at $\zeta = -iz/s_T$ and $k = 0, \pm 1, \pm 2, \ldots$. The last term is nothing but $S(z)$ itself, and therefore,

$$S(z) = -\frac{\pi}{2s_T}\coth(\pi z/s_T).$$

Combining this with equation (3), we arrive at

$$W(z) = U_\infty\left[\frac{\mu}{4s_T U_\infty}\coth(\pi z/s_T) + z\right]$$

so that

$$W'(z) = u - iv = \left[1 - \frac{\mu\pi}{4s_T^2 U_\infty \sinh^2(\pi z/s_T)}\right] U_\infty$$

where $u = Re(W'(z))$ and $v = -Im(W'(z))$. The stagnation points are $z = \pm\beta$, namely $W'(\pm\beta) = 0$. This latter condition yields $\beta = s_T/\pi \sinh^{-1}(\mu\pi/4s_T^2 U_\infty)^{1/2}$ with which we can eliminate the parameter, μ. Finally, we arrive at:

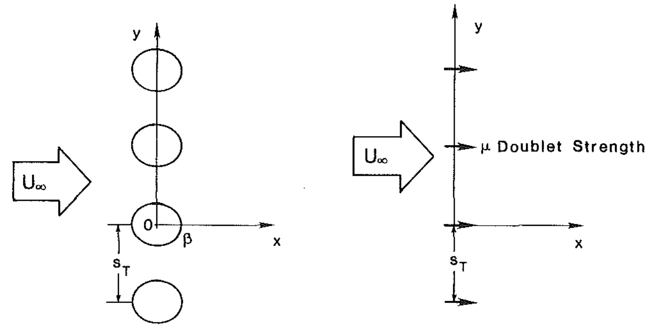

Fig. 1 Row of ovals and doublets

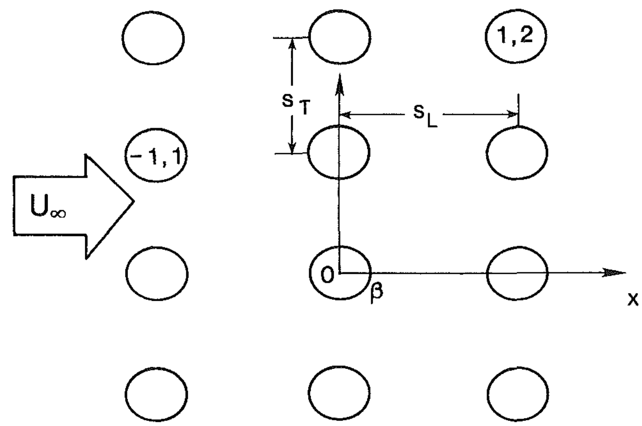

Fig. 2 Aligned oval bank

$$W(z) = U_\infty\left[\frac{s_T}{\pi}\sinh^2(\pi\beta/s_T)\coth(\pi z/s_T) + z\right] \qquad (4)$$

and

$$W'(z) = U_\infty\left[1 - \frac{\sinh^2(\pi\beta/s_T)}{\sinh^2(\pi z/s_T)}\right]. \qquad (5)$$

The complex potential used by Gostelow (1963, 1984) in his study of cascade airfoils can be obtained as a special case of equation (4), i.e., for $s_T = \pi$.

Aligned Tube Bank

The potential cross flow over an aligned tube bank is merely an extension of the foregoing analysis in the streamwise direction. The geometry is shown in Fig. 2. The complex potential of this flow field should be:

$$W(z) = -\sum_{m,n=-\infty}^{\infty} \frac{\mu}{2\pi(z - ms_L - ins_T)} + U_\infty z$$

$$= -\frac{\mu}{2\pi}\sum_{m=-\infty}^{\infty} S(z - ms_L) + U_\infty z$$

$$= \frac{\mu}{4s_T}\sum_{-\infty}^{\infty}\coth\frac{\pi(z-ms_L)}{s_T} + U_\infty z. \qquad (6)$$

The numbering scheme (m,n) is also shown in Fig. 2. Define $T(z)$ as:

$$T(z) \equiv \sum_{-\infty}^{\infty}\coth\frac{\pi(z-ms_L)}{s_T}. \qquad (7)$$

Using equation (2), $T(z)$ can be written as

$$T(z) = -\sum_{\text{poles}}\text{Res}\left[\pi\cot\pi\zeta\coth\frac{\pi(z-\zeta s_L)}{s_T}\right]. \qquad (8)$$

Poles are at $\zeta = l$ $(l = 0, \pm 1, \pm 2, \ldots)$ and $\zeta = z/s_L$. It is readily found that

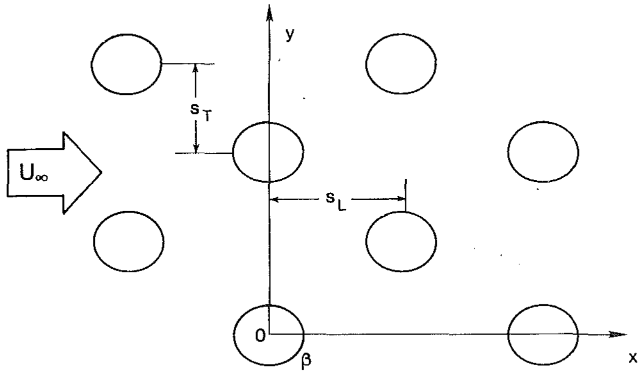

Fig. 3 Staggered oval bank

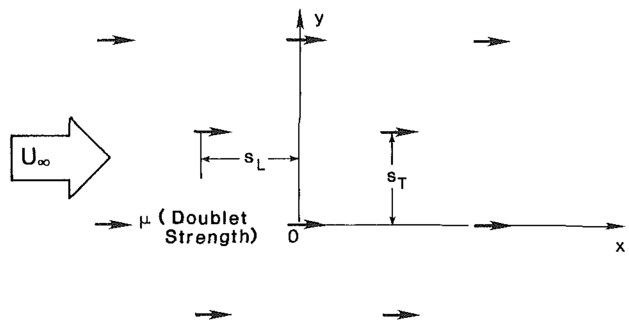

Fig. 4 Distribution of doublets corresponding to Fig. 3

$$T(z) = -\left[\sum_{-\infty}^{\infty} \coth \frac{\pi(z - ls_L)}{s_T} - \frac{s_T}{s_L} \cot \pi z/s_L\right].$$

Since the first term is $T(z)$ itself, we obtain the following expression for $T(z)$:

$$T(z) = (s_T/2s_L)\cot \pi z/s_L.$$

Substituting this expression into equation (7) gives

$$W(z) = \frac{\mu}{8s_L} \cot \frac{\pi z}{s_L} + U_\infty z$$

and

$$W'(z) = \frac{-\mu\pi}{8s_L^2 \sin^2 \pi z/s_L} + U_\infty$$

$$W'(\pm\beta) = 0 \text{ yields } \frac{\mu\pi}{8s_L^2 U_\infty} = \sin^2 \frac{\pi\beta}{s_L}.$$

Expressing μ in terms of β, we get:

$$W(z) = U_\infty \left[\frac{s_L}{\pi} \sin^2 \frac{\pi\beta}{s_L} \cot \frac{\pi z}{s_L} + z\right] \tag{9}$$

and

$$W'(z) = u - iv = U_\infty \left[1 - \frac{\sin^2 \pi\beta/s_L}{\sin^2 \pi z/s_L}\right]. \tag{10}$$

It is interesting to see the similarity between equations (4), (5) and equations (9), (10), respectively. Another interesting observation is that the potential flow field has no dependence on the transverse spacing, s_T, when the number of rows becomes infinite.

Staggered Tube Bank

The staggered tube bank is depicted in Fig. 3 and singularities representing the tubes are shown in Fig. 4. The complex potential for this flow field can be obtained from the preceding result for the cross flow over an aligned tube bank by the following replacements in equation (9):

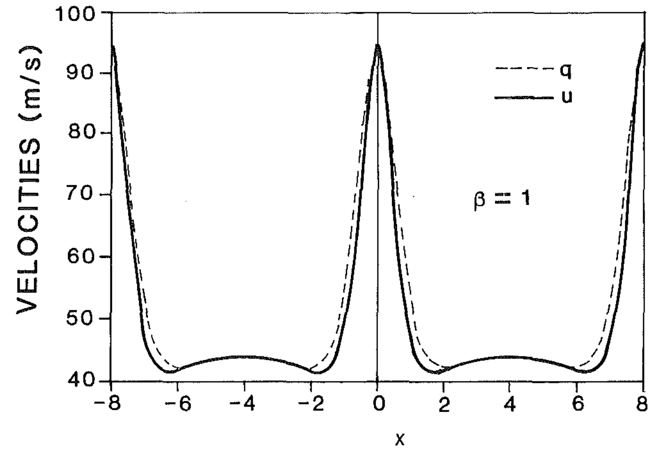

Fig. 5 Velocity fields at $y=1$ for the aligned tube bank; $s_L = 8\beta$ and $U_\infty = 50$ m/s

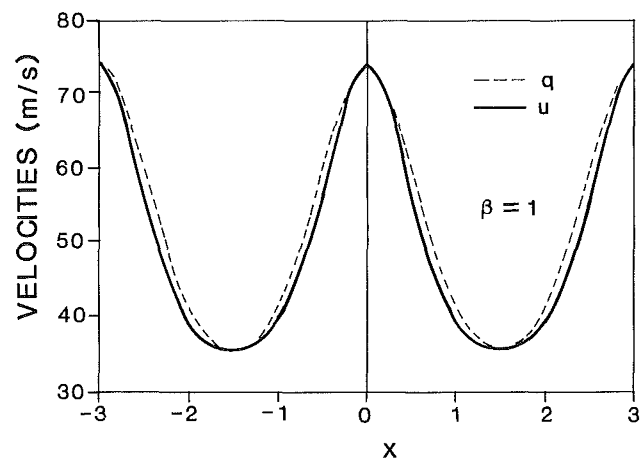

Fig. 6 Velocity fields at $y=1$ for the aligned tube bank; $s_L = 3\beta$ and $U_\infty = 50$ m/s

s_L by $2s_L$,

s_T by $2s_T$,

z by $z + c$, where $c = -(s_L + is_T)$.

This yields

$$W(z) = U_\infty\left\{\frac{2s_L}{\pi} \sin^2 \frac{\pi\beta}{2s_L}\left[\cot \frac{\pi z}{2s_L} + \cot \frac{\pi[z - (s_L + is_T)]}{2s_L}\right] + z\right\} \tag{11}$$

and

$$W'(z) = u - iv = U_\infty\left\{1 - \sin^2 \frac{\pi\beta}{2s_L}\left[\csc^2 \frac{\pi z}{2s_L} + \csc^2 \frac{\pi}{2s_L}[z - (s_L + is_T)]\right]\right\}. \tag{12}$$

Results and Discussion

The results for the velocity fields in an inviscid flow over both aligned and staggered tube banks were obtained from the aforementioned expressions. Figures 5 and 6 show the magnitudes of the absolute velocity, $q = (u^2 + v^2)^{1/2}$, as well as the streamwise component, u, for the aligned tube bank case. The flow field has a periodicity in s_L as should be the case. The flow field for the staggered tube bank, on the other hand, has

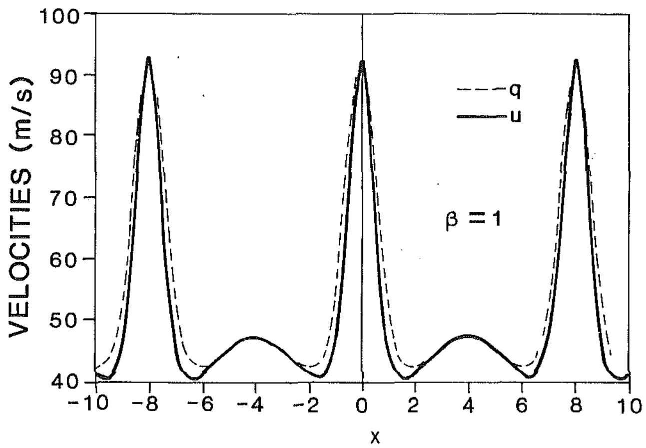

Fig. 7 Velocity fields at $y=1$ for the staggered tube bank; $s_L = s_T = 4\beta$

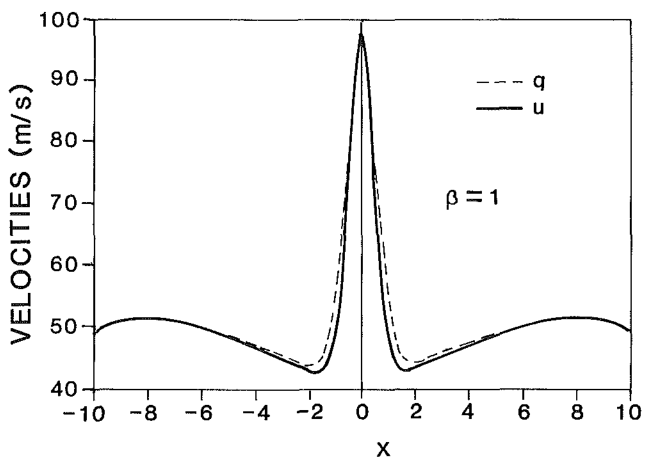

Fig. 8 Velocity fields at $y=1$ for the staggered tube bank; $s_L = 8\beta$ and $s_T = 5\beta$

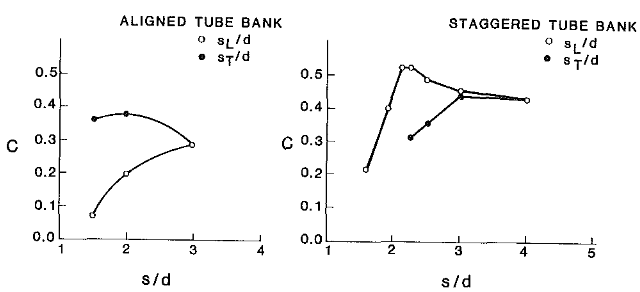

Fig. 9 Strong dependence of C on s_L for aligned and staggered tube banks

a weak dependence on the transverse spacing, s_T, compared with the dependence on s_L. This dependence on s_T is physically feasible since the flow field should have some dependence on the protuberances. The variation of the absolute velocity, q, and u are shown in Figs. 7 and 8, which clearly show the periodicity in $2s_L$. Grimison (1937) gives the following heat transfer correlation:

$$\overline{\mathrm{Nu}_D} = 1.13\ C Re^m_{d,\max} \mathrm{Pr}^{1/3} \begin{bmatrix} N \geq 10 \\ 2000 < Re_{d,\max} < 40{,}000 \\ \mathrm{Pr} \geq 0.7 \end{bmatrix} \tag{13}$$

where $Re_{d,\max} = U_{\max} d/\nu$ and N is the number of rows in the tube bank and $U_{\max}$ is the maximum velocity within the tube bank. All the properties for the previous correlation are evaluated at the film temperature. The constants C and m are tabulated in (Grimison 1937). Figure 9 illustrates the dependence of C on $s_{L(T)}$ parameters (for $s_{T(L)} = 3d$). As can be seen, the s_L-dependence dominates over the s_T-dependence, especially for the aligned tube banks. In actuality the viscosity effect, such as boundary layer separation and wake interactions, have to be considered in the flow field. Using the expressions for u and v given by equations (10) and (12), the pressure gradient along the tube contour can be evaluated.

Acknowledgment

Financial support for (YBS) from the Center for Energy and Mineral Resources (CEMR), Texas A&M University, is gratefully acknowledged. We would also like to thank the reviewers for their very useful comments.

References

Gostelow, J. P., 1963, "Potential Flow Through Cascades: A Comparison Between Exact and Approximate Solutions," ARC CP 807.

Gostelow, J. P., 1984, *Cascade Aerodynamics*, Pergamon Press, p. 99.

Grimison, E. D., 1937, "Correlation and Utilization of New Data on Flow Resistance and Heat Transfer for Cross Flow of Gases Over Tube Banks," *ASME Transactions*, Vol. 59, pp. 583–594.

Morse, P. M., and Feshback, H., 1953, *Methods of Theoretical Physics*, Part I, McGraw-Hill, New York, pp. 413–414.

Zhukauskas, A., 1972, "Heat Transfer from Tubes in Cross Flow," *Advances in Heat Transfer*, Vol. 8, Academic Press, pp. 93–160.

Linear Elastic Materials Sustaining a Prescribed Deformation

S. A. Silling[4]

Suppose that B is a body and $\mathbf{u}$ is a twice continuously differentiable displacement field on B. This paper concerns the following questions: Is there a linear elastic material such that $\mathbf{u}$ satisfies the equilibrium equation in the absence of body forces if B is homogeneous and composed of this material? If so, what is the totality of all such materials? If there is such a material, then the material will be said to *sustain* the deformation.

1 Method

It will be assumed that the only eligible materials are characterized by

$$\sigma_{ij} = c_{ijkl}\epsilon_{kl}, \tag{1}$$

$$\epsilon_{ij} = \frac{1}{2}(u_{i,j} + u_{j,i}), \tag{2}$$

$$c_{ijkl} = c_{jikl} = c_{ijlk} = c_{klij}. \tag{3}$$

Under the assumption that the symmetries in equation (3) hold, it is well known that there are at most 21 independent elastic constants. These will be referred to using the Voigt notation: $C_{11} = c_{1111}$, $C_{12} = c_{1122}$, $C_{13} = c_{1133}$, $C_{14} = c_{1123}$, $C_{15} = c_{1131}$, $C_{16} = c_{1112}$, $C_{21} = c_{2211}$, . . . , C_{66}, $= c_{1212}$. By (3), $C_{IJ} = C_{JI}$, $I = 1, \ldots, 6$, $J = 1, \ldots, 6$.

In the absence of body forces, the equilibrium equation is

$$\sigma_{ij,j} = 0. \tag{4}$$

[4]Division of Engineering, Brown University, Providence, R.I., 02912. Assoc. Mem. ASME.

Manuscript received by the ASME Applied Mechanics Division, April 11, 1988; final revision, November 9, 1988.

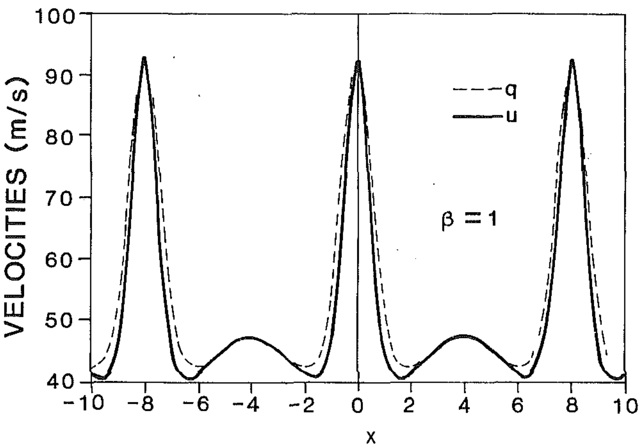

Fig. 7 Velocity fields at $y=1$ for the staggered tube bank; $s_L=s_T=4\beta$

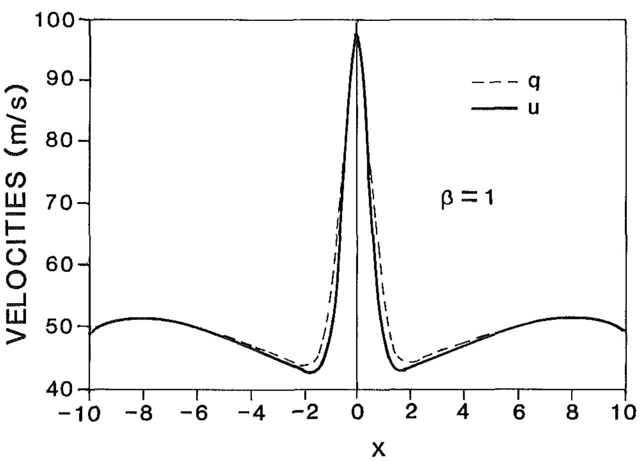

Fig. 8 Velocity fields at $y=1$ for the staggered tube bank; $s_L=8\beta$ and $s_T=5\beta$

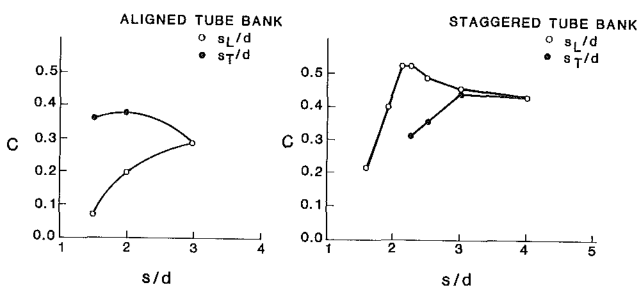

Fig. 9 Strong dependence of C on s_L for aligned and staggered tube banks

a weak dependence on the transverse spacing, s_T, compared with the dependence on s_L. This dependence on s_T is physically feasible since the flow field should have some dependence on the protuberances. The variation of the absolute velocity, q, and u are shown in Figs. 7 and 8, which clearly show the periodicity in $2s_L$. Grimison (1937) gives the following heat transfer correlation:

$$\overline{\mathrm{Nu}_D}=1.13\ CRe^{m}_{d,\max}\mathrm{Pr}^{1/3}\begin{bmatrix} N\geq 10 \\ 2000<Re_{d,\max}<40{,}000 \\ \mathrm{Pr}\geq 0.7 \end{bmatrix} \tag{13}$$

where $Re_{d,\max}=U_{\max}d/\nu$ and N is the number of rows in the tube bank and $U_{\max}$ is the maximum velocity within the tube bank. All the properties for the previous correlation are evaluated at the film temperature. The constants C and m are tabulated in (Grimison 1937). Figure 9 illustrates the dependence of C on $s_{L(T)}$ parameters (for $s_{T(L)}=3d$). As can be seen, the s_L-dependence dominates over the s_T-dependence, especially for the aligned tube banks. In actuality the viscosity effect, such as boundary layer separation and wake interactions, have to be considered in the flow field. Using the expressions for u and v given by equations (10) and (12), the pressure gradient along the tube contour can be evaluated.

Acknowledgment

Financial support for (YBS) from the Center for Energy and Mineral Resources (CEMR), Texas A&M University, is gratefully acknowledged. We would also like to thank the reviewers for their very useful comments.

References

Gostelow, J. P., 1963, "Potential Flow Through Cascades: A Comparison Between Exact and Approximate Solutions," ARC CP 807.

Gostelow, J. P., 1984, *Cascade Aerodynamics*, Pergamon Press, p. 99.

Grimison, E. D., 1937, "Correlation and Utilization of New Data on Flow Resistance and Heat Transfer for Cross Flow of Gases Over Tube Banks," *ASME Transactions*, Vol. 59, pp. 583–594.

Morse, P. M., and Feshback, H., 1953, *Methods of Theoretical Physics*, Part I, McGraw-Hill, New York, pp. 413–414.

Zhukauskas, A., 1972, "Heat Transfer from Tubes in Cross Flow," *Advances in Heat Transfer*, Vol. 8, Academic Press, pp. 93–160.

Linear Elastic Materials Sustaining a Prescribed Deformation

S. A. Silling[4]

Suppose that B is a body and $\mathbf{u}$ is a twice continuously differentiable displacement field on B. This paper concerns the following questions: Is there a linear elastic material such that $\mathbf{u}$ satisfies the equilibrium equation in the absence of body forces if B is homogeneous and composed of this material? If so, what is the totality of all such materials? If there is such a material, then the material will be said to *sustain* the deformation.

1 Method

It will be assumed that the only eligible materials are characterized by

$$\sigma_{ij}=c_{ijkl}\epsilon_{kl}, \tag{1}$$

$$\epsilon_{ij}=\frac{1}{2}(u_{i,j}+u_{j,i}), \tag{2}$$

$$c_{ijkl}=c_{jikl}=c_{ijlk}=c_{klij}. \tag{3}$$

Under the assumption that the symmetries in equation (3) hold, it is well known that there are at most 21 independent elastic constants. These will be referred to using the Voigt notation: $C_{11}=c_{1111}$, $C_{12}=c_{1122}$, $C_{13}=c_{1133}$, $C_{14}=c_{1123}$, $C_{15}=c_{1131}$, $C_{16}=c_{1112}$, $C_{21}=c_{2211}$, . . . , C_{66}, $=c_{1212}$. By (3), $C_{IJ}=C_{JI}$, $I=1,\ldots,6$, $J=1,\ldots,6$.

In the absence of body forces, the equilibrium equation is

$$\sigma_{ij,j}=0. \tag{4}$$

[4]Division of Engineering, Brown University, Providence, R.I., 02912. Assoc. Mem. ASME.

Manuscript received by the ASME Applied Mechanics Division, April 11, 1988; final revision, November 9, 1988.

In terms of the 21 elastic constants for a homogenous body, the $i = 1$ equation is

$$C_{11}N_{111}+C_{12}N_{221}+C_{13}N_{331}+2C_{14}N_{231}+2C_{15}N_{311}$$
$$+2C_{16}N_{121}+C_{61}N_{112}+C_{62}N_{222}+C_{63}N_{332}+2C_{64}N_{232}$$
$$+2C_{65}N_{312}+2C_{66}N_{122}+C_{51}N_{113}+C_{52}N_{223}+C_{53}N_{333}$$
$$+2C_{54}N_{233}+2C_{55}N_{313}+2C_{56}N_{123}=0 \qquad (5)$$

for all points in the region, where N_{ijk} are the components of the tensor field of order 3 defined by $N_{ijk}=\epsilon_{ij,k}$. Similar forms of the equilibrium equation hold for $i=2, 3$. Since $\mathbf{u}$ is given everywhere in the region, the N_{ijk} are known. For fixed $\mathbf{x}$, the three equations of the form (5) comprise a homogeneous linear algebraic system in the 21 unknowns, $C_{11}, \ldots, C_{66}$. This system may be written as

$$[E(\mathbf{x})]\mathbf{C}=\mathbf{0} \qquad (6)$$

where $[E(\mathbf{x})]$ is the 3×21 matrix of coefficients from the system and $\mathbf{C}=\mathrm{col}(C_{11}, C_{12}, \ldots, C_{66})$. Let R^{21} denote the 21-dimensional vector space consisting of column vectors of 21 real numbers. Let an orthonormal basis for R^{21} be given by $\mathbf{e}_{11} = \mathrm{col}(1, 0, 0, \ldots, 0), \ldots, \mathbf{e}_{66} = \mathrm{col}(0, 0, 0, \ldots, 1)$ where the basis vectors are labeled according to the Voigt notation.

Let Z be the set of all vectors $\mathbf{C}$ which satisfy (6) for all $\mathbf{x}$. Thus Z consists of the moduli of all materials which sustain the deformation. If we choose any two vectors in Z, then any linear combination of these vectors is also in Z since (6) is a linear system. Thus Z is a subspace of R^{21}. The problem may be regarded as that of finding the dimension of Z and finding a basis for Z.

The following describes a method for finding Z for a given deformation. The method relies partially on a numerical method. First, note that if a candidate for Z is given, it is essentially trivial to confirm whether or not each vector in this set sustains the deformation. This is merely a matter of confirming (6) for all $\mathbf{x}$ and for each basis vector in the set. The algorithm is as follows:

Step 0. Choose arbitrarily n points $\mathbf{x}^1, \ldots, \mathbf{x}^n$ in B, where n is any positive integer.

Step 1. Let Z^n be the subspace of R^{21} containing all vectors $\mathbf{C}$ which satisfy (6) at $\mathbf{x}=\mathbf{x}^1, \ldots, \mathbf{x}^n$. In order to find Z^n, form the following linear algebraic system:

$$[A]\mathbf{C}=\mathbf{0}, \quad [A] = \begin{bmatrix} [E(\mathbf{x}^1)] \\ [E(\mathbf{x}^2)] \\ \cdot \\ \cdot \\ \cdot \\ [E(\mathbf{x}^n)] \end{bmatrix}. \qquad (7)$$

$[A]$ is a $3n\times 21$ matrix. Z^n consists of all solutions to (7). All such solutions may be found numerically by the technique known as singular value decomposition (Press et al., 1986). The result of application of this method is the dimension of Z^n and a basis in R^{21} which spans Z^n.

Step 2. Test all basis vectors for Z^n for whether or not they solve (6) for all $\mathbf{x}$. If they do, then the problem is solved, and $Z=Z^n$. If some basis vector fails to solve (6) for some point in B, let $\mathbf{x}^{n+1}$ be any point at which such failure occurs. Replace n by $n+1$ and go back to Step 1.

Note that the dimension of Z^{n+1} must be less than the dimension of Z^n. Therefore the iteration must converge within 21 passes. If $Z^n=\{\mathbf{0}\}$ for some n, then there are no materials which sustain the deformation.

Any positive n may be used to start the iteration, but a great deal of effort is saved by an advantageous choice. Experience has shown that $n\geq 7$ works best, and if the $\mathbf{x}^n$ are chosen at random, convergence is usually obtained on the first pass.

Let $\bar{Z}$ be the orthogonal complement of Z, consisting of all vectors in R^{21} which are orthogonal to every vector in Z. Let L be the dimension of Z and let $\bar{L}$ be the dimension of $\bar{Z}$. Then $\bar{L}=21-L$. Let $\mathbf{C}^{(1)}, \mathbf{C}^{(2)}, \ldots, \mathbf{C}^{(L)}$ be a basis for Z. Every linear combination of these basis vectors represents a material which sustains the deformation. Let $\bar{\mathbf{C}}^{(1)}, \bar{\mathbf{C}}^{(2)}, \ldots, \bar{\mathbf{C}}^{(\bar{L})}$ be a basis for $\bar{Z}$. Note that an interpretation of $\bar{L}$ is that there are $\bar{L}$ restrictions on the moduli of the materials which sustain the deformation. This follows because a material with moduli $\mathbf{C}$ sustains the deformation if and only if $\mathbf{C}\cdot\bar{\mathbf{C}}^{(1)} = \mathbf{C}\cdot\bar{\mathbf{C}}^{(2)} = \ldots = \mathbf{C}\cdot\bar{\mathbf{C}}^{(\bar{L})} = 0$.

2 Homogeneous Deformations

As an application of the above section, assume that $u_i = H_{ij}x_j$ for some nine constants H_{ij}. Then the strain tensor ϵ_{ij} is constant, so $N_{ijk}\equiv 0$. Therefore $[E(\mathbf{x})]=[0]$ for all $\mathbf{x}$. Trivially, in this case $L = 21$, and any homogeneous linear elastic material sustains the deformation. The same result holds for nonlinear elastic materials as well: any compressible material sustains any homogeneous deformation.

The following converse of the last result also holds in both linear and finite elasticity: If a deformation is sustained by every elastic material, then the deformation is homogeneous. This may be proved for linear elasticity by requiring equation (6) to hold for each of the choices $\mathbf{C}=\mathbf{e}_{11}$, $\mathbf{C}=\mathbf{e}_{12}$, $\ldots$, $\mathbf{C}=\mathbf{e}_{66}$. These various choices force each of the N_{ijk} to vanish, proving that the deformation is homogeneous. Related (and stronger) results in finite elasticity were established by Ericksen (1955) and Shield (1971). However, neither the linear nor the nonlinear version is true if one considers only isotropic *incompressible* materials (Ericksen, 1954).

3 Quadratic Deformations

A useful class of deformations consists of those in which each component of displacement is expressible as a quadratic form in $\mathbf{x}$, i.e., $u_i=M_{ijk}x_jx_k$ for some 27 constants M_{ijk}. This means that each component of ϵ_{ij} varies linearly with $\mathbf{x}$. Hence, $N_{ijk}(\mathbf{x})$ and $[E(\mathbf{x})]$ are independent of $\mathbf{x}$ and $L\geq 18$. One such field will now be examined in detail.

Assume that the displacement field is

$$u_1=0,\ u_2=-2Tx_3x_1,\ u_3=2Tx_2x_1, \qquad (8)$$

for all $\mathbf{x}$ in B where T is some nonzero constant. The only nonzero components of N_{ijk} are $N_{123} = N_{213} = -T$, $N_{132} = N_{312} = T$. A field of the form (8) provides a solution to the problem of the torsion of a homogeneous isotropic linear elastic rod of constant circular cross-section.

The analysis just described yields $L=19$ and a basis for Z is provided by

$$\begin{array}{llll} \mathbf{C}^{(1)} = \mathbf{e}_{11} & \mathbf{C}^{(7)} = \mathbf{e}_{22} & \mathbf{C}^{(13)} = \mathbf{e}_{35} & (9) \\ \mathbf{C}^{(2)} = \mathbf{e}_{12} & \mathbf{C}^{(8)} = \mathbf{e}_{23} & \mathbf{C}^{(14)} = \mathbf{e}_{44} & \\ \mathbf{C}^{(3)} = \mathbf{e}_{13} & \mathbf{C}^{(9)} = \mathbf{e}_{24} & \mathbf{C}^{(15)} = \mathbf{e}_{55} & \\ \mathbf{C}^{(4)} = \mathbf{e}_{14} & \mathbf{C}^{(10)} = \mathbf{e}_{26} & \mathbf{C}^{(16)} = \mathbf{e}_{56} & \\ \mathbf{C}^{(5)} = \mathbf{e}_{15} & \mathbf{C}^{(11)} = \mathbf{e}_{33} & \mathbf{C}^{(17)} = \mathbf{e}_{66} & \\ \mathbf{C}^{(6)} = \mathbf{e}_{16} & \mathbf{C}^{(12)} = \mathbf{e}_{34} & \mathbf{C}^{(18)} = \mathbf{e}_{25}+\mathbf{e}_{46} & \end{array}$$

$$\mathbf{C}^{(19)}=\mathbf{e}_{36}+\mathbf{e}_{45}.$$

Also $\bar{L}=2$ and a basis for $\bar{Z}$ is

$$\bar{\mathbf{C}}^{(1)}=\mathbf{e}_{25}-\mathbf{e}_{46} \quad \bar{\mathbf{C}}^{(2)}=\mathbf{e}_{36}-\mathbf{e}_{45}. \tag{10}$$

Thus, the only restrictions on the material properties are $C_{25}=C_{46}$ and $C_{36}=C_{45}$. For anisotropic materials, this displacement field does not, in general, solve the torsion problem for a circular rod, because the traction-free condition on the lateral surface may not be satisfied.

4 Arbitrary Radial Deformations

Suppose that there is some spherical coordinate system in which a deformation is described by $u_r(r, \theta, \phi)=f(r)$, $u_\theta \equiv u_\phi \equiv 0$, where f is a smooth function. In rectangular coordinates, this is $u_i=f(r)x_i/r$, $r=|\mathbf{x}|$. One finds

$$N_{ijk}=r^{-3}(rf'(r)-f(r))(x_i\delta_{jk}+x_j\delta_{ki}+x_k\delta_{ij}) + r^{-5}(r^2f''(r)-3rf'(r)+3f(r))x_ix_jx_k, \quad r>0. \tag{11}$$

There are two special cases. First, the case $f(r)=\alpha r$, where α is a constant, is a homogeneous deformation. Hence $L=21$ and there are no restrictions on the moduli. The second is $f(r)=\alpha r^{-2}$, which will be discussed next.

After carrying out the analysis for an arbitrary f other than these special cases one finds that $L=6$ and a basis for Z is given by

$$\begin{array}{lll} \mathbf{C}^{(1)}=2\mathbf{e}_{12}-\mathbf{e}_{66} & \mathbf{C}^{(3)}=2\mathbf{e}_{23}-\mathbf{e}_{44} & \mathbf{C}^{(5)}=2\mathbf{e}_{25}-\mathbf{e}_{46} \\ \mathbf{C}^{(2)}=2\mathbf{e}_{13}-\mathbf{e}_{55} & \mathbf{C}^{(4)}=2\mathbf{e}_{14}-\mathbf{e}_{56} & \mathbf{C}^{(6)}=2\mathbf{e}_{36}-\mathbf{e}_{45}. \end{array} \tag{12}$$

The equilibrated stress fields arising from the deformation of the materials in this Z are by no means trivial, nor are they radially symmetric. It is perhaps surprising that there are *any* materials which can sustain an arbitrary radial deformation.

For the special case $f(r)=\alpha r^{-2}$, $\alpha \neq 0$, one finds $L=7$ and the basis for Z given in (12) is augmented by

$$\mathbf{C}^{(7)}=5(\mathbf{e}_{11}+\mathbf{e}_{22}+\mathbf{e}_{33})+2(\mathbf{e}_{44}+\mathbf{e}_{55}+\mathbf{e}_{66})+\mathbf{e}_{12}+\mathbf{e}_{23}+\mathbf{e}_{13}. \tag{13}$$

This special case is sustained by an isotropic material, which may be represented by

$$\mathbf{C}=\frac{\lambda+2\mu}{5}\mathbf{C}^{(7)}+\frac{2\lambda-\mu}{5}(\mathbf{C}^{(1)}+\mathbf{C}^{(2)}+\mathbf{C}^{(3)}) \tag{14}$$

where λ and μ are the Lamé moduli. Applications of this deformation include the Lamé problem.

5 A Nonsustainable Deformation

It is easy to find deformations which are not sustained by any material. An example is the following:

$$u_1=x_1^2x_2^3x_3^{-1},\ u_2=x_1^3x_2^4x_3^{-2},\ u_3=x_1^4x_2^5x_3^{-3}. \tag{15}$$

If the analysis is carried out for this deformation, one finds $L=0$, Z contains only the null vector, and $\bar{Z}=R^{21}$.

6 Discussion

Evidently L, the dimension of Z, is related to the degree of symmetry present in a deformation. Perhaps it could be exploited in quantifying this property.

The issue discussed in this note may have application to the design of experiments for the testing of anisotropic materials. Such an experiment might, for example, require all materials to undergo the same deformation in response to prescribed displacement boundary conditions.

Acknowledgment

The author gratefully acknowledges the support of the National Science Foundation through 1987 Presidential Young Investigator Award MSM-8658107.

References

Ericksen, J. L., 1954, "Deformations Possible in Every Isotropic, Incompressible Perfectly Elastic Body," *ZAMP*, Vol. 5, pp. 466–489.

Ericksen, J. L., 1955, "Deformations Possible in Every Compressible, Isotropic, Perfectly Elastic Material," *Journal of Mathematics and Physics*, Vol. 34, pp. 126–128.

Press, W. H., Flannery, B. P., Teukolsky, S. A., and Vetterling, W. T., 1986, *Numerical Recipes*, Cambridge University Press, Cambridge, U.K., p. 52.

Shield, R. T., 1971, "Deformations Possible in Every Compressible, Isotropic, Perfectly Elastic Material," *Journal of Elasticity*, Vol. 1, pp. 91–92.

The Normality Rule in Linear Elastic Bifurcation Problems

John Roorda[5] and Robert Maaskant[5]

An interesting and potentially useful analogy exists between plasticity theory and its yield surfaces, and elastic stability theory of the title problem with its stability boundary. Of particular interest in this regard are the convexity properties of these surfaces and their associated normality conditions.

In plasticity theory the normality condition leads to a useful "flow law" based on an assumed convexity of the yield surface. In brief, stress combinations (σ_{ij}) are elastic, plastic, or nonexistent depending on the value of a function $F(\sigma_{ij})$ which, when it takes on a critical value, represents the yield surface. It is possible to express the "flow law" algebraically as $\dot{\epsilon}_{ij}^p=\mu\partial F/\partial\sigma_{ij}$, where $\dot{\epsilon}_{ij}^p$ is the plastic part of the strain rate and μ is an arbitrary positive scalar. In regions where the yield surface is differentiable, a one-to-one correspondence is established between stress and strain rate direction. At corners or vertices the strain rate vector may have any direction within the fan or cone defined by the normals of the contiguous surfaces.

A close parallel to the aforementioned ideas is found in connection with linear elastic structures that become unstable through bifurcation under multiple independent loads. The entirety of the critical load combinations associated with an initial loss of stability is called the stability boundary. The region of stability bounded by this curve has been shown to be convex if there are no pre-buckling deformations, the loads are conservative, and the equilibrium equations are linear in the loads (Papkovich, 1963; Renton, 1967). A proof for discrete systems and a variation of it for vibrating systems are presented by Huseyin (1975) and Huseyin and Roorda (1971). The stability boundary of a linear bifurcating elastic system is generally an open surface with no critical values present in regions of load space where the structural elements are placed in tension.

Let the independent loads on the structure be denoted by p_i, $(i=1, 2, 3, \ldots, m)$, and let the corresponding displacement of a loaded point, in the direction of the load, be given by e_i. The fundamental and buckled components of the corresponding displacements, taken together, make up the total displacement

$$e_i=e_i^f+e_i^b. \tag{1}$$

The stability boundary can generally be expressed in terms of the independent loads as

$$\Phi(p_i)=0. \tag{2}$$

The existence of a normality condition between the stability boundary and the buckled components of the corresponding

[5]Department of Civil Engineering, University of Waterloo, Waterloo, Ontario, Canada.

Manuscript received by the ASME Applied Mechanics Division, June 10, 1988; final revision, November 15, 1988.

Also $\bar{L}=2$ and a basis for $\bar{Z}$ is

$$\bar{\mathbf{C}}^{(1)}=\mathbf{e}_{25}-\mathbf{e}_{46} \quad \bar{\mathbf{C}}^{(2)}=\mathbf{e}_{36}-\mathbf{e}_{45}. \tag{10}$$

Thus, the only restrictions on the material properties are $C_{25}=C_{46}$ and $C_{36}= C_{45}$. For anisotropic materials, this displacement field does not, in general, solve the torsion problem for a circular rod, because the traction-free condition on the lateral surface may not be satisfied.

4 Arbitrary Radial Deformations

Suppose that there is some spherical coordinate system in which a deformation is described by $u_r(r, \theta, \phi)=f(r)$, $u_\theta \equiv u_\phi \equiv 0$, where f is a smooth function. In rectangular coordinates, this is $u_i=f(r)x_i/r$, $r=|\mathbf{x}|$. One finds

$$N_{ijk}=r^{-3}(rf'(r)-f(r))(x_i\delta_{jk}+x_j\delta_{ki}+x_k\delta_{ij})$$
$$+r^{-5}(r^2f''(r)-3rf'(r)+3f(r))x_ix_jx_k, \quad r>0. \tag{11}$$

There are two special cases. First, the case $f(r)=\alpha r$, where α is a constant, is a homogeneous deformation. Hence $L=21$ and there are no restrictions on the moduli. The second is $f(r)=\alpha r^{-2}$, which will be discussed next.

After carrying out the analysis for an arbitrary f other than these special cases one finds that $L=6$ and a basis for Z is given by

$$\begin{array}{lll}\mathbf{C}^{(1)}=2\mathbf{e}_{12}-\mathbf{e}_{66} & \mathbf{C}^{(3)}=2\mathbf{e}_{23}-\mathbf{e}_{44} & \mathbf{C}^{(5)}=2\mathbf{e}_{25}-\mathbf{e}_{46}\\ \mathbf{C}^{(2)}=2\mathbf{e}_{13}-\mathbf{e}_{55} & \mathbf{C}^{(4)}=2\mathbf{e}_{14}-\mathbf{e}_{56} & \mathbf{C}^{(6)}=2\mathbf{e}_{36}-\mathbf{e}_{45}.\end{array} \tag{12}$$

The equilibrated stress fields arising from the deformation of the materials in this Z are by no means trivial, nor are they radially symmetric. It is perhaps surprising that there are *any* materials which can sustain an arbitrary radial deformation.

For the special case $f(r)=\alpha r^{-2}$, $\alpha \neq 0$, one finds $L=7$ and the basis for Z given in (12) is augmented by

$$\mathbf{C}^{(7)}=5(\mathbf{e}_{11}+\mathbf{e}_{22}+\mathbf{e}_{33})+2(\mathbf{e}_{44}+\mathbf{e}_{55}+\mathbf{e}_{66})+\mathbf{e}_{12}+\mathbf{e}_{23}+\mathbf{e}_{13}. \tag{13}$$

This special case is sustained by an isotropic material, which may be represented by

$$\mathbf{C}=\frac{\lambda+2\mu}{5}\mathbf{C}^{(7)}+\frac{2\lambda-\mu}{5}(\mathbf{C}^{(1)}+\mathbf{C}^{(2)}+\mathbf{C}^{(3)}) \tag{14}$$

where λ and μ are the Lamé moduli. Applications of this deformation include the Lamé problem.

5 A Nonsustainable Deformation

It is easy to find deformations which are not sustained by any material. An example is the following:

$$u_1=x_1^2x_2^3x_3^{-1},\ u_2=x_1^3x_2^4x_3^{-2},\ u_3=x_1^4x_2^5x_3^{-3}. \tag{15}$$

If the analysis is carried out for this deformation, one finds $L=0$, Z contains only the null vector, and $\bar{Z}=R^{21}$.

6 Discussion

Evidently L, the dimension of Z, is related to the degree of symmetry present in a deformation. Perhaps it could be exploited in quantifying this property.

The issue discussed in this note may have application to the design of experiments for the testing of anisotropic materials. Such an experiment might, for example, require all materials to undergo the same deformation in response to prescribed displacement boundary conditions.

Acknowledgment

The author gratefully acknowledges the support of the National Science Foundation through 1987 Presidential Young Investigator Award MSM-8658107.

References

Ericksen, J. L., 1954, "Deformations Possible in Every Isotropic, Incompressible Perfectly Elastic Body," *ZAMP*, Vol. 5, pp. 466–489.

Ericksen, J. L., 1955, "Deformations Possible in Every Compressible, Isotropic, Perfectly Elastic Material," *Journal of Mathematics and Physics*, Vol. 34, pp. 126–128.

Press, W. H., Flannery, B. P., Teukolsky, S. A., and Vetterling, W. T., 1986, *Numerical Recipes*, Cambridge University Press, Cambridge, U.K., p. 52.

Shield, R. T., 1971, "Deformations Possible in Every Compressible, Isotropic, Perfectly Elastic Material," *Journal of Elasticity*, Vol. 1, pp. 91–92.

The Normality Rule in Linear Elastic Bifurcation Problems

John Roorda[5] and Robert Maaskant[5]

An interesting and potentially useful analogy exists between plasticity theory and its yield surfaces, and elastic stability theory of the title problem with its stability boundary. Of particular interest in this regard are the convexity properties of these surfaces and their associated normality conditions.

In plasticity theory the normality condition leads to a useful "flow law" based on an assumed convexity of the yield surface. In brief, stress combinations (σ_{ij}) are elastic, plastic, or nonexistent depending on the value of a function $F(\sigma_{ij})$ which, when it takes on a critical value, represents the yield surface. It is possible to express the "flow law" algebraically as $\dot{\epsilon}_{ij}^p=\mu\partial F/\partial\sigma_{ij}$, where $\dot{\epsilon}_{ij}^p$ is the plastic part of the strain rate and μ is an arbitrary positive scalar. In regions where the yield surface is differentiable, a one-to-one correspondence is established between stress and strain rate direction. At corners or vertices the strain rate vector may have any direction within the fan or cone defined by the normals of the contiguous surfaces.

A close parallel to the aforementioned ideas is found in connection with linear elastic structures that become unstable through bifurcation under multiple independent loads. The entirety of the critical load combinations associated with an initial loss of stability is called the stability boundary. The region of stability bounded by this curve has been shown to be convex if there are no pre-buckling deformations, the loads are conservative, and the equilibrium equations are linear in the loads (Papkovich, 1963; Renton, 1967). A proof for discrete systems and a variation of it for vibrating systems are presented by Huseyin (1975) and Huseyin and Roorda (1971). The stability boundary of a linear bifurcating elastic system is generally an open surface with no critical values present in regions of load space where the structural elements are placed in tension.

Let the independent loads on the structure be denoted by p_i, $(i=1, 2, 3, \ldots, m)$, and let the corresponding displacement of a loaded point, in the direction of the load, be given by e_i. The fundamental and buckled components of the corresponding displacements, taken together, make up the total displacement

$$e_i=e_i^f+e_i^b. \tag{1}$$

The stability boundary can generally be expressed in terms of the independent loads as

$$\Phi(p_i)=0. \tag{2}$$

The existence of a normality condition between the stability boundary and the buckled components of the corresponding

[5]Department of Civil Engineering, University of Waterloo, Waterloo, Ontario, Canada.

Manuscript received by the ASME Applied Mechanics Division, June 10, 1988; final revision, November 15, 1988.

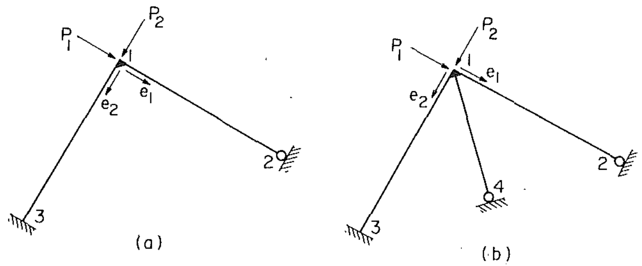

Fig. 1 Experimental test models: (a) Two-member frame and (b) three-member frame

displacements has been formally established (Huseyin, 1975; Masur, 1972), i.e.,

$$e_i^b = -\mu \frac{\partial \Phi}{\partial p_i}. \tag{3}$$

The negative sign in equation (3) is required because $\Phi(p_i)$ derives from the second variation of potential energy, which decreases through the stability boundary. The "bifurcation flow law" of equation (3) indicates that the vector e_i^b, when suitably projected into the load (p_i) subspace, is orthogonal to the stability boundary in the direction of the outward normal at the point where the load "ray" touches the boundary.

The bifurcation flow law, being rooted in the convexity of the stability boundary with its normality condition, can be interpreted in terms of elastic post-buckling work. The actual load vector, i.e., the vector to a point where the buckled component of the corresponding displacement vector is normal to the stability boundary, yields the maximum value of external post-buckling work. In other words, if $\mathbf{p}$ is the correct load vector to be associated with the displacement vector $\mathbf{e}^b$ and $\mathbf{p}'$ is any other load vector which lies inside or on the stability boundary, then $\mathbf{p} \cdot \mathbf{e}^b \geq \mathbf{p}' \cdot \mathbf{e}^b$. Simply put, the rate at which a bifurcating elastic structure absorbs strain energy is maximized.

Experiments

Some experimental evidence is now presented to corroborate the properties of convexity and normality in bifurcating elastic systems. Two different model frames, made of high strength steel members, were used.

***(a)* Two-Member Frame (Fig. 1*(a)*).** Both members in this frame were 604.6 mm long, 25.4 mm wide, and 1.6 mm thick, and were rigidly connected at right angles at joint 1, with a clamped support at 3 and a pinned support at 2.

***(b)* Three-Member Frame (Fig. 1*(b)*).** The members were connected in a common rigid joint at 1 with 45 deg subtended between them. Members 1-2 and 1-4 were 25.4 mm wide and 1.6 mm thick, and member 1-3 was 25.4 mm wide and 2.0 mm thick. The length of members 1-2 and 1-3 was 604.6 mm, and that of member 1-4 was 427.5 mm. The model had a clamped support at 3 and pin supports at 2 and 4.

Each frame, being fixed on a supporting structure mounted on a shaft to allow rotation of the frame to achieve different loading vectors, was loaded vertically at the rigid joint through a knife edge and via a long wire attached by means of a loading nut to a proving ring fixed to a firm base. The vertical and horizontal movements of the loaded joint were measured by means of displacement transducers attached to the knife edge, which was seated in a horizontally adjustable V-groove to allow the introduction of a small load eccentricity to offset any initial geometrical shape imperfections present in the model frame.

Tests were done for several loading vectors, each vector producing a different point on the stability boundary of the system. Two directions of buckling are possible at the critical load, represented by clockwise and counterclockwise joint rotation. At the critical load, a perfect frame is equally able to buckle in either direction. To compensate for the initial geometrical imperfections in the frame, the eccentricity of the load was adjusted to achieve a near perfect situation in which the effect of the load eccentricity more or less cancelled the opposing effect of the initial geometrical imperfections. The load was applied in suitable increments along the natural load path. After completion of the natural buckling path, the model was manually rotated into the opposite buckling direction to come to rest on the complementary path after suitable adjustment of the load. Readings along this path were then recorded. Four to

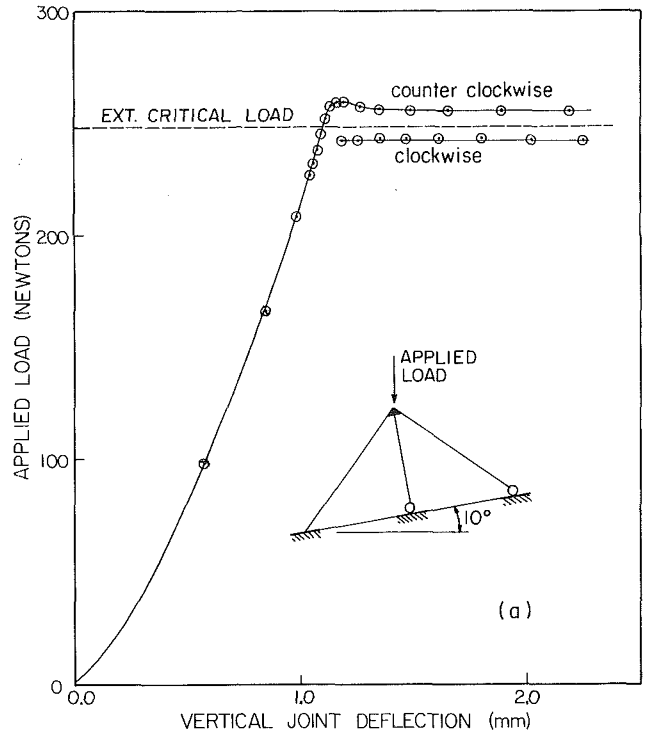

Fig. 2(*a*)

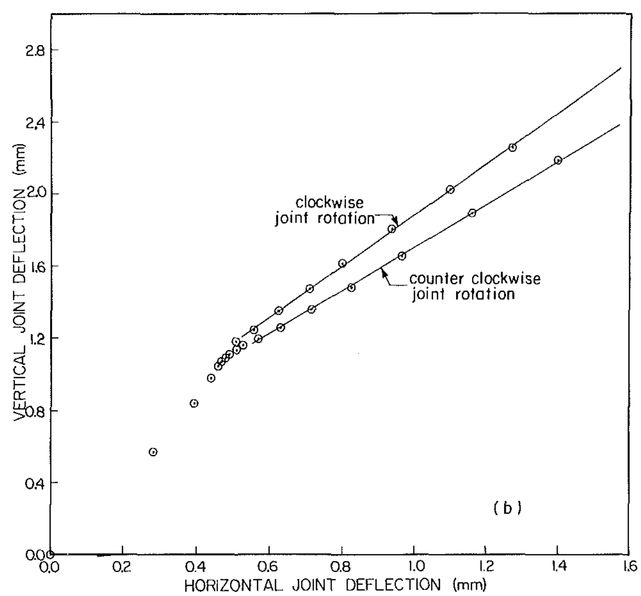

Fig. 2(*b*)

Fig. 2 Typical test measurements for the three-member frame: (*a*) applied load versus vertical deflection of the loaded joint and (*b*) horizontal versus vertical joint displacements

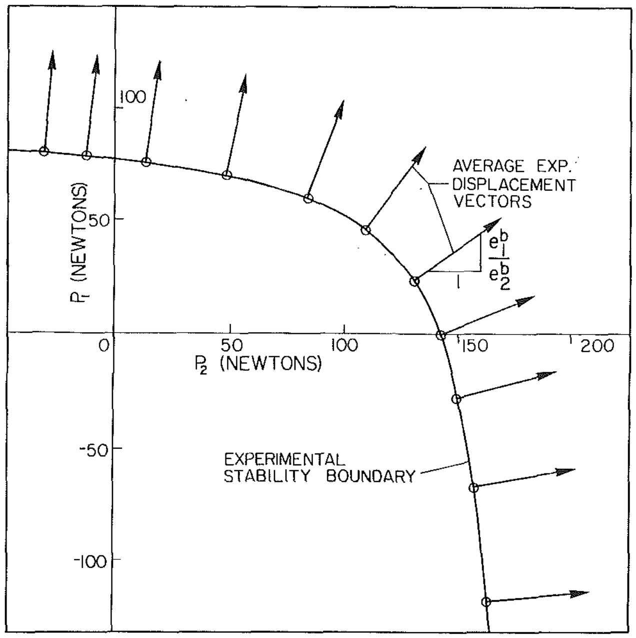

Fig. 3 Experimental stability boundary and corresponding buckling displacement vectors for the two-member frame

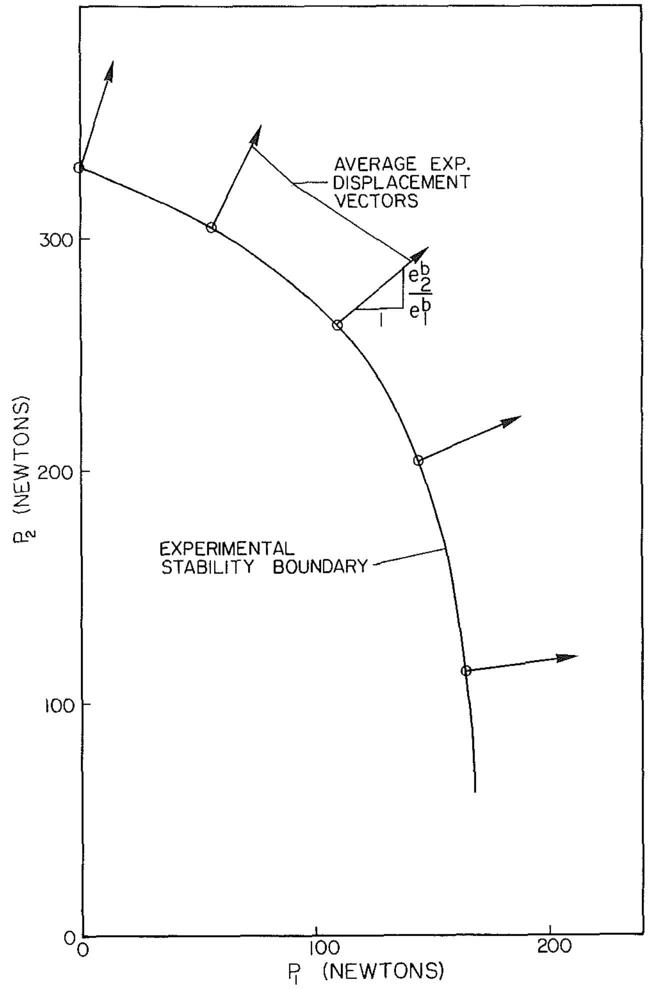

Fig. 4 Experimental stability boundary and corresponding buckling displacement vectors for the three-member frame

six tests were done for each load vector, each test yielding load and displacement measurements for both buckling directions.

The results of a typical test on the three-member frame are shown in Fig. 2. Some deflections occur before the critical load is reached. These may be attributed to settling in of the knife edge and supports under load, elastic axial deformation of the members, and a small amount of pre-buckling axial deformation due to out-of-straightness of the members and load eccentricity. Figure 2(*a*) indicates that the initial post-buckling deflections grow at almost constant load. Two branches are evident in post-buckling: one obtained from the natural loading path and the other from the complementary path. The experimental critical load is taken to be the average load for the two branches. Figure 2(*b*) shows the corresponding buckled branches in deflection space. Theoretically, for a structure without imperfections, these should coincide in location and slope, at least initially, and veer outward in a cusplike fashion due to nonlinear post-buckling behavior as the structure continues to buckle. The presence of imperfections, however, causes these branches to separate in practice, each with a slightly different slope. The average slope is taken to represent the vector of post-buckling deflections for the corresponding ideal system.

Resolving the experimental, vertically applied load into two components directed along the perpendicular members of the frame (see Fig. 1), and plotting the experimental critical values in load space (p_1 versus p_2), gives the plot shown in Fig. 3 for the two-member frame and Fig. 4 for the three-member frame. These experimental points represent the average critical value measured in 4 to 6 separate tests for a number of different load vectors obtained by rotating the model frame to specific angles. The curve drawn through these points represents the inferred experimental stability boundary for the perfect structure. In both experiments the stability boundary appears to be smoothly curved and the region of stability appears to be convex.

In a similar way the averaged buckling displacement vectors are resolved into components e_1 and e_2 (see Fig. 1). Superimposing the resultant displacement vectors on $p_1 - p_2$ load space at the corresponding experimental points on the stability boundary gives the vector directions shown in Figs. 3 and 4.

For both test models the experimental displacement vectors are practically normal to the experimentally obtained stability boundary, in harmony with the theory.

Concluding Remarks

The concepts of convexity and normality as they apply to bifurcating linear elastic structures have been presented in analogy with similar ideas in plasticity theory. The bifurcation flow law, or normality rule, which is rooted in these concepts has been corroborated in a conclusive manner by experimental evidence obtained from elastic buckling tests on continuous steel frames. The analogue found in plasticity theory, where convexity and the normality rule have provided a solid foundation for limit theorems, requires no further elaboration. How useful similar concepts will be in elastic buckling theory remains to be seen.

References

Huseyin, K., 1975, *Nonlinear Theory of Elastic Stability*, Noordhoff International Publishing, Leyden, p. 169.

Huseyin, K., and Roorda, J., 1971, "The Loading-Frequency Relationship in Multiple Eigenvalue Problems," ASME Journal of Applied Mechanics, Vol. 38, pp. 1007-1011.

Masur, E. F., 1972, discussion of a paper by Huseyin and Roorda, ASME Journal of Applied Mechanics, Vol. 39, p. 635.

Papkovich, P. F., 1963, *Works on the Structural Mechanics of Ships*, Vol. 4, Moscow, (in Russian).

Renton, J. D., 1967, "Buckling of Frames Composed of Thin-Walled Members," *Thin-Walled Structures*, Ed. A. H. Chilver et al., eds., London, pp. 1-59.

Column Buckling When Support Stiffens Under Compression

R. H. Plaut[6]

Introduction

The base of a column is often modeled as a pinned support with a rotational spring having stiffness coefficient K. For ideal pinned or clamped conditions, $K=0$ or $K=\infty$, respectively. In an actual column, K may vary as the column rotates (e.g., see Picard and Beaulieu, 1985), and this variation may have a significant effect on the behavior of the column (e.g., see Souza, 1987).

If the column is subjected to a compressive load P, the support condition may also depend on P. This has been demonstrated in recent experiments reported by Picard and Beaulieu (1985) and Picard, Beaulieu, and Pérusse (1987), in which the resistance to rotation increased as P increased. The effect of such support stiffening on column buckling is examined here. In this initial analysis, K is assumed to increase linearly with P. Results are presented for columns whose top ends are either pinned or clamped.

Analysis

Consider a uniform elastic column with bending stiffness EI and length L. It is subjected to a vertical load P at the top. The base is pinned and has a rotational spring with stiffness K. The column deflection is denoted $W(X)$, $0 \le X \le L$.

Define the nondimensional quantities

$$p=PL^2/EI,\ q=\sqrt{p},\ k=KL/EI,$$

$$x=X/L,\ w=W/L. \tag{1}$$

The equilibrium equation is

$$w''''(x)+pw''(x)=0 \tag{2}$$

with boundary conditions

$$w(0)=0,\ w''(0)-kw'(0)=0,\ w(1)=0,$$
$$\text{and either } w''(1)=0 \text{ or } w'(1)=0 \tag{3}$$

depending if the top is pinned or clamped.

The characteristic equation for the buckling loads is given by (Simitses, 1976)

$$(q^2+k)\sin q - kq\cos q = 0 \tag{4}$$

if the top is pinned, and

$$(1-k)q\sin q-(q^2+2k)\cos q+2k=0 \tag{5}$$

if the top is clamped. The nondimensional critical load p_{CR} is the square of the lowest positive root q of the characteristic equation.

Assume, for simplicity, that the support stiffens according to the linear relation

$$k=\beta+\gamma p \tag{6}$$

where $\beta \ge 0$, $\gamma \ge 0$. Equation (6) is substituted into (4) and (5), and critical loads are determined numerically. Results are presented in Figs. 1 and 2, where the initial stiffness β is fixed and the critical load is plotted as a function of the stiffening parameter γ. If the top is pinned (Fig. 1), $p_{CR}=\pi^2$ when $\beta=\gamma=0$, and $p_{CR}\rightarrow 20.2$ as $\beta\rightarrow\infty$ or $\gamma\rightarrow\infty$. If the top is clamped (Fig. 2), $p_{CR}=20.2$ when $\beta=\gamma=0$, and $p_{CR}\rightarrow 4\pi^2$ as $\beta\rightarrow\infty$ or $\gamma\rightarrow\infty$. These results demonstrate quantitatively how column buckling loads are affected by supports which stiffen when they are compressed.

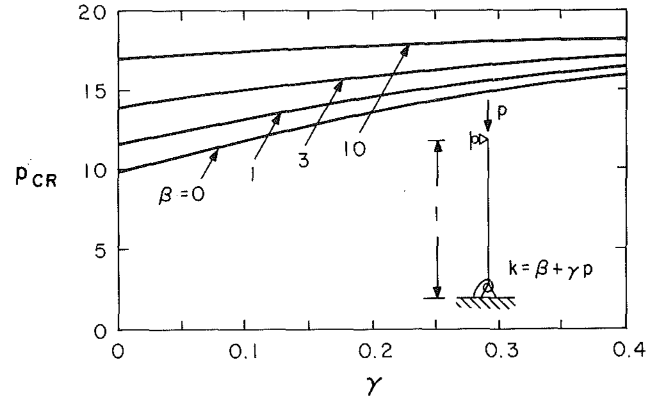

Fig. 1 Critical loads for columns pinned at the top

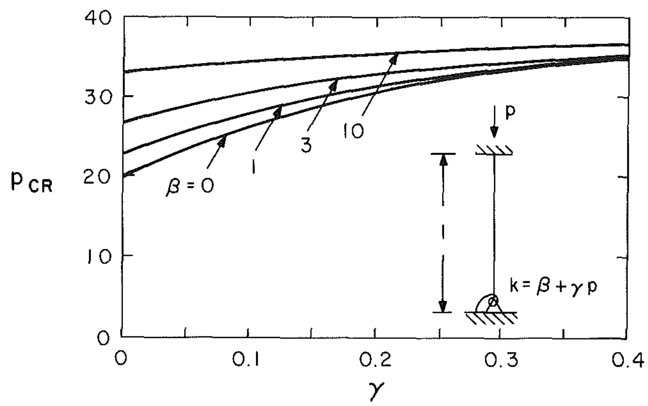

Fig. 2 Critical loads for columns clamped at the top

References

Picard, A., and Beaulieu, D., 1985, "Behaviour of a Simple Column Base Connection," *Canadian Journal of Civil Engineering*, Vol. 12, pp. 126–136.

Picard, A., Beaulieu, D., and Pérusse, B., 1987, "Rotational Restraint of a Simple Column Base Connection," *Canadian Journal of Civil Engineering*, Vol. 14, pp. 49–57.

Simitses, G. J., 1976, *An Introduction to the Elastic Stability of Structures*, Prentice-Hall, Englewood Cliffs, N.J.

Souza, M. A., 1987, "The Effects of Initial Imperfection and Changing Support Conditions on the Vibration of Structural Elements Liable to Buckling," *Thin-Walled Structures*, Vol. 5, pp. 411–423.

A Necessary Condition on the Strain-Energy Density for a Circular, Rubber-Like Plate to Have a Finite Deflection Under a Concentrated Load[7]

J. G. Simmonds[8]

[6]Professor, Department of Civil Engineering, Virginia Polytechnic Institute and State University, Blacksburg, VA 24061. Mem. ASME.

Manuscript received by the ASME Applied Mechanics Division, August 8, 1988; final revision, December 2, 1988.

[7]This research was supported by the National Science Foundation under Grant No. MSM-8618657.

[8]Department of Applied Mathematics, University of Virginia, Thornton Hall, Charlottesville, Va. 22903.

Manuscript received by the ASME Applied Mechanics Division, January 18, 1988; final revision, January 13, 1989.

Journal of Applied Mechanics

Book Reviews

Shock and Vibration Handbook, 3rd ed., edited by C. M. Harris. McGraw-Hill Book Co., New York, 1988. 1312 Pages. Price: $76.50.

REVIEWED BY C. W. BERT[1]

Since the appearance of the first edition, edited by C. M. Harris and C. E. Crede, in 1961, this handbook has become well established as "the" handbook of the whole field of shock and vibration. The present edition contains the same number of chapters (44) as did the second edition (1976). Of these, thirteen are completely new, seven are completely rewritten versions, six are minor revisions, and nineteen are essentially the same as in the second edition. In a sense, the appearance of whole new chapters (and vanishing of old ones) is a measure of the dynamicism of the field. New topics to which whole new chapters are devoted include modal analysis, ground motion-induced vibration, vibration induced by fluid flow and by wind, piezoelectric/piezoresistive transducers, signal analyzers, special purpose transducers, condition monitoring of machinery, and seismic qualification of equipment.

This book ranges the gamut from fundamental theory to analysis, design, application, standardization, instrumentation, and data reduction. It is intended primarily as a working reference book for engineers and scientists in the acoustic, aerospace, chemical, civil, electrical/electronic, and manufacturing fields. This reviewer believes that it fulfills this objective very well, especially for those just entering the shock and vibration field. It also may be useful as a supplemental reference for advanced courses in shock and/or vibration.

Nonlinear Water Waves, edited by K. Horikawa and H. Maruo. (Proceedings of IUTAM Symposium, Tokyo, Japan, August 25–28, 1987), Springer-Verlag, New York, 1987. 466 Pages.

REVIEWED BY A. D. D. CRAIK[2]

This volume records the proceedings of a IUTAM Symposium on *Nonlinear Water Waves*, comprising three "keynote lectures", 33 contributed papers, and 15 posters. Authors' camera-ready contributions, in the usual variety of typefaces, are acceptably reproduced; there is a brief editors' introduction and a full list of participants. The wide international representation included many leading water-wave researchers: The number of Japanese participants was naturally large, but numbers from the U.S.A. (8) and U.K. (2) were surprisingly small.

In the editors' words: "The Symposium has intended to provide a wide scope of analytical and numerical methods as well as experimental studies for the analysis of the nonlinear phenomena related to water waves . . . . . the scope of the presented papers includes the following topics: (1) Theoretical and experimental studies of nonlinear water waves, (2) Nonlinear instability and deformation of water waves, (3) Wave breaking, (4) Nonlinear wave-current interaction, (5) Nonlinear water waves around structures and ships, (6) Wave-body interaction, and (7) Nonlinear internal waves."

The keynote lectures were by C. C. Mei on nonlinear diffraction effects, D. H. Peregrine on modeling of unsteady and breaking waves, and O. M. Faltinsen on nonlinear interactions between waves and bodies. The emphasis on nonlinear effects reflects recent theoretical and computational advances. These, in turn, are mainly motivated by the need to understand and predict the complex interactions of waves with ships, moored structures, and underwater topography.

As a whole, the contributions are an interesting sample of current research, including such topics as shallow-water solutions, standing waves in closed basins, breaking and spilling waves, resonant interactions, wave propagation over bodies and varying topography, second-order wave-induced forces on bodies, nonlinear ship waves, and simulation of wave spectra. With few exceptions, each paper is restricted in length to eight pages: Inevitably, some are tantalizingly brief and others are mercifully so. Equally inevitably, many have been, or will be, published in greater detail in referred journals. One paper contains the first recorded occurrence (and hopefully the last!) of the word "serendipiditiously."

The usefulness of this collection is transient: For a few years it will provide a convenient, though incomplete and disconnected, survey of current strands of water-wave research, of use to specialists in this and related areas. It would be a worthwhile, but not indispensible, addition to research libraries. I, for one, have learned something from reading it.

Micromechanics of Defects in Solids, Second Rev. Ed., by T. Mura, Martinus Nijhoff Publishers, Boston, MA, 1987. 587 Pages.

REVIEWED BY T. C. T. TING[3]

This is a very well written book. The central theme of the book is the concept of eigenstrain, originally due to Eshelby, which has been systematically employed by Professor Mura in

[1]Benjamin H. Perkinson Chair Professor of Engineering, School of Aerospace and Mechanical Engineering, The University of Oklahoma, Norman, Okla. 73019. Fellow ASME.

[2]Professor, Department of Applied Mathematics, University of St. Andrews, Fife, Scotland, U.K.

[3]Professor of Applied Mechanics, Department of Civil Engineering, Mechanics, and Metallurgy, University of Illinois at Chicago, Box 4348, Chicago, Ill. 60680.